

**Handbook of Spectroscopy**

*Edited by G. Gauglitz and T. Vo-Dinh*

**Related Titles from WILEY-VCH**

H. Günzler and H.-U. Gremlich (eds)

**IR Spectroscopy**

2002. ca. 361 pages.

Hardcover. ISBN 3-527-28896-1

H. W. Siesler, Y. Ozaki, S. Kawata and H. M. Heise (eds)

**Near-Infrared Spectroscopy**

**Principles, Instruments, Applications**

2001. ca. 348 pages.

Hardcover. ISBN 3-527-30149-6

H. Günzler and A. Williams (eds)

**Handbook of Analytical Techniques**

2001. 2 Volumes, 1182 pages.

Hardcover. ISBN 3-527-30165-8

J. F. Haw (ed)

**In-situ Spectroscopy in Heterogeneous Catalysis**

2002. ca. 276 pages.

Hardcover. ISBN 3-527-30248-4

# **Handbook of Spectroscopy**

*Edited by G. Gauglitz and T. Vo-Dinh*



**WILEY-VCH GmbH & Co. KGaA**

*Handbook of Spectroscopy*. Edited by Günter Gauglitz and Tuan Vo-Dinh  
Copyright © 2003 WILEY-VCH Verlag GmbH & Co. KGaA, Weinheim  
ISBN 3-527-29782-0

**Prof. Dr. Guenter Gauglitz**  
Institute for Physical and Theoretical  
Chemistry  
University of Tübingen  
Auf der Morgenstelle 8  
72976 Tübingen  
Germany

**Prof. Dr. Tuan Vo-Dinh**  
Advanced Biomedical Science  
and Technology Group  
Oak Ridge National Laboratory  
P. O. Box 2008  
Oak Ridge, Tennessee 37831-6101  
USA

This book was carefully produced. Nevertheless, editors, authors and publisher do not warrant the information contained therein to be free of errors. Readers are advised to keep in mind that statements, data, illustrations, procedural details or other items may inadvertently be inaccurate.

**Library of Congress Card No.: applied for**  
A catalogue record for this book is available  
from the British Library.

**Bibliographic information published by**  
**Die Deutsche Bibliothek**  
Die Deutsche Bibliothek lists this publication  
in the Deutsche Nationalbibliografie;  
detailed bibliographic data is available in the  
Internet at <http://dnb.ddb.de>.

© 2003 WILEY-VCH Verlag GmbH & Co.  
KGaA, Weinheim

All rights reserved (including those of  
translation in other languages). No part of  
this book may be reproduced in any form –  
by photoprinting, microfilm, or any other  
means – nor transmitted or translated into  
machine language without written permis-  
sion from the publishers. Registered names,  
trademarks, etc. used in this book, even  
when not specifically marked as such, are  
not to be considered unprotected by law.

Printed in the Federal Republic of Germany.

Printed on acid-free paper.

**Typesetting** Hagedorn Kommunikation,  
Viernheim  
**Printing** Strauss Offsetdruck GmbH,  
Mörlenbach  
**Bookbinding** J. Schäffer GmbH & Co. KG,  
Grünstadt

**ISBN** 3-527-29782-0

## Contents

### Volume 1

Preface XXVIII

List of Contributors

### Section I Sample Preparation and Sample Pretreatment 1

Introduction 3

1 Collection and Preparation of Gaseous Samples 4

1.1 Introduction 4

1.2 Sampling considerations 5

1.3 Active vs. Passive Sampling 8

1.3.1 Active Air Collection Methods 8

1.3.1.1 Sorbents 9

1.3.1.2 Bags 11

1.3.1.3 Canisters 11

1.3.1.4 Bubblers 12

1.3.1.5 Mist Chambers 13

1.3.1.6 Cryogenic Trapping 13

1.3.2 Passive Sampling 13

1.4 Extraction and Preparation of Samples 14

1.5 Summary 15

2 Sample Collection and Preparation of Liquid and Solids 17

2.1 Introduction 17

2.2 Collection of a Representative Sample 17

2.2.1 Statistics of Sampling 18

2.2.2 How Many Samples Should be Obtained? 21

2.2.3 Sampling 22

2.2.3.1 Liquids 22

2.2.3.2 Solids 23

2.3 Preparation of Samples for Analysis 24

2.3.1	Solid Samples	24
2.3.1.1	Sample Preparation for Inorganic Analysis	25
2.3.1.2	Decomposition of Organics	28
2.3.2	Liquid Samples	29
2.3.2.1	Extraction/Separation and Preconcentration	29
2.3.2.2	Chromatographic Separation	31

## **Section II Methods 1: Optical Spectroscopy** 37

<b>3</b>	<b>Basics of Optical Spectroscopy</b>	39
3.1	Absorption of Light	39
3.2	Infrared Spectroscopy	41
3.3	Raman Spectroscopy	43
3.4	UV/VIS Absorption and Luminescence	44
<b>4</b>	<b>Instrumentation</b>	48
4.1	MIR Spectrometers	48
4.1.1	Dispersive Spectrometers	49
4.1.2	Fourier-Transform Spectrometers	50
4.1.2.1	Detectors	53
4.1.2.2	Step-scan Operation	53
4.1.2.3	Combined Techniques	54
4.2	NIR Spectrometers	54
4.2.1	FT-NIR Spectrometers	55
4.2.2	Scanning-Grating Spectrometers	55
4.2.3	Diode Array Spectrometers	56
4.2.4	Filter Spectrometers	56
4.2.5	LED Spectrometers	56
4.2.6	AOTF Spectrometers	56
4.3	Raman Spectrometers	57
4.3.1	Raman Grating Spectrometer with Single Channel Detector	57
4.3.1.1	Detectors	59
4.3.1.2	Calibration	60
4.3.2	FT-Raman Spectrometers with Near-Infrared Excitation	61
4.3.3	Raman Grating Polychromator with Multichannel Detector	61
4.4	UV/VIS Spectrometers	63
4.4.1	Sources	64
4.4.2	Monochromators	64
4.4.3	Detectors	64
4.5	Fluorescence Spectrometers	66
<b>5</b>	<b>Measurement Techniques</b>	70
5.1	Transmission Measurements	71
5.2	Reflection Measurements	73
5.2.1	External Reflection	73

5.2.2	Reflection Absorption	75
5.2.3	Attenuated Total Reflection (ATR)	75
5.2.4	Reflection at Thin Films	77
5.2.5	Diffuse Reflection	78
5.3	Spectroscopy with Polarized Light	81
5.3.1	Optical Rotatory Dispersion	81
5.3.2	Circular Dichroism (CD)	82
5.4	Photoacoustic Measurements	83
5.5	Microscopic Measurements	84
5.5.1	Infrared Microscopes	85
5.5.2	Confocal Microscopes	85
5.5.3	Near-field Microscopes	86
<b>6</b>	<b>Applications</b>	89
6.1	Mid-Infrared (MIR) Spectroscopy	89
6.1.1	Sample Preparation and Measurement	89
6.1.1.1	Gases	90
6.1.1.2	Solutions and Neat Liquids	91
6.1.1.3	Pellets and Mulls	92
6.1.1.4	Neat Solid Samples	94
6.1.1.5	Reflection–Absorption Sampling Technique	94
6.1.1.6	Sampling with the ATR Technique	95
6.1.1.7	Thin Samples	96
6.1.1.8	Diffuse Reflection Sampling Technique	97
6.1.1.9	Sampling by Photoacoustic Detection	97
6.1.1.10	Microsampling	98
6.1.2	Structural Analysis	98
6.1.2.1	The Region from 4000 to 1400 $\text{cm}^{-1}$	102
6.1.2.2	The Region 1400–900 $\text{cm}^{-1}$	102
6.1.2.3	The Region from 900 to 400 $\text{cm}^{-1}$	102
6.1.3	Special Applications	103
6.2	Near-Infrared Spectroscopy	104
6.2.1	Sample Preparation and Measurement	105
6.2.2	Applications of NIR Spectroscopy	110
6.3	Raman Spectroscopy	112
6.3.1	Sample Preparation and Measurements	112
6.3.1.1	Sample Illumination and Light Collection	113
6.3.1.2	Polarization Measurements	118
6.3.1.3	Enhanced Raman Scattering	119
6.3.2	Special Applications	120
6.4	UV/VIS Spectroscopy	125
6.4.1	Sample Preparation	125
6.4.2	Structural Analysis	129
6.4.3	Special Applications	132
6.5	Fluorescence Spectroscopy	135

6.5.1	Sample Preparation and Measurements	138
6.5.1.1	Fluorescence Quantum Yield and Lifetime	138
6.5.1.2	Fluorescence Quencher	139
6.5.1.3	Solvent Relaxation	144
6.5.1.4	Polarized Fluorescence	148
6.5.2	Special Applications	152

## Section III Methods 2: Nuclear Magnetic Resonance Spectroscopy 169

### Introduction 171

#### 7 An Introduction to Solution, Solid-State, and Imaging NMR Spectroscopy 177

7.1	Introduction	177
7.2	Solution-state $^1\text{H}$ NMR	179
7.3	Solid-state NMR	187
7.3.1	Dipolar Interaction	188
7.3.2	Chemical Shift Anisotropy	190
7.3.3	Quadrupolar Interaction	191
7.3.4	Magic Angle Spinning (MAS) NMR	194
7.3.5	$T_1$ and $T_{1\rho}$ Relaxation	195
7.3.6	Dynamics	198
7.4	Imaging	199
7.5	3D NMR: The HNCA Pulse Sequence	204
7.6	Conclusion	207

#### 8 Solution NMR Spectroscopy 209

8.1	Introduction	209
8.2	1D (One-dimensional) NMR Methods	210
8.2.1	Proton Spin Decoupling Experiments	211
8.2.2	Proton Decoupled Difference Spectroscopy	212
8.2.3	Nuclear Overhauser Effect (NOE) Difference Spectroscopy	212
8.2.4	Selective Population Transfer (SPT)	213
8.2.5	$J$ -Modulated Spin Echo Experiments	213
8.2.5.1	INEPT (Insensitive Nucleus Enhancement by Polarization Transfer)	214
8.2.5.2	DEPT (Distortionless Enhancement Polarization Transfer)	215
8.2.6	Off-Resonance Decoupling	216
8.2.7	Relaxation Measurements	217
8.3	Two-dimensional NMR Experiments	218
8.3.1	2D $J$ -Resolved NMR Experiments	219
8.3.2	Homonuclear 2D NMR Spectroscopy	223
8.3.2.1	COSY, Homonuclear Correlated Spectroscopy	223
8.3.2.2	Homonuclear TOCSY, Total Correlated Spectroscopy	226
8.3.2.3	NOESY, Nuclear Overhauser Enhancement Spectroscopy	228

8.3.2.4	ROESY, Rotating Frame Overhauser Enhanced Spectroscopy	230
8.3.2.5	NOESY vs. ROESY	231
8.3.2.6	Other Homonuclear Autocorrelation Experiments	231
8.3.3	Gradient Homonuclear 2D NMR Experiments	232
8.3.4	Heteronuclear Shift Correlation	234
8.3.5	Direct Heteronuclear Chemical Shift Correlation Methods	234
8.3.5.1	HMQC, Heteronuclear Multiple Quantum Coherence	234
8.3.6	HSQC, Heteronuclear Single Quantum Coherence Chemical Shift Correlation Techniques	236
8.3.6.1	Multiplicity-edited Heteronuclear Shift Correlation Experiments	237
8.3.6.2	Accordion-optimized Direct Heteronuclear Shift Correlation Experiments	239
8.3.7	Long-range Heteronuclear Chemical Shift Correlation	240
8.3.7.1	HMBC, Heteronuclear Multiple Bond Correlation	242
8.3.7.2	Variants of the Basic HMBC Experiment	243
8.3.7.3	Accordion-optimized Long-range Heteronuclear Shift Correlation Methods.	244
8.3.7.4	$^{2J}J$ -HMBC	248
8.3.7.5	Relative Sensitivity of Long-range Heteronuclear Shift Correlation Experiments	251
8.3.7.6	Applications of Accordion-optimized Long-range Heteronuclear Shift Correlation Experiments	252
8.3.8	Hyphenated-2D NMR Experiments	252
8.3.9	One-dimensional Analogues of 2D NMR Experiments	255
8.3.10	Gradient 1D NOESY	255
8.3.11	Selective 1D Long-range Heteronuclear Shift Correlation Experiments	257
8.3.12	Small Sample NMR Studies	257
8.4	Conclusions	262
<b>9</b>	<b>Solid-State NMR</b>	269
9.1	Introduction	269
9.2	Solid-state NMR Lineshapes	272
9.2.1	The Orientational Dependence of the NMR Resonance Frequency	272
9.2.2	Single-crystal NMR	273
9.2.3	Powder Spectra	275
9.2.4	One-dimensional $^2\text{H}$ NMR	278
9.3	Magic-angle Spinning	280
9.3.1	CP MAS NMR	281
9.3.2	$^1\text{H}$ Solid-State NMR	285
9.4	Recoupling Methods	287
9.4.1	Heteronuclear Dipolar-coupled Spins: REDOR	287
9.4.2	Homonuclear Dipolar-coupled Spins	290
9.4.3	The CSA: CODEX	291
9.5	Homonuclear Two-dimensional Experiments	292

9.5.1	Establishing the Backbone Connectivity in an Organic Molecule	293
9.5.2	Dipolar-mediated Double-quantum Spectroscopy	295
9.5.3	High-resolution $^1\text{H}$ Solid-state NMR	298
9.5.4	Anisotropic – Isotropic Correlation: The Measurement of CSAs	300
9.5.5	The Investigation of Slow Dynamics: 2D Exchange	303
9.5.6	$^1\text{H}$ – $^1\text{H}$ DQ MAS Spinning-sideband Patterns	305
9.6	Heteronuclear Two-dimensional Experiments	307
9.6.1	Heteronuclear Correlation	307
9.6.2	The Quantitative Determination of Heteronuclear Dipolar Couplings	310
9.6.3	Torsional Angles	312
9.6.4	Oriented Samples	313
9.7	Half-integer Quadrupole Nuclei	315
9.8	Summary	319

## Section IV Methods 3: Mass Spectrometry 327

<b>10</b>	<b>Mass Spectrometry</b>	329
10.1	Introduction: Principles of Mass Spectrometry	329
10.1.1	Application of Mass Spectrometry to Biopolymer Analysis	330
10.2	Techniques and Instrumentation of Mass Spectrometry	331
10.2.1	Sample Introduction and Ionisation Methods	331
10.2.1.1	Pre-conditions	331
10.2.1.2	Gas Phase (“Hard”) Ionisation Methods	331
10.2.1.3	“Soft” Ionisation Techniques	332
10.2.2	Mass Spectrometric Analysers	335
10.2.2.1	Magnetic Sector Mass Analysers	335
10.2.2.2	Quadrupole Mass Analysers	337
10.2.2.3	Time-of-Flight Mass Analysers	338
10.2.2.4	Trapped-Ion Mass Analysers	339
10.2.2.5	Hybrid Instruments	340
10.2.3	Ion Detection and Spectra Acquisition	340
10.2.4	High Resolution Fourier Transform Ion Cyclotron Resonance (ICR) Mass Spectrometry	341
10.2.5	Sample Preparation and Handling in Bioanalytical Applications	344
10.2.5.1	Liquid–Liquid Extraction (LLE)	344
10.2.5.2	Solid Phase Extraction (SPE)	345
10.2.5.3	Immunoaffinity Extraction (IAE)	345
10.2.5.4	Solid-phase Microextraction	345
10.2.5.5	Supercritical-Fluid Extraction (SFE)	346
10.2.6	Coupling of Mass Spectrometry with Microseparation Methods	346
10.2.6.1	Liquid Chromatography-Mass Spectrometry Coupling (LC-MS)	347
10.2.6.2	Capillary Electrophoresis (CE)-Mass Spectrometry	348
10.3	Applications of Mass Spectrometry to Biopolymer Analysis	349

10.3.1	Introduction	349
10.3.2	Analysis of Peptide and Protein Primary Structures and Post-Translational Structure Modifications	349
10.3.3	Tertiary Structure Characterisation by Chemical Modification and Mass Spectrometry	353
10.3.4	Characterisation of Non-Covalent Supramolecular Complexes	354
10.3.5	Mass Spectrometric Proteome Analysis	356

## Section V Methods 4: Elemental Analysis 363

<b>11</b>	<b>X-ray Fluorescence Analysis</b>	<b>365</b>
11.1	Introduction	365
11.2	Basic Principles	367
11.2.1	X-ray Wavelength and Energy Scales	367
11.2.2	Interaction of X-rays with Matter	367
11.2.3	Photoelectric Effect	369
11.2.4	Scattering	371
11.2.5	Bremsstrahlung	372
11.2.6	Selection Rules, Characteristic Lines and X-ray Spectra	373
11.2.7	Figures-of-merit for XRF Spectrometers	376
11.2.7.1	Analytical Sensitivity	376
11.2.7.2	Detection and Determination Limits	377
11.3	Instrumentation	380
11.3.1	X-ray Sources	380
11.3.2	X-ray Detectors	384
11.3.3	Wavelength-dispersive XRF	390
11.3.4	Energy-dispersive XRF	393
11.3.5	Radioisotope XRF	397
11.3.6	Total Reflection XRF	398
11.3.7	Microscopic XRF	399
11.4	Matrix Effects	401
11.4.1	Thin and Thick Samples	401
11.4.2	Primary and Secondary Absorption, Direct and Third Element Enhancement	403
11.5	Data Treatment	404
11.5.1	Counting Statistics	404
11.5.2	Spectrum Evaluation Techniques	405
11.5.2.1	Data Extraction in WDXRF	406
11.5.2.2	Data Extraction in EDXRF: Simple Case, No Peak Overlap	407
11.5.2.3	Data Extraction in EDXRF, Multiple Peak Overlap	408
11.5.3	Quantitative Calibration Procedures	409
11.5.3.1	Single-element Techniques	412
11.5.3.2	Multiple-element Techniques	413
11.5.4	Error Sources in X-ray Fluorescence Analysis	415

11.5.5	Specimen Preparation for X-ray Fluorescence	416
11.6	Advantages and Limitations	417
11.6.1	Qualitative Analysis	417
11.6.2	Detection Limits	418
11.6.3	Quantitative Reliability	418
11.7	Summary	419
<b>12</b>	<b>Atomic Absorption Spectrometry (AAS) and Atomic Emission Spectrometry (AES)</b>	<b>421</b>
12.1	Introduction	421
12.2	Theory of Atomic Spectroscopy	421
12.2.1	Basic Principles	421
12.2.2	Fundamentals of Absorption and Emission	426
12.2.2.1	Absorption	429
12.2.2.2	Line Broadening	430
12.2.2.3	Self-absorption	431
12.2.2.4	Ionisation	432
12.2.2.5	Dissociation	434
12.2.2.6	Radiation Sources and Atom Reservoirs	434
12.3	Atomic Absorption Spectrometry (AAS)	436
12.3.1	Introduction	436
12.3.2	Instrumentation	436
12.3.2.1	Radiation Sources	437
12.3.2.2	Atomisers	440
12.3.2.3	Optical Set-up and Components of Atomic Absorption Instruments	453
12.3.3	Spectral Interference	454
12.3.3.1	Origin of Spectral Interference	454
12.3.3.2	Methods for Correcting for Spectral Interference	455
12.3.4	Chemical Interferences	462
12.3.4.1	The Formation of Compounds of Low Volatility	463
12.3.4.2	Influence on Dissociation Equilibria	463
12.3.4.3	Ionisation in Flames	464
12.3.5	Data Treatment	465
12.3.5.1	Quantitative Analysis	465
12.3.6	Hyphenated Techniques	466
12.3.6.1	Gas Chromatography-Atomic Absorption Spectrometry	467
12.3.6.2	Liquid Chromatography-Atomic Absorption Spectrometry	469
12.3.7	Conclusion and Future Directions	470
12.4	Atomic Emission Spectrometry (AES)	471
12.4.1	Introduction	471
12.4.2	Instrumentation	471
12.4.2.1	Atomisation Devices	471
12.4.2.2	Optical Set-up and Detection	480
12.4.2.3	Instrumentation for Solid Sample Introduction	483

12.4.3	Matrix Effects and Interference	486
12.4.3.1	Spectral Interferences	486
12.4.3.2	Matrix Effects and Chemical Interferences	487
12.4.4	Quantitative and Qualitative Analysis	488
12.4.5	Advantages and Limitations	491
12.4.5.1	Absolute and Relative Sensitivity	491
12.4.5.2	Hyphenated Techniques	491
12.5	Summary	493

## **Section VI Methods 5: Surface Analysis Techniques** 497

<b>13</b>	<b>Surface Analysis Techniques</b>	<b>499</b>
13.1	Introduction	499
13.2	Definition of the Surface	501
13.3	Selection of Method	501
13.4	Individual Techniques	506
13.4.1	Angle Resolved Ultraviolet Photoelectron Spectroscopy	506
13.4.1.1	Introduction	507
13.4.1.2	Instrumentation	507
13.4.1.3	Sample	507
13.4.1.4	Analytical Information	507
13.4.1.5	Performance Criteria	507
13.4.1.6	Applications	508
13.4.1.7	Other Techniques	508
13.4.2	Appearance Potential Spectroscopy	508
13.4.2.1	Introduction	508
13.4.2.2	Instrumentation	508
13.4.2.3	Sample	509
13.4.2.4	Analytical Information	509
13.4.2.5	Performance Criteria	509
13.4.2.6	Applications	509
13.4.2.7	Other Techniques	510
13.4.3	Atom Probe Field Ion Microscopy	510
13.4.3.1	Introduction	510
13.4.3.2	Instrumentation	510
13.4.3.3	Analytical Information	510
13.4.3.4	Performance Criteria	510
13.4.3.5	Applications	510
13.4.4	Attenuated Total Reflection Spectroscopy	511
13.4.4.1	Introduction	511
13.4.4.2	Instrumentation	511
13.4.4.3	Analytical Information	511
13.4.4.4	Performance Criteria	511
13.4.4.5	Applications	512

13.4.5	Auger Electron Spectroscopy	512
13.4.5.1	Introduction	512
13.4.5.2	Instrumentation	512
13.4.5.3	Sample	513
13.4.5.4	Analytical Information	513
13.4.5.5	Performance Criteria	513
13.4.5.6	Applications	514
13.4.5.7	Other Techniques	514
13.4.6	Auger Photoelectron Coincidence Spectroscopy	514
13.4.6.1	Introduction	514
13.4.6.2	Instrumentation	515
13.4.6.3	Sample	515
13.4.6.4	Analytical Information	515
13.4.6.5	Performance Criteria	515
13.4.6.6	Applications	516
13.4.6.7	Other Techniques	516
13.4.7	Charge Particle Activation Analysis	516
13.4.7.1	Introduction	516
13.4.7.2	Instrumentation	516
13.4.7.3	Sample	517
13.4.7.4	Analytical Information	517
13.4.7.5	Performance Criteria	517
13.4.7.6	Application	518
13.4.7.7	Other Technique	518
13.4.8	Diffuse Reflection Spectroscopy	518
13.4.8.1	Introduction	518
13.4.8.2	Instrumentation	518
13.4.8.3	Analytical Information	519
13.4.8.4	Performance Criteria	519
13.4.8.5	Applications	519
13.4.9	Elastic Recoil Detection Analysis	520
13.4.9.1	Introduction	520
13.4.9.2	Instrumentation	520
13.4.9.3	Sample	520
13.4.9.4	Analytical Information	520
13.4.9.5	Performance Criteria	521
13.4.9.6	Applications	522
13.4.9.7	Other Techniques	522
13.4.10	Electron Momentum Spectroscopy	522
13.4.10.1	Introduction	523
13.4.10.2	Instrumentation	523
13.4.10.3	Sample	523
13.4.10.4	Analytical Information	523
13.4.10.5	Performance Criteria	523
13.4.10.6	Applications	523

- 13.4.11 Electron Probe Microanalysis 524
  - 13.4.11.1 Introduction 524
  - 13.4.11.2 Instrumentation 524
  - 13.4.11.3 Sample 524
  - 13.4.11.4 Analytical Information 524
  - 13.4.11.5 Performance Criteria 525
  - 13.4.11.6 Applications 525
- 13.4.12 Electron Stimulated Desorption 525
  - 13.4.12.1 Introduction 525
  - 13.4.12.2 Instrumentation 525
  - 13.4.12.3 Sample 526
  - 13.4.12.4 Analytical Information 526
  - 13.4.12.5 Performance Criteria 526
  - 13.4.12.6 Applications 526
- 13.4.13 Electron Stimulated Desorption Ion Angular Distributions 526
  - 13.4.13.1 Introduction 526
  - 13.4.13.2 Instrumentation 527
  - 13.4.13.3 Sample 527
  - 13.4.13.4 Analytical Information 527
  - 13.4.13.5 Performance Criteria 527
  - 13.4.13.6 Applications 527
- 13.4.14 Ellipsometry 528
  - 13.4.14.1 Introduction 528
  - 13.4.14.2 Instrumentation 528
  - 13.4.14.3 Sample 528
  - 13.4.14.4 Analytical Information 528
  - 13.4.14.5 Performance Criteria 529
  - 13.4.14.6 Applications 529
- 13.4.15 Extended Energy Loss Fine Structure 529
  - 13.4.15.1 Introduction 529
  - 13.4.15.2 Instrumentation 530
  - 13.4.15.3 Analytical Information 530
  - 13.4.15.4 Performance Criteria 530
  - 13.4.15.5 Applications 530
  - 13.4.15.6 Other Techniques 530
- 13.4.16 Evanescent Wave Cavity Ring-down Spectroscopy 530
  - 13.4.16.1 Introduction 531
  - 13.4.16.2 Instrumentation 531
  - 13.4.16.3 Performance Criteria 531
  - 13.4.16.4 Applications 531
- 13.4.17 Glow Discharge Optical Emission Spectrometry 531
  - 13.4.17.1 Introduction 531
  - 13.4.17.2 Instrumentation 532
  - 13.4.17.3 Sample 532
  - 13.4.17.4 Analytical Information 532

- 13.4.17.5 Performance Criteria 532
- 13.4.17.6 Application 533
- 13.4.17.7 Other Techniques 533
- 13.4.18 High Resolution Electron Energy Loss Spectroscopy 533
  - 13.4.18.1 Introduction 533
  - 13.4.18.2 Instrumentation 533
  - 13.4.18.3 Sample 534
  - 13.4.18.4 Analytical Information 534
  - 13.4.18.5 Performance Criteria 534
  - 13.4.18.6 Applications 535
  - 13.4.18.7 Other Techniques 535
- 13.4.19 Inelastic Electron Tunneling Spectroscopy 535
  - 13.4.19.1 Introduction 535
  - 13.4.19.2 Instrumentation 536
  - 13.4.19.3 Sample 536
  - 13.4.19.4 Analytical Information 536
  - 13.4.19.5 Performance Criteria 536
  - 13.4.19.6 Applications 536
- 13.4.20 Inverse Photoelectron Spectroscopy 536
  - 13.4.20.1 Introduction 536
  - 13.4.20.2 Instrumentation 537
  - 13.4.20.3 Sample 537
  - 13.4.20.4 Analytical Information 537
  - 13.4.20.5 Performance Criteria 538
  - 13.4.20.6 Applications 538
- 13.4.21 Ion Neutralization Spectroscopy 538
  - 13.4.21.1 Introduction 538
  - 13.4.21.2 Instrumentation 538
  - 13.4.21.3 Sample 539
  - 13.4.21.4 Analytical Information 539
  - 13.4.21.5 Performance Criteria 539
  - 13.4.21.6 Applications 539
  - 13.4.21.7 Other Techniques 539
- 13.4.22 Ion Probe Microanalysis 539
  - 13.4.22.1 Introduction 540
  - 13.4.22.2 Instrumentation 540
  - 13.4.22.3 Sample 540
  - 13.4.22.4 Analytical Information 540
  - 13.4.22.5 Performance Criteria 541
  - 13.4.22.6 Application 541
  - 13.4.22.7 Other Techniques 541
- 13.4.23 Low-energy Ion Scattering Spectrometry 542
  - 13.4.23.1 Introduction 542
  - 13.4.23.2 Instrumentation 542
  - 13.4.23.3 Sample 542

- 13.4.23.4 Analytical Information 542
- 13.4.23.5 Performance Criteria 543
- 13.4.23.6 Application 543
- 13.4.23.7 Other Technique 543
- 13.4.24 Near Edge X-ray Absorption Spectroscopy 544
  - 13.4.24.1 Introduction 544
  - 13.4.24.2 Instrumentation 544
  - 13.4.24.3 Sample 544
  - 13.4.24.4 Analytical Information 544
  - 13.4.24.5 Performance Criteria 544
  - 13.4.24.6 Applications 545
  - 13.4.24.7 Other Techniques 545
- 13.4.25 Neutron Depth Profiling 545
  - 13.4.25.1 Introduction 545
  - 13.4.25.2 Instrumentation 545
  - 13.4.25.3 Sample 545
  - 13.4.25.4 Analytical Information 545
  - 13.4.25.5 Performance Criteria 546
  - 13.4.25.6 Application 546
  - 13.4.26 Particle Induced Gamma Ray Emission 546
- 13.4.26.1 Introduction 547
  - 13.4.26.2 Instrumentation 547
  - 13.4.26.3 Sample 547
  - 13.4.26.4 Analytical Information 547
  - 13.4.26.5 Performance Criteria 547
  - 13.4.26.6 Applications 548
- 13.4.27 Particle Induced X-ray Emission 548
  - 13.4.27.1 Introduction 548
  - 13.4.27.2 Instrumentation 548
  - 13.4.27.3 Sample 549
  - 13.4.27.4 Spectrum 549
  - 13.4.27.5 Analytical Information 549
  - 13.4.27.6 Performance Criteria 550
  - 13.4.27.7 Application 550
  - 13.4.27.8 Other Techniques 550
- 13.4.28 Penning Ionisation Electron Spectroscopy 551
  - 13.4.28.1 Introduction 551
  - 13.4.28.2 Instrumentation 551
  - 13.4.28.3 Sample 551
  - 13.4.28.4 Analytical Information 551
  - 13.4.28.5 Performance Criteria 552
  - 13.4.28.6 Applications 552
  - 13.4.28.7 Other Techniques 552
  - 13.4.29 Photoacoustic Spectroscopy 552
- 13.4.29.1 Introduction 552

- 13.4.29.2 Instrumentation 553
- 13.4.29.3 Analytical Information 553
- 13.4.29.4 Performance Criteria 553
- 13.4.29.5 Application 553
- 13.4.30 Photoemission Electron Microscopy 553
- 13.4.30.1 Introduction 554
- 13.4.30.2 Instrumentation 554
- 13.4.30.3 Sample 554
- 13.4.30.4 Analytical Information 554
- 13.4.30.5 Performance Criteria 554
- 13.4.30.6 Applications 555
- 13.4.31 Positron Annihilation Auger Electron Spectroscopy 555
- 13.4.31.1 Introduction 555
- 13.4.31.2 Instrumentation 555
- 13.4.31.3 Sample 556
- 13.4.31.4 Analytical Information 556
- 13.4.31.5 Performance Criteria 556
- 13.4.31.6 Applications 557
- 13.4.31.7 Other Techniques 557
- 13.4.32 Raman Spectroscopy 557
- 13.4.32.1 Introduction 557
- 13.4.32.2 Instrumentation 557
- 13.4.32.3 Sample 557
- 13.4.32.4 Analytical Information 558
- 13.4.32.5 Performance Criteria 558
- 13.4.32.6 Application 558
- 13.4.33 Reflection-absorption Spectroscopy 559
- 13.4.33.1 Introduction 559
- 13.4.33.2 Instrumentation 559
- 13.4.33.3 Sample 559
- 13.4.33.4 Analytical Information 560
- 13.4.33.5 Performance Criteria 560
- 13.4.33.6 Limitations 560
- 13.4.33.7 Applications 560
- 13.4.33.8 Other techniques 561
- 13.4.34 Reflection Electron Energy Loss Spectroscopy 561
- 13.4.34.1 Introduction 561
- 13.4.34.2 Instrumentation 561
- 13.4.34.3 Sample 561
- 13.4.34.4 Analytical Information 562
- 13.4.34.5 Performance Criteria 562
- 13.4.34.6 Applications 562
- 13.4.34.7 Other Techniques 562
- 13.4.35 Resonant Nuclear Reaction Analysis 563
- 13.4.35.1 Introduction 563

- 13.4.35.2 Instrumentation 563
- 13.4.35.3 Sample 564
- 13.4.35.4 Analytical Information 564
- 13.4.35.5 Performance Criteria 564
- 13.4.35.6 Application 564
- 13.4.35.7 Other Techniques 565
- 13.4.36 Rutherford Backscattering Spectrometry 565
  - 13.4.36.1 Introduction 565
  - 13.4.36.2 Instrumentation 565
  - 13.4.36.3 Sample 565
  - 13.4.36.4 Analytical Information 565
  - 13.4.36.5 Performance Criteria 566
  - 13.4.36.6 Applications 567
  - 13.4.36.7 Other Techniques 567
- 13.4.37 Scanning Electron Microscopy 567
  - 13.4.37.1 Introduction 568
  - 13.4.37.2 Instrumentation 568
  - 13.4.37.3 Sample 569
  - 13.4.37.4 Analytical Information 569
  - 13.4.37.5 Performance Criteria 569
  - 13.4.37.6 Applications 570
- 13.4.38 Scanning Tunneling Spectroscopy 570
  - 13.4.38.1 Introduction 570
  - 13.4.38.2 Instrumentation 570
  - 13.4.38.3 Sample 571
  - 13.4.38.4 Analytical Information 571
  - 13.4.38.5 Performance Criteria 571
  - 13.4.38.6 Applications 571
  - 13.4.38.7 Other Techniques 571
- 13.4.39 Secondary Ion Mass Spectrometry 571
  - 13.4.39.1 Introduction 571
  - 13.4.39.2 Instrumentation 572
  - 13.4.39.3 Sample 572
  - 13.4.39.4 Analytical Information 572
  - 13.4.39.5 Performance Criteria 573
  - 13.4.39.6 Application 573
  - 13.4.39.7 Other Techniques 573
- 13.4.40 Spectroscopy of Surface Electromagnetic Waves 574
  - 13.4.40.1 Introduction 574
  - 13.4.40.2 Instrumentation 574
  - 13.4.40.3 Performance Criteria 574
  - 13.4.40.4 Applications 574
- 13.4.41 Spin Polarized Electron Energy Loss Spectroscopy 575
  - 13.4.41.1 Introduction 575
  - 13.4.41.2 Instrumentation 575

13.4.41.3	Sample	575
13.4.41.4	Analytical Information	575
13.4.41.5	Performance Criteria	575
13.4.41.6	Applications	576
13.4.41.7	Other Techniques	576
13.4.42	Spin Polarized Ultraviolet Photoelectron Spectroscopy	576
13.4.42.1	Introduction	576
13.4.42.2	Instrumentation	576
13.4.42.3	Sample	577
13.4.42.4	Analytical Information	577
13.4.42.5	Performance Criteria	577
13.4.42.6	Applications	577
13.4.43	Sum-Frequency Generation Vibrational Spectroscopy	578
13.4.43.1	Introduction	578
13.4.43.2	Instrumentation	578
13.4.43.3	Analytical Information	578
13.4.43.4	Performance Criteria	578
13.4.43.5	Applications	579
13.4.43.6	Other Methods	579
13.4.44	Surface Plasmon Resonance Spectroscopy	579
13.4.44.1	Introduction	579
13.4.44.2	Instrumentation	579
13.4.44.3	Analytical Information	579
13.4.44.4	Performance Criteria	580
13.4.44.5	Applications	580
13.4.45	Total Reflection X-ray Fluorescence Spectroscopy	580
13.4.45.1	Introduction	580
13.4.45.2	Instrumentation	580
13.4.45.3	Sample	581
13.4.45.4	Analytical Information	581
13.4.45.5	Performance Criteria	581
13.4.45.6	Applications	582
13.4.46	Transmission Spectroscopy	582
13.4.46.1	Introduction	582
13.4.46.2	Instrumentation	582
13.4.46.3	Performance Criteria	582
13.4.46.4	Applications	582
13.4.47	Ultraviolet Photoelectron Spectroscopy	583
13.4.47.1	Introduction	583
13.4.47.2	Instrumentation	583
13.4.47.3	Sample	583
13.4.47.4	Analytical Information	583
13.4.47.5	Performance Criteria	583
13.4.47.6	Applications	584
13.4.47.7	Other Techniques	584

13.4.48	X-ray Absorption Fine Structure	584
13.4.48.1	Introduction	584
13.4.48.2	Instrumentation	585
13.4.48.3	Analytical Information	585
13.4.48.4	Performance Criteria	585
13.4.48.5	Applications	585
13.4.48.6	Other Techniques	586
13.4.49	X-ray Photoelectron Diffraction	586
13.4.49.1	Introduction	586
13.4.49.2	Instrumentation	586
13.4.49.3	Sample	587
13.4.49.4	Analytical Information	587
13.4.49.5	Performance Criteria	587
13.4.49.6	Applications	587
13.4.50	X-ray Photoelectron Spectroscopy	587
13.4.50.1	Introduction	588
13.4.50.2	Instrumentation	588
13.4.50.3	Sample	589
13.4.50.4	Analytical Information	589
13.4.50.5	Performance Criteria	590
13.4.50.6	Applications	590
13.4.50.7	Other Techniques	591
13.4.51	X-ray Standing Wave	591
13.4.51.1	Introduction	591
13.4.51.2	Instrumentation	591
13.4.51.3	Sample	592
13.4.51.4	Analytical Information	592
13.4.51.5	Performance Criteria	592
13.4.51.6	Applications	593
13.5	Further Information	593
13.6	Appendix: List of Acronyms Related to Surface Analysis	594

**Volume 2****Section VII Applications 1: Bioanalysis 1**

14	<b>Bioanalysis</b>	3
14.1	General Introduction	3
14.1.1	Spectroscopy in the Biosensor and Genomics Age	3
14.1.2	Genomics, Proteomics and Drug Discovery	4
14.1.3	Biosensor Technologies	5
14.1.4	Biomolecular Structure Determination	6
14.1.5	Bioinformatics	6
14.2	Optical Spectroscopy in Bioanalysis	7
14.2.1	Introduction	7
14.2.2	VIS/NIR Fluorescence Spectroscopy in DNA Sequencing and Immunoassay	10
14.2.2.1	Introduction	10
14.2.2.2	Chemistry of VIS/NIR Dyes	28
14.2.2.3	Bioanalytical Applications of NIR and Visible Fluorescent Dyes	36
14.2.2.4	Fluorescence Polarisation Methods	54
14.2.2.5	Time-resolved Fluorescence	55
14.2.2.6	Fluorescence Excitation Transfer	56
14.2.2.7	Bioanalytical Applications of Fluorescent Proteins	57
14.2.3	Bioanalytical Applications of Multi-photon Fluorescence Excitation (MPE)	58
14.2.3.1	Introduction	58
14.2.3.2	MPE Fluorescence Dyes	59
14.2.3.3	Two-photon Excitation Immunoassays	61
14.2.3.4	MPE in Gel and Capillary Electrophoresis	61
14.2.3.5	MPE in Tissue Imaging	63
14.2.3.6	Future Prospects of MPE Fluorescence Spectroscopy	63
14.2.4	Bioluminescence, Chemiluminescence and Electrochemiluminescence	65
14.2.5	Bioanalytical Applications of NIR Absorption Spectroscopy	68
14.2.6	Bulk Optical Sensing Techniques	69
14.2.7	Evanescence Wave Spectroscopy and Sensors	71
14.2.7.1	Introduction	71
14.2.7.2	Theory of Total Internal Reflection	72
14.2.7.3	Measurement Configurations	81
14.2.7.4	Surface Plasmon Resonance (SPR)	85
14.2.7.5	Reflectometric Interference Spectroscopy (RIFS)	89
14.2.7.6	Total Internal Reflection Fluorescence (TIRF) and Surface Enhanced Fluorescence	91
14.2.8	Infrared and Raman Spectroscopy in Bioanalysis	92
14.2.8.1	FTIR, FTIR Microscopy and ATR-FTIR	92

14.2.8.2	Raman Spectroscopy	92
14.2.8.3	Surface Enhanced Raman Spectroscopy (SERS)	93
14.2.9	Circular Dichroism	93
14.3	NMR Spectroscopy of Proteins	94
14.3.1	Introduction	94
14.3.2	Protein Sample	95
14.3.2.1	Solubility and Stability	95
14.3.2.2	Isotope Labeling	97
14.3.2.3	Dilute Liquid Crystals	99
14.3.3	Proton NMR Experiments	102
14.3.3.1	One-dimensional NMR Experiment	103
14.3.3.2	Correlation Experiments	105
14.3.3.3	Cross-relaxation Experiments	110
14.3.4	Heteronuclear NMR Experiments	113
14.3.4.1	Basic Heteronuclear Correlation Experiments	113
14.3.4.2	Edited and Filtered Experiments	117
14.3.4.3	Triple Resonance Experiments	119
14.4	Bioanalytical Mass Spectroscopy	122
14.4.1	Introduction	122
14.4.2	MALDI-TOF	122
14.4.3	Electrospray Methods (ESI-MS)	123
14.4.4	Tandem-MS	124
14.4.5	TOF-SIMS	125
14.4.6	MS in Protein Analysis	126
14.4.7	MS in Nucleic Acid Analysis	130
14.5	Conclusions	130

## **Section VIII Applications 2: Environmental Analysis 149**

### **Introduction 151**

<b>15</b>	<b>LC-MS in Environmental Analysis</b>	<b>152</b>
15.1	Introduction	152
15.1.1	Historical Survey of the Development of LC-MS	152
15.1.2	First Applications of LC-MS	153
15.2	Applications of LC-MS Interfaces in Environmental Analyses	155
15.2.1	Moving Belt Interface (MBI)	156
15.2.2	Direct Liquid Introduction (DLI)	156
15.2.3	Particle Beam Interface (PBI)	157
15.2.4	Fast Atom Bombardment (FAB) and Continuous Flow FAB (CF-FAB)	160
15.3	LC-MS Interfaces Applied in Environmental Analysis During the Last Decade	163
15.3.1	Achievements and Obstacles	163
15.3.2	Soft Ionisation Interfaces (TSP, APCI and ESI)	168

15.3.3	The Applications of Soft Ionising Interfaces	172
15.3.3.1	Applications Using Thermospray Ionization Interface (TSP)	172
15.3.3.2	Atmospheric Pressure Ionization Interfaces (API)	183
15.4	Conclusions	226
<b>16</b>	<b>Gas Chromatography/Ion Trap Mass Spectrometry (GC/ITMS) for Environmental Analysis</b>	<b>244</b>
16.1	Introduction	244
16.2	Practical Aspects of GC/ITMS	245
16.2.1	Historical survey	245
16.2.2	Principles of Operation	245
16.2.3	Ionization and Scanning Modes	247
16.2.3.1	Electron Ionization	247
16.2.3.2	Chemical ionization	249
16.2.3.3	Full Scan Versus Selected-Ion Monitoring	251
16.2.4	Advances in GC/ITMS	251
16.2.4.1	Methods for Improving Performances: Increasing the Signal-to-Background Ratio	252
16.2.4.2	External Ion Sources	252
16.2.4.3	GC/MS/MS	253
16.3	Examples of Applications of GC/ITMS	254
16.3.1	Requirements for Environmental Analysis	254
16.3.2	Determination of Volatile Organic Compounds in Drinking Water; EPA Methods	256
16.3.3	Detection of Dioxins and Furans	257
16.3.4	Other Examples	258
16.4	Future Prospects in GC/Chemical Ionization-ITMS	260
16.4.1	Chemical Ionization in Environmental Analysis	260
16.4.2	Examples of Unusual Reagents for Chemical Ionization	261
16.4.3	Ion Attachment Mass Spectrometry	262
16.4.3.1	Principle	262
16.4.3.2	Sodium Ion Attachment Reactions with GC/ITMS	263
16.5	Conclusion	265
16.6	Appendix: List of Main Manufacturers and Representative Products for GC/ITMS	266

## **Section IX Application 3: Process Control** 268

### **Introduction** 269

<b>17</b>	<b>Optical Spectroscopy</b>	<b>279</b>
17.1	Introduction	279
17.2	Mid-infrared	281
17.3	Non-dispersive Infrared Analysers	281
17.4	Near-infrared Spectroscopy	282

17.5	Ultraviolet/Visible Spectroscopy	286
17.6	Raman Spectroscopy	287
17.7	Laser Diode Techniques	291
17.8	Fluorescence	293
17.9	Chemiluminescence	293
17.10	Optical Sensors	294
17.11	Cavity Ringdown Spectroscopy	294
<b>18</b>	<b>NMR</b>	297
18.1	Introduction	297
18.2	Motivations for Using NMR in Process Control	297
18.3	Broadline NMR	301
18.4	FT-NMR	307
18.5	Conclusion	314
<b>19</b>	<b>Process Mass Spectrometry</b>	316
19.1	Introduction	316
19.2	Hardware Technology	317
19.2.1	Sample Collection and Conditioning	319
19.2.2	Sample Inlet	319
19.2.2.1	Direct Capillary Inlets	320
19.2.2.2	Membrane Inlets	320
19.2.2.3	Gas Chromatography (GC)	320
19.2.3	Ionization	321
19.2.4	Mass Analyzers	322
19.2.4.1	Sector Mass Analyzers	322
19.2.4.2	Quadrupole Mass Analyzers	323
19.2.4.3	Choice of Analyzer	324
19.2.5	Detectors	325
19.2.6	Vacuum System	325
19.2.7	Data Analysis and Output	325
19.2.8	Calibration System	327
19.2.9	Gas Cylinders	328
19.2.10	Permeation Devices	328
19.2.11	Sample Loops	329
19.2.12	Maintenance Requirements	329
19.2.13	Modes of Operation	329
19.3	Applications	330
19.3.1	Example Application: Fermentation Off-gas Analysis	331
19.4	Summary	334
<b>20</b>	<b>Elemental Analysis</b>	336
20.1	Applications of Atomic Spectrometry in Process Analysis	336
20.1.1	Catalyst Control	337
20.1.2	Corrosion Monitoring	339

20.1.3	Reducing Environmental Impact	341
20.1.4	Troubleshooting Process Problems	342
20.2	On-stream/at-line Analysis	343
20.2.1	X-ray Fluorescence (XRF)	344
20.2.1.1	Liquid Process Streams	348
20.2.1.2	Trace Analysis and Corrosion Monitoring	351
20.2.1.3	Analysis of Slurries and Powders	352
20.2.1.4	Direct Analysis	354
20.2.2	Atomic Emission Spectrometry	356
20.2.2.1	Plasma Spectrometry	356
20.2.2.2	Laser Based Techniques	362
20.3	Conclusions	368

## **Section X Hyphenated Techniques** 377

### **Introduction** 379

<b>21</b>	<b>Hyphenated Techniques for Chromatographic Detection</b>	381
21.1	Introduction	381
21.2	Electronic Spectral Detection	383
21.3	MS Detection	400
21.4	NMR Detection	412
21.5	FTIR Detection	415
21.6	Atomic Spectrometric Detection	421
21.7	Other Types of Detection	428
21.8	Serial or Parallel Multiple Detection	430

## **Section XI General Data Treatment: Data Bases/Spectral Libraries** 437

### **Introduction** 439

<b>22</b>	<b>Optical Spectroscopy</b>	441
22.1	Introduction	441
22.2	Basic Operations	442
22.2.1	Centering	442
22.2.2	Standardization (Autoscaling)	443
22.3	Evaluation of Spectra	444
22.3.1	Introduction	444
22.3.2	Qualitative Evaluation of Spectra	446
22.3.2.1	Spectral Data Banks	446
22.3.2.2	Data Banks Containing Spectroscopic Information	452
22.3.2.3	Interpretation of Spectra by Means of Group Frequencies and of Characteristic Bands	452
22.3.2.4	PCA (Principal Component Analysis)	452
22.3.2.5	Cluster Analysis	455

22.3.2.6	Discriminant analysis	455
22.3.2.7	SIMCA Soft Independent Modeling of Class Analogy (SIMCA)	455
22.3.3	Quantitative Evaluation of Spectra	455
22.3.3.1	Univariate Methods	456
22.3.3.2	Multivariate Methods	459
<b>23</b>	<b>Nuclear Magnetic Resonance Spectroscopy</b>	469
23.1	Introduction	469
23.2	Comparison of NMR-Spectroscopy with IR and MS	470
23.3	Methods in NMR Spectroscopy	471
23.4	Spectral Similarity Search Techniques	471
23.5	Spectrum Estimation, Techniques	473
23.6	Spectrum Prediction, Quality Consideration	474
23.7	Spectrum Prediction and Quality Control, Examples	475
23.8	Spectrum Interpretation and Isomer Generation	481
23.9	Ranking of Candidate Structures	484
23.10	Conclusions	484
<b>24</b>	<b>Mass spectrometry</b>	488
24.1	Introduction	488
24.2	Mass Spectrometry Databases	489
24.2.1	NIST/EPA/NIH Mass Spectral Library	490
24.2.2	Wiley Registry of Mass Spectral Data	491
24.2.3	SpecInfo/SpecData	491
24.2.4	SDBS, Integrated Spectra Data Base System for Organic Compounds	492
24.2.5	Other Smaller Collections	492
24.2.5.1	Pfleger/Maurer/Weber: Mass Spectral and GC Data of Drugs, Poisons, Pesticides, Pollutants and Their Metabolites	494
24.2.5.2	Ehrenstorfer	494
24.2.5.3	Wiley-SIMS	494
24.2.5.4	American Academy of Forensic Sciences, Toxicology Section, Mass Spectrometry Database Committee	494
24.2.5.5	The International Association of Forensic Toxicologists (TIAFT)	494
24.3	Mass Spectrometry Search Software	495
24.3.1	INCOS	496
24.3.2	Probability Based Matching (PBM)	496
24.3.3	MassLib/SISCOM	497
24.3.4	AMDIS	498
24.3.5	Mass Frontier	499
24.3.6	The WebBook	500
24.3.7	General Spectroscopy Packages	501
24.4	Biological Mass Spectrometry and General Works	502
<b>Index</b>		505

## Preface

The *Handbook of Spectroscopy* is intended to serve as an authoritative reference source for a broad audience involved in the research, teaching, learning, and practice of spectroscopic technologies. Spectroscopy is defined as the science that deals with interactions between electromagnetic radiation and matter. This research field has recently experienced an explosive growth as a result of innovations in methodologies and instrumentation, which offer the possibilities for new applications and novel methods of analysis to solve common analytical problems as well as address new challenges. Research scientists, analytical scientists, environmental investigators, and industrial engineers, who are often confronted with the ever-increasing complexity of real-life sample analysis, need a readily accessible source of information and an authoritative guidance on how to best apply currently available spectroscopic techniques to their particular fields of interest and to their specific applications.

To address this important need, the *Handbook of Spectroscopy* is designed to provide a straightforward introduction to spectroscopy, what this field can do, and how an investigator can use it effectively. The Handbook also provides a clear, integrated, and objective account of the wealth of information that can be derived from spectra. The sequence of chapters covers the entire range of the electromagnetic spectrum and the physical mechanisms involved, from rotation processes in molecules to phenomena in the nucleus.

The Handbook is not designed to be just another treatise on the theory of spectroscopy, but rather a practical day-to-day laboratory guide. The academic level is appropriate for the newcomer to the various fields of spectroscopy; no special knowledge beyond the standard level of a graduate student in the physical or life sciences is required.

In addition to the introductory material, the Handbook provides a comprehensive guide to the state-of-the-art practices in all major fields of spectroscopy. The treatment of each field of spectroscopy presents the most up-to-date developments in methodologies, techniques, instrumentation, and data treatment. The Handbook indicates to the researcher and the practicing spectroscopist how to select the most suitable technique for a specific application, how to adopt the optimal methods of sample preparation and spectra recording, and how to interpret the re-

sults. Where appropriate, the Handbook also guides the reader to selected compilations of important data.

The Handbook represents the work of over 40 leading scientists and engineers in their field of research. The handbook contains 24 chapters, which are grouped in 11 sections:

- (1) Sample Preparation and Sample Pretreatment
- (2) Methods 1: Optical Spectroscopy
- (3) Methods 2: Nuclear Magnetic Resonance Spectroscopy
- (4) Methods 3: Mass Spectroscopy
- (5) Methods 4: Elemental Analysis
- (6) Methods 5: Surface Analysis Techniques
- (7) Applications 1: Bioanalysis
- (8) Applications 2: Environmental Analysis
- (9) Applications 3: Process Control
- (10) Hyphenated Techniques
- (11) General Data Treatment: Data Bases/Spectra Libraries

The goal of this Handbook is to provide a comprehensive forum that integrates interdisciplinary research and development of interest to scientists, engineers, manufacturers, teachers, and students. The Handbook is designed to present, in a single source, the most recent advances in instrumentation and methods, as well as applications in important areas of bioanalysis, environmental analysis, and process control. Because light is rapidly becoming an important diagnostic tool, it is our hope that the Handbook will be a valuable companion to the practicing spectroscopist and will stimulate a greater appreciation of the usefulness, efficiency, and potential of spectroscopy.

*Guenter Gauglitz*  
University of Tuebingen  
Tuebingen  
Germany

*Tuan Vo-Dinh*  
Oak Ridge National Laboratory  
Oak Ridge, Tennessee  
U. S. A.

## List of Contributors

Dr. Willem M. Albers  
 VTT Automation, Measurement  
 Technology, Sensing Materials  
 P. O. Box 13041  
 33101 Tampere  
 Finland

Dr. Arto Annila  
 VTT Biotechnology and Food  
 Research, Biomolecules,  
 Molecular Structure  
 P. O. Box 56  
 00014 University of Helsinki  
 Finland

Dr. Damia Barceló  
 Institut d'Investigation Químiques  
 i Ambientals  
 de Barcelona (IIQAB-CSIC)  
 Department of Environmental  
 Chemistry  
 Jordi Girona, 18–26  
 08034 Barcelona  
 Spain

Dr. Les Butler  
 Department of Chemistry  
 Louisiana State University  
 Baton Rouge, LA 70803-1804  
 USA

Dr. Jim S. Crighton  
 BP Chemicals  
 Research & Engineering Centre  
 Chertsey Road  
 Sunbury-on-Thames  
 Middlesex TW16 7LN  
 U. K.

Dr. Brian Cullum  
 Advanced Monitoring Development Group  
 Oak Ridge National Laboratory  
 Oak Ridge, TN 37831-6101  
 USA

Dr. Antony N. Davies  
 Institut für Spektrochemie  
 und Angewandte Spektroskopie  
 Bunsen-Kirchhoff-Str. 11  
 44139 Dortmund  
 Germany

Dr. Lyndon Emsley  
 Laboratoire de Stereochemie  
 et des Interactions Moleculaires  
 Ecole Normale Supérieure de Lyon  
 46 Allée d'Italie  
 69364 Lyon cedex 07  
 France

Dr. John C. Fetzer  
 Chevron Research and Technology Company  
 576 Standard Avenue  
 P. O. Box 1627  
 Richmond, CA 94804  
 USA

Dr. Thilo A. Fligge  
 Boehringer Ingelheim Pharma KG  
 Department of Lead Discovery  
 55216 Ingelheim  
 Germany

Dr. Toshihiro Fujii  
 National Institute for Environmental Studies  
 Japan Environment Agency  
 16-2 Onogawa, Tsukuba  
 Ibaraki 305-0053  
 Japan

Dr. Nicholas J. Goddard  
 University of Manchester  
 Institute of Science and Technology  
 Department of Instrumentation  
 and Analytical Science (DIAS)  
 P. O. Box 88  
 Manchester, M60 1QD  
 U. K.

Dr. John Green  
 33 Molescroft Road  
 Beverley  
 East Yorkshire HU17 7EG  
 U. K.

Dr. Chad E. Hadden  
 Rapid Structure Characterization Group  
 Pharmaceutical Development  
 Pharmacia Corporation  
 Kalamazoo, MI 49001-0199

Dr. Edward W. Hagaman  
 Chemical Sciences Division  
 Oak Ridge National Laboratory  
 Oak Ridge, TN 37831-6201  
 USA

Dr. Christian Hassell  
 Analytical Chemistry Sciences  
 Los Alamos National Laboratory  
 Los Alamos, NM 87545  
 USA

Dr. Martin Hof  
 J. Heyrovsky Institute of Physical Chemistry  
 Academy of Science of the  
 Czech Republic  
 Dolejskova 3  
 18223 Prague 8  
 Czech Republic

Prof. Dr. Koen Janssens  
 University of Antwerp  
 Department of Chemistry  
 Universiteitsplein 1  
 610 Antwerp  
 Belgium

Dr. Douglas A. Lane  
 Environment Canada  
 Atmospheric Research Directorate  
 Process Research Division  
 4905 Dufferin Street  
 Toronto, Ontario M3H 5T4  
 Canada

Dr. Anna Mackova  
 Nuclear Physics Institute of Academy  
 of Sciences of the Czech Republic  
 Rez near Prague, 250 68  
 Czech Republic

Dr. Gary E. Martin  
 Rapid Structure Characterization Group  
 Pharmaceutical Development  
 Pharmacia Corporation  
 Kalamazoo, MI 49001-0199  
 USA

Dr. Simon Morton  
 Advanced Light Source  
 Lawrence Berkeley National Laboratory  
 MS 7-222  
 1 Cyclotron Road  
 Berkeley, CA 94607  
 USA

Dr. Ulrich Panne  
 Laboratory for Applied Laser Spectroscopy  
 Technical University Munich  
 Institute of Hydrochemistry  
 Marchionistr. 17  
 81377 Munich  
 Germany

Prof. Dr. Gabor Patonay  
 Georgia State University  
 Department of Chemistry  
 University Plaza  
 Atlanta, Georgia 30303-3083

Prof. Dr. Michael Przybylski  
 University of Konstanz  
 Department of Chemistry  
 78457 Konstanz  
 Germany

Prof. Dr. Wolfgang Robien  
 Institute of Organic Chemistry  
 University of Vienna  
 Währingerstrasse 38  
 1090 Vienna  
 Austria

Dr. Erwin Rosenberg  
 Institute of Analytical Chemistry  
 Vienna University of Technology  
 Getreidemarkt 9  
 1060 Vienna  
 Austria

Dr. David J. Russell  
Rapid Structure Characterization Group  
Pharmaceutical Development  
Pharmacia Corporation  
Kalamazoo, MI 49001-0199  
USA

Dr. Valdas Sablinskas  
Department of Physics  
Vilnius University  
Universiteto str. 3  
Vilnius 2734  
Litauen

Dr. Michel Sablier  
Université Pierre et Marie Curie  
UMR 7613 du CNRS  
4 place Jussieu  
75005 Paris  
France

Prof. Dr. Reiner Salzer  
Technical University Dresden  
Institute of Analytical Chemistry  
Zellescher Weg 19  
01062 Dresden  
Germany

Prof. Dr. Horst Friedrich Schroeder  
Institut für Siedlungswasserwirtschaft  
Umweltanalytisches Labor  
Krefelder Str. 299  
52070 Aachen  
Germany

Prof. Dr. Erkki Soini  
Laboratory of Biophysics  
Institute of Biomedicine  
University of Turku  
P. O. Box 123  
20521 Turku  
Finland

Dr. Gerald Steiner  
Technical University Dresden  
Institute of Analytical Chemistry  
Zellescher Weg 19  
01062 Dresden  
Germany

Dr. Steffen Thiele  
Institute of Analytical Chemistry  
Technical University Dresden  
Zellescher Weg 19  
01062 Dresden  
Germany

Dr. Kurt Varmuza  
Laboratory for Chemometrics  
Institute of Food Chemistry  
Vienna University of Technology  
Getreidemarkt 9/160  
1060 Vienna  
Austria

Prof. Dr. Tuan Vo-Dinh  
Advanced Biomedical Science and  
Technology Group  
Oak Ridge National Laboratory  
P. O. Box 2008  
Oak Ridge, TN 37831-6101  
USA

Prof. Dr. Karel Volka  
Vysoka Skola Chemicko-Techn. v Praze  
Ustav Analyticke Chemie  
Technika 5  
16628 Praha 6 – Dejvice  
Czech Republic

Dr. Christopher G. H. Walker  
Bornpfad 26  
65232 Taunusstein  
Germany

Dr. Wolfgang Weinmann  
University of Freiburg  
Institut für Rechtsmedizin  
Albertstr. 9  
79104 Freiburg  
Germany

Dr. Loring A. Weisenberger  
Celanese Chemicals  
1901 N. Clarkwood Road  
Corpus Christi, Texas 78409

## **Section I**

### **Sample Preparation and Sample Pretreatment**

## **Introduction**

*Douglas A. Lane*

In order to obtain high-quality analytical data, the primary objective of the analytical scientist must be, ideally, to obtain an artifact-free sample for the analysis. This is seldom a simple matter and presents many challenges to the investigator. It is often the case that many sampling programs frequently select the sampling methods based on what equipment is available rather than on what question is to be answered or what problem is to be addressed. It is important that sampling objectives be defined first and then a suitable method be selected. The question, "Can the sampling method I select provide me with the answers I am looking for?" must always be answered in the affirmative.

Sampling methodology differs greatly depending upon whether the sample is in the gaseous, liquid or solid phase. If the sample is in the liquid or solid phase, is the sample an aerosol or particle that exists in a particular gaseous phase? In or on what medium shall the sample be collected and retained? How shall the sample be stored and/or transported prior to analysis? Must the sample be processed before the analysis to concentrate or isolate the analyte(s) of interest from the sample matrix before analysis? If the sample is to be used for legal purposes, a chain of custody (not discussed here) needs to be developed. A Quality Assurance/Quality Control (QA/QC) program will likely have to be developed for the analytical method.

In situations where the analyte is present in trace quantities (as usually occurs in environmental samples), it is vitally important to maximize the recovery of the analyte from the sample matrix and to lose as little of the analyte as possible during any subsequent processing or "work-up" stages in the analytical process. Extensive recovery testing is usually required to determine the efficiency of the collection and processing procedures.

The following two chapters address the question of sampling methods for the three phases in which a sample may occur — gaseous, liquid and solid. Different sampling approaches (active vs. passive) are considered as are the specific approaches for a wide variety of sample types and matrices.

# 1

## Collection and Preparation of Gaseous Samples

*Douglas A. Lane*

### 1.1

#### Introduction

The collection of artifact-free gas phase samples is not a simple process. Unless the gas is a highly filtered and purified gas, it will most likely be a complex mixture of gases and vapors, liquids (aerosols) and solids (particles). For example, one of the most sampled, yet most complex sources is the earth's atmosphere. The atmosphere is a mixture of gases (both organic and inorganic), liquids (such as rain droplets and aerosols) and solids (particles such as windblown dusts, pollens and fly ash from a myriad of combustion processes). The atmosphere is also irradiated with sunlight, which can initiate many photochemical reactions. It can truly be said that the atmosphere is like a giant chemical reactor in which all but the most inert compounds are chemically modified, dispersed and eventually deposited to the earth [1]. It is not a simple matter to collect atmospheric samples, or other gaseous samples for that matter, without modifying the sample during the collection process. After all, one really wants to know the gaseous composition at the time of collection, not as modified by a particular sampling process.

Prior to using the sophisticated techniques described in the rest of this book to analyze a sample, one must first collect the sample and then prepare it for the final analysis. Analytical techniques have become incredibly sophisticated and more selective and sensitive over the past 20 to 30 years. Sampling methods, unfortunately, have not kept pace with the advances in the analytical technology despite the fact that a poorly collected sample, no matter how sophisticated the analytical method, will still yield a poor result. To borrow an expression from the computer industry: "Garbage in equals garbage out". The ultimate challenge is to collect a sample that reflects the composition of the sample at the time of collection. To achieve this objective, the sample collection method selected must be as free as possible from all artifacts of the sampling procedure and be appropriate for the objective of the program for which the measurements are made. It is just as important to maintain the integrity of the sample after the sampling has been completed and during any work-up procedure to prepare the sample for analysis.

An artifact is something not naturally present in the sample but is introduced during the sampling or work-up procedure. Artifacts include the oxidation of the collected sample during the sampling process, adsorption of gas phase compounds by a particle collection filter, volatilization of particle associated compounds that subsequently are trapped by an adsorbent and assessed as gas phase material, irreversible adsorption or reaction of the gases or vapors with the sampling substrate, condensation of water on the sample, loss of adsorbed sample during sampling, transport or sample work-up and chemical alteration of the sample during sample extraction and/or preparation. There are many other potential artifacts, all of which should be minimized. Part of this process is the selection of the proper sampling method for the problem at hand.

Since the focus of this book is the analysis of collected samples, only integrated samples will be considered here. Furthermore, this chapter will look only at the collection and preparation of gaseous samples. The collection of particle and liquid samples will be considered in the following chapter. Because of their complexity, most of the discussions in this chapter will center on the collection and analysis of atmospheric samples, however, the principles involved relate to any gaseous sample.

The most important aspect of sampling is to know what problem is to be solved or addressed and then to select the appropriate method. Proper selection of sampling method is critical to the solution of a problem.

## 1.2 Sampling considerations

In the atmosphere, gases and vapors co-exist as gas phase material. Each chemical has its own vapor pressure and saturated vapor concentration. Chemical compounds that have a subcooled liquid phase vapor pressure greater than approximately  $10^{-2}$  Pa will exist entirely in the gas phase. These compounds include gases such as ozone, oxides of nitrogen, carbon monoxide, carbon dioxide and sulfur dioxide and vapors from volatile organic compounds (VOCs), such as methylene chloride, acetone, and isoprene, low molecular weight aliphatic compounds and aromatic compounds such as benzene, toluene and xylene. Contaminants with subcooled liquid phase vapor pressures less than  $10^{-5}$  Pa will exist almost entirely in the particle phase, while contaminants with vapor pressures between  $10^{-2}$  and  $10^{-5}$  Pa will partition themselves between the gaseous and particulate phases. These are the so-called semivolatile organic compounds (SVOCs), and include many of the polychlorinated biphenyls (PCBs), some of the polycyclic aromatic compounds, many of the dioxins and many pesticides. Semivolatile compounds exist in the atmosphere at or near equilibrium between the gaseous and particulate phases. In Fig. 1.1, the gas phase fraction of SVOC components is plotted versus the log of the subcooled liquid phase vapor pressure ( $\log P_L$ ) of the SVOCs. This shows graphically that compounds with a  $\log P_L$  between approximately  $10^{-2}$  and  $10^{-5}$  Pa will partition between the gaseous and particulate phases in the atmo-

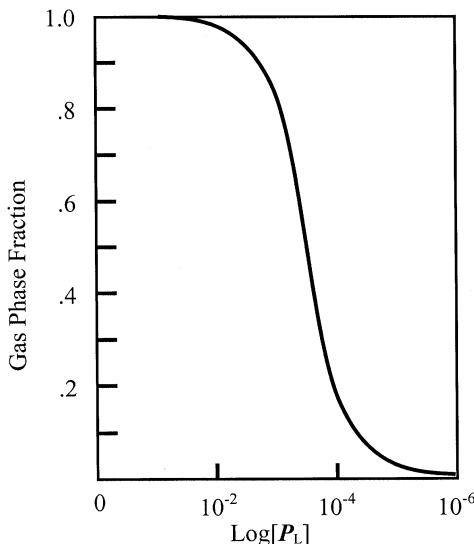


**Fig. 1.1** Gas Phase fraction as a function of the log of the subcooled liquid vapor pressure (Pa) of SVOCs.

sphere. First described by Junge [2], the theory has been greatly developed by Pankow [3, 4] and Pankow and Bidleman [5].

The sampling method selected must be sensitive to the vapor pressure of the compound, the temperature at which sampling is to take place, the stability of the compound during sampling and the anticipated concentration of the compound in the air. The act of drawing an air sample through a sampler requires a pressure drop across the sampler and this will disturb the equilibrium between the gas and particle phases. Sampling methods must endeavor to minimize this disruption of the equilibrium if gas particle partition measurements are being made.

Since gaseous samples are about 800 times less dense than liquid or solid samples and, since the vast majority of these gases and vapors exist in the atmosphere in extremely low concentrations (often at nanogram to sub-nanogram per cubic meter concentrations), it is necessary to collect large volumes of air in order to collect sufficient material to permit both qualitative and quantitative analyses. For example, in gas chromatographic/mass spectrometric analyses, 1  $\mu\text{L}$  of a 1 mL sample will typically be injected onto the column of the gas chromatograph. If the instrument has sufficient sensitivity to permit quantitation on 50 pg of analyte, then there must be 50,000 pg or 50 ng of the analyte in the 1 mL sample. This, in turn, requires that 50 ng of sample be collected from the air (assuming no losses during the work-up procedure). If the sample exists in the air at a concentration of  $1 \text{ ng m}^{-3}$ , then it follows that one would need to collect a minimum of  $50 \text{ m}^3$  of air for the analysis. Likewise, if the compound exists in the air at a concentration of  $100 \text{ ng m}^{-3}$ , then one need only collect a  $0.5 \text{ m}^3$  sample. It is, thus, important to have some knowledge of the anticipated concentration of the analyte in the gas mixture prior to selecting the sampling method and sampling time.

To collect such large volumes of air, ambient air sampling is frequently conducted over many hours, usually 12 h or 24 h. These are termed integrated air samples. Air samplers frequently draw air through a filter to remove the particles, then through a sorbent material to trap the gaseous components. In this filter/sorbent geometry air sampler, it is now well known that artifacts are produced, the most serious of which is the volatilization of the particle adsorbed semivolatile compounds due to the pressure drop across the filter. These volatilized compounds pass through the filter and are trapped on the adsorbent where they are analysed as though they were gaseous compounds. Temperature variations during sampling will also influence the gas/particle partitioning of the SVOCs. The filter sorbent geometry should be restricted to determining the total combined gas and particle burden of a particular air sample but should not be used to determine gas/particle partition ratios of semivolatile compounds. If the gas/particle partition ratios are to be determined, it is preferable to remove the gas phase first, and then to remove the particles, as is done in the annular diffusion denuder samplers.

The sample must subsequently be extracted from the trapping medium and processed before it is analysed by the desired analytical method. Very often the processing requires a series of steps to isolate a particular compound or compound class for the analysis to be effective. If the work-up steps are ignored, the collected sample is usually too complex for even the most selective and sensitive analytical methods available today.

If the concentration of the analyte fluctuates with time, then the result of the sampling is a concentration averaged over the sampling time period. The shorter the sampling period, the greater will be the temporal resolution of the concentration variations of the analyte.

Many chemical species found in the atmosphere are chemically and/or photochemically reactive. If such compounds are present, inert sample inlets and surfaces must be employed since there is a strong potential for the formation of artifacts. This is not a simple problem to overcome. It is also necessary to prevent further chemical degradation of the compounds during and after the sampling has been completed. The sample must not react with the sampling surfaces, filters or adsorbents. When adsorbents are used, the efficiency of extraction of the compounds from the adsorbents must be determined for each compound. If the gases and vapors pass through particle filters, the gases and vapors must not be adsorbed by, or react with the material from which the filters are made. Glass fiber and quartz fiber filters, for example, are well known to adsorb organic compounds whereas Teflon-coated glass fiber filters are much less likely to adsorb organic vapors. On the other hand, if the primary objective of the sampling is to determine the elemental carbon content of the collected particles, then a Teflon-coated glass fiber filter would obviously be a poor choice since the Teflon coating would become part of the analyte during the high temperature heating of the sample. As stated previously, it is imperative that the sampling system suits the problem that is to be solved. If adsorbents or diffusion denuders are used, it is possible that gas phase material adsorbed on the surfaces of the adsorbents might break through the collector. This must be investigated and, if significant, then either a different

adsorbing material must be used or a breakthrough factor must be statistically determined. All potential artifacts must be considered and minimized, if not eliminated, through proper sampler design and analytical process control. This often necessitates lengthy quality assurance (QA) and quality control (QC) programs.

### 1.3

#### Active vs. Passive Sampling

There are two basic means of collecting a gaseous sample: active sampling and passive sampling.

In active sampling procedures, air is drawn through an absorbing or adsorbing medium by a pump in order to trap the gas phase material. It is important that the sampler has an accurate, calibrated means to determine the total volume of the gaseous sample and the rate at which the gas is being sampled. This is most easily accomplished by the use of calibrated mass flow controllers.

In passive sampling devices, an adsorbing material is placed at a fixed distance away from the air being sampled. Gas phase molecules must pass through a membrane or filter and diffuse across this distance and be trapped on or react with the collecting medium. The principles of diffusion are utilized to calculate the concentration of the specified contaminant in the ambient air. The diffusion rate across the passive sampler (and/or through the membrane) is analogous to the flow rate in an active sampler.

##### 1.3.1

#### Active Air Collection Methods

There are many active air sampling methods available. Each method utilizes different ways to collect gaseous samples and each sampling method has its own particular inherent artifacts, and, thus, each method has its own strengths and weaknesses. It cannot be stated too often that the appropriate sampling method must be selected to address a particular question or problem.

There are several basic mechanisms whereby gases and vapors may be collected for subsequent analysis. Gaseous samples may be adsorbed on the surface of various substances, which have large surface areas and are specifically designed to collect the gaseous chemical species desired. They may react chemically with some chemical adsorbed on the surface of the collection device or on particles in the collector. Gases may be collected in bags or canisters or trapped in bubblers, in mist chambers or cryogenically. Each of these methods will be described briefly below.

### 1.3.1.1 Sorbents

Sorbents come in many varieties and may be used as beds (packed in glass or metal tubes), surfaces (deposited on tubular or annular surfaces) or in chemically treated filters designed to trap compounds selectively. They may be organic polymers, inorganic materials or made from activated carbon. Each sorbent material has specific advantages and disadvantages in specific sampling situations. Some sorbents are chemically treated to react with a single component and are used in specific gas samplers. They indicate the presence of a gas by a color change and the concentration of the gas by the length of the color developed in the adsorbent column. Since these sorbents give a direct indication of the gas concentration, no further analysis is performed. As a consequence, they are outside the scope of this book and will not be considered further.

Other sorbents are not compound specific and, as a result, trap a wide range of compounds. Unless specifically desired (see later in this section the discussion of DNPH-coated sorbents), it is vitally important that the compounds collected do not react with the sorbent. It is an unfortunate reality that the efficiency of recovery of most adsorbed compounds from the sorbents is less than 100 %. For this reason, the efficiency of the sorbent for the desired compounds and the extraction or desorption efficiency of the compounds from the sorbent must be determined.

Organic polymers have proven themselves to be effective adsorbents for many organic chemical species. They include materials such as Tenax<sup>TM</sup> (2,4-diphenyl-*p*-phenylene oxide), XAD (styrene-divinylbenzene copolymer) and polyurethane foam (PUF). Tenax and XAD are available as small beads (less than 1 mm in diameter) and have large surface areas for effective adsorption of organic chemicals. These materials are hydrophobic which makes them suitable for the collection of organic vapors in gases that contain a significant relative humidity. As water moisture causes significant problems for gas chromatographic analysis, the use of hydrophobic adsorbents can be a significant advantage. These resins are particularly effective for neutral and aromatic organics but are less effective in the trapping of highly polar organics. Under extremely moist conditions, however, these adsorbents may lose their efficiency, particularly if water condenses on the sorbent. PUF is suitable for the retention of polychlorinated organics such as the PCBs but is ineffective in trapping low molecular weight organics. PUF is not effective for trapping aromatics such as naphthalene, acenaphthene and acenaphthylene.

Although Tenax has good thermal stability it has a major disadvantage in that it is notoriously difficult to clean. The XAD resins also have good thermal stability but are still difficult to clean. If not manufactured from pure materials, solvent extraction or thermal desorption of the polymer will release the impurities present in the starting materials or produced during the manufacturing process. This problem is not easy to eliminate. For that reason, the sorbents must be exhaustively extracted or thermally desorbed prior to use. Tenax is cleaned by thermal treatment whereas the XAD resins are usually solvent extracted. Blanks are necessary to establish the level of interferences to the analytical procedure. In addition, the sorbents, although extremely efficient for the trapping of the higher molecular weight organics, are less effective in trapping and retaining the lower molecular weight VOCs.

Carbon-based traps have a lower affinity for water than does Tenax, but they must be purged with ultra-pure helium while being heated to drive off adsorbed impurities. Surrogates should be added before this clean-up procedure to determine the efficiency of the purge. After activation, sorbents must be handled with care as they may adsorb organic vapors from the air, thus resulting in adsorption artifacts.

Because of their physical structure and specific surface area, polymeric sorbents have a finite capacity for the collection of organic compounds. It is, therefore, necessary to determine the capacity of a particular sorbent under the particular sampling conditions desired. The minimum sampling duration will be defined by the concentration of the organics in the sampled gas and the sampling rate. If the capacity of a sorbent is exceeded, breakthrough of the sample will occur. In practice, it is wise, if not necessary, to use two sorbents in tandem. Any compounds which break through the first sorbent will be trapped by the second sorbent. This will indicate the extent to which breakthrough is a problem.

Adsorbents such as XAD can be ground to sub-micron sized particles thus greatly increasing their surface area and capacity. When these particles are properly applied to concentric glass tubes called annular diffusion denuders, they provide a large surface area for the collection of gases and vapors. Passing air through these devices will result in the gases and vapors being adsorbed to the walls of the denuder. The particles, because of their greater mass and momentum, pass through the denuder and are trapped by a filter. This sorbent/filter geometry greatly reduces the artifacts inherent in the filter/sorbent geometry.

PUF has commonly been used downstream of a particle filter to collect the gas phase material that passes through the filter. PUF is reasonably effective in trapping the higher molecular weight organics, but, like the resins, it is much less effective in trapping the low molecular weight organics. PUF is also notoriously difficult to clean and is well known to undergo chemical degradation when exposed to atmospheric oxidants. This can be seen over the course of a single 12 h sample by a yellowing of the foam that remains after solvent extraction.

Inorganic sorbents include silica gel, alumina and molecular sieves. Because they are polar substances, they are particularly effective in trapping polar vapors. For these sorbents, it is the degree of polarity which determines how well a particular gas or vapor is retained. A source of potential error is that very polar gases may displace less polar compounds from the adsorbent. For atmospheric sampling this presents a significant problem in that these sorbents are also very efficient in collecting water, which can cause serious deactivation of the sorbents. As a result, these compounds are not often used for the collection of organic vapors.

An adsorbent such as silica may be treated chemically with, for example, 2,4-dinitrophenylhydrazine (DNPH). When an air sample is passed through this material, organic carbonyls react with the DNPH to form the dinitrophenylhydrazone which can then be extracted and easily detected. In such a system, the sorbent simply acts as a large area substrate for the chemical reactant.

Activated carbon in beds and impregnated in glass fiber mats has been used to collect organic vapors. These sorbents are relatively non-polar and trap a wide

range of organics. It is extremely difficult to remove adsorbed organic compounds from activated carbon sorbents. This limits their applicability in air sampling unless the sole purpose of the adsorbent is to remove organics from an air stream.

#### 1.3.1.2 **Bags**

Bags made of aluminum/plastic or of plastic laminates can be used to collect gaseous samples. They are filled either with inert surface pumps or indirectly by placing the bag in a non-flexible, closed container and evacuating the space between the bag and the container. When the space between the bag and the rigid container is evacuated, the bag will inflate, drawing in the air sample. Bags must be carefully cleaned and examined and tested for leaks prior to sampling. Loss of organics to the walls can be a significant problem. Diffusion of gases and vapors through the walls has been greatly reduced by the use of the laminated plastics. The use of bags allows a grab sample of air, usually less than a cubic meter in volume, to be collected. Because a relatively small volume of air is collected, the compound of interest must be in sufficiently high concentration that it can be detected and quantified. Bag collectors can be bulky and difficult to transport.

If the collected sample is to be analysed by a technique such as gas chromatography-mass spectrometry, the sample must be passed through an adsorbent to concentrate the hydrocarbon gases and vapors. The sample must then be released from the adsorbent, either by solvent extraction or thermal desorption, prior to injection into the gas chromatograph.

#### 1.3.1.3 **Canisters**

Air may be collected in glass or steel containers. Glass containers may be evacuated prior to sample collection or the air sample may be drawn through the container. Glass containers, because of their small size, allow only the collection of a grab sample. Steel canisters with electropolished or chemically deactivated interiors may also be used to collect air samples. Inner surface treatment is necessary, as stainless steel is an adsorptive medium. Most canisters are designed to be evacuated in the laboratory then transported to the sampling site. However, prior to use, the canisters must be cleaned. This is a laborious procedure that requires that the canisters be evacuated to below 0.05 Torr and heated for several hours. The procedure may have to be repeated several times if the canister was previously exposed to a “dirty” sample. Even this may not satisfactorily clean a “dirty” canister. The canister may have to be wet cleaned to remove some polar compounds.

A valve in the canister is opened to allow the air sample to leak into the canister at a defined rate. The leak rate is fixed, often by a use of a suitable critical orifice. Depending on the leak rate, the size of the canister and the initial vacuum, the canisters may collect short-term grab samples or may extend the collection process up to as long as 48 hours, although sampling times of 6 to 8 hours are more common. Canisters have been used primarily to collect VOCs. Water management is a major problem with canisters and, to reduce its effects, Nafion drying tubes may have to

be used in the sampling inlet. The gases collected in these canisters remain stable and do not alter their concentrations over several weeks of storage. Canisters can be much larger than glass containers and come in sizes from 1 to about 35 L.

Some canisters have been designed to be pressurized to approximately 30 psi. However, this necessitates that the air sample passes through the sampling pump. As a result, the sampling pump has a great potential to contaminate the sample.

Prior to analysis, the collected sample must be treated in a manner similar to that for bags. The collected sample must be concentrated on a suitable sorbent trap, then eluted or desorbed from the trap before it is injected into the separation and analysis instrumentation.

#### 1.3.1.4 Bubblers

Gases that are not easily adsorbed on an adsorbent may be more easily collected in a liquid bubbler or impinger. Air is drawn into the bubbler or impinger and is scrubbed by the trapping liquid. The air frequently passes through a glass frit to form tiny bubbles. This increases the surface area of the bubbles and promotes effective exposure of the gas to the trapping liquid. The gases or vapors may simply be dissolved in the liquid, or they may react chemically to form more stable complexes. If the rate of uptake of the analyte is faster than the time needed for the bubbles to pass through the bubbler, then the gas will be retained. Impingers may contain as little as about 5 mL of liquid up to several hundred mL of liquid. For long sampling periods, there is the danger that the sorbing liquid may evaporate. This may, in turn, limit the effective sampling time. To counter this problem, devices have been developed to maintain a constant volume of liquid in the bubbler. Alternatively, organic solvents may be placed in sub-ambient temperature baths to minimize evaporation losses. It is necessary to have an *a priori* knowledge of the concentration of the contaminant in the air so that an appropriate impinger size can be selected. It is, of course, vitally important that the solution used in the bubbler does not freeze under the sampling conditions.

As in the case of sorbent tubes, breakthrough may pose a problem, particularly if the gas flow rate is too high and an efficient scrubbing of the gas does not occur. To avoid such a problem, two or more bubblers may be placed in series.

With increasing attention being paid to the chemical nature of particles and the effect that they may have on gas analysis, it may be necessary to remove particles from the air sample upstream of the bubbler. In fact, it may also be necessary to remove undesired gases before the bubbler if they are known to interfere with the determination of a particular analyte.

The sample from bubblers is already in the liquid phase but the sample may have to be reduced in volume to concentrate further the compounds of interest prior to injection into the separation and analysis instrumentation. If the sample is collected in an aqueous solvent and water poses a problem for the analytical instrumentation, the chemicals of interest will have to be extracted into an alternative solvent that is compatible with the analytical instrumentation.

#### 1.3.1.5 Mist Chambers

Mist chambers function in a manner very similar to that of bubblers. In the mist chamber, a fine mist of water or other chemical is generated. The air sample is drawn into the mist chamber and the analyte is scavenged by the mist droplets. In these chambers it is not clear to what extent particles are scavenged. If particles are not to be sampled, then particle filters may be placed before the mist chamber. This, however, may result in the volatilization of particle-associated organics, as described previously. If water is used as the scavenging mist, the analytical method must be able to accommodate water.

#### 1.3.1.6 Cryogenic Trapping

Cryogenically trapping contaminants from air is attractive since a wide range of gases, both organic and inorganic, are collected. In addition, contamination problems, inherent in many types of samplers, are eliminated and compound recoveries are consistent. Problems may occur if using liquid nitrogen as the cryogenic medium. Under liquid nitrogen temperatures, oxygen, water and carbon dioxide from the air will liquefy and be trapped as well. Organic and inorganic compounds may undergo oxidation under these conditions. Water and carbon dioxide may cause significant problems in chromatographic systems.

Prior to analysis, the cryogenically trapped compounds must be warmed and released while trapping the compounds of interest. The analytes may be taken up in a liquid or passed through an adsorbent for concentration before injection into the analysis instrumentation.

### 1.3.2

#### Passive Sampling

Passive samplers place an adsorptive surface (frequently charcoal-based) a fixed distance from a windshield or semipermeable membrane in an enclosure in which the windshield or membrane is exposed to the air being sampled. These devices generally require that a minimum air movement across the windshield or membrane occurs in order to ensure that the device is sampling properly. The concentration of the contaminants of interest will determine the minimum exposure time of the passive sampler. The major advantages of this type of sampler are that the collection devices are small, require no electrical power and are very easy to use. After exposure, which can, for some devices, extend to periods as long as 6 months or more, the adsorbent is removed and extracted. The extract may have to be reduced in volume prior to analysis. As with other non-specific adsorbents, the passive sampler adsorptive surface will trap a wide variety of compounds. Oxidation of the adsorbed compounds may be a problem if the passive sampler is left for a long period in a gas that contains oxidants.

**1.4****Extraction and Preparation of Samples**

Regardless of the method of collection of an air sample, the ultimate objective is to remove the collected sample and prepare it for analysis. Adsorbents such as carbon, XAD, alumina, and silica gel are usually solvent extracted with solvents appropriate for the desired analytes, whereas Tenax is usually thermally desorbed. Carbon and carbon-based adsorbents may also be thermally desorbed. Regardless of the removal mechanism, the efficiency of the retrieval of each compound must be determined.

Solvent extraction of adsorbents is usually relatively efficient and reproducible. Large volumes of solvent may be necessary to extract the sample from some adsorbents. The greater the volume of solvent, the more dilute will be the analytes. Consequently, the extract must be reduced in volume (see below). The advantage of solvent extraction is that only a single aliquot of the final reduced extract is consumed in the analytical procedure. The disadvantage is that only 0.1% to about 0.5% of the sample can be analysed at a time. This, in turn, means that large sample volumes must be collected in order to get sufficient material to detect and quantify.

It is important to know the efficiency of the solvent extraction process. Aliquots of solutions of perdeuterated chemical standards can be spiked onto the sorbents prior to extraction. The perdeuterated analogs of the analytes of interest have different retention times in chromatographic systems so that they are easy to detect. By evaluating the amount of standard extracted, one can determine the extraction efficiency of the compounds of interest.

Thermal desorption of analytes from sorbents such as Tenax and carbon has the advantage that the entire sample can be used in the analysis. The disadvantage is that one gets only a single chance to analyze the sample, replicate samples are not possible. Smaller sample volumes can, however, be collected. The desorption temperature must be selected carefully to avoid decomposition or pyrolysis of the analytes. If the desired analytes are labile, then thermal desorption is not a viable removal method.

Liquid extracts will have to be reduced in volume prior to analysis to concentrate the extracted analytes to a level that can be detected in the analytical devices. Solvent reduction is usually done in an evaporation device in which the liquid is heated under vacuum. Because reduction under vacuum and heat can result in the loss of the more volatile analytes and possibly chemical reactions, internal standards with similar properties to the analytes should be added before the reduction is commenced.

Class separation or clean-up as it is also termed, may or may not be included in the analytical procedure. If the sample extract is exceedingly complex, containing hundreds of compounds, then a class separation may be desirable. This may be accomplished using column chromatographic methods, high-pressure liquid chromatographic techniques or solid-phase, micro-extraction methods. The objective is to separate the sample into a range of compound classes such as non-polar compounds and polar compounds. Subsequent analysis of the fractions collected will simplify the chromatographic steps needed to analyze the sample.

## 1.5 Summary

In this chapter, the basic methods for the collection of gases and vapors have been discussed. Although the primary examples are drawn from atmospheric sampling, the general principles should apply to the sampling of any gas or vapor for subsequent analysis.

One of the unavoidable consequences of collecting a gaseous sample for detailed chemical analysis is that there is, in all likelihood, no 100 % artifact-free sampling method, particularly if one is dealing with SVOCs. It is very difficult to ensure that a collected sample is truly representative of how things existed in the original gaseous sample. The basic objective of sampling must be to understand the complexity of the gas being sampled, define the problem that is to be solved, select a sampling method best suited to the sampling objectives and finally to understand and to minimize the occurrence of artifacts.

There are many excellent books and articles describing collection and analytical methods for specific gases and vapors. Below, are listed only a few of the many possible sources that treat the subject of collection and treatment of gases and vapors [6–10].

## References

- 1 W.H. Schroeder, D.A. Lane, *Environ. Sci. Technol.*, 22(3), (1988) 240.
- 2 C.E. Junge, *Adv. Environ. Sci. Technol.*, 8(1), (1977) 7.
- 3 J.F. Pankow, *Atmos. Environ.*, 21(11), (1987) 2275.
- 4 J.F. Pankow, *Atmos. Environ.* 22(7), (1988) 1405.
- 5 J.F. Pankow, T.F. Bidleman, *Atmos. Environ., Part A*, 26(4), (1992) 1071.
- 6 L.H. Keith, M.M. Walker, *Handbook of Air Toxics: Sampling, Analysis and Properties*, CRC Lewis Publishers, 1995, 614 pp.
- 7 J.P. Lodge, Jr., *Methods of Air Sampling and Analysis*, Intersociety Committee, Lewis Publishers, 3rd edition, 1989, 763 pp.
- 8 1998 *Annual Book of ASTM Standards*, Section 11, Water and Environmental Technology, Volume 11.03: Atmospheric Analysis; Occupational Health and Safety; Protective clothing, ASTM, 1998, 1122 pp.
- 9 D.A. Lane, *Gas and Particle Phase Measurements of Atmospheric Organic Compounds*, ed. D.A. Lane, Volume 2 in *Advances in Environmental, Industrial and Process Control Technologies*, ed. T. Vo-Dinh, Gordon and Breach, New York, 1999, 404 pp.
- 10 A.C. Stern, *Air Pollution*, Academic Press, New York, 1976, Vol. I–V.

## **2**

# **Sample Collection and Preparation of Liquid and Solids**

*Brian M. Cullum and Tuan Vo-Dinh*

### **2.1**

#### **Introduction**

Sampling and sample preparation of liquids and solids often present many challenges for quantitative analyses using spectrometric techniques (e.g., UV–VIS and infrared absorption, luminescence and Raman spectroscopies). Very often, the native form of a sample is inappropriate for analysis. This could be due to: (1) the complex nature of the object which could provide false measurements due to interferences or masking agents, (2) the size of the object being too large to analyze in its entirety (e.g. ocean water measurements), or (3) the awkward shape of the object, preventing it from fitting in the instrument within which the measurement is to be made. To overcome the first problem, some sort of sample preparation must be performed. To overcome the latter two problem, a representative sampling of the object must be performed prior to any measurements. In many cases, both representative sampling and sample preparation are required prior to any quantitative analysis.

This chapter presents an overview of the various methods used for collecting and treating liquid and solid samples. These topics have been described extensively in a variety of manuscripts and review chapters in the literature [1–6]. This chapter contains two main sections. the first deals with obtaining a representative sample from either solid or liquid objects that cannot be analyzed in their entirety, and the second deals with the preparation of these samples for spectrometric analyses.

### **2.2**

#### **Collection of a Representative Sample**

In the ideal case, all analyses would be performed on homogenous samples, therefore presenting no problem in obtaining a “representative sample.” However, due to the complex nature of the real world, this is not typically the case. Thus, the first

step that researchers often have to consider is the collection of a sub-unit of the original sample that has the same characteristic features as the bulk. This sub-unit is termed a representative sample. Two different procedures that are typically used to create a representative sample from the bulk, or lot, are known as (1) random sampling and (2) composite sampling.

In the case where the original object is larger than can be introduced into the instrument to be used for analysis, yet not too large to be homogenized, random sampling is performed. Random sampling is achieved by first mixing the bulk thoroughly, and then removing sub-units of the mixture at random. An example of random sampling can be found in the analysis of a heterogeneous solid. The bulk can be ground into a powder and mixed prior to the random removal of aliquots necessary for analysis.

The second method for obtaining a representative sample from a heterogeneous object, known as composite sampling, is generally used when the original object to be analyzed is too large for introduction into the analyzing instrument. Representative sampling is also used when the original sample is too large for simple homogenization of the entire object. Composite sampling is generally performed when the object to be analyzed is clearly segregated into various sections with different compositions. In such a case, smaller portions of the different sections are collected in the same proportions as the original object. For example, if the original object contains four regions of distinctly different composition, in the proportions of 2:1:3:5, then small subsections of the original regions will be taken with the overall ratio of the different regions being 2:1:3:5. Once the composite sample is constructed, it can then be homogenized prior to analysis. Regardless of the sampling method used (random sampling or composite sampling) the overall goal is to produce a smaller portion of the original object that contains the same proportion of components and can be readily analyzed.

### 2.2.1 **Statistics of Sampling**

In general, a sample of a heterogeneous object does not have the exact composition of the original object. Therefore, it is important to determine the appropriate sample size or number of samples to achieve an acceptable representation of the composition of the original object. In addition, since the sample is different than the object, any analysis of the sample would produce errors with respect to the original object. These errors can be categorized into two different types, systematic or random. Systematic errors are those errors that tend to always give results that are either uncharacteristically high or uncharacteristically low relative to the true object composition. These errors are typically due to a procedural error in the sampling process. In order to quantify systematic errors, the accuracy of the analysis is determined. Accuracy is regarded as the closeness of the sample composition to the actual composition of the original object. This value is often difficult to determine as it depends on analyzing the original object in its entirety by several different techniques.

Random errors are the most common type of errors that occur during sampling, and these lead to results that sometimes show higher component concentrations of some constituents and sometimes lower concentrations of those constituents, relative to the true composition of the original sample. In the case of random errors, given enough samples, the most probable composition of the original object can be determined based on probability. Two measures of random errors are (1) variance and (2) standard deviation. Given a large enough sample population, the results of the individual samples will follow a normal distribution curve. This normal distribution curve can then be described by a Gaussian profile, whose maximum, or mean, represents the most likely true composition of the original object. Many different methods have been used to describe the spread of the measured values with respect to this mean. The most common methods involve calculating either the sample standard deviation ( $\sigma_s$ ) or the variance of the sample ( $v$ ). These values can be described as shown below:

$$\sigma_s = \sqrt{\frac{(\chi - \bar{\chi})^2}{n - 1}} \quad (1)$$

$$v = \sigma^2 = \left[ \frac{(\chi - \bar{\chi})^2}{n - 1} \right] \quad (2)$$

where  $\chi$  is the value of an individual sample;  $\bar{\chi}$  is the mean value determined from multiple samples; and  $n$  is the total number of samples analyzed. These two related values, the sample standard deviation and the sample variance, are quantitative measures of the precision of the sample. The values of  $\pm \sigma_s$  represents the inflection points of the Gaussian profile that is used to describe the sample distribution. The values spanned by  $\bar{\chi} \pm \sigma_s$  therefore describe a range within which approximately 67% of the individual sample values will fall. Since this range only describes 67% of the samples, several other means of stating the precision of a measurement are often used, including confidence intervals and  $t$ -values.

Confidence intervals are similar to the standard deviation of a measurement in the sense that they provide a range (surrounding the mean value) within which a certain stated percentage of the samples will fall. The most common confidence interval described is the 95 % confidence interval, which can be determined by the values  $\bar{\chi} \pm 1.96 \sigma_s$ , and describes 95 % of the samples that are taken from the original object. The alternative point of view of a confidence interval is to determine the probability of obtaining a value outside a certain set of limits. For a given distribution of samples, the probability that an individual sample will fall within a particular range can be described by  $\bar{\chi} \pm t \sigma_s$ , where  $t$  is a factor whose magnitude varies based upon the confidence desired by the interval and the number of degrees of freedom ( $n-1$ ).

Tables such as Tab. 2.1 that list the values of  $t$  for all probabilities and degrees of freedom are available. However,  $t$  values can also be calculated by the equation:

$$t = \frac{\text{true value} - \text{experimental value}}{\sigma} \quad (3)$$

If the “true value” of the original sample is known,  $t$  can provide a measure of accuracy for a specific sampling procedure, however, as it is typically unknown; the “true value” is often substituted with  $\bar{x}$  when calculating  $t$ . Upon calculating a  $t$ -value, tables based on the  $t$ -value and the degrees of freedom ( $n-1$ ) can be used

**Table 2.1** List of  $t$ -values for various confidence intervals.

<i>Degrees of Freedom (n-1)</i>	<i>Confidence Interval</i>				
	<b>50%</b>	<b>80%</b>	<b>90%</b>	<b>95%</b>	<b>99%</b>
1	1.000	3.078	6.314	12.706	63.657
2	0.816	1.886	2.920	4.303	9.925
3	0.765	1.638	2.353	3.182	5.841
4	0.741	1.533	2.132	2.776	4.604
5	0.727	1.476	2.015	2.571	4.032
6	0.718	1.440	1.943	2.447	3.707
7	0.711	1.415	1.895	2.365	3.500
8	0.706	1.397	1.860	2.306	3.355
9	0.703	1.383	1.833	2.262	3.250
10	0.700	1.372	1.812	2.228	3.169
11	0.697	1.363	1.796	2.201	3.106
12	0.695	1.356	1.782	2.179	3.055
13	0.694	1.350	1.771	2.160	3.012
14	0.692	1.345	1.761	2.145	2.977
15	0.691	1.341	1.753	2.131	2.947
16	0.690	1.337	1.746	2.120	2.921
17	0.689	1.333	1.740	2.110	2.898
18	0.688	1.330	1.734	2.101	2.878
19	0.688	1.328	1.729	2.093	2.861
20	0.687	1.325	1.725	2.086	2.845
21	0.686	1.323	1.721	2.080	2.831
22	0.686	1.321	1.717	2.074	2.819
23	0.685	1.319	1.714	2.069	2.807
24	0.685	1.318	1.711	2.064	2.797
25	0.684	1.316	1.708	2.060	2.787
26	0.684	1.315	1.706	2.056	2.779
27	0.684	1.314	1.703	2.052	2.771
28	0.683	1.313	1.701	2.048	2.763
29	0.683	1.311	1.699	2.045	2.756
30	0.683	1.310	1.697	2.042	2.750
$\infty$	0.674	1.282	1.645	1.960	2.576

to determine the probability that an individual sample falls outside a certain range of values. In most cases probabilities of  $< 0.05$  are desired, which translates to a probability that less than 1 out of every 20 samples will provide an incorrect value.

In the case of an individual sample that is providing values that are inconsistent with the remainder of the samples, an objective means of determining whether or not that sample is representative of the original object must often be determined. This determination is based on limits that are typically defined by values exceeding either  $\bar{x} \pm 2\sigma_s$  or  $\bar{x} \pm 3\sigma_s$ . The most stringent and commonly accepted of these two values is  $\bar{x} \pm 3\sigma_s$ , since  $\geq 99.7\%$  of all representative samples should fall within this range. If an individual sample falls outside these limits, it can be rejected from the sample population due to its non-representative nature.

### 2.2.2

#### How Many Samples Should be Obtained?

One of the important questions that a researcher needs to ask himself when sampling any object for analysis is how many samples should be taken to obtain a measurement. The general answer to this question is the more samples that can be taken, assuming only random error in the sampling process, the closer the mean of the results from the various samples will be to the true value. However, to obtain a more quantitative value for the number of samples that must be obtained to achieve a particular certainty in the measurements, it is possible to rearrange the equations used in the confidence interval determination to the form:

$$t = \frac{t^2 \sigma_s^2}{e^2} \quad (4)$$

where  $e$  represents the absolute error that is acceptable in decimal form. Therefore, assuming once again that the error associated with the sampling process is random, and given the standard deviation of the sampling operation, it is possible to determine the number of samples that should be necessary to achieve a specific error. Since the number of samples is unknown, an initial approximation of  $t$  from the students  $t$  table can be obtained using  $n = \infty$ . For example, the number of samples that would be necessary to achieve an error of 5 % when analyzed at a 95 % confidence interval and having a sampling standard deviation of 9 % could be determined as follows.

$$n \approx \frac{(1.960)^2 (0.09)^2}{(0.05)^2} = 12 \quad (5)$$

Now with a better estimate of the number of samples required, a better value for  $t$  can be obtained and the process can be iterated until  $n$  converges to a single value.

$$n \approx \frac{(2.201)^2(0.09)^2}{(0.05)^2} = 16 \quad (6)$$

$$n \approx \frac{(2.131)^2(0.09)^2}{(0.05)^2} = 15$$

$$n \approx \frac{(2.145)^2(0.09)^2}{(0.05)^2} = 15$$

Therefore, the number of samples that must be obtained to achieve these stipulations is 15.

### 2.2.3

#### **Sampling**

Samples collected for spectral analysis, can typically be classified into three categories: (1) solids, (2) liquids, and (3) gases. This chapter deals strictly with the collection and preparation of solid and liquid samples as other chapters describe the collection and sample preparation of gases.

##### 2.2.3.1 **Liquids**

Liquid samples generally fall into one of three different categories:

- Homogeneous solutions
- Liquids in a flowing sample
- Immiscible mixtures

The first of these categories is that of homogeneous solutions. These are the simplest type of object to sample, as a single aliquot can typically be taken from any point in the solution and provide a representative sample. The second category of liquid that is often encountered is a flowing sample that is constantly changing (e.g. a polluted stream, a process stream at a plant, etc.). To account for these constantly changing samples, small aliquots should be taken at regular time intervals. In addition to sampling at various time intervals, it is often necessary to sample various locations of the stream at each of these times. By collecting samples at various locations, it is possible to account for heterogeneity that may occur due to turbulent flows, eddies and other irregular flow phenomena. The final type of liquid specimen that can be encountered in the real world is an immiscible mixture. In such cases, either a composite sample can be obtained by removing each of the different layers, or a random sample can be obtained following a thorough mixing.

In addition to simply obtaining a representative sample of the original liquid, storage is also an important consideration. Depending upon the particular type of analysis that is going to be performed on the sample, various types of sample containers are recommended. In the case of the analysis of organic solutions, it

is important to ensure that no reaction or partitioning can occur due to the sample container. Therefore, containers for samples that are being stored for organic analysis are typically made of glass or an inert plastic such as Teflon. Containers with dark colored walls could minimize the photodegradation of samples. In the case of trace inorganic analysis (as in typical seawater measurements), the walls of glass containers have been found to provide an excellent site for ion partition interactions. Because of these interactions, inert plastic containers are commonly used for storing liquids for inorganic analyses.

With the advent of faster and more sensitive detectors and analysis systems, the possibility of real-time analyses being performed on samples has dramatically improved. To obtain representative samples for such analyses, short bypasses are often introduced into flow lines. These can divert a small amount of the total liquid into the particular instrument being used for analysis (e.g. spectrophotometers, etc.). When such bypasses are inserted into the overall flow of the reaction process, it is important to ensure that they do not change the flow of the original system, possibly skewing the sample that is being analyzed.

#### 2.2.3.2 Solids

Methods for sampling solids can vary more than the types of sampling of any other phase, as solid samples come in many different forms. Solid samples can exist as either a large single unit, large chunks of sample, or fine powder. Fine powders of solids are often the easiest to sample. Most often these powders already exist in a homogeneous state. However, if this is not the case, either a composite sample can be obtained or a random sampling of the powder can be performed following a thorough mixing process. When the solid to be sampled is composed of large chunks of various compositions, a representative sample is typically obtained via a composite sampling method. In such a case, the overall ratio of the various types of materials in the whole object must be determined and small chunks of each type of material must be collected in the same ratio. This ratio can be based upon mass, volume, or any other parameter; however, it is important to ensure that the units chosen do not cause the analysis to be skewed.

A type of material that is often encountered in solid sampling is the large heterogeneous single unit. Examples of this type of solid include the earth's crust, ice from the polar caps and many others. These types of samples represent the most difficult solids to sample, as they require a means of coring to different depths of the original object. In addition, as it is not possible to examine the heterogeneity of the internal layers of the object, many different core samples must be taken from various locations on the object. Due to the size of the core samples that are taken from the original object, further processing of the sample must generally occur prior to analysis. These further processing procedures will be elaborated upon in the following section on solid sample preparation. Metals represent a form of solid object that often falls into the category of a large single unit. As with other large single unit solid samples, metal sampling is often performed by

coring the object. However, unlike most other materials, metals require a few additional guidelines when sampling. Due to the strong oxidation of many types of metals, it is important to obtain a sample from the center of the object that has not been exposed to the air. Such a core sample is generally obtained equidistant from the various sides of the object. By obtaining a core of both the outside and the inside of the metal, the overall oxidation state of the entire object can be retained. Once the solid sample has been obtained from the original object, it is important to once again determine the appropriate container for storage of the sample. In the case of a metal sample where oxidation is a concern, the sample should be stored under an inert gas such as helium or argon. For other samples of different composition and reactivity, various other precautions should be observed during storage to ensure that the representative sample does not change from its original composition.

### **2.3 Preparation of Samples for Analysis**

Once a representative sample has been obtained from the object of interest, the next step is to prepare the sample for analysis. Since sample preparation depends upon both the analyte (e.g. iron in water, polycyclic aromatic compounds in benzene, etc.) and the instrumentation used to perform the spectroscopic measurement (e.g. UV–VIS or IR absorption, luminescence, Raman, HPLC-fluorescence, and GC-MS, etc.), details of the preparation process will vary from analysis to analysis. Many general procedures have been developed over the years for the preparation of various types of samples prior to analysis. Most of these procedures can be classified based upon the types of samples that are to be analyzed, either solids or liquids. Within each of these categories exist several subcategories based upon the type of analyte to be measured.

#### **2.3.1 Solid Samples**

The first of the two categories that we will discuss is solid sample preparation. The various types of solid samples that are most often encountered have been discussed previously in Section 2.2.3.2 (i.e., powders, chunks or cores). In the case of the latter two sample types (chunks and cores), the first preparation step involves grinding the larger pieces into a powder which is much easier to deal with and introduce into an instrument. The most common method for obtaining powders from these samples involves grinding a solid sample into a powder using either a mortar and pestle or a ball mill. Mortars typically come in two different types: the agate version (or ceramic), for relatively soft solid materials (e.g. large crystalline substances) that must be ground into a fine powder; or steel mortars, that are used for crushing much harder materials. Agate mortars are used by placing the material to be ground in the depression of the mortar and then simply pressing down on the

sample with the pestle in a rotating fashion. When using agate or ceramic mortars and pestles, it is important to clean them thoroughly to avoid sample contamination. Less expensive mortars are typically softer and hence can be scratched more easily than more expensive ones. This is especially the case for ceramic mortars. Once scratched, they are much more difficult to clean, and may require the use of an abrasive or even a strong HCl solution. Steel mortars, also known as percussion mortars, have a hardened steel sleeve and pestle that fit snuggly into the mortar and a hammer is then used to strike the pestle and subsequently crush the sample.

Another grinding tool that is often used to grind solid samples is the ball mill. A ball mill is a ceramic drum within which is placed the sample and many small balls made of hard ceramic. To grind the sample, the drum is then rotated, and a very fine powder is produced. Ball mills are often used on softer solids, as the time it takes for grinding is directly proportional to the hardness of the material. To ensure that none of the material that is being ground sticks to the walls of the mill during the grinding process, thereby producing larger pieces, the samples are typically dried to 100–110 °C prior to grinding to expel any water.

#### 2.3.1.1 Sample Preparation for Inorganic Analysis

Most conventional quantitative analyses are best suited for the analysis of liquid samples. Because of this, solid samples that are to be analyzed are typically dissolved in a suitable solvent. The solvent chosen may be either polar (e.g. water) or non-polar (e.g. benzene) depending on the polarity and reactivity of the sample. In order to ensure that the entire analyte has been dissolved, a solvent is chosen that can dissolve the entire solid sample (analyte as well as other materials). If the sample cannot be readily dissolved in these mild conditions, many other techniques are available for dissolution. As inorganic materials often represent the greatest difficulty in dissolution, this section will deal primarily with these materials.

**Acid digestion** Acid digestion of inorganic materials is a common alternative to the mild solvents used for dissolution, as described above. When using acids to digest metallic materials, great care should be taken not to change the speciation of the metal or metallic species to be analyzed. When analyzing a reduced state of a metal or metallic species, several non-oxidizing acids can be used. These include HF, HCl, HBr,  $\text{H}_3\text{PO}_4$ , dilute  $\text{H}_2\text{SO}_4$ , and dilute  $\text{HClO}_4$ . These acids dissolve most metals with negative reduction potentials. However, in some cases (i.e. aluminum) a protective oxide layer is formed that prevents the metal from being dissolved. Substances that cannot be dissolved in the non-oxidizing acids described above, are often soluble in the oxidizing acids;  $\text{HNO}_3$ , hot and concentrated  $\text{H}_2\text{SO}_4$ , and hot and concentrated  $\text{HClO}_4$ .

In most cases, the solubility of a metal dramatically increases by heating the acid. To improve the dissolution of samples in hot acids, a device often referred to as a “digestion bomb” has been developed. This device is comprised of a Teflon-lined

sample container that can be sealed and placed in a microwave oven for heating. An alternative to using the digestion bomb is to heat the acids in an open container, thereby allowing volatile species created during the reaction (e.g. H<sub>2</sub>S, H<sub>3</sub>BO<sub>3</sub>, etc.) to escape. However, in rare cases, some metal halides (e.g., SnCl<sub>4</sub>, HgCl<sub>2</sub>, OsO<sub>4</sub>, and RuO<sub>4</sub>) are volatile and can escape as gases.

**Nonoxidizing acids** HCl and HBr are typically used for the dissolution of most metals, oxides, sulfides, phosphates and carbonates. HCl and HBr digestions are typically performed with a concentration of 37% and 48–65%, respectively. When using hot acids, HCl has a constant boiling composition of 20% at 109 °C, and HBr has a constant boiling composition of 48% at 124 °C. H<sub>2</sub>SO<sub>4</sub> is an excellent solvent for most materials when used at its boiling point, 338 °C. The composition of H<sub>2</sub>SO<sub>4</sub> for digestion purposes is typically 95–98%. Heating H<sub>2</sub>SO<sub>4</sub> causes the sample to become dehydrated while dissolving the metals and, in addition, causes any organic material to become oxidized. To dissolve refractory oxides that are insoluble in other acids, hot H<sub>3</sub>PO<sub>4</sub> can be used at a concentration of 85%. As the temperature of the acid is increased, it dehydrates. At temperatures above 150 °C, it becomes anhydrous; at temperatures greater than 200 °C, it dehydrates to pyrophosphoric acid; and finally at temperatures greater than 300 °C, it is converted to meta-phosphoric acid. A 50% HF solution is often used for the dissolution of silicates. Since glass is comprised primarily of silica, HF must be used in Teflon, silver or platinum containers. At 112 °C, HF has a constant boiling composition of 38%.

**Oxidizing acids** HNO<sub>3</sub> is capable of dissolving most metals, with the exception of gold and platinum. To dissolve these two metals, a 3:1 volumetric mixture of HCl and HNO<sub>3</sub> (also known as *aqua regia*) can be used. As described above, H<sub>2</sub>SO<sub>4</sub> is typically considered a non-oxidizing acid with respect to metals, however, it provides a useful means of oxidizing organic material in the sample. When organic material in the sample cannot be oxidized by either HNO<sub>3</sub> or H<sub>2</sub>SO<sub>4</sub>, a 60–72% solution of hot HClO<sub>4</sub> can be used. In either cold or dilute conditions, HClO<sub>4</sub> is not oxidizing, however, at high temperatures, HClO<sub>4</sub> becomes an explosive oxidizer. Because of this extreme oxidizing potential, it is important to evaporate and destroy as much organic material as possible with hot HNO<sub>3</sub> prior to using HClO<sub>4</sub>.

It should be noted that mineral acids used to digest solid samples may contain a large number of metals in different concentration ranges (usually ppm or sub-ppm levels) themselves. This could provide a source of contamination, especially significant for trace analysis work. One way to account for this contamination source is to include a blank preparation with the digestion procedure. This involves exposing an extra beaker or flask, identical to the one containing the sample, to the same digestion treatment (added acids, thermal treatment, dilutions, etc.) to which the sample was exposed. The blank solution prepared this way will contain an approximately equal amount of contaminants introduced to the sample by the acid digestion.

**Fusion reactions** Fusion is a process by which a finely powdered sample is mixed with 5–10 times its mass of inorganic material (flux) and heated in a platinum crucible to temperatures of 300–1200 °C thereby melting the flux and the sample. While in the molten state, chemical reactions between the flux and the sample produce new species that are more soluble. After the sample has been thoroughly melted, the molten solution is allowed to cool slowly. During this cooling process, the crucible is swirled to create a thin layer of solidified material on the walls of the container. The newly solidified material is then dissolved in a dilute acid. Many different flux materials have been used over the years, with  $\text{Na}_2\text{CO}_3$ ,  $\text{Li}_2\text{B}_4\text{O}_7$ ,  $\text{LiBO}_2$ ,  $\text{Na}_2\text{B}_4\text{O}_7$ ,  $\text{NaOH}$ ,  $\text{KOH}$ ,  $\text{Na}_2\text{O}_2$ ,  $\text{K}_2\text{S}_2\text{O}_7$ ,  $\text{B}_2\text{O}_3$ , and a 2:1 mixture (wt/wt) of  $\text{Li}_2\text{B}_4\text{O}_7$  and  $\text{Li}_2\text{SO}_4$  being the most common. Fluxes are typically classified as either acidic, basic or amphoteric, with basic fluxes being best suited to the dissolution of acidic oxides of silicon and phosphorous and acidic fluxes being best suited to the dissolution of basic oxides, alkali metals, alkaline earths, lanthanides and aluminum. The basic fluxes listed above include:  $\text{Na}_2\text{CO}_3$ ,  $\text{LiBO}_2$ ,  $\text{NaOH}$ ,  $\text{KOH}$ , and  $\text{Na}_2\text{O}_2$ . The acidic fluxes include:  $\text{Li}_2\text{B}_4\text{O}_7$ ,  $\text{K}_2\text{S}_2\text{O}_7$ ,  $\text{B}_2\text{O}_3$ , and  $\text{Na}_2\text{B}_4\text{O}_7$ .

$\text{Na}_2\text{CO}_3$  is one of the most common fluxes, and is typically used for dissolving silicates (e.g. clays, rocks, minerals, glasses, etc.) as well as refractory oxides and insoluble sulfates and phosphates. To dissolve aluminosilicates, carbonates, and samples with high concentrations of basic oxides,  $\text{Li}_2\text{B}_4\text{O}_7$ ,  $\text{LiBO}_2$ , or  $\text{Na}_2\text{B}_4\text{O}_7$  are typically used. Analysis of both silicates and SiC based materials can be performed using a flux of either  $\text{NaOH}$  or  $\text{KOH}$ . When using these two fluxes, however, frothing may occur in the absence of water. Therefore, best results are often achieved by first melting the flux and then adding the sample. It is also important to note that when using  $\text{NaOH}$  and  $\text{KOH}$  as fluxes, either a gold or silver crucible should be used for the reaction. For silicates that cannot be dissolved using  $\text{Na}_2\text{CO}_3$ , a more powerful oxidant of  $\text{Na}_2\text{O}_2$  can be used. This flux is good for dissolving iron and chromium alloys, and should be used in a nickel crucible. Due to the strong oxidizing and basic properties of  $\text{Na}_2\text{O}_2$  the crucible used for this reaction should be coated with a thin layer of  $\text{Na}_2\text{CO}_3$ , which melts at a higher temperature than the peroxide and therefore protects the crucible. To dissolve refractory oxides and not silicates,  $\text{K}_2\text{S}_2\text{O}_7$  is the flux of choice. The  $\text{K}_2\text{S}_2\text{O}_7$  is prepared by either heating  $\text{KHSO}_4$  until all of the water is driven off and all of the foaming has stopped or decomposing  $\text{K}_2\text{S}_2\text{O}_8$  with heat.  $\text{B}_2\text{O}_3$  is a very useful flux for the dissolution of oxides and silicates. Its main advantage over the other fluxes listed previously is that the flux can be removed from the crucible completely, following reaction with the sample, as a volatile methyl borate, by simply washing several times with  $\text{HCl}$  in methanol. For relatively fast dissolution of refractory silicates and oxides (10–20 min at 1000 °C), a 2:1 mixture (wt/wt) of  $\text{Li}_2\text{B}_4\text{O}_7$  and  $\text{Li}_2\text{SO}_4$  works well. 1 g of this flux can dissolve 0.1 g of sample, and the resulting material can be easily dissolved in hot  $\text{HCl}$ . While fusion has proven to be a necessary method for the dissolution of many compounds, it should be used only as a last resort, due to the possibility of introducing impurities into the sample as well as being a very time-consuming process.

### 2.3.1.2 Decomposition of Organics

**Ashing** When elemental analysis of an organic sample or quantitative analysis of inorganic species complexed with organic species is desired, the first step of the process is to decompose the organic material. This process of decomposition of organic matter is often termed ashing. Ashing is typically subdivided into two different categories; those processes that do not require the use of a liquid, dry ashing, and those processes that rely on liquids for the decomposition, wet ashing. Fusion can be used as one type of ashing, with the most common fluxes used in these processes being  $\text{Na}_2\text{O}_2$  and alkali metals. Another common form of dry ashing is combustion analysis. In this procedure, organic material is burned in a stream of oxygen gas, with catalysts added for more complete combustion. The released  $\text{CO}_2$  and  $\text{H}_2\text{O}$  are then trapped and analyzed quantitatively. Variations in this procedure are also used to perform quantitative analyses of nitrogen, sulfur, and halogens in organic matter.

Wet ashing methods have existed for over several hundred years. One such method, which has been used since 1883, is known as the Kjeldahl procedure. This procedure is one of the most accurate and widely applicable methods for determining the nitrogen composition of organic matter. The first step in this procedure is to digest the organic matter in boiling  $\text{H}_2\text{S}_2\text{O}_4$  which converts the nitrogen to  $\text{NH}_4^+$ , while oxidizing other elements such as carbon and hydrogen. To speed up the process,  $\text{K}_2\text{SO}_4$  can be added, which increases the boiling point of the  $\text{H}_2\text{S}_2\text{O}_4$  to 338 °C. Another common procedure that has been developed is known as the Carius method. This procedure, which involves the digestion of organics in fuming  $\text{HNO}_3$ , is carried out in a heavy-walled sealed glass container that is heated to 200–300 °C. A very powerful technique that can be widely applied to the decomposition of organic matter is refluxing the sample in a mixture of  $\text{HNO}_3$  and  $\text{HClO}_4$ . However, perchloric acid is a strong explosive, and great care should be taken by the experimentalist to shield himself/herself from the digestion process. In this procedure, the sample is first heated in boiling  $\text{HNO}_3$  and the solution is then evaporated until almost dry. This process is repeated several times to remove any easily oxidized material which might explode in the presence of  $\text{HClO}_4$ . The sample is then collected and the process is repeated with  $\text{HClO}_4$ . One of the fastest, and easiest methods of wet ashing organic matter involves the use of a Teflon™-lined digestion bomb (described earlier in Section 2.3.1.1) and a microwave oven for heating. While many different procedures have been developed for various analyses, they all generally involve the addition of the sample and a liquid into the digestion bomb, which is then placed in the microwave and heated. An example of such a procedure is the decomposition of animal tissue using a 1:1 mixture of  $\text{HNO}_3$  and  $\text{H}_2\text{SO}_4$  and heating in a microwave oven for 1 min. Another example is a modified version of the Kjeldahl reaction in which  $\text{H}_2\text{S}_2\text{O}_4$  and  $\text{H}_2\text{O}_2$  are mixed in a Teflon™-lined bomb and heated, thereby reducing the digestion time to approximately 15 min. In contrast to other wet ashing procedures which rely on concentrated acids, a mild form of wet ashing has also been developed. This procedure uses hydroxyl radicals that are produced using Fenton's reagent, a com-

**Table 2.2** Various sample preparation methods for solid samples.**Dissolution of Solids:**

Acid Digestion:

Nonoxidizing acids:

HF, HCl, HBr,  $H_3PO_4$ , dilute  $H_2SO_4$ , dilute  $HClO_4$ 

Oxidizing acids:

 $HNO_3$ , hot and concentrated  $H_2SO_4$ , hot and concentrated  $HClO_4$ 

Fusion Reactions:

Basic Fluxes:

 $Na_2CO_3$ ,  $LiBO_2$ ,  $NaOH$ ,  $KOH$ , and  $Na_2O_2$ 

Acidic Fluxes:

 $Li_2B_4O_7$ ,  $K_2S_2O_7$ ,  $B_2O_3$ , and  $Na_2B_4O_7$ **Decomposition of Organics:**

Ashing Methods:

Dry Ashing:

Combustion in  $O_2$ , and Fusion with  $Na_2O_2$  or alkali metals

Wet Ashing Reagents:

Hot  $H_2SO_4$ , fuming  $HNO_3$ ,  $HClO_4$ , hydroxyl radicals ( $H_2O_2$  and  $Fe(NH_4)_2(SO_4)_2$ )

bination of  $H_2O_2$  and  $Fe(NH_4)_2(SO_4)_2$ , to oxidize the organic materials. The mixture is then heated to 50 °C with the organic material present, allowing the radicals to oxidize the sample.

The various sample preparation methods for solid samples are summarized in Tab. 2.2.

**2.3.2****Liquid Samples****2.3.2.1 Extraction/Separation and Preconcentration**

Once a liquid sample has been obtained, either from an original liquid object or by dissolution of a solid object, the various species of interest must be isolated for analysis. In the case of a liquid suspension, filtration, or centrifugation are often performed prior to analysis to remove any solid particles. In the case of a solution, there are many methods available for isolating analytes, including: complexation, separation or extraction. These procedures are performed prior to analysis, for many reasons. Most often these procedures are performed either to remove any species which may cause interferences in the particular analysis or to provide a means of concentrating the analyte prior to analysis.

**Extraction** Extraction is a common means of isolating a particular species from a solution. Several different types of extraction are commonly used for analyte isolation, including liquid/liquid extraction and solid phase extraction. In any extraction

procedure, the isolation of particular components is based upon the affinity of the particular species for two different phases. In liquid/liquid extractions, the two phases are both liquid and are immiscible in each other (e.g. an aqueous phase and an organic phase), creating two layers with a distinct boundary. The affinity of the various components within the sample for each of the two layers is used to separate them. The distribution of the analyte, or solute, between the two different phases is described as the partition coefficient (the ratio of the solute's concentration in one solvent to its concentration in the second). Therefore, the ideal extraction would happen with either a very large or a very small partition coefficient. When this is not the case, and the solute is only slightly more soluble in one solvent than the other, multiple extractions may have to be performed to remove most of the solute. In addition, as this extraction is based on fractional partitioning of the solute, it is impossible to extract 100 % into any one phase. Therefore, to determine the amount of analyte that has been extracted, one needs to keep track of the number of extractions that were performed and the partition coefficient of the process.

Another type of extraction commonly used on liquid samples is based upon the partitioning of an analyte between the liquid in which it is dissolved and a solid support. Such extractions are typically based upon adsorption of the solute onto the solid. An example of such an extraction is the adsorption of hydrocarbons in aqueous solution onto activated charcoal. This process has long been used in such areas as pollution control (e.g. oil spills in water), and now is beginning to be implemented more in trace analysis procedures as a technique called solid phase micro-extraction. The main disadvantage of extraction techniques is typically the time that is required to recover the majority of the solute. Because of this problem the use of extraction techniques in quantitative analyses is typically performed as a last choice.

**Complexation** To increase the specificity of a particular analysis, it is often necessary to remove components from the solution that could produce erroneous results. One means of performing this task is through complexation reactions. One such procedure, known as masking, involves the complexation of an interfering species with a chelating agent. The reaction between the two species forms a stable complex which cannot undergo certain chemical reactions that are essential for quantification of the analyte. Therefore, by complexing possible interferents, a more selective measurement can be obtained. Another form of complexation that is often employed for the removal of interferences is precipitation. In precipitation reactions, an insoluble complex is selectively formed with either the interfering species or the analyte itself. Once the precipitate is formed, it can be removed, and discarded in the case of an interfering species or analyzed in the case of the analyte. Complexation reactions typically involve elaborate procedures, and depend upon many parameters such as the chemical composition of the solution, its pH and the temperature. When these factors are considered, complexation procedures can provide excellent results. For example, uranium can be isolated from associated metals in solution, with the addition of carbonates. Carbonates form a soluble com-

**Table 2.3** Common masking agents.

<b>Masking Agent</b>	<b>Ions of Elements Complexed</b>
1. Ethylenediaminetetra-Acetic acid (EDTA)	Mg, Al, Ca, Sc, Mn, Fe, Co, Ni, Cu, Zn, Ga, Sr, Y, Cd, Ba, La, Pb, Bi, Ce, Th
2. Oxo and hydride	Be, B, Al, P, V, Cr, Mn, Zn, Ga, Ge, As, Se, Mo, Ru, Sn, Sb, Te, W, Re, Os, Pb
3. Carbonate	Be, Th, U
4. Sulfide	As, Sn, Sb
5. Cyanide and Amine	Co, Ni, Cu, Zn, Ru, Rh, Pd, Ag, Cd, Os, Ir, Pt, Au, Hg
6. Citrates and Tartrates	Be, Mg, Ca, Sc, Ti, Cr, Mn, Fe, Ga, Sr, Y, Zr, Nb, Mo, In, Sb, Ba, La, Hf, Ta, W, Re, Tl, Pb, Bi, Ce, Th, U
7. Halides ( $\text{Cl}^-$ , $\text{Br}^-$ , $\text{I}^-$ )	Ge, As, Ru, Rh, Pd, Cd, Sn, Os, Ir, Pt, Au, Hg, Tl
8. Fluoro ( $\text{F}^-$ ) agents	B, Al, Si, Ti, Zr, Nb, Mo, Hf, Ta, W
9. Peroxo agents	Ti, V, Zr, Nb, Hf, Ta, U
10. Oxalate	V, Cr, Fe, Co, Ni, Ge, In, Re, Tl, Bi

plex with uranium while most other metals form an insoluble carbonate of hydroxide precipitates. Although complexation of a particular species is dependent on the chemical equilibria of the various species involved, Tab. 2.3 provides a general list of the most common complexing agents and the species with which they react.

Using Tab. 2.3 and the particular formation constants and solubility constants of the involved species, at the correct pHs and temperatures, determination of the best complexing agents for a liquid sample should be possible. In the case where two agents form complexes with the same elements, the particular solution parameters (e.g. pH) should be used to determine which is most suitable. For instance, citrates usually form more stable complexes in acidic solutions, where tartrates are typically more stable in alkaline solutions.

### 2.3.2.2 Chromatographic Separation

A common alternative to extraction of a particular component from a liquid sample is separation using chromatography. The combination of chromatography and spectroscopy is described in detail in Chapter 21 on Hyphenated Techniques. This section only provides a brief discussion of separation methods used in sample treatment prior to spectrochemical analysis. As with solid extraction procedures, chromatographic separation is based upon the partitioning of the various solutes between two different phases, a liquid phase and a solid phase. However, unlike extractions, the two different phases are not separated to allow removal of the component of interest. Instead, the liquid containing the solute is flowed across the solid phase, and the partitioning of the various components in the liquid between the two phases causes them to be retained temporarily, and elute from the solid matrix at different times. The time of elution from the solid matrix, or retention time, is determined by the partitioning coefficient of the particular component between the solid and the liquid. Many chromatographic techniques exist for separating various solutes in liquids. These techniques are generally classified by the

types of interactions that occur between the analytes and the solid phase, or matrix. These categories include: (1) adsorption, (2) ion exchange, (3) partition, (4) thin layer, and (5) size exclusion. In adsorption chromatography, the separation is based upon the polarity of the solid matrix and the solutes. Solid matrices for adsorption chromatography can include: alumina, charcoal, clay, diatomaceous earth, silica, silica gels, cellulose or starch that are packed into a glass column. In the case of alumina, which is a polar matrix, the sample would be flowed down the column with the non-polar solutes eluting first and the polar solutes eluting later, due to stronger interactions with the matrix.

Ion exchange chromatography is similar to adsorption chromatography, with the exception that elution of the various components is based upon the affinity of ions for the solid matrix. The solid support matrix for such separations is some form of ion exchange resin, depending upon the materials to be separated. The mobile, or liquid phase, in ion exchange chromatography is generally an aqueous solution. Ion exchange chromatography is used to separate solute molecules based upon their charge. Under optimum conditions, ions of equal charge such as the alkali metals can even be separated in an ion exchange column. In particular separations, the effectiveness of ion exchange chromatography can be enhanced by the addition of chelating agents to the mobile phase, thus reducing the ionic interactions of particular species and making them elute earlier in time.

The third type of liquid chromatography, partition chromatography, is performed by placing the sample on a column of solid support that has been impregnated with a liquid. The sample is then flowed down the column with a second liquid as the mobile phase that is immiscible in the liquid used to moisten the column. Therefore, as the sample flows down the column, the various components are partitioned between the solid and liquid phases, based upon their solubility in the two solvents, and thus elute at different times.

Thin-layer chromatography is performed using a glass plate that has been evenly coated with an absorbent such as alumina or silica gel. To ensure binding of the adsorbent to the glass; starch, plaster of Paris, collodion or a plastic dispersion are often added. The coated plates are then dried in an oven prior to use. Once dried, the sample is spotted on one end of the plate, which is then placed in a dish containing a solvent. The solvent then travels up the plate, via capillary action and the various components in the sample travel different distances, depending upon their solubility in the solvent. Therefore, by changing the solvent used, the separation of the components can be varied until the particular analyte of interest is separated out from other components.

Another form of liquid chromatography that can be used for separation of components in a solution is known as size exclusion chromatography. In this technique, the solid matrix, which has well defined pore sizes, is placed in a column through which the liquid sample is flowed. The size of the pores varies from matrix to matrix, and it is these pore sizes that are used to separate compounds. As the components travel down the column, their elution times are based upon their size. This technique typically works best for larger molecules such as biomolecules or polymers.

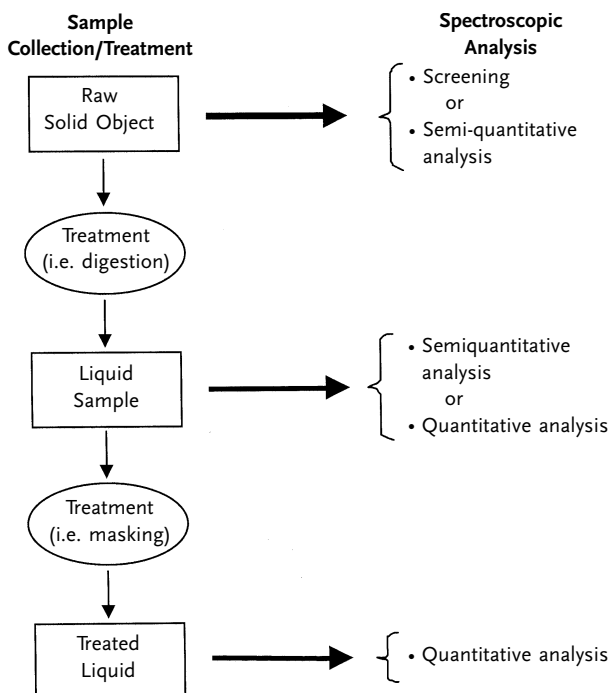


**Fig. 2.1** Schematic diagram depicting generalized sample preparation and analysis.

Another more recently developed means of separating components in a solution, is known as electrophoresis. This technique is used for the separation of components based upon their ability to travel in an electric field. Many different matrices have been used for electrophoretic separations, including buffered solutions, and gels (e.g. agarose gel). Gel electrophoresis has been used extensively for the separation of biomolecules, however, it is often slow and irreproducible. A faster more reliable form of electrophoretic separation is known as capillary electrophoresis. In this technique, a buffer filled capillary is used to span the distance between two containers of the same buffer solution. A potential of 20–30 kV is typically applied between the two containers, and a small amount of sample is injected into the capillary. The individual components of the sample are then separated, based upon the combination of their overall charge and their friction within the solvent. The individual components can then either be collected or detected upon elution from the column.

**Acknowledgements**

This research is jointly sponsored by the Federal Bureau of Investigation (Project No. 2051-II18-Y1) and by the U.S. Department of Energy at Oak Ridge National Laboratory, which is managed by UT-Battelle, LLC, for the U.S. Department of Energy under contract DE-AC05-00OR22725. In addition, B.M. Cullum is also supported by an appointment to the Oak Ridge National Laboratory Postdoctoral Research Associates Program administered jointly by the Oak Ridge National Laboratory and Oak Ridge Institute for Science and Education.

## References

- 1 Ayres, G. H. *Quantitative Chemical Analysis*, Harper and Row, New York, 2nd edition, 1968.
- 2 Harris, D. C. *Quantitative Chemical Analysis*, W. H. Freeman, New York, 3rd edition, 1991.
- 3 Minczewski, J.; Chwastowska, J.; Dybczynski, R. *Separation and Preconcentration Methods in Inorganic Trace Analysis*, New York, 1982.
- 4 Miller, J. C.; Miller J. N. *Statistics for Analytical Chemistry*, Ellis Horwood, New York, 2nd edition, 1992.
- 5 Pickering, W. F. *Fundamental Principles of Chemical Analysis*, Elsevier, New York, 1966.
- 6 Skoog, D. A.; Leary, J. J. *Principles of Instrumental Analysis*, Harcourt Brace Jovanovich, Fort Worth, TX, 1992.

## **Section II**

### **Methods 1: Optical Spectroscopy**

## 3

### Basics of Optical Spectroscopy

*Martin Hof*

#### 3.1

##### Absorption of Light

The theoretical description of light can be given in two ways: light can be regarded as a stream of corpuscles (photons) or as an electromagnetic wave. In the case of the corpuscle description, the behavior of the photons, and in particular the interaction between photons and molecules, may be described by the laws of quantum optics. In the case of the electromagnetic wave description, the interaction of the electromagnetic wave with a medium is described by the electromagnetic theory comprising *Maxwell's* equations.

In the first case, corpuscular description, the energy of the photons is

$$E = h v. \quad (1)$$

where  $h$  is the Planck constant ( $h = 6.626 \times 10^{-34}$  J s) and  $v$  is the frequency of light. The light velocity in vacuum  $c$  and the wavelength  $\lambda$  are related by

$$v = \frac{c}{\lambda}. \quad (2)$$

Thus, the energy of electromagnetic waves is directly proportional to the reciprocal wavelength. In particular in vibrational spectroscopy, the reciprocal wavelength is used and denoted as wavenumber  $k$ :

$$E = hc \tilde{v}. \quad (3)$$

Usually, the wavenumber  $k$  is written in the form

$$\tilde{v} [\text{cm}^{-1}] = \frac{10000}{\lambda [\mu\text{m}]} . \quad (4)$$

In the second case, describing light as an electromagnetic wave, its propagation may be written as

$$A(\varphi) = A_0(\varphi) e^{i(\omega t - \delta)}, \quad (5)$$

where  $A$  is the amplitude,  $\omega$  the circular frequency,  $t$  the time,  $\delta$  the phase angle and  $\varphi$  the polarization angle. The circular frequency may be expressed by the wavelength  $\lambda$  and the refractive index  $n$ :

$$\omega = \frac{c}{\lambda n}. \quad (6)$$

Equation (5) applies for the propagation of light in a non-absorbing medium. In the case of an absorbing medium Eq. (5) has to be modified by replacing the refractive index  $n$  by its complex form  $n^*$ :

$$n^* = n + ik, \quad (7)$$

where  $n$  and  $k$  are always non-negative. In the case of an absorbing medium the absorption coefficient  $\alpha$  is often used:

$$\alpha = \frac{4\pi\kappa}{\lambda}. \quad (8)$$

Based on Eq. (5), the light intensity  $I$  can now be described as:

$$I = I_0 e^{-\alpha l}, \quad (9)$$

where  $l$  is the path length of light within the absorbing medium. The Beer–Lambert law results directly from Eq. (9):

$$I = I_0 e^{-\epsilon cl}, \quad (10)$$

where  $\epsilon$  is the molar absorption coefficient and  $c$  the concentration of the absorbing compound. The Beer–Lambert law is usually expressed in its logarithmic form:

$$\log\left(\frac{I_0}{I}\right) = A = \epsilon cl \quad (11)$$

Note that the absolute value of  $\epsilon$  changes by a factor of 2.303 if “ln” was used instead of “log” (this happened often in former years).

In the medium, the absorption of light causes a transition from an energetic ground state to a particular excited state. Depending on the energy of light and on the chemical nature of the interacting compound, the excited states may differ very much in nature (cf. Fig. 3.1). Rotations and vibrations are excited in the infra-

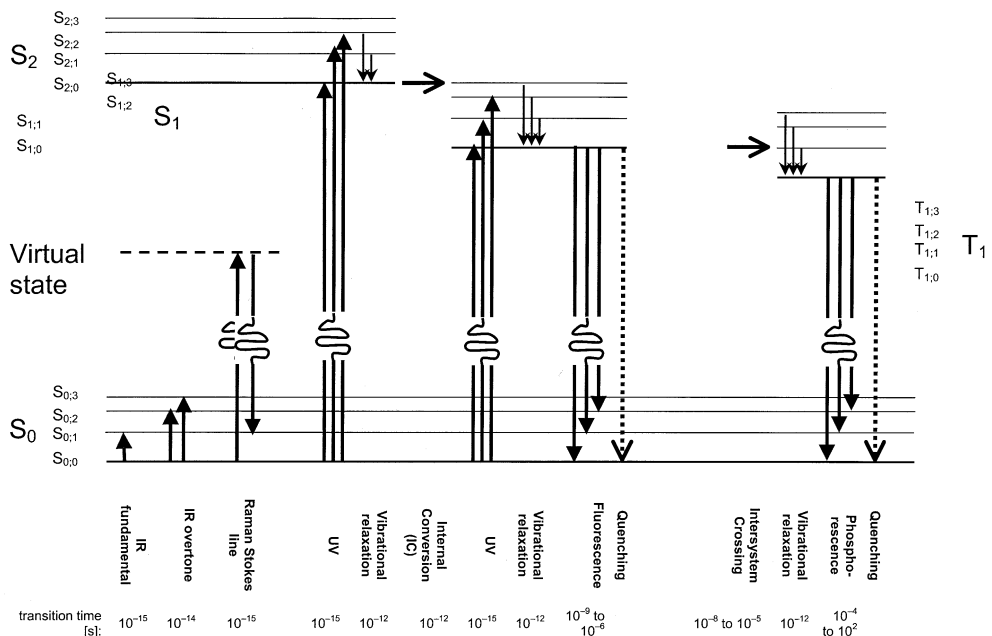


**Fig. 3.1.** Schematic depiction of vibrational and electronic transitions described in this chapter. The distance between electronic states has been compressed by a factor of at least 10 compared to the distance between vibrational states. fund: fundamental; harm: overtone; Fluo: fluorescence; Phospho: phosphorescence

red spectral range. In the UV/VIS range, absorption of light causes electronic and vibrational excitations. Relaxation of excited states back to the ground state may cause emission or luminescence, which are also evaluated spectroscopically. Electronic and vibrational transitions can be excited simultaneously (vibronic transitions), but due to the large differences in their transition energies the different types of optical excitation (electronic transitions, vibrational, and rotational motions) can be discussed separately (Born–Oppenheimer approximation). Spectral band parameters are the position of the band maximum (wavenumber  $\tilde{\nu}$  or wavelength  $\lambda$ ), the intensity of the band (height or area above the baseline), and the band shape (influenced by the environment of the vibrating group).

### 3.2 Infrared Spectroscopy

The mid- (fundamental) infrared region (IR or MIR) extends from  $4000\text{ cm}^{-1}$  ( $\lambda = 2.5\text{ }\mu\text{m}$ ) to  $400\text{ cm}^{-1}$  ( $25\text{ }\mu\text{m}$ ). It is surrounded by the far-IR region (FIR) from  $400\text{ cm}^{-1}$  ( $25\text{ }\mu\text{m}$ ) to  $10\text{ cm}^{-1}$  ( $1\text{ mm}$ ) and the very important near-IR region (NIR) from  $12500\text{ cm}^{-1}$  ( $800\text{ nm}$ ) to  $4000\text{ cm}^{-1}$  ( $2.5\text{ }\mu\text{m}$ ). Infrared spectroscopy is the

most commonly used spectroscopic method. There are a number of reasons for its great success and dissemination. The method is rapid, sensitive, easy to handle and provides many different sampling techniques for gases, liquids and solids. Important aspects are the convenient qualitative and quantitative evaluation of the spectra.

The standard format of an IR spectrum is transmittance [%T] versus wavenumber [ $\text{cm}^{-1}$ ]. According to IUPAC recommendations the values of the wavenumber axis decrease towards its right-hand end. The features of an IR spectrum (number of infrared absorption bands, their intensities and their shapes) are directly related to the molecular structure of a compound. The IR spectrum is a unique physical property of an individual compound, it is its molecular fingerprint.

The IR region comprises fundamental vibrations of bound atoms. Whenever such bound atoms vibrate, they absorb infrared energy, i. e. they exhibit IR absorption bands. The condition for a normal vibration  $j$  to be IR active is a change in molecular dipole moment  $\mu$  during vibration:

$$\mu_j = \mu_0 + \left( \frac{\delta\mu}{\delta q_j} \right) q_j + \frac{1}{2} \left( \frac{\delta^2 \mu}{\delta q_j^2} \right) q_j^2 + \dots \quad (12)$$

$q$  stands for the normal coordinate describing the motion of atoms during a normal vibration.

With respect to the direction of the vibrational movement we may distinguish between stretching vibrations (changes of bond lengths) and deformation vibrations (changes of bond angles). Deformation vibrations may be subdivided into bending modes, twisting or torsion modes, wagging modes and rocking modes. Further subdivision refers to the symmetry of the vibration (e. g., symmetric or antisymmetric, in-plane or out-of-plane).

Complications in evaluation of IR spectra are the overlapping of individual bands and the appearance of additional bands, e. g. overtone and combination bands, which may be caused by anharmonicity of some vibrations. In the NIR region, all bands are overtone or combination bands. They are always weaker in intensity than the corresponding fundamental bands. Originally considered as a drawback, the weak intensity of the NIR bands turned out to be the background for the large success of NIR spectroscopy in process analysis.

The concept of characteristic vibrations is used for qualitative analysis of polyatomic molecules. In organic compounds, characteristic vibrations occur usually between 4000 and 1500  $\text{cm}^{-1}$ . Inorganic compounds containing heavy atoms may exhibit characteristic vibrations at much lower frequencies. Characteristic vibrations are based on motions, mostly stretching vibrations, that are localized in and characteristic of typical functional groups. While individual bands are not sufficient to confirm the identity of a molecule, they provide useful information about the type and abundance of the substructures that make up a molecule. All frequencies of organic compounds below 1500  $\text{cm}^{-1}$  involve molecular vibrations, usually bending motions, that represent a characteristic fingerprint of the entire molecule or large fragments of the molecule. The comparison of the spectrum of an un-

known compound with spectra stored in spectral libraries together with corresponding search programs are an excellent possibility for qualitative analysis. Today these programs offer search routines based on complete spectra, compound information, molecular structures and substructures (see Chapter 13).

The intensities of the bands in pure components and in mixtures are proportional to the concentrations of the components. The relation between measured intensities and concentration is expressed in the Lambert–Beer law (Eq. (11)). Thus it is possible to carry out quantitative investigations by methods based on band heights or preferably by methods based on integrated intensities. Both single component analysis and multicomponent analysis by multivariate methods (see Chapter 13) can be performed.

### 3.3 Raman Spectroscopy

The Raman effect is a light-scattering effect. The exciting monochromatic beam has to be of high intensity (laser beam) in order to induce in the molecule a virtual energy state (cf. Fig. 3.1). Most of the molecules relax directly back to the  $S_{0;0}$  state, whereby light of the same wavelength as the exciting light is emitted (Rayleigh scattering). Only a very small percentage of the excited molecules relax back to a vibrationally excited state, hence the emitted photons are smaller than the exciting photons (Raman shift, Stokes lines). Because only a very small percentage of molecules use this relaxation pathway, Raman scattering is always of very low intensity, its investigation requires high-quality instrumentation. The Raman effect can be excited in the UV region, the visible region or in the NIR region.

The condition for a molecule to be Raman active is a change in the polarization (deformation) of the electron cloud during the interaction with the incident radiation. In case of Raman scattered radiation, the magnitude of the field vector E of the exciting radiation is modulated by the molecular vibrations. The induced dipole moment  $\mu'$  is

$$\mu' = \alpha E + \frac{1}{2}\beta E^2 + \frac{1}{6}\gamma E^3 + \dots \quad (13)$$

$\alpha$  is the molecular polarizability, a three-dimensional (tensor) term, whereas the dipole moment is a two-dimensional (vector) term. At commonly employed field strength values (laser output up to 1 kW per line), Eq. (13) can be reduced to its linear term. Non-linear terms have to be taken into account only in case of very high intensity of the exciting light (above 1 MW per line). Based on this situation, the conventional Raman effect is often denoted “linear Raman effect”, in contrast to “non-linear Raman effects” observed with very strong laser excitation (hyper-Raman effect, stimulated Raman effect, coherent anti-stokes Raman spectroscopy – CARS, cf. Section 6.3.2)

The Raman method is the complementary method to IR spectroscopy, where the excited vibrational state is directly approached. The Raman spectrum is the plot of Raman intensity versus Raman shift. Raman band parameters are the band position in the spectrum (Raman shift), the intensity of the band and the band shape. As in the case of the IR spectrum, the features of a Raman spectrum (number of Raman bands, their intensities and their shapes) are directly related to the molecular structure of a compound.

The complementarity of IR and Raman spectra is based on the different excitation conditions: change of dipole moment (vector quantity) in the case of an IR spectrum, change of polarization (tensor quantity) in the case of a Raman spectrum. Since a tensor is a three-dimensional quantity, the depolarization ratio  $\varrho$  can be obtained by measuring Raman spectra with polarized light (polarization directions parallel and perpendicular to the optical plane):

$$\varrho = \frac{I_{II}}{I_{\perp}} \quad (14)$$

The qualitative analysis by group frequencies and the quantitative analysis procedures for single and multicomponent analysis are, in principle, the same as in IR. A severe limitation in the application of Raman is the fluorescence phenomenon. Fluorescence is  $10^7$  times stronger than Raman scattering. Even trace impurities may fluoresce so strongly that it is often impossible to observe the Raman spectrum of the analyte. In order to avoid masking of Raman scattering by fluorescence, the gap between the virtual energy state and the electronically excited state  $S_1$  has to be sufficiently large (choice of excitation wavelength between UV, MIR and NIR). NIR excitation is often preferred, because there are very few electronic transitions in the NIR. The drawback of NIR excitation is the severely reduced Raman scattering intensity (proportional to  $\lambda_{\text{exc}}^{-4}$ ).

### 3.4 UV/VIS Absorption and Luminescence

UV/VIS absorption and luminescence spectra are related to electronic and vibrational transitions. The term luminescence summarizes a combination of basic processes like fluorescence or phosphorescence, which are described below. Transitions occur between energy levels described like  $S_{n,\nu}$  where  $S$  indicates an electronic singlet state and  $n,\nu$  the corresponding electronic ( $n$ ) and vibrational ( $\nu$ ) excitation levels. The intensity of a transition from an electronic and vibrational ground state  $S_{0,0}$  to a corresponding excited state  $S_{n,\nu}$  is proportional to the square of the transition dipole moment  $M$ , which itself can be separated into an electronic part  $M_{0,n}$  and the vibrational contribution  $F_{0,0;n,\nu}$ :

$$M = M_{0;n} F_{0,0;n,\nu} \quad (15)$$

$F_{0,0;n,v}$  represents the so-called vibrational overlap integral of the vibronic wavefunctions  $\chi_{0,0}$  and  $\chi_{n,v}$ , given by

$$F_{0,0;n,v} = \int \chi_{0,0} \chi_{n,v} dr, \quad (16)$$

where  $r$  is the internuclear distance. The square of  $F_{0,0;n,v}$  is known as the “Franck–Condon factor”, which is a measure of the transition probability between the vibrational ground state of  $S_0$  and a vibrational excited state of  $S_n$ . Individual Franck–Condon factors are directly related to the intensity of the vibrational bands and thus determine the vibrational fine structure of the absorption spectrum. The electronic transition dipole moment  $M_{0,n}$  is defined as

$$M_{0,n} = \psi_0 \mu \psi_n dq_e, \quad (17)$$

where  $\psi_0$  and  $\psi_n$  are the electronic wavefunctions of the ground and excited states, respectively,  $\mu$  is the electric dipole moment operator and  $q_e$  are the electron coordinates. The probability of an electronic transition is directly related to the square of the value of  $\cos \zeta$ , where  $\zeta$  is the angle between the plane of oscillation of the electrical vector of light and the direction of the electronic transition dipole moment  $M_{0,n}$ .

After the creation of the so-called “Franck–Condon state”  $S_{n,v}$  by “ultrafast” absorption of light ( $10^{-15}$  s), the molecule relaxes within  $10^{-12}$  s usually into the lowest excited state ( $S_{1,0}$ ). Though some rare examples of direct fluorescence from the  $S_{2,0}$  exist, they are considered as curiosities and do not find application in material or life sciences [1]. The photophysical processes populating the  $S_{1,0}$  are vibrational relaxation and internal conversion (e.g.  $S_{2,0} \rightarrow S_{1,v}$ ). Subsequently, the molecule can return back to the ground state  $S_{0,v}$  by fluorescence (typically between  $10^{-9}$  and  $10^{-6}$  s). Since the vibrational fine structure of the fluorescence spectrum is again determined by the Franck–Condon factors for the possible  $S_{1,0} \rightarrow S_{0,v}$  transitions, the emission is, for most chromophores, the mirror image of the  $S_{0,0} \rightarrow S_{1,v}$  transition. Alternatives to the light emission are several radiationless deactivation pathways from the  $S_{1,0}$  states. The most fundamental processes are the intramolecular processes of internal conversion ( $S_{1,0} \rightarrow S_{0,v}$ ) and intersystem crossing ( $S_{1,0} \rightarrow T_{n,v}$ ), as well as intermolecular interactions like collisional quenching or resonance energy transfer. After the population of an excited triplet level  $T_{n,v}$  by intersystem crossing, again vibrational relaxation and internal conversion lead to the population of the lowest triplet excited state  $T_{1,0}$ . The luminescence from the  $T_{1,0}$  state is called phosphorescence and is spin forbidden, hence it is relatively low in intensity and relatively slow (typically between  $10^{-4}$  and  $10^2$  s). It is quite common at temperatures cold enough for liquid nitrogen or helium, but rare at room temperature and even rarer at physiological temperatures. Thus, phosphorescence [2, 3] as well as the rare process of delayed fluorescence will be skipped when further discussing practical limits and possibilities of luminescence. It has to be stressed that the above described picture (summarized in Fig. 3.1.) only holds for measurements in the gas phase and in non-polar solvents as well as in

the absence of special intramolecular photochemical processes. The real situation of a chromophore in interacting solvents is much more complicated. One must include interaction with the surrounding molecules, transfer of the excitation energy from one molecule to another, variety of photochemical processes, effects of polarized excitation and detection, the different mechanisms of quenching, and relaxation of the solvent. Those of these processes that yield information when applied in material and life sciences are discussed in Section 6.5 Fluorescence Spectroscopy.

## References

- 1 Herzberg G., *Molecular Spectra and Molecular Structure: Spectra of Diatomic Molecules*, Krieger, 1989.
- 2 Herzberg G., *Molecular Spectra and Molecular Structure : Infrared and Raman of Polyatomic Molecules Vol. 2*, Krieger, 1991.
- 3 Griffiths P. R., Haseth J. A., *Fourier Transform Infrared Spectrometry*, John Wiley & Sons, Chichester 1986.
- 4 Hollas J. M., *Modern Spectroscopy*, John Wiley & Sons, Chichester 1996.
- 5 Günzler H. and Gremlich H.-U., *IR Spectroscopy. An Introduction*, Wiley-VCH, Weinheim 2002.
- 6 *Infrared and Raman Spectroscopy. Methods and Applications*, ed. B. Schrader, Wiley-VCH, Weinheim 1995.
- 7 Diem M., *Introduction to Modern Vibrational Spectroscopy*, John Wiley & Sons – Interscience, 1993.
- 8 *Modern Techniques in Raman Spectroscopy*, ed. J. J. Laserna, John Wiley & Sons, Chichester 1996.
- 9 Painter C., Coleman M. M., Koenig J. L., *The Theory of Vibrational Spectroscopy and Its Application to Polymeric Materials*, John Wiley and Sons, Chichester 1991.
- 10 Twardowski J., Anzenbacher P., *Raman and IR spectroscopy in Biology and Biochemistry*, Ellis Horwood, Chichester 1994.
- 11 Barrow G. M., *Molecular Spectroscopy*, McGraw-Hill, New York 1962.
- 12 *Applied Laser Spectroscopy Techniques, Instrumentation, and Applications*, ed. D. L. Andrews, John Wiley & Sons, Chichester 1992.
- 13 Lakowicz J. R., *Principles of Fluorescence Spectroscopy*, 2nd edition, Kluwer Academic/Plenum, 1999.
- 14 Silverstein R. M., Bassler G. C., Morrill T. C., *Spectrometric Identification of Organic Compounds*, 5th edition, John Wiley & Sons, Chichester 1998.

## 4

# Instrumentation

*Valdas Sablinskas*

There are a few basic types of instruments which are used in optical spectroscopy for the determination of absorption, fluorescence or Raman spectra of condensed and gaseous samples. These basic types are monochromators, interferometers and polychromators. The wavelength range of optical spectroscopy extends from 200 nm (UV) to 500 μm (FIR). It is impossible to build one single spectral instrument capable of covering the region completely and providing information about the different processes of absorption, emission and scattering of light. Light sources, detectors and other optical components have limited operational ranges, caused by the underlying physical work principles. The choice of the appropriate instrument type depends on the application. The interaction process of light with the material and the spectral interval of interest have to be taken into account. Traditionally, spectrometers for absorption measurements are optimized for ultraviolet/visible (UV/VIS) (175–750 nm), near-infrared (NIR) (0.8–2.5 μm), mid-infrared (MIR) (2.5–25 μm) and far-infrared (FIR) (25–1000 μm) ranges. Some commercial spectrometers are capable of covering neighboring spectral regions (for instance, UV/VIS/NIR or MIR/FIR).

Spectrometers for investigation of scattering and emission of light belong to different classes of instruments. Raman and fluorescence spectrometers belong in this group.

### 4.1

#### MIR Spectrometers

There are two types of MIR spectrometers, dispersive and Fourier-transform (FT) spectrometers. Today FT spectrometers are used predominantly. The most significant advantage of FT spectrometers is that radiation from all wavelengths is measured simultaneously, whereas in dispersive spectrometers all wavelengths are measured consecutively. Therefore, a FT spectrometer is much faster and

more sensitive. Dispersive MIR spectrometers are no longer available on the market, but they are still in use in laboratories.

Information about the absorption of infrared radiation in the sample is obtained by measuring the intensity ratio of the radiation “before” and “after” the sample. In order to obtain this ratio with sufficient accuracy, infrared absorption spectrometers should be double channel instruments.

#### 4.1.1

##### Dispersive Spectrometers

Basically, dispersive instruments are much simpler than Fourier Transform ones, since they measure the spectrum directly (Fig. 4.1). The IR beam from the source of infrared radiation is directed both to a sample and to a reference position inside the sample chamber (double-beam principle). After passing the sample chamber, both beams are combined into one common path by means of a rotating chopper mirror. The beams enter the grating monochromator and, finally, reach the detector. By turning the grating, all spectral elements are eventually directed to the detector. The spectrum is recorded in real time as the ratio of the sample beam intensity ( $I$ ) to the reference beam intensity ( $I_0$ ). Usually, one grating is not sufficient to cover the complete MIR spectral range. Up to four different gratings are subsequently used for the region  $4000\text{--}400\text{ cm}^{-1}$ .

The great advantage of the double-beam principle is the automatic compensation in the spectra of most of the external disturbances, such as contributions from optical components or absorptions due to solvents or atmospheric water and  $\text{CO}_2$ . Regardless of this automatic compensation, no meaningful results are obtained if the absorption due to these disturbances is too strong. Such regions are called dead spectral regions. For instance, because of the strong absorption of  $\text{CO}_2$  around  $2364\text{ cm}^{-1}$ , this region may be blocked in conventional MIR spectrometers. The problem of dead spectral regions can be overcome by purging the spectrometer with dry and  $\text{CO}_2$ -free air or evacuating it. An air dryer can be installed on any MIR spectrometer as an option. Vacuum spectrometers are usually more expensive than purged ones, moreover vacuum-tight sample cells have to be used.

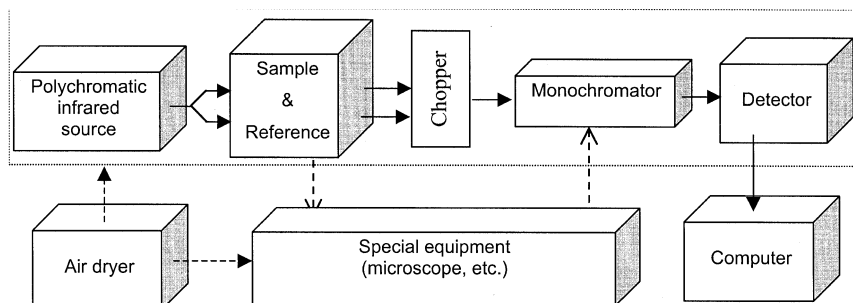


**Fig. 4.1** Block diagram of a dispersive spectrometer.

The most common source in MIR spectrometers is a glowing ceramic bar, a so-called glowbar (or globar). More intense emission is provided by the Nernst glower due to its higher operation temperature (black body radiator). A thermocouple or a thermopile is commonly used as detector. The response behaviour of such detectors is slow, which prevents rapid scanning by dispersive MIR spectrometers.

#### 4.1.2

#### Fourier-Transform Spectrometers

FT-IR spectrometers cannot be built as double-beam instruments. Unlike dispersive instruments, FT-IR spectrometers acquire single channel spectra of sample and reference and their ratio is calculated afterwards (Fig. 4.2). Sample and reference may automatically be replaced by a sample slider, or the IR beam may be switched between sample and reference by flip-mirrors. In the case of higher accumulation numbers, the instrument switches repeatedly between sample and reference scan.

The heart of any FT-IR spectrometer is an interferometer. The Michelson interferometer consists basically of a beamsplitter and two flat mirrors. One of the mirrors is fixed in one interferometer arm, the other mirror is movable in the second interferometer arm. Most common MIR beamsplitters are made of KBr with a multilayer coating. The beamsplitter should have a reflectivity of 50% and no absorption across its range of use.

The functionality of a Michelson interferometer is based on a collimated IR beam. The latter is directed to the beamsplitter, which divides the beam into two parts of equal intensity (in the ideal case). The divided beams are reflected, by the fixed and the movable mirrors, back to the beamsplitter, where they recombine

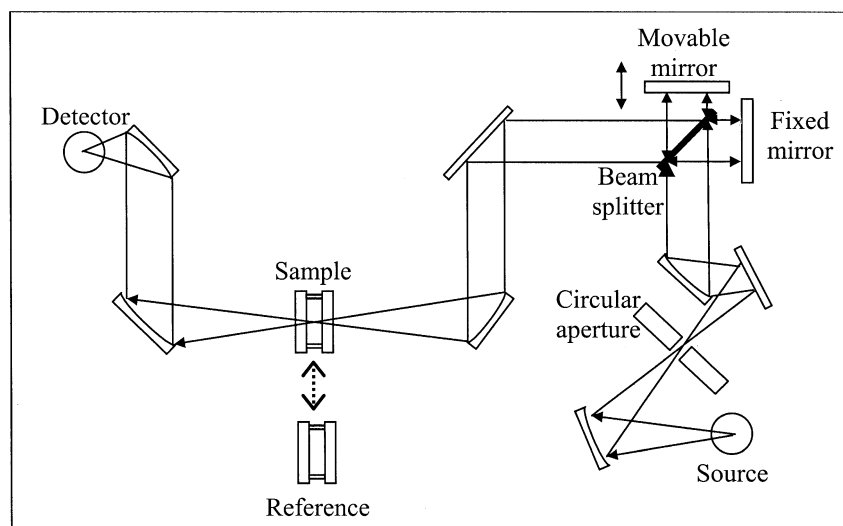


**Fig. 4.2** Diagram of a FT-IR spectrometer with Michelson interferometer.

and interfere. The displacement of the movable mirror causes changes in the optical pathlength between the two beams, so that the conditions for constructive and destructive interference, as well as all intermediate states between the two, are consecutively met. The recombined IR beam passes the sample (or the reference) and reaches the detector. The position and movement of the movable mirror are controlled by a helium–neon laser ( $\lambda_{\text{HeNe}}=632.8 \text{ nm}$ ). The interferogram of the helium–neon laser is used to control the sampling of the IR interferograms in steps down to  $\lambda_{\text{HeNe}}/2=316.4 \text{ nm}$ .

The mathematical procedure, which is employed to convert the IR interferogram (intensity versus time, also called time domain) to an IR spectrum (intensity versus frequency, also called frequency domain), is called Fourier transformation. Sample and reference interferograms are separately transformed. Afterwards, the ratio of both is automatically calculated and displayed as instrument-independent IR transmission spectrum (Fig. 4.3).

Resolution in an FT-IR spectrometer is mainly defined by the maximum path difference between the interferometer arms. It is crucial to maintain the optical alignment of the interferometer during mirror movement, hence the efficiency of the device for moving the mirror (the so-called scanner) is very important. Most interferometers employ either a mechanical pivot bearing, a mechanical slide bearing, or an air bearing to translate the mirror along a linear path. Alternatively, an optical retardation can be introduced by rotating a pair of planar mirrors

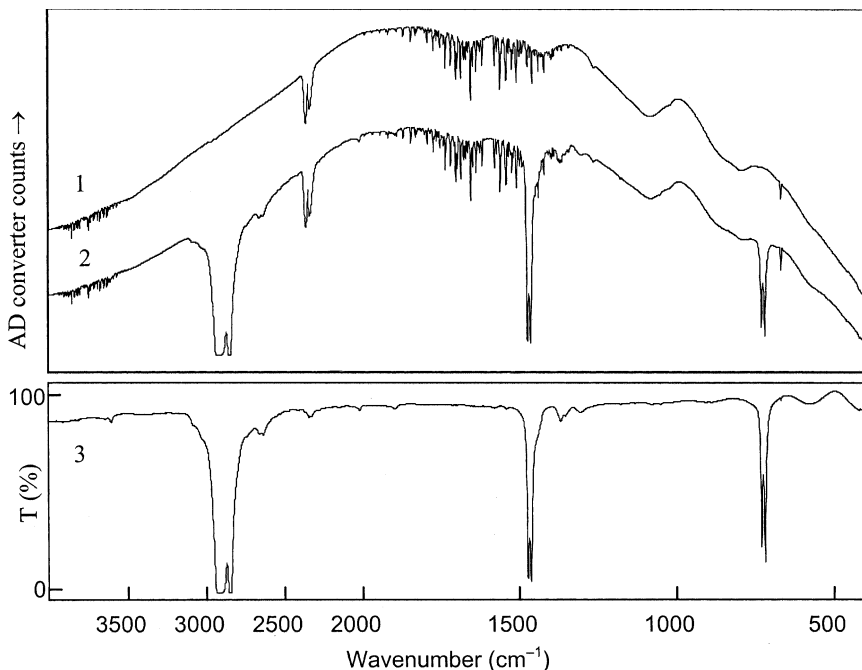


**Fig. 4.3** IR absorption spectrum of polyethylene: 1. Single-beam reference spectrum (without sample); 2. single-beam sample spectrum; 3. ratioed transmission spectrum.

instead of translating one mirror. The larger the angle of the mirror rotation, the greater the achieved optical retardation. Regardless of the type of mirror drive, it moves continuously and does not stop during data collection at each interferogram sampling point (continuous-scan operation). In order to correct for alignment errors during mirror movement, newer interferometers employ fast-response piezoelectric crystals to align the position of the fixed mirror during the scan. Moving mirror tilt may also be eliminated optically by using so-called corner cube mirrors. This method is preferable for high resolution instruments, where the moving mirror displacement may be as large as a few meters.

Traditionally, FT-IR spectrometers used to be divided into two groups, routine and research spectrometers. Both have an affiliated PC for the data processing and handling. Routine spectrometers usually have a resolution limit of ca.  $1\text{ cm}^{-1}$ . Research spectrometers can achieve resolution as high as  $0.001\text{ cm}^{-1}$ . Sources, beamsplitters and detectors are exchangeable in research spectrometers, so one could use these spectrometers from 40000 down to  $20\text{ cm}^{-1}$  (from the UV to far-IR range). In some spectrometers different sources and detectors are installed permanently. They can be switched on or off by means of flip mirrors. Nowadays there are no designated limits between routine and research instruments.

The high efficiency of FT-IR spectrometers is mainly due to the so-called Jacquinot advantage, i. e. the optical throughput is no longer limited by a relatively narrow monochromator slit. Interferometers have circular apertures, whose diameter depends only on the desired spectral resolution. In general, the beam cross-section of an FT instrument is usually 75 to 100 times larger than the slit opening of a dispersive instrument. Correspondingly, a much larger amount of IR radiation reaches the detector of an FT instrument. The diameter of the aperture in FT instruments is limited by the chosen spectral resolution. The better the resolution required the smaller the computer-controlled diameter of the aperture, and eventually the signal at the detector.

Another important advantage of FT-IR spectrometers is their outstanding frequency accuracy (Connes advantage), the basis for all achievements in difference spectroscopy. This accuracy of spectral frequencies is due to the precise and stable collection of the interferogram signal, triggered by the helium–neon laser. An accuracy in wavenumber of better than  $0.01\text{ cm}^{-1}$  can be achieved.

The third advantage is high speed and/or high sensitivity (Felgett advantage). The time needed by the movable mirror for one scan cycle varies between 0.01 and 1 s, depending on the spectral resolution as well as the detector response. Typically, 20–200 scans are accumulated in one measurement to acquire a sufficient signal-to-noise ratio. The number of accumulations depends on the experimental conditions and can be much higher if few spectral effects have to be studied.

#### 4.1.2.1 Detectors

The standard detector in routine FT-IR instruments is the pyroelectric DTGS (deuterated triglycine sulfate) detector, whose response in the MIR range is wavelength independent. The detector operates at ambient temperature and shows good linearity across the whole transmittance scale. The DTGS detector responds to signal frequencies of up to several thousand Hz, hence the time needed to scan one spectrum at a resolution of  $4\text{ cm}^{-1}$  is of the order of 1 s.

The MCT (mercury cadmium telluride) detector is much more sensitive and faster than the DTGS detector. The operation of MCT detectors is based on an internal photo effect. Each IR radiation quantum excites one bound electron of the detector material to a free state, i. e. the electrical conductivity of the MCT detector element increases. A serious drawback of the MCT detector is its spectral working range. Low energy photons are not able to promote the bound electrons to the free state (low wavenumber cut-off of MCT detector at  $600\text{ cm}^{-1}$ ). In some MCTs this cut-off is even higher ( $750\text{ cm}^{-1}$ ) due to absorption in the detector optical window. Due to its low operating temperature, the detector element is covered by a vacuum enclosure with an optical window in front of the detector element. The vacuum housing makes the MCT detector rather expensive. Furthermore, the MCT detector shows nonlinear response, which can be minimised by special electronics and software. The time needed to scan one spectrum is only 0.01 s, i. e. rates of 100 scans per second are achieved. The MCT is the detector of choice for experiments in conditions of low radiation levels.

FT-IR spectrometers with array detectors can be considered a new class of IR instruments. The size of an array detector chip with its sensitive elements placed in one plane (so-called focal plane array (FPA)) is usually ca.  $4\times 4\text{ mm}^2$  and, depending on the number of single MCT detectors in the array, a large number of interferograms are collected simultaneously. For instance, in the case of a  $64\times 64$  FPA detector, 4096 interferograms are collected simultaneously. With such a detector IR spectral imaging of the sample area  $4\times 4\text{ mm}^2$  can be done in a few seconds. By combining the FT-IR imaging spectrometer with an IR microscope, images from areas as small as  $250\times 250\text{ }\mu\text{m}$  can be acquired. Since the read-out electronics need some time to collect signals from all MCT elements of the FPA detector, the scanner speed has to be reduced substantially. For this reason, interferometers in imaging instruments are commonly operated in the step-scan mode.

#### 4.1.2.2 Step-scan Operation

In step-scan mode, the moving mirror of the interferometer is stopped at each data acquisition point and held for some time (seconds to minutes) during which data are acquired. In step-scan mode the collected interferograms contain the same information as in continuous-scan mode, only the time required for the complete experiment is much longer. Under stroboscopic measuring conditions, a time resolution of 100 ns can be achieved. This technique can be applied to processes which can repeatedly be started under highly reproducible conditions. The step-scan technique can also be applied for the acquisition of voluminous data. This

is the case for FPA detectors, where data points from a vast number of individual detector elements have to be collected.

#### 4.1.2.3 Combined Techniques

Many FT-IR spectrometers have external ports for optical coupling to dedicated accessories. The IR radiation is conveniently directed to/from the external ports by computer-controlled flip mirrors. A large variety of accessories, like an IR microscope, interfaces for gas chromatography (GC/FT-IR), liquid chromatography (HPLC/FT-IR), thin layer chromatography FT-IR (TLC/FT-IR), etc., is commercially available. This type of method combination is usually called a hyphenated technique. FTIR spectrometers can even be supplemented by a FT-Raman accessory. The versatile combination of FT-IR spectrometers with other instruments has substantially contributed to their abundance in most analytical laboratories.

## 4.2

### NIR Spectrometers

Absorption of electromagnetic radiation in the NIR region is caused by overtone and combination vibrations. Polyatomic molecules exhibit many overtone and combination vibrations, their spectral bands overlap and make typical NIR bands look very broad and featureless. Nevertheless, NIR spectra contain molecular information about the sample, and this information can be extracted by means of chemometric methods (cf. Chapter 13). A prerequisite for chemometric evaluations is high quality of the collected spectral data. Therefore, wavelength precision, resolution, photometric precision and signal-to-noise ratio are important criteria for the selection of an NIR spectrometer.

Among all optical spectroscopic methods, NIR offers the greatest diversity of instrumentation principles, and the market for commercially available instruments is undergoing continuous change and growth. NIR has an enormous variety of applications, e. g. in agriculture, in food processing, in medical and in pharmaceutical applications, in polymer and plastics processing, in environmental analysis, in material recycling, and in satellites or aircraft for remote sensing. Commercial NIR spectrometers vary remarkably with respect to cost, size and portability, measurement time and environmental conditions for on-line applications in industry. According to their measurement principles, NIR spectrometers fall into one of six categories:

1. Fourier-Transform spectrometers
2. Scanning-Grating spectrometers
3. Diode array spectrometers (fixed-grating spectrometers)
4. Filter spectrometers
5. LED (light-emitting diode) spectrometers
6. AOTF (acousto-optical tuneable filter) spectrometers

**Table 4.1** NIR detectors and their application ranges.

<b>Detector</b>	<b>Working temperature/K</b>	<b>Application range/nm</b>
Ge detector	77	600 to 1800
Si detector	300	400 to 1100
InGaAs detector	300	900 to 1700
PbS detector	196	1100 to 3500
InAs detector	77	1500 to 3500
Extended InGaAs detector	300	1100 to 2800
Ge detector	300	600 to 1900
InSb detector	77	2000 to 4000
PbS detector	300	1000 to 3000
PbSe detector	300	1100 to 4000

#### 4.2.1

##### **FT-NIR Spectrometers**

These are identical to the FT spectrometers already described in Section 4.1. The most commonly used light source for FT-NIR spectrometry is the tungsten–halogen lamp which delivers high and constant energy throughout the NIR range, is very stable and has a long lifetime. Beamsplitters for FT-NIR spectrometers are usually made from  $\text{CaF}_2$  with working range  $10000\text{--}1600 \text{ cm}^{-1}$  (1000–6000 nm). There is no detector available to cover the complete NIR range or to suit all types of NIR spectrometers. A list of detectors and their application ranges is given in Tab. 4.1. Most detectors used in the range 1100 to 2500 nm are PbS and PbSe detectors, whereas Si diodes are preferred in the range 400 to 1100 nm.

#### 4.2.2

##### **Scanning-Grating Spectrometers**

These spectrometers and their basic construction have already been described in Section 4.1. Scanning-Grating NIR spectrometers often permit continuous scans from the UV through the VIS to the NIR region, therefore they have two detectors, one for the UV/VIS (Si) and one for the NIR regions (mostly PbS). Because NIR spectral bands of solid or liquid samples are rather broad, NIR spectrometers usually do not provide high spectral resolution. For many NIR applications a resolution of 10 nm is sufficient. This allows rapid scans across the entire NIR range in only 0.1–1 s. The broad spectral range of such spectrometers, their speed and accuracy are the great advantages of these instruments. Full-range spectrometers are rather expensive, hence they are mainly found in research laboratories.

#### 4.2.3

##### **Diode Array Spectrometers**

These have no moving parts. NIR radiation is spread by a fixed grating across the diode array detector so that a definite wavelength range is directed towards each detector element. Diode arrays usually consist of 256 or 512 InGaAs and InSb detector elements. The spectral resolution depends upon the number of elements in the array and the wavelength range. The great advantage of these spectrometers is the possibility of miniaturisation. Such spectrometers can fit on a PC plug-in card. NIR radiation is delivered from the lamp via the sample to the detector by optical fibre cables (single fibre of 50–1000 µm diameter or bundles of up to 80 single fibres). If the wavelengths to be investigated are known in advance, one may use a set of bandpass filters to send radiation of only discrete wavelengths through the sample to the detector array.

#### 4.2.4

##### **Filter Spectrometers**

These may have several filters mounted on a rotating wheel. The wheel has either a set of filters with predefined wavelength regions for a specific application or a set of filters for the NIR region of interest. The advantages of these spectrometers are their robustness and low cost.

#### 4.2.5

##### **LED Spectrometers**

These work at predefined wavelengths, they have no moving parts. Because LEDs emit radiation of discrete wavelengths, these instruments do not need any wavelength selector (filter, monochromator etc.). Additional interference filters can be used in order to limit the spectral bandwidth. Advantages are the possibility of miniaturisation and the high stability of these light sources.

#### 4.2.6

##### **AOTF Spectrometers**

These are built around a birefringent crystal, which is used for rapid and precise wavelength selection. Usually it is a TeO<sub>2</sub> crystal with one or more piezoelectric transducers. The working principle is based on a phonon–photon scattering mechanism. Broadband randomly polarized light is incident on the AOTF crystal, where it is separated into ordinary and extraordinary polarized components. When radio frequency acoustic waves are coupled into the crystal via a piezoelectric transducer, the refractive index is spatially modulated, producing a phase grating that diffracts one specific wavelength of the incident light. This light is symmetrically deflected on exit from the crystal into two orthogonal polarized beams, one of which is imaged on to the detector, all other wavelengths travel through

the crystal without being diffracted along the incident ray. By changing the frequency of the acoustic waves, the wavelength of the diffracted light is changed. Spectral resolution depends on the size of the crystal. Advantages of such a spectrometer over a filter wheel or grating monochromator include high resolution, high speed, random or sequential wavelengths access, no moving parts, compact size, and imaging capabilities. A disadvantage is the high cost of the instrument.

Some types of the described spectrometers can be applied for NIR imaging purposes. FT-NIR and AOTF imaging spectrometers are already available on the market.

### 4.3

#### Raman Spectrometers

Raman spectrometers are used to analyze light scattered by molecules. A major advantage of Raman spectroscopy is the high spatial resolution that can be obtained, typically of the order of 1  $\mu\text{m}$  (compared to approx. 10  $\mu\text{m}$  with FT-IR).

In conventional Raman experiments the sample is illuminated by monochromatic light. The registration of low intensity Raman scattering in the presence of strong Tyndall and Rayleigh scattering implies special requirements for Raman spectrometers. A Raman spectrometer has to combine very good filter characteristics for eliminating Rayleigh and Tyndall scattering with high sensitivity for detecting very weak Raman bands. Currently, there are three types of Raman instruments available on the market:

1. Raman grating spectrometer with single channel detector
2. FT-Raman spectrometer with near infrared excitation
3. Raman grating polychromator with multichannel detector

All three types of instruments have particular advantages and disadvantages for a given analytical task.

##### 4.3.1

###### Raman Grating Spectrometer with Single Channel Detector

A Raman grating spectrometer with single channel detector is the conventional type of Raman instrument. It consists of three main parts: a monochromatic light source, a grating monochromator and a single channel detection system. Light sources in Raman spectrometers are lasers. The laser power impinging on the sample may vary between 10 and 1000 mW depending on its thermal stability. The laser may be continuous or quasi-continuous. The longer the wavelength of the laser the lower the probability of generating fluorescence. On the other hand, the Raman scattering intensity diminishes proportionally to the fourth power of the laser wavelength. A list of most frequently used lasers in dispersive Raman instruments is given in Tab. 4.2.

**Table 4.2** Lasers used with dispersive Raman instruments.

<b>Laser</b>	<b>Type</b>	<b>Type of radiation</b>	<b>Wave-length/nm</b>	<b>Max. power/W</b>	<b>Beam diameter/mm</b>	<b>Price; Comments</b>
Ar <sup>+</sup>	Gas	CW	488.0 514.5	4 4	1.5	Medium; Standard source
Kr <sup>+</sup>	Gas	CW	647.1 725.5	4	1.8	Medium; Standard source
He–Ne	Gas	CW	632.8	0.05	1.1	Low; Not intense
Liquid dye	Liquid	CW, Pulsed, tunable	Depends on dye	0.1		Low; Used mainly for RRS*
Ti–sapphire	Solid	CW, Pulsed, tunable	720–980	2	0.95	High; Used mainly for RRS*
Diode	Solid	CW	700–900	0.5		Very low; Modern source

\* RRS: Resonance Raman scattering.

Lasers with short pulses are not used in Raman spectrometers, mainly because the detectors in Raman spectrometers are tuned to high sensitivity. Such detectors are very easy to saturate and this is a case where short and intense laser pulses are employed for excitation of Raman scattering. It must be noted, that gas lasers are not perfect sources of monochromatic radiation. Together with intense coherent radiation such lasers produce weak incoherent radiation, caused by a different transition between electronic energy levels of the gas. The intensity of this incoherent and noncollimated radiation can be suppressed by increasing the distance between the laser and the sample, by placing a spatial filter (consisting of two lenses and a pinhole) or a narrow-band filter (usually an interference filter) into the laser beam.

The monochromator is the main part of a grating Raman instrument. Single monochromators should not be used in Raman spectrometers because of their insufficient performance in eliminating Rayleigh and Tyndall scattering. Instead, double or even triple monochromator systems are well suited. The common configuration for double monochromator systems is the so-called Czerny–Turner arrangement (Fig. 4.4). Two identical monochromators are placed in such a way that their angular dispersions are co-added (additive mode). The slit between the monochromators (intermediate slit) acts as a filter to prevent stray light from the first monochromator entering the second one. In general, entrance, intermediate and exit slit widths in a double monochromator Raman spectrometer are of the same size. A triple monochromator is preferred when very low frequency Raman bands (frequency range close to laser frequency) have to be recorded. In addition to their very low stray light level, triple monochromators in additive mode have high angular dispersion and permit the recording of Raman spectra with very good resolution.

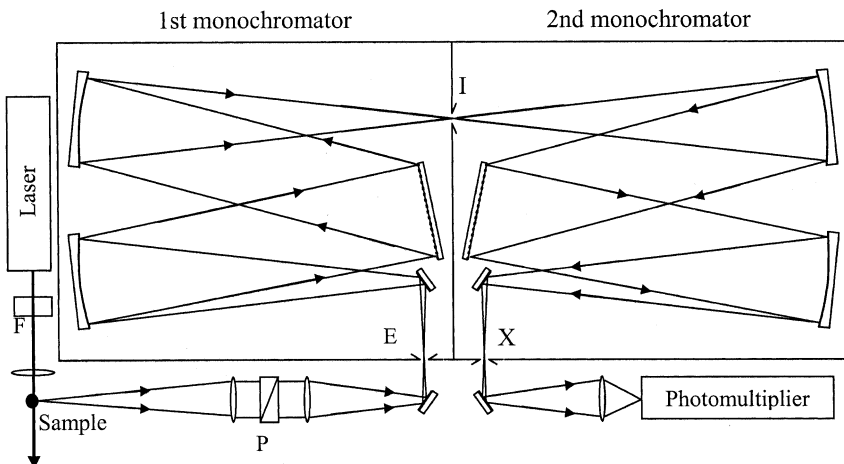


**Fig. 4.4** Dispersive grating Raman spectrometer with single channel detector and double monochromator in Czerny–Turner configuration. F, narrow band filter; P, polariser; E, entrance slit; I, intermediate slit; X, exit slit.

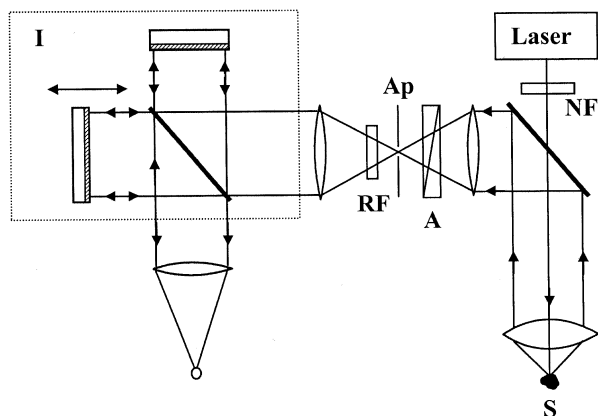


**Fig. 4.5** Basic diagram of a FT-Raman spectrometer. S, sample; NF, notch filter for rejecting non-lasing radiation from laser; RF, Rayleigh filter for rejecting radiation at laser frequency; Ap, aperture wheel; A, analyser; I, interferometer.

#### 4.3.1.1 Detectors

Detectors are crucial parts of Raman spectrometers due to the low intensity of Raman bands. Photomultipliers have excellent characteristics in the ultraviolet and visible spectral regions, hence they are the preferred detectors in a single channel dispersive Raman spectrometer. The sensitivity of photomultipliers is limited by their dark current (residual electrical detector signal observed in the absence of any light). The dark current increases with temperature, i.e., cooling increases the signal to noise ratio of photomultipliers. Liquid N<sub>2</sub> cooling provides the best performance, but for routine Raman experiments Peltier cooling is often sufficient.

### 4.3.1.2 Calibration

In the case of dispersive instruments, the Raman spectrum is obtained as a function of the rotation of the dispersive element (prism or grating). In modern dispersive Raman instruments a cosecant drive mechanism is used (usually, stepping motor), which provides a nearly linear relation between the grating angle and the Raman shift scale. In all cases, calibration of the Raman shift scale by recording a well-known spectrum with narrow spectral bands is necessary. Atomic emission spectra are also well suited. Very often an ordinary neon lamp is used, whose emission lines are narrow, intense and distributed over a wide range in the visible. The line positions can be found in any catalog of atomic emission spectra. A frequently used calibration is the use of the plasma lines of the Raman excitation laser itself: after setting-up the Raman experiment, the laser resonator mirrors are slightly de-adjusted. Under such conditions the laser emits weak atomic radiation whose in-

**Table 4.3** Intensities and positions of plasma lines of the  $\text{Ar}^+$  laser.

<b>Relative intensity, a. u.</b>	<b>Wavelength, <math>\lambda/\text{nm}</math> (in air)</b>	<b>Wavenumber, <math>\tilde{\nu}/\text{cm}^{-1}</math></b>	<b>Raman shift, <math>\Delta \tilde{\nu}/\text{cm}^{-1}</math> (<math>\lambda_{\text{exc}} = 488.0 \text{ nm}</math>)</b>	<b>Raman shift, <math>\Delta \tilde{\nu}/\text{cm}^{-1}</math> (<math>\lambda_{\text{exc}} = 514.5 \text{ nm}</math>)</b>
1120	487.9860	20486.67	0	
25	488.9033	20448.23	38.4	
16	490.4753	20382.70	104.0	
121	493.3206	20265.13	221.5	
14	494.2915	20225.33	261.3	
1	495.5111	20175.53	311.1	
120	496.5073	20135.07	351.6	
41	497.2157	20106.39	380.3	
190	500.9334	19957.16	529.5	
77	501.7160	19926.03	560.6	
155	506.2036	19749.39	737.3	
1	509.0496	19638.98	847.7	
45	514.1790	19443.06	1043.6	
125	514.5319	19429.73	1056.9	0
1	516.2745	19364.14	1122.5	65.6
4	516.5774	19352.79	1133.9	76.9
5	517.6233	19313.69	1173.0	116.0
3	521.6816	19163.44	1323.2	266.3
18	528.6895	18909.43	1577.2	520.3
2	530.5690	18842.45	1644.2	587.3
2	539.7522	18521.87	1964.8	907.9
1	540.2604	18504.45	1982.2	925.3
1	540.7348	18488.21	1998.5	941.5
2	545.4307	18329.04	2157.6	1100.7
2	549.5876	18190.47	2296.2	1239.3
2	549.8185	18182.76	2303.9	1247.0
2	550.0334	18175.66	2311.0	1254.1
3	555.4050	17999.88	2486.8	1429.8
3	555.8703	17984.81	2501.9	1444.9

tensity is usually strong enough to obtain an atomic calibration spectrum. Intensities and positions of the plasma spectral lines of the Ar<sup>+</sup> laser are listed in Tab. 4.3.

#### 4.3.2

#### **FT-Raman Spectrometers with Near-Infrared Excitation**

Interferometers are superior to monochromators for obtaining spectra of electromagnetic radiation, but technical problems prevent interferometers from being used in routine spectrometers at wavelengths shorter than the near-infrared. Fortunately, Raman excitation by near-infrared radiation is just possible ( $\lambda^{-4}$  law, cf. Section 3.3 of Chapter 3).

The laser in FT-Raman spectrometers (Fig. 4.5) is the continuous wave Nd<sup>3+</sup>/YAG system operating at 1064 nm with output power up to 2000 mW. The laser is optically pumped by either a lamp or diode system. In both cases, nonlasing lines are generated. They have to be removed by very effective notch filters (NF), otherwise they get mixed up with the Raman spectrum producing so-called laser line artifacts.

The scattered radiation in an FT-Raman spectrometer contains Rayleigh and Tyndall radiation at laser frequency. Usually, scattered radiation at laser frequency is up to eight orders of magnitude more intense than the Raman scattering, hence it can cause saturation or even damage of the detector. A so-called Rayleigh filter (RF) for filtering out radiation at laser frequency is an obligatory part of any FT-Raman spectrometer. The best Rayleigh filters have a cut-off frequency closer than 50–40 cm<sup>-1</sup> to the exciting laser frequency. Rayleigh filters remain the main limiting factor, preventing application of FT-Raman spectrometers in low frequency Raman spectroscopy.

#### 4.3.3

#### **Raman Grating Polychromator with Multichannel Detector**

Conventional multichannel Raman instruments consist of a double monochromator working in the subtractive mode, and a polychromator (Fig. 4.6). The double monochromator acts as a filter for rejection of stray light at laser frequency. Common detectors in such instruments are nitrogen cooled CCD cameras with up to 1024 pixels in a row. This limited number of the pixels in a row does not allow one to fully exploit the spectral resolution power of the polychromator in only one measurement. In order to obtain a complete Raman spectrum with spectral resolution 1 cm<sup>-1</sup>, the spectrum should be measured with the above configuration in at least four steps by measuring spectral intervals up to 1000 cm<sup>-1</sup> and mechanically rotating the monochromator grating between measurements. After completion of the successive measurements, the spectra from different spectral regions are merged by the instrument's software. In this kind of multichannel Raman instrument, rather sophisticated mechanical systems for rotating gratings and changing the opening of the slits of the monochromators and polychromator are used.

Recent achievements in the design of near-infrared diode lasers, of volume-phase transmission multiplexed holographic gratings and of sensitive CCD arrays allow

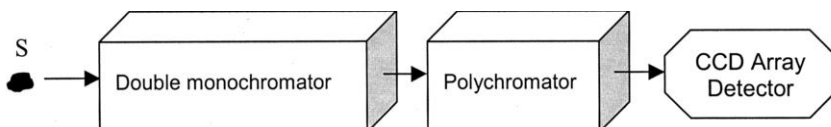


**Fig. 4.6** Block diagram of a conventional multichannel Raman spectrometer. S, sample. Note, the double monochromator is operating in subtractive mode.

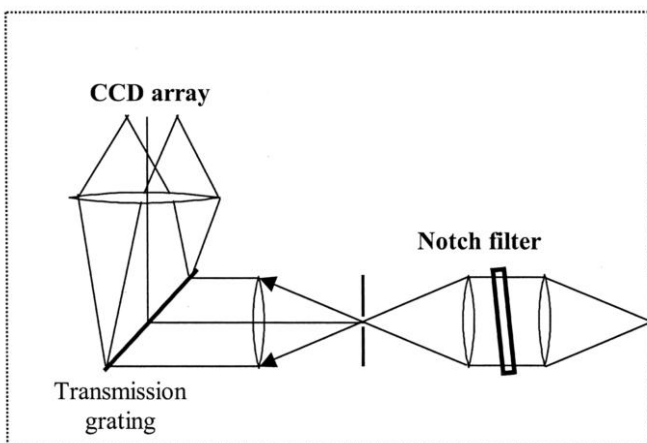


**Fig. 4.7** Basic diagram of axial transmissive multichannel Raman instrument.

one to build very efficient multichannel Raman grating spectrometers, which can be considered as a new class of Raman instruments. In such modern spectrometers a small holographic notch filter is used to reject the stray light at laser frequency instead of a large double monochromator (Fig. 4.7). The reflectivity of the notch filter is very high and its bandwidth very narrow. The transmission at the center of the notch is less than 0.0001% and half maximum of the notch corresponds to  $175\text{ cm}^{-1}$ . A notch filter is usually operated at normal incidence. Tilting the filter at a small angle (typically  $15^\circ$ ) shifts the rejection band to lower frequencies. This allows one to use the notch filter line for low frequency Raman applications as close as  $40\text{ cm}^{-1}$  to the exciting laser. The conventional polychromator is replaced by holographic transmission gratings. Several such gratings may be assembled in order to extend the operating range of the system. Each grating may deflect the light to different areas on the CCD array detector. In such a way, a modern multichannel Raman instrument permits the acquisition of complete Raman spectra at a spectral resolution of  $2\text{ cm}^{-1}$  at once without rotating any grating.

#### 4.4 UV/VIS Spectrometers

The UV/VIS spectral region extends from 190 to 400 nm (UV range) and from 400 to 780 nm (visible range). In order to obtain complete spectra in the UV/VIS range, dual beam dispersive scanning instruments or dispersive multi-channel instruments are employed. UV/VIS scanning spectrometers consist of a light source, a monochromator, a chopper (rotating sector mirror or rotating sector disc) to generate a sample and a reference beam as well as to recombine them, a sample and reference compartment, and a detector (Fig. 4.8). Spectrometers, which permit a synchronous measurement of sample and reference beams are denoted double beam instruments (cf. Section 4.2). Note the position of sample and reference after the monochromator in this type of UV/VIS spectrometer. There they are substantially less exposed to the high-energy UV radiation than directly after the source. The disadvantage of this optical layout is its sensitivity to ambient stray light, which may directly reach the detector if the sample chamber is not fully covered.

A multi-channel spectrometer has a light source with shutter, a sample and reference compartment, a grating polychromator and a diode array detector (Fig. 4.9). All spectral elements are recorded simultaneously by the array detector, i.e. the measuring time with the shutter in its open position is very short. The short illumination time permits the sample and reference positions to be positioned immediately after the light source. Multi-channel spectrometers may also be constructed as double beam instruments. For special measurements, e.g. rapid kinetic investigations, when the chopper frequency is too low with respect to the rate of

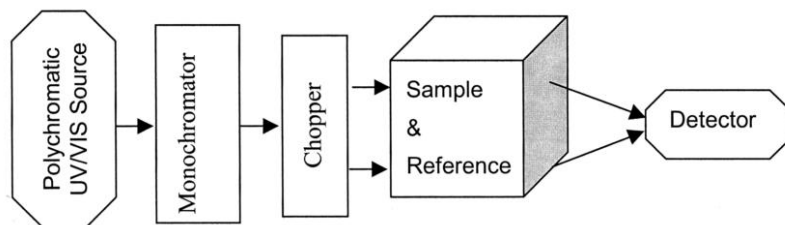


Fig. 4.8 Block diagram of a UV/VIS scanning spectrometer.

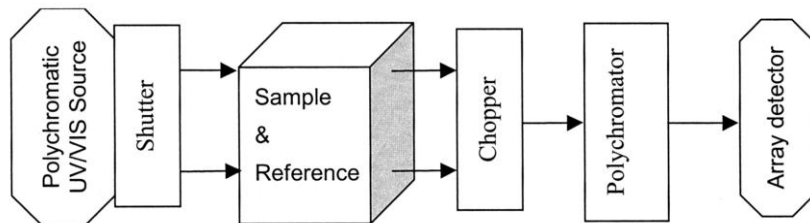


Fig. 4.9 Block diagram of a UV/VIS multichannel spectrometer.

the process under investigation, double beam instruments with two separate detectors are used.

UV/VIS absorption spectra may also be obtained with single beam instruments. In single beam spectrometers the background and sample spectra are measured one after the other. Since a chopper and reference chamber are not needed, single beam instruments are usually cheaper than double beam instruments.

#### 4.4.1

##### Sources

The most commonly used light sources are deuterium lamps in the region from 180 to 350 nm and tungsten filament and halogen lamps in the region from 330 to 900 nm. A light source for the complete range is the xenon arc from 175 to 1000 nm. Furthermore, for special applications such as high resolution studies, tunable lasers can be used. For time resolved measurements pulsed arc lamps can be used.

#### 4.4.2

##### Monochromators

The cheapest versions for dedicated applications are filter monochromators. Monochromators in routine spectrometers usually have a prism or diffraction grating. The complete spectrum can be measured by turning the prism or grating. The slit width and the dispersion of the monochromator determine the spectral slit function (SSF). The SSF of single monochromators does not extend below 5 nm. For applications, which require higher resolution, the use of double monochromators with SSFs down to 1 nm is necessary. In addition, double monochromators improve the stray light rejection and allow measurement of samples with high optical density. The drawback of double monochromator systems is their lower optical throughput, which causes the signal to noise ratio to deteriorate.

#### 4.4.3

##### Detectors

Standard UV/VIS detectors are photomultipliers and silicon diodes. Silicon diodes are smaller and cheaper, whereas photomultipliers have a higher sensitivity. Most research instruments are based on photomultipliers. A recent development is the use of photomultiplier arrays and CCD cameras as in all other spectroscopic methods.

An important consideration for all types of instruments is the linear absorption range, i.e. maximum absorption measured at a predetermined accuracy. The photometric accuracy depends on the instrument's electronics, which may be sensitive to ambient temperature and humidity. Spectrometers should be calibrated from time to time. Neutral density filters of well defined absorbance are commonly used for absorbance calibration. Solutions of potassium chromate and potassium

dichromate are also widely used as reference standards for validating the photometric scale. Current estimations for linear absorption limits are 1 absorption unit for multichannel instruments or scanning dispersive instruments with a single monochromator, 2.5 absorption units for dispersive instruments with a double monochromator.

The exit beam from the monochromator includes some amount of unwanted stray radiation. This is partly due to imperfections in the diffraction grating (or prism) and partly to undesired reflections at optical surfaces. For accurate measurements it is vital to use a spectrometer with stray light levels as low as possible. Hence it is necessary to have a method for measuring such levels. The usual method for the measurement of stray light in a spectrometer is to insert into the optical path a blocking filter that absorbs nearly completely at the wavelength of interest while passing radiation at other frequencies unattenuated. A signal observed by the detector under these conditions at the wavelength of interest is due to stray radiation. Materials for checking and calibration of UV/VIS spectrometers recommended by the U. S. National Bureau of Standards are listed in Tab. 4.4.

As in the case of dispersive Raman spectrometers (cf. Section 4.4.1), it is necessary to calibrate the wavelength scale of dispersive UV/VIS spectrometers. The most accurate standards for checking the UV/VIS wavelengths are lasers of various types. The inexpensive helium–neon laser can be used to check at 632.8 nm. For spectrometers with a deuterium source, spectral lines at 486.6 and 656.1 nm can be used for calibration. A common method for wavelength calibration is the use of optical filters. A filter of didymium glass has many sharp absorption peaks, which can be used as a second wavelength standard (precision within 0.5 nm).

If measurements have to be done in the UV region below 240 nm, it is necessary to purge the spectrometer with dry nitrogen gas in order to remove oxygen. Oxygen absorbs at wavelengths shorter than 240 nm and is transformed into ozone. Absorption by oxygen molecules inside the instrument can make measurements

**Table 4.4** Standard reference materials (SRMs) for UV/VIS spectrophotometry used at National Bureau of Standards (NBS)<sup>a</sup>.

SRM number	Type	Parameter checked	Wavelength range/nm
930D	Glass filters	Transmittance	440–635
931d	Liquid filters	Absorbance	302–678
932	Quartz cuvet	Pathlength	–
935	Potassium dichromate	UV absorbance	235–350
2009	Didymium oxide glass	Wavelength	400–760
2031	Metal-on-quartz filters	Transmittance	250–635
2032	Potassium iodide	Stray light	240–280
2034	Holmium oxide solution	Wavelength	240–650
936	Quinine sulfate dihydrate	Fluorescence	375–675

<sup>a</sup> A More complete description can be found in: R. Mavrodineanu, J. I. Schultz and O. Menis, *Accuracy in Spectrophotometry and Luminescence Measurements*, National Bureau of Standards Special Publication 378, Washington, DC 1973.

below 240 nm meaningless. Moreover, ozone is very reactive and can cause damage to optical and mechanical components of the spectrometer.

#### 4.5 Fluorescence Spectrometers

Basically, instruments for measuring fluorescence and phosphorescence spectra have similar construction and should be called luminescence spectrometers. However the group of molecules that exhibit fluorescence is by far larger than that exhibiting phosphorescence, hence the term fluorescence spectrometer is used. The main spectral features of luminescence are: spectral distribution, polarization and radiation lifetime. For analytical purposes spectral distribution and polarization are mainly used. Measuring the lifetimes requires a rather sophisticated time-resolved spectroscopic technique. It is very seldom used for analytical purposes and will not be discussed in this chapter.

Two basic types of spectra can be produced by a conventional fluorescence spectrometer. In the emission spectrum, the wavelength of the exciting radiation is held constant (at an absorption wavelength of the analyte) and the spectral distribution of the emitted radiation is measured. In the excitation spectrum, the fluorescence signal is measured at a fixed wavelength of the emission selector as the wavelength of the exciting radiation is varied. An analyte can fluoresce only after it has absorbed radiation, and an excitation spectrum identifies the wavelengths of light that the analyte is able to absorb. Thus, the excitation spectrum of a molecule should be the same as its UV/VIS absorption spectrum.

A general schematic of a fluorescent spectrometer is shown in Fig. 4.10. The instrument contains the source of UV/VIS radiation, an excitation wavelength selector, an emission wavelength selector, a sample chamber and a detector. Basically this is a single beam instrument. The fluorescence emitted by the sample is usually measured at 90° in order to avoid disturbances by non-absorbed excitation radiation.

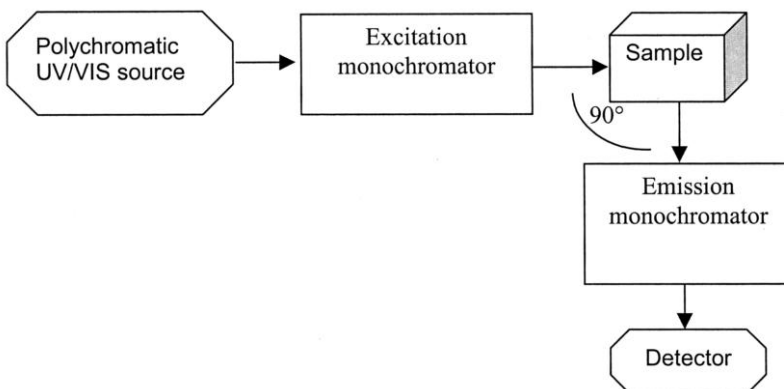


**Fig. 4.10** Block diagram of a fluorescence spectrometer.

The excitation wavelength selector can be either a filter or a monochromator. Filters offer better detection limits, but do not provide spectral scanning capabilities. Often, a filter is used in the excitation beam along with a monochromator in the emission beam to allow emission spectra to be acquired. Full emission and excitation spectral information can be acquired only if monochromators are used in both the excitation and emission beams. In modern instruments with array detectors, a polychromator is used in the emission beam instead of a monochromator. Recent research instruments are able to scan both wavelengths automatically and combine all data into a 2D excitation–emission spectrum. In lifetime spectrometers, a pulsed light source and a gated detector are synchronized in order to measure the time dependence of the luminescence emission.

The luminescence intensity is directly proportional to the intensity of the light source, and a high-intensity light source can therefore be used to increase the sensitivity and to lower the detection limits for luminescence analyses. The xenon arc lamp is a commonly used source. The Xe lamp emits continuously over a broad wavelength range and is therefore well suited for spectral scanning. Another common source is the high-pressure mercury arc lamp. Its output is a continuum with a line spectrum superimposed, making the mercury lamp better suited to non-scanning filter instruments. Other sources include halogen lamps and combined xenon–mercury lamps. Lasers are also used in luminescence experiments, in which continuous scanning of excitation is not required. Tunable lasers can be used to provide multiwavelength excitation capabilities. The excitation laser beam must often be greatly attenuated in order to avoid photodecomposition of the sample.

Pulsed sources, including both lamps and lasers, are used for special applications such as dynamic measurements of luminescence lifetimes and time-resolved elimination of background signals.

Photomultiplier tubes (PMTs) are the most commonly used detectors, various types are available for different applications. In general they are sensitive in the range from 200 to 600 nm, with maximum sensitivity obtained in the 300–500 nm range. Red-sensitive PMTs are also available for investigations beyond 600 nm. The PMT housings are sometimes cooled to temperatures as low as –40 °C to minimize temperature-dependent noise.

Among the more commonly used multichannel detectors are diode arrays, vidicons, silicon intensified target vidicons, charge-coupled and charge-injection devices, and numerous other devices made available by recent technological advances. The use of multichannel detectors in fluorescent spectrometers has increased the range of applications of luminescence experiments to include real-time experiments, kinetic measurements, and on-line detection for chromatography and other flow systems. The ability to acquire complete spectral information nearly instantaneously has also greatly facilitated qualitative analysis by reducing the time required per analysis.

Fluorescence spectrometers can be used to measure fluorescence polarization by placing polarizers in the excitation and emission beams. High quality instrumentation for polarized fluorescence measurements is commercially available.

Since most fluorescence spectrometers are single beam instruments, different kinds of distortions may be found in excitation and emission spectra. These distortions are mainly due to variations of source power or detector sensitivity with wavelength. Spectra of the same sample obtained using two different fluorescence spectrometers may therefore be quite different. Even changing the source or detector in a spectrometer may alter the apparent fluorescence or excitation spectrum of a compound. These artefacts can be eliminated instrumentally, several instruments that can produce corrected spectra are commercially available. Unfortunately, most published spectra are uncorrected, they cannot be fully reproduced by other investigators. There exist only a few extensive and broadly used databases of fluorescence spectra.

## References

### MIR

- Encyclopedia of Analytical Chemistry. Applications, Theory and Instrumentation*, ed. Meyers R. A., John Wiley & Sons, Chichester 2000.
- Griffiths P. R., Haseth J. A., *Fourier Transform Infrared Spectrometry*, J. Wiley & Sons, Chichester 1986.
- Analytical Chemistry*, ed. Kellner R., Mermet J.-M., Otto M., et al., Wiley-VCH, Weinheim, 1998.
- Handbook of Instrumental Techniques for Analytical Chemistry*, ed. Settle F., Prentice Hall, Englewood Cliffs, NJ 1997.
- Analytical Instrumentation Handbook*, ed. Ewing G. W., Marcel Dekker, New York 1990.
- Noble D., *Rev. Anal. Chem.*, 1995, 67, 381A–385A.
- Henry C., *Rev. Anal. Chem.*, 1998, 70, 273A–276A.

### NIR

- Near-Infrared Spectroscopy. Principles, Instruments, Applications*, ed. Siesler H. W., Ozaki Y., Kawata S., Heise H. M., Wiley-VCH, Weinheim 2001.
- Burns D. A., Ciurczak E. W., *Handbook of Near-Infrared Analysis*, Marcel Dekker, New York 1992.
- Murray, I., Cowe, I. A., *Making Light Work. Advances in Near Infrared Spectroscopy*, Wiley-VCH, Weinheim 1992.
- William, P., Norris, K., *Near Infrared Technology in the Agriculture and Food Industries*, The American Association of Cereal Chemists, St. Paul 1998.

### Raman

- Infrared and Raman spectroscopy. Methods and Applications*, ed. Schrader B., Wiley-VCH, Weinheim 1995.
- Mukamel S., *Principles of Nonlinear Optical Spectroscopy*, Oxford University Press, New York 1995.
- Modern Techniques in Raman Spectroscopy*, ed. Laserna J. J., John Wiley & Sons, Chichester 1996.
- Chang R. K., Furtak T. E., *Surface Enhanced Raman Scattering*, Plenum Press, New York 1982.
- Long D. A., *Raman Spectroscopy*, McGraw-Hill, New York 1977.

### UV/VIS and Fluorescence

- Lakowicz J. R., *Principles of Fluorescence Spectroscopy*, 2nd edition, Kluwer Academic/Plenum Publishers, New York 1999.
- Clark B. J., Frost T., Russell M. A., *Techniques in Visible and Ultraviolet Spectrometry*, Vol. 4, UV Spectroscopy, Chapman & Hall, London 1993.
- Burgess C., Knowles A., *Techniques in Visible and Ultraviolet Spectrometry*, Vol. 1. Standards in Absorption Spectrometry, Chapman & Hall, London 1981.
- Miller J. N., *Techniques in Visible and Ultraviolet Spectrometry*, Vol. 2. Standards in Fluorescence Spectrometry, Chapman & Hall, London 1981.
- Knowles A., Burgess C., *Techniques in Visible and Ultraviolet Spectrometry*, Vol. 3. Practical Absorption Spectrometry, Chapman & Hall, London 1984.

## 5

### Measurement Techniques

*Gerald Steiner*

Upon interacting with a sample, incident light of intensity  $I_0$  may be partly reflected at optical interfaces ( $I_R$ ), it may be scattered ( $I_S$ ) and absorbed in the sample ( $I_A$ ), the remaining part will be transmitted ( $I_T$ ), see Fig. 5.1.

According to the law of conservation of energy, the energy balance for the incident light may be written as

$$I_0 = I_A + I_T + I_R + I_S \quad (1)$$

The light intensities  $I_0$ ,  $I_T$ ,  $I_R$  and  $I_S$  can easily be measured by placing a detector at the corresponding position. All chemical information about the sample goes into  $I_A$ , but this value cannot be measured directly.  $I_A$  can only be accessed by evaluating Eq. (1). In all commercial spectrometers only one detector is used to measure a particular couple of intensity values ( $I_0$  and either  $I_T$ ,  $I_R$ , or  $I_S$ , cf. Table 5.1). It is the goal of sample preparation to bring the remaining intensities to zero (or at least very close to it). Neglecting these basic considerations will result in measurement errors, which can never be eliminated by subsequent digital data treatment.

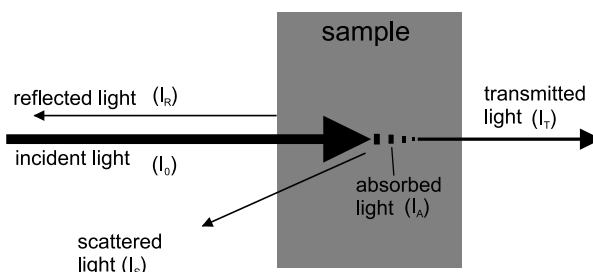


Fig. 5.1 Energy balance of incident light upon interaction with a sample.

**Table 5.1** Measured and illicit contributions of light.

<b>Measured</b>	<b>Aim of Sample Preparation</b>	<b>Evaluation</b>	<b>Exp. Technique</b>
$I_0, I_T$	$I_R = I_S = 0$	$I_A = I_0 - I_T$	Transmission measurements
$I_0, I_R$	$I_T = I_S = 0$	$I_A = I_0 - I_R$	Reflection measurements
$I_0, I_S$	$I_T = I_R = 0$	$I_A = I_0 - I_S$	Diffuse reflection measurements

**5.1****Transmission Measurements**

Transmission spectroscopy is the most widely used measurement technique. It is simple and can be applied to characterize gases, liquids and solids. Quantitative evaluations are based on the Beer–Lambert law as described in Chapter 3. Typical sample cells for gases and liquids are shown in Fig. 5.2. Note the polished windows in the light path, while the other cell walls may be opaque. Polished windows must not be touched or even scratched. Fingerprints in the light path cause light scattering, hence reducing the accuracy of the measurement. Normal incidence of the incoming light is required in order to minimize reflection.

The range of use of a particular cell depends on the window material. Most common materials for optical windows or fibers are summarized in Tab. 5.2. The refractive index of the window material should be very close to that of the sample in order to avoid reflection or scattering contributions.

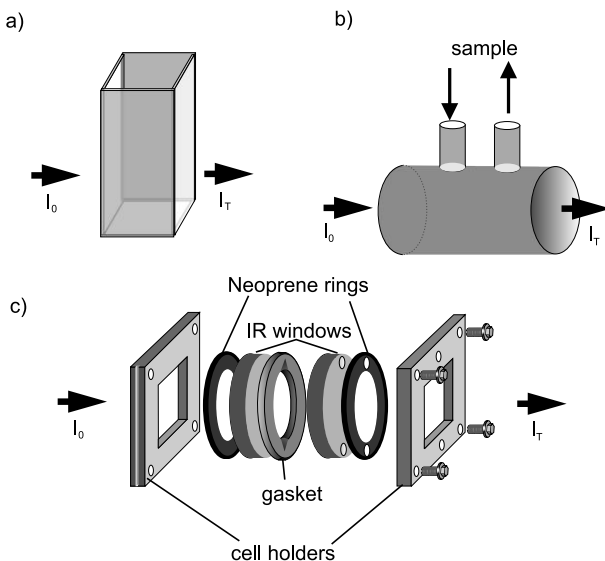


**Fig. 5.2** Cells for transmission measurements: (a) UV/VIS liquid cell, (b) flow cell for gases and liquids ; (c) demountable IR liquid cell.

**Table 5.2** Window or fiber material for optical spectroscopy

<b>Material</b>	<b>Transmission Range/<math>\mu\text{m}</math></b>	<b>Refractive Index (@ 20 °C)</b>	<b>Use</b>	<b>Solubility</b>
Optical glasses ( $\text{SiO}_2$ )	0.2–2.2	1.6 @ 0.2 $\mu\text{m}$ 1.5 @ 2 $\mu\text{m}$	windows, fibers	high resistance to acids (except hydrofluoric acid)
Quartz				
Fussed silica	0.2–2.5	1.55 @ 0.2 $\mu\text{m}$ 1.44 @ 2 $\mu\text{m}$		
Sapphire (single crystal $\text{Al}_2\text{O}_3$ )	0.2–4.5	1.73 @ vis, 1.65 @ 4 $\mu\text{m}$	fibers, ATR crystals	high resistance to acids and alkali at temperatures up to 1000 °C very hard
KBr	0.25–25	1.5	windows, pellets	soluble in water (53 g/100 ml $\text{H}_2\text{O}$ ) and alcohol
KRS-5 ( $\text{TlBr}/\text{TlI}$ )	0.3–40	2.4	windows	slightly soluble in water (0.02 g/100 ml $\text{H}_2\text{O}$ ), vulnerable to organic solvents, toxic
CsI	0.3–60		windows	soluble in water (44 g/100 ml $\text{H}_2\text{O}$ ) and alcohol
NaCl	0.3–16	1.55	windows	soluble in water (36 g/100 ml $\text{H}_2\text{O}$ ), slightly soluble in alcohol
$\text{CaF}_2$	0.2–10	1.4	windows	soluble in solutions of ammonium salts
Silicon (Si)	1.5–10	3.5 @ 1.5 $\mu\text{m}$ 3.4 @ 10 $\mu\text{m}$	ATR crystals	hard
Germanium (Ge)	2.0–15	4.1 @ 2 $\mu\text{m}$ 3.9 @ 15 $\mu\text{m}$	ATR crystals	soluble in mixtures of HCl and $\text{HNO}_3$ and $\text{H}_2\text{O}_2$
Zinc Selenide ( $\text{ZnSe}$ , Irtran-4)	0.6–15	2.5 @ 0.6 $\mu\text{m}$ 2.3 @ 15 $\mu\text{m}$	ATR crystals, windows	soluble in acids, solubility in water @296 K: 0.001 g / 100 ml $\text{H}_2\text{O}$
Zinc Sulfide ( $\text{ZnS}$ , Irtran-2)	0.5–18	2.3 @ 0.5 $\mu\text{m}$ 2.0 @ 18 $\mu\text{m}$	ATR crystals, windows	soluble in acids, slightly soluble in water
AMTIR-1 ( $\text{Ge}_{33}\text{As}_{12}\text{Se}_{55}$ )	1–14	2.5 – 2.6	ATR crystals, windows	high homogeneity, not soluble in water
Polyethylene	to 1000	1.5	window	not soluble in water, organic solvents and acids, used for far infrared
Silver halides	1–15	1.6	fibers, windows	soluble in $\text{NH}_3$ , sensitive to UV and visible light
Chalcogenides (e.g. $\text{As}_2\text{S}_3$ , $\text{As}_{40}\text{Se}_{35}\text{S}_{25}$ )	0.8–10	1.56	fibers	sensitive to water
Diamond (C)	0.2–20	2.4	ATR crystals, windows	extremely hard, high resistance to acids and alkalis at temperatures up to 120 °C

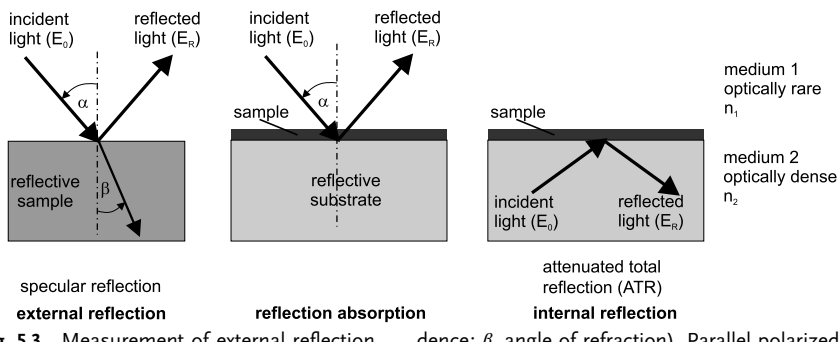


**Fig. 5.3** Measurement of external reflection, reflection absorption and internal reflection. Reflection and transmission of light at a plane optical interface with  $n_2 > n_1$  ( $\alpha$ , angle of incidence;  $\beta$ , angle of refraction). Parallel polarized light has its electric vector parallel to the plane of the figure.

## 5.2 Reflection Measurements

Reflection measurements at *optically flat interfaces* can be performed in two basic configurations, external and internal reflection. In the case of external reflection (also called specular reflection) the light propagates in the optically rare medium (e. g. air), whereas in the case of internal reflection (usually employed as attenuated total reflection (ATR)) the light propagates in the optically dense medium (Fig. 5.3).

### 5.2.1 External Reflection

The intensity distribution between reflected and transmitted light at plane optical interfaces is based on *Maxwell's theory* and *Fresnel's equations*. The reflectivity  $R$  relates the intensity  $I_R$  of the reflected light to the intensity  $I_0$  of the incident light:

$$R = |r|^2 = \frac{I_R}{I_0} \quad (2)$$

where  $r$  denotes the amplitude coefficient.

The measured reflectivity  $R$  is polarization dependent, the amplitude coefficients for parallel polarization  $r_{||}$  and perpendicular polarization  $r_{\perp}$  are:

$$r_{||} = \frac{n_2 \cos \alpha - n_1 \cos \beta}{n_2 \cos \beta + n_1 \cos \alpha} \quad (3)$$

$$r_{\perp} = \frac{n_1 \cos \alpha - n_2 \cos \beta}{n_2 \cos \beta + n_1 \cos \alpha} \quad (4)$$

At the *Brewster angle* or polarizing angle  $\alpha_B$ , no parallel polarized light is reflected ( $r_{||} = 0$ ). Beyond the critical angle  $\alpha_C$ , the incident light undergoes total reflection at the interface:

$$\alpha_C = \arcsin\left(\frac{n_1}{n_2}\right) \quad (5)$$

In order to calculate the transmitted intensity  $T = (1-R)$  immediately after the interface in a similar manner as in Eq. (2), the intensity in the different media has to be taken into account:

$$I_T = (1 - R) I_0 \quad (6)$$

In the usual case of absorbing media, the refractive index  $n$  has to be replaced by its complex form:

$$n^* = n(1 - ik) \quad (7)$$

where  $k$  denotes the absorption index, which is related to the absorption coefficient  $a$  [ $\text{cm}^{-1}$ ] and the decadic molar absorptivity  $\epsilon$  [ $\text{L mol}^{-1} \text{cm}^{-1}$ ] in the *Beer – Lambert law*  $A = ecd$ :

$$a = \frac{4\pi k}{\lambda} = \frac{\epsilon c}{\ln 10} \quad (8)$$

In an absorption region the real part  $n$  of the complex refractive index  $n^*$  exhibits an anomaly as shown schematically in Fig. 5.4.

This effect occurs especially in the infrared range, because narrower absorption bands effect a stronger anomaly of  $n$ . As a consequence, IR reflection spectra differ severely from the corresponding transmission spectra. The *Kramers–Kronig relation* can be used to analyze reflection spectra and to relate them to transmittance data.

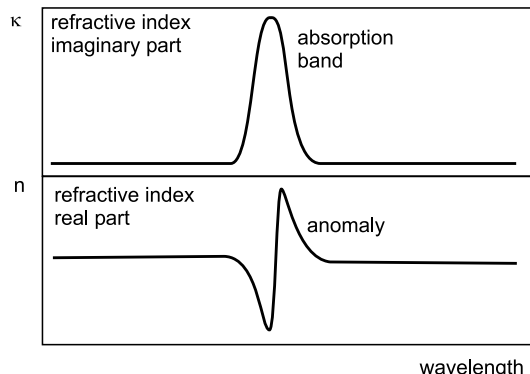


**Fig. 5.4** Anomaly in the real part of the complex refractive index within an absorption region.

### 5.2.2

#### Reflection Absorption

Reflection absorption measurements are performed by placing the analyte on a reflective substrate (Fig. 5.3). The reflective substrate may be either optically flat or diffusely reflecting. Incident light passes the analyte twice and a sort of transmission spectrum is obtained (sometimes called transfection spectrum). The greater the angle of incidence, the larger the effective path length in the analyte. The technique is known by the acronyms IRRAS (infrared reflection absorption spectroscopy) and RAIRS (reflection absorption infrared spectroscopy). The extreme case is the so-called grazing incidence technique, where the area illuminated by the incident beam is maximized (maximum number of molecules in the beam).

Reflection absorption experiments on samples with a thickness larger than the wavelength used give absorbance values corresponding to the enlarged effective path length described above. In the case of sample thickness of the order of the wavelength or even below, the Beer–Lambert law is no longer valid, because the field amplitude of the standing wave emerging during reflection varies regularly. In the case of a very thin sample layer, its transmission is not only dependent on its optical properties but also on the regular field variations in the vicinity of the reflecting surface. Additional enhancement factors may occur, which could provide sub-monolayer sensitivity. Since light of different polarization behaves differently upon reflection, a very complex situation results. In particular in the case of grazing incidence, only absorptions with components of the transition moments normal to the reflecting surface can be observed. Main application areas are surface coatings, very thin films and adhesives on reflective surfaces as well as molecular orientation studies.

### 5.2.3

#### Attenuated Total Reflection (ATR)

A beam propagation in an optically dense medium with refractive index  $n_2$  undergoes total reflection at the interface to the optically rare medium ( $n_1$ ) when the angle of incidence exceeds the critical angle  $\alpha_c$  (cf. Eq. (5)). Upon undergoing total reflection the electromagnetic wave propagates through the optical interface and generates an evanescent field, which penetrates the rare medium (Fig. 5.5).

The evanescent field is a non-transverse wave along the optical surface, whose amplitude can be expressed as an exponential function along the  $z$ -axis into the rare medium:

$$E_z = E_0 e^{-z \frac{2\pi n_2}{\lambda_0} \sqrt{\sin^2 \alpha - \left(\frac{n_1}{n_2}\right)^2}} \quad (9)$$

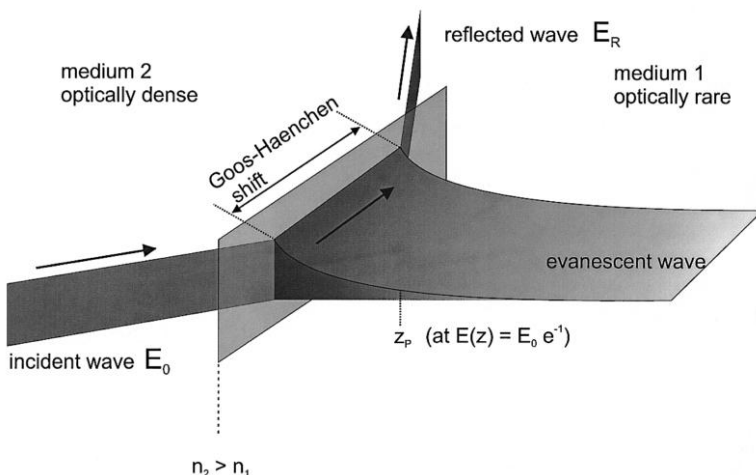


**Fig. 5.5** Strength and penetration of the evanescent field.

where  $E_z$  is the amplitude of the evanescent field at distance  $z$ ,  $\lambda_0$  the vacuum wavelength of the light used. A penetration depth  $z_p$  is defined as the distance at which the exponent is equal to one:

$$z_p = \frac{\lambda_0}{2\pi n_2 \sqrt{\sin^2 \alpha - \left(\frac{n_1}{n_2}\right)^2}} \quad (10)$$

If medium 1 is absorbing, the evanescent field will be absorbed and less intensity can be reflected (attenuated total reflection (ATR)). An ATR spectrum is similar to the conventional absorption spectrum except for the band intensities at longer wavelengths. At longer wavelengths the evanescent field penetrates ever deeper into the sample, equivalent to an increasing sample thickness. Sometimes an empirical so-called ATR correction is applied in order to compensate across the spectrum for the linear wavelength increase in Eq. (10):

$$R_{\text{corr}} \sim R \frac{1}{\lambda} \quad (11)$$

Other differences may occur due to surface effects between the sample and the optical crystal or due to absorption changes across the sample. Single-reflection or multi-reflection crystals may be used. The measured reflectivity depends on the number of reflections as well as on the efficiency of contact between sample and substrate surface.

An important advantage of the ATR technique is its applicability to turbid solutions, aqueous solutions included. Suspended particles are surrounded by a thin liquid film (hydrating shell). This shell forms also the phase boundary to the ATR crystal surface so that the evanescent field will not scatter by the particle.

ATR crystals for the UV, VIS and NIR ranges are usually made of quartz glass. Sapphire is used for special UV and NIR applications, it is one of the hardest of all optical materials so that the surface is more resistant to scratches (Tab. 5.2). In the mid IR, zinc selenide, silicon, germanium and diamond are used. Zinc selenide is currently the most popular material for ATR crystals. Its most important advantage is its low absorbance at wavelengths larger than 10 µm, but zinc selenide scratches more easily than germanium and silicon, and it is toxic. AMTIR-1 is a glass-like amorphous material with a high homogeneity. The low thermal change refractive index of  $7 \times 10^{-6} \text{ }^{\circ}\text{C}^{-1}$  is of advantage in optical systems.

#### 5.2.4

##### Reflection at Thin Films

Thin films can be investigated either by reflection absorption (cf. Section 5.2.2) or by a sort of internal reflection measurement using the occurrence of multiple reflections. In the case of plane, parallel-sided, homogeneous and isotropic thin films (Fig. 5.6), the amplitude of the reflected light can be expressed in the form

$$r \sim \frac{r_{12} + r_{23}e^{-2i\delta}}{1 + r_{12}r_{23}e^{-2i\delta}} \quad (12)$$

where  $r_{12}$  is the reflection coefficient for the interface 1–2 and  $r_{23}$  for the 2–3 interface (cf. Eq. (3) and (4)). The term  $\delta$  is given by

$$\delta = \frac{2\pi}{\lambda} n_2 l \cos(\beta) \quad (13)$$

where  $l$  is the layer thickness of the sample. For non-normal incidence, the amplitude of the reflected light depends on the state of polarization of the incident light. If the film itself or the surrounding medium is absorbing, the reflection coefficients  $r_{ij}$  become complex (cf. Eq. (7)).

Spectral features arises from two properties: (i) the intrinsic absorption strength and (ii) the orientation of the transition dipole with respect to the wave vector of the incident light. In samples with random distribution an averaged spectrum will be recorded. In highly ordered films the absorption depends upon the ordering within the film and the orientation of the sample. Therefore the angle of incidence and polarization of the light have to be chosen carefully.

The analysis of thin films is often performed by infrared spectroscopy. Compared to reflection absorption measurements on metal surfaces using p-polarized light at grazing incidence, investigation of self-supported thin films or of thin films on transparent substrates shows weaker infrared absorption bands. Weaker absorption bands are caused by the absence of the surface enhancement mechanism and the poorer reflectivity. On the other hand, due to the absence of the metal selection rule, spectra of p- and s-polarization can be recorded in the case of free-standing films or of transparent substrates. Complex spectral features may arise

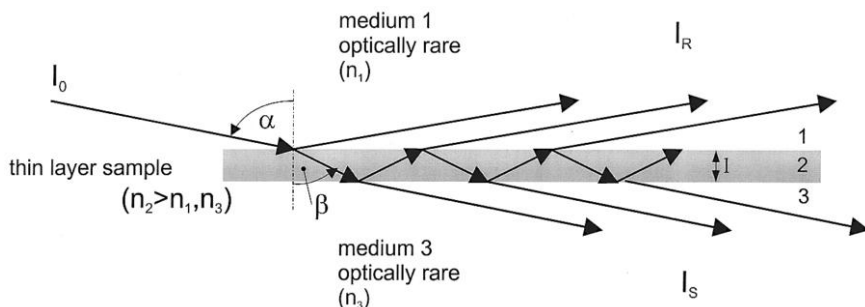


Fig. 5.6 Reflection and transmission of light in a thin film.

from optical features of the substrate or in the case of optical dispersion within the sample film.

### 5.2.5

#### Diffuse Reflection

Light incident at *optically scattering interfaces* (inhomogeneous samples like powders) with roughness down to the range of the wavelength may be partly reflected regularly, partly scattered diffusely, and partly enter the substrate. The latter part may undergo absorption within particles, undergo diffraction at grain boundaries, re-emerge at the sample surface and intermingle with reflected parts. The measured reflectivity includes contributions from all mechanisms, see Fig. 5.7.

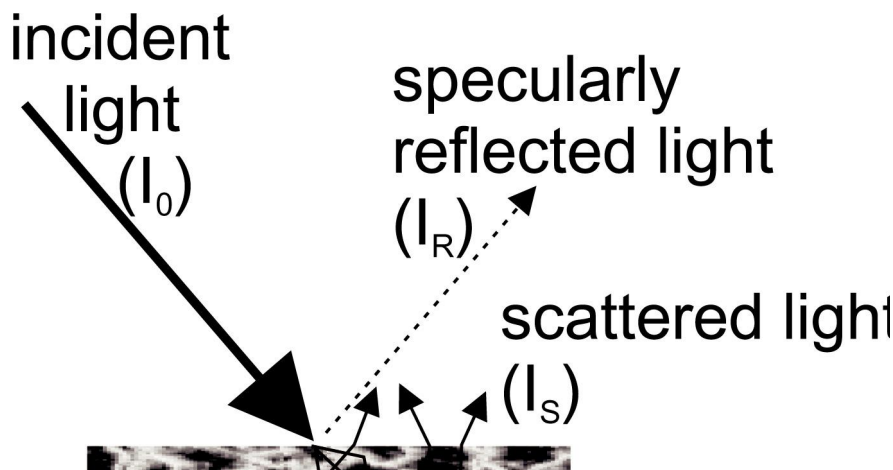


Fig. 5.7 Schematic illustration of light trajectories in a scattering sample.

Quantitative evaluation of diffuse reflectance spectra requires “optically indefinitely thick” samples ( $I_T = 0$ ; cf. Tab. 5.1). The reflectivity  $R_\infty$  of such a sample (in the IR its thickness does normally not exceed a few millimeters) is:

$$R_\infty = \frac{R_\infty(\text{sample})}{R_\infty(\text{reference})} \quad (14)$$

$R_\infty$  is transformed by the empirical *Kubelka–Munk* relation into the absorption-proportional parameter  $f(R_\infty)$ :

$$f(R_\infty) = \frac{1 - R_\infty}{2 R_\infty} = \frac{k}{s} \quad (15)$$

$k$  describes the absorbing and  $s$  the scattering properties. The parameters  $k$  and  $s$  vary with particle size and packing density. It is assumed that  $s$  does not depend on wavelength and that the sample is weakly absorbing. The former assumption has to be ensured by proper sample preparation, the latter by dilution of strong absorbers with non-absorbing substrate powder. In the case of  $R_\infty < 0.01$ , the transformation is often done by the simpler function  $-\log R_\infty$  or simply by  $1/R_\infty$ . Such small  $R_\infty$  values are usually found in the NIR region.

Measurement of diffuse reflection spectra has a much longer tradition in UV/VIS than in IR, because (i) the scattering is much more efficient at shorter wavelengths and (ii) an ideal non-absorbing scattering substrate is missing in the MIR.

UV/VIS and NIR diffuse reflection spectra are usually measured by an integrating sphere. The inner surface of the so-called “Ulbricht sphere” (Fig. 5.8) is coated by strongly scattering, non-absorbing powder. After repeated reflections at the inside of the sphere all radiation will eventually reach the detector.

Of practical importance is the sphere factor  $K$ :

$$K = \frac{\rho}{1 - \rho(1 - a)} \quad (16)$$

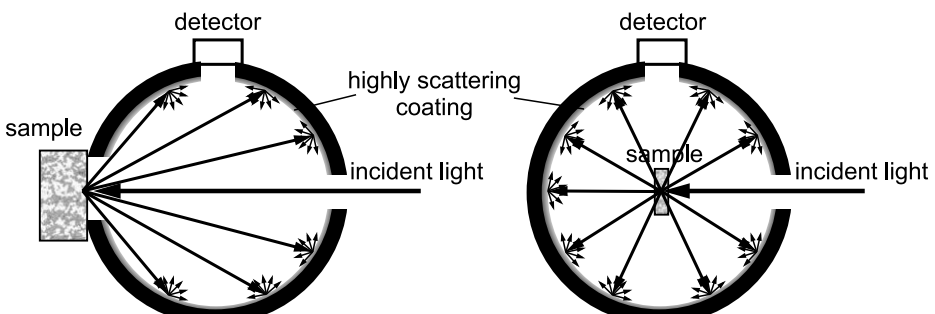
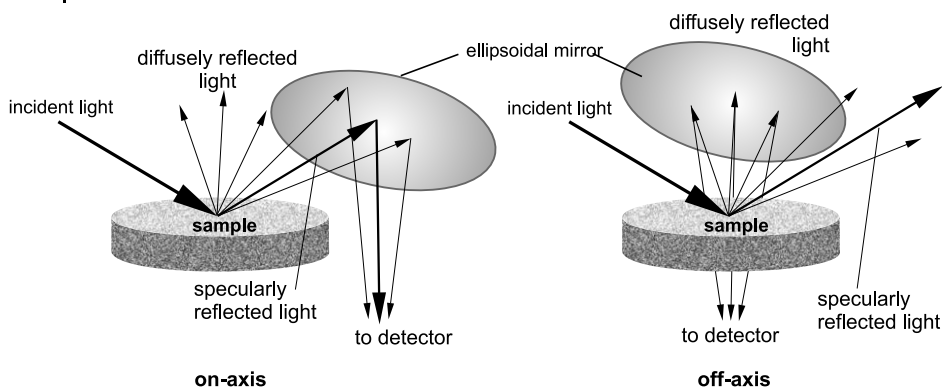


Fig. 5.8 Two configurations of Ulbricht spheres for diffuse reflectance measurement. Large or thick samples are usually positioned at a sphere port, small samples are mounted in the center.



**Fig. 5.9** Optical layout for measurements of diffuse reflection in the infrared range: on-axis arrangement with collecting mirror in the optical plane of incident and specularly reflected light; off-axis arrangement with collecting mirror out of the optical plane of incident and specularly reflected light.

where  $\rho$  is the reflectivity of the cover and  $a$  the ratio between the area of all holes and the total sphere area. If the factor  $a$  does not exceed a range of 5 to 10 %,  $K$  will essentially remain independent of sample properties.

Barium sulfate based coatings are mainly used in the UV/VIS range, they are characterized by a reflectivity of up to 80 % and an almost constant factor  $K$  throughout the VIS range. PTFE is suitable throughout the whole range from the UV to the NIR. In the NIR, a rough gold surface can also be used.

In the MIR, diffuse reflectance is very weak and could only be measured after routine FT-IR spectrometers became available (DRIFT spectroscopy, diffuse reflectance infrared Fourier-transform spectroscopy). Due to the lack of ideal non-absorbing scattering substrates in the MIR, the diffusely reflected MIR radiation is generally collected by large ellipsoidal mirrors, which cover as much area above the sample as possible. Two optical configurations are commercially available, on-axis and off-axis designs (Fig. 5.9).

In the Reflection configuration, the ellipsoidal mirror collects both diffusely and regularly reflected light. In the off-axis configuration, the ellipsoidal mirror is positioned off the plane of regular reflection, the latter influences the measurement much less. While the on-axis design has the advantage of much simpler alignment in the interferometer, superposition of regular and diffuse reflection leads to both inferior sensitivity and reduced accuracy in quantitative analysis. Reflection models provide superior sensitivity and accuracy at the expense of acquisition costs and laboratory experience. KBr or KCl powders are used as reference as well as diluent for strong absorbers.

### 5.3

#### Spectroscopy with Polarized Light

Chiral molecules occur in pairs related by a symmetry plane, their mirror images cannot be superimposed (enantiomers). Such molecules exhibit optical activity, i.e. they transmit left and right circularly polarized light in a different manner. The difference in the refraction indices for left and right circularly polarized light is called optical rotatory dispersion (ORD), the corresponding difference in absorption coefficients is called circular dichroism (CD). ORD and CD can be related to each other by the *Kramers–Kronig* transformation.

##### 5.3.1

###### Optical Rotatory Dispersion

Pairs of chiral molecules transmit left and right circularly polarized light with a different velocity. The two forms of chiral molecules have an asymmetric distribution of electrons, hence they interact with right and left polarized light in opposite ways. If the index of refraction for right polarized light is larger than for left polarized light, the plane of polarization will be rotated towards the left, and vice versa, Fig. 5.10.

The angle of rotation  $\alpha$  at the wavelength  $\lambda$  is directly proportional to the concentration  $c$ :

$$\alpha = [\alpha]_{\lambda}^T l c \quad (17)$$

where  $l$  is the path length of the sample cell.  $[\alpha]_{\lambda}^T$  is the specific angle of rotation [grad cm<sup>-3</sup>], it depends on wavelength and temperature. In polymer chemistry and biochemistry, the rotation is related to the molar mass, e.g. to the average mass of all amino acids of the protein (mean residue weight,  $M_0$ ):

$$[m] = \frac{\alpha M_0}{10 l c} \quad (18)$$

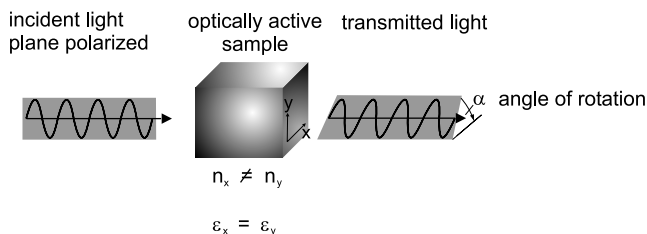


**Fig. 5.10** Optical rotatory dispersion: linearly polarized light can be considered as superposition of opposite circularly polarized light of equal amplitude and phase. The different velo-

cities of left and right circularly polarized light lead to optical rotation of the polarization plane of the transmitted light.

The obtained molar rotation  $[m]$  may be influenced by the refractive index  $n$  of the solvent. The corrected molar rotation is defined by

$$[m]_s = \frac{3}{n_s^2 + 2} \frac{\alpha M_0}{10 c l} \quad (19)$$

### 5.3.2

#### Circular Dichroism (CD)

CD is observed when refraction indices as well as absorption coefficients are different for left and right circularly polarized light, see Fig. 5.11.

CD is measured by passing left circularly polarized light ( $I_T^L$ ) and right circularly polarized light ( $I_T^R$ ) consecutively through the sample and subtracting the observed intensities:

$$\Delta I_T(\lambda) = I_T^L(\lambda) - I_T^R(\lambda) \quad (20)$$

The difference in left and right polarized absorbance is usually in the range of 0.0001, corresponding to an ellipticity of approximately  $0.01^\circ$ . The molar ellipticity is defined as

$$[\Phi] = \frac{M \Phi}{10 c l} \quad (21)$$

where  $\phi$  is the measured ellipticity,  $c$  is the concentration and  $l$  the path length of the sample cell.

CD is a very sensitive method to study molecular conformation, in particular for analyzing secondary structures of proteins and nucleic acids in solution. Because different conformations have their characteristic CD spectra, the CD spectrum of a protein gives quantitative information about each kind of secondary structure.

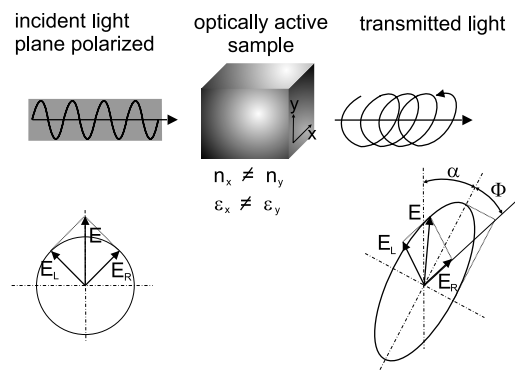


**Fig. 5.11** Principles of CD: As in ORD, linearly polarized light can be considered as the superposition of circularly polarized light of opposite direction of rotation but equal amplitude and phase. Differences in absorption of left and right polarized light lead to elliptic polarization of the transmitted light.

Moreover, CD is suited to a study of the rate of structural changes, and it can probe interactions such as protein–ligand, protein–protein or protein–nucleic acid.

## 5.4

### Photoacoustic Measurements

After selective absorption of radiation, excited molecules may relax either by emission of radiation or by non-radiative processes (cf. Chapter 3, Fig. 3.1). In photoacoustic measurements, the conversion of absorbed radiation into thermal energy is utilized. This type of conversion results in changes in the sample's thermodynamic parameters such as temperature or pressure. Changes in pressure generate acoustic waves, which eventually will be transferred to the surroundings of the sample (Fig. 5.12) where they can be measured by a sensitive microphone see Fig. 5.13 (photoacoustic spectroscopy (PAS)).

Acoustic waves are exclusively generated by the process of light absorption and subsequent relaxation, neither reflection nor scattering produce PAS signals. For this reason, optical absorption in high scattering samples and at optical interfaces can be more accurately measured by PAS. Moreover, the indirect measurement in PAS being more sensitive than optical transmission measurements, samples with low absorbance can be investigated. Concentrations below  $10^{-10}$  M or microsamples may even be measured. Some other key features are that PAS is non-destructive, non-contactive, and macro as well as micro samples can be investigated. The application range of PAS extends from the UV to the far IR. Because PA signals depend directly on light absorption, a PA spectrum looks like a conventional absorption spectrum. However, additional processes such as internal conversion, thermal diffusion and other thermal effects may occur and render the spectrum more or less distorted.

One important application of PAS is the depth-resolved measurement of layered samples. As the thermal waves propagate from the point where absorption occurs,

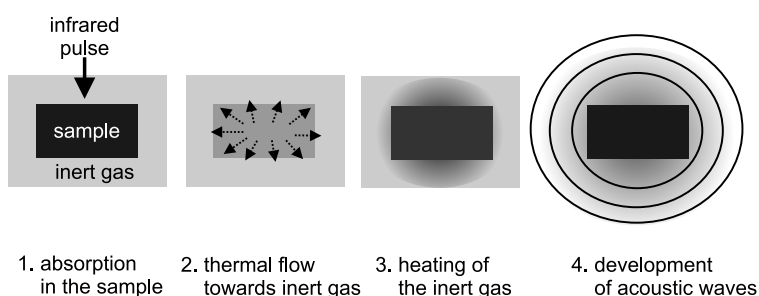


**Fig. 5.12** Photoacoustic signal generation:  
 1. IR pulses are absorbed by the sample,  
 2. the sample is heated and thermal pulses  
 are generated, 3. thermal pulses are transferred  
 from the sample to the surrounding gas,  
 4. thermal pulses cause pressure waves  
 (acoustic waves) within the surrounding gas.  
 The PAS cell does not need to be closed for  
 the measurement of the acoustic signal.

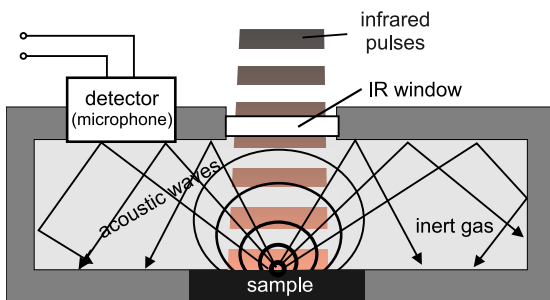


**Fig. 5.13** Schematic of photo-acoustic cell.

curred to the sample surface, they decay rapidly. The intensity of the thermal pulse is a square root function of the frequency at which the light is modulated (pulse repetition rate). The photoacoustic sampling depth  $l_{PA}$  is controlled by the modulation frequency:

$$l_{PA} = \sqrt{\frac{D}{\pi f}} \quad (22)$$

where  $f$  is the modulation frequency and  $D$  is the thermal diffusion parameter of the sample. Typical values of  $l_{PA}$  are between 0.5 and 500  $\mu\text{m}$ , depending on sample and wavelength.

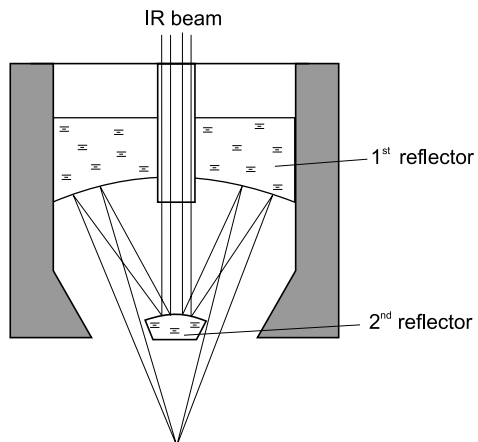
## 5.5 Microscopic Measurements

Microscopes focus the light beam at the sample position to a very small area. Microsamples may fully fit this small area. The minimum diameter of the light spot in a conventional microscope may reach the order of the wavelength of this light (diffraction limit), but the optical conductance of microscopes is usually considerably lower than that of the spectrometer alone.

Every microscope is characterized by its numerical aperture NA, which describes the angle between the optical axis and the most remote point of the sample which can be observed. NA is directly proportional to the energy throughput. Objectives with infinity correction provide advantages such as sharper images and better signal-to-noise ratio. Infinity corrected objectives are increasingly used, especially in microscopic imaging with array detectors.

Because of the different capabilities of the various optical spectroscopic techniques and their distinct demands, special types of microscopes have been developed.

**Fig. 5.14** Optical set-up of a Cassegrainian objective.



### 5.5.1

#### Infrared Microscopes

In contrast to VIS microscopes with a system of glass lenses, IR microscopes are built around reflecting components. The heart of most infrared microscopes is a Cassegrainian or Schwarzschild objective, see Fig. 5.14.

Common IR objectives have NA values between 0.5 and 0.7, typical magnification is 15x. Higher magnification objectives up to 36x are available. IR microscopic measurements can be done in transmission, in external reflection and in internal reflection. The latter requires a so-called ATR objective. ATR objectives permit *in situ* investigations of highly absorbing samples, even without sample preparation.

The sample position is controlled by visible light. Thus, IR microscopes must transmit both IR and VIS light, only small differences in coverage between the IR and the VIS images remain unavoidable due to aberration effects. Typical sample thickness in transmission is 5 to 50  $\mu\text{m}$ . Investigations of strongly absorbing or opaque samples are carried out in reflection mode which has the disadvantage of lower signals due to the splitting between incident and reflected beams.

### 5.5.2

#### Confocal Microscopes

Confocal microscopes provide particularly good spatial resolution. They are mainly used in Raman and fluorescence measurements. The basic idea of a confocal microscope is that all structures being out of focus are suppressed at the detector. This is achieved by point illumination and a pinhole in front of the detector. The optical layout of a confocal microscope is shown in Fig. 5.15.

In contrast to a conventional microscope, the whole object is not illuminated at the same time. The image will be reconstructed by stepwise movement of the sample. Scanning in the plane as well as along the optical axis allows three-dimensional investigations. Defocusing does not lead to blurring but it cuts out a part

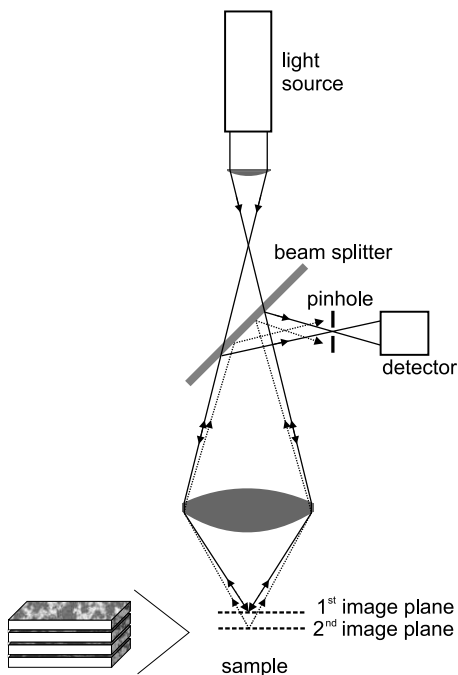


**Fig. 5.15** Optical layout of a confocal microscope.

of the sample image as one moves away from the focal plane so that these parts become darker or even disappear. This feature is also known as optical sectioning. The depth of the focus is determined by the objective's numerical aperture, the diameter of the pinhole and the wavelength.

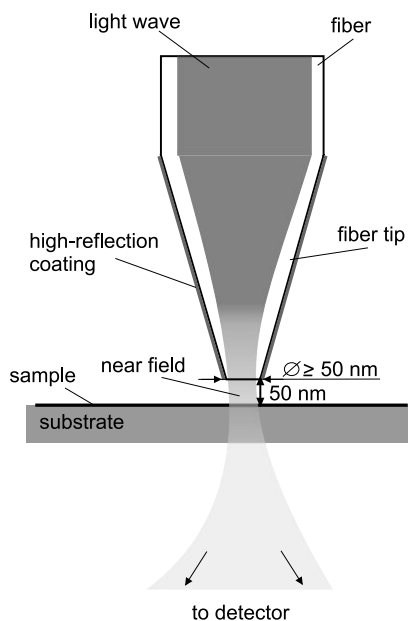
### 5.5.3

#### Near-field Microscopes

Near-field scanning optical microscopes (NSOM or SNOM) are mainly used in fluorescence and VIS measurements. They provide optical images with spatial resolution less than the *Abbe's* limit of  $\lambda/2$ . The high lateral resolution is commonly achieved by using the optical near-field, e. g. in close vicinity of a very narrow fiber tip. Figure 5.16 illustrates the design of a near-field microscope.

Light can leave the extremely narrow orifice of the fiber tip only by a tunneling mechanism, which results in the generation of an evanescent field (or near-field) outside the tip. The fiber tip must be positioned merely a few nanometers away from the sample surface by a device as used in atomic force microscopy (AFM). A spatial resolution of approximately  $\lambda/10$  can currently be achieved, limited by the signal-to-noise ratio obtained at the detector and the distance of the fiber tip from the sample. Because of the extreme damping of the fiber tip, lasers are commonly used as light sources. The development of new powerful NIR and IR lasers makes near-field IR microscopy feasible for the near future.

**Fig. 5.16** Scheme of a near-field microscope. Light emerges from a fiber tip with the diameter of the orifice below the refraction limit. The configuration shown employs near-field excitation/far-field detection. The alternative configuration is far-field excitation/near-field detection.



Near-field microscopy has been successfully applied in investigations of polymer surfaces, of biological samples and of advanced inorganic film materials. No special sample preparation is required.

## Literature

- F. M. Mirabella, *Modern Techniques in Applied Molecular Spectroscopy*, John Wiley & Sons, New York 1998.
- H. Gobrecht, *Lehrbuch der Experimentalphysik, Bd III Optik*, Walter de Gruyter, Berlin 1987.
- J. M. Hollas, *Modern Spectroscopy*, John Wiley & Sons, New York 1987.
- W. Schmidt, *Optische Spektroskopie*, VCH, Weinheim 1994.
- G. Kortüm, *Reflexionsspektroskopie*, Springer, Berlin 1969.
- H. Schilling, *Optik und Spektroskopie*, Fachbuchverl, Leipzig 1980.
- T. Buffeteau, B. Desbat, J. M. Turlet, *Appl. Spectrosc.*, 1991, 45(3), 380–389.
- U. C. Fischer, J. Koglin, A. Naber et al., Near-field Optics and Scanning Near-field Optical Microscopy, in *Quantum Optics of Confined Systems*, eds.
- M. Ducloy, D. Bloch, Kluwer Academic Publishers, Dordrecht 1996.
- Spectroscopy for Surface Science*, eds.
- R. J. H. Clark, R. E. Hester, John Wiley & Sons, Chichester 1998.
- N. J. Harrick, *Internal Reflection Spectroscopy*, Wiley, New York, 1986.
- W. Suetaka, *Surface Infrared and Raman Spectroscopy: Methods and Applications*, Plenum Press, New York, 1995.
- Internal Reflection Spectroscopy, Theory and Applications*, ed. F. M. Mirabella, Marcel Dekker, New York 1992.
- P. R. Griffiths, *Chemical Infrared Fourier Transform Spectroscopy*, Wiley, New York 1995.
- J. Michl, E. W. Thulstrub, *Spectroscopy with Polarized Light*, VCH, New York, 1986.
- J. R. Barker, B. M. Toselli, in *Photothermal Investigations in Solids and Fluids*, ed. J. A. Sell, Academic Press, New York 1998.
- E. Betzig, J. K. Trautman, *Science*, 1992, 257, 189–195.
- Infrared and Raman Spectroscopy*, ed. B. Schrader, VCH, Weinheim 1995.

# **6**

## **Applications**

*Valdas Sablinskas, Gerald Steiner and Martin Hof*

### **6.1**

#### **Mid-Infrared (MIR) Spectroscopy**

In the MIR spectral region we are dealing with transitions between various vibrational energy levels of molecules. Gaseous samples are a special case, because rotational fine-splitting of spectral bands can be observed. Fine-splitting is caused by simultaneous excitation of rotational and vibrational transitions.

The MIR spectral range extends from 4000 to 400  $\text{cm}^{-1}$ . Transitions can be observed by absorption or emission measurements. For analytical purposes, absorption measurements are usually preferred. The decision about an optimal sampling technique is very much dependent on the aggregate state of the sample under investigation.

##### **6.1.1**

##### **Sample Preparation and Measurement**

According to the Beer–Lambert law, the density of the analyte (or concentration of it in the case of mixtures or solutions) and the IR pathlength in the sample are crucial. These parameters have to be chosen in such a way that good measurable optical signals are obtained, in contemporary spectrometers between 20 and 60 %T for band maxima. In order to minimize the background in the spectrum, care should be taken with regard to the homogeneity of the sample, the level of impurities and absorptions in the solvent. The quality of the spectral data acquired depends very much on the sampling technique chosen. Detailed descriptions of sampling techniques can be found in [1–3]. A summary of common sampling techniques is given in Fig. 6.1.

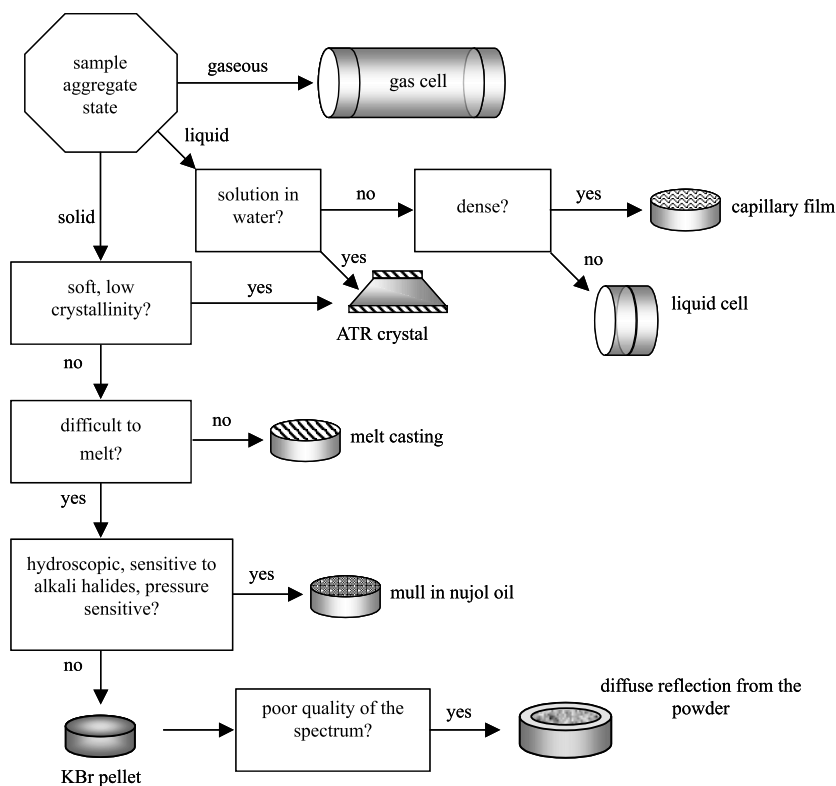


**Fig. 6.1** Summary of common IR sampling techniques.

### 6.1.1.1 Gases

Gas cells are essentially gas-tight containers fitted with IR transparent windows to enable the radiation to enter and exit the container. Gas cells should be equipped with inlets for introducing, pressurizing and evacuating the gas. Cell sizes vary from a cylinder of a few centimeters pathlength, typically 10–20 cm, constructed from glass or stainless steel, with windows at each end, to compact long-pathlength cells, which have internal gold mirrors (multipass gas cells) in order to provide an effective pathlength of many meters within the gas sample. At pressures down to 50 Torr many gases yield useful spectra in a standard 10 cm pathlength cell. Unfortunately, many molecular species have much lower saturated vapor pressure at room temperature, i. e. a longer pathlength is required for meaningful measurements.

A sketch of a gas cell with multipass optics in the so-called White arrangement is given in Fig. 6.2. It comprises three spherical mirrors, which can be adjusted for the desired number of passes. Four passes (as shown in Fig. 6.2(a)) is the minimum number of passes in such an arrangement. The achievable maximum number of passes depends on the reflectivity of the mirrors and on the quality of the incoming beam. The latter is partly defined by the size of the IR source. Commer-

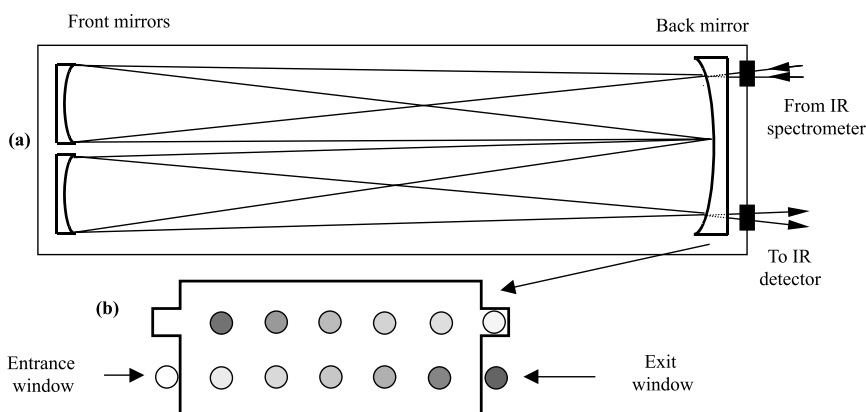


**Fig. 6.2** Multipass gas cell with White optics. (a) Ray diagram for four optical passes; (b) Front view of the back mirror with images of the IR source on it for 24 passes.

cial cells with White optics have an outer length of ca. 30–100 cm and provide a folded optical setup with total path of up to 100 m. Measurements with the multipass gas cells should be carried out in single beam mode. A drawback of multipass gas cells concerns cooling. It is very difficult to ensure stable alignment and prevention of atmospheric water condensation on the windows in low temperature experiments with such a cell.

High-resolution MIR spectrometers are required in order to resolve the rotational fine-structure of vibrational bands. MIR instruments providing resolution down to  $0.001\text{ cm}^{-1}$  are commercially available. The width of the rotational spectral lines of a gaseous analyte depends not only on its partial pressure, but also on the total pressure and temperature. Molecular collisions will broaden the rotational spectral lines, a phenomenon known as pressure broadening. The statistical distribution of velocities of the molecules causes the so-called Doppler broadening of the rotational lines, this broadening effect can be partly eliminated by cooling the gaseous sample.

Spectra of compounds with vapor pressure down to 0.001 Torr can be obtained using multipass gas cells. This technique has proved very useful for the detection of atmospheric impurities or trace components in waste and combustion gases.

#### 6.1.1.2 Solutions and Neat Liquids

Every solvent has its own absorption bands in the MIR region. For this reason, the most appropriate solvent for the given situation has to be chosen from a whole selection. Unfortunately this selection does not include water and alcohols, which exhibit broad and strong bands in their MIR spectra. Moreover, many optical materials used as MIR windows for liquid cells (e.g. alkali halides, such as KBr) are soluble in water and alcohol. The solvents with the largest absorption free areas in the MIR are carbon tetrachloride and carbon disulfide. Both solvents are quite toxic and must be handled carefully. A list of the most common MIR solvents is

given in Chapter 5. A comprehensive review of the spectral transmission of all solvents is given in [1].

Windows for liquid cells typically consist of NaCl or KBr for non-aqueous samples or CaF<sub>2</sub> for aqueous solutions. A list of common MIR window material is given in Chapter 5.

For the selection of optical windows, besides such parameters as useful spectral range, mechanical resistance and solubility, the refractive index also has to be taken into account. The refractive index of the windows should match that of the liquid sample in order to minimize reflection losses, stray light and distortions of band shapes (Christiansen effect). NaCl and KBr are very suitable for organic analytes. Inorganic analytes may have much higher refractive indices. The higher the refractive index, the higher the reflection losses for the incident IR radiation.

For solutions, the typical thickness of liquid cells is in the 0.05 to 1 mm range, which is provided by a Teflon gasket placed between the two windows. Both fixed thickness and variable thickness liquid cells are available commercially. Typically, solutions of 0.05 to 10% in concentration are handled in IR cells. In double-beam spectrometers, a reference cell is filled with pure solvent and placed in the reference beam in order to compensate for solvent bands and other background effects. In single-beam instruments, solvent bands and background effects are usually removed by computing the difference between the sample and solvent spectra. Both cell thickness and analyte concentration can be calculated from the measurements with high accuracy. This renders MIR spectroscopy very suitable for quantitative measurements.

Neat liquids require a film thickness in the 10 µm range. Since it would be difficult to fill a cell of such low thickness, and even more difficult to clean it, capillary films of such a sample are usually formed by squeezing a few drops of compound between two windows.

In the case of relatively low-melting solids it is also possible to prepare a thin film by melting and squeezing the sample between two windows. Thin films of nonvolatile liquids or solids can be deposited on the window by solvent evaporation. The sample is first dissolved in a volatile solvent. A few drops of the solution are placed on the window. After evaporation of the solvent, a thin film of sample is obtained on the window. The windows can usually be cleaned using carefully dried methylene chloride or acetone. Preparing a thin film from solution or solidification from the melt are methods well suited to the examination of amorphous materials, such as waxes or soft resins.

#### 6.1.1.3 Pellets and Mulls

Pellets are used for solid samples that are difficult to melt or dissolve in any suitable solvent, or which have to be measured in their native solid state. The sample is finely ground and mixed with dry potassium bromide (or other alkali halide) powder. The usual analyte/KBr ratio is ca. 1:100. Grinding and mixing can be done with an agate mortar and pestle or with a vibrating mill. The mixture is then pressed into a transparent disk in an evacuable die for 2 min at a pressure of

0.6 GPa (6 tons  $\text{cm}^{-2}$ ). Without evacuation (e.g. when moist air is present during pressing) it is impossible to obtain highly transparent pellets. The size of the ground particles should not exceed 2  $\mu\text{m}$ , otherwise scattering losses may result. IR spectra obtained by the pellet technique often exhibit bands at 3450 and 1640  $\text{cm}^{-1}$  due to adsorbed moisture. Without the addition of an internal standard the pellet technique is not suitable for quantitative measurements because the thickness is not precisely reproducible and the size of the IR bands depends on the dispersion of the sample (see Fig. 6.3).

Mulls are used as alternatives to pellets. The sample (1 to 5 mg) is carefully ground into a suspension using a couple of drops of a mulling agent. This mull is pressed between two IR transmitting windows to form a thin film. Common mulling agents are Nujol (liquid paraffin), Fluorolube (a chlorofluorocarbon poly-

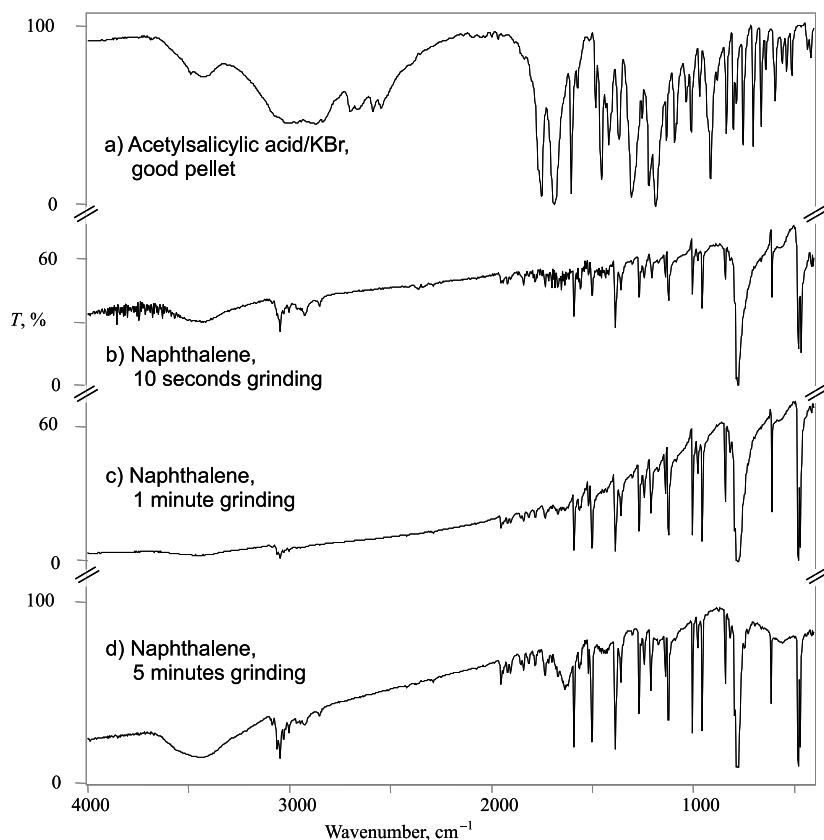


**Fig. 6.3** Examples of possible errors in the KBr pellet technique: (a) good spectrum of acetylsalicylic acid in a KBr pellet; (b) insufficient grinding results in light scattering (background shape of absorption bands; (d) too long grinding results in good size and shape of absorption bands but causes adsorption of larger amounts of water in the pellet (broad band at 3450  $\text{cm}^{-1}$ ).

mer) and hexachlorobutadiene. To obtain a complete IR spectrum that is free of mulling agent bands, experiments with various mulls are generally required. The mull technique is recommended for water-sensitive samples and for samples which interact with alkali halides.

A detailed description of all the techniques can be found in [1].

#### 6.1.1.4 Neat Solid Samples

Pellet or mull techniques cannot usually be applied to polymeric samples due to their softness. Samples of thermoplastic polymers can be prepared by using a so-called press tool for melt films. This tool consists of two heatable metal plates, which can be placed in a hydraulic press. The thickness of the squeezed film is defined by the thickness of the metal spacer placed between the heated plates. The metal plates may be wrapped in aluminum foil in order to prevent adhesion of the sample to the plates. The foils can be easily removed by dissolution in dilute HCl.

If the compound under investigation is both insoluble and non-meltable, it can be cut into slices of appropriate thickness using a microtome. Conventional sampling techniques require sample areas of a few square centimeters, which might hardly be achievable for slices of 20 and 50  $\mu\text{m}$  thickness. Samples of smaller area may advantageously be investigated by microATR (see below).

#### 6.1.1.5 Reflection–Absorption Sampling Technique

This technique is used to study thin (down to submonolayer) films adsorbed on reflective substrates such as metals. Experimentally it involves measuring the change in the reflectance spectrum of the substrate that accompanies thin film formation. Various acronyms for the technique are used: infrared reflection–absorption spectroscopy (IRRAS, IRAS) and reflection–absorption infrared spectroscopy (RAIRS). The Basics of IRRAS spectra are described in Chapter 5.2.

According to theory, the maximum sensitivity in reflection–absorption measurements should be achieved at grazing incidence angle (between 65 and 85 °). Various accessories are available, either with fixed angle of incidence or variable angle of incidence. It is necessary to record the reflectance spectrum of the substrate with a high signal-to-noise ratio both before and after formation of the thin film, the IRRA spectrum is then computed as the ratio of these two spectra. The range of incidence angles that can be effectively utilized is rather limited. The experiment has to be designed carefully, particularly with regard to source and detector types.

The depth of penetration of the electrical field from the surface of the metal substrate into the adsorbed sample is between 5 and 500 nm. This enables investigation of submonolayers. IRRA spectra differ from conventional transmission spectra of bulk compounds, because only vibrations with transition dipole moments perpendicular to the surface will be excited. Since the evanescent field decays rapidly, vibrating groups closer to the surface yield larger absorption bands. Moreover, the polarization status of incident radiation is crucial, only p-polarized light will interact.

Another practical consideration is film thickness. In the case of IRRAS of thick films, we observe a superposition of two spectra, one spectrum due to molecules close to the surface (with some enhanced spectral bands) and one due to the bulk sample (conventional transmission spectrum). In the case of very thick samples, the bulk spectrum dominates and the angle of incidence is not so important. In the case of thicknesses between 0.1 and 1  $\mu\text{m}$ , both types of spectra have to be taken into consideration.

Compared to other sampling techniques for surface investigations, a great advantage of IRRAS results from propagation of the probe photon in a non-vacuum environment. This enables the spectrometer to be set up outside an ultra-high vacuum chamber, which considerably simplifies operation.

#### 6.1.1.6 Sampling with the ATR Technique

Attenuated total reflectance (ATR) accessories are especially useful for obtaining IR spectra of samples that cannot be readily examined by common transmission methods. Such accessories are suitable for studying thick or highly absorbing solid and liquid samples, including films, coatings, powders, threads, adhesives, polymers, and aqueous samples. ATR requires only little sample preparation for most samples, it is one of the most versatile sampling techniques.

The basics of ATR have been described in Chapter 5.2.3. The sample has to be brought into good optical contact with the ATR crystal as shown in Fig. 6.4. The IR beam is directed towards the bevel edge of the ATR crystal and undergoes single or multiple internal reflections. ATR multireflection crystals may be trapezoidal or rod-shaped. The number of reflections and the penetration depth decrease with increasing angle of incidence. The resulting IR-ATR spectrum is similar to a conventional IR spectrum but the intensities of the bands at longer wavelengths are higher due to the larger penetration depth at longer wavelengths. ATR accessories fit easily into the sample compartment of any grating or FT-IR spectrometer, but high quality spectra can only be obtained by FT-IR spectrometers due to the energy limited condition.

ATR is a surface and interface investigation method. The penetration depth is of the order of a few tenths of the wavelength of investigation, in the IR between 0.5 and 10  $\mu\text{m}$  (cf. Eq. (10) in Chapter 5). A variety of ATR accessories is available including various kinds of liquid cells or even horizontal units for cell-less investiga-

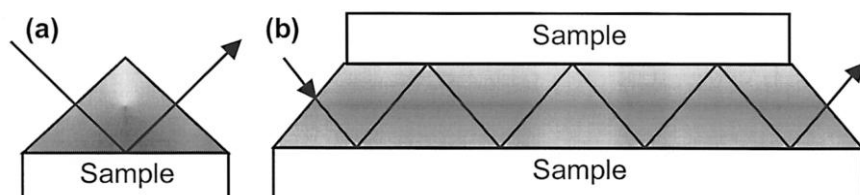


**Fig. 6.4** ATR sampling technique. (a) ATR crystal for single reflection measurement; (b) ATR crystal for multi reflection measurement.

tion of liquids. Heatable ATR cells are also commercially available. A special and meanwhile widespread ATR variety uses a single reflection diamond. The fields of application of ATR are metals, polymers, lacquers, rubbers, coatings, laminates, papers, textiles, fibres, jelly-like samples and interfaces of liquids and solids.

#### 6.1.1.7 Thin Samples

Part of the incident beam is reflected at each optical boundary (air-sample boundary in the case of a free-standing thin sample or air-window/window-sample boundaries in the case of a liquid cell), even at normal incidence. Of particular importance is that part of the radiation which undergoes multiple reflections at the two opposite surfaces of a plane-parallel sample. The double-reflected beam can interfere with the original beam, which results in sinusoidal type periodical features in the background of the spectrum (Fig. 6.5). Such features usually cause difficulties during evaluation of spectra. On the other hand, the interference provides access to the effective thickness of the sample as well as the optical quality of its boundaries (deviations from plane-parallelity cause reduced amplitudes of the interference fringes). The effective sample thickness can be calculated according to:

$$d = \frac{N \times 10000}{2 \times n_D \times (\tilde{\nu}_1 - \tilde{\nu}_2)} \text{ } (\mu\text{m})$$

where  $N$  is the number of interference fringes between  $\tilde{\nu}_1$  and  $\tilde{\nu}_2$ ,  $n_D$  is the refractive index of the medium inside the cell ( $n_D = 1$  in the case of an empty cell), 10000 is the conversion factor between wavenumber [ $\text{cm}^{-1}$ ] and thickness [ $\mu\text{m}$ ]. Usually, the pathlengths of liquid cells of thickness up to 1 mm are determined by evaluation of their interference fringes (cf. Fig. 6.5).

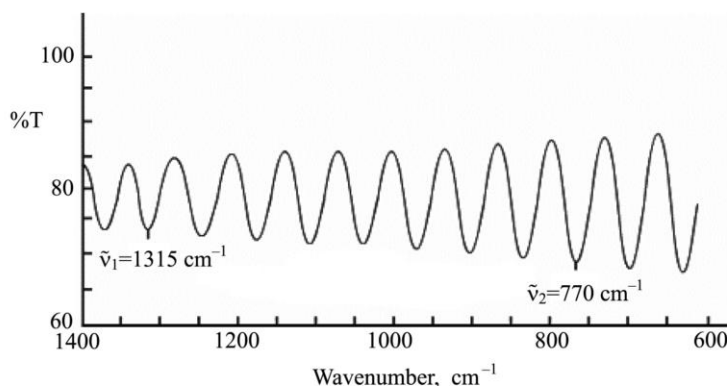


**Fig. 6.5** Interference fringes in an IR spectrum of an empty KBr cell. Eight fringes between 1315 and 770  $\text{cm}^{-1}$  correspond to a cell thickness of 73  $\mu\text{m}$ .

#### 6.1.1.8 Diffuse Reflection Sampling Technique

There is a large group of solid samples (like powders, pastes, pellets with rough and scattering sample surface) which do not give good-quality spectra by any of the above described sampling techniques. In these cases, measurement of the diffuse reflection may be an alternative. Diffuse reflection means scattering of a large part of the radiation in all directions. The penetration depth of incident IR radiation into the scattering sample is usually between 10 and 500  $\mu\text{m}$ . Even in the case of rough surfaces, a small contribution of specularly reflected radiation always persists. Specularly reflected IR radiation does not contain much information about the sample (very short path within the sample), it mainly decreases the accuracy of the quantitative measurement and increases detector noise.

Diffuse reflection accessories are commercially available. They collect the diffusely scattered IR radiation by means of large ellipsoid mirrors. Even the largest mirrors only permit the collection of a part of the scattered radiation, therefore the use of diffuse reflection accessories is restricted to FT-IR spectrometers (diffuse reflection in IR by FT spectrometer – DRIFT). The Kubelka–Munk transformation has to be performed in order to linearize the ordinate of the obtained spectra. Integrating spheres (so-called Ulbricht spheres) are no longer used in MIR due to the lack of non-absorbing and uniformly high-scattering coatings for the inside of the sphere.

DRIFT spectra depend on both the scattering and the absorbing properties of the sample (Kubelka–Munk theory). DRIFT spectra are considerably complex, they are influenced by particle size, crystallite orientation, sample homogeneity and analyte concentration. The bigger the particle size the larger the contribution from specular reflection and absorption. Both contributions have to be minimized for quantitative evaluation. The ideal particle size is between 2 and 10  $\mu\text{m}$ . Larger particles have to be ground before measurement. Low absorbance is achieved by dilution in a non-absorbing matrix, usually KBr powder in a ratio from 1:3 to 1:100. A special variation for compact materials is the abrasion technique. Nickel–diamond abrasive pads are used to rub off a part of the sample, for example a varnish. The pad is then inserted into the DRIFT accessory and measured directly.

An excellent description of all aspects of diffuse reflectance can be found in [4].

#### 6.1.1.9 Sampling by Photoacoustic Detection

The basics of photoacoustic spectroscopy (PAS) are described in Chapter 5. PAS is useful for examining highly absorbing samples that are difficult to analyze by other IR techniques. Minor or even no sample preparation is required here. The size and shape of the sample are not critical. PA spectra can be obtained from a wide variety of samples such as powders, polymer pellets, viscous glues, single crystals, and single fibres.

PA spectra are generally similar to conventional IR spectra except that strong spectral bands will often be saturated (truncated). However, the presence of such truncated bands does not appreciably limit the practical use of PAS. Depth resolved

measurements are an important feature of the FT-IR PAS technique. Depth resolution can be varied from 1 to 20  $\mu\text{m}$  simply by changing the velocity of the moving mirror inside the interferometer. Multilayer samples such as polymer composites can easily be studied by PA spectroscopy.

#### 6.1.1.10 Microsampling

Microsampling techniques have to be applied when either small amounts or small sizes of analytes have to be investigated. Microsampling techniques may be derived from conventional techniques by miniaturisation. For all such miniaturized sampling techniques a beam condenser (micro-illuminator) is needed. Standard beam condensers are made of a pair of ellipsoidal mirrors. Micropellets for solids have a diameter of 0.5 and 1.5 mm with sample amounts of 5 to 10  $\mu\text{g}$  in 4 mg KBr. For liquids and solutions, microcells with volume down to 0.3  $\mu\text{l}$  are commercially available. A special case of microsampling is the so-called diamond anvil cell, where a tiny drop of liquid analyte is squeezed between two diamond crystals. Even solidification of sample between the diamonds can be achieved by applying pressures up to 100 bar. Usual dimensions of the diamond surfaces are below one millimeter. This technique is very useful for conformational analysis.

Nowadays, microsampling is performed by the use of IR microscopes (see also Chapter 5.5). They permit easy access to spectra from small sample areas down to ca.  $10 \times 10 \mu\text{m}^2$ . This size limit is given by the basic diffraction theory, spectral information from smaller areas can be obtained only by investigating wavelengths closer to the NIR spectral range. IR microscopes equipped with an X,Y-motorized stage permit the 2D mapping of chemical properties with good lateral resolution (e.g., distribution of impurities). Recently, a MIR instrument with array detectors has become commercially available. Such instruments permit the collection of IR images in only a few seconds by direct imaging.

All microsampling techniques require very thorough sample preparation. To obtain meaningful results in either transmission or reflection mode of an IR microscope, sufficient skills in microscopic sample preparation are required.

A wide range of compounds can be investigated by IR microscopy. The broad scale of sampling accessories for IR microspectroscopy even includes objectives for ATR or grazing angle measurements.

#### 6.1.2 Structural Analysis

Every chemical compound has its own characteristic IR spectrum. The IR spectrum contains the entire information about the molecular structure of the investigated sample. The main problem is the assignment of experimental spectral bands. In addition to fundamental vibration bands, very often so-called combination and overtone bands are present. Fermi resonance can cause intensity changes and frequency shifts of the bands involved. Intermolecular interactions (such as hydrogen bonding) can cause additional bands. Furthermore, the influences of solvents, tem-

perature and pressure have to be considered. There are two different approaches for the assignment of vibrational bands.

The most convenient tool for identification of molecules from their vibrational spectrum are spectral databases (cf. Chapter 22). The matching process is very much accelerated by computerized search programs. If an exact match cannot be found, these programs usually list the reference compounds that numerically match the unknown spectrum very closely. Attention: close proximity in a search hit list does not guarantee close similarity of molecular structures.

A more chemical approach is the evaluation of characteristic or group frequencies. Some chemical groups exhibit very characteristic bands regardless of the kind of molecule in which they are included. The group frequency approach is very useful for structural analysis. From the frequencies and intensities of some spectral bands it is possible to predict what kind of chemical groups are present in the molecule, how they are connected to other groups and, finally, the structure of the molecule under investigation may be guessed.

According to the theory of molecular vibrations in any  $N$ -atomic molecule there are  $3N-6$  ( $3N-5$  in the case of linear molecules) fundamental vibrations. By the group frequency approach one takes into account only the movements of atoms with the largest amplitude and neglects atoms with much smaller vibration amplitude. Vibrations can be subdivided into two groups: stretching vibrations (when the bond lengths are changing during vibration, also called valence vibrations) and deformation vibrations (when the bond angles are changing). Deformation vibrations are subdivided further into scissoring, wagging, rocking and twisting modes. Vibrations of  $\text{CH}_2$  and  $\text{CH}_3$  groups are summarized in Fig. 6.6.

Each normal vibration has particular symmetry properties, described by the symmetry elements of the point group to which the molecule under investigation belongs. Symmetry considerations are very useful for the assignment of the spectral bands. So-called character tables may be used to derive the symmetry of each normal vibration and to deduce the IR and Raman activity of a given vibration. A vibration is infrared active if the total molecular dipole moment changes during vibration. It is Raman active, if the molecular polarizability changes during vibration. From symmetry considerations it can be deduced whether dipole moment or polarizability changes occur during vibration. IR or Raman activity merely indicates the appearance of a particular band in the spectrum. In order to further predict the intensity of vibrational bands, detailed information about the magnitude of the transition moment is needed.

Not all vibrations exhibit characteristic frequencies. For instance, vibrational frequencies of the various C–C bonds of the carbon backbone in aliphatic molecules are very much coupled to each other (so-called skeleton modes), and they depend very much on the chemical groups connected to the aliphatic chain. This behavior can also be used for spectrum interpretation. A short list of group frequencies of some chemical groups is given in Tab. 6.1. A more comprehensive list of characteristic bands can be found in spectral correlation tables and charts, for example in [5,6].

For practical evaluation, the IR spectrum is often divided into three regions (a) from 4000 to  $1400 \text{ cm}^{-1}$ , (b) from  $1400$  to  $900 \text{ cm}^{-1}$  and (c) from  $900$  to  $400 \text{ cm}^{-1}$ .

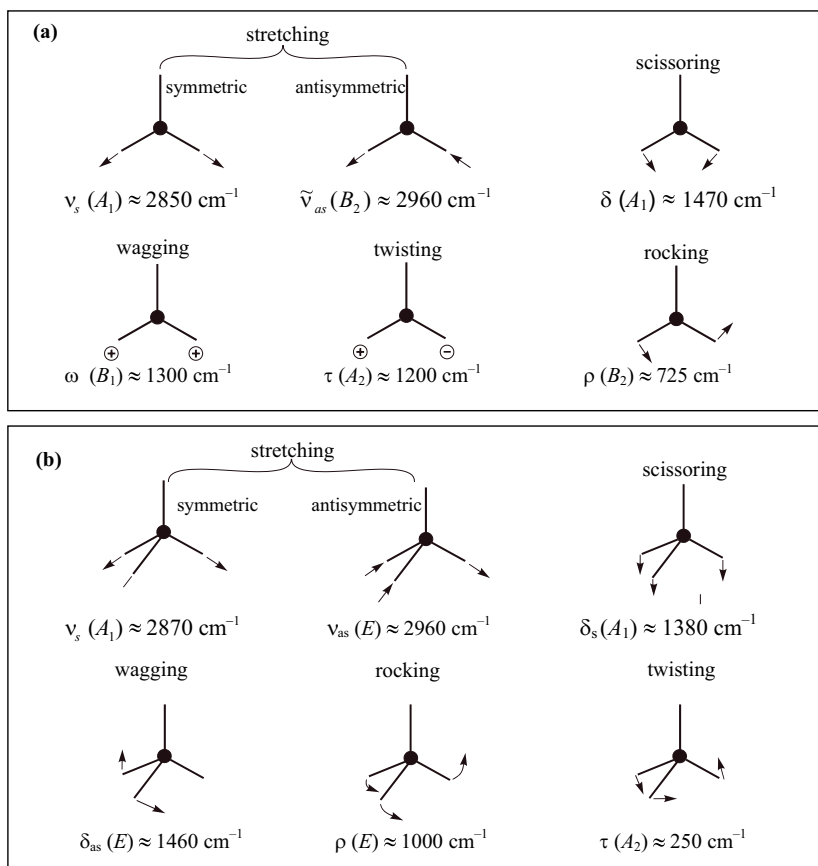


**Fig. 6.6** Group frequencies of (a)  $\text{CH}_2$  and (b)  $\text{CH}_3$  groups. The name of each type of vibration (abbreviated by a greek letter) reflects the kind of movement. The italic letters given in parentheses are used to fully describe the symmetry properties of the oscillator.

**Table 6.1** Selection of vibrational group frequencies.

Spectral Range, $\text{cm}^{-1}$	Chemical Group	Group Vibration
3700–3200	$-\text{OH}$	O–H stretching
3400–3330	$-\text{NH}_2$	Antisymmetric stretching
3300–3250	$-\text{NH}_2$	Symmetric stretching
3065–3030	$-\text{C}-\text{H}_{\text{aromat}}$	C–H stretching
3020–2950	$-\text{CH}_3$	Antisymmetric stretching
2960–2910	$-\text{CH}_2$	Antisymmetric stretching
2970–2860	$-\text{CH}_3$	Symmetric stretching
2860–2840	$-\text{CH}_2$	Symmetric stretching
2590–2560	$-\text{SH}$	S–H stretching
2600–2350	$-\text{B}-\text{H}$	B–H stretching
2450–2275	$-\text{P}-\text{H}$	P–H stretching

**Table 6.1** (continued)

<b>Spectral Range, <math>\text{cm}^{-1}</math></b>	<b>Chemical Group</b>	<b>Group Vibration</b>
2300–2230	$-\text{C}\equiv\text{C}-$	$\text{C}\equiv\text{C}$ stretching
2260–2230	$-\text{C}\equiv\text{N}$	$\text{C}\equiv\text{N}$ stretching
2250–2100	$-\text{Si}-\text{H}$	$\text{Si}-\text{H}$ stretching
2250–2100	$-\text{C}-\text{D}$	$\text{CD}, \text{CD}_2, \text{CD}_3$ stretching
1760–1720	$-\text{C}=\text{O}$	In organic acids
1740–1700	$-\text{N}-\text{C}=\text{O}$	In ketones
1660–1650	$-\text{C}=\text{O}$	In amides
1660–1640	$-\text{C}=\text{N}-$	Stretching
1700–1625	$-\text{C}=\text{O}$	Amide I
1660–1640	$-\text{C}=\text{C}-$	Stretching
1600–1595	$-\text{COO}^-$	Antisymmetric $-\text{COO}^-$ stretching
1600–1450	$-\text{N}=\text{O}$	$\text{N}=\text{O}$ stretching in organic nitrates
1470–1440	$-\text{CH}_3$	Antisymmetric deformation
1470–1440	$-\text{CH}_2$	Symmetric and antisymmetric deformation
1430–1420	$-\text{CO}-\text{OH}$	CO stretching in organic acids
1410–1390	$-\text{COO}^-$	Symmetric $-\text{COO}^-$ stretching
1400–1310	$-\text{S}=\text{O}_2-$	Antisymmetric stretching
1390–1370	$-\text{CH}_3$	Symmetric deformation
1380–1300	$-\text{CF}_3$	Stretching
1340–1250	$-\text{CO}-\text{NH}$	Amide III
1330–1250	$-\text{CH}$	Deformation
1265–1250	$-\text{CO}-\text{OH}$	$\text{CO}-\text{OH}$ deformation in organic acids
1280–1250		Oxirane, breathing of the ring
1300–1140	$-\text{P}=\text{O}$	Stretching
1300–1120	$-\text{CF}_2$	Stretching
1200–1120	$-\text{S}=\text{O}_2-$	Symmetric stretching
1120–1060	$-\text{C}-\text{F}$	Stretching
1300–1100	$-\text{C}-\text{O}-$	Stretching
1150–950	$-\text{C}-\text{C}-$	Stretching
1070–1040	$-\text{S}=\text{O}$	Stretching
1040–980	$-\text{C}_6\text{H}_5$	In-plane deformations of benzene ring
900–670	$-\text{CCH}_{\text{aromat}}$	Aromatic C–H out-of-plane bend
930–830	$-\text{COC}-$	Symmetric stretching in ethers
760–680	$-\text{C}-\text{Cl}$	Stretching
780–720	$-\text{CCl}_2$	Symmetric stretching
700–660	$-\text{CCl}_3$	Symmetric stretching
650–600	$-\text{C}-\text{Br}$	Stretching
620–600	$-\text{CBr}_2$	Symmetric stretching
560–540	$-\text{CBr}_3$	Symmetric stretching
560–500	$-\text{C}-\text{I}$	Stretching

### 6.1.2.1 The Region from 4000 to 1400 cm<sup>-1</sup>

This region comprises stretching vibrations involving movements of light atoms (molar mass below 20 g mol<sup>-1</sup>). O—H and N—H stretching bands are located in the region from 3700 to 2500 cm<sup>-1</sup>. These groups very often participate in the formation of hydrogen bond complexes. The formation of such complexes results in red shifted and very broad spectral bands. C—H stretching bands are found in the 3300–2800 cm<sup>-1</sup> spectral range. Bands in the 2700–1850 cm<sup>-1</sup> spectral region usually belong to C≡C, C≡N, N≡N or some groups containing hydrogen and a heavier atom (S—H, P—H and Si—H). The 1950–1450 cm<sup>-1</sup> region exhibits IR absorption from a wide variety of double-bonded chemical groups, in particular C=O. This region is of particular importance for investigations of biological molecules. Conjugation, ring size, hydrogen bonding, steric and electronic effects often result in significant shifts in absorption frequencies.

### 6.1.2.2 The Region 1400–900 cm<sup>-1</sup>

This is called the fingerprint region. Many chemical groups with single bonds have group frequencies in this region. These vibrations usually couple very strongly, i. e. particular bands in this region can hardly be attributed to a single chemical bond or group. On the other hand, bands caused by complex interacting vibrations constitute a unique fingerprint for each compound. If two spectra exhibit identical fingerprint patterns in this region, the corresponding samples are generally considered to be identical.

### 6.1.2.3 The Region from 900 to 400 cm<sup>-1</sup>

Some characteristic bands of aromatics occur in this region. These bands are due to aromatic C—H out-of-plane bending vibrations. The absence of absorption bands in the 900 to 650 cm<sup>-1</sup> region usually indicates the lack of aromatic rings in the molecule under investigation. Some organic molecules containing halogen atoms can also contribute in this region.

Based on extensive experience, the following scheme for interpretation of IR spectra based on group frequencies was worked out. No systematic procedure of general validity exists, a reasonable way to proceed is the following:

- |                            |  |
|----------------------------|--|
| 1. Carbon backbone:        | evaluation of C—H str, C—H def, C—C str<br>presence of aromatic,<br>—C—C—, —C=C—, —C≡C— groups<br>compare with NMR data! |
| 2. O-containing compounds: | evaluation of C=O str, O—H str<br>interactions with<br>—C—H str, —N—H str, —O—H str.                                     |
| 3. N-containing compounds: | evaluation of N—H str, C≡N str<br>compare with MS data!  |

4. S-, P-, Hal-containing  
compounds:

evaluation of S–H str, S=O str, –SO<sub>2</sub> str

P=O str, C–Hal str

compare with chemical analysis and MS data!

It should always be recalled that the aim of structural analysis based on characteristic IR frequencies is to identify structural groups, not to ascertain the total molecular structure of the analyte. Even the identification of structural groups should be based on different chemical and physical data, not just on a single IR spectrum. In general, it is impossible to deduce the total molecular structure of a molecule solely by interpretation of IR spectra by means of correlation tables. Sometimes, the absence of a particular absorption may be more informative than its presence.

A very general approach is the comparison of experimental spectra with calculated spectra. For small molecules (up to 30–40 atoms) it is possible to predict their structure and infrared and Raman spectra with reasonable precision by quantum chemical (*ab initio*) methods. By comparing theoretical and experimental spectra, bands can be assigned. If calculated and experimental spectra fit each other, the structure used for calculation should be the correct one.

Nowadays, spectra of polymers and other large molecules can only be computed by semiempirical or molecular mechanics calculations. Such calculations allow one to predict the molecular structure, but do not give (or give too little) information about the vibrational frequencies and cannot be used for interpretation of spectra.

#### 6.1.3

#### **Special Applications**

Various modern accessories (ATR crystals, acoustic detectors, infrared microscopes, polarization modulation technique) as well as hyphenation techniques have substantially expanded the field of application of infrared spectroscopy. Applications of IR spectroscopy to surface investigations (characterization of the surface, physisorption and chemisorption studies, catalytic properties) are reviewed in [7–9]. Applications of hyphenated techniques, in particular combinations with chromatography, are given in [8].

IR spectroscopy retains its importance in the field of *industrial applications*, Raman spectroscopy regains its attraction. A detailed summary of applications can be found in [10]. The industrial environment requires special conditions for the instruments such as rapid measurements, a high degree of automation and reliability, robustness and special software. Of importance are the sampling methods, the data transfer to computer networks and the software for quantitative analysis. A major field is quality assurance, for example in the pharmaceutical and semiconductor industry. A very new field is the use of IR for industrial combinatorial chemistry. The most rapidly growing area is on- and in-line process control in almost all industrial applications. For the investigation of inorganic substances and coordination and organometallic compounds IR techniques are also

suitable. In [11] is given an excellent survey of the experimental aspects and the applications with many examples.

In recent years the use of IR spectroscopy for *medical applications* such as the analysis of human tissues and fluids such as blood has substantially increased. In such kinds of measurements all modern spectroscopic methods like mapping, ATR microscopy, and the chemometric evaluation of the data by statistical and multivariate analysis are needed. IR spectroscopy is very sensitive to structure and concentration changes in biological macromolecules such as nucleic acids, proteins and lipids. A summary of this field is given in [12]. Examples of successful applications of IR are the monitoring of cellular metabolism and the identification of tumors. Photoacoustic spectroscopy applications in life science studies as well as on solids, liquids and gases are described in [13]. A new method for applications in biology, medicine and industry (semiconductors) is IR imaging spectroscopy, a combination of IR microscopy with a focal plane array detector. Another new method is 2D spectroscopy where the spectral intensity is obtained as a function of two independent spectral variables. A short description of the method is given in [14] and the literature cited therein.

The *analysis of polymers* is one of the most important application fields for IR spectroscopy. This kind of spectroscopy can be successfully used for the determination of chemical structures like stereo-regularity, chain conformation, orientation and crystallinity, for identification of complex polymeric systems, for monitoring reaction processes and for the study of dynamic properties like diffusion. All these applications are discussed in [15].

For *forensic analysis* IR spectroscopy is a commonly used method. A description of all application fields with many samples is described in [16]. Specific analyses are those of paints, paper, inks, gemstones, polymers, fibers, food and the analysis of physiological samples and environmental samples. The main methods of investigation are the ATR diamond cell and all reflectance techniques as well as the GC-IR technique.

An excellent summary of the use of IR spectroscopy in the *study of works of art* is given by Edwards [9]. So it is possible to investigate plastics, glass, pottery, biomaterials, paintings, medieval manuscripts and wall paintings and to determine the origin and the age of all these art objects. Fringeli [17] describes the basics, the possibilities and applications of ATR and reflectance IR spectroscopy including new applications like the single beam sample reference (SBSR) ATR technique, modulated excitation spectroscopy and 2D IR spectroscopy (see Reference Data Table 1 on page 106/107).

## 6.2 Near-Infrared Spectroscopy

The near infrared (NIR) spans the range from  $12500\text{--}4000\text{ cm}^{-1}$  ( $800\text{--}2500\text{ nm}$ ) and is dominated by overtones and combinations of O–H, N–H, C–H and C=O vibrations. Overtone and combination bands are rather weak. Band intensities

**Table 6.2** NIR absorption regions of important groups and vibrations.

<b>Group</b>	<b>Type of Vibration (<math>\nu</math>, stretching, <math>\delta</math>, bending)</b>	<b>Wavenumber, <math>\text{cm}^{-1}</math></b>	<b>Wavelength, nm</b>
free OH	$3\nu$ (2nd overtone)	10400–10200	960–980
bound OH	$3\nu$ (2nd overtone)	10000–8850	1000–1130
C–H ( $\text{CH}_3$ , $\text{CH}_2$ )	$3\nu$ (2nd overtone) and combination $2\nu + 2\delta$	8700–8200 7350–7200	1150–1220 1360–1390
free OH	$2\nu$ (1st overtone)	7140–7040	1400–1420
C–H ( $\text{CH}_3$ , $\text{CH}_2$ )	combination $2\nu + \delta$	7090–6900	1410–1450
free NH	$2\nu$ (1st overtone)	6710–6500	1490–1540
hydrogen bonded NH	$2\nu$ (1st overtone)	6620–6250	1510–1600
S–H	$2\nu$ (1st overtone)	5780–5710	1730–1750
$\text{CH}_3$ and $\text{CH}_2$	$2\nu$ (1st overtone)	6020–5550	1660–1800
C=O	$3\nu$ (2nd overtone)	5230–5130	1910–1950
free OH	combination $\nu + 2\delta$ and $3\delta$	5210–5050	1920–1980
C–H ( $\text{CH}_3$ , $\text{CH}_2$ )	combination $\nu + \delta$	4440–4200	2250–2380

usually drop by a factor between 10 and 100 from excitation level to excitation level. The low absorbance of overtones and combinations usually restricts the application range of NIR spectroscopy to liquids and solids. Absorption regions for some important groups and vibrations are given in Tab. 6.2. In addition, the short wavelength NIR range covers lowest-energy electronic transitions. Fermi and other resonances occur in the region as well [18].

NIR is increasingly used in process and environmental analysis, the food industry, agriculture, the pharmaceutical industry and polymer analysis. In-line measurement with fiber optics and rapid multi-component quantification are the most important advantages of NIR spectroscopy. In comparison to mid-infrared, NIR analysis is much faster and more versatile. Most samples are analysed in one minute or less. Often chemometric methods must be applied to determine the parameter of interest.

### 6.2.1

#### Sample Preparation and Measurement

One of the greatest advantages of NIR spectroscopy is the ease of sample handling. Often, common transmission and reflection techniques can be used for nondestructive analysis. Thus, NIR analysis eliminates the sampling errors caused by manual handling and reagent or solvent contamination.

For liquids, quartz cells like those used in UV/VIS can be used. Because of the weak absorption coefficients most samples need not be diluted, and a cell of large pathlength, up to some centimeters, can be used. NIR spectra of some common solvents are represented in Fig. 6.7. Tetrachloromethane is very suitable because all C–Cl vibrations occur far away from the NIR range. In contrast, water and ethanol are not suitable due to their strong O–H absorption bands. For the

**Reference Data Table 1**  
**Method Parameter Reference Sheet**

<b>Method:</b>	IR spectroscopy
<b>Characterized Parameter</b>	Absorbance
<b>Type of Information:</b>	Functional groups, structure, concentration, identity
<b>Required User Skills</b>	Unskilled for routine measurements

### Sample

	Excellent	Good	Fair	Poor	Problems
Pure compound	+				
Multi-analyte	+				
Gaseous		+			
Liquid	+				
Solid	+				
Matrix effects / matrix assisted			+		
Size		+			
Trace			+		
Cross sensitivity	+				
Identification	+				
Quantification	+				

**Equipment (typical data):**

CW/Fourier	Fourier
Internal/external reference	External reference
Single/double beam	Single and dual beam
Destroying sample	Non-invasive
Sequential / simultaneous	Simultaneous
Source	Glowbar
Dispersion by:	
filter / monochromator	
nondispersing	Nondispersing
Absorption / emission / scattering	Absorption
Ratio recording	Yes

**Spectrometer (typical parameter)**

Frequency / wave number / wavelength range	4000 cm <sup>-1</sup> to 400 cm <sup>-1</sup> (2.5 μm to 25 μm)
Time per spectrum	0.5 to 10 minutes
Noise Signal/noise at high/low concentr. limit	1000 : 1 at high concentration 5 : 1 at low concentration
Reproducibility (wavelength, signal)	± 1 cm <sup>-1</sup>
Spectra overlay (single/multi)	Multi
Sampling (number of times)	64 to 1024
Resolution (nm, s <sup>-1</sup> , cm <sup>-1</sup> , molecular weight)	1 cm <sup>-1</sup>
Limit of detection	mM
Time required for analysis Preparation	0 to 10 minutes
Measurement	0.5 to 10 minutes
Evaluation	10 to 30 minutes
Cost per sample (Euro)	10 (estimated)

**Techniques yielding similar information:** Raman spectroscopy

**Typical features of attached computers:**

Computers (not built-in) are part of modern MIR spectrometer. The supplied software manages data acquisition and analysis. Additional software for chemometric evaluation is available.

**Typical application (as demonstrated in chapter):** Qualitative and quantitative analysis, in-situ measurements, process control.

**Preferable samples:** Solutions in percent concentration

**Problematic samples:** Water as solvent, weakly absorbing samples

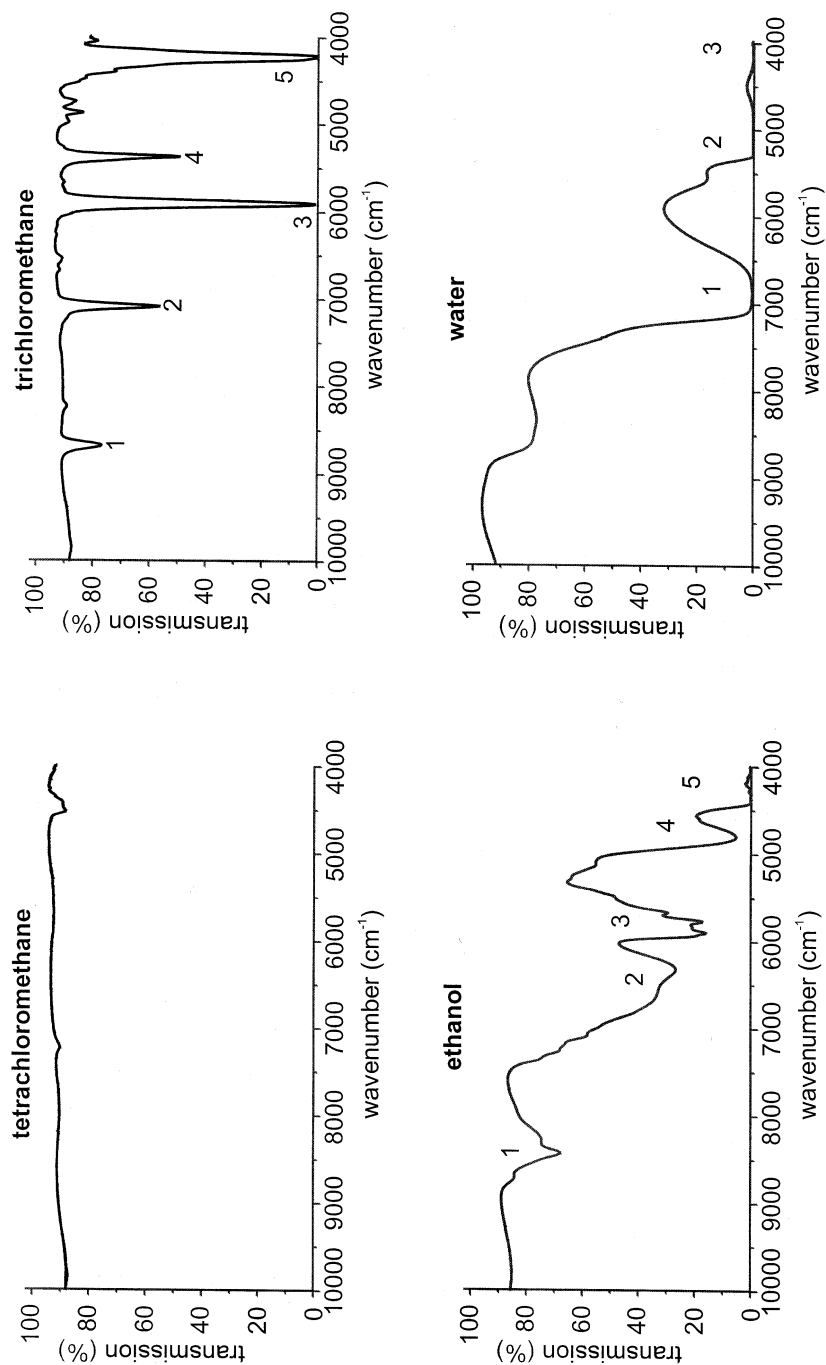


Fig. 6.7 NIR spectra of some typical solvents, recorded in 2 mm quartz cells. For band assignments see Tab. 6.3.

same reason, drying may be necessary for native samples (agriculture and food analysis).

Weakly scattering solids can be investigated by transmission techniques. For strongly scattering samples, diffuse reflection accessories must be used.

Slight temperature variations may lead to a shift in band positions and to changes in absorbance. This is of particular importance for quantitative evaluation of NIR spectra. The NIR spectra of water at several temperatures, shown in Fig. 6.8, reveal band shifts towards shorter wavelengths, which arise from changes in the average size of molecular clusters and from weakening of strongly H-bonded states [19]. Temperature effects of this size in aqueous samples can easily overlap weak absorption signals from weakly concentrated analyte.

The availability of low-cost, highly transmitting NIR fibers has led to the widespread application of NIR fiber sensors. Fibers may simply be used as a light guide between the NIR spectrometer and the measuring point, or they may serve as a sensor by using the evanescent field of light totally reflected inside

**Table 6.3** Assignments of the most pronounced absorption bands of solvents shown in Fig. 6.7.

<b>Water</b>	<b>Ethanol</b>	<b>Trichloromethane</b>
1 2v O–H	1 3v C–H, combination C–H	1 3v C–H
2 combination	2 2v O–H, combination CH <sub>2</sub> /CH <sub>3</sub>	2 combination C–H
3 v O–H	3 2v C–H 5 combination CH <sub>2</sub> /CH <sub>3</sub> , vO–H	3 2v C–H 5 combination C–H

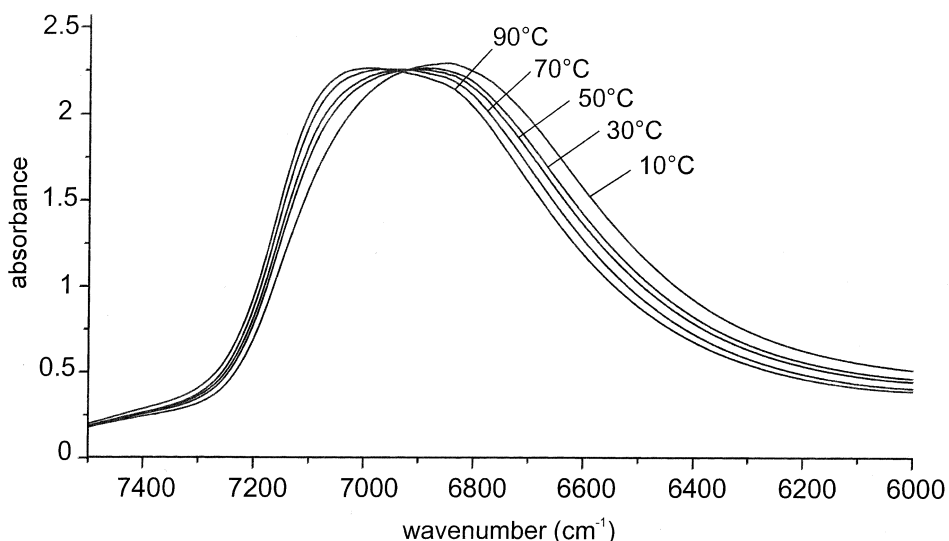


**Fig. 6.8** NIR spectra of water at different temperatures, recorded in a 2 mm quartz cell.

the fiber. NIR fiber optic sensors combined with statistical data evaluation are increasingly used for in-line monitoring of chemical compounds or reactions.

### 6.2.2

#### Applications of NIR Spectroscopy

Fiber optic sensors provide access to real-time reaction profiles and to careful control of the reactions. The need to measure product quality during a production process has driven the development of NIR fiber optic sensors. Gas, liquid and solid material can be analyzed. An important field is *environmental monitoring*. NIR in combination with fiber optics is applied to achieve information about volatile organic compounds in water and waste water, sediments, mud and solid samples. The polymer cladding (e.g. silicone) of optical fibers acts as a hydrophobic membrane that enriches non-polar compounds in water. Chlorinated hydrocarbons and aromatic substances in water can be detected by using evanescent field absorption of the fiber guided light up to the sub-ppm concentration range [18].

NIR spectroscopy has been used for more than 30 years in the *food industry and agriculture*. The main applications are determination of moisture and characterization of other compounds, e.g. protein content in grain and milk products. Usually diffuse reflection is measured because then the samples need not be prepared extensively. Compared to wet chemical analysis or other instrumental methods of analysis, NIR in particular allows rapid detection even under field conditions. Some basic characteristic wavelengths are listed in Tab. 6.4.

Moisture and hydroxyl number are important parameters, which are determined by measuring either the first overtone at  $6890\text{ cm}^{-1}$  or the combination band at  $5180\text{ cm}^{-1}$ . A few details about chemical structure are accessible by interpretation of these bands. Changes in hydrogen bonding lead to changes in the band shape and band location. Difference spectra or second derivatives must be calculated in order to detect minor chemical interactions of OH with other molecular species in the sample. The number of double bonds is another important parameter to describe the properties of fats and oils, e.g. their degree of unsaturation.

NIR spectroscopy can also be used to identify different makes or different charges of the same product. Chemometric evaluation even of very similar looking spectra provides access to the parameter of interest or enables distinction between

**Table 6.4** Typical wavelengths for NIR characterization of food [20].

Wavenumber, $\text{cm}^{-1}$	Compound
4400	lignin
4330	oil
4280	cellulose
4590	protein
4760	carbohydrate
5150	moisture

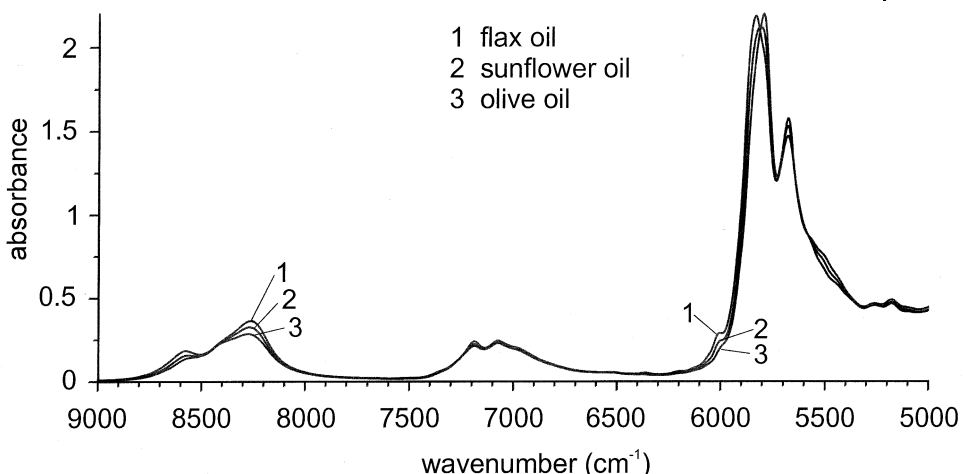


**Fig. 6.9** NIR spectra of three different edible oils. The spectra are dominated by C–H and O–H bands.

similar samples. Spectra of different edible oils are shown in Fig. 6.9. Despite the similarity of their spectra, samples can be well discriminated by statistical data analysis.

In the food industry NIR spectroscopy is the most common in-line method to monitor moisture, oil, fat and protein to analyze grains, feeds, meat, dairy and other products. Metabolites in leaves of spice plants can be determined by using NIR reflection measurements [21]. Accuracy and precision achieved are better than  $\pm 0.2\%$  [22]. On-line measurements are also made for diverse snack food products.

NIR spectroscopy is applied in the *pharmaceutical industry* to analyze raw material and drugs, and to identify packing materials. The effect of drugs, among other things, depends on the crystalline form in which the drug exists. While structural information is available in MIR, secondary interactions between several groups are often seen in NIR. Thus, polymorphism of drugs as well as isomeric purity of optically active substances can be monitored by NIR.

In the *polymer industry*, packing material, laminates including multilayer films, pellets or molded products can be analyzed by NIR. Even polymer latex particles with up to 99 % water content may be analyzed. NIR provides information about reaction mechanisms, polymerization, crystallinity, orientation, water content and hydrogen bonding, even during the process of polymer manufacture. For example the disappearance of the double bonds in polyethylene and polypropylene can be monitored. In the NIR spectrum C=C bonds lead to a combination band at about 4740  $\text{cm}^{-1}$  and a first overtone at about 6170  $\text{cm}^{-1}$ . NIR spectroscopy is applied to characterize ester-, nitrile-, or amide-based acrylic and methacrylic polymers. Other examples are the identification of polyvinylchloride, polyvinyl alcohol and polyvinyl acetates or the analysis of polymerization in epoxy and phenolic resins.

NIR is applied in many areas of *medicine, biology and biotechnology*. Optical fibers for the near-infrared and new fiber optic compact process spectrometer as well as NIR light emitting diodes (LED) permit new applications in medical diagnosis [23]. Proteins [24], blood glucose [25], cholesterol and fatty acids have been subjected to the investigations. Although *in-vivo* NIR has many problems, such as high water absorbance in tissue, light scattering, peak shift caused by temperature changes and peak overlap, the advantages of NIR are evident in the application to living tissues and cells [26]. Optical tomography systems use NIR spectroscopy to image the cerebral cortex and the level of oxygenated blood in the tissue [27]. In biotechnology NIR spectroscopy is mainly used to monitor fermentation processes and to measure biomass, nutrient products or the concentration of byproducts in real time.

NIR spectroscopy is an important method for rapid on-line monitoring of *oil and petrol production* processes. It has become an essential component in hydrocarbon processing. NIR reflection spectrometers are also used to analyze oil sand in the petroleum industry. NIR spectroscopy is used for *in-situ* quantification of liquid natural gas. Feed streams can also be monitored. Finally, NIR reflection spectroscopy is also used to determine pollution and contamination of oil and other petrochemical products in sand, and earth [28] (see Reference Data Table 2 on page 114/115).

### 6.3 Raman Spectroscopy

Raman spectroscopy is a spectroscopic method, which is complementary to IR spectroscopy. It offers various advantages over MIR and NIR spectroscopy. Since water is a weak scatterer in the VIS range, no special accessories are needed for measuring aqueous solutions. Furthermore, atmospheric gases are very weak scatterers, therefore purging of the Raman instrument is not needed. Ordinary glass is transparent in the visible and near-infrared spectral regions, where Raman spectra are excited so inexpensive liquid sample cells made from glass can be used for most Raman measurements. For remote analysis glass fiber optics can be used. The standard Raman spectral range extends down to  $10\text{ cm}^{-1}$ , so the technique is ideal for both organic and inorganic samples.

The limitations of Raman spectroscopy in comparison to IR are sensitivity and undesired fluorescence. Relatively expensive and sophisticated instrumentation also should be taken into account.

#### 6.3.1 Sample Preparation and Measurements

The alignment of optics used for delivering the laser beam to the sample and for collecting Raman scattered radiation towards the spectrometer entrance slit is very important for the effective application of Raman spectroscopy, since Raman scattering is very weak. In conventional Raman instruments this procedure is rather

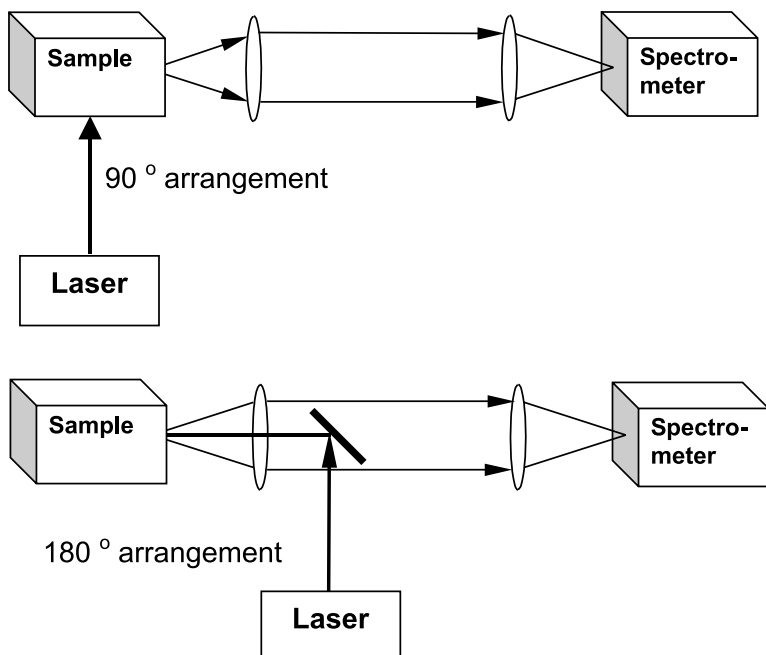


Fig. 6.10 Common sampling geometries in Raman spectroscopy.

tedious and requires some experience. In FT-Raman instruments this is a more routine task, because the alignment is based on the observation of the Raman interferogram. To collect the Raman scattering, various set-ups can be used. The most common ones are 90° collection and 180° collection (back scattering) geometry (Fig. 6.10). 0° scattering geometry is also possible, but is rarely used.

#### 6.3.1.1 Sample Illumination and Light Collection

Sample illumination and methods for collecting Raman scattered light can be subdivided into three groups: the use of conventional optics like lenses and mirrors, the use of fiber optics, and the use of optical microscopes.

A comprehensive overview of cells and sample illumination methods in Raman spectroscopy is given in [29]. Rectangular cells, spherical cells, NMR tubes or light pipes may be used. The most popular arrangements for sample illumination are shown in Fig. 6.11.

Optical fibers are increasingly used for remote Raman probing, for example to monitor chemical processes in-line or inside a reactor. The laser beam is guided to the probe head by an excitation fiber, and the Raman signal is returned to the detector by a collection fiber. Probe heads usually work in the 180° arrangement. There are two different types of fiber probes for common use in Raman spectroscopy: the concentric unfiltered fiber bundle and the filtered probe. The fiber bun-

**Reference Data Table 2**  
**Method Parameter Reference Sheet**

<b>Method:</b>	NIR spectroscopy
<b>Characterized Parameter</b>	Absorbance
<b>Type of Information:</b>	Concentration, structure
<b>Required User Skills</b>	Unskilled for routine measurements

### Sample

	Excellent	Good	Fair	Poor	Problems
Pure compound	+				
Multi-analyte	+				
Gaseous				+	
Liquid	+				
Solid		+			
Matrix effects / matrix assisted			+		
Size			+		
Trace				+	
Cross sensitivity				+	
Identification			+		
Quantification	+				

**Equipment (typical data):**

CW/Fourier	cw
Internal/external reference	External reference
Single/double beam	Single and double beam
Destroying sample	Non-invasive
Sequential / simultaneous	Sequential
Source	Tungsten lamp
Dispersion by:	
filter / monochromator	Filter or monochromator
nondispersing	
Absorption / emission / scattering	Absorption
Ratio recording	Yes

**Spectrometer (typical parameter)**

Frequency / wave number / wavelength range	12500 cm <sup>-1</sup> to 4000 cm <sup>-1</sup> (800 nm to 2500 nm)
Time per spectrum	0.5 to 5 minutes
Noise Signal/noise at high/low concentr. limit	500 : 1 at high concentration 5 : 1 at low concentration
Reproducibility (wavelength, signal)	± 5 cm <sup>-1</sup>
Spectra overlay (single/multi)	Single
Sampling (number of times)	Once
Resolution (nm, s <sup>-1</sup> , cm <sup>-1</sup> , molecular weight)	4 cm <sup>-1</sup>
Limit of detection	mM
Time required for analysis Preparation	0 to 10 minutes
Measurement	0.5 to 5 minutes
Evaluation	10 to 30 minutes
Cost per sample (Euro)	10 (estimated)

**Techniques yielding similar information:** IR spectroscopy**Typical features of attached computers:**

Computers (not built-in) are part of modern NIR spectrometer. The supplied software manages data acquisition and analysis. Additional software for chemometric evaluation is available.

**Typical application (as demonstrated in chapter):** In-line measurements, process control, quantitative analysis

**Preferable samples:** Solutions in percent concentration

**Problematic samples:** Water as solvent, weakly absorbing samples

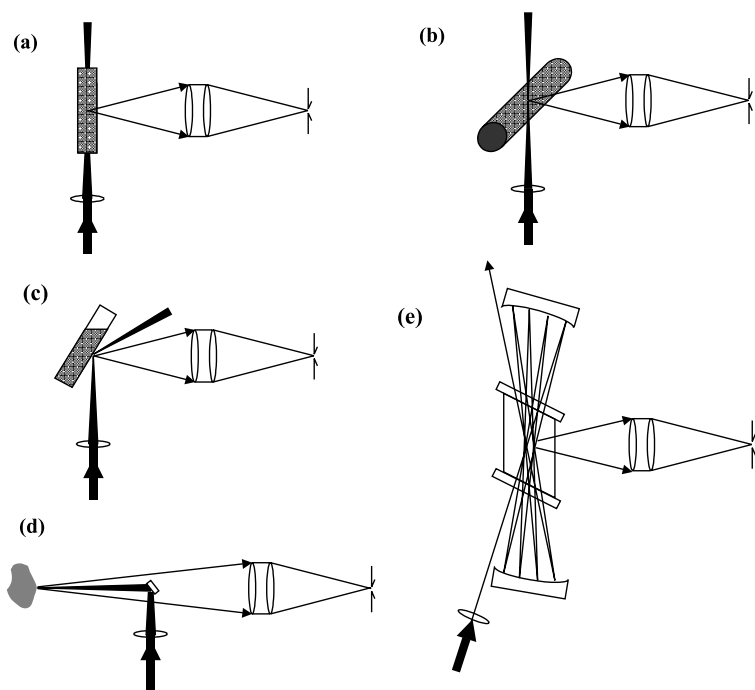


**Fig. 6.11** Sample illumination in Raman spectroscopy: (a), (b) liquid sample; (c) liquid or solid sample; (d) solid sample; (e) gaseous sample by multipath.

dle is less expensive, while the filtered probe offers better signal-to-background ratio in certain applications.

Usually the fiber bundles consist of fibers of  $100\text{ }\mu\text{m}$  core diameter, which are cemented into a cylindrical holder and then polished. The central fiber (excitation fiber) delivers laser light to the sample, while the surrounding fibers collect Raman radiation. The laser beam is focussed into the excitation fiber by a microscope objective. For coupling to the entrance slit of a dispersive spectrometer, the output ends of the collection fibers are arranged in a row, as shown in Fig. 6.12. Matching optics is only needed in the case of a difference in f/numbers between fiber and spectrometer. The fiber bundle can be immersed into liquid samples or held at a short distance from the surface of a solid sample. Fibers are usually made from silica, which itself generates Raman as well as fluorescence signals. In most cases fiber signals can be eliminated, but some noise may be introduced and weak Raman signals may be obscured. These problems are avoided by filtered probes. The basic diagram of such a probe is given in Fig. 6.13. Light emerging from the excitation fiber is collimated and diffracted by a transmission grating. All signals except the laser light are blocked by the pinhole. The laser light is then reflected from the first filter of the notch filter pair towards the sample. The excited Raman and Rayleigh scattering as well as the reflected laser light are passed back to the notch filters. These filters remove reflected laser light in order to avoid any

**Fig. 6.12** Sketch of an eight-around-one fiber probe, showing both ends of fibers.

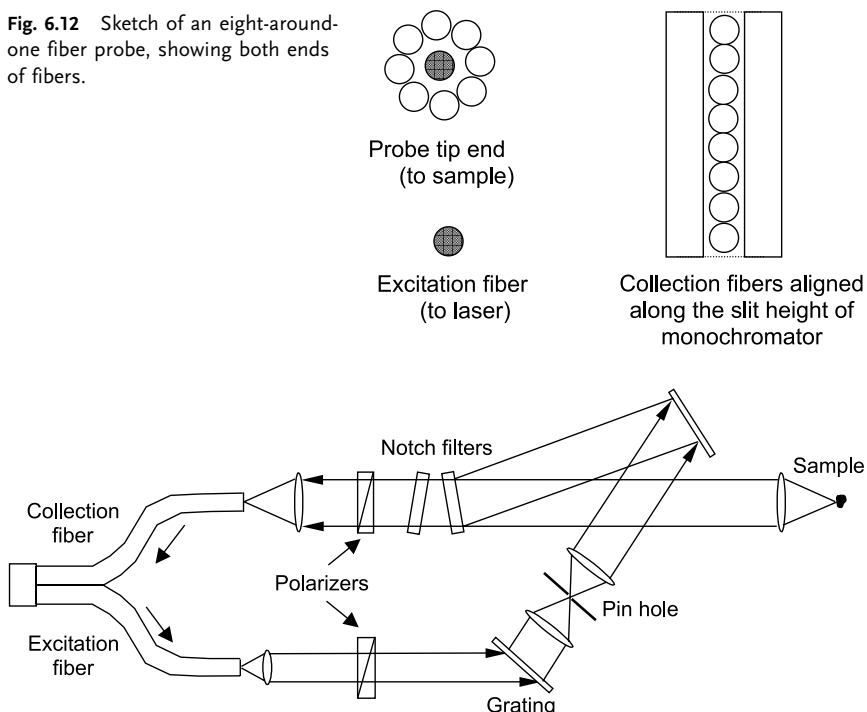


**Fig. 6.13** Basic diagram of filtered Raman fiber probe.

fiber background generation as the collected Raman light travels to the spectrometer. The use of lenses allows efficient delivery and collection with a single fiber. The advantage of such an arrangement is that once the coupling between the fibers, the laser and the spectrometer has been optimized, the fiber probe will permit spectral acquisition from a variety of liquid or solid samples without any optical realignment. Advanced fiber optics is available, in particular in the NIR region.

A sampling technique of distinctly growing importance is the Raman microscope that uses a microscope. It permits the collection of Raman images by mapping or imaging. These techniques allow investigation of samples or sample regions at 1  $\mu\text{m}$  lateral resolution and 2  $\mu\text{m}$  depth resolution. Depth resolution usually depends on the sample, in the case of transparent samples it is worse than the lateral resolution. Depth resolution can be enhanced by decreasing the depth of the focus by using a confocal Raman microscope (cf. Chapter 5.5.2).

The lateral step size in Raman mapping experiments can be as small as 100 nm. In the case of imaging, the Raman signal from the observed sample area is directed by the microscope to a CCD array detector. The wavelength range for investigation has to be selected by a tuneable filter or a set of changeable filters.

### 6.3.1.2 Polarization Measurements

The depolarization ratio  $\rho$  is usually measured in  $90^\circ$  geometry. The experimental set-up for Raman polarization measurements is shown in Fig. 6.14. Four different spectra can be measured:  $I_{VV}$ ,  $I_{VH}$ ,  $I_{HV}$  and  $I_{HH}$ , with the first index denoting the polarization of laser radiation and the second the polarization of the Raman scattered light. Actually, the last three polarized Raman spectra contain the same information ( $I_{VH} = I_{HV} = I_{HH}$ ) and the depolarization factor is defined as  $\rho = I_{VH}/I_{VV}$  (cf. Eq. (14) in Chapter 3.3). These two spectra are usually measured one after the other with the corresponding positions of the analyzer. Polarization measurements have significant value for chemical analysis. They can give important information about the molecular symmetry of an unknown (symmetry of molecular packing in crystal cell in the case of mono-crystalline samples) or give additional arguments for assignment of Raman bands.

In the case of highly symmetrical molecules (e.g. molecules having symmetry axes higher than 2nd order), the depolarisation factor  $\rho$  is equal to zero for total symmetric normal vibrations. In the case of molecules of low symmetry,  $\rho$  can vary between 0 and  $\frac{3}{4}$  for the corresponding Raman bands. For non-fully symmetric vibration of any molecule,  $\rho$  is equal to  $\frac{3}{4}$  (or to  $6/7$  in the case of excitation with nonpolarized light). This polarization rule is valid for liquids and gases. i.e. for samples with chaotically oriented molecules. In solids the situation is more complex. The spectral intensities  $I_{VV}$  and  $I_{VH}$  of crystalline samples depend on the orientation of the crystal axis with respect to the polarization of the incident light. In polycrystalline samples consisting of many small crystallites of different orientation, the scattered light undergoes multireflection at the crystallites, and the polarization information of the Raman bands is lost.

In any anisotropic system, the depolarization factor may be used as a valuable source of information about the orientation of molecules, e.g. about the orientation of polymer chains in fibers or the orientation of adsorbed molecules on surfaces.

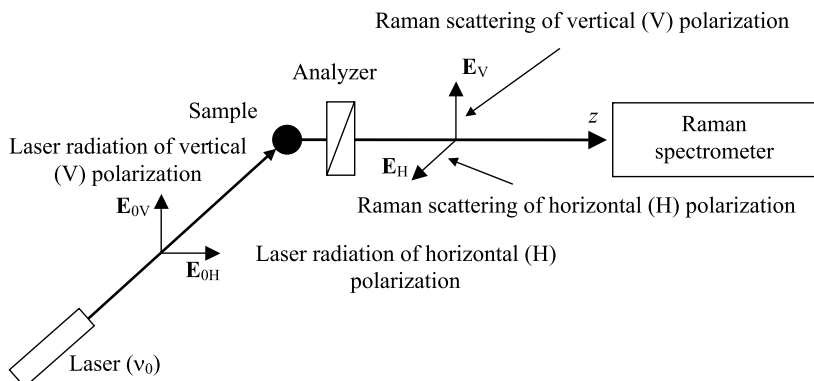


Fig. 6.14 Set-up for measuring depolarization ratios of Raman bands in  $90^\circ$  geometry.

### 6.3.1.3 Enhanced Raman Scattering

The quantum yield of the classical (or so-called linear) Raman effect is rather poor. Only a fraction of  $10^{-6}$  to  $10^{-8}$  of the exciting photons are converted into Raman photons. This excludes the detection of low concentration analytes. Moreover, due to the quantum yield of fluorescence, even traces of fluorescent impurities may mask the Raman signal by their fluorescence. Therefore, there has been much scientific effort towards the development of Raman based methods which allow one to overcome this problem. Methods to overcome these problems are Resonance Raman Scattering and Surface Enhanced Raman Scattering.

**Resonance Raman scattering (RRS)** In linear Raman spectroscopy the energy of the exciting photon is assumed to be much lower than the energy of the lowest electronic transition. If the energy of the exciting photon approaches the energy of the electronic transition, the intensity of some Raman spectral bands increases by a factor of  $10^2$  to  $10^4$  due to resonance between electronic and vibrational excitation. The selection rules RRS are completely different from those in linear Raman scattering. Overtones of normal vibrations with  $\Delta\nu = 1, 2, 3, 4, \dots$  can be observed in RRS spectra. Figure 6.15 shows the RRS of  $I_2$ , whose spontaneous Raman spectrum has only one spectral band at  $211\text{ cm}^{-1}$  with a low intensity of ca. 100 photon counts per second.

There are two physical reasons for the enhancement in RRS, the Franck–Condon enhancement and the vibronic enhancement. Both mechanisms are complicated, a detailed description is given in [30]. An application of RRS is the investigation of biological molecules like metalloporphyrins and carotenoids. These molecules have very strong electronic transitions in the VIS. The vibrations of the chromophoric part become resonance enhanced but the vibrations of the surrounding protein matrix do not. This allows observation of the chromophoric site without spectral interference from the surrounding protein. RRS is suitable

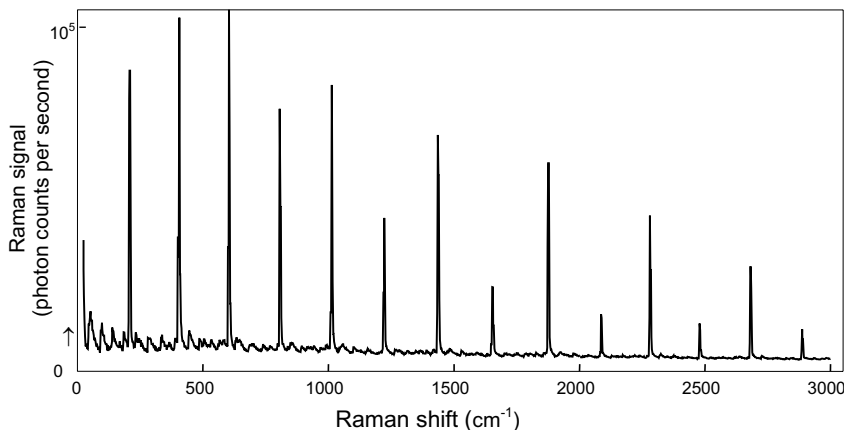


**Fig. 6.15** Resonance Raman spectrum of gaseous iodine. Argon ion laser line at  $\lambda = 514.5\text{ nm}$  was used for the excitation.

for molecules with strong VIS absorptions like fullerenes or polydiacetylenes. RRS can also be exploited in the UV, where many molecules absorb, however the high cost of equipment (lasers, optics, spectrometers) has limited UV-RRS spectroscopy to a small number of specialists.

**Surface-enhanced Raman scattering (SERS)** This effect gives rise to an enhancement of the Raman signal by up to six (or even more) orders of magnitude. As yet there is no complete theoretical understanding of this type of enhancement. Two mechanisms are taken into account to explain the SERS effect.

The first is an enhanced electromagnetic field formed at the surface of the metal. Molecules adsorbed on the metal surface experience a large increase in electromagnetic field strength compared to the strength of the incident radiation. The extent of the electromagnetic enhancement depends upon a number of factors, including the electric properties of metal, the distance of the molecule from the surface, the orientation of the molecule with respect to the normal of the surface, the energy of the incident radiation, the morphology of the surface, and the size and geometry of the surface roughness. Of particular importance is the surface roughness, which can be tailored electrochemically or by use of solid or island films. The best morphologies are small particles of less than 100 nm in size or atomic rough surfaces. Only particular metals such as silver, copper or gold can be used as the substrate in SERS technology.

The second mechanism of SERS enhancement consists in the formation of a charge-transfer complex between the metal surface and the molecule. Molecules with lone pair electrons or  $\pi$  clouds, such as aromatic amines or phenols, show the strongest SERS effect. The effect can also be seen in other electron-rich compounds like carboxylic acids.

The selection rules for SERS are essentially the same as those for the linear Raman effect. However, because the local electrical field at the surface is highest in the direction normal to the surface, only vibrations perpendicular to the surface are strongly enhanced. In order to optimise the surface enhancement effect, the laser frequency has to match the frequency of a plasma resonance. A large variety of SERS substrates are reported in the literature. The most common substrates are electrodes, colloids, metal films and silver island metal films.

Because of the huge signal enhancement, SERS is particularly useful for trace analysis and for in-situ investigations of various interfacial processes or of monolayers adsorbed on metals. However, sample preparation is a rather tedious procedure. For this reason, SERS is still more an academic tool rather than a routine analytical instrument. Some applications of SERS are given in [31].

### 6.3.2

#### Special Applications

The traditional application field of Raman spectroscopy as a complementary method to IR spectroscopy is structural analysis. In the case of molecules featuring a center of inversion, the combined evaluation of Raman and IR spectra is vital due

to the so-called mutual exclusion rule: in such molecules one part of the fundamental vibrations is IR active, the other part is Raman active only. The basics of structural analysis are described in Section 6.1 and will not be repeated here.

In a number of experimental situations, Raman is superior to IR spectroscopy, i.e. the vibrational fingerprints obtained by Raman spectroscopy are more informative:

1. A Raman spectrum from 4000 to  $10\text{ cm}^{-1}$  can be acquired in one scan, unlike the IR experiment.
2. In the case of hydrogen-bonded or wet samples, IR bands are often diffuse and broad, whereas Raman equivalents are sharp.

A survey of the advantages and special applications of FT-Raman spectroscopy is given in [32]. FT-Raman has widespread applications in biology, medicine, pharmacy, art, forensic science, inorganic materials, geology and polymers. Applications of non-linear Raman techniques (hyper-Raman effect, stimulated Raman effect, coherent anti-Stokes Raman spectroscopy (CARS)) are described in [33]. The main applications for non-linear Raman techniques are the study of gases and their temperature dependence. The particular advantage of CARS is its intense signal in the anti-Stokes spectral region, which enables investigation of fluorescent and luminescent samples.

Water is an ideal solvent for Raman studies; this is reflected in the large volume of published work on organic and inorganic compounds in *aqueous solutions*. Both identification of species present and evaluation of their concentration are feasible, thus providing information on chemical processes in aqueous solution and their rate constants, often as a function of temperature and pressure. Raman spectroscopy is an appropriate method to analyze hydrogen bonding in aqueous solution. Intramolecular interactions caused by hydrogen bond formation, or very weak intermolecular forces indicated by very low frequency vibrations (down to  $10\text{ cm}^{-1}$ ) can be investigated directly.

Rapid advances in *semiconductor technology*, including thin film formation by deposition, interface preparation or microstructuring, demand characterization techniques that provide understanding of the fundamental processes involved, including information on structural order-disorder and spatial inhomogeneity. Raman spectroscopy is used both in process control and quality assessment [34]. Typical examples of semiconductor applications are composition determination, analysis of crystal structure, surface and interface analysis, phase determination, doping, point defects, temperature influence and mechanical stress.

The most commonly used material in the semiconductor industry is silicon. The Raman spectra of crystalline and amorphous silicon differ quite markedly in the region  $\Delta\nu = 600\text{--}100\text{ cm}^{-1}$  (the region of the phonon bands), the two phases can be well characterized. For other semiconductors this difference is smaller. One should keep in mind that Raman bands from polycrystalline sample areas are similar to those from monocrystalline areas. The effect of strain can also be assessed, local stress can be studied via a Raman microscope. Silicon–metal interfaces are amenable to examination. For instance, it is possible to identify the

PtSi layer, estimate its thickness and describe its crystallographic order. Zinc blende type semiconductors, particularly gallium arsenide (GaAs) and related materials such as GaAlAs, can be studied. Concentrations of free carrier may be determined, together with the width of the space charge layer. The effect of an amorphous phosphorus overlayer on n-type GaAs can be studied. The spectroscopic information usefully complements what has been deduced from the electric properties of the material. Alloy semiconductors can be studied effectively by Raman spectroscopy, e.g. in a system like  $\text{Ga}_{1-x}\text{Al}_x\text{As}$  the value of  $x$  can be determined. As with the zinc blende type semiconductors, it is possible to determine carrier concentrations and assess the effect of ion implantation and annealing. Similarly, in the case of  $\text{Hg}_{1-x}\text{Cd}_x\text{Te}$ , the value of  $x$  may be determined.

Important targets for *biochemical and biomedical investigations* are proteins, nucleic acids and biomembranes. It is also possible to investigate the dynamics of biological systems such as living cells or to study biological interfaces. Tissue differentiation has a great potential for clinical use in the near future. The most promising medical areas for Raman applications are angiology, lithiasis, orthopedics, dentistry, ophthalmology, dermatology and pathology.

Spectra obtained with a Raman microscope can be used to investigate nerve cells containing a one-layer membrane composed mainly of proteins and long-chain phospholipids. A field, where Raman microscopy may make a major contribution, is characterization of tumors. The Raman spectra of carcinomas are dissimilar from those of the surrounding healthy tissue.

For studies by Raman spectroscopy of biomolecules, which are often not available in large amounts, SERS and RRS can be used. Raman spectra of molecules with a solubility even lower than  $5 \times 10^{-4}$  g per 100 g H<sub>2</sub>O can be obtained by means of SERS. In the case of biopolymers with chromophoric groups, Raman bands are both resonance and surface enhanced and high-resolution Raman spectra from very dilute solutions down to  $10^{-8}$  mol l<sup>-1</sup> can be measured. Summaries of biochemical and biomedical applications of Raman spectroscopy are given in [35] and [36]. A review of pharmaceutical applications of Raman spectroscopy is given in [37].

When using the SERS technique for large molecules one has to keep in mind that SERS activity decays very fast with increasing distance from the surface. In small molecules of approximate size 0.6 nm (benzene), all vibrations are enhanced. In large biomolecules with approximate size 5 nm (hemoglobin protein), only groups which are attached directly to the surface will yield surface enhancement. Native DNA in solution exhibits some 30–40 Raman bands. The most intense bands are caused by vibrations of the base residues, adenine, guanine, cytosine and thymine. DNA consists of a double-stranded helix with weak Raman scattering groups (sugar-phosphate groups) at the outside of the helix and strong Raman scattering groups (nucleic bases) located at the center of the helix. The distance from the center of DNA to the phosphate group is about 1 nm. These building blocks of DNA, when adsorbed onto a silver surface, exhibit strong SER bands. The interaction of DNA with other molecules, e.g. antitumor anthracyclines, can also be investigated by means of SERS.

There are many Raman applications in the *pharmaceutical industry* ranging from structural testing to chemical imaging. The ability to analyze samples without sample preparation leads to fast and specific identification tests for raw materials, finished products, package components and packaged products. In the *food industry*, the degree of hydrogenation of fats (number of C=C bonds in the skeletal backbone of fat molecules) can be measured in seconds. No sample preparation is needed, in contrast to the chromatographic techniques still employed for this type of analysis.

Raman spectroscopy can be useful in the synthesis and characterization of *catalytic* materials, in examining adsorbates and their reactivity on metals, metal oxide surfaces and zeolites [38]. Thin films can be characterized using the waveguide technique. SERS in combination with RRS and microRaman spectroscopy offer the possibility of detecting amounts of substance in the ng range. The sensitivity can reach detection limits at the level of highly sensitive fluorescence spectroscopy, maintaining the high structural sensitivity of Raman spectroscopy. Small metallic particles with a diameter of 10 nm, e.g. Raney nickel or platinum black, can be used for Raman enhancement. Silica- and alumina-supported particles, consisting of 10 nm particles covered with 3 nm diameter metallic islands, can also be used. An enhancement of  $10^3$ – $10^4$  was observed for molecules like CO, C<sub>2</sub>H<sub>4</sub> and C<sub>6</sub>H<sub>6</sub>. The spectra consist of a series of sharp lines of the excited vibrational modes of the adsorbed molecules superimposed on a broad, enhanced background. Ethylene has been used to study the formation of intermediates on catalytic surfaces. Ethylene is chemisorbed dissociatively as acetylene at room temperature. This is revealed by the appearance of the C=C stretching vibration at 1204 cm<sup>-1</sup> and was confirmed by inelastic electron loss spectroscopy applied to acetylene chemisorbed on Ni(111) surfaces. The strongest line in the spectrum of benzene chemisorbed at room temperature is the totally symmetric ring-breathing mode at 990 cm<sup>-1</sup>. All molecules with ring systems exhibit this characteristic band, it is the most strongly enhanced mode.

One important catalytic reaction cycle which starts from a primary gas mixture of carbon monoxide and hydrogen is the Fischer–Tropsch synthesis. Depending on the reaction parameters (temperature of the catalytic surface, gas pressure and composition of the gas mixture) a great variety of aliphatic, aromatic and even oxygen-containing compounds can be obtained. The understanding of reaction mechanisms in terms of the appearance of intermediates on the surface, their structure and symmetry, is of fundamental interest for the development of well-defined reaction pathways. The frequency of the C–H stretching Raman band is a measure of the state of hybridization of the adsorbed molecule.

The fact that Raman measurements can usually be made through glass and plastic packaging, eliminating the need to prepare samples prior to analysis, makes Raman spectroscopy very attractive for *forensic science*. The availability of commercial portable instrumentation and extended fiber optic probes makes Raman suitable for on-site forensic use, minimizing the risk of exposure of investigating personnel to potentially hazardous chemicals. For identification of explosives the SERS method has proved to be very useful. A tiny amount of explosive, diluted

in colloid solution with silver particles, is enough to produce a SERS spectrum sufficient for analysis.

Raman spectra of drugs are full of information and are unique to each substance. Very similar chemicals, e. g. amphetamine  $\times$  HCl and amphetamine sulfate or heroin and morphine, yield very different spectra. Usually such samples consist of many constituents, hence multivariate analysis (cf. Chapter 13) should be used to obtain quantitative models of drug concentrations in solid mixtures. The ability to correctly identify unknowns also depends upon the availability of high-quality reference spectra.

Raman spectroscopy has proven useful also in areas like identification of *gems*, and *art* works. A summary of the use of Raman spectroscopy for studies of art works is given in [39]. Investigations of paintings, medieval manuscripts and wall paintings, of glass, pottery, plastics, biomaterials are working fields of Raman spectroscopy. The origin and the age of such objects can be determined.

*Polymer science* is an area, where Raman methods have found their widest application. Progress has been reported across the field from synthetic thermoplastics through elastomers, including vulcanizates and biopolymers. Virtually any polymer, degraded or loaded with filler, will give a superb Raman spectrum. Liquid crystalline polymers change their structure as they are heated, which in turn gives rise to changes in their Raman spectra. A review of Raman applications in polymer science is given in [40]. Applications include polymer identification, multivariate quantitative analysis of composition, analysis of polymer microstructure such as isomers, chain sequence and endgroups, analysis of morphology such as conformation, crystallinity and molecular orientation. Furthermore, it is possible to investigate curing and degradation. Polymeric reactions (kinetics and degree of polymerization) can even be characterized in-line.

Sulfur or sulfur-containing organic compounds produce particularly intense Raman bands. This fact is employed to monitor the reaction occurring during mastication of elastomers with vulcanization agents (sulfur, ZnO and accelerators). Isomerization frequently occurs during vulcanization. Since *cis-trans* and vinylic moieties of C=C groups oscillate at distinctly different frequencies, they can conveniently be kept separate in Raman spectroscopy. A serious limitation for Raman investigations of polymeric samples is set by carbon black. Only 1 % content of carbon black renders Raman spectroscopy impossible. If it is attempted, the sample starts to burn due to strong absorption of laser light and no spectra are obtained.

Further *industrial applications* of Raman spectroscopy include identification, quality assurance, reaction monitoring and on-line process control and the analysis of gases. These applications require special conditions for the instruments like rapid measurements, a high degree of automation, reliability and robustness. Raman spectrometers equipped with multiple-fiber optics can simultaneously record data collected at several remote locations, even in a chemically hazardous environment for on-site monitoring in chemical plants. Advantages and disadvantages of Raman applications for industrial use are described in [41, 42] (see Reference Data Table 3 on page 126/127).

## 6.4

### UV/VIS Spectroscopy

Absorptions in the UV/VIS are associated with electronic transitions from the ground level to an excited state. The strongest transitions are  $\sigma \rightarrow \sigma^*$ , they are observed below 200 nm (vacuum UV). Typical examples are C–C and C–H bonds. Because all molecules include  $\sigma$  electrons,  $\sigma \rightarrow \sigma^*$  transitions constitute the short-wavelength cut-off of the routine UV/VIS range. Saturated compound with pairs of free electrons exhibit  $n \rightarrow \sigma^*$  transitions in a wavelength range from 150 to 250 nm, their absorption coefficients do not exceed  $1000 \text{ l cm}^{-1} \text{ mol}^{-1}$ . Most UV/VIS investigations are based on  $n \rightarrow \pi^*$  or  $\pi \rightarrow \pi^*$  transitions, which occur across the UV/VIS range and result from unsaturated groups. Typical absorption coefficients of  $n \rightarrow \pi^*$  transitions are below  $100 \text{ l cm}^{-1} \text{ mol}^{-1}$ , while absorption coefficients of  $\pi \rightarrow \pi^*$  transitions exceed  $1000 \text{ l cm}^{-1} \text{ mol}^{-1}$ . Absorptions of transition metal ions are caused by their 3d and 4d electrons, whereas 4f and 5f electrons are excited in lanthanide and actinide ions. Absorption bands of d and f electrons are sharper than those of most chromophores because the inner orbitals are largely shielded from external influences. Transitions of donor electrons to an acceptor orbital (charge transfer complexes) originate in inorganic as well as organic compounds, their absorption coefficients usually exceed  $10000 \text{ l cm}^{-1} \text{ mol}^{-1}$ . Band transitions in solids also lead to UV/VIS absorptions. Such transitions may occur between valence and conduction bands or between a band and a localized energy level in the forbidden zone. Such conditions may occur for instance in the case of lattice defects or point defects.

A number of historic terms are still used in UV/VIS spectroscopy:

- Chromophore: system which is responsible for the absorption.
- Auxochrome: substituent which leads to shift of the absorption maximum.
- Bathochromic effect: red shift (towards longer wavelength) of an absorption maximum.
- Hypsochromic effect: blue shift (towards shorter wavelength) of an absorption maximum.
- Hyperchromic effect: increasing absorption intensity.
- Hypochromic effect: decreasing absorption intensity.

#### 6.4.1

##### Sample Preparation

Samples are prepared as described in the preceding subchapters, mostly by dilution with a suitable solvent. The application range of solvents is given by their short wavelength cut-off (Tab. 6.5).

Water and ethanol are good solvents for most samples. Both are cheap and transparent down to about 210 nm. Hexane and other hydrocarbons are more suitable for less polar samples. The latter solvents interact only weakly with the solute, so that the fine structure of the absorption band may be revealed much better.

**Reference Data Table 3**  
**Method Parameter Reference Sheet**

<b>Method:</b>	Raman spectroscopy
<b>Characterized Parameter</b>	Intensity of Raman scattering
<b>Type of Information:</b>	Functional groups, structure, concentration, identity
<b>Required User Skills</b>	Skilled in preparation of samples and carrying out the measurements

### Sample

	Excellent	Good	Fair	Poor	Problems
Pure compound	+				
Multi-analyte	+				
Gaseous				+	
Liquid		+			
Solid		+			
Matrix effects / matrix assisted			+		
Size	+				
Trace				+	
Cross sensitivity	+				
Identification	+				
Quantification		+			

**Equipment (typical data):**

CW/Fourier	CW
Internal/external reference	Internal reference
Single/double beam	Single beam
Destroying sample	Non-invasive, can be destructive for absorbing samples
Sequential / simultaneous	Simultaneous
Source	Laser
Dispersion by:	
filter / monochromator	Polychromator
nondispersing	
Absorption / emission / scattering	Scattering
Ratio recording	No

**Spectrometer (typical parameter)**

Frequency / wave number / wavelength range	Raman shift from 50 cm <sup>-1</sup> to 4000 cm <sup>-1</sup>
Time per spectrum	0.5 to 10 minutes
Noise Signal/noise at high/low concentr. limit	500 : 1 at high concentration 5 : 1 at low concentration
Reproducibility (wavelength, signal)	± 1 cm <sup>-1</sup>
Spectra overlay (single/multi)	Multi
Sampling (number of times)	64 to 1024
Resolution (nm, s <sup>-1</sup> , cm <sup>-1</sup> , molecular weight)	1 cm <sup>-1</sup>
Limit of detection	µM
Time required for analysis Preparation	0 to 10 minutes
Measurement	0.5 to 10 minutes
Evaluation	10 to 30 minutes
Cost per sample (Euro)	30 (estimated)

**Techniques yielding similar information:** IR spectroscopy**Typical features of attached computers:**

Computers (not built-in) are part of modern MIR spectrometer. The supplied software manages data acquisition and analysis. Additional software for chemometric evaluation is available.

**Typical application (as demonstrated in chapter):** Qualitative and quantitative analysis, in-situ and in-vivo measurements, process control.

**Preferable samples:** Neat liquids and solids

**Problematic samples:** Fluorescent and totally absorbing (black or umbra) compounds

**Table 6.5** Cut-off wavelengths of common solvents.

At the cut-off, the transmission drops below 60% at an optical path of 1 cm.

Solvent	Cut-off wavelength (nm)
hexane	200
ethanol	210
water	210
methanol	210
acetonitrile	215
cyclohexane	215
chloroform	250
carbon tetrachloride	280
benzene	280
pyridine	310

All solvents influence the position of the absorption bands.  $n \rightarrow \pi^*$  absorption bands are shifted towards shorter wavelengths upon increasing solvent polarity, whereas  $\pi \rightarrow \pi^*$  transitions become red shifted upon increasing solvent polarity. Forces between the solvent and the sample lead to a lower energy level of both the excited and unexcited levels. The effect also influences  $n \rightarrow \pi^*$  transitions but the stronger blue shift resulting from solvation of lone pairs may cover the weaker red-shift (Fig. 6.16).

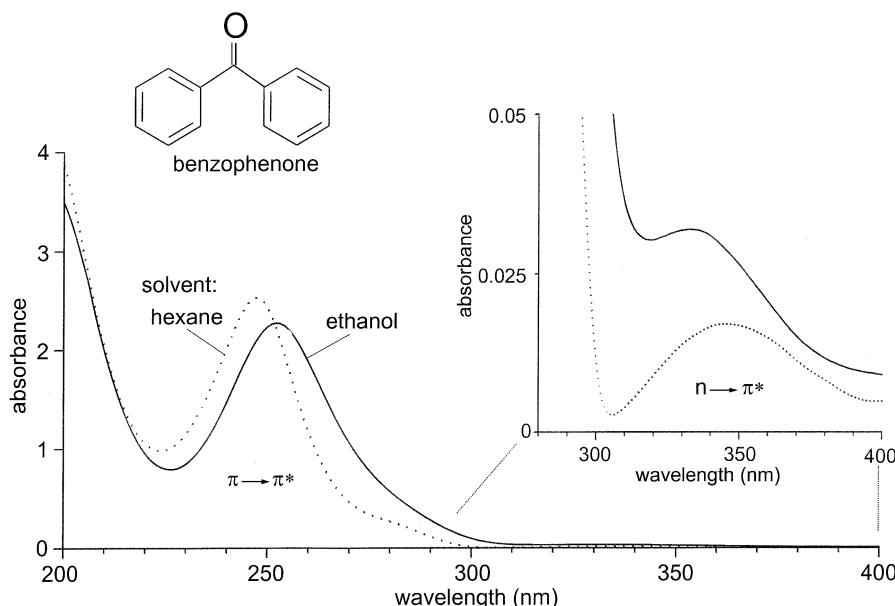


**Fig. 6.16** Shift in absorption bands of benzophenone dissolved in either ethanol or in hexane. The more polar ethanol leads to a red-shift of  $\pi \rightarrow \pi^*$  and to a blue-shift of  $n \rightarrow \pi^*$  transitions.

## 6.4.2

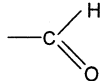
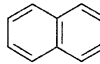
**Structural Analysis**

Locations of the typical UV absorption bands of representative chromophores are listed in Tab. 6.6. Substitution leads to a bathochromic shift of the band maximum. Conjugation of  $\pi$  electrons leads to lower  $\pi^*$  energy levels. As the number of double bonds in conjugation increases, the absorption maximum will shift towards longer wavelengths. In coincidence with the spectral shift the absorption coefficient will increase (Fig. 6.17). Besides the number of double bonds in a long chain polyenes, changes from *cis*- to *trans*-configuration may also lead to red shift and increasing absorbance.

The Woodward rules provide values for the estimation of positions of absorption bands for dienes. The calculation is based on typical parent compounds and takes into account the red-shift increments by additional conjugated double bonds and by further auxochromes:

Parent diene: acyclic	217 nm
heteroannular	214 nm
homoannular	253 nm
$\alpha, \beta$ -unsaturated carbonyl	222 nm

**Table 6.6** Absorption of representative chromophores.

<i>Chromophore</i>	<i>Band maxima, nm</i>
$-\text{C}\equiv\text{C}-$	175 195 225
$>\text{C}=\text{C}<$	175
$>\text{C}=\text{O}$	160 185 280
	210 280
	184 205
	255 220 275 310
$\text{R}-\text{NO}_2$	205
$\text{R}-\text{ONO}$	225

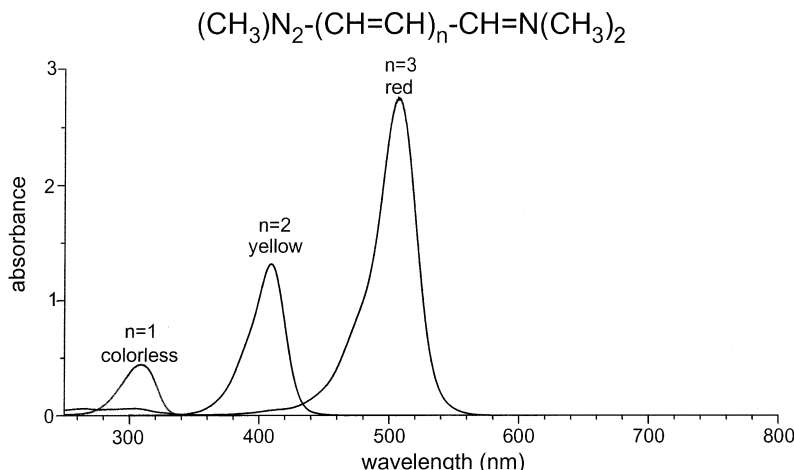


**Fig. 6.17** UV/VIS spectra of polymethines. Due to the increasing number of double bonds the absorption maximum shifts towards longer wavelengths and the absorbance increases.

Additions for each substituent:

double bond extending the conjugation	30 nm
exocyclic double bond	5 nm
each alkyl group or ring residue	5 nm
-OR	6 nm
-SR	30 nm
-NR <sub>2</sub>	60 nm
-Cl, -Br	5 nm

A weak band in the 275–300 nm range is an indicator of a ketone or aldehyde carbonyl group. Substituents like OH, NH<sub>2</sub>, NHR or halogen shift the n → π\* transition towards shorter wavelengths. Conjugation of a C=O group with C=C bonds shifts the π → π\* transition towards the VIS range.

The π → π\* transitions in *benzene* and *benzene derivates* lead to absorption bands in the range 160–270 nm. Although four transition  $\pi_{2/3} \rightarrow \pi_{4/5}^*$  are expected in benzene, only three bands can be observed due to a degenerate state. The band at 250 nm also shows vibrational fine structure as Fig. 6.18.

In *disubstituted benzenes*, *p*-substitution causes a red shift of the main absorption bands, whereas *o*- or *m*-substitution does not shift the bands much (Fig. 6.19).

Spectra of *polycyclic aromatic hydrocarbons* may be used as fingerprints for identification of the compounds. Highest and lowest orbitals are not degenerate so that four transitions may occur. Upon increasing annulation, the bands shift towards longer wavelengths. *Heteroaromatic compounds* show roughly the same effects as their corresponding hydrocarbons. Spectroscopic effects caused by the heteroatom depend on the electronic properties and on the orientation of the substituent.

*Proteins* show typical absorptions in the range 190–350 nm. Peptide bonds have an intense π → π\* transition between 190 and 210 nm. The n → π\* transition at

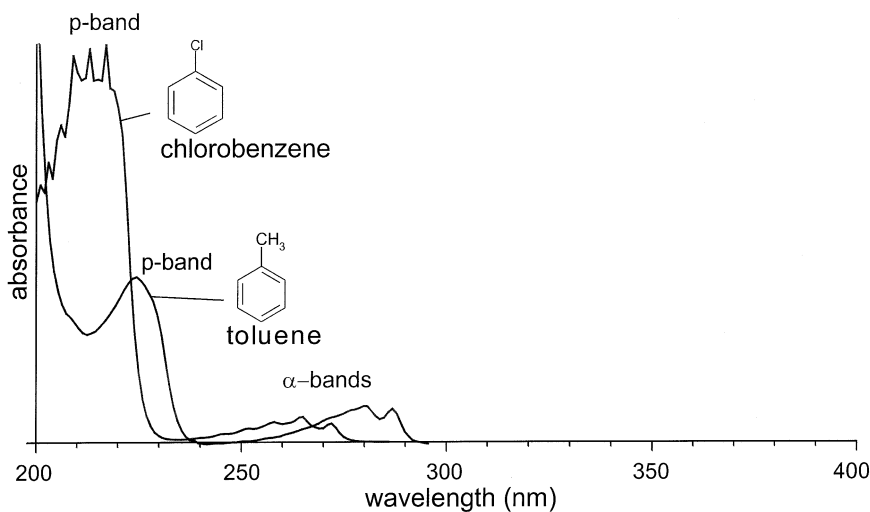


**Fig. 6.18** UV/VIS absorption spectra of chlorobenzene and toluene. Both p- and  $\alpha$ -bands show vibrational fine structure. Toluene was 5-fold less concentrated than chlorobenzene. Solvent: n-hexane.

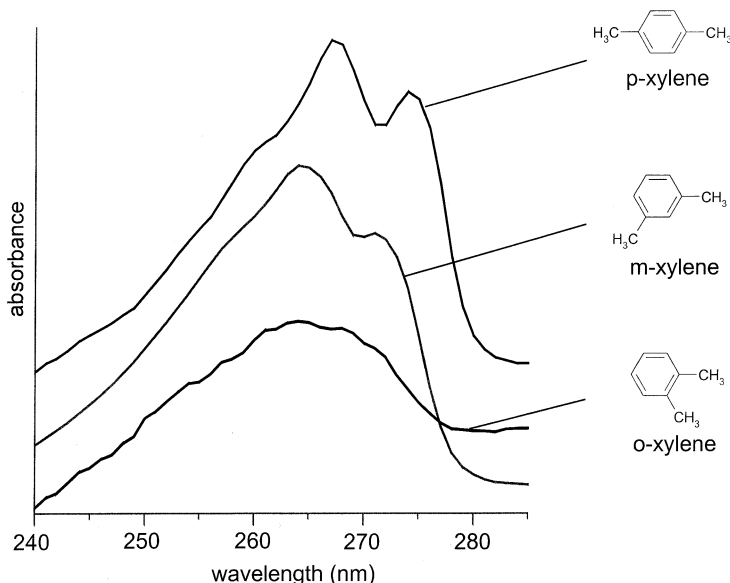


**Fig. 6.19** UV/VIS spectra of xylenes. The red shift increases from *o*- via *m*- to *p*-substitution.

210–220 nm is weak, as it is forbidden, and forms a shoulder on the  $\pi \rightarrow \pi^*$  absorption band.

Aromatic amino acids have bands between 210 and 280 nm. These bands are commonly used to determine the total protein concentration in solution. Proteins may have colored prosthetic groups, such as heme, Cu complexes and covalently

**Table 6.7** Absorption maxima of some amino acids.

Amino acid		Band maxima, nm
histidine		210
tryptophan		220, 280
tyrosine		195, 222, 275
L-cysteine		235
L-cystine		250
phenylalanine		190, 205, 255

bound coenzymes. Some proteins show absorption due to changes in the pH. For example the chromophore of tyrosine is the phenolic group. Upon decreasing the pH the maximum absorption is shifted from 275 to 295 nm. Proteins show a slight sensitivity to the polarity of the environment; this arises from the aromatic side chains and their interaction with polar groups. An increase in non-polar constituents leads to a red shift of the absorption maximum. Tyrosine and tryptophan, especially, show such environmental sensitivity which can be used to detect conformational differences in different states of a protein (Tab. 6.7).

The aromatic l-amino-acids tryptophan, tyrosine and phenylalanine are responsible for protein absorption in the UV. The aromatic side-chains of amino acids often have characteristic spectra. UV/VIS spectroscopy offers the advantages of being non-degrading to the sample.

#### 6.4.3 Special Applications

The color of metal complexes is basically controlled by three kinds of transition: charge-transfer,  $\pi \rightarrow \pi^*$  and  $n \rightarrow \pi^*$  transitions in complexes with organic ligands, d-d transitions within the metal ion. The latter are usually weaker than the former two, nevertheless the color of aqueous solutions of transition metals is caused by

d–d transitions. Due to splitting of d-orbitals in a ligand field or crystal field, (Fig. 6.20), absorptions at longer wavelengths may occur. UV/VIS spectra of Ti ions with and without ligand field splitting are shown in Fig. 6.21.

The degree of splitting depends on several factors: the charge on the metal, the size of the metal and the nature of the ligand. It is possible to correlate empirically the various ligands in a sequence according to their ability to split the orbital. The cyanide anion has the strongest ligand field in the so-called spectrochemical series:

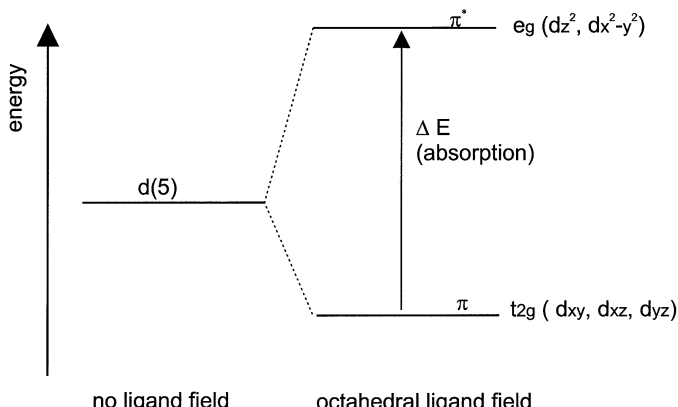


**Fig. 6.20** The octahedral ligand field splits the d orbital into two levels, which give rise to a new absorption band.

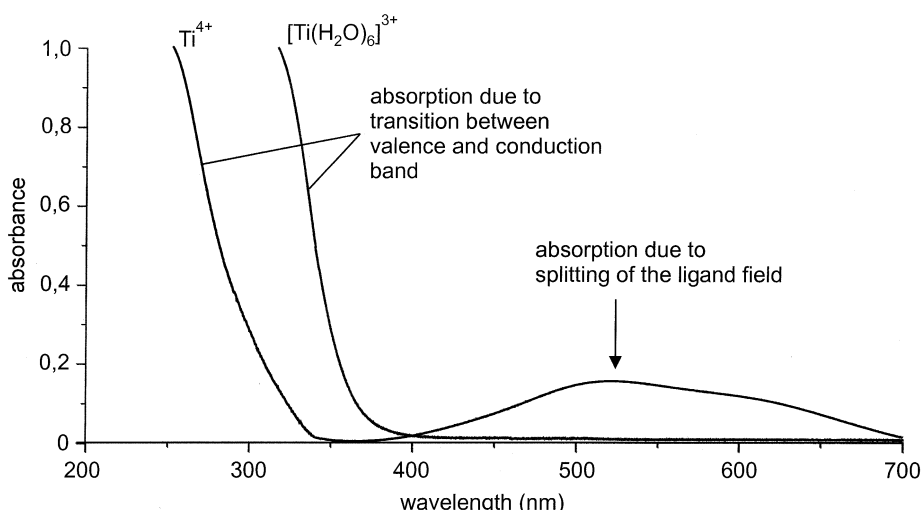


**Fig. 6.21** UV/VIS spectra of  $\text{Ti}^{4+}$  and  $\text{Ti}^{3+}$  complexes.  $\text{Ti}^{3+}$  has an octahedral ligand field where the d-level is split into two levels. Transitions between the latter cause an additional absorption band at 510 nm. The absorption edges around 300 nm arise from a transition between the valence and the conduction band.

Metal complexes with organic ligands show different spectroscopic effects, dependent upon whether the metal–ligand bonds are covalent or ionic. If the metal–ligand bond is essentially ionic only small changes occur, the spectrum of the complex being similar to that of the protonated ligand. On the other hand, the spectrum is significantly changed for complexes with strong covalent metal–ligand bonds, such complexes are highly colored.

Charge-transfer transitions may occur in the case of covalently bound ligand orbitals and empty or anti-bonding metal orbitals. Organic ligands forming charge transfer complexes are often used in the analysis of ions such as Fe, Cu, Cd or Zn.

The porphyrin dyes hemoglobin and chlorophyll are biologically important. Both are octahedral metal complexes, the proteins being bound to the central atom. In the hemoglobin molecule there are five ligand positions occupied by histidine.

In most *semiconductors* the gap between the valence and conduction bands gives rise to a transition in the UV/VIS range. Such transitions produce a UV/VIS absorption edge (Fig. 6.22).

The absorption edge  $\lambda_{\text{gap}}$  may be expressed by

$$\lambda_{\text{gap}} = \frac{h}{W_0} c$$

where  $W_0$  is the binding energy,  $h$  is the Planck constant and  $c$  is the speed of light in vacuum. If  $W_0 > 3.1$  eV, the semiconductor is transparent, whereas crystals with  $W_0 < 1.5$  eV absorb across the whole UV/VIS range and look like metals. Gap transition energies and corresponding wavelengths for a range of semiconductors are given in Tab. 6.8.

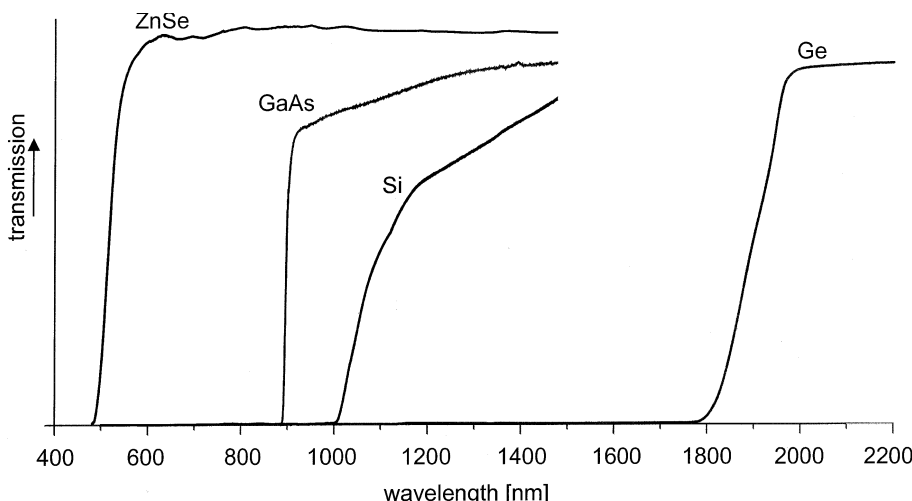


Fig. 6.22 UV/VIS absorption edges of selected semiconductors.

**Table 6.8** Gap transition energies of relevant semiconductors.

<i>Semiconductor</i>	$\lambda_{\text{gap}} \text{ eV}$	<i>nm</i>
ZnO	3.44	360
SiC	3.0	413
CuO	2.15	576
GaAs	1.40	885
Si	1.17	1059
ZnS	0.91	1362
GaSb	0.81	1530
Ge	0.66	1875
InAs	0.36	3443
PbS	0.29	4274
InSb	0.23	5390

In UV/VIS spectra of semiconductors with an indirect band transition (photon-phonon excitation), the absorption band edge may indicate a higher binding energy  $W_0$ . Additional energy levels may occur in imperfect semiconductor crystals. These energy levels are often situated between the valence and conduction band and lead to absorption at greater wavelengths. Other processes like the electronic interaction between an excited electron and a hole may lead to intrinsic band changes. A well-known example is the absorption band edge of CuO where additional narrow absorption bands occur.

Band structure details of *insulators* can be determined from their UV/VIS spectra. Defects in the crystal produce electronic levels within the gap between the conduction and the valence bands. Spectroscopic measurements at low temperature allow the investigation of the phonon structure of a crystal. Absorptions due to lattice or point defects can be used to describe the optical and electronic properties of the insulator. For example, Cr in  $\text{Al}_2\text{O}_3$  crystals leads to an intense color change of the crystal. Many so-called *color centers* are based on lattice defects caused by intercalation of atoms in the crystal lattice.

For further reading please see [43, 44] (see Reference Data Table 4 on page 136/137).

## 6.5

### Fluorescence Spectroscopy

After the appearance of the first book on fluorescence in 1951 [45], fluorescence spectroscopy became a widely used scientific tool in biochemistry, biophysics, and in material science. In the last few years, however, several new applications based on fluorescence have been developed, promoting fluorescence spectroscopy from a primarily scientific to a more routine method. The phenomena of fluorescence is for example exploited in simple analytical assays in environmental science and clinical chemistry, in cell identification and sorting in flow cytometry, and in imaging of single cells in medicine. The analyte, whose light emission is investi-

**Reference Data Table 4**  
**Method Parameter Reference Sheet**

<b>Method:</b>	UV/VIS spectroscopy
<b>Characterized Parameter</b>	Absorbance
<b>Type of Information:</b>	Concentration, structure
<b>Required User Skills</b>	Unskilled for routine measurements

### Sample

	Excellent	Good	Fair	Poor	Problems
Pure compound	+				
Multi-analyte		+			
Gaseous					+
Liquid	+				
Solid	+				
Matrix effects / matrix assisted			+		
Size		+			
Trace		+			
Cross sensitivity				+	
Identification				+	
Quantification	+				

**Equipment (typical data):**

CW/Fourier	cw
Internal/external reference	External reference
Single/double beam	Single and double beam
Destroying sample	Non-invasive
Sequential / simultaneous	Sequential
Source	Tungsten lamp, D <sub>2</sub> lamp
Dispersion by:	
filter / monochromator	Filter or monochromator
nondispersing	
Absorption / emission / scattering	Absorption
Ratio recording	Yes

**Spectrometer (typical parameter)**

Frequency / wave number / wavelength range	200 nm to 800 nm
Time per spectrum	0.5 to 5 minutes
Noise Signal/noise at high/low concentr. limit	10000 : 1 at high concentration 5 : 1 at low concentration
Reproducibility (wavelength, signal)	± 0.1 nm
Spectra overlay (single/multi)	Single
Sampling (number of times)	Once
Resolution (nm, s <sup>-1</sup> , cm <sup>-1</sup> , molecular weight)	1 nm
Limit of detection	μM
Time required for analysis Preparation Measurement Evaluation	1 to 10 minutes 0.5 to 5 minutes 20 to 60 minutes
Cost per sample (Euro)	10 (estimated)

**Techniques yielding similar information:****Typical features of attached computers:**

Computers (not built-in) are part of modern UV/VIS spectrometer. The supplied software manages data acquisition and analysis.

**Typical application (as demonstrated in chapter):** Characterization of organic compounds, biological samples, semiconductors, quantitative analysis

**Preferable samples:** Molar till micromolar solutions

**Problematic samples:** Gaseous samples, highly absorbing samples, scattering samples

**Table 6.9** References for fluorescence data evaluation.

<b>Spectroscopic method</b>	<b>Basic parameter characterized</b>	<b>References</b>
Steady-state fluorescence	Quantum yield	48
Time-resolved fluorescence	Lifetime	46, 47
Fluorescence correlation spectroscopy	Particle number, diffusion time	216
Fluorescence recovery after photobleaching	Rate and extent of recovery	166
Application of total internal reflection fluorescence	Dependent on the combined method	171

gated, is often called a “dye”. Fluorescence measurements give information about the photophysical properties of the dye as well as about the chemical and physical nature of the surroundings of the dye.

### 6.5.1

#### Sample Preparation and Measurements

Beside the classical sampling techniques using different types of cuvettes, there are several advanced ways of detecting the fluorescence signal. The use of fiber optics allows the measurement of fluorescence in whole organs *in vivo*. When looking at cells one can use cell culture plates or flow cytometry. Selected spots within a cell can be monitored using classical, confocal, or multiphoton microscopy (see Chapter 5).

Since each of the measurement techniques provides different information based on different ways of detecting the fluorescence signal, the data evaluation is different for each method. Table 6.9 lists the references dealing with the mathematical data treatment and evaluation of the basic fluorescence techniques. Some details of fluorescence data treatment are outlined in Chapter 13.

##### 6.5.1.1 Fluorescence Quantum Yield and Lifetime

In the gas phase or in non-interacting solvents and in the absence of other photophysical processes (cf. Fig. 6.23) the fluorescence intensity  $F$  detected over a certain emission wavelength range decays following a mono-exponential decay law with an average lifetime  $\tau$ . The rate constant of this fluorescence decay  $k$  ( $= 1/\tau$ ) represents the sum of the emissive rate of the fluorophore  $k_0$  ( $= 1/\tau_0$ ) and the rate constants of the two radiationless processes, internal conversion and intersystem crossing,  $k_{ic}$  and  $k_{isc}$ , respectively. The radiative lifetime  $\delta_0$  can be correlated with the transition dipole moment  $M$  by

$$\tau_0 \approx \text{constant} / k_{\text{ave}}^3 n^2 |M|^2 \quad (1)$$

where  $n$  is the refractive index of the solvent and  $k_{\text{ave}}$  the average wavenumber of the center of gravity of the fluorescence emission spectrum. The natural lifetime  $\tau_0$

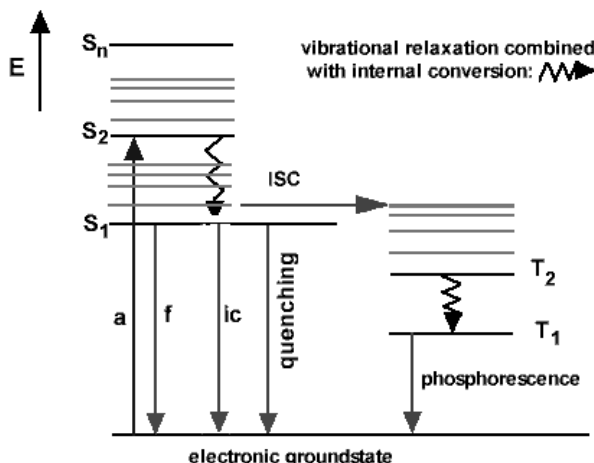


**Fig. 6.23** Jablonski diagram illustrating the creation and fate of an excited singlet state, including absorption (a), fluorescence (f), internal conversion (ic), intersystem crossing

(isc), vibrational relaxation, and collisional quenching. Not included are processes like solvent relaxation, energy transfer, and photochemical reactions.

can be considered as a photophysical constant of a chromophore surrounded by a defined solvent shell. In the case of planar aromatic systems it appears to be temperature-independent [46]. Since the internal conversion and intersystem crossing processes compete with fluorescence for deactivation of the lowest excited singlet state, not all will return to the ground state by fluorescence (Fig. 6.23). The fraction of excited molecules that do fluoresce is called the quantum yield  $\phi$ . In terms of the above defined rate constants and lifetimes,  $\phi$  is given by:

$$\phi = k_0 / (k_0 + k_{\text{ic}} + k_{\text{isc}}) = \tau / \tau_0 \quad (2)$$

The fluorescence lifetime  $\tau$  can be determined directly by monitoring the decay curve of fluorescence intensity following a brief excitation pulse [48] or by detecting the emission delay of intensity modulated excitation light [47]. Using a standard steady-state fluorometer the quantum yield  $\phi$  is determined, usually by comparison with standard compounds of known quantum yield [49].

#### 6.5.1.2 Fluorescence Quencher

A fluorescence quencher is a compound, the presence of which leads to a decrease in the fluorescence quantum yield and lifetime of the examined chromophore. The quenching system can be molecules or ions added to the solution which come into molecular contact with the chromophore, introducing new or promoting already existing non-radiative pathways (solute quenching). Further possibilities are self-quenching by other molecules of the same dye type and quenching by solvent molecules. In any case the quenching term  $k_Q [Q]$  has to be added to Eq. (2), yielding

$$\phi = k_0 / (k_0 + k_{ic} + k_{isc} + k_Q [Q]) \quad (3)$$

where  $k_Q$  is the bimolecular quenching constant and  $[Q]$  the concentration of the quencher.

**Solute quenching** Solute quenching reactions are a very valuable tool for the study of proteins, membranes, and other supra- or macromolecular assemblies and can provide information about the location of fluorescent groups in the examined molecular structure. A fluorophore that is located on the surface of such a structure will be relatively accessible to a solute quencher (for a list of quenchers see Tab. 6.10). The quenching agent will quench a chromophore that is buried in the core of the molecular assembly to a lesser degree. Thus, the quenching experiment can be used to probe topographical features of the examined structure and to detect structural changes that may be caused by addition of external compounds or changed physical conditions. In normal quenching experiments the solute is added successively to the probe. The analysis of the dependence of the fluorescence intensity,  $F$ , quantum yield,  $\phi$ , or lifetime,  $\tau$ , yields quantitative information about the accessibility of the chromophore within the macro- or supramolecular structure.

Depending on the chemical nature of the quenching agent as well as that of the chromophore one has to distinguish between two forms of quenching: dynamic and static quenching. Static quenching results from the formation of a non-fluorescent complex between fluorophore and quencher already in the ground state. A characteristic of static quenching is that increasing quencher concentration decreases the fluorescence intensity or quantum yield, but does not affect the fluorescence lifetime. A further characteristic feature of static quenching is its decrease with increasing temperature, as the stability of the complexes between the fluorophore in the electronic ground state and the quencher is generally lower at higher

**Table 6.10** List of selected solute quenchers.

Type of fluorophore	Quencher	References
Indole	Carboxy groups, chlorinated compounds, Dimethylformamide	51–53
Tyrosine	Disulfides	54
Tryptophan	Acrylamide, histidin, succinimide, trifluoroacetamide, iodide, disulfides	55–58
Naphthalene	Halogens, nitroxides	59, 60
Anthracene	Amines, halogens, thiocyanate	61, 62
Anthranoyloxy probes	Tetracain	63–65
Quinolinium ions and their betains	Chloride, bromide, iodide	66
Pyrene	Halothane	67–69
Carbazole	Amines, chlorinated compounds, halogens	70
Common quencher for almost all dyes	Oxygen	71–74
		75, 76

temperatures. If quenchers act by competing with the radiative process (see Eq. (3) and Fig. 6.23), the ratio of the quantum yield in the absence,  $\phi_a$ , and the presence,  $\phi$ , of the quencher will be equal to the ratio of the corresponding lifetimes,  $\tau_a/\tau$  (see Eq. (2)). The concentration dependence of this so-called dynamic or collisional quenching is described by the Stern–Volmer equation, where the Stern–Volmer constant  $K_{sv}$  is equal to  $k_Q \tau_a$ :

$$\phi_a / \phi = \tau_a / \tau = F_a / F = 1 + K_{sv} [Q] = 1 + k_Q \tau_a [Q] \quad (4)$$

Thus from the plot of this ratio versus the quencher concentration and by knowing  $\delta_a$  separately, the bimolecular quenching constant,  $k_Q$ , can be determined. The magnitude of  $k_Q$  is given by:

$$k_Q = 4 \gamma \pi D r N' \times \quad (5)$$

where  $\gamma$  is the efficiency of the quenching reaction,  $D$  and  $r$  are the sums of the diffusion coefficients and the molecular radii, respectively, for the quencher and chromophore, and  $N' = 6.02 \times 10^{20}$ . The diffusion coefficient for a single species  $i$  can be calculated, by using the Stokes–Einstein relationship:

$$D_i = b T / 6 \pi \eta r_i \quad (6)$$

where  $b$  is Boltzmann's constant and  $\eta$  is the viscosity. Thus the quenching constant increases with increasing temperature  $T$  because of the diffusion control of dynamic quenching. The molecular mechanism of the fluorescence quenching depends on the chemical nature of the chromophore and solute. A quencher that possesses halogens or heavy atoms quenches by increasing the intersystem crossing rate induced by the spin–orbital coupling mechanism. Acrylamide quenching of tryptophans in proteins is probably due to excited state electron transfer from the indole to acrylamide. Paramagnetic species are believed to quench aromatic fluorophores by an electron spin exchange process. In many instances the fluorophore can be quenched both by dynamic and static quenching. The characteristic feature for mixed quenching is that the plot of the concentration dependence of the quantum yield or intensity ratios (see Eq. (40)) shows an upward curvature. In this case the Stern–Volmer equation has to be modified, resulting in an equation, which is second order in  $[Q]$ . More details on the theory and applications of solute quenching can be found in [50]. An overview of characterised fluorophore–quencher pairs is given in Table 6.10.

**Example of application of solute quenching in protein studies** One of the main aims in biophysical studies of the structure and function of proteins is to identify the protein domains which are responsible for the interaction of the entire protein with physiologically relevant binding partners. Proteins usually contain several tryptophan residues, which may be distributed among the different protein domains. Since each of these tryptophan residues is located in a distinct environ-

ment, each residue may exhibit a different fluorescence lifetime profile as well as different accessibilities to quenching molecules. Using picosecond time-resolved fluorescence spectroscopy the tryptophan fluorescence lifetime profile of proteins containing up to three tryptophan residues can be determined with high accuracy [55]. An example that may serve here is a picosecond tryptophan study of prothrombin fragment 1 (BF1), which is the 1–156 N-terminal peptide of a key blood coagulation protein, prothrombin. It is believed to be the region predominantly responsible for the metal ion and membrane binding properties of prothrombin. An important question to answer is to what extent the conformation of the two protein domains, the so-called Gla and kringle domain, are altered by the interaction with calcium ions and negatively charged phospholipid surfaces (see Fig. 6.24).

The analysis of the fluorescence decays of the three tryptophan residues (Trp42, Trp90, Trp126) in apo-BF1 resulted in a five exponential decay model, where the five fluorescence lifetimes are wavelength independent. Since structural data show a huge difference in solvent accessibilities for the kringle tryptophans ( $4 \times 10^{-20} \text{ m}^2$  for Trp90 and Trp126) and the Gla tryptophan ( $133 \times 10^{-20} \text{ m}^2$  for Trp42), acrylamide quenching studies were performed to assign the five lifetimes to the two types of tryptophans. Acrylamide was added successively up to a concentration of 0.7 M. The Stern–Volmer analysis of the fluorescence decays showed that the five lifetimes are basically due to two different types of tryptophans characterised by two different  $k_Q$ -values ( $0.2 \pm 0.2 \times 10^9 \text{ M}^{-1} \text{ s}^{-1}$  and  $1.1 \pm 0.3 \times 10^9 \text{ M}^{-1} \text{ s}^{-1}$  for the kringle and Gla tryptophan components, respectively). Note that the theoretical  $k_Q$ -value for a fully exposed polypeptide-tryptophan is about  $3 \times 10^9 \text{ M}^{-1} \text{ s}^{-1}$ . The resulting assignment of the lifetime compounds to the two types of tryptophans allowed for a separate investigation of conformational changes in the two protein domains without cleaving BF1 into the isolated Gla (containing Trp42) and kringle domains (containing Trp90 and Trp126) or modifying the protein by site-directed mutagenesis. Based on the assignment of the lifetimes to the two tryptophan types in BF1, further experiments led to the conclusion that the Gla domain is exclusively responsible for the interaction with calcium ions and negatively charged phospholipid. Moreover, the first experimental evi-

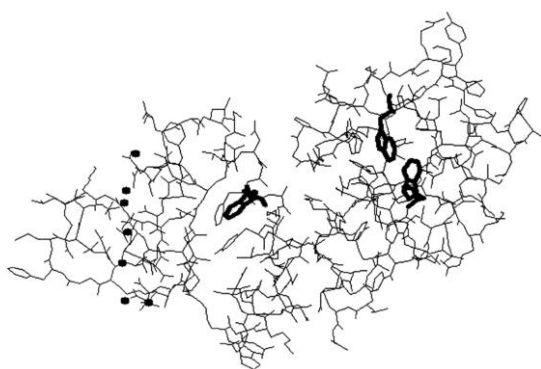


**Fig. 6.24** A depiction of the X-ray structure of Ca-BF1. The right part of the protein is the kringle-domain, where the solvent inaccessible tryptophan residues Trp90 and Trp126 are located. The Gla-domain is the left part of the protein, containing the solvent and quencher accessible Trp42 and seven calcium ions (dots).

dence for a lipid specific conformational change in the Gla domain of prothrombin was found, indicating an important role of this domain in the regulation of blood coagulation [77].

**Solvent quenching** The influence of solvent molecules on the fluorescence characteristic of a dye is certainly one of the most complex issues in fluorescence measurement. Eventually every chromophore shows some dependence of its quantum yield on the chemical structure of the surrounding solvent. This observation is to some extent due to fluorescence quenching by the solvent. One possibility is that the interaction of the chromophore with its solvent shell can promote non-radiative pathways, by changing the energy levels of the  $S_0^-$ ,  $S_1^-$  and  $T_1$ -states. The transition probabilities for the internal conversion and intersystem crossing processes are governed by the energy-gap law [78]. This law states that the rate constants  $k_{ic}$  or  $k_{isc}$  increase exponentially as the energy gap between the  $S_1^-$  and  $S_0^-$  or  $S_1^-$  and  $T_1$ -states, respectively, decrease [78]. Thus any change in those energy levels will strongly influence the fluorescence lifetime and quantum yield (see Eq. (2)). Some of the so-called hemicyanine dyes represent special cases for the promotion of non-radiative pathways by increasing solvent polarity [79]. These dyes undergo an intramolecular twist in the excited state. The intramolecular twist leads to an increase in the polarity and the twisted form of the  $S_1^-$  states is very effectively deactivated by fast internal conversion. Increasing solvent polarity promotes the intramolecular twist and, therefore, the non-radiative deactivation by internal conversion [79]. Moreover, evidence has been accumulated that quenching by interaction with solvent molecules can proceed by a vibrational mechanism. It has been speculated that the collision between dye and solvent molecules results in vibrational coupling that favors efficient internal conversion [80]. In this connection the solvent deuterium effect on the fluorescence lifetime, which has been observed for a variety of chromophores, should be mentioned [81–83]. It has been found that the quantum yield is substantially increased when using  $D_2O$  instead of  $H_2O$  as the solvent. Interestingly, this effect appears to be independent of the chemical nature of the dye. It is conceivable that the different energies of the OH versus OD stretching vibrations ( $3657\text{ cm}^{-1}$  and  $2670\text{ cm}^{-1}$ , respectively) are responsible for more effective solvent quenching by  $H_2O$  than by  $D_2O$ . Independent of the physical nature, this heavy atom effect in solvent quenching has been shown to be a very smart tool for the characterization of water accessibilities in supra- and macromolecular assemblies [81].

**Self-quenching** Self-quenching is the quenching of one fluorophore by another. It is a widespread phenomenon in fluorescence, but it requires high concentrations or labelling densities. The general physical treatment of self-quenching processes involves a combination of trap-site formation and energy transfer among fluorophores, with the possibility of migration of trap sites, which results in quenching. Trap-sites may be formal fluorophore complexes or aggregates, or may result from fluorophore proximity at sufficiently high concentrations. A mathematical model of such processes is given in [84]. Self-quenching experiments are frequently

exploited, by simply monitoring the increase in the fluorescence intensity  $F$  due to decrease in local dye concentrations. One example represents a self-quenching assay for the characterisation of leakage of aqueous contents from cells or vesicles as a result of lysis, fusion or physiological permeability. This assay is based on the fact that carboxyfluorescein is >95 % self-quenched at concentrations >100 mM [85]. Concentrated solutions of these water-soluble dyes are encapsulated in liposomes. Upon addition of a fusogen or other permeabilizing agent, dye release is accompanied by an increase in fluorescence. Further chromophores, the self-quenching properties of which are exploited in biochemical assays are NBD (derivatives of 7-nitrobenz-2-oxa-1,3-diazol-4-yl) [86, 87], Bodipy (derivatives of 4-bora-3a,4a-diaza-s-indacene) [88], and DPH (derivatives of 1,6-diphenyl-1,3,5-hexatriene) [89].

**Trivial quenching** Trivial quenching arises from attenuation of the exciting beam and/or the inability of a fluorescence photon to reach the detector. It occurs mainly when compounds that absorb strongly in the UV range are added. Though the added concentration may be small, the excitation light may be blocked completely. Another reason for trivial quenching can be the turbidity of the sample. True and trivial quenching, however, are easily differentiated, since in trivial quenching the lifetime and quantum yield remain constant.

#### 6.5.1.3 Solvent Relaxation

Any electronic excitation from the ground state  $S_0$  to the excited state  $S_1$  is paralleled by a change in the dipole moment  $\Delta\mu_c$  ( $\Delta\mu_c = \mu(S_1) - \mu(S_0)$ ). Since the time-scale of the electronic transition is much shorter than that of nuclear motion, the excitation causes an ultrafast change in the charge distribution of the probes but does not affect the position or orientation of the surrounding solvent molecules. The solvent molecules are, thus, forced to adapt to the new situation, and start to reorient themselves in order to find an energetically favored position with respect to the excited dye. The dynamic process starting from the originally created non-equilibrium Franck–Condon state (FC) and gradually establishing a new equilibrium in the excited state (R) is called solvent relaxation (SR). This relaxation redshifts the probe's emission spectrum continuously from the emission maximum frequency of the Franck–Condon state ( $v(0)$  for  $t = 0$ ) to the emission maximum of the fully relaxed R-state ( $v(\infty)$  for  $t = \infty$ ). Since a more polar solvent leads typically to a stronger stabilization of the polar R-state, the overall shift  $\Delta v$  ( $\Delta v = v(0) - v(\infty)$ ) increases with increasing solvent polarity for a given change in the solute's dipole moment  $\Delta\mu_c$ . The accurate mathematical description of this relationship depends on the choice of the dielectric solvation theories [90–95]. The fundamental 'dielectric continuum solvation model' [93–95] predicts a linear proportionality between  $\Delta v$  and a dielectric measure of solvent polarity for a large variety of solvents [96]. According to this model, changes in  $\Delta v$  directly reflect polarity changes in the dye environment, giving the first major information accessible by studies of the solvent relaxation process. The second information obtainable from the investigation of solvent relaxation processes is based on the fact that the SR kinetics is de-

terminated by the mobility of the dye environment. The response of solvent molecules to the electronic rearrangement of the dye is fastest in the case of water: more than half of its overall solvation response occurs within 55 fs [97]. If the dye is located in a viscous medium the solvent relaxation takes place on the nanosecond time scale [98]. In vitrified solutions, on the other hand, the dye may fluoresce before solvent relaxation towards the R-state is completed [99].

**Steady-state spectra** Non-viscous solvents at ambient temperature respond with a fast inertial (labilational) motion in the range between 50 and 500 fs to the ultrafast change in the dipole moment due to electronic excitation. After this initial period of solvation response, the diffusion of the solvent molecules, occurring on the pico- to subnanosecond timescale leads to further solvation energy relaxation towards the R-state [96, 97, 100, 101]. The fluorescence decay time  $\tau$  of chromophores is usually 1 ns or longer. Thus, almost the entire fluorescence in a steady-state experiment occurs from the equilibrium state R. Considering the above described connections between  $\Delta\mu_c$  and the dipole moments of the solute,  $\Delta\mu_c$ , and the polarity of the solvent, there are two basic consequences for the spectral position of the steady-state fluorescence spectrum: 1. Increased solvent polarity leads generally to a red-shift of the emission spectrum. For illustration, the influence of the solvent on the emission maximum of Prodan (6-propionyl-2-(dimethylamino)-naphthalene) is depicted in Fig. 6.25) The larger  $\Delta\mu_c$ , the more pronounced is the effect of solvent polarity on the position of the emission spectrum. Moreover, since solvent relaxation is much faster than fluorescence, the wavelength of the maximum

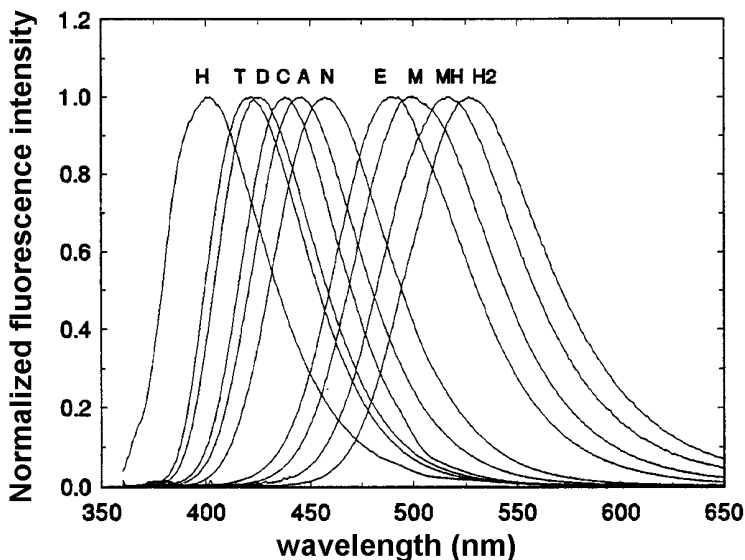


**Fig. 6.25** Fluorescence spectra of Prodan in different solvents at ambient temperature;  $\lambda_{ex} = 337$  nm; H = heptane; T = toluene; D = dioxane; C = chloroform; A = acetone; N = acetonitrile; E = ethanol; M = methanol; MH = methanol/water 1:1; H2 = water.

emission and the fluorescence lifetimes are independent of the excitation wavelength.

If the dye is located in a viscous medium, the solvent relaxation may take place on the nanosecond (ns) timescale. Thus, emission occurs to a substantial extent during solvent relaxation, and the emission spectrum represents an average of the partially relaxed emission. In this case, the maximum of the emission spectrum is no longer directly correlated with the polarity of the solvent. An increase in the temperature leads to a faster solvent reorientation process and, thus, to a red-shift of the maximum of the emission spectrum. Moreover, the wavelength of the emission band maximum of polar fluorophores in motionally restricted media, such as in very viscous solutions [102, 103] or membranes [98], shifts to longer wavelength by shifting the excitation wavelength toward the red-edge of the absorption band [104]. The observed shift should be maximal if the solvent relaxation is much slower than the fluorescence, and it should be zero if SR is fast and independent of the excitation wavelength for the entire fluorescence origins from the relaxed R-state. Thus, the red-edge excitation shift can serve as an indicator of the mobility of the probe's surroundings [102, 103, 105]. Usually, red-edge excitation shift values range from several up to 40 nm depending on the chosen solute and solvent system. The red-edge excitation shift is especially useful when using dyes the absorption and fluorescence maxima of which have linear correlations with the polarity of low-viscosity solvents [99, 106], because then the probed polarity as well as the hypothetical emission maximum of the fully relaxed R-state can be estimated from the absorption maximum. In vitrified solutions, such as sol–gel matrices [99], solvent relaxation becomes much slower than fluorescence and it arises from states close to the Franck–Condon state.

**Time-resolved emission spectra** Although there have been several attempts to simplify the characterisation of the SR process, the determination of time-resolved emission spectra (TRES) is certainly the most general and most precise way to quantitatively describe the solvent response. The time-resolved emission spectra are usually determined by 'spectral reconstruction' [96, 97, 106]. The time-resolved emission spectrum at a given time  $t$  is calculated from the wavelength dependent time-resolved decays by relative normalization to the steady-state spectrum [107]. By fitting the TRES at different times  $t$  by the empirical "log-normal" function, the emission maximum frequencies  $v(t)$  (or  $\lambda(t)$ : see Fig. 6.26) and the total Stokes-shift  $\Delta\nu$  (or  $\Delta\lambda$ ) are usually derived [106]. Since  $v(t)$  contains both information about the polarity ( $\Delta\nu$ ) and the viscosity of the reported environment, the spectral shift  $v(t)$  may be normalized to the total shift  $\Delta\nu$ . The resulting 'correlation functions'  $C(t)$  (Eq. (7)) describe the time course of the solvent response and allow for comparison of the SR-kinetic and, thus, of relative micro-viscosities, reported from environments of different polarities [96, 97, 106, 108, 109, 116, 117, 122]

$$C(t) = (v(t) - v(\infty)) / \Delta\nu \quad (7)$$

**Table 6.11** List of solvent relaxation probes.

<b>Dye or chromophore</b>	<b>References</b>
1,8-ANS (1-anilinonaphthalene-8-sulfonate)	111
2,6-ANS (2-anilinonaphthalene-6-sulfonate)	111
2,6-TNS (2-(p-toluidinylnaphthalene)-6-sulfonate)	112, 113
NPN ( <i>N</i> -phenyl-1-naphthylamine)	114
Dansyl Lysin ( <i>N</i> -e-(5-dimethylaminonaphthalene-1-sulfonyl)-L-lysine)	115
Prodan (6-propionyl-2-(dimethylamino)-naphthalene)	116, 117, 122
Laurdan (2-dimethylamino-6-lauroylnaphthalene)	118
Patman (6-palmitoyl-2-[[2-(triethylammonium)ethyl]methylamino]-naphthalene chloride)	116, 117, 122
NBD (7-nitrobenz-2-oxa-1,3-diazol-4-yl)	98
Coumarin 153	96, 99, 106
Nile red	119
hemicyanine dyes	105, 120
piperidine-bridged electron donor acceptor systems	120

Solvent relaxation probes used for the characterisation of micro-viscosities and polarities are listed in Tab. 6.11. They are characterized by a large change in the dipole moment  $\Delta\mu_c$  upon electronic excitation.

**Example for using solvent relaxation for probing micro-polarities** The benefit of the solvent relaxation techniques in probing micro-polarities may be demonstrated by the time-resolved emission spectra of the *n*-anthroyloxy fatty acids (*n*-AS) in small unilamellar vesicles [108]. These compounds constitute a unique set of fluorescent dyes with the advantage of having a common chromophore, which is covalently attached at different positions ( $n = 2, 6, 9, 12, 16$ ) along the acyl chain of the fatty acid (stearic acid for  $n = 2-12$ ; palmitic acid for  $n = 16$ ). The *n*-AS probes are known to insert into the membrane with the stearoyl chains parallel to the phospholipid acyl chains. While the total Stokes-shifts  $\Delta\tilde{\nu}$  (or  $\lambda$ ) in highly viscous, non-polar solvents like paraffin oil evoking from an intramolecular relaxation process are small and independent of the fluorophore position ( $\Delta\lambda = 7-10$  nm), the *n*-AS dyes show much larger  $\Delta\lambda$  values increasing within the series 16-AP < 12-AS < 9-AS < 6-AS < 2-AS (Fig. 6.26), when incorporated in phosphatidylcholine small unilamellar vesicles (PC-SUV). With 2-AS a total Stokes-shift  $\Delta\lambda$  of 39 nm was observed. Apparently, 2-AS, which is located closest to the membrane/water interface probes the most polar environment. The Stokes-shift of 6 nm observed for 16-AP is comparable to those detected in non-polar, viscous solvents, and indicates the absence of water molecules close to the center of the bilayer. The presented trends illustrate the  $\Delta\tilde{\nu}$ /solvent polarity relationship and show that the solvent relaxation is an excellent direct method for detecting externally induced polarity changes within the bilayer and other self-organizing systems.

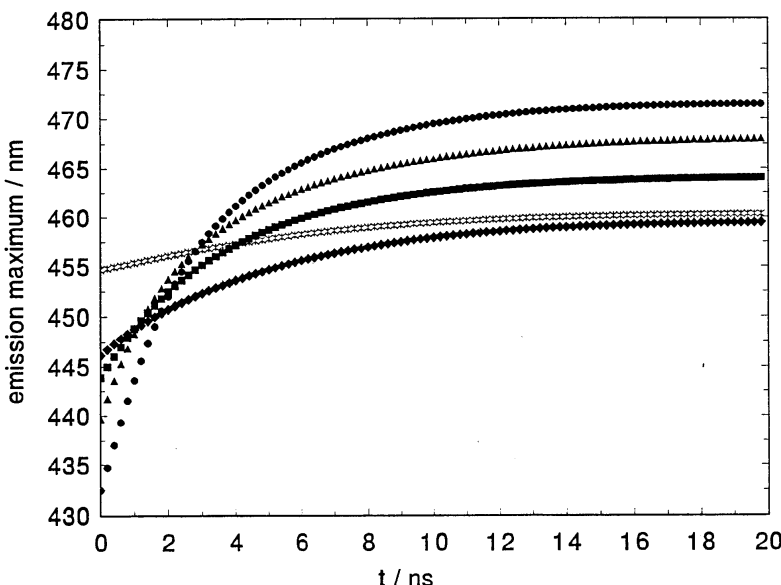


**Fig. 6.26** Time course of the emission maxima (in nm) as a function of time after excitation of the *n*-AS in PC-SUV at 25 °C. Circles: 2-AS; triangles: 6-AS; boxes: 9-AS; diamonds: 12-AS; asterisks: 16-AP recorded by equipment with a time-resolution of about 200 ps. For a fully quantitative description of the solvent relaxation process of the *n*-AS dyes see [122].

#### 6.5.1.4 Polarized Fluorescence

Excitation with linear polarized light, or to a lesser extent even unpolarized light, leads to an anisotropic spatial distribution of excited state molecules. Since this selection persists also in emission, the emitted light is also polarized. The degree of fluorescence polarization is largest when linear polarized light is used and depends on how well the effect of photoselection has been kept in the emission. The polarization can be diminished by excitation energy transfer and by rotational diffusion of the excited molecule. The latter process depends on the viscosity of the dye environment and on the size of the diffusing species. This connection represents the basis for the applications of fluorescence polarization studies. The depolarization by excitation energy transfer [125] is usually an undesirable process. Resonance energy transfer, however, occurs only in concentrated solution where the average distance between the dyes is typically near 5 nm (see Section 6.5.3.1). Thus, this depolarization mechanism can be avoided by the use of dilute solutions.

The polarization is conventionally characterized with reference to a system of laboratory coordinates defined by the directions of the linear polarized excitation ( $E_{\parallel}$ ) and of the fluorescence beam. It is customary to observe the fluorescence beam resolved in directions parallel ( $F_{\parallel}$ ) and perpendicular ( $F_{\perp}$ ) to the direction of the excitation light. The degree of fluorescence polarization  $P$  is defined as

$$P = (F_{\parallel} - F_{\perp}) / (F_{\parallel} + F_{\perp}) \quad (8)$$

An equivalent parameter used for the description of polarization of fluorescence is the anisotropy  $a$ :

$$a = (F_{\text{II}} - F_{\perp}) / (F_{\text{II}} + 2 F_{\perp}) \quad (9)$$

Though both parameters are equivalent for the description of polarised light, anisotropy is usually preferred. Following pulse excitation, the anisotropy of spherical particles in a homogeneous isotropic medium decays exponentially, given by:

$$a = a_0 \exp(-t/\tau_p) \quad (10)$$

where  $\tau_p$  is the rotational correlation time of a sphere and  $a_0$  is the anisotropy at  $t = 0$ . The initial value of the anisotropy  $a_0$  is constant if the fluorophore is fixed in space. Thus, it can be experimentally determined by measuring the steady-state anisotropy of the dye in a rigid and homogeneous medium, such as a vitrified solution. It depends on the angle between the absorption and transition moment of the dye,  $\beta$ . Since the orientations of the absorption and transition moments are characteristic for the corresponding electronic transitions, the angle  $\beta$  is a constant for a pair of electronic transitions of a dye. Fluorescence usually arises from a single transition. Thus  $a_0$  is supposed to be invariant with the emission wavelength. The presence of solvent relaxation occurring on the nanosecond timescale, however, can result in a wavelength dependent change of the emitting  $S_1$  state (see section Steady-state spectra, above), and thus to a substantial decrease in anisotropy across the emission spectrum. Since the excitation spectrum may be composed of several absorption bands corresponding to several transition moments, the polarization of fluorescence may change with the exciting light wavelength. Thus, polarization excitation spectra can be used to identify different overlapping electronic transitions. Using linear polarized light under one-photon excitation conditions (for multi-photon excitation see [123])  $a_0$  for a randomly orientated molecule is

$$a_0 = 0.6 \cos^2 \beta - 0.2 \quad (11)$$

For a collinear transition dipole moment, the theoretical maximum value  $a_0$  is equal to 0.4.

**Steady-state fluorescence anisotropy** In low-viscosity solvents the rotational depolarization of low molecular weight compounds occurs on the picosecond timescale [124]. Since in this case the rotation is much faster than the fluorescence, the steady-state emission is unpolarised. If the rotational motion of the fluorophore is on the same timescale as the fluorescence, a steady state polarisation is observed. In the simplest case for a spherical rotor and a single-exponential fluorescence intensity decay ( $\tau$ ), the measured anisotropy is given by

$$a = a_0 / [1 + (\tau / \tau_p)] \quad (12)$$

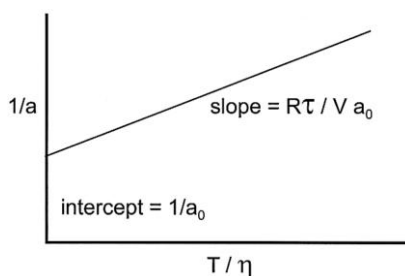


**Fig. 6.27** Illustration of a Perrin plot for the determination of the apparent hydrodynamic volume  $V$  by steady-state fluorescence anisotropy measurements.

The rotational correlation time of a sphere  $\tau_p$  is given by

$$\tau_p = \eta V / RT \quad (13)$$

where  $\eta$  is the viscosity,  $T$  the temperature,  $R$  the gas constant, and  $V$  the volume of the rotating unit. It is important to note that these relations only hold for spherically symmetrical molecules. A formal description of these relations for spherically unsymmetrical and ellipsoidal molecules can be found in the literature [125–128]. By combining Eq. (12) and (13) it can be seen that a plot of  $1/a$  versus  $T/\eta$  should be linear, with intercept equal to  $1/a_0$  and with a slope/intercept that is directly proportional to  $\tau$  and indirectly proportional to  $V$  (see Fig. 6.27). If one of the latter two parameters is known, the other can be calculated from such data. The absence of viscosity dependence indicates that some other depolarizing process dominates. A nonlinear plot of  $1/a$  versus  $T/\eta$  indicates the existence of more than one rotational mode.

Prior to the availability of time-resolved measurements, such so-called Perrin plots were used extensively to determine the apparent hydrodynamic volume of proteins [129–131]. Since protein association reactions usually affect the rotational correlation time of the protein label, such reactions have been characterized by steady state anisotropy measurements [132, 133].

**Time-resolved fluorescence polarization** As described by Eq. (10), the anisotropy of spherical particles in a homogeneous isotropic medium decays exponentially. Anisotropy decays, however, can be more complex. The three most important origins for non-monoexponential decays are described in the following:

(a) *Non-spherical particles in a homogenous isotropic medium*

The theory for rotational diffusion of non-spherical particles is complex. In theory the anisotropy decay of such a molecule can be composed of a sum of up to five exponentials [134]. The ellipsoids of revolution represent a smooth and symmetrical figure, which is often used for the description of the hydrodynamic properties of proteins. They are three-dimensional bodies generated by rotating an ellipse about one of its characteristic axes. In this case the anisotropy decay displays

only three rotational correlation times, which are correlated to the rotational diffusion coefficients  $D_{\parallel}$  and  $D_{\perp}$ . In this case, the indexes  $\parallel$  and  $\perp$  denote the rotation around the main and side axis, respectively [132]. The pre-exponential factors of the three exponentials depend on the angle between the emission transition moment and the main axis of the rotational ellipsoid. In practice, due to the limited time-resolution, one rarely resolves more than two exponentials [128].

(b) *Segmental mobility of the chromophore*

A more important fact is that the chromophore is not rigidly fixed to the biopolymer and, thus, rotates about the bond linking it to the biopolymer. Consequently, the anisotropy decay kinetics is found to be double or triple exponential, due to the contributions from internal and global rotation of the macromolecule. The same concept applies for the rotational wobble of that portion of the biopolymer in proximity to the fluorophore or in the more defined case for the rotation of a molecular domain [135].

(c) *Hindered rotors: fluorescent dyes in biological membranes*

If isotropic rotors are imbedded in an anisotropic environment, such as phospholipid bilayers, the decay of fluorescence anisotropy can be complex. Let us consider a dye, such as 1-(4-trimethylammonium-phenyl)-6-phenyl-1,3,5-hexatriene (TMA-DPH) or 1,6-diphenyl-1,3,5-hexatriene (DPH), intercalated inside the bilayer. The polarization of its fluorescence depends on the resistance to its motion, exerted by its molecular environment. In the case of a fixed hindrance to rotational relaxation motion, the value of anisotropy decreases exponentially, not to zero, but to a finite value  $a_{\infty}$ , yielding formula Eq. (14):

$$a = (a_0 - a_{\infty}) \exp(-t/\tau_p) + a_{\infty} \quad (14)$$

Thus, the time-resolved measurement of such membrane probes contains information on the dynamics of the hindered probe rotation, often interpreted as the micro-viscosity, and about the hindrance of this rotation, usually interpreted as the static packing arrangement of the lipids or the so-called membrane order [136, 137]. Fluorescence polarisation studies in membranes, however, exhibit some major limitations: the experimentally determined steady-state and time-resolved anisotropies characterize the motional restrictions of the ‘reporter’ molecule itself and give therefore only *indirect* information about the dye environment, with the consequence that, if the probe is bound covalently to the lipid (TMA-DPH), this attachment may dominate the recorded depolarisation behaviour. The membrane order parameters obtained from freely mobile probes like (DPH) result from a broad distribution of localisation within the hydrophobic interior, the detailed characterisation of which reveals inherent ambiguities [138].

Among the fluorescence techniques employed, the determination of fluorescence anisotropy has certainly been the dominating fluorescence method in studies of biological systems. For a detailed description of the theory and several examples of its application one may refer to two review articles [128, 137].

### 6.5.2

#### Special Applications

The fluorescence resonance energy transfer (FRET) is a nonradiative transfer of the excitation energy from a donor to an acceptor chromophore. It is governed by a long-range interaction between the emission and absorption transition dipole moments of the donor and acceptor, respectively. The rate of energy transfer depends on the extent of the spectral overlap of the emission and absorption spectra of the donor and acceptor, respectively, on the quantum yield of the donor, the relative orientation of the transition dipole moments, and the distance between the donor and acceptor molecules. The distance dependence has resulted in its widespread use to measure distances between donors and acceptors in macromolecular systems. The quality of a pair of a *donor/acceptor* pair is usually characterized by the parameter  $R_0$ , which is typically in the range 2–9 nm. It is defined as the distance at which the rate of resonance energy transfer is equal to what would be the decay rate of the donor in the absence of an acceptor and can be estimated, as follows:

$$R_0 \text{ (in nm)} = 979 (\kappa^2 n^4 \phi_0 J)^{1/6} \quad (15)$$

where  $n$  is the refractive index of the medium,  $\phi_0$  the fluorescence quantum yield of the donor,  $J$  the spectral overlap integral, and  $\kappa$  an orientation factor. The rate of energy transfer  $k_{\text{ET}}$  is given by

$$k_{\text{ET}} = 1/\tau_d (R_0/r)^6 \quad (16)$$

where  $\tau_d$  is the decay time of the donor in the absence of the acceptor, and  $r$  is the distance between the donor and the acceptor. Thus the rate depends strongly on distance, providing a spectroscopic ruler for determining distances in macromolecular assemblies.

The magnitude of  $k_{\text{ET}}$  can be determined from the efficiency of energy transfer,  $ET$ , via

$$k_{\text{ET}} = 1/\tau_d (ET / 1 - ET) \quad (17)$$

and  $ET$ , in turn, can be experimentally evaluated from the measurement of the decrease in the intensity  $F$  or lifetime  $\tau$  of the donor in the presence of the acceptor:

$$ET = 1 - F/F_d = 1 - \tau/\tau_d \quad (18)$$

Thus, determining  $ET$  and knowing  $R_0$  the separation distance one can calculate  $r$ . In such distance measurements there is often concern about the effects of the orientation factor  $\kappa^2$ , which depends on the relative orientation of the emission oscillator of the donor and the absorption oscillator of the acceptor. The value of  $\kappa^2$  varies from 4 (parallel orientation of the oscillators) to 0 (perpendicular orientation). Often a value of  $\kappa^2 = 2/3$  is assumed, which corresponds to the situation when there is rapid, isotropic rotation of the donor and acceptor molecules. Randomly oriented dipoles that remain fixed during the singlet lifetime give  $\kappa^2 = 0.476$ . When required, the range of values for  $\kappa^2$  can be estimated by polarization measurements [139]. A comprehensive discussion on the theory and effects of the orientation factor is given in [140].

When assuming the simplest case of a monoexponentially decaying donor  $\tau_d$ , a fixed distance  $r$  and a dynamically random orientation factor  $\kappa^2 = 0.476$ ,  $k_{ET}$  will be added to Eq. (3) and thus the energy transfer will simply result in a shortened, monoexponential decay of the donor  $\tau_d$ . In homogeneous solution, however, at low donor concentrations and without diffusion of the donor and acceptor within the fluorescence lifetime, the intensity decay is given by [141–144]:

$$F = F_0 \exp(-t/\tau_d) \exp[-\gamma(t/\tau_d)^\delta] ; \delta = \text{dim}/6 \quad (19)$$

For randomly distributed donor and acceptor molecules the value for the dimension dim is equal to 3 and  $\gamma$  is given by

$$\gamma = 4/3 g \pi^{3/2} c_a R_0, \text{ where } g = (3/2 \kappa^2)^{0.5} \quad (20)$$

with  $c_a$  the acceptor concentration. With knowledge of the acceptor concentration and on the condition that the donor fluorescence decays mono-exponentially in the absence of the acceptor, the  $R_0$  value and the dimension of the medium in which donor and acceptors are imbedded can be determined. Two-dimensional or so-called fractal energy transfer are of interest, if the dye molecules are bound to phospholipid membranes [145, 146] or imbedded in silicate networks [147]. One-dimensional energy transfer has been considered for dyes bound to DNA [148].

One application field of *fluorescence resonance energy transfer* is assays for the characterisation of fusion of cells or vesicles. Usually such membrane systems are labelled either by a donor or an acceptor molecule. Fusion leads to an intermixing of these membrane labels in the same bilayer, allowing resonance energy transfer to occur. Examples can be found in the literature [149–153]. Another membrane application of energy transfer has been the demonstration of lipid asymmetry in human red blood cells [154]. Moreover, energy transfer has been shown to be a very useful tool in elucidating the subunit structure of oligomeric assemblies in membranes. Examples are studies of the oligomerisation of ATPase of sarcoplasmic reticulum in phospholipid vesicles [155], on gramicidin A transmembrane channels [156], and of the aggregation state of bacteriorhodopsin [157]. Finally, the combination of energy transfer with flow cytometry [158] and its use in immu-

noassays should be mentioned [159]. More detailed information on the theory and application of energy transfer can be found in [140, 160].

The term excimer is used when the excited dye forms a transient fluorescent dimeric complex with another fluorophore of the same kind. The excimer fluorescence is usually red shifted with respect to that of the monomer (see Fig. 6.28). The most widely used types of *excimer-forming probes* are pyrene (see Fig. 6.28) and perylene and their derivatives. The ratio of the maxima of the excimer to the monomer spectra can be used to judge the efficiency of excimer formation. This (Ex/Mo)-ratio depends on the concentration of the dye and is controlled by the diffusion properties. It allows, when using pyrene or perylene labeled fatty acids or phospholipids (see Fig. 6.28), the estimation of the probe's lateral diffusion coefficients in lipid bilayer membranes. Thus, membrane fluidity can be measured by monitoring the fluorescence spectra of such an excimer probe.

Since increasing temperature leads to increased fluidity and thus to a faster probe diffusion, pyrene lipids have been frequently used to study phase transition in membranes [161,162]. Phospholipid phase separation increases the local concentration of dye labeled lipids and can, therefore, be investigated via the characterization of excimer formation. The binding of proteins or ions, however, may induce phase separation as well as decreasing lateral lipid diffusion. Since these two effects are opposing in terms of excimer formation, the binding of such proteins or ions cannot be studied by the (Ex/Mo)-ratio. The time-resolved analysis of the monomer fluorescence of the labeled lipid, however, allows for the separation of

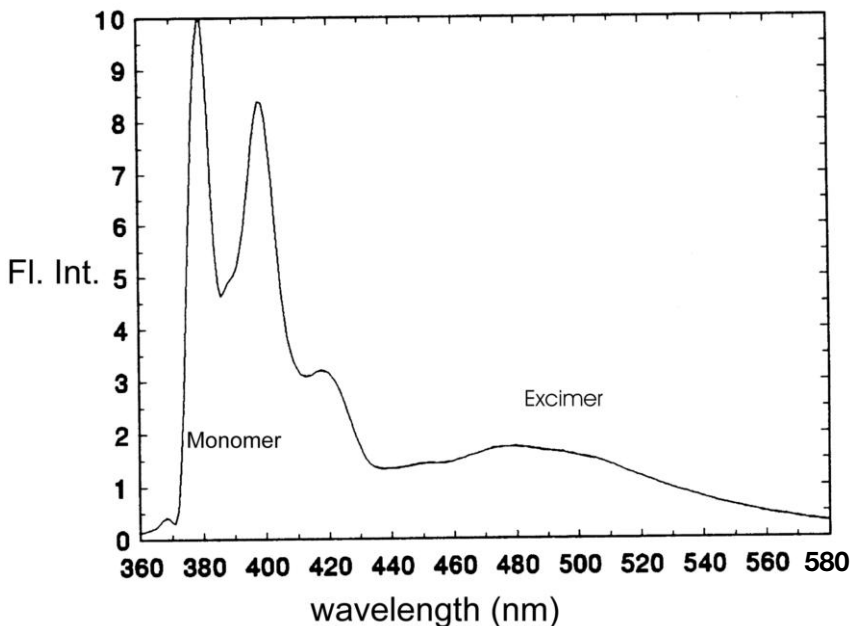


Fig. 6.28 Fluorescence spectrum of pyrene labeled phosphatidylglycerol (5 mol%) in phosphatidylcholine small unilamellar vesicles at ambient temperature;  $\lambda_{\text{ex}} = 337 \text{ nm}$ .

both effects [163]. A comprehensive treatise of theory and application of excimer probes in membrane research can be found in [164, 165].

'Fluorescence recovery after photobleaching' (FRAP) was introduced as a method to measure the local mobility of fluorescently labeled particles bound to the plasma membrane of living cells [166–168]. It has been used to study transport phenomena in a wide variety of biological membrane-bound systems, as well as to probe the photobleaching properties of fluorescent molecules [169]. FRAP is based on the principle of observing the rate of recovery of fluorescence due to the movement of a fluorescent marker into an area of the membrane which contains this same marker but which has been rendered non-fluorescent via an intense photobleaching pulse of laser light. The two-dimensional diffusion coefficient of the fluorophore is related to both its rate and extent of recovery. For a discussion of the photo-physical mechanism of photobleaching see [170]. In order to create a finite observation area, usually both laser beams, the single short pulse with rather high intensity leading to photobleaching and the less intense pulse monitoring the fluorescence recovery are focused by an epifluorescence or confocal microscope. A very elegant variation is to combine FRAP with total internal reflection fluorescence (TIRF) [171]. Here, a laser beam totally internally reflects at a solid/liquid interface, creating an evanescent field, which penetrates only a fraction of the wavelength into the liquid domain. When using planar phospholipid bilayer and fluorescently labeled proteins, this method allows the determination of adsorption/desorption rate constants and surface diffusion constants [171–173]. Figure 6.29 shows a representative TIRF-FPR curve for fluorescein-labeled prothrombin bound to planar membranes. In this experiment the experimental conditions are chosen such that the recovery curve is characterized by the prothrombin desorption rate. It should be mentioned that, similar to other applications of fluorescence microscopy, two and three photon absorption might be combined with FRAP in the near future.

Recent advances in ultrasensitive instrumentation have allowed the detection of individual atoms and molecules in solids [174, 175], on surfaces [176, 177], and in the condensed phase [178, 179] using laser-induced fluorescence. In particular, *single molecule detection* in the condensed phase enables scientists to explore new frontiers in many scientific disciplines, such as chemistry, molecular biology, molecular medicine and nanostructure materials. There are several optical methods to study single molecules, the principles and application of which have been reviewed by Nie and Zare [180]. These methods are listed in Tab. 6.12.

In contrast to the other listed single molecule techniques, measurements based on fluorescence correlation spectroscopy (FCS) can already be performed both routinely and rapidly. Moreover, FCS is applied in many scientific disciplines and the number of applications of this technique is growing very rapidly. Thus, its principles will be briefly outlined: Usually, a sharply focused laser beam illuminates a volume element of about  $10^{-15}$  l by using confocal or multi-photon microscopy. This volume is so small that at a given point in time, it can host only one fluorescent particle out of many under analysis. The illuminated volume is adjustable in 1  $\mu\text{m}$  steps in three dimensions, providing a high spatial resolution. The single fluorescent molecules diffusing through the illuminated volume give rise to bursts

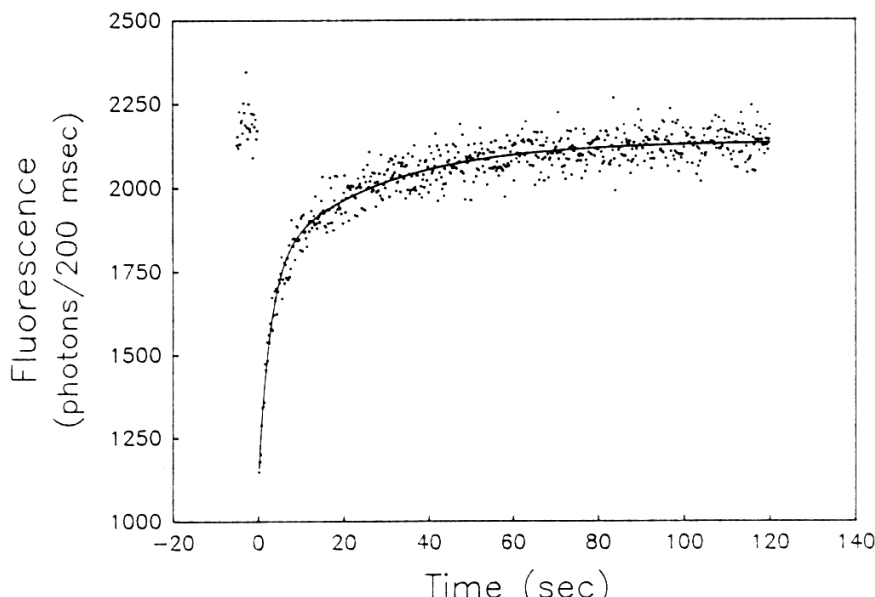


**Fig. 6.29** Representative TIRF-FPR curve for fluorescein-labeled prothrombin bound to planar membranes. Shown is a typical recovery curve for the binding of 1  $\mu\text{M}$  prothrombin (labeled with fluorescein) to a planar bilayer. The dotted points represent the experimental

data and the line the best fit, yielding the desorption rate. Note, that the fluorescence intensity does not recover fully. This effect is generally observed in photobleaching experiments and is one of the major drawbacks of this method.

**Table 6.12** Methods for studying single molecules using laser-induced fluorescence.

<b>Method for studying single molecules</b>	<b>References</b>
Solid matrices at low temperatures	181, 182
Liquid streams	183–185
Microdroplets	186
Near-field scanning optical microscopy	177, 188–190
Far-field confocal microscopy, including fluorescence correlation spectroscopy	191, 192
Microscopy combined with multi-photon excitation	193–195
Wide-field epi-illumination	196, 197
Evanescence wave excitation	198

of fluorescence light quanta. Each individual burst, resulting from a single molecule, can be registered. The photons are recorded in a time-resolved manner by a highly sensitive single photon counting device. The autocorrelation function of the time-course of the fluorescence signal gives information about the number of molecules in the illuminated volume element and their characteristic translational diffusion time. Since the size of the illuminated volume is known, the con-

**Table 6.13** Examples of fluorescence sensing.

Analyte	Sensing dye	Sensing mechanism	References
Oxygen	Several Ru-complexes (e.g. $[\text{Ru}(\text{Ph}_2\text{phen})_3]^{2+}$ )	Collisional quenching	213
Chloride	Sultons (betrains) of quinolinium and acridinium ions	Collisional quenching	69, 214
Calcium	Blue and green fluorescent proteins	Resonance energy transfer	216
pH	Fluoresceins	pH-dependent ionization	217, 218
Glucose	Fluorescein and rhodamine	Resonance energy transfer	219

centration and diffusion constant of the fluorescent species is determined. In the majority of applications the diffusion properties of two species with different molecular weight are analysed. In the case where the fluorescently labeled low molecular weight compound is bound to a high molecular weight compound, titration of the latter allows for the determination of equilibrium binding constants. This principle can be used for example for the characterisation of interactions between different proteins [199–202], proteins and membranes [203], xenobiotics and proteins [204], or polynucleotides and DNA [205]. Moreover, any chemical or biochemical reactions leading to a marked change in the molecular weight can be analysed in real time [206–208]. The high spatial resolution of FCS allows the characterisation of diffusion processes in different compartments of a cell [207–212].

Due to the high sensitivity, selectivity, and versatility of fluorescence spectroscopy, however, *fluorescence sensors* are the most highly developed. In many cases the sensing probe is placed on a carrier material. The analyte can be either in the gas phase or in solution. Interaction between the sensing probe and the analyte leads to a fluorescence change. The use of fiber optics allows one to perform fluorescence measurements on remote objects, which is especially useful in clinical applications. The required fluorescence change monitoring e.g. the pH, O<sub>2</sub> pressure, or the concentration of ions in blood can occur in the intensity, emission spectrum, anisotropy, or lifetime of the sensing probe. The mechanism for a change in the listed fluorescence parameters can be collisional quenching, resonance energy transfer, photo-induced electron transfer, or analyte induced change in the state of the sensing chromophore. Table 6.13 gives some examples of analyte, sensing probe and sensing mechanism. Since intensity measurements are dependent upon the concentration of the fluorophore, they are often not usable and they may be inaccurate if photobleaching occurs. Moreover, intensity-based systems suffer from other problems including turbidity, limited range of detection, low signal-to-noise ratios, and optical losses. Fluorescence lifetime-based sensing, on the other hand, does not suffer from these problems and it seems likely to become widely used in the near future. An up to date overview on this topic is given in the chapter ‘Fluorescence sensing’ in [220] (see Reference Data Table 5 on page 158/159, and Reference Data Table 6 on page 160/161).

**Reference Data Table 5**  
**Method Parameter Reference Sheet**

<b>Method:</b>	Steady-state spectrofluorometer
<b>Characterized Parameter</b>	Fluorescence intensity
<b>Type of Information:</b>	Concentration, structure
<b>Required User Skills</b>	Unskilled for routine measurements

### Sample

	Excellent	Good	Fair	Poor	Problems
Pure compound	+				
Multi-analyte		+			
Gaseous			+		
Liquid	+				
Solid	+				
Matrix effects / matrix assisted					+
Size	+				
Trace	+				
Cross sensitivity				+	
Identification				+	
Quantification				+	

**Equipment (typical data):**

CW/Fourier	CW
Internal/external reference	Internal reference photomultiplier
Single/double beam	Single beam
Destroying sample	Non-invasive
Sequential / simultaneous	sequential
Source	Arc lamps filled with xenon and/or mercury
Dispersion by:	
filter / monochromator	monochromator
nondispersing	
Absorption / emission / scattering	emission
Ratio recording	yes

**Spectrometer (typcal parameter)**

Frequency / wave number / wavelength range	200 nm to 900 nm
Time per spectrum	1 to 5 minutes
Noise Signal/noise at high/low concentr. limit	500 :1 at low concentration limit
Reproducibility (wavelength, signal)	± 0.5 nm
Spectra overlay (single/multi)	Single
Sampling (number of times)	Once
Resolution (nm, s <sup>-1</sup> , cm <sup>-1</sup> , molecular weight)	± 1 nm
Limit of detection	pM
Time required for analysis Preparation Measurement Evaluation	Strongly dependent on type of sample 1 to 5 minutes 3 minutes
Cost per sample (Euro)	10

**Techniques yielding similar information:** Time-resolved fluorescence**Typical features of built-in computers:**

Computers (not built-in) are part of modern spectrofluorometer. The supplied software manages data acquisition and analysis as well the control of optional accessories.

**Typical application (as demonstrated in chapter):** Characterization of quenching, spectral shifts, polarization, energy transfer, excited state reactions

**Preferable samples:** Micromolar solutions

**Problematic samples:** Scattering samples, solid samples, gaseous samples

**Reference Data Table 6**  
**Method Parameter Reference Sheet**

<b>Method:</b>	Time-resolved spectrofluorometer based on single photon counting
<b>Characterized Parameter</b>	Fluorescence lifetime
<b>Type of Information:</b>	Structure, relaxation
<b>Required User Skills</b>	Skilled in preparation of samples and carrying out the measurements

### Sample

	Excellent	Good	Fair	Poor	Problems
Pure compound	+				
Multi-analyte		+			
Gaseous			+		
Liquid	+				
Solid			+		
Matrix effects / matrix assisted					+
Size		+			
Trace		+			
Cross sensitivity				+	
Identification				+	
Quantification				+	

**Equipment (typical data):**

CW/Fourier	pulsed
Internal/external reference	External reference
Single/double beam	Single beam
Destroying sample	Non-invasive
Sequential / simultaneous	Sequential
Source	Lasers or flash lamps
Dispersion by:	
filter / monochromator	Filter or monochromator
nondispersing	
Absorption / emission / scattering	Emission
Ratio recording	No

**Spectrometer (typcal parameter)**

Frequency / wave number / wavelength range	250 nm to 900 nm
Time per decay curve	3 to 180 minutes
Noise Signal/noise at high/low concentr. limit	1000 : 1 at low concentration limit
Reproducibility (wavelength, signal)	± 0.1 ns for flashlamp excitation, ± 0.01 ns for laser excitation
Spectra overlay (single/multi)	Single
Sampling (number of times)	Once
Resolution (nm, s <sup>-1</sup> , cm <sup>-1</sup> , molecular weight)	0.3 ns for flashlamp excitation, 0.03 ns for laser excitation
Limit of detection	pm
Time required for analysis Preparation Measurement Evaluation	Strongly dependent on type of sample 3 till 180 minutes 1 till 60 minutes
Cost per sample (Euro)	100

**Techniques yielding similar information:** Steady-state fluorescence**Typical features of built-in computers:**

Built-in computers are not part of modern time-resolved spectrofluorometer. The supplied software manages data acquisition and analysis.

**Typical application (as demonstrated in chapter):** Characterisation of quenching, spectral shifts, polarisation, energy transfer, excited state reactions

**Preferable samples:** Micromolar solutions

**Problematic samples:** Scattering samples, solid samples, gaseous samples

**Acknowledgement**

Dr. Hof acknowledges the financial support given by the Ministry of Education, Youth and Sports of the Czech Republic (via LN 00A032).

## References

- 1 H. Günzler, H.-U. Gremlich, *IR Spectroscopy*, Wiley-VCH, Weinheim, 2002.
- 2 H. W. Siesler, K. Holland-Moritz, *Infrared and Raman Spectroscopy of Polymers*, Marcel Dekker, New York 1980.
- 3 *Infrared and Raman Spectroscopy*, ed. B. Schrader, B., VCH, Weinheim 1995.
- 4 E.-H. Korte, Infrarot-Spektroskopie Difus Reflektierender Proben, in *Analytiker Taschenbuch 9*, Springer, Berlin 1990.
- 5 G. Socrates, *Infrared Characteristic Group Frequencies*, Wiley, Chichester 1994.
- 6 L. J. Bellamy, *The Infrared Spectra of Complex Molecules*, Chapman and Hall, London 1975 and 1980, Vol. 1 and 2.
- 7 N. Sheppard, Surface Studies by IR Spectroscopy, in *Encyclopedia of Spectroscopy and Spectrometry*, Academic Press, San Diego 2000, Vol. 3, pp. 2320–2328.
- 8 R. L. White, Chromatography-IR, in *Encyclopedia of Spectroscopy and Spectrometry*, Academic Press, San Diego 2000, Vol. 1, pp. 288–293.
- 9 H. G. M. Edwards, Art Works Studied Using IR and Raman Spectroscopy, in *Encyclopedia of Spectroscopy and Spectrometry*, Academic Press, San Diego 2000, Vol. 1, pp. 2–17.
- 10 A. S. Gilbert, R. W. Lancaster, Industrial Applications of IR and Raman Spectroscopy, in *Encyclopedia of Spectroscopy and Spectrometry*, Academic Press, San Diego 2000, Vol. 2, pp. 881–893.
- 11 C. Pettinari, C. Santini, IR and Raman Spectroscopy of Inorganic, Coordination and Organometallic Compounds, in *Encyclopedia of Spectroscopy and Spectrometry*, Academic Press, San Diego 2000, Vol. 2, pp. 1021–1034.
- 12 M. Jackson, H. H. Mantsch, Medical Science Applications of IR, in *Encyclopedia of Spectroscopy and Spectrometry*, Academic Press, San Diego 2000, Vol. 2, pp. 1271–1281.
- 13 M. W. Sigrist, Photoacoustic Spectroscopy, Applications, in *Encyclopedia of Spectroscopy and Spectrometry*, Academic Press, San Diego 2000, Vol. 3, pp. 1800–1809.
- 14 I. Noda, in *Proceedings of the 12<sup>th</sup> ICOFTS*, ed. by K. Itoh and M. Tasumi, Waseda Univ. Press, Tokyo, 1999, 57–60.
- 15 C. M. Snively, J. L. Koenig, Polymer Applications of IR and Raman Spectroscopy, in *Encyclopedia of Spectroscopy and Spectrometry*, Academic Press, San Diego 2000, Vol. 3, pp. 1858–1864.
- 16 J. C. Lindon, Forensic Science, Applications of IR spectroscopy, in *Encyclopedia of Spectroscopy and Spectrometry*, Academic Press, San Diego 2000, Vol. 1, pp. 603–615.
- 17 U. P. Fringeli, ATR and Reflectance IR Spectroscopy, Applications, in *Encyclopedia of Spectroscopy and Spectrometry*, Academic Press, San Diego, 2000, Vol. 1, pp. 58–75.
- 18 H. W. Siesler, Y. Ozaki, S. Kawata, et al., Near-Infrared Spectroscopy, Wiley-VCH, Weinheim 2002.
- 19 F. O. Libnau, O. M. Kvalheim, A. A. Christy, et al., *Vib. Spectrosc.*, 1994, 7, 243–254.
- 20 D. A. Burns, E. W. Ciurczak, *Handbook of Near-Infrared Analysis*, Marcel Dekker, New York 1992.

- 21** H. Schulz, H. H. Drews, H. Krüger, *J. Essential Oil Res.*, **1999**, *11*, 185–190.
- 22** E. Baldwin, Z. *Lebensmitteltechnik*, **1992**, *43*, 502–508.
- 23** R. J. Dempsey, D. G. Davis, R. G. Buice Jr., et al., *Appl. Spectrosc.*, **1996**, *50*, 18A–33A.
- 24** A. Bittner, R. Marbach, H. M. Heise, *J. Mol. Struct.*, **1995**, *349*, 341–344.
- 25** R. Marbach, T. H. Koschinska, F. A. Gries, et al., *Appl. Spectrosc.*, **1993**, *47*, 875–881.
- 26** F. F. Jöbsis-vanderVliet, P. Jöbsis, *J. Biomed. Opt.*, **1999**, *4*, 397–402.
- 27** Y. Yamashita, A. Maki, H. Koizumi, *J. Biomed. Opt.*, **1999**, *4*, 414–417.
- 28** H. W. Zwanziger, H. Förster, *J. NIR Spectrosc.*, **1998**, *6*, 189–197.
- 29** *Infrared and Raman Spectroscopy*, ed. B. Schrader, VCH, Weinheim 1995.
- 30** A. B. Myers, R. A. Mathies, *Biological Applications of Raman Spectroscopy: Vol. 2: Resonance Raman Spectra of Polyenes and Aromatics*, Wiley & Sons, New York 1987.
- 31** W. E. Smith, C. Rodger, Surface-Enhanced Raman Scattering (SERS), Applications, in *Encyclopedia of Spectroscopy and Spectrometry*, Vol. 3, Academic Press, San Diego 2000, pp. 2329–2334.
- 32** R. H. Brody, E. A. Carter, H. G. M. Edwards, et al., FT-Raman Spectroscopy, Applications, in *Encyclopedia of Spectroscopy and Spectrometry*, Vol. 1, Academic Press, San Diego 2000, pp. 649–657.
- 33** W. Kiefer, Non-linear-Raman Spectroscopy, Applications, in *Encyclopedia of Spectroscopy and Spectrometry*, Vol. 2, Academic Press, San Diego 2000, pp. 1609–1623.
- 34** I. D. De Wolf, I. D., Semiconductors, in *Analytical Applications of Raman Spectroscopy*, Blackwell Science, London 1999, pp. 435–472.
- 35** P. Hildebrandt, S. Lecomte, Biochemical Applications of Raman Spectroscopy, in *Encyclopedia of Spectroscopy and Spectrometry*, Vol. 1, Academic Press, San Diego 2000, pp. 88–97.
- 36** Y. Guan, E. N. Lewis, I. W. Levin, Biomedical Applications of Raman Spectroscopy, in *Analytical Applications of Raman Spectroscopy*, Blackwell Science, London 1999, pp. 276–327.
- 37** C. J. Frank, Review of Pharmaceutical Applications of Raman Spectroscopy, in *Analytical Applications of Raman Spectroscopy*, Blackwell Science, London 1999, pp. 224–275.
- 38** N. J. Ortins, T. A. Kruger, P. K. Dutta, Recent Raman Spectroscopic Studies of Heterogeneous Catalysts, in *Analytical Applications of Raman Spectroscopy*, Blackwell Science, London 1999, pp. 328–366.
- 39** H. G. M. Edwards, Art Works studied using IR and Raman Spectroscopy, in *Encyclopedia of Spectroscopy and Spectrometry*, Vol. 1, Academic Press, San Diego 2000, pp. 2–17.
- 40** N. Everal, Raman Spectroscopy of Synthetic Polymers, in *Analytical Applications of Raman Spectroscopy*, Blackwell Science, London 1999, pp. 127–192.
- 41** A. S. Gilbert, R. W. Lancaster, Industrial Applications of IR and Raman Spectroscopy, in *Encyclopedia of Spectroscopy and Spectrometry*, Vol. 2, Academic Press, San Diego 2000, pp. 881–893.
- 42** E. D. Lipp, M. A. Leugers, Applications of Raman Spectroscopy in the Chemical Industry, in *Analytical Applications of Raman Spectroscopy*, Blackwell Science, London 1999, pp. 106–126.
- 43** H. H. Perkampus, *UV-VIS-Atlas of Organic Compounds*, VCH, Weinheim 1992.
- 44** D. H. Williams, I. Flemming, *Spectroscopic Methods in Organic Chemistry*, McGraw-Hill, London 1995.
- 45** T. Foerster, *Fluoreszenz organischer Verbindungen*, Vandenhoeck und Ruprecht, Goettingen 1951.
- 46** H. Lanig, M. Hof, G. Bringmann, et al., *Chem. Phys. Lett.*, **1997**, *272*, 478–483.
- 47** J. R. Lakowicz, I. Gryczynski, in *Topics in Fluorescence Spectroscopy: Techniques*, ed. J. R. Lakowicz, Plenum Press, New York 1991, pp. 293–336.
- 48** D. V. O'Connor, D. Philips, *Time Correlated Single Photon Counting*, Academic Press, London 1983.

- 49** C. A. Parker, W. T. Rees, *Analyst (London)*, **1960**, *85*, 587.
- 50** M. R. Eftink, in *Topics in Fluorescence Spectroscopy: Principles*, ed. J. R. Lakowicz, Plenum Press, New York 1991, pp. 53–126.
- 51** D. R. James, W. R. Ware, *J. Phys. Chem.*, **1985**, *89*, 5450–5458.
- 52** A. Namiki, N. Nakashima, K. Yoshihara, *J. Chem. Phys.*, **1979**, *71*, 925–930.
- 53** A. F. Fucaloro, L. S. Forster, M. K. Campbell, *Photochem. Photobiol.*, **1984**, *39*, 503–506.
- 54** J. K. Swadesh, P. W. Mui, H. A. Scheraga, *Biochemistry*, **1987**, *26*, 5761–5769.
- 55** M. Hof, G. R. Fleming, V. Fidler, *Proteins: Struct., Funct., Genet.*, **1996**, *24*, 485–494.
- 56** R. Vos, Y. Engelborghs, *Photochem. Photobiol.*, **1994**, *60*, 24–32.
- 57** M. R. Eftink, C. A. Ghiron, *Biochemistry*, **1984**, *23*, 3891–3899.
- 58** P. Midoux, P. Wahl, J. C. Auchet, et al., *Biochim. Biophys. Acta*, **1984**, *801*, 16–25.
- 59** S. S. Lehrer, , *Biochemistry*, **1971**, *10*, 3254–3263.
- 60** G. Sanyal, E. Kim, F. M. Thompson, et al., *Biochem. Biophys. Res. Commun.*, **1989**, *165*, 772–781.
- 61** P. K. Behera, T. Mukherjee, A. K. Mishra, *J. Lumin.*, **1995**, *65*, 131–136.
- 62** S. A. Green, D. J. Simpson, G. Zhou, et al., *J. Am. Chem. Soc.*, **1990**, *112*, 7337–7346.
- 63** I. E. Obyknovennaya, I. M. Vasileva, A. S. Cherkasov, *Opt. Spectrosc.*, **1986**, *60*, 169–171.
- 64** E. J. Bowen, W. S. Metcalf, *Proc. R. Soc. London, Ser.A*, **1951**, *206*, 437–447.
- 65** M. Mac, J. Najbar, D. Phillipis, et al., *J. Chem. Soc., Faraday Trans.*, **1992**, *88*, 3001–3005.
- 66** R. Hutterer, K. Krämer, F. W. Schneider, et al., *Chem. Phys. Lipids*, **1997**, *90*, 11–23.
- 67** S. C. Chao, J. Tretzel, F. W. Schneider, *J. Am. Chem. Soc.*, **1979**, *101*, 134.
- 68** E. Urbano, H. Offenbacher, O. S. Wolfbeis, *Anal. Chem.*, **1984**, *56*, 427–429.
- 69** O. S. Wolfbeis, E. Urbano, *Fresenius' Z. Anal. Chem.*, **1983**, *314*, 577–581.
- 70** K. Washington, M. M. Sarasua, L. S. Koehler, et al., *Photochem. Photobiol.*, **1984**, *40*, 693–701.
- 71** P. B. Bisht, H. B. Tripathi, *J. Lumin.*, **1993**, *55*, 153–158.
- 72** G. E. Johnson, *J. Phys. Chem.*, **1980**, *84*, 2940–2946.
- 73** D. Daems, N. Boens, F. C. Schryver, *Eur. Biophys. J.*, **1989**, *17*, 25–36.
- 74** A. Ahmed, G. Durocher, , *Photochem. Photobiol.*, **1981**, *34*, 573–578.
- 75** K. Kikuchi, C. Sato, M. Watebe, et al., *J. Am. Chem. Soc.*, **1993**, *115*, 5180–5184.
- 76** W. K. Subczynski, J. S. Hyde, A. Kusumi, *Proc. Natl. Acad. Sci. U. S. A.*, **1989**, *86*, 4474–4478.
- 77** M. Hof, *Biochim. Biophys. Acta*, **1998**, *1388*, 143–153.
- 78** E. W. Schlag, S. Schneider, S. Fischer, *Annu. Rev. Phys. Chem.*, **1971**, *22*, 465.
- 79** P. Fromherz, *J. Phys. Chem.*, **1995**, *99*, 7188–7192.
- 80** S. G. Schulman, *Fluorescence and Phosphorescence Spectroscopy: Physicochemical Principles and Practice*, Pergamon Press, New York 1977.
- 81** K. Brand, M. Hof, F. W. Schneider, *Ber. Bunsen-Ges. Phys. Chem.*, **1991**, *95*, 1511–1514.
- 82** T. Foerster, K. Rokos, *Chem. Phys. Lett.*, **1967**, *1*, 279.
- 83** R. Sriram, M. Z. Hoffman, *Chem. Phys. Lett.*, **1982**, *85*, 572.
- 84** J. Baumann, M. D. Fayer, *J. Chem. Phys.*, **1986**, *85*, 4087.
- 85** R. F. Chen, J. R. Knutson, *Anal. Biochem.*, **1988**, *198*, 119.
- 86** R. S. Brown, J. D. Brennan, U. J. Krull, *J. Chem. Phys.*, **1994**, *100*, 6019–6021.
- 87** A. Chattopadhyay, *Chem. Phys. Lipids*, **1990**, *53*, 1.
- 88** H. S. Hendrickson, et al., *Anal. Biochem.*, **1999**, *276*, 27.
- 89** D. Massenburg, B. R. Lentz, *Biochemistry*, **1993**, *32*, 9172.
- 90** B. Bagchi, S. D. Oxtoby, G. R. Fleming, *Chem. Phys.*, **1984**, *86*, 257.
- 91** I. Rips, J. Klafter, J. Jortner, *J. Chem. Phys.*, **1988**, *89*, 4288.
- 92** H. L. Friedman, F. O. Rainieri, F. Hirata, et al., *J. Stat. Phys.*, **1995**, *78*, 239.

- 93** N. G. Bakshiev, *Opt. Spectrosc. (USSR)*, **1964**, *16*, 446.
- 94** Y. T. Masurenko, N. G. Bakshiev, *Opt. Spectrosc. (USSR)*, **1970**, *28*, 490.
- 95** W. Liptay, in *Excited States Vol. 1*, ed. E. C. Lim, Academic Press, New York 1974, p. 129.
- 96** M. L. Horng, J. A. Gardecki, A. Papazyan, et al., *J. Phys. Chem.*, **1995**, *99*, 17320.
- 97** R. Jimenez, G. R. Fleming, P. V. Kumar, et al., *Nature*, **1994**, *369*, 471.
- 98** S. Mukherje, A. Chattopadhyay, *J. Fluorescence*, **1995**, *5*, 237.
- 99** M. Hof, P. Lianos, *Langmuir*, **1997**, *13*, 290.
- 100** H. Zhang, A. M. Jonkman, van der Meulen, et al., *Chem. Phys. Lett.*, **1994**, *236*, 587.
- 101** D. Bingemann, N. P. Ernsting, *J. Chem. Phys.*, **1995**, *102*, 2691.
- 102** A. P. Demchenko, in *Topics in Fluorescence Spectroscopy: Biochemical Applications*, J. ed. R. Lakowicz, Plenum Press, New York 1991, 65.
- 103** A. P. Demchenko, *Biochim. Biophys. Acta.*, **1994**, *1209*, 149.
- 104** W. C. Galley, R. M. Purkey, *Proc. Natl. Acad. Sci. USA*, **1970**, *67*, 1116.
- 105** M. Hof, P. Lianos, A. Laschewsky, *Langmuir*, **1997**, *13*, 2181.
- 106** M. Maroncelli, G. R. Fleming, *J. Chem. Phys.*, **1987**, *86*, 6221.
- 107** M. Hof, J. Schleicher, F. W. Schneider, *Ber. Bunsen-Ges. Phys. Chem.*, **1989**, *93*, 1377.
- 108** R. Hutterer, F. W. Schneider, H. Lanig, et al., *Biochim. Biophys. Acta*, **1997**, *1323*, 195.
- 109** R. Hutterer, M. Hof, in *Recent Research Developments in Lipids*, ed. S. G. Pandalai, Transworld Research Network, in press.
- 110** E. Blatt, K. P. Ghigginio, W. H. Sawyer, *J. Chem. Soc., Faraday Trans. 1*, **1981**, *77*, 2551.
- 111** J. Slavik, *Biochim. Biophys. Acta*, **1982**, *694*, 1.
- 112** J. R. Lakowicz, R. B. Thompson, H. Cherek, *Biochim. Biophys. Acta*, **1983**, *815*, 295.
- 113** M. Hof, R. Hutterer, N. Perez, et al., *Biophys. Chem.*, **1994**, *52*, 165.
- 114** E. D. Matayoshi, A. M. Kleinfeld, *Biochim. Biophys. Acta*, **1981**, *644*, 233.
- 115** R. M. Epand, B. T. C. Leon, *Biochemistry*, **1992**, *31*, 1550.
- 116** R. Hutterer, F. W. Schneider, H. Sprinz, et al., *Biophys. Chem.*, **1996**, *61*, 151.
- 117** R. Hutterer, F. W. Schneider, W. T. Hermens, et al., *Biochim. Biophys. Acta*, **1998**, *1414*, 155–164.
- 118** T. Parasassi, M. Di Stefano, M. Loiero, et al., *Biophys. J.*, **1994**, *66*, 763.
- 119** J. F. Deye, T. A. Berger, A. G. Anderson, *Anal. Chem.*, **1990**, *62*, 615.
- 120** P. Fromherz, *J. Phys. Chem.*, **1995**, *99*, 7185.
- 121** I. H. M. van Stokhum, T. Scherer, A. M. Brouwer, et al., *J. Phys. Chem.*, **1994**, *98*, 852.
- 122** J. Sykora, P. Kapusta, V. Fidler, et al., *Langmuir*, **2002**, *18*(3), 571–574.
- 123** P. R. Callis, *Annu. Rev. Phys. Chem.*, **1997**, *48*, 271–297.
- 124** J. E. Hansen, S. J. Rosenthal, G. R. Fleming, *J. Phys. Chem.*, **1992**, *96*, 3034–3029.
- 125** F. Perrin, *J. Phys. Radium*, **1926**, *7*, 390.
- 126** A. Jablonski, *Bull. Acad. Pol. Sci.*, **1960**, *8*, 529.
- 127** A. Kawska, *Crit. Rev. Anal. Chem.*, **1993**, *23*, 459–529.
- 128** R. F. Steiner, in *Topics in Fluorescence Spectroscopy: Principles*, ed. J. R. Lakowicz, Plenum Press, New York 1991, pp. 1–52.
- 129** B. Q. Ferguson, D. C. H. Yang, *Biochemistry*, **1986**, *25*, 529–539.
- 130** B. M. Gorovits, P. M. Horowitz, *J. Biol. Chem.*, **1995**, *270*, 13057–13062.
- 131** K. Lim, D. M. Jameson, C. A. Gentry, et al., *Biochemistry*, **1995**, *34*, 6975–6984.
- 132** T. J. Lukas, E. H. Burgess, F. G. Pendergast, et al., *Biochemistry*, **1986**, *25*, 1458–1464.
- 133** V. LeTilly, C. Royer, *Biochemistry*, **1993**, *31*, 7753–7758.
- 134** T. Tao, *Biopolymers*, **1969**, *8*, 609.
- 135** G. Lipari, A. Szabo, *Biophys. J.*, **1980**, *30*, 489.
- 136** F. Jaehnig, *Proc. Natl. Acad. Sci. USA*, **1980**, *76*, 6361.
- 137** B. R. Lentz, *Chem. Phys. Lipids*, **1989**, *50*, 171.

- 138** U. A. Van der Heide, G. van Ginkel, Y. K. Levine, *Chem. Phys. Lett.*, **1996**, 253, 118.
- 139** R. E. Dale, J. Eisinger, W. E. Blumberg, *Biophys. J.*, **1979**, 26, 161.
- 140** B. W. Van der Meer, G. Coker, S. Y. S. Chen, *Resonance Energy Transfer Theory and Data*, VCH, Weinheim 1994.
- 141** Th. Foerster, *Discuss. Faraday Soc.*, **1959**, 27, 7–17
- 142** U. Goesele, *Spectrosc. Lett.*, **1978**, 11, 445.
- 143** M. Hauser, U. K. A. Klein, U. Goesele, *Z. Phys. Chem.*, **1976**, 101, 255.
- 144** J. Klafter, A. Blumen, *J. Phys. Chem.*, **1984**, 80, 875.
- 145** P. Lianos, G. Duportail, *Biophys. Chem.*, **1993**, 48, 293–299.
- 146** L. M. M. Loura, A. Fedorov, M. Prieto, *Biophys. J.*, **1996**, 71, 1823–1836.
- 147** J. Schleicher, M. Hof, F. W. Schneider, *Ber. Bunsen-Ges. Phys. Chem.*, **1993**, 97, 172–176.
- 148** J. L. Mergny, A. Slama-Schwok, T. Monteney-Garestier, et al., *Photochem. Photobiol.*, **1991**, 53, 555–558.
- 149** R. I. MacDonald, *J. Biol. Chem.*, **1987**, 10392–10397.
- 150** P. M. Keller, S. Person, W. Snipes, *J. Cell. Sci.*, **1968**, 28, 167–177.
- 151** G. A. Gibson, L. M. Loew, *Biochem. Biophys. Res. Commun.*, **1979**, 88, 135–140.
- 152** D. K. Struck, D. Hoekstra, R. E. Pagano, *Biochemistry*, **1981**, 20, 4093–4099.
- 153** S. J. Morris, D. Bradley, *Biochemistry*, **1984**, 23, 4642–4650.
- 154** J. Connor, A. J. Schroit, *Biochemistry*, **1987**, 26, 5099–5105.
- 155** J. M. Vanderkoi, A. Ierokomas, H. Nakamura, et al., *Biochemistry*, **1977**, 16, 1262–1267.
- 156** W. Veatch, L. Stryer, *J. Mol. Biol.*, **1977**, 113, 89–102.
- 157** C. A. Hasselbacher, T. L. Street, T. G. Dewey, *Biochemistry*, **1984**, 23, 6445–6565.
- 158** L. Tron, J. Szoellosi, S. Damjanovich, et al., *Biophys. J.*, **1984**, 45, 939–946.
- 159** P. L. Khanna, E. F. Ullman, *Anal. Biochem.*, **1980**, 108, 156–161.
- 160** H. C. Cheung, in *Topics in Fluorescence Spectroscopy: Principles*, ed. J. R. Lakowicz, Plenum Press, New York 1991, pp. 127–176.
- 161** H. J. Galla, W. Hartmann, *Chem. Phys. Lipids*, **1980**, 27, 199.
- 162** S. Y. Chen, K. H. Cheng, D. M. Ortalano, *Chem. Phys. Lipids*, **1990**, 53, 321.
- 163** R. Hutterer, A. Haefner, F. W. Schneider, et al., in *Fluorescence Microscopy and Fluorescence Probes*, Vol. 2, ed. J. Slavik, Plenum Press, New York 1998, pp. 93–98.
- 164** P. K. J. Kinnunen, A. Koiv, P. Mustonen, in *Fluorescence Spectroscopy*, ed. O. S. Wolfbeis, Springer Verlag, Berlin 1993, pp. 159–171.
- 165** G. Duportail, P. Lianos, in *Vesicles*, ed. M. Rosoff, Marcel Dekker, New York 1996, pp. 296–372.
- 166** D. Axelrod, D. Koppel, J. Schlessinger, et al., *Biophys. J.*, **1976**, 16, 1055.
- 167** M. Edidin, M. Zagynsky, T. Lardner, *Science*, **1976**, 191, 466.
- 168** R. Peters, J. Peters, K. Tews, et al., *Biochim. Biophys. Acta*, **1974**, 367, 282–294.
- 169** N. Periasamy, S. Bicknese, A. Verkman, *Photochem. Photobiol.*, **1996**, 63, 265.
- 170** C. Eggeling, J. Widengren, R. Rigler, et al., in *Applied Fluorescence in Chemistry, Biology and Medicine*, eds. W. Rettig, B. Strehmel, S. Schrader, et al., Springer-Verlag, Berlin 1999, pp. 193–240.
- 171** N. L. Thompson, T. P. Burghardt, D. Axelrod, *Biophys. J.*, **1981**, 33, 435–454.
- 172** Z. P. Huang, K. H. Pearce, N. L. Thompson, *Biophys. J.*, **1994**, 67, 1754–1766
- 173** K. H. Pearce, M. Hof, B. R. Lentz, et al., *J. Biol. Chem.*, **1993**, 268, pp. 22984–22991.
- 174** W. P. Ambrose, W. E. Moerner, *Nature*, **1991**, 349, 225.
- 175** T. Plakhotnik, D. Walser, M. Pirotta, et al., *Science*, **1994**, 265, 364.
- 176** E. Betzig, R. J. Chichester, *Science*, **1993**, 262, 1422.
- 177** X. S. Xie, R. C. Dunn, *Science*, **1994**, 265, 361.
- 178** P. M. Goodwin, W. P. Ambrose, R. A. Keller, *Acc. Chem. Res.*, **1996**, 29, 607.
- 179** M. D. Barnes, C. Y. Kung, W. B. Whitten, et al., *Anal. Chem.*, **1997**, 69, 2115.

- 180** S. Nie, R. N. Zare, *Annu. Rev. Biophys. Biomol. Struct.*, **1997**, *26*, 567–596.
- 181** M. Orrie, J. Bernard, *Phys. Rev. Lett.*, **1990**, *65*, 2716–2719.
- 182** W. E. Moerner, T. Plakonik, T. Irmgartinger, et al., *J. Phys. Chem.*, **1994**, *98*, 7382–7389.
- 183** N. J. Dovichi, J. C. Martin, J. H. Jett, et al., *Science*, **1983**, *219*, 845–847.
- 184** D. Chen, N. J. Dovichi, *Anal. Chem.*, **1996**, *68*, 690–696.
- 185** S. A. Shopa, L. M. Davis, E. B. Shera, *J. Opt. Soc. Am. B*, **1992**, *9*, 1761–1769.
- 186** M. D. Barnes, W. B. Ramsay, W. B. Whitten, *Anal. Chem.*, **1995**, *67*, 418–423.
- 187** W. P. Ambrose, R. L. Affleck, P. M. Goodwin, et al., *Exp. Tech. Phys.*, **1995**, *41*, 1–12.
- 188** R. C. Dunn, G. R. Holton, L. Mets, et al., *J. Phys. Chem.*, **1994**, *98*, 3094–3098.
- 189** E. Betzig, J. K. Trautmann, *Science*, **1992**, *257*, 189–195.
- 190** J. K. Trautmann, J. J. Macklin, L. E. Bruns, et al., *Nature*, **1994**, *369*, 40–42.
- 191** M. Eigen, R. Rigler, *Proc. Natl. Acad. Sci. USA*, **1994**, *91*, 5740–5747.
- 192** S. Nie, D. T. Chiu, R. N. Zare, *Anal. Chem.*, **1995**, *67*, 2849–2857.
- 193** J. Mertz, C. Xu, W. W. Webb, *Opt. Lett.*, **1995**, *20*, 2532–2534.
- 194** E. B. Brown, J. B. Shear, S. R. Adams, et al., *Biophys. J.*, **1999**, *76*, 489–499.
- 195** P. Schwille, U. Haupis, S. Maiti, et al., *Biophys. J.*, **1999**, *77*, 2251–2265.
- 196** T. Schmidt, G. J. Schultz, W. Baumgartner, et al., *Proc. Natl. Acad. Sci. USA*, **1996**, *9*, 2926–2929.
- 197** R. N. Gosh, W. W. Webb, *Biophys. J.*, **1994**, *66*, 1301–1318.
- 198** R. D. Vale, T. Funatsu, D. W. Pierce, et al., *Nature*, **1996**, *380*, 451–453.
- 199** B. Rauer, E. Neumann, J. Widengren, et al., *Biophys. Chem.*, **1996**, *58*, 3–12.
- 200** L. O. Tjernberg, A. Pramanik, S. Björpling, et al., *Chem. Biol.*, **1999**, *6*, 53–62.
- 201** E. Van Crandenbroeck, Y. Engelborghs, *Biochemistry*, **1999**, *38*, 5082–5088.
- 202** M. Pitschke, R. Prior, M. Haupt, et al., *Nature Medicine*, **1998**, *4*, 832–834.
- 203** P. I. H. Bastiens, E. H. W. Pap, J. Widengren, et al., *J. Fluorescence*, **1994**, *4*, 377–383.
- 204** M. Benes, J. Hudecek, P. Anzenbacher, et al., *Coll Czech Chem. Commun.*, **2001**, *66*, 855–869.
- 205** S. Björpling, M Kinjo, Z. Foldes-Papp, et al., *Biochemistry*, **1998**, *15*, 12971–12978.
- 206** U. Kettling, A. Koltermann, P. Schwille, et al., *Proc. Natl. Acad. Sci. USA*, **1998**, *95*, 1416–1420.
- 207** J. Widengren, R. Rigler, *Cell. Mol. Biol.*, **1998**, *44*, 857–879.
- 208** Z. Foldes-Papp, P. Thyberg, S Björpling, et al., *Nucleosides Nucleotides*, **1997**, *16*, 781–787.
- 209** K. M Berland, P. T. So, E. Gratton, *Biophys. J.*, **1995**, *68*, 694–701.
- 210** J. C. Politz, E. S. Browne, D. E. Wolf, et al., *Proc. Natl. Acad. Sci. USA*, **1998**, *95*, 6043–6048.
- 211** R. Brock, T. M. Jovin, *Cell. Mol. Biol.*, **1998**, *44*, 847–856.
- 212** R. Brock, M. A. Hink, T. M. Jovin, *Biophys. J.*, **1998**, *75*, 2547–2557.
- 213** O. S. Wolfbeis, *Fiber Optic Chemical Sensors and Biosensors*, CRC Press, Boca Raton 1991.
- 214** A. S. Verkman, *Am. J. Physiol.*, **1990**, *253*, C375–C388.
- 215** N. L. Thompson, in *Topics in Fluorescence Spectroscopy: Techniques*, ed. J. R. Lakowicz, Plenum Press, New York 1991, pp. 337–378.
- 216** A. Miyawaki, J. Llopis, R. Heim, et al., *Nature*, **1997**, *388*, 882–887.
- 217** J. A. Thomas, R. N. Buchsbaum, A. Zimmniak, et al., *Biochemistry*, **1979**, *18*, 221–2218.
- 218** T. J. Rink, R. Y. Tsien, T. Pozzan, *J. Cell. Biol.*, **1982**, *95*, 189–196.
- 219** H. Szmacinski, J. R. Lakowicz, in *Topics in Fluorescence Spectroscopy: Probe Design and Chemical Sensing*, ed. J. R. Lakowicz, Plenum Press, New York 1994, pp. 295–334.
- 220** J. R. Lakowicz *Principles of Fluorescence Spectroscopy*, Plenum Press, New York 1999, pp. 531–572.

## **Section III**

### **Methods 2: Nuclear Magnetic Resonance Spectroscopy**

## Introduction

*Edward W. Hagaman*

The nuclei of all elements possess mass and charge. One or more isotopes of most nuclei also have spin, i. e., angular momentum. Since spinning charge creates a magnetic field, there is a magnetic moment,  $\mu$ , associated with the angular momentum. It is this property of matter that is exploited in nuclear magnetic resonance (NMR) spectroscopy. The magnetic moment, a vector quantity, can be aligned in the presence of an intense static magnetic field,  $H_0$ , then manipulated in space, i. e., caused to evolve in time under the influence of specific interactions and, finally, observed. The detected response can provide information about (1) the specific nuclear isotope present, (2) the local structure around the nucleus, and (3) motional dynamics of the matter containing the nuclei. As will be apparent in the following three chapters, the environment reported on by nuclear magnetization extends far beyond the immediate nuclear horizon, giving information on the bonding arrangement of neighboring nuclei many angstroms removed. Each magnetic nucleus in a molecule reports on itself and on its relationship to its neighboring nuclei such that the sum of the overlapping connectivity information from all nuclei redundantly determines a unique structure for the molecule. The goal of much of the research activity in NMR over the past 25 years has been the development of multi-dimensional NMR techniques that make it possible to extract the needed information from NMR spectra. With current, routine solution state  $^1\text{H}$  NMR capabilities it is possible to assign essentially every proton resonance in modest molecular weight proteins to a specific proton in a specific amino acid residue, determine the amino acid sequence, and determine the three dimensional structure of the folded protein. Such a tour de force requires high static magnetic field strengths (today's state of the art magnets have  $H_0 = 21.15$  T, i. e., 900 MHz proton frequency) and modern multi-dimensional correlation pulse sequences replete with their editing, filtering, and solvent suppression schemes. This stunning accomplishment represents one marker on the path of NMR progress that, 55 years after the birth of this spectroscopy, is still a healthy, burgeoning research area that provides one of the most exciting areas in science in which to work.

The quantum mechanical description of the NMR experiment tells us that the maximum observable component of the angular momentum is  $I\hbar/2\pi$ , where  $I$  is

the nuclear spin quantum number, or simply, the spin, and  $\hbar$  is Planck's constant. The magnetic moment is quantized along  $2I + 1$  orientations with respect to the static field. The magnitude of the moment vector is a measure of the strength of the nuclear magnet. It depends on the angular momentum and on the internal structure of the nucleus, i.e., the distribution of protons and neutrons and their associated angular momenta, according to Eq. (1):

$$\mu = \gamma I \hbar / 2\pi \quad (1)$$

where  $\gamma$ , the gyromagnetic ratio, is the proportionality factor between the magnetic moment and the angular momentum.

For  $I = \frac{1}{2}$  nuclei like  $^1\text{H}$ ,  $^{13}\text{C}$ , or  $^{15}\text{N}$ , there are two orientations of the moment in the applied field, aligned parallel and anti-parallel to the field. The force exerted by the static field on the moments causes them to precess about the static field direction. This motion is analogous to that of a toy top: the top spins with its angular momentum along its spinning axis and wobbles (precesses) about the earth's gravitational field. Nuclei with spin  $I > 0$  have isotope-specific nuclear magnetic moments and field dependent addresses,  $\omega_o$ , the precession frequency, given by the Larmor relation:

$$\omega_o = \gamma H_o \quad (2)$$

For typical magnetic field strengths the Larmor frequency is in the radiofrequency region of the electromagnetic spectrum. For protons in an 18.8 T field,  $\omega_o = 800$  MHz; for  $^{13}\text{C}$  in the same field  $\omega_o = 201.6$  MHz.

The NMR experiment consists of inducing transitions between the states of quantized magnetization. This is accomplished by irradiating the sample with radio frequency (rf) energy. The frequency of the rf must exactly match the precession frequency of the nuclei in order to cause the transition. This specificity is the resonance phenomenon, analogous to the tuned circuit in a radio receiver. The tuned receiver (the spin system composed of a specific nuclear isotope) is only capable of interacting with the broadcast signal whose frequency matches the Larmor frequency of the nuclei.

It is our good fortune that NMR has layers of complexity that are not explicitly revealed in Eqs. (1) and (2). Unraveling this complexity (shielding, coupling, relaxation) has been the preoccupation of NMR spectroscopists for more than half a century, and is the topic of this section of the Handbook. Three chapters on nuclear magnetic resonance spectroscopy are assembled. They are authored by outstanding experimentalists working at the forefront of NMR research.

In the opening chapter, "An Introduction to Solution, Solid-State, and Imaging NMR Spectroscopy" Leslie Butler (Louisiana State University) introduces the fundamental structure parameters in the NMR experiment through a discussion on solution state  $^1\text{H}$  NMR. The shielding of nuclei by core and valence electrons, gives rise to those structure-pregnant numbers called chemical shifts,  $\delta$ , that have been accrued and correlated since the earliest days of NMR. Scalar coupling,

$J$ , is the through-bond transmission of spin state orientation that historically has been the avenue through which chemists have established bonded atom relationships, configuration and conformation in molecules. This section is followed by a discussion of properties commonly studied through solid state NMR, namely, chemical shift anisotropy, dipolar coupling, and quadrupolar interactions. A section on spin-lattice relaxation precedes a discussion of the use of NMR to measure the dynamics of molecular motion. A short introduction to NMR imaging follows to acquaint the reader with spin density mapping using linear gradients. The chapter ends with a description of a 3D NMR experiment used to establish atom connectivity and provides an appropriate segue into the next chapter.

The chapter “Solution State NMR” by Gary Martin, Chad Hadden and David Russell (Pharmacia Corporation) begins with an exposition of the uses of scalar coupling in the context of one-dimensional (1D) experiments. Homonuclear decoupling experiments and nuclear Overhauser effect (NOE) difference spectroscopy are illustrated before moving on to heteronuclear coupling and the selective population transfer (SPT) experiment. SPT is the basis for enhanced signal intensity in the non-selective polarization transfer experiments, INEPT and DEPT,  $J$ -modulated experiments that sort  $^{13}\text{C}$  spectra into resonance subsets based on carbon multiplicity groups, e.g., C, CH,  $\text{CH}_2$ , and  $\text{CH}_3$  groups. The principles of two-dimensional (2D) NMR are introduced and illustrated in the context of 2D  $J$ -resolved spectroscopy in which the 2D spectrum correlates chemical shifts on one axis with scalar coupling on the second frequency axis. Homonuclear 2D NMR experiments in which both frequency axes are chemical shift and that reveal  $J$  coupling partners (COSY, TOCSY) or NOE connected partners (NOESY, ROESY) as off-diagonal elements are illustrated. The focus then shifts to heteronuclear chemical shift correlation and treats experiments based on one-bond coupling (HMQC, HSQC). Heteronuclear chemical shift correlation via long-range coupling (HMBC) is described in turn along with multiplicity-edited versions of these experiments. In current practice, most 2D NMR experiments are implemented using pulsed field gradients (PFGs) to select coherence transfer pathways in lieu of using phase cycling routines, as originally conceived, to successively add desired magnetization components and cancel unwanted magnetization components. Thus, gradient COSY (GCOSY), GHMQC and GHMBC, for example, are the modern experiments in use, giving the same experimental correlations, but with excellent artifact cancellation and time savings, in instances where sample size is not limiting. Pulse sequence modifications which optimize the HMBC experiment over a range of  $J$  coupling amplitudes are discussed and end with a description of  $^2J$ ,  $^3J$  HMBC, an experiment which makes possible the detection *and* differentiation of two-bond and three-bond proton couplings to protonated carbon and nitrogen centers. It is worth reflecting for a moment on the evolution in the use of three-bond coupling that has occurred since the early discovery of scalar coupling. Correlations of unambiguous  $^3J$  with structure, i. e., Karplus relations, dihedral angle dependence of three-bond coupling, were established in many molecular fragments. Karplus relationships have been used to make structural and conformational predictions in applicable systems, it being necessary to establish independently the correct designation of

similar magnitude two- and three-bond long-range couplings.  $^2J$ ,  $^3J$  HMBC now provides the long-range assignment capability, experimentally distinguishing  $^2J$  from  $^3J$ .

The chapter continues with an overview of inverse (proton-detected) ‘hyphenated’ 2D NMR techniques which join together two correlation experiments. HSQC-TOCSY, for example, first labels protons with the chemical shift of the directly bound heteronuclide,  $^{13}\text{C}$  say, in the HSQC part of the experiment, and after the magnetization is transferred back to the proton, homonuclear vicinal coupling is propagated between contiguous protons in the homonuclear TOCSY segment of the experiment. The proton magnetization ultimately acquired provides homonuclear correlated spin systems sorted by the chemical shift of the directly bound carbon(s) in question.

In cases in which just a select coupling or correlation is needed from a spectrum to complete an assignment or structure determination, a complete 2D analysis may not be required. There are one-dimensional analogues of 2D NMR experiments which can provide the specific information in a more time-efficient manner than performing a full 2D NMR analysis. Examples of 1D analogs for NOESY and HETCOR experiments are described that use field gradients to select the resonance of interest.

The chapter concludes with a discussion of NMR sensitivity using probes designed for small samples. 2D NMR data are presented for a submicro gradient (SMIDG) probe that demonstrate the current performance (10s of micrograms) for sample limited NMR analysis. The future in the area of small sample NMR studies is in the development of cold metal NMR probes, i.e., cryogenic probes, which have the potential to reduce analysis time by nearly an order of magnitude. A COSY spectrum on a 2.9  $\mu\text{g}$  sample of Taxol and an HSQC spectrum of the aliphatic region of strychnine (40  $\mu\text{g}$ ), recorded in 45 min. and <2 h, respectively, illustrate the state of the art in sensitivity using cryogenic probe technology.

The chapter “Solid State NMR” by Lyndon Emsley and Steven Brown (Ecole Normale Supérieure de Lyon) begins with sketches of the major interactions that lead to spectral broadening in the solid state. The motionally averaged spectrum observed in solution NMR is replaced in the solid phase with a more complex spectrum reflecting the tensor character of the chemical shift (CSA), dipolar coupling ( $D$ ), and quadrupolar coupling, ( $C_Q$ ). Each of these anisotropic interactions can broaden the NMR resonance beyond the normal limits of the isotropic chemical shift distribution. This, in and of itself, does not prevent analysis of the spectrum. The theoretical description of the spectrum is well known for each interaction and the appropriate parameters can be extracted, in principle, by fitting the experimental and calculated spectrum. However, this method fails for materials where many resonances overlap.

In typical applications, say of organic solids by  $^{13}\text{C}$  NMR, microcrystalline solids or amorphous samples are studied in which all orientations of molecules are present. Each  $^{13}\text{C}$  in a molecule is represented by a distribution of resonances, a powder pattern, which reflects the orientation dependence of the chemical shift and  $^1\text{H}$ – $^{13}\text{C}$  dipolar interactions. The experimental spectrum is the sum of powder patterns from all the resonances in the spectrum, and as such usually presents a

nearly featureless and uninterpretable solid state NMR spectrum. The authors present the principal line narrowing method used in solid state NMR, namely, magic angle spinning (MAS), in which the sample is mechanically spun along a unique axis, inclined at angle  $\theta = 54.74^\circ$  with respect to the static field axis. This coherent motion narrows the orientation dependent CSA and  $D$  interactions by the factor  $(1-3\cos^2\theta)$ . At the magic angle, the chemical shift tensor reduces to the isotropic chemical shift and the dipolar interaction vanishes, yielding a high-resolution spectrum. In practice, the sample cannot be spun fast enough using current technology to completely remove the broadening from dipolar interactions. MAS is used in concert with high power decoupling (dipolar decoupling) to eliminate the dipolar broadening.

Having demonstrated the achievement of high-resolution solid state NMR capability, the authors describe experiments that combine the high-resolution aspect of MAS NMR with methods that retain the structure and/or dynamic information inherent in the anisotropic interactions. Rotational-echo double resonance (REDOR) allows the determination of  $D$  between isolated heteronuclear spin pairs.  $D$  is related simply and without approximation to internuclear separation. Hence, REDOR makes possible the unambiguous direct determination of internuclear distance between the labeled spin pair, independent of pair orientation, i.e., in *amorphous* and /or *microcrystalline* solids, and extends our ability to quantitatively explore complex materials. It is also possible to extract internuclear distance from homonuclear dipolar coupled spin pairs, and these experiments are also reviewed.

As in solution state NMR, the extension of experiments into two or more dimensions is the path used to gain the resolution required to measure multiple, large anisotropic interactions (dipolar coupling, CSA) that are accessible in solids. Experiments that focus on homonuclear multi-dimensional experiments include  $J$ -mediated  $^{13}\text{C}$ – $^{13}\text{C}$  correlation and dipolar-mediated  $^1\text{H}$  2D double quantum (DQ) MAS spectroscopy. The authors give an example of the state of the art in solid state  $^1\text{H}$  NMR line narrowing experiments using combined rotation and multiple pulse decoupling (CRAMPS), and indicate that the newest variants of this experiment have yielded line widths as low as 60 Hz for the aliphatic protons resonances of the amino acid L-alanine.

The correlation of anisotropic and isotropic interactions in 2D NMR are illustrated with experiments that measure the chemical shift anisotropy of spin  $\frac{1}{2}$  nuclei. Results using the elegant magic angle turning experiment (MAT) are illustrated for the monoterpane verbenol that show the determination of the CSA tensor quantities for all carbons in this polymorphic substance. The usefulness of 2D NMR methods for characterizing chemical exchange processes is illustrated using static  $^2\text{H}$  NMR and MAS  $^{13}\text{C}$  NMR. In contrast to the rotor synchronized  $^1\text{H}$ – $^1\text{H}$  DQ MAS experiment referred to above, this experiment can also be performed using a large spectral width in the isotropic dimension, re-introducing the spinning sideband patterns in the spectrum. From their intensities it is possible to calculate  $D$  directly and, hence, inter-proton distances. The applications of this experiment and others that allow the measurement of proton–heteroatom distances situate NMR as a powerful method to quantitatively study hydrogen bonding.

The focus of the chapter then shifts to heteronuclear 2D correlation (HETCOR) experiments. The evolution of single quantum coherence (SQC) of two different nuclei in these experiments with a coherence transfer step provides the basic formula for these correlations. In  $^1\text{H}$ – $^{13}\text{C}$  WISE (wide line separation), a wide dipolar broadened  $^1\text{H}$  resonance is correlated with narrow  $^{13}\text{C}$  resonances in the isotropic  $^{13}\text{C}$  dimension. These experiments are used to distinguish rigid and mobile components of mixtures as the width of the  $^1\text{H}$  dipolar coupling in the  $^1\text{H}$  dimension is partially averaged by molecular motion.  $^1\text{H}$ – $^{13}\text{C}$  correlation with high resolution in both dimensions is useful for establishing one bond correlations using the dipolar coupling. In contrast to using  $D$ , experiments that use the isotropic  $J$  coupling for the coherence transfer are complementary signal assignment methods that only detect intra-molecular contributions to the correlations.

Experiments that allow the measurement of multiple heteronuclear dipolar couplings in a single experiment and, hence, the simultaneous measurement of multiple internuclear distances, are reviewed. Variations of these experiments are also reported that allow the determination of bond angles, e.g., the H–N–H bond angle in the  $\text{NH}_2$  group, and torsion angles in fragments like  $\text{H}^{\text{N}}-\text{N}-\text{C}^{\alpha}-\text{H}^{\alpha}$ . The application of heteronuclear 2D correlation experiments using  $^{15}\text{N}$  chemical shift and  $^{15}\text{N}$ – $^1\text{H}$  dipolar coupling in oriented samples, i.e., uniformly  $^{15}\text{N}$ -labeled membrane proteins in an oriented lipid bilayer, allows the determination of the tilt angle of a polypeptide helix with respect to the bilayer normal.

This chapter concludes with a section on measuring spectra of half-integer quadrupolar nuclei. For such nuclei the central transition,  $m_{\text{l}} = +1/2 \leftrightarrow m_{\text{l}} = -1/2$ , is not broadened by the quadrupolar coupling to first order, and is observable. The resonance is broadened to second order by a fourth rank tensor contribution that is not removed by MAS. This broadening often confuses the recognition of chemically or crystallographically distinct sites. Mechanical methods to eliminate this broadening, i.e., dynamic-angle spinning (DAS) and double rotation (DOR) are summarized. The 2D multiple quantum magic angle spinning (MQ/MAS) technique is an echo experiment that refocuses the second order quadrupolar broadening and yields 2D spectra from which both quadrupolar and chemical shift parameters can be extracted. The MQ/MAS experiment extends the effective domain of solid state NMR to dozens of half-integer quadrupolar nuclei using conventional MAS technology. This robust experiment has already proven itself capable of providing new insight into many inorganic systems.

It is an understatement to say that the manipulation of nuclear magnetization in physical and spin space described in the three chapters of this section on NMR constitute one of the most powerful spectroscopic approaches to the study of matter in solution and solid phases. NMR continues to evolve in delightful ways that keeps this spectroscopy fresh and applicable in solving structure and dynamics problems in complex materials.

## 7

# An Introduction to Solution, Solid-State, and Imaging NMR Spectroscopy

*Leslie G. Butler*

### 7.1

#### Introduction

Nuclear magnetic resonance is a flexible technique with many applications [1, 2]. For substances dissolved in solution, NMR observation of  $^1\text{H}$ ,  $^{13}\text{C}$ ,  $^{15}\text{N}$ , and  $^{31}\text{P}$  yields structures of organic molecules, organometallic complexes, proteins, and nucleic acid oligomers. For solid materials,  $^2\text{H}$  and  $^{13}\text{C}$  NMR yields polymer structure,  $^{27}\text{Al}$  and  $^{29}\text{Si}$  NMR spectra yield zeolite and cement structures, and  $^{17}\text{O}$  and  $^{63/65}\text{Cu}$  NMR yield properties of high- $T_c$  superconductors. For solids containing fluid inclusions,  $^1\text{H}$  NMR yields porosity and diffusivity information, even from thousands of meters below ground with *in situ* NMR instruments lowered through boreholes into petroleum formations. NMR is a fast, sensitive measure of magnetic fields; based on this, airborne NMR was used to detect submarines, and satellite-mounted NMR mapped the Earth's magnetic field. Adding a magnetic field gradient yields an imaging experiment:  $^1\text{H}$  and  $^{31}\text{P}$  MRI provide three-dimensional views of the human body, even showing specific brain activity. Even our breathing can be visualized with  $^{129}\text{Xe}$  MRI.

In synthetic organic and organometallic chemistry, solution-state NMR means a 300–500 MHz NMR spectrometer, high-precision glass sample tubes, 2 ml of deuterated solvent (typically fully deuterated chloroform, acetone, benzene, or dichlorobenzene), several milligrams of pure sample, and a basic suite of  $^1\text{H}$  and  $^{13}\text{C}$  NMR experiments [3–7]. With several hours of spectrometer time and data interpretation, the structures of new compounds with molecular weights up to 2000 Da can be determined, especially when analyzed along with results from NMR databases and mass spectroscopy.

The structure of a protein in solution usually compares well with a crystallographic determination. However, not all proteins crystallize, and crystals of membrane-bound proteins are especially rare. Hence, the 600–800 MHz and newly constructed 900 MHz NMR spectrometers are largely allocated for biological samples [8, 9]. Although most proteins are studied in solution, membrane-bound proteins may be studied in assembled bilayers. Currently, the greater part of NMR technol-

**Table 7.1** NMR spectrometers and applications.

<i><sup>1</sup>H Resonance</i>	<i>Magnet</i>	<i>Applications</i>
600–900 MHz	narrow-bore superconducting	biological NMR
100–500 MHz	narrow-bore superconducting	organic chemistry
200–750 MHz	wide-bore superconducting	materials science
40–100 MHz	benchtop permanent magnet	quality control
40 MHz	1 m open-access permanent magnet	whole body imaging
200 MHz	1 m bore superconducting	whole body imaging and spectroscopy
ca. 50 MHz	permanent magnet fringe field	borehole logging

ogy research and development efforts is directed towards new techniques in biological NMR, especially magnet development and software for data analysis.

In material science applications solid state NMR often employs a 200–750 MHz NMR spectrometer (Table 7.1) with a wide-bore magnet and high-power RF amplifiers and matching NMR probes [10–12]. This equipment is especially useful for analysis of polymer structures with  $^2\text{H}$  and  $^{13}\text{C}$  NMR and for analysis of zeolites with  $^{27}\text{Al}$  and  $^{29}\text{Si}$  NMR. In polymers, local dynamics can be studied with time scales ranging from seconds to picoseconds; phase separations can be studied with domain sizes from nanometers to micrometers. For zeolites, the structures are characterized in terms of silicon/aluminum ratios, aluminum–hydrogen distances, and the chemistry of catalytic sites.

Why is NMR so widely used? In brief, NMR gives detailed information for selected nuclei, information about the chemical bonding, the local electronic structure, and the local site dynamics. For example, in protein NMR, each of the 20 amino acids has a distinctive set of resonances. Also, these resonances shift slightly with a twist of the amide bond, and other interactions yield the distance between one amino acid and its neighbors, provided that the distance is less than about 8 Å.

What makes NMR such a unique analytical technique? NMR uses the very weak interaction between a nucleus and the rest of the universe. The interaction between the magnetic moment of a nucleus and the RF field of an NMR pulse/receiver circuit is extremely weak: of the order hundreds of MHz versus several eV for optical spectroscopy (500 MHz corresponds to about 2  $\mu\text{eV}$ ). At first glance, this seems to be an enormous disadvantage as, for an equivalent sample mass, NMR has a much lower signal-to-noise ratio relative to many other spectroscopic techniques. However, the weak interaction also yields extremely high resolution. The weak interaction isolates the nucleus from external perturbation for long periods; relaxation times of the order of seconds are common and, conversely, line widths can be less than 1 Hz. Small changes to the environment at an NMR-active nucleus can be detected and identified. Most other analytical techniques are burdened with broad line widths.

How sensitive is an NMR resonance to the environment at the nucleus? Consider these observations:

- In a material such as diamond, the NMR signal can be saturated, and it will be nearly a day before the signal is regained; the spin–lattice relaxation time for  $^{13}\text{C}$  in diamond is hours as the rare (1.08 atom%)  $^{13}\text{C}$  nuclei in diamond individually have weak interactions with the rest of the universe.
- Following pulse excitation, a coherent signal can typically be observed for 10–100 ms (solid) and 1–10 s (liquid samples). The natural line widths are roughly the inverse of these decay times.
- NMR spectroscopy of organic molecules relies on shifts and couplings between nuclei separated by several chemical bonds. The couplings between nuclei separated by two and three chemical bonds is especially important in protein NMR, even though the coupling is 10 Hz or less.

NMR theory is extensive: a working knowledge for materials science applications requires an understanding of these models and concepts:

- The rotating frame is used for simple descriptions of spin–lattice ( $T_1$ ) and spin–spin ( $T_2$ ) relaxation and some basic pulse sequences.
- Time-independent quantum mechanics gives transition frequencies and intensities for static systems (solids) or systems in the fast motion limit (solutions) subject to  $J$ -coupling, chemical shift, and quadrupolar coupling interactions.
- Motional averaging, for example, a two-site exchange, will affect both solution and solid state spectra.
- Time-dependent quantum mechanics can be used to describe the spin system evolution in multiple pulse experiments.

In this short introduction to NMR spectroscopy, a discussion of important NMR parameters will be presented through experiments that cover solution-state  $^1\text{H}$  NMR, solid-state NMR and magnetic resonance imaging.

## 7.2 Solution-state $^1\text{H}$ NMR

Consider the molecule in 1-chloroethene (vinyl chloride),  $\text{ClCHCH}_2$ , a carcinogenic gas (<http://toxnet.nlm.nih.gov/>) and a precursor for polyvinylchloride. If we study the most common isotopomer, all hydrogens are  $^1\text{H}$  (nuclear spin =  $1/2$ ), both carbons are  $^{12}\text{C}$  ( $S = 0$ ), and the chlorine is either  $^{35}\text{Cl}$  or  $^{37}\text{Cl}$  (both  $S = 3/2$ ). 1-Chloroethene will dissolve in chloroform, thus the solvent of choice is deuterated chloroform,  $\text{CDCl}_3$ , commonly available in solution-state NMR labs. The typical NMR tube is a thin-wall glass tube and too likely to break to risk a hazardous, volatile sample. A better choice is a thick-walled NMR tube sealed with an attached O-ring valve; flame sealing is sometimes used. Since detailed toxicological studies often use isotopic labels to follow the metabolic pathways of a toxin, let us note in the following discussion the ability of NMR to monitor the position of a

label, either  $^2\text{H}$  or  $^{13}\text{C}$ , in the 1-chloroethene molecule. In the following discussion, it should become obvious that NMR is an effective method for deducing subtle details of molecular structure and has distinct advantages over mass spectrometry or vibrational spectroscopy.

A typical solution-state  $^1\text{H}$  NMR spectrum of 1-chloroethene is shown in Fig. 7.1. We are first shocked by 11 peaks as we expected only three, one for each hydrogen. The physicist Murray Gell-Mann said at the discovery of the subatomic particle, the quark, "Who ordered this?" In general, spectroscopy should yield sufficient, but not overwhelming, information. Here, we will examine the 1-chloroethene spectrum and learn for ourselves if the 11 peaks are overwhelming or just what we might have ordered. A few general questions:

- Can chemical structure be used to predict the spectrum. Conversely, can the spectrum be used to predict the chemical structure?
- Can the spectrum be generated from a few parameters?
- Experimentally, can the adjustment of a few parameters modify the spectrum in a predictable manner?
- Do experimental procedures exist to simplify the spectrum?
- How does the spectrum change with deuteration or  $^{13}\text{C}$  labeling?
- How does the spectrum change with chemical modification, for example, fluorine for chlorine?

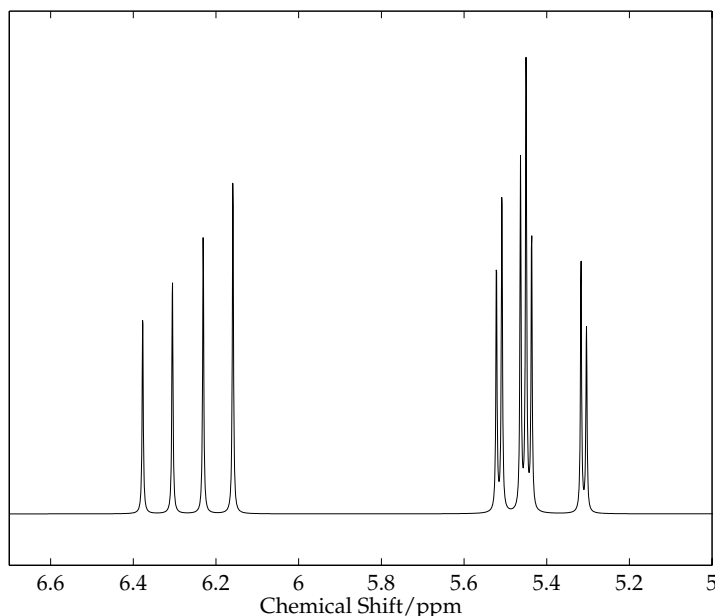


**Figure 7.1** Solution-state  $^1\text{H}$  NMR spectrum (3.33 ms per complex data point) and (simulated) of 1-chloroethene for  $B_0 = 2.3488 \text{ T}$ , 212 complex data points. At this resolution,  $\nu_{RF} = (1 - 6 \times 10^{-6}) \times 100 \text{ MHz}$ ,  $T_2 = 1 \text{ s}$ , 11 distinct peaks are observed.  
spectral width = 300 Hz (digitization rate =

The parameters which determine the 1-chloroethene spectrum are magnetic field ( $B_0$ ), detection frequency ( $\nu_{RF}$ ), nuclear spin, gyromagnetic ratio, chemical shift, and  $J$ -coupling constants.

Briefly, a  $^1\text{H}$  nucleus in a magnetic field of 2.3488 T will typically resonate within 1 kHz of 100 MHz. Because of the response of the molecule's core and valence electrons to the magnetic field, the actual field at the nucleus will be slightly different, that is, it will be "shifted" from 2.3488 T, hence the label "chemical shift", with the symbol  $\delta$  and in units of parts per million (ppm). Based on the asymmetric structure of 1-chloroethene, all three hydrogens will have slightly different chemical shifts, as shown in Fig. 7.2. For example, in 1-chloroethene,  $\text{H}_a$  has a chemical shift of 6.26 ppm, while for the analogous vinyl fluoride, the shift for the  $\text{H}_a$  is reduced to 6.17 ppm. On the basis of years of experience with NMR spectroscopy, chemical shift databases are available for  $^1\text{H}$ ,  $^{13}\text{C}$ ,  $^{15}\text{N}$ ,  $^{29}\text{Si}$ ,  $^{19}\text{F}$ , and most other  $S = 1/2$  nuclei. In many cases, approximate correlations are noted between chemical bonds, such as carbon–carbon single, double, and triple bonds; the electronegativity of substituents, such as F, Cl, and  $\text{NO}_3$ ; and other molecular features in organic and organometallic compounds. In practice, a synthetic chemist or structural biochemist may become a walking database of  $^1\text{H}$ ,  $^{13}\text{C}$ , and  $^{15}\text{N}$  chemical shifts. The definition of chemical shift is:

$$\delta = \frac{\nu - \nu_{\text{reference}}}{\nu_{\text{reference}}} \times 10^6 \text{ ppm} \quad (1)$$

where  $\nu$  is the observed NMR frequency and  $\nu_{\text{reference}}$  is the frequency at which a reference molecule has  $\delta = 0$  ppm in that magnetic field.

The  $J$ -coupling constants describe short-range, through-bond (as opposed to through-space) interactions which connect the spins of neighboring nuclei. An immensely positive result is connectivity information. A minor negative result is a visually complicated spectrum. However, there are experimental methods which simplify the spectrum: one method is to increase the magnetic field from 2.3488 T by a factor of four or eight, as will be discussed shortly.

The solution-state  $^1\text{H}$  NMR spectrum of 1-chloroethene (Fig. 7.1) is easily described by time-independent quantum mechanics using an uncoupled basis set of spin functions. The total Hamiltonian is

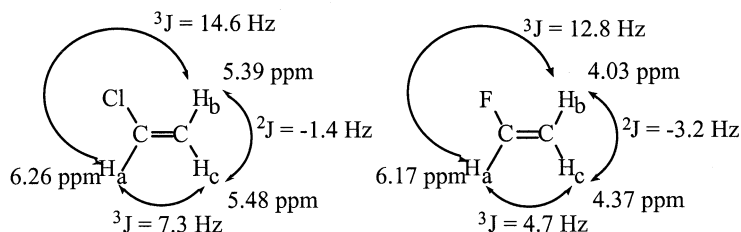


Fig. 7.2  $^1\text{H}$  NMR parameters, chemical shifts and  $J$ -coupling constants, for 1-chloroethene and 1-fluoroethene.

$$\begin{aligned}
 H_{\text{total}}[\text{Hz}] = & -\frac{\gamma_{\text{H}}B_0}{2\pi}(1 + \delta_A)S_{zA} - \frac{\gamma_{\text{H}}B_0}{2\pi}(1 + \delta_B)S_{zB} - \frac{\gamma_{\text{H}}B_0}{2\pi}(1 + \delta_c)S_{zC} + \dots \\
 J_{AB}[S_{xA} \times S_{xB} + S_{yA} \times S_{yB} + S_{zA} \times S_{zB}] + \dots \\
 J_{AC}[S_{xA} \times S_{xC} + S_{yA} \times S_{yC} + S_{zA} \times S_{zC}] + \dots \\
 J_{BC}[S_{xB} \times S_{xC} + S_{yB} \times S_{yC} + S_{zB} \times S_{zC}]
 \end{aligned} \tag{2}$$

where  $\gamma_{\text{H}}$  is the gyromagnetic ratio for hydrogen,  $B_0$  is the applied magnetic field, and  $S_{zA}$ , etc. are the spin functions for  $S=1/2$ . The chemical shifts and  $J$ -coupling constants are as defined in the line structure above. Evaluation of Eq. (2) in matrix form yields an  $8 \times 8$  matrix in bra-ket notation:

$$\left( \begin{array}{cccccccc} -150,000,851 & 0 & 0 & 0 & 0 & 0 & 0 & 0 \\ 0 & -50,000,306 & -0.7 & 0 & 3.65 & 0 & 0 & 0 \\ 0 & -0.7 & -50,000,319 & 0 & 7.3 & 0 & 0 & 0 \\ 0 & 0 & 0 & 50,000,225 & 0 & 7.3 & 3.65 & 0 \\ 0 & 3.65 & 7.3 & 0 & -50,000,236 & 0 & 0 & 0 \\ 0 & 0 & 0 & 7.3 & 0 & 50,000,316 & -0.7 & 0 \\ 0 & 0 & 0 & 3.65 & 0 & -0.7 & 50,000,311 & 0 \\ 0 & 0 & 0 & 0 & 0 & 0 & 0 & 150,000,862 \end{array} \right) \text{ Hz} \tag{3}$$

The off-diagonal elements from the  $J$ -coupling interaction are small and scarcely perturb the energy levels defined by the chemical shift and Zeeman interaction. On the other hand, the experimental resolution is frequently better than 1 Hz, so even small interactions can be observed. The allowed transitions are single quantum; for example, spin  $H_A$  will absorb a single quantum of energy near 100 MHz while  $H_B$  and  $H_C$  stay in one of four possible quantum configurations. Diagonalization of Eq. (3) yields the energy levels; the unitary matrix that performs the matrix diagonalization yields the relative transition probabilities. Listed in Tab. 7.2 are the 12 allowed transitions.

Of the 12 transitions listed, two are overlapping at the resolution of the spectrum shown in Fig. 7.1. The peaks have Lorentzian lineshapes. The full width at half of the maximum peak height (FWHM) is given by:

$$\Delta\nu = 1/\pi T_2 \tag{4}$$

In Fig. 7.1,  $T_2$  is set at 1 s, hence the peak widths are 0.3 Hz.

In Fig. 7.1, four peaks appear at frequencies just slightly greater than the detection frequency ( $\nu_{\text{RF}} = 100 \text{ MHz} + 6 \text{ ppm} = (1 + 6 \times 10^{-6}) \times 100 \text{ MHz}$ ) and seven resolved peaks occur at lower frequencies. The NMR parameters, chemical shifts and  $J$ -coupling constants, are given in Fig. 7.2 and cannot be determined precisely

**Table 7.2** Calculated  $^1\text{H}$  NMR transitions for 1-chloroethene at  $B_0 = 2.3488 \text{ T}$ .

$ abc\rangle$	$E(\text{i})/\text{MHz}$	$\langle abc $	$E(\text{f})/\text{MHz}$	$v \cdot v_{\text{RF}}/ \text{Hz}^a$	<b>Amplitude</b>	<b>Nucleus<sup>b</sup></b>	$\delta/\text{ppm}$
---	50,000,224	---	150,000,862	37.7	0.764	H <sub>A</sub>	6.38
+--	-50,000,320	--+	50,000,311	30.5	0.902	H <sub>A</sub>	6.31
++-	-50,000,306	-+-	50,000,317	23.1	1.052	H <sub>A</sub>	6.23
+++	-150,000,851	-++	-50,000,236	15.9	1.281	H <sub>A</sub>	6.16
-++	-50,000,236	-+-	50,000,317	-47.9	0.949	H <sub>C</sub>	5.52
--+	50,000,311	---	150,000,862	-49.2	1.235	H <sub>C</sub>	5.51
-++	-50,000,236	--+	50,000,311	-53.7	1.332	H <sub>B</sub>	5.46
-+-	50,000,317	---	150,000,862	-55.0	1.001	H <sub>B</sub>	5.45
+++	-150,000,851	++-	-50,000,306	-55.1	0.760	H <sub>C</sub>	5.45
-++	-50,000,320	++-	50,000,224	-56.4	1.057	H <sub>C</sub>	5.44
+++	-150,000,851	++-	-50,000,320	-68.3	0.959	H <sub>B</sub>	5.32
-+-	-50,000,306	++-	50,000,224	-69.6	0.707	H <sub>B</sub>	5.30

<sup>a</sup> $v_{\text{RF}} = 100 \text{ MHz} + 6 \text{ ppm} = (1 + 6 \times 10^{-6}) \times 100 \text{ MHz}$

<sup>b</sup>Transition dominated by spin function at this site.

by inspection of the spectrum in Fig. 7.1. Basically, the spectrum in Fig. 7.1 is difficult to interpret because the off-diagonal elements (Eq. (3)) are large with respect to the differences between diagonal elements. Since we can increase  $B_0$ , which then increases the magnitude of the diagonal elements, spectra acquired at higher magnetic field will show a closer, more obvious relationship with the NMR parameters such as chemical shifts and  $J$ -coupling constants. The NMR spectra of 1-chloroethene at increasing magnetic fields is shown in Fig. 7.3.

Here, the linear dependence of the diagonal components of  $H_{\text{total}}$  terms such as  $-\gamma B_0(1 + \delta_A)S_{zA}$ , causes the increased dispersion of peaks at higher magnetic fields. To observe the subtle effects of the  $J$ -coupling constants, it is convenient to replot the spectra on the chemical shift scale, Eq. (1), as shown in Fig. 7.4.

When solution-state NMR spectra are plotted on a chemical shift scale, the center-of-mass of a group of peaks defines the chemical shift for that nucleus, provided that the field is large enough to diminish the effect of the off-diagonal  $J$ -coupling terms. We can see above that good estimates of  $\delta(H_A)$  can be read from the plots at all magnetic fields but that values for  $\delta(H_B)$  and  $\delta(H_C)$  require a 400 MHz or larger NMR spectrometer. Thus, increasing the magnetic field is one experimental method for simplifying the NMR spectrum.

In addition to magnetic field, the two other experimental methods frequently used for spectral simplification and/or modification are selective decoupling and chemical modification. Selective decoupling can be done in a variety of ways; one method is the application of low power RF over a narrow frequency range during the time of NMR signal acquisition. Within a selected, narrow frequency range, low power RF causes the nuclei to undergo rapid absorption and stimulated emission. In simple terms, a nucleus, such as H<sub>B</sub>, will flip rapidly between spin up and spin down states. If the flip-rate is fast enough, the  $J$ -coupling terms involving

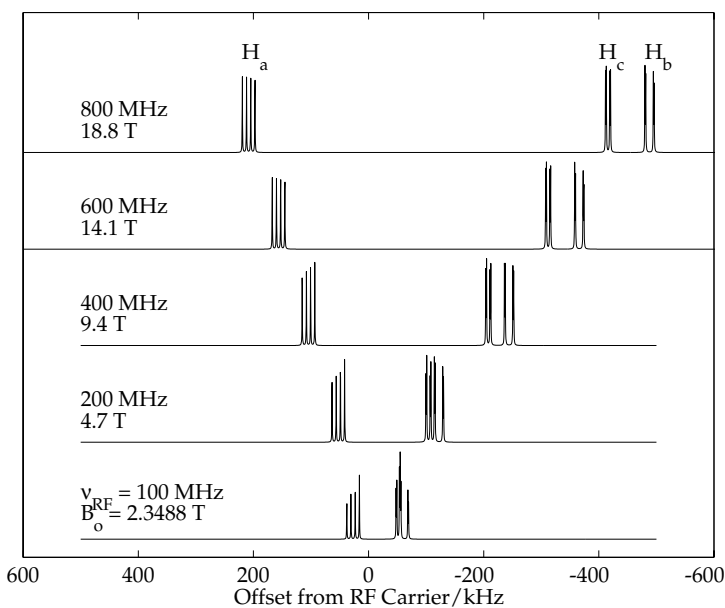


**Fig. 7.3** Solution-state  $^1\text{H}$  NMR spectrum of 1-chloroethene, plotted on the frequency scale. For each spectrum, the RF carrier,  $v_{\text{RF}}$ , is set to  $(1 + 6 \times 10^{-6}) \times 100 \text{ MHz}$ , 200 MHz, etc.

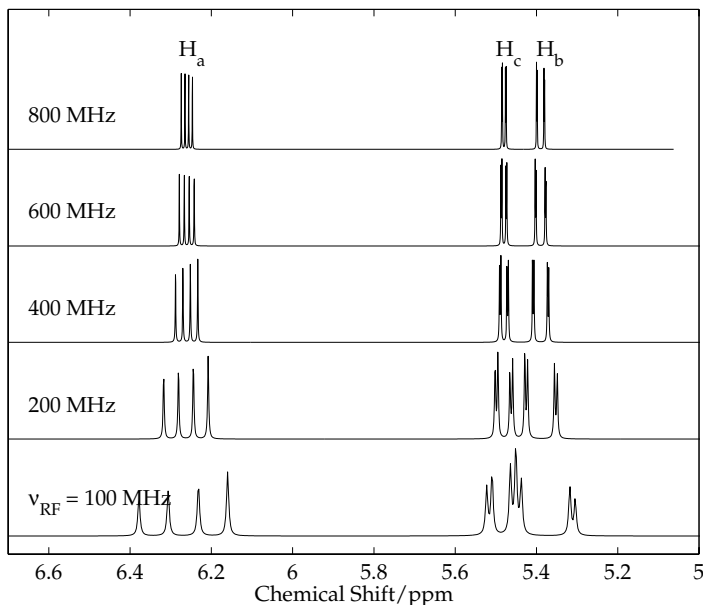


**Fig. 7.4** Solution-state  $^1\text{H}$  NMR spectrum of 1-chloroethene, plotted on the chemical shift scale. Here, the zero, 0 ppm, is set by  $v_{\text{reference}}$ , the frequency at which hydrogens of a chemical shift standard are resonant at  $B_0$ .

nucleus  $H_B$  in Eq. (2) average to zero; the NMR jargon is  $H_B$  is “decoupled” from the other spins. The effect of  $H_B$  decoupling is shown in Fig. 7.5b. Compared to the original 200 MHz spectrum for 1-chloroethene (Fig. 7.5a), the decoupled spectrum is quite simple, a four-line pattern which clearly shows two hydrogens with chemical shifts of 6.26 and 5.48 ppm and a  $J$ -coupling of 7.3 Hz. Similarly, the decoupling of  $H_C$  yields another four-line pattern, (Fig. 7.5c) showing resonances centered at 6.26 and 5.39 ppm, and a  $J$ -coupling of 14.6 Hz.

To explore the relationship between structure and NMR parameters, a series of similar molecules should be studied. Shown in Fig. 7.5d and e are 100 and 200 MHz  $^1H$  NMR spectra for the analogous 1-fluoroethene. To suppress the effect of  $J(^1H-^{19}F)$  coupling, this spectrum is shown as acquired with  $^{19}F$  decoupling. That is, during the experiment, RF power is applied to all  $^{19}F$  resonances. In NMR nomenclature,  $^1H[^{19}F]$  means  $^1H$  observation with  $^{19}F$  decoupling.

A few more details about the  $^1H$  NMR spectrum of 1-chloroethene are worthy of discussion. First, the  $J$ -coupling from  $^{35,37}Cl$  is averaged to zero because, in solution, the chlorine nucleus has a very short  $T_1$ ; in effect, the  $^{35,37}Cl$  nuclei are self-decoupled from the hydrogen spins. Second, selective deuteration of 1-chloroethene will yield spectra very similar to Fig. 7.5b and c for deuteration at the B and C sites, respectively. The values of  $J(^1H-^2H)$  are about one-sixth ( $= 15.351$  MHz/100 MHz) of the  $J(^1H-^1H)$  values shown in Fig. 7.2 and the

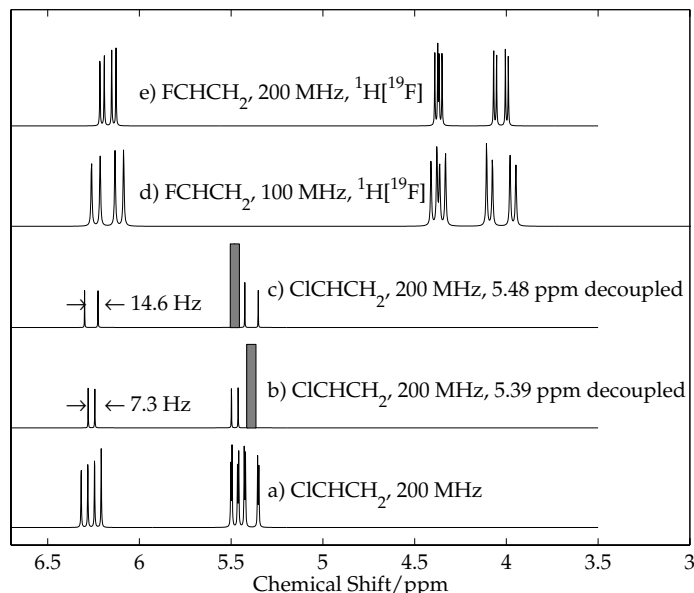


**Fig. 7.5** Solution-state  $^1H$  NMR spectrum of 1-chloroethene and 1-fluoroethene. The results of selective homonuclear decoupling are shown in (b) and (c). The results of heteronuclear decoupling are shown in (d) and (e). Not shown is the simple,  $^{19}F$  coupled  $^1H$  NMR spectrum (or the double negative “ $^{19}F$  undecoupled”) of 1-fluoroethene, which has twice as many  $^1H$  transitions as shown in (d) and (e) (each line is then a doublet from  ${}^nJ(^1H-^{19}F)$ ,  $n = 2, 3$ ).

$S=1$   $^2\text{H}$  nucleus creates triplets instead of doublets. The net results are slightly line-broadened versions of the spectra shown in Fig. 7.5b and c. Third,  $^{13}\text{C}$  labeling at one site will add coupling with the  $S=1/2$   $^{13}\text{C}$  nucleus to the  $^1\text{H}$  spectrum. The one-bond coupling,  $^1J(^1\text{H}-^{13}\text{C})$ , is about 150 Hz and the two-bond coupling,  $^2J(^1\text{H}-^{13}\text{C})$ , is about 10 Hz. So, the  $^{13}\text{C}$ -labeled site will cause a great change, due to  $^1J(^1\text{H}-^{13}\text{C})$  coupling, in either the  $\text{H}_\text{A}$  resonances or in both  $\text{H}_\text{B}$  and  $\text{H}_\text{C}$  resonances, depending on which carbon site is labeled.

Almost all NMR spectra are acquired with pulse methods. The  $^1\text{H}$  NMR spin system is excited with a short duration RF pulse, and the response of the spin system is measured, both the in-phase and out-of-phase components. Based on the terminology of complex numbers, these two components are referred to as the real and imaginary components. This NMR signal is called the free-induction decay, FID, a name which harks back to a classical viewpoint of a freely moving magnet precessing within a solenoidal coil, thus inducing a current. In fact, a current is measured in the NMR probe, which is often a coil of wire, and then digitized. When the raw data is viewed, it shows an exponentially decaying set of sinusoidal signals. Figure 7.6 shows the FID for 1-chloroethene, acquired under the conditions leading to the spectrum shown in Fig. 7.1.

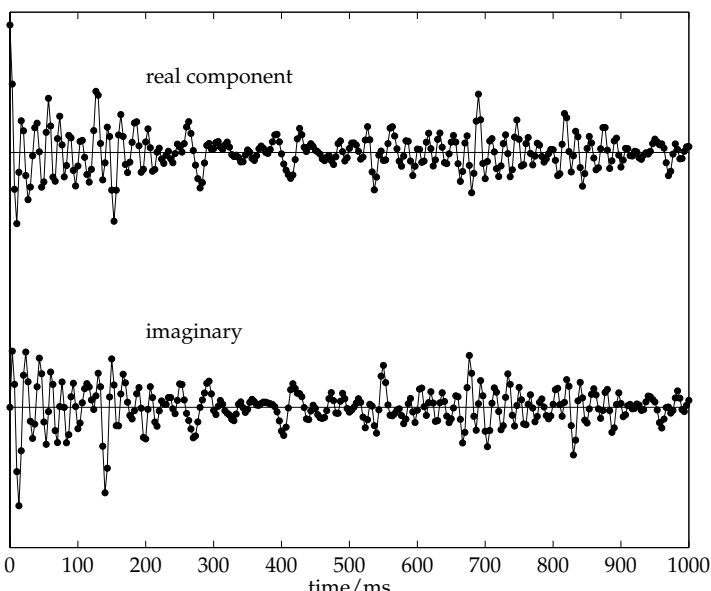


**Fig. 7.6** The first 1000 ms of the FID corresponding to the spectrum shown in Fig. 7.1. The digitization interval is 3.33 ms per complex data point, yielding a spectral width of 300 Hz, an unusually small spectral window. At 9.4 T,  $^1\text{H}$  NMR is usually done with a 10 kHz spectral window,  $^{13}\text{C}$  with 25–50 kHz, and solid-state  $^2\text{H}$  with 1 MHz (and a corresponding 1  $\mu\text{s}$  digitization rate).

While  $v_{\text{reference}}$  is fixed by the nucleus and the magnetic field,  $v_{\text{RF}}$  is adjustable, and usually set near the middle of the peaks of interest. The absolute values of the vertical scale are not used except to note whether or not the first data point is “clipped” by the NMR receiver system; clipping leads to unacceptable spectral distortion.

The data processing usually involves four user-intervention steps: 1. applying a smoothing function to the FID, 2. Fourier transformation, 3. phasing the frequency domain data into pure real and imaginary components, 4. setting the 0 ppm point for the chemical shift axis. A common smoothing function is a Lorentzian line broadening function, equivalent to point by point multiplication of the FID by an exponentially damped function. Phasing removes linear changes in phase within the spectrum, producing uniform absorption line shapes for all signals.

To summarize, solution NMR spectra of small organic, organometallic, and biological materials show well-resolved  $^1\text{H}$  NMR spectra. The two major interactions affecting the spectra are chemical shift and  $J$ -coupling; extensive databases of interactions aid the identification of the molecule and the assignment of the spectrum. Both low and high magnetic fields are functional, though there is a preference for higher fields which yield greater resolution between peaks and spectra which are easier to interpret.

### 7.3

#### Solid-state NMR

Consider hypothetical studies of the orientations and dynamics of a self-assembled monolayer (SAM) of organic thiols chemisorbed on a gold surface. Aside from the chemical information that comes from chemical shifts and  $J$ -coupling, NMR can also provide orientation information for selected sites within a molecule. Consider a related series of organic thiols and their  $^{13}\text{C}$ ,  $^2\text{H}$ , and  $^1\text{H}$  NMR spectra. The alkyne thiol derivatives shown in Fig. 7.7 will be used to demonstrate how to obtain orientation and dynamic information. We will first consider static samples, then samples in which the molecule is executing one of several modes of motion. For static samples, we seek information about the angle between the magnetic field and a labelled portion of the molecule. For molecules which are in motion, we seek the rate of motion, the activation energy, and the mode of motion. The mode of motion can be random, isotropic molecular motion; thermally-activated motion about a molecular axis; or rapid motion of the entire sample about a magic angle, a special angle with respect to the magnetic field.

NMR of solids differs from solution-state NMR in several important ways. First, the solution-state “tumbling” of molecules is, of course, restricted in the solid phase. In the absence of rapid isotropic motion, magnetic dipolar interaction between neighboring spins affects the NMR line shape. Second, the chemical shift interaction is not just a simple scalar, but is a tensor quantity. In solution-state NMR, only the scalar average is seen while in solid-state NMR, the tensor elements are observed. In the solid state, the chemical shift tensor yields a variety of possible NMR line shapes. Likewise, the quadrupolar interaction also creates a variety of line shapes. Third, a single molecular motion can dominate the process of thermal equilibration of the NMR spin system with its environment.

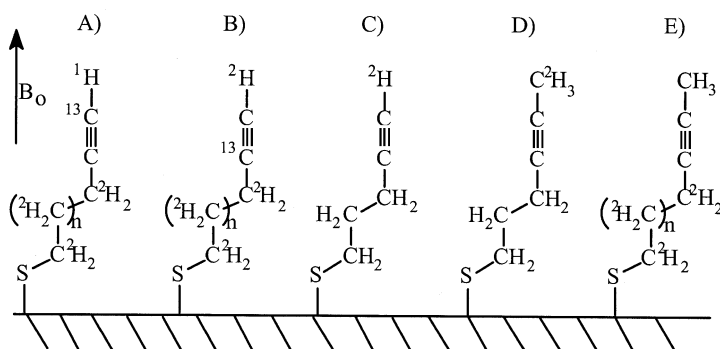


**Fig. 7.7** Alkyne thiol derivatives illustrating (A)  $^{13}\text{C}-^1\text{H}$  dipolar interaction, (B)  $^{13}\text{C}$  chemical shift anisotropy, (C)  $^2\text{H}$  quadrupolar interaction, (D) dynamics of a deuterated methyl site, and (E)  $^1\text{H} T_{1p}$  relaxation times. Assume a gold-coated glass slide that is uniformly covered with one of these molecules. Because of signal-to-noise considerations, a number of these slides may be stacked together in the NMR sample coil.

### 7.3.1

#### Dipolar Interaction

The alkyne thiol,  $\text{R}-\text{C}\equiv^{13}\text{C}-^1\text{H}$ , has two neighboring magnetic spins, both aligned with the large magnetic field,  $B_o$ . From the viewpoint of the  $^{13}\text{C}$  site, the magnetic field is a sum of  $B_o$  and the small magnetic field generated by the  $^1\text{H}$  nucleus. The magnetic field at  $^{13}\text{C}$  varies with the orientation of the  $^{13}\text{C}-^1\text{H}$  unit with respect to  $B_o$  and with the nuclear spin quantum state ( $m_s$ ) of the  $^1\text{H}$  site. When the  $^{13}\text{C}-^1\text{H}$  unit is parallel with  $B_o$  ( $\theta = 0^\circ$ ) and  $m_s(^1\text{H}) = +1/2$ , the total magnetic field at  $^{13}\text{C}$  is a maximum, yielding an absorption about 24 kHz above the isotropic  $^{13}\text{C}$  chemical shift, as shown in Fig. 7.8 by the leftmost vertical line to the dashed line. The dashed line represents the subspectrum for all  $^{13}\text{C}$  spins dipolar coupled to a  $^1\text{H}$  in the  $m_s = +1/2$  spin state. As the  $^{13}\text{C}-^1\text{H}$  unit is rotated to a perpendicular position, the dipolar magnetic field from  $^1\text{H}$  ( $m_s = +1/2$ ) decreases until the  $^{13}\text{C}$  peak is at -12 kHz (vertical bar to dashed line) relative to the  $^{13}\text{C}$  chemical shift. The  $^{13}\text{C}-^1\text{H}$  dipolar interaction is described by:

$$H_{\text{dipolar}}[J] = \left(\frac{\mu_0}{4\pi}\right) \hbar^2 \gamma_s \gamma_I \left[ \frac{\vec{S} \cdot \vec{I}}{r^3} - 3 \frac{(\vec{S} \cdot \vec{r})(\vec{I} \cdot \vec{r})}{r^5} \right] \quad (5)$$

$$\omega[^{13}\text{C} - ^1\text{H}] = \left(\frac{\mu_0}{4\pi}\right) \hbar \frac{\gamma_{^{13}\text{C}} \gamma_{^1\text{H}}}{r^3} = (2\pi)(23.6\text{kHz}) \quad \{\text{for } r = 108.5\text{ pm}\} \quad (6)$$

The NMR signal amplitude is larger for  $\theta = 90^\circ$  than  $\theta = 0^\circ$ . In a powder, there are many possible orientations of the molecule. For this axially-symmetric  $^{13}\text{C}-^1\text{H}$  unit, one can imagine the range of possible orientations as the Earth with an arrow pointing from the center to the surface. Only one arrow orientation points

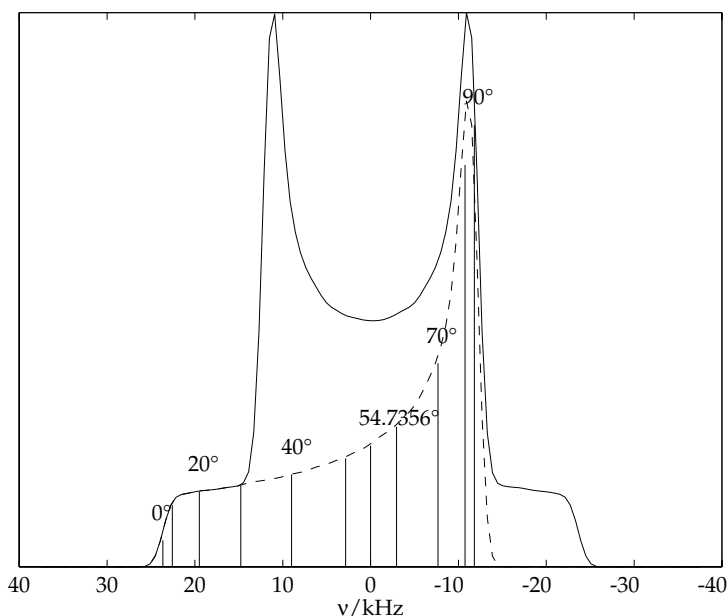


**Fig. 7.8** Solid-state  $^{13}\text{C}$  NMR “powder pattern” line shape for the case of  $^{13}\text{C}-^1\text{H}$  dipolar interaction and an ensemble of randomly oriented  $^{13}\text{C}-^1\text{H}$  units. The frequency axis is centered on the  $^{13}\text{C}$  resonance. The upper trace (—) is the observed line shape while the lower trace (---) is a subspectrum from  $^{13}\text{C}$  sites adjacent to a  $^1\text{H}$  site in the  $m_s = +1/2$  spin state. Not shown is the corresponding subspectrum for  $^1\text{H}$   $m_s = -1/2$ . Vertical bars show the  $^{13}\text{C}$  resonance frequency at  $\theta = 0^\circ, 10^\circ, \dots$  to  $90^\circ$ , including  $\theta = 54.7356^\circ$ , an orientation of the  $^{13}\text{C}-^1\text{H}$  unit for which the dipolar interaction is zero.

to the North Pole, but an infinite number of orientations point to the Equator (fortunately, the NMR sample has a finite number of molecules). Thus, relatively few  $^{13}\text{C}-^1\text{H}$  sites are oriented at  $\theta = 0^\circ$  and contribute to the absorption at +24 kHz; many more molecules contribute to the -12 kHz absorption corresponding to the  $\theta = 90^\circ$  orientation.

The  $^{13}\text{C}-^1\text{H}$  dipolar powder pattern has features which affect other NMR experiments. First, this is an inhomogeneously broadened line composed of many, narrow but homogenously broadened peaks. Second, the two subspectra generated by  $m_s(^1\text{H}) = \pm 1/2$  are mirror images of each other. Third, powder-pattern averages of axially-symmetric units, such as  $\text{C} \equiv ^{13}\text{C}-^1\text{H}$ , give the characteristic “Pake doublet”[1, 10–12]. The “Pake doublet” is obscured by interactions between three or more spins, hence the deuteration of the methylene chain in molecule A (see Fig. 7.7). Fourth, the orientation at which the dipolar interaction is zero,  $\theta = 54.7356^\circ$ , is a critical feature of the “magic angle spinning experiment”, to be discussed later.

Finally,  $^{13}\text{C}$  NMR of a stack of gold-coated glass slides will likely yield information about the orientation of the  $\text{R}-\text{C} \equiv ^{13}\text{C}-^1\text{H}$  molecules. This experiment is

easier at moderate fields than at high fields. If the R—C≡<sup>13</sup>C—H molecules are uniformly tilted with respect to the gold-coated glass slide, and the surface is perpendicular to  $B_0$ , then a pair of peaks should be seen in the <sup>13</sup>C NMR spectrum, one for each spin state of H, and the peak separation will yield the tilt angle. The experimental problems are surface roughness, low signal-to-noise because of the small number of <sup>13</sup>C spins in the NMR sample volume, and the range of magnetic fields at the <sup>13</sup>C nuclei due to the difference between the magnetic susceptibility of gold versus air, especially near the sides of the gold layers. This line-broadening effect increases linearly with the magnetic field strength, thus the optimum field strength is a field sufficient to obtain a signal.

For simplicity, the spectrum in Fig. 7.8 assumes an isotropic <sup>13</sup>C chemical shift. As it turns out, all known <sup>13</sup>C alkyne sites have highly anisotropic chemical shifts which are best described by tensors. This is a nice lead-in to a discussion of chemical shift anisotropy.

### 7.3.2

#### Chemical Shift Anisotropy

The chemical shift at a nucleus is due to the core and valence electrons near that nucleus. The bonding electrons in the axially-symmetric —C≡C unit (Fig. 7.7B) increase the field at the  $\theta = 0^\circ$  orientation, causing the <sup>13</sup>C resonance to occur at lower frequency than expected; on the chemical shift scale, the resonance is at —69 ppm. When the —C≡C unit has the more probable orientation of  $\theta = 90^\circ$ , the magnetic field is less at <sup>13</sup>C than for the chemical shift standard, tetramethylsilane (TMS), yielding a peak near 148 ppm, as shown in Fig. 7.9. The chemical shift anisotropy depends upon the bonding at carbon, as can be seen in the other traces in Fig. 7.9 which shows the predicted <sup>13</sup>C[<sup>1</sup>H] NMR powder pattern line shapes for aromatic, olefinic, and methyl sites. As can be seen, the extraction of molecular orientation from the line shape is particularly straightforward for the alkyne.

The chemical shift anisotropy is usually described in a principal axis system, which is usually not the molecular axis system. In the principal axis system, the chemical shift tensor is diagonal. The elements of this tensor contribute to the NMR spectrum via these two equations:

$$\delta^{lab} = R^{-1}(\phi, \theta, \psi) \begin{vmatrix} \delta_{xx}^{PAS} & 0 & 0 \\ 0 & \delta_{yy}^{PAS} & 0 \\ 0 & 0 & \delta_{zz}^{PAS} \end{vmatrix} R(\phi, \theta, \psi) \quad (7)$$

$$H_{\text{total}}[\text{Hz}] = H_{\text{Zeeman}} + H_{\text{Chemical Shift}} = -\frac{\gamma B_0}{2\pi} (1 + \delta_{zz}^{lab}) S_z \quad (8)$$

In summary, orientation of R—C≡C—H molecules (Fig. 7.7B) chemisorbed on gold surfaces can be obtained from <sup>13</sup>C[<sup>1</sup>H] NMR of a stack of gold-coated glass

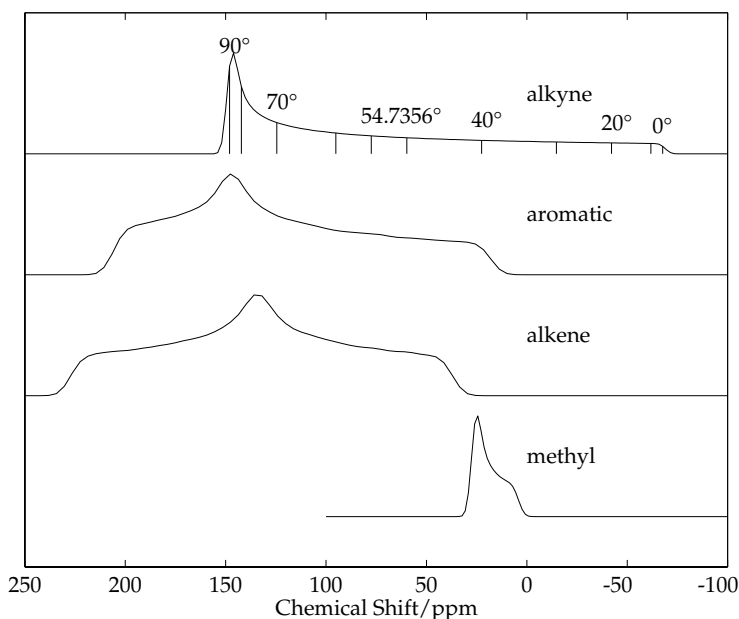


**Fig. 7.9** Solid-state  $^{13}\text{C}[^1\text{H}]$  NMR “powder pattern” line shape for  $^{13}\text{C}$  chemical shift anisotropy and an ensemble of randomly oriented  $^{13}\text{C}\equiv\text{C}$  (alkyne) units. Vertical bars show the  $^{13}\text{C}$  resonance frequency at  $\theta = 0^\circ, 10^\circ, \dots$  to  $90^\circ$ , including  $\theta = 54.7356^\circ$ , an orientation of sites. the  $-13\text{C}\equiv\text{C}$  unit for which the peak position corresponds to the isotropic chemical shift observed in solution-state NMR. Also shown are the typical chemical shift anisotropy powder patterns for  $^{13}\text{C}$  aromatic, alkene, and methyl

slides. The same issues of signal-to-noise and magnetic susceptibility line-broadening discussed earlier will also apply to the  $^{13}\text{C}[^1\text{H}]$  NMR experiment.

### 7.3.3

#### Quadrupolar Interaction

The quadrupolar interaction occurs for nuclei with  $S \geq 1$  and tends to align the nucleus with the electric charge distribution near the nucleus. While there are many more  $S \geq 1$  nuclei than  $S = 1/2$  nuclei, the typical NMR spectrometer is equipped to observe with ease only  $^2\text{H}$  ( $S = 1$ ),  $^{27}\text{Al}$  ( $5/2$ ), and maybe  $^{17}\text{O}$  ( $5/2$ ),  $^{11}\text{B}$  ( $3/2$ ),  $^7\text{Li}$  ( $3/2$ ), and  $^{23}\text{Na}$  ( $3/2$ ). Less common are experiments for  $^{63,65}\text{Cu}$  (both  $3/2$ ),  $^{91}\text{Zr}$  ( $5/2$ ),  $^{93}\text{Nb}$  ( $9/2$ ),  $^{35,37}\text{Cl}$  ( $3/2$ ),  $^{79,81}\text{Br}$  ( $3/2$ ), and  $^{127}\text{I}$  ( $5/2$ ).

In short, the electric charge asymmetry of the nucleus and asymmetry of the charge distribution around the nucleus causes the electric quadrupolar interaction. In electrostatics, magnetic and electric interactions can be described in a progression of moments: monopole, dipole, quadrupole, etc. For an  $S = 1/2$  nucleus such as  $^1\text{H}$ , the relevant moments are: a non-zero electric monopole moment (+1 charge), a small magnetic dipole moment, and zero values for nuclear magnetic monopole, nuclear magnetic quadrupole and nuclear electric dipole moments.

As more protons and neutrons are added to the nucleus, the nuclear electric quadrupole moment can become non-zero. In much the same way that the magnetic dipole aligns with a magnetic field, an electric quadrupole moment aligns with the electric field gradient. The quadrupolar interaction can be small, about 170 kHz for many  $^2\text{H}$  sites, to over 1 GHz for some  $^{127}\text{I}$  sites. The electric field gradient can be computed from the positions of all charges, both electrons and neighboring nuclei, near the quadrupolar nucleus. In practice, most molecular orbital programs can calculate accurate electric field gradients for  $^2\text{H}$ ,  $^{14}\text{N}$ ,  $^{17}\text{O}$ , and other nuclei in medium size molecules such as nitrobenzene. Thus, the observation of quadrupolar spectra and comparison with calculated electric field gradients can aid investigations of many different structural questions.

The quadrupolar interaction is described by a tensor. The electric field gradient (EFG) is described with size, shape, and orientation parameters: The size of the EFG tensor is given by the quadrupolar coupling constant in Hz, variously labeled as  $C_Q$ ,  $e^2q_{zz}Q/h$ , and QCC (not recommended). The shape of the EFG tensor is given by the asymmetry parameter,  $\eta$ . The EFG tensor has a well-defined orientation with respect to the molecular or crystal structure. For the quadrupolar nucleus, the important nuclear properties are spin and quadrupole moment:  $S = 1, 3/2, 5/2, 3, 7/2$ , and  $9/2$  are frequently encountered. The nuclear electric quadrupole moment is given by  $Q$  in units of  $\text{m}^2$ . So, for a given materials science study, one generally selects a nucleus ( $S, Q$ ), and then measures  $C_Q$  and  $\eta$  as a function of structure with frequent comparisons to calculated electric field gradient tensors from molecular orbital calculations ( $C_Q$ ,  $\eta$ , orientation). The quadrupolar hamiltonian is:

$$H_{\text{Quadrupolar}}[\text{Hz}] = \frac{1}{6J(2I-1)} \sum_{\alpha\beta}^{x,y,z} Q_{\alpha\beta}^{\text{lab}} \left[ \frac{3}{2}(I_\alpha I_\beta + I_\beta I_\alpha - \delta_{\alpha\beta} I^2) \right] \quad (9)$$

$$Q^{\text{lab}} = R^{-1}(\phi, \theta, \psi) C_q \begin{vmatrix} \frac{\eta-1}{2} & 0 & 0 \\ 0 & -\frac{\eta-1}{2} & 0 \\ 0 & 0 & 1 \end{vmatrix} R(\phi, \theta, \psi) \quad (10)$$

Representative quadrupolar nuclei and some quadrupolar interaction data are listed in Tab. 7.3. Simulated spectra for several of these sites are shown in Fig. 7.10 as if the spectra were acquired on a 9.4 T (400 MHz) NMR spectrometer with a probe having a fantastically wide spectral width. In practice, the  $\alpha$ -alumina spectrum can barely be acquired and the andalusite and nitro spectra are essentially unobservable. Even the  $^2\text{H}$  spectrum can be difficult to acquire without distortion from probe ringdown effects.

The deuterated alkyne thiol, Fig. 7.7C, is a relatively easy molecule to prepare at levels of  $>80\%$  deuteration and, in general, the  $^2\text{H}$  NMR experiment yields spectra with good signal-to-noise ratios. Thus, it is reasonable to expect a  $^2\text{H}$  quadrupolar powder pattern NMR spectrum showing a combination of the features of the  $^2\text{H}$  NMR (Fig. 7.10) with the orientational aspects of the Pake doublet (Fig. 7.8).

**Table 7.3** Representative  $C_Q$  and  $\eta$  for  $^2\text{H}$  in some sites [13].

Site	$C_Q/\text{kHz}$	$\eta$
$\text{C(sp}3\text{)}-^2\text{H}$	170–175	~0
$\text{C(aromatic)}-^2\text{H}$	180–185	~0.1
$\text{C(sp)}-^2\text{H}$	200–210	0
$\text{O}-^2\text{H}$	50–320	0–1
$\text{N}-^2\text{H}$	50–280	0–1

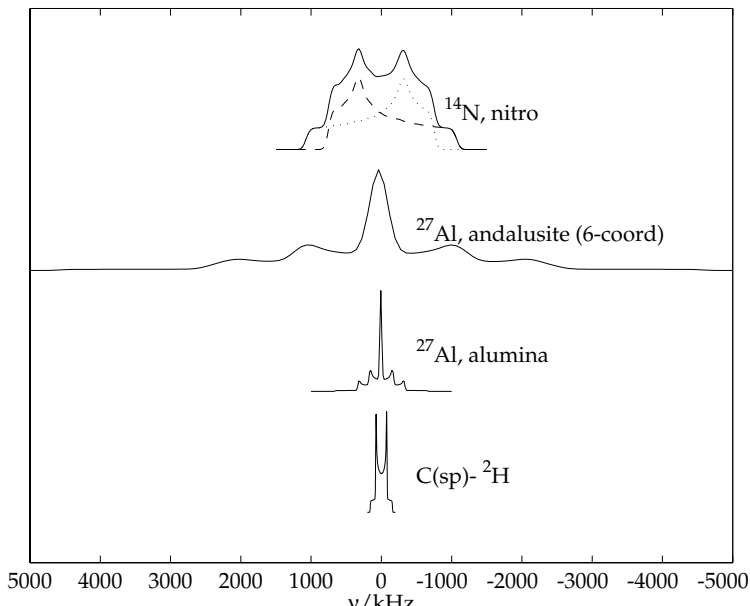


**Fig. 7.10** Static, solid-state quadrupolar NMR line shapes for some  $^2\text{H}$ ,  $^{27}\text{Al}$ , and  $^{14}\text{N}$  sites in andalusite or nitro sites. Also shown for  $^{14}\text{N}$  are andalusite or nitro sites. Also shown for  $^{14}\text{N}$  are subspectra making up the total line shape: the powder (non-oriented) samples at a field of transition  $|+1\rangle \rightarrow |0\rangle$  yields the subspectrum 9.4 T (400 MHz for  $^1\text{H}$ ). The useful bandwidth (--) and the transition  $|0\rangle \rightarrow |-1\rangle$  yields the of a solid-state NMR spectrometer is typically 1 MHz, thus spectra cannot be acquired for the

subspectrum making up the total line shape: the transition  $|+1\rangle \rightarrow |0\rangle$  yields the subspectrum (--) and the transition  $|0\rangle \rightarrow |-1\rangle$  yields the subspectrum (...).

If a SAM has high orientational order and an oriented sample is studied (stacks of glass slides), then the  $^2\text{H}$  spectrum could show two peaks corresponding to the  $|+1\rangle \rightarrow |0\rangle$  and  $|0\rangle \rightarrow |-1\rangle$  transitions. The frequency difference between the two peaks would then give the angle between the  $\text{C}-^2\text{H}$  bond and  $B_0$  (see Fig. 7.8). Conversely, a random orientation between the  $\text{C}-^2\text{H}$  bonds and  $B_0$  yields a line shape like the Pake doublet (Fig. 7.8 and 7.10).

## 7.3.4

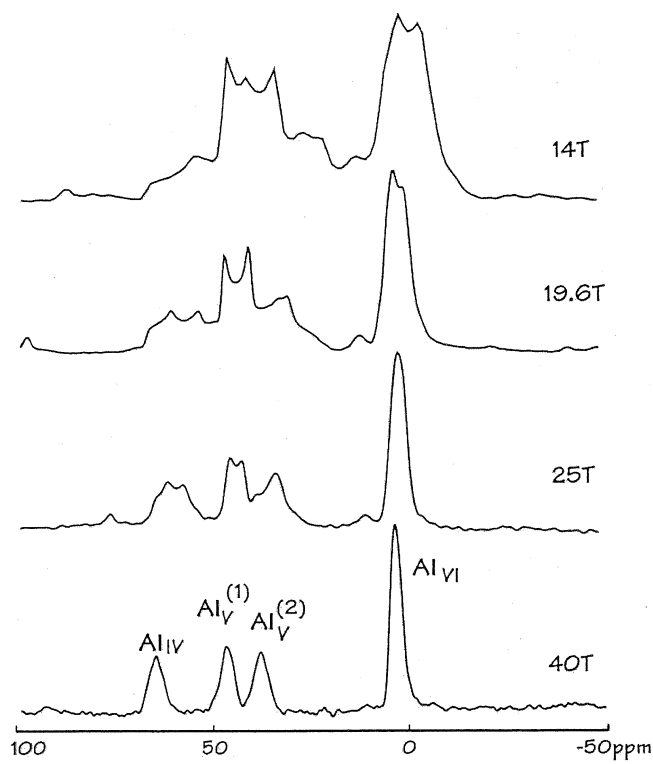
**Magic Angle Spinning (MAS) NMR**

The quadrupolar powder patterns of Fig. 7.10 and the chemical shift powder patterns of Fig. 7.9 provide much insight into local chemical structure and dynamics. However, if the sample contains two or more different  $^2\text{H}$  or  $^{13}\text{C}$  sites, say, then overlapping patterns can be difficult to interpret. Therefore, we seek a method which can “turn off” the quadrupolar interaction and the chemical shift tensor effects. A clue is obtained from solution NMR; the line widths are much narrower because the rapid molecular tumbling averages the interactions. For the chemical shift tensor, the average is the isotropic chemical shift,  $\delta_{\text{iso}}$ , as introduced in the solution NMR section. For the quadrupolar interaction, the average is zero. Given a solid sample, the question is how to quickly average the orientation of each nuclear site with respect to  $B_0$ , and to do so with a simple instrument modification. A clue comes from the orientations of sites detailed in Fig. 7.8 and 7.9. At an orientation of  $54.7356^\circ$ , the dipolar and quadrupolar interactions are zero and the chemical shift tensor average is  $\delta_{\text{iso}}$ .

Magic angle spinning (MAS) NMR of solids consists of rapid rotation of the sample about an axis set at  $54.7356^\circ$  relative to  $B_0$ . The rotational velocity should be greater than the static (non-spinning) line width. For  $^{13}\text{C}$  and  $B_0 = 9.4$  T, typical rotation rates are about 10 kHz, i.e., 600,000 rpm. At these high rotation rates, the strength of the sample holder (the rotor) is critical, with zirconia a common material. To further reduce stress, the maximum diameter of the rotor is often reduced to 5 mm or less. The drive mechanism is compressed air, and compressed air is also used for all of the bearing surfaces. Obviously, failure of the bearing air supply is very likely to cause destruction of the zirconia rotor and perhaps the rest of the MAS probe.

When the MAS experiment is applied to  $S=1/2$  nuclei such as  $^{13}\text{C}$ ,  $^{29}\text{Si}$ , and  $^{31}\text{P}$ , advantage is taken of the  $^1\text{H}$  spin system, assuming the sample also contains abundant  $^1\text{H}$  sites. A pulse sequence incorporating dipolar decoupling and cross polarization is used for two reasons: (a) to reduce the  $^{13}\text{C}$ ,  $^{29}\text{Si}$ , and  $^{31}\text{P}$  line width because the MAS rotational rate is usually not fast with respect to dipolar coupling (see Fig. 7.8 for an example of  $^1\text{H}$ – $^{13}\text{C}$  dipolar coupling) and (b) to increase the signal-to-noise ratio. More details and examples of the CP/MAS experiment are given in a following chapter.

When the MAS experiment is applied to quadrupolar nuclei such as  $^{27}\text{Al}$ , the quality of the NMR spectrum depends dramatically on the magnitude of  $C_q$  compared with both the MAS spin rate and the magnetic field,  $B_0$ . Excellent spectra are obtained for small  $C_q$  sites when studied with high-speed MAS spin rates at high  $B_0$ . Conversely,  $^{27}\text{Al}$  sites can be “invisible” for high  $C_q$  values and modest MAS spin rates and  $B_0$ ; note the evolution in line shapes for the  $^{27}\text{Al}$  MAS NMR spectra in Fig. 7.11. Likewise, the four-coordinate  $\text{AlO}_4$  sites in an aluminum isopropoxide complex, with  $C_q = 12.3$  MHz, are observable at 20 kHz and 19.6 T while three-coordinate aluminum sites in related complexes, with  $C_q > 30$  MHz, are not observable [14].



$^{27}\text{Al}$  MAS Spectra of  $9\text{Al}_2\text{O}_3 + 2\text{B}_2\text{O}_3$

**Figure 7.11**  $^{27}\text{Al}$  MAS NMR line shapes as a function of magnetic field. The spectra of the ceramic  $9\text{Al}_2\text{O}_3 + 2\text{B}_2\text{O}_3$  have been acquired with a spin rate of 35 kHz. Figure courtesy of Dr. Zhehong Gan, National High Magnetic Field Laboratory [15]. Reprinted with permission.

### 7.3.5

#### $T_1$ and $T_{1\rho}$ Relaxation

Whenever we talk about spins aligning with  $B_0$ , we know that the spin system must release energy. For the  $^1\text{H}$  spins in a  $-\text{CH}_3$  group in a 400 MHz NMR spectrometer, the alignment of each  $^1\text{H}$  will release a 400 MHz quantum of energy. At 400 MHz, the spontaneous release of energy by photon emission is extremely slow; for comparison, the emission of a visible photon from an excited rhodamine dye molecule is much faster. Instead, at 400 MHz, energy release is stimulated by the motion of neighboring magnetic dipole moments, that is, the three  $^1\text{H}$  spins in a methyl group contribute to the relaxation of each other, provided the methyl group is moving. In most R- $\text{CH}_3$  groups, the methyl group rotates quite fast, with rotation rates of the order of GHz, and correlation times of the order of picoseconds, at room temperature. At very low temperature,  $^1\text{H}$  NMR of methyl groups can provide detailed information of motional processes, both classical motion and

quantum-mechanical tunnelling. In the more common room temperature and  $-100$  to  $200\text{ }^{\circ}\text{C}$  experiments, relaxation experiments will probe motions with thermal activation energies of about  $5$  to  $30\text{ kJ mol}^{-1}$ .

There are many relaxation paths and experiments to measure the relaxation kinetics. Three common relaxation pathways are:

- $T_1$ , spin–lattice relaxation. Measures the rate of energy exchange between the spin system and the vibrational and phonon modes of the lattice. Has  $B_0$  dependence.
- $T_2$ , spin–spin relaxation. Measures the loss of coherence of the NMR signal during a FID.
- $T_{1p}$ , spin–lattice in the rotating frame relaxation. While an on-resonance RF pulse is applied, this parameter is a measure of the rate of energy exchange between the spin system and the vibrational and phonon modes of the lattice.  $T_{1p}$  depends upon the magnitude of both  $B_0$  and  $B_1$ , where  $B_1$  is the amplitude of the RF pulse.

For common experiments in the solid-state,  $T_1$  is critical to determining the length of the experiment. It can happen that raising or lowering the sample temperature can dramatically improve the experimental set-up. Also, in some cases, measurement of  $T_1$  or  $T_{1p}$  values can yield insight into molecular motion. Shown in Fig. 7.12 are idealized  $T_1$  and  $T_{1p}$  values for three different thermal activation energies. There are several obvious features. The most efficient spin–lattice relaxation, i.e., shortest  $T_1$  value, occurs when the correlation time is approximately equal to the inverse of the resonance frequency,  $\tau\omega_0 \sim 1$ , as listed in Tab. 7.4. Second, the slopes of the  $T_1$  and  $T_{1p}$  curves are determined by the activation energy; the plot shows relaxation times for activation energies of  $5$ ,  $15$ , and  $30\text{ kJ mol}^{-1}$ . Third, when slow frequency motions are suspected, i.e., moderate temperatures and high activation energies, then  $T_{1p}$  experiments at variable  $B_1$  fields are more convenient than switching from magnet to magnet to access  $T_1$  data.

The correlation times shown in Fig. 7.13 range from  $1\text{ ps}$  to  $10\text{ s}$ . The corresponding  $T_1$  and  $T_{1p}$  values are all accessible given a range of magnets, variable temperature probes, and appropriate RF pulse sequences. Thus, the ability of NMR to measure dynamic processes is quite powerful; quick survey experiments can be done with any NMR signal and more detailed studies can be done with specifically labeled samples. To return to the SAM samples, compound E of Fig. 7.7 may be expected to show two  $T_1$  minima, the first in the range of  $10$  to  $50\text{ K}$  corresponding to thermal activation of methyl group rotation and a second minimum at higher temperature due to a larger motion of the alkyl chain. There is one significant problem with the use of relaxation methods to monitor kinetic processes: while the rate constants and activation energies can be measured, often the mode of motion is not clearly determined. In the case of compound E, the higher temperature minimum could be assigned to a simple motion at the end of the alkyl chain or to a cooperative motion of all of the alkyl chains. With only relaxation methods, the mode of motion remains ambiguous.

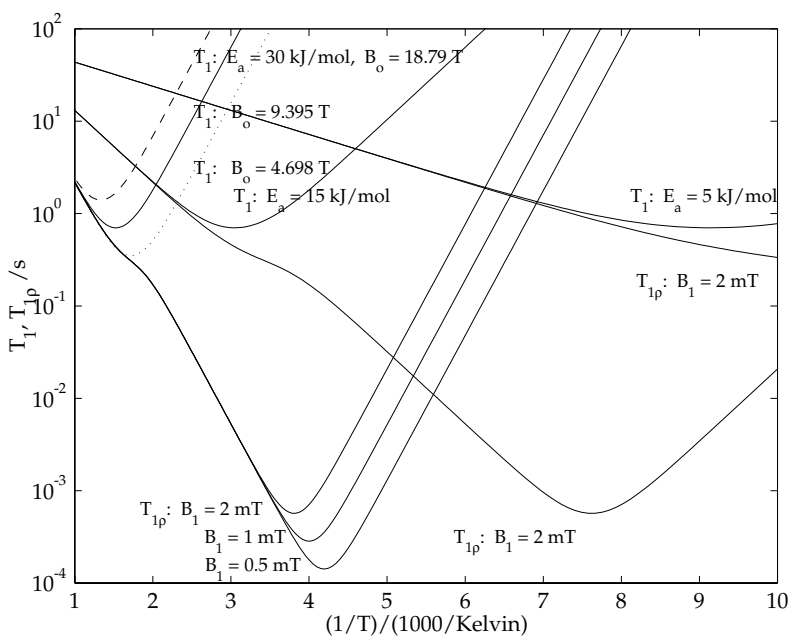


**Figure 7.12** Simulated spin–lattice ( $T_1$ ) and spin–lattice in the rotating frame ( $T_{1p}$ ) relaxation times for a  ${}^1\text{H}$  moving with respect to the molecular structure, for example, methyl group (...) and 18.79 T rotation. Shown here, from left to right, are three sets of curves corresponding to  $E_a = 30, 15$ , and  $5 \text{ kJ mol}^{-1}$ .  $B_o = 9.395 \text{ T}$  ( ${}^1\text{H} = 400 \text{ MHz}$ ) except for  $T_1$  at  $B_o = 4.698 \text{ T}$  ( ${}^1\text{H} = 200 \text{ MHz}$ ) and  $18.79 \text{ T}$  ( ${}^1\text{H} = 800 \text{ MHz}$ ), respectively.

**Table 7.4** Activation energies and temperatures of  $T_1$  minima, correlation times, and magnetic field (given as the resonant frequency in radians per second).

$E_a/\text{kJ mol}^{-1}$	$T_{\min}/\text{K}$	$\tau_{\min}/\text{ps}$	$\omega_o/10^9 \text{ rad s}^{-1}$
30	750	120	5.0265
30	660	240	2.5133
30	580	500	1.2566
15	330	240	2.5133
5	110	240	2.5133

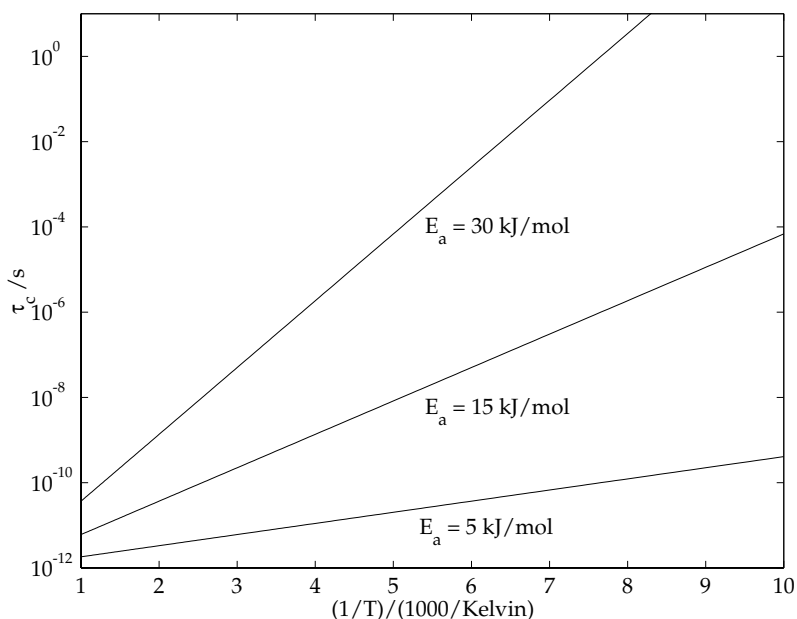


**Fig. 7.13** Correlation times used to generate the  $T_1$  and  $T_{1\rho}$  values of the previous figure from the Arrhenius relationship  $\tau = \tau_0 \exp(-E_a/RT)$  where  $\tau_0 = 10-12 \text{ s}$ .

### 7.3.6 Dynamics

In solid-state NMR, a common technique for measuring the rate of molecular motion, and the mode of motion, is  $^2\text{H}$  NMR. For C– $^2\text{H}$  bonds, the value of  $C_q$  is usually known, and for a static system yields a predictable powder pattern. Recall that each orientation of the C– $^2\text{H}$  bond with respect to  $B_0$  yields a discrete pair of transition frequencies. If the C– $^2\text{H}$  bond orientation should change, then the transition frequencies may change. For modes of motion such as methyl group rotation, the transition frequencies average to new values, but still offset from the Zeeman frequency. With increasing rate of methyl group rotation, the  $^2\text{H}$  NMR evolves smoothing to a new, motionally-averaged, line shape, as shown in Fig. 7.14. For compound D (Fig. 7.7), this experiment could show the onset of fast methyl group rotation and then the onset of more complex molecular motions such as chain motion or migration of the chain across the surface.

Solid-state  $^2\text{H}$  NMR is, among techniques which measure molecular motion, capable of measuring an extremely wide range of motional rates. When  $^2\text{H}$   $T_1$  measurements are included, rate constants of more than 10 orders of magnitude are accessible. In addition to methyl group rotation, the combination of deuteration and solid-state  $^2\text{H}$  NMR has yielded molecular dynamic information on phenyl groups, aliphatic chains, and ethene bound to transition metal centers.

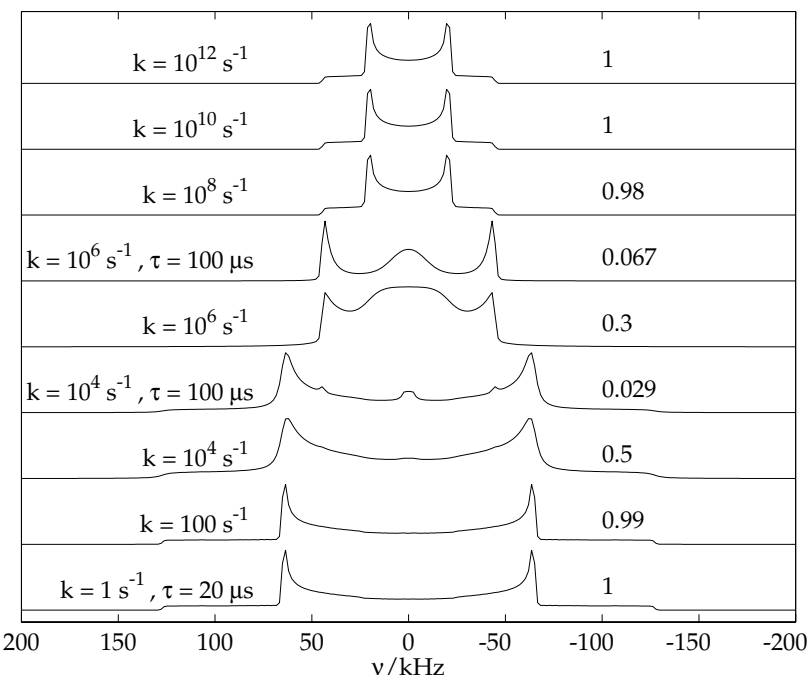


**Fig. 7.14** Simulated  $^2\text{H}$  NMR line shapes of a methyl group as a function of methyl group rotation rate,  $k$ . The interpulse spacing,  $\tau$ , is  $20 \mu\text{s}$ , unless otherwise specified. The relative amplitudes of each spectrum are given on the right.

#### 7.4 Imaging

Magnetic resonance imaging (MRI) is NMR spectroscopy with magnetic field gradients applied to the sample. Thus, every volume element within a sample can be exposed to a specific magnetic field. Since RF and magnetic fields can penetrate many samples, NMR is a widely applicable imaging technique. However, the most convenient NMR imaging methods work only with narrow NMR resonances, such as the  $^1\text{H}$  NMR resonances of water and lipids or the  $^3\text{He}$  and  $^{129}\text{Xe}$  resonances of helium and xenon [8].

In any imaging experiment, the critical issues are sample preparation, image contrast, spatial resolution, field of view, and total time of the experiment. Relative to other imaging techniques, the NMR spectroscopist's control over the image contrast mechanisms is exceptional. Of course, MRI images are affected by the number of nuclei in each volume element. In addition, the NMR relaxation dynamics,  $T_1$  and  $T_2$ , can be used to control image contrast, especially for the soft tissues in the human body. Sample preparation is perfectly simple for the patient: remove metal objects and lie still. For inanimate objects, sample preparation of

this simplicity enables many unique experiments: variable temperature, variable pressure and/or flow, and measurements as a function of time. The other NMR interactions discussed earlier find modest applications in MRI. The chemical shift interaction is used in  $^{31}\text{P}$  MRI of muscle tissue to monitor metabolism via phosphocreatine/ATP concentrations.

An MRI pulse sequence, spin-warp, is shown here as a 2D imaging sequence (Fig. 7.15). An initial  $^1\text{H}$   $90_x$  pulse converts  $^1\text{H}$   $z$ -magnetization to magnetization aligned with the  $y'$ -axis of the rotating frame. In this chapter, this is the first NMR pulse sequence to be described with the rotating frame concept. The description of other pulse sequences, such as two pulse sequences used for  $T_1$  and  $T_2$  measurement are given in many textbooks. We chose the rotating coordinate system to have  $B_o \parallel$  to the  $z$ -axis; the  $x'$  and  $y'$  axes are chosen to be synchronized with the RF frequency of the initial pulse in a pulse sequence. The primes denote the two moving axes; primes are generally omitted from labels such as " $90_x$ " since it is understood that the RF pulse is referenced to the rotating coordinate system.

To visualize the effect of a pulse sequence with the rotating frame description, one makes the following assumptions:

- The magnetization vector,  $\mathbf{M}$ , represents the vector sum of all the magnetic moments in the sample.
- The coordinate system chosen is rotating about an axis parallel to  $B_o$  at a rate equal to the  $^1\text{H}$  resonance frequency.
- In the rotating frame, the initial orientation of  $\mathbf{M}$  is along the  $+z$  axis (denoted as  $\mathbf{M}_z$ ) and a  $90_x$  pulse results from the application of a magnetic field along the  $x'$ -axis (denoted as  $B_{1x}$ ).
- The motion of  $\mathbf{M}_z$  in response to  $B_{1x}$  is a torque which causes  $\mathbf{M}$  to precess towards the  $y'$ -axis. Of course, when  $\mathbf{M}$  is aligned with the  $y'$ -axis, the RF pulse is terminated. Then,  $\mathbf{M}'_y$  will stay aligned with the  $y'$ -axis until: (a) its resonance frequency changes or (b) another RF pulse is applied to the sample.

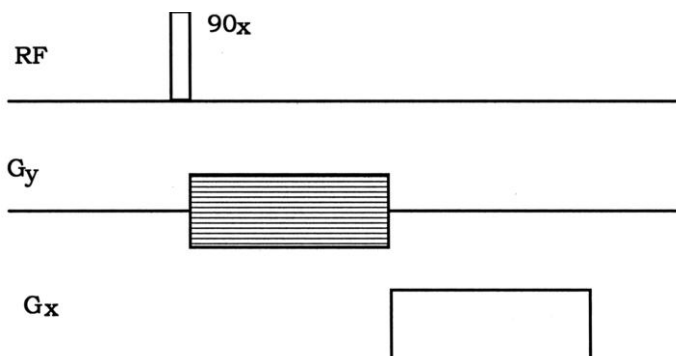


**Fig. 7.15** Spin-warp pulse sequence for 2D imaging. In successive experiments, the amplitude of  $G_y$  is varied while the amplitude of  $G_x$  is fixed. The NMR signal is acquired during the application of  $G_x$ .

- The detected NMR signal is described with complex numbers.  $M_y'$  is positive, real magnetization along the  $x$ -axis,  $M_x'$ , is imaginary. Note: When pulse sequences are analyzed in greater detail, and with more regard to sign conventions, the axis labels will change. Nevertheless, the rotating frame model remains quite useful.

A hypothetical sample is shown in Fig. 7.16. This sample has 5 spins at  $x = -3$ ,  $y = +2$  cm and 1 spin at  $x = 1$ ,  $y = 0$  cm. We assume that all spins will, in the absence of any magnetic field gradients, have exactly the same resonance frequency. The evolution of the magnetization in the rotating frame illustrates how the sample spin density distribution is imaged.

Shown in Fig. 7.17 are plots of  $M_x$  and  $M_y$  starting immediately after the  $90_x$  pulse of the spin-warp 2D imaging pulse sequence. For  $G_y = 0 \text{ mT m}^{-1}$  (Fig. 7.17A), magnetization stays aligned with the  $+y$  axis for 10 ms; the resonant frequency is exactly equal to the rotating frame frequency. Then, with the application of the  $G_x$  gradient, the resonant frequency changes for spins at sample sites with nonzero  $x$ -coordinates. For  $G_y = +0.1175 \text{ mT m}^{-1}$  and  $y = +2 \text{ cm}$ , the change in resonant frequency is +100 Hz,

$$\Delta\nu = \frac{\gamma}{2\pi} \Delta x G_y = (42.57 \text{ MHz/T}) (+0.02 \text{ m}) (+0.1175 \text{ mT/m}) = +100 \text{ Hz} \quad (11)$$

creating the sinusoidal dependence in the magnetization along the  $y$ -axis (rotating frame) in Fig. 7.17B, and, separated in phase by  $\pm 90^\circ$ , a component along the  $x$ -axis. An even larger gradient increases the offset frequency. The phase of the

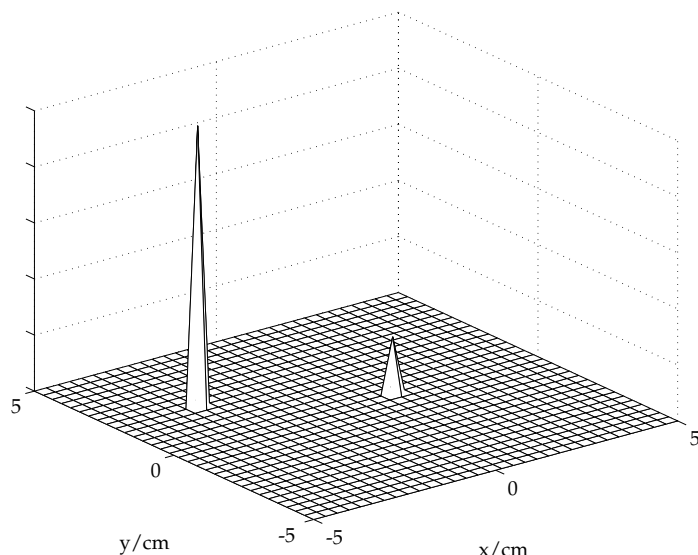


**Fig. 7.16** Hypothetical sample with five  $^1\text{H}$  nuclei at  $x = -3$ ,  $y = 2$  cm, and one  $^1\text{H}$  nucleus at  $x = 1$ ,  $y = 0$  cm.

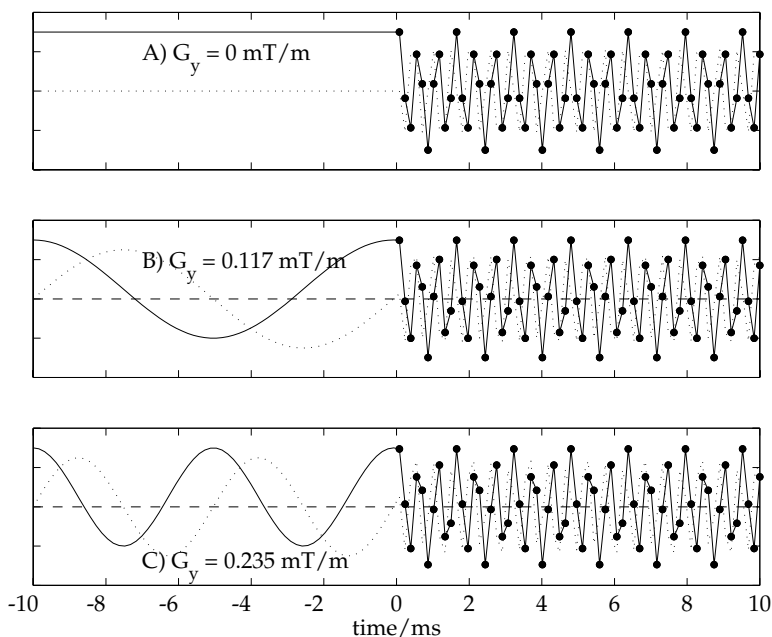


**Fig. 7.17** Magnetization in the rotating frame:  $M_y$  (—) and  $M_x$ (...). The acquired data (•) is taken during the application of the  $G_x$  gradient.

imaginary component changes by  $180^\circ$  for  $G_y < 0 \text{ T m}^{-1}$  or sample position  $< 0 \text{ cm}$ . The digitized values are indicated (•) in Fig. 7.17 and again, the frequency of the signal depends upon  $G_x$  and the location of the spins in the sample. A complete 2D spin–warp experiment consists of  $2^n$  different values of  $G_y$  and, for each  $G_y$  value, a digitized FID with  $2^n$  data points.

For the purpose of image filtering, a smoothing function is often applied to the 2D FID data set. Shown in Fig. 7.18 is the smoothed 2D FID data array (real component). This surface plot shows both the oscillation set by  $G_x$  and the variable phase of that oscillation set by  $G_y$ . This last point, the phase encoding by a pulse or gradient, is a key feature of multidimensional NMR experiments.

Lastly, 2D Fourier transformation of the smoothed 2D FID data set yields the image (Fig. 7.19), which corresponds quite well to the original distribution of spin density through the field of view.

Besides the spin–warp sequence, the echo planar sequence is widely used in biomedical applications. Figure 7.20 shows an image recently acquired of a young girl’s sprained knee. The instrument used a permanent magnet system configured to reduce the claustrophobic feeling of a more traditional solenoidal magnet.

Besides imaging, pulsed magnetic field gradients are also used to study self-diffusion of solutes and solvents. Basically, the pulsed field gradients “encode” a structure on the spin system, and the evolution of this structure yields the rate of trans-

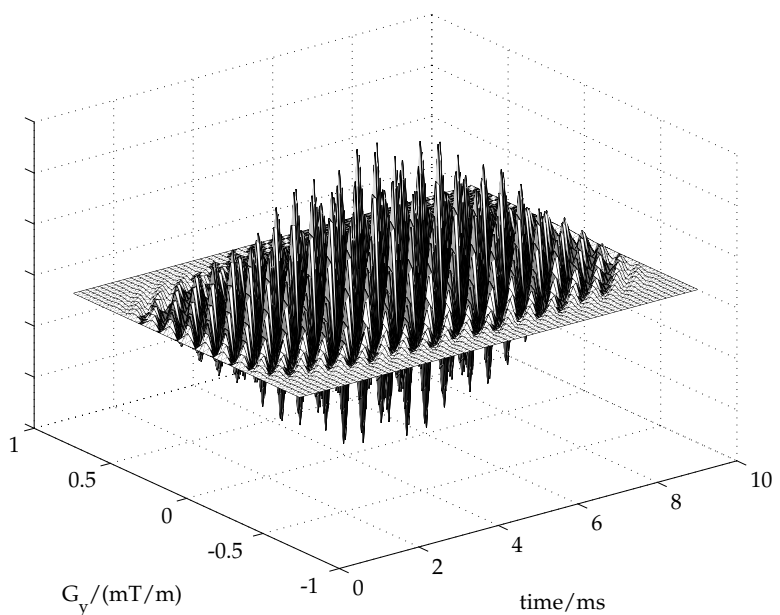


**Fig. 7.18** The real ( $M_y$ ) component 2D FID data set after smoothing with a sine function. The oscillation frequency along the time axis is set by  $G_x$  and the initial phase of each oscillation is set by  $G_y$ .

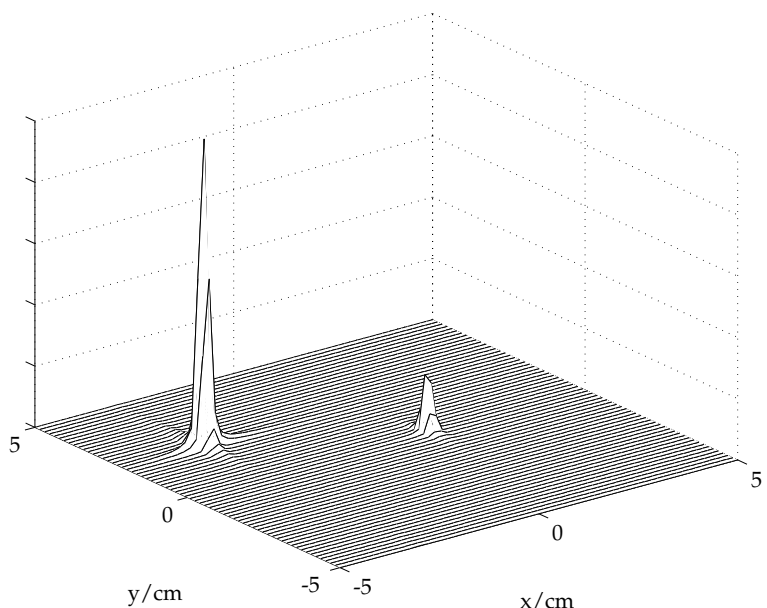


**Fig. 7.19** The MRI image, obtained by 2D FFT of the smoothed 2D FID array.

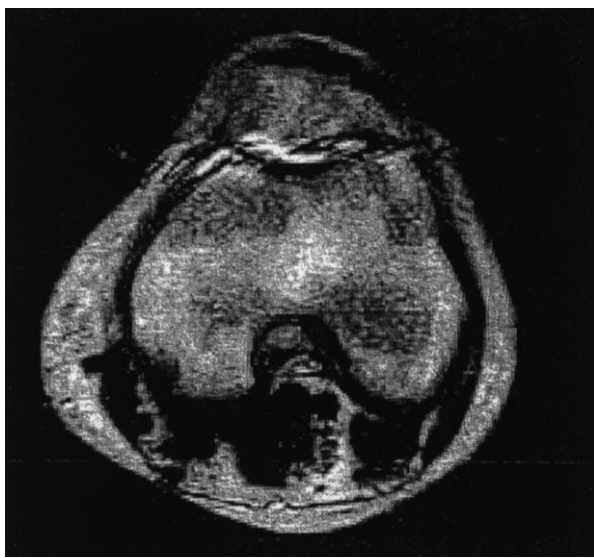


**Fig. 7.20** An MRI image of a knee. The high intensity region shows a small amount of fluid concentration following a sprain.

lational motion in the solution. Since magnetic field gradients can be quite large and the time of application can be of the order of milliseconds, the structure can be created at sub-micron resolution. Therefore, quite small translational motions are measured.

## 7.5 3D NMR: The HNCA Pulse Sequence

Multiple pulse NMR sequences for the solution-state can be modeled with either product operator or density matrix calculations. Here, we use the latter for analyzing a pulse sequence for three-dimensional NMR, the HNCA pulse sequence. The HNCA pulse sequence is used to establish connectivity between the amide hydrogen, the amide nitrogen, and the alpha carbon in an amino acid in a polypeptide sequence. The detected  $^1\text{H}$  NMR signal shows a modulation which is dependent upon  $^1\text{J}(^1\text{H}-^{15}\text{N})$  and  $^2\text{J}(^1\text{H}-^{13}\text{C})$ , a modulation which will be simulated with density matrix calculations. Because a polypeptide has many amide hydrogens, amide nitrogens, and alpha carbons, a necessary step for assigning the NMR spectra is identifying neighboring atoms. Fortunately, these three nuclei are coupled by unique and nearly uniform  $J$ -coupling constants (Fig. 7.21).

The HNCA pulse sequence has groups of three pulse sequences optimized for the  $J$ -coupling constants. The rotating frame description can be applied to parts of the pulse sequence (Fig. 7.22), but is insufficient to describe the entire sequence. With tools such as Mathematica or Matlab, it is straightforward to simulate the pulse sequence (Fig. 7.23). These tools allow for the evaluation of the exponent of a Hermitian matrix, a common step in time dependent quantum mechanics.

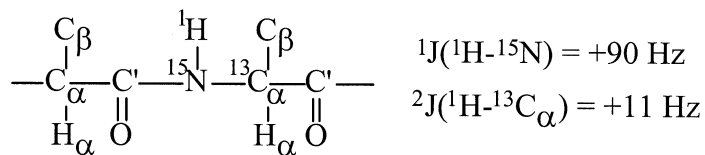


**Fig. 7.21** A portion of a polypeptide structure focusing on the amide hydrogen and alpha carbon.

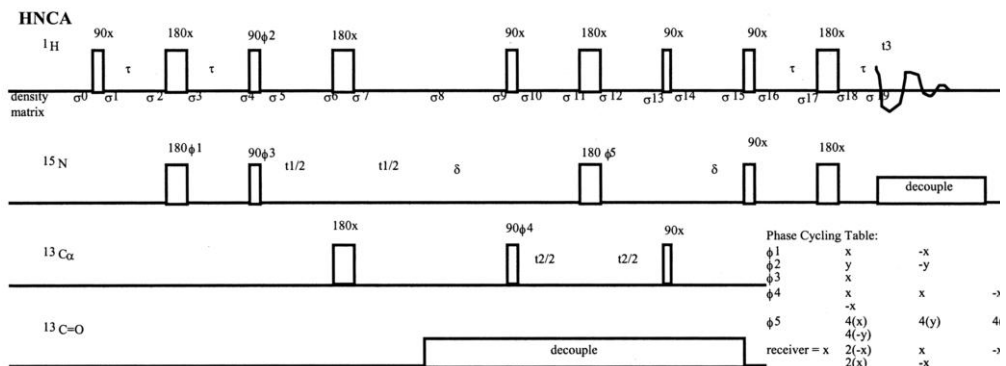


**Fig. 7.22** The HNCA 3D NMR pulse sequence. The objective is to correlate the detected  $^1\text{H}$  NMR signal of an amide hydrogen with adjacent  $^{15}\text{N}$  and  $^{13}\text{C}_\alpha$  sites. The labels below the  $^1\text{H}$  RF pulses refer to density matrices used in the pulse sequence simulation.

```

U = MatrixExp[ -π/2 i × SxH ];
σ1 = U. σ0 . Transpose[Conjugate[U]] ;

Hinteraction = -(νH - νHRef) Szh - (νN - νNRef) SzN - (νC - νCRef) SzC
            + JHN (Szh.SzN) + JNC (SzN.SzC);
U = MatrixExp[-i×(2 π τ)×Hinteraction];
σ2 = U. σ1 . Transpose[Conjugate[U]] ;

Hpulse = -π i × SxH + -π i × φ1;
U = MatrixExp[Hpulse];
σ3 = U. σ2 . Transpose[Conjugate[U]] ;

U = MatrixExp[-i×(2 π τ)×Hinteraction];
σ4 = U. σ3 . Transpose[Conjugate[U]] ;

```

**Fig. 7.23** A brief portion of a Mathematica program used to simulate the HNCA pulse sequence. The complete program is given at <http://www.chem.lsu.edu> (see Butler's publications). With an analysis such as this, it is possible to follow the basic features of a complex

pulse sequence, in particular, how the detected signal changes with the magnitude of the  $J$ -coupling constants. The program is long, but repetitive, with commands as shown above repeated from the first pulse to the last pulse.

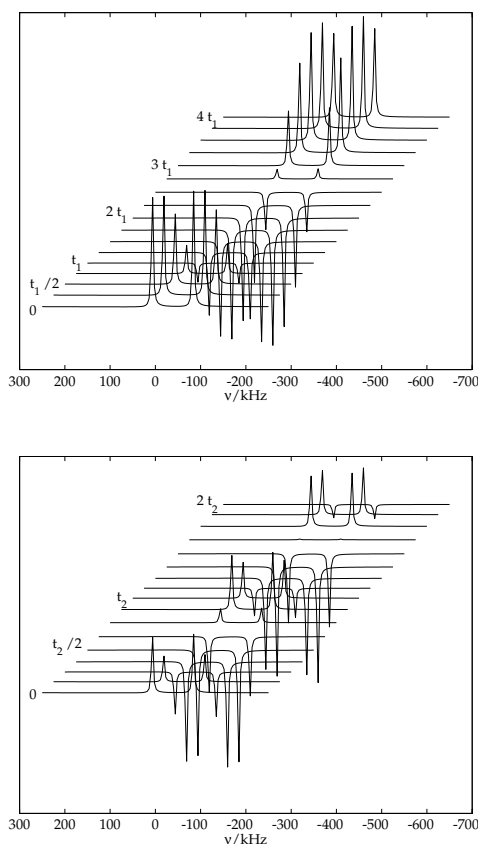


**Fig. 7.24** Simulated amide  $^1\text{H}$  NMR spectra from an HNCA pulse sequence, shown here without  $^{15}\text{N}$  decoupling. On the top is the  $^1\text{H}$  NMR signal as a function of  $t_1$  evolution, and on the bottom,  $t_2$  evolution. These evolutions will only be seen for  $^1\text{H}$   $J$ -coupled to  $^{15}\text{N}$  and  $^{13}\text{C}$ .

In this 3D NMR pulse sequence, two time increments,  $t_1$  and  $t_2$ , are successively incremented. Because of the  $J$ -coupling, each time increment leads to a modulation of the detected  $^1\text{H}$  NMR signal. Shown here (Fig. 7.24) are simulated  $^1\text{H}$  NMR spectra acquired at various time increments. A large array of these spectra, processed in total by 3D FFT, will lead to a cube of data, which is typically analyzed slice by slice.

NMR of proteins uses a suite of 2D and 3D NMR pulse sequences like HNCA with the objective of acquiring connectivity information. Besides the signal-to-noise ratio for the detected signal, other issues are the separation of one  $^{15}\text{N}$  resonance from another, and likewise, the separation of one  $^{13}\text{C}_\alpha$  resonance from another. The S/N and resolution issues both push the experiment to higher and higher magnetic fields.

### 7.6 Conclusion

NMR spectroscopy is a very effective method to examine the interactions between nuclei and their environments. NMR spectra yield information which can be used to determine the structure of complex organic, organometallic, and biological molecules as these structures exist in solution. For similar molecules in the solid state, the hierarchy of dominant NMR interactions changes, and other information becomes available, yielding more emphasis on chemical bonding and molecular dynamics. The application of magnetic field gradients enables imaging experiments such as MRI and self-diffusion measurements. The NMR interactions are well-described by time-independent and time-dependent quantum mechanics.

## References

- 1 Abragam, A. *The Principles of Nuclear Magnetism*, Oxford University Press, Oxford 1961.
- 2 *Encyclopedia of Nuclear Magnetic Resonance*, eds. Grant, D. M.; Harris, R. K., John Wiley & Sons, Chichester 1996.
- 3 Becker, E. D. *High Resolution NMR: Theory and Chemical Applications*, 3rd edition, Academic Press, New York 1999.
- 4 Evans, J. N. S. *Biomolecular NMR Spectroscopy*, Oxford University Press, Oxford 1995.
- 5 Friebolin, H. *Basic One- and Two-Dimensional NMR Spectroscopy*, 3rd edition, John Wiley & Sons, Chichester 1998.
- 6 Braun, S.; Kalinowski, H.-O.; Berger, S. *150 And More Basic NMR Experiments: A Practical Course*, 2nd edition, John Wiley & Sons, Chichester 1998.
- 7 Sanders, J. K. M.; Hunter, B. K. *Modern NMR Spectroscopy : A Guide for Chemists*, Oxford University Press, Oxford 1993.
- 8 Ernst, R. R.; Bodenhausen, G.; Wo-kun, A. *Principles of Nuclear Magnetic Resonance in One and Two Dimensions*, Oxford Science Publications, Oxford 1987.
- 9 *Two-Dimensional NMR Spectroscopy: Applications for Chemists and Biochemists*, eds. Croasmun, W. R.; Carlson, R. M. K., 2nd edition, John Wiley & Sons, Chichester 1994.
- 10 Fukushima, E.; Roeder, S. B. W. *Experimental Pulse NMR a Nuts and Bolts Approach*; Addison-Wesley, 1981.
- 11 Stejskal, E. O.; Memory, J. D. *High Resolution NMR in the Solid State: Fundamentals of CP/MAS*, Oxford University Press, Oxford 1994.
- 12 Schmidt-Rohr, K.; Spiess, H. W. *Multi-dimensional Solid-State NMR and Polymers*; Academic Press, New York 1997.
- 13 Butler, L. G.; Keiter, E. A., *J. Coord. Chem.*, 1994, 32, 121–134 (Note: Eq. (4) is missing plus signs.).
- 14 Bryant, P. L.; Harwell, C. R.; Mrse, A. A. et al., *J. Am. Chem. Soc.*, 2001, 123, 12009–12017.
- 15 Cron, Z.; Gorikov, P.; Cross, T. A.; Samoson, A.; Massiot, O. *J. Am. Chem. Soc.*, 2002, 124, 5634–5635.

# 8

## Solution NMR Spectroscopy

*Gary E. Martin, Chad E. Hadden, and David J. Russell*

### 8.1

#### Introduction

NMR, or nuclear magnetic resonance spectroscopy, affords one of the richest sources of molecular connectivity information available to the structural chemist. Since the inception of NMR, which originated as a curiosity of the physicist when the principle was first discovered just over 50 years ago [1, 2], the discipline has gone on to become universally recognized for its unique capability to precisely define molecular structures through a variety of fundamental parameters. It is entirely safe to say that NMR has become the cornerstone technique for the elucidation of chemical structure.

The fundamental parameters of the NMR experiment have been covered in a previous chapter and will be mentioned here only briefly. Structure elucidation by NMR at the simplest level may simply entail a comparison of the chemical shifts of the molecule of interest with a database library of chemical shift information. Commonly studied nuclides include,  $^1\text{H}$ ,  $^{13}\text{C}$ ,  $^{19}\text{F}$ , and  $^{31}\text{P}$  for organic molecules; less commonly, for reasons of sensitivity, other nuclides such as  $^{15}\text{N}$  may be investigated. In addition to the nuclides just cited, which are of primary interest to investigators working with organic and bio-organic molecules, studies of the diverse array of metallic nuclides that comprise the periodic table are also possible [3–12]. The assumption will be made that individuals reading this chapter have the ability to utilize NMR chemical shift data bases and we will thus focus our attention on the utilization of experiments that “exploit” fundamental NMR parameters. At the next level of complexity, an investigator is likely to take an interest in scalar ( $J$ ) spin coupling interactions between appropriate nuclide pairs, which may include  $^1\text{H}$ – $^1\text{H}$ ,  $^1\text{H}$ – $^{13}\text{C}$ , or more recently  $^1\text{H}$ – $^{15}\text{N}$ . Homo- or heteronuclear scalar (through bond) couplings may either be directly observable, probed by decoupling techniques, or alternatively, they may provide the basis for performing homo- or heteronuclear chemical shift correlation experiments. On a similar plane are through-space connectivity and molecular motion measurements such as the nuclear Overhauser enhancement (NOE), molecular diffusion measurements, and others.

A convenient collection of explanations of some of the terminology of NMR spectroscopy to which some may wish to refer is the monograph, *A Handbook of Nuclear Magnetic Resonance*, by Freeman [13]. In addition, there are also numerous monographs dealing with various aspects of NMR that have appeared over the last 10–15 years that are worthy of note [14–32]. Those cited are by no means intended to be an exhaustive compilation, but rather are those volumes that the authors have found useful.

Beyond simple one-dimensional (1D) NMR spectra, users will generally begin to consider multidimensional NMR experiments. Such experiments allow the segregation of information between two discrete frequency domains. The earliest two-dimensional (2D) NMR experiments were homonuclear experiments in which both frequency domains were used for proton chemical shift information. Here, the scalar coupling between two protons in a chemical structure is exploited to generate off-diagonal responses in a diagonally symmetric data matrix (spectrum) to correlate protons to one another in a fashion analogous to correlating proton resonances with homonuclear decoupling. These experiments are called COSY experiments, which is an acronym for COrrelated SpectroscopY. A diverse array of two-dimensional NMR experiments exist in which proton chemical shift information may be relegated to one axis while  $^{13}\text{C}$  or even  $^{15}\text{N}$  chemical shift information may be on the other axis of the experiment, to give just two examples. These techniques will be treated following the presentation of simpler, one-dimensional NMR methods.

## 8.2 1D (One-dimensional) NMR Methods

The simplest 1D NMR experiments involve the application of a pulse followed by observation of the resulting signal in the time domain, with subsequent Fourier transformation of the data to the frequency domain for presentation in a format that we, as chemists, can understand. Pulsed NMR methods had their inception in 1966 [33] and have almost completely supplanted earlier continuous wave (CW) methods. For reasons of sensitivity, only  $^1\text{H}$  1D NMR spectra were typically acquired prior to the 1970s. The advent of pulsed Fourier transform NMR instruments made it possible to acquire natural abundance  $^{13}\text{C}$  NMR spectra on a routine basis in the early 1970s. With the routine availability of  $^{13}\text{C}$  NMR data came the compilation of chemical shift data bases and a very different way of approaching chemical structure elucidation.

We will briefly consider in this section various aspects of homonuclear spin-decoupling experiments and nuclear Overhauser effect (NOE) difference spectra. Obviously any detailed treatment is far beyond the size limitations of this chapter. Moving next to 1D  $^{13}\text{C}$  NMR techniques, we will briefly consider the utilization of selective spin-population transfer (SPT) and experiments which rely on these principles such as INEPT and DEPT, off-resonance proton decoupling techniques, decoupler gating experiments, and finally spin–lattice or  $T_1$  relaxation techniques,

which also have application to proton NMR spectroscopy in many instances to establish acquisition parameters for 2D NMR experiments, *etc.*

### 8.2.1

#### Proton Spin Decoupling Experiments

Proton spins interact with one another through scalar ( $J$ ) coupling mechanisms. These processes give rise to the familiar multiplets seen in proton spectra, for example the quartet for the methylene and a triplet for the methyl signal of an ethyl group. In the case of simple molecules, spin multiplets are likely to be well separated. Alphabetically, a system of two sets of spins that are widely separated, *i.e.*  $\Delta\nu \gg J$  (where  $\Delta\nu$  is the difference in the chemical shifts of the two spin-coupled nuclides) will be referred to as an AX spin system. Such a system is also referred to as a first order spectrum. As molecular complexity increases, spectral congestion generally increases in parallel. With increasing spectral congestion, chemical shift differences between coupled spins frequently decrease. As  $\Delta\nu$  begins to become comparable to  $J$ , spin systems become less first order in nature, making spectral interpretation by visual inspection progressively more difficult.

Prior to the advent of two-dimensional NMR methods in the mid-1970s, it was common to use spin decoupling as a method of deciphering which proton was coupled to another, the second located perhaps in a congested region of a spectrum. This experiment uses radiofrequency (rf) irradiation, at a frequency coinciding with a proton resonance of interest, to alter the spectral response of the protons coupled to the target resonance. As a function of the strength of the rf field applied, a range of phenomena can be observed. In order of increasing rf field strength, one begins from selective population transfer (SPT) in which a single resonance line of a multiplet, or a  $^{13}\text{C}$  satellite resonance for that matter, is selectively irradiated without perturbing other resonance lines of the same multiplet. A more intense field will give a result known as “spin tickling.” The interested reader is referred to the monograph of Freeman for a discussion of this phenomenon [13]. At higher rf field strength complete spin-decoupling occurs. Applying rf irradiation at this field strength to a proton that is resolved will collapse the scalar coupling(s) of the proton(s) to which the irradiated proton is  $J$ -coupled. Spin decoupling is well documented in any of the monographs cited above, and the interested reader is referred to these sources for further discussion. If an investigator can see the collapsed spin multiplets by simple visual inspection of the resulting spectrum, he or she is finished and can move on with the investigation of the structure. In more complex spectra, the location of the protons affected by the irradiation of one proton may not be easily discerned. In such cases, one may wish to resort to decoupled difference spectra.

### 8.2.2

#### Proton Decoupled Difference Spectroscopy

Difference spectroscopy, as the name implies, requires spectral subtraction. Two spectra are acquired. One in which the proton of interest is decoupled and a second reference spectrum in which the irradiation is applied in an isolated region far from the nearest proton resonance. The two spectra are then subtracted from one another, the resulting difference spectrum highlighting protons that were affected by the decoupling process [34]. Several excellent examples of applications of this technique are found in the monograph by Nakanishi [24].

### 8.2.3

#### Nuclear Overhauser Effect (NOE) Difference Spectroscopy

The nuclear Overhauser effect or NOE is a spatial phenomenon involving two magnetically active nuclides in close proximity. Generally, we think of these experiments in terms of  $^1\text{H}$ – $^1\text{H}$  interactions, but heteronuclide pairs also exhibit these effects. In the  $^1\text{H}$ – $^1\text{H}$  homonuclear case, given two protons in spatial proximity that are not coupled to one another through bonds, the irradiation of one proton (saturation) will lead to an observable enhancement in the signal of the neighboring proton through dipolar cross-relaxation mechanisms. Simplified in the extreme, this is the nuclear Overhauser effect or an NOE. Two excellent monographs treat these experiments in considerable detail. The aging volume by Noggle and Schrimmer [35], while dated, is still an excellent reference. The more recent and comprehensive monograph by Neuhaus and Williamson is probably the best source of information on the NOE currently available [36].

While homonuclear NOEs may range to as great as 50 % enhancements of signal intensity, it is much more common to observe NOEs of only a few percent. Visually observing perhaps what may only be a 2–3 % enhancement of the intensity of a signal is very difficult. In contrast, by using a difference approach, in which only signals enhanced by a given irradiation remain in the spectrum, it is a facile process to determine which protons exhibit a NOE when a neighbor is irradiated. The principle is the same as that used in preparing difference-decoupled spectra. Two spectra are acquired, one in which the proton of interest is irradiated and a second in which the irradiation is in an isolated region of the spectrum. The reference spectrum is subtracted and the difference spectrum is examined. Applications for the use of NOEs are widely varied. NOEs may be used to determine stereochemical relationships, to measure distances between a pair of protons, and for many other purposes. The interested reader is referred to the monographs cited above for further information and examples.

## 8.2.4

**Selective Population Transfer (SPT)**

Applying rf fields of lower intensity to selectively perturb a single resonance or satellite line is the basis of the SPT or selective population transfer experiment. Perhaps the most interesting example of the utilization of SPT experiments, which form the basis for the INEPT, DEPT and other spectral editing experiments that have been developed, is found in the consideration of an AX heteronuclear spin system, *e.g.*  $^1\text{H}$ – $^{13}\text{C}$  or  $^1\text{H}$ – $^{15}\text{N}$  where the heteronuclear spin is insensitive relative to the proton. The energy level diagram for such a spin system will have four transition lines corresponding to the four resonance lines in the spectra of the two nuclides; the proton resonance will be a doublet due to  ${}^nJ_{\text{CH}}$ . The observed  $^1\text{H}$  spectrum will consist of three lines, actually, the central line comprising ~98.9 % of the total resonance intensity will arise from  $^1\text{H}$ – $^{12}\text{C}$ ; the  $^{13}\text{C}$  satellite lines will be separated from the central resonance by  $\pm {}^nJ_{\text{CH}}/2$ , and will have an aggregate intensity of ~1.1 %. Based on the gyromagnetic ratios of the heteronuclides,  $\gamma_{\text{H}}$  and  $\gamma_{\text{C}}$  in this case, the four transitions associated with the energy level diagram of this heteronuclear AX spin system can be assigned numerical values. In the case of the Boltzmann equilibrium state, the two resonance lines for  $^{13}\text{C}$  will each have an intensity of +1. By selectively inverting one of the proton transitions, and then sampling the perturbed system, the  $^{13}\text{C}$  resonance can be observed with transition intensities of +5 and –3 (this special case is termed spin population inversion (SPI)). This signal enhancement is the basis for the sensitivity improvements obtained with the INEPT and DEPT experiments. SPT has also been employed as a means of making resonance assignments. Nagel et al. [37], have reported an excellent example in the course of determining the structure of the complex alkaloid oxaline. When this technique is applied to  $^{15}\text{N}$ , even larger enhancement of the involved resonances is observed because of the greater difference between the gyromagnetic ratios of  $^1\text{H}$  and  $^{15}\text{N}$ .

## 8.2.5

***J*-Modulated Spin Echo Experiments**

While the SPT experiment has obvious utility, it is cumbersome to use unless the selective nature of the experiment is specifically being exploited for structure elucidation purposes. A group of experiments that may be categorized as *J*-modulated spin echo experiments allows the simultaneous investigation of the entire spectrum. As the name of this group of experiments implies, they utilize a spin echo of the type shown in Eq. (1), over which a scalar coupling driven process (using  ${}^1J_{\text{CH}}$  most commonly) is superimposed.

$$\tau - 180^\circ - \tau \quad (1)$$

Experiments that fall into this category include INEPT, DEPT, and APT. These experiments are discussed in considerable detail in any of the monographs cited in

the Introduction to this chapter to which the interested reader is referred. Below, we will focus briefly on the INEPT and DEPT experiments since these are conceptually useful for the development of two-dimensional heteronuclear shift correlation spectroscopy.

### 8.2.5.1 INEPT (Insensitive Nucleus Enhancement by Polarization Transfer)

While the SPT method, as the name indicates, is a selective experiment, techniques derived from the principle of population transfer of a non-selective nature are also available. The first of these to appear was the INEPT experiment [38]. The pulse sequence schematics for INEPT and refocused INEPT are shown in Fig. 8.1. As with the SPT experiment described above, INEPT and its successor, the DEPT experiment, both operate with enhanced sensitivity through the perturbation of the Boltzmann populations. This prototypical non-selective experiment is now relatively seldom used as more refined variants have been developed. The INEPT experiment ( $\tau = (4J)^{-1}$ , Fig. 8.1A) generates antiphase responses analogous to those observed with SPT experiments. The antiphase components of magnetization can, however, be refocused by adding a delay of  $2\Delta$  with a  ${}^1\text{H}/{}^{13}\text{C}$  180° pulse sandwich in the center of the interval where  $\Delta = 1/x^n J_{\text{CH}}$  ( $x = 4–8$ ) [39, 40]. This modification, since the antiphase components of magnetization are refocused, also allows the utilization of broadband decoupling during acquisition.

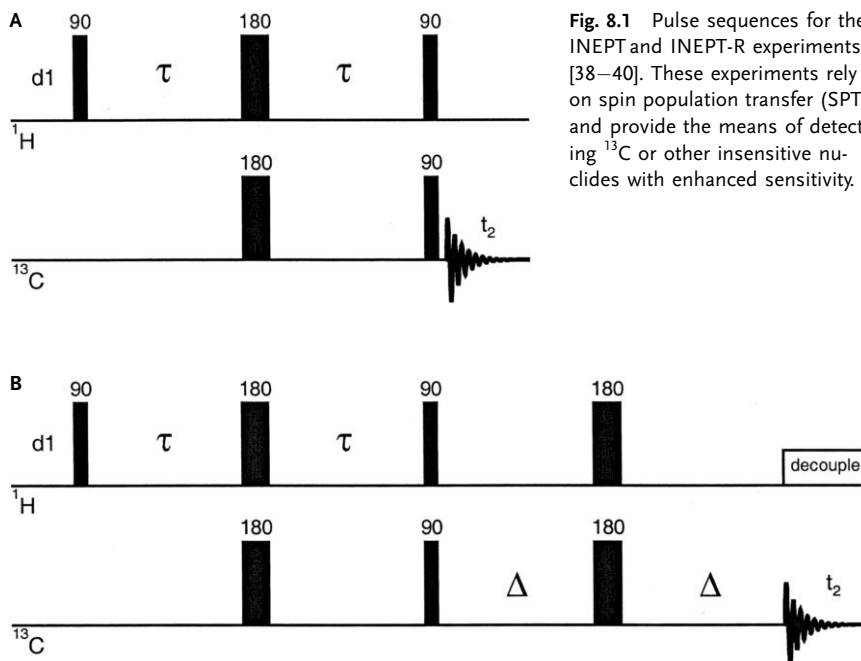


**Fig. 8.1** Pulse sequences for the INEPT and INEPT-R experiments [38–40]. These experiments rely on spin population transfer (SPT) and provide the means of detecting  ${}^{13}\text{C}$  or other insensitive nuclides with enhanced sensitivity.

### 8.2.5.2 DEPT (Distortionless Enhancement Polarization Transfer)

The next level of refinement in non-selective polarization transfer experiments was the DEPT experiment developed by Doddrell and co-workers [41, 42]. The DEPT pulse sequence schematic shown in Fig. 8.2 employs a variable flip angle read pulse,  $\theta$ , as the last proton pulse of the sequence. By varying the flip angle of this pulse, edited subspectra based on resonance multiplicity ( $\text{CH}$ ,  $\text{CH}_2$ , and  $\text{CH}_3$ ) can be readily generated. When  $\theta = 45^\circ$ , a spectrum in which all protonated carbons have positive intensity is produced; quaternary carbons are suppressed and absent. When  $\theta = 90^\circ$ , only methine carbons are observed and have positive intensity. Finally, when  $\theta = 135^\circ$ , a spectrum in which methine and methyl resonances have positive intensity while methylenes are negative is obtained. Given these three spectra, plotting the result with  $\theta = 90^\circ$  gives a  $\text{CH}$ -only spectrum. Plotting the difference spectrum obtained by subtracting the  $\theta = 135^\circ$  spectrum from the  $\theta = 45^\circ$  spectrum gives a methylene-only spectrum. A methyl-only spectrum can be generated by adding the results of the  $\theta = 45^\circ$  and  $135^\circ$  experiments and subtracting the result of the  $\theta = 90^\circ$  experiment. Simple subtraction will give residual responses in the edited subspectra, which can be eliminated by using multiplication coefficients if necessary. Residual responses, however, rarely confuse the sorting of carbon resonance by multiplicity. Examples of DEPT-edited subspectra are shown in Fig. 8.3.

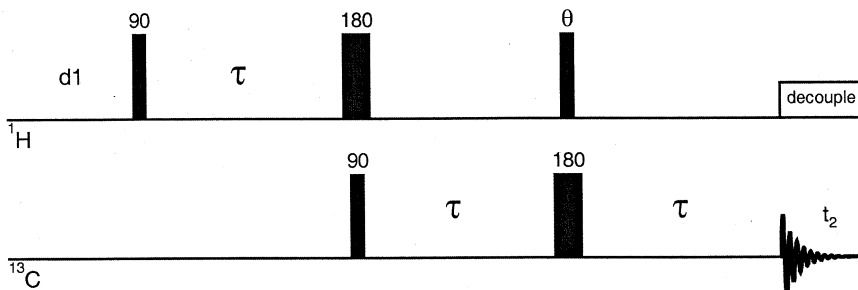


**Fig. 8.2** Pulse sequence for the DEPT experiment [41, 42]. By adjusting the variable flip angle read pulse,  $\theta$ , it is possible to generate edited subspectra based on resonance multiplicity ( $\text{CH}$ ,  $\text{CH}_2$ , and  $\text{CH}_3$ ). When  $\theta = 45^\circ$ , all protonated carbons will exhibit positive intensity. When  $\theta = 90^\circ$ , only methine carbons are observed and have positive intensity. When  $\theta = 135^\circ$  a spectrum is produced in which methine and methyl resonances have positive intensity

while methylene resonances have negative intensity. Plotting the  $\theta = 90^\circ$  spectrum gives a methane-only subspectrum; the difference spectrum obtained by subtracting the  $\theta = 135^\circ$  spectrum from the  $\theta = 45^\circ$  spectrum gives a methylene-only spectrum; finally, a methyl-only spectrum can be generated by adding the experimental results of the  $\theta = 45^\circ$  and  $135^\circ$  experiments. An example of the edited subspectra of a model compound are shown in Fig. 8.3.

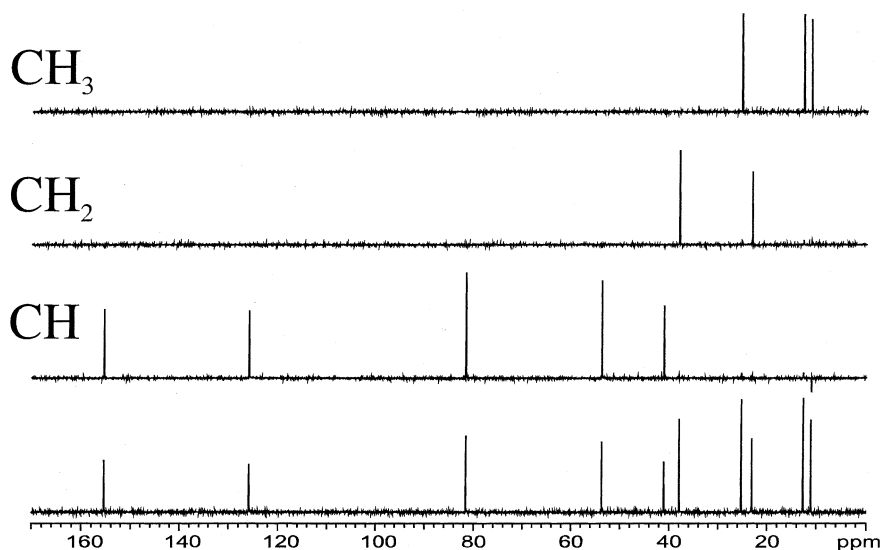


**Fig. 8.3** Multiplicity-edited DEPT spectra recorded at 125 MHz for a sample of santonin (1).

### 8.2.6

#### Off-Resonance Decoupling

If a low power rf field is selectively applied to a specific proton resonance and a  $^{13}\text{C}$  spectrum is subsequently recorded, the resulting spectrum will nominally be proton coupled, with the exception of the carbon associated with the selected proton. In this fashion, by performing a series of such experiments, it is possible to correlate carbon resonances with their directly attached protons. As the decoupling frequency is moved off-resonance, residual coupling,  $J_{\text{R}}$ , will be observed in the carbon spectrum with  $J_{\text{R}}$  a function of the strength of the applied rf field and how far off resonance it is applied. By preparing a series of such experiments, various carbon multiplets will successively collapse and reappear as the frequency of the applied proton decoupling field is systematically varied from one experiment to the next. Such experiments were an early forerunner of two-dimensional heteronuclear shift correlation experiments. Perhaps it is worthy of note that a whole qualitative dimension of spectral information is available from inspecting multiplicity shape as a function of  $J_{\text{R}}$ . Such information frequently allows specific assignment of resonances within multiplicity groups. This information is lost, however, in spectral editing sequences like INEPT and DEPT that rely on sign and intensity variation of the coupled or decoupled resonance [43].

## 8.2.7

**Relaxation Measurements**

Following the application of a pulse or pulses to an NMR sample and the acquisition of whatever data are of interest, time is required for the system to return to some level of equilibrium. Two fundamental relaxation processes govern the return of a perturbed spin system to equilibrium. These processes are spin–lattice or  $T_1$  relaxation, and spin–spin or  $T_2$  relaxation. A variety of means are available to measure both of these fundamental processes [27, 29, 31]. We will limit the discussion here to the former.

Spin–lattice relaxation is the time constant for the recovery of magnetization along the  $z$ -axis in a NMR experiment. Various methods are available for the measurement of spin–lattice relaxation times. The interested reader is referred to the series of monographs edited by Levy on Carbon-13 NMR spectroscopy [44, 45] for more details. The energy transfer between nuclear moments and the “lattice”, the three-dimensional system containing the nuclei, provides the mechanism to study molecular motion, *e.g.* rotations and translations, with correlation times of the order of the nuclear Larmour frequencies, tens to hundreds of MHz. We will limit our discussion here to the simple inversion-recovery  $T_1$  relaxation time measurement experiment, which, in addition to providing a convenient means for the quick estimation of  $T_1$  to establish the necessary interpulse delay in two-dimensional NMR experiments, also provides a useful entry point into the discussion of multi-dimensional NMR experiments.

The inversion recovery experiment, applies a  $180^\circ$  pulse to align the magnetization along the  $-z$ -axis using the pulse sequence shown in Fig. 8.4. A variable delay,  $\tau$ , follows, which is adjusted across a range of values in a series of experiments, generally beginning with periods much shorter than the actual relaxation time through delays which are several times longer than the relaxation time to be measured. Following the  $\tau$  interval, the evolved state of the magnetization is sampled using a  $90^\circ$  pulse. The intensity of the observed response can range from fully negative intensity, when  $\tau$  is much shorter than  $T_1$ , through full positive responses when  $\tau > 5T_1$ , as shown in Fig. 8.5. The signal intensity will be zero at the cross-over point when  $\tau = 0.69 T_1$ . Each data point represents a separate experiment differing from the other experiments in the series by the duration of  $\tau$ . The  $T_1$  relaxation time is encoded in the signal intensity in this series of experiments through the successive variation of the duration of  $\tau$ . This process is exactly analogous to the encoding of chemical shift information, or other spectral parametric information, in a 2D NMR experiment.

To establish interpulse delays for two-dimensional NMR experiments, it is frequently convenient to run a very quick proton  $T_1$  relaxation measurement. Given the sensitivity of modern spectrometers, this can usually be done with only a single or a few transients for each of the  $\tau$  values in the series, and typically requires 10 min or less. By visual inspection, the  $T_1$  relaxation time can be estimated from the  $\tau$  value at which response intensity is zero. A knowledge of the  $T_1$  relaxation time is also useful for establishing mixing times for NOESY and ROESY experiments,

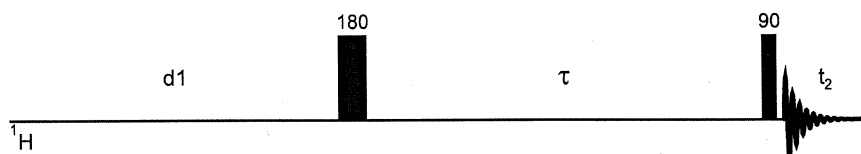


**Fig. 8.4** Spin–lattice ( $T_1$ ) inversion recovery pulse sequence. The  $180^\circ$  pulse inverts magnetization, allowing it to recover along the  $z$ -axis. The duration of the delay,  $\tau$ , is varied from  $\ll T_1$  to several times the longest expected  $T_1$  relaxation time in the molecule. The resulting, varying states of relaxation are sampled by the  $90^\circ$  pulse. The “null point,” when there is essentially no signal intensity corresponds to  $0.69 T_1$ . The results of an inversion recovery experiment applied to  $^1\text{H}$  for strychnine (2) are shown in Fig. 8.5.

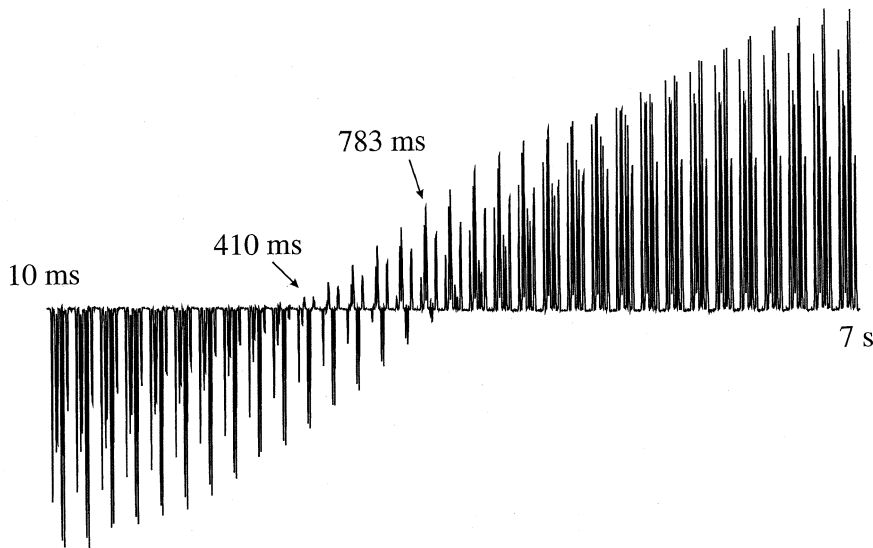


**Fig. 8.5** Inversion recovery experiment results for strychnine (2) shown as a horizontal stack plot where the duration of the delay,  $\tau$ , between the  $180^\circ$  and  $90^\circ$  pulses is increased from right to left.

which empirically can generally be performed by setting the mixing time to  $\sim 0.7T_1$  and  $\sim 0.5T_1$ , respectively.

### 8.3 Two-dimensional NMR Experiments

Two-dimensional NMR spectroscopy has been the topic of numerous monographs [14–17, 23–27, 29–31]. It is the intent here to provide the reader with a brief introduction and the means of accessing key aspects of what has become a voluminous literature on the subject. Briefly, 2D NMR experiments are comprised of several fundamental segments or building blocks. Three periods are obligatory in a 2D NMR experiment. These consist of a preparation period, the evolution period,  $t_1$ , which corresponds to what will be the indirectly digitized time domain, and a

detection period,  $t_2$ , which is the directly detected time domain. In addition, some 2D NMR experiments contain a fourth period for “mixing” that is inserted between evolution and detection. Double Fourier transformation of the resulting data matrix affords a two-dimensional frequency matrix in which responses are a function of two frequencies as shown by Eq. (2)

$$S(t_1, t_2) \rightarrow s(F_1, F_2) \quad (2)$$

The two frequency axes may consist of a diverse assortment of pairs of fundamental NMR parameters. Examples might include chemical shift on one axis and a frequency axis for scalar couplings on the second as in the 2D  $J$ -resolved NMR experiments. Both axes may be proton chemical shift, in which responses may be correlated by scalar ( $J$ ) coupling as in the COSY experiment [46–48], by dipolar relaxation pathways as in the NOESY [35, 36, 49–51] and ROESY [35, 36, 52, 53] experiments, or by chemical exchange pathways as in the EXSY experiment [54–59]. Other examples may involve chemical shift on one axis and a multiple quantum frequency on the second axis. Examples here would include proton double [60–62] and zero quantum spectroscopy [63–67],  $^{13}\text{C}$ – $^{13}\text{C}$  INADEQUATE [68, 69], etc. The available axes in a 2D NMR experiment may also be used for heteronuclear chemical shift correlation, e.g.  $^1\text{H}$ – $^{13}\text{C}$  or  $^1\text{H}$ – $^{15}\text{N}$ , where the respective nuclide pairs are correlated via their one-bond ( $^1J_{\text{XH}}$ ) or multiple bond ( $^nJ_{\text{XN}}$ ) heteronuclear couplings [14, 16, 17, 23–27, 29–31, 70–72].

While the subject of 2D NMR spectroscopy may initially appear a daunting one, the simplest point of entry into 2D NMR is undoubtedly via  $J$ -resolved experiments [73, 74]. From a fundamental understanding of the segregation of spectral parameter information between frequency domains in a 2D  $J$  experiment, the reader can successfully begin to delve into homo- and heteronuclear 2D NMR techniques.

### 8.3.1

#### 2D $J$ -Resolved NMR Experiments

2D  $J$ -resolved NMR experiments are a conceptual amalgamation of two topics discussed above, the  $J$ -modulated spin echo and the two-dimensional characteristic of the spin–lattice relaxation experiments. As the name of these experiments implies, scalar coupling information,  $J$ , will be displayed in the one frequency domain; chemical shift information will be presented in the second frequency domain. The simplest 2D  $J$  experiments sort  $^{13}\text{C}$  chemical shift information in the detected time domain, labeled  $t_2$  by convention, while the heteronuclear scalar couplings of each carbon are sorted into the indirectly determined time domain,  $t_1$  (do not be confused lower case  $t_1$  with the spin–lattice relaxation time,  $T_1$ ).

The pulse sequence for an amplitude modulated heteronuclear 2DJ experiment is shown in Fig. 8.6 [75]. The experiment consists of a  $90^\circ$   $^{13}\text{C}$  pulse to rotate magnetization into the  $xy$ -plane where it begins to evolve with the decoupler turned on. After the first half of the evolution time has elapsed,  $t_1/2$ , a  $180^\circ$   $^{13}\text{C}$  pulse is applied and the decoupler is gated off for the second half of the evolution period.

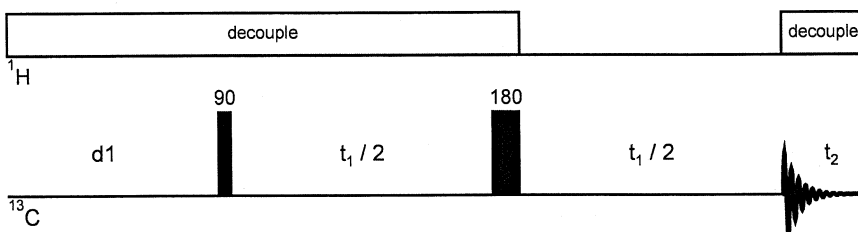


**Fig. 8.6** Pulse sequence for the amplitude modulated 2D  $J$ -resolved NMR experiment. The experiment is based on a  $J$ -modulated spin echo. The first  $90^\circ$  pulse tips magnetization into the  $xy$ -plane where it evolves during the first half of the evolution period,  $t_1/2$ . The  $180^\circ$  pulse is applied and the decoupler is simultaneously gated off for the second half of evolution.

Decoupling is resumed when acquisition is started. The evolution of magnetization under the influence of the heteronuclear coupling during the second half of the evolution period leads to a 2D spectrum in which heteronuclear couplings are scaled by a factor of 2 and sorted as a function of the  $^{13}\text{C}$  chemical shift as shown by the contour plot presented in Fig. 8.9.

As might be expected at this point, two processes are ongoing in the second half of the evolution period. First, having applied a  $180^\circ$   $^{13}\text{C}$  pulse at  $t_1/2$ , we should expect that magnetization will be refocused in a spin-echo at time =  $t_1$ . Second, since the decoupler has been gated off for the second half of the evolution period, the spin echo will be  $J$ -modulated by the evolution of heteronuclear couplings during the second  $t_1/2$  interval.

A 2D  $J$  experiment, or any 2D NMR experiment for that matter, consists of a series of 1D experiments in which the duration of the evolution time,  $t_1$ , is systematically incremented in some fashion from one experiment to the next. In the specific case of a 2D  $J$  experiment, the incremented parameter is the dwell time, which corresponds to  $1/\text{sw}_1$ , where  $\text{sw}_1$  is the desired spectral width of the second frequency domain,  $F_1$ , in Hz. Typical one-bond heteronuclear couplings range from about 125 to 160 Hz for aliphatic to aromatic compounds, respectively, with some heteroaromatics having one-bond couplings ranging up to about 210 Hz. In most cases, the spectral width in the second frequency domain of a 2D  $J$  experiment can be set to a total of 100 Hz, keeping in mind that couplings will be scaled by  $J/2$  since  $J$ -modulation occurs for only half of the evolution time.

Experimentally, the results of performing a 2D  $J$  experiment such as that shown in Fig. 8.6 are represented by the following several figures. First, as shown in Fig. 8.7, response intensity is amplitude modulated for a given carbon from one experiment to the next as the evolution time,  $t_1$  is incremented. The amplitude modulated resonance corresponds to the data arising from the first Fourier transformation as defined by Eq. (3).

$$S(t_1, t_2) \rightarrow s(t_1, F_2) \quad (3)$$

Transposition of the 2D data matrix, as defined by Eq. (4) allows us to look at the modulation of response intensity in the time domain, which is analogous to looking at a free induction decay (FID). These data are shown in Fig. 8.8.

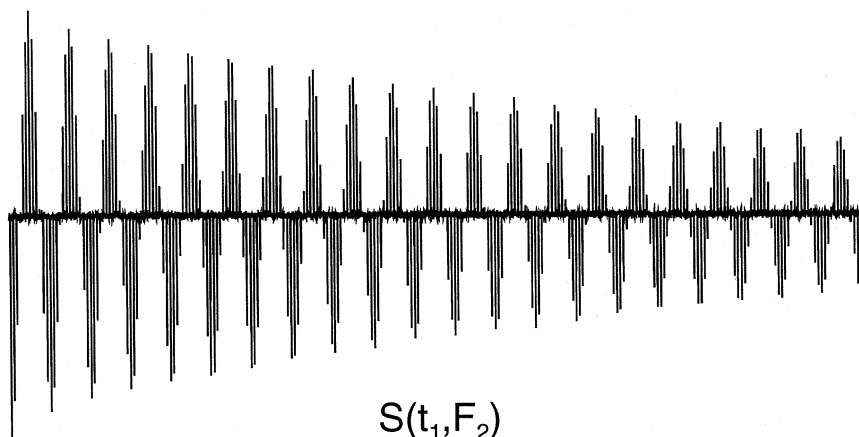


**Fig. 8.7** Amplitude modulation of a single  $^{13}\text{C}$  resonance extracted from a partially processed amplitude modulated 2D  $J$ -resolved experiment. The data set was subjected to the first Fourier transform to give a data set of the form  $S[t_1, F_2]$  from which the data shown were extracted. Successive incrementation of the duration of the evolution period,  $t_1$ , leads to the amplitude modulation of the  $^{13}\text{C}$  signal observed. The

heteronuclear coupling information is encoded into the modulation frequency. Each peak in this horizontal stack plot is obtained for a different value of the evolution time,  $t_1$ . Generally, these data would be shown in a stack plot of the type shown in Fig. 8.8. They are shown here as a simple horizontally plotted series of 256 spectra to emphasize the amplitude modulation of the carbon resonance.

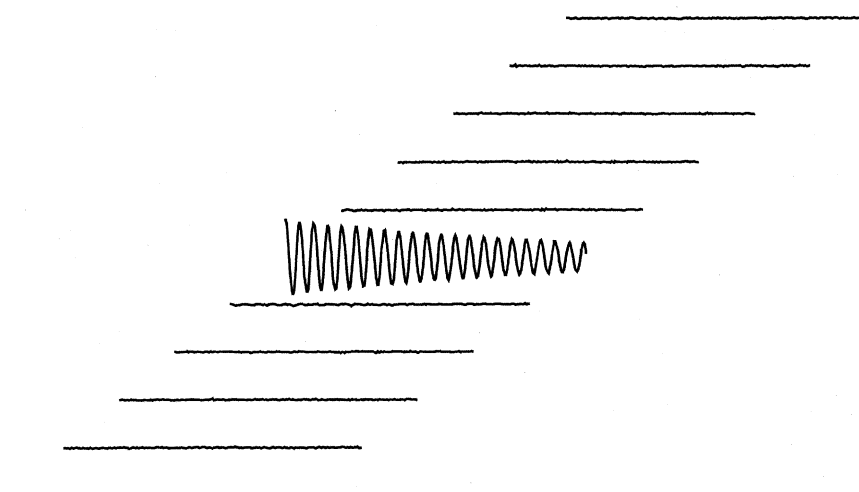


**Fig. 8.8** Interferograms from the region surrounding the amplitude modulated resonance shown in Fig. 8.7. These data would correspond to transposition of the  $S[t_1, F_2]$  data set to the form  $S[F_2, t_1]$ . Fourier transformation of the interferograms extracts the heteronuclear cou-

pling information encoded into the amplitude modulation of the resonance, sorted by  $^{13}\text{C}$  chemical shift. The final, Fourier transformed result of the amplitude modulated 2D  $J$ -resolved experiment is shown in Fig. 8.9.

$$S(t_1, F_2) \rightarrow s(F_2, t_1) \quad (4)$$

Completion of the second Fourier transform Eq. (5) gives the resulting 2D  $J$  spectrum, which is shown as a contour plot in Fig. 8.9.

$$S(F_2, t_1) \rightarrow s(F_2, F_1) \quad (5)$$

The data shown in Fig. 8.9 were acquired for santonin (**1**). The  $^{13}\text{C}$  chemical spectrum of the sesquiterpene is shown plotted along the  $F_2$  axis. If a projection were done through the  $F_1$  or second frequency domain, a so-called “ $J$  spectrum” would be obtained, which in this case is not especially useful. Each of the carbons contains, at its respective chemical shift in  $F_2$ , responses due to the scalar ( $J$ ) couplings of that carbon. For protonated carbons, the larger spacing arises from the  $^1J_{\text{CH}}$  coupling; the smaller spacings, when clearly resolved in this presentation, e.g. the carbon near 80 ppm just downfield of the chloroform response, are a result of the  $^nJ_{\text{CH}}$  coupling, where  $n = 2$  or 3. The non-protonated carbons, e.g. the two non-protonated vinyl carbons, exhibit responses centered on the axis  $F_1 = 0$  Hz due to  $^nJ_{\text{CH}}$  couplings but do not have larger  $^1J_{\text{CH}}$  responses.

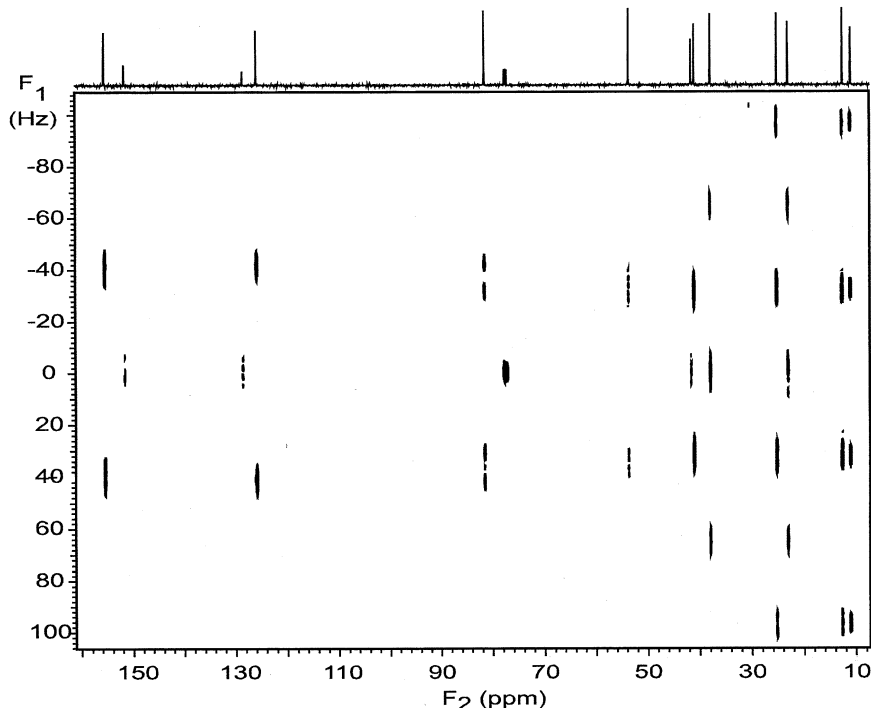
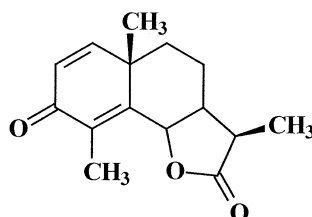


**Fig. 8.9** Contour plot of the amplitude modulated 2D  $J$ -resolved NMR spectrum of the simple alkaloid santonin (**1**) recorded at 400 MHz. The  $^{13}\text{C}$  reference spectrum is plotted along the horizontal axis; the so-called “ $J$ -spectrum” (not shown) is obtained by projection through the data matrix. Heteronuclear couplings are scaled by a factor of 2 since they evolve without decoupling for only half of the evolution period,  $t_1$ .



1

In addition to the use of *J* spectroscopy for <sup>1</sup>H–<sup>13</sup>C heteronuclear coupling, there are also homonuclear variants of the experiment [76]. For the most part, however, the 2D *J*-resolved experiments have fallen into disuse as there are more efficient means of deriving the same spectral information.

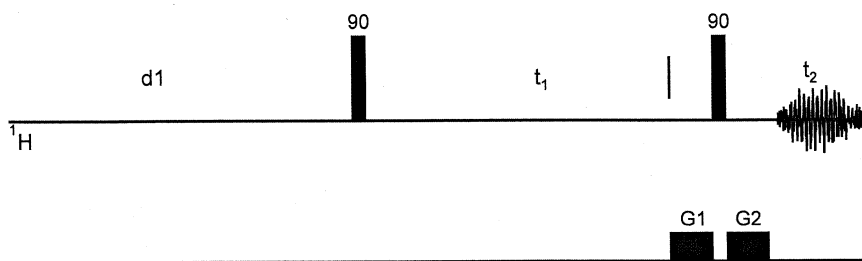
### 8.3.2

#### Homonuclear 2D NMR Spectroscopy

There are probably, at present, about four homonuclear 2D NMR experiments in common usage for small molecules. These include COSY (COrelatEd SpectroscopY) [46–48], TOCSY (TOtal Correlation SpectroscopY) [77–79], NOESY [35, 36, 49–51], and ROESY [35, 36, 52, 53], the latter two corresponding to nuclear Overhauser and spin-locked Overhauser correlated experiments, respectively. Several less frequently employed homonuclear 2D experiments are also possible and include: <sup>13</sup>C–<sup>13</sup>C [68, 69]; <sup>1</sup>H double quantum spectroscopy [60–62]; <sup>1</sup>H zero quantum spectroscopy [63–67], and others<sup>1</sup>H. We will discuss the primary experiments in the category briefly in turn, and we will direct the reader interested in other homonuclear 2D variants to the appropriate literature.

##### 8.3.2.1 COSY, Homonuclear Correlated Spectroscopy

The COSY experiment was developed early in the history of 2D NMR [46–48]. Both frequency axes in the experiment are used to display proton chemical shift information in most cases. The actual proton spectrum of these experiments resides along the diagonal in the 2D spectrum. Individual proton resonances in the experiment are correlated to one another via scalar (*J*) coupling through off-diagonal correlation responses. Geminal (<sup>2</sup>*J*<sub>HH</sub>) and vicinal (<sup>3</sup>*J*<sub>HH</sub>) correlations will almost always be observed if the scalar coupling between the protons in question is of a reasonable size. Depending on the extent of digitization in the second frequency domain, weak vicinal couplings (those for protons whose couplings are weak because of Karplus considerations) and longer – range couplings may or may not be observed. The observation of weaker responses is also, in part, a function of the mathematical weighting functions used in processing the data. It is entirely possible through data processing procedures to retain or eliminate weak vicinal and longer-range proton–proton correlation responses.



### Z-Gradient

**Fig. 8.10** Pulse sequence for homonuclear correlation spectroscopy, COSY/GCCOSY [46–48]. Although the gradient version of the experiment is shown, the pulse sequences are the same except for the two gradients and their associated delays. The non-gradient experiment employs a four-step phase cycle; the gradient experiment allows the acquisition of data with a

single transient/ $t_1$  increment since the coherence transfer pathway is selected by the gradients. The proton spectrum appears along the diagonal of the diagonally symmetric data matrix. Correlations between scalar ( $J$ ) coupled resonances are denoted by off-diagonal elements in the spectrum, as shown in Fig. 8.11.

The pulse sequence used for the COSY experiment is extremely simple, consisting of a pair of  $90^\circ$  pulses separated by the incremented evolution period,  $t_1$ , as shown in Fig. 8.10. The incrementation of the evolution time is generally set to afford a square data matrix since it is desirable to have both frequency axes identical in homonuclear correlation experiments. In the case of macro-driven modern NMR instruments, setting the spectral width in the second frequency domain of an experiment like COSY is usually transparent. In general, for a survey experiment, it is useful to acquire perhaps 2K points in the observed time domain ( $t_2$ ; 1K points after Fourier transformation) and  $\sim 1/6$ th as many points in the second time domain,  $t_1$ , as the transformed result in  $F_2$ . Generally, for a survey COSY experiment we find it convenient to acquire 128 to 160 files in the second time domain. After processing, these data will yield a spectrum in which geminal and most vicinal correlation responses will be observed. When weaker or long-range homonuclear correlation responses are sought, higher levels of digitization of  $t_1$  are necessary, up to a maximum of half the number of points acquired in  $t_2$ .

Processing COSY data usually employs sinebell multiplication, with zero filling in the second frequency domain to yield a square data matrix. As an example, consider the COSY spectrum of the aliphatic region of strychnine (2) shown in Fig. 8.11. The COSY data shown were acquired using the general survey conditions suggested above. The data are presented as a contour plot, which is analogous to a topographic map. Peaks are defined by contours; weak responses in the spectrum may be represented by one or only a few contour levels while stronger peaks may require numerous contours for representation. The diagonal in this presentation corresponds to the proton reference spectrum that is plotted above the contour plot. Protons in the molecular structure that are scalar coupled to one another are correlated in the experimental spectrum by the off-diagonal responses. Several correlation pathways are shown in Fig. 8.11. A full discussion of the interpretation

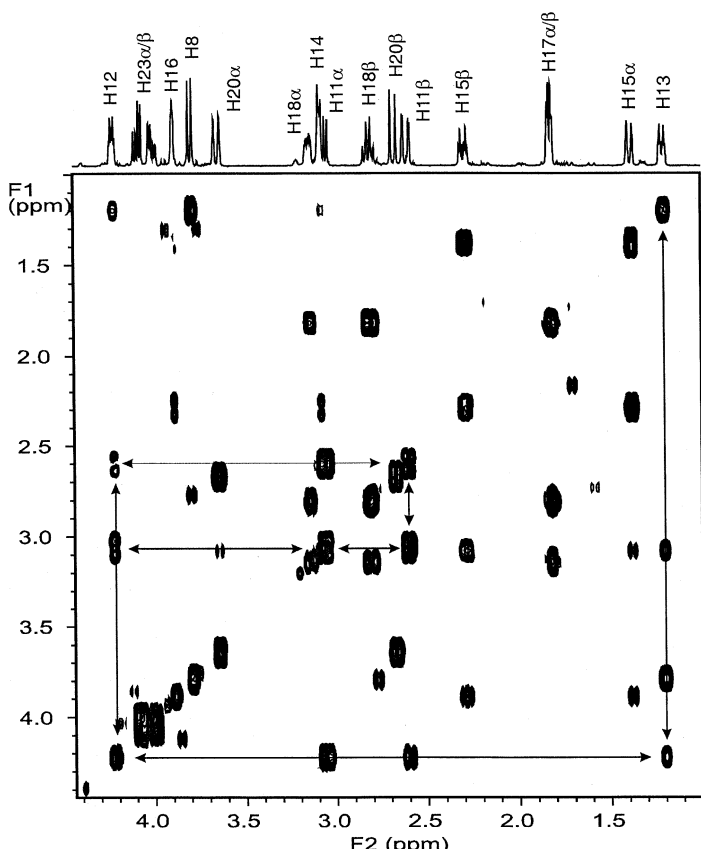
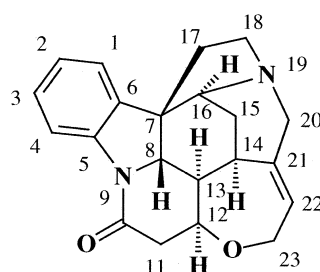


**Fig. 8.11** COSY spectrum of the aliphatic region of the strychnine (**2**)  $^1\text{H}$  spectrum. Connectivities are shown from the anisochronous, geminal H11 resonances to H12, and in turn to the H13 resonance. The COSY spectrum is essentially the equivalent to the simultaneous

acquisition of all possible selective homonuclear spin decoupling experiments. The COSY experiment has become one of the fundamental cornerstone experiments used in the determination of natural product structures and for many related structural studies.

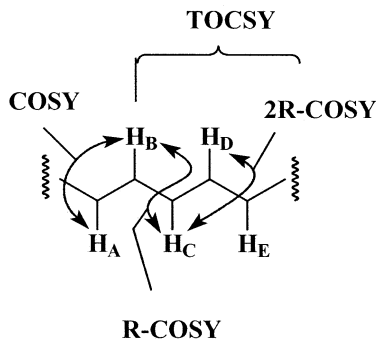
and or utilization of COSY data is beyond the scope of this treatment and the interested reader is referred to any of the monographs on the subject of 2D NMR cited in the introduction to this chapter. Briefly, however, referring to the H11 $\alpha/\beta$  geminal proton resonances at 3.11 and 2.6 ppm, we note that these protons are correlated to one another in the spectrum with correlations also observed to the H12 proton resonating at 4.23 ppm. If one were to continue from the H12 correlation on the diagonal, in a step-wise fashion, the H13 methine resonance at 1.3 ppm could next be assigned, as shown in Fig. 8.11. Continuing in this fashion, the contiguous proton spin system can be constructed as far as it is possible to follow correlations from one proton to the next, in principle to the H16 resonance.



2

### 8.3.2.2 Homonuclear TOCSY, Total Correlated Spectroscopy

In an effort to extend the correlation ability of the COSY experiment just described, the Relayed- or R-COSY experiment [80, 81] was developed. While the COSY experiment correlates  $H_A \rightarrow H_B$  in the hypothetical structural fragment shown by 3, the R-COSY experiment ideally extends the correlation a step further  $H_A \rightarrow H_B \rightarrow H_C$  via an additional delay following the evolution period and a  $90^\circ$  pulse. Double relayed or 2R-COSY is a trivial extension of the RCOSY experiment that repeats the relay process, giving correlation from  $H_A$  ultimately to  $H_D$ , assuming that the delays were set appropriately for the intervening homonuclear couplings. Likewise, the so-called long-range or LR-COSY experiment [82] used a fixed delay to emphasize long-range homonuclear couplings in much the same sense as in long-range heteronuclear shift correlation experiments which are described below. The assemblage of experiments has been largely supplanted by a single experiment known as homonuclear TOCSY, which is the experimental amalgamation of the series of ideas just advanced.



3

The homonuclear TOCSY experiment [77, 79] utilizes the fundamental COSY pulse sequence and evolution time followed by a delay and then an isotropic mixing period; the pulse sequence is shown in Fig. 8.12. Homonuclear vicinal

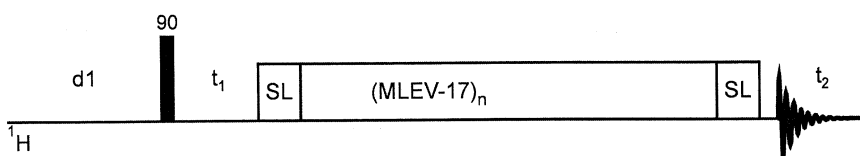


**Fig. 8.12** Homonuclear TOCSY pulse sequence [77–79]. Isotropic mixing is provided by a pulse train, and serves to propagate magnetization from a given proton to its scalar coupled neighbor. The extent to which coherence will be transferred along a series of coupled, homonuclear spins, is a function of the duration of the mixing time.

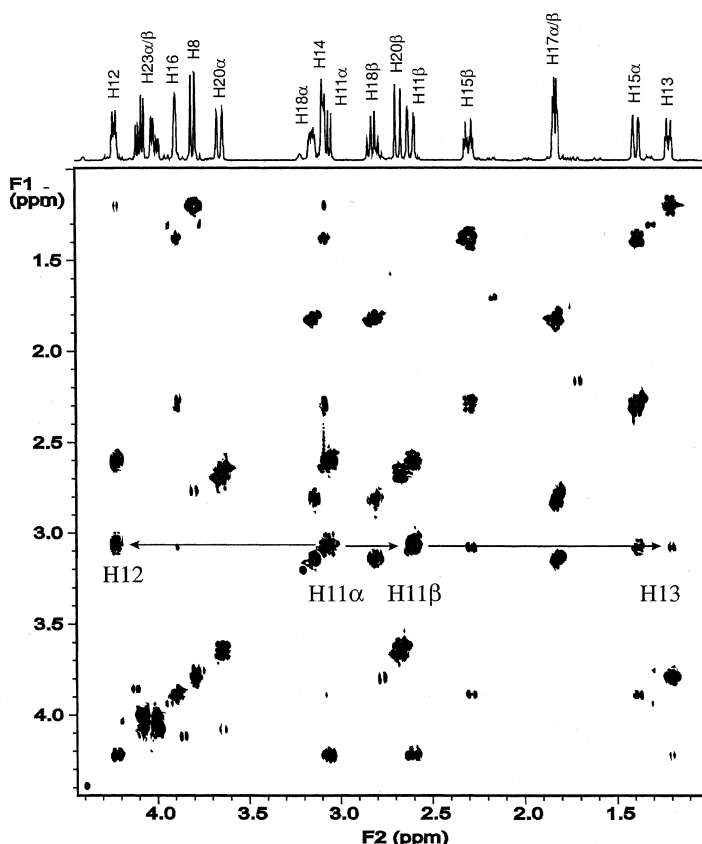


**Fig. 8.13** TOCSY spectrum of the aliphatic region of the strychnine (**2**) proton spectrum recorded with a mixing time of 30 ms. Correlations from the H11 protons are shown as in the COSY spectrum shown in Fig. 8.11. The off-diagonal elements from the H11

resonances correlate them to each other (geminally) and to the H12 resonance as in the COSY spectrum. However, in addition, the 30 ms mixing time is long enough to propagate magnetization from the H11 resonances to H12 and then on to the H13 resonance.

coupling coherence is established during the evolution period; magnetization is propagated from the vicinal neighbor to its vicinal neighbor, and so on. The extent to which magnetization is propagated is a function of the mixing time and the size of the homonuclear coupling constants between the vicinally coupled protons in question. The longer the mixing time, the further magnetization is propagated through the contiguous homonuclear vicinal coupling network. Shorter mixing times, e.g. ~12 ms for aromatic systems and 18–24 ms for aliphatic or alicyclic systems will establish correlations to protons one or two bonds removed from the starting resonance. In the case of 3, shorter mixing times will establish correlations from  $H_A$  to protons as far removed as  $H_C$  or  $H_D$  depending on the size of the intervening homonuclear couplings. Longer mixing times, e.g. 18–24 ms for aromatic compounds and 24–36 ms for aliphatic/alicyclic molecules will transfer magnetization still further. It should be remembered, however, that these are only approximations.

Returning to the example of strychnine (2), a 30 ms TOCSY spectrum of the aliphatic region of the proton spectrum at 500 MHz is shown in Fig. 8.13. Again, starting from the  $H_{11}$  geminal methylene pair, correlations are established as far as  $H_{13}$  through the intervening protons.

### 8.3.2.3 NOESY, Nuclear Overhauser Enhancement Spectroscopy

The NOESY experiment is another of the homonuclear autocorrelated experiments in which both frequency axes display chemical shift information (usually  $^1H$ , although  $^{19}F$  experiments are certainly possible in perfluorinated compounds, and possibly  $^{13}C$  for molecules biosynthesized using 1,2- $^{13}C$  acetate). The experiment begins in a fashion analogous to the COSY experiment and again employs a mixing period to permit the dipolar relaxation processes to occur, which are being sampled to correlate resonances (see Fig. 8.14) [35, 36, 49–51]. As noted above, a convenient means of establishing the duration of the mixing period is afforded from a simple spin–lattice ( $T_1$ ) inversion–recovery relaxation experiment. The “null” point in the inversion–recovery experiment is ~0.69  $T_1$ , which is a useful rule-of-thumb for setting the duration of the mixing time in a NOESY experiment. The NOESY spectrum of strychnine (2) recorded with a 350 ms mixing time,

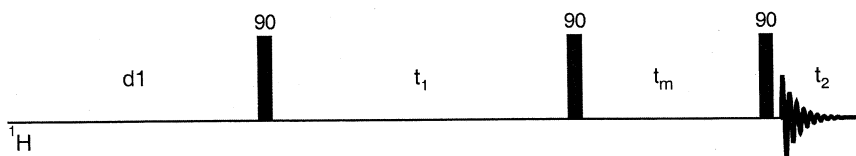


**Fig. 8.14** NOESY pulse sequence. The NOESY  $\tau_m$ , allows dipolar cross relaxation to occur, experiment is one which uses a mixing period,  $\tau_m$ , in addition to the obligatory preparation, evolution and detection periods. Protons are labeled with the individual chemical shifts during the evolution period,  $t_1$ . The mixing period,  $\tau_m$ , is detected with the final 90° pulse of the sequence. The duration of the mixing time is usually set to about 0.7  $T_1$ , which corresponds to the null point when an inversion recovery  $T_1$  relaxation measurement is done.

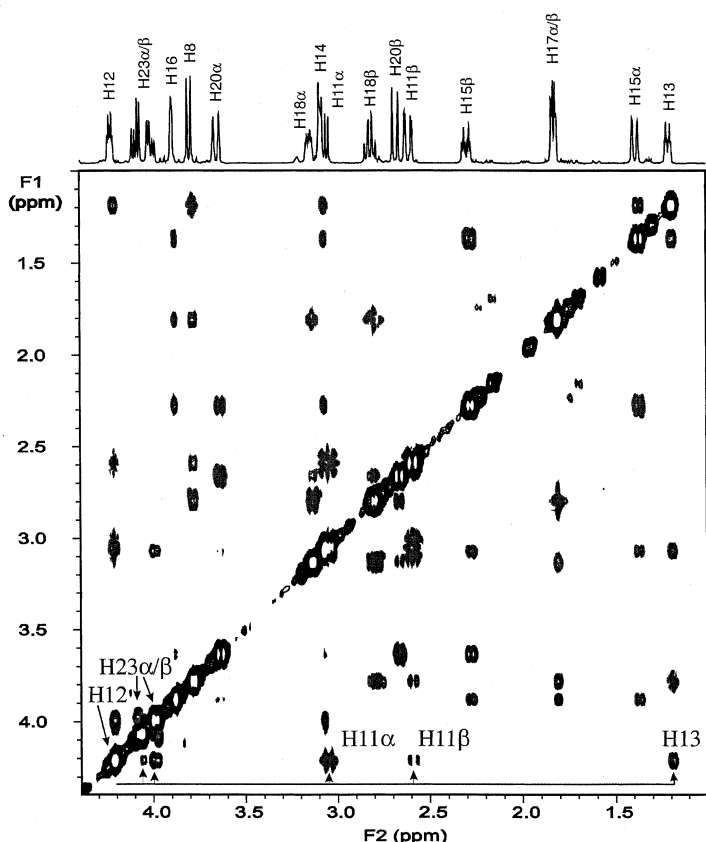


**Fig. 8.15** NOESY spectrum of the aliphatic region of the strychnine (**2**) proton spectrum recorded with a 350 ms mixing time. These data are useful, in establishing correlations between protons that are not scalar coupled, e.g. the correlation between the 23- and 12-methine proton, as shown by the labeled connectivities in the spectrum. In addition, these data also

show that the H12 methine and H13 methine resonance are located on the same side of the molecule. The more intense response of the 23- and 11-anisochronous methylene resonances are also located on the same side of the molecule, *a*, as the H12 resonance, providing a convenient means of differentiating and assigning these resonances.

is shown in Fig. 8.15. Several brief observations concerning the spectrum shown are warranted. First, the relative orientation of the H12 resonance relative to the H11 $\alpha$  and H11 $\beta$  protons is readily established from the data. In addition, it is also possible to establish a correlation across the oxepin ether linkage from the 11- to 23-position in the molecule. This affords new structural connectivity information, which is probably very difficult to obtain via a homonuclear scalar coupling, if it is observable at all.

### 8.3.2.4 ROESY, Rotating Frame Overhauser Enhanced Spectroscopy

The ROESY experiment combines ideas drawn from the TOCSY and NOESY experiments. Protons are correlated to one another via ROEs (rotating frame Overhauser effect) [35, 36, 52, 53]. ROEs are developed in the ROESY experiment through the use of a spin-locking field in a manner analogous to the propagation of magnetization in the homonuclear TOCSY experiment (see Fig. 8.16). The dura-

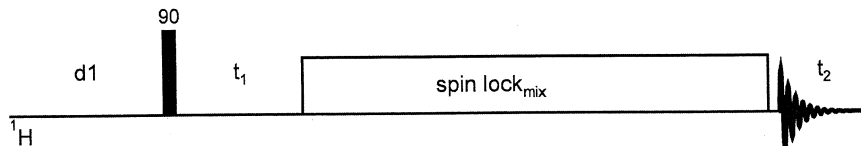


**Fig. 8.16** ROESY pulse sequence [35, 36, 52, 53]. Protons are labeled with their respective chemical shifts during the evolution time,  $t_1$ , as with the COSY and NOESY experiments.

ROEs are developed by the isotropic mixing sequence applied during the mixing time,  $t_m$ , which is generally set to about 0.5  $T_1$ .

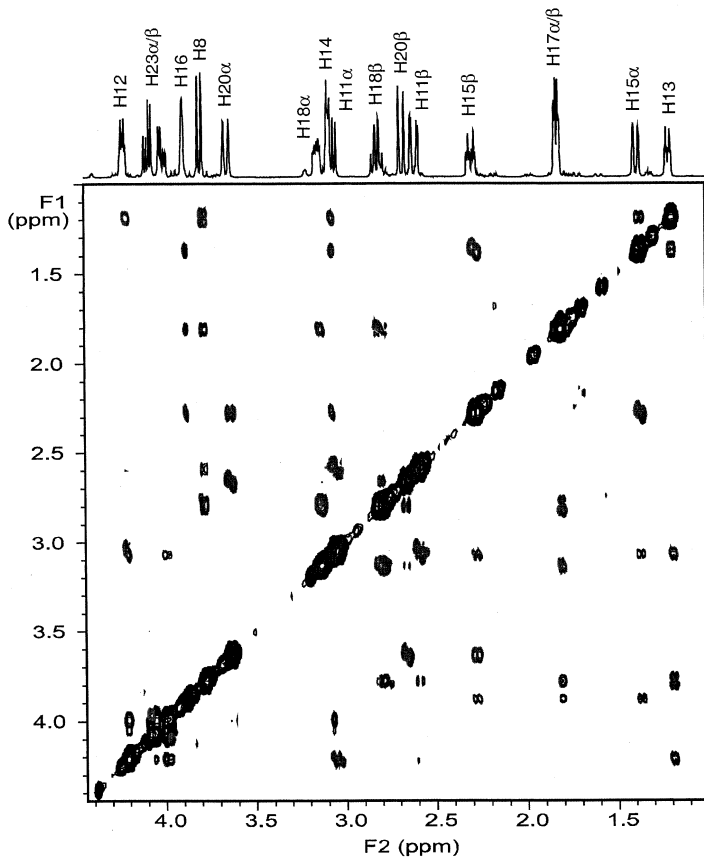


**Fig. 8.17** ROESY spectrum of the aliphatic region of strychnine (2) recorded with a 250 ms mixing time. The correlations observed and the assignment information which can be derived from them is the same as for the NOESY experiment presented in Fig. 8.15.

tion of the mixing time in a ROESY experiment can also be conveniently set from a simple inversion–recovery experiment. Recalling that the “null” point in the inversion recovery experiment is  $\sim 0.69 T_1$ , the rough approximation of the average  $T_1$  relaxation time for the proton(s) of interest can be easily determined. As a general rule of thumb, setting the mixing time in a ROESY experiment to  $\sim 0.5 T_1$  will generally provide usable data.

Again returning to strychnine (2) as a structural model, the ROESY spectrum with a mixing time of 250 ms is shown in Fig. 8.17. Comparison of the correlations observed in the ROESY spectrum shows them to be qualitatively similar to those seen in the NOESY experiment shown in Fig. 8.15.

### 8.3.2.5 NOESY vs. ROESY

The comparable responses in the NOESY and ROESY experiment obviously beg the question of which experiment is preferable? Dipolar relaxation processes are dependent on molecular motion (tumbling), as defined by the reorientational correlation time,  $\tau_c$ . Very small molecules will generally afford quite usable NOESY spectra as they tumble quite rapidly in solution. Larger “small” molecules will generally reorient in solution more slowly; dipolar relaxation processes are consequently less efficient. Correspondingly, the size of the NOE response diminishes, making them more difficult to observe. Eventually, when molecules are large enough, they are tumbling slowly enough that the sign of the NOE is reversed and they begin again to exhibit progressively larger but negative NOEs. As a general guideline, when the molecular weight is approximately the same as the spectrometer observation frequency, NOEs will generally be weaker and more difficult to observed. In the intermediate condition, ROESY experiments, which rely on a spin-lock rather than being dependent on molecular tumbling, will still give reliable data. Fundamentally, there is no reason why ROESY experiments cannot be performed on very small molecules as well. The choice becomes one of preference and perhaps the prior experience of the spectroscopist doing the work.

### 8.3.2.6 Other Homonuclear Autocorrelation Experiments

In addition to the homonuclear autocorrelated experiments just described, there are numerous additional autocorrelated experiments, the description of which is beyond the scope of this chapter. What follows is a brief, non-exhaustive listing of some of these experiments that will provide the interested reader with some entry points into the literature.

Previous sections have exploited the scalar coupling,  $J$ , and dipolar relaxation mechanisms for purposes of autocorrelation. It is certainly possible, however, to correlate resonances via other fundamental processes. Some examples include exchange processes. As a group, these experiments are sometimes collectively referred to as EXSY (EXchange SpectroscopY) experiments [54–59].

Resonances can also be correlated via multiple quantum frequencies. One seminal example is found in the work of Müller [83] in which heteronuclear multiple

quantum coherence was used for heteronuclear shift correlation. We will discuss this further in the sections on heteronuclear shift correlation experiments later in this chapter. For homonuclear correlation of resonances via multiple quantum coherence, Freeman and co-workers pioneered the development of the  $^{13}\text{C}$ – $^{13}\text{C}$  INADEQUATE experiment [68, 69]. Remarkably, the INADEQUATE experiment allows an investigator to trace out the carbon skeleton of a molecule using adjacent  $^{13}\text{C}$ – $^{13}\text{C}$  resonant pairs at natural abundance. Unfortunately the statistical probability of such molecules in a sample is about 1 molecule in 10,000 at the natural abundance of  $^{13}\text{C}$  which is ~1.1%. Thus,  $^{13}\text{C}$ – $^{13}\text{C}$  INADEQUATE requires very large samples, frequently making the experiment inappropriate for natural product structure elucidation when sample sizes are limited.

Applying the idea of using multiple quantum coherence to correlate protons has also been explored. Mareci and Freeman [60] reported the first experimental demonstration of proton double quantum correlated spectroscopy. The  $F_2$  axis in these experiments is used to present  $^1\text{H}$  chemical shift in the usual fashion. In contrast, the  $F_1$  axis is used for the double quantum frequency axis. Protons correlated to one another via double quantum coherence will exhibit a response in  $F_1$  at the algebraic sum of the offsets of the coupled resonances relative to the transmitter frequency. A scant few applications have been reported including an exploratory study of strychnine (2) [61] and the structural characterization of the marine natural product plumericin [62].

Correlation in the second frequency domain using zero quantum coherence has also been described by Müller [63] and in work by Hall and co-workers [84–87]. Unlike higher quantum coherence experiments, zero quantum spectroscopy is insensitive to magnetic field inhomogeneities. Responses in the second frequency domain are observed at the zero quantum frequency, which is the algebraic difference of the coupled resonances relative to the transmitter. Again, only a scant few examples appear in the literature, including an exploratory study of strychnine (2) [64] and the characterization of several marine natural products [65]. One area of potential utility for zero quantum correlated spectroscopy is in the characterization of molecules with heavily congested proton spectra, for example polynuclear aromatics [66, 67] although this area has yet to receive much attention from investigators.

### 8.3.3

#### Gradient Homonuclear 2D NMR Experiments

Traditionally, coherence transfer pathway selection has been accomplished by phase cycling routines. The desired components of magnetization are successively added to the memory storage location while undesired components are alternately added and then subtracted on subsequent scans such that at the end of the phase cycle they are ideally eliminated [88, 89]. The two most common phase cycling prescriptions are probably the CYCLOPS [90] and EXORCYCLE [91] routines. As an alternative to phase cycling, coherence transfer pathways can also be selected through the use of pulsed field gradients (PFGs) [92–94]. The gradient-selection procedure allows the selected coherence to remain in phase and the signal for it

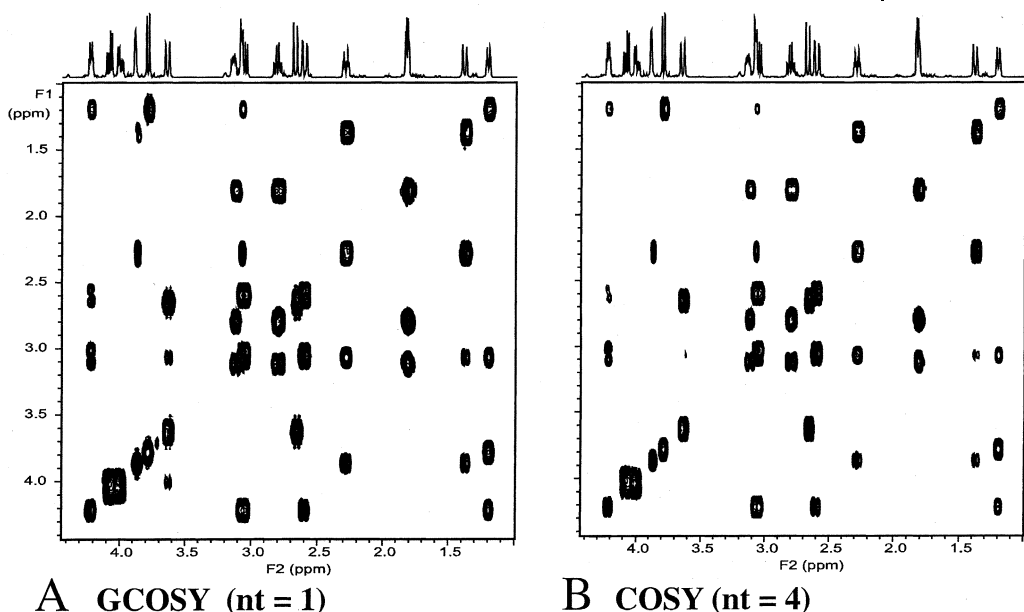


**Fig. 8.18** Comparative presentation of the GCOSY (A) and COSY (B) spectra of the aliphatic region of strychnine (2). The spectra differ only in that the former data were acquired

by accumulating a single transient/ $t_1$  increment while the latter required the acquisition of 4 transients/ $t_1$  increment to satisfy phase cycling requirements.

to thus be acquired while unwanted coherences are dephased and not detected. Essentially no, or minimal, phase cycling is required to generate largely artifact-free spectra. The spectral quality of gradient-selected experiments is not, however, without penalty. Since only one coherence transfer pathway is selected, other comparable pathways are not selected and thus do not contribute to the detected signal, resulting in a sensitivity loss when compared to phase cycle-based experiments [95]. This shortcoming of using gradients can be partially circumvented by using PEP (preservation of equivalent pathways) methods as suggested in the work of Cavanaugh and co-workers [96–98]. When not severely sample limited [99, 100], the use of gradient NMR experiments is strongly recommended.

Gradient homonuclear 2D NMR experiments give results (albeit with the exception of noise) that are indistinguishable from phase-cycled experiments. Experiments such as GCOSY [101, 102] can be performed by accumulating a single transient per  $t_1$  increment when not sample limited rather than using the obligatory four-step phase cycle of the conventional COSY experiment. A comparison of the COSY and GCOSY spectra of the aliphatic region of strychnine (2) recorded by accumulating 4 and 1 transient per  $t_1$  increment, respectively, are shown in Fig. 8.18. GTOCSY [102–104], GNOESY (also known as GOESY) [102, 105], and GROESY [102–104] experiments can be performed with similar minimal phase cycling and corresponding time savings and reduced artifact response intensity. Gradient heteronuclear and gradient selective 1D NMR experiments are discussed below.

### 8.3.4

#### Heteronuclear Shift Correlation

The development of heteronuclear 2D shift correlated spectroscopy began, indirectly, with the idea of “walking” the decoupler through the  $^1\text{H}$  spectrum with the decoupler operating to collapse a single frequency while acquiring  $^{13}\text{C}$  spectra. As successive experiments are recorded, each with the decoupler repositioned, resonances will begin to collapse from multiplets, will appear as a singlet when the decoupler is on resonance, and will then resume multiplet structures as the decoupler moves away again. The SPT (spin population transfer) experiments discussed above represented the next level of sophistication in this development saga. Finally, heteronucleus detected 2D heteronuclear shift correlation experiments evolved through a series of steps that are discussed in chronological detail in the monograph by Martin and Zektzer [16].

Initially, heteronuclear shift correlation experiments exploited the large one-bond ( $^1J_{\text{CH}}$ ) heteronuclear coupling to afford direct correlation spectra. Long-range heteronuclear shift correlation, via  $^nJ_{\text{CH}}$  couplings was proposed but not experimentally realized in the visionary communication of Hallenga and van Binst [106]. It remained for Reynolds and co-workers in 1984 [107] to report the first experimental demonstration of this important experiment. Reynold’s seminal report sparked a flurry of activity to develop new heteronucleus-detected long-range heteronuclear shift correlation experiments which were the topic of a 1986 review by one of the authors [108].

Heteronucleus-detected shift correlation experiments have now been largely supplanted by far more sensitive proton- or “inverse”-detected methods. The heteronucleus-detected experiments are now largely reserved, in laboratories with modern NMR spectrometers, for those occasions when very high digital resolution is needed in the carbon frequency domain because of high spectral congestion [109, 110]. The remainder of this section will focus on the now widely utilized proton-detected heteronuclear shift correlation methods.

### 8.3.5

#### Direct Heteronuclear Chemical Shift Correlation Methods

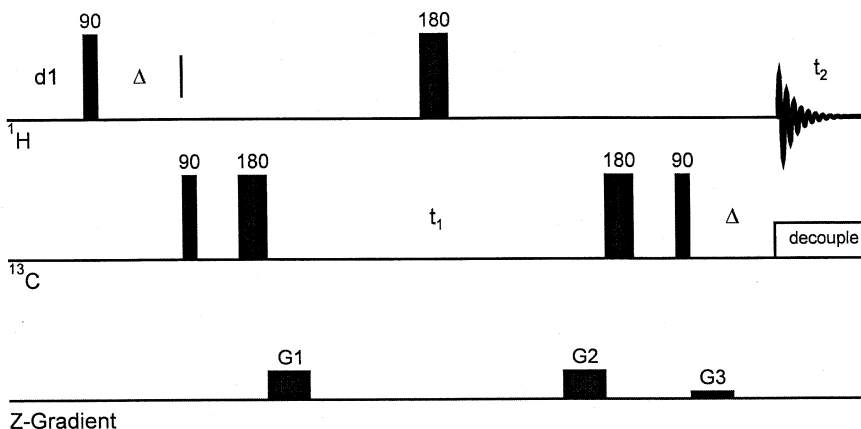
The “direct” heteronuclear shift correlation experiments exploit the one-bond ( $^1J_{\text{CH}}$ ) heteronuclear coupling as the basis of establishing chemical shift correlations. The concept of using multiple quantum coherence was developed by Müller in 1979 [83]; that of using single quantum coherence came out of the work of Bodenhausen and Ruben in 1980 [111].

##### 8.3.5.1 HMQC, Heteronuclear Multiple Quantum Coherence

From the standpoint of experimental complexity, the HMQC experiment for direct correlation purposes is much simpler than the HSQC experiment described below. The HMQC experiment has its origins in the work of Bax, Griffey, and Hawkins in

1983 [112], which was directed at establishing  $^1\text{H}$ – $^{15}\text{N}$  correlations. The version of the experiment that came into common usage was that described by Bax and Subramanian in 1986 [113]. The gradient version of this experiment shown in Fig. 8.19 was reported in 1991 by Hurd and John [114]. In general, the gradient version of the heteronuclear shift correlation experiment will be the preferred method, with the exception of very small samples, when it will be preferable to revert to the non-gradient version of the experiment to avoid signal losses associated with the use of the gradient methods [95, 99, 100]. The topic of gradient heteronuclear shift correlation experiments was the topic of an early benchmark paper by Ruiz-Cabello and co-workers [115] and also of a more recent review by Parella [116]. The interested reader is referred to these excellent reports, to the various monographs cited in Section 8.1, or to the reviews cited in the section dealing with selective 1D experiments below.

Figure 8.19 shows the gradient version of the HMQC experiment since in most cases users will want to opt for the improved performance of the gradient experiment. Following a preparation period, heteronuclear multiple quantum coherence (zero and double) is created by the  $90^\circ$  X-nucleus pulse applied at the initiation of the evolution period,  $t_1$ . Evolution occurs and the  $180^\circ$   $^1\text{H}$  pulse serves to refocus



#### Z-Gradient

**Fig. 8.19** Schematic representation of the gradient heteronuclear multiple quantum coherence or GHMQC pulse sequence. The gradient version of this experiment now in use [114] is derived from the earlier non-gradient experiment described by Bax and Subramanian [113]. Coherence pathway selection is obtained by the application of gradients in a ratio of 2:2:1 as shown. Other ratios are also possible, as considered in the reports of Ruiz-Cabello et al. [115] and Parella [116]. The experiment creates heteronuclear multiple quantum coherence with the  $90^\circ$   $^{13}\text{C}$  pulse that precedes evolution. Both zero and double quantum coherences are created and begin to evolve through the first half

of the evolution period. The  $180^\circ$   $^1\text{H}$  pulse midway through evolution interchanges zero and double quantum coherence terms in addition to “decoupling” proton chemical shift evolution during evolution. Antiphase proton single quantum coherence is recreated by the final  $90^\circ$   $^{13}\text{C}$  pulse which is then allowed to refocus before acquisition and the application of broadband heteronuclear decoupling. The GHMQC experiment is infrequently used in the author’s laboratory relative to the GHSQC experiment which gives substantially better resolution in the second frequency domain [70, 117–119] (see Fig. 8.20–8.22).

proton chemical shift evolution and interchanges zero and double quantum coherence terms. At the end of the evolution period, unobservable heteronuclear multiple quantum coherence is reconverted to observable, antiphase single quantum coherence by the 90° X-nucleus pulse the ends the evolution period. The three coherence pathway selection gradients are nominally applied in a 2:2: $\pm 1$  ratio for  $^1\text{H}$ - $^{13}\text{C}$  heteronuclear shift correlation measurements and in a 5:5: $\pm 1$  for  $^1\text{H}$ - $^{15}\text{N}$  correlation. (Note: other gradient ratios are possible, e.g. 5:3:4 for  $^1\text{H}$ - $^{13}\text{C}$ , etc. See the work of Ruiz-Cabello et al., [115] or that of Parella for a further discussion on this point [116].) At this point, the antiphase proton single quantum coherence is labeled with the chemical shift of the directly bound  $^{13}\text{C}$ . Magnetization is refocused and acquisition and broadband heteronuclear decoupling are initiated simultaneously.

The HMQC/GHMQC experiments are quite useful and were treated in an early review by Martin and Crouch [71]. Relative to the single quantum variant of the experiment discussed below, the effective  $F_1$  resolution of the multiple quantum experiment suffers due to homonuclear coupling modulation during the evolution period, which leads to broadened responses being observed in the  $F_1$  dimension. The difference in the effective resolution of the HMQC vs. HSQC experiments was noted in a review on applications of inverse-detection in alkaloid chemistry by Martin and Crouch [70] and has since been treated in more detail by Reynolds and others [117–119]. On this basis, the HSQC/GHSQC experiments discussed in the following section should be preferentially used on a routine basis in the opinion of the authors.

### 8.3.6

#### **HSQC, Heteronuclear Single Quantum Coherence Chemical Shift Correlation Techniques**

The idea of heteronuclear single quantum coherence experiments derives from the early work of Bodenhausen and Ruben [111]. The contemporary variant of their experiment is shown in Fig. 8.20. The fundamental concept of the experiment, regardless of refinements to augment the performance of the experiment, is unchanged. The experiment utilizes an INEPT step to transfer single quantum magnetization from proton to the heteronuclide immediately prior to the beginning of the evolution time. During evolution chemical shift labeling for the heteronuclide occurs; proton chemical shift evolution is reversed by the 180°  $^1\text{H}$  pulse applied midway through the evolution period. Following evolution, magnetization is transferred back to the protons and refocused to allow data acquisition with broadband decoupling.

The gradient or GHSQC version of the experiment applies a pair of gradients rather than the three gradients used in the GHMQC experiment (see Fig. 8.19). Gradients are applied in the ratio of 4:1 for  $^1\text{H}$ - $^{13}\text{C}$  heteronuclear correlation. The first gradient, G1, is applied during the evolution period while the second gradient, G2, is applied during the final refocusing delay following the 180° pulse sandwich just prior to acquisition. More sophisticated variants of the experiment

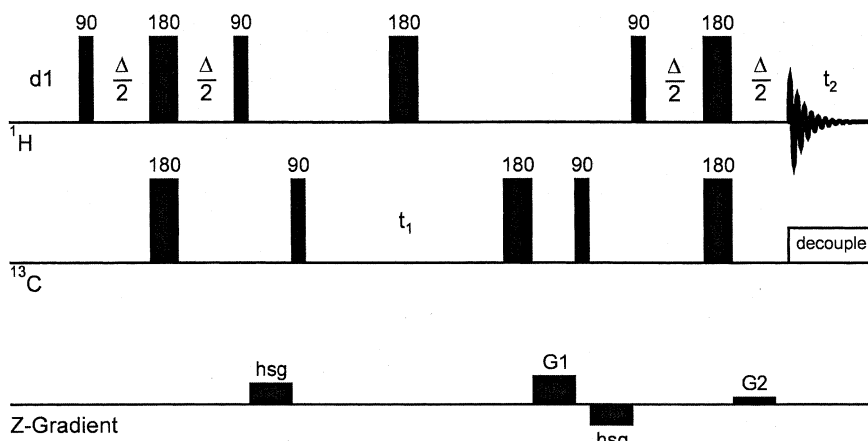


**Fig. 8.20** Schematic representation of the gradient heteronuclear single quantum coherence or GHSQC pulse sequence. The non-gradient version of this experiment was described originally by Bodenhausen and Ruben [111]. Heteronuclear single quantum coherence is created by the first INEPT segment of the experiment which evolves during the evolution period,  $t_1$ . The reverse INEPT step following evolution converts the heteronuclear single quantum coherence to proton single quantum coherence which is then detected. The gradient version of the experiment currently in use in the author's

laboratory is shown. While phase-sensitive, the experiment offers only about half the sensitivity of the non-gradient variant since only one of the two equivalent coherence pathways is selected by the simple gradient version of the experiment [95]. More complex variants of the experiment developed by Cavanaugh and co-workers [96–98] utilize a technique known as preservation of equivalent pathways or PEP to recover both coherence pathways giving a  $\sqrt{2}$  improvement in signal-to-noise for methine resonances.

use a process known as PEP or preservation of equivalent pathways [96–98] to record high sensitivity, phase-sensitive 2D HSQC spectra. The PEP variant of the experiment employs a second reverse INEPT “block” to reclaim both orthogonal components of magnetization thereby giving a  $\sqrt{2}$  improvement in signal-to-noise. The phase of one of the  $90^\circ$  X pulses and that of the G2 gradient are inverted on alternate scans and the data are stored separately to provide a phase-sensitive final result.

The phase-sensitive GHSQC spectrum of strychnine is shown in Fig. 8.21A.

### 8.3.6.1 Multiplicity-edited Heteronuclear Shift Correlation Experiments

Heteronuclear chemical shift correlation methods establish the direct link between protons and the respective, directly attached carbons (or nitrogens). In the case of methylenes with inequivalent (anisochronous) protons, the “multiplicity” of the carbon in question is irrefutably obvious. For isotropic methylenes and other resonances, the multiplicity of the resonance ( $\text{CH}$ ,  $\text{CH}_2$  or  $\text{CH}_3$ ) in question may be less obvious. Early work by Kessler and co-workers addressed this issue via the development of the DEPT-HMQC experiment. [120] Multiplicity editing is also available for experiments such as GHSQC. An extra pair of delays and pulses, with the flip angle of the proton pulse being adjustable, allow the acquisition of data in

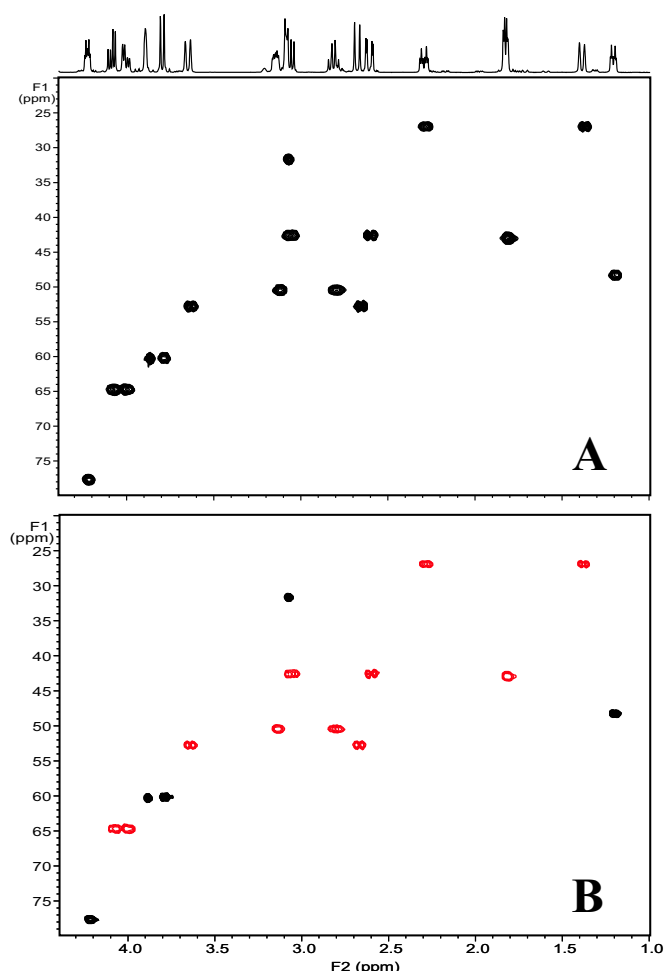


**Fig. 8.21** A. GHSQC spectrum of the aliphatic region of the strychnine (2) spectrum recorded using the pulse sequence shown in B. multiplicity-edited GHSQC [120–123] spectrum of strychnine showing methylene resonances in red and opposite in phase from

methine and methyl resonances that are shown in black (no methyls are in the strychnine structure). These data were acquired using the pulse sequence shown in Fig. 8.22 with the multiplicity editing step following the reverse-INEPT portion of the experiment.

which the response phase is indicative of resonance multiplicity [121–123]. The multiplicity-edited GHSQC sequence presently in use in the author's laboratory is shown in Fig. 8.22; the framed segment of the pulse sequence provides the multiplicity editing. Adjusting the flip angle  $\alpha$  of the proton pulse to  $180^\circ$  affords a spectrum in which the phase of the methine/methyl resonances is opposite to that of the methylenes. By setting the "adjustable" pulse to  $\alpha = 90^\circ$  a spectrum con-

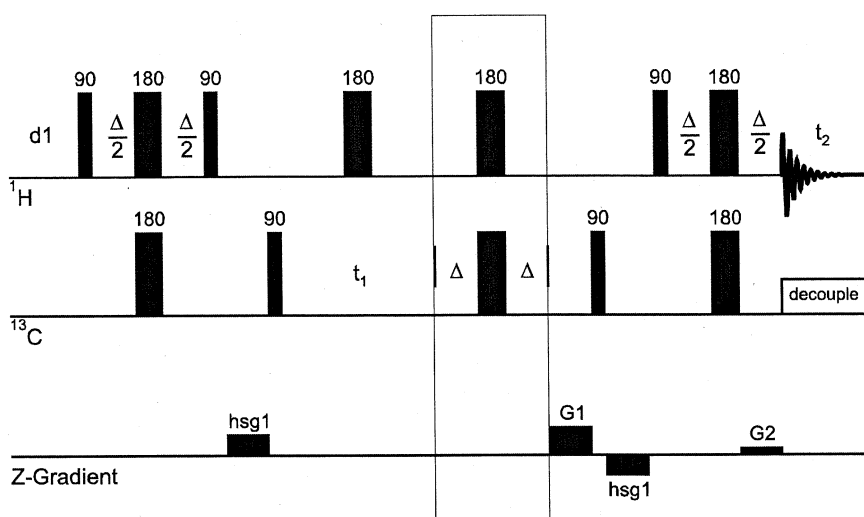


**Fig. 8.22** Schematic representation of the multiplicity edited GHSQC pulse sequence in use in the author's laboratory with the multi-

plicity editing step following the evolution period [120–123].

taining only methine resonances is obtained. The multiplicity edited GHSQC spectrum of the aliphatic region of the spectrum of strychnine (2) is shown in Fig. 8.21B; responses plotted in red denote inverted methylene resonances while black responses denote positive methine resonances (there are no methyl groups in strychnine).

#### 8.3.6.2 Accordion-optimized Direct Heteronuclear Shift Correlation Experiments

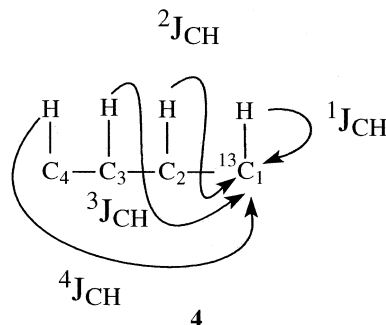
Following the development of accordion-optimized long-range heteronuclear shift correlation experiments (see Section 8.3.7.3 below), Hadden and Angwin [124] have recently reported the development of an accordion-optimized direct correlation experiment, ADSQC. Additionally, Zangerer and Armitage also reported the accordion-HMQC experiment [125]. These experiments provide a convenient means of circumventing the choice of optimization in the direct correlation experiments. Under most circumstances a one-bond correlation experiment is not problematic; survey optimization of the one-bond delays for ~140 Hz provides quite reliable results. However, molecules containing some heterocyclic moieties, e.g. furans and other species having proton–carbon pairs with exceptionally large one-bond coupling constants may fail to give direct correlation responses under standard survey conditions. As an example, the 2-position of furan has a 208 Hz  $^1J_{CH}$  coupling that reproducibly fails to give a direct correlation response under standard survey conditions. By optimizing the ADSQC or accordion-HMQC over a range of one-bond couplings, e.g. 120–210 Hz, this problem can be avoided.

## 8.3.7

**Long-range Heteronuclear Chemical Shift Correlation**

Successful exploitation of the use of one-bond ( $^1J_{\text{CH}}$ ) heteronuclear coupling constants in the development of direct heteronuclear shift correlation experiments in the late 1970s prompted the visionary suggestion of Hallenga and van Binst [106] in 1980 of doing the same experiment using instead the long-range heteronuclear coupling,  $^nJ_{\text{CH}}$ . Unfortunately, the long-range heteronuclear chemical shift correlation experiment was not realized in their seminal work. Rather, it remained for Reynolds and co-workers [107] in 1984 to demonstrate experimentally the viability of long-range heteronuclear chemical shift correlation experiments.

Reynolds' initial report sparked the development of numerous long-range heteronuclear shift correlation experiments that continued through about 1986. Experiments developed included the constant time COLOC experiment [126, 127], experiments designed to decouple one-bond modulation effects [128, 129], and the XCORFE experiment of Reynolds and co-workers [130] that allowed the differentiation of  $^2J_{\text{CH}}$  from  $^3J_{\text{CH}}$  long-range couplings to protonated carbon resonances (see 4). The heteronucleus-detected long-range shift correlation experiments are the topic of a 1986 review by Martin and Zektzer [108].



Bax and Summers 1986 report of the proton-detected HMBC experiment [131] essentially ushered to a close the development of new, heteronuclide-detected long-range chemical shift correlation experiments. Aside from the development of a gradient-enhanced GHMBC experiment [132, 133] there was a nearly decade-long hiatus in the development of new, inverse-detected, long-range heteronuclear shift correlation methods. More recently, the reported development of new proton-detected long-range experiments has resumed and is treated briefly in the following sections of this chapter.

The increase in sensitivity afforded by the proton-detected HMBC experiment revolutionized structure elucidation studies. The utilization of HMBC data in the characterization of alkaloid structures has been reviewed [70] and is also treated in a more general review of the application of inverse-detected methods in natural products structure elucidation [71]. Other applications of the experiment are quite

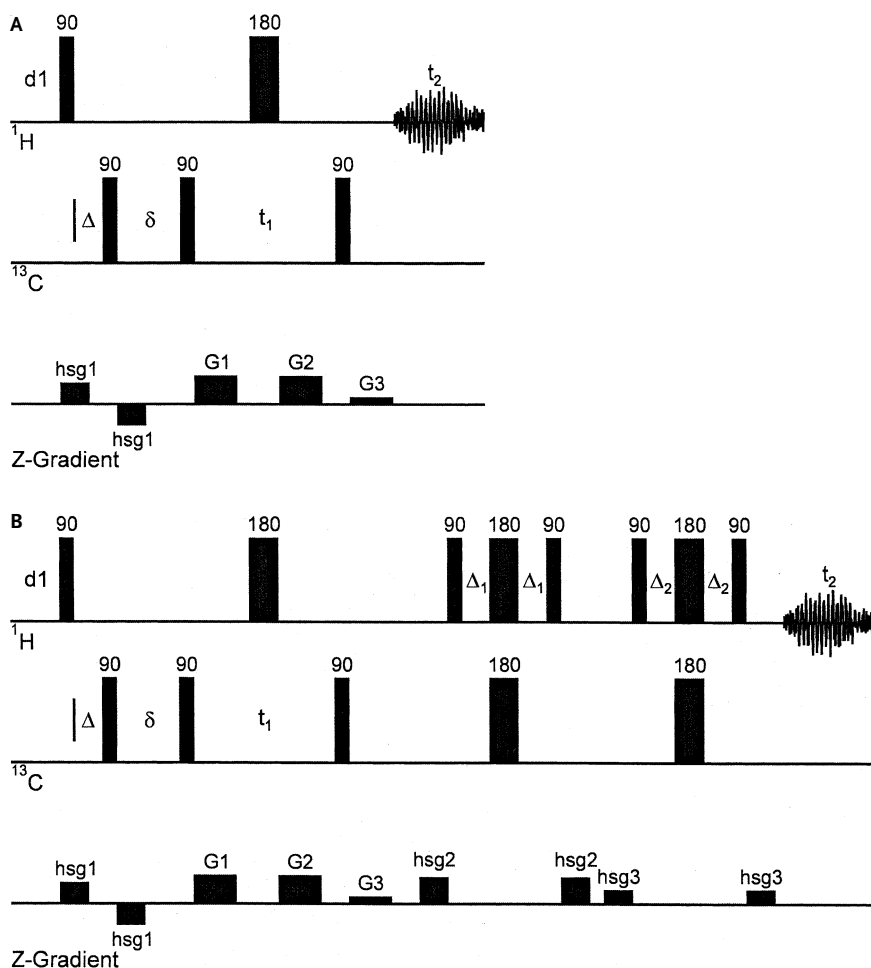


**Fig. 8.23** A. Schematic representation of the original HMBC experiment of Bax and Summers [131]. The experiment begins with a low-pass *J*-filter. The phase of the first 90° <sup>13</sup>C pulse is alternated 0202 while the receiver phase is cycled as 0022. In this fashion, the magnetization arising from the direct correlation responses is alternately added and subtracted in memory and ultimately canceled. Much like the HMQC experiment, HMBC creates zero and double quantum coherences but does so for the long-range couplings rather than the direct couplings. Given that long-range couplings are typically in the range of about 6 to 10 Hz, delays

in the range from 83 to 50 s, respectively, are typical. The HMBC experiment has been largely replaced by the gradient or GHMBC experiment [126, 127] in many NMR laboratories. B. The version of the GHMBC experiment currently in use in the author's laboratories is shown here and employs a double pulsed field gradient spin echo (DPFGSE) [136] to suppress the residual, unwanted direct correlation responses. For very weak samples, recent work has shown that it is actually preferable to utilize the non-gradient phase cycled version of the HMBC experiment rather than the newer gradient versions of the experiment [100].

numerous and any complete survey is beyond the scope of this chapter. It should also be noted here that within the past five years it has become feasible to perform long-range  $^1\text{H}$ – $^{15}\text{N}$  heteronuclear shift correlation experiments at natural abundance, which is the subject of a recent review by two of the authors [72].

### 8.3.7.1 HMBC, Heteronuclear Multiple Bond Correlation

The original pulse sequence for the HMBC experiment, as reported in 1986 by Bax and Summers [131] is shown in Fig. 8.23A. The sequence begins with a pulse sequence operator known as a low-pass  $J$ -filter. Alternatively, dual stage gradient low-pass  $J$ -filters [134, 145] or double pulsed field gradient spin echoes (DPGSEs) [136] can be substituted for the low-pass  $J$ -filter and afford substantially better suppression of residual direct response signals. This component of the experiment is designed to remove unwanted direct correlation responses. While the  $90^\circ$  X-pulse in the low pass  $J$ -filter is phase cycled as 0022, the receiver phase is cycled 0202, which effectively adds and subtracts the unwanted direct response component of magnetization. The first delay,  $\Delta$ , is optimized as a function of  $\frac{1}{2}(^1J_{\text{CH}})$ . The second  $90^\circ$  X-pulse, which is applied after a delay,  $\delta$ , of  $\frac{1}{2}(^nJ_{\text{CH}})$ , where  $n = 2$  or 3 and corresponds to an optimization in the range of 6–10 Hz, creates heteronuclear zero and double quantum coherence that begins to evolve through the evolution period,  $t_1$ . The  $180^\circ$   $^1\text{H}$  pulse interchanges zero and double quantum coherence terms and simultaneously removes proton chemical shift evolution. The last  $90^\circ$  X-pulse pulse converts the heteronuclear multiple quantum coherences back into observable single quantum coherence, which is then detected. Gradient versions of the experiment were developed in the early 1990s by Willker and co-workers [132] and by Rinaldi and Keifer [133] and are now generally used *in lieu* of the original, non-gradient version of the experiment (see Fig. 8.23B).

The aliphatic region of the 6 Hz optimized GHMBC spectrum of strychnine is shown in Fig. 8.24A. In the specific case of the H-12 resonance of strychnine, only a single long-range correlation of the several possible long-range couplings (shown in 5) is observed in the spectrum. We will use the H12 correlations as a performance comparison for several of the more recently developed, accordion-optimized long-range experiments described below. Correlations which predominate in

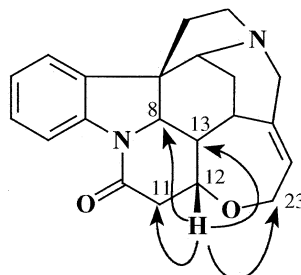
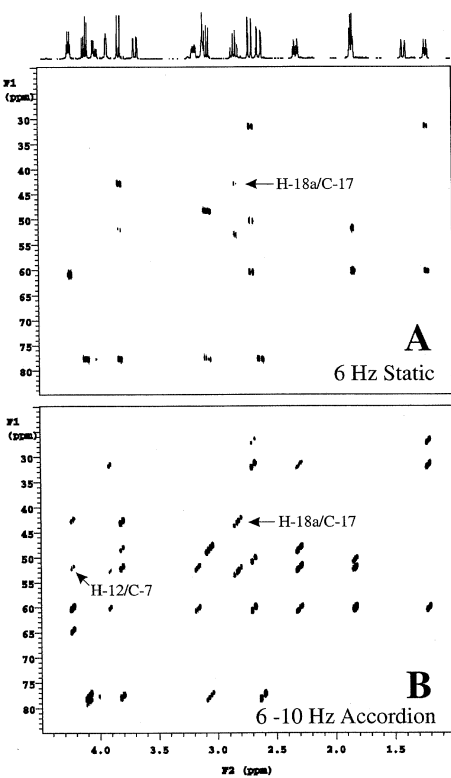


**Fig. 8.24** A. GHMBC experiment recorded using the gradient variant of the pulse sequence shown in Fig. 8.23A. The spectrum shown is the aliphatic region of the strychnine (**2**) spectrum; the long-range delays in the GHMBC sequence delays in the experiment were optimized for 6 Hz. Note that for the H12 resonance (furthest downfield at 4.27 ppm) only one response is observed in the data shown, which correlates H12 to C8. Care must be exercised when interpreting weak responses in HMBC/GHMBC experiment such as that denoted with the arrow that correlates the H18a resonance via two bonds to C17. B.) Data from a 6–10 Hz optimized ACCORD-HMBC (see Fig. 8.25) experiment [144, 145] for the same region of the strychnine (**2**) spectrum. The ability to sample a broad range of potential long-range couplings in a single experiment is well demonstrated by these data. When compared to the GHMBC spectrum shown in Fig. 8.24A, the H12 resonance, for instance, shows four correlation responses. While the H18a–C17 correlation response was weak in the GHMBC data, it is now quite strong. Furthermore, the characteristic  $F_1$  “skew” of the ACCORD-HMBC data provides a convenient means of response authentication: legitimate long-range correlations will be skewed, making them readily distinguishable from weak noise peaks.  
(Reproduced with permission – Wiley-VCH).



HMBC/GHMBC spectra are  $^2J_{\text{CH}}$  and  $^3J_{\text{CH}}$  with  $^4J_{\text{CH}}$  long-range correlations observed only occasionally. In the specific case of strychnine, four  $^4J_{\text{CH}}$  couplings are typically observed in the 10 Hz optimized GHMBC spectrum.

Structure elucidation strategies that employ long-range heteronuclear shift correlation experiments generally use the correlations observed to position quaternary atoms relative to protonated carbon fragments, e.g. in the case of a correlation from H-12 to the C-8 quaternary carbon, or to bridge heteroatoms, e.g. the correlation from H-12 to C-23 across the oxepin ether linkage, as shown above.

### 8.3.7.2 Variants of the Basic HMBC Experiment

Beginning in 1995, a number of reports of variants of the HMBC/GHMBC experiment began to appear. The inclusion of a refocusing delay to allow broadband decoupling during acquisition was described by Bermel, Wagner and Griesinger [137]; Furihata and Seto subsequently described this experiment giving it the acronym D-HMBC experiment [138], apparently unaware of the prior work by Bermel,

Wagner and Griesinger. A report of a pseudo-3D variant followed, each plane of the third dimension having a different long-range optimization [139]. Projection of the  $F_2/F_3$  plane gave, albeit rather inefficiently, the equivalent of an accordion-optimized spectrum. Marek and co-workers [140] described a phase-sensitive single quantum long-range experiment, GSQMBc, that allowed in the case of some multiplets, the measurement of long-range heteronuclear couplings. Another phase-sensitive method was reported in 1998 by Sheng and van Halbeek [141] for the purpose of extracting long-range heteronuclear couplings. Later in 1998, Furihata and Seto [142] described several constant time variants of the basic HMBC experiment in an effort to suppress homonuclear coupling modulations that arise during the incrementation of the evolution time,  $t_1$ . These experiments set the stage for the subsequent development of accordion-optimized long-range experiments.

### 8.3.7.3 Accordion-optimized Long-range Heteronuclear Shift Correlation Methods.

The idea of accordion-optimization is by no means new [143]. The idea of applying this method to the optimization of the long-range delay of HMBC-type experiments, however, was only reported in 1998 by Wagner and Berger [144] in their description of the ACCORD-HMBC experiment. The ACCORD-HMBC pulse

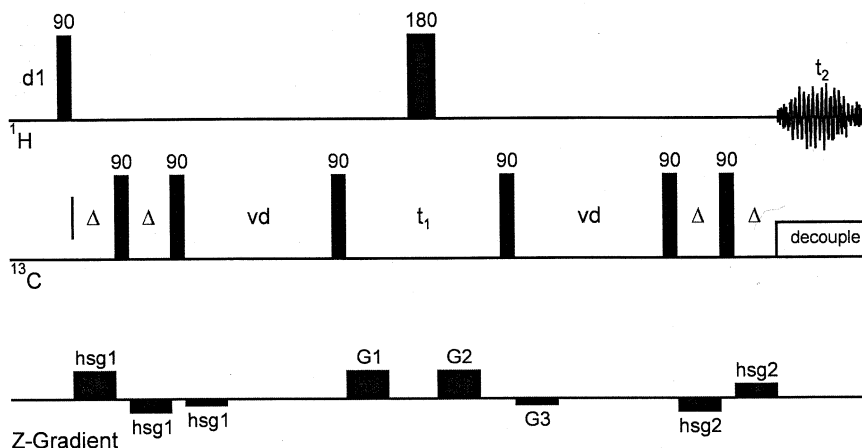


**Fig. 8.25** Pulse sequence schematic for the ACCORD-HMBC experiment pioneered by Wagner and Berger [144]. The experiment begins with a gradient dual-stage low-pass  $J$ -filter to suppress unwanted direct correlation responses. A variable duration delay,  $Vd$ , follows, the duration of which is decremented from  $1/2''J_{\min}$  to  $1/2''J_{\max}$  ( $\tau_{\max}$  and  $\tau_{\min}$ , respectively) in successive increments of the evolution time,  $t_1$ . In this fashion, all possible long-range couplings in the user-selected range are sampled in a single experiment. The  $90^\circ$   $^{13}\text{C}$  pulse following the variable delay functions in the usual fashion

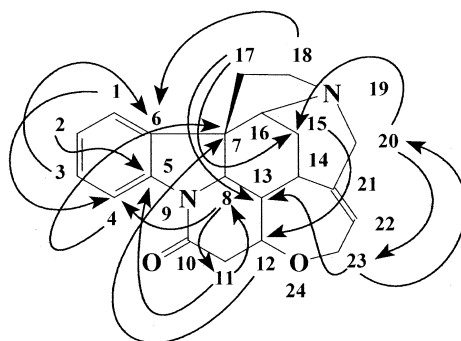
to create heteronuclear zero and double quantum coherences which are manipulated as in the HMBC/GHMBC experiment (see Fig. 8.23). To allow broadband heteronuclear decoupling during acquisition, Wagner and Berger originally proposed a symmetric experiment so that all long-range couplings are refocused immediately prior to acquisition. In practice, we have found that it is actually desirable to initiate acquisition following the final coherence pathway selection gradient to avoid potential signal losses due to the long, variable delay.

sequence is shown in Fig. 8.25. Quite simply, the ACCORD-HMBC experiment is governed by the limits  $\frac{1}{2}^n J_{\min}$  to  $\frac{1}{2}^n J_{\max}$ , which correspond to  $\tau_{\max}$  to  $\tau_{\min}$ , respectively. As the evolution time,  $t_1$ , is systematically incremented, the duration of the variable delay,  $Vd$ , is decremented from  $\tau_{\max}$  to  $\tau_{\min}$  in increments of  $(\tau_{\max} - \tau_{\min})/n_i$ , where  $n_i$  is the number of increments of the evolution period. In this fashion, the ACCORD-HMBC experiment essentially integrates across a range of potential long-range couplings, allowing the complete range to be sampled in a single experiment.

A drawback of accordion-optimization of the long-range delay in the ACCORD-HMBC experiment is  $F_1$  “skew” caused by homonuclear coupling modulation occurring during the variable delay, which serves as a pseudo-evolution period for these processes [145]. Conversely,  $F_1$  skew also serves as a determinant of response authenticity for weak long-range responses since noise or other random signals cannot exhibit  $F_1$  skew.

Comparison of the performance of a statically-optimized GHMBC (i.e. optimized for a single value of the long-range delay) experiment with ACCORD-HMBC is shown by comparing the spectral segments shown in Fig. 8.24. The 6 Hz optimized GHMBC results are shown in Fig. 8.24A. A single correlation from the H12 resonance is observed in this data. In contrast, for the 6–10 Hz optimized ACCORD-HMBC spectrum presented in Fig. 8.24B, four correlations, those shown by 5, are observed from the H12 resonance. In addition, some correlations, such as the H18a–C17 correlation, which is observed with weak response intensity in the 6 Hz optimized GHMBC spectrum, are observed with much better response intensity in the accordion-optimized experiment.

An ACCORD-HMBC spectrum of the aliphatic region of strychnine optimized over the range 2–25 Hz is shown in Fig. 8.26. It is interesting to note that while only four  $^4J_{\text{CH}}$  long-range couplings are observed in the 10 Hz GHMBC spectrum of strychnine, 17 such couplings are observable in this very aggressively optimized ACCORD-HMBC spectrum, as shown in **6** [145].



## 6

Homonuclear coupling modulation during the variable delay in the ACCORD-HMBC experiment prompted the development of a constant time variable delay

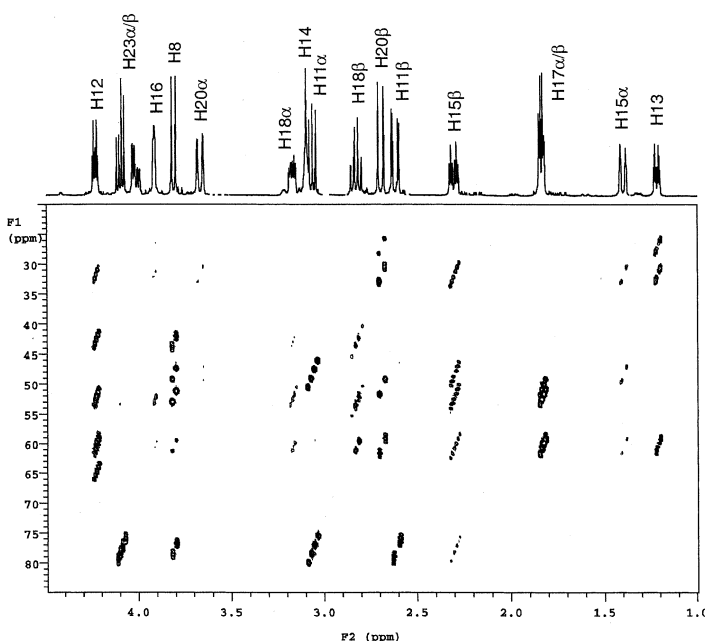


**Fig. 8.26** Results of an aggressively optimized 2–25 Hz ACCORD-HMBC experiment performed on strychnine (**2**) are presented here. Such data might be used when it becomes necessary to resort to relatively uncommon four-bond ( $^4J_{\text{CH}}$ ) long-range couplings to solve a structural problem. In the 10 Hz optimized

GHMBC spectrum of strychnine (**2**) a total of four four-bond long-range couplings are observed. In contrast, the 2–25 Hz ACCORD-HMBC experimental data shown identified 17 four-bond long-range couplings as shown by **6**. (Reproduced with permission – Wiley-VCH).

to replace the simple variable delay in the ACCORD-HMBC experiment. This pulse sequence element was incorporated into the IMPEACH-MBC experiment [146]. The constant time variable delay segregates the manipulation of homo- and heteronuclear components of magnetization. First, by keeping the overall duration of this pulse sequence operator constant, homonuclear coupling modulation can be made to occur in constant time, thereby rendering the effect of this modulation unobservable. This then requires a modification of the delay to maintain its variable character for long-range heteronuclear couplings. This task is accomplished by adding a second variable delay,  $D$ , within the overall constant time variable delay which contains the following element:

$$D/2 - 180^\circ {^{13}\text{C}} - D/2 - \text{Vd} \quad (6)$$

$| \leftarrow "J_{\text{CH}} \text{ refocused} \rightarrow | \leftarrow "J_{\text{CH}} \text{ evolves} \rightarrow |$ .

The variable delay,  $D$ , is halved about a  $180^\circ {^{13}\text{C}}$  pulse which serves to refocus  $^nJ_{\text{CH}}$  components of magnetization at  $D$ . These same components of magnetization then experience a variable delay,  $\text{Vd}$ , during which they are sampled. The accordion

range is determined as in the ACCORD-HMBC experiment. However, as the duration of Vd is decremented from  $\tau_{\max}$  by  $(\tau_{\max} - \tau_{\min})/n_i$ , rather than allowing the overall duration of the delay to be decremented, the interval  $[(\tau_{\max} - \tau_{\min})/n_i]/2$  is instead added to each of the  $D/2$  intervals keeping the total duration constant. Thus, while homonuclear coupling processes evolve in a constant time,  $^nJ_{\text{CH}}$  components of magnetization are refocused at  $D$  and evolve only during the variable delay, Vd, thereby eliminating  $F_1$  skew with the exception of that which arises due to the incrementation of the evolution period,  $t_1$ , which is identical to what one observes in the HMBC/GHMBC experiments.

While uncontrolled  $F_1$  response skew of the type encountered in the ACCORD-HMBC experiment is undesirable [145], user-defined  $F_1$  skew can be a useful determinant of response authenticity. A further generation accordion-optimized long-range experiment, CIGAR-HMBC, was developed to provide this flexibility. The constant time variable delay from the IMPEACH-MBC experiment was further modified as follows:

$$(D/2 + \Delta/2) - 180^\circ {}^{13}\text{C} - (D/2 + \Delta/2) - \text{Vd} \quad (7)$$

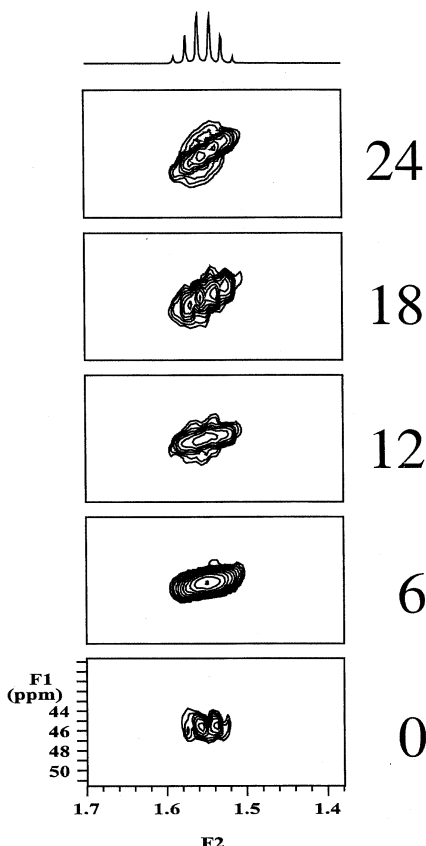


**Fig. 8.27**  $F_1$  skew inherent to responses in ACCORD-HMBC spectra is only partially user controllable. These properties prompted the development of the IMPEACH-MBC experiment [146], which suppresses  $F_1$  skew. Further modification to re-introduce user-controlled  $F_1$  skew was incorporated into the CIGAR-HMBC experiment using a parameter called  $J_{\text{scale}}$  [147]. The effect of adjusting the  $J_{\text{scale}}$  parameter in the CIGAR-HMBC experiment is shown for the 3-methylene group of 2-pentanone over a range of  $J_{\text{scale}}$  settings from 0 to 24.

The range of optimization is defined as in the previous experiments;  $V_d$  is decremented and  $D$  is incremented as in the IMPEACH-MBC experiment [146]. The interval  $\Delta_2$  is used to provide user-defined  $F_1$  skew. The CIGAR-HMBC experiment uses a new parameter  $J_{scale}$  to control the extent of  $F_1$  skew introduced [147]. The duration of  $\Delta_2$  is incremented by the interval  $(J_{scale} - 1) * t_1$ . There are three possible conditions:  $J_{scale} = 0, 1, >1$ . When  $J_{scale} = 0$ , the interval  $\Delta_2$  will actually be decremented as the evolution time,  $t_1$  is incremented, keeping the total duration of the experiment completely constant. This results in the suppression of homonuclear coupling modulation occurring during the incremented evolution period and gives the highest possible  $F_1$  resolution as in the CT-HMBC experiment described by Furihata and Seto [142]. When  $J_{scale} = 1$ , results identical to an IMPEACH-MBC experiment are obtained. Finally, and most interestingly, when  $J_{scale} > 1$ , the overall duration of the modified constant time variable delay becomes “non-constant” in a user-defined manner. Incrementation of the  $\Delta_2/2$  intervals in the experiment reintroduces  $F_1$  skew to a user-determined extent. The degree of  $F_1$  skew is determined by the setting of the parameter  $J_{scale}$  as illustrated in Fig. 8.27.

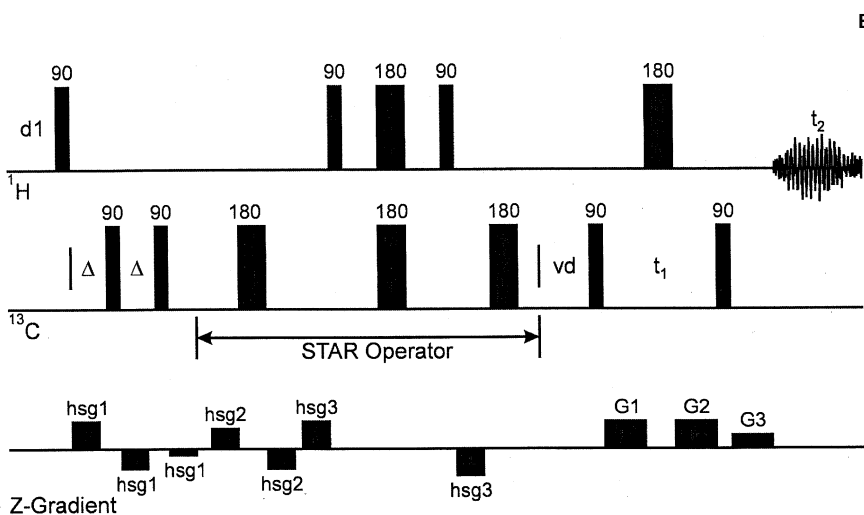
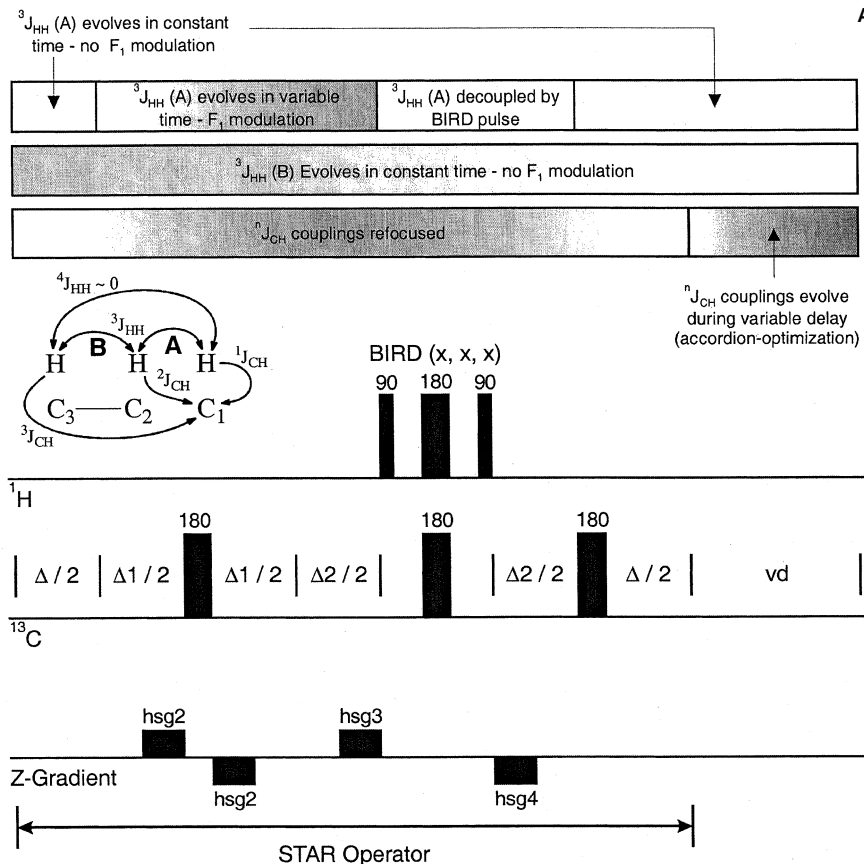
#### 8.3.7.4 $^2J, ^3J$ -HMBC

The most sophisticated accordion-optimized long-range shift correlation experiment to be developed to date is the  $^2J, ^3J$ -HMBC experiment [148]. For the first time in an inverse-detected experiment, it is possible to differentiate two-bond from three-bond long-range correlations to protonated carbon or nitrogen resonances. This capability was last available for protonated carbons via the heteronucleus-detected XCORFE sequence pioneered by Reynolds and co-workers in 1985 [130].

Selective manipulation of the various components of magnetization to allow the differentiation of two-bond from three-bond long-range correlations is through the application of a new pulse sequence operator given the acronym STAR (selectively tailored accordion  $F_1$  refocusing) shown schematically in Fig. 8.28A while the full  $^2J, ^3J$ -HMBC pulse sequence is shown in Fig. 8.28B. Homonuclear couplings evolve through the  $D$  interval, while heteronuclear couplings are refocused by the  $180^\circ {^{13}C}$  pulse prior to the second  $D/2$  segment. The interval  $\Delta_1$  is incremented from zero

**Fig. 8.28** The  $^2J, ^3J$ -HMBC experiment is the most sophisticated accordion-optimized long-range heteronuclear shift correlation experiment reported to date [148]. The experiment uses a pulse sequence operator known as a STAR (selectively tailored  $F_1$  accordion refocusing) to selectively manipulate two-bond and three-bond long-range correlations to protonated carbon or nitrogen resonances. A. STAR operator used in the  $^2J, ^3J$ -HMBC experiment. The experiment takes advantage of the ability of a BIRD(x,x,x) pulse to refocus the one-bond heteronuclear coupling of a protonated carbon. By doing this, the  $^2J_{CH}$  coupling to this proton

labeled “A” in 7 is effectively decoupled. Within ▶ the STAR operator, the consequence of this event is to cause the  $^2J_{CH}$  long-range coupling to evolve in variable time (see evolution bars above the operator schematic), leading this response to selectively exhibit  $F_1$  skew. B. Incorporation of the STAR operator into the  $^2J, ^3J$ -HMBC pulse sequence. Some of the detail in the expansion of the operator in A. is eliminated for clarity. The schematic representation of the expectation of the results of using the STAR operator in the  $^2J, ^3J$ -HMBC experiment are shown in Fig. 8.29.



by  $J_{\text{scale}} * t_1 J_{\text{scale}} * t_{1\max}$  while conversely, the  $\Delta 2$  delay is decremented from  $J_{\text{scale}} * t_{1\max}$  to zero. Hence, the sum of the  $\Delta 1 + \Delta 2$  intervals is constant. All homonuclear couplings evolve through  $\Delta 1$ ; all long-range heteronuclear couplings are refocused by

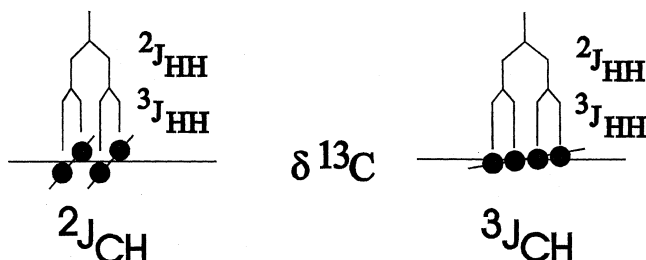


**Fig. 8.29** Schematic representation of expectations for two-bond (left, e.g. the H11 $\alpha$ -C12) and three-bond long-range couplings (right, e.g. the H11 $\alpha$ -C13) long-range couplings in strychnine (2). The staggered  $F_1$  skew is typical

of what would be expected from the function of the STAR operator. Experimental verification of these anticipated results is shown in Fig. 8.30. (Reproduced with permission – Academic Press).

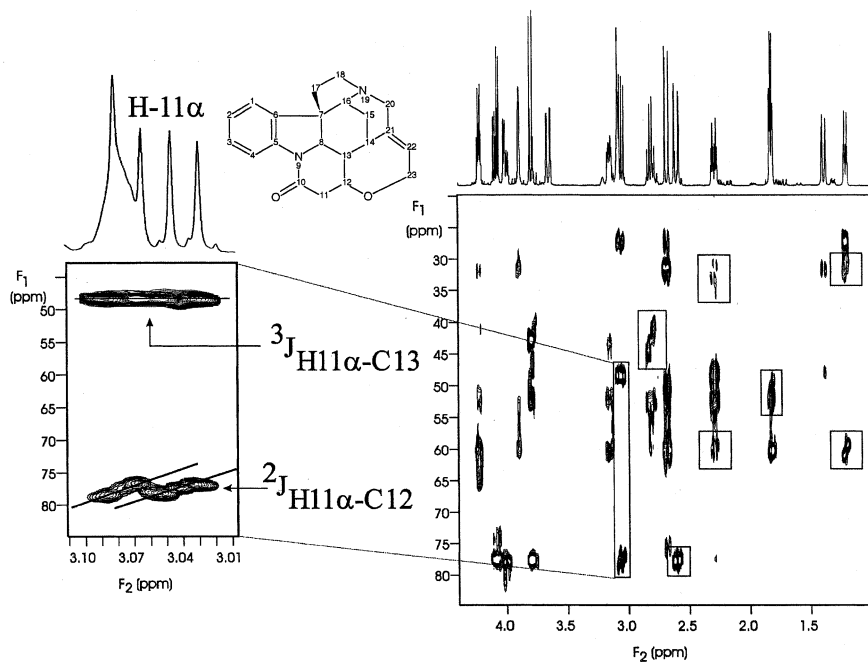
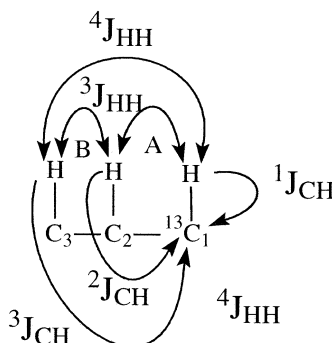


**Fig. 8.30** Results obtained with the  $^2J, ^3J$ -HMBC using strychnine (2) as a model compound [148]. The aliphatic region is shown. The expanded region shows the two- and three-bond correlations from H11 $\alpha$  to C12 and C13. The staggered  $F_1$  skew exhibited for the H11 $\alpha$ -C12 two-bond correlation is consistent with the schematic shown in Fig. 8.29. The experiment

utilizes an accordion-optimization range (6–10 Hz) as in predecessor experiments. The parameter  $J_{\text{scale}}$  is also employed to allow a user-selected degree of  $F_1$  skew to be introduced into the two-bond correlation responses ( $J_{\text{scale}} = 16$ ). (Reproduced with permission – Academic Press).



7

the  $180^\circ$   $^{13}\text{C}$  pulse at  $\Delta 1/2$ . The BIRD pulse located at  $\Delta 2/2$  serves as a  $180^\circ$  pulse for  $^1\text{H}-{}^{13}\text{C}_1$  and as a  $360^\circ$  pulse for other couplings. This results in a selective refocusing of the  $^3J_{\text{HH}}$  coupling between  $\text{H}_2-\text{H}_1{}^{13}\text{C}$ . As a consequence of the incrementation of  $\Delta 1$  and the decrementation of  $\Delta 2$ , the sum of the two intervals serves as a variable delay for this homonuclear coupling, causing the  $^2J_{\text{CH}_2}$  coupling response to be selectively skewed in  $F_1$  while other long-range correlations have the appearance of what would be the corresponding response in the IMPEACH-MBC experiment with  $J_{\text{scale}} = 1$ . The appearance of the long-range couplings from  $\text{H}11\alpha-\text{C}12$  ( $^2J_{\text{CH}}$ ) and from  $\text{H}11\alpha-\text{C}13$  ( $^3J_{\text{CH}}$ ) are shown schematically in Fig. 8.29; experimental results are presented in Fig. 8.30. The “staggered skew” exhibited by the two-bond  $\text{H}11\alpha-\text{C}12$  correlation response is typical of two-bond long-range correlations in the  $^2J, {}^3J$ -HMBC experiment. The setting for the parameter  $J_{\text{scale}}$  as in the predecessor CIGAR-HMBC experiment, [147] allows user control over the degree of staggered  $F_1$  skew of two-bond responses in the experiment.

### 8.3.7.5 Relative Sensitivity of Long-range Heteronuclear Shift Correlation Experiments

Relative to direct correlation experiments, the various long-range correlation experiments now available are all lower in sensitivity. It is generally accepted that the HMBC experiment ranges from 1/4th to 1/8th the sensitivity of a direct correlation experiment. While comparative data are not available for all of the available long-range experiments, all of the accordion-optimized long-range experiments have been directly compared to the HMBC experiment in the recent description of the  $^2J, {}^3J$ -HMBC experiment [148]. It is likely that the other available experiments will range in sensitivity from that of HMBC downward, with the 3D-HMBC experiment of Furihata and Seto [139] likely to have the lowest sensitivity of any of the available experiments.

### 8.3.7.6 Applications of Accordion-optimized Long-range Heteronuclear Shift Correlation Experiments

To date, aside from the papers reporting the development of the accordion-optimized long-range experiments there have only been two reported applications, although more will doubtless follow. Two of the authors have reported a comparison of accordion-optimized experiments for long-range  $^1\text{H}$ – $^{15}\text{N}$  heteronuclear shift correlation at natural abundance to avoid problems inherent to the optimization of these experiments with more conventional experiments [149]. Zannegar and Armitage [125] have also reported the utilization of an accordion-optimized HMQC experiment for the observation of the possible long-range  $^1\text{H}$ – $^{113}\text{Cd}$  couplings in a metalloprotein. Most recently, Sørensen and co-workers [150] have reported a method for measuring long-range  $^1\text{H}$ – $^{31}\text{P}$  coupling constants in nucleic acids which utilizes the accordion methods just described.

### 8.3.8 Hyphenated-2D NMR Experiments

The inverse-detected 2D NMR experiments that have been discussed to this point have all been discrete, single-purpose experiments, e.g. correlating protons with their directly bound heteronuclide (typically  $^{13}\text{C}$  or  $^{15}\text{N}$ ). There are another class of inverse-detected 2D NMR experiments that are generally referred to as “hyphenated” 2D experiments. These are experiments that first establish one type of correlation, followed by an additional experiment segment that then pursues a further spectroscopic task. Predecessors of the inverse-detected variants of these experiments were the HC-RELAY (proton–carbon heteronuclear relayed coherence transfer) experiments pioneered by Bolton [151–155]. Examples of these include, but are by no means limited to HXQC-COSY and -TOCSY [156–158], -NOESY [159], -ROESY [160], and more recent gradient variants [161] etc., where X = S (single) or M (multiple) quantum variants of the experiments.

Hyphenated 2D NMR experiments utilize the obligatory three fundamental experiment segments (preparation, evolution, and detection) with a fourth period, e.g. a mixing period, inserted between evolution and detection. Probably the most commonly encountered member of this class of experiments is HSQC- or HMQC-TOCSY (there are, of course, non-gradient predecessor versions of these experiments) [156–158]. Using the modern GHSQC-TOCSY experiment as an example, the experiment begins with the usual preparation period followed by an evolution period which labels amenable protons (the experiment does not work for protons on oxygen, or nitrogen, for example if a proton–carbon correlation experiment is being performed) with the chemical shift of the directly bound heteronuclide. After magnetization is transferred back to the proton in question, homonuclear vicinal coupling is propagated between contiguous protons as in a homonuclear TOCSY experiment. The proton magnetization ultimately acquired provides homonuclear TOCSY correlated proton spin systems sorted by the chemical shift of the directly bound carbon(s) in question. In similar fashion, the -COSY,

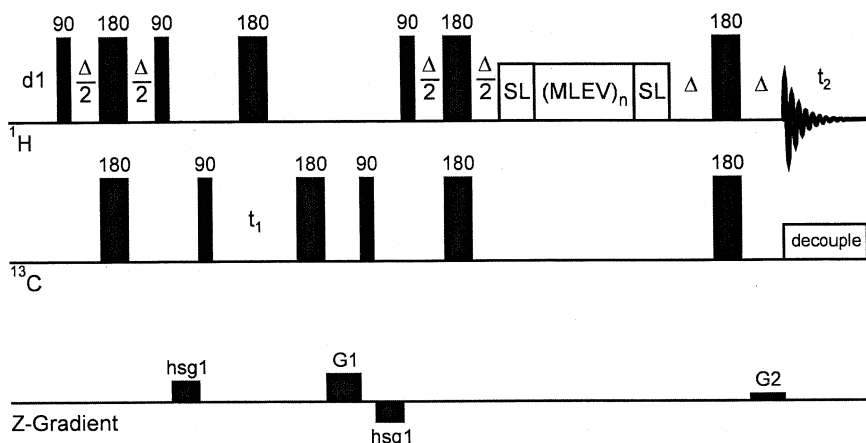


**Fig. 8.31** Pulse sequence schematic for the inverted direct response GHSQC-TOCSY experiment. After labeling protons with the respective, directly bound carbon chemical shifts, magnetization is propagated from a given proton to its vicinal and further removed neighboring protons through the isotropic mixing period. The number of bonds through which magnetization is propagated is a function of the duration of the mixing time.

-NOESY, -ROESY related experiments provide the corresponding homonuclear correlation data sorted by heteronuclide chemical shift.

Direct response-edited variants of the HSQC- and HMQC-TOCSY experiments and their gradient analogues have been developed following the initial, pioneering report of the HSQC-TOCSY experiment by Domke [162]. Possible choices include inverted direct response (IDR) and suppressed direct response (SDR) variants [163] and gradient variants of the experiment [164], which can be quite useful when dealing with homonuclear spin systems that contain direct and relayed correlation responses with AB character. In the case of molecules with AB spin systems, the ability to either invert (IDR) or suppress (SDR) the direct response increases the certainty of observing the relayed correlation response, which is not always true in the original version of the heteronuclear relayed coherence experiments. The GHSQC-TOCSY pulse sequence with multiplicity-editing capability is presented in Fig. 8.31.

Unfortunately, the relative sensitivity of the hyphenated 2D NMR experiments, as a group, is not high. The more sensitive experiments, e.g. GHSQC-TOCSY, are lower in sensitivity than the long-range experiments such as GHMBC by at least a factor of two in the experience of the authors. The -NOESY and -ROESY hyphenated variants are much lower in sensitivity since the S/N ratio in the data set must be high enough to allow the observation of NOE or ROE (rotating frame Overhauser effect) responses with intensities of only a few percent of the direct responses to be observed. Despite the inherent insensitivity of these techniques they have still found a number of useful applications. Examples include the application of inverted direct response GHSQC-TOCSY in the total assignment of the proton and carbon NMR spectra of complex marine polyether toxins such as brevetoxin-2

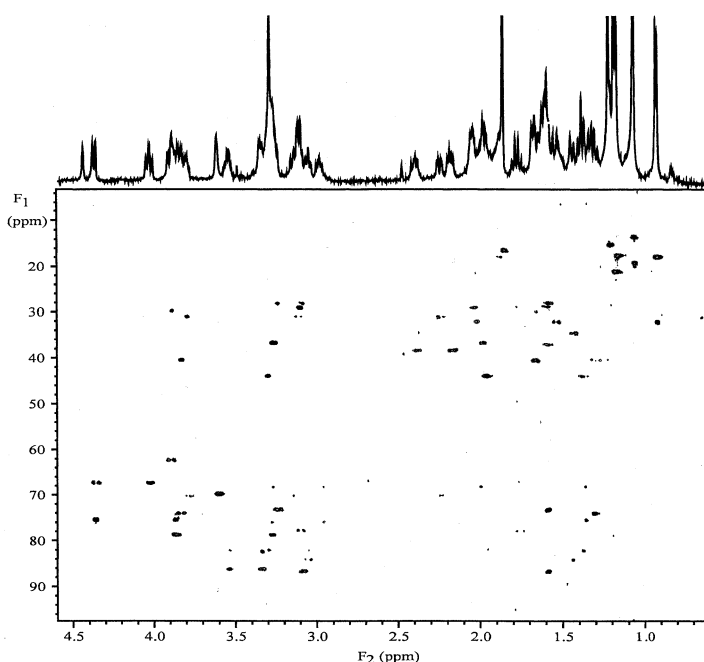
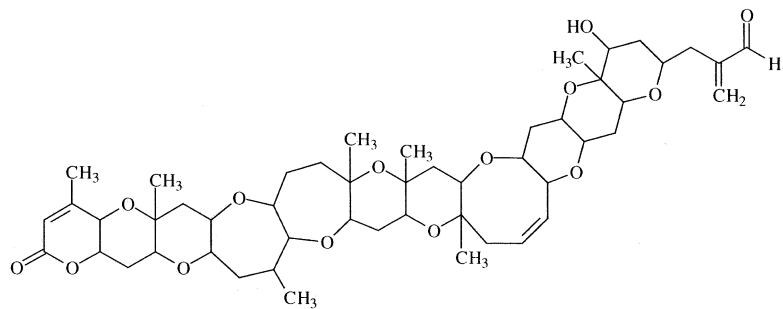


**Fig. 8.32** IDR-GHSQC-TOCSY spectrum of a 500 µg sample of brevetoxin-2 (**8**) in 30 µL of  $d_6$ -benzene. Data were acquired at 600 MHz using a Varian INOVA spectrometer equipped with a Nalorac SMIDG-600-1.7 submicro gra-

dient inverse detection probe. Data were acquired overnight. Direct responses are inverted and plotted in red; relayed responses have positive intensity and are denoted by black responses.

(**8**) [165] (Fig. 8.32); the observation of couplings between overlapped protons [166]; ROEs between “equivalent” protons in C2 symmetric molecules [160, 167–170]; and the unequivocal determination of the structure of complex polynuclear heteroaromatics [168, 169] to list a few of the applications contained in the literature.



### 8.3.9

#### One-dimensional Analogues of 2D NMR Experiments

Frequently, a single piece of correlation data such as an NOE or ROE, or a long-range heteronuclear coupling is sufficient to complete the structural characterization of a molecule. To provide these data, a number of selective, one-dimensional analogues of 2D NMR experiments have been devised. Early work in this area has been reviewed by Kessler and co-workers in 1991 [171]. More recently, Parella [172] in 1996 and Berger [173] in 1997, have reviewed the combined use of selective pulses and gradients in NMR experiments. Specialized, shaped rf pulses frequently used in selective 1D NMR experiments have also been reviewed by Freeman [174]. At present, in the author's experience, the most frequently employed selective 1D NMR experiments are the gradient 1D NOESY experiment and selective 1D analogues of the HMBC experiment. These techniques are discussed in the following sections of this chapter.

### 8.3.10 Gradient 1D NOESY

Gradient selected experiments [105, 136, 175] are finding increased use in structural characterization. The gradient 1D NOESY experiment [175], in particular, is robust and has been very useful in the author's laboratory. The pulse sequence employs a DPFGSE (double pulsed field gradient spin-echo) element to select the resonance for which NOEs will be developed and sampled in the experiment. The gradient 1D NOESY pulse sequence is shown in Fig. 8.33. The selected resonance is refocused by the selective  $180^\circ$  pulses while other resonances are left in random orientations in the  $xy$ -plane. The resonance of interest is ultimately rotated to the  $-z$  axis by the second  $90^\circ$  pulse. The NOE develops during the ensuing mixing delay,  $t_m$ , and is sampled by the final  $90^\circ$  pulse. Results that can be obtained with the

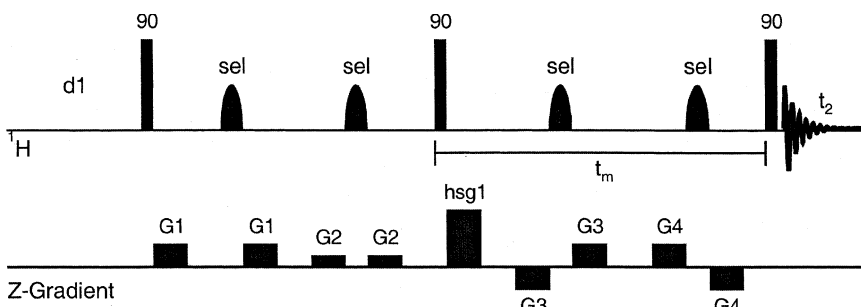


**Fig. 8.33** Pulse sequence schematic for the gradient 1D NOESY experiment. The double pulsed field gradient spin echo (DPFGSE) refocuses only for that resonance subject to the selective pulse. All other magnetization is left defocused in the  $xy$ -plane. Ultimately, a NOESY spectrum is recorded only for the selected re-

sonance. In general 1D gradient NOESY data are substantially free of subtraction artifacts, etc. than the older 1D NOE difference experiment data (see Fig. 8.34). In essence, 1D gradient NOESY represents a selected "slice" of what would otherwise be a normal 2D NOESY experiment.

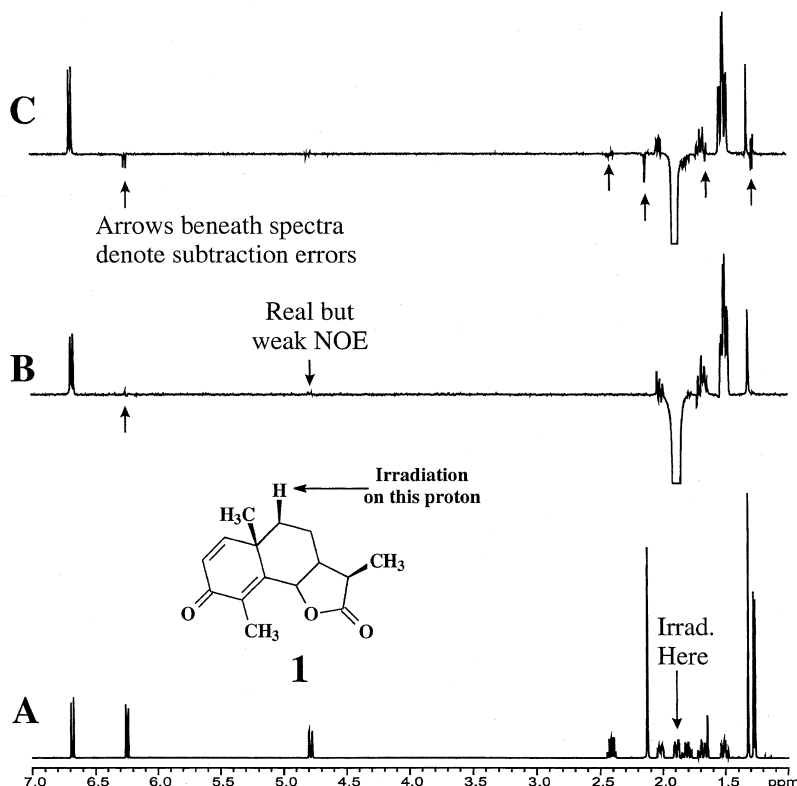


**Fig. 8.34** Application of the 1D gradient NOESY experiment to santonin (**1**). Comparison reference spectrum (A), 1D gradient NOESY (B), and 1D NOE difference (C) spectra. The proton shown on the structure inset was selected for both the 1D gradient NOESY data shown in trace (B) and the 1D NOE difference data shown in trace (C). The gradient 1D NOESY data shown in trace (B) is sub-

stantially free of artifacts with the exception of the one response denoted by an arrow below the trace and potential strong coupling effects for the geminal coupling partner of the selected resonance. In comparison, the 1D NOE difference data shown in trace (C) have a substantial number of subtraction artifacts, as denoted by arrows below the trace.

gradient 1D NOESY experiment are shown in Fig. 8.34 and are compared to results from a conventional NOE difference experiment. Gradient 1D NOESY experiments are particularly useful in that they do not require the calculation of difference spectra to observe the NOEs being sought and they cleanly remove signals not arising from NOEs making them more readily interpretable. These data are very useful for qualitative determinations of stereochemical orientation.

Unlike steady-state NOEs calculated from difference spectra, the transient NOEs determined using the 1D gradient NOESY technique have some attributes associated with responses that are worthy of mention. Responses are sensitive to mixing time choices and may vary markedly as a function of this parameter choice.

The NOE enhancement will depend on the degree of inversion, which can be influenced by pulse calibration. This can lead to the absolute percentage enhancement that is observed being smaller than in a NOE difference experiment, necessitating a “recalibration” of what the spectroscopist may consider to be a reliable response. Despite the potential shortcomings just noted, gradient 1D NOESY experiments are extremely useful and will probably see more widespread use with time.

### 8.3.11 Selective 1D Long-range Heteronuclear Shift Correlation Experiments

Situations frequently arise where one or a few heteronuclear correlations are all that is needed to complete the elucidation of a given structure. Often this missing information is a consequence of an inappropriate choice for the optimization of the long-range delay if HMBC/GHMBC experiments are being employed. In such situations, rather than acquiring another full, long-range 2D experiment, it is far more expedient to consider the acquisition of a selective long-range heteronuclear correlation experiment.

Following the description of the non-gradient SIMBA (selective inverse multiple bond analysis) experiment by one of the authors in 1991 [176], a number of reports describing related methods appeared [177–183]. There have been a few successful applications of SIMBA experiments reported in the literature [70, 184–186] used to establish specific correlations to complete structure assignments.

With the advent of gradient NMR methods, there have been several reports of gradient analogs of the SIMBA method [187–190]. Most recently, a double-selective J-HMBC method has been reported [191] and used to extract long-range couplings to the selectively excited resonances of the alkaloid harmane. Given the potential utility of SIMBA-type experiments augmented by PFGs, it is probable that this class of experiments will see expanded use in the future.

### 8.3.12 Small Sample NMR Studies

All NMR experiments detect signals from the sample being studied using some form of probe. Conventionally, NMR spectrometers have generally utilized 5 mm probes. There have, however, been a number of early reports of studies utilizing small sample NMR probes. A number of pioneering reports by Shoolery using 1.7 mm probe designs were reported in the late 1970s [192–194]. Following these studies, there was a hiatus of more than a decade before interest in small volume NMR probes was rekindled. In 1992, the collaborative development of 3 mm “micro” NMR probes was reported by one of the authors; comparative evaluation of 3 mm probes relative to 5 mm probes with identical quantities of material showed that the former achieved a given S/N ratio in roughly a quarter the time required for a conventional 5 mm probe [195, 196]. There followed a number of natural product studies utilizing 3 mm probes through the mid 1990s [196–205].

The development of the magic angle, liquid Nano-probe™ by Varian was reported in the mid 1990s [206–209]. A number of studies utilizing this probe technology have been reported and there have been a few comparative comments made regarding 3 mm micro probes vs. the Nano-probe design [201, 202]. At about the same time, Sweedler and colleagues [210] began to report the results of their development of what they referred to as  $\mu$ -coil NMR probes [211]. A number of subsequent studies have been reported by these authors including the development of  $\mu$ -coil inverse probe designs [212, 213] and probes with multiple  $\mu$ -coils contained in a single probehead [214]. The 1.7 mm probe format was revisited in 1998 by one of the authors when the development of the submicro gradient or SMIDG probe design was reported [215, 216]. A number of small sample  $^1\text{H}$ – $^{13}\text{C}$  and  $^1\text{H}$ – $^{15}\text{N}$  studies utilizing this probe design have also been reported [216–222]. To illustrate the capabilities of the 1.7 mm submicro NMR probe, GHSQC spectra of a 750  $\mu\text{g}$

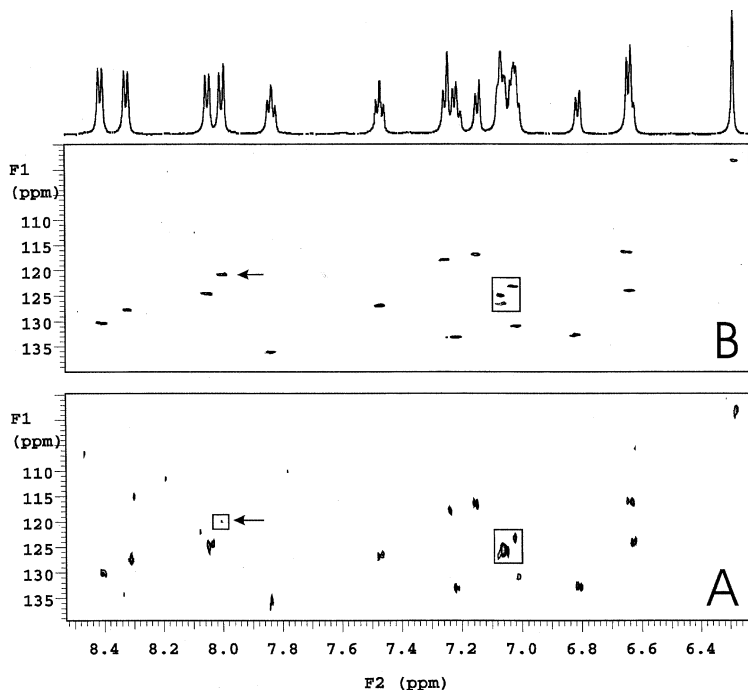


**Fig. 8.35** GHSQC spectra obtained using a 750  $\mu\text{g}$  sample ( $\sim 1.5 \mu\text{mol}$ ) of cryptospirolepine (9) in 30  $\mu\text{L}$  of  $\text{DMSO-d}_6$  [221]. The data shown in panel A were acquired in a scant 34 s as  $16 \times 2$  hypercomplex files with one transient accumulated/ $t_1$  increment. The weak, boxed response denoted by the arrow is the weakest correlation in the spectrum (see Fig. 8.36). The other boxed region of the spectrum that is not well resolved under the data acquisitions used

to acquire the 34 s spectrum shown should contain responses for three correlations. B. GHSQC spectrum acquired in approximately 5 min with  $48 \times 2$  hypercomplex files with 2 transients accumulated/ $t_1$  increment. The weak boxed response in panel A is now clearly identifiable as a legitimate correlation and the three responses in the boxed region of panel A are now clearly resolved. (Reproduced with permission – HeteroCorp.).

sample of the alkaloid cryptospirolepine (**9**) (MW 505 Da) recorded in 34 s and <5 min are shown in Fig. 8.35A and B, respectively [210]. The trace containing weakest response in the 34 s GHSQC spectrum of the alkaloid is plotted above a proton reference spectrum in Fig. 8.36. Despite the extremely short acquisition time, the S/N ratio even for the weakest response is adequate. Work in the area of small sample NMR is the subject of a recent review by Sweedler and co-workers [223].

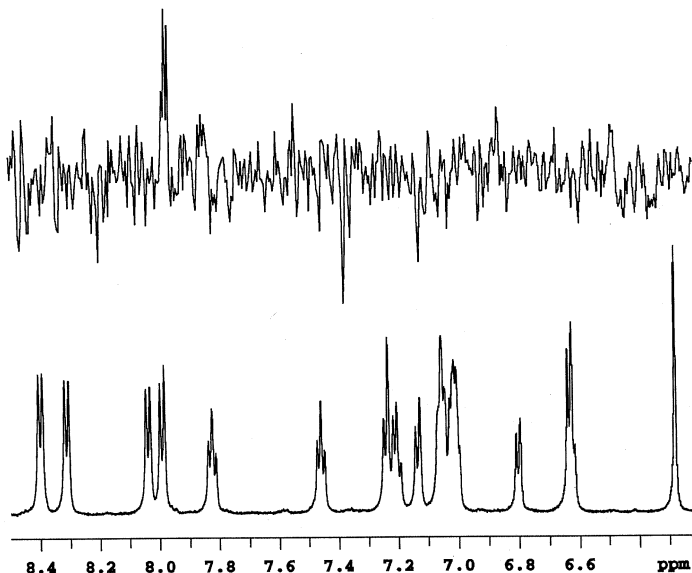
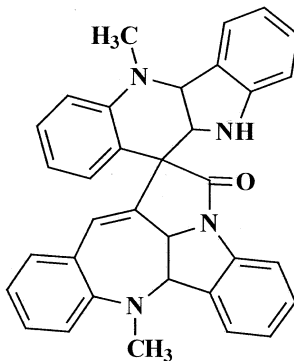


**Fig. 8.36** Proton reference spectrum and the S/N ratio of the weakest peak is still ~3:1, trace from the 2D GHSQC spectrum shown in which when coupled with the multiplet Fig. 8.34A of the weakest response in the 34 s appearance, makes it easy to validate this as a spectrum of **9**. Despite the extremely short real response from the examination of the slice. acquisition time for the GHSQC spectrum, (Reproduced with permission – HeteroCorp.).



What will undoubtedly have the greatest impact on small sample NMR studies will be the development of small volume cold metal NMR probes. Probes of this type have rf coils designed to operate in the range of about 8–25 K [224–227]. Efforts in this area have only begun to be reported within the past year [228], but the initial results are quite promising. Sensitivity for 2.5 or 3 mm versions of these probes have reported gains of as much as four-fold relative to conventional probes operating at ambient magnet bore temperatures [229, 230]. To illustrate the potential of cold metal NMR probes, two examples are shown. The 45 min COSY spectrum of a 2.9  $\mu\text{g}$  sample of paclitaxel (**10**, Taxol<sup>TM</sup>) acquired using a 3 mm cryogenic NMR probe is shown in Fig. 8.37 [231]. An HSQC spectrum of the aliphatic region of strychnine (**2**) acquired using a 3 mm cryogenic NMR probe is shown for a 40  $\mu\text{g}$

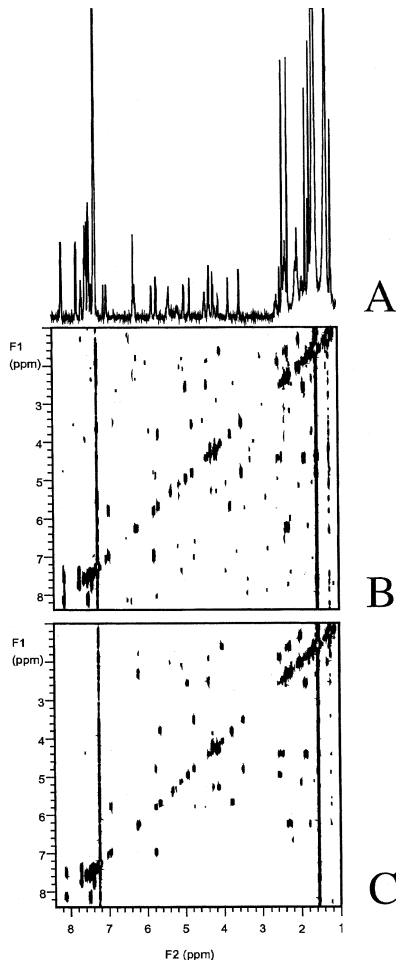


**Fig. 8.37** Spectra recorded with a 2.9  $\mu\text{g}$  sample of paclitaxel (Taxol<sup>TM</sup>, **10**, ~3.4 nanomol) dissolved in 165  $\mu\text{L}$   $\text{CDCl}_3$ , [219]. A. Proton reference spectrum recorded in 32 transients. B. COSY spectrum recorded in 46 min as a 2048  $\times$  128 point file accumulating 12 transients/ $t_1$  increment. All of the expected correlations are observable in the spectrum and are discernible from the noise. C. COSY spectrum recorded in 3 h 4 min as a 2048  $\times$  192 point file accumulating 32 transients/ $t_1$  increment. The spectrum is essentially noise-free.

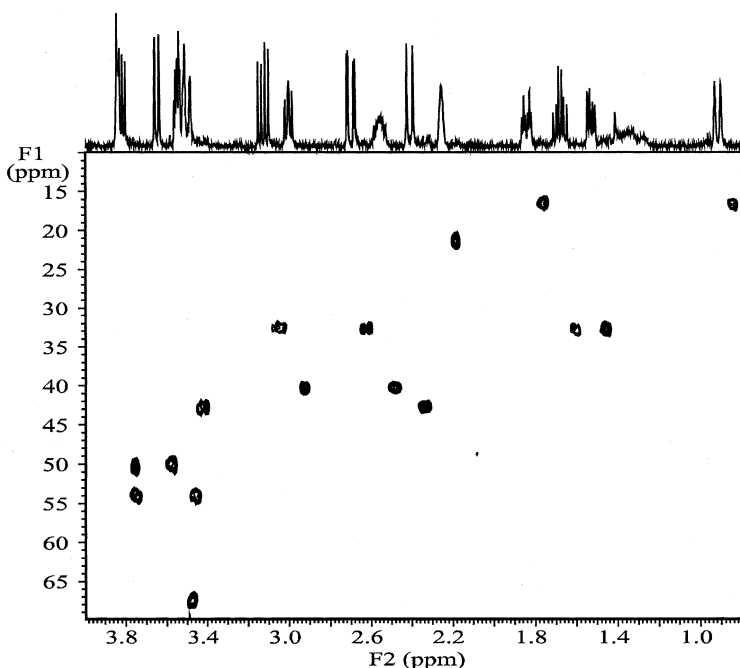
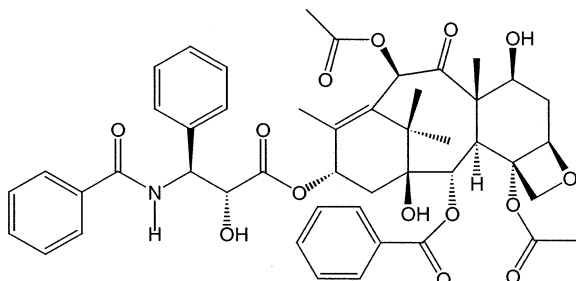


**Fig. 8.38** HSQC spectrum of a 40  $\mu\text{g}$  sample (120 nmol) of strychnine (**2**) dissolved in 160  $\mu\text{L}$  benzene-d<sub>6</sub> in a 3 mm NMR tube. The data were acquired in 90 min using a Varian INOVA 500 MHz instrument equipped with a Nalorac 3 mm Cryo-Spec® NMR probe. The acquisition of an HSQC spectrum with comparable signal-to-noise using a conventional 3 mm NMR probe required 17 h [232].

(0.12  $\mu\text{mol}$ ) sample. The data, shown in Fig. 8.38 were acquired in < 2 h [232]. Comparable data acquired in a conventional 3 mm micro NMR probe required a 17 h acquisition. Full characterization of a sample of this size, if it required the acquisition of an HMBC or GHMBC spectrum in addition to the HSQC spectrum, would consume approximately 100 h of spectrometer time. In contrast, using a 3 mm cryogenic NMR probe, it should be possible to acquire all of the



necessary data in approximately 10 h. Consequently, it is likely that the use of small volume cryogenic NMR probes will be an area of intense research in the coming years.

#### 8.4 Conclusions

NMR experiments performed in the solution state are capable of providing a wealth of chemical structure information both through bonds and through space. The array of experiments available to the spectroscopist with which to probe chemical structure is vast. Many of the issues relating to the inherent insensitivity of the NMR experiment have been addressed through increases in magnetic field strength, with 600 MHz instruments now frequently available for the determination of small molecule structures. Sample limitations have been largely circumvented by small volume NMR probes, specialized NMR cells, and by the very recent availability of 3 mm cryogenic NMR probes. When the available technology is used in concert and in conjunction with data from other analytical spectroscopic techniques such as mass spectrometry and vibrational methods, most chemical structures can be solved in reasonable periods of time even if only submicromole quantities of material are available for analysis.

## References

- 1 E. M. Purcell, H. C. Torrey, R. V. Pound, *Phys. Rev.*, **1946**, *69*, 37–38.
- 2 F. Bloch, W. W. Hansen, M. E. Packard, *Phys. Rev.*, **1946**, *69*, 127.
- 3 R. K. Harris, B. E. Mann, *NMR and the Periodic Table*, Academic Press, New York, 1981.
- 4 C. Brevard, P. Granger, *Handbook of High Resolution Multinuclear NMR*, John Wiley & Sons, New York, 1986.
- 5 R. K. Harris, *Nuclear Magnetic Resonance Spectroscopy*, John Wiley & Sons, New York, 1986.
- 6 J. Mason, *M multinuclear NMR*, Plenum Press, N. Y., 1987.
- 7 *Transition Metal Nuclear Magnetic Resonance*, ed. P. Pregosin, Elsevier, Amsterdam, 1991.
- 8 T. Fäcke, R. Wagner, S. Berger, *Concepts Magn. Reson.*, **1994**, *6*, 293–306.
- 9 H. Günther, in *Advanced Applications of NMR to Organometallic Chemistry*, eds. M. Gielen, R. Willem, B. Wrackmeyer, Wiley & Sons, New York, 1996, pp. 247–290.
- 10 J. J. van der Klink, H. B. Brom, *Annu. Rep. NMR Spectrosc.*, **1999**, *36*, 89–201.
- 11 K. G. Orrell, *Annu. Rep. NMR Spectrosc.*, **1999**, *37*, 1–74.
- 12 D. Gudat, *Annu. Rep. NMR Spectrosc.*, **1999**, *38*, 139–202.
- 13 R. Freeman, *A Handbook of Nuclear Magnetic Resonance Spectroscopy*, John Wiley & Sons, New York, 1987.
- 14 A. Bax, *Two-Dimensional Nuclear Magnetic Resonance in Liquids*, D. Reidel Publishing Co., Boston, MA, 1982.
- 15 *Pulse Methods in 1D and 2D Liquid-Phase NMR*, ed. W. S. Brey, Academic Press, New York, 1988.
- 16 G. E. Martin, A. S. Zektzer, *Two-Dimensional NMR Methods for Establishing Molecular Connectivity: A Chemist's Guide to Experiment Selection, Performance, and Interpretation*, VCH, New York, 1989.
- 17 *Two-Dimensional NMR Spectroscopy, Applications for Chemists and Biochemists*, 2nd edition, eds. W. R. Croasmun, R. M. K. Carlson, VCH, New York, 1994.
- 18 T. C. Farrar, E. D. Becker, *Pulse and Fourier Transform NMR*, Academic Press, New York, 1971.
- 19 E. Fukushima, S. B. W. Roeder, *Experimental Pulse NMR: A Nuts and Bolts Approach*, Addison-Wesley, New York, 1981.
- 20 T. C. Farrar, *Introduction to Pulse NMR Spectroscopy*, Farragut Press, Madison, WI, 1997.
- 21 E. Breitmaier, W. Voelter, *Carbon-13 NMR Spectroscopy*, 3rd edition, VCH, New York, 1987.
- 22 F. W. Fehrli, A. P. Marchand, S. Wehrli, *Interpretation of Carbon-13 NMR Spectra*, 2nd edition, John Wiley & Sons, New York, 1983.
- 23 R. S. Macomber, *A Complete Introduction to Modern NMR Spectroscopy*, John Wiley & Sons, New York, 1998.
- 24 K. Nakanishi, *One-Dimensional and Two-Dimensional NMR Spectra by Modern Pulse Techniques*, University Science Books, Mill Valley, CA, 1990.
- 25 H. Frieboe, *Basic One- and Two-Dimensional NMR Spectroscopy*, 3rd edition, Wiley-VCH, New York, 1998.
- 26 S. Braun, H.-O. Kalinowski, S. Berger, *150 and More Basic NMR Experi-*

- ments – A Practical Course, 2nd edition, Wiley-VCH, New York, 1998.
- 27 A. E. DeRome, *Modern NMR Techniques for Chemistry Research*, Pergamon Press, New York, 1987.
- 28 S. Berger, S. Braun, H.-O. Kalinowski, *NMR Spectroscopy of the Non-Metallic Elements*, New York, 1997.
- 29 H. Günther, *NMR Spectroscopy*, 2nd edition, John Wiley & Sons, New York, 1992.
- 30 R. R. Ernst, G. Bodenhausen, A. Woekaun, *Principles of Nuclear Magnetic Resonance in One and Two Dimensions*, Clarendon Press, Oxford, 1987.
- 31 T. D. W. Claridge, *High-Resolution NMR Techniques in Organic Chemistry*, Pergamon, Amsterdam, 1999.
- 32 R. Freeman, *Spin Choreography*, Oxford University Press, Oxford, 1998.
- 33 R. R. Ernst, W. A. Anderson, *Rev. Sci. Instrum.*, 1966, 37, 93–102.
- 34 J. K. M. Sanders, J. D. Mersh, *Prog. Nucl. Magn. Reson.*, 1982, 13, 355–361.
- 35 J. H. Noggle, R. E. Schrimmer, *The Nuclear Overhauser Effect – Chemical Applications*, Academic Press, New York, 1971.
- 36 D. Neuhaus, M. Williamson, *The Nuclear Overhauser Effect in Structural and Conformational Analysis*, VCH, New York, 1989.
- 37 D. W. Nagel, K. G. Pachler, P. S. Steyn, et al., *Tetrahedron*, 1976, 32, 2625–2631.
- 38 G. A. Morris, R. Freeman, *J. Am. Chem. Soc.*, 1979, 101, 760–762.
- 39 G. A. Morris, *J. Am. Chem. Soc.*, 1980, 102, 428–429.
- 40 D. M. Doddrell, D. T. Pegg, *J. Am. Chem. Soc.*, 1980, 102, 6388–6390.
- 41 D. M. Doddrell, D. T. Pegg, M. R. Bendall, *J. Magn. Reson.*, 1982, 48, 323–327.
- 42 D. M. Doddrell, D. T. Pegg, M. R. Bendall, *J. Chem. Phys.*, 1982, 77, 2745–2752.
- 43 E. W. Hagaman, *Org. Magn. Res.*, 1976, 8, 389–398.
- 44 J. R. Lyerla, Jr., G. C. Levy, Carbon-13 Nuclear Spin Relaxation, in *Topics in Carbon-13 NMR Spectroscopy*, ed. G. C. Levy, Wiley-Interscience, New York, 1974, 79–149, vol. 1.
- 45 F. W. Wehrli, Organic Structure Assignments using  $^{13}\text{C}$  Spin-Relaxation Data, in *Topics in Carbon-13 NMR Spectroscopy*, ed. G. C. Levy, Wiley-Interscience, New York, 1976, 343–391, vol. 2.
- 46 J. Jenner, Ampere International Summer School, Basko Polje, Jugoslavia, 1971.
- 47 W. P. Aue, E. Bartholdi, R. R. Ernst, *J. Chem. Phys.*, 1976, 64, 2229–2246.
- 48 A. Bax, R. Freeman, G. A. Morris, *J. Magn. Reson.*, 1981, 42, 164–168.
- 49 S. Macura, Y. Huang, D. Suter, R. R. Ernst, *J. Magn. Reson.*, 1981, 43, 259–281.
- 50 E. T. Olejniczak, J. C. Hoch, C. M. Dobson, et al., *J. Magn. Reson.*, 1985, 64, 199–206.
- 51 N. H. Andersen, K. T. Nguyen, C. J. Hartze, et al., *J. Magn. Reson.*, 1987, 74, 195–211.
- 52 A. A. Bothner-By, R. L. Stephens, J. Lee, et al., *J. Am. Chem. Soc.*, 1984, 106, 811–813.
- 53 A. Bax and D. G. Davis, *J. Magn. Reson.*, 1985, 63, 207–213.
- 54 J. Jeener, B. H. Beier, P. Bachmann et al., *J. Chem. Phys.*, 1979, 71, 4546–4553.
- 55 K. G. Orrell, V. Šik, D. Stephenson, *Prog. Nucl. Magn. Reson. Spectrosc.*, 1990, 22, 141–208.
- 56 C. L. Perrin and T. J. Dwyer, *Chem. Rev.*, 1990, 90, 935–967.
- 57 K. G. Orrell, V. Šik, *Annu. Rep. NMR Spectros.*, 1993, 27, 103–171.
- 58 J. Sandström, *Dynamic NMR Spectroscopy*, Academic Press, London, 1982.
- 59 M. Oki, *Applications of Dynamic NMR Spectroscopy to Organic Chemistry*, VCH, Weinheim, 1985.
- 60 T. H. Mareci, R. Freeman, *J. Magn. Reson.*, 1983, 51, 531–535.
- 61 D. A. Craig, G. E. Martin, *J. Nat. Prod.*, 1986, 49, 456–465.
- 62 G. E. Martin, R. Sandjua, M. Alam, *J. Org. Chem.*, 1985, 50, 2383–2387.
- 63 L. Müller, *J. Magn. Reson.*, 1984, 59, 326–331.
- 64 A. S. Zekterz and G. E. Martin, 1987, 50, 455–462.

- 65** D. E. Barnekow, J. H. Cardellina, II, A. S. Zektzer et al., *J. Am. Chem. Soc.*, **1989**, *110*, 3511–3517.
- 66** A. S. Zektzer, G. E. Martin, R. N. Castle, *J. Heterocycl. Chem.*, **1987**, *24*, 879–884.
- 67** A. S. Zektzer, J. G. Stuart, G. E. Martin et al., *J. Heterocycl. Chem.*, **1986**, *23*, 1587–1593.
- 68** A. Bax, R. Freeman, S. P. Kempsell, *J. Am. Chem. Soc.*, **1980**, *102*, 4849–4851.
- 69** A. Bax, R. Freeman, T. A. Fremkiel, *J. Am. Chem. Soc.*, **1980**, *102*, 2102–2104.
- 70** G. E. Martin, R. C. Crouch, Inverse-Detected 2D NMR Applications in Alkaloid Chemistry, in *Modern Methods of Plant Analysis*, eds. H. F. Linskens, J. F. Jackson, Springer-Verlag, Berlin, 1994, 25–89, vol. 15.
- 71** G. E. Martin, R. C. Crouch, *J. Nat. Prod.*, **1991**, *54*, 1–70.
- 72** G. E. Martin and C. E. Hadden, *J. Nat. Prod.*, **2000**, *63*, 543–585.
- 73** G. E. Martin and A. S. Zektzer, *Two-Dimensional NMR Methods for Establishing Molecular Connectivity: A Chemist's Guide to Experiment Selection, Performance, and Interpretation*, VCH, New York, 1989, 19–29.
- 74** T. D. W. Claridge, *High-Resolution NMR Techniques in Organic Chemistry*, Pergamon, Amsterdam, 1999, 259–276.
- 75** R. Freeman, G. A. Morris, D. L. Turner, *J. Magn. Reson.*, **1977**, *26*, 373–378.
- 76** W. P. Aue, J. Karhan, R. R. Ernst, *J. Chem. Phys.*, **1976**, *64*, 4226–4227.
- 77** A. Bax and D. G. Davis, *J. Magn. Reson.*, **1985**, *63*, 207–213.
- 78** A. Bax and D. G. Davis, *J. Magn. Reson.*, **1985**, *65*, 355–360.
- 79** L. Braunschweiler, R. R. Ernst, *J. Magn. Reson.*, **1983**, *53*, 521–528
- 80** G. Eich, G. Bodenhausen, R. R. Ernst, *J. Am. Chem. Soc.*, **1982**, *104*, 3731–3732.
- 81** A. Bax, G. Drobny, *J. Magn. Reson.*, **1985**, *61*, 306–320.
- 82** A. Bax, R. Freeman, *J. Magn. Reson.*, **1981**, *44*, 542–561.
- 83** L. Müller, *J. Am. Chem. Soc.*, **1979**, *101*, 4481–4484.
- 84** L. D. Hall, T. J. Norwood, *J. Chem. Soc., Chem. Commun.*, **1986**, 44–46.
- 85** L. D. Hall, T. J. Norwood, *J. Magn. Reson.*, **1986**, *69*, 391–396.
- 86** L. D. Hall, T. J. Norwood, *J. Magn. Reson.*, **1986**, *69*, 585–590.
- 87** L. D. Hall, T. J. Norwood, *J. Magn. Reson.*, **1987**, *74*, 171–176.
- 88** A. Bain, *J. Magn. Reson.*, **1984**, *56*, 418–427.
- 89** G. Bodenhausen, H. Kogler, R. R. Ernst, *J. Magn. Reson.*, **1984**, *58*, 370–388.
- 90** D. I. Hoult and R. E. Richards, *Proc. R. Soc. London, Ser. A*, **1975**, *344*, 311.
- 91** G. Bodenhausen, R. Freeman, D. L. Turner, *J. Magn. Reson.*, **1977**, *27*, 511–514.
- 92** A. A. Maudsley, A. Wokaun, R. R. Ernst, *Chem. Phys. Lett.*, **1978**, *55*, 9–14.
- 93** A. Bax, P. G. De Jong, A. F. Mehlkopf et al., *Chem. Phys. Lett.*, **1980**, *69*, 567–570.
- 94** P. B. Baker, R. Freeman, *J. Magn. Reson.*, **1985**, *64*, 334–338.
- 95** G. Kontaxis, J. Stonehouse, E. D. Laue, J. Keeler, *J. Magn. Reson., A*, **1994**, *111*, 70–76.
- 96** J. Cavanaugh, A. G. Palmer, III, P. E. Wright et al., *J. Magn. Reson.*, **1991**, *91*, 429–436.
- 97** A. G. Palmer, III, J. Cavanaugh, P. E. Wright, M. Rance, *J. Magn. Reson.*, **1991**, *93*, 151–170.
- 98** J. Cavanaugh, M. Rance, *Annu. Rep. NMR Spectrosc.*, **1993**, *27*, 1–58.
- 99** D. J. Russell, C. E. Hadden, G. E. Martin, **1999**, unpublished results.
- 100** W. F. Reynolds, R. G. Enriquez, *Magn. Reson. Chem.*, **2001**, *39*, 531–538.
- 101** M. A. Bernstein, L. A. Trimble, *Magn. Reson. Chem.*, **1994**, *32*, 107–110.
- 102** C. Dalvit, *J. Magn. Reson., A*, **1995**, *113*, 120–123.
- 103** P. Adell, T. Parella, F. Sánchez-Ferrando et al., *J. Magn. Reson., B*, **1995**, *108*, 77–80.
- 104** C. Dalvit, G. Bovermann, *Magn. Reson. Chem.*, **1995**, *33*, 156–159.
- 105** J. Stonehouse, P. Adell, J. Keele et al., *J. Am. Chem. Soc.*, **1994**, *116*, 6037–6038.
- 106** K. Hallenga, G. van Binst, *Bull. Magn. Reson.*, **1980**, *2*, 343.

- 107** W. F. Reynolds, R. G. Enriquez, L. I. Escobar et al., *Can. J. Chem.*, **1984**, *62*, 2421–2425.
- 108** G. E. Martin, A. S. Zektzer, *Magn. Reson. Chem.*, **1988**, *26*, 631–652.
- 109** W. F. Reynolds, S. McLean, H. Jacobs et al., *Can. J. Chem.*, **1999**, *77*, 1922–1930.
- 110** W. F. Reynolds, M. Yu, R. G. Enriquez, *Magn. Reson. Chem.*, **1997**, *35*, 614–618.
- 111** G. Bodenhausen, D. J. Ruben, *Chem. Phys. Lett.*, **1980**, *69*, 185–188.
- 112** A. Bax, R. H. Griffey, B. L. Hawkins, *J. Magn. Reson.*, **1983**, *55*, 3301–315.
- 113** A. Bax, S. Subramanian, *J. Magn. Reson.*, **1986**, *67*, 565–569.
- 114** R. E. Hurd, and B. K. John, *J. Magn. Reson.*, **1991**, *91*, 648–653.
- 115** J. Ruiz-Cabello, G. W. Vuister, C. T. W. Moonen et al., *J. Magn. Reson.*, **1992**, *100*, 282–302.
- 116** T. Parella, *Magn. Reson. Chem.*, **1998**, *36*, 467–495.
- 117** W. F. Reynolds, S. Mclean, L. L. Tay et al., *Magn. Reson. Chem.*, **1997**, *35*, 455–462.
- 118** D. M. Eastwick, K. O. Pascoe, *Magn. Reson. Chem.*, **1997**, *35*, 455–462.
- 119** T. D. W. Claridge, *High-Resolution NMR Techniques in Organic Chemistry*, Pergamon, Amsterdam, 1999, 229–230.
- 120** H. Kessler, P. Schmeider, M. Kurz, *J. Magn. Reson.*, **1989**, *85*, 400–405.
- 121** T. Parella, J. Belloc, F. Sánchez-Ferrando et al., *Magn. Reson. Chem.*, **1998**, *36*, 715–519.
- 122** T. Parella, F. Sánchez-Ferrando, A. Virgili, *J. Magn. Reson.*, **1997**, *126*, 274–277.
- 123** T. D. W. Claridge, *High-Resolution NMR Techniques in Organic Chemistry*, Pergamon, Amsterdam, 1999, 239–240.
- 124** C. E. Hadden, D. T. Angwin, *Magn. Reson. Chem.*, **2001**, *39*, 1–8.
- 125** K. Zanniger, I. M. Armitage, *Magn. Reson. Chem.*, **2000**, *38*, 452–458.
- 126** H. Kessler, C. Griesinger, J. Zarbock et al., *J. Magn. Reson.*, **1984**, *37*, 331–336.
- 127** H. Kessler, C. Criesinger, J. Lautz, *Angew. Chem., Int. Ed., Engl.*, **1984**, *23*, 444–445.
- 128** V. V. Krishnamurthy, J. E. Casida, *Magn. Reson. Chem.*, **1987**, *25*, 837–842.
- 129** M. J. Quast, A. S. Zektzer, G. E. Martin et al., *J. Magn. Reson.*, **1987**, *71*, 554–560.
- 130** W. F. Reynolds, S. McLean, M. Perpick-Dumont et al., *Magn. Reson. Chem.*, **1989**, *27*, 162–169.
- 131** A. Bax, M. F. Summers, *J. Am. Chem. Soc.*, **1986**, *108*, 2093–2094.
- 132** W. Willker, D. Leibfritz, R. Kerssebaum et al., *Magn. Reson. Chem.*, **1993**, *31*, 287–292.
- 133** P. L. Rinaldi, P. A. Keifer, *J. Magn. Reson., A*, **1994**, *108*, 259–262.
- 134** O. W. Sørensen, N. C. Nielsen, H. Bildso et al., *J. Magn. Reson.*, **1986**, *70*, 54–70.
- 135** A. Meissner, D. Moskau, N. C. Nielsen et al., *J. Magn. Reson.*, **1997**, *124*, 245–249.
- 136** K. Stott, J. Stonehouse, J. Keeler et al., *J. Am. Chem. Soc.*, **1995**, *117*, 4199–4200.
- 137** W. Bermel, G. Wagner, C. Griesinger, *J. Magn. Reson.*, **1989**, *83*, 223–232.
- 138** K. Furihata, H. Seto, *Tetrahedron Lett.*, **1995**, *36*, 2817–2820.
- 139** K. Furihata, H. Seto, *Tetrahedron Lett.*, **1996**, *37*, 8901–8904.
- 140** R. Marek, L. Králík, V. Sklenář, *Tetrahedron Lett.*, **1997**, *38*, 6654–558.
- 141** S. Sheng, H. van Halbeek, *J. Magn. Reson.*, **1998**, *130*, 296–299.
- 142** K. Furihata, H. Seto, *Tetrahedron Lett.*, **1998**, *39*, 7337–7340.
- 143** G. Bodenhausen, R. R. Ernst, *J. Am. Chem. Soc.*, **1982**, *104*, 1304–1309.
- 144** R. Wagner, S. Berger, *Magn. Reson. Chem.*, **1998**, *36*, S44–S46.
- 145** G. E. Martin, C. E. Hadden, R. C. Crouch et al., *Magn. Reson. Chem.*, **1999**, *37*, 517–528.
- 146** C. E. Hadden, G. E. Martin, V. V. Krishnamurthy, *J. Magn. Reson.*, **1999**, *140*, 274–280.
- 147** C. E. Hadden, G. E. Martin, V. V. Krishnamurthy, *Magn. Reson. Chem.*, **2000**, *38*, 143–147.
- 148** V. V. Krishnamurthy, D. J. Russell, C. E. Hadden et al., *J. Magn. Reson.*, **2000**, *146*, 232–239.

- 149** G. E. Martin and C. E. Hadden, *Magn. Reson. Chem.*, **2000**, *38*, 251–256.
- 150** C. H. Gotfredsen, A. Meissner, J. Ø. Duus et al., *Magn. Reson. Chem.*, **2000**, *38*, 692–695.
- 151** P. H. Bolton, *J. Magn. Reson.*, **1982**, *48*, 336–340.
- 152** P. H. Bolton, G. Bodenhausen, *Chem. Phys. Lett.*, **1982**, *89*, 139–144.
- 153** A. Bax, *J. Magn. Reson.*, **1983**, *53*, 149–153.
- 154** H. Kessler, M. Bernd, H. Kogler et al., *J. Am. Chem. Soc.*, **1983**, *105*, 6944–6952.
- 155** P. Bigler, W. Ammann, R. Richarz, *Org. Magn. Reson.*, **1984**, *22*, 109–113.
- 156** P. H. Bolton, *J. Magn. Reson.*, **1985**, *62*, 143–146.
- 157** L. Lerner, A. Bax, *J. Magn. Reson.*, **1986**, *69*, 375–380.
- 158** D. Brühwiler, G. Wagner, *J. Magn. Reson.*, **1986**, *69*, 546–551.
- 159** K. Sohn, S. J. Opella, *J. Magn. Reson.*, **1989**, *82*, 193–197.
- 160** J. Kawabata, E. Fukushi, J. Mizutami, *J. Am. Chem. Soc.*, **1992**, *114*, 1115–1117.
- 161** R. E. Hoffman, R. Shenhar, I. Willner et al., *Magn. Reson. Chem.*, **2000**, *38*, 311–314.
- 162** T. Domke, *J. Magn. Reson.*, **1991**, *95*, 174–177.
- 163** R. C. Crouch, T. D. Spitzer, G. E. Martin, *Magn. Reson. Chem.*, **1992**, *30*, S71–73.
- 164** R. C. Crouch, A. O. Davis, G. E. Martin, *Magn. Reson. Chem.*, **1995**, *33*, 889–892.
- 165** R. C. Crouch, G. E. Martin, R. W. Dicke et al., *Tetrahedron*, **1995**, *51*, 8409–8422.
- 166** R. C. Crouch, R. B. McFadyen, S. M. Daluge et al., *Magn. Reson. Chem.*, **1990**, *28*, 792–796.
- 167** J. Kawabata, E. Fukushi, M. Hara et al., *Magn. Reson. Chem.*, **1992**, *30*, 6–10.
- 168** L. W. Castle, M. D. Johnston, C. L. Camoutsis et al., *J. Heterocycl. Chem.*, **1992**, *29*, 1869–1871.
- 169** R. E. Hoffman, R. Shenhar, I. Willner et al., *Magn. Reson. Chem.*, **2000**, *38*, 311–314.
- 170** J. Kawabata, E. Fukushi, J. Mizutani, *Phytochemistry*, **1993**, *32*, 1347–1349.
- 171** H. Kessler, S. Mronga, G. Gemmecher, *Magn. Reson. Chem.*, **1991**, *29*, 527–557.
- 172** T. Parella, *Magn. Reson. Chem.*, **1996**, *34*, 329–347.
- 173** S. Berger, *Prog. Nucl. Magn. Reson. Spectrosc.*, **1997**, *30*, 137–156.
- 174** R. Freeman, *Prog. Nucl. Magn. Reson. Spectrosc.*, **1998**, *32*, 59–106.
- 175** K. Stott, J. Keeler, Q. N. Van et al., *J. Magn. Reson.*, **1997**, *125*, 302–324.
- 176** R. C. Crouch, G. E. Martin, *J. Magn. Reson.*, **1991**, *92*, 189–192.
- 177** M. A. Keniry, G. A. Poulton, *Magn. Reson. Chem.*, **1991**, *29*, 46–48.
- 178** L. Poppe, H. van Halbeek, *J. Magn. Reson.*, **1991**, *92*, 636–641.
- 179** L. Poppe, H. van Halbeek, *Magn. Reson. Chem.*, **1991**, *29*, 848–851.
- 180** J. M. Nuzillard, J. M. Bernassau, *J. Magn. Reson., B*, **1994**, *103*, 284–287.
- 181** L. Poppe, S. Sheng, H. van Halbeek, *J. Magn. Reson., A*, **1994**, *111*, 104–107.
- 182** L. Poppe, S. Sheng, H. van Halbeek, *Magn. Reson. Chem.*, **1994**, *32*, 97–100.
- 183** D. Uhrín, A. Mele, K. E. Köver et al., *J. Magn. Reson., A*, **1994**, *108*, 160–170.
- 184** S. A. Morris, R. E. Schwartz, D. F. Sesin et al., *J. Antibiotics*, **1994**, *47*, 755–764.
- 185** D. O. Hensens, M. A. Goetz, J. M. Liesch et al., *Tetrahedron Lett.*, **1995**, *36*, 2005–2008.
- 186** W. S. Horn, M. S. J. Simmonds, R. E. Schwartz et al., *Tetrahedron*, **1995**, *51*, 3969–3978.
- 187** T. Parella, F. Sánchez-Ferrando, A. Virgili, *J. Magn. Reson., A*, **1995**, *112*, 106–108.
- 188** T. Parella, F. Sánchez-Ferrando, A. Virgili, *J. Magn. Reson., A*, **1995**, *114*, 32–38.
- 189** S. Stelten, D. Leibfritz, *Magn. Reson. Chem.*, **1995**, *33*, 827–830.
- 190** F. G. Vogt, A. J. Benesi, *J. Magn. Reson., B*, **1998**, *132*, 214–219.
- 191** H. Seki, T. Tokunaga, H. Utsumi et al., *Tetrahedron*, **2000**, *56*, 2935–2939.
- 192** J. N. Shoolery, *Varian Instrum. Appl.*, **1977**, *10*, 19–20.
- 193** J. N. Shoolery, R. E. Majors, *Am. Lab.*, **1977**, *9*, 51–61.
- 194** J. N. Shoolery, in *Topics in Carbon-13 NMR Spectroscopy*, ed. G. C. Levy, Ed.,

- Wiley-Interscience, New York, 1979, 28–38, vol.3.
- 195** R. C. Crouch, G. E. Martin, *J. Nat. Prod.*, **1992**, *55*, 1343–1347.
- 196** R. C. Crouch, G. E. Martin, *Magn. Reson. Chem.*, **1992**, *30*, S66–S70.
- 197** J. P. Shockcor, R. M. Wurm, I. S. Silver et al., *Tetrahedron Lett.*, **1994**, *35*, 4919–4922.
- 198** R. C. Crouch, A. O. Davis, T. D. Spitzer et al., *Heterocycl. Chem.*, **1995**, *32*, 1077–1080.
- 199** J. Kawabata, E. Fukushi, *J. Magn. Reson., A*, **1995**, *117*, 88–90.
- 200** M. H. M. Sharaf, P. L. Schiff, Jr., A. N. Tackie et al., *Magn. Reson. Chem.*, **1995**, *33*, 767–778.
- 201** R. C. Crouch, G. E. Martin, S. M. Musser et al., *Tetrahedron Lett.*, **1995**, *36*, 6827–6830.
- 202** S. M. Musser, R. M. Eppley, E. P. Mazzola et al., *J. Nat. Prod.*, **1995**, *58*, 1392–1397.
- 203** W. F. Reynolds, M. Yu, R. G. Enriquez, *Magn. Reson. Chem.*, **1997**, *35*, 614–618.
- 204** E. Kolehmainen, J. Voivisto, K. Laihia et al., *Magn. Reson. Chem.*, **1999**, *37*, 359–364.
- 205** S. J. Logusch, P. C. C. Feng, H. Fujiwara et al., *J. Agric. Food Chem.*, **1999**, *47*, 2125–2129.
- 206** T. Barbara, *J. Magn. Reson., A*, **1994**, *109*, 265–269.
- 207** W. L. Fitch, G. Degre, C. P. Holmes et al., *J. Org. Chem.*, **1994**, *59*, 7955–7956.
- 208** J. N. Shoolery, *Prog. Nucl. Magn. Reson. Spectrosc.*, **1995**, *28*, 37–52.
- 209** P. A. Keifer, L. Baltusis, D. M. Rice et al., *J. Magn. Reson.*, **1996**, *119*, 65–75.
- 210** D. L. Olson, T. L. Peck, A. G. Webb et al., *Science*, **1995**, 1967–1970.
- 211** D. L. Olson, M. E. Lacey, J. V. Sweedler, *Anal. Chem.*, **1998**, *70*, A257–A264.
- 212** D. L. Olson, M. E. Lacey, J. V. Sweedler, *Anal. Chem.*, **1998**, *70*, 645–650.
- 213** R. Subramanian, J. V. Sweedler, A. G. Webb, *J. Am. Chem. Soc.*, **1999**, *121*, 2333–2334.
- 214** Y. Li, A. M. Wolters, P. V. Malawry et al., *Anal. Chem.*, **1999**, *71*, 4815–4820.
- 215** G. E. Martin, R. C. Crouch, A. P. Zens, *Magn. Reson. Chem.*, **1998**, *36*, 551–557.
- 216** G. E. Martin, J. E. Guido, R. H. Robins et al., *J. Nat. Prod.*, **1998**, *61*, 555–559.
- 217** C. E. Hadden, G. E. Martin, *J. Nat. Prod.*, **1998**, *61*, 969–972.
- 218** C. E. Hadden, G. E. Martin, *Magn. Reson. Chem.*, **1999**, *37*, 385–388.
- 219** C. E. Hadden, G. E. Martin, A. N. Tackie et al., *J. Heterocycl. Chem.*, **1999**, *36*, 1115–1117.
- 220** G. E. Martin, C. E. Hadden, *Magn. Reson. Chem.*, **1999**, *37*, 721–729.
- 221** G. E. Martin, C. E. Hadden, A. N. Tackie et al., *Magn. Reson. Chem.*, **1999**, *37*, 529–537.
- 222** C. E. Hadden, M. H. M. Sharaf, J. E. Guido et al., *J. Nat. Prod.*, **1999**, *62*, 238–240.
- 223** M. E. Lacey, R. Subramanian, D. L. Olson et al., *Chem. Rev.*, **1999**, *99*, 3133–3152.
- 224** P. Styles, N. F. Soffe, C. A. Scott et al., *J. Magn. Reson.*, **1983**, *60*, 397–404.
- 225** P. Styles, N. F. Soffe, C. A. Scott, *J. Magn. Reson.*, **1989**, *84*, 376–378.
- 226** W. A. Anderson, W. W. Brey, A. L. Brooke et al., *Bull. Magn. Reson.*, **1995**, *17*, 98–102.
- 227** H. D. W. Hill, *IEEE Trans. Appl. Superconduct.*, **1997**, *7*, 3750–3755.
- 228** T. M. Logan, N. Murali, G. Want et al., *J. Magn. Reson.*, **1999**, *37*, 762–765.
- 229** J. Pease, R. Withers, R. Nast et al., 40<sup>th</sup> Experimental NMR Conference, Orlando, FL, February 28–March 5, 1999, Abstr. W&Th P202.
- 230** Y. Liu, J. Pease, B. Potts et al., SMASH 2000 Small Molecule NMR Conference, Argonne, IL, July 16–19, 2000, Poster 21.
- 231** D. J. Russell, C. E. Hadden, G. E. Martin et al., unpublished results.
- 232** D. J. Russell, C. E. Hadden, G. E. Martin et al., *J. Nat. Prod.*, **2000**, *63*, 1047–1049.

## 9

# Solid-State NMR

*Steven P. Brown and Lyndon Emsley*

### 9.1

#### Introduction

For the chemist today, the importance of solution-state NMR is well established. Individual nuclei within a molecule are differentiated on account of their chemical shift, while connectivities, which permit spectral assignment, are identified by through-bond  $J$  couplings. Through-space proximities, which yield information about three-dimensional structure, are accessible by experiments which exploit the nuclear Overhauser effect (NOE). Moreover, a host of multi-dimensional experiments have been developed which further enhance the information content [1, 2]. In many cases, however, the most appropriate sample to study molecular structure and dynamics is the solid. The purpose of this article is to give an overview of the different solid-state NMR methods which are available in such cases. Our focus is on the structural and dynamic information which a particular method can deliver, and, at most, only a simple qualitative explanation of how the experiment works will be given, although the relevant literature will always be cited, such that the interested reader can find details about, e.g., the experimental implementation.

Firstly, it is necessary to consider how and why NMR of solid samples differs from the solution-state case. High-resolution solution-state spectra are a result of fast isotropic molecular tumbling. In the solid state, this motion is (usually) absent, and anisotropic interactions, i.e., the chemical shift anisotropy (CSA), and the dipolar and quadrupolar couplings, lead to a broadening, see Section 9.2, of the resonances [3–5]. These anisotropic interactions, on the one hand, have the significant disadvantage of hindering the resolution of distinct sites, but, on the other hand, contain valuable structural and dynamic information. Specifically, the CSA and quadrupolar interactions provide insight into electronic structure and bonding, while the dipolar coupling offers direct access to internuclear distances. Moreover, all three anisotropic interactions are formidable probes of dynamics. As will be demonstrated in this article a number of ingenious experimental approaches have been developed which provide access to the information inherent to the anisotropic

interactions particular to the solid state, while retaining the site specificity associated with high-resolution NMR.

Tables 9.1 and 9.2 list the NMR-active nuclei (i.e., those with  $I > 0$ ) of most relevance for organic and inorganic solids, respectively, together with their nuclear spin quantum numbers, their magnetogyric ratios ( $\gamma$ ), and natural abundances. (For a comprehensive listing of all NMR-active nuclei, the reader is referred to [6]) For spin  $I = 1/2$  nuclei, the two most important anisotropic interactions are

**Table 9.1** The properties of the NMR-active nuclei of most relevance for organic solids [6].

Nucleus	$I$	$\gamma/10^7 \text{ rad T}^{-1} \text{ s}^{-1}$	Natural Abundance (%)
$^1\text{H}$	1/2	26.8	99.99
$^2\text{H}$	1	4.1	0.02
$^{13}\text{C}$	1/2	6.7	1.10
$^{14}\text{N}$	1	1.9	99.63
$^{15}\text{N}$	1/2	-2.7	0.37
$^{17}\text{O}$	5/2	-3.6	0.04
$^{19}\text{F}$	1/2	25.2	100.00

**Table 9.2** The properties of the NMR-active nuclei of most relevance for inorganic solids [6].

Nucleus	$I$	$\gamma/10^7 \text{ rad T}^{-1} \text{ s}^{-1}$	Natural Abundance (%)
$^6\text{Li}$	1	3.9	7.50
$^7\text{Li}$	3/2	10.4	92.50
$^{11}\text{B}$	3/2	8.6	80.10
$^{17}\text{O}$	5/2	-3.6	0.04
$^{23}\text{Na}$	3/2	7.1	100.00
$^{25}\text{Mg}$	5/2	-1.6	10.00
$^{27}\text{Al}$	5/2	7.0	100.00
$^{29}\text{Si}$	1/2	-5.3	4.67
$^{31}\text{P}$	1/2	10.8	100.00
$^{33}\text{S}$	3/2	2.1	0.75
$^{45}\text{Sc}$	7/2	6.5	100.00
$^{47}\text{Ti}$	5/2	-1.5	7.30
$^{49}\text{Ti}$	7/2	-1.5	5.50
$^{51}\text{V}$	7/2	7.0	99.75
$^{55}\text{Mn}$	5/2	6.6	100.00
$^{59}\text{Co}$	7/2	6.3	100.00
$^{67}\text{Zn}$	5/2	1.7	4.10
$^{71}\text{Ga}$	3/2	8.2	39.89
$^{87}\text{Rb}$	3/2	8.8	27.83
$^{93}\text{Nb}$	9/2	6.6	100.00
$^{113}\text{Cd}$	1/2	-6.0	12.22
$^{119}\text{Sn}$	1/2	-10.0	8.59
$^{133}\text{Cs}$	7/2	3.5	100.00
$^{195}\text{Pt}$	1/2	5.8	33.80
$^{207}\text{Pb}$	1/2	5.6	22.10

the anisotropy of the chemical shielding interaction and the dipolar coupling between the dipole moments of two or more spins. This is to be compared to the case of nuclei with  $I \geq 1$ , which possess a quadrupole moment and whose spectra are dominated by the interaction of the quadrupole moment with the electric field gradient at the nucleus. Thus, a separate methodology exists for quadrupolar nuclei. Moreover, it is further necessary to distinguish between quadrupolar nuclei with integer (only  $I = 1$ ) and half-integer ( $I = 3/2, 5/2, 7/2, 9/2$ ) spin, since in the latter case the presence of a “central transition”, which is not broadened by the quadrupolar interaction to a first-order approximation, modifies the experimental approach. Solid-state NMR methods suitable for half-integer quadrupolar nuclei, e.g.  $^{17}\text{O}$ ,  $^{23}\text{Na}$ , and  $^{27}\text{Al}$ , which are of much importance in inorganic systems, are therefore discussed separately in Section 9.7.

Nuclei can be further classified as to their natural abundance: nuclei with 99+% natural abundance, e.g.,  $^1\text{H}$ ,  $^{19}\text{F}$ , and  $^{31}\text{P}$ , are referred to as being abundant, while nuclei with low natural abundances, e.g.  $^2\text{H}$ ,  $^{13}\text{C}$ , and  $^{15}\text{N}$ , are termed dilute or rare. For dilute nuclei, there exists the possibility of achieving site selectivity by means of selective isotopic labelling. In an NMR experiment, the sensitivity, i.e., the signal-to-noise ratio (S/N), depends on the natural abundance, i.e., the number of NMR-active nuclei in the sample, as well as the magnetogyric ratio, which determines the Larmor frequency of the nucleus at a particular magnetic field. Of all the naturally occurring nuclei, the proton,  $^1\text{H}$ , thus, has the best sensitivity. However, unlike in solution-state NMR where  $^1\text{H}$  NMR is of central importance, in the solid-state there exists a major complication with  $^1\text{H}$  NMR primarily due to its high natural abundance; namely, the abundance of protons in organic solids means that there exist strongly dipolar-coupled proton networks, which lead to static line broadenings of the order of 50 kHz. As a consequence, as far as organic solids are concerned, attention has rather focused on dilute spin  $I = 1/2$  nuclei, e.g.,  $^{13}\text{C}$  and  $^{15}\text{N}$ . However, as will be discussed briefly in this article, new high-resolution  $^1\text{H}$  solid-state NMR methods have recently been developed [7], such that the importance of  $^1\text{H}$  solid-state NMR is expected to increase significantly in the coming years.

In this chapter, we will first illustrate how anisotropic interactions lead to a broadening of the NMR resonances (Section 9.2), and then describe the principal line-narrowing method in solid-state NMR, namely magic-angle spinning (MAS), in Section 9.3. As stated above, achieving high-resolution is not the only goal in solid-state NMR, and ideally the spectroscopist would like to combine this with the retention of the structural and dynamic information inherent to the anisotropic interactions responsible for the line broadening. Recoupling methods [8, 9] are the subject of Section 9.4. As in solution-state NMR, the extension of the experiment to a second (and higher) dimension is of much importance in solid-state NMR; homonuclear and heteronuclear multi-dimensional experiments are discussed in Sections 9.5 and 9.6, respectively. Finally, methods applicable to half-integer quadrupolar nuclei are introduced in Section 9.7.

## 9.2

## Solid-state NMR Lineshapes

## 9.2.1

## The Orientational Dependence of the NMR Resonance Frequency

In solid-state NMR, a very important concept is that *the resonance frequency of a given nucleus within a particular crystallite depends on the orientation of the crystallite* [3–5]. Considering the example of the CSA of a  $^{13}\text{C}$  nucleus in a carboxyl group, Fig. 9.1 illustrates how the resonance frequency varies for three particular orientations of the molecule with respect to the static magnetic field,  $B_0$ . At this point, we note that the orientation dependence of the CSA, dipolar, and first-order quadrupolar interactions can all be represented by what are referred to as second-rank tensors. This simply means that the interaction can be described mathematically in Cartesian space by a  $3 \times 3$  matrix (this is to be compared with scalar and vector quantities, which are actually zero- and first- rank tensors, and are specified by a single element and a  $3 \times 1$  matrix, respectively). For such a second-rank tensor, there exists a principal axes system (PAS) in which only the diagonal elements of the matrix are non-zero. Indeed, the orientations illustrated in Fig. 9.1 correspond to the orientation of the three principal axes of the chemical shift tensor with respect to the axis defined by  $B_0$ .

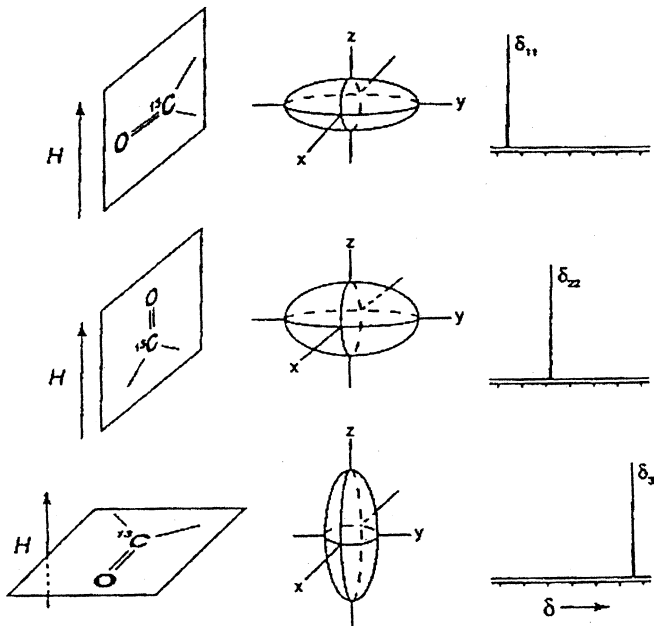


**Fig. 9.1** The dependence of the resonance frequency upon orientation for an anisotropic interaction, namely the CSA of a  $^{13}\text{C}$  nucleus in a carboxyl group. The orientations illustrated

correspond to the alignment of the three principal axes of the chemical shift tensor with the axis defined by  $B_0$ . (Reproduced by permission of the Società Italiana di Fisica from [5].)

To fully characterise the CSA and the first-order quadrupolar coupling, it is necessary to determine the three principal values (corresponding to the diagonal elements in the PAS) as well as the two angles (referred to as Euler angles) which describe the rotation of the PAS onto a fixed reference frame, e.g., that are specified by  $B_0$ . The mathematical expression for the dependence of the resonance frequency of a given nucleus in a crystallite on these parameters is given in the Appendix. It should be noted that the dipolar coupling between a pair of spins is always axially symmetric, and is fully specified by a single principal value and a single angle (see also the Appendix). Since the principal values and Euler angles for a given anisotropic interaction contain valuable chemical information, e.g., about the electronic environment, one of the principal aims of solid-state NMR is the development of methods by which these parameters can be determined.

### 9.2.2

#### **Single-crystal NMR**

One approach by means of which the principal values and orientations of the different anisotropic interactions can be determined involves the measurement of the change in the observed resonance frequencies upon rotating a single crystal in a well-defined fashion [10]. This is illustrated in Fig. 9.2 for the case of  $^2\text{H}$  NMR of a single crystal of the peptide *N*-acetyl-D, L-valine (NAV) for which the exchangeable amide and carboxyl hydrogens were deuterated [11]. The quadrupolar coupling leads to an inequivalence of the two single-quantum (SQ) transitions associated with a spin  $I = 1$  nucleus such that a doublet is observed for each distinct deuterium. There are two molecules in the unit cell of NAV, and thus two crystallographically distinct hydrogen positions for both the amide and carboxyl groups, yielding four different deuterons, and therefore eight separate lines are observed (see Fig. 9.2(a)).

The change in the resonance frequencies of these eight lines upon rotating the crystal in  $10^\circ$  steps around two orthogonal axes is shown in Fig. 9.2(b) and (c). These results can then be analysed to yield the principal values and orientations of both the  $^2\text{H}$  CSA and quadrupolar tensors for both the amide and carboxyl hydrogens in NAV. As described in [11], it was found that, while the eigenvectors corresponding to the largest and intermediate principal values of the quadrupolar interaction are aligned (within experimental error) with the NH bond direction and the normal to the peptide plane, respectively, small but significant deviations are observed for the orientation of the CSA tensor.

Although the power of the single crystal method is evident, it suffers from a couple of significant limitations. Firstly, a single crystal of sufficient size, several mm in each dimension, with a typical volume of  $50 \text{ mm}^3$ , is necessary. Secondly, a specialised NMR probe incorporating a goniometer is required for the well-defined rotation of the sample, and such equipment is available in only a handful of laboratories worldwide. If, however, both the crystal and the equipment are available, this kind of study yields very precise measurements of parameters that are not available from diffraction techniques.

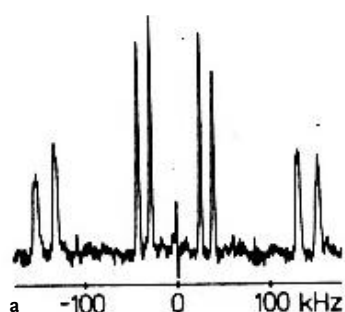
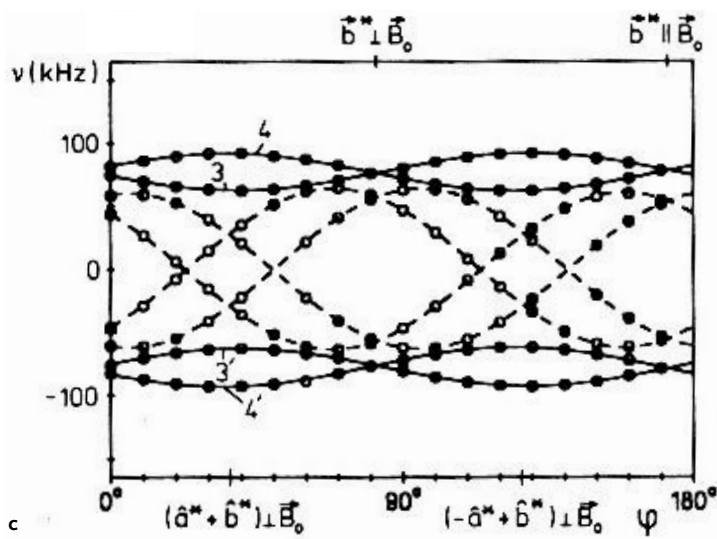
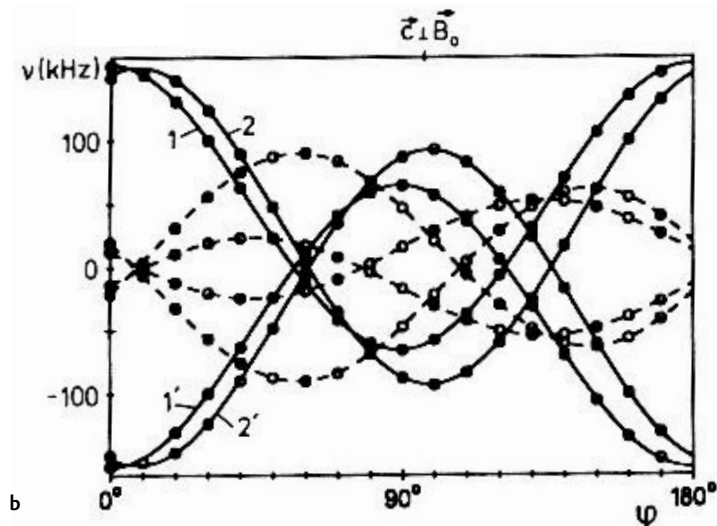


**Fig. 9.2** (a)  $^2\text{H}$  NMR spectrum for a particular orientation of a single crystal of the peptide *N*-acetyl-D,L-valine (NAV) for which the exchangeable amide and carboxyl hydrogens were deuterated. (b), (c) The change in the resonance frequencies of the eight lines upon rotating the crystal in  $10^\circ$  steps around two orthogonal axes. (Reproduced by permission of the American Chemical Society from [11].



At this point, we mention a related class of sample, namely oriented samples. In the case of a perfect macroscopic ordering, each equivalent nucleus is oriented identically, and the situation is the same as that in a single crystal. Specific oriented samples of relevance (with varying degrees of ordering) include polymer fibres [4], liquid crystals (LC), [12, 13] and membrane proteins in oriented lipid bilayers [14]. We will return to the latter two cases in the discussion of two-dimensional experiments in Sections 9.5 and 9.6.

### 9.2.3

#### Powder Spectra

In solid-state NMR, it is more usual to deal with a powdered sample, where there is a uniform distribution of molecular orientations over three-dimensional space. The NMR spectrum for a powdered sample, therefore, consists of a superposition of many lines, corresponding to all the possible resonance frequencies,

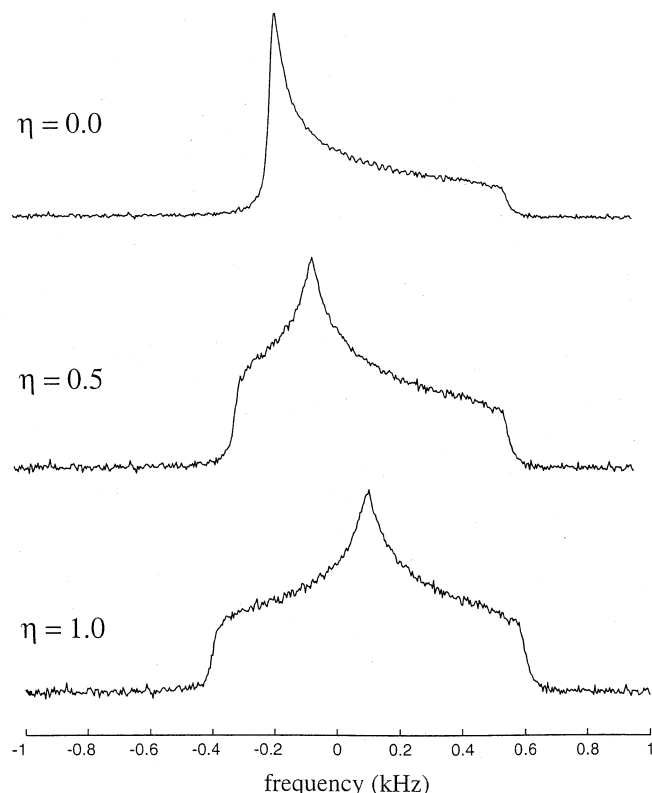


**Fig. 9.3** Simulated static powder spectra (with added noise) for the anisotropic broadening due to the CSA of a spin  $I = 1/2$  nucleus, e.g.,  $^{13}\text{C}$ . Spectra are shown for three different values of the asymmetry parameter,  $\eta$  (see Appendix). (Reproduced by permission of the Società Italiana di Fisica from [5].)

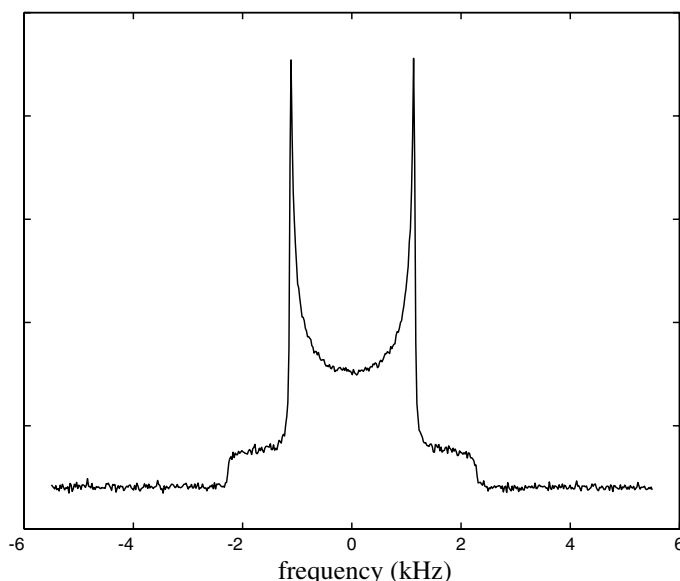


**Fig. 9.4** Simulated static powder spectrum (with added noise) for the anisotropic broadening due either to a dipolar coupling between an isolated pair of spin  $I = 1/2$  nuclei or to the first-order quadrupolar coupling of a spin  $I = 1$  nucleus, e.g.,  $^2\text{H}$ . (Reproduced by permission of the Società Italiana di Fisica from [5].)

where each line originates from a given nucleus in a particular crystallite. Examples of powder spectra are shown in Fig. 9.3 and 9.4. In Fig. 9.3, the anisotropic broadening is due to the CSA of a spin  $I = 1/2$  nucleus, e.g.,  $^{13}\text{C}$ , (for three different values of the asymmetry parameter,  $\eta$  (see Appendix)), while Fig. 9.4 corresponds either to a dipolar coupling between an isolated pair of spin  $I = 1/2$  nuclei or to the first-order quadrupolar coupling of a spin  $I = 1$  nucleus, e.g.,  $^2\text{H}$ .

If powder spectra of the type shown in Fig. 9.3 and 9.4 can be obtained experimentally, the principal values of the anisotropic interaction in question (though *not* the orientation of the PAS with respect to a fixed frame) can be obtained by a straightforward lineshape analysis. However, to obtain such spectra, it is necessary that there is only one distinct nucleus, and that one anisotropic interaction dominates. Usually, the static NMR lineshape is a “broad featureless hump” due to the overlapping of many powder patterns as well as the interplay of the different broadening mechanisms. As an example of this, Fig. 9.5 presents a  $^1\text{H}$  NMR spectrum of a representative organic solid, together with, for comparison, the corresponding solution-state  $^1\text{H}$  spectrum. It is to be noted that the problem in such a case is not a lack of information, but rather there is essentially an overload, such that the net effect is the virtual loss of all information. In the remainder of this article, solid-state NMR approaches by which this information can be recovered will be demonstrated.

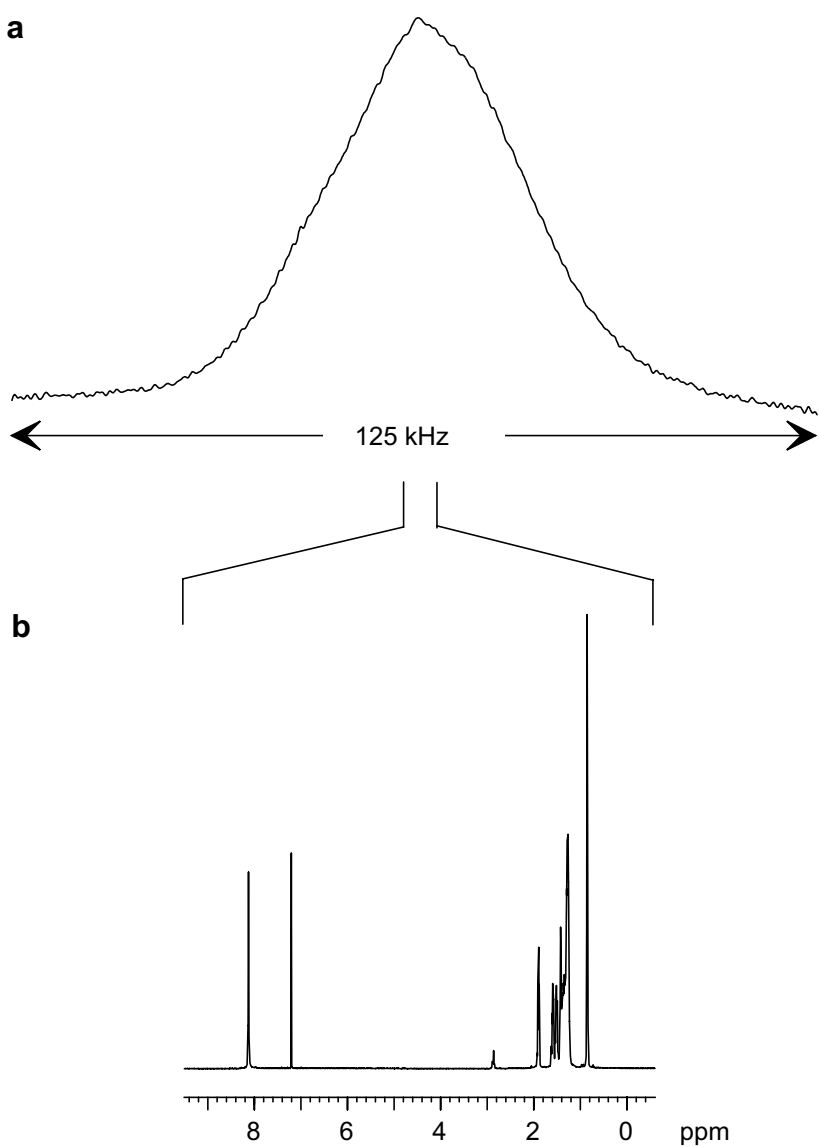


**Fig. 9.5** A comparison of the (a) static solid-state and (b) solution-state  $^1\text{H}$  NMR spectra of a typical organic compound. (Reproduced by permission of the American Chemical Society from [7].)

## 9.2.4

**One-dimensional  $^2\text{H}$  NMR**

One notable case where it is possible to obtain powder spectra due to a single resonance for the case where one broadening mechanism dominates is  $^2\text{H}$  NMR. Since the natural abundance of deuterium is very low (see Tab. 1), the  $^2\text{H}$  NMR spectrum of a sample which has been selectively deuterated at a particular hydrogen position contains, to an extremely good approximation, only the response of that particular  $^2\text{H}$  nucleus. Moreover,  $^2\text{H}$  is a spin  $I = 1$  nucleus, and it, therefore, possesses a quadrupole moment. Although the  $^2\text{H}$  quadrupolar coupling ( $\sim 200$  kHz) is relatively small compared to other quadrupolar nuclei, it still dominates the other anisotropic interactions in diamagnetic compounds, i.e., the CSA and the dipolar coupling.

The applications of  $^2\text{H}$  NMR usually relate to the investigation of dynamic processes [4]. Indeed, one of the most important facets of solid-state NMR, in general, is its ability to probe molecular dynamics with atomic site selectively. This ability to probe dynamics is a direct consequence of the orientational dependence of the NMR resonance frequency: a given motional process leads to a particular crystallite experiencing a range of different orientations and hence a range of different frequencies. The motion is thus reflected in a marked change in the NMR spectrum as compared to the static case, with an extreme example of this phenomenon being the complete removal of anisotropic broadening as a consequence of isotropic molecular tumbling in solution. Notably, solid-state NMR spectra are not only sensitive to the *rates* of dynamic processes but also the *geometry*.

In  $^2\text{H}$  NMR of a selectively labelled molecule, the one-dimensional (1D) powder spectrum depends only on the quadrupolar interaction for a single resonance. Moreover, the quadrupolar interaction for a deuteron bonded to a carbon atom is invariably axially symmetric and aligned with the bond direction. By recording a series of spectra at different temperatures, it is therefore possible, by means of a relatively straightforward lineshape analysis based on computer simulations, to determine the kinetic parameters, i.e., the rate constants and the activation energy, as well as the motional mechanism for the dynamic process under investigation. Moreover, such investigations are aided by the fact that the experiment can be performed over a very wide temperature range, since the sample is static and in the solid-state (i.e., there is no problem with a solvent freezing or evaporating). It should be noted that it is usual practice to record  $^2\text{H}$  powder spectra using the quadrupolar (or solid) echo technique [15].

As a specific example, consider the  $^2\text{H}$  NMR spectra shown in Fig. 9.6, which were recorded for a sample of  $[18\text{-CD}_3]\text{-}6\text{-s-cis-retinoic acid}$ , such that the motion of the methyl hydrogens could be investigated [16]. Marked changes in the spectra are apparent upon increasing the temperature. In particular, as well as changing its shape, the linewidth is observed to narrow by approximately a factor of two, when comparing the spectra for the lowest (top) and highest (bottom) temperatures. The rate constant for a model invoking a three-site jump motion was determined at each temperature by means of a lineshape analysis, and in Fig. 9.6, the best-fit si-

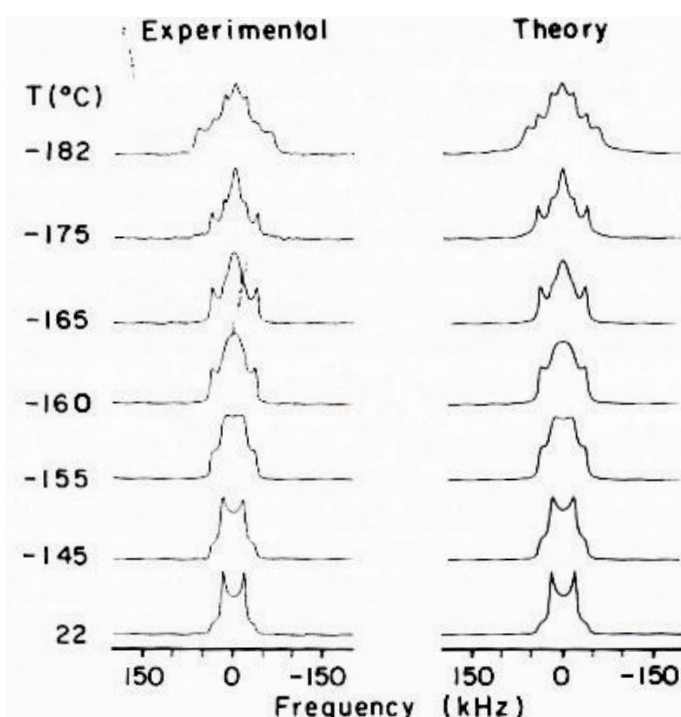


**Fig. 9.6** Variable-temperature  $^2\text{H}$  NMR spectra recorded for a sample of  $[18\text{-CD}_3]\text{-}6\text{-s-cis-retinoic acid}$ . Best-fit spectra simulated for a model invoking a three-site jump motion are shown to the right of the corresponding experimental spectra. (Reproduced by permission of the American Chemical Society from [16].)

mulated spectra are shown to the right of the corresponding experimental spectra. For the lowest (top) and highest (bottom) temperatures investigated, the rate-constant was determined to be  $2.3 \times 10^4$  and  $1.5 \times 10^{10} \text{ s}^{-1}$ , respectively. These two temperatures, therefore, correspond to a motion which is, respectively, “slow” and “fast” compared to the relevant timescale of this NMR experiment (corresponding, in this case, to the time required to record the free-induction decay (FID)). From the knowledge of the rate constant for each temperature, it was possible to determine an activation energy of  $14.5 \text{ kJ mol}^{-1}$ . By additionally investigating the methyl group jump motion in the corresponding *trans* model compound as well as in the membrane protein bacteriorhodopsin, Copié et al. were able to postulate the existence of a 6-s-*trans* chromophore in the protein [16].

**9.3****Magic-angle Spinning**

The above example of the effect of dynamics on a  $^2\text{H}$  NMR powder spectrum illustrates that motion leads to line narrowing. Moreover, as noted above, in solution, fast isotropic tumbling of the molecules causes the averaging *to zero* of the line broadening due to the anisotropic interactions. To achieve high resolution, the solid-state NMR spectroscopist would like to mimic this averaging process. Rather than requiring random isotropic motion of each molecule, it can be shown that a physical rotation of the whole sample around an axis inclined at an angle of  $\arctan(\sqrt{2}) = 54.7^\circ$  (referred to as the magic angle) to  $B_0$  suffices to average any second-rank tensor interaction to zero [17, 18].

To understand why so-called magic-angle spinning (MAS) is so successful as a means of line narrowing, it is first necessary to recognise that the CSA, dipolar, and first-order quadrupolar interaction all have basically the same orientational dependence: for an axially symmetric tensor (this is always the case for the dipolar interaction, and corresponds to a CSA or first-order quadrupolar interaction with a zero asymmetry parameter), the orientationally dependent part of the frequency of a particular crystallite can be expressed in the form

$$\omega \propto 1/2 (3 \cos^2 \theta - 1), \quad (1)$$

where  $\theta$  denotes the angle between the tensor PAS direction and  $B_0$  (see the Appendix for the full mathematical expressions). For a static sample, there is thus no anisotropic frequency shift for those crystallites with  $\theta = 54.7^\circ$ .

To illustrate the effect of MAS, we consider in Fig. 9.7 the specific example of a dipolar coupling between two spins. The four cones represent the range of positions adopted over the course of one rotor period for four different orient-

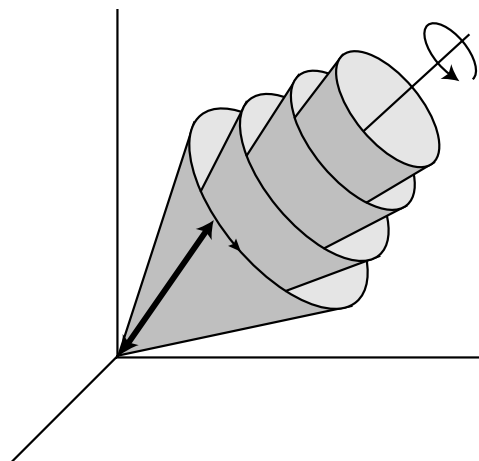


**Fig. 9.7** The effect of MAS for the specific example of a dipolar coupling between two spins. The four cones represent the range of positions adopted over the course of one rotor period for four different orientations of the inter-nuclear vector relative to the rotor axis. The double-headed arrow represents an arbitrary position of one of the inter-nuclear vectors.

tations of the internuclear vector relative to the rotor axis. In each case, the sample rotation leads to those components *perpendicular* to the rotation axis being zero on average, and only the component *parallel* to the rotation axis remains non-zero on average. Thus, for any original orientation, rotation around an axis yields an “average orientation” parallel to the axis of rotation. If the rotation axis is inclined at the magic angle to  $B_0$ , this parallel component has an anisotropic frequency shift equal to zero for all cases. Thus, under MAS, the anisotropic broadening is averaged to zero by the sample rotation for all crystallite orientations.

### 9.3.1

#### CP MAS NMR

For solid-state NMR of a dilute spin  $I = 1/2$  nucleus, e.g.  $^{13}\text{C}$  or  $^{29}\text{Si}$ , MAS is usually combined with the method of cross polarisation (CP) [19, 20], whereby a sensitivity enhancement results as a consequence of the transfer of polarisation from an abundant nucleus with a high magnetogyric ratio, usually  $^1\text{H}$ ; the approach is referred to as CP MAS NMR [21]. High-power proton decoupling is normally applied during the acquisition of the FID to remove broadenings due to dipolar couplings involving the protons, such that the dominant anisotropic broadening is the CSA.

The simulated spectra in Fig. 9.8 illustrate the effect of MAS for the case of a CSA interaction. Upon rotating the sample, the static lineshape is seen to break up into a centreband and spinning sidebands, separated by the rotor frequency. At a low MAS frequency,  $v_R$ , the sideband manifold is observed to map out the shape of the static pattern. As the  $v_R$  is increased, the signal intensity is increasingly concentrated at the centreband position, which corresponds to the isotropic chemical shift. It is to be noted that the linewidths are narrow and independent of  $v_R$  [22].

In principle, it is possible to extract the anisotropy and asymmetry of the CSA by fitting the observed MAS sideband intensities. This is referred to as a Herzfeld–Berger analysis [23]. Such an approach is restricted to relatively small molecules, since it is necessary to be able to resolve, at a low  $v_R$ , the sidebands of different resonances. As the number of distinct resonances increases, the 1D spectrum becomes increasingly more crowded; the advantage of extending the experiment to a second dimension in such cases will be discussed in Section 9.5.

The main interest of the CP MAS technique is that it can provide high-resolution purely isotropic spectra. As is apparent from Fig. 9.8, as  $v_R$  is increased such that it becomes large as compared to the static linewidth, the signal is increasingly concentrated in the centreband position. The spectrum is obviously much simplified if there is only one narrow resonance line, at the isotropic chemical shift, for each distinct nucleus. As an example, Fig. 9.9 presents a  $^{13}\text{C}$  CP MAS spectrum of powdered cyclosporin A, a cyclic 11-residue peptide. In this case, the isotropic spectrum is obtained by employing a  $v_R$  of 33.3 kHz, and there are virtually no spinning sidebands. (MAS probes capable of supporting such a  $v_R$  have only be-

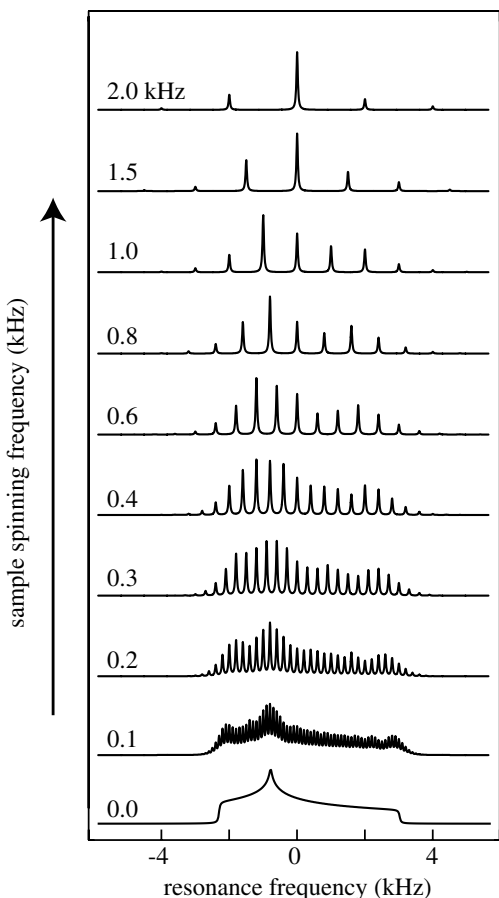


**Fig. 9.8** Simulated spectra showing the effect of MAS on the anisotropic lineshape due to a CSA interaction. (Reproduced by permission of the American Institute of Physics from [178].)

come available in the last 2–3 years. It is to be noted that at such a fast  $v_R$ , it is necessary to employ a modified CP procedure, which is referred to as ramped CP [24, 25].) An alternative means by which a purely isotropic spectrum without spinning sidebands can be achieved for the case of a moderate  $v_R$  is to employ a specially designed sequence of radiofrequency (rf) pulses to suppress the spinning sidebands; the classic example is the TOSS (total suppression of sidebands) sequence [26, 27] which involves the application of four (or  $2n + 2$ ) appropriately spaced  $180^\circ$  pulses before the start of acquisition.

In solid-state NMR experiments, a central theme is that of resolution. For  $^{13}\text{C}$  CP MAS NMR, a critical factor in this respect is the efficiency of  $^1\text{H}$  decoupling. The simplest method, which is termed continuous wave (CW) decoupling, involves the application of a continuous rf pulse of fixed phase for the duration of the acquisition of the FID [28]. Recently, more sophisticated decoupling methods, such as TPPM [29] or other sequences possessing a  $RN_n^\nu$  symmetry [30], have been introduced; an explanation of why these methods yield narrower  $^{13}\text{C}$  linewidths than

conventional CW decoupling is given in [30, 31]. In simple terms, the efficiency of  $^1\text{H}$  decoupling increases as the rf field strength increases (note that NMR literature usually refers to the inherent nutation frequency of the pulse,  $|\omega_1| = |\gamma B_1|$ , where  $B_1$  is the rf field strength). Experimentally, care must of course be taken to find the power level which gives the optimum decoupling performance without damaging the probe. In Fig. 9.9, it is shown that current state-of-the-art  $^1\text{H}$  decoupling, namely TPPM at a  $\omega_1$  of 200 kHz, yields a  $^{13}\text{C}$  linewidth (full-width at half-maximum height, FWHM) of 14 Hz (see the inset for a methyl carbon in cyclosporin A). The spectrum in Fig. 9.9 was recorded at a  $B_0$  of 11.8 T (corresponding to  $^1\text{H}$  and  $^{13}\text{C}$  Larmor frequencies of 500 and 125 MHz). Today, solid-state NMR is being performed at  $B_0$  fields approaching 20 T; provided that the same or narrower linewidths (in Hz) can be achieved at the higher  $B_0$ , and this can certainly not be taken for granted in solid-state NMR, the resolution of resonances with different chemical shifts will be further improved at higher  $B_0$ .

For small molecules, some of the  $^{13}\text{C}$  resonances can usually be assigned by reference to an assigned solution-state spectrum, since  $^{13}\text{C}$  chemical shifts are relatively insensitive to the through-space effects of importance in the solid phase. As the molecular size increases, however, this is no longer the case. To assign a complicated  $^{13}\text{C}$  CP MAS spectrum, such as that in Fig. 9.9, spectral editing me-

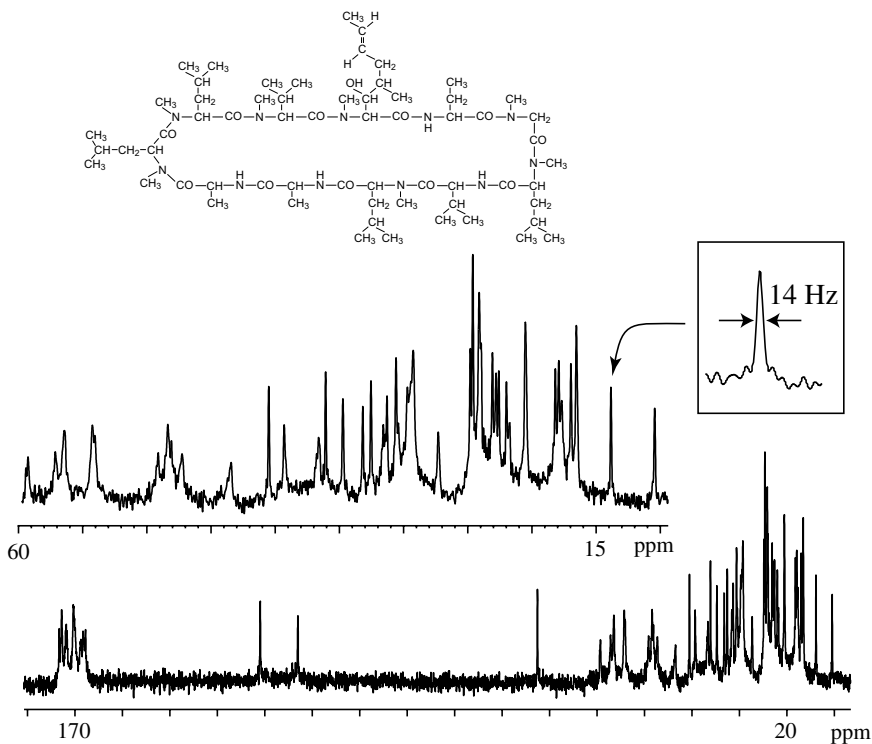


**Fig. 9.9** A  $^{13}\text{C}$  CP MAS ( $\nu_R = 33.3$  kHz) spectrum of powdered cyclosporin A, a cyclic 11-residue peptide, at natural abundance. (Courtesy of A. Lesage and P. Charmont.)

thods which can distinguish between  $\text{CH}_3$ ,  $\text{CH}_2$ ,  $\text{CH}$ , and quaternary carbons are of much help [32–35]. As a specific example, Fig. 9.10 shows a 1D  $^{13}\text{C}$  spectrum of L-histidine monohydrochloride monohydrate recorded using the SS-APT (solid-state attached proton test) method [33]: resonances due to carbons with an even (i.e., quaternary and  $\text{CH}_2$  moieties) or odd (i.e.,  $\text{CH}$  and  $\text{CH}_3$  moieties) number of attached protons are positive or negative, respectively. It is to be noted that the SS-APT method is based on through-bond  $J$  couplings, and thus has the advantage of being unaffected by molecular motion, which can lead to the erroneous interpretation of spectra obtained with the other spectral editing methods which exploit through-space dipolar couplings.

*1D CP MAS is the workhorse solid-state NMR experiment*, a fact which is apparent from the very wide range of applications, with specific examples including fossil fuels [36], i.e., coals [37] and cokes [38], food science, e.g. polysaccharides [39], pharmaceuticals [40], polymer blends [41] and soil science [42]. In addition to  $^{13}\text{C}$  and, to a lesser extent,  $^{15}\text{N}$ , another much investigated nucleus is  $^{29}\text{Si}$ , with  $^{29}\text{Si}$  solid-state NMR being of much importance in materials science and geology [43, 44]. Although  $^{31}\text{P}$  has a 100 % natural abundance, the relatively large separation between phosphorus atoms in a typical solid means that  $^{31}\text{P}$  often has the characteristics of a rare spin.  $^{31}\text{P}$  CP MAS NMR is of importance in, e.g., the investigation of glasses [45].

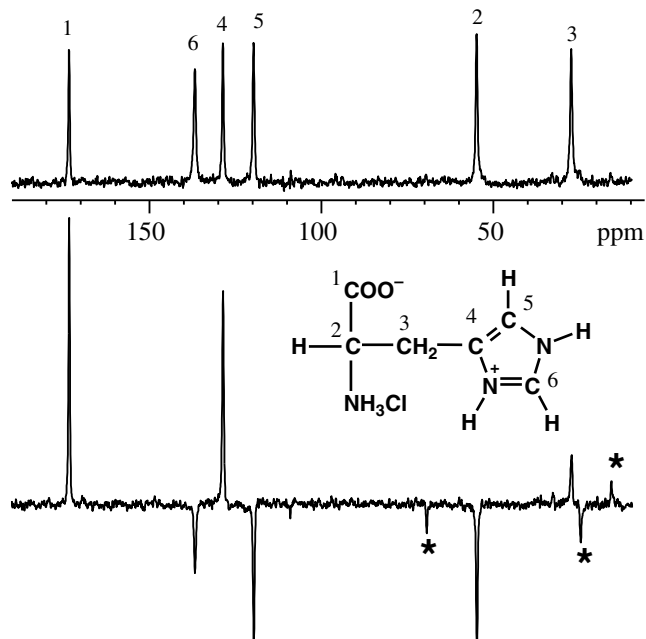
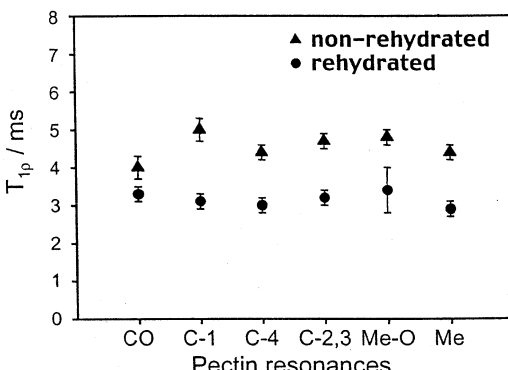


**Fig. 9.10** 1D  $^{13}\text{C}$  spectrum of L-histidine monohydrochloride monohydrate recorded using the SS-APT method. Resonances due to carbons with an even (i.e., quaternary and  $\text{CH}_2$  moieties) or odd (i.e.,  $\text{CH}$  and  $\text{CH}_3$  moieties) number of attached protons are positive or

negative, respectively. Spinning sidebands are labelled by asterisks. For comparison, the  $^{13}\text{C}$  CP MAS spectrum is shown at the top. (Reproduced by permission of the American Chemical Society from [33].)

**Fig. 9.11** Fitted  $^1\text{H}$   $T_{1p}$  relaxation time constants as read out at the various assigned  $^{13}\text{C}$  resonances for 10% hydrated (triangles) and 35% hydrated (circles) onion cell-wall material. The difference directly reflects the increased mobility in the hydrated sample. (Reproduced by permission of Elsevier Science Publishers from [46].)



Valuable information can often be obtained by simple experiments which determine the relaxation times, in particular the spin–lattice (or longitudinal) relaxation times in the laboratory or rotating frame, namely the  $^{13}\text{C}$   $T_1$  and the  $^1\text{H}$   $T_{1p}$ , respectively, for the different resolved resonances in a 1D CP MAS spectrum. In simple terms, a faster relaxation time is due to an increase in molecular mobility. As a specific example, Fig. 9.11 shows the  $^1\text{H}$   $T_{1p}$  relaxation time constants, as read out at the  $^{13}\text{C}$  resonances, for the pectin resonances in onion cell-wall material [46]. It is apparent that increasing the sample hydration from 10 to 35 % leads to a clearly faster relaxation.

### 9.3.2

#### $^1\text{H}$ Solid-State NMR

In the discussion of Fig. 9.8, it was noted that the linewidths of the centreband and spinning sidebands are narrow and independent of  $\nu_R$ . This is a general feature of *rare spin* spectra. A different situation is usually encountered in  $^1\text{H}$  solid-state NMR. Figure 9.12 shows the effect of increasing  $\nu_R$  upon the centreband in the  $^1\text{H}$  MAS NMR spectrum of a medium-sized organic solid. In particular, it is apparent that the linewidth is dependent on  $\nu_R$ , with a line narrowing being observed upon increasing  $\nu_R$ . Even at 35 kHz, the linewidths ( $\text{FWHM} \approx 750$  Hz) are, however, much larger than those observed in  $^{13}\text{C}$  MAS spectra.

The different effect of MAS in  $^1\text{H}$  and  $^{13}\text{C}$  NMR is a consequence of the central importance and relative insignificance of homonuclear (i.e., between like spins) dipolar couplings in the respective two cases. The homonuclear dipolar coupling between a pair of protons is approximately 16 times larger than that between two  $^{13}\text{C}$  nuclei at the same internuclear separation. Moreover, the natural abundance of  $^{13}\text{C}$  is only 1 % as opposed to nearly 100 % for  $^1\text{H}$ , such that (except for the case of isotopically enriched samples) very few  $^{13}\text{C}$  nuclei have a nearby  $^{13}\text{C}$  neighbour.

For a typical organic solid, there exists a strongly dipolar-coupled multi-proton network, and the effect of MAS is quite different as compared to the case of the CSA interaction. This difference is explained in a classic paper by Maricq and Waugh [22]. The CSA is an example of an interaction where the anisotropic broad-

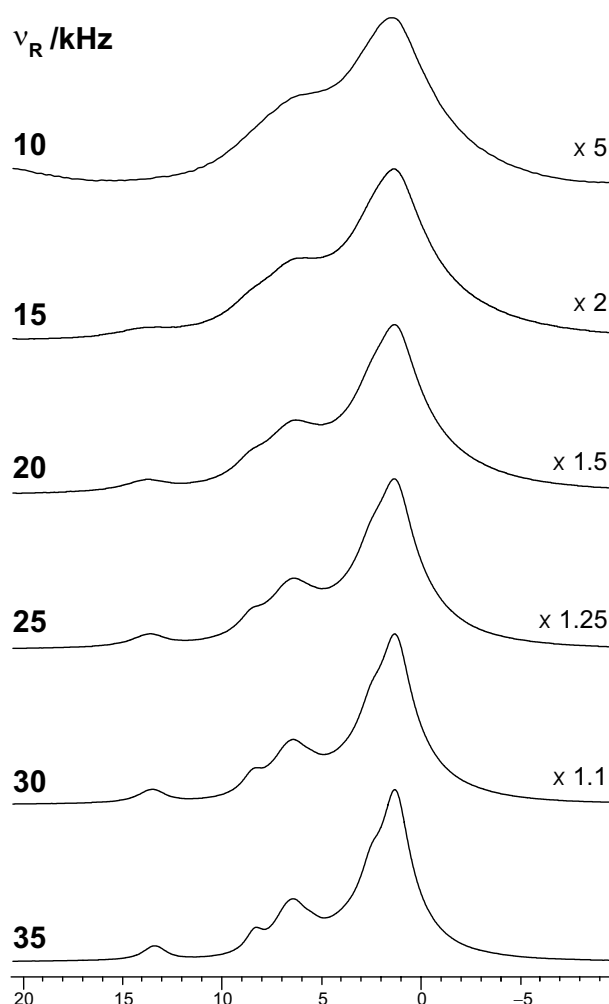


**Fig. 9.12** The effect of increasing the MAS frequency,  $\nu_R$ , on the centreband of a  $^1\text{H}$  MAS spectrum of a typical organic compound. (Reproduced by permission of the American Chemical Society from [47].)

ening is perfectly refocused at the end of each rotor period,  $\tau_R$ , (in the language of quantum mechanics, the corresponding Hamiltonian for a given crystallite commutes with itself at all times). By comparison, when there are three or more dipolar-coupled protons, the perturbing influence of the other dipolar-coupled protons upon a particular dipolar-coupled pair means that the Hamiltonian does not commute with itself at all times, and the evolution under the dipolar coupling of a particular pair is no longer refocused at the end of each  $\tau_R$ .

It was noted in the previous section, that a  $\nu_R$  in excess of 20 kHz has only become possible in the last 2–3 years. The advantage in terms of the enhanced line

narrowing in a  $^1\text{H}$  MAS NMR spectrum is evident in Fig. 9.12. Indeed, it has been shown that a  $\nu_R$  of 30+ kHz at a  $^1\text{H}$  Larmor frequency of 500+ MHz is sufficient to allow some  $^1\text{H}$  resonances due to particular chemically distinct protons to be resolved in  $^1\text{H}$  MAS NMR spectra of small to moderately sized organic solids [47–50]. The line narrowing achieved by MAS alone at a  $\nu_R$  equal to 30 kHz is, however, still far from the limiting case, where all residual dipolar broadening has been removed.

Brute-force fast MAS is not the only means by which line narrowing can be achieved in solid-state NMR. A particularly ingenious alternative approach, first presented over 30 years ago by Waugh and co-workers, involves the removal of the dipolar broadening by specific multiple-pulse techniques, where radiofrequency pulses achieve rotations in spin space [51, 52]. These rotations can complement the effect of the physical rotation of the sample; combined rotation and multiple-pulse spectroscopy (CRAMPS) [53–55] yields well-resolved  $^1\text{H}$  spectra [56]. We will discuss the CRAMPS approach in more detail in Section 9.5.3.

An inspection of Table 9.1 reveals that  $^{19}\text{F}$  has similar NMR properties to  $^1\text{H}$ . Thus, methods which deal with the residual broadening due to homonuclear dipolar couplings are also of much relevance in  $^{19}\text{F}$  solid-state NMR [57]. Although fluorine is much less commonly encountered in chemistry than the omnipresent hydrogen,  $^{19}\text{F}$  solid-state NMR has found a number of important applications, with recent examples including fluoropolymers [58] and biomembranes [59].

## 9.4 Recoupling Methods

Anisotropic interactions present both problems and opportunities. On the one hand, there is the significant disadvantage of hindering the resolution of distinct sites, and methods, such as MAS, which remove the line broadening due to the anisotropic interactions are essential to allow the recovery of the isotropic chemical shift information. On the other hand, they contain valuable structural and dynamic information. This information can be accessed while maintaining high resolution by employing a so-called recoupling method [8, 9] to recover the anisotropic interaction during part of the NMR experiment. In simple terms, recoupling involves the application of rf pulses to counteract the effect of the physical rotation. The conceptually most simple technique to illustrate the principle is REDOR.

### 9.4.1 Heteronuclear Dipolar-coupled Spins: REDOR

In the rotational-echo double-resonance (REDOR) [60–62] technique, the distance between two heteronuclei is determined by comparing the signal intensity in two closely related experiments. The interpretation of the experimental results assumes the existence of isolated spin pairs, and there is thus usually a requirement for selective isotopic labelling at the two sites, the distance between which is of interest.

In a reference experiment, an echo corresponding to the refocusing of the evolution under both the chemical shift and the heteronuclear dipolar coupling is formed. The echo intensity in the reference experiment,  $S_0$ , is then compared to that in a second experiment where the application of  $180^\circ$  pulses at intervals of  $\tau_R/2$  on the channel where there is no transverse magnetisation interferes with the refocusing by MAS of the evolution due to the heteronuclear dipolar coupling, and hence results in a reduced signal intensity,  $S_r$ . For an isolated spin pair, the ratio  $S_r/S_0$  depends solely and in a straightforward manner on the product of the evolution time and the heteronuclear dipolar coupling. The REDOR master curve applicable to all heteronuclear spin pairs is plotted in Fig. 9.13. Note that it is common to see the REDOR literature referring to the difference,  $\Delta S = S_0 - S_r$ . By simple reference to this master curve, it is possible to determine the hetero-

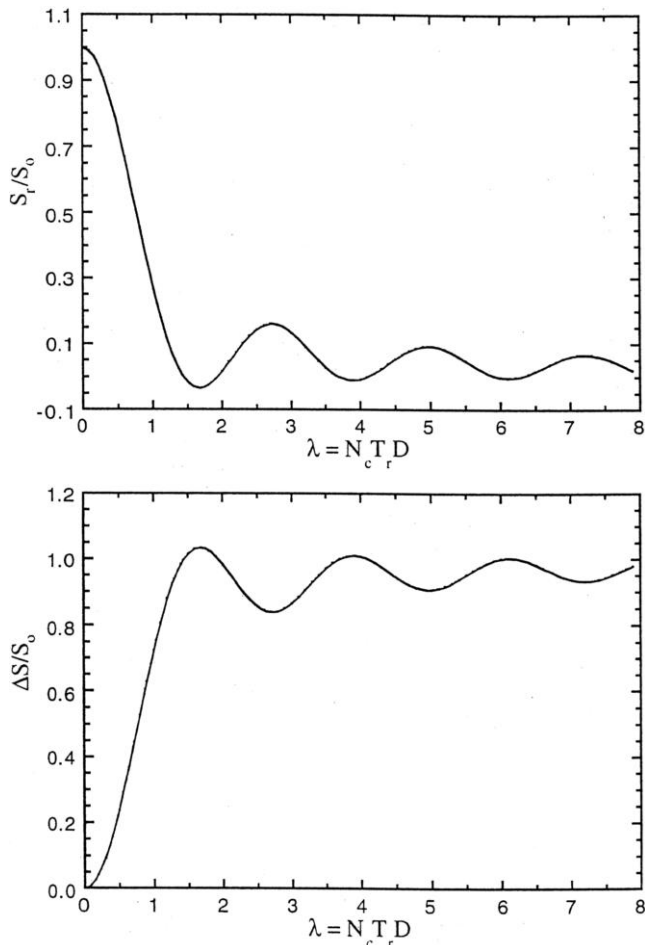


**Fig. 9.13** REDOR master curves for an isolated dipolar-coupled spin pair showing the dependence of the ratios  $S_r/S_0$  and  $\Delta S/S_0$  upon the product of the evolution time and the heteronuclear dipolar coupling. (Reproduced from [62].)

nuclear dipolar coupling between the spin pair under consideration. It is of course advisable to determine two or more  $S_r$  values to ensure the reliability of the analysis. Since the dipolar coupling depends on the internuclear distance to the inverse cubed power (see Appendix), this method allows the determination of internuclear distances for heteronuclear spin pairs.

A number of interesting applications of the REDOR method have been presented (see Table 1 of [9]), with a particular emphasis on samples of biological relevance. A specific example is shown in Fig. 9.14, where the distance be-

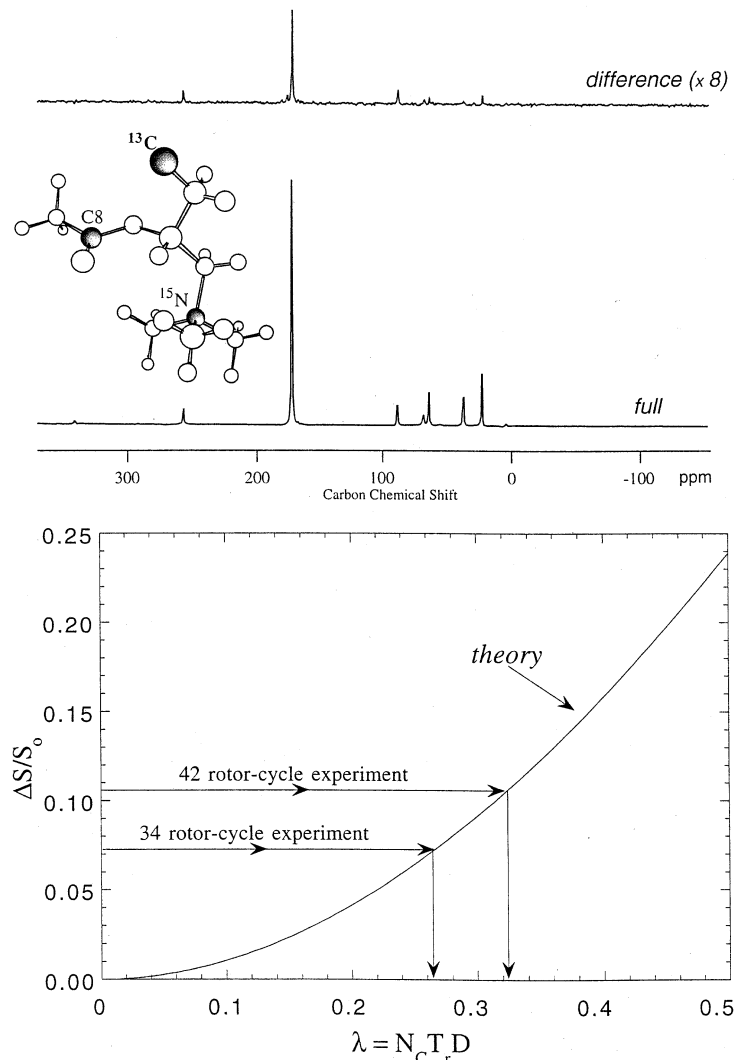


**Fig. 9.14** The determination of the distance between the specific spin labels in [<sup>1</sup>-<sup>13</sup>C, <sup>15</sup>N]acetyl-L-carnitine by the REDOR technique. The difference,  $\Delta S$ , and reference,  $S_0$ , REDOR spectra are shown for the 34- $\tau_R$  experiment. (Reproduced from [62].)

tween the specific spin labels in [ $1\text{-}^{13}\text{C}$ ,  $^{15}\text{N}$ ]acetyl-L-carnitine is determined to be 0.496 nm [62]. In this particular case, a distance determination was possible even though the C1 resonance is not resolved from that of the indicated C8 carbon. As well as  $^{13}\text{C}$  and  $^{15}\text{N}$ , other spin  $I = 1/2$  nuclei studied by REDOR include  $^{19}\text{F}$ ,  $^{29}\text{Si}$ , and  $^{31}\text{P}$ . For example, Holl et al. have demonstrated the measurement of a 0.8 nm  $^{13}\text{C}$ – $^{19}\text{F}$  internuclear distance in a nine-residue fragment of the peptide antibiotic emerimicin [63]. Extensions of the REDOR method to measure distances where one or even both of the nuclei are quadrupolar have also been proposed. For quadrupolar nuclei, the large quadrupolar interactions present significant problems, in particular a simple  $180^\circ$  pulse does not achieve a uniform inversion for all crystallites for the case of a broad quadrupolar lineshape. Various methods, e.g. TRAPDOR [64] and REAPDOR [65], have been introduced which attempt to address this problem.

#### 9.4.2

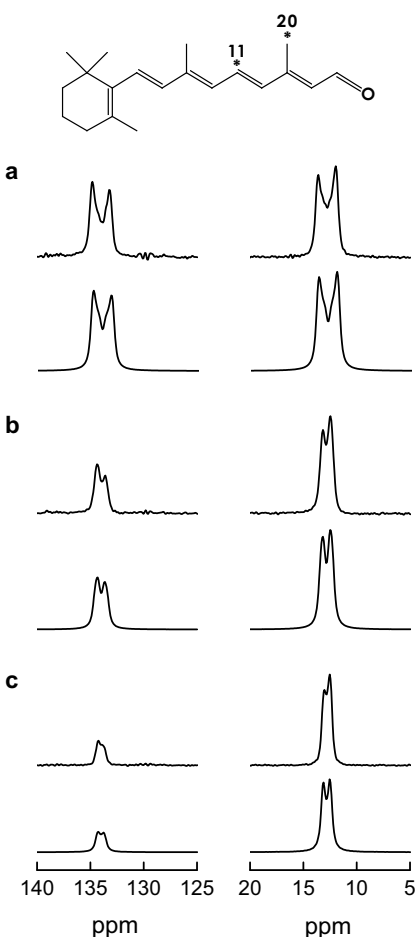
#### Homonuclear Dipolar-coupled Spins

There are small but important differences between the evolution of a given spin under a homonuclear as opposed to a heteronuclear dipolar coupling [3–5]. As a consequence, a different methodology is required for the determination of the internuclear distance between a homonuclear dipolar-coupled pair of spins.

Rotational resonance (RR) is an intriguing phenomenon which is observed when  $\nu_R$  is equal to a small integer multiple of the difference in the isotropic chemical shift frequencies of two resonances in the spectrum [66, 67]. The most apparent effect of RR is that the normally narrow spectral peaks acquire splittings and broadenings, the nature of which depend on the dipolar coupling between the two spins. As a specific example, experimental spectra (together with best-fit simulations) corresponding to the  $n = 1$ , 2, and 3 RR conditions for all-*E*-[11,20- $^{13}\text{C}_2$ ]-retinal are shown in Fig. 9.15 [68]. In this case, it was possible to determine that the internuclear distance between the two  $^{13}\text{C}$  labels is  $0.301 \pm 0.008$  nm.

In the last decade, a large number of methods for recoupling the homonuclear dipolar coupling have been developed, with specific examples including DRAMA [69], RFDR [70], HORROR [71], C7 [72], BABA [73], DRAWS [74] and DREAM [75] (for a comprehensive account see [8, 9]). We note that Levitt and coworkers have recently introduced a very helpful classification system, based on symmetry principles, which explains how many of these sequences work and provides a framework for generating other sequences [30, 76]. Rather than allowing the accurate determination of internuclear distances, these sequences, as will be illustrated in Section 9.5, are usually employed to establish correlations or to select dipolar-coupled spin pairs in multi-dimensional homonuclear experiments.

**Fig. 9.15**  $^{13}\text{C}$  rotational-resonance experimental spectra (top), together with best-fit simulations (bottom), corresponding to the  $n =$  (a) 1, (b) 2, and (c) 3 RR conditions for all-*E*-[11,20- $^{13}\text{C}_2$ ]-retinal. (Reproduced by permission of Elsevier Science Publishers from [68].)



#### 9.4.3

##### The CSA: CODEX

It was stated above that MAS causes the evolution under the CSA to be refocused at the end of each  $\tau_{\text{R}}$ . If a  $180^\circ$  pulse is applied every  $\tau_{\text{R}}/2$ , the refocusing of the CSA evolution is prevented (the same principle applies for the case of the heteronuclear dipolar coupling in the REDOR experiment (see Section 9.4.1) or the homonuclear dipolar coupling in the RFDR [70] sequence). Recently, deAzevedo et al. have shown how an experiment incorporating two periods of such CSA recoupling separated by a mixing time,  $\tau_m$ , allows the detection of slow dynamic processes [77, 78]. The method is applicable at fast MAS, and is termed centreband-only detection of exchange (CODEX). The principle of the experiment is that a loss of signal intensity is observed if the orientation of the CSA tensor for a particular carbon changes during  $\tau_m$ . By subtracting the signal intensity from that measured in a reference experiment, a pure-exchange CODEX spectrum is obtained.

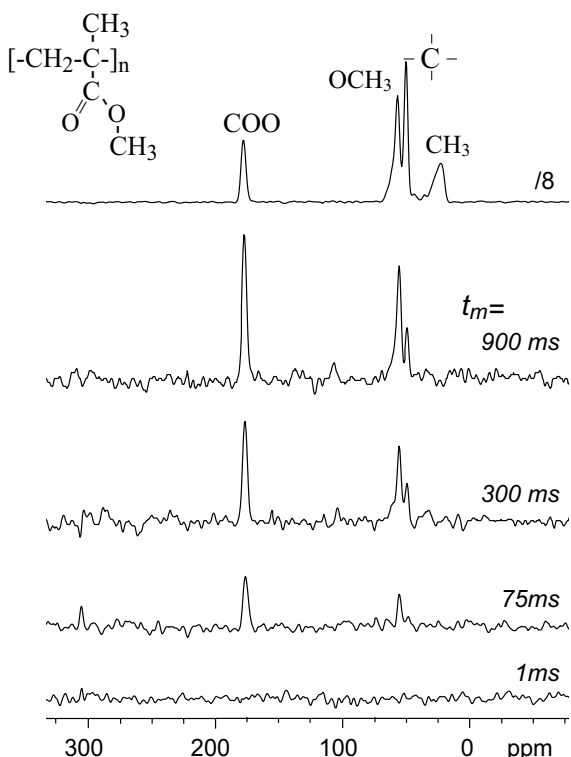


**Fig. 9.16** Pure-exchange CODEX  $^{13}\text{C}$  NMR spectra, recorded for a sample of amorphous PMMA, (at natural abundance in  $^{13}\text{C}$ ) at 300 K with different  $\tau_m$ . A  $^{13}\text{C}$  CP MAS spectrum is shown at the top. (Reproduced by permission of the American Chemical Society from [77].)

As a specific example, Fig. 9.16 shows pure-exchange CODEX  $^{13}\text{C}$  NMR spectra, recorded for a sample of amorphous poly(methyl methacrylate), PMMA, (at natural abundance in  $^{13}\text{C}$ ) at 300 K with different  $\tau_m$  [77]. For the very small mixing time,  $\tau_m$ , of 1 ms, no intensity is observed, indicating the absence of dynamics on this timescale. For a longer  $\tau_m$ , intensity is seen to build up at the COO and OCH<sub>3</sub> positions as well at the quaternary C position due to side group and backbone motion, respectively, in the polymer. From a series of CODEX experiments, it is possible to determine the reorientation angle, the correlation time, as well as the fraction of mobile segments.

## 9.5 Homonuclear Two-dimensional Experiments

The importance of solution-state NMR today owes much to the extension of the experiment to a second (and higher) dimension [1]. Two-dimensional (2D) NMR spectroscopy is also of much significance in solid-state NMR. In attempting to classify the many important different 2D solid-state NMR experiments which have been proposed to date, we make, in this article, a distinction between homonuclear (i.e., those involving only one kind of nucleus) and heteronuclear experiments.

## 9.5.1

**Establishing the Backbone Connectivity in an Organic Molecule**

In Section 9.3.1, the problem of assigning the many resolved  $^{13}\text{C}$  resonances in a 1D MAS spectrum was mentioned, and 1D spectral editing methods were introduced. In this section, we describe homonuclear  $^{13}\text{C}$ – $^{13}\text{C}$  2D correlation experiments in which a selection is usually made such that 2D peaks are only observed for pairs of directly-bonded carbons (or at least these peaks are significantly more intense). In this way, it is possible to trace out the connectivity along the backbone of the organic molecule, and thus assign the  $^{13}\text{C}$  resonances. As a consequence of the significant sensitivity problems associated with the very low probability of finding a pair of directly bonded  $^{13}\text{C}$  nuclei in a sample at natural abundance, these experiments are usually performed on fully or partially  $^{13}\text{C}$ -enriched (normally globally, i. e. at all carbon positions) samples.

In the first class of  $^{13}\text{C}$ – $^{13}\text{C}$  2D correlation experiments described here, SQ coherence (SQC), i. e., that which is detected in a conventional 1D NMR experiment, evolves in both dimensions of the NMR experiment. A mixing time is inserted between the two evolution periods during which a pulse sequence is applied which recouples the homonuclear dipolar coupling (see Section 9.4.2), such that coherence transfer occurs between  $^{13}\text{C}$  nuclei which are close together in space. As a specific example, Fig. 9.17 shows the region corresponding to the  $\text{C}_\alpha$  and aliphatic side-chain carbons of a  $^{13}\text{C}$ – $^{13}\text{C}$  SQ–SQ correlation spectrum of  $^{13}\text{C}$  globally-labelled antanamide (a cyclic decapeptide), recorded using the DREAM [75] recoupling sequence. The indicated negative off-diagonal peaks are due to one-bond correlations among the aliphatic side-chains.

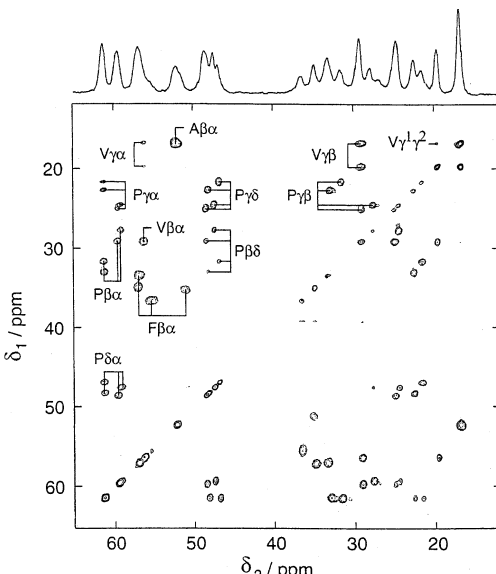


**Fig. 9.17** The region corresponding to the  $\text{C}_\alpha$  and aliphatic side-chain carbons of a  $^{13}\text{C}$ – $^{13}\text{C}$  SQ–SQ correlation spectrum of  $^{13}\text{C}$  globally-labelled antanamide (Val-Pro-Pro-Ala-Phe-Phe-Pro-Pro-Phe-Phe), recorded at a magnetic field of 14.1 T and  $\nu_R = 30$  kHz. Mixing was achieved using a DREAM [75] recoupling sequence of duration 7 ms. Positive and negative peaks are shown as dark- and light-shaded lines, respectively. The indicated negative off-diagonal peaks are due to one-bond correlations among the aliphatic side-chains. (Courtesy of B. H. Meier.)

By using very-high magnetic fields, ever larger biopolymers are becoming accessible to solid-state NMR. As an example, Fig. 9.18 presents a  $^{13}\text{C}$ – $^{13}\text{C}$  SQ–SQ correlation spectrum of a solid 62 residue  $^{13}\text{C}$  and  $^{15}\text{N}$  globally-labelled protein containing the  $\alpha$ -spectrin SH3 domain, recorded at 17.6 T [79]. In this case, mixing was achieved using proton-driven spin diffusion; a long mixing time of 15 ms was employed such that longer-range correlations are also observed. Using this and other experiments, it was possible to assign all the  $^{13}\text{C}$  and  $^{15}\text{N}$  resonances.

Emsley and co-workers have recently suggested an alternative approach for establishing carbon–carbon connectivities, namely the solid-state INADEQUATE experiment [80]. It is so termed because of the analogy to the solution-state experiment of the same name [81]. Unlike the experiments described above which utilise through-space dipolar couplings, this approach is based on the through-bond  $J$  coupling. A further important difference is that double-quantum (DQ) coherence (DQC) as opposed to SQC evolves during the  $t_1$  (or indirect) dimension of the experiment. Experiments involving the creation of DQC and multiple-quantum coherence (MQC) in general are of much importance in both solution-state and solid state NMR. For example, in pioneering work, Pines and co-workers have shown that the analysis by so-called spin-counting experiments of the very high MQC orders excitable in static  $^1\text{H}$  solid-state NMR provides valuable information about large clusters (often up to 100 nuclei) of dipolar-coupled protons [82, 83].

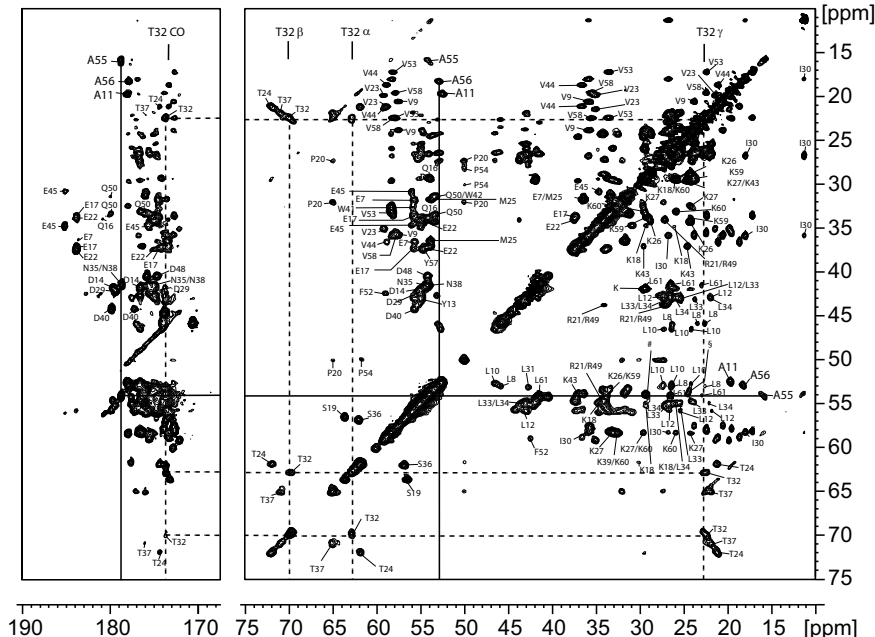
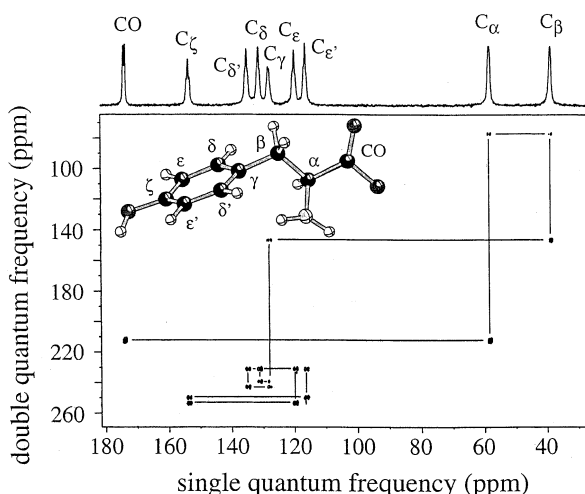


**Fig. 9.18** A 2D  $^{13}\text{C}$ – $^{13}\text{C}$  SQ–SQ correlation spectrum of a solid 62 residue  $^{13}\text{C}$  and  $^{15}\text{N}$  globally-labelled protein containing the  $\alpha$ -spectrin SH3 domain, recorded at 17.6 T. Mixing was achieved using proton-driven spin diffusion; a long mixing time of 15 ms was employed such that longer-range correlations are also observed. (Reproduced from [79].)

**Fig. 9.19** A 2D  $^{13}\text{C}$ – $^{13}\text{C}$  INADEQUATE spectrum of L-tyrosine.



For a detailed discussion of the concept of MQC, the reader is referred to e.g., [1, 84]. Here, we simply note two relevant features: firstly, a MQC cannot be directly detected in an NMR experiment, i.e., an experiment involving a MQ evolution period is inherently at least 2D, since the MQC must be converted into detectable SQC; and, secondly, for spin  $I=1/2$  nuclei, MQC can only be created for coupled nuclei. As illustrated by the specific example of L-tyrosine in Fig. 9.19, an advantage over the SQ–SQ correlation spectra in Fig. 9.17 and 9.18 is the absence of signal along the diagonal. Furthermore, by using the  $J$  coupling, the observation of a pair of correlated peaks can only be due to directly-bonded  $^{13}\text{C}$  nuclei. However, the signal-to-noise ratio (S/N) of the  $J$ -coupled INADEQUATE experiment is invariably worse than that of the dipolar-based experiments used for Fig. 9.17 and 9.18, although refocused INADEQUATE experiments [85, 86] reduce the signal loss and are applicable to disordered systems.

### 9.5.2 Dipolar-mediated Double-quantum Spectroscopy

DQ spectroscopy is not only useful for homonuclear  $^{13}\text{C}$ – $^{13}\text{C}$  correlation experiments which allow the identification of the backbone connectivity. In this section, the utility of other 2D DQ experiments which provide insight into, e.g., through-space proximities will be illustrated. As opposed to the solid-state INADEQUATE experiment introduced in the previous section, the experiments described in this section are based on the dipolar as opposed to the  $J$  coupling of spins.

A  $^1\text{H}$  2D DQ MAS spectrum [87] recorded in a rotor-synchronised fashion in  $t_1$  (i.e., the  $t_1$  increment is set equal to one rotor period such that all spinning sidebands in the DQ dimension ( $F_1$ ) fold back onto the centreband position) is shown in Fig. 9.20a. To create DQC as well as to allow its conversion into observable SQC, the BABA [73] recoupling sequence (see Section 9.4.2) was used. This is a robust

sequence which is suitable for the fast  $v_R$  of 35 kHz employed. The ability of the  $^1\text{H}$  DQ MAS experiment to identify proton–proton proximities lies in the fact that both the excitation and subsequent reconversion of DQC relies on the presence of a dipolar coupling between a particular two spins. Since the dipolar coupling is proportional to the internuclear distance to the inverse cubed power, a peak is, hence, only observed in the DQ MAS spectrum if the corresponding two protons are close together in space. As a rule of thumb, the presence of a peak in a  $^1\text{H}$  DQ MAS spectrum implies a proton–proton proximity of under 0.35 nm.

For this particular example, which corresponds to the aromatic protons of an alkyl-substituted polycyclic aromatic system ( $\text{HBC-C}_{12}$ ) [48], three resonances (labelled A, B, and C) can be identified in the corresponding 1D  $^1\text{H}$  (500 MHz) MAS spectrum, which is shown at the top of Fig. 9.20a. The six possible DQ peaks in this case are shown in Fig. 9.20b. Since the DQ frequency corresponding to a given DQC is simply the sum of the two SQ frequencies, DQCs between like (AA) and unlike (AB) spins can, in general, be distinguished in that, in the former

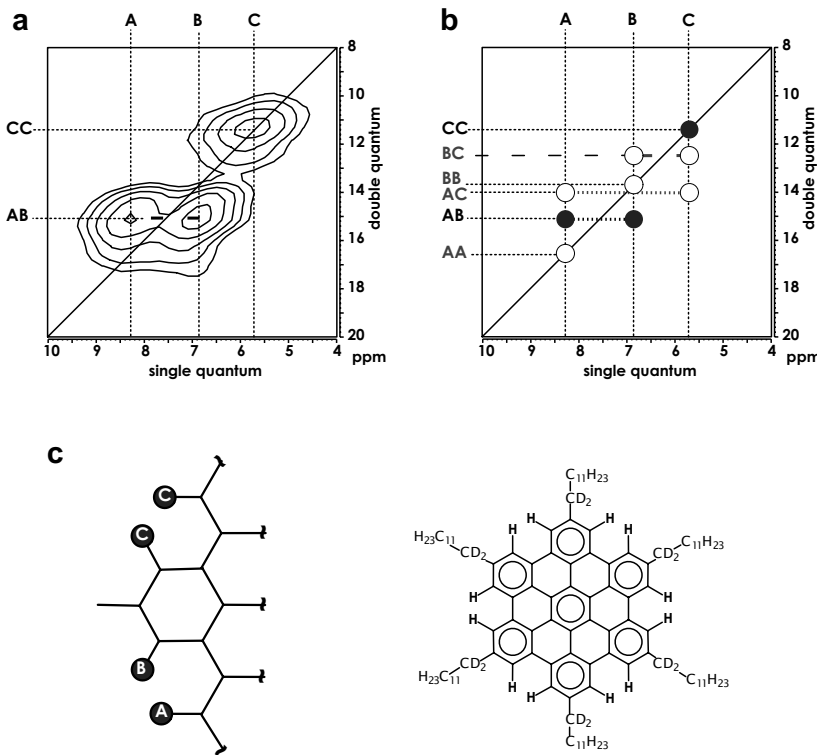


**Fig. 9.20** (a) A representative rotor-synchronised  $^1\text{H}$  DQ MAS spectrum, corresponding to the aromatic protons in  $\text{HBC-C}_{12}$ . (b) A schematic representation showing the positions of the six possible DQ peaks; the observed AB and CC peaks (filled circles) imply the proton–proton proximities indicated in (c). (Reproduced by permission of Elsevier Science Publishers from [49].)

case, a single peak at  $(2\nu_A, \nu_A)$  is observed, while, in the latter case, two peaks at  $(\nu_A + \nu_B, \nu_A)$  and  $(\nu_A, \nu_B + \nu_B)$  are observed. (The notation  $(\nu_1, \nu_2)$  refers to a DQ peak centred at  $\nu_1$  and  $\nu_2$  in the  $F_1$  and  $F_2$  dimensions, respectively.) Note that for the anisotropic dipolar coupling, it is, unlike for the isotropic  $J$  coupling, possible to observe an auto peak for a DQC between two like spins. It should be noted that an advantage of the DQ approach over a spin diffusion experiment [4,88] in which a mixing time is inserted between two SQ evolution periods is that an auto peak is only observed if there is a close proximity of two protons. By contrast, in the spin diffusion experiment, strong auto peaks are seen for all resonances, regardless of whether there is a close proximity.

Of the six possible DQ peaks, only two, namely AB and CC, are observed in the experimental spectrum in Fig. 9.20a. For this system, the aromatic protons are arranged into well-isolated pairs of 'bay protons'; the observed DQ peaks thus correspond to these bay protons pairs. As discussed in [48], the implied presence of only two types of pairs of aromatic protons,  $H_A-H_B$  and  $H_C-H_C$  (see Fig. 9.20c) is a consequence of intermolecular ring current effects; for an isolated molecule, the six-fold symmetry leads to all aromatic protons being equivalent. Using quantum-chemical calculations of  $^1H$  chemical shifts, the experimental data could be assigned in a fully quantitative manner to a particular structural model [89]. Such effects of ring currents on NMR chemical shifts are, of course, well established [90]; however, it is only recently, with the development of solid-state NMR methods allowing the resolution of  $^1H$  resonances, that the widespread importance of these effects in organic solids is gaining attention; other clear examples of the phenomenon can be found in, e.g., [91, 92]. It is to be noted that, although the absolute shifts due to ring currents are similar for both  $^1H$  and  $^{13}C$ , the much smaller range of chemical shifts (~20 ppm as opposed to 200 ppm) means that the influence is much more evident in  $^1H$  NMR. In addition, protons are normally located at the more exposed parts of the structure.

$^1H$  NMR is well suited for the investigation of hydrogen bonding, with it being well known that hydrogen bonding leads to a marked lowfield (to a high ppm value) chemical shift. For example, for a general hydrogen bond O–H...O, a clear correlation between the  $^1H$  isotropic chemical shift and the hydrogen-bond strength as given by the O...H and O...O distances determined by single-crystal diffraction studies has been established [93–95]. By identifying specific proton–proton proximities, rotor-synchronised 2D  $^1H$  DQ MAS spectra have been shown to differentiate between distinct hydrogen-bonded structures [47].

Applications of dipolar-mediated DQ spectroscopy are not limited to  $^1H$  NMR. For example,  $^{31}P$ – $^{31}P$  DQ MAS spectra have provided valuable insight into the structure of inorganic phosphates [96] and glasses [97]. In addition, Nielsen et al. and Hong have presented dipolar analogues of the  $J$ -coupled  $^{13}C$ – $^{13}C$  DQ MAS correlation experiment described in Section 9.5.1 [98, 99]. Finally, we note that Schmidt-Rohr and co-workers have elegantly demonstrated that 2D  $^{13}C$ – $^{13}C$  DQ spectra recorded for static samples can identify the chain conformation statistics for  $^{13}C$ -labelled polymer samples [100]. Remembering that the frequency of a given  $^{13}C$  resonance depends on the orientation of the CSA tensor (see Section

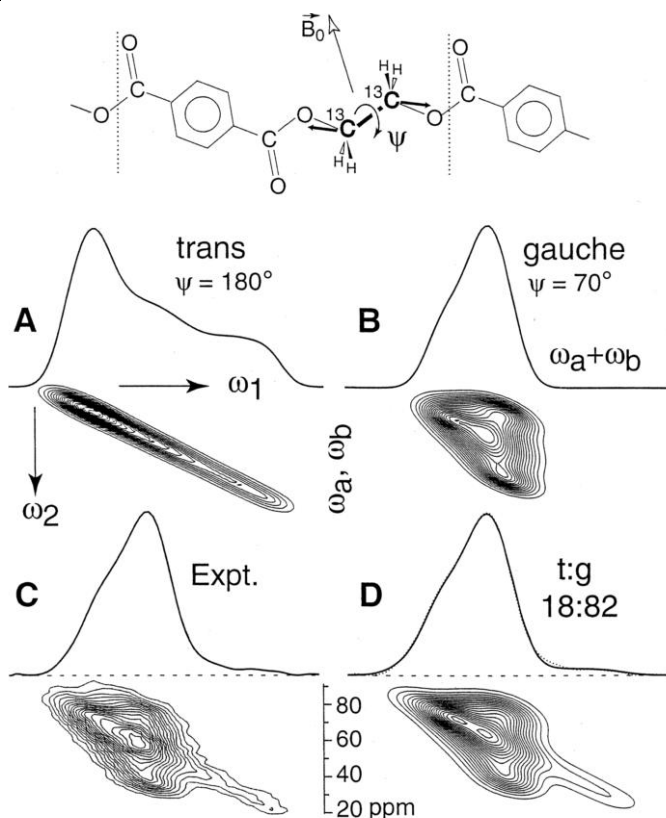


**Fig. 9.21** 2D  $^{13}\text{C}$ - $^{13}\text{C}$  DQ static spectra allow the determination of the chain conformation statistics for  $^{13}\text{C}$ -labelled polymer samples. The simulated spectra show that (A) *trans* and (B) *gauche* conformations lead to very different 2D DQ powder spectra. For the experimental spectrum (C) obtained for amorphous PET, a best-fit simulation (D) revealed a 18:82 *trans*:*gauche* distribution. (Reproduced by permission of the American Association for the Advancement of Science from [100].)

9.2.1), the method relies on the fact that the adoption of a particular torsional angle along the chain results in DQ peaks for only specific pairs of  $^{13}\text{C}$  frequencies. As illustrated in Fig. 9.21, *trans* and *gauche* conformations lead to very different 2D DQ powder spectra, and it was thus possible to quantitatively determine the conformation statistics for a sample of amorphous poly(ethylene terephthalate) (PET).

### 9.5.3

#### High-resolution $^1\text{H}$ Solid-state NMR

The previous section has illustrated that the resolution in a  $^1\text{H}$  DQ MAS spectrum provided by a combination of very-fast MAS and a high magnetic field as well as the extension to a second frequency dimension is sufficient to allow the differentiation of some particular  $^1\text{H}$  resonances. However, as noted in Section 9.3.2, the

line narrowing achieved by MAS alone at a  $\nu_R$  equal to 30 kHz is still far from the limiting case, where all residual dipolar broadening has been removed. Section 9.3.2 also briefly introduced experiments which provide homonuclear  $^1\text{H}$  decoupling by combining multiple (rf) pulse sequences with MAS. In this section, we demonstrate that a marked line narrowing as compared to MAS alone can be achieved by this CRAMPS approach.

In this section, we consider “windowless” homonuclear decoupling sequences. Specific examples are the Lee–Goldburg (LG) technique [101] and refinements, namely the frequency switched and phase-modulated LG (FSLG [102, 103] and PMLG [104]) sequences, as well as the computer-optimised sequence, DUMBO-1

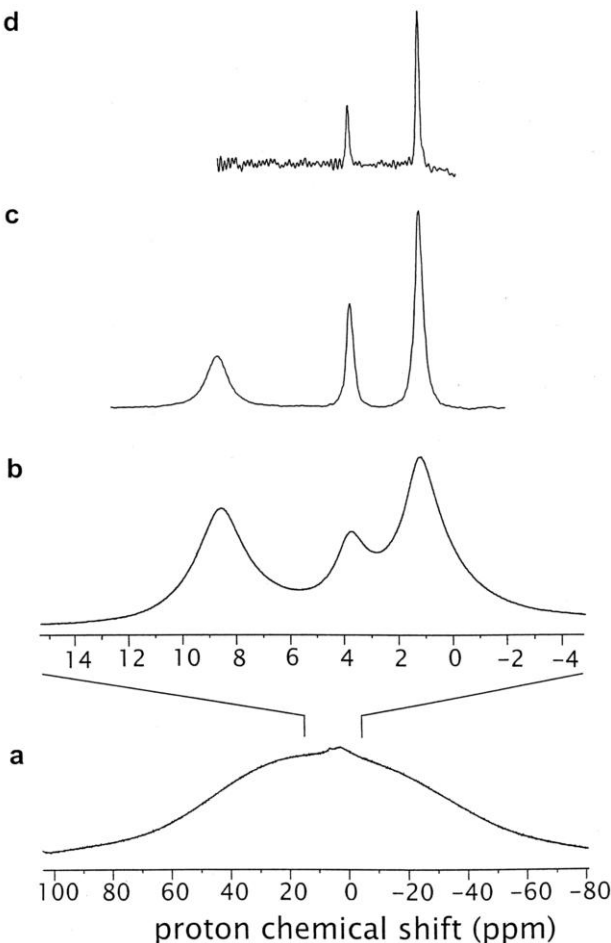


**Fig. 9.22**  $^1\text{H}$  (500 MHz) NMR spectra of natural abundance powdered L-alanine, recorded with (a and b) a one-pulse experiment for (a) a static sample and (b) under MAS at a  $\nu_R = 30$  kHz, (c) the 2D FSLG ( $\nu_R = 12.5$  kHz) experiment, and (d) the CT-CRAMPS ( $\nu_R = 12.5$  kHz) experiment using FSLG decoupling. (Reproduced by permission of the American Chemical Society from [106].)

[105]. For a discussion of these different decoupling sequences, the interested reader is referred to, e.g., [7]. Such sequences are so-called because no windows during which acquisition of the FID would be possible are built into the sequence. NMR experiments incorporating evolution under the application of a windowless homonuclear decoupling are thus inherently multi-dimensional. For example, Vinogradov et al. have presented a 2D experiment in which a high-resolution  $^1\text{H}$  dimension, incorporating PMLG homonuclear decoupling, is correlated with  $^1\text{H}$  acquisition, with only moderate MAS (10–15 kHz) providing line narrowing in the direct dimension [104].

Using Lee–Goldburg based decoupling methods, a FWHMH of 150–170 Hz has been reported for the aliphatic  $^1\text{H}$  resonances in L-alanine [106]; this is demonstrated in Fig. 9.22c, where, for comparison, the (a) static and (b) MAS ( $\nu_R = 30$  kHz) spectra are also shown. Lesage et al. have further shown that the frontiers of high-resolution  $^1\text{H}$  solid-state NMR can be pushed back yet further; using the constant-time (CT) CRAMPS experiment [106] a FWHMH as low as 60 Hz can be obtained for the aliphatic resonances in L-alanine (see Fig. 9.22d).

#### 9.5.4

#### Anisotropic–Isotropic Correlation: The Measurement of CSAs

In section 3.1, it was stated that it is possible to extract the anisotropy and asymmetry of the CSA by fitting the observed MAS sideband intensities. It is, however, necessary to be able to resolve, at a low  $\nu_R$ , the sidebands of the different resonances. The problem of the 1D spectrum becoming increasingly more crowded as the number of distinct resonances increases can be overcome by extending the NMR experiment to a second dimension.

In a first class of experiment, a 2D spectrum is obtained in which a separate anisotropic powder lineshape (corresponding to either the static case or a slow spinning frequency) is associated with each resolved resonance in an isotropic dimension. Two elegant approaches have been presented by which this can be achieved, namely magic-angle hopping (MAH) [107] and magic-angle turning (MAT) [108]. In the MAH experiment,  $t_1$  consists of the sample making three hops of  $120^\circ$  about an axis inclined at the magic angle to  $B_0$ , with a period of evolution of the same incremented duration (during which the sample is static) before each hop. In this way, the evolution periods correspond to each crystallite adopting three orthogonal positions relative to  $B_0$ ; for this case, it can be shown that the average chemical shift evolution equates to the isotropic chemical shift. The same effect is achieved in the MAT experiment under conditions of very slow (typically < 100 Hz) continuous sample rotation by rotations in spin space, i.e., by the application of rf pulses. Moreover, related experiments such as switched angle sample spinning (SASS) [109, 110] and variable angle correlation spectroscopy (VACSY) [111], which involve a change in the orientation of the rotor axis with respect to  $B_0$ , have also been presented.

For the original MAH and MAT techniques, a significant drawback was the long measuring time (1–2 days) that was required even when up to 5 g of sample was used. However, modified versions of the MAT approach employing  $180^\circ$  rather than

90° pulses and using a faster  $v_R$  have been presented, which offer a better experimental sensitivity [112, 113]. For example, Fig. 9.23 shows the anisotropic CSA patterns for each resolved resonance in a selected region of the isotropic  $^{13}\text{C}$  spectrum of the terpene verbenol [114]. Six resonance lines are resolved for both the C2 and C3 carbons, with the CSA tensor spinning-sideband patterns being remarkably similar. Supported by quantum-chemical calculations of the  $^{13}\text{C}$  CSA tensors, the solid-state NMR analysis demonstrated that verbenol exhibits polymorphism, with, however, only minor conformational variations in the distinct

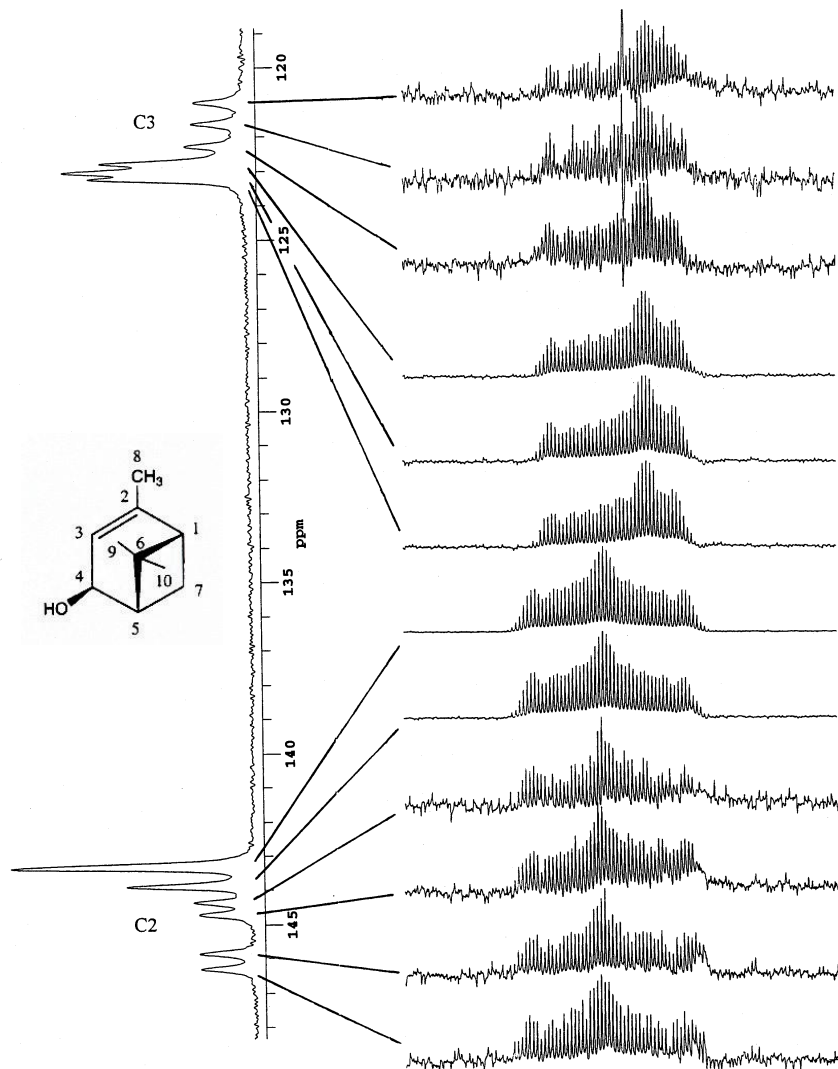


**Fig. 9.23** The anisotropic CSA patterns for each resolved resonance in a selected region of the isotropic  $^{13}\text{C}$  spectrum as obtained from a FIREMAT experiment recorded for a sample of the terpene verbenol. (Reproduced by permission of the American Chemical Society from [114].)

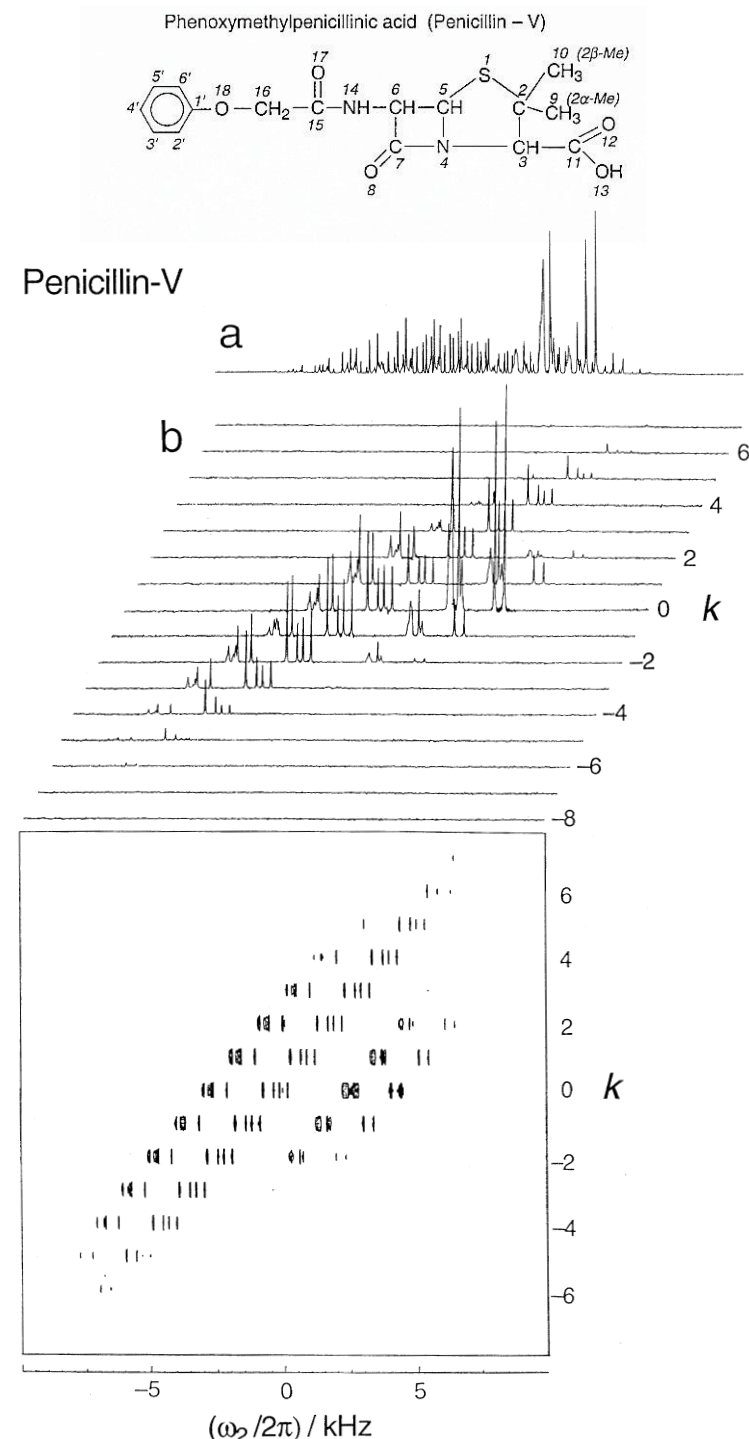


**Fig. 9.24** A 2D  $^{13}\text{C}$  PASS spectrum recorded for the antibiotic, penicillin-V. The 1D CP MAS spectrum is shown in (a). (Reproduced by permission of Academic Press from [116].)

solid-state environments. It is to be noted that single crystals suitable for an X-ray diffraction analysis could only be obtained for the major crystalline form.

An alternative means by which the isotropic and anisotropic chemical shift interactions can be separated is the 2D PASS (phase-adjusted spinning sidebands) experiment due to Levitt and co-workers [115]. By changing the timings of the application of five  $\pi$  pulses in the  $t_1$  dimension, it is possible to separate the spinning sidebands by order. As a specific example, Fig. 9.24 shows the 2D  $^{13}\text{C}$  PASS spectrum for the antibiotic, penicillin-V. [116] An analysis of this spectrum allowed the determination of the CSA principal values for all the  $^{13}\text{C}$  resonances. A distinct advantage of this approach is that only very few (typically 16) increments must be made in the indirect dimension.

### 9.5.5

#### The Investigation of Slow Dynamics: 2D Exchange

The basic principle of 2D exchange NMR involves the measurement of the frequency of the same molecular segment at two different times. A slow dynamic process is detected on account of the change, during a mixing time between the two evolution periods, in the NMR frequency caused by a reorientation of the molecular segment. In this section, we describe  $^2\text{H}$  static and  $^{13}\text{C}$  MAS 2D exchange experiments [4].

In static  $^2\text{H}$  2D exchange NMR, advantage is taken of the simplification resulting from both the presence of a single  $^2\text{H}$  resonance and the fact that the quadrupolar interaction dominates (see Section 9.2.4). Without any slow dynamics in the mixing time, the frequency of each molecular segment remains unchanged, and the intensity in the 2D frequency-domain spectrum is restricted to a ridge along the  $v_1 = v_2$  diagonal. If a reorientation occurs, off-diagonal intensity is observed as a consequence of the frequency change. In particular, a well-defined motion yields an elliptical off-diagonal pattern which is characteristic of the reorientation angle. The beauty of the static  $^2\text{H}$  exchange experiment is illustrated in Fig. 9.25, which shows a spectrum recorded for a sample of methyl-deuterated isotactic polypropylene (iPP) [117]. The observed elliptical ridges are characteristic of the helical chain reorientation illustrated in the inset.

A 2D exchange experiment can also be recorded under MAS, although care must be taken to ensure that pure absorption-mode spinning sidebands are obtained. As compared to a static experiment, both the resolution and sensitivity are improved, which is of much importance for  $^{13}\text{C}$  NMR. These gains are, however, at the expense of the ease with which information about the reorientation process can be accessed. As in the static case, a reorientation is associated with the observation of off-diagonal intensity. As a specific example, Fig. 9.26 presents a  $^{13}\text{C}$  2D MAS exchange spectrum recorded for polyoxymethylene (POM) [118]. In addition to probing the motion of a particular molecular moiety, 2D exchange experiments are well suited to the investigation of slow chemical exchange processes; for example, Titman et al. have studied the hydrogen shift and/or  $\pi$  flip which occurs in solid tropolone [119].

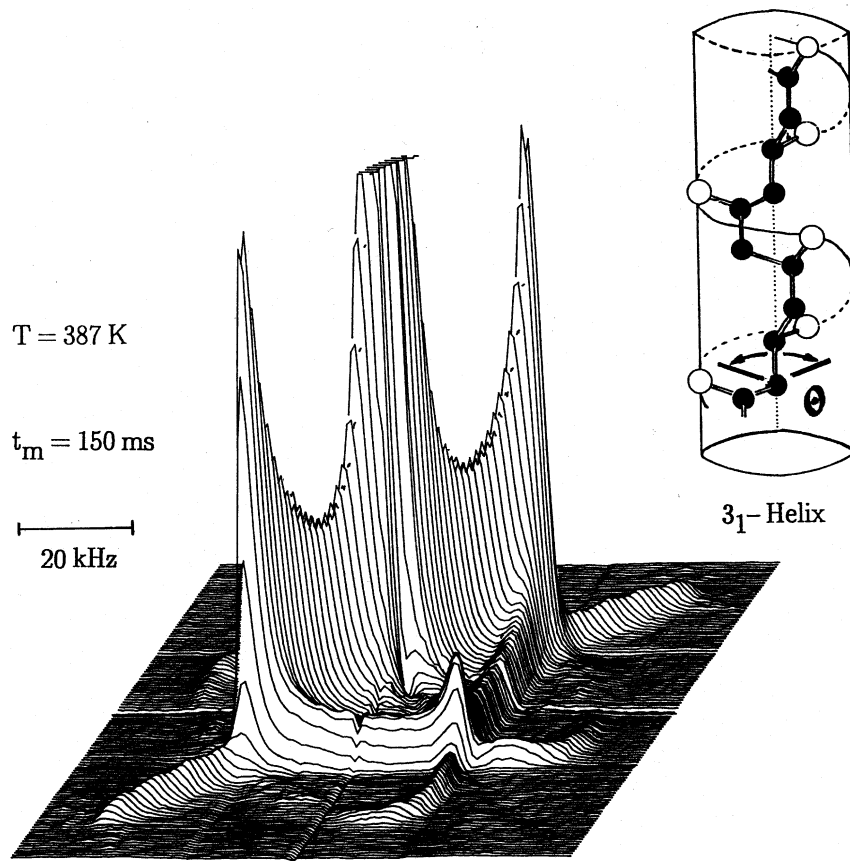


**Fig. 9.25** A static  $^2\text{H}$  exchange experiment recorded for a sample of methyl-deuterated isotactic polypropylene (iPP) at  $T = 387\text{ K}$ . The observed elliptical ridges are characteristic of the helical chain reorientation illustrated in the inset. (Reproduced by permission of the American Chemical Society from [117].)

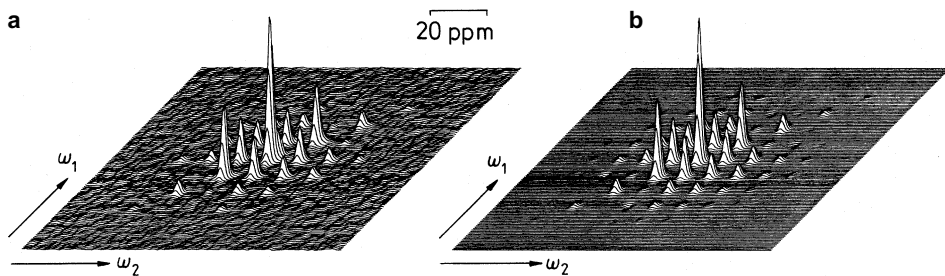


**Fig. 9.26** (a) Experimental and (b) theoretical  $^{13}\text{C}$  2D MAS pure absorption-mode exchange spectra recorded for polyoxymethylene (POM). The experimental spectrum corresponded to  $T = 360\text{ K}$  and a mixing time of 1.5 s. (Reproduced by permission of Academic Press from [118].)

## 9.5.6

 $^1\text{H}$ - $^1\text{H}$  DQ MAS Spinning-sideband Patterns

In Section 9.5.2, a rotor-synchronised  $^1\text{H}$ - $^1\text{H}$  DQ MAS spectrum was presented (Fig. 9.20). The 2D DQ MAS can be performed in an alternative fashion; if the  $t_1$  increment is reduced, which corresponds to an increase in the DQ spectral width, a DQ MAS spinning-sideband pattern is observed [120, 121]. Such DQ MAS sideband patterns exhibit characteristic unusual features. In particular, the observed patterns are very sensitive to the product of the dipolar coupling constant,  $D$ , and the recoupling time,  $\tau_{\text{rcpl}}$ , with an increase in this product leading to the appearance of higher-order spinning sidebands.

Importantly, since  $\tau_{\text{rcpl}}$  is known, the absolute value of  $D$  can be extracted by an analysis of DQ MAS spinning-sideband patterns. As a specific example, Fig. 9.27 presents experimental  $^1\text{H}$ - $^1\text{H}$  DQ MAS spinning sideband patterns for the aromatic protons in (a) the crystalline and (b) the LC phases of the same alkyl-substi-

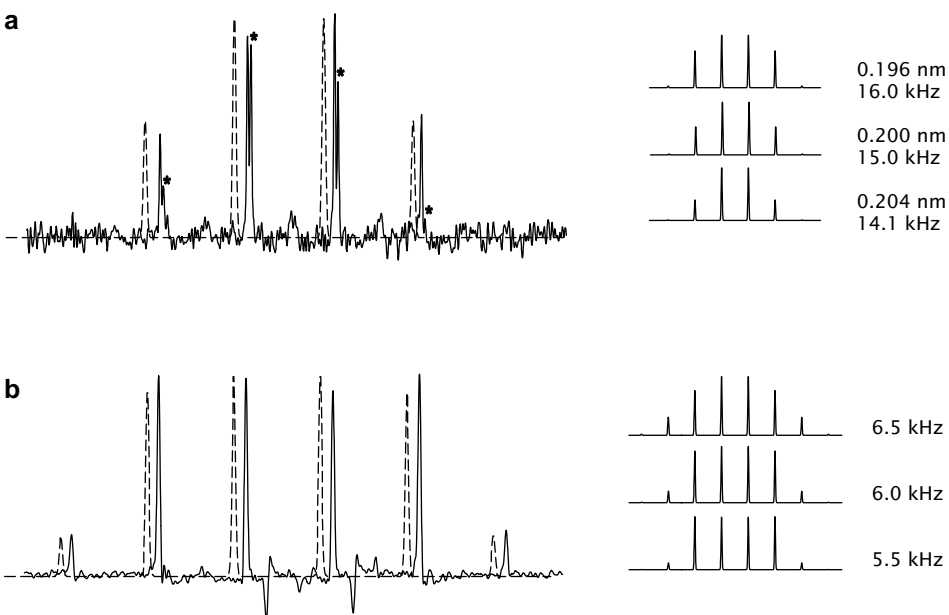


**Fig. 9.27** Extracted columns from  $^1\text{H}$  (500.1 MHz) DQ MAS spectra of HBC-C<sub>12</sub>, showing the DQ spinning sideband patterns for (a) the aromatic protons at 8.3 ppm in the solid phase ( $T = 333\text{ K}$ ), and (b) the aromatic protons at 6.2 ppm in the LC phase ( $T = 386\text{ K}$ ). In each case, best-fit spectra, generated according to the analytical expression for a spin pair, are shown (shifted to the left to allow a better comparison) as dotted lines. A spinning frequency,  $v_R$ , equal to 35 and 10 kHz was used for

the solid and LC phases, respectively, with the two rotor-period compensated BABA recoupling sequence being used for the excitation and reconversion of DQCs in both cases. In (a), additional peaks corresponding to DQCs between aromatic and residual undeuterated  $\alpha$ -carbon protons are marked by \*. The insets to the right of the experimental spectra show the sensitivity of the spinning-sideband patterns to the product  $D \tau_{\text{rcpl}}$ . (Reproduced by permission of the American Chemical Society from [48].)

tuted polycyclic aromatic system, HBC-C<sub>12</sub>, discussed in Section 5.2 [48]. The dotted lines represent best-fit spectra simulated using the analytical time-domain expression for an isolated spin pair. As is evident from the insets on the right of Fig. 9.27, the DQ MAS spinning sideband patterns are very sensitive to the product of  $D$  and  $\tau_{\text{rcpl}}$ . The best-fit spectra for the solid and LC phases then correspond to  $D/(2\pi)$ s equal to  $15.0 \pm 0.9$  and  $6.0 \pm 0.5$  kHz, respectively.

Comparing the evaluated  $D$  values for the crystalline and LC phases, a reduction of  $D$  by a factor of  $0.40 \pm 0.04$  is observed, corresponding to an order parameter [122] of  $0.80 \pm 0.08$ . This could be explained by postulating the presence of out-of-plane motion in addition to the axial rotation of the molecule about an axis perpendicular to the ring. The good agreement with the value of 0.84 obtained from an analysis of <sup>2</sup>H 1D NMR lineshapes is to be noted [123]. It is to be emphasised, however, that the <sup>1</sup>H DQ MAS method is applicable to as-synthesised samples, i.e., there is no reliance upon isotopic labelling.

As well as the investigation of dynamics, an analysis of <sup>1</sup>H DQ MAS spinning-sideband patterns can be used to determine proton–proton distances. For example, it was possible to determine that the distance between the lactam and pyrrole NH protons in the complex hydrogen-bonding arrangement in the biologically important molecule bilirubin is  $0.186 \pm 0.002$  nm [124]. In this respect, it is to be noted that structure determination by single-crystal X-ray diffraction methods, being based on the diffraction of X-rays by electrons, is not well suited to the localisation of lighter atoms. This is of particular relevance with regards to the localisation of hydrogen-bonded protons, in which case a neutron diffraction study is to be preferred [125]. Moreover, neutron diffraction is not the perfect solution: as well as the requirement for both larger crystals and very expensive facilities, the investigation of protons is complicated by their large incoherent cross section, such that deuteration, which may cause a change in the hydrogen-bonding arrangement, is often required. Thus, solid-state NMR methods which can provide inter-proton and proton–heteroatom distance constraints, by means of which the localisation of the important protons in the single crystal structure can be refined, are of much value.

Finally, we note that 1D DQ-filtered MAS experiments (corresponding to setting  $t_1 = 0$ ) can also provide insight into dynamic processes. The principle, in this case, is that signal is only observed for pairs of protons which remain dipolar coupled for the timescale of the experiment, which in this case is the time required to excite and reconvert the DQC. For example, in [126], the kinetics of hydrogen bond breaking and formation is quantitatively analysed for a carboxylic acid dimer on the basis of the fall off in the DQ intensity with increasing temperature.

## 9.6

### Heteronuclear Two-dimensional Experiments

#### 9.6.1

##### Heteronuclear Correlation

In a 2D heteronuclear correlation (HETCOR) experiment, the  $t_1$  and  $t_2$  periods correspond to the evolution of SQC of two different nuclei, e.g.,  $^1\text{H}$  and  $^{13}\text{C}$ . A number of different HETCOR experiments have been proposed which differ with respect to, e.g., the means by which coherence transfer is achieved, the type of coherence which evolves during  $t_1$ , as well as the application of homonuclear decoupling sequences.

One of the simplest HETCOR experiments is the  $^1\text{H}$ – $^{13}\text{C}$  WISE (wideline separation) experiment [127]. After the  $t_1$  period, during which  $^1\text{H}$  transverse magnetisation created by a  $90^\circ$  pulse evolves, coherence transfer to  $^{13}\text{C}$  SQC, which is detected in  $t_2$ , is achieved by a simple CP step. The experiment is performed under MAS. At a low to moderate  $\nu_R$ , a wide dipolar-broadened  $^1\text{H}$  lineshape in  $F_1$  (see Section 9.3.2) is correlated with a narrow resonance line in a well-resolved isotropic  $^{13}\text{C}$  dimension ( $F_2$ ). Remembering that motion leads to a narrowing of the  $^1\text{H}$  resonance due to the reduction in the dipolar broadening, the WISE experiment has found a number of applications in polymer chemistry on account of its ability to distinguish between rigid and mobile chemical moieties [4]. For example, in Fig. 9.28, narrow and broad lines in the  $^1\text{H}$  dimension are observed for the resonances due to the mobile poly(butyl methacrylate) (PbuA) and the rigid PMMA, respectively, in a core–shell system [128]. Furthermore, as illustrated by the investigation of onion cell-wall material in Ref. [46], the information provided by WISE spectra complements that yielded by an analysis of  $^{13}\text{C}$   $T_1$  and the  $^1\text{H}$   $T_{1p}$  relaxation times.

$^1\text{H}$ – $^{13}\text{C}$  HETCOR spectra incorporating a high-resolution  $^1\text{H}$  dimension can be achieved. As early as 1982, Caravatti et al. presented an experiment which employed a multiple-pulse sequence at a low  $\nu_R$  (as in the conventional CRAMPS approach) to achieve homonuclear decoupling in  $t_1$  [129, 130]. Recently, various alternative high-resolution HETCOR experiments applicable at a fast or a very-fast  $\nu_R$  have been proposed. Two methods which utilise the through-space dipolar coupling to achieve coherence transfer are those due to van Rossum et al. [131] and Saalwächter et al. [132, 133]. In the former case, coherence transfer occurs via CP, while FSLG  $^1\text{H}$  homonuclear decoupling (see Section 9.5.3) is applied during the evolution of transverse  $^1\text{H}$  magnetisation in  $t_1$ . This is to be compared with the latter recoupled polarisation transfer (REPT) methods, which employ REDOR recoupling under very-fast MAS (see Section 9.4.1) to create a heteronuclear SQC (HSQC) or a heteronuclear MQC (HMQC), the evolution of which is followed during  $t_1$ . The analogy to the well-known solution-state heteronuclear single-quantum correlation (HSQC) [134] and heteronuclear multiple-quantum correlation (HMQC) [135] experiments (dilute-spin, e.g.  $^{13}\text{C}$ , detected) is to be noted.

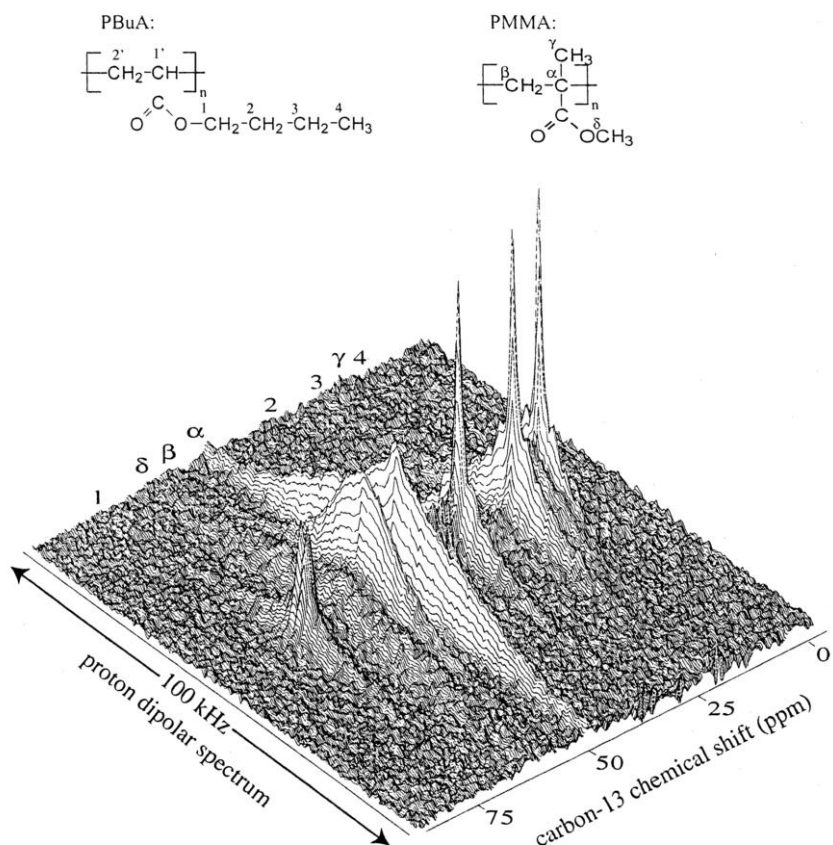


**Fig. 9.28** A  $^1\text{H}$ - $^{13}\text{C}$  WISE experiment recorded for a core–shell system comprising mobile poly(butyl methacrylate) (PbuA) and rigid PMMA. (Reproduced by permission of the American Chemical Society from [128].)

Alternatively, the MAS- $J$ -HMQC [136, 137] and MAS- $J$ -HSQC experiments [138] utilise the isotropic through-bond  $J$  coupling. The primary aim of recording a  $^1\text{H}$ - $^{13}\text{C}$  correlation spectrum is usually the establishing of one-bond correlations, such that the  $^1\text{H}$  chemical shifts can be identified. For correlation methods based on the dipolar coupling, it is necessary to ensure that the observed peaks are then not due to close through-space proximities. This problem is obviously avoided by utilising through-bond  $J$  couplings. As an example, Fig. 9.29 presents  $^1\text{H}$ - $^{13}\text{C}$  and  $^1\text{H}$ - $^{15}\text{N}$  MAS- $J$ -HMQC spectra recorded for 20 mg of a tripeptide sample at natural abundance [137]. The recording of  $^1\text{H}$ - $^{13}\text{C}$  MAS- $J$ -HMQC spectra which reveal one- and multiple-bond connectivities allowed the complete assignment of the  $^1\text{H}$ ,  $^{13}\text{C}$ , and  $^{15}\text{N}$  resonances for the tripeptide.

It should be noted that the existence of methods based on both dipolar and  $J$  couplings opens up the possibility for distinguishing through-bond connectivities and through-space proximities on a medium- to long-range, such that insight into in-

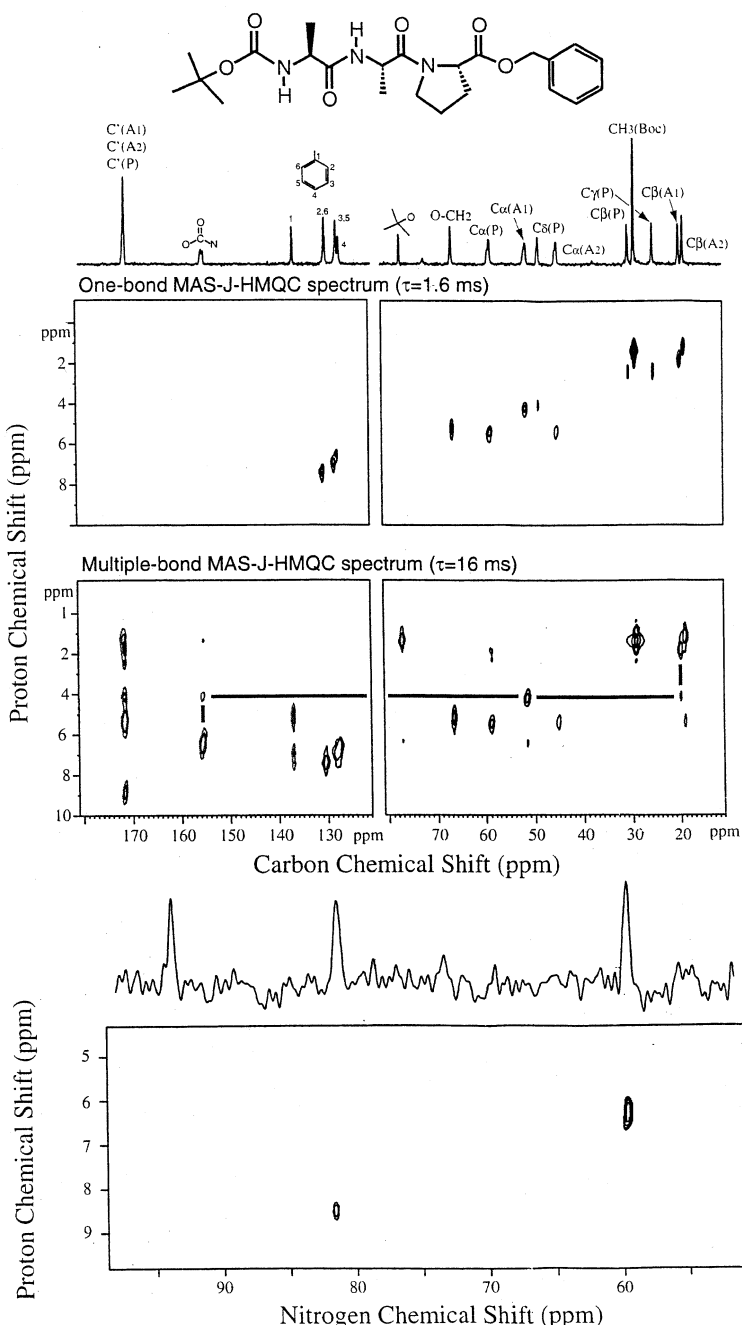


**Fig. 9.29**  $^1\text{H}$ - $^{13}\text{C}$  and  $^1\text{H}$ - $^{15}\text{N}$  MAS-J-HMQC spectra recorded for a tripeptide sample at natural abundance. Two different  $^1\text{H}$ - $^{13}\text{C}$  experiments were performed, with the use of a short ( $\tau = 1.6$  ms) and a long ( $\tau = 16$  ms) evolution period selecting in the former case

one-bond correlations, while the latter case allowed the identification of multiple-bond correlations.  $^{13}\text{C}$  and  $^{15}\text{N}$  CP MAS spectra are presented above the relevant 2D spectra. (Reproduced by permission of the American Chemical Society from [137].)

termolecular packing arrangements is provided. In this way, the two approaches are complimentary in a similar way to the case of the COSY and NOESY [1, 2] solution-state NMR experiments.

### 9.6.2

#### The Quantitative Determination of Heteronuclear Dipolar Couplings

As described in Section 9.4.1, the REDOR experiment, by allowing the quantitative determination of dipolar couplings, accurately yields the distance between two heteronuclei. Indeed, REDOR is currently the workhorse experiment for structure determination. The method does, however, rely on selective isotopic labelling. As well as measuring internuclear distances, Section 9.5.6 showed how probing the change in the dipolar coupling provides insight into a dynamic process. In this section, 2D experiments which have the aim of measuring multiple heteronuclear dipolar couplings (as opposed to only one in the REDOR experiment) are described.

In a separated local field (SLF) experiment [139–142] the basic principle is that a spinning-sideband pattern, from which the heteronuclear dipolar coupling can be extracted, is obtained in the indirect dimension for each resolved resonance in the direct dimension, i.e., the dipolar interaction is separated from the chemical shift interaction (the experiment is sometimes referred to as the DIPSHIFT experiment). In the original SLF papers, a homonuclear decoupling method is applied in  $t_1$ , but recently McElheny et al. have shown that fast MAS alone at a  $\nu_R$  of at least 12 kHz (much faster MAS should be avoided since the higher-order spinning sidebands become too weak to allow a reliable fitting) provides sufficient proton dipolar decoupling such that relatively reliable  $^1\text{H}$ – $^{13}\text{C}$  dipolar couplings can be extracted [143].

Alternatively, in a modification of the original SLF method, Hohwy et al. have presented a sophisticated experiment in which a pulse sequence is applied during  $t_1$  which actively recouples the weak heteronuclear dipolar coupling while decoupling the homonuclear  $^1\text{H}$ – $^1\text{H}$  dipolar coupling [144]. Instead of giving a spinning-sideband pattern, a powder line shape is obtained in the indirect dimension. It is shown that this experimental approach allows the accurate determination of both N–H distances as well as the H–N–H bond angle in an  $\text{NH}_2$  group. Another state-of-the-art method which has recently been proposed involves performing CP from  $^1\text{H}$  to  $^{13}\text{C}$  with the rf pulse on the  $^1\text{H}$  channel fulfilling the Lee–Goldburg condition mentioned in Section 9.5.3 [145]. The suppression of the homonuclear  $^1\text{H}$  dipolar couplings means that a LG–CP signal builds up in an oscillatory manner, reflecting coherent heteronuclear transfer. The Fourier transformation of such build-up curves yields powder spectra with marked singularities from the separation of which the heteronuclear dipolar coupling can be determined. Alternatively, it is to be noted that an analysis of a standard CP build-up curve under fast MAS can, in some cases, allow the determination of the heteronuclear dipolar coupling [146].

In direct analogy to the homonuclear DQ MAS experiment (see Section 9.5.6), if the  $t_1$  increment in the REPT pulse sequences (see Section 9.6.1) is not set

equal to  $\tau_R$ , a spinning-sideband pattern rotor-encoded by the heteronuclear dipolar coupling is obtained [132, 133, 147]. An advantage of the heteronuclear  $^1\text{H}$ – $^{13}\text{C}$  approach is that it benefits from the better resolution in a  $^{13}\text{C}$  SQ dimension. An example of this is provided by the hexa(*para*-n-dodecylphenyl)-substituted HBC (hereforth referred to as HBC-PhC<sub>12</sub>) [147]. In this case,  $^1\text{H}$  solid-state NMR is unable to distinguish the core and exo-phenyl protons. By comparison, as shown in the  $^{13}\text{C}$  CP MAS spectrum at the top right of Fig. 9.30, the corresponding  $^{13}\text{C}$  resonances are well resolved. It is, thus, possible to use the heteronuclear approach to probe separately the dynamics of the core and the outer phenyl rings. For example, the right-hand-side of Fig. 9.30 presents  $^1\text{H}$ – $^{13}\text{C}$  spinning-sideband patterns obtained at the core aromatic CH  $^{13}\text{C}$  resonance for the solid and LC phases of HBC-PhC<sub>12</sub>, using the REPT-HMQC experiment.

A comparison of the spinning-sideband patterns obtained for the LC phases of HBC-C<sub>12</sub> and HBC-PhC<sub>12</sub> reveals that the third-order spinning sidebands are significantly higher in the latter case; they are of the same height as the first-order spinning sidebands for HBC-PhC<sub>12</sub>. Since the same experimental conditions

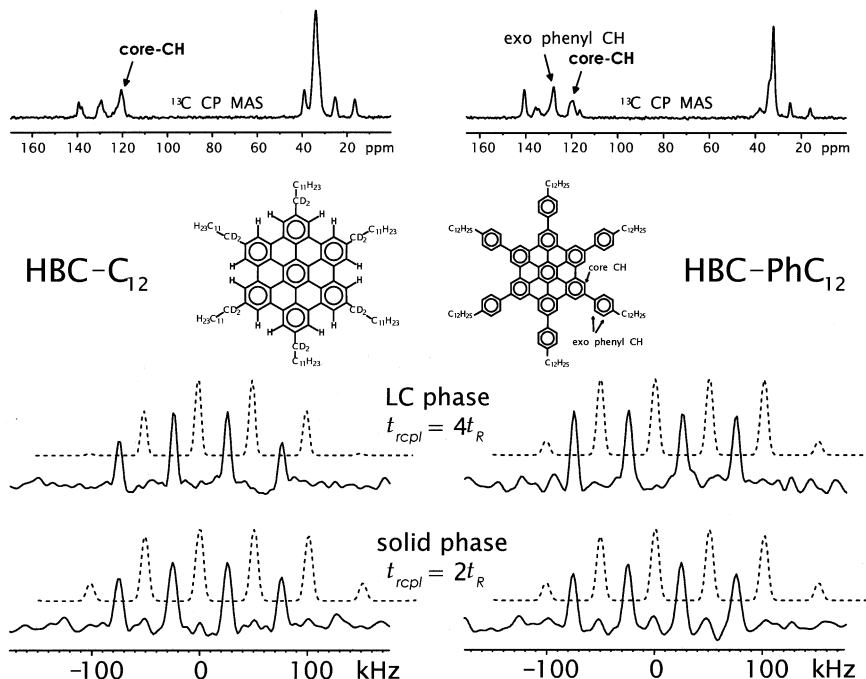


**Fig. 9.30**  $^1\text{H}$ – $^{13}\text{C}$  heteronuclear MQ MAS spinning-sideband patterns, obtained at a  $\gamma_R = 25$  kHz, using the REPT-HMQC experiment. The patterns correspond to the sum projections over the  $^{13}\text{C}$  resonance due to the aromatic core CH in the 2D spectra of HBC-C<sub>12</sub>, and HBC-PhC<sub>12</sub>. The spectra for the room temperature (solid) and high temperature LC phases were

recorded at 35 °C and 120 °C, respectively. The dashed traces represent simulated spectra, obtained by taking into account the best-fit  $D$ s for the CH groups. At the top,  $^{13}\text{C}$  CP-MAS ( $\gamma_R = 15$  kHz) spectra are presented, with the signal positions of the aromatic CH resonances being identified. (Reproduced from [147].)

were used in both cases, this result immediately indicates a larger dipolar coupling and, hence, a larger order parameter for HBC-PhC<sub>12</sub>. Indeed, the order parameter is determined to be  $0.93 \pm 0.09$ , indicating less out-of-plane mesogen mobility. It is interesting that this NMR result is correlated with an improved intra- and inter-columnar packing as evidenced by powder X-ray diffraction patterns [147].

### 9.6.3

#### Torsional Angles

In an extension to experiments which measure internuclear distances, Levitt and co-workers and Griffin and co-workers have presented ingenious methods which allow the measurement of torsional angles [148, 149]. The methods involve the creation of MQC between a pair of nuclei (selective isotopic labelling is required), which may be homonuclear, e.g. <sup>13</sup>C–<sup>13</sup>C, or heteronuclear, e.g. <sup>13</sup>C–<sup>15</sup>N. A spinning-sideband pattern is observed due to the evolution of the two spins which make up the MQC under the dipolar couplings to the directly attached nuclei. As a specific example, consider the H<sup>N</sup>–N–C<sup>α</sup>–H<sup>α</sup> moiety in <sup>15</sup>N-labelled NAV [149]. By incrementing a period of <sup>1</sup>H homonuclear decoupling, a *t*<sub>1</sub> FID (Fig. 9.31a) is obtained which depends on the evolution under the N–H<sup>N</sup> and C<sup>α</sup>–H<sup>α</sup>

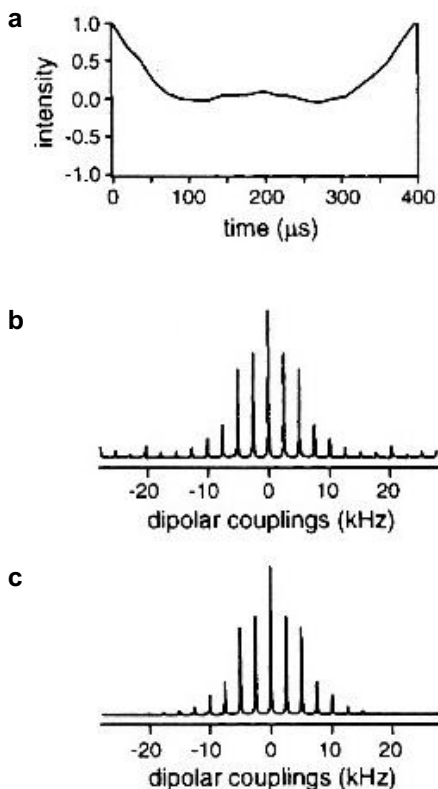


**Fig. 9.31** The measurement of the H<sup>N</sup>–N–C<sup>α</sup>–H<sup>α</sup> torsional angle in <sup>15</sup>N-labelled NAV. The (a) *t*<sub>1</sub> FID and (b) frequency-domain spinning-sideband pattern depend on the evolution under the N–H<sup>N</sup> and C<sup>α</sup>–H<sup>α</sup> dipolar coupling, and in particular the relative orientation of the two bonds. The (c) best-fit simulation corresponds to a torsional angle of  $-135^\circ$ . (Reproduced by permission of the American Chemical Society from [149].)

dipolar coupling, and in particular the relative orientation of the two bonds. From the best-fit simulation (Fig. 9.31c) of the experimental frequency-domain spinning-sideband pattern (Fig. 9.31b), the torsional angle was determined to be  $-135^\circ$ .

#### 9.6.4

#### Oriented Samples

The difficulties associated with the preparation of samples suitable for diffraction studies has led to much interest in the application of solid-state NMR to the investigation of the three-dimensional structure adopted by membrane proteins in their functional environment of phospholipid bilayers [14]. As an oriented sample, the NMR spectrum of a membrane protein is much simplified as compared to the case of a powder sample; for perfect ordering, all structurally equivalent nuclei have the same orientation with respect to  $B_0$ , and hence the same anisotropic resonance frequency (see Section 9.2.1). This phenomenon is taken advantage of in the PISEMA (polarisation inversion with spin exchange at the magic angle) experiment [150]. This technique is closely related to the experiments described in Section 9.6.2, although it is to be noted that it is applied to static samples.

Figure 9.32a presents a 2D PISEMA spectrum of a uniformly  $^{15}\text{N}$ -labelled polypeptide in an oriented lipid bilayer [151]. For each  $^{15}\text{N}$  resonance, the  $^{15}\text{N}$  chemical shift (horizontal axis) is correlated with the corresponding  $^{15}\text{N}-^1\text{H}$  dipolar coupling, with both the chemical shift and the dipolar coupling depending on the orientation of the particular nitrogen containing moiety. Making the assumption that the local chemical environment leads to only slight variations in the principal values and orientations of the CSA and dipolar tensors, the observed PISEMA pattern

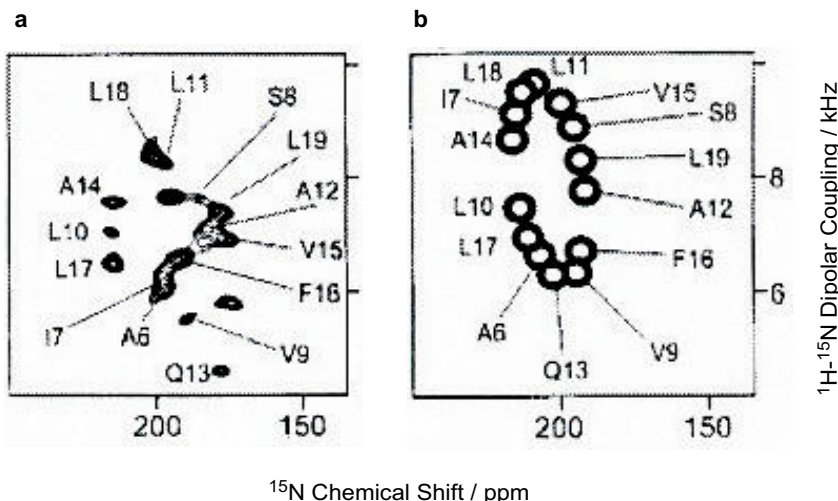


**Fig. 9.32** (a) A 2D PISEMA spectrum of a uniformly  $^{15}\text{N}$ -labelled polypeptide in an oriented lipid bilayer. (b) The best-fit simulated spectrum corresponds to a helix tilt angle of  $12^\circ$ . (Reproduced by permission of Academic Press from [151].)

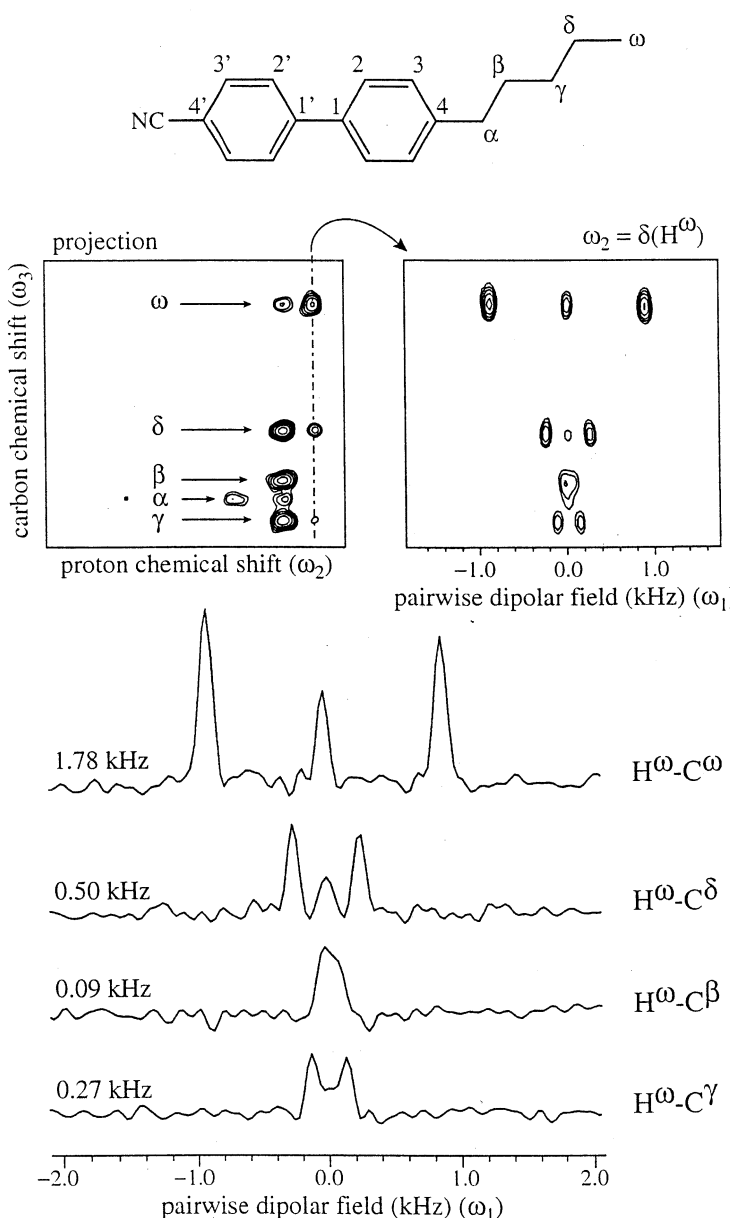


**Fig. 9.33** The aliphatic region of the 3D pair-wise local field spectrum of the nematic LC, 5CB. A projection onto the  $\omega_2-\omega_3$  plane yields a  ${}^1\text{H}-{}^{13}\text{C}$  correlation spectrum (upper left), and a plane taken perpendicular to this at a particular  ${}^1\text{H}$  chemical shift yields a  $\omega_3-\omega_1$  slice (upper right) that contains a series of pair-wise local fields for each carbon atom. The pair-wise local fields obtained for  $\text{H}^\omega$  are shown, which demonstrate that couplings to carbons all the way down the chain to  $\text{C}\beta$  can be measured. (Reproduced by permission of the American Chemical Society from [158].)

allows the tilt angle of the polypeptide helix with respect to the bilayer normal to be determined. For example, the best-fit simulated spectrum in Fig. 9.32b corresponds to a helix tilt angle of 12°.

PISEMA experiments yield the local dipolar field experienced by the  $^{13}\text{C}$  or  $^{15}\text{N}$  nucleus. Perhaps counter intuitively, it has been shown that better resolution is obtained by using experiments which detect the local dipolar field on protons [129, 152, 153, 154]. As specific examples, the  $^1\text{H}$  detected local field experiment has recently successfully been applied to the characterisation of liquid crystals [155, 156] and membranes [157]. As illustrated by Fig. 9.33, this approach has even been shown to yield sufficient resolution in 3D versions to allow the direct measurement of internuclear dipolar couplings between nuclei separated by up to five bonds in liquid crystals, thereby providing very strong conformational constraints [158].

## 9.7

### Half-integer Quadrupole Nuclei

An inspection of Tab. 9.2 reveals that many nuclei of relevance in inorganic systems, e. g.  $^{23}\text{Na}$  (spin  $I = 3/2$ ),  $^{27}\text{Al}$  (spin  $I = 5/2$ ), and  $^{17}\text{O}$  (spin  $I = 5/2$ ), are quadrupolar with a half-integer nuclear spin. For such nuclei, an important result is that the  $|m_l = +s\rangle \leftrightarrow |m_l = -s\rangle$  transitions are not broadened by the quadrupolar coupling to first order (for a spin  $I = 3/2$  nucleus, the energy levels are labelled  $-3/2$ ,  $-1/2$ ,  $+1/2$ , and  $+3/2$ ). As a consequence, for the usual case that the quadrupolar coupling is large (typically of the order of MHz), only the central transition,  $|m_l = +1/2\rangle \leftrightarrow |m_l = -1/2\rangle$ , is observed in the normal spectrum, since the broadened satellite transitions ( $|m_l = +3/2\rangle \leftrightarrow |m_l = +1/2\rangle$  and  $|m_l = -1/2\rangle \leftrightarrow |m_l = -3/2\rangle$  for a spin  $I = 3/2$  nucleus) are lost in the baseline. It should be noted that various groups have presented ingenious methods which use the satellite transitions to enhance the sensitivity of the central transition spectrum [159–161].

The central transition of a half-integer quadrupolar nucleus is, however, broadened to second order. In contrast to the CSA, and dipolar and first-order quadrupolar couplings, the orientation dependence of the broadening associated with second-order quadrupolar coupling is no longer purely a second-rank tensor. In particular, there is a fourth-rank tensor contribution, which is not fully removed by MAS (regardless of what  $\nu_R$  is used). The residual second-order quadrupolar broadening of the central transition often prevents the resolution of resonances due to chemically or crystallographically distinct sites [162]. For example, Fig. 9.34b shows the  $^{87}\text{Rb}$  (spin  $I = 3/2$ ) MAS spectrum of  $\text{RbNO}_3$ ; the presence of residual second-order quadrupolar broadening precludes the resolution of the three crystallographically distinct sites.

Since the fourth-rank anisotropic broadening can be removed by sample rotation at an angle of 30.6° or 70.1° with respect to  $B_0$ , high-resolution spectra corresponding to the removal of the residual second-rank quadrupolar broadening can be achieved by the methods of double rotation (DOR) [163] and dynamic-angle spin-

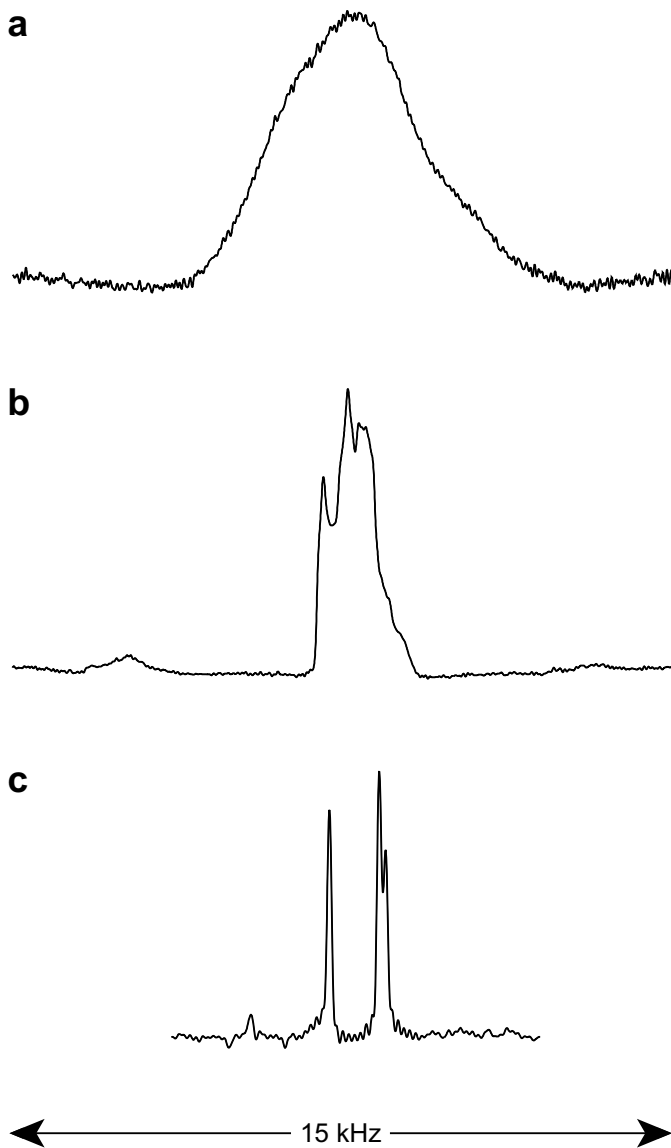


**Fig. 9.34**  $^{87}\text{Rb}$  (130.9 MHz) (spin  $I = 3/2$ ) (a) static, (b) MAS, and (c) isotropic MQMAS spectra of  $\text{RbNO}_3$ .

ning (DAS) [164], which, respectively, involve the simultaneous and sequential rotation of the sample about two axes [165]. As a specific example, Fig. 9.35a presents a  $^{17}\text{O}$  2D DAS spectrum of the bridging oxygen ( $\text{Si}-\text{O}-\text{Si}$ ) resonances in a  $\text{K}_2\text{Si}_4\text{O}_9$  glass [166,167]. Residual second-order quadrupolar broadening is removed from the isotropic dimension such that the broadness of the isotropic lineshape reflects a continuous variation in the  $^{17}\text{O}$  isotropic frequency. The selected anisotropic cross

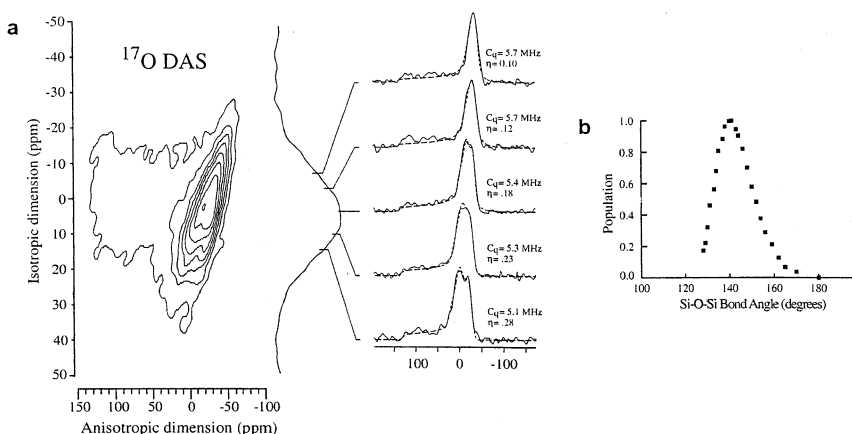


**Fig. 9.35** (a) A  $^{17}\text{O}$  2D DAS spectrum of the bridging oxygen (Si—O—Si) resonances in a  $\text{K}_2\text{Si}_4\text{O}_9$  glass. Selected anisotropic cross sections corresponding to different  $^{17}\text{O}$  isotropic frequencies are shown. (b) The Si—O—Si bond angle distribution in the glass, as determined by the use of quantum chemical calculations to interpret the experimental information about the  $^{17}\text{O}$  quadrupolar interactions. (Reproduced from [167].)

sections demonstrate that the quadrupolar coupling parameters vary as the isotropic frequency changes. In combination with quantum chemical calculations, the information about the  $^{17}\text{O}$  quadrupolar interactions allows the determination of the Si—O—Si bond angle distribution in the glass (Fig. 9.35b). Although a number of impressive applications of both the DAS and DOR methods have been presented, the technical complexity of both experiments has meant that their use is not widespread.

In 1995, Frydman and Harwood presented a 2D MQMAS experiment, which, by means of the formation of an echo corresponding to the refocusing of the fourth-rank second-order quadrupolar broadening, yields 2D spectra in which anisotropically broadened ridges are resolved on the basis of their different isotropic shifts [168]. The resolution of the three distinct Rb sites in  $\text{RbNO}_3$  in an isotropic MQMAS spectrum is demonstrated in Fig. 9.34c. It is to be noted that the experiment is only applicable for odd MQ orders (e.g. 3Q or 5Q), for which there is no first-order quadrupolar broadening. Moreover, as compared to the spin  $I = 1/2$  MQ methods described earlier in this article, MQC can be excited for a single isolated nucleus.

The MQ MAS technique has the big advantage of requiring only conventional MAS hardware. In the last five years, much attention has been devoted to the optimisation of the technique, with respect to e.g., obtaining pure absorption-mode lineshapes, improving the sensitivity, and extending the applicability to nuclei with ever greater quadrupolar couplings; various groups have carried out studies to compare the different variants which have been proposed [169–171]. The development has been so rapid that MQMAS NMR of nuclei such as  $^{23}\text{Na}$ ,  $^{27}\text{Al}$  and  $^{17}\text{O}$  can now be considered to be routine, with many applications having been presented, which encompass, e.g., glasses, minerals, and microporous materials [172–177].

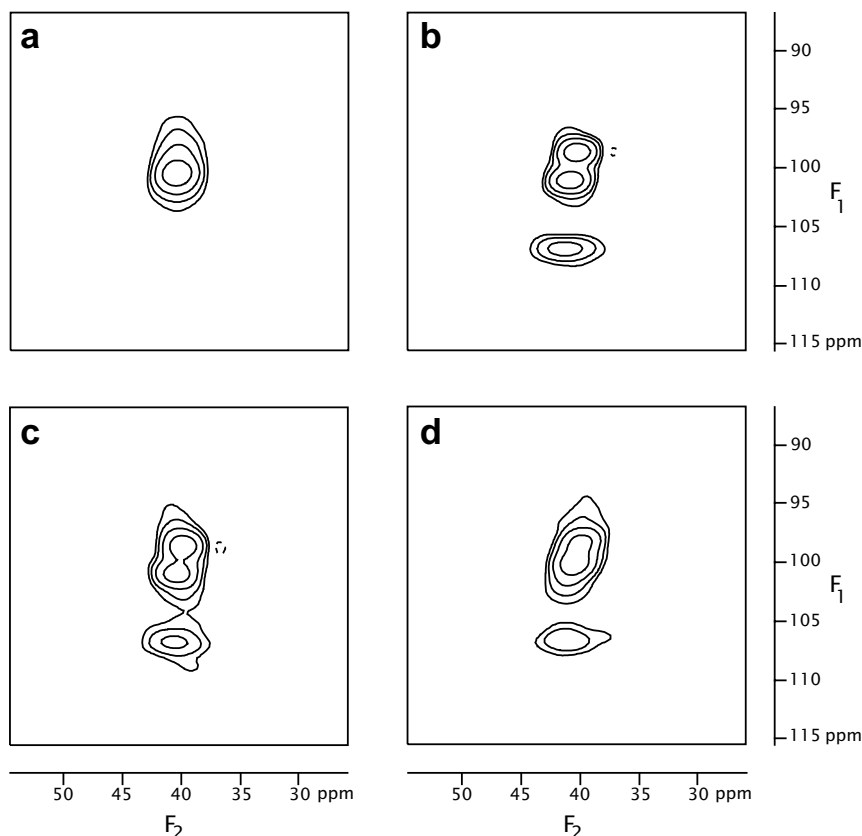


**Fig. 9.36**  $^{27}\text{Al}$  (104.3 MHz) 5Q MAS spectra corresponding to the tetrahedral aluminium sites in the microporous aluminium methylphosphonates (a) AlMePO- $\alpha$  and (b) AlMePO- $\beta$ , as well as (c) a physical mixture of the two

forms, and (d) a sample in which the thermal transformation between the two forms was interrupted. (Reproduced by permission of the American Chemical Society from [175].)

As a specific example, Fig. 9.36 shows  $^{27}\text{Al}$  5Q MAS spectra corresponding to the tetrahedral aluminium sites in the microporous aluminium methylphosphonates (a) AlMePO- $\alpha$  and (b) AlMePO- $\beta$  [175]. In Fig. 9.36b, three distinct sites can be distinguished in the isotropic ( $F_1$ ) dimension. In a MAS experiment (this corresponds to the projection onto the  $F_2$  dimension), only a single peak is observed in the tetrahedral region. AlMePO- $\beta$  can be converted by a thermal transformation into AlMePO- $\alpha$ . As discussed in [175], insight into this process is provided by the subtle but significant differences between the 5Q MAS spectra for a physical mixture of the two forms (Fig. 9.36c) and for a sample in which the thermal transformation was interrupted (Fig. 9.36d).

## 9.8 Summary

This article has given an overview of the wide range of solid-state NMR experiments available today. The central role of anisotropic interactions, e.g. the CSA and the dipolar and quadrupolar couplings, has become evident. Through the orientation dependence imparted to the resonance frequency, access is made available to valuable structural and dynamic information. However, for a powder sample, the associated line broadening hinders the resolution of distinct sites. Achieving high-resolution NMR while retaining access to the information inherent to the anisotropic interactions particular to the solid state is a key aim of many of the described experimental methods.

A number of NMR methods applicable to small amounts (10–20 mg) of a powdered sample at natural abundance have been presented. In particular, recent advances in both NMR hardware and the development of new pulse sequences means that  $^1\text{H}$  solid-state NMR is becoming routinely feasible. In this way, insight into the structure and dynamics of, in particular, hydrogen-bonded systems as well as aromatic  $\pi-\pi$  interactions can be provided. A further important new class of experiments are those which exploit the  $J$  coupling to establish through-bond connectivities. As a general strategy, as much information as possible should be first gleaned for the sample at natural abundance (for large biological systems, global isotopic labelling is unavoidable). If pertinent questions remain unanswered, a strategy involving the synthesis of a sample incorporating selective isotopic labelling can be considered.

Solid-state NMR spectroscopy should certainly not be used in isolation. For example, the assignment of solid-state spectra is aided by the existence of solution-state NMR spectra, while if dynamic processes are to be investigated, it is very useful if differential scanning calorimetry (DSC) curves can be first obtained, so that the temperatures at which phase transitions occur are known in advance. In addition, the advances in computing power as well as the development of methodology means that the use of quantum chemical calculations of NMR parameters in the interpretation of experimental results will become ever more popular.

Solid-state NMR should not be considered as a replacement for the established diffraction methods. Instead, the two methods should be thought of as being complementary, since they have much to offer each other. For example, the existence of a single-crystal X-ray structure for a related system aids the interpretation of NMR spectra obtained for a system, where it is not possible to obtain a single crystal suitable for an X-ray analysis. In addition, solid-state NMR is of use when an X-ray single-crystal structure is available. For example, since structure determination by single-crystal X-ray diffraction methods, being based on the diffraction of X-rays by electrons, is not well suited to the localisation of lighter atoms, the ability of solid-state NMR to provide distance constraints, which can be used in the optimisation of a crystal structure, in particular the very relevant hydrogen-bonded part, is of much importance. Furthermore, solid-state NMR is extremely well suited to the investigation of dynamic processes. It can also detect polymorphic forms, which

may be overlooked when selecting single crystals for X-ray diffraction analysis. Finally, by probing the CSA and quadrupolar interactions, solid-state NMR provides electronic information which is not accessible to X-ray studies.

### Acknowledgements

SPB is supported by a Marie Curie Fellowship of the European Community programme "Improving Human Research Potential and the Socio-economic Knowledge Base" under contract number "HPMFCT-2000-00525". The information published does not represent the opinion of the Community, and the Community is not responsible for any use that might be made of data appearing therein.

## Appendix

### Anisotropic Interactions: The Orientation Dependence of the Resonance Frequency [4]

For the CSA,

$$\omega_{\text{CS}} = \omega_0 \left( \sigma_{xx}^{\text{PAS}} \cos^2 \phi \sin^2 \theta + \sigma_{yy}^{\text{PAS}} \sin^2 \phi \sin^2 \theta + \sigma_{zz}^{\text{PAS}} \cos^2 \theta \right) \quad (\text{A1})$$

where  $\omega_0$  is the Larmor frequency,  $\sigma_{xx}^{\text{PAS}}$ ,  $\sigma_{yy}^{\text{PAS}}$ , and  $\sigma_{zz}^{\text{PAS}}$  are the principal values (eigenvalues) in the PAS, and  $\phi$  and  $\theta$  are polar angles defining the transformation of the PAS onto the laboratory frame defined by  $B_0$ .

The CSA is more commonly expressed as a sum of an isotropic and an anisotropic part. The isotropic chemical shift is given by

$$\sigma_{\text{iso}} = \frac{1}{3} \left( \sigma_{xx}^{\text{PAS}} + \sigma_{yy}^{\text{PAS}} + \sigma_{zz}^{\text{PAS}} \right) \quad (\text{A2})$$

while the anisotropic frequency is

$$\omega_{\text{aniso}} = \frac{\delta}{2} (3 \cos^2 \theta - 1 - \eta \sin^2 \theta \cos 2\phi) \quad (\text{A3})$$

where  $\delta$  and  $\eta$  describe the anisotropy and the asymmetry of the interaction, respectively.

An important feature of solid-state NMR is that the orientation dependence of the CSA, dipolar, and first-order quadrupolar interactions can all be represented by what are referred to as second-rank tensors. As a consequence, Eq. (A3) can be considered as a general expression which applies to all three interactions. It should be noted that the isotropic part is zero for both the dipolar coupling and the first-order quadrupolar interaction.

For the dipolar coupling between a pair of spins, the interaction is always axially symmetric and thus  $\eta = 0$ . It is necessary to distinguish between a heteronuclear and a homonuclear dipolar coupling. For the heteronuclear case,

$$\delta = D, \quad (\text{A4})$$

while for the homonuclear case,

$$\delta = 3D/2, \quad (\text{A5})$$

where  $D$  is the dipolar coupling constant:

$$D = \frac{\mu_0 \eta \gamma_I \gamma_S}{4\pi r^3}. \quad (\text{A6})$$

$r$  denotes the internuclear distance, while  $\gamma$  corresponds to the magnetogyric ratio.

For the first-order quadrupolar interaction,

$$\delta = \frac{3\pi C_Q}{2I(2I-1)}, \quad (\text{A7})$$

where the quadrupolar coupling constant,  $C_Q$ , (in units of Hz) is given by

$$C_Q = \frac{e^2 q Q}{h}. \quad (\text{A8})$$

$eq$  corresponds to the electric field gradient at the nucleus and  $Q$  to the nuclear quadrupole moment.

## References

- 1 R. R. Ernst, G. Bodenhausen, A. Wo-kau, *Principles of Nuclear Magnetic Resonance in One and Two Dimensions*, Clarendon Press, Oxford 1987.
- 2 T. D. W. Claridge, *High-Resolution NMR Techniques in Organic Chemistry*, Pergamon Press, Amsterdam 1999.
- 3 M. Mehring, *Principles of High Resolution NMR in Solids*, Springer, Berlin 1983.
- 4 K. Schmidt-Rohr, H. W. Spiess, *Multi-dimensional Solid-State NMR and Polymers*, Academic Press, New York 1994.
- 5 L. Emsley, D. D. Laws, A. Pines, Lectures on Pulsed NMR (3rd edition), in *The Proceedings of the International School of Physics "Enrico Fermi"*, Course CXXXIX, ed. B. Maraviglia, IOS Press, Amsterdam, 1999, p. 45.
- 6 R. K. Harris, in *Encyclopedia of Nuclear Magnetic Resonance*, eds. D. M. Grant, R. K. Harris, Wiley, Chichester, 1996, Vol. 5, p. 3301.
- 7 S. P. Brown and H. W. Spiess, *Chem. Rev.*, **2001**, *101*, 4125.
- 8 A. E. Bennett, R. G. Griffin, S. Vega, in *NMR Basic Principles and Progress*, Springer-Verlag, Berlin 1994, Vol. 33, p. 1.
- 9 S. Dusold, A. Sebald, *Annu. Rep. NMR Spectrosc.*, **2000**, *41*, 185.
- 10 M. H. Sherwood, in *Encyclopedia of Nuclear Magnetic Resonance*, eds. D. M. Grant, R. K. Harris, Wiley, Chichester 1996, Vol. 2, p. 1322.
- 11 R. Gerald II, T. Bernhard, U. Haeberlen et al., *J. Am. Chem. Soc.*, **1993**, *115*, 777.
- 12 R. Y. Dong, *Nuclear Magnetic Resonance of Liquid Crystals*, Springer, New York, 1994.
- 13 J. W. Emsley, in *Encyclopedia of Nuclear Magnetic Resonance*, eds. D. M. Grant and R. K. Harris, Wiley, Chichester 1996, Vol. 4, p. 2788.
- 14 J. H. Davis, M. Auger, *Prog. NMR Spectrosc.*, **1999**, *35*, 1.
- 15 J. H. Davis, K. R. Jeffrey, M. Bloom et al., *Chem. Phys. Lett.*, **1976**, *42*, 390.
- 16 V. Copié, A. E. McDermott, K. Beshah et al., *Biochemistry*, **1994**, *33*, 3280.
- 17 E. R. Andrew, A. Bradbury, R. G. Eades, *Nature*, **1958**, *182*, 1659.
- 18 I. Lowe, *Phys. Rev. Lett.*, **1959**, *2*, 285.
- 19 S. R. Hartmann, E. L. Hahn, *Phys. Rev.*, **1962**, *128*, 2042.
- 20 A. Pines, M. G. Gibby, J. S. Waugh, *J. Chem. Phys.*, **1972**, *56*, 1776.
- 21 J. Schaefer, E. O. Stejskal, *J. Am. Chem. Soc.*, **1976**, *98*, 1031.
- 22 M. M. Maricq, J. S. Waugh, *J. Chem. Phys.*, **1979**, *70*, 3300.
- 23 J. Herzfeld, A. E. Berger, *J. Chem. Phys.*, **1980**, *73*, 6021.
- 24 G. Metz, X. Wu, S. O. Smith, *J. Magn. Reson. A*, **1994**, *110*, 219.
- 25 S. Hediger, B. H. Meier et al., *Chem. Phys. Lett.*, **1994**, *223*, 283.
- 26 W. T. Dixon, *J. Magn. Reson.*, **1981**, *44*, 220.
- 27 W. T. Dixon, *J. Chem. Phys.*, **1982**, *77*, 1800.
- 28 F. Bloch, *Phys. Rev.*, **1958**, *111*, 841.
- 29 A. E. Bennett, C. M. Rienstra et al., *J. Chem. Phys.*, **1995**, *103*, 6951.
- 30 M. Carravetta, M. Edén, X. Zhao et al., *Chem. Phys. Lett.*, **2000**, *321*, 205.
- 31 M. Ernst, H. Zimmermann, B. H. Meier, *Chem. Phys. Lett.*, **2000**, *317*, 581.
- 32 X. Wu, S. T. Burns, K. W. Zilm, *J. Magn. Reson. A*, **1994**, *111*, 29.

- 33** A. Lesage, S. Steuernagel, L. Emsley, *J. Am. Chem. Soc.*, **1998**, *120*, 7095.
- 34** J. Z. Hu, J. K. Harper, C. Taylor et al., *J. Magn. Reson.*, **2000**, *142*, 326.
- 35** D. Sakellariou, A. Lesage, L. Emsley, *J. Magn. Reson.*, **2001**, *151*, 40.
- 36** R. E. Botto, in *Encyclopedia of Nuclear Magnetic Resonance*, eds. D. M. Grant, R. K. Harris, Wiley, Chichester 1996, Vol. 3, p. 2101.
- 37** R. J. Pugmire, in *Encyclopedia of Nuclear Magnetic Resonance*, eds. D. M. Grant, R. K. Harris, Wiley, Chichester 1996, Vol. 2, p. 1355.
- 38** M. Pruski, in *Encyclopedia of Nuclear Magnetic Resonance*, eds. D. M. Grant, R. K. Harris, Wiley, Chichester 1996, Vol. 2, p. 1378.
- 39** H. Saitô, in *Encyclopedia of Nuclear Magnetic Resonance*, eds. D. M. Grant, R. K. Harris, Wiley, Chichester 1996, Vol. 6, p. 3740.
- 40** R. K. Harris, in *Encyclopedia of Nuclear Magnetic Resonance*, eds. D. M. Grant, R. K. Harris, Wiley, Chichester 1996, Vol. 6, p. 3734.
- 41** W. S. Veeman, in *Encyclopedia of Nuclear Magnetic Resonance*, eds. D. M. Grant, R. K. Harris, Wiley, Chichester 1996, Vol. 6, p. 3655.
- 42** R. H. Newman, in *Encyclopedia of Nuclear Magnetic Resonance*, eds. D. M. Grant, R. K. Harris, Wiley, Chichester 1996, Vol. 2, p. 738.
- 43** H. C. Marsmann, in *Encyclopedia of Nuclear Magnetic Resonance*, eds. D. M. Grant, R. K. Harris, Wiley, Chichester 1996, Vol. 7, p. 4386.
- 44** G. Engelhardt, in *Encyclopedia of Nuclear Magnetic Resonance*, eds. D. M. Grant, R. K. Harris, Wiley, Chichester 1996, Vol. 7, p. 4398.
- 45** H. Eckert, *NMR Basic Principles and Progress*, **1994**, *33*, 125.
- 46** S. Hediger, L. Emsley, M. Fisher, *Carbohydr. Res.*, **1999**, *322*, 102.
- 47** I. Schnell, S. P. Brown, H. Y. Low et al., *J. Am. Chem. Soc.*, **1998**, *120*, 11784.
- 48** S. P. Brown, I. Schnell, J. D. Brand et al., *J. Am. Chem. Soc.*, **1999**, *121*, 6712.
- 49** S. P. Brown, I. Schnell, J. D. Brand et al., *J. Mol. Struct.*, **2000**, *521*, 179.
- 50** K. Yamauchi, S. Kuroki, K. Fujii et al., *Chem. Phys. Lett.*, **2000**, *324*, 435.
- 51** J. S. Waugh, L. M. Huber, U. Haeberlen, *Phys. Rev. Lett.*, **1968**, *20*, 180.
- 52** U. Haeberlen, J. S. Waugh, *Phys. Rev.*, **1968**, *175*, 453.
- 53** B. C. Gerstein, R. G. Pemberton, R. C. Wilson et al., *J. Chem. Phys.*, **1977**, *66*, 361.
- 54** G. Scheler, U. Haubenreisser, H. Rosenberger, *J. Magn. Reson.*, **1981**, *44*, 134.
- 55** G. E. Maciel, C. E. Bronnimann, B. Hawkins, *Adv. Magn. Reson.*, **1990**, *14*, 125.
- 56** S. F. Dec, C. E. Bronnimann, R. A. Wind et al., *J. Magn. Reson.*, **1989**, *82*, 454.
- 57** J. M. Miller, *Prog. NMR Spectrosc.*, **1996**, *28*, 255.
- 58** S. Ando, R. K. Harris, J. Hirschinger et al., *Macromolecules*, **2001**, *34*, 66.
- 59** S. L. Grage, A. S. Ulrich, *J. Magn. Reson.*, **2000**, *146*, 81.
- 60** T. Gullion, J. Schaefer, *J. Magn. Reson.*, **1989**, *81*, 196.
- 61** T. Gullion, J. Schaefer, *Adv. Magn. Reson.*, **1989**, *13*, 57.
- 62** T. Gullion, *Concepts Magn. Reson.*, **1998**, *10*, 277.
- 63** S. M. Holl, G. R. Marshall, D. D. Beußen et al., *J. Am. Chem. Soc.*, **1992**, *114*, 4830.
- 64** C. P. Grey, W. S. Veeman, A. J. Vega, *J. Chem. Phys.*, **1993**, *98*, 7711.
- 65** T. Gullion, *Chem. Phys. Lett.*, **1995**, *246*, 325.
- 66** D. P. Raleigh, M. H. Levitt, R. G. Griffin, *Chem. Phys. Lett.*, **1988**, *146*, 71.
- 67** M. H. Levitt, D. P. Raleigh, F. Creuzet et al., *J. Chem. Phys.*, **1990**, *92*, 6347.
- 68** X. Feng, P. J. E. Verdegem, Y. K. Lee et al., *Solid State Nucl. Magn. Reson.*, **1999**, *14*, 81.
- 69** R. Tycko, G. Dabbagh, *J. Am. Chem. Soc.*, **1991**, *113*, 9444.
- 70** A. E. Bennett, J. H. Ok, R. G. Griffin et al., *J. Chem. Phys.*, **1992**, *96*, 8624.
- 71** N. C. Nielsen, H. Bildse, H. J. Jakobsen et al., *J. Chem. Phys.*, **1994**, *101*, 1805.
- 72** Y. K. Lee, N. D. Kurur, M. Helmle et al., *Chem. Phys. Lett.*, **1995**, *242*, 304.
- 73** W. Sommer, J. Gottwald, D. E. Demco et al., *J. Magn. Reson. A*, **1995**, *113*, 131.
- 74** D. M. Gregory, G. Wolfe, T. Jarvie et al., *Mol. Phys.*, **1996**, *89*, 1835.

- 75** R. Verel, M. Baldus, M. Ernst et al., *Chem. Phys. Lett.*, **1998**, 287, 421.
- 76** A. Brinkmann, M. Edén, M. H. Levitt, *J. Chem. Phys.*, **2000**, 112, 8539.
- 77** E. R. deAzevedo, W.-G. Hu, T. J. Bonagamba et al., *J. Am. Chem. Soc.*, **1999**, 121, 8411.
- 78** E. R. deAzevedo, W.-G. Hu, T. J. Bonagamba et al., *J. Chem. Phys.*, **2000**, 112, 8988.
- 79** J. Pauli, M. Baldus, B. van Rossum et al., *Chem. Biochem.*, **2001**, 2, 272.
- 80** A. Lesage, C. Auger, S. Caldarelli et al., *J. Am. Chem. Soc.*, **1997**, 119, 7867.
- 81** A. Bax, R. Freeman, T. A. Frenkiel, *J. Am. Chem. Soc.*, **1981**, 103, 2102.
- 82** Y.-S. Yen, A. Pines, *J. Chem. Phys.*, **1983**, 78, 3579.
- 83** J. Baum, M. Munowitz, A. N. Garroway et al., *J. Chem. Phys.*, **1985**, 83, 2015.
- 84** P. J. Hore, J. A. Jones, S. Wimperis, *NMR: The Toolkit*, Oxford University Press, Oxford 2000.
- 85** A. Lesage, M. Bardet, L. Emsley, *J. Am. Chem. Soc.*, **1999**, 121, 10987.
- 86** R. Verel, J. D. van Beek, B. H. Meier, *J. Magn. Reson.*, **1999**, 140, 300.
- 87** H. Geen, J. J. Titman, J. Gottwald et al., *Chem. Phys. Lett.*, **1994**, 227, 79.
- 88** P. Caravetti, P. Neuenschwander, R. R. Ernst, *Macromolecules*, **1985**, 18, 119.
- 89** C. Ochsenfeld, S. P. Brown, I. Schnell et al., *J. Am. Chem. Soc.*, **2001**, 123, 2597.
- 90** P. Lazzeretti, *Prog. NMR Spectrosc.*, **2000**, 36, 1.
- 91** B.-J. van Rossum, G. J. Boender, F. M. Mulder et al., *Spectrochim. Acta, Part A*, **1998**, 54, 1167.
- 92** S. P. Brown, T. Schaller, U. P. Seelbach et al., *Angew. Chem. Int. Ed. Engl.*, **2001**, 40, 717.
- 93** B. Berglund, R. W. Vaughan, *J. Chem. Phys.*, **1980**, 73, 2037.
- 94** G. A. Jeffrey, Y. Yeon, *Acta Crystallogr. Sect. B*, **1986**, 42, 410.
- 95** R. K. Harris, P. Jackson, L. H. Merwin et al., *J. Chem. Soc., Faraday Trans.*, **1988**, 84, 3649.
- 96** M. Feike, R. Graf, I. Schnell, C. Jäger et al., *J. Am. Chem. Soc.*, **1996**, 118, 9631.
- 97** R. Witter, P. Hartmann, J. Vogel et al., *Solid State Nucl. Magn. Reson.*, **1998**, 13, 189.
- 98** N. C. Nielsen, F. Creuzet, R. G. Griffin et al., *J. Chem. Phys.*, **1992**, 96, 5668.
- 99** M. Hong, *J. Magn. Reson.*, **1999**, 136, 86.
- 100** K. Schmidt-Rohr, W. Hu, N. Zumbulyadis, *Science*, **1998**, 280, 714.
- 101** M. Lee, W. I. Goldburg, *Phys. Rev. A*, **1965**, 140, 1261.
- 102** A. Bielecki, A. C. Kolbert, M. H. Levitt, *Chem. Phys. Lett.*, **1989**, 155, 341.
- 103** A. Bielecki, A. C. Kolbert, H. J. M. de Groot et al., *Adv. Magn. Reson.*, **1990**, 14, 111.
- 104** E. Vinogradov, P. K. Madhu, S. Vega, *Chem. Phys. Lett.*, **1999**, 314, 443.
- 105** D. Sakellarou, A. Lesage, P. Hodgkinson et al., *Chem. Phys. Lett.*, **2000**, 319, 253.
- 106** A. Lesage, L. Duma, D. Sakellarou et al., *J. Am. Chem. Soc.*, **2001**, 123, 5747.
- 107** A. Bax, N. M. Szeverenyi, G. E. Maciel, *J. Magn. Reson.*, **1983**, 52, 147.
- 108** Z. Gan, *J. Am. Chem. Soc.*, **1992**, 114, 8307.
- 109** A. Bax, N. M. Szeverenyi, G. E. Maciel, *J. Magn. Reson.*, **1983**, 55, 494.
- 110** T. Terao, T. Fujii, T. Onodera et al., *Chem. Phys. Lett.*, **1984**, 107, 145.
- 111** L. Frydman, G. C. Chingas, Y. K. Lee et al., *J. Chem. Phys.*, **1992**, 97, 4800.
- 112** S. L. Gann, J. H. Baltisberger, A. Pines, *Chem. Phys. Lett.*, **1994**, 210, 405.
- 113** D. W. Alderman, G. McGeorge, J. Z. Hu et al., *Mol. Phys.*, **1998**, 95, 1113.
- 114** J. K. Harper, D. M. Grant, *J. Am. Chem. Soc.*, **2000**, 122, 3708.
- 115** O. N. Antzutkin, S. C. Shekar, M. H. Levitt, *J. Magn. Reson. A*, **1995**, 115, 7.
- 116** O. N. Antzutkin, Y. K. Lee, M. H. Levitt, *J. Magn. Reson.*, **1998**, 135, 144.
- 117** D. Schaefer, H. W. Spiess, U. W. Suter et al., *Macromolecules*, **1990**, 23, 3431.
- 118** A. Hagemeyer, K. Schmidt-Rohr, H. W. Spiess, *Adv. Magn. Reson.*, **1989**, 13, 85.
- 119** J. J. Titman, Z. Luz, H. W. Spiess, *J. Am. Chem. Soc.*, **1992**, 114, 3756.
- 120** H. Geen, J. J. Titman, J. Gottwald et al., *J. Magn. Reson. A*, **1995**, 114, 264.
- 121** J. Gottwald, D. E. Demco, R. Graf et al., *Chem. Phys. Lett.*, **1995**, 243, 314.

- 122** *Handbook of Liquid Crystals*, eds. D. Demus, J. W. Goodby, G. W. Gray et al., Wiley-VCH, Weinheim 1998.
- 123** P. Herwig, C. W. Kayser, K. Müllen et al., *Adv. Mater.*, **1996**, *8*, 510.
- 124** S. P. Brown, X. X. Zhu, K. Saalwächter et al., *J. Am. Chem. Soc.*, **2001**, *123*, 4275.
- 125** G. A. Jeffrey, W. Saenger, *Hydrogen Bonding in Biological Structures*, Springer-Verlag, New York 1991.
- 126** S. P. Brown, I. Schnell, J. D. Brand et al., *Phys. Chem. Chem. Phys.*, **2000**, *2*, 1735.
- 127** K. Schmidt-Rohr, J. Clauss, H. W. Spiess, *Macromolecules*, **1992**, *25*, 3273.
- 128** K. Landfester, C. Boeffel, M. Lambla et al., *Macromolecules*, **1996**, *29*, 5972.
- 129** P. Caravatti, G. Bodenhausen, R. R. Ernst, *Chem. Phys. Lett.*, **1982**, *89*, 363.
- 130** P. Caravatti, L. Braunschweiler, R. R. Ernst, *Chem. Phys. Lett.*, **1983**, *100*, 305.
- 131** B.-J. Van Rossum, H. Förster, H. J. M. De Groot, *J. Magn. Reson.*, **1997**, *124*, 516.
- 132** K. Saalwächter, R. Graf, H. W. Spiess, *J. Magn. Reson.*, **1999**, *140*, 471.
- 133** K. Saalwächter, R. Graf, H. W. Spiess, *J. Magn. Reson.*, **2001**, *148*, 398.
- 134** G. Bodenhausen, D. J. Ruben, *Chem. Phys. Lett.*, **1980**, *69*, 185.
- 135** L. Müller, *J. Am. Chem. Soc.*, **1979**, *101*, 4481.
- 136** A. Lesage, D. Sakellariou, S. Steuer-nagel et al., *J. Am. Chem. Soc.*, **1998**, *120*, 13194.
- 137** A. Lesage, P. Charmont, S. Steuer-nagel et al., *J. Am. Chem. Soc.*, **2000**, *122*, 9739.
- 138** A. Lesage, L. Emsley, *J. Magn. Reson.*, **2001**, *148*, 449.
- 139** R. K. Hester, J. L. Ackerman, B. L. Neff et al., *Phys. Rev. Lett.*, **1976**, *36*, 1081.
- 140** M. G. Munowitz, R. G. Griffin, G. Bodenhausen et al., *J. Am. Chem. Soc.*, **1981**, *103*, 2529.
- 141** M. G. Munowitz, R. G. Griffin, *J. Chem. Phys.*, **1982**, *76*, 2848.
- 142** J. E. Roberts, G. S. Harbison, M. G. Munowitz et al., *J. Am. Chem. Soc.*, **1987**, *109*, 4163.
- 143** D. McElheny, E. DeVita, L. Frydman, *J. Magn. Reson.*, **2000**, *143*, 321.
- 144** M. Hohwy, C. P. Jaroniec, B. Reif et al., *J. Am. Chem. Soc.*, **2000**, *122*, 3218.
- 145** B.-J. van Rossum, C. P. de Groot, V. Ladizhansky et al., *J. Am. Chem. Soc.*, **2000**, *122*, 3465.
- 146** S. Hediger, PhD Thesis, ETH Zurich, 1997.
- 147** A. Fechtenkötter, K. Saalwächter, M. A. Harbison et al., *Angew. Chem. Int. Ed. Engl.*, **1999**, *38*, 3039.
- 148** X. Feng, Y. K. Lee, D. Sandström et al., *Chem. Phys. Lett.*, **1996**, *257*, 314.
- 149** M. Hong, J. D. Gross, R. G. Griffin, *J. Phys. Chem. B*, **1997**, *101*, 5869.
- 150** C. H. Wu, A. Ramamoorthy, S. J. Opella, *J. Magn. Reson. A*, **1994**, *109*, 270.
- 151** F. M. Marassi, S. J. Opella, *J. Magn. Reson.*, **2000**, *144*, 150.
- 152** D. P. Weitekamp, J. R. Garbow, A. Pines, *J. Chem. Phys.*, **1982**, *77*, 2870.
- 153** K. Schmidt-Rohr, D. Nanz, L. Emsley et al., *J. Phys. Chem.*, **1994**, *98*, 6668.
- 154** S. Caldarelli, M. Hong, L. Emsley et al., *J. Phys. Chem.*, **1996**, *100*, 18696.
- 155** B. M. Fung, K. Ermolaev, Y. Yu, *J. Magn. Reson.*, **1999**, *138*, 28.
- 156** H. Sun, B. M. Fung, *Liq. Cryst.*, **2000**, *27*, 755.
- 157** S. Massou, M. Tropis, A. Milon, *J. Chim. Phys. Phys.-Chim. Bio.*, **1999**, *96*, 1595.
- 158** S. Caldarelli, A. Lesage, L. Emsley, *J. Am. Chem. Soc.*, **1996**, *118*, 12224.
- 159** J. Haase, M. S. Conradi, *Chem. Phys. Lett.*, **1993**, *287*, 209.
- 160** A. P. M. Kentgens, R. Verhagen, *Chem. Phys. Lett.*, **1999**, *300*, 435.
- 161** Z. Yao, H.-T. Kwak, D. Sakellariou et al., *Chem. Phys. Lett.*, **2000**, *327*, 85.
- 162** S. Ganapathy, S. Schramm, E. Oldfield, *J. Chem. Phys.*, **1982**, *77*, 4360.
- 163** A. Samoson, E. Lippmaa, A. Pines, *Mol. Phys.*, **1988**, *65*, 1013.
- 164** K. T. Mueller, B. Q. Sun, G. C. Chingas et al., *J. Magn. Reson.*, **1990**, *86*, 470.
- 165** A. Llor, J. Virlet, *Chem. Phys. Lett.*, **1988**, *152*, 248.
- 166** I. Farnan, P. J. Grandinetti, J. H. Baltisberger et al., *Nature*, **1992**, *358*, 31.
- 167** P. J. Grandinetti, in *Encyclopedia of Nuclear Magnetic Resonance*, eds. D. M. Grant, R. K. Harris, Wiley, Chichester 1996, Vol. 3, p. 1768.

- 168** L. Frydman, J. S. Harwood, *J. Am. Chem. Soc.*, **1995**, *117*, 5367.
- 169** S. P. Brown, S. Wimperis, *J. Magn. Reson.*, **1997**, *128*, 42.
- 170** T. Vosegaard, P. Florian, P. J. Grandinetti et al., *J. Magn. Reson.*, **2000**, *143*, 217.
- 171** M. Pruski, J. W. Wiench, J.-P. Amouroux, *J. Magn. Reson.*, **2000**, *147*, 286.
- 172** J. Rocha, A. P. Esculas, C. Fernandez et al., *J. Phys. Chem.*, **1996**, *100*, 17889.
- 173** P. J. Dirken, S. C. Kohn, M. E. Smith et al., *Chem. Phys. Lett.*, **1997**, *266*, 568.
- 174** Z. Xu, H. Maekawa, J. V. Oglesby, J. F. Stebbins, *J. Am. Chem. Soc.*, **1998**, *120*, 9894.
- 175** S. P. Brown, S. E. Ashbrook, S. Wimperis, *J. Phys. Chem. B*, **1999**, *103*, 812.
- 176** S. Caldarelli, F. Ziarelli, *J. Am. Chem. Soc.*, **2000**, *122*, 12015.
- 177** L. B. Alemany, R. L. Callender, A. R. Barron et al., *J. Phys. Chem. B*, **2000**, *104*, 11612.
- 178** P. Hodgkinson, L. Emsley, *J. Chem. Phys.*, **1997**, *107*, 4808.

## **Section IV**

### **Methods 3: Mass Spectrometry**

## 10

### Mass Spectrometry

*Michael Przybylski, Wolfgang Weinmann, and Thilo A. Fligge*

#### 10.1

##### Introduction: Principles of Mass Spectrometry

Mass spectrometry (MS) is an analytical method in which free gaseous ions are produced and subsequently subjected to magnetic and electric fields in a high vacuum for analysis of mass/charge ratios. Although initially developed predominantly for physico-chemical investigations, mass spectrometry has found broad application since the 1950s in the analysis of more complex organic and small biochemical molecules [1–3]. Initial applications of mass spectrometry to the study of biological processes date back to the 1940s with stable isotope ratio measurements. Complex mixtures of compounds that were either volatile or could be derivatised to enhance volatility could be analysed by combined gas chromatography-mass spectrometry (GC-MS). However, access of mass spectrometry to applications in life sciences only became possible after solving one of the central problems, the generation and gas phase transfer of intact, structurally relevant ions of biomacromolecules [4–6]. In recent years, dramatic analytical developments and advances in instrumentation have rendered mass spectrometry central to many problems in modern biopolymer analysis. These advances make it possible to determine molecular masses of large biomacromolecules to isotopic accuracies (see Section 10.2.4); this gives the possibility of identifying, e.g. minute yet functionally critical posttranslational modifications of proteins, supramolecular biopolymer interactions and biomolecular recognition processes, using small and even impure samples [5, 7].

Since the 1980s a revolution in the use of mass spectrometry for biological analyses has occurred and continues today. A major reason for this development was the introduction of new ionisation techniques such as fast atom bombardment (FAB), plasma desorption (PD) and thermospray (TSP) permitting the production of gas phase ions from charged and polar biopolymers [7–10]. It has reached a first culmination with the recent award of the 2002 Nobel prizes in chemistry to two scientists pioneering the development of electrospray-ionisation and laser desorption mass spectrometry, John Fenn and Kuichi Tanaka [11, 12].

## 10.1.1

**Application of Mass Spectrometry to Biopolymer Analysis**

The development of efficient “soft”-ionisation methods has led to a breakthrough for the direct, molecular characterisation of biopolymers, such as proteins and nucleic acids [5–7]. While fast atom bombardment and 252-Cf-plasma desorption (PD) have enabled accurate mass determinations of polypeptides and small proteins, mass determinations for biopolymers considerably beyond 100 kDa have become feasible by electrospray-ionisation (ESI-MS) and matrix-assisted laser desorption (MALDI-MS) [11, 12]. In addition to molecular weight determinations, desorption-ionisation MS methods already have defined applications to the *primary structure* analysis of proteins, characterisation of intracellular processing pathways and the identification of post-translational structure modifications. Beyond these, recent approaches to the characterisation of higher-order (tertiary) structures, to structure–function studies and even specific *non-covalent* interactions of proteins have been recently emerging as exciting new areas of mass spectrometry [13–15]. Furthermore, the feasibility of soft-ionisation-MS methods for the analysis of multi-component proteolytic mixtures (peptide mapping) has been demonstrated successfully for the molecular characterisation of chemical modification sites in proteins, providing useful structural information, e.g. on surface topology, tertiary structure micro-environment and specific antigenic binding sites (epitopes) to antibodies [15–19].

In this chapter, classical and modern ionisation techniques and instrumental developments of mass spectrometry are described, first in order to provide an overview and understanding, particularly, of its current feasibility and application in life sciences. In a subsequent section (Section 10.2.5) an overview of important sample preparation and handling techniques for bioanalytical applications is given. Today, amounts of samples down to the attomole ( $10^{-11}$  M) range and molecular masses of proteins and biopolymer complexes over the MDa range can be measured with accuracies thousands of times greater than by classical gel electrophoresis; moreover, today’s analyser and electronics developments enable some of these powerful mass spectrometers to be relatively small and easy to use. This performance is presently experiencing a further, unrivalled breakthrough with the development of Fourier transform ion cyclotron resonance mass spectrometry (FTICR-MS; Section 10.2.4). Selected application examples are then used (Section 10.3) to illustrate the feasibility, and perspectives of mass spectrometric methods for biopolymer analyses; the most recent offspring, *proteome analysis*, has been included as a final part to illustrate a fascinating new application area [20]. This part, however, is by no means intended to provide a comprehensive review of the entire field; rather it should provide perspectives to today’s mass spectrometry instrumentation and applications of a highly dynamic area of biomolecular analysis.

## 10.2

### Techniques and Instrumentation of Mass Spectrometry

#### 10.2.1

##### Sample Introduction and Ionisation Methods

###### 10.2.1.1 Pre-conditions

In mass spectrometry ions are subjected to magnetic and electric fields in a vacuum. For this purpose, a compound has to be in a charged state, or must be ionised prior to mass spectrometric analysis. Additionally, these ions have to be transferred to the gas-phase in the vacuum system of a mass spectrometer. Mass spectrometry in general is used to analyse free ions in a high vacuum. The main problem for its biochemical application during the past decades has been the non-destructive transfer of polar and thermally labile molecules into the gas-phase, especially in the presence of suitable matrices. Gaseous or heat-volatile samples can be easily handled but many compounds are not capable of being heated without decomposition.

Therefore, special ionisation methods providing desolvation or desorption of the analyte of different matrices, and the simultaneous ionisation had to be developed. The choice of an ionisation method depends on the analyte characteristics and the required type of analytical information. Classically, “hard ionisation” methods such as *electron ionisation* (EI) or *chemical ionisation* (CI) make use of their fragmentation capabilities to gain structural information, typically of small organic molecules. In contrast, “soft ionisation” techniques such as electrospray ionisation or laser desorption are used to obtain mass spectra of intact molecules with little or no fragmentation, being capable of analysing complex multi-component mixtures.

###### 10.2.1.2 Gas Phase (“Hard”) Ionisation Methods

**Electron impact ionisation (EI)** This classical “hard” ionisation method employs an electron beam passing through the sample in the gas-phase [21]. When colliding with neutral analyte molecules another electron can be knocked off resulting either in a positively charged molecular ion of the intact analyte molecule or, more often, producing fragment ions corresponding to a certain molecular substructure. Typically, electron beams of 70 eV are used for EI (Fig. 10.1). Decreasing this energy may result in reduced fragmentation but also causes reduced sensitivity.

The samples are usually introduced through a heated direct insertion probe or, for extremely volatile samples, through a gas chromatograph. EI is the oldest and best characterised ionisation method and can be applied to all volatile and thermally stable compounds. EI mass spectra show a high reproducibility (“fingerprinting”) often used in combination with mass spectral libraries [22]. Additionally, structural information can be obtained by the fragmentation pattern produced.

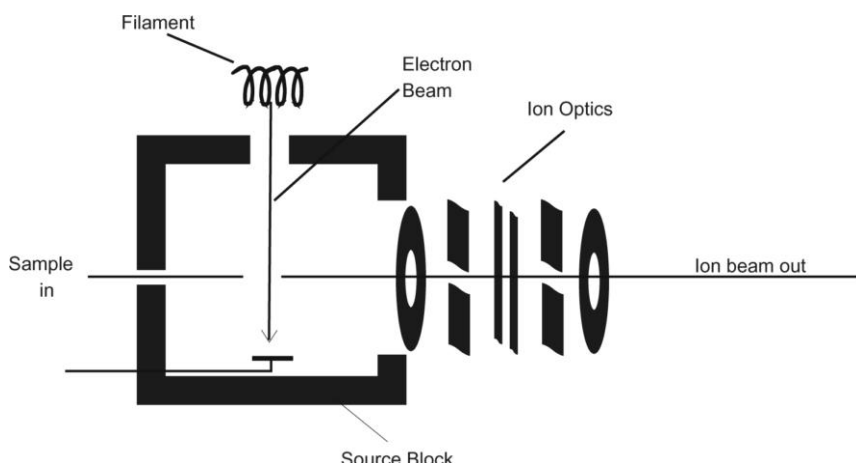


**Fig. 10.1** Set-up of an ion source for electron ionisation (EI). The analyte sample has to be available in the gaseous state within the ion source. Sample admission may be performed by gaseous and liquid inlet systems or with a heatable solid insertion probe.

**Chemical ionisation (CI)** In chemical ionisation a reagent gas such as ammonia or methane is ionised by electron impact [23]. Ion–molecule reactions between ions and neutrals of the reagent gas occur due to a high reagent gas pressure within the source. Some of these ions can react with analyte molecules to form analyte ions. The reagent gas is an energy mediator reducing the energy transfer to the sample molecules. Therefore, compared to EI, fragmentation is reduced and molecular ions such as  $[M+H]^+$  are obtained.

Samples can be introduced into the ion source through a heated direct insertion probe or by a gas chromatograph. As a variation on CI, the analyte can be placed on a filament and rapidly heated in the CI plasma in the presence of reagent gas. This so-called desorption CI reduces fragmentation and is applicable to samples that cannot be thermally desorbed without decomposition.

#### 10.2.1.3 “Soft” Ionisation Techniques

In order to detect intact molecular ions “soft” ionisation techniques had to be developed. Field desorption (FD) was the first ionisation technique established to produce mass spectra with little or no fragment-ion content. FD is based on electron tunnelling from an emitter biased at a high electrical potential [24]. The filament of the emitter is heated and the sample is evaporated into the gas-phase. Typically, intact molecular ions are detected. This method is limited to relatively low molecular weight compounds, which additionally have to be thermally stable to some extent.

As a further soft ionisation method plasma desorption (PD) has been developed [25]. The nucleic decay of  $^{252}\text{Cf}$  results in two 100 MeV products that desorb the analyte molecules from a nitrocellulose-coated film and also give the starting signal for the pulsed time-of-flight detection.

**Fast atom bombardment (FAB)** Fast atom bombardment is particularly capable of studying polar molecules with molecular weights up to c. 10 kDa [26]. The sample is dissolved in a liquid matrix with low volatility such as glycerol or *m*-nitrobenzyl alcohol and deposited on a target. The target is bombarded with a continuous beam of fast, heavy atoms (e.g. Xe) or ions (e.g.  $^{131}\text{Cs}^+$ ). In the latter case this ionisation method is also referred to as secondary ion mass spectrometry (SIMS). Molecular ions and fragments of the analyte are desorbed together with cluster ions from the liquid matrix. The latter is responsible for the chemical background in the mass spectra.

Besides the direct insertion probe, liquid chromatography (LC) has also been interfaced to FAB-MS [27]. This rapid and simple ionisation method is relatively tolerant of variations in sampling and is suitable for a large variety of compounds. It is limited by a high chemical background and therefore by difficulty in distinction between low molecular weight components and the background.

**Electrospray ionisation (ESI)** Electrospray ionisation is a method in which the analyte is sprayed at atmospheric pressure into an interface to the vacuum of the mass spectrometric ion source [28]. The sample solution is sprayed across a high potential difference (1–4 kV) from a needle tip into an orifice of the mass spectrometer. Heat and gas flows (e.g. a counter-current gas) may assist in the desolvation of the charged droplets containing the analyte molecular-ions. Finally, ion emission (Taylor-cone-model) leads to the formation of multiply protonated or deprotonated ions (Fig. 10.2).

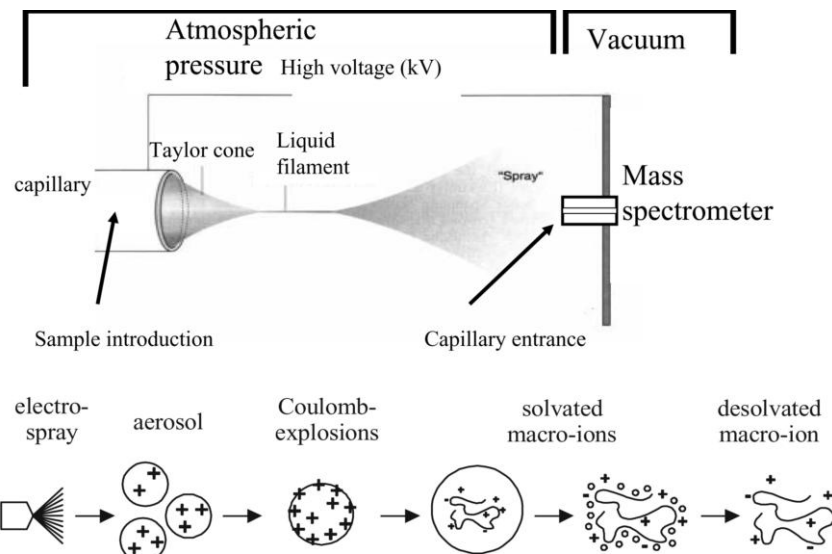


**Fig. 10.2** Principle of ionisation source and mechanism of gaseous ion formation in ESI-MS. The sample solution is admitted through a small capillary from which the spray is formed at atmospheric pressure. The charged aerosol is evaporated due to Coulomb explosions to smaller droplets which finally result in desolvated macro-ions.

The extremely soft desolvation and ionisation in ESI allows the detection of tertiary structure-related biopolymer ions, and even intact non-covalent complexes comprising specific interactions (see Section 10.3.3). Typically, multiply charged molecular ions are produced. The number of charges increases with increasing molecular weight and surface structure; ion composition correlates with, e.g. a basic or acidic analyte structure. Results of several model studies and applications have provided evidence for a correlation of *charge structures* of ions, and solution structures of biopolymers [15, 31]. This feasibility for the characterisation of higher-order biopolymer structures is one of the outstanding features of ESI-MS, among other ionisation methods [15–17].

Solution flow rates can range from microlitres to several millilitres making this ionisation method very suitable for interfacing to chromatographic separation methods. Within the last few years several microflow devices have been developed to meet the needs in protein analysis caused by the availability of only low amounts of sample [29, 30]. Especially nanoelectrospray has been shown to be feasible for protein analysis and also for the characterisation of non-covalent complexes [31]. The small nanospray-droplets enable a higher ionisation efficiency at significantly reduced spray potentials. The low flow rates enable enhanced experimental variation which is especially useful for MS/MS experiments and reaction monitoring [32, 33].

In atmospheric pressure chemical ionisation (APCI), a corona discharge is used to ionise the analyte in the source of the mass spectrometer [31]. Complementary to ESI, which is especially suitable for charged, basic or polar analytes, APCI can be used for analysis of uncharged or low-polarity compounds (e.g. steroids).

**Matrix assisted laser desorption/ionisation (MALDI)** For laser desorption methods a pulsed laser is used to desorb species from a target surface. Therefore, a mass analyser compatible with pulsed ionisation methods has to be used. Typically, time-of-flight (TOF) analysers are employed, but several hybrid systems (Q-TOF) and, recently, high resolution Fourier transform ion cyclotron resonance (FT-ICR) analysers have been successfully adapted (see Section 10.2.4). Direct laser desorption relies on the very rapid heating of the sample or sample substrate to vapourise molecules without decomposition. The more recent development of MALDI relies on the absorption of laser energy by a solid, microcrystalline matrix compound such as  $\alpha$ -cyano-4-hydroxy cinnamic acid or sinapinic acid [8, 34]. MALDI has become an extremely popular method for the rapid and sensitive analysis of high-molecular-weight compounds [4].

The analyte is typically dissolved in a solution containing an excess of the matrix that contains a chromophore absorbing at the laser wavelength. UV lasers are mainly used for protein analysis, but for certain biopolymer classes such as polynucleotides IR lasers are also employed [8, 34]. Several sample preparation techniques have been developed to place a small amount of solution on the target. The MALDI process is depicted schematically in Fig. 10.3. Although details of the mechanism are unknown at present, it is generally accepted that the matrix ab-

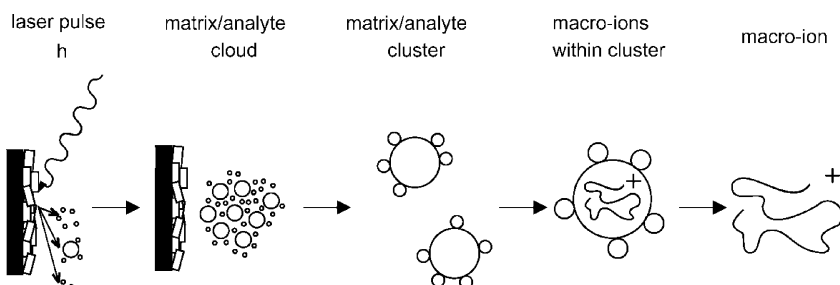


**Fig. 10.3** Principle of ionisation/desorption in MALDI-MS. A matrix/analyte-cloud is desorbed from the microcrystalline matrix/sample preparation by a laser pulse. Proton-transfer from matrix ions is thought to be primarily responsible for the subsequent generation of analyte ions.

sorbs energy from the laser pulse and produces a plasma, resulting in desorption of matrix–analyte clusters and also in ionisation of the analyte molecules [35]. Notably, low charges are generally produced, even in large biopolymers (e.g. singly and doubly protonated ions), in contrast to the multiply-charged ion structures in ESI-MS [31].

### 10.2.2

#### Mass Spectrometric Analysers

In a mass spectrometer ion formation, mass analysis, and ion detection are combined. Various mass analysers have been developed to separate ions according to their mass-to-charge ratio. Each analyser has its own special characteristics and field of application. No mass analyser can match all possible requirements. The choice of the analyser should generally be based upon the application, the performance desired, and cost.

All commonly used mass analysers use electric and/or magnetic fields to apply a force to charged molecules. The acceleration force is mass dependent, as well as dependent on the ionic charge. Therefore, it should be understood that mass spectrometers separate ions according to their mass-to-charge ratio ( $m/z$ ). The principles of all  $m/z$  analysers depend on ion energies, with the exception of FT-ICR. Since kinetic energy differences are crucial for biopolymer ions and limit the analyser performance, this renders FT-ICR-MS a prominent tool for high resolution analysis of large biopolymers (see Section 10.2.4).

##### 10.2.2.1 Magnetic Sector Mass Analysers

In a magnetic deflection mass spectrometer, ions leave the ion source and are accelerated to a high velocity. The ions subsequently pass through a magnetic sector in which the magnetic field is applied in a direction perpendicular to the direction of ion motion. By applying an acceleration perpendicular to the direction of motion of an object, the velocity of the object remains constant, but the object travels in a

circular path. Therefore, the magnetic sector follows an arc; the radius and angle of the arc vary with different optical designs.

A magnetic sector alone will separate ions according to their mass-to-charge ratio, but the resolution is limited by the fact that ions leaving the ion source do not all have exactly the same energy and therefore do not have exactly the same velocity. To focus ions according to their kinetic energy, it is necessary to add an electric sector to achieve higher resolution. Like the magnetic sector, the electric sector applies a force perpendicular to the direction of ion motion, and therefore has the form of an arc.

A schematic representation of a double-focussing mass spectrometer is shown in Fig. 10.4. For historical reasons, this set-up is referred to as a “reverse-geometry” magnetic sector mass spectrometer, which means that the magnetic sector precedes the electric sector [1].

The simplest mode of operation of a magnetic sector mass spectrometer keeps the accelerating potential and the electric sector at a constant potential and varies the magnetic field. Ions that have a constant kinetic energy, but different mass-to-charge ratio are brought into focus at the detector slit at different magnetic field strengths. The working equation of a magnetic sector mass spectrometer shows the dependence of  $m/z$  on the magnetic field  $B$  and the kinetic energy of the ions resulting from a certain acceleration voltage  $V$ :

$$\frac{m}{z} = \frac{B^2 r^2}{2V}$$

Typically, the electric sector is held constant at a value which passes only ions having the specific kinetic energy. Therefore, the parameter that is most commonly varied is the magnetic field strength  $B$ . A magnetic field scan can be used to

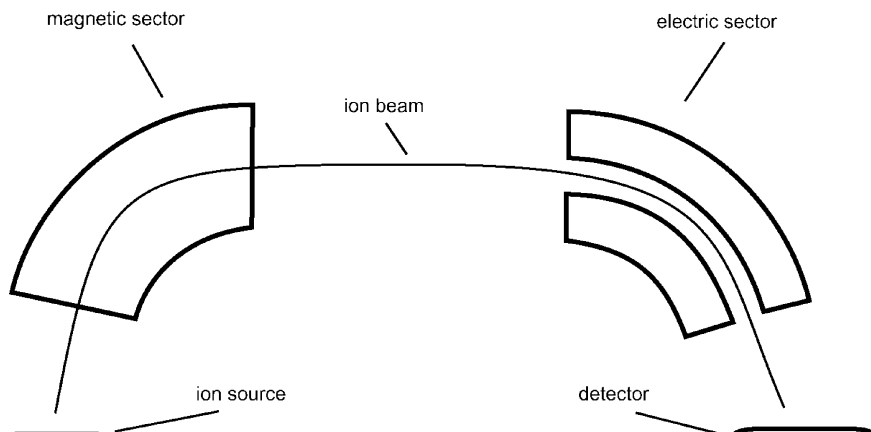


**Fig. 10.4** Scheme of a double-focussing magnetic sector instrument with BE configuration. Dependent on the mass-to-charge ratio the ions are distracted by the magnetic field to circular arcs with different radii.

cover a wide range of mass-to-charge ratios with a sensitivity that is essentially independent of the mass-to-charge ratio. The maximum ion transmission and sensitivity occur at the maximum working accelerating voltage for a given magnetic sector mass spectrometer, whereas the effective mass range of the mass spectrometer can be increased by decreasing the accelerating voltage.

The resolving power of a magnetic sector mass spectrometer is determined by the slit widths. Higher resolution is obtained by decreasing the slit widths, thereby decreasing the number of ions that reach the detector.

Linked scans, in which the magnetic and electric fields are scanned together, can be used to perform MS/MS experiments (product, precursor, and neutral loss) with a double focussing mass spectrometer.

Focal plane (array) detectors can detect a range of masses simultaneously. This provides a multichannel advantage that can improve the sensitivity for magnetic sectors, and detection limits can be improved if the analysis is limited by the analyte ion current instead of the chemical background level. This is the case for experiments such as MS/MS, electrospray ionisation, and field desorption. Array detectors can be used with pulsed ionisation methods, but the array detectors for commercial magnetic sector mass spectrometers can only detect a portion of the entire mass range at any given instant.

Double focussing magnetic sector mass analysers provide a very high reproducibility, high resolution, and a high dynamic range. Their use is limited due to their size and higher cost compared to other mass analysers.

#### 10.2.2.2 Quadrupole Mass Analysers

The quadrupole mass analyser is a “mass filter”. Combined DC and RF potentials on the quadrupole rods can be set to pass only a selected mass-to-charge ratio [36]. All other ions do not have a stable trajectory through the quadrupole mass analyser and will collide with the quadrupole rods, never reaching the detector. The operation of a quadrupole mass analyser is usually treated in terms of a stability diagram that relates the applied DC potential and the applied RF potential, and the RF frequency to a stable vs unstable ion trajectory through the quadrupole rods. A schematic diagram of a quadrupole mass filter is shown in Fig. 10.5.

Increasing the resolution decreases the number of ions that reach the detector. Good resolution also depends on the quality of the machining for the quadrupole rods. Quadrupole rods can have other functions besides their use as a mass filter. An RF-only quadrupole will act as an ion guide for ions within a broad mass range. For example, the collision region of a triple quadrupole mass spectrometer uses an RF ion guide. A DC-only quadrupole is used as a lens element in some ion optical systems.

Quadrupole mass analysers provide good reproducibility and represent a relatively small and low-cost system. Low-energy collision-induced dissociation (CID) MS/MS experiments are enabled in triple quadrupole and hybrid mass spectrometers and have efficient conversion of precursor to product. These spectra depend strongly on energy, collision gas, pressure, and other factors. Quadrupole mass

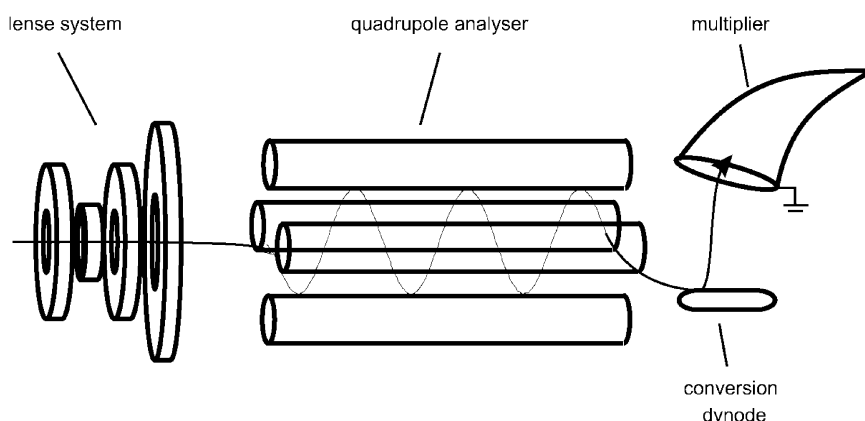


**Fig. 10.5** Scheme of a quadrupole mass analyser. Only ions with selected mass-to-charge ratio pass the combined DC and RF potentials on the quadrupole rods to reach the detector.

analysers are limited due to their comparatively low resolution. Additionally, they are not well suited for pulsed ionisation methods. Quadrupole mass analysers are employed in the majority of benchtop GC/MS and LC/MS systems due to their low cost and stable operation.

#### 10.2.2.3 Time-of-Flight Mass Analysers

A time of flight (TOF) mass spectrometer measures the mass-dependent time it takes ions of different masses to move from the ion source to the detector. This requires that the starting time (the time at which the ions leave the ion source) is well-defined. Therefore, ions are either formed by a pulsed ionisation method (usually matrix-assisted laser desorption ionisation, or MALDI), or various kinds of rapid electric field switching are used as a ‘gate’ to release the ions from the ion source in a very short time.

The working equation for the time-of-flight mass spectrometer is

$$\frac{m}{z} = \frac{2Vt^2}{L^2}$$

The ions leaving the ion source of a time-of-flight mass spectrometer have neither exactly the same starting times nor exactly the same kinetic energies. Various time-of-flight mass spectrometer designs have been developed to compensate for these differences. A linear-field reflectron allows ions with greater kinetic energies to penetrate deeper into the reflectron than ions with smaller kinetic energies. The ions that penetrate deeper will take longer to return to the detector. If a packet of ions of a given mass-to-charge ratio contains ions with varying kinetic energies, then the reflectron will decrease the spread in the ion flight times, and therefore improve the resolution of the time-of-flight mass spectrometer. A curved-field reflectron en-

sures that the ideal detector position for the time-of-flight mass spectrometer does not vary with mass-to-charge ratio. This also results in improved resolution for time-of-flight mass spectrometers.

Time-of-flight analysers are the fastest MS analysers making them especially suitable for application in high throughput LC/MS. They are well suited for pulsed ionisation methods (method of choice for the majority of MALDI mass spectrometer systems). MS/MS information can be obtained from post-source decay. TOF analysers also provide the highest practical mass range of all MS analysers, but require pulsed ionisation method or ion beam switching. For most MS/MS experiments the ion selectivity is limited.

#### 10.2.2.4 Trapped-Ion Mass Analysers

There are two principle trapped-ion mass analysers: three-dimensional quadrupole ion traps (“dynamic” traps), and ion cyclotron resonance mass spectrometers (“static” traps, see Section 10.4). Both operate by storing ions in the trap and manipulating the ions by using DC and RF electric fields in a series of carefully timed events. This provides several unique capabilities, such as extended MS/MS experiments, very high resolution, and high sensitivity. The trade-off is that trapping the ions for long periods of time (milliseconds to hours) provides sufficient time for the ions to degrade spontaneously (unimolecular decomposition), to experience unwanted interactions with other ions (space charge effects), neutral molecules (ion–molecule reactions), or perturbations in the ion motion due to imperfect electric fields [36]. This can lead to artefacts and unexpected changes in the mass spectrum (so called “non-classical mass spectra”).

Quadrupole ion traps ions are dynamically stored in a three-dimensional quadrupole ion storage device (Fig. 10.6) [37]. The RF and DC potentials can be scanned to eject successive mass-to-charge ratios from the trap into the detector (mass-selective ejection). Ions are formed within the ion trap or injected into an ion trap from an external source. The ions are dynamically trapped by the applied RF potentials (a common trap design also makes use of a “bath gas” to help contain the ions in the trap). The trapped ions can be manipulated by RF events to perform ion ejection, ion excitation, and mass-selective ejection. This provides MS/MS and  $MS^n$  experiments, which are eminently suited for structure determinations of biopolymers [38] (see Section 10.4).

Space-charge effects (ion–ion repulsion) limit the inherent dynamic range of the ion trap. This is usually handled by auto-ranging: a pre-scan is performed to determine the ion current and the ionising electron current is then adjusted to reduce the number of ions formed to within the working range. This can be done whenever the ion formation event can be manipulated to control the number of ions formed.

### 10.2.2.5 Hybrid Instruments

Hybrid time-of-flight mass spectrometers make use of a TOF analyser placed orthogonal to a beam of ions. Ions are deflected at right angles into the TOF analyser by a pulsed electrical potential from an electrode placed alongside the beam.

By having a quadrupole analyser as a gate in conjunction with an orthogonal TOF analyser, a full mass spectrum of all ions from an ion source may be obtained if the ‘gate’ is open. Alternatively, precursor ions can be selected for MS/MS so as to give a fragment ion spectrum characteristic of the precursor ions chosen, which gives structural information [39].

Combining an ion trap instrument with an orthogonal time-of-flight instrument leads to a hybrid with high sensitivity in both MS and MS/MS modes and a rapid switching between the two [40]. The combination is particularly useful for biochemical analyses because of its high sensitivity and the ease of obtaining MS/MS structural information from very small amounts of material. In either case, the TOF analyser is used to obtain the mass spectrum. Furthermore, this hybrid provides high sensitivity and a linear mass scale to 10,000 at full sensitivity. The digitised accumulation of spectra provides a better signal-to-noise ratio than can be obtained from one spectrum alone.

### 10.2.3

#### **Ion Detection and Spectra Acquisition**

After the mass analyser has dispersed the ions in space or in time according to their various  $m/z$  values, they may be collected by a detector. In modern mass spectrometry, a detector consists of a planar assembly of small electron multipliers, called an array in one case (spatial separation) and a microchannel plate in the other (temporal separation). These collectors can either detect the arrival of all ions sequentially at a point (a point ion collector) or detect the arrival of all ions simultaneously (an array or multipoint collector).

Quadrupole mass spectrometers (mass filters) allow ions at each  $m/z$  value to pass through the analyser sequentially. Therefore, the ion collector at the end of the quadrupole unit needs only to cover one point or focus in space and can be placed immediately behind the analyser. A complete mass spectrum is recorded over a period of time (temporally), which is set by the voltages on the quadrupole analyser. The resolution of  $m/z$  values is dependent solely on the analyser and not on the detector.

A multipoint ion collector (also called the detector) consists of a large number of miniature electron multiplier elements assembled side by side over a plane. A multipoint collector may be an array, which detects a dispersed beam of ions simultaneously over a range of  $m/z$  values and is frequently used with a sector type mass spectrometer. Alternatively, a microchannel plate collector detects all ions of one  $m/z$  value. When combined with a time-of-flight analyser, the microchannel plate affords an almost instantaneous mass spectrum. Because of their construction and operation, microchannel plate detectors are cheaper to fit and maintain.

Other types of mass spectrometer may use point or array or both types of ion detection. Ion trap mass spectrometers may detect ions sequentially or simultaneously and, in some cases, may not use a formal electron multiplier type of ion collector at all; the ions can be detected by their different electric field frequencies in flight, according to their  $m/z$  values.

#### 10.2.4

#### **High Resolution Fourier Transform Ion Cyclotron Resonance (ICR) Mass Spectrometry**

Ions move in a circular path in a magnetic field. The cyclotron frequency of the ion's circular motion is mass-dependent. By measuring the cyclotron frequency, one can determine an ion's mass [41].

The working equation for ICR can be quickly derived by equating the centripetal force and the Lorentz force experienced by an ion in a magnetic field:

$$f_c = \frac{zB}{2\pi m}$$

A group of ions of the same mass-to-charge ratio will have the same cyclotron frequency  $f_c$ , but they will be moving independently and out-of-phase at roughly thermal energies. If an excitation pulse is applied at the cyclotron frequency, the "resonant" ions will absorb energy and be brought into phase with the excitation pulse. As ions absorb energy, the size of their orbit also increases.

The packet of ions passes close to the receiver plates in the ICR cell and induces image currents that can be amplified and digitised. The signal induced in the receiver plates depends on the number of ions and their distance from the receiver plates.

If several different masses are present, then one must apply an excitation pulse that contains components at all of the cyclotron frequencies. This is done by using a rapid frequency sweep ("chirp"), an "impulse" excitation, or a tailored waveform. The image currents induced in the receiver plates will contain frequency components from all of the mass-to-charge ratios. The various frequencies and their relative abundances can be extracted mathematically by using a Fourier transform which converts a time-domain signal (the image currents) to a frequency-domain spectrum (the mass spectrum).

A cubic ICR cell consists of three pairs of parallel plates (see Fig. 10.7). The functions of the excitation and receiver plates are apparent from the preceding discussion. A small potential is applied to the trapping plates to keep the ions contained within the ICR cell because the magnetic field does not constrain the ion motion along the direction of the applied magnetic field. Besides the cubic cell, many other ICR cell designs have been evaluated and used in FTICR instruments, and each has its own special characteristics.

Excitation events can be used to increase the kinetic energy of ions, or to eject ions of a given mass-to-charge ratio from the cell by increasing the orbital radius until ions are lost by collisions with the cell plates. The background pressure of an

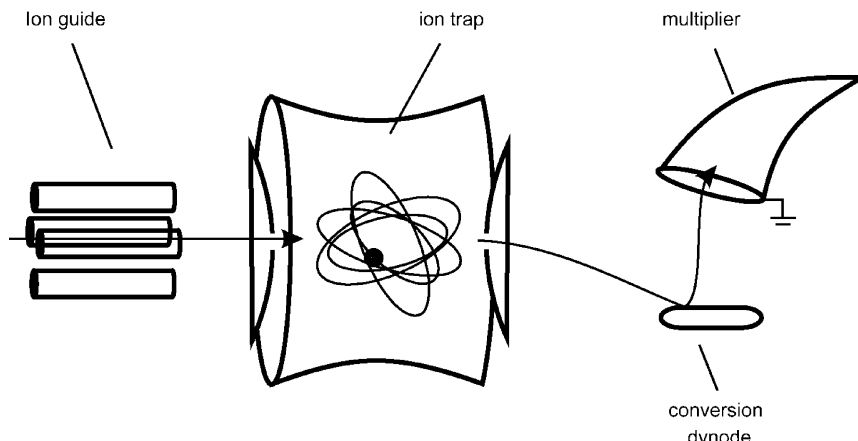


**Fig. 10.6** Scheme of an ion trap mass spectrometer. A defined ion beam is admitted into the trap through a focussing ion guide, e.g. quadrupole.

FTICR should be very low to minimise ion–molecule reactions and ion–neutral collisions that dampen the coherent ion motion. A variety of external ion source designs have been developed to deal with this problem, and each design has its own performance characteristics [42].

Most FTICR mass spectrometers use superconducting magnets, which provide a stable calibration over a long period of time. Although some mass accuracy can be obtained without internal calibrant, mass accuracy and resolution are inversely proportional to  $m/z$ , and the best accurate mass measurements require an internal calibrant. Unlike the quadrupole ion trap, the FTICR mass spectrometer is not operated as a scanning device.

The above working equation of FTICR shows that the  $m/z$  measurement is only dependent on the external magnetic field and, in contrast to all other mass spectrometric analyser systems, independent of the ion's kinetic energy [41]. This feature provides the basis for the intrinsic high resolution capability of the FTICR method for the analysis of biopolymers.

FT-ICR-MS has recently enabled a breakthrough in the ultra-high resolution mass spectrometric analysis of biopolymers using both ESI and MALDI ionisation. A unique attribute of FT-ICR-MS in comparison to other MS methods is its ability to simultaneously provide high mass resolution ( $> 10^6$ ), mass determination accuracy ( $< 1$  ppm), and sensitivity. A schematic diagram of a commercial FTICR mass spectrometer (Bruker Apex II with ESI and MALDI ionisation sources) is shown in Fig. 10.7. Of particular interest is the versatility of FT-ICR-MS<sup>n</sup>-techniques for structure determination using fragmentation by CID or IR laser irradiation (IRMPD) [43], and the coupling with micro/nano-ESI. As an example of the ESI-FTICR performance, the spectrum of the protein ubiquitin (Fig. 10.8) provides a mass determination accuracy of c. 1 ppm at a mass resolution of c. 80,000 [44]. The charge states of the multiply protonated ions are readily defined from the

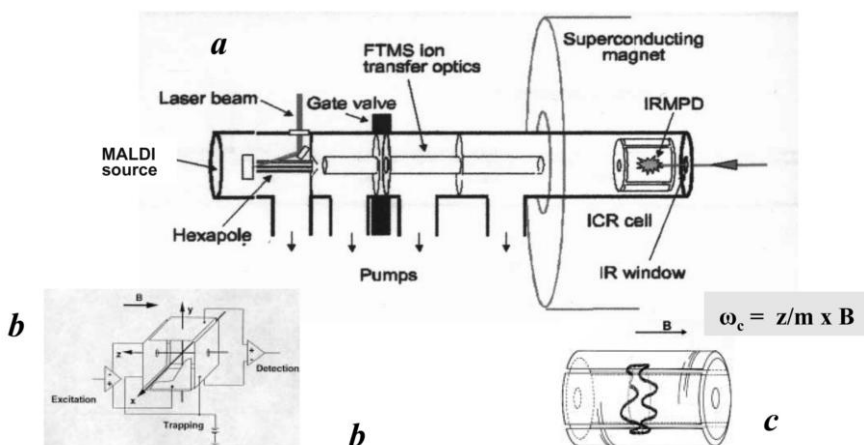


**Fig. 10.7** Scheme of the Bruker Apex-II FT-ICR mass spectrometer (a) with MALDI ionisation source and subsequent hexapole ion retardation, ion transfer optics/high vacuum system, and ICR cell with IRMPD system through a rear exit IR window. (b), (c) schematic illustration of cubic and cylindrical ICR cell configurations with excitation, trapping and detection plates.

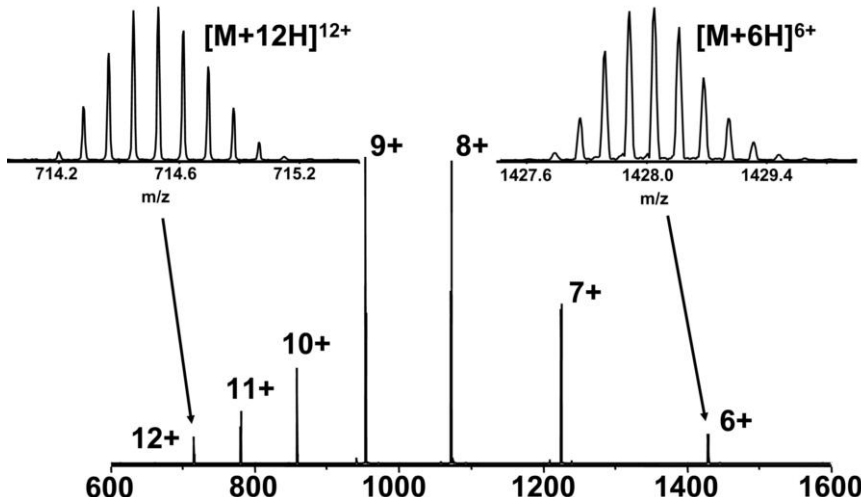


**Fig. 10.8** ESI-FT-ICR mass spectrum of bovine ubiquitin. A sample solution of ca.  $0.01 \text{ mg ml}^{-1}$  (monoisotopic molecular weight, determined: 8559,5912; calculated: 8559,6162;  $\Delta m$ : 3 ppm). The inserts show isotopic separa-

mass difference of two adjacent isotopes, without the need for deconvolution techniques. This is of importance, e.g. for the ESI-MS analysis of non-covalent complexes where a low charge distribution may yield only a few peaks that are difficult to deconvolute [31].

### 10.2.5

#### Sample Preparation and Handling in Bioanalytical Applications

Most biological samples analysed by GC/MS or LC/MS need sample preparation, depending on the matrix content and concentration of the analyte. In clinical and forensic toxicology, for example, body fluids such as blood/serum and urine have to be analysed as well as tissue samples (organs, muscle), stomach contents, and hair [45]. In environmental toxicology, sewage sludge, sediments, waste water, or plant material contain only traces of the analytes of interest, thus concentration and clean-up steps are necessary prior to analysis.

For the determination of drugs in plasma, extraction and concentration are also necessary in most cases. Matrix effects can influence the chromatographic separation in GC- or LC/MS, and also the ionisation process in ESI mass spectrometry [45, 46].

##### 10.2.5.1 Liquid–Liquid Extraction (LLE)

Liquid–liquid extraction of organic, non-polar analytes for subsequent mass spectrometric analysis is still a common method in clinical, pharmaceutical, and environmental analysis, especially for the analysis of aqueous phases such as plasma and urine, but also for tissue samples. Major goals of the methodology development in the last ten years have been miniaturisation, automation [47] and the removal of solvents with high toxicity (e.g. benzene and halogenated solvents). Liquid–liquid extraction is usually a robust method because only two natural constants are relevant for the extraction efficiency, the distribution constant between the organic and aqueous phases and the dissociation constant of the acidic or basic analyte; furthermore, pH and temperature can be optimised and controlled easily. LLE can provide high selectivity for the analytes of interest. Some efforts at automation have been made for the high-throughput pharmacokinetic analysis of human plasma samples, by using deep-well 96-well plates for extraction (e.g. in the determination of the anticancer drug methotrexate [48]), or an automated liquid handling system customised with integrated mechanical shaker and valve systems [47].

For systematic clinical toxicological analysis, also known as “general-unknown screening”, Pfleger et al. have developed extraction and derivatisation methods for GC/MS analysis for subsequent electron impact mass spectra library searching [49]. In their procedure urine (plasma or gastric content) is extracted directly or after acidic hydrolysis (for the cleavage of phase-II-metabolites) with solvent mixtures containing ethyl acetate, diethyl ether and dichloromethane. The hydrolysed fraction is acetylated prior to GC/MS, to convert amines and hydroxides into volatile derivatives. Other derivatisation methods have also been used, such as alkylation with phase-transfer catalysis and silylation, e.g. for the detection of carboxylic acids. In other liquid–liquid extraction procedures for drugs from plasma or urine samples, 1-chlorobutane has been used for subsequent GC/MS or HPLC-analysis [50, 51].

### 10.2.5.2 Solid Phase Extraction (SPE)

In contrast to liquid–liquid extraction, solid phase extraction is considerably more complex and is based on a sorbent with specific affinity for the analyte. Several sorbents have been developed, most being silica-based with different modifications (reversed phase, ion exchange, diol- and amino-phases) or polymer-based (e.g. polystyrene–divinylbenzene copolymer). SPE methods for screening toxicological analysis have been reviewed by Franke et al. [52] who concluded, that although silica-bonded phases (especially mixed-bonded phases with reversed-phase C8 or ion-exchange functions) were used for screening analysis, no single extraction procedure provides optimum results for different sample types and detection techniques. Sample pre-treatment is highly dependent on the sample type: For example, whole blood or tissue homogenate cannot be applied directly onto SPE columns, whereas plasma or urine can be applied directly or after simple dilution.

Using SPE disks or small bead-volume cartridges for miniaturisation of sample volumes and robotics with 96-well plates, automation is facilitated for large numbers of plasma and urine samples, especially in combination with LC/MS/MS detection [53, 54]. On-line sample concentration by trapping-columns for automated LC/MS-analysis will be discussed in Section 10.2.6.

### 10.2.5.3 Immunoaffinity Extraction (IAE)

Immunoaffinity extraction (IAE) is probably the most effective way of extracting trace amounts of analytes from biosamples, especially if coupled directly to LC/MS/MS. Henion et al. published a method for automated IAE-LC/LC-MS/MS-analysis for the detection of LSD metabolites and beta-agonists in urine, and benzodiazepines from chemical libraries [55, 56], whereas Maurer et al. used IAE for the determination of amatoxins in urine [57]. Approximately 20-fold higher sensitivity was achieved in these studies by IAE compared to the standard SPE method. However, a disadvantage of IAE is the narrow linear range due to the fact that the antibodies are easily overloaded.

### 10.2.5.4 Solid-phase Microextraction

Solid-phase microextraction (SPME) is currently under investigation in many laboratories for its usefulness for a large variety of bioanalytical applications. SPME involves extraction and pre-concentration with a fused silica fibre or tubing coated with a polymeric stationary phase. SPME can be performed in two-phase (sample–fibre coating) and three-phase (sample–headspace–fibre coating) systems [58].

Desorption for GC-analysis is performed directly in the GC-injector by increasing the temperature. For HPLC analysis an interface has been constructed for solvent extraction of the analyte from the fibre, followed by introduction of the solvent into the LC injector [59].

Besides applications to volatiles from solid samples, liquids and gaseous samples, polar and less volatile compounds are increasingly under study as analytical targets and difficulties with small partition coefficients and long equilibration

times have been identified. Headspace methods minimise interactions between sample and fibre and have proven useful for semivolatile analytes such as amphetamines from urine, and free volatile fatty acids in waste water [60, 61]. Several experimental concepts have been pursued for optimisation of the method, including matrix modification by heating, addition of salt, and pH buffering.

Automated “in-tube” solid-phase microextraction (SPME) has recently been coupled with liquid chromatography/electrospray ionisation mass spectrometry (LC/ESI-MS), e.g. for the determination of drugs in urine [60, 62]. In-tube SPME is an extraction technique in which analytes are extracted from the sample directly into an open tubular capillary by repeated draw/eject cycles of sample solution. The analyte is then desorbed with methanol and transferred to an analytical HPLC-column.

The solid-phase microextraction (SPME) device has been also employed as a time-weighted average (TWA) sampler for gas-phase analytes [63]. This was performed by retracting the coated fibre a known distance into its needle housing during the sampling period. Unlike in conventional spot sampling with SPME, the TWA sampling approach does not allow the analytes to reach equilibrium with the fibre coating, but rather they diffuse through the opening in the needle to the location of the sorbent. The amount of analytes accumulated over time gives the average concentration to which the device was exposed to. Depending on the sorbent used, TWA sampling is possible for 15 min up to 12 h.

#### 10.2.5.5 Supercritical-Fluid Extraction (SFE)

SFE has been automated for serial extraction of samples. Fields of applications of SFE with supercritical carbondioxide and additional modifiers have been environmental (sewage sludge [64]) and forensic toxicology (drugs [65, 66]), as well as food and plant analysis [67]. On-line coupling to different analytical methods (IR, NMR, fluorescence detection, MS) has recently been reviewed [68], but most bioanalytical applications are based on the off-line extraction with subsequent analysis by GC/MS or LC/MS.

#### 10.2.6

#### Coupling of Mass Spectrometry with Microseparation Methods

A detailed review of interfacing microseparation methods with mass spectrometry has been recently published by Tomer [69]. This covers the development of interfaces for micro- and nano-LC, capillary electrophoresis (CE), capillary electrochromatography (CEC), micellar electrokinetic chromatography (MECC), and capillary isotachophoresis (ITP) and mass spectrometry in the recent past. Furthermore, multidimensional chromatography/MS, microfabricated microfluidic devices (microchip)/MS, LC/MALDI-MS, affinity chromatography/MS and supercritical fluid chromatography/MS were discussed in this article. Although GC/MS is often considered a mature field, new developments in GC/MS have been covered including fast GC/MS using TOF-MS and supersonic molecular beam-GC/MS. In the follow-

ing an overview is given of the miniaturisation of LC/MS which has become a routine technique in many bioanalytical laboratories, as well as for the structural identification of biopolymers.

#### 10.2.6.1 Liquid Chromatography-Mass Spectrometry Coupling (LC-MS)

GC/MS with capillary columns has been the gold standard for more than 20 years, but LC/MS has become a complementary method due to the success in interface development with atmospheric pressure ionisation (API) for low molecular weight compounds and the application to biopolymers. For many areas of analytical chemistry, LC/MS has become indispensable due to its advantages over GC/MS for polar and thermolabile analytes. A limiting factor for LC/MS has been the incompatibility between the liquid eluting from the LC and the mass spectrometer vacuum. This could be overcome in electrospray ionisation with the use of a nebuliser gas ("ion spray") or additional heated drying gas ("turbo ion spray") [70, 71]. Due to its high sensitivity and selectivity, API-MS has become a standard tool for the structure elucidation of analytes from complex mixtures.

Standard electrospray is limited to flow rates below  $10 \mu\text{l min}^{-1}$ , whereas nebuliser assisted ESI can handle up to  $100 \mu\text{l}$  (ion spray); turbo-ionspray, orthogonal or Z-spray (from different instrument manufacturers) can handle flow rates up to  $2 \text{ ml min}^{-1}$  without split. APCI is normally used with flow rates of  $0.2\text{--}1 \text{ ml min}^{-1}$  and can be used with normal- and narrow-bore columns without splitting the eluent, whereas ESI can also be used with microseparation methods. Microseparation methods such as nanocapillary-HPLC, capillary electrophoresis (CE) and capillary electrochromatography (CEC) have the advantage that higher separation efficiencies are achieved, yielding narrow analyte peaks and high peak concentrations. Drawbacks of the microseparation methods are that only low sample amounts are applicable [72] and only a short path length can be used for detection. The advantage of low flow-rates is that the complete effluent can be transferred to the mass spectrometer thus yielding high detection sensitivity. Several ESI parameters such as the diameters of the spray tip and positions relative to the sampling orifice can be optimised to improve ionisation efficiency and ion sampling. As noted in Section 10.2.1.3 the use of microspray systems enhances sampling efficiency. Another way to increase the number of ions sampled to the mass spectrometer is the use of larger entrance skimmers or capillaries; however, this requires a higher gas flow entering the mass spectrometer. The relationship of flow rate and sensitivity has been investigated by Hopfgartner et al. and Oosterkamp et al. [73, 74], who showed that optimum flow rates for conventional ESI range from  $1$  to  $10 \mu\text{l min}^{-1}$ , while rates for ion-sprays range from  $50$  to  $1000 \mu\text{l min}^{-1}$  using a heated drying gas. Micro-LC/ESI-MS can be performed with conventional ESI-sources with ESI-emitters of small internal diameter [75], whereas for nano-LC (flow-rates  $< 2 \mu\text{l min}^{-1}$ ) micro-ESI interfaces with custom-made ESI-emitters have been used [76]. Low diameter ESI-emitters have been produced by different techniques, e.g. by electropolishing of metal needles, treatment of silica-capillaries with HF or drawing with a laser-puller with subse-

quent surface coating (gold sputtering) [77]. However, most promising is the coupling of nanoscale capillary-LC with nanospray-MS using a coaxial sheath flow interface. Flow rates below  $200 \text{ nl min}^{-1}$  [78] can be achieved, yielding high sensitivity, e.g. for peptide mixture analysis. With the downscaling of LC-separation and ESI interfaces, detection limits down to the low femtomole range have been obtained; however, on-line separations with flow rates  $> 100 \text{ nl min}^{-1}$  are still less sensitive than continuous sample flow from nanoelectrospray tips [79, 80] which typically have flow rates of 1 to  $20 \text{ nl min}^{-1}$ . Furthermore, on-line pre-concentration by column-switching prior to micro- or nano-LC/MS has been shown to improve concentration detection limits [76, 81] and can be used to overcome limited sample volumes. During the last years, ESI-emitters for nano-flow LC or CE separations have become commercially available. A major drawback of nano-LC/MS is still its lack of robustness due to capillary plugging; however, miniaturised LC/MS systems are likely to be further optimised in the near future.

#### 10.2.6.2 Capillary Electrophoresis (CE)-Mass Spectrometry

In contrast to HPLC, flow rates of capillary zone electrophoresis (CE) are in the low nanolitre-per-minute range. Migration of analytes between the buffer reservoirs at both ends of a fused-silica capillary is effected by electromigration and electro-osmosis [82]. Electrophoretic migration occurs with positively charged species from anode (high positive potential) migrating to the cathode (low or ground potential) or vice versa. Electro-osmotic flow (EOF) occurs when an electrical potential is applied across a liquid-filled porous medium, it acts to sweep all solutes through the capillary and does not promote separation. Surface deactivation can lead to suppression of the EOF so that the flow of solvent from the capillary is minimised.

For CE-MS coupling different sheath-flow interfaces have been designed ([82–84] in addition to a liquid-junction interface [85] (using a liquid reservoir for electrical contact without a make-up flow of liquid and a porous glass joint [86]. Furthermore, off-line coupling devices have been developed for the coupling of MALDI to CE, basically by means of sheath-flow interfaces for sample collection and subsequent target-preparation [87–89]. To overcome the low amounts of analyte in CE, capillary transient isotachophoresis (tITP) has been used for analyte concentration [90–92]. The high separation efficiency of CE makes it attractive for the analysis of complex mixtures after sample clean-up and concentration; a main drawback still being the limited amount of sample load onto the CE capillary.

In capillary electrochromatography (CEC) a liquid flow through a packed capillary is created by application of an electric field. Several interfaces have been designed for coupling to ESI-MS, and current applications have been reviewed [93, 94]. CEC is a good alternative for neutral analytes in combination with mass spectrometric detection, since no interferences with micellar matrix can occur [95]. The combination with LC, resulting in an electrically and a pneumatically driven flow of solvent, has been called pressurised CEC. This combination offers new opportunities for the separation of complex mixtures.

### 10.3

#### Applications of Mass Spectrometry to Biopolymer Analysis

##### 10.3.1

###### Introduction

As pointed out in Section 10.1.1, the development of “soft”-ionisation mass spectrometry has caused a revolution in both the range of bioanalytical application areas and particularly, the possibilities for molecular structure–function analysis of biopolymers. The two currently dominant techniques, ESI-MS and MALDI-MS have driven the development and perfection of several high-resolution separation techniques, particularly 2D-gel electrophoresis and HPLC, for mass spectrometric applications. Combinations of these mass spectrometric approaches, with suitable protein-chemical and biochemical procedures, have become feasible for molecular studies of even highly complex mixtures, and heterogeneous forms of biopolymers [6, 15]. Thus, mass spectrometric approaches are now suitable for the identification of low levels of specific sequence mutations, post-translational modifications and other subtle covalent structural changes, frequently hitherto undetectable [5–7]. Moreover, MS approaches have been recently developed for new applications with great demand, and/or lack of molecular-biochemical techniques, the characterisation of tertiary structure and conformational states, specific *non-covalent* biopolymer complexes, and *molecular recognition* structures (epitopes; receptor ligands) [31].

In the following sections, illustrations of *some* of these applications are presented, including an outline of mass spectrometric *proteome* analysis as an area which is presently exerting a dramatic impact on biotechnology and biomedical research. Furthermore, the particular role of high-resolution, FT-ICR-MS as a molecular tool in biopolymer analysis will be illustrated. Within these bioanalytical applications, studies employing the combination of specific protein-chemical modification reactions and mass spectrometric peptide mapping have been included [15, 16] to illustrate the wide variety of useful structural information amenable to biopolymer mass spectrometry, e.g. on surface topology and tertiary structure micro-environment.

##### 10.3.2

###### Analysis of Peptide and Protein Primary Structures and Post-Translational Structure Modifications

Mass spectrometric methods have been effectively developed recently to sequence determinations (partial or complete) of polypeptides, and even *de-novo* sequencing of proteins [7, 96, 97]. The two general strategies for peptide sequencing, (i) mass spectrometric fragmentation of a peptide backbone, particularly using tandem-MS methodologies and (ii) specific enzymic or chemical cleavage and subsequent mass spectrometric analysis of truncated peptide ion mixtures, are complementary. Different types of MS/MS instrumentation with triple quadrupole and tandem

magnetic sector spectrometers have been successfully employed, and have been summarised in reviews [97, 98]. Fragmentations at the peptide backbone produce major types of sequence-specific ions from both the N- and C-terminal end (e.g. “b”- and “y”-ions, see Fig. 10.9) which have been named according to a nomenclature first proposed by Roepstorff et al. [99]. Such fragmentations can occur as a result of the ionisation method directly, such as capillary-skimmer voltage-induced dissociation of molecular ions in ESI-MS ( $\Delta$ CS), or by collision-induced decomposition (CID) with a neutral gas molecule; they are, in principle, suitable both for sequence determinations and the identification of post-translational modifications.

Sequence determinations have been performed by FAB-MS/MS fragmentations of  $[M+H]^+$  ions with magnetic sector and triple-quadrupole instruments. A major disadvantage of the tandem magnetic sector is the relatively large and expensive instrumentation, while triple-quadrupole MS/MS systems as smaller, low resolution instruments have been shown to be effective for rapid sequencing of smaller peptides [7, 29, 97]. Electrospray ionisation has also been used effectively for peptide sequencing, both with triple-quadrupole MS/MS and with ion trap systems [96, 99]. Most recently, FTCIR-MS has been shown to provide substantial advances in the high mass determination accuracy and high sensitivity over a wide mass range; the possibility of simultaneous excitation and detection of *in-source* fragment ions of all mass-to-charge ratios, and of collision induced dissociation (CID) in the ICR ion cell enables the acquisition of detailed primary structure data [41, 43, 44, 100–102]. This is illustrated in Fig. 10.9 by the capillary-skimmer fragmentation in the ESI-FT-ICR spectrum of a cytosolic polypeptide domain of the Alzheimer amyloid precursor protein, APP(723–767). It has been shown that the cleavage of APP to amyloidogenic products involves a complex pathway that is mediated by intracellular targeting sequences located in the cytosolic tail, hence knowledge of

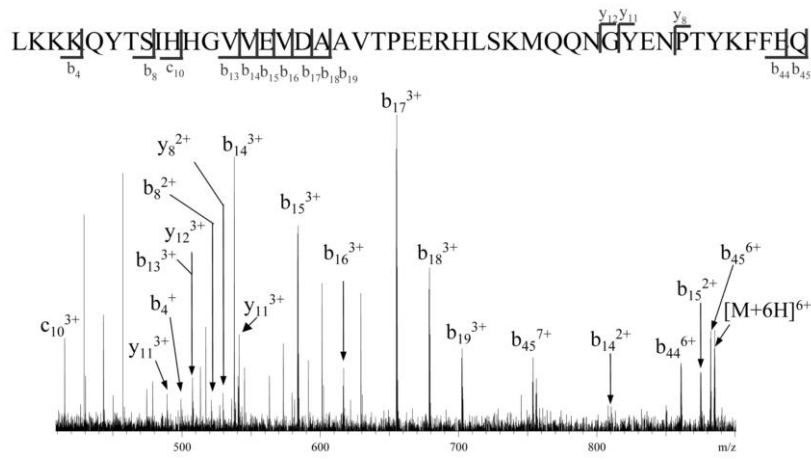


**Fig. 10.9** ESI-FT-ICR spectrum showing capillary-skimmer fragmentation of the cytosolic polypeptide domain of Alzheimer amyloid-precursor protein, APP(723–767). Sequence-specific b- and y-ions are indicated with sequence positions and charge states in the spectrum, and partially in the sequence. Capillary exit voltage, 130 V; sample concentration c. 0.01  $\mu\text{g}\ \mu\text{l}^{-1}$  [105].

the cytoplasmic APP structure is important for understanding the amyloid formation at the molecular level [103, 104]. The accuracy of fragment ion mass determinations (Fig. 10.9) yields detailed structural information by b- and y-sequence ions [105]. In addition, fragmentation by ESI-FTICR using collision-induced dissociation (SORI-CID) in the ICR cell provides fragment ions covering the complete sequence.

A second general approach consists of successive chemical and/or enzymatic exopeptidolytic cleavage, in combination with mass spectrometric analysis of the truncated peptide mixture [7]. This approach has been quite successful in obtaining *partial* sequence determinations with a variety of carboxypeptidases and aminopeptidases of broad specificity (such as carboxypeptidase Y), and by using ESI-MS and MALDI-MS, as well as other ionisation methods (FAB) for oligo- and polypeptides, and is suitable for identification of modified amino acids in peptides [106–108]. Limitations of this approach are (i) that isobaric residues cannot be determined (Leu/Ile), Gln/Lys require high resolution-MS with isotopic mass accuracy [109] and (ii) the difficulty in producing homogeneous stepwise truncated peptide series. For the latter reason, techniques employing N-terminal Edman degradation and mass spectrometric analysis of the stepwise shortened peptide have been introduced [110, 111]. For example, addition of a small amount of the reaction-terminating phenyl-isocyanate has been employed in Edman degradation to produce a homogeneous truncation series (“ladder sequencing”), and has been successful for determination of shorter peptide sequences [112].

Mass spectrometric sequencing, and specific fragmentation methods have been developed with considerable success (in some cases as key techniques) for the identification of covalent post-translational modifications in proteins, such as glycosylation, acylation, intramolecular disulfide linkages, phosphorylations etc. [113–118]. Using suitable chemical procedures for (i) selective cleavage of the modification group from the peptide backbone and (ii) partial sequencing, in conjunction with mass spectrometry, the modification position within the polypeptide chain can often be identified, even in cases where a complete structure determination is not directly feasible [117, 118]. Such approaches may include the mass spectrometric analysis of the intact protein before and after removal of a modification group, and/or Edman degradation and mass spectrometric analysis of the modified sequence. While these methods have been successful for identification of single-site modifications such as alkylated or fatty-acylated residues [119, 120], more complex modification structures such as glycosylations [121–123] require a specific set-up of chemical reactions in combination with mass spectrometric analysis. For the analysis of glycosylations the identification of attachment sites of carbohydrates to proteins (N- and O-linked) is a first tedious task, aided by the consensus Asn-tripeptide motif for possible N- (but not O-) glycosylation. However, the considerable heterogeneity and structural complexity of (e.g. branched, multi-antennary) glycosylations make it frequently necessary to use separate analytical strategies and procedures for the carbohydrate analysis [6, 7]. Mass spectrometric determinations of carbohydrate structures in protein glycosylations have been summarised in reviews [4, 6, 7].

The characterisation of phosphorylated protein structures is discussed in the following to illustrate the use and requirements of specific mass spectrometric strategies and analytical procedures for post-translational modifications. Phosphorylation is a key step, not only for the replication control, but also for the regulation of gene expression and protein synthesis controlling cell growth, division and differentiation, hence the identification of the specific phosphorylation sites is essential in order to understand the molecular basis of these regulatory mechanisms. Due to the low level, and complexity (multiplicity) of many phosphorylations, the use of immobilised metal ion affinity (IMAC) enrichment of phosphopeptides, e.g. from proteolytic mixtures has been shown to be an efficient step for their identification by MALDI-MS and ESI-MS [124, 125]. The adsorption in IMAC is based on a reversible complex between the phosphate and Ga(III) under acidic conditions which dissociates at slightly alkaline pH. Enzymatic cleavage by alkaline phosphatase, in combination with Ga(III) IMAC and MALDI-MS provides the identification of phosphopeptides by observation of 80 amu mass shifts, and of phosphorylation sites by analysis of metastable fragmentations (loss of  $\text{HPO}_3$  and  $\text{H}_3\text{PO}_4$ ) [126].

The selectivity of Ga(III)- IMAC for phosphopeptides, combined with the specificity of mass determination by MALDI-MS often enables the identification of phosphopeptide candidates, by comparing the predicted proteolytic peptide masses to experimentally determined mass values. However, the high mass

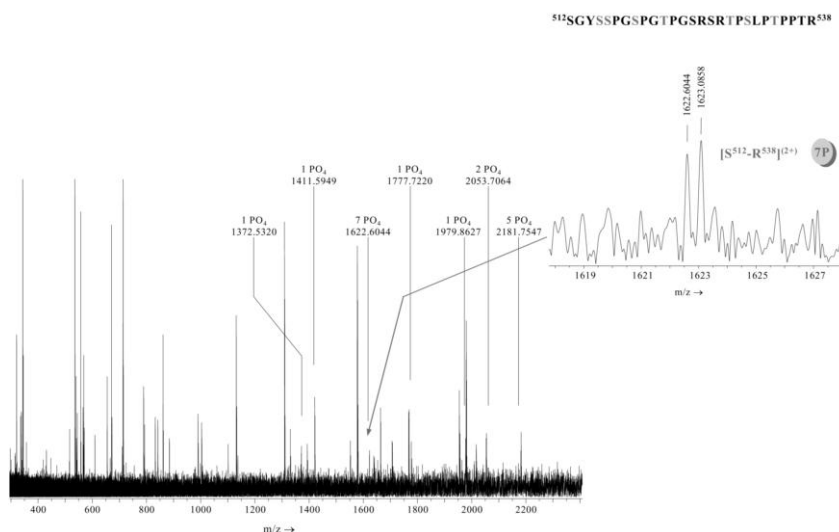


**Fig. 10.10** ESI-FTICR mass spectrum of tryptic digest mixture of multi-phosphorylated human neurofibrillary tau protein. Peak assignments within the  $m/z$  detection range, 200–2500, are shown for phosphorylated peptides. The insert shows the peptide fragment of the phosphorylation domain (512–538); the seven phosphorylation sites, identified using information from the NiceProt View of Swiss Prot database (primary accession number P10636), are indicated in red (C113, H191, N36, P7, doubly protonated; calc. 1622.55513, found 1622.60435,  $\Delta = 30$  ppm) [44].

determination accuracy of FT-ICR-MS may enable the *direct* (without enrichment) characterisation of phosphorylation structures, as shown recently in a study of the multi-phosphorylated, neuronal Tau protein [44, 127]. Tau is a microtubule-associated protein which is involved in promoting microtubule assembly and has recently gained widespread interest as a target protein in neurofibrillary tangles characteristic of Alzheimer's disease [128]; the pathophysiological aggregation of tau in brain tissue has been shown to be associated with hyper-phosphorylation. In the ESI-FT-ICR spectrum of a tryptic peptide mixture of human neurofibrillary tau the complete primary structure, including a total of 18 serine- and threonine-phosphorylations, could be directly identified, demonstrating the high analytical utility of the high resolution FT-ICR-MS; in the tryptic peptide 7 and 5 phosphorylation sites could be directly identified in the multiphosphorylation domains (512–538) and (382–398), respectively (Fig. 10.10).

### 10.3.3

#### Tertiary Structure Characterisation by Chemical Modification and Mass Spectrometry

Chemical modification reactions have long been employed in structure–function studies of proteins, e. g. for modifying enzymatic properties and immunological reactivity [15, 129]. Although a number of specific reactions for amino acid residues have been evaluated (see [13, 15] for reviews), their full development has long been impeded by the lack of specific methods for characterising the multiple reaction products [129]. In contrast to conventional methods based on electrophoretic or chromatographic procedures, mass spectrometric peptide mapping of proteolytic digest mixtures has been found highly suitable for the rapid and sensitive identification of multiple chemical modification sites [130]. A general analytical scheme has been developed for the characterisation of “native-like” chemically modified proteins [15] which involves, in a first step, the determination of the extent of modification (i. e. number and distribution of modified residues) by direct mass spectrometric molecular weight determination. Here, an additional level of information is provided by ESI-MS by the distribution of multiply charged ions (“charge structures” [13,31]) due to their correlation with conformation states in solution [13]. In a second step, denaturation and proteolytic digestion is performed, and the sites of modifications are identified by mass spectrometric peptide mapping of the fragment mixtures [131]. Furthermore, assignments of relative reactivities at specific residues can be obtained from series of partially modified proteins [130].

Such mass spectrometric determinations of reactive sites in intact protein structures by chemical modifications in proteins have been found highly useful in structure–function studies of proteins [15], such as for ion-channel proteins (porins; see Fig. 10.11). The structures of several bacterial porins have been determined by X-ray crystallography, such as the porin from *Rhodobacter capsulatus* (R. c.-porin) [132] which forms a trimeric complex of 16–18-stranded  $\beta$ -barrels. A characteristic structure element of R. c.-porin is a central constriction loop inside the  $\beta$ -barrel, which has been suggested as the central site determining cation/anion permeability and

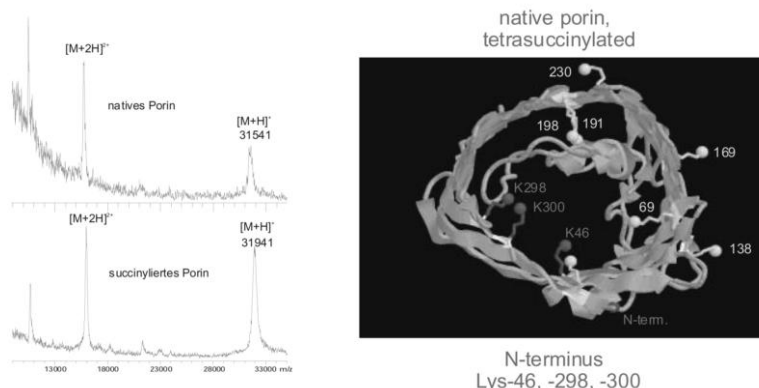


**Fig. 10.11** MALDI mass spectra (left) of native and tetra-succinylated *Rhodobacter capsulatus* porin, and X-ray structure (right) of the succinylated porin [133]. The modified residues Lys-46, -298 and -300 and the N-terminus are indicated in red; unmodified Lys residues are shown in yellow.

transport selectivity [15]. The R. c.-porin was succinylated at conditions that provide native-like acylation of amino groups [133]. The structure of the succinylated porin was identified by X-ray crystallography at 2.4 Å resolution (see Fig. 10.11); however, the electron density maps did not permit an assignment of the succinylated groups, although ion transport experiments revealed substantial single channel conductance. The precise extent and the sites of succinylations were determined by MALDI-MS which showed a predominantly tetra-succinylated protein (Mw 31941 Da; Fig. 10.11) [133]. The identification of the succinylation sites by MALDI-MS peptide mapping revealed the selective modification of three Lys-amino groups at the inner channel surface (K-46, K-298, K-300), and of Lys-46 at the channel constriction loop. This specific pattern was well compatible with a point charge model to explain the concomitant increase in single-channel conductance and cation selectivity.

#### 10.3.4

#### Characterisation of Non-Covalent Supramolecular Complexes

Beyond the characterisation of primary structures, the direct analysis tertiary structure states and even non-covalent supramolecular complexes by mass spectrometry have not been considered feasible in previous work. In a few cases tertiary structure-dependences have been found, e. g. specific fragmentations in FAB mass spectra of  $\alpha$ -helical polypeptides and some MALDI and PD mass spectra of proteins suggesting some “native-like” structure of macromolecular ions [106, 107]. This situation has changed drastically recently with the analytical development of ESI-MS. A substantial number of ESI-MS studies have demonstrated the identification of supramolecular complexes of biopolymers, as well as specific non-covalent complexes with low-molecular weight constituents [15–18, 31]. In contrast to other ionisation methods in which, predominantly, *singly charged* ions are produced (FAB,

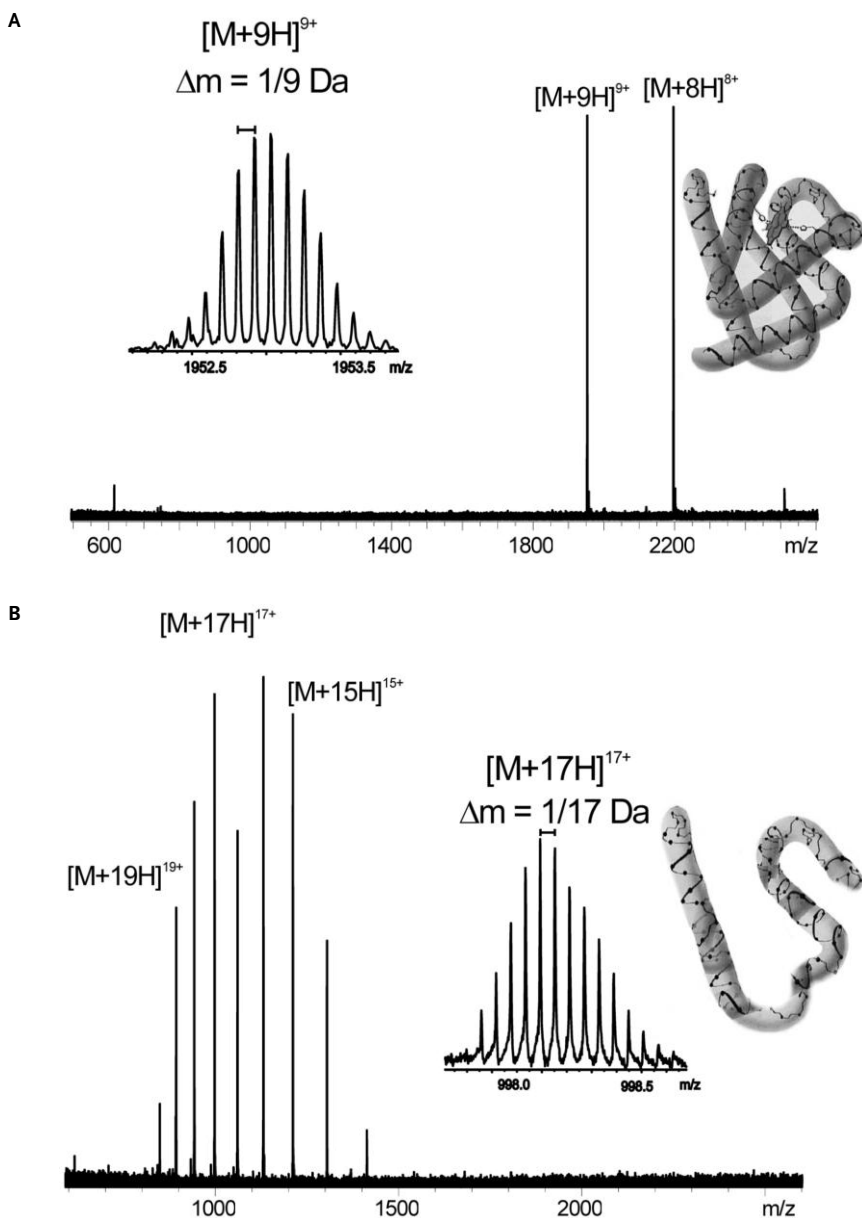


**Fig. 10.12** ESI-FT-ICR mass spectra of (a) the native intact hem-protein complex of horse heart myoglobin; (b) spectrum of the denatured apoprotein upon dissociation of hem in trifluoroacetic acid, pH 3. The inserts show isotopic resolutions for the 9- and 17-fold protonated molecular ions [146].

MALDI), the continuous series of *multiply charged* macro-ions in ESI-MS reflects charge states and distributions characteristic of the solution structure (“charge structure”; cf. Section 10.2.1) [31]. Moreover, ESI-MS can be readily carried out with aqueous solutions at physiological solution conditions, enabling comparative studies with other structure determination methods such as NMR [134]. This feasibility for the direct mass spectrometric characterisation of non-covalent complexes has opened new analytical perspectives for supramolecular chemistry and biochemistry [16, 31, 135].

Although the mechanism of ion formation in ESI-MS has not yet been elucidated in detail, a number of different non-covalent interactions (e. g. ionic, hydrophobic) have been successfully characterised and results discussed with regard to application areas in biochemistry and supramolecular chemistry. Experimental parameters and criteria employed for the identification of non-covalent complexes based on chemical conditions of complex formation, and their effects on the ion formation in ESI-MS, have been summarised [31]. These include the identification of a specific stoichiometry of complex ions, modification of the stoichiometry of solution components, and modification of the ESI-MS conditions (interface temperature, declustering potential). Further evidence is provided by competition experiments with complex components and analysis of the specificity of pH or concentration changes. An illustrative example demonstrating the close correlation of solution structures and charge structures of molecular ions are the pH-dependent ESI spectra of myoglobin [13]. The high resolution ESI-FTICR spectrum in aqueous solution at pH 6 reveals a most abundant  $[M + 9H]^{9+}$  ion of the intact heme-protein complex, whereas under acidic conditions (pH 2) complete dissociation occurs, with molecular ions of high charge states (up to 20+) and the ion of the free heme group (Fig. 10.12). A particularly attractive feature of the FTICR-MS is the complete isotopic resolution and direct characterisation of charge states [44, 136].

Thus, although the quantitative characterisation of equilibria of complex formation has not yet been established, the large number of already successful applications indicates broad potential for the analysis of non-covalent complexes by ESI-MS.

### 10.3.5

#### Mass Spectrometric Proteome Analysis

During the past decade, large amounts of protein sequence data have been deposited in a number of databases as a result of different genome projects [137]. Only a minor part of these sequence data has been from expressed proteins, whereas a major portion has been deduced from corresponding gene acid sequences. The sequence determination of several genomes in recent years has reached a first culmination point in the completion of the human genome in 2000/2001 [138]. It has now become clear that functions from such protein sequences are frequently only predicted and remain unclear for a substantial part of structural genes, *inter alia* due to processes such as alternative splicing, RNA editing and post-trans-

lational protein modifications [137, 139]. The field of *proteomics*, using the term “proteome” to define the PROTEin complement of the genOME [137], has recently created an explosion of interest with the use of mass spectrometry as the key technology for the large-scale identification of proteins from cellular expression material [140]. The reader is referred to recent reviews in this new area (cf. also the generation of several new international journals [139–141]).

Within the last years several combinations of high performance separation techniques with mass spectrometric peptide mapping have been developed and employed for the identification of proteins from complex biological systems, such as whole cell lysates [141]. At present, one of the most efficient techniques is the proteolytic degradation of proteins, separated by 2D-gel electrophoresis [142], within the gel matrix and subsequent mass spectrometric analysis of eluted peptide fragments. Both MALDI-MS and ESI-MS have been extensively employed for these studies [141]. The unequivocal identification of proteins from sequence databases using peptide mass fingerprint data only, without any additional sequence information such as a sequence tags and MS/MS data [141, 143], typically requires a set of ten to twenty peptide masses with high mass determination accuracy (< 200 ppm mass error) [144]. Furthermore, a high sequence coverage by the observed peptide molecular ions is an important criterion for the certainty of protein identification.

In recent proteome studies, the combination of 2D-gel electrophoresis with high resolution FT-ICR-MS has been employed as a powerful tool [145, 146]; the high (low- to sub-ppm) mass determination accuracy and isotopic fine structure obtained by FT-ICR-MS provide particular advantages for the identification of cellular proteins expressed with minor or very low abundance. The accurate masses obtained by FT-ICR-MS allow the use of low tolerance thresholds in database searches and greatly improve the selectivity of protein identification, compared to standard techniques using MALDI-TOF-MS [141]. The identification of a protein component, TNF $\alpha$ -IgG in a serum cryoprecipitate from a patient with cryoglobulinemia by MALDI-FTICR-MS is illustrated in Fig. 10.13 and requires only a minimum number of peptides [146]. Cryoglobulins are cold-precipitable serum immunoglobulins associated with a number of infectious, autoimmune and neoplastic disorders such as hepatitis C [147, 148]; their characterisation using high performance proteomics tools has become of considerable interest as described above. The main protein components in a serum cryoprecipitate from a patient with type II cryoglobulinemia have been recently identified by MALDI-FTICR-MS as IgG and IgM  $\mu$ - and  $\gamma$ -heavy chains,  $\kappa$ - and  $\lambda$ -light chains, and  $\jmath$ -chains [149].

One major shortcoming in the application of the combination of 2D-gel electrophoresis with mass spectrometry is the loss of information about specific protein–protein interactions and molecular recognition processes due to the denaturing electrophoretic conditions. At present, only a few, but promising, attempts have been made to directly analyse interactions in proteome studies [19, 141, 150]. Recently, a new approach for the identification of affinity bound proteins by proteolytic generation and mass spectrometric analysis of its antibody-bound

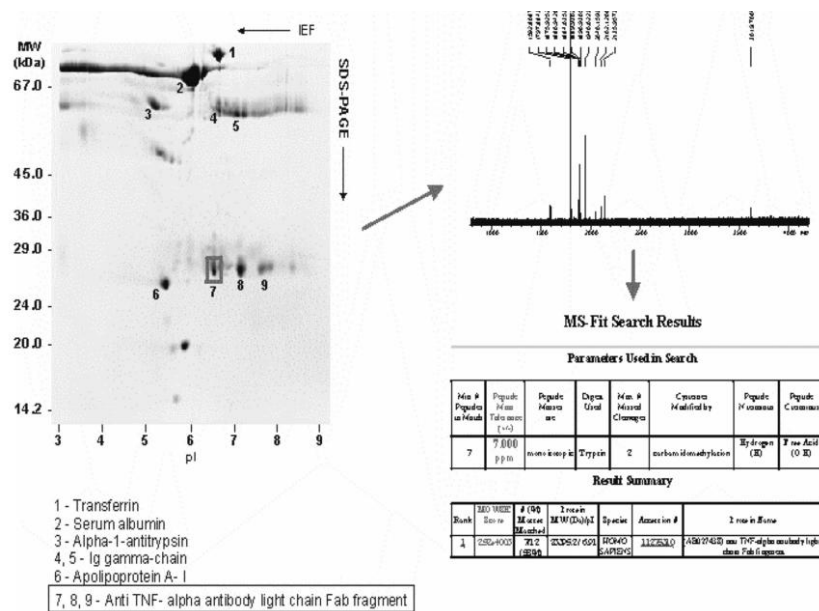


**Fig. 10.13** 2D-PAGE Separation of a cryoglobulin isolated from serum of a patient with glomerulonephritis (left) and MALDI-FT-ICR-MS of tryptic in-gel digest mixture of spot 7 (right). The MS-fit search using SwissProt database yields identification of anti-TNF-alpha-light chain fragment [149].

epitope peptides has been described [151]. The selectivity of identification of antibody-bound proteins by the combination of antigen–antibody specificity with the redundancy of epitope peptide sequences should render this “affinity-proteomics” approach a powerful tool for the mass spectrometric identification of proteins from complex biological material.

## References

- 1 R. O. Nier, *J. Am. Soc. Mass Spectrom.* **1991**, *2*, 447–452.
- 2 J. W. Amy, W. Baitinger, R. G. Cooks, *J. Am. Soc. Mass Spectrom.* **1990**, *1*, 119–128.
- 3 R. S. Gohlke, F. W. McLafferty, *J. Am. Soc. Mass Spectrom.* **1993**, *4*, 367–371.
- 4 A. L. Burlingame, S. A. Carr, *Mass Spectrometry in the Biological Sciences*, Humana Press, Totowa, N.J. 1996.
- 5 G. Siuzdak, *Proc. Natl. Acad. Sci. USA* **1994**, *91*, 11290–11297.
- 6 A. L. Burlingame, J. A. McCloskey, *Biological Mass Spectrometry*, Elsevier, Amsterdam 1990.
- 7 T. Matsuo, R. Caprioli, M. Gross, *Biological Mass Spectrometry: Present and Future*, Wiley, New York 1994.
- 8 M. Karas, U. Bahr, U. Giessmann, *Mass Spectrom. Rev.* **1991**, *19*, 335–381.
- 9 M. Przybylski, *Fresenius' Z. Anal. Chem.* **1983**, *315*, 402.
- 10 R. Sundquist, R. D. McFarlane, *Mass Spectrom. Rev.* **1985**, *4*, 421.
- 11 J. B. Feng, M. Mann, C. K. Meng et al., *Science* **1989**, *246*, 46–49.
- 12 K. Tanaka, H. Waki, Y. Ido et al., *Mass Spectrom.* **1988**, *2*, 151–153.
- 13 M. Przybylski, *Adv. Mass. Spectrom.* **1995**, *13*, 257–283.
- 14 O. N. Jensen, M. R. Larsen, P. Roepstorff, *Proteins* **1998**, *Suppl 2*, 74–89.
- 15 M. Przybylski, V. Schnaible, J. Kast et al., in *New Methods for the Study of Biomolecular Complexes*, eds. W. E. et al., Kluwer Academic Publishers, Amsterdam 1998, pp. 17–43.
- 16 R. T. Aplin, in *New Methods for the Study of Biomolecular Complexes*, eds. W. Ens, K. G. Standing, Kluwer Academic Publishers, Amsterdam 1998.
- 17 J. A. Loo, *Mass Spectrom. Rev.* **1997**, *16*, 1–23.
- 18 R. D. Smith, J. E. Bruce, Q. Wu, et al., *Chem. Soc. Rev.* **1997**, *26*, 191–202.
- 19 D. Suckau, J. Kohl, G. Karwath et al., *Proc. Natl. Acad. Sci. U S A* **1990**, *87*, 9848–9852.
- 20 P. James, *Quart. Rev. Biophys.* **1997**, *30*, 279–331.
- 21 H. Budzikiewicz, C. Djerassi, D. H. Williams, *Mass Spectrometry of Organic Compounds*, Holden Day, San Francisco 1967.
- 22 F. W. McLafferty, *The Wiley/NBS Registry of Mass Spectral Data*, Wiley-Interscience, New York 1989.
- 23 M. S. B. Munson, F. H. Field, *J. Am. Chem. Soc.* **1966**, *88*, 2621–2630.
- 24 H. D. Beckey, *Int. J. Mass Spectrom. Ion Phys.* **1969**, *2*, 500–503.
- 25 R. D. Macfarlane, D. F. Torgerson, *Science* **1976**, *191*, 920–925.
- 26 M. Barber, R. S. Bordoli, R. D. Sedgwick et al., *J. Chem. Soc. Chem. Commun.* **1981**, 325–327.
- 27 Y. Ito, T. Takeuchi, D. Ishi et al., *J. Chromatogr.* **1985**, *346*, 161–166.
- 28 J. B. Fenn, M. Mann, C. K. Meng et al., *Science* **1989**, *246*, 64–71.
- 29 M. R. Emmett, R. M. Caprioli, *J. Am. Soc. Mass Spectrom.* **1994**, *5*, 605–613.
- 30 M. S. Wilm, M. Mann, *Int. J. Mass Spectrom. Ion Processes* **1994**, *136*, 167–180.
- 31 M. Przybylski, M. O. Glocker, *Angew. Chem. Int. Ed. Engl.* **1996**, *35*, 806–826.
- 32 R. Körner, M. Wilm, K. Morand et al., *J. Am. Soc. Mass Spectrom.* **1996**, *7*, 150–156.

- 33** T. A. Fligge, J. Kast, K. Bruns et al., *J. Am. Soc. Mass Spectrom.* **1999**, *10*, 112–118.
- 34** M. Karas, F. Hillenkamp, *Anal. Chem.* **1988**, *60*, 2299–2301.
- 35** M. Dey, J. Grotemeyer, *Eur. Mass Spectrom.* **1995**, *1*, 95–103.
- 36** P. H. Dawson, *Quadrupole Mass Spectrometry and Its Applications*, Elsevier, New York, 1976.
- 37** R. G. Cooks, R. E. Kaiser, *Acc. Chem. Res.* **1990**, *23*, 213–219.
- 38** U. Bahr, A. Pfenninger, M. Karas et al., *Anal. Chem.* **1997**, *69*, 4530–4535.
- 39** H. R. Morris, T. Paxton, A. Dell et al., *Rapid Commun. Mass Spectrom.* **1996**, *10*, 889–896.
- 40** M. G. Qian, D. M. Lubman, *Rapid Commun. Mass Spectrom.* **1996**, *10*, 1911–1920.
- 41** A. G. Marshall, C. L. Hendrickson, G. S. Jackson, *Mass Spectrom. Rev.* **1998**, *17*, 1–35.
- 42** M. E. Belov, E. N. Nikolaev, G. A. Anderson et al., *J. Am. Soc. Mass Spectrom.* **2001**, *12*, 38–48.
- 43** G. Baykut, R. Jertz, M. Witt, *Rapid Commun. Mass Spectrom.* **2000**, *14*, 1238–1247.
- 44** J. S. Rossier, N. Youhnovski, N. Lion et al., *Angew. Chem. Int. Ed. Engl.* **2002**, in press.
- 45** R. Bonfiglio, R. C. King, T. V. Olah et al., *Rapid Commun. Mass Spectrom.* **1999**, *13*, 1175–1185.
- 46** R. C. King, R. Bonfiglio, C. Fernandez-Metzler et al., *J. Am. Soc. Mass Spectrom.* **2000**, *11*, 942–950.
- 47** W. Mueck, D. Leitner, W. Marter et al., *Am. Biotechnol. Lab.* **1999**, *27*, 78–91.
- 48** S. Steinborner, J. Henion, *Anal. Chem.* **1999**, *71*, 2340–2345.
- 49** K. Pfleger, H. H. Maurer, A. Weber, *Mass Spectral and GC Data on Drugs, Poisons, Pesticides, and Pollutants and Their Metabolites*, 2nd and 3rd editions, Verlag Chemie, Weinheim 1999.
- 50** E. R. Cairns, B. R. Dent, J. C. Ouwerkerk et al., *J. Anal. Toxicol.* **1994**, *18*, 1–6.
- 51** P. M. Kabra, N. A. Mar, L. J. Marton, *Clin. Chim. Acta* **1981**, *111*, 123–132.
- 52** J. P. Franke, R. A. De Zeeuw, *J. Chromatogr. B* **1998**, *713*, 51–59.
- 53** H. Simpson, A. Berthemy, D. Buhrmann, et al., *Rapid Commun. Mass Spectrom.* **1998**, *12*, 75–82.
- 54** J. Zweigenbaum, K. Heinig, S. Steinborner et al., *Anal. Chem.* **1999**, *71*, 2294–2300.
- 55** J. Cai, J. Henion, *Anal. Chem.* **1996**, *68*, 72–78.
- 56** M. L. Nedved, S. Habibi-Goudarzi, B. Ganem et al., *Anal. Chem.* **1996**, *68*, 4228–4236.
- 57** H. H. Maurer, T. Kraemer, O. Ledvinka et al., *J. Chromatogr. B Biomed. Sci. Appl.* **1997**, *689*, 81–89.
- 58** J. Pawliszyn, *Solid Phase Microextraction – Theory and Practice*, Wiley VCH, Weinheim, 1997.
- 59** K. Jinno, T. Muramatsu, Y. Saito et al., *J. Chromatogr. A* **1996**, *754*, 137–144.
- 60** H. L. Lord, J. Pawliszyn, *Anal. Chem.* **1997**, *69*, 3899–3906.
- 61** M. Abalos, J. M. Bayon, J. Pawliszyn, *J. Chromatogr. A* **2000**, *873*, 107–115.
- 62** H. Kataoka, S. Narimatsu, H. L. Lord et al., *Anal. Chem.* **1999**, *71*, 4237–4244.
- 63** P. A. Martos, J. Pawliszyn, *Anal. Chem.* **1999**, *71*, 1513–1520.
- 64** J. D. Berset, R. Holzer, *J. Chromatogr. A* **1999**, *852*, 545–558.
- 65** C. Staub, *Forensic Sci. Int.* **1997**, *84*, 295–304.
- 66** J. C. Spell, K. Srinivasan, J. T. Stewart et al., *Rapid Commun. Mass Spectrom.* **1998**, *12*, 890–894.
- 67** F. J. Senorans, E. Ibanez, S. Caverio et al., *J. Chromatogr. A* **2000**, *870*, 491–499.
- 68** J. Amador-Hernandez, M. D. Luque De Castro, *J. Biochem. Biophys. Methods* **2000**, *43*, 329–343.
- 69** K. B. Tomer, *Chem. Rev.* **2001**, *101*, 297–328.
- 70** A. P. Bruins, *Trends Anal. Chem.* **1994**, *13*, 37–43.
- 71** A. P. Bruins, *J. Chromatogr. A* **1998**, *794*, 345–357.
- 72** K. B. Tomer, M. A. Moseley, L. J. Deterding, C. E. Parker, *Mass Spectrom. Rev.* **1994**, *13*, 431–457.
- 73** G. Hopfgartner, T. Wachs, K. Bean et al., *Anal. Chem.* **1993**, *65*, 439–446.
- 74** J. Abian, A. J. Oosterkamp, E. Gelpi, *J. Mass Spectrom.* **1999**, *34*, 244–254.

- 75** J. Cai, J. Henion. *Anal. Chem.* **1996**, *68*, 72–78.
- 76** A. J. Oosterkamp, E. Gelpi, J. Abian, *J. Mass Spectrom.* **1998**, *33*, 976–983.
- 77** K. Vanhoutte, W. van Dongen, E. L. Esmans, *Rapid Commun. Mass Spectrom.* **1998**, *12*, 15–22.
- 78** M. A. Moseley, in *Mass Spectrometry in Biology and Medicine*, Humana Press Totowa, NJ **2000**, pp. 179–196.
- 79** M. S. Wilm, M. Mann, *Int. J. Mass Spectrom. Ion Processes* **1994**, *136*, 167–180.
- 80** M. Mann, M. Wilm, *Anal. Chem.* **1994**, *66*, 4390–4399.
- 81** M. Zell, C. Husser, G. Hopfgartner, *Rapid Commun. Mass Spectrom.* **1997**, *11*, 1107–1114.
- 82** R. D. Smith, C. J. Barinaga, H. R. Udseth, *Anal. Chem.* **1988**, *60*, 1948–1952.
- 83** K. B. Tomer, M. A. Moseley, in *Continuous-flow Fast Atom Bombardment Mass Spectrometry*, ed. R. M. Caprioli, John Wiley & Sons Ltd, New York, 1990, pp. 121–136.
- 84** E. Parker, J. R. Perkins, K. B. Tomer et al., *J. Am. Soc. Mass Spectrom.* **1992**, *5*, 563–574.
- 85** T. Wachs, R. L. Sheppard, J. Henion, *J. Chromatogr. B, Biomed. Appl.* **1996**, *685*, 335–342.
- 86** R. E. Settlage, P. S. Russo, J. Shabanowitz et al., *J. Microcolumn* **1998**, *10*, 281–285.
- 87** W. Weinmann, C. E. Parker, K. Baumeister et al., *Electrophoresis* **1994**, *15*, 228–233.
- 88** W. Weinmann, C. Maier, K. Baumeister et al., *J. Chromatogr. A* **1994**, *664*, 271–275.
- 89** W. Weinmann, C. E. Parker, L. J. Deterding et al., *J. Chromatogr. A* **1994**, *680*, 353–361.
- 90** T. J. Thompson, F. Foret, P. Vouros et al., *Anal. Chem.* **1993**, *65*, 900–906.
- 91** E. M. Javerfalk-Hoyes, U. Bondesson, D. Westerlund et al., *Electrophoresis* **1999**, *20*, 1527–1532.
- 92** Q. Tang, A. K. Harrata, C. S. Lee, *Anal. Chem.* **1995**, *67*, 3515–3519.
- 93** S. J. Lane, M. G. Tucker, *Rapid Commun. Mass Spectrom.* **1998**, *12*, 947–954.
- 94** Apffel, H. Yin, W. S. Hancock, D. McManigill et al., *J. Chromatogr. A* **1999**, *832*, 149–163.
- 95** J. Ding, T. Barlow, A. Dipple et al., *J. Am. Soc. Mass Spectrom.* **1998**, *9*, 823–829.
- 96** D. F. Hunt, T. Krishnamurthy, J. Shabanowitz et al., in *Mass Spectrometry of Peptides*, ed. D. M. Desiderio, CRC Press, Boca Raton, FL **1991**, 139–158.
- 97** K. Biemann, in *Methods in Enzymology: Mass Spectrometry*, ed. J. A. McCloskey, Academic Press, San Diego, CA **1991**, 455–479.
- 98** *Methods in Protein Sequence Analysis*, eds. K. Imahori, F. Sakiyama, Plenum Press, New York **1993**, 167–171.
- 99** P. Roepstorff, J. Fohlman, *Biomed. Mass Spectrom.* **1984**, *11*, 601.
- 100** M. E. Belov, M. V. Gorshkov, H. R. Udseth et al., *J. Am. Soc. Mass Spectrom.* **2000**, *11*, 19–23.
- 101** M. R. Emmett, F. M. White, C. L. Hendrickson et al., *J. Am. Soc. Mass Spectrom.* **1998**, *9*, 333–340.
- 102** S. H. Bauer, M. F. Wiechers, K. Bruns et al., *Anal. Biochem.* **2001**, *298*, 25–31.
- 103** T. A. Ramelot, L. N. Gentile, L. K. J. Nicholsen, *Biochemistry* **2000**, *39*, 2714–2718.
- 104** H. Steiner, A. Capell, C. Haass, *Biochem. Soc. Trans.* **1999**, *27*, 234–242.
- 105** X. Tian, R. Cecal, E. Amstalden et al., *J. Peptide Sci.* **2003**, in press.
- 106** P. Roepstorff, P. F. Nielsen, B. Klarskov et al., *Biomed. Environ. Mass Spectrom.* **1988**, *16*, 9–24.
- 107** M. Przybylski, I. Manz, P. Fonrobert et al., *Adv. Mass Spectrom.* **1986**, *10*, 1519–1521.
- 108** R. M. Caprioli, T. Fan, *Anal. Biochem.* **1986**, *154*, 596–603.
- 109** E. Windberg, F. Hudecz, A. Marquardt et al., *Rapid Commun. Mass Spectrom.* **2002**, *16*, 834–839.
- 110** K. Biemann, in *Protein Sequencing – A Practical Approach*, eds. J. B. C. Findley, M. J. Geisow, IRL, Oxford, 1989, pp. 99–121.
- 111** P. F. Nielsen, B. Landis, M. Svoboda et al., *Anal. Biochem.* **1990**, *191*, 202–312.

- 112** B. T. Chait, R. Wang, R. C. Beavis et al., *Science* **1993**, *262*, 89–92.
- 113** R. G. Krishna, F. Wold, in *Methods in Protein Sequence Analysis*, eds. K. Ima-hori, F. Sakiyama, Plenum Press, New York 1993, pp. 167–171.
- 114** S. A. Martin, J. E. Vath, W. Yu et al., in *Biological Mass Spectrometry: Present and Future*, eds. T. Matsuo, R. Caprioli, M. Gross, et al., Wiley, New York 1993, pp. 313–330.
- 115** D. L. Smith, Z. Zhou, in *Methods in Enzymology: Mass Spectrometry*, ed. J. A. McCloskey, Academic Press, San Diego 1990, vol. 193, pp. 374–389.
- 116** T. Kinumi, H. Niwa, H. Matsumoto, *Anal. Biochem.* **2000**, *277*, 177–186.
- 117** H. Jaffe, P. H. C. Veeranna, *Biochemistry* **1998**, *37*, 16211–16234.
- 118** J. J. Lennon, K. A. Walsh, *Protein Sci.* **1999**, *8*, 2487–2493.
- 119** M. Przybylski, C. Maier, K. Haegele et al., in *Peptides – Chemistry, Structure and Biology*, eds. R. S. Hodges, J. A. Smith, Escom, Leiden 1994, pp. 338–340.
- 120** T. Voss, K. P. Schäfer, P. F. Nielsen et al., *Biochim. Biophys. Acta* **1992**, *1138*, 261–270.
- 121** C. Albach, R. A. Klein, B. Schmitz, *Biol. Chem.* **2001**, *382*, 187–194.
- 122** S. H. Bauer, X. Y. Zhang, W. Van Dongen et al., *Anal. Biochem.* **1999**, *274*, 69–80.
- 123** N. E. Zachara, R. N. Cole, G. W. Hart et al., *Curr. Protocols Mol. Biol.* **2002**, *3*, 1761–62.
- 124** M. C. Posewitz, P. Tempst, *Anal. Chem.* **1999**, *71*, 2883–92.
- 125** P. Cao, J. T. Stults, *J. Chromatogr. A* **1999**, *853*, 225–235.
- 126** M. Wind, H. Wesch, W. D. Lehmann, *Anal. Chem.* **2001**, *73*, 3006–3011.
- 127** J. S. Becker, S. F. Boulyga, J. Su et al., *Int. J. Mass Spectrom.* **2003**, in press.
- 128** J. Goetz, S. Chen, J. van Dorpe et al., *Science* **2001**, *293*, 1491–1495
- 129** A. N. Glazer, in *The Proteins 2*, eds. H. Neurath, R. L. Hill, Academic Press, New York 1976, pp. 1–103.
- 130** D. Suckau, M. Mak, M. Przybylski, *Proc. Natl. Acad. Sci. USA* **1992**, *89*, 5630–5634.
- 131** M. O. Glocker, C. Borchers, W. Fiedler et al., *Bioconj. Chem.* **1994**, *5*, 583–590.
- 132** W. Welte, U. Nestel, T. Wacker et al., *Kidney Int.* **1995**, *48*, 930–940.
- 133** M. Przybylski, M. O. Glocker, U. Nestl et al., *Protein Sci.* **1996**, *5*, 1477–1489.
- 134** L. J. Smith, M. J. Sutcliff, C. Refield, et al., *Biochemistry* **1991**, *30*, 986–994.
- 135** A. A. Rostom, C. V. Robinson, *Curr. Opin. Struct. Biol.* **1999**, *9*, 135–141.
- 136** T. A. Fligge, C. Reinhard, C. Harter et al., *Biochemistry* **2000**, *39*, 8491–8496.
- 137** M. R. Wilkins, K. L. Williams, *Proteome Research: New Frontiers in Functional Genomics*, Springer, Berlin 1997.
- 138** <http://www.ncbi.nlm.nih.gov/> genome/seq/.
- 139** J. Godovac-Zimmermann, L. R. Brown, *Mass Spectrom. Rev.* **2001**, *20*, 1–57.
- 140** N. G. Anderson, A. Matheson, N. L. Anderson, *Proteomics* **2001**, *1*, 3–12.
- 141** F. Lottspeich, *Angew. Chem. Int. Ed. Engl.* **1999**, *38*, 2476–2492.
- 142** S. D. Patterson, R. Aebersold, *Electrophoresis* **1995**, *16*, 1791–1814.
- 143** M. Wilm, A. Shevchenko, T. Honthaeve, et al., *Nature* **1996**, *379*, 466–469.
- 144** P. Jungblut, B. Thiede, *Mass Spectrom. Rev.* **1997**, *16*, 145–62.
- 145** D. R. Goodlett, J. E. Bruce, G. A. Anderson et al., *Anal. Chem.* **2000**, *72*, 1112–1118.
- 146** M. Przybylski, N. Youhnovski, N.-E. Damoc et al., *Electrophoresis* **2003**, in press.
- 147** J. D. Tissot, D. H. Vu, V. Aubert, P. Schneider, F. Vuadens, D. Crettaz, M. A. Duchosal, *Proteomics* **2002**, *2*, 813–24.
- 148** J. D. Tissot, J. C. Sanchez, F. Vuadens et al., *Electrophoresis* **2002**, *23*, 1203–1206.
- 149** E. Damoc, S. Buddrus, J. Su, Becker et al., *Proteomics*, **2003**, in press.
- 150** A. L. McCormack, *Anal. Chem.* **1997**, *69*, 767–776.
- 151** M. Macht, M. Wochner, U. Krawinkel, et al., in *Peptides*, Akademiai Kiado, Budapest 1999, pp. 74–75.

## **Section V**

### **Methods 4: Elemental Analysis**

# 11

## X-ray Fluorescence Analysis

*K. Janssens*

### 11.1 Introduction

X-ray fluorescence (XRF) analysis is a powerful analytical tool for the spectrochemical determination of almost all the elements present in a sample. XRF radiation is induced when photons of sufficiently high energy, emitted from an X-ray source, impinge on a material. These primary X-rays undergo interaction processes with the analyte atoms. High-energy photons induce ionization of inner shell electrons by the photoelectric effect and thus electron vacancies in inner shells (K, L, M, ...) are created. The prompt transition of outer shell electrons into these vacancies within some 100 fs can cause the emission of characteristic fluorescence radiation. Not all transitions from outer shells or subshells are allowed, only those obeying the selection rules for electric dipole radiation. The creation of a vacancy in a particular shell results in a cascade of electron transitions, all correlated with the emission of photons with a well-defined energy corresponding to the difference in energy between the atomic shells involved. The family of characteristic X-rays from each element including all transitions allows the identification of the element. Next to this radiative form of relaxation, a competing process can take place: the emission of Auger electrons. Both processes have Z-dependent probabilities that are complementary: the Auger yield is high for light elements and the fluorescence yield is high for heavy elements.

The working principle of XRF analysis is the measurement of wavelength or energy and intensity of the characteristic photons emitted from the sample. This allows the identification of the elements present in the analyte and the determination of their mass or concentration. All the information for the analysis is stored in the measured spectrum, which is a line spectrum with all characteristic lines superimposed above a certain fluctuating background. Other interaction processes, mainly the elastic and inelastic scattering of the primary radiation on sample and substrate, induce the background.

Measurement of the spectrum of the emitted characteristic fluorescence radiation is performed using wavelength-dispersive (WD) and energy-dispersive (ED)

spectrometers. In wavelength-dispersive X-ray fluorescence analysis (WDXRF), the result is an intensity spectrum of the characteristic lines versus wavelength measured with a Bragg single crystal as dispersion medium while counting the photons with a Geiger–Müller, a proportional or scintillation counter. In energy-dispersive X-ray fluorescence analysis (EDXRF), a solid-state detector is used to count the photons, simultaneously sorting them according to energy and storing the result in a multi-channel memory. The result is an X-ray energy vs. intensity spectrum. The range of detectable elements ranges from Be ( $Z = 4$ ) for the light elements and goes up to U ( $Z = 92$ ) on the high atomic number  $Z$  side. The concentrations that can be determined with standard spectrometers of WD or ED type lie are situated in a wide dynamic range: from the percent to the  $\mu\text{g g}^{-1}$  level. In terms of mass the nanogram range is reached with spectrometers having the standard excitation geometry.

By introducing special excitation geometries, optimized sources and detectors, the picogram and even femtogram range of absolute analyte detection capacity can be reached; in terms of concentrations, the same improvement factor can be attained, i. e. from the  $\mu\text{g g}^{-1}$  towards the  $\text{pg g}^{-1}$  level under the best conditions.

In principle, XRF analysis is a multi-element analytical technique and, in particular, the simultaneous determination of all the detectable elements present in the sample is inherently possible with EDXRF. In WDXRF both sequential and simultaneous detection modes are possible.

The most striking feature of XRF analysis is that this technique allows the qualitative and quantitative analysis of almost all the elements (Be–U) in an unknown sample. The analysis is, in principle, nondestructive, has high precision and accuracy, has simultaneous multi-element capacity and requires only a short irradiation time so that a high sample throughput is possible; on-line analysis is also possible and the running costs are low. The technique is extremely versatile for applications in many fields of science, research and quality control, has low detection limits and a large dynamic range of concentrations covering up to 9 orders of magnitude. The physical size of an XRF spectrometer ranges from handheld, battery-operated field units to high-power laboratory units with compact tabletop units and larger ones requiring several cubic meters of space including a 10–20 kW electrical power supply and efficient cooling units with high pressure water and a heat sink.

In contrast to all these attractive properties there are some disadvantages. The absorption effects of the primary radiation and the fluorescence radiation created in the analyte result in a shallow layer a few tenths of a millimeter deep that provides information on its composition. This requires a perfectly homogeneous sample, which often occurs naturally but must sometimes be produced by acid dissolution into liquids or by grinding and the preparation of pressed pellets. In both instances the feature of non-destructiveness is lost. Thin films or small amounts of microcrystalline material on any substrate are the ideal analyte where also the quantification process is simple because there is linearity between fluorescence intensity and concentration. In thick samples corrections for absorption and enhancement effects are necessary.

While the roots of the method go back to the early part of this century, where electron excitation systems were employed, it is only during the last 30 years or so that the technique has gained major significance as a routine means of elemental analysis.

Some references for further study are listed at the end of this chapter [1–16].

## 11.2 Basic Principles

### 11.2.1 X-ray Wavelength and Energy Scales

The X-ray or Röntgen region of the electromagnetic spectrum start at ca. 10 nm and extends towards the shorter wavelengths. The energies of X-ray photons are of the same order of magnitude as the binding levels of inner-shell electrons (K, L, M, ... levels) and therefore can be used to excite and/or probe these atomic levels. The wavelength  $\lambda$  of an X-ray photon is inversely related to its energy  $E$  according to:

$$\lambda \text{ (nm)} = 1.24/E \text{ (keV)}$$

where 1 eV is the kinetic energy of an electron that has been accelerated over a voltage difference of 1 V ( $1 \text{ eV} = 1.602 \times 10^{-19} \text{ J}$ ). Accordingly, the X-ray energy range starts at ca. 100 eV and continues towards higher energies. X-ray analysis methods most commonly employ radiation in the 1–50 keV (1–0.02 nm) range.

### 11.2.2 Interaction of X-rays with Matter

When an X-ray beam passes through matter, some photons will be absorbed inside the material or scattered away from the original path, as illustrated in Fig. 11.1. The intensity  $I_0$  of an X-ray beam passing through a layer of thickness  $d$  and density  $\rho$  is reduced to an intensity  $I$  according to the well-known Lambert–Beer law:

$$I = I_0 e^{-\mu\rho d} \quad (1)$$

The number of photons (the intensity) is reduced but their energy is generally unchanged. The term  $\mu$  is called the *mass attenuation coefficient* and has the dimension  $\text{cm}^2 \text{ g}^{-1}$ . The product  $\mu_L = \mu\rho$  is called the *linear absorption coefficient* and is expressed in  $\text{cm}^{-1}$ .  $\mu(E)$  is sometimes also called the total cross section for X-ray absorption at energy  $E$ .

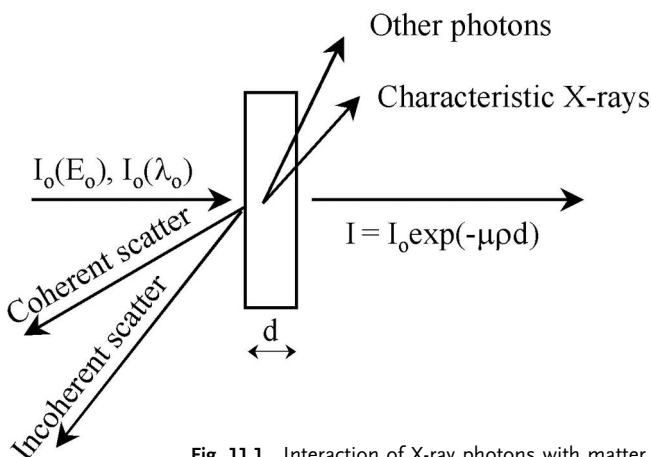


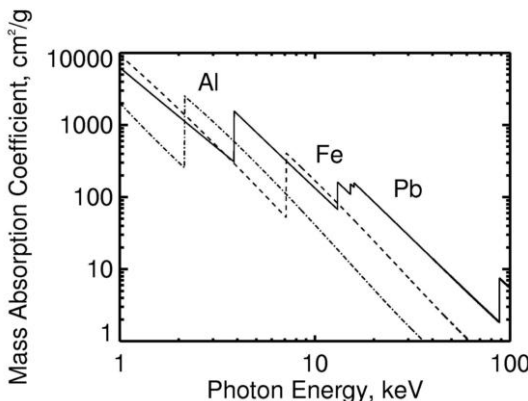
Fig. 11.1 Interaction of X-ray photons with matter.

Figure 11.2 shows a log–log plot of the energy dependence of the mass attenuation coefficient of several chemical elements in the X-ray energy range between 1 and 100 keV. The absorption edge discontinuities (due to photoelectric absorption, see below) are clearly visible. Low-Z materials attenuate X-rays of a given energy less than high-Z materials. A given material will attenuate high energy (i.e. hard) X-rays less than low energy (soft) X-rays.

The mass absorption coefficient  $\mu(M)$  of a complex matrix M consisting of a mixture of several chemical elements (e.g., an alloy such as brass), can be calculated from the mass attenuation coefficients of the  $n$  constituting elements:

$$\mu(M) = \sum_{i=1}^n w_i \mu_i \quad (2)$$

where  $\mu_i$  is the mass attenuation coefficient of the  $i$ th pure element and  $w_i$  its mass fraction in the sample considered. This is called the *mixture rule*.

Fig. 11.2 Energy dependence of the mass absorption coefficient  $\mu$  of several elements.

The mass absorption coefficient  $\mu$  plays a very important role in quantitative XRF analysis. Both the exciting primary radiation and the fluorescence radiation are attenuated in the sample. To relate the observed fluorescence intensity to the concentration, this attenuation must be taken into account.

As illustrated in Fig. 11.1, the absorption of radiation in matter is the cumulative effect of several types of photon–matter interaction processes that take place in parallel. Accordingly, in the X-ray range the mass attenuation coefficient  $\mu_i$  of element  $i$  can be expressed as:

$$\mu_i = \tau_i + \sigma_i \quad (3)$$

where  $\tau_i$  is the cross section for photoelectric ionization and  $\sigma_i$  the cross section for scattering interactions. All above-mentioned cross sections are energy (or wavelength) dependent. Except at the absorption edges (see below),  $\mu$  is more or less proportional to  $Z^4\lambda^3$ .

### 11.2.3

#### Photoelectric Effect

In the photoelectric absorption process (see Fig. 11.3), a photon is completely absorbed by the atom and an (inner shell) electron is ejected. Part of the photon is used to overcome the binding energy of the electron and the rest is transferred in the form of kinetic energy. After the interaction, the atom (actually an ion now) is left in a highly excited state since a vacancy has been created in one of the inner shells. The atom will almost immediately return to a more stable electron configuration by emitting an Auger electron or a characteristic X-ray photon. The latter process is called X-ray fluorescence. The ratio of the number of emitted characteristic X-rays to the total number of inner-shell vacancies in a particular atomic shell that gave rise to it, is called the fluorescence yield of that shell (e. g.,  $\omega_K$ ). For light elements ( $Z < 20$ ), Auger electrons are produced predominantly during the relaxation upon K-shell ionisation ( $\omega_K < 0.2$ ) while the medium to heavy elements relax preferentially in a radiative manner ( $0.2 < \omega_K < 1.0$ ).

Photoelectric absorption can only occur if the energy of the photon  $E$  is equal or higher than the binding energy  $\phi$  of the electron. For example, an X-ray photon with an energy of 15 keV can eject a K-electron ( $\phi_K = 7.112$  keV) or an L<sub>3</sub>-electron ( $\phi_{L3} = 0.706$  keV) out of a Fe atom. However, a 5 keV electron can only eject L-shell electrons from such an atom.

Since photoelectric absorption can occur at each of the (excitable) energy levels of the atom, the total photoelectric cross section  $\tau_i$  is the sum of (sub)shell-specific contributions:

$$\tau_1 = \tau_{i,K} + \tau_{i,L} + \tau_{i,M} + \dots = \tau_{i,K} + (\tau_{i,L1} + \tau_{i,L2} + \tau_{i,L3}) + (\tau_{i,M1} + \dots + \tau_{i,M5}) + \dots \quad (4)$$

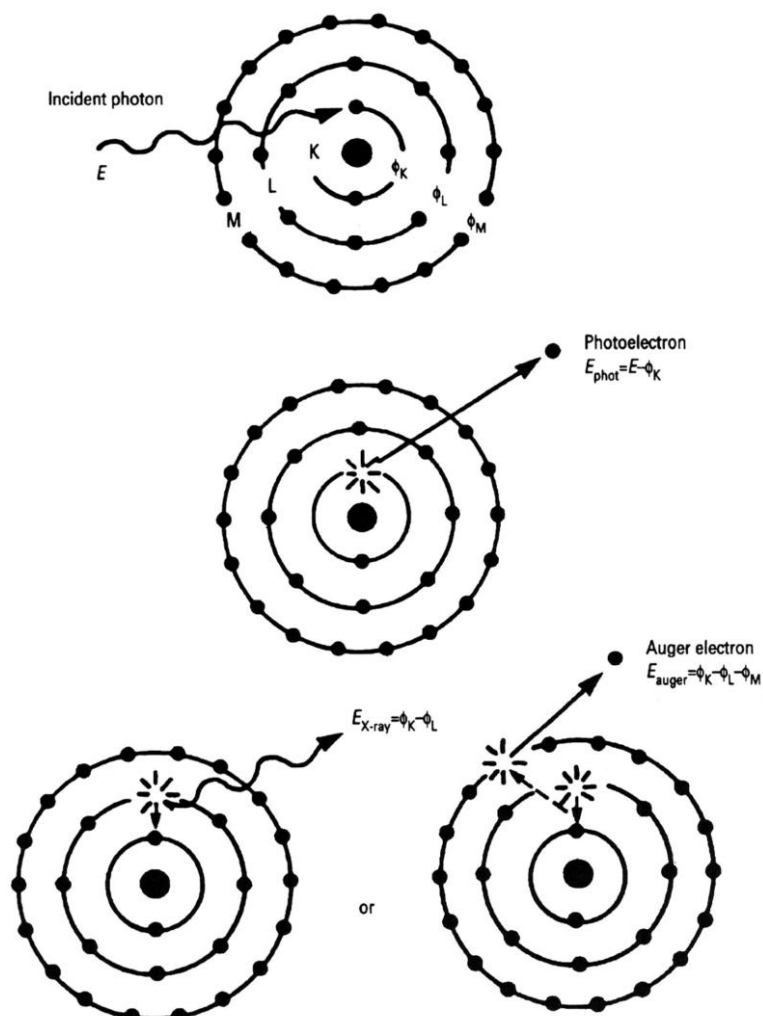
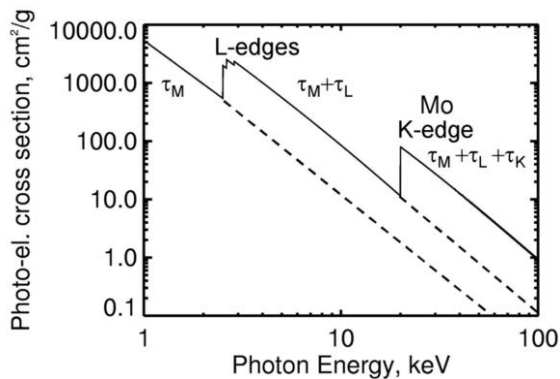


**Fig. 11.3** Photoelectric ionization can be followed by either radiative relaxation, causing the emission of characteristic fluorescent X-rays or non-radiative relaxation, involving the emission of Auger electrons.

In Fig. 11.4, the variation of  $\tau_{\text{Mo}}$  with energy is plotted. At high energy, e.g., above 50 keV, the probability for ejecting a K-electron is rather low and that for ejecting an L<sub>3</sub>-electron is even lower. As the energy of the X-ray photon decreases, the cross section increases, i.e., more vacancies are created. At the binding energy  $\phi_K = 19.99$  keV there is an abrupt decrease in the cross section because X-rays with lower energy can no longer eject electrons from the K-shell. However, these photons continue to interact with the (more weakly bound) electrons in the L and M-shells. The discontinuities in the photoelectric cross section are called absorption edges. The ratio of the cross section just above and just below the absorption edges.

**Fig. 11.4** Variation of  $\tau_{Mo}$  as a function of X-ray photon energy. The K, L<sub>1</sub>, L<sub>2</sub> and L<sub>3</sub> absorption edges are clearly visible.



tion edge is called the jump ratio,  $r$ . As X-ray fluorescence is the result of selective absorption of radiation, followed by spontaneous emission, an efficient absorption process is required. An element can therefore be determined with high sensitivity by means of XRF when the exciting radiation has its maximum intensity at an energy just above an absorption-edge of that element.

#### 11.2.4 Scattering

Scattering is the interaction between radiation and matter which causes the photon to change direction. If the energy of the photon is the same before and after scattering, the process is called elastic or Rayleigh scattering. Elastic scattering takes place between photons and bound electrons and forms the basis of X-ray diffraction. If the photon loses some of its energy, the process is called inelastic or Compton scattering.

Accordingly, the total cross section for scattering  $\sigma_i$  can be written as the sum of two components:

$$\sigma_i = \sigma_{R,i} + \sigma_{C,i} \quad (5)$$

where  $\sigma_{R,i}$  and  $\sigma_{C,i}$  respectively denote the cross sections for Rayleigh and Compton scatter of element  $i$ .

Compton scattering occurs when X-ray photons interact with weakly bound electrons. After inelastic scattering over an angle  $\phi$ , a photon (see Fig. 11.5), with initial energy  $E$ , will have a lower energy  $E'$  given by the Compton equation:

$$E' = \frac{E}{1 + \frac{E}{m_0 c^2} (1 - \cos \phi)} \quad (6)$$

where  $m_0$  denotes the electron rest mass.

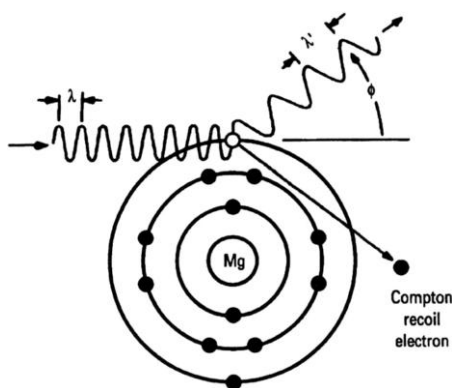


**Fig. 11.5** Geometry for Compton scattering of X-ray photons.

### 11.2.5 Bremsstrahlung

When an energetic electron beam impinges upon a (high-Z) material, X-rays in a broad wavelength band are emitted. This radiation is called *Bremsstrahlung* as it is released during the sudden deceleration of the primary electrons, as a result of their interaction with the electrons of the lattice atoms in the target. At each colli-

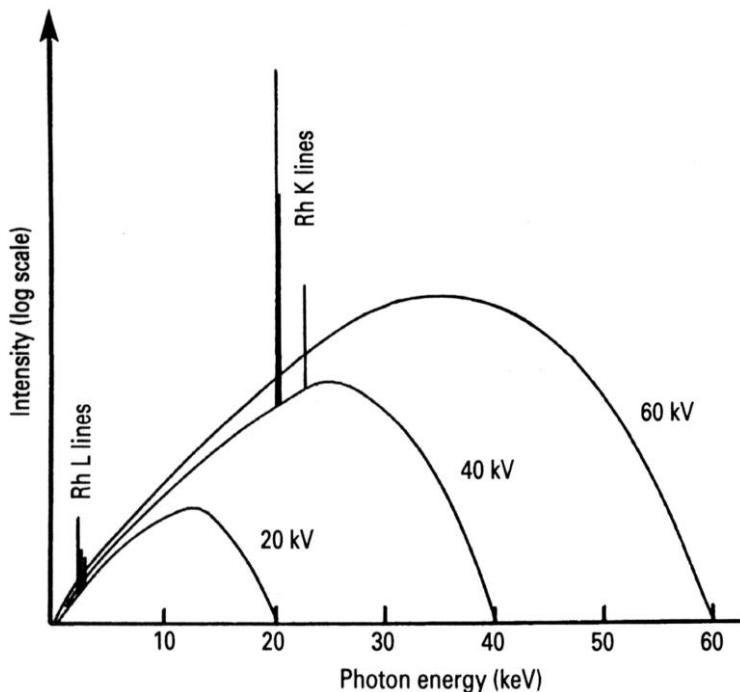


**Fig. 11.6** Polychromatic excitation spectra emitted by a Rh X-ray tube operated at various accelerating voltages. The excitation spectrum consists of a *bremsstrahlung* continuum upon which the characteristic lines of the anode material are superimposed (adapted from [12]).

sion, the electrons are decelerated and part of the kinetic energy lost is emitted as X-ray photons. (In addition, characteristic X-ray lines (see below) of the target materials are also produced.) Since during one collision, an electron of energy  $E$  can lose any amount between zero and  $E$ , the resulting *bremsstrahlung* continuum features photons with energies in the same range. On a wavelength scale, the continuum is characterized by a minimal wavelength  $\lambda_{\min}$  (nm) =  $1.24/E_{\max}$  (keV) =  $1.24/V$  (kV) where  $E_{\max}$  is the maximum energy of the impinging electrons and  $V$  the potential used to accelerate them. The continuum distribution reaches a maximum at  $1.5-2 \times \lambda_{\min}$  so that an increase in the accelerating potential  $V$  causes a shift of the continuum towards shorter wavelengths. In Fig. 11.6 *bremsstrahlung* spectra emitted by X-ray tubes operated at different accelerating potentials are shown.

### 11.2.6

#### Selection Rules, Characteristic Lines and X-ray Spectra

Characteristic X-ray photons are produced following the ejection of an inner orbital electron from an excited atom, and subsequent transition of atomic orbital electrons from states of high to low energy. Each element present in the specimen will produce a series of characteristic lines making up a polychromatic beam of characteristic and scattered radiation coming from the specimen. The systematic (IUPAC) name of the X-ray line arising from a vacancy in the K-shell of an atom, which is filled by an electron originally belonging to the L<sub>3</sub>-shell of that atom is the K–L<sub>3</sub> transition. However, this transition is more commonly referred to as the K<sub>α1</sub>-line (non-systematic or Siegbahn nomenclature); similarly, fluorescent X-rays resulting from L<sub>3</sub>–M<sub>5</sub> transitions are better known as L<sub>α1</sub>-photons. Table 11.1 lists a number of observed X-ray lines and their corresponding IUPAC and Siegbahn names.

Moseley first established the relationship between the wavelength  $\lambda$  of a characteristic X-ray photon and the atomic number  $Z$  of the excited element (see Fig. 11.7). Moseley's law is written as:

$$1/\lambda = K(Z - s)^2 \quad (7)$$

where  $Z$  is the atomic number and  $K$  and  $s$  are constants.  $s$  is the shielding constant and takes a value close to one.  $K$  has a different value for each of the line series considered (e.g., the K<sub>α</sub>-lines, the L<sub>α</sub>-lines, see Table 11.1). Each unique atom has a number of available electrons that can take part in the transfer and, since millions of atoms are typically involved in the excitation of a given specimen, all possible de-excitation routes are taken. These de-excitation routes can be defined by a simple set of selection rules that account for the majority of the observed wavelengths.

Each electron in an atom can be defined by four quantum numbers. The first of these quantum numbers is the principal quantum number  $n$ , which can take all integral values. When  $n$  is equal to 1, the level is referred to as the K level;

**Table 11.1** Principal X-ray lines (IUPAC and Siegbahn notations) and their approximate intensities relative to the major line in each subshell.

Series	IUPAC name	Siegbahn name	Relative Intensity
K-lines	K-L <sub>3</sub>	K <sub>α1</sub>	100
	K-L <sub>2</sub>	K <sub>α2</sub>	~50
	K-M <sub>3</sub>	K <sub>β1</sub>	~17
	K-M <sub>2</sub>	K <sub>β2</sub>	~8
L <sub>3</sub> -lines	L <sub>3</sub> -M <sub>5</sub>	L <sub>α1</sub>	100
	L <sub>3</sub> -M <sub>4</sub>	L <sub>α2</sub>	~10
	L <sub>3</sub> -N <sub>5,4</sub>	L <sub>β2,15</sub>	~25
	L <sub>3</sub> -M <sub>1</sub>	L <sub>η</sub>	~5
	M <sub>3</sub> -N <sub>1</sub>	L <sub>β6</sub>	~1
L <sub>2</sub> -lines	L <sub>2</sub> -M <sub>4</sub>	L <sub>β1</sub>	100
	L <sub>2</sub> -N <sub>4</sub>	L <sub>γ1</sub>	~20
	L <sub>2</sub> -M <sub>1</sub>	L <sub>η</sub>	~3
	L <sub>2</sub> -O <sub>1</sub>	L <sub>γ6</sub>	~3
L <sub>1</sub> -lines	L <sub>1</sub> -M <sub>3</sub>	L <sub>β3</sub>	100
	L <sub>1</sub> -M <sub>2</sub>	L <sub>δ4</sub>	~70
	L <sub>1</sub> -N <sub>3</sub>	L <sub>γ3</sub>	~30
	L <sub>1</sub> -N <sub>2</sub>	L <sub>γ2</sub>	~30
M-lines	M <sub>5</sub> -N <sub>7</sub>	M <sub>α1</sub>	
	M <sub>5</sub> -N <sub>6</sub>	M <sub>α2</sub>	
	M <sub>5</sub> -N <sub>6</sub>	M <sub>β</sub>	

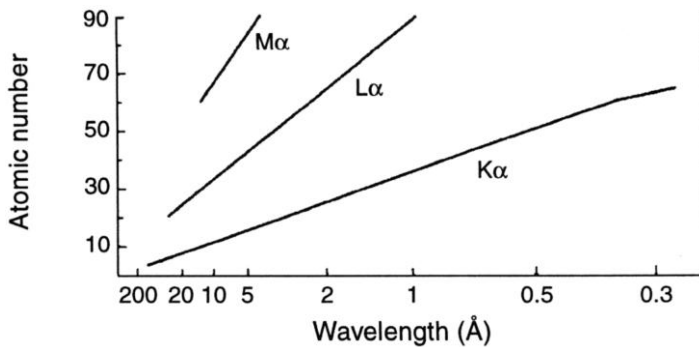


**Fig. 11.7** Moseley's law: relation between (inverse of the) wavelength of the K<sub>α</sub>, L<sub>α</sub> and M<sub>α</sub> lines of the elements and their atomic number (adapted from [8]).

when  $n$  is 2, the L level, and so on.  $l$  is the angular quantum number and this can take all values from  $(n-1)$  to zero.  $m$  is the magnetic quantum number and can take values from  $+l$  to  $-l$ .  $s$  is the spin quantum number with a value of  $\pm\frac{1}{2}$ . The total momentum  $J$  of an electron is given by the vector sum of  $l + s$ . Since no two electrons within a given atom can have the same set of quantum numbers, a series of levels or shells can be constructed. Table 11.2 lists the atomic structures of the first three principal shells. The first shell, the K-shell, has a maximum of two electrons and these are both in the 1s level (orbital). Since the value of  $J$  must be

**Table 11.2** Atomic structures of the first three principal shells.

<b>Shell (number of electrons)</b>	<b>n</b>	<b>l</b>	<b>m</b>	<b>s</b>	<b>Orbitals</b>	<b>J</b>
K (2)	1	0	0	$\pm \frac{1}{2}$	1s	$\frac{1}{2}$
L (8)	2	0	0	$\pm \frac{1}{2}$	2s	$\frac{1}{2}$
	2	1	1	$\pm \frac{1}{2}$	2p	$\frac{1}{2}, \frac{3}{2}$
	2	1	0	$\pm \frac{1}{2}$	2p	$\frac{1}{2}, \frac{3}{2}$
	2	1	-1	$\pm \frac{1}{2}$	2p	$\frac{1}{2}, \frac{3}{2}$
M (18)	3	0	0	$\pm \frac{1}{2}$	3s	$\frac{1}{2}$
	3	1	1	$\pm \frac{1}{2}$	3p	$\frac{1}{2}, \frac{3}{2}$
	3	1	0	$\pm \frac{1}{2}$	3p	$\frac{1}{2}, \frac{3}{2}$
	3	1	-1	$\pm \frac{1}{2}$	3p	$\frac{1}{2}, \frac{3}{2}$
	3	2	2	$\pm \frac{1}{2}$	3d	$\frac{3}{2}, \frac{5}{2}$
	3	2	1	$\pm \frac{1}{2}$	3d	$\frac{3}{2}, \frac{5}{2}$
	3	2	0	$\pm \frac{1}{2}$	3d	$\frac{3}{2}, \frac{5}{2}$
	3	2	-1	$\pm \frac{1}{2}$	3d	$\frac{3}{2}, \frac{5}{2}$
	3	2	-2	$\pm \frac{1}{2}$	3d	$\frac{3}{2}, \frac{5}{2}$

positive in this instance the only allowed value is  $+\frac{1}{2}$ . In the second shell, the L shell, there are eight electrons: two in the 2s level and six in the 2p levels. In this instance  $J$  has a value of  $\frac{1}{2}$  for the 2s level and  $\frac{3}{2}$  or  $\frac{1}{2}$  for the 2p level, thus giving a total of three possible L transition levels. These levels are referred to as  $L_1$ ,  $L_2$  and  $L_3$  respectively. In the M level, there are a maximum of 18 electrons: 2 in the 3s level, 8 in the 3p level and 10 in the 3d level. Again, with the values of  $\frac{3}{2}$  or  $\frac{1}{2}$  for  $J$  in the 3p level and  $\frac{5}{2}$  and  $\frac{3}{2}$  in the 3d level, a total of five M transition levels are possible ( $M_1$  to  $M_5$ ). Similar rules can be used to build up additional levels: N, O, etc.

The selection rules for the production of normal (diagram) lines require that the principal quantum number must change by at least one ( $\Delta n \geq 1$ ), the angular quantum number must change by only one ( $\Delta l = \pm 1$ ), and the  $J$  quantum number must change by zero or one ( $\Delta J = 0, \pm 1$ ). Application of the selection rules indicates that in, for example, the K series, only  $L_2 \rightarrow K$  and  $L_3 \rightarrow K$  transitions are allowed for a change in the principal quantum number of one. There are equivalent pairs of transitions for  $n = 2$ ,  $n = 3$ ,  $n = 4$ , etc. Figure 11.8 shows the lines that are observed in the K series. Three groups of lines are indicated. The normal lines are shown on the left-hand side, consisting of three pairs of lines from the  $L_2/L_3$ ,  $M_1/M_3$  and  $N_2/N_3$  sub-shells respectively. While most of the observed fluorescent lines are normal, certain lines may also occur in X-ray spectra that, at first sight, do not abide by the basic selection rules. These lines are called forbidden lines; they arise from outer orbital levels where there is no sharp energy distinction between orbitals. As an example, in the transition elements, where the 3d level is only partially filled and is energetically similar to the 3p levels, a weak forbidden transition (the  $\beta_5$ ) is observed. A third type are satellite lines arising from dual ionizations. Following the ejection of the initial electron in the photoelectric process, a short, but finite, period of time elapses before the vacancy is filled. This time period is called the lifetime of the excited state. For the lower atomic number

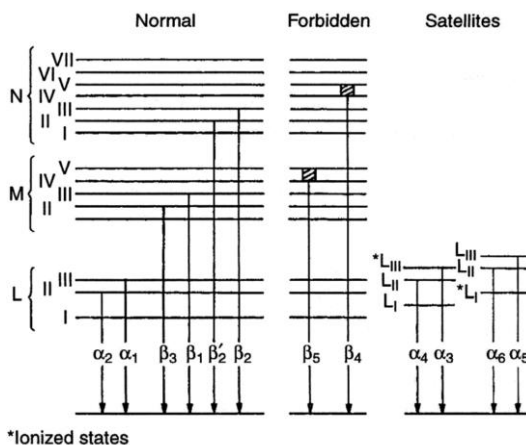


**Fig. 11.8** Observed lines in the K-series.

elements, this lifetime increases to such an extent that there is a significant probability that a second electron can be ejected from the atom before the first vacancy is filled. The loss of the second electron modifies the energies of the electrons in the surrounding sub-shells, and thus X-ray emission lines with other energies are produced. For example, instead of the  $K\alpha_1/K\alpha_2$  line pair, a double ionized atom will give rise to the emission of satellite lines such as the  $K\alpha_3/K\alpha_4$  and the  $K\alpha_5/K\alpha_6$  pairs. Since they are relatively weak, neither forbidden transitions nor satellite lines have great analytical significance; however, they may cause some confusion in the qualitative interpretation of spectra and may sometimes be misinterpreted as being analytical lines of trace elements.

### 11.2.7

#### Figures-of-merit for XRF Spectrometers

##### 11.2.7.1 Analytical Sensitivity

When XRF analysis of thin film samples is performed (i.e., in samples where the product  $\rho d$  of sample thickness  $d$  and sample density  $\rho$  is so small that absorption of the incoming exciting and of the outgoing fluorescent radiation in the material can be neglected, see Section 11.4.), there is a linear relation between the collected net X-ray intensity  $N_i$  of a given characteristic line of element  $i$  and the irradiated mass  $m_i$ , which usually is also proportional to the concentration  $c_i$  of that element in the sample:

$$N_i = S_i^* m_i t = S_i c_i t \quad (8)$$

The proportionality constants  $S_i$  for the various elements are called the sensitivity coefficients of the XRF spectrometer for determination of these elements (expressed in counts  $s^{-1}$   $(g/cm^3)^{-1}$ ) and are important figures-of-merit of the instrument. In Fig. 11.9, the variation with atomic number of the sensitivity of a

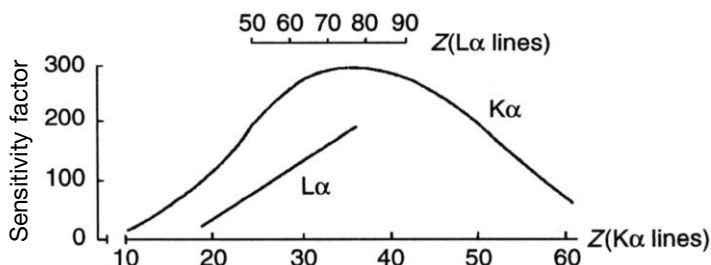


Fig. 11.9 Variation of sensitivity coefficients with atomic number for a WDXRF spectrometer (adapted from [9]).

WDXRF spectrometer is plotted, for the case where either the K<sub>α</sub> ( $10 < Z_i < 60$ ) or L<sub>α</sub> ( $40 < Z_i < 80$ ) peak intensities are used as analytical signals. By selection of the excitation conditions (tube anode material, excitation voltage), the shape and location of the maximum in the sensitivity curve can be influenced to suit the needs of the application at hand.

Instead of using the X-ray intensity collected during a specific time  $t$ , it is often more convenient to use the net X-ray count rate  $R_i$ :

$$R_i = N_i / t = S_i c_i \quad (9)$$

#### 11.2.7.2 Detection and Determination Limits

In reality, it is not possible to directly measure the net peak intensity  $N_i$ ; rather, a total intensity  $T_i = N_i + B_i$  is measured (see also Fig. 11.27). The background intensity  $B_i$  can be written as the sum of various contributions:

$$B_i = B_i^{\text{scatter}} + B_i^{\text{detector}} + \sum_{j \neq i} B_{i,j}^{\text{overlap}} + B_i^{\text{blank}} \quad (10)$$

where  $B_i^{\text{scatter}}$  denotes the contribution to the spectral background below the analytical line of element  $i$  due to scattering of the primary radiation in the sample itself, in the sample environment gas (air or helium, if any) and (in some cases) on the sample holder materials. These phenomena cause a continuous background upon which the characteristic peaks are superimposed.  $B_i^{\text{detector}}$  denotes the background contribution in the same energy/wavelength region due to detector artifacts,  $B_{i,j}^{\text{overlap}}$  is the contribution to the peak intensity resulting from unresolved overlap between lines of an element  $j \neq i$  and the analytical line of element  $i$  and  $B_i^{\text{blank}}$  denotes the contributions to the peak intensity of element  $i$  not originating from the sample, i.e. a blank value.

When the magnitude of  $B_i$  is experimentally determined and this measurement is repeated  $n$  times, the results will be distributed around a mean value  $\langle B_i \rangle$  with a standard deviation  $s_B$ . In modern instruments, most sources of systematic and random errors (e.g. due to mechanical or electrical instabilities) are small compared to the inherent uncertainty of the intensity measurements resulting from

counting statistics. When  $B_i$  is obtained by means of a counting procedure (which usually is the case), Poisson (or counting) statistics govern the measurements so that  $s_B^2 = \langle B_i \rangle$ .

The Union of Pure and Applied Chemistry (IUPAC) defines the limit of detection as “the lowest concentration level than can be determined to be statistically significant from an analytical blank”. The lowest net X-ray intensity  $N_{i,LD}$  that still can be distinguished in a statistically significant manner from the average background level can be written as:

$$N_{i,LD} = \langle B_i \rangle + k s_B \quad (11)$$

where  $k$  is a constant depending on the significance level considered.

The limit of detection concentration  $c_{i,LD}$  corresponding to  $N_{i,LD}$  can be written as:

$$c_{i,LD} = \frac{N_{i,LD} - \langle B_i \rangle}{S_i t} = \frac{ks_B}{S_i t} = \frac{k\sqrt{R_B}}{S_i \sqrt{t}} \quad (12)$$

where  $R_B = \langle B_i \rangle / t$  is the background count rate. When the irradiation of a standard sample (with known concentration  $c_i$ ) during a time  $t$  results in net and background intensities  $N_i^{\text{std}}$  and  $B_i^{\text{std}}$ , so that the sensitivity  $S_i$  can be approximated by the ratio  $N_i^{\text{std}}/c_i^{\text{std}}/t$ , it follows that the lowest detectable concentration (or relative detection limit)  $c_{i,LD}$  can be estimated from this measurement by using the relation:

$$c_{i,LD} \cong c_i^{\text{std}} \frac{k \sqrt{B_i^{\text{std}}}}{N_i^{\text{std}}} \quad (13)$$

When during such an experiment, a known mass  $m_i^{\text{std}}$  was irradiated, the lowest detectable mass (or absolute detection limit)  $m_{i,LD}$  is can be calculated by means of:

$$m_{i,LD} \cong m_i^{\text{std}} \frac{k \sqrt{B_i^{\text{std}}}}{N_i^{\text{std}}} \quad (14)$$

Relative detection limits are useful figures-of-merit for bulk XRF equipment, where it is usually relevant to know the lowest concentration level at which the spectrometer can be used for qualitative or quantitative determinations. In instruments where very small sample masses are being irradiated (e.g., in the pg range for microscopic XRF ( $\mu$ -XRF) and total-reflection XRF (TXRF)), the absolute detection limit is another useful figure-of-merit since that provides information on the minimal sample mass than can be analysed in a given set-up.

In the literature, usually detection limit values for  $k = 3$  (corresponding to a statistical confidence level of 99 %) are reported. A related figure-of-merit is the *determination limit* which is defined as the lowest concentration (or mass) at which a

**Table 11.3** WDXRF obtained relative detection limits (in  $\mu\text{g g}^{-1}$ ) in various matrixes and using different instruments.

Matrix	Element	$c_{LD}$
Terephthalic acid	Fe	0.15
	Co	0.18
Aluminum	Mg	10.5
	P	1.3
Al–Mg alloy	Mg	7
	Si	5
	Ti	3
	Mn	2
	Cu	1
Cement	$\text{Na}_2\text{O}$	36
	$\text{MgO}$	27
	$\text{Al}_2\text{O}_3$	22
	$\text{SiO}_2$	50
	$\text{SO}_3$	24
Low-alloy steel	$\text{P}_2\text{O}_5$	32
	C	80
	Al	4
	Si	2
Copper alloys	Cr	2
	Be	0.20 %

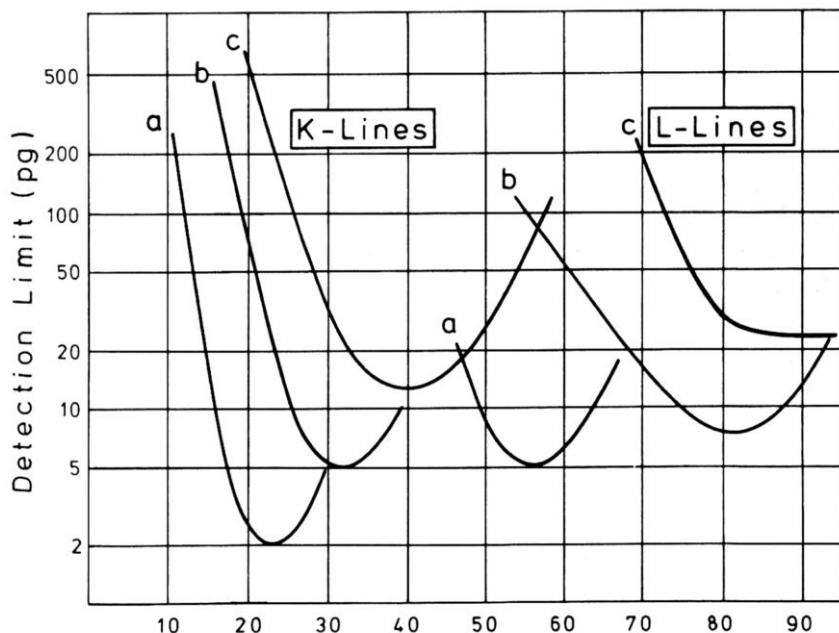


**Fig. 11.10** Typical absolute detection limit values for TXRF spectrometers. The labels a, b and c refer to different instrument settings (adapted from [15]).

quantitative determination with a relative uncertainty of at least 10 % is possible. This quantity can be calculated by setting  $k = 10$  in the above expressions.

In Tab. 11.3, as an example, relative LD values for trace elements obtained by means of WDXRF in different matrices are listed. In Fig. 11.10, a plot of typical absolute LD values for TXRF spectrometers is shown.

### 11.3 Instrumentation

While most of the early work in X-ray spectrometry was carried out using electron excitation, today, use of electron-excited X-radiation is restricted mainly to X-ray spectrometric attachments to electron microscopes. Most modern stand-alone X-ray spectrometers use X-ray excitation sources rather than electron excitation. All conventional X-ray spectrometers are comprised of three parts: the primary source unit, the spectrometer itself and the measuring electronics.

X-ray fluorescence spectrometry typically uses a polychromatic beam of short wavelength/high energy photons to induce the emission of longer wavelength/lower energy characteristic lines in the sample to be analyzed. Modern X-ray spectrometers may use either the diffracting power of a single crystal to isolate narrow wavelength bands (wavelength-dispersive XRF (WDXRF)) or an energy-selective detector may be employed to isolate narrow *energy* bands (energy-dispersive XRF (EDXRF)) from the polychromatic radiation (including characteristic radiation) that is produced in the sample.

Because the relationship between emission wavelength and atomic number is known, isolation of individual characteristic lines allows the unique identification of an element to be made and elemental concentrations can be estimated from characteristic line intensities. Thus this technique is a means of material characterization in terms of chemical composition.

Wavelength-dispersive XRF instrumentation is almost exclusively used for (highly reliable and routine) bulk-analysis of materials, e.g., in industrial quality control laboratories. In the field of energy-dispersive XRF instrumentation, next to the equipment suitable for bulk analysis, several important variants have evolved in the last 20 years. Both total reflection XRF (TXRF) and micro-XRF are based on the spatial confinement of the primary X-ray beam so that only a limited part of the sample (+ support) is irradiated. This is realized in practice by the use of dedicated X-ray sources, X-ray optics, and irradiation geometries.

#### 11.3.1 X-ray Sources

Four different types of X-ray sources are employed in X-ray analysis: (a) sealed X-ray tubes and (b) radioactive sources are the most commonly employed, while to a lesser extent primary X-rays produced in (c) rotating anode tubes and (d) synchrotron radiation facilities are also utilized for analytical purposes.

Most commercially available X-ray spectrometers utilize a sealed X-ray tube as an excitation source, and these tubes typically employ a heated tungsten filament to induce the emission of thermionic electrons in a vacuum chamber. After acceleration by means of a high voltage  $V$ , the electrons are directed towards a layer of high purity metal (e.g., Cr, Rh, W, Mo, Rh, Pd, ...) that serves as anode. In the metal layer, a *bremssstrahlung* continuum is produced, onto which the characteristic lines of the anode material are superimposed. The broad band radiation is well suited for the excitation of the characteristic lines of a wide range of atomic numbers. The higher the atomic number of the anode material, the more intense the beam of radiation produced in the tube. Fig. 11.11 shows a schematic cross-section of a sealed X-ray tube.

In typical X-ray tubes employed in XRF spectrometers, accelerating voltages of 25–50 kV are used, while electron currents in the range 20–50 mA are employed. For WDXRF, frequently, 3 kW X-ray tubes are used; in EDXRF spectrometers, depending on the manner of sample excitation, tubes in the 50–1000 W range are used. The efficiency of an X-ray tube is relatively low: only about 1 % of the electric power is converted into X-rays, the rest is dissipated as heat. Accordingly, the tube anode of high power tubes ( $> 100$  W) is usually water-cooled to avoid meltdown of the metal block. A key factor in the design of an X-ray tube is the maximum powder loading (expressed in  $\text{W mm}^{-2}$ ) it can stand. The high-voltage power supplies used together with X-ray tubes are highly stable so that a wide conical X-ray beam of nearly constant intensity (to within a few% relative) is emitted. For applications requiring higher power levels such as 3 kW, rotating rather than fixed anode tubes are employed. In these devices, the anode is a fast-spinning water-cooled metal cylinder covered with the desired anode material. During each revolution of the anode, only a small area on the surface is bombarded by the electrons

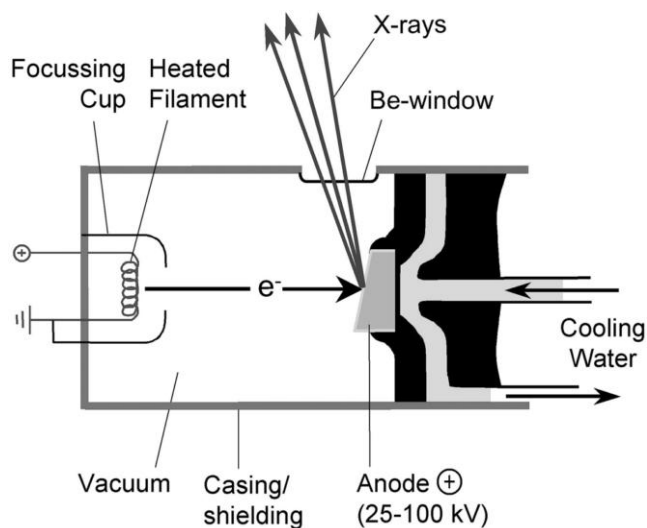


Fig. 11.11 Cross-section of a sealed X-ray tube.

during a short fraction of the time, so that the rest of the period can be used for heat removal. Rotating anode tubes that can be operated up to a total power of 18 kW are commercially available.

The emission spectrum of an X-ray tube (see Fig. 11.6) consists of two components: a *bremstrahlung* continuum upon which the characteristic lines of the anode material (that becomes ionized as a result of the electron bombardment) are superimposed. The shape of the emission spectrum can be modified by changing the electron acceleration voltage.

Radioactive  $\alpha$ -,  $\beta$ -, and  $\gamma$ -sources may also be employed for (ED)XRF analysis. Generally, these sources are very compact compared to X-ray tubes and can, e.g., be used in portable analysis systems.  $\alpha$ -sources are suitable for the analysis of low atomic number elements. Frequently used sources are  $^{244}\text{Cm}$ , with a half-life ( $t_{1/2}$ ) of 17.8 years that emits 5.76 and 5.81 MeV  $\alpha$ -particles, and  $^{210}\text{Po}$ , having a half-life of 138 days and emitting 5.3 MeV  $\alpha$ -particles.

$\beta$ -sources can also be employed, either for direct EDXRF excitation of a sample or for producing *bremstrahlung* radiation in a target to be used for subsequent sample excitation.  $^{22}\text{Na}$  ( $t_{1/2} = 2.6$  years),  $^{85}\text{Kr}$  ( $t_{1/2} = 10.7$  years) and  $^{63}\text{Ni}$  ( $t_{1/2} = 100$  years) are  $\beta$ -emitters that can be used for the former purpose, emitting, respectively,  $\beta^-$ -particles of ca. 550, 670 and 66 keV. For *bremstrahlung* production,  $^{147}\text{Pm}$  ( $t_{1/2} = 2.6$  years, 225 keV) in combination with a Zr target and  $^3\text{H}$  ( $t_{1/2} = 12.4$  years, 19 keV, Ti target) are useful.

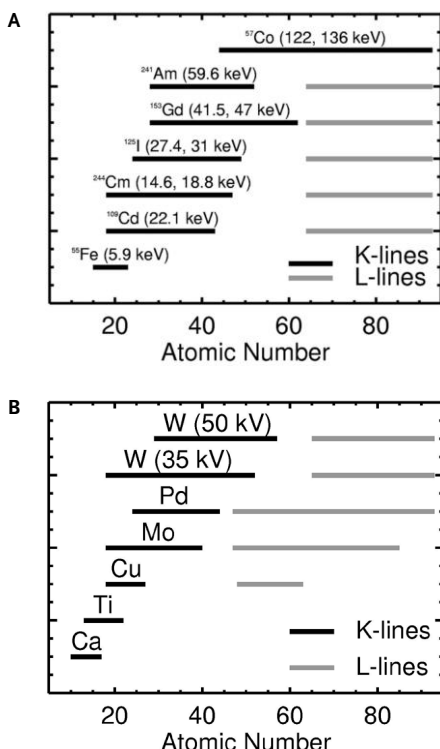
In Tab. 11.4, some characteristics of radio sources emitting X-ray or  $\gamma$ -ray lines are listed. The X-ray emitting sources usually contain nuclides that decay by means of the electron-capture mechanism. During the decay, an inner shell electron is captured by the neutron-deficient nucleus, transforming a proton into a neutron. This results in a daughter nuclide that has a vacancy in one of its inner shells, which results in the emission of corresponding characteristic radiation. For example, when a  $^{55}\text{Fe}$ -nucleus (26 protons and 29 neutrons) captures a K-electron and becomes a  $^{55}\text{Mn}$  nucleus, a Mn K-L<sub>3,2</sub> (Mn-K $\alpha$ ) or K-M<sub>3,2</sub> (Mn-K $\beta$ ) photon will be emitted. Other sources (such as  $^{241}\text{Am}$  or  $^{57}\text{Co}$ ) emit  $\gamma$ -rays of suitable energy as a result of different nuclear transformations.

In Fig. 11.12, the range of elements that can be usefully analyzed by means of various radioactive and X-ray tubes sources is summarized.

**Table 11.4** Radioactive sources used for XRF analysis (flux in photons  $\text{s}^{-1} \text{sr}^{-1}$ ).

<b>Radio</b>	<b>Half-life</b>	<b>X-ray or <math>\gamma</math>-ray energy</b>	<b>Flux</b>
<b>isotope</b>	<b>(years)</b>	<b>(keV)</b>	
$^{55}\text{Fe}$	2.7	5.9–6.5 (Mn-K X-rays)	$7 \times 10^6$
$^{244}\text{Cm}$	88	14.6–22 (U L X-rays)	
$^{109}\text{Cd}$	1.3	22–25 (Ag K X-rays)	$8 \times 10^6$
$^{125}\text{I}$	0.16	27–32 (Te K X-rays)	
$^{241}\text{Am}$	433	59.6 ( $\gamma$ -ray)	$6 \times 10^7$
$^{153}\text{Gd}$	0.66	41.48 (Eu-K X-rays)	$4 \times 10^8$
$^{57}\text{Co}$	0.74	122.136 ( $\gamma$ -ray)	$4 \times 10^6$

**Fig. 11.12** Range of elements that can be analyzed using (a) radioactive sources, (b) X-ray tubes with different anodes, showing excitation of K- and L-lines.



In a number of specialized cases, XRF experiments also make use of synchrotron sources. Synchrotron radiation (SR) is produced by high-energy (GeV) relativistic electrons or positrons circulating in a storage ring. This is a very large, quasi-circular vacuum chamber where strong magnets force the particles on closed trajectories. X-radiation is produced during the continuous acceleration (change in velocity vector in this case) of the particles. SR-sources are several (6–12) orders of magnitude brighter than X-ray tubes, have a natural collimation in the vertical plane and are linearly polarized in the plane of the orbit. The spectral distribution is continuous, and the simplest way of employing SR is to use the full white beam to irradiate the sample (see section 11.3.7: micro-XRF). By proper monochromatization, it is possible to employ selective excitation of a series of elements in the sample, yielding optimal detection conditions (see section 11.3.6: TXRF). An additional advantage is the high degree of polarization of SR, causing spectral backgrounds due to scatter to be greatly reduced when the detector is placed at 90° to the primary beam and in the storage ring plane. The combination of a high primary beam intensity and low spectral background causes DL values of SRXRF to go down to the ppb level (see, e.g., Fig. 11.24). A disadvantage of the use of SR is that the source intensity decreases with time (due to a gradual loss of orbiting particles between ring refills) so that measurement of unknown samples must be bracketed between standards and/or by continuously monitoring the primary beam intensity.

## 11.3.2

**X-ray Detectors**

As any radiation detector, an X-ray detector is a transducer for converting X-ray photon energy into easily measurable and countable voltage pulses. All detector types work through a process of photoionization in which interaction between the entering X-ray photon and the active detector material produces a number of electrons. By means of a capacitor and a resistor, the current produced by the electrons is converted to a voltage pulse, in such a way that one digital voltage pulse is produced for each X-ray photon that enters the detector.

Next to being sensitive to photons of the appropriate energy range, there are two other important properties that the ideal detector should possess: proportionality and linearity. A detector is said to be proportional when the height of the voltage pulse that is produced upon entry of a photon, is proportional to the energy of the photon. Proportionality is needed when, through pulse-height selection, only pulses of a particular height, i. e. corresponding to X-ray photons within a specific energy band, are to be measured.

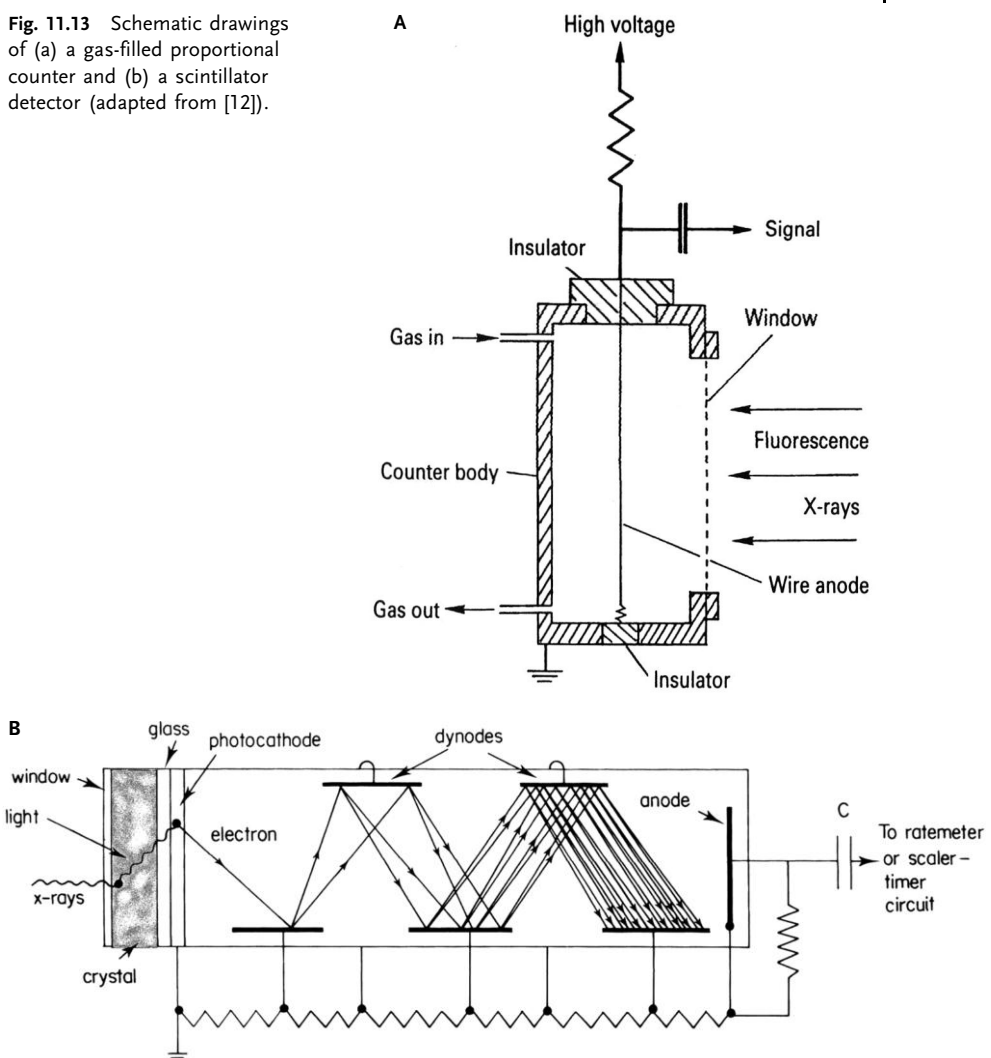
When the rate at which voltage pulses are being recorded is the same as the rate at which X-ray photons enter the detector, the latter is said to have a linear response. This property is important when the recorded count rates of various X-ray lines are to be used as measures of the photon intensities of these lines produced in a sample.

The detector resolution is the precision/repeatability with which the energy of a specific type of X-ray photons (e. g., the Mn-K<sub>α</sub> line at 5.9 keV) can be determined and is therefore a measure of the capability of the detector to distinguish between X-rays of very similar energy but different origin (e. g., the As- K<sub>α1</sub> line at 10.543 keV and the Pb-L<sub>α1</sub> line at 10.549 keV).

In wavelength-dispersive spectrometers, gas flow proportional counters (for long wavelengths,  $\lambda > 0.2$  nm) and scintillation counters (for wavelengths shorter than 0.2 nm) are used to count X-rays. Both types of detectors are usually combined in a tandem detector that covers the entire wavelength range used in WDXRF spectrometry. Since neither of these detectors has sufficient resolution to separate multiple wavelengths/energies on its own, they are employed together with an analyzing crystal. In the case of energy-dispersive spectrometry, solid-state detectors of higher resolution are used.

A gas flow proportional counter (see Fig. 11.13a) consists of a cylindrical tube about 2 cm in diameter, carrying a thin (25–50 mm) wire along its radial axis. The tube is filled with a mixture of inert gas and quench gas, typically 90% argon/10% methane (P-10). The cylindrical tube is grounded and a voltage of ca 1400–1800 V is applied to the central wire. The wire is connected to a resistor shunted by a capacitor. An X-ray photon entering the detector produces a number of ion pairs ( $n$ ), each comprising one electron and one Ar<sup>+</sup> ion. The first ionization potential for argon is about 16 eV, but competing processes during the conversion of photon energy to ionization cause the average energy required to produce an ion pair to be greater than this amount. The fraction relating the average energy to pro-

**Fig. 11.13** Schematic drawings of (a) a gas-filled proportional counter and (b) a scintillator detector (adapted from [12]).



duce one ion pair, to the first ionization potential, is called the Fano factor  $F$ . For argon,  $F$  is between 0.5 and 0.3 and the average energy  $\epsilon$  required to produce one primary ion pair is equal to 26.4 eV. The number of ion pairs produced by a photon of energy  $E$  will equal:

$$n = E/\epsilon \quad (15)$$

Following ionization, the charges separate, with the electrons moving towards the (anode) wire and the argon ions to the grounded cylinder. As the electrons approach the high field region close to the anode wire they are accelerated sufficiently

to produce further ionization of argon atoms. Thus a much larger number  $N$  of electrons will actually reach the anode wire. This effect is called gas gain, or gas multiplication, and its magnitude is given by  $M = N/n$ . For gas flow proportional counters used in X-ray spectrometry  $M$  typically has a value of around  $10^5$ . Provided that the gas gain is constant the size of the voltage pulse  $V$  produced is directly proportional to the energy  $E$  of the incident X-ray photon. In practice not all photons arising from photon energy  $E$  will be exactly equal to  $V$ . There is a random process associated with the production of the voltage pulses and the resolution of a counter is related to the variance in the average number of ion pairs produced per incident X-ray photon.

While the gas flow proportional counter is ideal for measurement of longer wavelengths, it is rather insensitive to wavelengths shorter than about 0.15 nm. For this shorter wavelength region it is common to use a scintillation counter (see Fig. 11.13b). The scintillation counter consists of two parts, the phosphor (scintillator) and the photomultiplier. The phosphor is typically a large single crystal of sodium iodide that has been doped with thallium, denoted as a NaI(Tl) crystal. When X-ray photons fall onto the phosphor, blue light photons are produced (with a wavelength of 410 nm), where the number of blue light photons is related to the energy of the incident X-ray photon. These visual light photons produce electrons by interaction with the surface of the photocathode in the photomultiplier, and the number of electrons is linearly increased by a series of secondary surfaces, called dynodes, inside the photomultiplier. The current produced by the photomultiplier is then converted to a voltage pulse, as in the case of the gas flow proportional counter. Since the number of electrons is proportional to the energy of the incident X-ray photon, the scintillation counter also has a proportional response. Because of inefficiencies in the X-ray/visual-light/electron conversion processes, the average energy to produce a single event within a scintillation counter is more than a magnitude greater than the equivalent process in a flow counter. For this reason, the resolution of scintillation counters is much worse than that of flow counters.

The output pulses produced by both above-mentioned detectors are further processed by a linear amplifier and a discriminator circuit. Usually the number of pulses is counted during a preset amount of time and the accumulated counts stored in computer memory for display and further processing. The processing of an X-ray event by the detector and its associated electronics takes a finite amount of time. After the arrival of one X-ray the detection system is said to be 'dead' during this length of time, because X-rays arriving within this dead period will not be counted. The dead time is of the order of 200 to 300 ns after the arrival of each photon; this implies that count rates up to  $10^6$  photons per second can be handled.

The detectors used in the various forms of EDXRF are semiconductor detectors. Conventionally, two types, i. e. lithium drifted silicon (Si(Li)) and hyperpure germanium (HP-Ge) detectors are used. Their main advantages are their compact size, the non-moving system components, and relatively good energy resolution, which optimally is of the order of 120 eV at 5.9 keV. Because of their operation prin-

ciples, these detectors have an inherent simultaneous multi-element capacity, which leads to a short measuring time for all elements as the detectors select the energy and collect counts at the same time. Disadvantages include the need for liquid nitrogen ( $\text{LN}_2$ ) cooling during operation, the necessity of having a relatively thin (8–25  $\mu\text{m}$ ) Be window and the fact that the maximum processable number of counts is limited to about 40,000 cps. This figure can be increased to 100,000 cps, but with loss of optimal performance characteristics.

The detector crystal itself is a disk of very pure Si or Ge with dimensions of 4–10 mm diameter and 3–5 mm thickness. Even careful production of the Si ingots from which the disks are cut will still leave some trace impurities in the Si lattice. To compensate and bind all free electrons, lithium ions are drifted (allowed to diffuse at elevated temperature) into the silicon crystal to neutralize the Si crystal defects in a particular zone, the so-called intrinsic zone. Then the Au contacts are evaporated onto the crystal and a reverse voltage applied. In the crystal, the energy difference  $\epsilon$  (band gap) between the valence and conduction band is 3.8 eV. At room temperature, the conduction band is partially populated so that the crystal is a semiconductor. To keep the leakage current as low as possible, the crystal is cooled with  $\text{LN}_2$  by placing it in a vacuum cryostat. At  $-196^\circ\text{C}$  almost all electrons remain in the valence band. The radiation to be measured needs to enter the cryostat through a thin entrance window, usually made of Be. By applying a reverse voltage to the charge-carrier-free intrinsic zone, an absorbed X-ray photon is converted into charge by ionization. Electrons are promoted from the valence to the conduction band, leaving “positive holes” in the valence band; thus the crystal temporarily becomes conducting.  $n = E/\epsilon$  electron–hole pairs are created. The electrons and holes are quickly swept to the contact layers by the electric field created by the applied reverse bias on the crystal.

Figure 11.14 shows the operation principle schematically. The charge induces a signal at the gate of a cooled field effect transistor (FET) that is the input stage of a charge sensitive preamplifier. The output signal is fed to a pulse processor that shapes the pulse and amplifies it further. This signal is in the range up to 10 V and is proportional to the energy of the absorbed photon. The pulse height is digitized by means of an analog-to-digital converter (ADC) and the resulting digital value stored in a multi-channel analyzer (MCA). This is an array of memory cells, called channels; by using the digital value associated with a single event as address offset into the memory array, the content of the appropriate channel is incremented with one count. Thus, all detector events having the same pulse height are stored in the same channel. For example, upon entry in the detector of a  $\text{Cu-K}_{\alpha 1}$  photon ( $E = 8.05 \text{ keV}$ ), 2117 electron–hole pairs will be generated, which may lead to the formation of a preamplifier voltage pulse of, e.g., 42.0 mV. After further amplification and shaping, this is converted into a bell-shaped pulse of 4.20 V; the pulse-height is then digitized by an ADC, resulting for instance in a digital number of 420. Ultimately, this causes the content of channel 420 to be incremented with one count. After readout, the MCA memory (typically 1024 or 2048 channels in size, each corresponding to a 10–20 eV wide energy range) yields a pulse-height

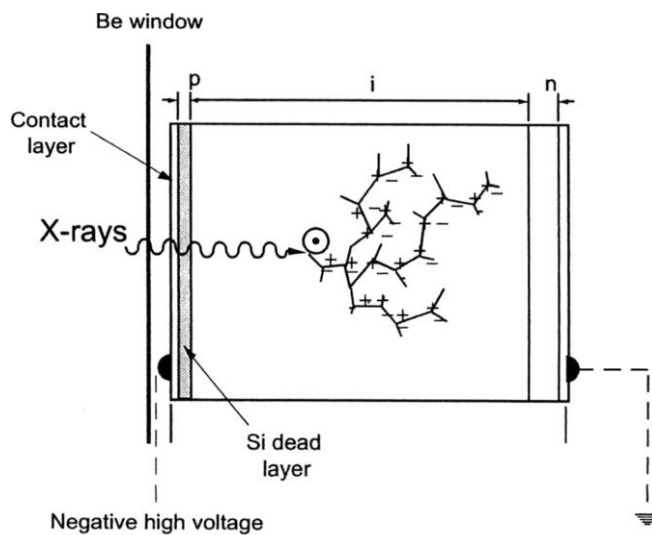


Fig. 11.14 Scheme of the working principle of a Si(Li) detector.

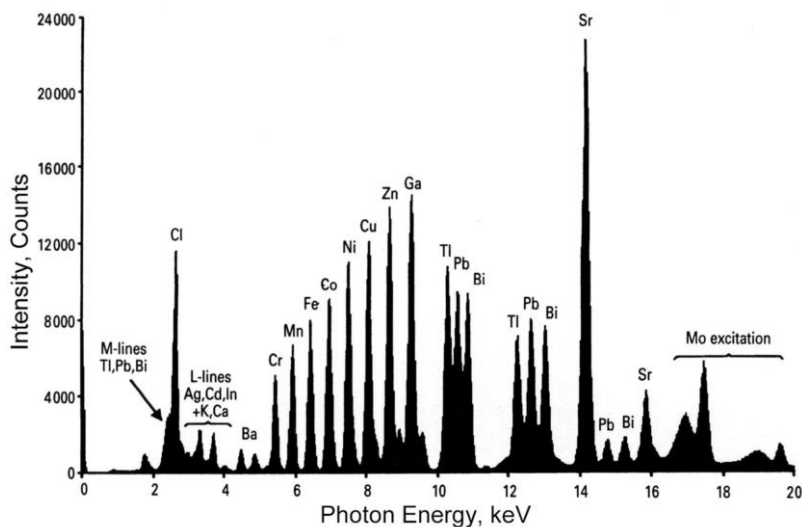


Fig. 11.15 Energy-dispersive XRF spectrum of a multi-element standard, obtained in a TXRF spectrometer.

distribution of the detected events or an energy-dispersive X-ray spectrum, as shown in Fig. 11.15.

In the spectra, a broadening of the X-ray lines can always be observed, i.e. the counts associated with photons of a specific energy, which normally should end up in a single channel, are distributed in a quasi-gaussian fashion over several adjacent channels in the spectrum, thus giving rise to a bell-shaped X-ray peak

in the spectrum. This line-broadening is caused by statistical fluctuations in the number of electron–hole pairs created when an X-ray photon of a given energy enters the detector; electronic noise in the amplifiers cause the uncertainty in the pulse-height to increase further. Even under conditions in which all noise contributions in the electronics are minimized, the line broadening remains a significant phenomenon, causing frequent peak overlap to occur in X-ray spectra, e.g., between lines of adjacent elements such as the Mn-K<sub>β</sub> and Fe-K<sub>α</sub> peaks. The resolution of energy-dispersive detectors conventionally is expressed as the full-width-at-half-maximum of the Mn-K<sub>α</sub> (Mn K-L<sub>2,3</sub>) peak (at 5.98 keV) and typically is around 150 eV. In the most optimal case, this value can be also low as 120 eV. The time to process an X-ray event (dead time) is of the order of 10 to 30 μs; conventional EDXRF spectrometers can therefore only operate at count rates up to 40,000 counts per second. In view of the presence of a Be window in the detector cryostat, X-ray photons below 2 keV are hard to detect in a conventional Si(Li) detector, although thin-window models are commercially available.

Since about 1995, several types of compact and thermoelectrically cooled ED detectors have become available. The most significant advantage of these detectors is that they do not require liquid nitrogen cooling, allowing the instrument they are incorporated in to be much smaller. This type of detector is suitable for employment in portable equipment.

Thermoelectrically cooled Si-PIN, Cd<sub>1-x</sub>Zn<sub>x</sub>Te (CZT) and HgI<sub>2</sub> detectors are fairly inexpensive devices. The currently available Si-PIN diode detectors mostly have a thickness of about 300 μm which makes the detector useful up to X-ray energies of 20 keV and an energy resolution in the range 180–200 eV at Mn-K<sub>α</sub> i.e., slightly worse than that of Si(Li) or HPGe detectors. Versions with 500 μm thickness or larger active areas (up to 25 mm<sup>2</sup> vs. the standard 5–10 mm<sup>2</sup>) are now (2001) becoming available, but still have resolutions in the 200–250 eV range at Mn-K<sub>α</sub>. CZT detectors are targeted towards the higher energy range with a thickness of up to 2 mm, allowing efficient detection of X-rays up to 150 keV with a resolution of ca. 250 eV at Mn-K<sub>α</sub> (5.9 keV) and 1 keV at 60 keV. Similarly, HgI<sub>2</sub> detectors (with thicknesses of a few millimeters) can also be used in this range with a resolution of ca. 200 eV at Mn-K<sub>α</sub>.

A very promising type of solid-state detector is the solid-state drift chamber (SSD) detector, featuring excellent energy resolution at high count rates. A FWHM below 140 eV at 5.9 keV can be achieved with thermoelectrical cooling (Peltier effect). SSDs exist in a large variety of sizes up to 2 cm<sup>2</sup> diameter. They still show excellent spectroscopic behaviour at count rates as high as  $2 \times 10^6$  counts cm<sup>-2</sup> s<sup>-1</sup>. The compact design, the relatively low price, the absence of the need for liquid nitrogen for cooling, the high count rate capability and the non-sensitivity to noise pick-up make these systems attractive alternatives to conventional semiconductor detectors.

The resolution of a number of different of X-ray detectors in the range 1–100 keV (ca. 1–0.01 nm) is compared in Fig. 11.16. It is clear that scintillators and proportional counters are not even able to separate the K<sub>α</sub>-lines of adjacent elements whereas most of the solid-state detectors can do this.

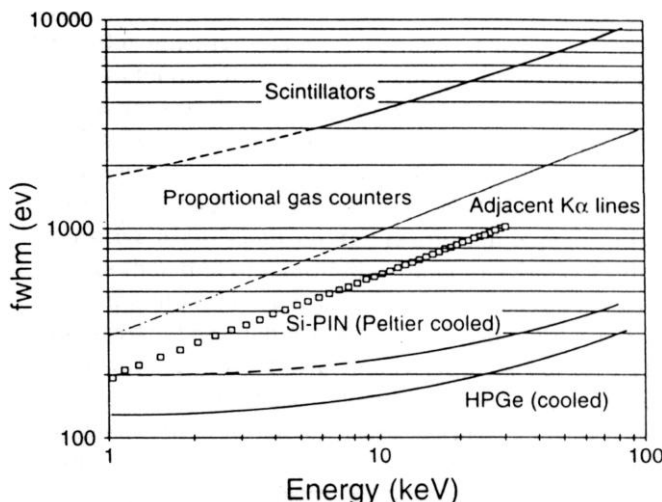


**Fig. 11.16** Energy-resolution (expressed as FWHM of the  $K_{\alpha}$  line of a given energy), of different X-ray detectors in the 1–100 keV range. The difference in  $K_{\alpha}$  line energy between adjacent elements is also shown (symbols) (adapted from [3]).

### 11.3.3

#### Wavelength-dispersive XRF

A typical WDXRF system consists of an X-ray tube, a specimen support holder, a primary collimator, an analyzing crystal and a tandem detector. The typical WDXRF irradiation/detection geometry is shown in Fig. 11.17. Wavelength-dispersive spectrometers employ diffraction by a single crystal to separate characteristic wavelengths emitted by the sample. A single crystal of known interplanar spacing  $d$  is used to disperse the collimated polychromatic beam of characteristics wavelengths that is coming from the sample, such that each wavelength  $\lambda$  will diffract at a specific angle  $\theta$ , given by Braggs law:

$$n\lambda = 2d \sin \theta \quad (16)$$

where  $n$  is an integer number denoting the order of the diffracted radiation. A goniometer is used to maintain the required  $\theta/2\theta$  relationship between sample and crystal/detector.

Prior to impinging on the analyzer crystal, by means of a collimator or slit, the spread in initial directions of the sample-to-crystal beam is limited. Since the maximum achievable angle on a typical WDXRF spectrometer is around  $73^{\circ}$ , the maximum wavelength that can be diffracted by a crystal of spacing  $d$  is equal to ca.  $1.9d$ .

The angular dispersion  $d\theta/d\lambda$  of a crystal with spacing  $2d$  is given by:

$$\frac{d\theta}{d\lambda} = \frac{n}{2d \cos \theta} \quad (17)$$

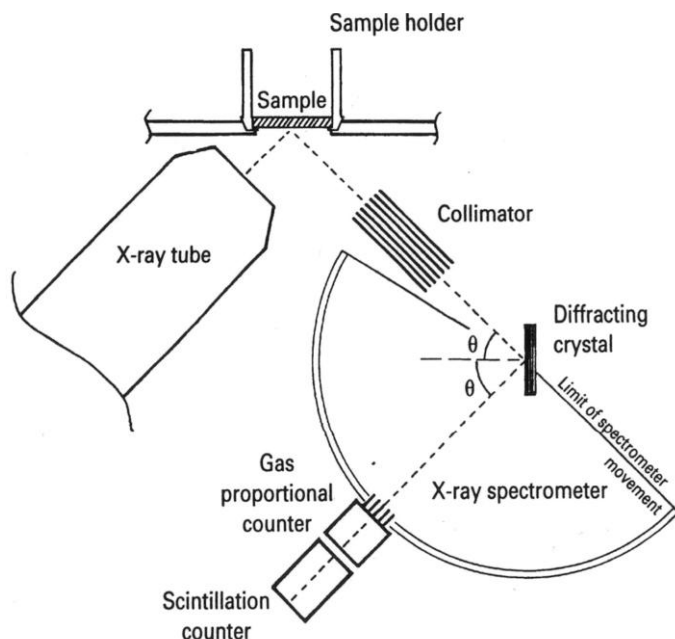


Fig. 11.17 Schematic drawing of a wavelength-dispersive XRF spectrometer (adapted from [12]).

and is therefore inversely proportional to its  $d$ -spacing. Thus, high dispersion can only be obtained at the expense of reducing the wavelength range covered by a particular crystal. Several crystals therefore are likely to be employed for covering a number of analyte elements. Typically, 4 to 6 different analyzer crystals (with different  $d$ -spacings) and two different collimators are provided in this type of instrument, allowing for a wide choice in dispersion conditions. The smaller the  $d$ -spacing of the crystal, the better the separation of the lines, but the smaller the wavelength range that can be covered. The separating power of the crystal spectrometer is dependent upon the divergence allowed by the collimators (which mainly determine the width of the diffracted lines) in the  $2\theta$  spectrum, but the angular dispersion of the analyzing crystal itself and the intrinsic width of the diffraction lines also play a role.

In Tab. 11.5, some characteristics of a few commonly employed analyzer crystals are listed. Classically, large single crystals have been used as dispersive elements. For dispersion of long wavelengths ( $> 0.8$  nm), only a limited number of natural materials are available; the most commonly employed is thallium acid phthalate (TAP,  $2d = 2.63$  nm), allowing measurement of the Mg, Na, F and O-K lines. As an alternative, several other materials with large  $2d$ -spacings have been used and since the 1980s layered synthetic multilayers (LSMs) have been in use. These consist of stacks of alternate electron-rich (e.g., W) and electron-poor (e.g., graphite) layers of atoms or molecules, deposited on a sufficiently smooth substrate. Since the composition and interplanar distance of the LSM to a certain extent can be optimized for particular applications, a factor of four to six improvement in peak intensities compared to TAP crystals can be achieved.

**Table 11.5** Analyzing crystals used in wavelength-dispersive X-ray spectrometry.

Crystal	Planes	2d (nm)	K-line range	L-line range
Lithium fluoride (LiF)	220	0.2848	> Ti	> La
Lithium fluoride (LiF)	200	0.4028	> K	> Cd
Pentaerythritol (PET)	002	0.8742	Al–K	—
Thallium acid phthalate (TAP)	001	2.64	F–Na	—
LSMs	—	5–12	Be–F	—

Among wavelength-dispersive spectrometers, a distinction can be made between single-channel instruments and multi-channel spectrometers. In the former type of instrument, a single dispersive crystal/detector combination is used to sequentially measure the X-ray intensity emitted by a sample at a series of wavelengths when this sample is irradiated with the beam from a high power (2–4 kW) X-ray tube. In a multi-channel spectrometer, many crystal/detector sets are used to measure many X-ray lines/elements simultaneously.

Single-channel instruments are also referred to as scanning spectrometers; this type is the most common. During an angular scan, the angle  $\theta$  between sample and analyzer crystal is continuously varied; in order to maintain an identical angle between analyzer crystal and detector, the latter moves at double the angular speed of the crystal. In this manner, X-ray intensity vs.  $2\theta$  diagrams are obtained. By means of tables, the recorded peaks can be assigned to the characteristic lines of one or more elements. In Fig. 11.18, a typical  $2\theta$ -spectrum obtained from a brass sample is shown.

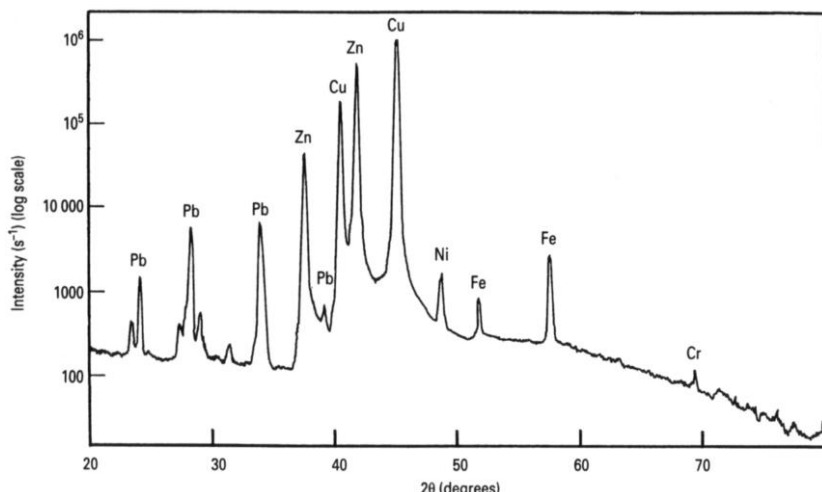


**Fig. 11.18** Wavelength-dispersive XRF of a brass sample recorded with a LiF analyzer crystal, showing the characteristic lines of the major elements Cu and Zn and the lines of Cr, Fe, Ni and Pb superimposed on a continuous background (adapted from [12]).

Simultaneous wavelength-dispersive spectrometers were introduced in the early 1950s, and sequential systems about a decade later. At this time, about 30,000 or so wavelength-dispersive instruments have been supplied commercially. The two major categories of wavelength-dispersive X-ray spectrometers differ mainly in the type of source used for excitation, the number of elements that they are able to measure at one time, the speed at which they collect data and their price range. For high specimen throughput quantitative analysis where speed is of the essence, and where high initial cost can be justified, simultaneous wavelength-dispersive spectrometers are optimal. For more flexibility, where speed is important but not critical and where moderately high initial cost can be justified, sequential wavelength-dispersive spectrometers are probably more suitable. Both of the instruments are, in principle at least, capable of measuring all elements in the periodic classification from  $Z = 9$  (F) and upwards, and most modern wavelength-dispersive spectrometers can do some useful measurements down to  $Z = 6$  (C). Both can be fitted with multi-sample handling facilities and automated. Both are capable of precision of the order of a few tenths of 1% and both have sensitivities down to the ppm level. Single-channel wavelength-dispersive spectrometers are typically employed for both routine and nonroutine analysis of a wide range of products, including ferrous and nonferrous alloys, oils, slags and sinters, ores and minerals and thin films. These systems are very flexible but, relative to multi-channel spectrometers, are somewhat slow. The multi-channel wavelength-dispersive instruments are used almost exclusively for routine, high throughput analyses where there is need of fast accurate analysis, but where flexibility is of no importance.

#### 11.3.4

#### Energy-dispersive XRF

Energy-dispersive spectrometers became commercially available in the early 1970s with the advent of high resolution solid state detectors; today there are of the order of 20,000 units in use. In principle, EDXRF instruments have a much simpler mechanical design than WDXRF instruments, as the detection system does not include any moving parts and the solid-state detector (most commonly a Si(Li) detector) itself acts as a dispersion agent. The high geometrical efficiency of the semiconductor detector permits a great variety in excitation conditions. The manner in which the radiation that originally exits from the X-ray tube is 'pretreated' before it reaches the sample varies according to the type of EDXRF instrument. The final analytical capabilities, and in particular the LD values that can be attained by the instrument, depend strongly on the sophistication with which this is done.

In Fig. 11.19a, the most simple of ED-XRF instrumental configurations is shown. A low power X-ray tube (e.g., 50 W) and a Si(Li) detector are both placed at an angle of  $45^\circ$  with respect to the sample. Collimators are used to confine the excited and detected beam to a sample area between 0.5 and  $2\text{ cm}^2$ . In such a 'direct-excitation' configuration, the distance between the components can be fairly small (typically a few cm) and since both the tube anode lines and the *bremsstrahl-*

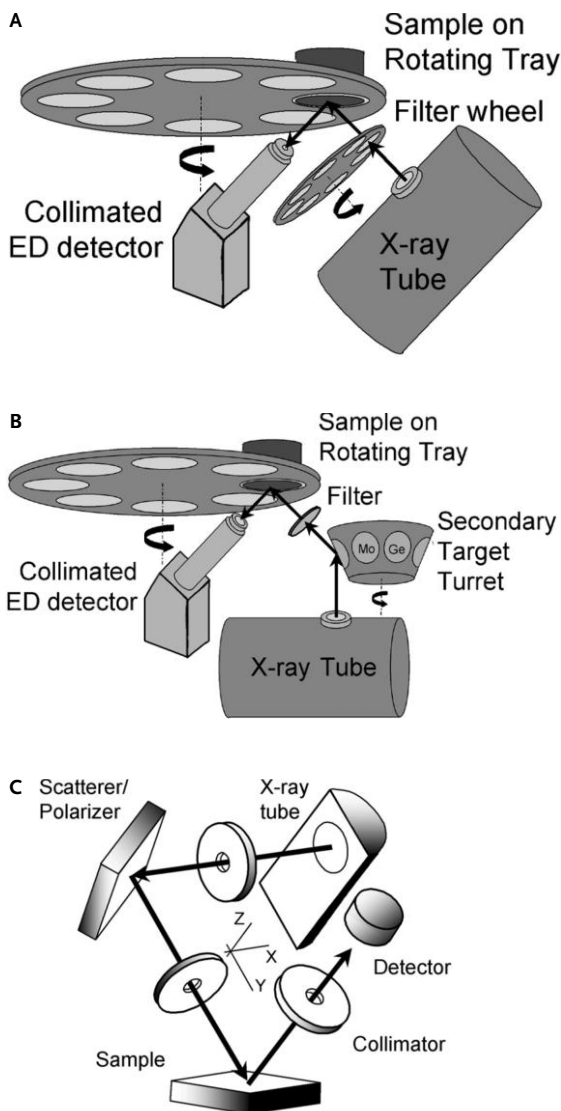


**Fig. 11.19** Schematic drawings of (a) a direct-excitation XRF instrument, (b) a secondary target XRF instrument, (c) a polarized XRF instrument employing a cartesian (XYZ) irradiation geometry.

lung-component of the tube output spectrum are used to irradiate the sample, only a limited tube power is required. Since the *bremsstrahlung* continuum not only ensures a uniform excitation of many elements, but also causes a significant scatter background to be present in the recorded EDXRF spectra, most direct-excitation systems are equipped with a set of primary beam filters to alter the tube spectrum. By selection of an appropriate filter, the excitation conditions for a particular range of elements can be optimized. In order to facilitate the determination of low-Z elements, commercial systems can be either evacuated or flushed with He, thus reducing the absorption of low energy radiation and scatter.

The schematic of a ‘secondary target’ EDXRF system is shown in Fig. 11.19b. In such a configuration, a high power (1 kW) X-ray tube irradiates a metal disk (the secondary target, e.g., made of Mo), causing it to emit its own characteristic radiation lines ( $\text{Mo-K}_\alpha$  and  $\text{Mo-K}_\beta$ ). This ‘bichromatic’ fluorescent radiation is then used to excite the sample to be examined. The advantage of the secondary target scheme is that, as a result of the bichromatic excitation, the background in the resulting EDXRF spectra is significantly lower than in the direct excitation case. This leads to better detection limits. By using a filter that preferentially absorbs the  $\text{K}_\beta$  component of the secondary target radiation (e.g., a Zr foil in case of a Mo target), a quasi-monochromatic form of sample excitation can be realized. By interchanging the target (and matching filter), different element ranges can be excited optimally. For example, to obtain the best conditions for determination of trace concentrations of the elements Rb–Nb in geological samples, a Rh secondary target may be selected while for optimal detection of Cr in the same material, a Cu target would be more beneficial.

The ability to simultaneously measure a wide range of elements is one of the greatest advantages of EDXRF. This advantage is strongly reduced when the count rate limitation of the ED detection electronics is taken into consideration. This is due to simultaneous recording of the entire primary source radiation scattered on the specimen and is especially true for examinations on samples with light matrices.

The stationary arrangement of components used in EDXRF is ideally suited for geometrical configurations that exploit polarization phenomena to reduce background and thereby improve signal-to-noise ratios.

Figure 11.19c shows a configuration employed to achieve a reduction in the background level of EDXRF spectra obtained in direct excitation conditions. In this case, one or more energy bands of the tube emission spectrum are scattered and/or diffracted under (nearly)  $90^\circ$  by means of a suitable scatterer material and/or diffraction crystal. Because scattering rather than fluorescence is used to ‘reflect’ the primary tube spectrum onto the sample, the X-ray beam that impinges on the sample is linearly polarized in the (YZ) plane perpendicular to the tube–scatterer–sample plane (XY). When the Si(Li) detector is also positioned in the YZ plane at  $90^\circ$  relative to the scatterer–sample axis, the lowest background level will be recorded. The reason for this background reduction is that the polarized photons will be preferentially scattered out of the plane of polarization and therefore will not reach the detector. The optimal geometrical configuration is therefore that tube, scatterer, sample and detector are arranged in an XYZ (also called ‘cartesian’) geometry, as shown in Fig. 11.19c. For polarization of medium-to-hard radiation ( $E > 10$  keV) by Barkla-scattering, fairly thick slabs of low-Z materials such as  $\text{Al}_2\text{O}_3$ ,  $\text{B}_4\text{C}$  and  $\text{B}_3\text{N}$  are suitable. For polarization of softer radiation, the above-mentioned materials are not suitable since for  $E < 10$  keV, photoelectric absorption dominates over scattering. In the region 1–10 keV, radiation can be polarized through Bragg diffraction over  $2\theta \approx 90^\circ$  by using a suitable crystal. For example, HOPG (highly oriented pyrolytic graphite) is an excellent Bragg polarizer for the (002) reflection of the Rh- $\text{L}_\alpha$  radiation ( $\theta = 43.2^\circ$ ).

Multiple-layer scatterers, for example consisting of a thin layer of HOPG glued on top of an  $\text{Al}_2\text{O}_3$  substrate, in combination with a Rh tube are useful to determine a wide range of elements simultaneously with good detection limits and sensitivities.

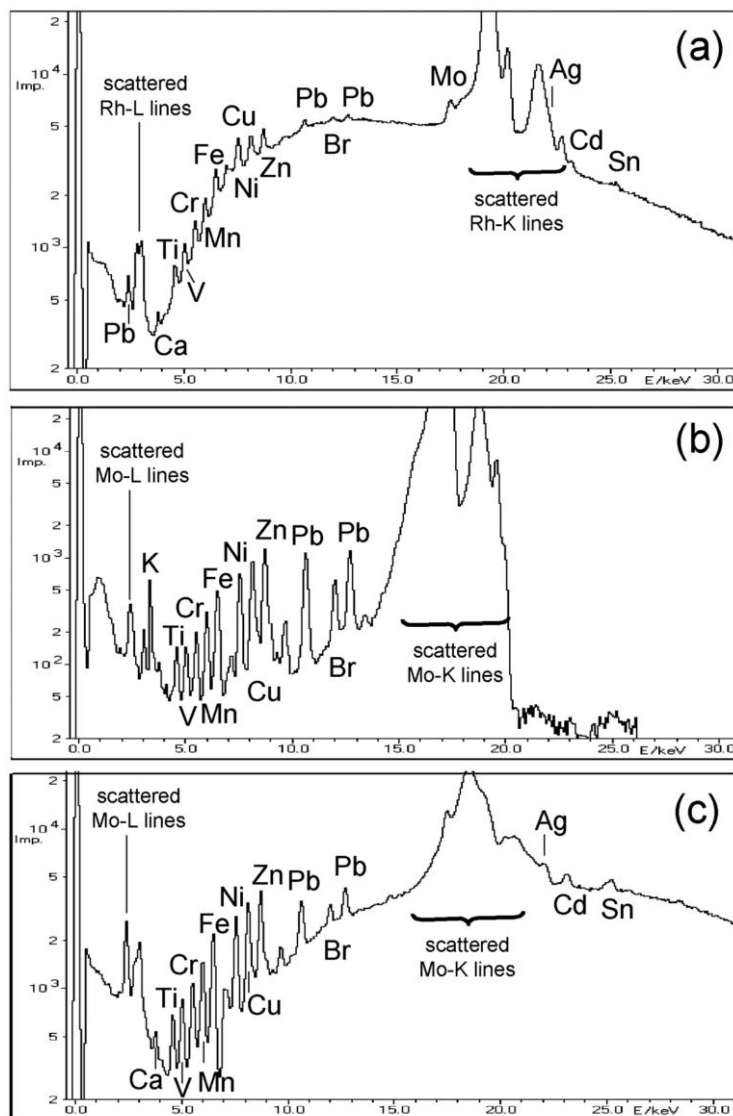


**Fig. 11.20** Comparison of EDXRF spectra of an oil standard containing 21 elements (e.g. Ca, Ti, V, Cr, Mn, Fe, Ni, Cu, Zn, Mo, Ag, Cd, Sn, Ba and Pb) with concentrations of  $30 \mu\text{g g}^{-1}$ . The spectra (log. scale) are (a) non-polarized, direct excitation by radiation from rhodium anode X-ray tube; (b) molybdenum secondary excitation; (c) polarized excitation by scatter from a HOPG/ $\text{Al}_2\text{O}_3$  target. The measuring time amounts to 200 s for each spectrum. In all cases a Rh end-window tube was used (adapted from [1]).

**Table 11.6** Limits of detection (LD) (n. d. = not detectable), for some elements in base oil using direct excitation, monochromatic excitation using a Mo secondary target and direct excitation with linearly polarized X-rays (175 W for a measuring time of 200 s and an incident pulse density of about 60,000 cps). (\* overlapping with Rh K<sub>β2</sub>). (Adapted from [1]).

<b>Element</b>	<b>Limits of Detection, in <math>\mu\text{g g}^{-1}</math></b>		
	<b>Direct excitation</b>	<b>Mo-secondary target</b>	<b>Polarization</b>
Ca	13	8.8	4.1
Ti	3.8	2.9	1.6
Cr	3.1	2	0.78
Mn	2.6	1.2	0.51
Cu	1.7	0.31	0.34
Zn	1.7	0.3	0.33
Mo	2.3	n. d.	0.95
Cd	18.0*	n. d.	1.6
Sn	12	n. d.	2
Pb	3.9	0.31	0.79

In Fig. 11.20, the spectra that result from direct excitation, secondary excitation and polarized direct excitation of a standard oil sample are compared, containing 21 elements at the  $30 \mu\text{g g}^{-1}$  level. The relative detection limits obtained from the three spectra are summarized in Tab. 11.6; they indicate that the DL values by means of polarized excitation are on average 5 times better than those determined with direct excitation. The secondary target results are better by a factor of 2.5 than the polarized excitation values for elements efficiently excited by the Mo-Ka line (e. g. Pb); however, elements such as Sn and Cd cannot be determined with the Mo secondary target while they are well excited by the polarized *bremsstrahlung* radiation.

### 11.3.5

#### Radioisotope XRF

Besides EDXRF spectrometers that are intended for use in the laboratory, a number of portable EDXRF instruments are also available. These devices are used in various fields for on-site analysis of works of art, environmental samples, forensic medicine, industrial products and waste materials etc. In their simplest form, the instruments consist of one or more radioisotope sources combined with a scintillation or gas proportional counter. However, combinations of radio-sources with thermoelectronically cooled solid-state detectors are also available in compact and light-weight packages (below 1 kg). In Fig. 11.21, schematics of various types of radio-source based EDXRF spectrometers are shown. In Fig. 11.21a, the X-ray source is present in the form of a ring; radiation from the ring irradiates the sample from below while the fluorescent radiation is efficiently detected by a solid-state detector positioned at the central axis. Shielding prevents radiation from the source from entering the detector. In Fig. 11.21b and c, the X-ray source has another

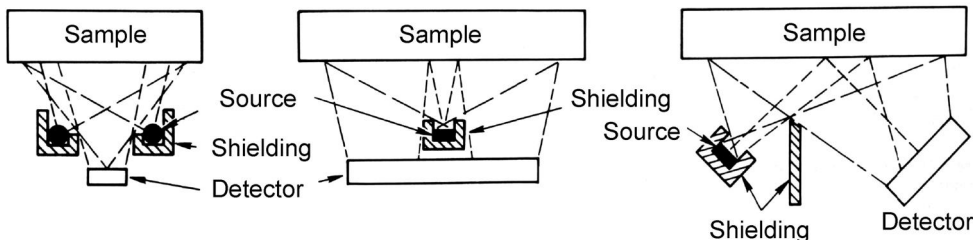


**Fig. 11.21** Radioisotope-excited X-ray fluorescence analysis by means of (a) an annular source, (b) a central source and (c) a side-looking source (adapted from [15]).

shape, requiring a different type of shielding. Besides equipment using radioisotopes as X-ray source, portable equipment that includes miniature low power X-ray tubes is also available; in such devices, the direct excitation form of EDXRF is almost exclusively employed.

#### 11.3.6 Total Reflection XRF

When X-rays impinge upon an (optically) flat material under a very small angle (typically a few mrad), i.e. nearly grazing the surface, total external reflection occurs. This means that instead of penetrating the material, the X-ray photons will only interact with the top few nm of the material and then be reflected. Material that is present on top of the reflecting surface will be irradiated in the normal manner, and will interact with both the primary and the reflected X-rays. The major difference between conventional EDXRF and TXRF therefore is the excitation geometry. In the standard case of EDXRF the angle between the primary incident radiation and the sample is  $45^\circ$  while the detector is placed normal to the incident beam so that the angle between sample and detector is also  $45^\circ$ . The principle set-up of TXRF is shown in Fig. 11.22. A narrow, almost parallel, beam impinges at angles below the critical angle on the surface of the reflector that carries the sample (is the form of randomly distributed microcrystals) in the center part of its surface. Since the X-rays scarcely penetrate the reflector, the contribution from scattered primary radiation from the substrate is minimized. As a result of the double excitation of the sample by both the primary and the reflected beam, the fluorescent signal is practically twice as intense as in the standard EDXRF excitation mode. The largest angle at which total external reflection still takes place is called the critical angle of total reflection  $\phi_{\text{crit}}$ . The critical angles are in the range of a few milliradians for typical reflector materials such as quartz or Si and primary radiation of 9.4 keV (from a W-L tube) or 17.5 keV (from a Mo-anode X-ray tube). With higher energies in the exciting spectrum, adjustments must be made for the proper incident angle below the critical angle, which is given by:

$$\phi_{\text{crit}} \text{ (mrad)} = 20.7/E \text{ (keV)} \rho^{1/2} \text{ (g cm}^{-3}\text{)} \quad (18)$$

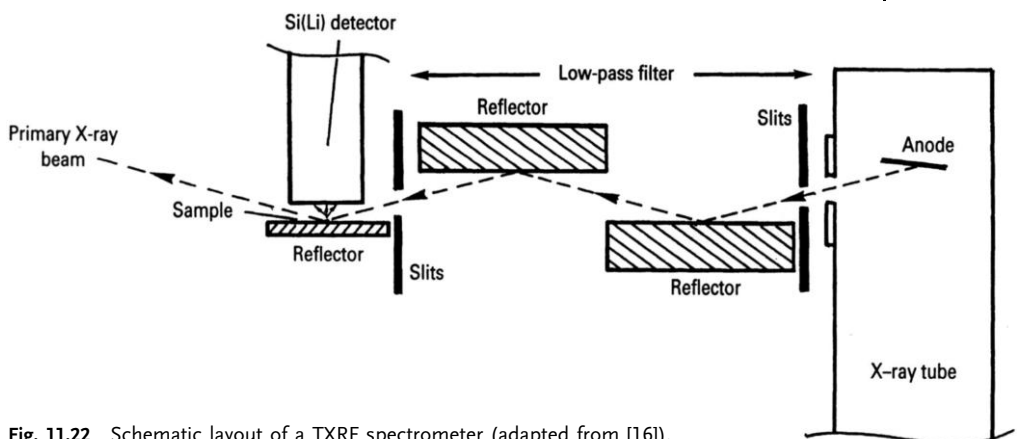


**Fig. 11.22** Schematic layout of a TXRF spectrometer (adapted from [16]).

The main advantages of TXRF are:

- The background caused by scattering of the primary radiation on the substrate is reduced.
- The fluorescence intensity is doubled as the primary and reflected beams pass through the sample giving rise to efficient excitation.
- The distance between the sample on the reflector surface and the detector can be made small, thus the solid angle for detection is large.

All these advantages lead to lower limits of detection (LD) compared to the standard EDXRF mode.

Depending on the X-ray source and the spectral modification devices, the LD are in the pg range for 2–3 kW X-ray tubes and in the fg range with excitation by means of synchrotron radiation. Figure 11.15 shows a typical TXRF spectrum; the absolute detection limit values of typical TXRF instruments are shown in Fig. 11.10. Thus, TXRF permits to simultaneously determine trace elements in samples of small volume. Additional advantages are insensitivity to matrix effects, easy calibration, fast analysis times and low cost. In practice, the method is in particular applied for multi-element determinations in water samples of various nature and for the routine analysis of Si-wafer surfaces employed in the microelectronics industry.

### 11.3.7

#### Microscopic XRF

The basic measuring strategy of microscopic X-ray fluorescence analysis ( $\mu$ -XRF) is illustrated in Fig. 11.23. This microanalytical variant of bulk EDXRF is based on the localized excitation and analysis of a microscopically small area on the surface of a larger sample, providing information on the lateral distribution of major, minor and trace elements in the material under study. Essentially, a beam of primary X-rays with (microscopically) small cross-section irradiates the sample and in-

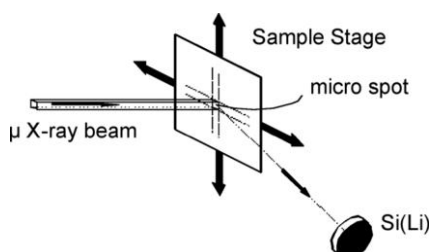


**Fig. 11.23** Principle of  $\mu$ -XRF.

duces the emission of fluorescent X-rays from a micro-spot. A suitable detector system collects the fluorescent radiation that carries information on the local composition of the sample. When the sample is moved, either manually or under computer control, in the X-ray beam path, either spot analyses, line-analysis or image collection is possible.

The difficulties in the exploitation of this method reside with the production of sufficiently intense X-ray beams to allow sensitive microanalysis. Techniques to do this have only recently appeared; in the past, X-rays were considered to be notably difficult to focus to a small dimension beam. Any variants on the basic mode of operation either reside with the method employed for X-ray beam concentration/focusing or with the source type employed: conventional X-ray tubes or synchrotron radiation sources. Especially the increased performance of compact and relatively inexpensive X-ray focusing devices and in particular the development of (poly)capillary X-ray focusing optics, permitting X-ray beams to be focused to below 10  $\mu\text{m}$  diameter spots, has made the development of  $\mu$ -XRF possible. When used in combination with X-ray tubes, absolute detection limits in the pg area are obtained for thin samples. In massive samples, relative LD values around 10 ppm have been reported. At synchrotron facilities, the capabilities of the  $\mu$ -XRF method (both regarding spot sizes and detection limits) are significantly better: fg to ag-level absolute detection limits are obtained with beams that are between 0.5 and 2  $\mu\text{m}$  in diameter. By the use of monochromatic beams of polarized radiation, optimal peak-to-background ratios in the resulting EDXRF spectra can be obtained,

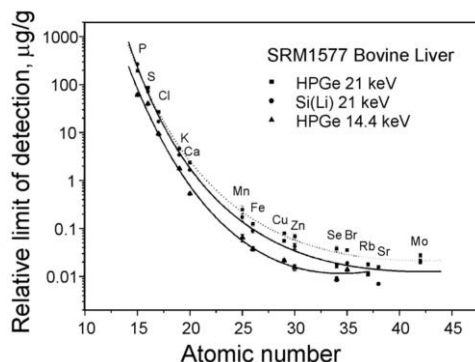


**Fig. 11.24** Relative LD values obtained by irradiation of NIST SRM 1577 Bovine Liver by means of 14.4 and 21 keV synchrotron microbeams and Si(Li) or HPGe detectors.

resulting in relative LD levels in the 10–100 ppb range in biological materials. As an example, Fig. 11.24 shows the LD values obtained within 1000 s by using 14 and 21 keV synchrotron microbeams (of  $2 \times 15 \mu\text{m}$  diameter) to irradiate NIST SRM 1577 Bovine Liver. The application of  $\mu$ -XRF to a great variety of problems and materials has been described, including geochemistry, archaeology, industrial problems and environmental studies. Especially the fact that quantitative data on (trace) constituents can be obtained at the microscopic level without sample damage is of use in many different circumstances.

## 11.4 Matrix Effects

### 11.4.1 Thin and Thick Samples

The simple linear relation between observed count rate  $R_i$  of analyte element  $i$  and its concentration  $c_i$  shown in Eq. (9) is only valid in a limited number of cases. In general, for monochromatic forms of excitation (with energy  $E_0$ ) and in the absence of enhancement phenomena, the observed XRF count rate  $R_i$  of an element  $i$  (with fluorescent energy  $E_i$ ) is related to the sample thickness  $d$  and its concentration  $c_i$  in the following manner (see also Eq. (34)–(36)):

$$R_i = S_i c_i \frac{1 - e^{-\chi(E_0, E_i)\rho d}}{\chi(E_0, E_i)\rho d} = S_i c_i A_i \quad \text{with } \chi(E_0, E_i) = \mu(E_0) \csc \alpha + \mu(E_i) \csc \beta \quad (19)$$

where  $\alpha$  and  $\beta$  are the angles under which the X-rays impinge and take-off relative to the sample surface (see Fig. 11.25) and  $\rho$  is the sample density. The absorption factor  $A_i$  is obtained by adding all contributions to  $R_i$  produced in a series of infinitesimal sample volumes at various depths  $z$  inside the sample and by considering an attenuation factor  $\exp[-\mu(E_0)\rho z \csc \alpha]$  for the primary radiation while penetrating into the sample until this depth and an attenuation factor  $\exp[-\mu(E_i)\rho z \csc \beta]$  for the fluorescent radiation when emerging from the sample towards the detector. When polychromatic forms of excitation are used, Eq. (19) is more complicated and involves an integral over the intensity distribution of the X-ray source (see below, Eq. (36)).

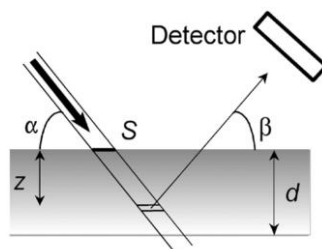


**Fig. 11.25** Basic XRF irradiation geometry.

As a result of the attenuation of both primary and fluorescent radiation within the sample, there is a critical depth in the sample  $d_{\text{thick}}$  below the surface, beyond which any emitted photon is essentially absorbed and therefore will not make a significant contribution to the detected fluorescent intensity. This critical penetration depth varies as a function of matrix composition and is also strongly dependent on the energy of the (primary and) fluorescent radiation. Samples that have a thickness greater than the critical penetration depth for a specific kind of fluorescent radiation are sometimes referred to as ‘infinitely thick’ or ‘massive’ samples. In Tab. 11.7 values for  $d_{\text{thick}}$  in a geological (a silicate rock) and metallurgical (steel) matrix are listed for various fluorescent line energies. For low-energy photons (e.g., the  $K_{\alpha}$ -photons of low- $Z$  elements such as Al or Na), the critical penetration depth is very small (a fraction to a few  $\mu\text{m}$ ) so that compositional information that exclusively pertains to the surface layers of the sample is obtained. When more penetrating fluorescent radiation is used (e.g. Rb- $K_{\alpha}$  at 13.39 keV), having  $d_{\text{thick}}$  values of several mm, compositional information from much deeper in the sample is obtained.

In many practical situations, it is important to ensure that the sample presented for analysis is sufficiently thick (i.e. thicker than the highest critical penetration depth among the various fluorescent signals being used), so that the observed analytical signals no longer depend on sample thickness but only on analyte concentration.

Next to the critical penetration depth  $d_{\text{thick}}$ , it is also useful to define a critical thickness  $d_{\text{thin}}$  below which absorption and enhancement effects can be neglected. For analysis of such ‘thin-film’ samples, the calibration relations of Eq. (8) and (9) are valid and matrix effect corrections need not be applied. By convention,  $d_{\text{thin}}$  corresponds to the situation where the total attenuation in the sample is equal to 1%. Table 11.7 lists typical  $d_{\text{thin}}$  values for various fluorescent line energies in two matrices.

**Table 11.7** Critical penetration depth and thin film thickness of various fluorescent lines in two matrices. (Adapted from [17]).

<b>Element</b>	<b>Energy/Wavelength of <math>K_{\alpha}</math> line</b>		<b>Excitation Spectrum</b>	<b>Critical Penetration Depth <math>d_{\text{thick}}/\mu\text{m}</math></b>		<b>Thin Film Thickness <math>d_{\text{thin}}/\mu\text{m}</math></b>	
	<b><math>E/\text{keV}</math></b>	<b><math>\lambda/\text{nm}</math></b>		<b>Silicate</b>	<b>Steel</b>	<b>Silicate</b>	<b>Steel</b>
C	0.28	4.4	Cr	—	0.1	—	0.002
Na	1.04	1.19	Cr	4.8	0.4	0.09	0.009
Si	1.74	0.713	Cr	13	1.6	0.2	0.03
Ca	3.69	0.336	Cr	36	9.6	0.7	0.2
Cr	5.41	0.229	Rh	90	30	1.7	0.7
Fe	6.4	0.194	Rh	180	43	3.4	0.9
Rb	13.39	0.0927	Rh	900	40	16	0.9
Nb	16.61	0.0748	Rh	1400	62	25	1.3
Rh	20.21	0.0614	W	3900	161	72	3.5
La	33.44	0.0373	W	10600	580	190	13
Eu	41.53	0.0301	W	15400	886	280	19

## 11.4.2

**Primary and Secondary Absorption, Direct and Third Element Enhancement**

In the context of X-ray fluorescence analysis, matrix effects are caused by attenuation and enhancement phenomena that influence the intensity of the fluorescent X-ray lines observed from a sample. As the magnitude of the matrix effects varies with elemental composition, the observed XRF intensity is no longer linearly proportional to the concentration of the analyte (Eq. (9)). Corrections must therefore be applied to the measured intensity data to account for:

(a) Primary absorption (see Fig. 11.26a): this occurs because all atoms of the specimen matrix will absorb photons from the primary source. Since there is competition for these primary photons by the atoms making up the specimen, the intensity/wavelength distribution of these photons available for the excitation of a given analyte element may be modified by other matrix elements. In this manner, the intensity and spectral distribution of the X-ray flux available to excite the sample

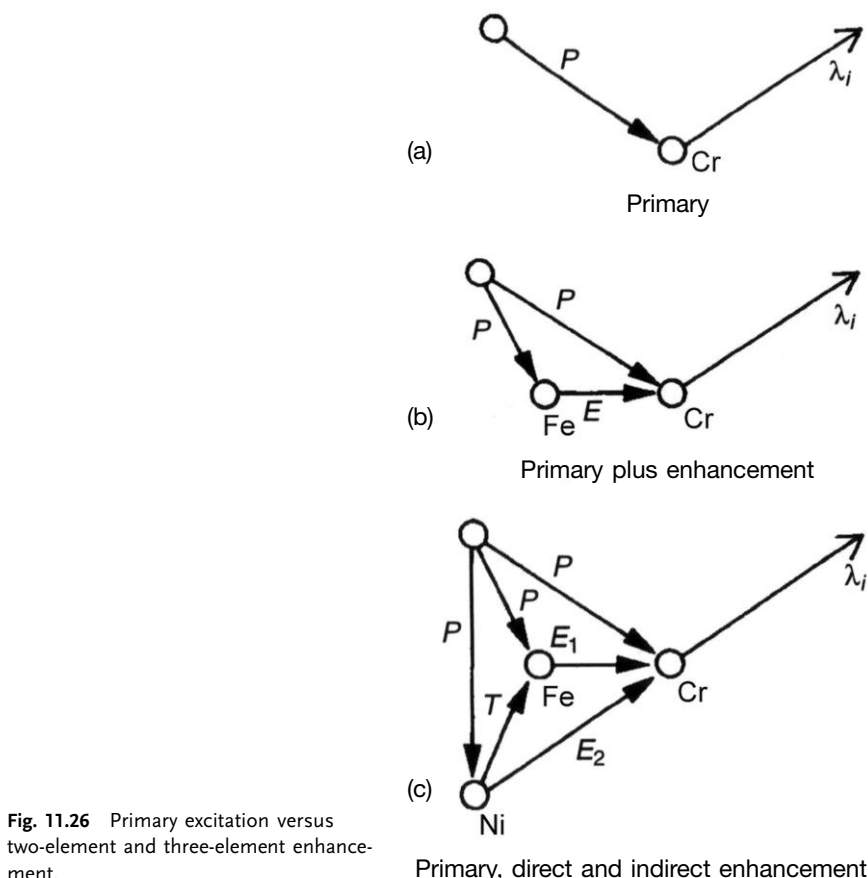


**Fig. 11.26** Primary excitation versus two-element and three-element enhancement.

Primary, direct and indirect enhancement

atoms can change with penetration depth. This phenomenon is known as ‘beam hardening’.

(b) Secondary absorption: this refers to the effect of the absorption of characteristic analyte radiation by the specimen matrix. As characteristic radiation passes out from the specimen in which it was generated, it will be absorbed by all matrix elements, by amounts relative to the mass absorption coefficients of these elements;

(c) Direct (or second-element) enhancement (see Fig. 11.26b): in situations where the energy of a fluorescent photon (e.g., Ni-K $\alpha$  at 7.47 keV) is immediately above the absorption edge of a second element (e.g., the K-edge of Fe at 7.11 keV), the fluorescence intensity of the second element (here: Fe-K $\alpha$  and Fe-K $\beta$  radiation) will be enhanced as a result of the preferential excitation (here: by Ni-K $\alpha$  radiation) within the sample. The magnitude of this effect is not always significant but is readily observable in alloys of specific combinations of elements (e.g., Cr–Fe–Ni steels) and in multilayer thin film samples.

(d) Indirect (or third-element) enhancement (see Fig. 11.26c): For example in a stainless steel matrix, the observed intensity of the Cr-K characteristic radiation (Cr-K absorption edge at 5.99 keV) is enhanced by secondary excitation due to Fe-K (K $\alpha$  at 6.40 keV) and Ni-K radiation. Since the intensity of the Fe-K radiation is itself enhanced (see above), part of the Cr enhancement due to Fe is a tertiary effect originating from Ni.

## 11.5 Data Treatment

The process to convert experimental XRF data into analytically useful information (usually in the form of concentration values of elemental constituents whose X-ray peaks are visible above the background in the spectrum) can be divided into two steps: first the evaluation of the spectral data, whereby the net height or the net intensity of the X-ray peaks is determined, taking care to correct for peak overlap (if any) between X-ray lines of different elements and secondly the conversion of the net X-ray intensities into concentration data, i.e. the quantification. In this last step, especially, the appropriate correction of matrix effects is a critical issue.

### 11.5.1 Counting Statistics

The production of X-rays is a random process that can be described by a Gaussian distribution. Since the number of photons counted is nearly always large, typically thousands or hundreds of thousands, rather than a few hundred, the properties of the Gaussian distribution can be used to predict the probable error for a given count measurement. There will be a random error  $s_I$  associated with a measured intensity value  $I$ , this being equal to  $I^{1/2}$ . As an example, if  $10^6$  counts are taken, the 1s standard deviation will be  $[10^6]^{1/2} = 10^3$ , or 0.1 %. The measured parameter

in wavelength-dispersive X-ray spectrometry is generally the counting rate  $R=I/t$  and, based on what has been already stated, the magnitude of the *relative* random counting error  $RSD(R)$  associated with a given measured rate  $R$  can be expressed as:

$$RSD(R)(\%) = 100\% \frac{S_R}{R} = 100\% \frac{S_I}{I} = 100\% \frac{\sqrt{I}}{I} = \frac{100\%}{\sqrt{Rt}} \quad (20)$$

Care must be exercised in relating the counting error (or indeed any intensity related error) with an estimate of the error in terms of concentration. Provided that the sensitivity of the spectrometer in counts per second per percent, is linear, a count error can be directly related to a concentration error. However, where the sensitivity of the spectrometer changes over the range of measured response, a given fractional count error may be much greater when expressed in terms of concentration.

### 11.5.2

#### Spectrum Evaluation Techniques

Spectrum evaluation is a crucial step in X-ray analysis, as important as sample preparation and quantification. As with any analytical procedure, the final performance of X-ray analysis is determined by the weakest step in the process. Spectrum evaluation in EDXRF analysis is more critical than in WDXRF spectrometry because of the relatively low resolution of the solid-state detectors employed.

In general, it is possible to distinguish between amplitude and energy noise in (ED)X-ray spectra. Amplitude noise is the result of the statistical nature of the counting process in which random events (the arrival of X-ray photons in the detector) are observed during a finite time interval. Poisson statistics cause the typical channel-to-channel fluctuations observed in X-ray spectra. Energy noise, on the other hand, causes the characteristic X-ray lines in EDXRF spectra to appear much wider (of the order of 120–150 eV) than their natural line widths (typically 5–10 eV). It results partly from the photon-to-charge conversion process in the detector and partly from the electronic noise that is introduced in the amplification and processing steps that follow it. Accordingly, characteristic X-ray lines appear as nearly Gaussian peaks in EDXRF spectra.

In WDXRF spectra, where at least one of these noise contributions is usually absent (the noise in the energy/wavelength dimension is significantly lower as a result of the much higher resolution of the dispersion systems used), spectrum evaluation, in principle, is much more simple and sometimes can be discarded altogether. Because the X-ray lines appear as narrow, well-defined peaks, their net X-ray intensities and that of the background in the same region can be determined with great accuracy. The few cases of peak overlap (e.g., between  $\text{As-K}_\alpha$  and  $\text{Pb-L}_\alpha$ , where the separation of 8 eV is less than the natural line width of  $\text{As-K}_\alpha$ ) can be dealt with on a case-by-case basis or avoided by the use of another, non-overlapped, X-ray line of the elements involved as analytical signals (e.g., the  $\text{As-K}_\beta$  line).

In both WDXRF and EDXRF, the net number of counts under a characteristic X-ray line (i.e., the integrated peak *intensity*) is proportional to the concentration of the analyte. At constant resolution, this proportionality also exists between concentration and net peak *height*. In EDXRF (where the detector resolution is low and changes considerably with energy and many peaks are low in intensity), the use of the net peak area as analytical signal is preferred, since this also results in a lower statistical uncertainty for the small peaks. In WDXRF (where the detector resolution is high and much less dependent on the wavelength, while sharp and intense peaks are often encountered), the acquisition of the entire peak profile is often too time consuming so that the count rate is frequently measured only at the peak maximum.

#### 11.5.2.1 Data Extraction in WDXRF

In WDXRF, the count rate  $R_{\max}$  at the angle of the peak maximum, corrected for background is most often used as the analytical signal. In order to estimate the appropriate background below the line, the background count rate at slightly lower and higher  $2\theta$ -values is measured and the average calculated. If  $T$  is the number of counts accumulated during a time interval  $t_T$  at the top of the peak and  $B$  is the corresponding background level (observed during a time  $t_B$ ), the net count rate  $R$  is given by the difference of the total and background count rates  $R_T$  and  $R_B$ :

$$R = R_T - R_B = \frac{T}{t_T} - \frac{B}{t_B} \quad (21a)$$

and, considering that  $s^2_T = T$  and  $s^2_B = B$ , the uncertainty  $s_R$  on the net count rate  $R$  is given by:

$$s_R^2 = \frac{T}{t_T^2} + \frac{B}{t_B^2} = \frac{R_T}{t_T} + \frac{R_B}{t_B} \quad (21b)$$

Accordingly, in WDXRF, several counting strategies may be employed to keep this number as low as possible. In the ‘optimum fixed time’ strategy, the minimum uncertainty is obtained within a time interval  $t = t_T + t_B$  when  $t_T$  and  $t_B$  are chosen in such a way that :

$$\frac{t_T^2}{t_B^2} = \frac{R_T}{R_B} \quad (22)$$

In this case, the uncertainty  $s_R$  can be written as:

$$s_R = \frac{\sqrt{R_T} + \sqrt{R_B}}{\sqrt{t}} \quad (23)$$

### 11.5.2.2 Data Extraction in EDXRF: Simple Case, No Peak Overlap

The most straightforward method to obtain the net area of an isolated, non-overlapped peak in an EDXRF spectrum is to interpolate the background under the peak and to sum the net channel contents in a window enclosing the peak. Thus, the net peak area  $N$  is given by:

$$N = \sum_j [y_j - y_B(j)] = \sum_j y_j - \sum_j y_B(j) = T - B \quad (24)$$

where the summation runs over the spectral window (containing  $n_T$  channels) under consideration. Thus, the uncertainty  $s_N$  can be written as:

$$s^2 N = s^2 T + s^2 B = T + B \quad (25)$$

The background height  $y_B(j)$  in channel  $j$  of the peak window can be interpolated between the average background height left and right of the peak ( $y_{B,L} = B_L/n_L$  and  $y_{B,R} = B_R/n_R$  where  $B_L$  and  $B_R$  are the integrals of the left and right background windows and  $n_L$ ,  $n_R$  their widths in channels) (see Fig. 11.27):

$$y_B(j) = y_{B,L} + \frac{y_{B,R} - y_{B,L}}{j_{B,R} - j_{B,L}} (j - j_{B,L}) \quad (26)$$

where  $j_{B,L}$  and  $j_{R,L}$  represent the channels between which the background is linearly interpolated. When both background windows around the peak have equal width

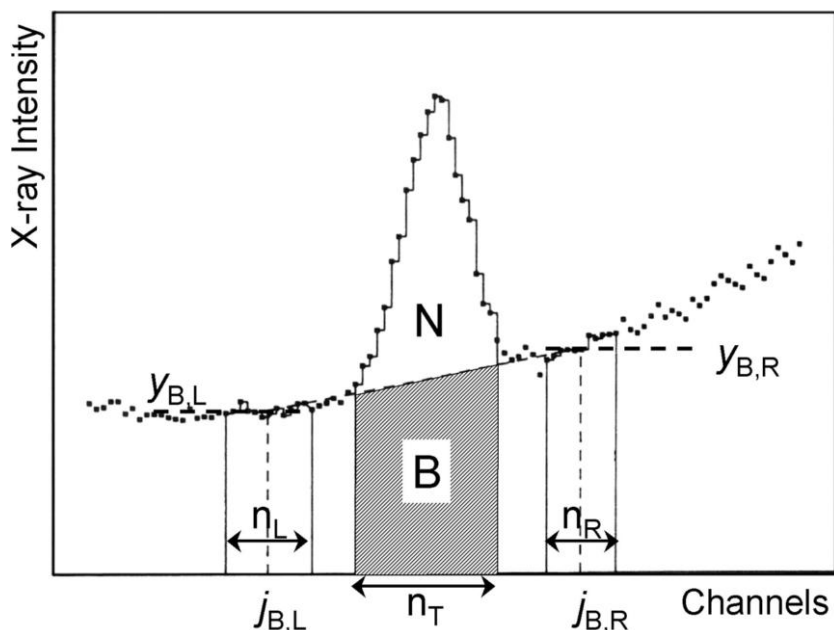


Fig. 11.27 Background estimation below an isolated photo peak.

(i.e.,  $n_L = n_R = n_B/2$  channels) and are positioned symmetrically around the maximum, the uncertainty on  $N$  is given by:

$$s_N^2 = T + \left(n_T^2/n_B^2\right) (B_L + B_R) \quad (27)$$

### 11.5.2.3 Data Extraction in EDXRF, Multiple Peak Overlap

The above-described simple integration procedure is very useful for explorative data analysis but implicitly assumes that within the energy window used, a single, non-overlapped peak is present with a high peak-to-background ratio. In general, these assumptions are not valid: peak overlap frequently occurs in energy-dispersive X-ray spectra while, especially for peaks corresponding to trace constituents, the background intensity below the peak may be of the same order or larger than the net peak intensity. In these cases, the use of too simple spectrum evaluation procedures may negate all the efforts that are made both during the data collection and during the further quantitative processing of the data to increase the reliability of the final (trace) element concentrations. An established way of proceeding is to use a non-linear least squares strategy to minimize the weighted difference  $\chi^2$  between the experimental data  $y_i$  and a mathematical fitting function  $y_{\text{fit}}$

$$\chi^2 = \frac{1}{n - m} \sum_i \left( \frac{[y_i - y_{\text{fit}}(i)]^2}{y_i} \right) \quad (28)$$

where  $y_i$  is the observed content of channel  $i$  in the spectrum being processed and  $y_{\text{fit}}(i)$  is the calculated fitting function in this channel.  $n$  is the total number of channels in the fitting window while  $m$  represents the number of parameters in the fitting function. The latter consists of two parts, describing respectively the spectral background and the photo peaks:

$$y_{\text{fit}}(i) = y_{\text{back}}(i) + y_{\text{peak}}(i) = y_{\text{back}}(i) + \sum_j y_j(i) \quad (29)$$

where the index  $j$  runs over all characteristic line groups which appear in the spectrum. For each line group  $j$  (e.g., Fe-K, Pb-L<sub>3</sub>), the contribution  $y_j(i)$  to the  $i$ th channel is calculated as:

$$y_j(i) = A_j \left( \sum_{k=1}^{N_j} r_{jk} G(E_{jk}, i) t(E_{jk}) \right) \quad (30)$$

where  $A_j$  represents the total area of all photo peaks in line group  $j$  (comprised, e.g., of the Fe-K <sub>$\alpha$</sub>  and -K <sub>$\beta$</sub>  lines); these are optimizable parameters during the least squares fitting process. The index  $k$  runs over all lines in group  $j$ , each line having a relative abundance  $r_{jk}$  (with  $\sum_k r_{jk} = 1$ ).  $G_{jk}$  represents a Gaussian function centered around  $E_{jk}$ ;  $t(E_{jk})$  denotes the total attenuation factor for X-rays with energy

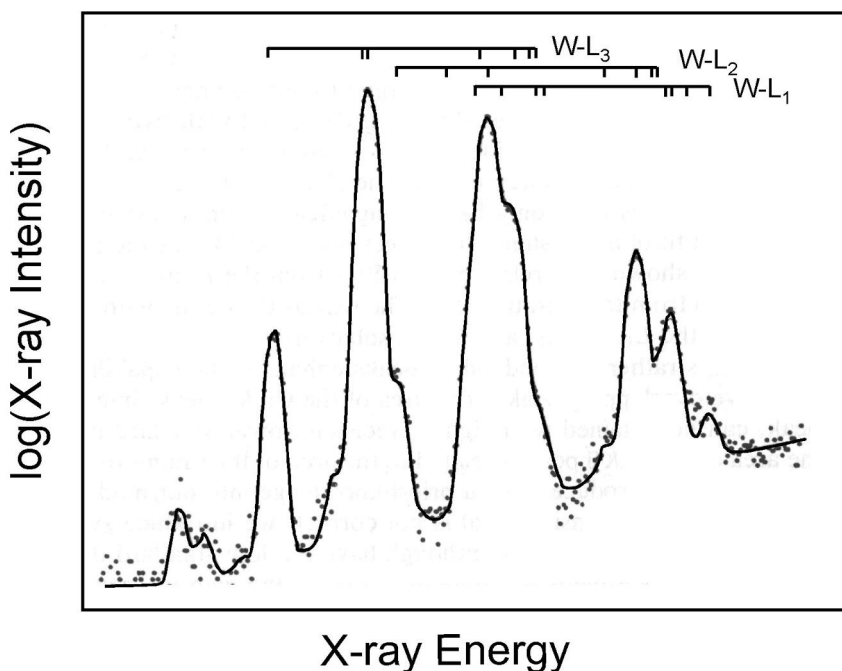


**Fig. 11.28** Spectral deconvolution in the case of complex multiplets.

$E_{jk}$  as defined by the absorption of radiation in the detector, in absorbers placed between sample and detector and in the sample itself. This model can also be expanded to account for spectral artifacts that are generated in the solid-state detector. In Fig. 11.28, the result of non-linear deconvolution of the complex multiplets constituted by the W-L<sub>1</sub>, L<sub>2</sub> and L<sub>3</sub>-lines is shown.

The background in ED-XRF spectra is the result of many processes and therefore can have a fairly complex shape. Although it is not impossible to calculate/predict this shape, during spectrum evaluation, usually a more empirical (and faster) approach is favored. Either the background shape is estimated *a priori* so that it can be subtracted from the experimental data before the actual fitting ('background estimation') or it is described by a suitable mathematical function (usually a polynomial of some kind), of which the coefficients are optimized together with the other parameters of the fitting model ('background modeling').

### 11.5.3

#### Quantitative Calibration Procedures

In the X-ray analytical laboratory the quantitative method of analysis employed will be typically determined by a number of circumstances of which probably the four most common are: the complexity of the analytical problem; the time allowable; the data processing and calibration software present and the number of standards

available. It is convenient to break quantitative analytical methods down into two major categories: single-element methods and multiple-element methods.

- Single-element Methods: Internal standardization  
Standard addition
- Multiple-element Methods: Type standardization  
Use of influence coefficients  
Fundamental parameter techniques

The simplest quantitative analysis situation to handle is the determination of a single element in a known matrix. A slightly more difficult case might be the determination of a single element where the matrix is unknown. As shown in the table, three basic methods are commonly employed in this situation: use of internal standards, use of standard addition, or use of a scattered line from the X-ray source.

The most complex case is the analysis of all, or most, of the elements in a sample about which little or nothing is known. In this case a full qualitative analysis would be required before any attempt is made to quantify the matrix elements. Once the qualitative composition of the sample is known, again, one of three general techniques is typically applied: use of type standardization, use of an influence coefficient method, or use of a fundamental parameter technique.

The correlation between the characteristic count rate  $R_i$  of an analyte element and the concentration  $c_i$  of that element is typically non-linear over wide ranges of concentration, due to inter-element effects between the analyte element and other elements making up the specimen matrix. However, the situation can be greatly simplified in the case of homogeneous specimens, where severe enhancement effects are absent, and here, the slope of a calibration curve  $S_i$  is inversely proportional to the total absorption factor  $A_i$  of the specimen for the analyte wavelength:

$$S_i = R_i c_i^{-1} A_i^{-1} \quad (31)$$

As an example, the data in Tab. 11.8 show how the net intensity of the Fe-K $\alpha$  line (Fe K-L<sub>3,2</sub> transition) resulting from a concentration of 1% iron depends strongly on the matrix composition: the Fe-intensity obtained from a graphite sample, in which virtually no absorption takes place ( $A \approx 1$ ) of the Fe-K $\alpha$  radiation is ca. 600 times higher than that obtained from the same Fe concentration in a strongly absorbing lead sample. With the Ni sample, a higher intensity than in the Cr sample is observed, even though the absorption in the Ni matrix is higher. This is caused by the enhancement effect due to the Ni characteristic X-rays that additionally excite the Fe atoms. The combination of matrix absorption and enhancement effects causes the calibration curves in XRF to be nonlinear. Figure 11.29 shows calibration curves for Pb and Sn in binary Pb–Sn alloys. Different quantitative analysis schemes are used depending on the type of matrix, the concentration range and the availability of the standards.

**Table 11.8** Count rate (in cps) of the Fe-K $\alpha$  line obtained from a 1% concentration of Fe in various matrices.

Matrix	Intensity
C	1200
Al	108
Cr	22
Ni	79
Pb	20

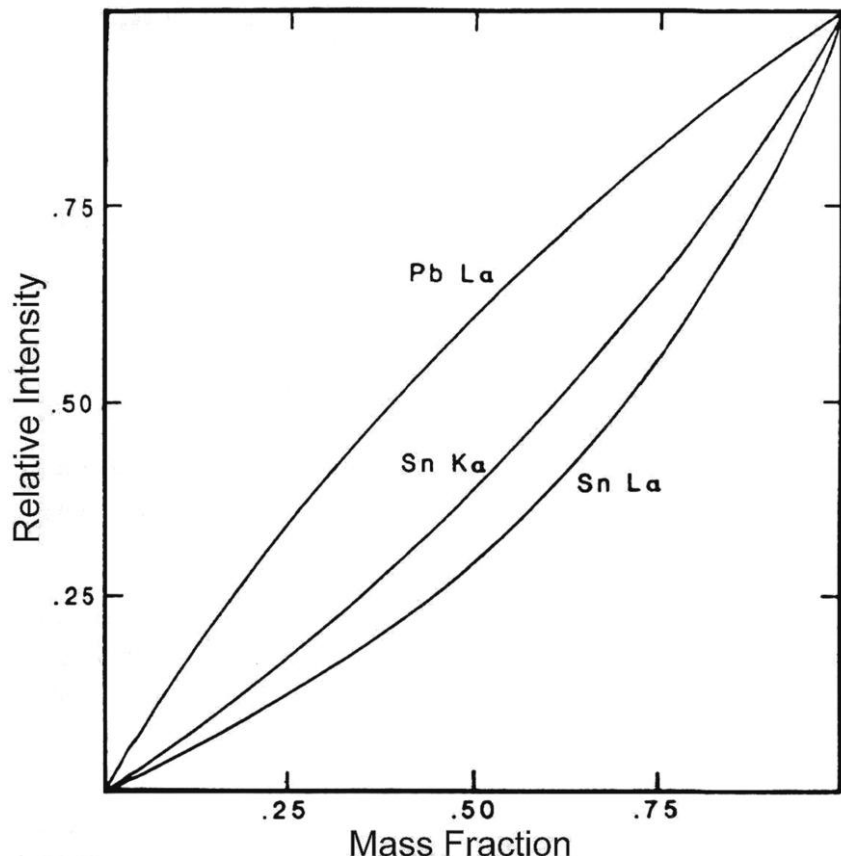


**Fig. 11.29** Calibration curves for Pb-L $\alpha$ , Sn-K $\alpha$  and Sn-L $\alpha$  in Pb-Sn binaries. The Pb-L $\alpha$  intensity shows a slight enhancement effect (due to the Sn-K lines); the Sn-K $\alpha$  and Sn-L $\alpha$  curves indicate different degrees of absorption in the sample. In case of Sn-L $\alpha$ , the absorption effect apparently dominates over the enhancement of the Sn-L $\alpha$  intensity by both the Pb-L and Sn-K lines.

### 11.5.3.1 Single-element Techniques

Single-element techniques reduce the influence of the absorption term  $\mu$  in Eq. (31), generally by referring the intensity of the analyte wavelength to a similar wavelength, arising either from an added standard or from a scattered line from the X-ray tube. In certain cases, limiting the concentration range of the analyte may allow the assumption to be made that the absorption value does not significantly change over the concentration range and the calibration curve is essentially linear.

**Thin film approach** Quantitative analysis of thin films, such as filters loaded with aerosol particles, can be done by simply comparing the count rate for a particular element in the sample with the count rate observed in a thin film standard, because matrix effects are virtually absent. Special reference standards may be made up for particular purposes, and these may serve the dual purpose of instrument calibration and establishing working curves for analysis. As an example, two thin glass film standard reference materials (SRMs) specially designed for calibration of X-ray spectrometers are available from the National Institute of Standards and Technology in Washington as SRMs 1832 and 1833. They consist of a silica-based film deposited by focused ion-beam coating onto a polycarbonate substrate. SRM 1832 contains aluminum, silicon, calcium, vanadium, manganese, cobalt and copper, and SRM 1833 contains silicon, potassium, titanium, iron and zinc.

**Internal standardization** One of the most useful techniques for the determination of a single analyte element in a known or unknown matrix is to use an internal standard. The technique is one of the oldest methods of quantitative analysis and is based on the addition of a known concentration of an element that features an X-ray line with a wavelength/energy close to that of the analyte wavelength. The assumption is made that the effect of the matrix on the internal standard is essentially the same as the effect of the matrix on the analyte element. Internal standards are best suited for the measurement of analyte concentrations below ca. 10 %. The reason for this limit arises because it is generally advisable to add the internal standard element at about the same concentration level as that of the analyte. When more than 10 % of the internal standard is added, it may significantly change the specimen matrix and introduce errors into the determination. Care must also be taken to ensure that the particle sizes of specimen and internal standard are about the same, and that the two components are adequately mixed. Where an appropriate internal standard cannot be found it may be possible to use the analyte itself as an internal standard. This method is a special case of standard addition (spiking).

**Type standardization** Provided that the total specimen absorption does not vary significantly over a range of analyte concentrations, and provided that enhancement effects are absent and that the specimen is homogeneous, a linear relationship will be obtained between analyte concentration and measured characteristic line intensity. Where these provisos are met, type standardization techniques can be employed.

In this way, linear calibration curves can be used to determine trace and minor element concentrations in alloys, mineral pellets and liquids provided that the major element concentrations of standards and unknowns are very similar. In this case, the matrix effect remains the same.

It will also be clear from the previous discussion that by limiting the range of analyte concentrations to be covered in a given calibration procedure, the range in absorption can also be reduced. Type standardization is probably the oldest of the quantitative analytical methods employed, and the method is usually evaluated by taking data from a well-characterized set of standards, and, by inspection, establishing whether a linear relationship is indeed observed. Where this is not the case, the analyte concentration range may be further restricted. Many hundreds of good reference standards are commercially available. While the type standardization method is not without its pitfalls, it is nevertheless extremely useful and especially for quality control type applications where a finished product is being compared with a desired product.

#### 11.5.3.2 Multiple-element Techniques

To determine major and minor elements in complex samples, more elaborate matrix correction algorithms need to be applied. They can be roughly divided into two categories: the influence coefficient methods and the fundamental parameter method.

**Influence coefficient methods** All these models have essentially the same form:

$$c_i/R'_i = K_i + \text{model-dependent term(s)} \quad (32)$$

describing the (empirical) relation between an analyte concentration  $c_i$ , its X-ray intensity ratio  $R'_i$ , an instrument-dependent term  $K_i$  that is equal to the inverse of the sensitivity of the spectrometer for the analyte in question ( $K_i = 1/S_i$ ), and a term that corrects this sensitivity term for the effect of the matrix.  $R'$  is the ratio of the analyte intensity in the unknown sample to that obtained from a pure element standard, measured under identical circumstances. The different methods only vary in the form of the correction term. Below, the relations used by some of the commonly employed influence methods are listed:

$$\text{Linear model } c_i/R'_i = K_i \quad (33a)$$

$$\text{Lachance-Traill } c_i/R'_i = K_i + \sum_j a_{ij} c_j \quad (33b)$$

$$\text{Claisse-Quintin } c_i/R'_i = K_i + \sum_j a_{ij} c_j + \sum_j \gamma_{ij} c_j^2 \quad (33c)$$

$$\text{Rasberry-Heinrich } c_i/R'_i = K_i + \sum_j a_{ij} c_j + \sum_{k \neq j} \beta_{ijk} [c_k/(1 + c_i)] \quad (33d)$$

$$\text{Lachance-Claisse } c_i/R'_i = K_i + \sum_j a_{ij} c_j + \sum_j \sum_{k > j} a_{ijk} c_j c_k \quad (33e)$$

where all concentrations are expressed as mass fractions.

All the models are concentration correction models in which the product of the influence coefficient ( $\alpha$ ,  $\beta$ , or  $\gamma$  in the above equations) and the concentration of the interfering element are used to correct the slope of the analyte calibration curve. The Lachance–Traill model is the earliest model; after that, in the Rasberry–Heinrich model, the influence of the absorbing and enhancing elements is separated by the use of the  $\alpha$  and  $\beta$  coefficients respectively. When the physics of the X-ray excitation are thoroughly studied, it becomes clear that the above-mentioned models are too simple and that all binary coefficients (the  $\alpha_{ij}$ s and  $\beta_{ij}$ s) are systematically dependent on the composition. Both the Claisse–Quintin and the Lachance–Claisse models use higher order cross-terms to correct for enhancement and third element effects. Accordingly, these models are in general more suited for use over a very wide concentration range.

**Fundamental parameter method** The fundamental parameter method is based on the physical theory of X-ray production rather than on empirical relations between observed X-ray count rates and concentrations of standard samples. In general, the observed XRF count rate  $R_{i,K\alpha}$  of (the  $K_\alpha$  line of) an element  $i$ , obtained by polychromatic excitation of a sample with thickness  $d$  and density  $\rho$ , can be written as:

$$R_{i,K\alpha} = \int_{E=E_{i,\text{abs}}}^{E_{\max}} \int_{z=0}^d I_0(E) \frac{G_1}{\sin\varphi} \sigma_{i,K\alpha}(E) c_i H_i(E) e^{-\chi(E, E_{i,K\alpha})\rho z} G_2 B(E, E_{i,K\alpha}) \varepsilon(E_{i,K\alpha}) dz dE \quad (34)$$

where the quantity  $\sigma_{i,K\alpha}$  is the effective cross section for production of  $K_\alpha$ -radiation of element  $i$ :

$$\sigma_{i,K\alpha}(E) = \tau_{i,K\alpha}(E) \omega_{i,K} p_{i,K\alpha} \quad (35)$$

(with  $p_{i,K\alpha}$  the probability of producing a  $K_\alpha$ -fluorescent photon from a vacancy in the K-shell and  $\omega_{i,K}$  its fluorescence yield).  $E_{i,\text{abs}}$  is the absorption edge energy and  $E_{i,K\alpha}$  the  $K_\alpha$ -line energy of element  $i$ ,  $I_0(E)dE$  is the spectral distribution of the exciting radiation with  $E_{\max}$  its maximum energy (see Fig. 11.6),  $G_1$  and  $G_2$  are geometry constants,  $\chi(E, E_{i,K\alpha})$  is defined in Eq. (19).  $H_i(E, E_{i,K\alpha})$  is a factor describing secondary and higher order excitation (at low concentrations,  $H_i = 1$ ) while the factor  $B(E, E_{i,K\alpha})$  describes the absorption of the radiation in the medium between tube, sample and detector (e.g., air, He).  $\varepsilon(E_{i,K\alpha})$  is the efficiency of the detector. After integration over the sample depth, Eq. (34) becomes:

$$R_{i,K\alpha} = \int_{E=E_{i,\text{abs}}}^{E_{\max}} I_0(E) \frac{G_1 \rho d}{\sin\varphi} \sigma_{i,K\alpha}(E) c_i \frac{1 - e^{-\chi(E, E_{i,K\alpha})\rho d}}{\chi(E, E_{i,K\alpha})\rho d} G_2 B(E, E_{i,K\alpha}) \varepsilon(E_{i,K\alpha}) dE \quad (36)$$

**Table 11.9** Analysis of Tool Steels obtained by means of a fundamental parameter program and one calibration standard. Min., max.: minimum and maximum concentrations in the series of analyzed samples. Standard deviation on the basis of the difference between calculated and certified concentrations. (Adapted from [18])

Element	Min (%)	Max (%)	Standard Deviation (%)
Si	0.14	0.27	0.03
S	0.015	0.029	0.003
P	0.022	0.029	0.003
Mo	0.2	9.4	0.04
Mn	0.21	0.41	0.01
Cr	2.9	5	0.13
Co	0	10	0.2
C	0.65	1.02	0.16
W	1.8	20.4	0.52

The above fundamental parameter equation relates the intensity of one element to the concentration of all elements present in the sample. A set of such equations can be written, one for each element to be determined. This set of equations can only be solved in an iterative way, making the method computationally complex. Moreover, an accurate knowledge of the shape of the excitation spectrum  $I_0(E)dE$ , of the detector efficiency  $\epsilon$  and of the fundamental parameters  $\mu$ ,  $\tau$ ,  $\omega$  and  $p$  is required. The fundamental parameter method is of interest because it allows for semi-quantitative (5–10 % deviation) analysis of completely unknown samples and is therefore of use in explorative phases of investigations. Several computer programs are available that allow one to perform the necessary calculations at various levels of sophistication. As an example, in Tab. 11.9, the relative standard deviation between certified and calculated concentration of the constituents of a series of tool steels are listed.

#### 11.5.4 Error Sources in X-ray Fluorescence Analysis

Table 11.10 lists the four main categories of random and systematic error encountered in X-ray fluorescence analysis. The first category includes the selection and preparation of the sample to be analyzed. Two stages are generally involved before the actual prepared specimen is presented to the spectrometer, these being sampling and specimen preparation. The actual sampling is rarely under the control of the spectroscopist and it generally has to be assumed that the container containing the material for analysis does, in fact, contain a representative sample. It can be seen from the table that, in addition to a relatively large random error, inadequate sample preparation and residual sample heterogeneity can lead to very large systematic errors. For accurate analysis these errors must be reduced by use of a suitable specimen preparation method. The second category includes errors arising from the X-ray source. Source errors can be reduced to less than 0.1 % by the use of the ratio counting technique, provided that high frequency transients are

**Table 11.10** Sources of error in X-ray fluorescence analysis.

<b>Source</b>	<b>Random (%)</b>	<b>Systematic (%)</b>
1 Sample preparation	0–1	0–5
Sample inhomogeneity	—	0–50
2 Excitation source fluctuations	0.05–0.2	0.05–0.5
Spectrometer instability	0.05–0.1	0.05–0.1
3 Counting statistics	time dependent	—
Dead time correction	—	0–25
4 Primary absorption	—	0–50
Secondary absorption	—	0–25
Enhancement	—	0–15
Third element effects	—	0–2

absent. The third category involves the actual counting process and these errors can be both random and systematic. System errors due to detector dead time can be corrected either by use of electronic dead time correctors or by some mathematical approach. The fourth category includes all errors arising from inter-element effects. Each of the effects listed can give large systematic errors that must be controlled by the calibration and correction scheme.

### 11.5.5

#### Specimen Preparation for X-ray Fluorescence

Because X-ray spectrometry is essentially a comparative method of analysis, it is vital that all standards and unknowns be presented to the spectrometer in a reproducible and identical manner. Any method of specimen preparation must give specimens which are reproducible and which, for a certain calibration range, have similar physical properties including mass attenuation coefficient, density, particle size, and particle homogeneity. In addition the specimen preparation method is preferred to be rapid and cheap and must not introduce extra significant systematic errors; for example, the introduction of trace elements from contaminants in a diluent. Specimen preparation is an all-important factor in the ultimate accuracy of any X-ray determination, and many papers have been published describing a multitude of methods and recipes for sample handling. In general samples fit into three main categories:

1. Samples that can be handled directly following some simple pretreatment such as pelletizing or surfacing. For example, homogeneous samples of powders, bulk metals or liquids.
2. Samples that require significant pretreatment. For example, heterogeneous samples, samples requiring matrix dilution to overcome inter-element effects and samples exhibiting particle size effects.
3. Samples that require special handling treatment. For example, samples of limited size, samples requiring concentration or prior separation, and radioactive samples.

The ideal specimen for X-ray fluorescence analysis is one in which the analyzed volume of specimen is representative of the total specimen, which is, itself, representative of the sample submitted for analysis. There are many forms of specimen suitable for X-ray fluorescence analysis, and the form of the sample as received will generally determine the method of pretreatment. It is convenient to refer to the material received for analysis as the sample, and the material actually analyzed in the spectrometer as the specimen. While the direct analysis of certain materials is certainly possible, more often than not some pretreatment is required to convert the sample to the specimen. This step is referred to as specimen preparation. In general, the analyst would prefer to analyze the sample directly because, if it is taken as received, any problems arising from sample contamination that might occur during pretreatment are avoided. In practice, however, there are three major constraints that may prevent this ideal circumstance from being achieved: sample size, sample size homogeneity and sample composition heterogeneity. Problems of sample size are frequently severe in the case of bulk materials such as metals, large pieces of rock, etc. Problems of sample composition heterogeneity will generally also occur under these circumstances, and in the analysis of powdered materials heterogeneity must almost always be considered. The sample as received may be either homogeneous or heterogeneous; in the latter case, it may be necessary to render the sample homogeneous before an analysis can be made. Heterogeneous bulk solids are generally the most difficult kind of sample to handle, and it may be necessary to dissolve or chemically react the material in some way to give a homogeneous preparation. Heterogeneous powders are either ground to a fine particle size and then pelletized, or fused with a glass-forming material such as borax. Solid material in liquids or gases must be filtered out and the filter analyzed as a solid. Where analyte concentrations in liquids or solutions are too high or too low, dilution or preconcentration techniques may be employed to bring the analyte concentration within an acceptable range.

## 11.6 Advantages and Limitations

### 11.6.1 Qualitative Analysis

Qualitative analysis is, in principle, very simple with XRF and is based on the accurate measurement of the energy, or wavelength, of the fluorescent lines observed. Since many WD-XRF spectrometers operate sequentially, a  $2\theta$  scan needs to be performed. The identification of trace constituents in a sample can sometimes be complicated by the presence of higher order reflections or “satellite” lines from major elements. With energy-dispersive XRF, the entire X-ray spectrum is acquired simultaneously. The identification of the peaks, however, is rendered difficult by the comparatively low resolution of the ED detector. In qualitative analysis programs, the process is simplified by overplotting so called “KLM” markers onto

an (unknown) spectrum. These markers indicate the theoretical position of the K, L and M lines of a specific element; when these observed peaks coincide with the line markers, an element is positively identified.

### 11.6.2

#### **Detection Limits**

For a particular element, the detection limit depends on the sensitivity and on the count rate of the continuum below the peak and is inversely proportional to the measurement time. Detection limits can be improved by increasing the sensitivity (optimization of the excitation and detection efficiency), by reducing the background (as is done in TXRF) or by counting a longer period of time. The value of the attainable detection limits thus depends very much upon the sample, the element considered and the experimental conditions. In wavelength-dispersive instruments, values range from 0.1 ppm to 10 ppm are obtained for medium-Z elements (such as Fe) up to 1–5 % for the lightest elements (B, Be). Detection limits for unpolarized ED-XRF are typically a factor of 5 to 10 worse, except for TXRF that has absolute detection limits in the pg range. Using synchrotron sources, the detection limits of XRF are generally several orders of magnitude better than in the case where conventional X-ray sources are employed.

### 11.6.3

#### **Quantitative Reliability**

The great flexibility, sensitivity and range of the various types of X-ray fluorescence spectrometer make them ideal for quantitative analysis. In common with all analytical methods, quantitative X-ray fluorescence analysis is subject to a number of random and systematic errors that contribute to the final accuracy of the analytical result. Like all instrumental methods of analysis, the potential high precision of X-ray spectrometry can only be translated into high accuracy if the various systematic errors in the analysis process are taken care of. The precision of a wavelength-dispersive system for the measurement of a single, well separated line is typically of the order of 0.1 %, and about 0.25 % for the energy-dispersive system. An expression useful to estimate the expected standard deviation  $\sigma$  at an analyte concentration level  $c$  is given by:

$$\sigma = K (c + 0.1)^{1/2} \quad (37)$$

where  $K$  varies between 0.005 and 0.05. For example, at a concentration level  $c \approx 25\%$ , the expected value of  $\sigma$  would be between about 0.025 % and 0.25 %. A  $K$  value of 0.005 would be considered very high quality analysis and a value of 0.05 rather poor quality. The value of  $K$  actually obtained under routine laboratory conditions depends upon many factors but with reasonably careful measurements a  $K$  value of around 0.02 to 0.03 can be obtained.

## 11.7 Summary

When a chemical element is bombarded by high-energy particles, orbital electrons may be ejected creating inner orbital atomic vacancies. These vacancies may be filled by transition of outer level electrons giving rise to characteristic X-radiation. X-ray fluorescence spectrometry provides the means of identification of an element by measurement of its characteristic X-ray emission wavelength or energy.

The method allows the quantization of a given element by first measuring the emitted characteristic line intensity and then relating this intensity to element concentration.

While the roots of the method go back to the early part of this century, where electron excitation systems were employed, it is only during the last 30 years or so that the technique has gained major significance as a routine means of elemental analysis. Wavelength-dispersive spectrometers employ diffraction by a single crystal to separate characteristic wavelengths emitted by the sample. Today, nearly all commercially available X-ray spectrometers use the fluorescence excitation method and employ a sealed X-ray tube as the primary excitation source. The first commercial X-ray spectrometer became available in the early 1950s and although these earlier spectrometers operated only with an air path, they were able to provide qualitative and quantitative information on all elements above atomic number 22 (titanium). Later versions allowed the use of helium or vacuum paths that extended the lower atomic number cut-off to around atomic number 9 (fluorine). X-ray detectors used include the flow counter, the scintillation counter and the Si(Li) detector.

The X-ray method has good overall performance characteristics. In particular, the speed, accuracy and versatility of X-ray fluorescence are the most important features among the many that have made it the method of choice in over 30,000 laboratories all over the world.

Most wavelength-dispersive spectrometers fall into two broad categories: single channel and multi-channel. Single channel spectrometers are typically employed for both routine and non-routine analysis of a wide range of products, including ferrous and nonferrous alloys, oils, slags and sinters, ores and minerals, thin films, and so on. These systems are very flexible but relative to multi-channel spectrometers are somewhat slow. The multi-channel wavelength-dispersive instruments are used almost exclusively for routine, high-throughput analysis where the great need is for fast accurate analysis, but where flexibility is of no importance. Energy-dispersive spectrometers exist in various forms, some designed for (on-site or laboratory) bulk analysis, others for surface-specific or microscopic analysis.

Interelement (matrix) effects often complicate quantitative analysis by X-ray fluorescence. However, a wide selection of methods is now available for minimizing these effects, allowing excellent accuracy to be obtained in many cases. Detection limits are achievable down to the low parts per million (ppm) range and it is possible to obtain reasonable responses from as little as a few milligrams of material.

## References

- 1 Hechel J., Ryon R.W.: Polarized Beam X-ray Fluorescence Analysis, in *Handbook of X-ray Spectrometry*, 2nd edition, eds. R. E. Van Grieken and A. A. Markowicz, Marcel Dekker, New York 2001, Chapter 10.
- 2 Bertin E.P.: *Principles and Practice of X-ray Spectrometric Analysis*, 2nd edition, Plenum Press, New York 1975.
- 3 Cesareo R., Gigante G. E., Castellano A., Iwanczyk J. S.: Portable Systems for Energy-dispersive X-ray Fluorescence, in *Encyclopedia of Analytical Chemistry*, ed. R. A. Meyers, John Wiley & Sons, Chichester 2000, 13327–13338.
- 4 Janssens K. H., Adams F. C., Rindby A.: *Microscopic X-ray Fluorescence Analysis*, John Wiley & Sons, Chichester 2000.
- 5 Janssens K., Adams F.: X-ray Techniques: Overview, in *Encyclopedia of Analytical Science*, ed. A. Townshend, Academic Press, London 1995, Vol. 9, 5560–5574.
- 6 Jenkins R., *X-ray Fluorescence Spectrometry*, John Wiley & Sons, New York 1988.
- 7 Jenkins R., Gould R. W., Gedcke D.: *Quantitative X-ray Spectrometry*, Marcel Dekker, New York 1981.
- 8 Jenkins R.: X-ray Techniques: Overview, in *Encyclopedia of Analytical Chemistry*, ed. R. A. Meyers, John Wiley & Sons, Chichester 2000, 13269–13268.
- 9 Jenkins R.: Wavelength-dispersive X-ray Fluorescence Analysis, in *Encyclopedia of Analytical Chemistry*, ed. R. A. Meyers, John Wiley & Sons, Chichester 2000, 13422–13444.
- 10 Klockenkämper R.: *Total Reflection X-ray Fluorescence Analysis*, John Wiley & Sons, Chichester 1997.
- 11 Potts P.: X-ray Fluorescence: Basic Theory, in *Encyclopedia of Analytical Science*, ed. A. Townshend, Academic Press, London 1995, Vol. 9, 5601–5611.
- 12 Potts P.: Wavelength-dispersive X-ray Fluorescence, in *Encyclopedia of Analytical Science*, ed. A. Townshend, Academic Press, London 1995, Vol. 9, 5611–5622.
- 13 Potts P.: Energy-dispersive X-ray Fluorescence, in *Encyclopedia of Analytical Science*, ed. A. Townshend, Academic Press, London 1995, Vol. 9, 5622–5633.
- 14 Selin-Lindgren E.: Energy-dispersive X-ray Fluorescence Analysis, in: *Encyclopedia of Analytical Chemistry*, ed. R. A. Meyers, John Wiley & Sons, Chichester 2000, 13315–13327.
- 15 *Handbook of X-ray Spectrometry*, eds. Van Grieken R. E., Markowicz A. A., Marcel Dekker, New York 1993, 453–489.
- 16 Wobrauschek P., Streli C.: Total Reflection X-ray Fluorescence, in *Encyclopedia of Analytical Chemistry*, ed. R. A. Meyers, pp. 13384–13414, John Wiley & Sons, Chichester 2000, 13384–13414.
- 17 P. Potts: *Handbook of Silicate Rock Analysis*, Blackie, Glasgow 1987.
- 18 *Handbook of X-ray Spectrometry*, eds. R. E. Van Grieken and A. A. Markowicz, 1st edition, Chapter 5, p. 320.

## **12**

### **Atomic Absorption Spectrometry (AAS) and Atomic Emission Spectrometry (AES)**

*Erwin Rosenberg and Ulrich Panne*

#### **12.1**

##### **Introduction**

Atomic absorption and atomic emission spectrometry were the first instrumental techniques to be established for elemental analysis. They are based on the pioneering work of Bunsen and Kirchhoff [1] in the middle of the 19th century who discovered that elements which are brought into a hot flame emit light of a characteristic wavelength. On the other hand, this characteristic emission can be absorbed again by the vapor of the same element. These two discoveries formed the basis for atomic absorption and emission spectrometry and demonstrate the close interrelation and complementary nature of these two techniques. Atomic absorption and atomic emission spectrometry have many theoretical and practical considerations in common, and they can be described by the same formalism. The theory of AAS and AES will thus be treated together.

#### **12.2**

##### **Theory of Atomic Spectroscopy**

###### **12.2.1**

###### **Basic Principles**

The development of atomic spectroscopic techniques and their application to fundamental studies fostered the concurrent development of atomic theory and quantum mechanics. In turn, the better understanding of atomic theory has led to the implementation of many beneficial techniques and instrumental features in atomic spectroscopy, particularly for the reduction or elimination of interferences and background.

A first step toward the interpretation of atomic spectra was made in 1885, when Balmer found a formula describing the different emission lines of hydrogen in the visible region:

$$\lambda = k \frac{n^2}{n^2 - 4} \quad (1)$$

where  $\lambda$  is the wavelength (in nm),  $k$  a constant, and  $n = 3, 4, 5, \dots$  represents the spectroscopic lines  $H_\alpha, H_\beta, H_\gamma, \dots$

Eq. (1) may be expressed in wavenumbers,

$$\nu' = \frac{1}{\lambda} = R \left( \frac{1}{2^2} - \frac{1}{n^2} \right) \quad (2)$$

where  $\nu'$  is the frequency of the radiation in wavenumbers ( $\text{cm}^{-1}$ ) and  $R$  the Rydberg constant ( $109,677 \text{ cm}^{-1}$ ). Eq. (2) may be generalised to give the wavelength of the lines in all series of the hydrogen atom:

$$\nu' = R \left( \frac{1}{n_1^2} - \frac{1}{n_2^2} \right) \quad (3)$$

where  $n_1 > n_2$ . The numbers  $n_1 = 1, 2, 3$  represent the Lyman, Balmer, and Paschen series, respectively. Eq. (3) was further extended by Rydberg to yield:

$$\nu' = R Z^2 \left( \frac{1}{n_1^2} - \frac{1}{n_2^2} \right) \quad (4)$$

$Z$  stands for the effective charge of the atomic species which now gives the possibility of calculating the wavelength of lines of atoms other than the hydrogen atom. The two numbers  $n_1$  and  $n_2$  are the so-called spectral terms of the particular atom. These terms describe the defined energy levels of the electrons in their orbits around the nucleus. According to Bohr's theory of the atomic structure, no energy is taken up or emitted as long as the electron remains in its given orbit. Energy ( $E$ ) is only taken up or emitted in the form of electromagnetic radiation when the transition of an electron between two energetic states occurs. The wavelength of this radiation is given by:

$$E = h\nu = hc/\lambda \quad (5)$$

with  $h = 6.626 \times 10^{-34} \text{ J s}$ : Planck's constant;  $\nu$ : frequency (in  $\text{s}^{-1}$ ),  $c = 3 \times 10^8 \text{ m s}^{-1}$  speed of light, and  $\lambda$ : wavelength (m). The energy difference accompanying such a transition is thus:

$$\nu' = \frac{1}{\lambda} = \frac{E}{hc} = \frac{E_1}{hc} - \frac{E_2}{hc} = T_1 - T_2 \quad (6)$$

$T_1$  and  $T_2$  are the Bohr energy levels. Considering systems with a single valence electron, the energy of this electron can be expressed as:

$$E = \frac{2\pi Z^2 e^4 \mu}{n^2 h^2} \quad (7)$$

where  $\mu$  is the reduced mass of the system,  $\mu = m \times M / (m + M)$  with  $m$  representing the mass of the electron and  $M$  the mass of the nucleus, and  $n$  is the principal quantum number ( $n = 1, 2, 3, \dots$ ).

The orbital quantum number,  $l$ , with  $l = 0, 1, 2, \dots (n - 1)$  determines the orbital angular momentum  $\mathbf{L}$ :

$$||\mathbf{L}|| = \frac{\hbar}{2\pi} \times \sqrt{l(l+1)} \quad (8)$$

For an elliptical orbit, the possible orientations relative to an external electric or magnetic field are:

$$\mathbf{L}_z = \frac{\hbar}{2\pi} m_l \quad (9)$$

where  $\mathbf{L}_z$  is the component of the orbital angular momentum of  $\mathbf{L}$  that is parallel to the external field with  $m_l = \pm 1, \pm(n-1), \dots, 0$ .  $m_l$  has  $(2l+1)$  values. When an absorbing or emitting atom is brought into a strong magnetic field, the spectral lines display a hyperfine structure, called the Zeeman effect. The explanation of this effect requires the assumption that the electron rotates around its axis, thus exhibiting a spin angular momentum  $\mathbf{S}$ :

$$||\mathbf{S}|| = \frac{\hbar}{2\pi} \times \sqrt{S(S+1)} \quad (10)$$

The spin quantum number  $m_s$  describes the orientation of the axis of rotation of the electron and the external field:

$$s_z = \frac{\hbar}{2\pi} m_s \quad (11)$$

$m_s$  may assume the values of  $\pm 1/2$ .

The total angular momentum of an electron  $\mathbf{J}$  results from the vector sum of the orbital angular momentum and the spin angular momentum:

$$\vec{\mathbf{J}} = \vec{\mathbf{L}} + \vec{\mathbf{S}} \text{ with } ||\mathbf{J}|| = \frac{\hbar}{2\pi} \times \sqrt{j(j+1)} \quad (12)$$

$j = l \pm s$  is the total internal quantum number.

All electrons of an atom must differ in their energetic states. These are given by the quantum number in the following notation:

$$n^m l_j \quad (13)$$

where  $n$  stands for the principal quantum number;  $m$  for the multiplicity of the signal ( $m = 2s + 1$ ), and  $l$  ( $l = 0, 1, 2, \dots$ ) for the orbital quantum number. The corresponding terms are denoted by the symbols s (sharp), p (principal), f (fundamental), d (diffuse) etc., which were initially used to describe the appearance of the different spectral lines.  $j$  is the total internal quantum number.

These term schemes are useful for expressing the energy levels of each element. They also allow one to define which transitions between energy levels are allowed, and which are forbidden. This is expressed by the so-called selection rules. These are:

- $\Delta n = 0 \pm 1 \pm 2, \dots$  (the principal quantum number may change by any integer value)
- $\Delta l = \pm 1$  (the orbital quantum number must change by one integer)
- $\Delta j = 0$  or  $\pm 1$  (the total internal quantum number may either remain unchanged or change by one integer, however the transition  $J = 0 \rightarrow J = 0$  is forbidden)
- $\Delta s = 0$  (the spin quantum number must change by one integer)

For larger systems (heavy atoms), however, the selection rules  $\Delta l = \pm 1$  and  $\Delta s = 0$  are sometimes violated.

The spectroscopic notation is easy to derive for elements with one valence electron, e.g. the Na atom: Its electron configuration in the ground state is:  $1s^2 2s^2 2p^6 3s^1$  or  $3^2S_{1/2}$  which results from  $l = 0$  (s);  $m = 2(1/2)+1 = 2$  (with  $s = 1/2$ ), and  $j = ||l \pm s|| = ||0 \pm 1/2|| = 1/2$ . The spectroscopic notation corresponding to the excited states with the 3s electron being lifted to the 3p level is  $3^2P_{1/2}$  and  $3^2P_{3/2}$  (since  $l = 1(p)$ ;  $m = 2(1/2)+1 = 2$  (with  $s = 1/2$ ), and  $j = ||l \pm s|| = ||1 \pm 1/2|| = 1/2$  and  $3/2$ ).

The term schemes of the elements have been compiled by Grotrian [2]. Two examples are given in Fig. 12.1. The energy level diagram of the singly charged magnesium ion differs comparatively little from that of the uncharged sodium atom (or of other alkaline metal atoms). A significant difference, however, consists in the energy difference between the 3p and 3s states which is almost double for  $Mg^+$  in comparison to  $Na^0$  as a consequence of the larger charge of the nucleus of Mg.

For atoms with more than one valence electron, coupling of the spin- and orbital angular momentum must be considered (Russel–Saunders- or  $L-S$ -coupling). The orbital momenta of all electrons have to be coupled to the total orbital momentum, as have the spin momenta. The total quantum number  $L$  is obtained by replacing  $L = \sum l$ ,  $S = \sum s$ , and  $J = L - S, \dots, L + S$ . The term symbol thus becomes:

$$^M L_J \quad (14)$$

As an example, the ground state of Mg is denoted as  $3^1S_0$  (electron configuration:  $1s^2 2s^2 2p^6 3s^2$ , corresponding to  $L = 0$  as  $l_1 = 0$  and  $l_2 = 0$ ;  $S = 0$  as  $s_1 = 1/2$  and  $s_2 = -1/2$ ; and  $J = L + S = 0$ ). The notation for the first excited state ( $1s^2 2s^2 2p^6 3s$

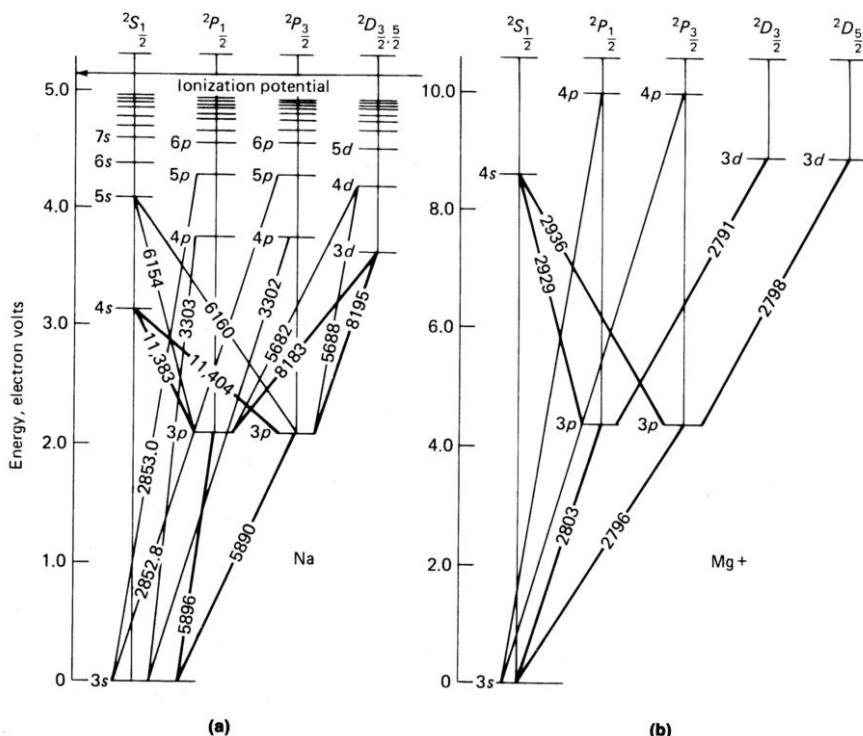
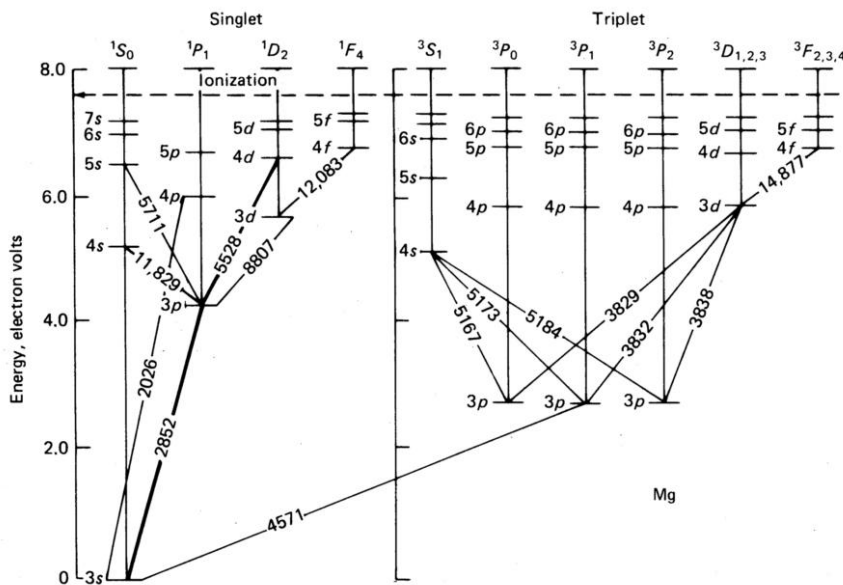


Fig. 12.1 Energy level (Grotrian) diagrams for (a) atomic sodium and (b) magnesium (I) ion.

$3p$ ) is, depending on the spin quantum number of the two valence electrons,  $3^1P_1$  (with  $L = 1$  as  $l_1 = 0$  and  $l_2 = 1$ ;  $S = 0$  as  $s_1 = 1/2$  and  $s_2 = -1/2$ ; and  $J = L + S = 0$  and  $J = |L + S| = 1$ ), as well as  $3^3P_2$ ,  $3^3P_1$ , and  $3^3P_0$  (corresponding to parallel spins  $s_1 = 1/2$  and  $s_2 = 1/2 \Rightarrow S = 1$  and consequently  $J = 0, 1, 2$ ). The energy level diagrams for ionic magnesium with one valence electron (Fig. 12.1(b)) and atomic magnesium (Fig. 12.2) differ significantly. For atoms with two outer electrons, two different term schemes exist upon excitation, the singlet and the triplet state with considerably different excitation energies. In the excited singlet state the spins of the two electrons are of opposed orientation and they are paired. In the triplet state the spins are parallel or unpaired. For this reason, the triplet excited state is of lower energy than the corresponding singlet state.

While the energy level diagrams and the corresponding spectroscopic transitions are relatively straightforward for light elements, they become very complex for heavier elements. The number of observed lines listed by Harvey [3] increases from the alkali metals with 30 (for lithium) to 645 (for caesium) to several thousand lines for the transition elements (chromium: 2277, iron: 4757, and cerium 5755 lines, respectively).



**Fig. 12.2** Energy level diagram for atomic magnesium. Strong lines indicate greater line intensities. The singlet/triplet transition has a significantly lower probability for occurrence than the singlet/singlet transition.

### 12.2.2

#### Fundamentals of Absorption and Emission

Atomic absorption and emission require the prevalence of free atoms which, in most instances, is achieved in a plasma or a plasma-like state. When a plasma is contained in a closed system and is in thermal equilibrium, the population of the excited levels may be described for one species by Boltzmann's law:

$$\frac{N_q}{N_0} = \frac{g_q}{g_0} \exp(-E_q/kT) \quad (15)$$

with  $N_q$ : number of particles in the excited state,  $N_0$ : number of particles in the ground state,  $g_q$  and  $g_0$ : statistical weights of the corresponding energy levels;  $E_q$ : excitation energy of the state  $q$ ;  $k$ : Boltzmann's constant ( $= 1.38 \times 10^{-23} \text{ J K}^{-1}$ ), and  $T$ : absolute temperature.

When the plasma is in the steady-state, the number of particles that leave an energy level per time unit is equal to that of those that arrive at this level. A number of phenomena are responsible for the transition of species between energy levels in a plasma:

- (a) collisions of atoms, leading to the excitation of one species to a higher energy level (collisions of the first kind)

- (b) collisions of an excited species with another particle, leading to radiationless relaxation (collisions of the second kind)
- (c) excitation by collision with electrons
- (d) de-excitation with the transfer of energy to an electron
- (e) excitation of atoms or ions by the absorption of radiation
- (f) de-excitation of atoms or ions by spontaneous or stimulated emission

Assuming the presence of two species, with  $n$  being the concentration of one species and  $N$  that of the second species that is in large excess ( $N \gg n$ ), we can set up the following equations:

$$\alpha N n_0 = \beta N n_q \quad (16)$$

$$\alpha_e n_e n_0 = \beta_e n_e n_q \quad (17)$$

$$B' \rho_\nu n_0 = (A + B \rho_\nu) n_q \quad (18)$$

$A$ ,  $B$ , and  $B'$  are the Einstein transition probabilities for spontaneous emission, stimulated emission, and absorption, respectively; and  $\alpha_e$ ,  $\alpha$ ,  $\beta_e$ , and  $\beta$  are the cross sections of the respective processes (which are also a function of the velocity distribution of the particles involved).  $n_e$  is the electron density;  $\rho_\nu$  is the radiation density at a given frequency  $\nu$ .

When the system is in thermodynamic equilibrium, the rate of formation and disappearance of charged particles and neutrals is equal, and at a given temperature  $T$  we can state:

$$\frac{n_q}{n_0} = \frac{\alpha}{\beta} = \frac{\alpha_e}{\beta_e} = \frac{B'}{A/\rho_\nu + B} = \frac{g_q}{g_0} \exp(-E_q/kT) \quad (19)$$

The number of charged and uncharged species remains constant through excitation and de-excitation by collisions with neutrals, ions and electrons. Absorption and emission, as they occur in a real radiation source, certainly also have to be considered, but they normally contribute only very little to the energy balance which is in the so-called local thermal equilibrium (LTE):

$$\alpha N n_0 + \alpha_e n_e n_0 + B' \rho_\nu n_0 = \beta N n_q + \beta_e n_e n_q + (A + B \rho_\nu) n_q \quad (20)$$

From Eq. (20),  $n_q/n_0$  can be calculated. In the radiation source, the population of excited states is determined by the excitation process, as may be deduced from Eq. (20): Thus, for example, a d.c. arc source (that is said to be in LTE),  $\alpha N \gg (\alpha_e n_e + B' \rho_\nu)$ , and  $\beta N \gg [\beta_e n_e + (A + B \rho_\nu) n_q]$ .

As long as the radiation density is low (which is the case for the d.c. arc) the plasma can be assumed to operate under local thermal equilibrium. This is not the case for low-pressure discharges where both collisions with electrons and radiative de-excitation are very important. Also, for low-pressure plasmas, the assumption of a Maxwellian velocity distribution of the particles is no longer valid.

Species can decay from excited states through a number of processes, including collision with uncharged (molecules, atoms) or charged (ions, electrons) particles, or by the emission of electromagnetic radiation. In the case of radiative decay, the wavelength of emission is given by Planck's law. For the spontaneous decay from level  $q$  to level  $p$ , the number of events per unit time is:

$$-\frac{dN_q}{dt} = A_{qp}N_q \quad (21)$$

$A_{qp}$  is the Einstein coefficient for spontaneous emission ( $s^{-1}$ ). Equation (21) must be adapted when several transitions starting from level  $q$  are to be considered:

$$-\frac{dN_q}{dt} = N_q \sum_p A_{qp} = N_q v_q \quad (22)$$

$v_q$  is here the lifetime of the excited state  $q$ . The typical lifetime of an excited state from which a species decays through an allowed radiative transition is of the order of  $10^{-8}$  s. When radiative transitions are not allowed, the excited states are metastable (as is the case, e.g. for the Ar 11.5 and 11.7 eV states), and relaxation can only occur through collisions with other particles.

Absorption of electromagnetic radiation of frequency  $\nu_{qp}$  and radiation density  $\rho_\nu$  increases the number density of excited particles  $N_q$  to:

$$\frac{dN_q}{dt} = B'_{qp}N_0\rho_\nu \quad (23)$$

Stimulated emission takes place when atoms in the excited state  $q$  decay upon interaction with radiation of wavelength  $\lambda_{qp}$  and leads to a reduction in the number density of excited species according to:

$$-\frac{dN_q}{dt} = B_{qp}N_q\rho_\nu \quad (24)$$

Under conditions of thermal equilibrium:

$$g_q B_{qp} = g_p B_{pq} \quad (25)$$

where  $g_q$  and  $g_p$  are the statistical weights (degeneration factors) of levels  $p$  and  $q$ .

When species emit, the intensity of the emitted spectral line (denoted by the subscript  $a$ ) is proportional to the number density of atoms in the excited state  $q$ :

$$I_{qp} = A_{qp}n_{aq}h\nu_{qp} \quad (26)$$

$n_{aq}$  may be substituted using the Boltzmann equation:

$$I_{qp} = A_{qp} h \nu_{qp} n_a \frac{g_q}{Z_a} \exp(-E_q/kT) \quad (27)$$

The sum  $Z_a = \sum_a g_a \exp(-E_a/kT)$  is the partition function. It is a function of temperature, and the coefficients of this function are tabulated in the literature for a large number of atoms and ions. When the intensities of two emission lines  $a$  and  $b$  from the same ionisation state of an element are used, the excitation temperature  $T$  may be calculated from:

$$T = \frac{5040(E_a - E_b)}{\log[(g_a A_a)/(g_b A_b)] - \log(\lambda_a/\lambda_b) - \log(I_a/I_b)} \quad (28)$$

In this equation, energies are in eV, and  $E_a$  and  $E_b$  denote the excitation energies (in eV) of lines  $a$  and  $b$ . The line pair Zn 307.206 nm/Zn 307.59 nm is very often used for calculating the excitation temperature. It is particularly suitable, as ionisation of zinc is generally low (due to its high ionisation energy), the difference between the two wavelengths is not too large, ensuring a uniform detector response, and the  $gA$  factors are precisely known.

### 12.2.2.1 Absorption

Between absorption and the number density of the absorbing atoms the following relation holds:

$$\int K_\nu d\nu = \frac{\pi e^2}{mc} N f \quad (29)$$

where  $K_\nu$  is the absorption coefficient at frequency  $\nu$ ,  $m$  is the electron mass and  $e$  its charge,  $c$  is the velocity of light,  $N$  the number density of atoms, and  $f$  the oscillator strength. As this relation is only strictly valid for monochromatic light, the use of a source that emits radiation with a very narrow spectral linewidth is required. Normally, atomic emission sources like hollow cathode lamps or electrodeless discharge lamps fulfil this condition. The relation between the absorption  $A$  and the concentration  $c$  is given by the law of Lambert and Beer which states that the intensity of incident radiation  $I_0$  is diminished by the fraction  $dI$  by absorption in the incremental length  $dl$  (with  $l$  being the total optical pathlength):

$$-dI = k I_0 c dl \quad (30)$$

Integration of Eq. (30) in the limits  $I = I_0$  to  $I$  and  $l = 0$  to  $l$ :

$$-\int_{I=I_0}^I \frac{dI}{I} = k c \int_{l=0}^l dl \quad (31)$$

$$\log\left(\frac{I_0}{I}\right) = k c l \quad (32)$$

As  $\log(I_0/I)$  equals the absorbance  $A$ , Eq. (32) can finally be written as:

$$A = k c l \quad (33)$$

The Lambert–Beer law is only valid within a restricted concentration range. Deviations from linearity are commonly observed and may be due to a number of reasons.

### 12.2.2.2 Line Broadening

Due to the contribution of various broadening mechanisms, the linewidths typically observed in atomic spectrometry are significantly broader than the natural width of a spectroscopic line which can be theoretically derived. The natural width of a spectral line is a consequence of the limited lifetime  $\tau$  of an excited state. Using Heisenberg's uncertainty relation, the corresponding half-width expressed as frequency is:

$$\Delta v_N = \frac{1}{2\pi\tau} \quad (34)$$

From this equation, a typical half-width of ca.  $10^{-2}$  pm is obtained for most spectroscopic lines.

The first important line broadening mechanism is *Doppler line broadening*. It results from the movement that emitting species make towards or away from the point of observation. The contribution to line broadening is:

$$\Delta v_D = 2\sqrt{\ln(2)} c v_0 \sqrt{2RT/M} \quad (35)$$

where  $c$  is the velocity of light,  $v_0$  the frequency of the emission maximum,  $R$  the gas constant and  $M$  the atomic mass. Eq. (35) suggests that Doppler line broadening is strongly temperature dependent. It has therefore also often been termed temperature broadening. It may thus be used to determine the kinetic energy of the emitting atoms or ions. For example, Doppler broadening is about 0.8 nm for the Ca(I) 422.6 nm emission at 300 K and reduced pressure (0.1 kPa), while it approaches 2 pm at 3000 K.

*Pressure or Lorentz broadening* is the second important factor for line broadening. It is a result of the interaction of the emitting species and other, non-emitting particles. Its contribution to line broadening is:

$$\Delta\nu_L = (2/\pi)\sigma_L^2 N \sqrt{\left[2\pi RT\left(\frac{1}{M_1} + \frac{1}{M_2}\right)\right]} \quad (36)$$

where  $M_1$  and  $M_2$  are the atomic masses of the two interacting species.  $N$  is the concentration of the foreign atom species and  $\sigma_L$  is its cross-section. At low pressure, the contribution of pressure broadening is low, e.g. for the Ca(I) 422.6 nm line only about 0.02 pm at 300 K and 0.9 kPa. However, with increasing pressure, this contribution becomes the dominant factor for line broadening.

Other factors contributing to line broadening are *isotopic effects* and *hyperfine structure* (as a result of the interaction between radiating and non-radiating atoms of the same species) and *Stark broadening* which are due to the interaction with electric fields.

#### 12.2.2.3 Self-absorption

Self-absorption occurs when radiation emitted by the source is absorbed by atoms of the same species in the ground state. Since the probability of re-emission of an absorbed photon is always smaller than unity, self-absorption results in a reduction of the radiation produced. The intensity distribution of an emission line is  $I_0 P_E(v)$ , where  $I_0$  stands for the intensity emitted at the line maximum, and  $P_E(v)$  for the profile function. After passage through a layer of absorbing species with a number density  $n_A$  of absorbing species, the intensity distribution is:

$$I(v) = I_0 P_E(v) \exp[-\rho P_A(v) / P_A(v_0)] \quad (37)$$

Where  $v_0$  is the intensity in the line centre,  $P_A(v)$  the absorption profile function,  $P_A(v_0)$  its value at the line centre and  $\rho$  an absorption parameter given by:

$$\rho \sim BP_A(v)n_A \quad (38)$$

$\rho$  increases with increasing Einstein coefficient for absorption and consequently is larger for transitions that are based on excitation from the ground state. It also becomes larger when the number density of species  $n_A$  increases in the source. Self-absorption is strongest in the centre of the line where absorption reaches its maximum. Thus, flatter line profiles are observed in this case. When self-absorption is so pronounced that it leads to a minimum in the intensity profile and  $\rho > 1$ , this is called *self-reversal*. Self-reversal is only seen when the radiation source exhibits a strong temperature gradient and the number densities of the analyte are high in both the hotter and the cooler zones of the source.

### 12.2.2.4 Ionisation

When the plasma is sufficiently energetic, atoms may be ionised. The degree of ionisation depends on the temperature of the plasma and the ionisation energy of the considered element. In particular, for easily ionisable species, ionic spectra also contribute to the emission spectra observed in a plasma to a great extent. The ionisation of atoms  $a$  of a particular element into ions  $i$  with liberation of electrons  $e$  is an equilibrium reaction,



whose equilibrium constant  $S_n(T)$  is the so-called Saha constant:

$$S_n(T) = \frac{n_i n_e}{n_a} \quad (40)$$

The degree of ionisation  $\alpha$  for the considered element is:

$$\alpha = \frac{n_i}{n_{\text{total}}} = \frac{n_i}{n_i + n_a} \quad (41)$$

$n_i$  and  $n_a$  are the concentrations of ions and atoms in the plasma, respectively, and can be expressed as fractions of the total element concentration:

$$n_a = (1 - \alpha) n_{\text{total}} \text{ and } n_i = \alpha n_{\text{total}} \quad (42)$$

This can be substituted into the Saha equation:

$$S_n(T) = \frac{\alpha}{1 - \alpha} n_e \quad (43)$$

The Saha equation can also be expressed in partial pressures  $p$ :

$$S_p(T) = \frac{p_i p_e}{p_a} = \frac{[(2\pi m)^{3/2} (kT)^{5/2}]}{h^3 (2Z_i / Z_a [\exp(-E_i/kT)])} \quad (44)$$

The factor 2 is the statistical weight of the free electron (which has two possible orientations for its spin),  $k$  is the Boltzmann constant ( $1.38 \times 10^{-23}$  J K $^{-1}$ ),  $m$  the mass of an electron ( $9.11 \times 10^{-28}$  g),  $h$  is Planck's constant ( $6.63 \times 10^{-34}$  J s). With the conversion to eV (1 eV =  $1.6 \times 10^{-19}$  J) the Saha equation reads:

$$\log S_p = \frac{5}{2} \log \frac{T - 5040}{T} E_i + \log \frac{Z_i}{Z_a} - 6.18 \quad (45)$$

where  $E_i$  is the ionisation energy in eV.

The Saha equation is only valid when the plasma is in (at least local) thermal equilibrium. The temperature resulting from the Saha equation is then the ionisation temperature. Under these conditions, the degree of ionisation can be calculated from the intensity of the atom and ion lines of the same element,  $I_{qp}$  and  $I_{qp}^+$ :

$$\log \left( \frac{a}{1-a} \right) = \log \left( \frac{I_{qp}^+}{I_{qp}} \right) - \log \left( \frac{g_q^+ A_{qp}^+ v_{qp}^+}{g_q A_{qp} v_{qp}} \right) + \frac{5040}{T} (E^+ - E_q) + \log \left( \frac{Z_i}{Z_a} \right) \quad (46)$$

The temperature of the plasma must be precisely known and controlled for the calculation of the degree of ionisation, as the partition functions  $Z_a$  and  $Z_i$  for the atom and ion species, respectively are strongly temperature dependent. The accuracy of the values of  $gA$  determines the accuracy of the calculation of the degree of ionisation. The line pairs Mg(II) 279.6 nm/Mg(I) 278.0 nm and Mg(II) 279.6 nm/Mg(I) 285.2 nm are very often used to calculate the degree of ionisation of an element in a plasma. When the degree of ionisation  $a$  is known, the electron pressure in the plasma can be determined. Starting from

$$\log \left( \frac{a}{1-a} \right) = \log \left( \frac{S_p(T)}{p_e} \right) \quad (47)$$

one can derive:

$$\log p_e = -\log \left( \frac{a}{1-a} \right) + \log S_p(T) \quad (48)$$

This equation may be rephrased to:

$$\log p_e = -\log \left( \frac{I_{qp}^+}{I_{qp}} \right) + \log \left( \frac{g_q^+ A_{qp}^+ v_{qp}^+}{g_q A_{qp} v_{qp}} \right) - \frac{5040}{T} (E_i + E_q^+ - E_q) + \frac{5}{2} \log T - 6.18 \quad (49)$$

which indicates that the intensity ratio of the atom and ion lines of an element changes remarkably with the electron pressure. This is particularly true for elements with low ionisation energy, such as the alkaline metals. An important consequence of this fact is the occurrence of so-called ionisation interferences.

From the above it can be concluded that there exists for each spectral line emitted by a radiation (plasma) source an optimum temperature at which its emission intensity reaches a maximum. This so-called standard temperature depends on the energy of ionisation and excitation of this element, and on the electron pressure and temperature in the plasma. The standard temperatures for many atom lines are around 4000 K, while the standard temperature of ionic lines is often around 10000 K.

## 12.2.2.5

**Dissociation**

Although atomic spectroscopy requires the presence of free atoms, highly stable radicals or molecules are also present in a radiation source and contribute to the background emission. The atomic and ionic lines are then superimposed on the molecular bands. Common species encountered in plasmas are CN, NH, NO OH, and N<sub>2</sub> or N<sub>2</sub><sup>+</sup>, but refractory reaction products may also be observed (e.g. AlO<sup>+</sup>, TiO<sup>+</sup>, or YO<sup>+</sup>). The dissociation of the molecular species within the plasma is an equilibrium reaction. It can be described by a formula similar to the Saha equation:

$$K_n = \left[ \left( \frac{2\pi}{h^2} \right) \left( \frac{m_x m_y}{m_{xy}} \right) (kT)^{3/2} \right] \left( \frac{Z_x Z_y}{Z_{xy}} \right) [\exp(-E_d/kT)] \quad (50)$$

where  $K_n$  is the equilibrium constant and the indices  $x$  and  $y$  denote the species that are produced from the dissociation of  $xy$ .

$$K_n = \frac{n_x n_y}{n_{xy}}$$

If we take the example of a metal oxide in the plasma, the degree of dissociation can be calculated from the plasma temperature, the partial pressure of the reactant (oxygen, in this case) and the dissociation energy  $E_d$ .

12.2.2.6 **Radiation Sources and Atom Reservoirs**

In the discussion of the elementary steps of atomic spectroscopy, it is essential to distinguish between “radiation sources” and “atom reservoirs”. In the former, radiation is generated which is used for the spectroscopic measurement. The latter serve to produce free atoms (or ions) from the sample. The two devices may be separated, as is the case for atomic absorption (and also atomic fluorescence), or the atom reservoir may also be the radiation source, as for atomic emission.

The volatilisation (vaporisation) and dissociation of the sample usually require highly energetic conditions to be as complete as possible. This is essential to maximise sensitivity while minimising matrix interferences at the same time. The effectiveness of volatilisation, atomisation, and excitation is dependent upon the supply of energy to the sample and is characterised by different spectroscopic temperatures. They represent an important diagnostic tool for the characterisation of atomisation conditions in the plasma:

**Rotational temperature** This is important for all processes where molecules or radicals are involved. It can be determined from the intensity distribution from the rotational lines in rotational–vibrational spectra. In most cases, diatomic molecules or radicals such as OH and CN are used as thermometric probes.

**Gas temperature** This depends on the kinetic energy of the atoms and ions in the plasma. It can be determined from the Doppler peak broadening. This is however not completely straightforward, as the contributions of Doppler and temperature line broadening have to be separated by mathematical deconvolution. Together with the rotational temperature it is an indicator for the vaporisation and atomisation capability of a plasma.

**Electron temperature** This is characteristic for the kinetic energy of the electrons. It is important for all excitation and ionisation processes that are initiated by collision with electrons. Electron temperatures are often determined from the intensity of the recombination continuum or from the energy distribution of the bremsstrahlung.

**Excitation temperature** This characterises the population of the excited levels of atoms or ions and is thus of fundamental importance for spectroscopic measurements. It can be determined from the intensity ratio of two lines of a given element in the same atomic or ionic state. Alternatively, it may be determined from a plot of the emission intensity at different lines over their excitation energies for the particular element at a defined state of ionisation.

**Ionisation temperature** This describes the equilibrium between atoms, ions and electrons in a plasma. When thermal equilibrium applies, the Saha equation can be used to calculate the ionisation temperature from the intensity ratio of an ion and an atom line of the same element. Another possibility is to calculate the ionisation temperature from the  $n_e$  value that can be obtained from Stark broadening.

In plasmas that are in thermal equilibrium, all the above temperatures are equal. That means that:

- The velocity distribution of all species in the plasma (molecules, atoms, ions, and electrons) can be described by the Maxwell equation
- The population of the different energy levels follows the Boltzmann equation
- The equilibrium between electrons, ions, and neutrals of the different species obeys the Saha equation

Real plasmas provide, even in the best cases, just an approximation to local thermal equilibrium. However, their spatial inhomogeneity is very large as concerns temperature and number density distributions of the different species. Consequently, the equilibria occur only within very small volume elements of the plasma. Table 12.1 gives an overview of the different temperatures observed in the most common excitation sources and reservoirs for atomic spectrometry.

**Table 12.1** Temperatures of different excitation sources and atom reservoirs used in atomic spectrometry.

Source	Temperature / K				State
	Rotational, $T_{rot}$	Excitation, $T_{ex}$	Electron, $T_e$	Ion, $T_i$	
Arc (d. c.)	5000	5000	5500	5000	LTE
Spark		20000	20000	20000	LTE
Inductively coupled plasma	4800	5000	6000	6000	$\approx$ LTE
Microwave plasma	2000	4000	6000	6000	non-LTE
Low-pressure discharge	600	20000	30000	30000	non-LTE

## 12.3 Atomic Absorption Spectrometry (AAS)

### 12.3.1 Introduction

Atomic absorption spectrometry (AAS) is nowadays one of the most important instrumental techniques for quantitative analysis of metals (and some few metalloids) in various types of samples and matrices. The history of atomic absorption spectrometry dates back to the discovery of dark lines in the continuous emission spectrum of the sun by Wollaston in 1802. The lines are caused by the absorption of the elements in the atmosphere of the sun. His work was taken up and further pursued by Fraunhofer in 1814. In 1860, Kirchhoff and Bunsen demonstrated that the yellow line emitted by sodium salts when introduced into a flame is identical with the so-called D-line in the emission spectrum of the sun. However, it took nearly one century before this important discovery was transferred into a viable analytical technique. In 1955, Alan Walsh published the first paper on atomic absorption spectroscopy [4]. At the same time, and independently of Walsh, Alkemade and Wilatz published the results of their fundamental AAS experiments [5, 6]. But it was the vision of Walsh and his indefatigable efforts that eventually led to the general acceptance and commercialisation of AAS instrumentation in the mid-1960s. Further instrumental achievements, such as the introduction of the graphite furnace and the hydride generation technique, in the second half of the 1960s further promoted the popularity and applicability of the technique.

### 12.3.2 Instrumentation

The instrumental requirements of atomic absorption spectrometry will be discussed in the following section. In Fig. 12.3, the essential components of an atomic absorption spectrometer are depicted schematically: a suitable radiation source, an

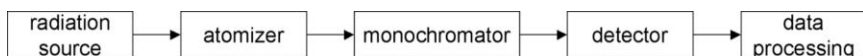


**Fig. 12.3** The essential components of an atomic absorption spectrometer.

atomiser, some optics and a monochromator, and a detector including suitable electronic signal processing [7, 8]. The individual components of an AAS instrument will be discussed in this order.

#### 12.3.2.1 Radiation Sources

For absorption-based optical methods, one has to consider the linewidth of the excitation source in relation to the linewidth of the respective transition of the absorbing species.

The half width of elemental lines is of the order of 0.002 nm when observed by emission spectroscopy with flame or electrothermal atomisation. A number of reasons can cause broadening of the linewidth, of which the most important and best understood are natural, pressure, resonance, and Doppler broadening. If a stable and sensitive detection is to be achieved, the linewidth of the excitation radiation must be narrower than the full width at half maximum (FWHM) of the analyte line. Under these conditions, the entire radiant energy produced by the excitation source will be available for absorption by the analyte. The typical line sources used for atomic absorption are element specific excitation sources such as the hollow cathode lamp or the electrodeless discharge lamp. But even continuum sources can be used with appropriate instrumental designs.

**The hollow-cathode lamp** Initially described in 1916 by Paschen, the hollow cathode lamp (HCL) is probably the most versatile excitation source for atomic absorption spectrometry. A schematic of this excitation source is given in Fig. 12.4. It consists of a Pyrex glass tube in which the cathode and anode are located under an

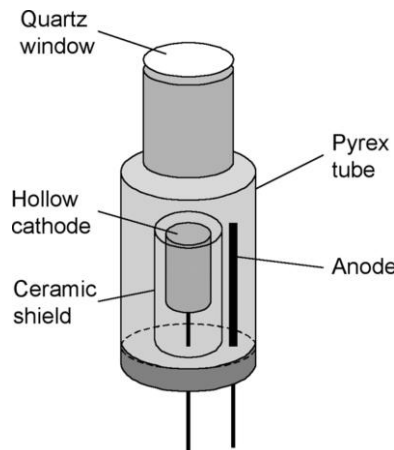


**Fig. 12.4** Schematic of a hollow-cathode lamp.

inert gas atmosphere (neon or argon) at a pressure of typically 1–5 torr. The hollow cathode is made from (or coated with) the respective element, and the anode is a strong nickel or tungsten wire. The two electrodes are separated by a ceramic shield. At the front end of the hollow cathode lamp, a quartz window transparent in the UV/vis spectral range is attached.

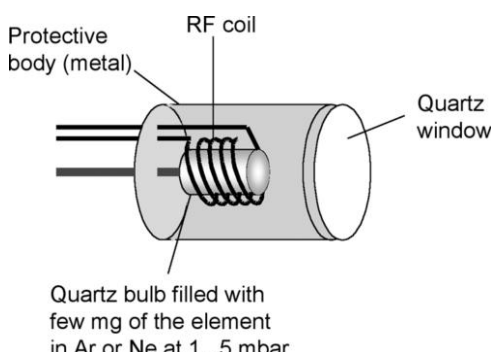
The emission is generated by applying a voltage of typically 350 V to 500 V across the electrodes which leads to a current of 1 to 50 mA, resulting in an electrical discharge. Positive noble gas ions are accelerated towards the hollow cathode where their impact sputters atoms of the element to be determined from the hollow cathode. The sputtered metal ions are then excited through collisions with Ne or Ar ions in the gas phase. The metal ions return to the ground state by emitting radiation at characteristic wavelengths. The typical half-width of an atomic emission line produced by a HCL is approximately 0.0002 nm which fully complies with the requirements for an AAS line source discussed above.

The intensity of radiation produced by a HCL is proportional to the number of sputtered and excited atoms and will thus depend on the kinetic energy of the inert gas ions which is controlled by the lamp current. Although the increase in lamp current produces a higher radiance and thus provides a higher sensitivity, there is, however, an upper limit for the HCL current for practical reasons: At high lamp currents, a large number of metal atoms are sputtered and brought into the gas phase. In this dense cloud of gas phase metal atoms self-absorption reduces the intensity of the element-specific radiation, resulting in a reduction in sensitivity. Ideally, the sputtered metal atoms are re-deposited on the hollow cathode upon radiative de-excitation. However, the metal atoms may also be transported and be deposited on the glass walls of the HCL which reduces the lifetime of the lamp. For this reason, the geometry of the cathode walls is optimised and a protective shield is placed around the cathode.

In addition to single-element hollow cathode lamps, multi-element HCLs are also available and provide multi-element excitation capabilities with one single hollow cathode lamp at a price that is comparable to a single-element HCL. Their principle of operation is the same as for single element lamps, with the cathode being made either from an alloy or from pressed powders of the respective elements. Although they represent a significant improvement for multi-element AAS measurements (and make the exchange of HCLs obsolete when several elements are to be determined) they have some practical drawbacks: Their lifetime is typically shorter than that of single-element HCLs, since the elements used for the production of the HCL have different volatilities. The element with the highest volatility will be preferentially sputtered and, with time, it will cover all other elements in the HCL, making them inaccessible to sputtering by accelerated gas ions. This will cause the sensitivity of the less volatile elements to diminish over time and will eventually shorten the effective lifetime of the HCL.

**The boosted hollow-cathode lamp** A very intense radiation source for AAS is the boosted hollow-cathode lamp. It has been developed from the regular hollow-cathode lamp and includes a second pair of electrodes between which a boosted

**Fig. 12.5** Scheme of an electrodeless discharge lamp.



discharge is initiated, using the existing instrument lamp current supply. Via this discharge, the excitation of the sputtered atoms is increased significantly while self-absorption is minimised. As a result, the emission intensity is 5–15 times higher than for a standard HCL, which significantly improves the signal-to-noise ratio.

**The electrodeless discharge lamp** The electrodeless discharge lamp (EDL) is another atomic line source that allows one to produce a highly effective excitation source for elements that cannot be cast into hollow cathodes, such as mercury, arsenic, antimony, and some other elements.

The EDL is produced by filling a small quartz bulb with some few milligrams of the respective element under an inert gas atmosphere (usually argon) at reduced pressure and then sealing this tube. The quartz bulb is located in the center of a radio frequency (RF) coil (Fig. 12.5). When a RF field, typically oscillating at 27.12 MHz, is applied to the coil, the argon atoms are ionised. The collision of free atoms of the particular element in the gas phase with the electrons produced by ionisation of the argon leads to their excitation and subsequent radiative relaxation. While the EDL produces element-specific radiation of greater intensity than the HCL, its use is restricted to the more volatile elements. It also requires a separate power supply that provides the RF current.

**Continuum sources** The disadvantage of having to change hollow cathode lamps for every new element to be determined explains the interest in continuum light sources in AAS. However, as the line width of the absorbing species (0.0002 nm) is typically much smaller than the bandpass of common monochromators (0.1 to 0.2 nm) this approach is limited in practice [9]. This would mean that a large fraction of the light reaching the detector is not at the characteristic wavelength of the element. The small fraction of light that is actually absorbed by the atoms at their characteristic excitation wavelength would result in only a low analytical sensitivity. Echelle grating monochromators with their smaller spectral bandpass have, in part, overcome this shortcoming of continuum light source AAS, but still the sensitivity that can be reached is smaller than with narrow linewidth atomic line sources. Continuum sources that are currently used are the high-intensity xenon arc

lamp and the deuterium lamp, the former being preferred owing to its higher brilliance.

Although the presently realised continuum-source AA spectrometers are still operated sequentially for multi-element detection, it may be anticipated that, with use of suitable optics and multi-array detectors, this method will become a truly simultaneous multi-element technique [10].

**Diode laser sources** Already in 1980, lasers had been suggested as excitation sources for atomic absorption spectrometry [11]. Tunable dye lasers can provide virtually any atomic line between 213 and 900 nm with a bandwidth corresponding to the natural line width of an atomic line and with a comparatively high intensity. However, they have not found widespread acceptance for this application so far due to their cost and complex operation compared to hollow cathode or electrodeless discharge lamps. This situation seems to have changed with the advent of inexpensive, mass produced diode lasers (DL) [12, 13].

DLS provide a radiant output which can be several orders of magnitude higher than that of common HCLs. Together with their excellent stability (both in terms of wavelength and intensity), this accounts for an improvement in signal-to-noise ratio which brings about a 1–2 orders of magnitude improvement in the detection limit when compared with HCLs.

The typical line width of a commercial DL is approximately two orders of magnitude lower than that of atomic absorption lines in flames and furnaces. This allows one to expand the linear dynamic range of the method by tuning the DL to the wings of the absorption line where optically thin conditions prevail. Also, due to the simplicity of DL emission (which basically emit one single line) the requirements for the monochromator are much lower, allowing the construction of simpler instruments.

The possibility of modulating the emitted wavelength of DLs at GHz frequencies by the modulation of the diode current allows one to reduce the low-frequency (flicker) noise in the baseline, which again improves the detection limit. Emission wavelength modulation also permits to correct for unspecific background absorption, thereby improving the selectivity of the technique.

Constraints for the use of DLs in AAS arise from their limited availability with emission wavelengths in the range 190–315 nm, which is also inaccessible with frequency doubling techniques. This however will most likely not remain a fundamental limitation, as the development of short wavelength diode lasers is driven by the telecommunication and electronics industry.

### 12.3.2.2 Atomisers

Atomic absorption spectrometry requires that the species under investigation prevails in the gaseous and atomic state so that absorption of free atoms can be observed. The two most common methods for the production of atoms in the gas phase make use of thermal energy to vaporise and atomise the analyte. The sample transfer efficiency, i. e. how much of the sample is reaching the actual atomisation zone,

and the atomisation efficiency that tells which fraction of the analyte is released in atomic form from its compounds, determine the overall efficiency. These two factors are important and directly related to the sensitivity that can be achieved with the particular method of atomisation.

**Flame atomisation** In flame atomisation, the sample solution is introduced into the flame with a particularly designed nebuliser (Fig. 12.6). The function of the nebuliser is to disrupt the continuous sample stream into a mist of fine droplets of typically 5–20 µm diameter which are swept into the mixing chamber. The aerosol is then mixed with the fuel gas and the oxidant gas before reaching the burner head. As a number of physical and chemical reactions, e.g., vaporisation, dissociation, reduction, or oxidation, may occur, it becomes evident that precise control of the operating conditions of flame atomisation is required to obtain stable and sensitive signals. Optimisation of flame atomic absorption measurements has thus the double role of maximising the element's response while minimising the undesired side-reactions.

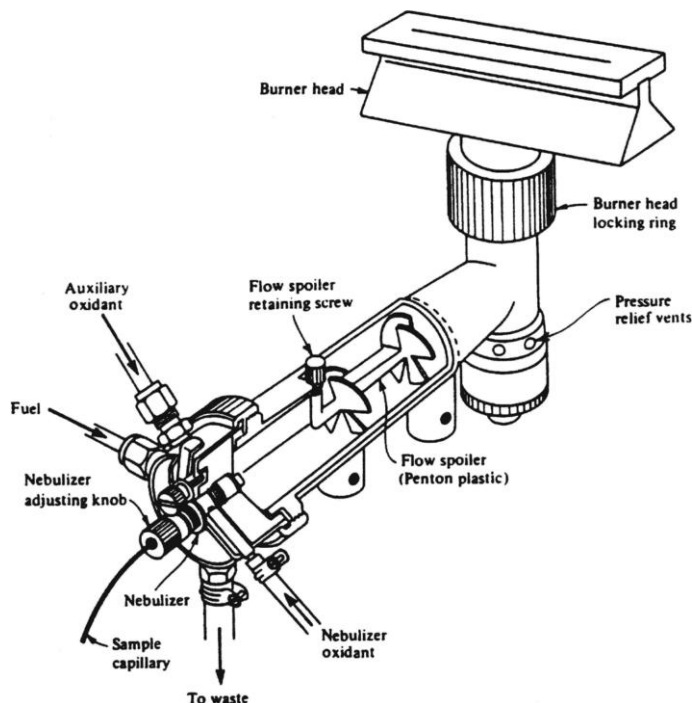


Fig. 12.6 Design of a laminar flow burner (Courtesy of the Perkin-Elmer Corporation, Norwalk, CT).

### Nebulisers

The most common type of nebuliser is the concentric tube nebuliser which consists of a capillary through which the liquid is introduced and an outer tube of larger diameter with a nozzle at its end. Through this outer tube, the nebuliser gas stream is directed at high pressure and achieves both transport of the liquid sample stream by aspiration and disruption of the continuous supply of sample. The advantage of this nebuliser type is its simple construction and the fact that it is self-aspirating. Other nebuliser types are in use, such as the cross-flow nebuliser where the high pressure gas flow is directed perpendicular to the capillary from which the liquid emerges. This type of nebuliser requires the liquid to be pumped through the capillary which reduces the effect of viscosity on sample introduction. The high pressure gas is usually the oxidant, while the fuel gas is mixed subsequently to the sample aerosol.

### Burner design

The aerosol is sprayed into the mixing chamber which serves two functions: First, the fuel gas and additional oxidant gas are added (if required) and pre-mixed to achieve optimum flame conditions. Second, droplets larger than ca. 20 µm in diameter are prevented from reaching the flame by arranging flow spoilers inside the mixing chamber. As a concentric tube nebuliser produces an aerosol of rather wide droplet size distribution, it is important to preclude the droplets of larger diameter from being transported into the flame. Due to the short residence time of the sample in the flame, large diameter droplets are not completely desolvated and atomised and thus increase the background noise of the flame. They are separated from the smaller diameter droplets by impacting on baffles and are drained to waste. Therefore, only less than 10 % of the actual sample being converted to an aerosol reaches the burner head.

The burner head is constructed in the form of a long narrow slit (“laminar flow burner”). The long slit through which the flame expands (typically 10 or 5 cm) increases the absorption path length and thus also the sensitivity.

A point of critical importance in the AAS system is the optimisation of fuel and oxidant gas flow ratios. Although fuel and oxidant gases are usually combined in approximately stoichiometric ratios, the determination of certain elements may require significantly different ratios.

Typical flame gas mixtures and resulting flame temperatures are given in Tab. 12.2. Early AAS work was carried out with natural gas/air- and hydrogen/air-flames and was focused mainly on those elements that, although easy to atomise, were difficult to excite due to the short excitation wavelengths, i.e., Zn (213.8 nm), Cd (228.8 nm), Ni (232.0 nm), and Pb (283.3 nm). The use of hotter flames became necessary, however, as it was realised that a higher temperature is required for complete atomisation (particularly for Al, Ti, or Si). While oxygen/natural gas or oxygen/acetylene mixtures can easily produce significantly higher flame temperatures, they require a particular burner head design that allows stable and safe operation even at the very high burning velocities of these gas mixtures.

**Table 12.2** Typical gas mixtures and flame properties for flame-AAS.

<b>Fuel</b>	<b>Oxidant</b>	<b>Flame Temperature/°C</b>	<b>Maximum Burning Velocity/cm s<sup>-1</sup></b>	<b>Burner Slot/mm</b>
Natural gas	Air	1700–1900	39–43	100 x 1.5
Natural gas	Oxygen	2700–2800	370–390	
Hydrogen	Air	2000–2100	300–440	
Hydrogen	Oxygen	2550–2700	900–1400	
Acetylene	Air	2100–2400	158–266	100 x 1.5
Acetylene	Oxygen	3050–3150	1100–2480	
Acetylene	Nitrous oxide	2600–2800	285	50 x 0.5

The burning velocity is the velocity at which the flame expands in a premixed fuel/oxidant gas mixture. If the burning velocity is larger than the flow rate of the burner gas mixture, the flame propagates back into the burner, resulting in a flashback and potentially causing ignition of the explosive mixture in the mixing chamber. At higher flow rates a point is reached where the flow velocity equals the burning gas velocity, so that a stable operation of the flame is achieved. If the flow velocity is further increased, the flame rises and eventually reaches a point where the flame is blown off the burner head. The extremely high burning velocities of oxygen/natural gas or oxygen/acetylene mixtures make their use in flame AAS very inconvenient and hazardous. A significant breakthrough was the introduction of the nitrous oxide/acetylene flame which permits operation at reasonable burning velocities. However, the burner design has still to be modified for nitrous oxide/acetylene flames in contrast to air/acetylene- or air/natural gas flames, that is, both the length and width of the burner head slit are of particular dimensions. This design provides a more efficient heat sink for the flame than with the larger dimension slit and thus reduces the risk of flashback.

Flames that operate in fuel-rich conditions are sometimes called “yellow” flames, while flames that are operated under fuel-lean conditions are often called “blue” flames. While the latter are oxidising flames, the former provide reducing conditions which may be advantageous for the determination of certain elements. The atomisation of an analyte is not homogenous throughout the flame, as the production of free atoms in the flame is governed by the variation in temperature in the different zones of the flame, as well as by the rate of diffusion of the flame gases that dilute the free atom population in the observation zone. For highest sensitivity, the radiation from the light source must be directed through the zone of the flame that contains the highest concentration of free atoms. To meet this condition, the height and alignment of the burner head relative to the light path must be carefully optimised.

**Electrothermal atomisation** In the late 1950s, L'vov made the first attempts to use a graphite furnace for the atomisation of the sample in AAS [14]. It did however take until the early 1970s before the first graphite furnace (GF) or electrothermal (ET) atomisers were introduced onto the market. Measurements by electrothermal

AAS are discontinuous, and an analysis cycle comprises the following four steps: (1) The sample is introduced into the cold graphite furnace, (2) the solvent is evaporated at temperatures of around 100 °C, (3) the sample is ashed and any volatile sample constituents are removed by keeping the sample for ca. 1 min at 450–900 °C before (4) the temperature is rapidly increased to 2000–3000 °C to vapourise and atomise the sample in a very short interval (milliseconds to a few seconds). The entire cycle can be accomplished in about 1 min due to the fast heating rates achieved by direct electrical (resistive) heating of the graphite furnace at currents of up to 400 A and a voltage in the order of 8 V (see Fig. 12.10).

The graphite furnace (Fig. 12.7) comprises the following features: The cylindrical graphite tube is open at both ends and has, typically, a length of 18–28 mm and an internal diameter of 6–10 mm. At its centre, it has a small hole through which the sample (typically 5–20 µL) is introduced automatically. At its ends, the graphite tube is tightly fitted into a pair of water-cooled graphite ring electrodes through which the heating current is provided. The entire furnace is purged with argon to exclude air from the graphite tube and to prevent its incineration at high temperatures. An additional argon gas stream is directed from both ends of the tube towards the centre to purge vapors from the sample matrix generated during the vaporisation and ashing step. Argon has excellent optical transparency in the UV region which is important for the detection of elements at short wavelength. Despite the use of an inert gas atmosphere, the graphite tubes are severely affected during the heating cycles and must routinely be replaced after about 100 analyses.

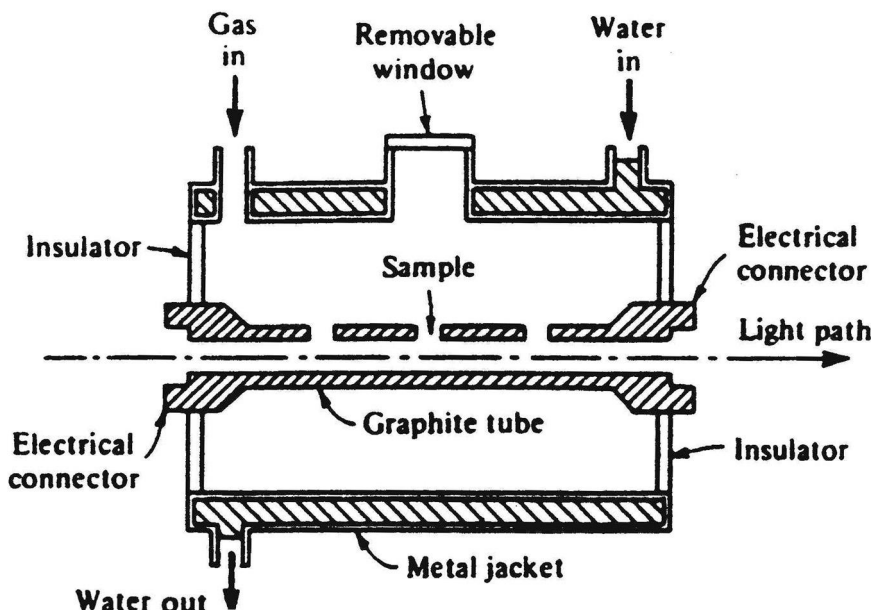
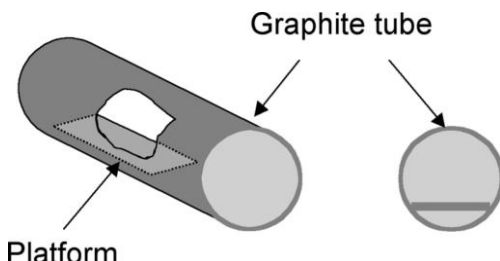


**Fig. 12.7** Cross-sectional view of a graphite furnace (Courtesy of the Perkin-Elmer Corporation, Norwalk, CT).

**Fig. 12.8** The L'vov platform and its position in the graphite furnace (redrawn after W. Slavin, *Anal. Chem.*, 54, 1982, 689A)



Although this technique offers a much improved sensitivity in comparison with flame AAS, due to the fact that the entire sample is atomised and that the concentration of free atoms is very high in the restricted volume of the graphite tube (ca. 2 mL), some disadvantages arise from the use of graphite tubes with the above-mentioned design. As the graphite tube is rapidly heated, it will be considerably hotter than the gas phase in the centre of the tube. Thus analyte atoms are evaporated into a significantly cooler zone where they may recombine and further condense. This disadvantage has been alleviated by the introduction of the sample onto a small platform (L'vov platform) of graphite that is located in the centre of the graphite tube (Fig. 12.8). The heating characteristics of the modified graphite tube remain essentially unaltered compared to those without a platform. However, since the platform has only a limited heat capacity, it will basically be heated by radiation from the tube walls. This will cause the temperature of the platform to lag somewhat behind the platform of the tube walls. The analyte will thus be volatilised with delay when compared to a graphite tube without platform, and it will also evaporate into an atmosphere that is significantly hotter than with wall atomisation. In this way the platform reduces interferences that arise from temporal non-isothermality. However, graphite furnaces of this design still have a remarkable spatial non-isothermality due to the water cooled electrical contacts acting as effective heat sinks. The graphite tube has its highest temperature in the centre and becomes cooler towards its ends. Elements of low volatility may therefore condense after initial volatilisation or adsorb on cooler wall regions located away from the tube centre. During a subsequent atomisation sequence, re-vaporisation of the analyte may occur and lead to memory effects since the ends of the tube initially also attain higher temperatures. For this reason, the transversely heated atomiser has been introduced that provides spatial isothermality through which condensation and memory effects are notably reduced (Fig. 12.9).

It has, furthermore, been observed that some of the sample matrix effects and the poor reproducibility sometimes associated with graphite furnace atomisation can be improved by reducing the natural porosity of the graphite tube. It appears that part of the analyte and matrix diffuse into the pores of the tube. This slows down the atomisation process and causes smaller analyte signals or memory effects due to re-vaporisation in a subsequent analysis cycle. To reduce the porosity, the graphite surfaces are covered with a thin layer of pyrolytic carbon through which the pores of the graphite tube are sealed.

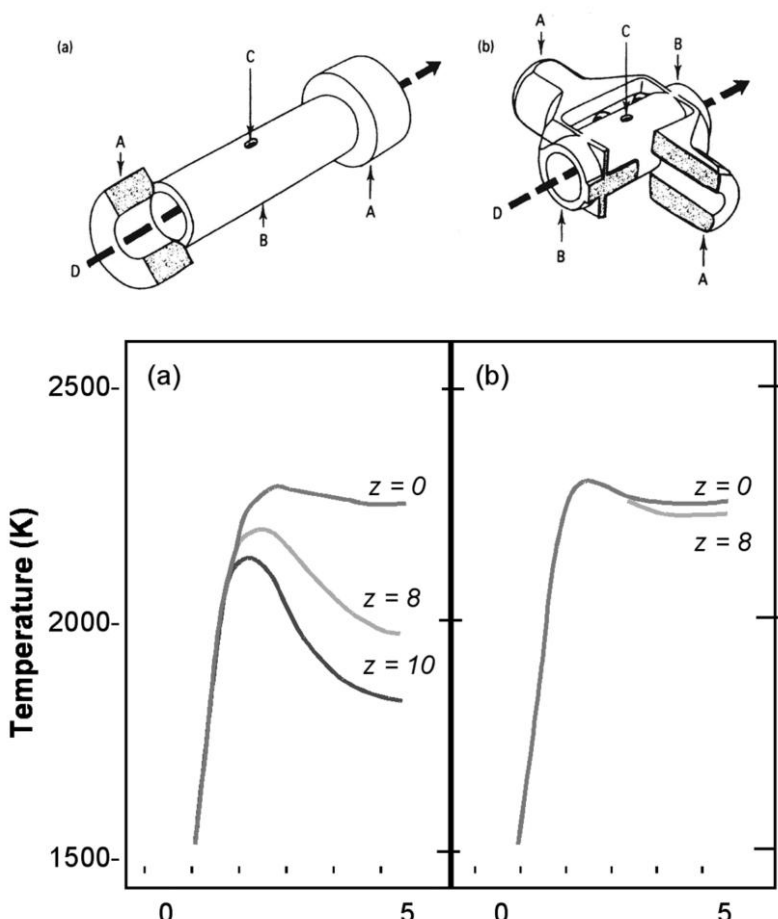


**Fig. 12.9** End-heated (a) and side-heated (b) electrothermal atomiser configuration and temperature profiles associated with these furnace designs. A, water-cooled electrical graphite contact cylinders; B, graphite tube; C, sample injection port; D, light path of the spectrometer. The value of  $z$  denotes the distance from the centre (in mm) at which the temperature profiles have been recorded for a graphite tube of 28 mm length.

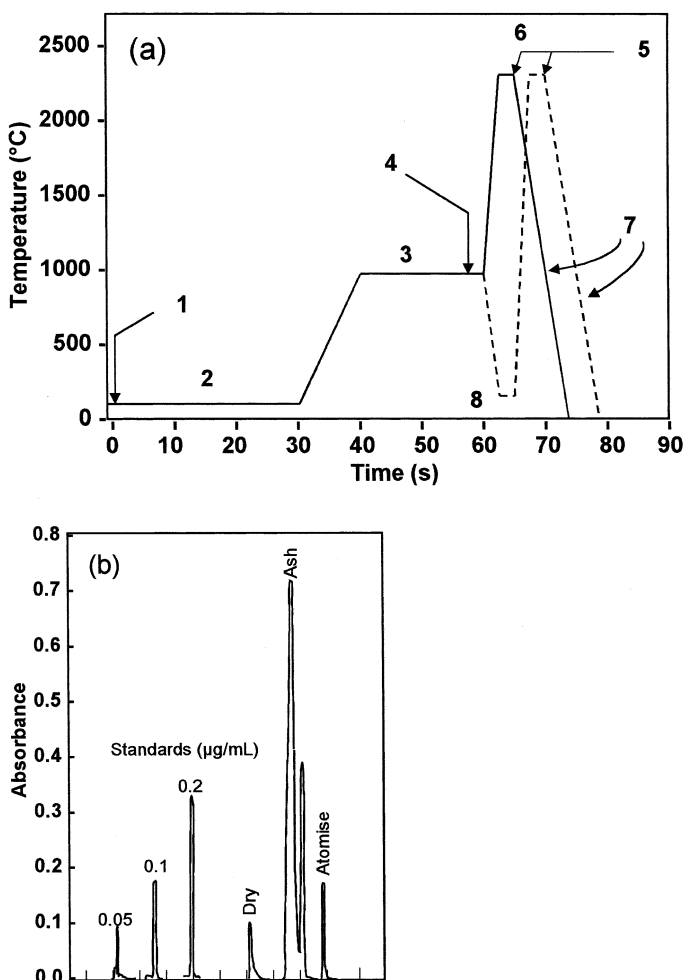


**Fig. 12.10** (a) Schematic temperature program of the graphite furnace (1, Ar flow on; 2, drying; 3, ashing; 4, Ar flow off; 5, Ar flow on; 6, atomisation step; 7, cooling period; 8, cool-down-procedure) and (b) typical signal output of a graphite furnace AAS measurement.

**Vapor generation techniques** The generation of gaseous analytes from the sample and their introduction into atomisation cells for subsequent absorption spectrometric determination offers a number of advantages over the conventional sample introduction by pneumatic nebulisation of the sample solution. These include the elimination of the nebuliser, the enhancement of the transport efficiency, which approaches 100 %, and the presentation of a homogenous sample vapor to the atomiser. The most common and versatile techniques for the formation of volatile compounds are the hydride generation technique and the cold vapor technique.

Other techniques for the formation of volatile compounds, such as volatile chlorides or volatile organic complexes (e.g.  $\beta$ -diketonates or dithiocarbamates) have also been used, although rarely, and will thus not be discussed in the following.

The versatility and general acceptance of vapor formation techniques in AAS result from the various advantages that they offer:

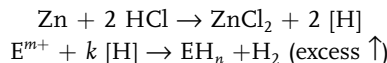
- Separation of the analyte from the matrix is achieved which improves the accuracy of the determination.
- Preconcentration of the analytes is easily implemented and allows one to improve concentration detection limits significantly.
- Different chemical species can be discriminated in some cases.
- The procedures are readily accessible to automation.

Only a few disadvantages are quoted for vapor generation techniques. These include the (chemical) interferences, notably in the presence of transition metals, a pronounced pH-effect on the reaction, and its dependence on the oxidation state of the element, which, however, can also be advantageously used for speciation analysis, and finally gas-phase atomisation interferences which may be caused by the presence of other volatile hydrides.

Vapor-generation techniques comprise the following three steps: (1) Transformation of the analyte into a volatile form, (2) its collection or preconcentration (if necessary) and transfer to the atomiser, and (3) decomposition of the volatile compounds to liberate the free analyte atom (not necessary for mercury) with subsequent measurement of the atomic absorption signal.

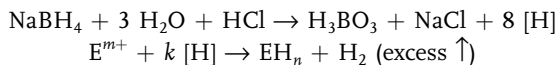
#### **Hydride generation technique**

A number of different reactions have been described for the formation of covalent volatile metal hydrides, which all have as a common denominator that they rely on the formation of atomic hydrogen as reducing agent [15]. For the generation of volatile hydrides of arsenic, antimony, and selenium ( $\text{AsH}_3$ ,  $\text{SbH}_3$  and  $\text{H}_2\text{Se}$ ) the well-known reaction of Zn with concentrated hydrochloric acid may be employed:



In the above equation, E represents the analyte element, and  $m$  may be, but need not necessarily be, equal to  $n$  (e.g. when the analyte occurs in various oxidation states). Reduction by Zn/HCl requires that the analytes be present in their lower oxidation states prior to reaction. When this is not the case, the analytes must be reduced, e.g. by  $\text{SnCl}_2$  in an acidic medium. The formation of volatile hydrides (and of excess hydrogen) is then initiated by the addition of zinc metal. This reaction is rather inconvenient, since it is slow, difficult to automate, and subject to high blank values due to the impurities of the zinc. Also its efficiency is limited as a consequence of incomplete reaction and the possibility of adsorption or entrapment in the zinc sludge of the volatile metal hydrides formed. Due to these disadvantages, the use of this procedure has nowadays been practically abandoned.

Instead, the far more effective sodium tetrahydroborate reagent is used that reacts according to:



The higher reactivity of this reagent allows its use for the formation of volatile hydrides of antimony, arsenic, bismuth, germanium, lead, selenium, tellurium, and tin. This method is not only superior to the Zn/HCl method due to the wider range of elements that are accessible, but also with respect to speed, efficiency of the reaction, and reduced contamination. The reaction is essentially completed within 10–30 s, and the reagent is typically added into the acidified samples as 0.1–10% (w/v) solution. These factors contribute to the ease of automation which has been a key factor in the success of the hydride generation technique.

The preferred acid for this application is hydrochloric acid,  $\text{HNO}_3$  and  $\text{H}_2\text{SO}_4$  have also been used, although less frequently. The optimum acid concentration is a parameter of careful optimisation and may vary considerably, depending on the element and the matrix. It may range from as low as 0.1–0.2 mol L<sup>-1</sup> for tin and lead to up to 9 mol L<sup>-1</sup> for antimony, arsenic, and bismuth. Only two disadvantages have to be mentioned for the tetrahydroborate reduction: The reagent is not completely free from contaminants (particularly tin) which limits the achievable detection limits, and the generation of a large excess of hydrogen may be a significant hindrance, although this is usually not the case for atomic absorption rather than for other spectroscopic techniques.

Hydride generation-AAS may be carried out in batch systems (where the  $\text{NaBH}_4$  may even be added as pellets), in continuous generation systems where the sample and the reducing agent are pumped continuously into the reaction chamber, and then further to a gas–liquid phase separator, and into a flow injection (FI) system. In such a system, discrete amounts of sample are injected into a flowing carrier stream which is merged with the reagent streams. Reaction takes place in a reaction coil, and the volatile hydrides are purged in a gas–liquid phase separator and carried to the atomisation cell (Fig. 12.11).

The most widely used atomiser for hydride generation is the heated quartz T-tube atomiser with a typical diameter of 10 mm and a length of 100–150 mm, making it compatible with the optical path of most AA spectrometers. The quartz tube is electrically heated to 700–1000 °C which permits one to optimise the atomisation temperature for each element. The quartz tube may either have open ends, or these ends are sealed by removable quartz windows, and holes at the extreme ends of the quartz tube provide the gas flow outlets. This set-up increases the residence time of the atoms in the light path and thus improves sensitivity. With continued use the performance of the quartz tube atomiser invariably deteriorates in terms of sensitivity and precision. This is attributed both to devitrification of the inner surface of the quartz tube to a less inert modification, and to contamination of the inner atomiser surface by deposition of small particles and droplets that were not efficiently removed by the gas–liquid phase separator.

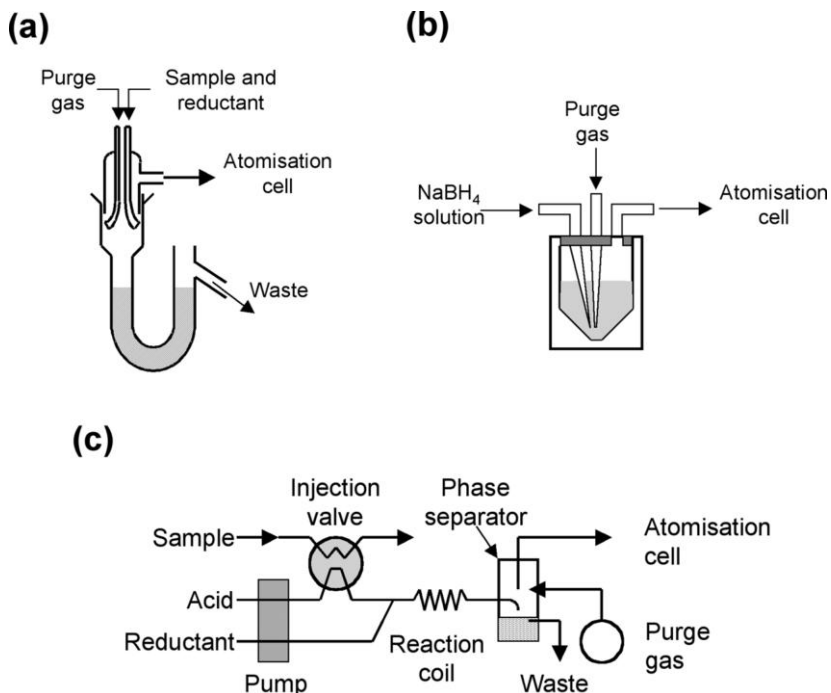
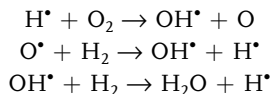
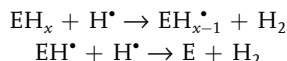


**Fig. 12.11** Hydride generation systems. (a) Batch generation, (b) continuous generation, and (c) flow injection generation.

The decomposition of hydrides to form free atoms is mainly due to the reaction with hydrogen radicals, but oxygen also plays an active role. The following reactions may take place within a quartz tube atomiser:



The concentration of the hydrogen radical in the atomiser tube is several orders of magnitude higher than that of the hydroxyl radical. Thus if a metal hydride is introduced into the quartz tube, it will undergo the following subsequent reactions, leaving finally the free atom in the gas phase:



In addition to this process, thermal decomposition of the hydrides is also supposed to take place, however, only if the oxygen supply to the atomiser is insufficient. Thermal decomposition is the dominant atomisation process in the graphite furnace.

### Cold vapor generation technique

Mercury is the only metallic element that is liquid and sufficiently volatile at room temperature. These particular properties make this element uniquely suited for determination without an atomiser after reduction to the elemental state and transfer into the vapor phase and into the optical path of the absorption spectrometer [16]. As is the case for hydride generation systems, the technique lends itself to both batch and flow injection procedures which are becoming increasingly popular. A typical cold vapor generation system is depicted in Fig. 12.12. For historical reasons, tin(II)chloride has been widely used as reducing reagent, but it is now being replaced by  $\text{NaBH}_4$ . Since the latter is a more powerful reducing reagent, particular precautions must be taken to avoid interferences which may have adverse effects on the preconcentration (amalgamation) trap which is normally used. Helium is preferred to purge the elemental mercury from the sample solution. Either a chemical desiccant or a glass fibre filter is positioned between the reaction vessel and the amalgamation trap to prevent small water droplets from reaching the trap (which is more tolerant to water vapor). The material for the reaction vessels and all tubing must be selected with particular consideration to avoid permeation or adsorption of mercury. Quartzware and fluorinated ethylene/propylene (FEP) are suitable materials showing only little adsorption of mercury, while polytetrafluoroethylene (PTFE) is said to be the most appropriate material for the transport of gaseous mercury.

Similar to hydride generation, the mercury vapor can be directly introduced into the absorption cell. However, due to the fact that vapor formation from the liquid phase is rather slow, requiring a period of typically 1–2 min, this would result in broad peaks of low intensity. Consequently, a trap is used to preconcentrate the generated Hg vapor and to improve the concentration detection limit for analysis

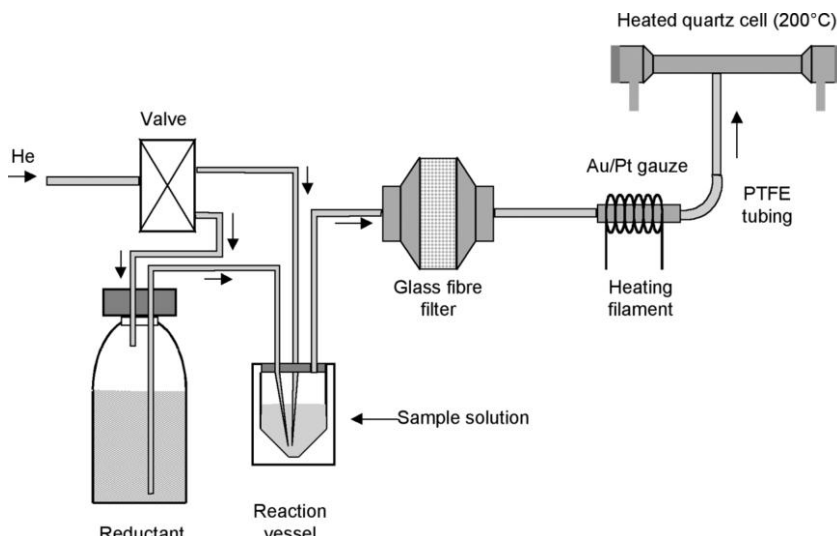


**Fig. 12.12** Scheme of a cold vapor generation system for mercury (redrawn from [17]).

in solution [17]. This is achieved by amalgamating mercury on a noble metal trap, from which it is subsequently thermally desorbed at 500–700 °C. In many instances, a gold–platinum gauze (90 % Au, 10 % Pt) is used for this purpose. It provides a high surface area, excellent thermal conductivity, ease of cleaning, and good physical stability. This results in excellent performance in terms of reproducibility and signal enhancement.

Since mercury is present already in the atomic state in the cold vapor technique, there is no need for an atomiser as such. The sample vapor is swept directly from the reduction cell or the amalgamation trap in the carrier gas stream to a 10 cm length T-shaped quartz tube that is moderately heated (to ca. 200 °C to prevent condensation of mercury). This quartz cell is located in the light path of a conventional AA spectrometer where the attenuation of a characteristic Hg line source is measured. Dedicated AA spectrometers (which, in this case, often have a continuum light source) may also be used with longer absorption cells (300 mm pathlength) to increase the sensitivity.

**Direct introduction of solid samples** Both flame and electrothermal AAS principally allow the direct introduction of solid samples. For flame AAS, cups may be used to introduce the solid sample, as suggested initially by Delves [18]. Alternatively, organic samples may be combusted and the vapors directed directly into the flame. Although the direct introduction of solid powders into the graphite furnace was already reported in the early 80s [19], the analysis of sample slurries is preferable. Slurry sample introduction has been pioneered for flame AAS by Ebdon and Cave [20] who also demonstrated its applicability to graphite furnace AAS. Solid sample introduction must, however, be used with particular attention: Since the amount of sample introduced is normally small, a few milligrams are normally used, sample homogeneity and the avoidance of potential sampling errors become an important issue. For this reason, the use of larger furnaces which may accept larger sample sizes has been suggested. Calibration for solid sample analysis is generally difficult, since the nature and particle size of the solid affect analyte volatilisation, transport and consequently its response.

For the analysis of solid samples without prior digestion, the combination of cathodic sputtering with AAS has been proposed [21]. Jet-enhanced sputtering gives a high analyte number density and the atom vapor cloud is introduced into the flame or electrothermal atomiser. This approach is particularly feasible for the analysis of samples which are difficult to dissolve, such as refractory oxide-forming metals and alloys.

Laser ablation-AAS is also useful for insulating samples, where AA analysis is performed directly in the laser plume. Due to the production of various particles in the measurement zone (solid particles, molecules, radicals) and the resulting background emission, appropriate techniques for the correction of spectral interferences must be used.

### 12.3.2.3 Optical Set-up and Components of Atomic Absorption Instruments

Instruments for atomic absorption spectrometry can generally be divided into single- and double beam designs. The sophistication and consequently the cost of the instruments span a very wide range.

The optical system of an AA spectrometer must provide a spectral resolution sufficient to separate the chosen analytical line from other lines that may interfere. Only in the case of some alkali metals which have some few widely spaced resonance lines across the visible spectrum, may this be achieved by simple filter monochromators. For the determination of most elements, however, high quality UV/VIS monochromators are required that are capable of achieving a spectral bandwidth of the order of 0.1 nm. Such monochromators are nowadays implemented in most commercial AA instruments. The optical components used (particularly, monochromators and detectors) are very similar to those used for emission spectroscopy and will be discussed in more detail later.

**Single beam spectrophotometer** The typical design of a single-beam spectrophotometer is shown in Fig. 12.13. It is constructed using an absolute minimum of optical components with the evident advantage of high optical throughput and relatively low cost. The simplicity of this system is however at the price of limited stability of the system, since any fluctuation in light source intensity will result in baseline variation.

**Double beam spectrophotometer** The optical set-up of a double-beam spectrophotometer is given in Fig. 12.14. The beam from the light source is divided into two paths of light, one of which passes through the flame, while the other is directed around the atomiser. These two light beams are subsequently recombined and modulated by a rotating (mirrored) chopper that alternately transmits the beams to the Czerny–Turner grating monochromator. The two signals are detected by a photomultiplier tube and ratioed before further amplification and electronic signal processing. Double beam spectrophotometers, being more complex and costly, offer the advantage of compensating any variations in light source intensity. However, radiant power loss through absorption and scattering effects in the flame are

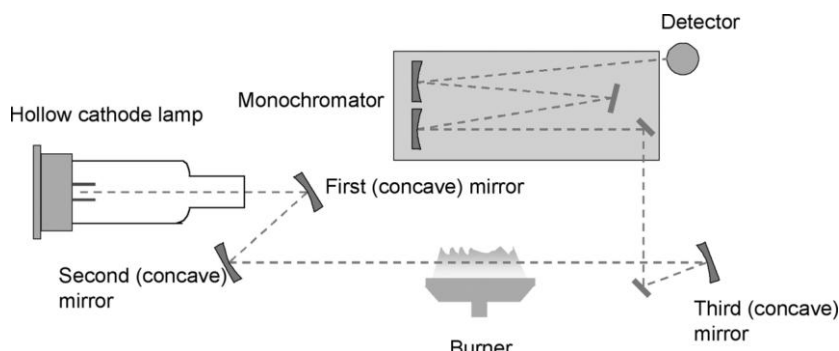
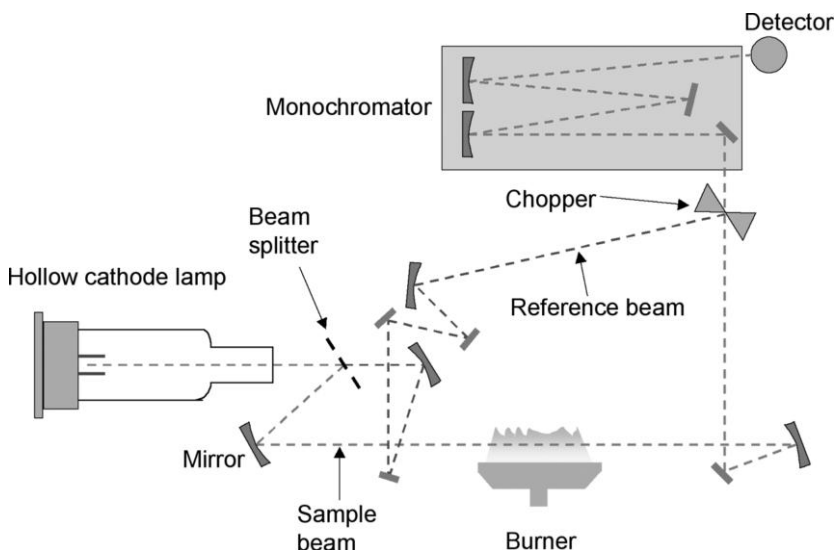


Fig. 12.13 Optical system for a single-beam atomic absorption spectrophotometer.



**Fig. 12.14** Optical system for a double-beam atomic absorption spectrophotometer.

still not accounted for, since the reference beam bypasses the flame. Methods for the correction of these optical losses are discussed in the following section.

Detection is normally done with photomultiplier tubes, or, for instruments that incorporate echelle-grating based polychromators, with solid state detectors consisting of a two-dimensional array of photodiodes.

### 12.3.3

#### Spectral Interferences

Two types of interference are encountered in atomic absorption spectroscopy: *Spectral interference* is a result of the absorption of an interfering species that either completely overlaps with the signal of interest or lies so close to this signal that it cannot be resolved by the monochromator. *Chemical interference* may be a consequence of the various chemical processes that occur during atomisation and alter the absorption characteristics of the analyte.

Spectral interferences can, to a certain degree, be compensated or eliminated by suitable instrumental designs and analytical procedures.

##### 12.3.3.1 Origin of Spectral Interference

As the emission lines of hollow cathode lamps are very narrow, interference due to overlapping lines is rather unlikely. The separation between two spectral lines would have to be less than typically 0.01 nm for such an interference to occur. As an example, the vanadium absorption line at 308.211 nm interferes in the anal-

ysis of aluminum at 308.215 nm. A simple alternative is to carry out the measurement at a different (intense) aluminum absorption line, e.g. at 309.270 nm.

Spectral interferences may also result from combustion products that exhibit broad-band absorption or particulate matter that causes scattering of the incident radiation. As both reduce the spectral radiance of the light source, they may erroneously lead to an overestimation of the absorbance and, consequently, the concentration. When the combustion or the particulate products arise from the fuel and oxidant mixture, they may be determined by measuring the absorbance while a blank is aspirated into the flame. The situation is more complicated if the absorption or scattering arises from a product associated with the sample or its matrix. For example an elemental absorption line can be interfered by a molecular absorption line from reaction products of co-existing elements in the sample. In the case of Ba determination in the presence of Ca the elemental absorption line at 553.6 nm can be overlapped by a broad CaOH absorption band in the range 548.0 nm to 558.0 nm. In many cases such interference can be eliminated by replacing air as oxidant by nitrous oxide. The resulting higher flame temperature leads to the decomposition of the CaOH and eliminates the absorption band.

In flame AA determination of elements such as Ti, Zr, and W spectral interferences from the formation of refractory oxide particles with diameters greater than the wavelength of the light can increase the scattering. Interference due to scattering may also be observed when organic solvents are used. When these are combusted incompletely, carbonaceous particles may be generated and cause light scattering. This interference is, however, not very frequently observed in flame AA or can easily be eliminated by the judicious choice and optimisation of the analytical conditions. Alternatively, one may add the interfering substance (if this is known) in large excess to the sample. In that case, the interference due to the compound initially present in the sample will become insignificant in comparison to that of the compound added. Such a procedure is sometimes referred to as *spectral buffering*.

While electrothermal AA was considered to be more susceptible than flame AA to the interferences discussed above, this appears no longer to true with the instrumental developments that have been realised over the past decades. Nowadays, graphite furnace AA may be considered as being affected by interferences to a level not higher than observed with flame AA.

#### 12.3.3.2 Methods for Correcting for Spectral Interference

A number of methods have been developed for correcting spectral interference caused by matrix products. Perfect background correction can only be achieved when the background absorbance measurement corresponds exactly in space, time, and wavelength with the atomic absorbance measurement. Since this exact matching of all three parameters is impossible, it is common to give priority to the equality in space and to make the difference in wavelength and/or time as small as possible. This is due to the fact that the background absorption can never be assumed to be completely constant over the considered (spectral or temporal) range.

In general, any type of background correction requires two measurements to be made, one of which is the measurement of the gross or total absorbance at the wavelength of the resonance line  $A_{\text{total}}$ . Then, the background attenuation,  $A_{\text{background}}$ , is subtracted from the total absorbance to yield the absorbance of the analyte,  $A_{\text{analyte}}$ .

**Two-line background correction** The two-line correction method, which was proposed in the late 1970s [22], is based on measuring the absorption at a second, non-resonant line. This line should be close to the resonance line of the element that is measured but should not be absorbed by the analyte. If these conditions are met sufficiently well, it can be assumed that the attenuation at this second line is only due to the background absorption in the sample.

The reference line may e.g. be a neon or argon line from the gas in the hollow cathode lamp, or it may stem from an impurity in the hollow cathode material. Alternatively, another source of an element that is not present in the sample may be used for background measurement. The closer the reference line is to the analytical line, the better the background correction will be. In reality, this is not always easy to achieve. Particularly for short wavelengths of resonance absorption, the spectral distance of the two lines should not be more than 1 nm, otherwise significant errors may arise from inadequate background correction since scattering is strongly depending on wavelength (and increases proportionally to  $\lambda^{-4}$ ).

**Continuum source background correction** In a second, more widely used, method for background correction, a deuterium lamp provides a source of continuous emission throughout the UV region. Deuterium lamps consist of an arc that is sustained in a deuterium atmosphere. They provide enough energy in the wavelength range between 190 and 330 nm with an emission maximum near 250 nm. For longer wavelengths, a halogen lamp is used alternatively.

The radiation from the hollow cathode lamp and the deuterium lamp are directed alternately through a chopper to the (flame or graphite furnace) atomiser. The rotating chopper wheel allows the radiation of either source to pass alternately while the absorption is detected for either of the two beams (Fig. 12.15). The absorbance of the deuterium lamp is then subtracted from the absorbance of the element-specific line source.

The continuous-source emission of the deuterium lamp is passed through a bandpass filter that has a transmission window of 0.2–1 nm. Since the half-width of an atomic absorption line is only about 2–5 pm, the attenuation of the comparatively wide spectral window of the continuous emission source due to the specific absorption of the analyte will be negligible. It is thus possible to assume the attenuation of the continuous light source as being due only to the background absorption and scattering, while the additional attenuation observed at the resonance wavelength is caused by element-specific absorption (Fig. 12.16). In continuous-source background correction, it is assumed that the background is constant over the considered spectral range. If this is not the case, significant positive or negative correction errors may occur.

**Fig. 12.15** Schematic of a system used for continuous-source background correction. The chopper may be eliminated when each lamp is pulsed alternately.

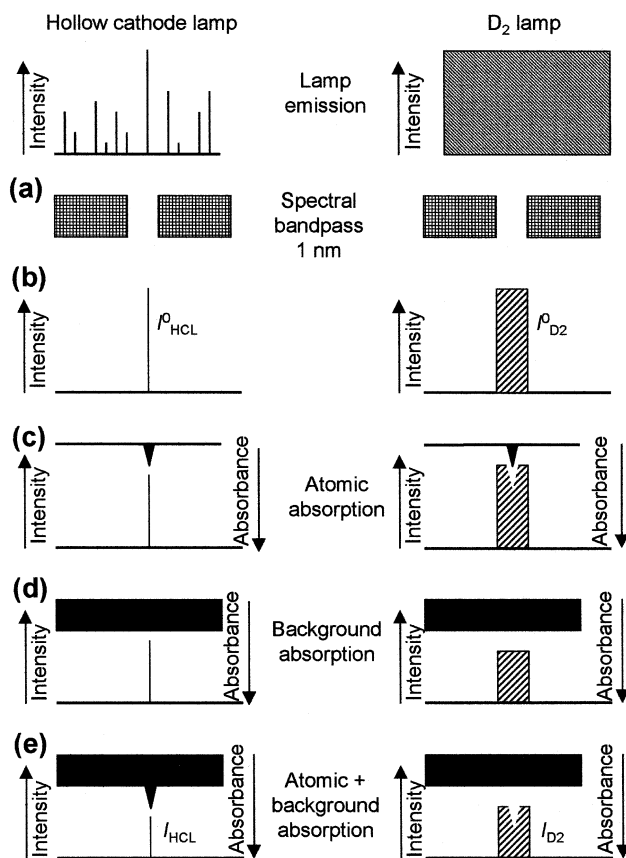
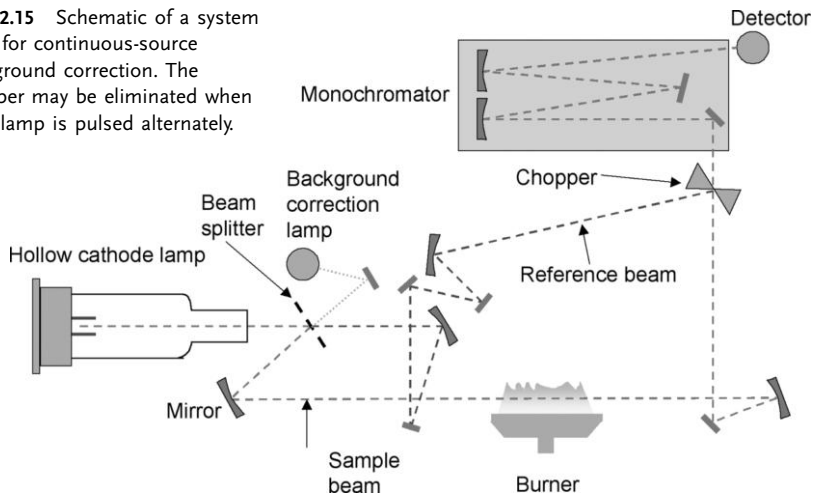


**Fig. 12.16** Principle of background-correction using a continuous-source, e.g. a deuterium lamp.

Since the alteration between the two light sources is fast, continuum-source background correction can conveniently be used even with graphite furnace AA instruments that produce fast transient signals. Few disadvantages are claimed for this type of background correction: These include the more complex (and thus more expensive) instrumental set-up with two light sources, and the fact that even if the two light sources are perfectly aligned, they will illuminate different sample volumes due to different light source geometries and also the differing intensity profiles across the beam.

However, continuum-source background correction is implemented in many commercial instruments and is particularly useful in combination with flame atomisation or hydride generation.

**Zeeman background correction** In 1897 Zeeman observed a splitting of the electronic energy levels of a free atom which is introduced into a strong magnetic field (of 0.1 to 1 T). For each electronic transition the Zeeman effect produces several absorption lines with a splitting of the order of 10 pm. The sum of the integrated absorbance of all lines equals the absorbance of the original line from which they derive. Different types of splitting exist, depending on the electronic state from which absorption occurs. In the simplest case (for singlet transitions) a single line is split into three components under the action of the magnetic field. The central ( $\pi$ ) line is at the wavelength of the original line, while the other two ( $\sigma$ ) lines are located symmetrically around this line. The absorbance of the  $\pi$  line is twice that of each  $\sigma$  line. With other transitions the splitting pattern becomes more complex which is often termed “anomalous Zeeman effect” (in contrast to the “normal Zeeman effect” observed for the simpler systems). Zeeman patterns are observed in both absorption and emission.

Use is made of the Zeeman effect for background correction as the response of the two types of absorption peaks ( $\pi/\sigma$ ) to polarised radiation is different: While the  $\pi$ -peaks absorb only radiation that is polarised in a plane parallel to the external magnetic field, the  $\sigma$ -peaks absorb only radiation that is polarised in a plane perpendicular to this field (Fig. 12.17).

Generally the non- or only slightly shifted  $\pi$ -components are used to measure the total absorbance of the analyte atoms and the background while the shift of the  $\sigma$ -components is used to measure the background absorbance. For the *background correction by the transverse Zeeman effect* a strong magnetic field is aligned perpendicular to the graphite furnace (Fig. 12.18(a)). The element-specific absorption takes place only within the  $\pi$ -component of the absorption line profile, while the  $\sigma$ -components of the absorption line are shifted to different wavelengths  $\lambda_1$  and  $\lambda_2$ . When a polariser is inserted in the light path that rejects the  $\pi$ -component, and the magnetic field is switched on and off at a sufficiently high frequency (e. g. at 50 Hz) by an alternating current, the gross absorbance and the background absorbance can be measured alternately. The net absorbance is obtained by subtracting the background absorbance from the gross absorbance. In this way, the background absorption is obtained at a single analyte wavelength  $\lambda_a$ , so that the background absorbance is measured correctly even for a structured background.

**Fig. 12.17** Principle of Zeeman background correction: The lower curve in each graph represents the emission of the hollow cathode lamp ( $I_{HCL}$ ) while the upper line shows the absorption coefficient of the analyte ( $k^a$ ) at wavelength  $\lambda$  in the presence of a background absorbance  $k_b$ . (a) conventional AAS, no magnetic field applied; (b) in the presence of a transverse magnetic field; (c) in the presence of a longitudinal magnetic field.

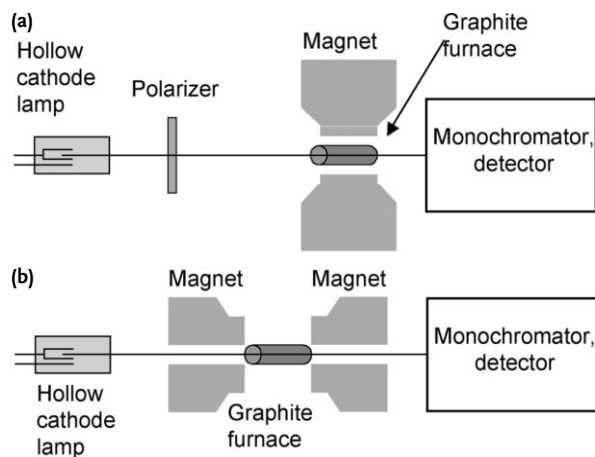
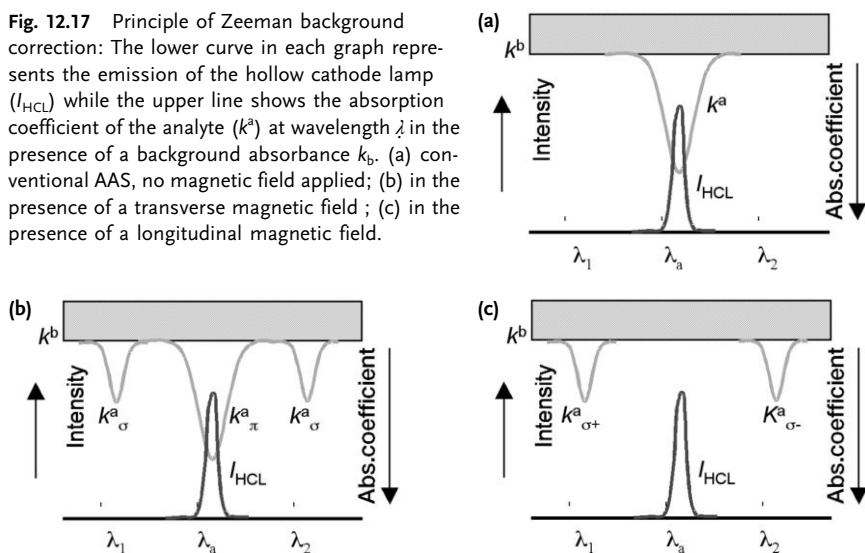


**Fig. 12.18** Schematic diagram of different Zeeman background correction systems for AAS: (a) Transverse magnetic field, i.e. the magnetic field is perpendicular to the optical axis of the spectrometer. The rotating polariser provides alternately p- and s-polarised radiation when the magnetic field is constant or trans-

mits only p-polarised radiation if the magnetic field is modulated periodically by an AC current. (b) Instruments in which the longitudinal magnetic field is oriented parallel to the optical axis of the spectrometer do not require a polariser.

Alternatively, a permanent or direct current magnet be used in combination with a rotating polariser. This allows alternate measurements with  $\pi$ - and  $\sigma$ -polarised radiation. The  $\pi$ -polarised radiation is absorbed by both the background and the element to be determined, providing the gross absorbance. In contrast, the  $\sigma$ -polarised radiation is absorbed by the background only, as these lines are shifted away from the resonance absorption wavelength  $\lambda_a$ . The net analyte absorbance again results from the difference of these two measurements.

The *longitudinal Zeeman effect* for *background correction* employs a longitudinal magnetic field instead of the transverse magnetic field. In this case (Fig. 12.18(c)), the original atomic absorption line is split only into the two  $\sigma$ -components which are circularly polarised. When the longitudinal magnetic field is modulated by application of an alternating current, then the gross absorbance is measured at zero field strength while the absorbance of the background is measured with the magnetic field. The advantage of the longitudinal Zeeman effect background correction is that no polariser is required. For this reason, the full intensity of the hollow cathode lamp can be used in both measurement phases.

Principally, Zeeman background correction can be applied to either the source or the atomiser. When the magnetic field is located around the element specific line source, its emission lines will be split into  $\sigma$ - and  $\pi$ -components. Depending on the polariser orientation relative to the magnetic field, these will account for either only background absorption or the absorption of analyte and background. For practical reasons, however, the arrangement is preferred where the graphite furnace is located in the magnetic field, since smaller magnets can be used. This is also the reason why Zeeman background correction is particularly popular with electro-thermal AAS but hardly used with flame AAS, since the magnet would have to be large enough for the burner head to fit into its gap.

The use of the Zeeman effect for background correction in AAS was initially proposed in 1969 [23]. Six years later, the first commercial instruments became available [24]. Zeeman background correction is nowadays widely used in ET-AAS instruments. It is capable of reliably handling even high nonspecific absorption. In particular the more volatile elements Pb and Cd are preferably measured by ET-AAS with Zeeman background correction, since the relative volatility of the elements does not allow high temperatures to be used in the pyrolysis step to remove interferences.

Zeeman effect background correction is effective at any wavelength. There are, however, some disadvantages: A slight decrease in the sensitivity can be observed (ca. 20 %) and a bending of the calibration curve ("rollover") is also encountered.

**Pulsed lamp background correction** A very simple method of background correction has been proposed by Smith and Hieftje [25] and is therefore known as the Smith–Hieftje method. It is based on the self-reversal behaviour of the radiation emitted by hollow cathode lamps when they are operated at high currents. This effect is seen when a large number of non-excited atoms are brought into the vapor phase. These atoms absorb the characteristic radiation emitted by the excited species. At the same time, a significant broadening of the emission line is observed.

Altogether, this results in a broad emission line that has a minimum in intensity at its centre, that is exactly at the position of the atomic absorption line. Thus, at low lamp current, the sum of the specific and the unspecific absorption is measured, while at high lamp currents effectively only background emission is determined due to the intensity minimum at the wavelength of specific absorption and the significantly broadened peak profile which is attenuated by the non-specific absorption to the left and right of the characteristic absorption of the analyte. The difference between the two signals yields the background-corrected absorption of the analyte (Fig. 12.19).

Background correction is thus achieved by modulating the lamp current to generate a longer pulse at low current (e.g. 9 ms at 5–10 mA), followed directly by a short pulse at high lamp current (for example, 0.3 ms at 200–300 mA). As the atom cloud persists in the hollow cathode lamp for several milliseconds, a minimum pulse repetition time of typically 50 ms is required to allow the atom cloud to clear before the next measurement cycle is started.

Background correction by self-reversal is instrumentally very simple to implement and has consequently been used with flame and electrothermal atomisation and with hydride generation systems. It is particularly attractive since, like the Zeeman background correction, it does not require an additional radiation source. The efficiency of pulsed lamp background correction depends on the degree of band broadening that can be achieved. This however differs from element to element and also varies strongly (increases) with lamp current. At the same time, high lamp currents significantly reduce their lifetime. Thus, specially designed hollow cathode lamps and lamp current modulation circuits must be used to achieve an acceptable compromise.

It is assumed that only the background absorption is measured at high lamp current (which is an only partially valid assumption), however, the broadening of the line profile is limited and self-reversal is not complete. Thus, radiation is still emitted at the centre of the emission line and is absorbed by the analyte, and will subsequently be subtracted from the gross absorption of the analyte. This significantly reduces the sensitivity of the determination, with an average loss of sensitivity of ca. 45 % being observed for the elements most commonly determined by

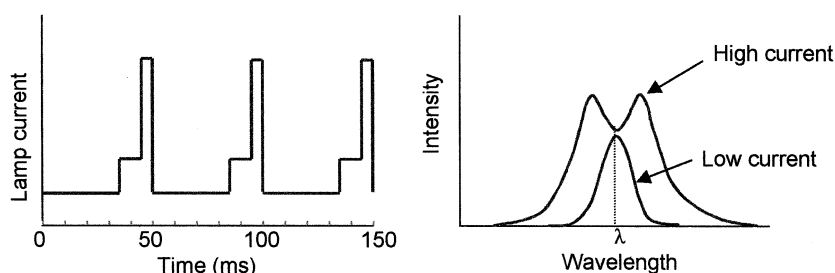


**Fig. 12.19** Background correction by source self-reversal. (a) Modulation of the lamp current that drives the hollow cathode lamp; (b) resulting hollow cathode lamp emission line profiles generated at high and low current operation.

AAS. Also the efficiency of background correction becomes insufficient, particularly at high absorbance values ( $A > 2$ ).

**Wavelength-modulation correction methods** When a broad-band continuous emission source is used, background correction can easily be performed by measuring the background absorbance in the direct vicinity of the resonant absorption line. When a constant spectral background absorption can be assumed, it is sufficient to measure the absorption at the position of the resonance line and at one point next to this wavelength. If the spectral background is sloping, two points on either side are required to interpolate the background at the position of the absorption line (cf. Fig. 12.33 in Section 12.4.3). The analytical signal is then obtained as the difference of the gross absorption signal and the background absorption. It is evident that for a structured background this method would provide inadequate results, but as long as the wavelengths used as baseline points are close to the analytical line, the error is usually small. This method of background correction was first described by Snelleman in 1968 [26] and developed further by Zander et al. [27].

Its instrumental realisation is achieved by a wavelength modulator, a vibrating mirror, driven by an AC current, that is inserted in the light path between the atomiser and the monochromator. By the periodic movement of the wavelength modulator, a very narrow wavelength across the analytical resonance line is scanned, resulting in a modulated absorption signal as output. Phase-sensitive detection allows one to discriminate the background (DC) signal from the first harmonic AC component of the signal (due to specific absorption) and to calculate the net absorption as the difference of the two signals.

Background correction by wavelength-modulation is not widely used, but seems to have considerable potential for simultaneous multi-element AAS with continuum sources. Alternatively, high-resolution echelle gratings may be used that can detect both the elemental line and the background at the same time.

It becomes evident that there is no ideal method of background correction. Since each of the presented methods has its individual advantages and shortcomings, the choice of the most suitable technique depends on the instrumental design and particularly on the type of atomiser, as well as on the analyte and matrix.

#### 12.3.4

#### Chemical Interferences

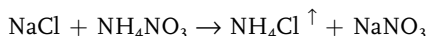
In addition to spectral interferences, chemical interferences are also significant in AA spectrometry. Although in many instances, they can be reduced by judicious optimisation of the operating conditions. Chemical interferences are observed in atomic absorption spectrometry as a consequence of (a) formation of compounds of low volatility, (b) influence on dissociation equilibria, and (c) ionisation of the analytes.

### 12.3.4.1 The Formation of Compounds of Low Volatility

This is perhaps the most common type of chemical interference. The presence of certain anions may cause refractory compounds to be formed with the analyte. As a consequence, its atomisation is hindered and a decrease in response is observed. A well-known example is the suppression of the response of Ca with increasing concentrations of phosphate or sulfate. When the anion concentration in the flame is increased while keeping the calcium concentration constant, the absorbance decreases to about half its original value which is attributed to the formation of hardly dissociated calcium phosphate or sulfate. At high anion concentrations, the analyte response again becomes independent of the anion concentration.

The co-occurrence of cations may also contribute to the formation of refractory compounds. The presence of aluminum has such an effect on the determination of magnesium. It is assumed that a refractory aluminium–magnesium oxide is formed which reduces the sensitivity of the magnesium determination.

While an increase in atomiser temperatures (when possible) is an obvious way to reduce chemical interference, a second possibility is the use of matrix modifiers. An example of this is e.g. the addition of salts whose cations react preferentially with the interfering anion and thereby prevent their reaction with the analyte. The addition of Sr or La ions may, for instance, reduce the interference of phosphate in the analysis of calcium by forming a thermally stable compound with phosphate, with the effect that Ca will be released to form free atoms. An opposite approach is used when certain salts such as  $\text{NH}_4\text{NO}_3$  are added to remove chloride salts by volatilisation:

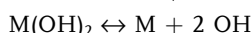
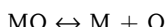


In this case,  $\text{NH}_4\text{Cl}$  is removed during the ashing step and the residual  $\text{NaNO}_3$  does not interfere during the atomisation.

In a further approach, protective agents may be added to prevent the interfering substance from reacting with the analyte. Stable, but volatile complexes or compounds are formed between the analyte and the protective agent. These protective agents are very often complexing agents, such as ethylenediamine tetraacetate (EDTA), ammonium pyrrolidone-dithiocarbamate (APDC), or 8-hydroxyquinoline.

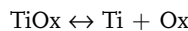
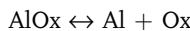
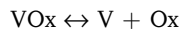
### 12.3.4.2 Influence on Dissociation Equilibria

The influence of other elements present in the flame or graphite furnace on the dissociation equilibria of the analyte can be a significant cause of chemical interference. As the absorption requires that the analyte prevails in the atomic state, dissociation of its compounds must occur, following for example the equations:



However, since the alkaline earth metal oxides in particular are comparatively stable, molecular bands, arising from metal oxides or hydroxides, are frequently observed in the spectra of these elements. In contrast to this, the oxides of alkali metals are less stable, resulting in strong atomic lines.

A similar mechanism of interaction explains the increase in the response of vanadium in the presence of aluminum or titanium. This effect is observed more markedly in fuel rich flames and depends critically on the concentration of oxygen-containing species (Ox), such as O and OH, in the flame. In the flame, the dissociation equilibria of the three metals



co-exist. The concentration of Ox is comparatively low in rich flames, so that the presence of Al or Ti in the flame shifts the dissociation equilibrium of the first equation to the right-hand side. The consequent increase in free metal concentration is accompanied by an increase in the absorption for vanadium. On the other hand, the concentration of Ox is high enough in lean combustion mixtures so that no significant shift is observed in the presence of Al or Ti. Thus, no particular shift of the dissociation equilibrium for vanadium is observed in flames with high oxidant concentration.

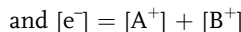
#### 12.3.4.3 Ionisation in Flames

This is a third mechanism that is largely responsible for chemical interference. In combustion mixtures that include air as oxidant, flame temperatures are usually not high enough to achieve a significant degree of ionisation of the analyte. At the higher flame temperatures achievable with oxygen or nitrous oxide as oxidant, ionisation is no longer negligible. Ionisation can be treated as an equilibrium process according to the equation:



If we accept the treatment of ionisation as an equilibrium process it is evident that the degree of ionisation will be affected by the presence of other ionisable species in the flame. As this interfering species B is also ionised to a certain degree in the flame, the degree of ionisation of the analyte atom A will be decreased, due to the law of mass-action, by the electrons formed from B. The charge balance now requires consideration of the ionisation of both species:





It can thus be concluded that in the presence of an easily ionisable element B in the flame the degree of ionisation of the analyte A is reduced and thereby its absorption is increased. Note, that at higher flame temperatures ionisation is increased which may counterbalance the increase in atomisation. Thus, a hotter flame does not necessarily result in an improved sensitivity of AAS measurements.

The addition of an easily ionisable element at relatively high concentration as an *ionisation buffer* allows one to reduce the effect of shifts in ionisation equilibria. The ionisation buffer (often an alkali metal salt such as potassium chloride) creates a high concentration of electrons in the flame, resulting in suppression of the ionisation of the analyte.

A generally useful and common approach to eliminate chemical interference in AAS is to use standard addition for quantitation. This will be described in more detail in the following section.

### 12.3.5

#### Data Treatment

##### 12.3.5.1 Quantitative Analysis

Due to its principle and instrumental realisation, atomic absorption spectrometry is a technique for quantitative analysis and is practically unsuitable for qualitative analysis. Quantitative response is governed by the law of Lambert and Beer, i. e. the absorption  $A$  is proportional to the optical pathlength  $l$ , the absorption coefficient  $k$  at the observed wavelength, and the concentration  $c$  of the species.

$$A = k c l \quad (33)$$

In contrast to many other spectroscopic techniques, atomic absorption however often possesses only a very limited linear range. This deviation from linearity is the result of a combination of factors, including the finite width of the absorbing and the exciting lines, secondary lines within the bandpass of the spectrometer, and stray light that reaches the detector. Also spatial inhomogeneities of the excitation radiation and the atom cloud in the atomiser have been held responsible for these non-linearities. The operating software of most spectrometers nowadays provides tools for curve fitting of non-linear curves to optimise the useful dynamic range.

**Quantitation by external calibration** The most common and straightforward method of calibration in atomic absorption spectrometry is the use of an external calibration with suitable standard solutions. It is based on the assumption that the standard solution matches the composition of the sample sufficiently well. This is an assumption that must always be examined with care, since, for example, samples of different viscosity may be aspirated at different rates in flame AAS,

resulting in different sensitivities. Flame AAS normally produces step-function-like response curves due to the continuous introduction of sample or standard for a certain period of time (until a stable signal is reached). The height of this signal is evaluated. In electrothermal AAS, the transient signal is produced by subjecting the sample to a defined thermal cycle which produces a comparatively narrow signal of some few seconds (cf. Fig. 12.10).

**Quantitation by the standard addition technique** Matrix interferences result from the bulk physical properties of the sample, e.g. viscosity, surface tension, and density. As these factors commonly affect nebulisation efficiency, they will lead to a different response of standards and the sample, particularly with flame atomisation. The most common way to overcome such matrix interferences is to employ the method of standard additions. This method in fact creates a calibration curve in the matrix by adding incremental sample amounts of a concentrated standard solution to the sample. As only small volumes of standard solutions are to be added, the additions do not alter the bulk properties of the sample significantly, and the matrix remains essentially the same. Since the technique is based on linear extrapolation, particular care has to be taken to ensure that one operates in the linear range of the calibration curve, otherwise significant errors may result. Also, proper background correction is essential. It should be emphasised that the standard addition method is only able to compensate for proportional systematic errors. Constant systematic errors can neither be uncovered nor corrected with this technique.

#### 12.3.6 Hyphenated Techniques

The determination of the different forms (e.g. compounds or complexes) in which an element occurs (often referred to as the speciation of an element and speciation analysis, respectively [28]) is in most cases performed by hyphenated techniques. These are the combination of a high-performance separation technique such as gas or liquid chromatography, or electrophoresis, and an element- or compound-specific detector [29]. While the former provides the separation of the different elemental species prevalent in the sample, the latter brings selective and sensitive detection. In the case of AAS, only the hyphenation with gas and liquid chromatography, respectively, has gained importance. The combination of atomic absorption spectrometry and electrophoresis has never proven successful, obviously due to the incompatibility of the extremely low flow rates of electrophoretic separations with the aspiration volumes of flame atomisers and the difficulties of interfacing the two techniques.

### 12.3.6.1 Gas Chromatography-Atomic Absorption Spectrometry

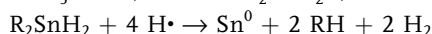
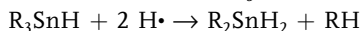
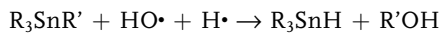
The combination of flame AAS and gas chromatography represents probably the first example of a hyphenated technique used for speciation analysis [30]. It is particularly favorable since the analytes arrive at the detector already in the gaseous state. Interfacing is straightforward, and in most cases a simple heated transfer line is used to direct the analytes to the atomiser. However, despite its apparent simplicity, the design of such a transfer line is critical since peak broadening due to dead volumes, cold spots, or lack of chemical inertness have to be avoided. In many cases, heated stainless steel capillaries or deactivated quartz capillaries inside a stainless steel tube of the shortest possible length are used, or the chromatographic column is directly interfaced to the premixing chamber of a flame atomiser. As the analytes are in the gaseous state, the transfer efficiency is in this case close to 100 %. Capillary columns, as nowadays predominantly used in gas chromatography, are easier to interface than packed columns. They offer improved resolution, however chromatographic peak width becomes much smaller, which poses higher demands on the speed of the data acquisition system. Also, capillary columns have a significantly smaller sample capacity than packed columns, which may result in less favorable relative detection limits.

The hyphenation of flame-AAS and GC is easy to achieve, however, it does not provide adequate sensitivity for most problems of environmental relevance.

Graphite furnace AAS would provide trace level sensitivity, however, GF-AAS instruments are not designed for continuous operation. This prevents their use as on-line detectors for continuous chromatographic separation.

Hyphenated GC-AAS became successful by the introduction of quartz furnace-(QF)-AAS with an electrothermally heated quartz T-tube furnace atomiser by Van Loon and Radziuk [31]. The system is designed for continuous operation, since the quartz tube can stand temperatures of up to ca. 1000 °C for an extended period, and combines the advantages of high sensitivity and low operation costs. QF-AAS appears to be an ideal detector for speciation analysis as long as the analytes are introduced in the vapor form. In most instances, the quartz furnaces are operated at temperatures of 700–950 °C (Fig. 12.20). For metal hydrides, atomisation in the graphite furnace takes place according to the equations given already. Generally the addition of O<sub>2</sub> and H<sub>2</sub> is required which leads to the formation of H· and OH· radicals that initiate the atomisation reaction.

For organometallic species, the decomposition of a molecule takes place via a series of electrophilic and nucleophilic reactions of the alkylated (or otherwise organically substituted) molecule with the hydroxyl and hydrogen radicals. For the example of an alkylated triorganotin compound, atomisation can be described by the following reaction sequence:



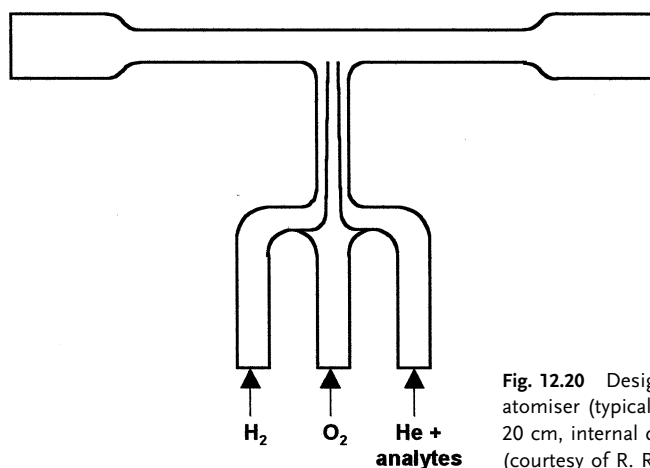


**Fig. 12.20** Design of a quartz-T-tube atomiser (typical dimensions: length 20 cm, internal diameter 0.8 cm). (courtesy of R. Ritsema)

The lifetime of the quartz tube atomiser is variable and can range up to several months. New tubes initially perform poorly and must be conditioned by several runs before achieving optimum sensitivity. Contamination of the quartz surface may result in significant signal suppression. As the electrothermal quartz furnace atomiser is comparatively robust and offers high overall efficiency and sensitivity at relatively low cost, it has found widespread application for the analysis of organometallic species of the elements Sn, Se, As, Sb, Pb, and Hg.

A simple, yet very efficient alternative to hyphenated GC-AAS is the use of a cryotrapping-AAS system [32]. This technique combines an on-line aqueous derivatisation of the ionic analytes, a preconcentration by cryofocussing, and chromatographic separation with detection by atomic absorption spectrometry. Details of

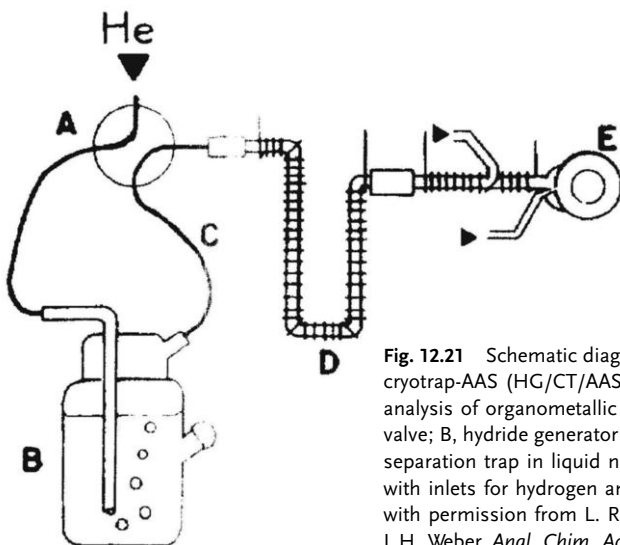


**Fig. 12.21** Schematic diagram of a hydride generation cryotrap-AAS (HG/CT/AAS) system for speciation analysis of organometallic compounds: A, four-way valve; B, hydride generator; C, heated transfer lines; D, separation trap in liquid nitrogen; E, quartz furnace with inlets for hydrogen and oxygen gas (reproduced with permission from L. Randall, O. F. X. Donard, J. H. Weber, *Anal. Chim. Acta*, 184, 1986, 197–203).

the instrumental set-up are presented in Fig. 12.21. The analytes are derivatised *in situ* by NaBH<sub>4</sub> or NaBEt<sub>4</sub> and are purged to the cryotrap. Removal of the water vapor by a suitable dryer is required to avoid blocking of the trap at cryogenic temperatures. The cryotrap is a stainless steel U-tube (typically 300–450 mm long, 6 mm i.d.) that is packed with a suitable adsorbent and immersed in liquid nitrogen and it serves to trap the derivatised analytes. After removal of the liquid nitrogen, the trap eventually warms up or is actively heated, and the analytes are evaporated according to their volatility and transported with the carrier gas stream to the quartz furnace atomiser. Although the short packed column is only capable of achieving limited resolution (less than 1500 theoretical plates), this is often sufficient for speciation analysis of low molecular weight organometallic analytes such as organotin or organolead compounds. Due to the preconcentration effect which can be achieved by cryotrapping, detection limits in the low ng L<sup>-1</sup> range can be achieved for the analysis of samples of 100–500 mL volume.

#### 12.3.6.2 Liquid Chromatography-Atomic Absorption Spectrometry

With its different modes of operation, high-performance liquid chromatography (HPLC) is a most suitable technique for the separation of less volatile, polar, or even ionic analytes. HPLC separation provides a continuous eluent flow of typically up to 1 mL min<sup>-1</sup> which can easily be introduced into the nebuliser of a flame AAS system. The interface design generally is a critical factor, since it may induce additional peak broadening which reduces both sensitivity and resolution.

The column effluent is directly introduced into the mixing chamber of the flame atomiser. Since the transport efficiency of flame AAS is usually only 5–10%, this explains why the sensitivity of this type of coupling is limited, particularly in comparison with GC-AAS.

In part, this disadvantage can be overcome by using post-column derivatisation for HPLC-FAAS. The most versatile reaction is hydride generation, but aqueous phase ethylation has also been employed to form volatile derivatives *in situ* after liquid chromatographic separation. These are purged from the liquid phase in a nitrogen gas stream and carried into the flame atomiser. The advantage is not only that the analytes are converted to volatile forms and the transport efficiency is significantly increased thereby, but also that a separation from the matrix is achieved. However, the application of this technique is obviously limited to hydride-forming elements or elements that can be alkylated by alkylborate reagents. Detection limits comparable to those of GF-AAS can be reached, e.g. less than 1 ng absolute for Pb.

Graphite furnace AAS generally offers highly sensitive detection for small sample amounts, however the sequential nature of the drying, ashing, and atomisation steps make it difficult to interface it to a continuous separation technique like HPLC. As a simple solution, the autosampler of a commercial GF-AAS instrument may be modified in such a way that the effluent is passed through a PTFE flow-through cell from which the autosampler periodically injects a small aliquot (10–50 µL) into the furnace. Of course, this does not provide a continuous on-

line signal, but the resulting discrete signals will allow one to reconstruct the chromatographic trace of the analytes.

Despite the better sensitivity of GF-AAS the coupling with HPLC has only found limited use, mainly due to the difficulties of coupling a continuous flow separation technique with the discrete nature of GF-AAS. Improvements may be expected by coupling HPLC and GF-AAS after on-line hydride generation as outlined for HPLC-FAAS, however, these techniques has not been thoroughly investigated.

### 12.3.7

#### Conclusion and Future Directions

Both flame and GF-AAS can now be considered mature techniques. Flame-AAS is very common, particularly in routine laboratories, as it is easy to use, inexpensive, and reliable. The technique is well understood, only little affected by interference and provides satisfactory limits of detection. Where these are not sufficient, the use of GF-AAS is recommended. Atomic absorption spectrometry is certainly the most widely employed method for elemental analysis.

Since AAS is classically a single-element technique, there is an increasing trend to overcome this limitation by the development of simultaneous multi-element spectrometers with multichannel detection. Such instruments are presently available on the market, and allow the simultaneous determination of up to six elements. As these are GF instruments, they must however be used under compromise conditions for the ashing and atomisation steps.

Great interest has arisen in the direct introduction of solids in AAS: This technique has been introduced for GF-AAS [33], however, it has never been widely accepted due to the obvious difficulties in quantitative analysis. The introduction of solid suspensions (slurries) into the graphite furnace seems to be a further promising approach that has found better acceptance among users: After introduction of the sample slurry into the GF, it is subjected to a modified temperature program in the presence of modifiers as they are common for GF analysis of solutions. Thus, sample throughput is largely increased as there is no need for digestion of the sample material. It should be emphasised again that, since only very small sample amounts are analysed, a problem arises for quantitative analysis from the inhomogeneity of the original sample. However, as there is no need for sample digestion or dissolution, the advantage of this technique is still convincing and it has consequently been applied to a great variety of sample types such as biological materials, polymers, industrial, and environmental samples.

## 12.4

### Atomic Emission Spectrometry (AES)

#### 12.4.1

#### Introduction

Atomic emission spectrometry has considerable potential for qualitative and quantitative analysis since all elements can, upon excitation, emit radiation at characteristic wavelengths. Unfortunately, the conditions for excitation are so variable that until now no single source exists to excite all elements [34–38]. Historically, atomic emission spectrometry dates back to the pioneering work of Bunsen and Kirchhoff in the mid1800s. However, it was not before 1920 that flame emission spectrometry was established as a quantitative method. Arc and spark discharges were developed for solid samples by 1940 and continue to be a valuable tool for today's metallurgical analysis. With the increasing interest in plasma sources in the 1960s, a new era began with the inductively coupled plasma (ICP) commercially introduced in the mid-1970s. Due to its commercial success and widespread use in research and routine analysis, the discussion in many sections will be devoted mostly to ICP-AES.

#### 12.4.2

#### Instrumentation

##### 12.4.2.1 Atomisation Devices

An atomic emission source serves a twofold purpose, the atomisation of analytes with high efficiency and the supply of energy to excite all analytes of interest. In addition, it would be desirable for an 'ideal source' to control the excitation energy in order to optimise the analytical conditions (see Fig. 12.22). Atomisation and excitation should occur in an inert atmosphere to minimise formation of interfering species and reduce background emission. The source should tolerate the introduction of solid, liquid, or gaseous samples, while organic solvents can be accepted as well as aqueous samples with a high salt or particulate load. Further, the ideal source should provide reproducible atomisation and excitation conditions to facilitate a high precision for multi-element analysis at a reasonable cost and maintenance. Naturally, none of the atomisers described below fulfils all the criteria.

**Flame atomiser** Historically, flames have been employed as atomisation source for various elements. Flames as they are typically used for spectrochemical analysis are characterised through a chemical reaction between a fuel, such as hydrogen, acetylene, or propane, and an oxidant, such as oxygen, air, or nitrous oxide. The burners are usually operated with premixed flames, in which fuel and oxidant are mixed prior to the combustion region. The sample is nebulised into the high-temperature region of the flame, where desolvation, volatilisation, atomisation and excitation take place. The hotter flames, for example acetylene–oxygen

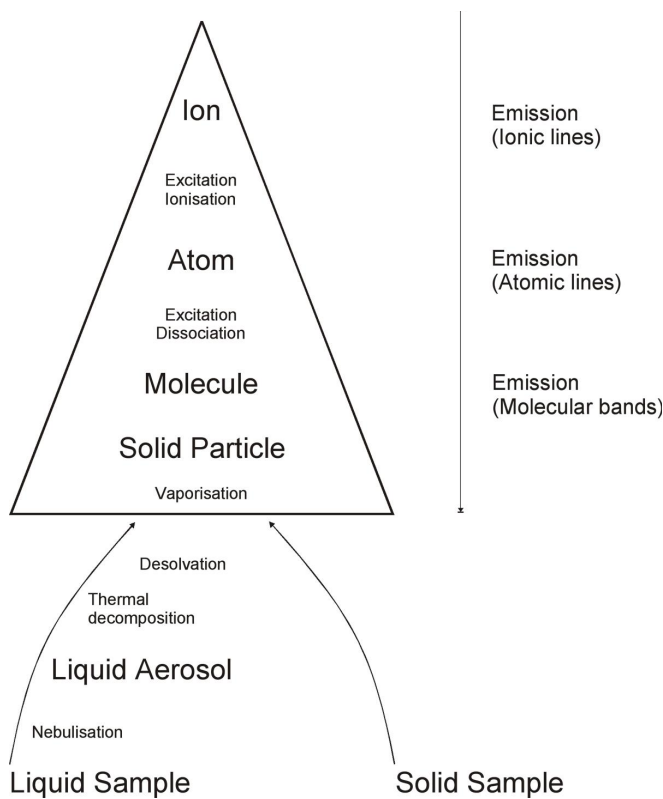


**Fig. 12.22** The main steps leading from a sample to atomic emission.

flames, generally produce a higher background emission, more ionisation and line rich spectra of analytes and interferences. The background emission is typically reduced in cooler flames, for example flames with hydrogen as fuel. However, problems can arise from non-volatile matrix components. The fraction of excited atoms in a flame atomiser is rather. Less than 0.1 % of all atoms are excited at temperatures around 2000 K and emit in the UV/vis region.

For multi-element analysis, the significantly more energetic plasma sources are therefore by far superior to flames in most regards. Today, flames are only used for the determination of alkali metals, as these can be excited at low temperatures and give simple spectra free of interferences. The determination of these metals is especially important for the analysis of biological fluids, so that emission in acetylene–air flames is still routinely used in highly automated, and simplified systems based on single or multiple interference filters and photomultiplier detection (see Fig. 12.23). The systems often also include automatic addition of an internal standard and dilution [39].

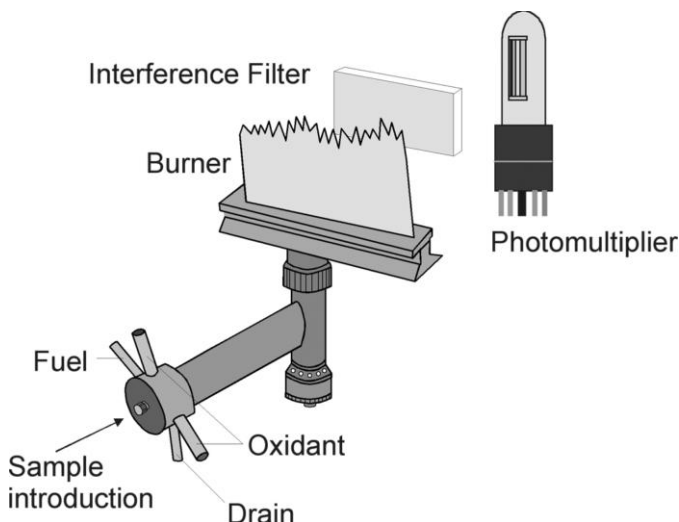
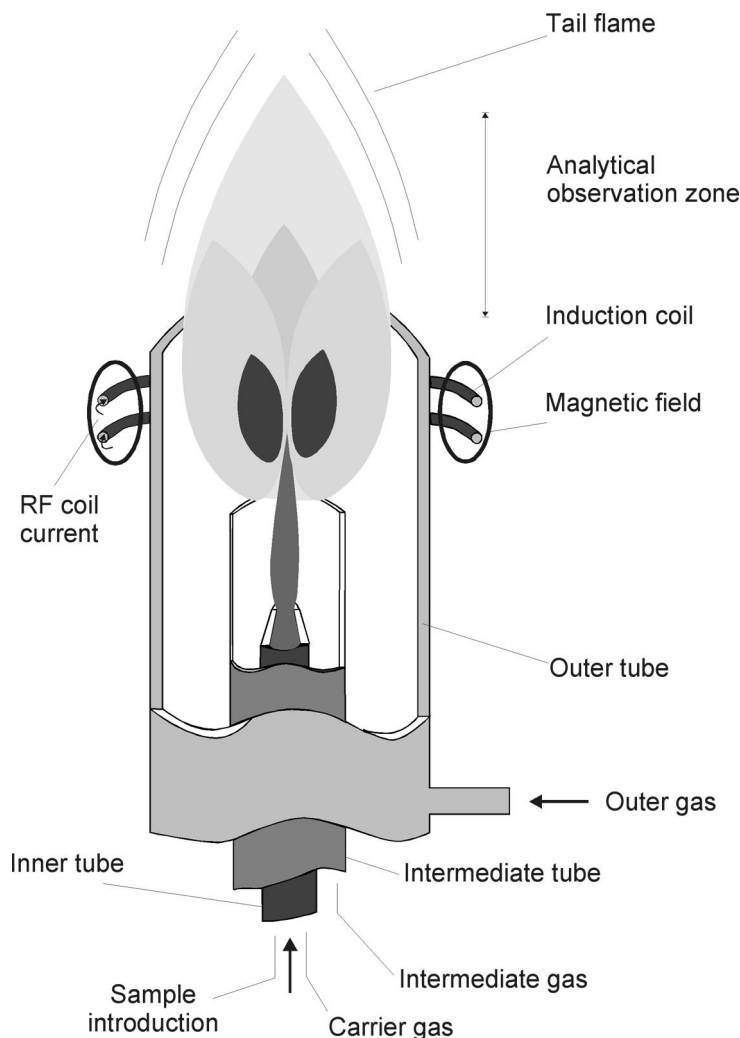


Fig. 12.23 Schematic diagram of a simple flame photometer.

**Inductively coupled plasma** Early types of plasmas that were the predecessors of the current inductively coupled plasma (ICP) appeared in the early 1960s and were first reported independently by Fassel and Greenfield around 1964/65 [40]. The inductively coupled plasma nowadays is probably the most common source in atomic emission spectroscopy and has been widely used in routine elemental analysis since its commercial introduction in 1974. An inductively coupled plasma (ICP) is formed within the confines of three concentric quartz tubes, called a torch, through which a total flow of argon between 5 and 20 L min<sup>-1</sup> is established. Figure 12.24 shows a schematic diagram of a torch with the outer tube, the intermediate tube, and the inner or carrier gas tube. A two- or three-turn, water cooled induction coil around the torch produces an intense oscillating magnetic field around the coil via a radio-frequency (RF) generator. The RF generators, producing 0.5–2 kW, are oscillators generating an alternating current at the desired frequency, typically at 27.12 or 40.68 MHz. In free running oscillators the frequency is fixed by the impedance of the components in the circuit itself. Alternatively, a piezoelectric crystal can stabilise the frequency through feedback. A higher frequency of oscillation leads to a lower excitation temperature and a lower electron density, which can result in a lower background emission, and improved detection limits. With seed electrons and ions from a Tesla discharge, the ionisation of the argon begins and a plasma is initiated in the toroidal region around the induction coil. The plasma is then sustained by inductive heating. The power delivered to the plasma will determine its temperature, with higher power resulting in higher excitation temperatures. Typical gas-kinetic temperatures in the ICP are about 5000–6000 K, while the excitation temperature is between 6500 and 7000 K and the electron temperature about 10000 K. Due to the high temperatures inside the coil (about 5000 K), a vortex gas flow of about 10 L min<sup>-1</sup> between the outer



**Fig. 12.24** Schematic diagram of an inductively coupled plasma.

and the intermediate tube thermally isolates the outer tube and centres the plasma in a radial direction. The toroidal plasma core extends a few millimetres above the tube and emits a continuum which originates from ion–electron recombination and bremsstrahlung. On top of this continuum emission, atomic argon lines are superimposed. Between 10 and 30 mm above the core, the continuum background is reduced by several orders of magnitude so that the plasma is optically thin. The background in this second zone consists primarily of argon lines, OH bands, and some molecular bands. Due to the large temperature gradient, emission in this zone is observed from elements with a wide range of excitation energies. Above this zone, a flame tail is observed with temperatures similar to ordinary combus-

tion flames, which can be used for easily excitable elements. Traditionally, the emission is viewed laterally through the plasma (side-on) and has the advantage of providing immediate venting of exhaust gases and heat to an overhead extraction system. Newer instruments also allow axial viewing, which permits a longer path length in the central channel and improved detection limits, by a factor of four to ten. For a long time, axial viewing had a poor reputation with regard to matrix effects as the atomisation zone within the coil and the recombination zone at the top of the plasma is also probed by the observation system. Recently, systems have appeared on the market that displace the cooler tail flame of the plasma away from the optical path either by a sampling cone or a directed gas flow. In this way, most of the original problems mentioned above can be solved.

The sample enters the plasma as an aerosol through the inner tube at a flow rate of about  $1 \text{ L min}^{-1}$  and has a residence time of about 2 ms in the plasma at temperatures between 4000 and 8000 K after which it enters the observation zone above the core. The carrier flow shapes the plasma into the characteristic toroidal form. The intermediate gas flow is optional and can be employed for example for the analysis of samples in organic solvents to prevent soot deposition on the torch.

The nebuliser or carrier gas flow affects not only the residence time in the plasma and the plasma conditions, but also the size of the aerosols produced. With conventional nebulisers, the aerosol size increases at a low nebuliser gas flow, reducing the transport efficiency and decreasing the emission from all lines. However, lower flow rates also increase the residence time and the excitation temperature enhancing the emission of ionic lines. For atomic lines, the excitation is improved either by the increased residence time. On the other hand also the ionisation rate is increased, resulting in a net decrease of atomic line emission.

The temperatures of an ICP are significantly higher than those in any combustion flame and the atomisation occurs in an inert gas atmosphere, which tends to enhance the lifetime of the free atoms by preventing oxide formation. As the temperature across the plasma is fairly uniform, self-absorption and self-reversal are not observed, thus permitting a considerable dynamic range (five orders of magnitude). Normally, the background intensities are rather low compared to other sources, which results in good detection limits in the ppb-range.

**Direct current plasma** The direct current plasma (DCP) is an electrical discharge between two graphite anodes and a tungsten cathode, which are arranged in such a way that a tangentially flowing argon stream from the two anodes forms an inverted V-shaped plasma (see Fig. 12.25). The cathode is located above the central apex into which the sample aerosol is directed. The plasma jet is built up by bringing the cathode and anodes into contact, resulting in ionisation of the argon and development of a current (about 13–15 A). Although excitation temperatures of 6000 K can be reached, the sample volatilisation is often not complete due to the relatively short residence times in the plasma. Spectra from a DCP generally have less lines than those from an ICP and the lines are largely from atomic species. Problems arise from the small triangular region in which an optimal signal-to-background ratio can be achieved. The main advantage is the good stability and

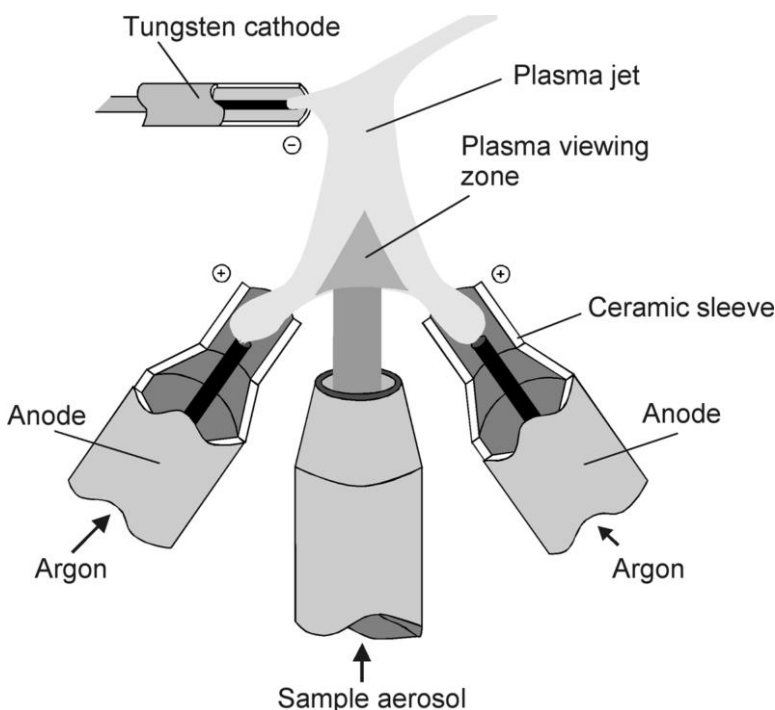


**Fig. 12.25** Schematic diagram of direct current plasma (DCP)

the ability to tolerate organic solvents as well as aqueous solutions and solutions with high solid contents. In addition, the power requirement is only 700 W and the argon consumption is, compared to the ICP, moderate at  $7 \text{ L min}^{-1}$ .

**Microwave plasmas** Microwave plasmas can be differentiated into microwave induced plasmas (MIPs) and capacitively coupled microwave plasma (CMPs). In the case of MIPs, the plasma is usually generated in a flat, cylindrically shaped Beenakker-type cavity resonator (Fig. 12.26) which is connected to a magnetron by coaxial or cavity waveguides. The power consumption is between 50 and 200 W at 2.45 GHz. A dielectric (quartz) capillary of 1–2 mm inner diameter is located in the centre of the cavity in an axial direction. The plasma is formed within the capillary and ignited by a Tesla coil or an electrical spark. The sample is introduced into the capillary at a flow of  $0.05\text{--}1 \text{ L min}^{-1}$  with a carrier gas such as helium, nitrogen or argon. The MIP is characterised by a high excitation temperature (4000–7000 K depending upon the carrier gas), which favours the atomic emission of non-metals, but a low gas temperature (about 1000 K). Thus, there is little kinetic energy for dissociation of thermally stable compounds or high solvent loads, and the atomisation efficiency is not much better than that of common flames. MIPs have been extensively used for detection of non-metals in species separated by gas chromatography or supercritical fluid chromatography [49].

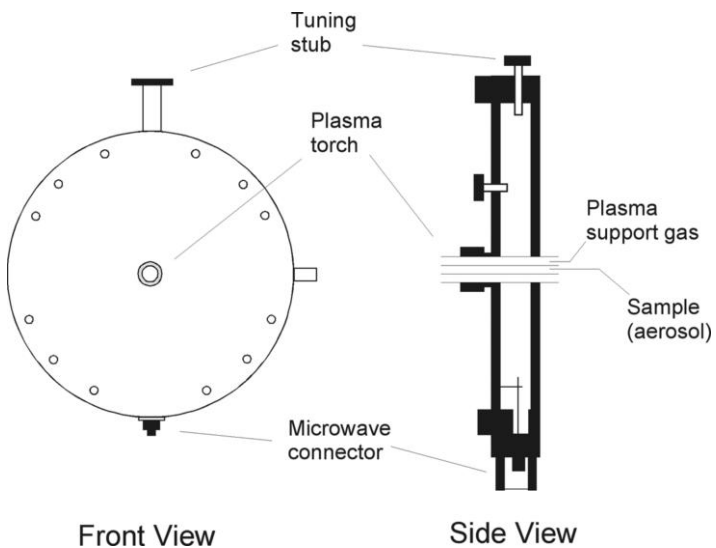


**Fig. 12.26** Schematic diagram of a Beenakker resonant cavity for microwave induced plasmas.

CMPs are operated at higher powers (0.5–3 kW) than MIPs, while the same frequency is used. A waveguide system transfers the energy into a plasma tube, where the plasma is ignited via a spark discharge. While excitation temperatures between 4900 and 8200 K, similar to MIPs, are achieved, gas temperatures between 4500 and 5700 K can be reached due to the higher power, so that CMPs are better suited for direct solution analysis.

**Arc and spark plasmas** Arc and spark discharges have been the workhorses for qualitative and quantitative emission spectrometry since the 1920s. Electrical discharges, classified into arcs and sparks, allow one to remove material from a sample surface and to excite it at the same time. Depending on the experimental conditions the material is vaporised, eroded, or sputtered, usually in an argon atmosphere, for concurrent or consequent excitation. The sample must be conductive, either naturally or through addition of a conductive material such as powdered copper or graphite. Arcs are formed between a pair of metal or graphite electrodes a few millimetres apart. The DC arc, the most commonly used type, is ignited by a low-current spark and then sustained by thermal ionisation. The kinetic temperature, typically between 4000 and 7000 K, depends upon the resistance between the electrodes and thus is a function of the atomisation of material from the sample and the electrodes. Samples are generally introduced into the arc by evaporation from a cup-shaped electrode. Alternatively, liquid samples can be deposited on a graphite electrode and evaporated to dryness. The emission spectra contain mainly atomic lines and are interfered by the formation of CN radicals from the electrodes, even in an inert gas atmosphere. Due to the different rates of volatilisation and excitation, the spectra of different species are time dependent and long integration times are needed to record all species under study. On the other hand, selective vo-

labilisation can be used advantageously to enhance the signal-to-background ratio. The low-temperature outer regions of the arc contain high densities of ground state species and are therefore prone to self-absorption and self-reversal. With the DC arc about 70–80 elements can be excited, the analysis is mainly qualitative or semi-quantitative due to the moderate precision of the arc.

Due to their good precision (RSD of the order of 1%), high voltage spark source emission spectrometry is still popular for analysis of metallic samples down to concentrations of 1 ppm. For light elements spark source AES easily outperforms X-ray fluorescence spectrometry. The high-voltage discharge is an intermittent discharge and lasts typically a few microseconds at a repetition rate of 100–1000 Hz. The sparking includes two phases: In the first phase a low energy discharge is produced by a primary circuit applying a potential difference  $> 10$  kV for a few microseconds across the electrodes to ionise the argon and create a conducting plasma. In the second phase, the main circuit of the spark generator discharges with an energy of 100 to 400 W at a moderate voltage of 300 to 500 V. In this phase, the sample is melted and evaporated at the impact point of the spark, while the different species are excited in the first phase in which excitation temperatures above 20000 K can be reached for a short time. While in early spark systems the current waveform of the discharge was determined by the circuit resistance, inductance, and capacitance, today's systems allow excellent control of the waveform to improve detection limits and precision. Ionic spectra are more pronounced in a high-voltage spark source than in an arc. With a spark, electrode material is randomly sampled by many successive discharges on the surface, resulting in a spatial averaging. To overcome changes in the surface, the integration is usually postponed for a pre-spark time of 1–2 min. Metallic samples for spark excitation are most often machined into the proper geometry to serve as electrodes.

**Laser plasmas** Laser ablation (LA) atomic emission spectroscopy is employed in two major fields of applications: bulk analysis with a spatial resolution between 100 and 1000  $\mu\text{m}$  and local microanalysis with a spatial resolution of 5–50  $\mu\text{m}$  [41]. In the case of atomic emission spectroscopy with the laser plasma, the technique is often denoted as laser induced breakdown spectroscopy (LIBS) or laser-induced plasma spectroscopy (LIPS). For LIPS an intense, pulsed laser beam (typically a Nd:YAG or excimer laser) is focused on the sample of interest, resulting in evaporation, atomisation, and partial ionisation of the sample in an expanding plasma cloud. After a delay of some hundred nanoseconds to discriminate from the background, the elemental composition of the sample can be determined via the spectrally and temporally resolved detection of the characteristic atomic and ionic emissions. Due to the minimal sample preparation, the low cost for a single measurement, and the potential for extensive automation, LIPS is an attractive approach to environmental screening and monitoring, and process analysis of solid, liquid, and gaseous samples. In addition, remote sensing is also possible either directly over a distance of some meters, or with fibre optics over a distance of 10–30 m. A microanalytical approach, either under atmospheric pressure or with Ar as buffer gas, has a considerable advantage compared to other beam tech-

niques due to the higher sampling rate achievable with the laser. Quantitative determinations are often hampered by the lack of suitable matrix matched standards or reference materials as well as elemental fractionation.

**Reduced pressure discharges** In addition to its widespread use as a light source for AAS, the hollow cathode discharge can also be used for atomic emission spectroscopy. The sample is positioned in the hollow cathode and volatilised thermally and by cathode sputtering. The analyte vapor has a long residence time in the negative glow region of the plasma and is very efficiently excited, while the signal-to-background is very good due to the low electron densities. The time consuming evacuation and gas-filling operation does not allow a fast throughput of samples, which makes the approach more suitable for solid samples, especially refractory materials.

Glow discharges with planar electrodes were introduced by Grimm in 1968 [42]. In this case the glow discharge is confined to the sample, operating as cathode. The distance between the cathode and the anode block is below the mean free path of the electrons, so that the sample is volatilised by cathodic sputtering. Due to the absence of thermal evaporation and separate atomisation and excitation, matrix effects are low. Glow discharges are suitable for depth profiling solid samples in the ppm range. Recently, glow-discharge emission spectrometry experienced a further impetus by the development of radio-frequency sources (see Fig. 12.27), which allow direct analysis of non-conducting samples.

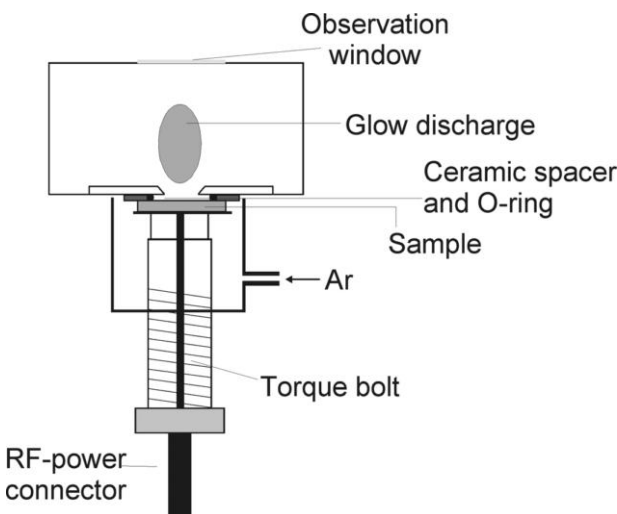


**Fig. 12.27** Schematic diagram of a discharge cell for RF-glow discharge atomic emission spectroscopy.

### 12.4.2.2 Optical Set-up and Detection

In atomic emission spectroscopy the number of detectable elements is related to the wavelength coverage of the collimating and dispersive optical system. Alkali metal elements are usually observed above 500 nm, while elements such as Cl, Br, N, or As are detected in the VUV region between 130 and 190 nm. In addition, the selectivity is related to the spectral resolution of the system, which minimises spectral interference from elements with line rich spectra and the overall signal-to-background ratio. However, high spectral resolution is accompanied by reduced light throughput, which can degrade the detection limits.

There are more than 50,000 documented spectral lines in ICP-AES, which makes a high resolution spectrometer mandatory for analysis, especially when matrix effects have to be considered. The most versatile detection systems are characterised by large spectral coverage (120–770 nm) and high spectral resolution. The best spectral resolution achieved for the Ba(II) indicator line (see below) at 230.424 nm is currently below 5 pm. For high spectral resolution, all systems have to compensate thermal and mechanical drifts by periodic spectral recalibration.

Design goals for an atomic emission spectrometer are (1) low spectral bandpass ( $\lambda/\Delta\lambda > 40,000$ ) and low stray light level, (2) simultaneous measurement of the background and analyte line intensity, (3) a detector with noise characteristics that are not the limiting noise sources, (4) precise intensity reading  $< 1\% \text{ RSD}$  at concentration levels five hundred times the detection limit of the analyte under study, and (5) large dynamic range (six orders of magnitude) of the detection system to record the emission intensity of major, minor, and trace components simultaneously.

**Sequential instruments** Sequential systems are often based on a classical grating monochromator in a Czerny–Turner or comparable configuration with a holographic grating with 2400 to 3600 lines per millimetre. Scanning is performed by rotating the grating with a stepper motor, so that the different wavelengths are sequentially focused on the exit slit of the monochromator. Photomultiplier tubes (PMTs) are usually employed as detectors, some instruments use dedicated photomultipliers for the UV and vis region. In comparison with conventional linear scanning monochromators, slew-scan monochromators provide significant savings in analysis time and sample consumption. Slew-scan systems can be programmed to scan slowly over or to stop momentarily at a wavelength region of interest, while the instrument moves rapidly between such regions.

To a certain extent, the linear dispersion and resolution can be improved by a finer ruled grating and a larger focal length. However, high-resolution is more easily achieved with an echelle monochromator which utilises diffraction orders greater than 80. The echelle grating provides high dispersion and a constant blaze at all wavelengths. The spectral coverage is much lower so that a low dispersion grating or a prism is needed as order sorter or cross disperser (see Fig. 12.29 below). Ambiguities in order overlap can be solved with a separate predispersion system, which also improves the overall optical throughput by removing the

entrance slit height restrictions [43]. This results in a bandpass of the order of 0.007 nm at 200 nm with an accessible spectral range of 165–900 nm.

**Multichannel instruments** In general, two types of multichannel instruments can be identified: polychromator instruments with several independent detectors such as photomultipliers or small linear CCD (charge coupled device) arrays and echelle spectrographs with solid state array detectors such as CCDs or CIDs (charge injection device). Polychromators, such as the Rowland spectrometer in Fig. 12.28, are based on a concave grating, which does both imaging and dispersion. This reduces the cost of optical components in the instrument, reduces alignment time and also minimises reflective and refractive losses. The spectral lines appear as astigmatically extended images of the entrance slit in a curved focal area. The entrance slit, the grating surface, and several exit slits with photomultipliers are arranged

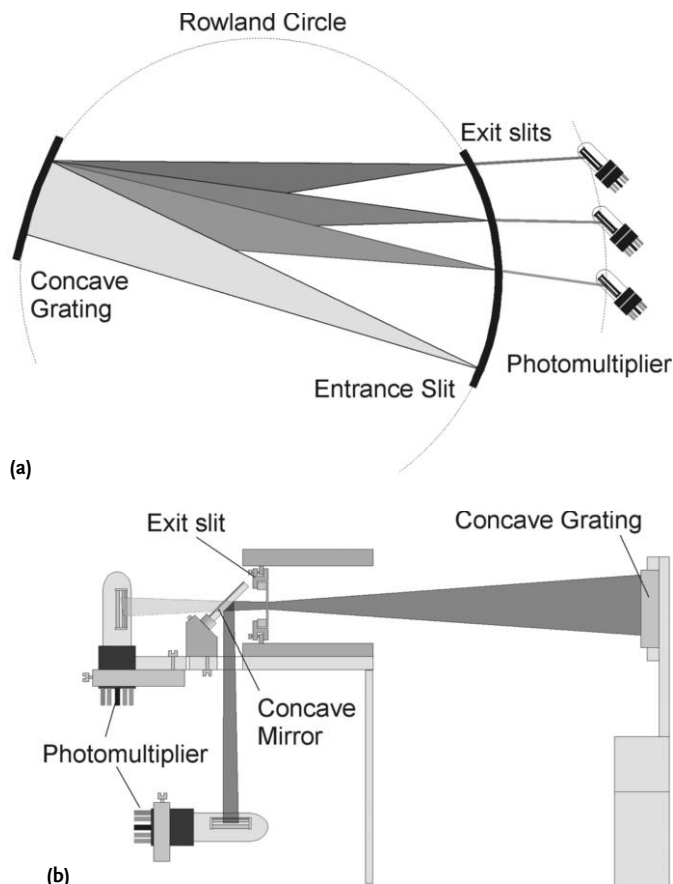


**Fig. 12.28** Schematic diagram of a polychromator based on a Paschen–Runge mount and photomultiplier detection. (a) General optical set-up; (b) side view and arrangement of the photomultiplifiers.

along the circumference of the Rowland circle. The circle diameter equals the radius of curvature of the grating. With holographic gratings with non-equidistant, curved grooves a nearly flat focal plane can be achieved for a defined spectral range. Then, an arrangement of small linear CCDs tangential to the circumference of the Rowland circle becomes possible, as employed in recent commercial systems. By moving the entrance slit tangentially to the Rowland circle, emission signals can be scanned and a background recorded. The dispersed light from the exit slits is directed with small mirrors to the corresponding photomultipliers (compare Fig. 12.28), whose signals are processed by individual analogue integrators. This allows a very fast read-out of the detectors, while the dynamic range and sensitivity for each line can be adjusted individually. Up to 60 elements can be determined simultaneously (with a 1-m–Paschen–Runge spectrometer equipped with a 20 µm slit and a sampling time of 1 min), which makes polychromators the standard instrumentation for arc and spark analysers.

In cases where no a priori information about the elemental composition is available, a more flexible approach is needed to cope with numerous emission lines and a potentially variable background. Echelle spectrographs (see Fig. 12.29), based on an echelle grating and an order sorter, for example a prism or second grating, disperse the spectrum in two dimensions in the focal plane [43]. With solid state array detectors, a large spectral range can be addressed simultaneously with superior spectral resolution. Although CIDs have a poorer signal-to-noise ratio compared to CCDs, their intermediate, i.e. during an exposure, read-out capability allows an improved dynamic range ( $> 10^5$ ).

Simultaneous detection permits in this way an increased sample throughput and a significant reduction in source flicker noise. Disadvantages of the two-dimensional dispersion are the reduced optical-throughput and the fact that certain element combinations can be measured only in sequential groups due to different plasma conditions needed for their optimum determination. In addition, the dynamic range of the ICP-AES system itself ( $10^5$ – $10^6$ ) is larger than the dynamic range of today's CCDs (about  $10^4$ ), so that multiple exposures with different

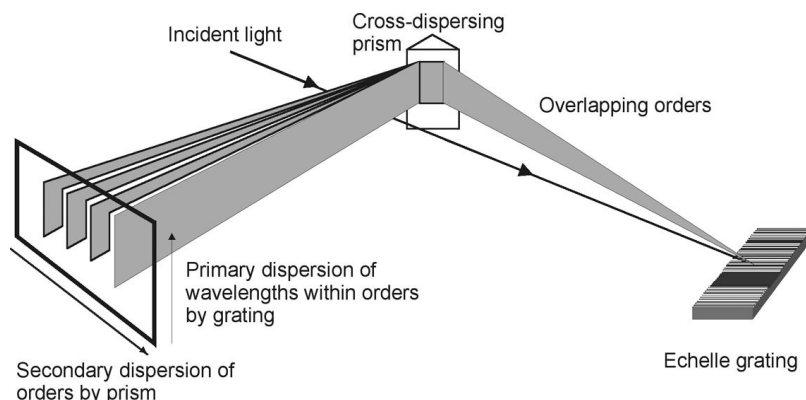


**Fig. 12.29** Principle of an echelle spectrograph.

exposure times are needed for determination of trace, minor, and major components. This can also complicate the use of an internal standard if the elements under study are present in very different concentrations.

#### 12.4.2.3 Instrumentation for Solid Sample Introduction

Although most samples are commonly presented as liquids for atomic emission spectroscopy, direct solid sample analysis has the advantage that no major pre-treatment or dissolution steps are required [44]. This minimises dilution errors or contamination from reagents and reduces the reagent and manpower cost per sample. In addition, improved detection limits may be obtained if microsamples or microanalysis are possible without any further dilution. However, the analyst has to ensure that the solid material sampled is representative of the bulk material. ICP-AES has generally a remarkable tolerance for total dissolved solids compared to ICP-MS or flame AAS so that, depending on the overall matrix, between 2 and 25 % suspended solids can be coped with. Therefore, most of the solid sample introduction devices described below are dedicated for ICP-AES.

**Direct insertion** The sample, ground into a powder, dried, and weighed, can be deposited on a probe, made of graphite, tantalum, or tungsten, and be directly introduced into the plasma. An ICP torch can be modified for example by replacing the inner tube with a quartz tube that also guides the sample probe. The insertion process can be carried out in one or several defined steps by automatic positioning devices. Positioning the probe at successively closer positions to the plasma enables sample pre-treatment and atomisation steps, analogous to drying, ashing, and atomisation in a graphite furnace. The signal is recorded as time-dependent intensity due to the differential volatilisation of the sample. A typical precision of 7–15 % is achieved because of the sample heterogeneity, irreproducible vaporisation and sample insertion, or reactions of the sample with the probe material.

**Slurry nebulisation** Conventional pneumatic nebulisers are prone to serious losses and blockage if solids in the form of slurries are introduced. Usually Babington-type nebulisers are employed, where the sample solution is pumped along a V-shaped groove and nebulised via a gas stream centred in this groove. Slurry nebulisation is very suitable for small particles (particle diameter < 6 µm) and narrow size distributions. In this case, simple aqueous solutions can be used for calibration. The plasma conditions for slurries can differ considerably from solutions and a separate optimisation is needed. Apart from difficulties in the reproducible preparation of slurries, the inherent problem is the effect of particle size on evaporation and excitation. Slurry nebulisation is especially interesting for fast monitoring studies, e.g. geochemical and geological screening [45].

**Electrothermal vaporisation** Electrothermal vaporisation, analogous to the approach utilised in AAS, can be performed by resistive heating of sample devices such as boats, ribbons, rods, or tubes from graphite or a refractory element [46].

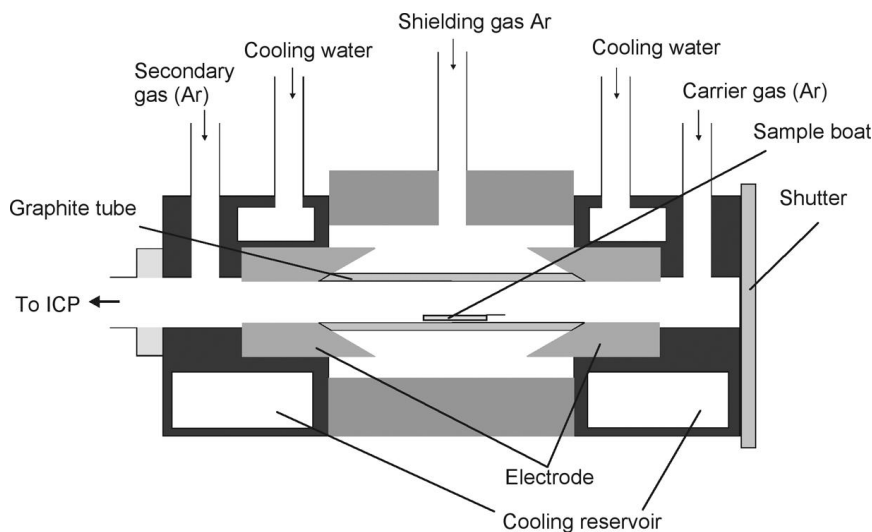


**Fig. 12.30** Platform boat for electrothermal vaporisation.

Usually the vaporiser, exemplarily illustrated in Fig. 12.30, can be sequenced through several heating stages, so that the solvent and matrix components can be temporally separated from each other and do not disturb the plasma conditions. The dry, highly dispersed aerosol produced under these conditions is swept into the plasma by an appropriate carrier gas stream. Due to the highly efficient sample vaporisation and transport efficiency (30–80 % compared to the typical 2 % efficiency of a conventional cross-flow nebuliser), detection limits for aqueous solutions are generally improved by a factor of ten to a hundred. For solid samples, the maximum load is limited to 0.5 mg, with which absolute detection limits in the nanogram to picogram range can be achieved.

**Arc and spark ablation** Arc and spark ablation systems for sample introduction are similar to the respective atomisation sources described above [47]. The dc arc equipped with metal or graphite electrodes is the most widely used form of the arc. Spark sources, as depicted in Fig. 12.31, are frequently used for conducting samples due to their instantaneous high temperature whereas the arc temperature will increase during a measurement cycle, which can lead to fractionation effects.

**Laser ablation** Laser ablation (LA) in combination with the ICP atomiser has become a powerful and flexible technique for solid sample introduction [47]. LA-AES has found its niche primarily as a bulk sampling technique for the analysis of bulk solid materials with a large focal spot (500–1000 µm). It offers comparable detection capability to spark ablation/emission but is not dependent on the sample being conductive. The experimental set-up, revealed in Fig. 12.32, consists in its simplest form of a pulsed laser (excimer- or Nd:YAG-laser) with a defined pulse energy, some focusing optics, and a sample cell with a continuous Ar flow con-

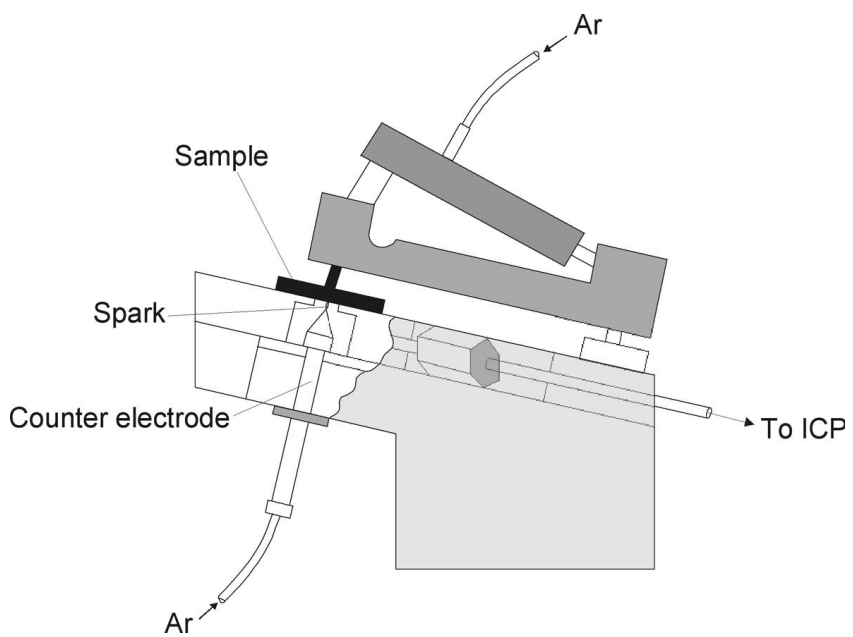


Fig. 12.31 Spark chamber for solid sample introduction.

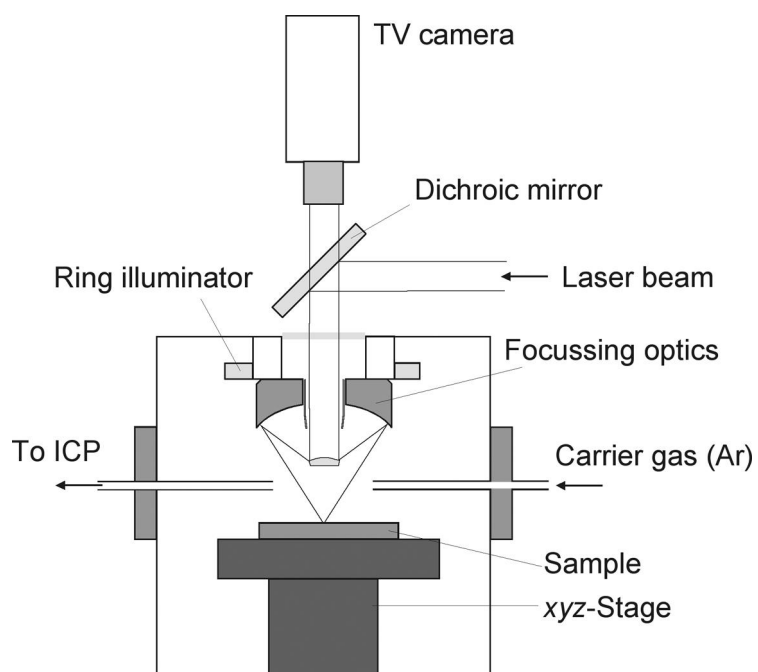


Fig. 12.32 A laser ablation set-up for solid sample introduction.

nected to the ICP torch with a simple plastic tube of 1–5 m length. For microanalysis, considerable efforts have been described in the literature to provide a homogeneous beam profile and suitable focusing optics for focal spots below 10 µm. Due to the superior sensitivity of ICP-MS, microanalysis with ICP-AES is usually limited to minor and main components. Calibration is typically based on solid reference standards, if possible with a suitable internal standard. Problems can arise from fractionation, i. e. not all elements exhibit similar ablation and transport characteristics. The fractionation is related to the key parameters of a laser ablation system, i. e. laser wavelength, irradiance, and pulse width, and possibly transport phenomena or subsequent processes in the atomiser itself, and of course also depends on the sample itself. Laser ablation can be also used favourably in combination with other excitation sources such as microwave plasmas. The experimental set-up is similar to that of LA-ICP-AES systems.

#### 12.4.3

##### Matrix Effects and Interference

In the early phase of ICP use, this technique was claimed to be free of matrix interference. Although the ICP was superior to earlier employed excitation sources and was less prone to interference than for example arc and sparks, matrix interference and spectral interference can still be observed.

###### 12.4.3.1 Spectral Interference

Spectral interference has been well studied and are probably best understood in atomic emission spectroscopy. The usual remedy to alleviate a spectral interference is to either increase the spectral resolution of the spectrometer (which often is not possible with a given type of instrument) or to select an alternative emission line. Three types of spectral interference can be discriminated: 1. Direct wavelength coincidence with another emission line, 2. partial overlap of the line under study with an interfering line in close proximity, 3. a linear or non-linear increase or decrease in background continuum (see Fig. 12.33).

Interferences of types 1 and 2 can occur not only from another element in the matrix but also from an argon line or molecular species such as OH or N<sub>2</sub>. An example of a type 1 interference is the Zn(I) line at 213.856 nm overlapping with the Ni(I) line at 213.858 nm. As type 2 can be eliminated only by improved spectral resolution, mathematical algorithms are used on a routine basis to solve this type. If the interference can be identified and quantified, then interelement correction factors can be inferred in a simple manner: First, a calibration for the analyte is constructed in the usual way and then different concentrations of the interfering element are studied and the apparent analyte concentration calculated at the emission line(s) of interest.

Type 3 is easily solved by registering the background on either side of the line and modelling the background by an appropriate mathematical function. Provided that no fine structure is present, this approach should prove to be satisfactory. In

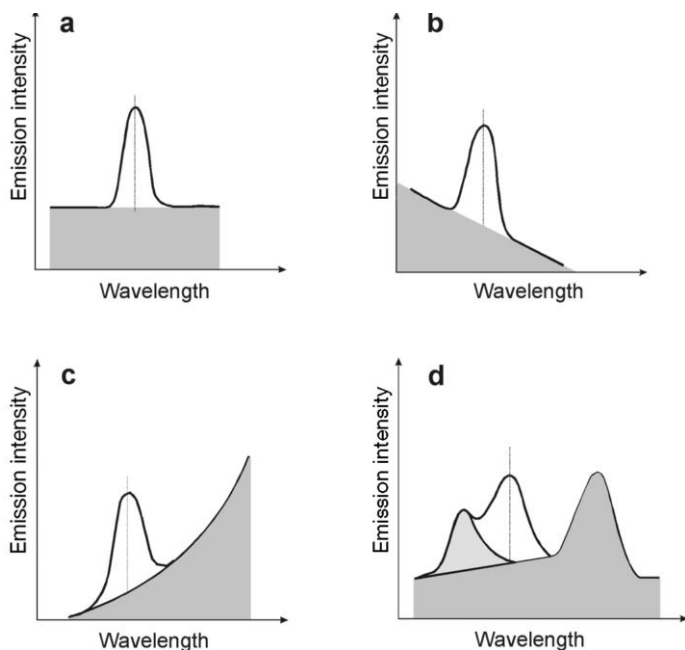


**Fig. 12.33** Typical spectral interferences and spectral background. (a) flat background, (b) sloped linear background, (c) non-linear background, (d) structured background.

general the background emission decreases with wavelength, so most useful analytical lines are found in the UV region.

The selection of non-interfered lines is more critical for polychromator systems due to the limited number of channels. The major requirement is that the line is not spectrally interfered and provides sufficient sensitivity. However, for the determination of minor and major components less sensitive lines must also be included to allow for a better dynamic range.

#### 12.4.3.2 Matrix Effects and Chemical Interferences

Matrix effects include nebulisation interference, transfer and desolvation interference, chemical or ionisation interference, and atomisation and volatilisation interference. Although the primary indication is a change in the emission intensity, it is often difficult to determine the origin of the interference.

As the spray chamber, through which samples are most commonly introduced into the ICP, can significantly affect the aerosol size distribution solely by its design, the trend is to use a direct injection nebuliser (DIN). Matrix constituents, such as salts, organic compounds or solvents altering the viscosity, surface tension, or solution density can considerably change the quantity of the sample nebulised as a function of time. Interference by desolvation is due to the differences in volatility between the matrix and the analyte and is accompanied by a change in the analyte concentration in the aerosol during desolvation. Memory effects may be re-

lated to large tubing lengths or vessel surfaces used in the nebulisation or desolvation system.

Mineral acids are widely used for sample preparation and solution storage and are therefore common matrices in atomic emission spectroscopy. Depending on the nature and concentration of the acid, the atomic emission in ICP can be influenced. At low concentrations (< 1% v/v) an increase in the analyte signal is observed, whereas higher acid concentrations lead to a decrease in net signal intensity. Possible explanations for this observation are a decrease in the sample uptake rate as a result of increased viscosity, a modified vapor pressure in the spray chamber, a change in the aerosol size distribution or transport efficiency, or a change in the ICP atomisation and excitation conditions. Regarding the nature of the acid, it has been found that sulfuric and phosphoric acid result in an increased aerosol size due to the increased viscosity of the solution, while nitric, perchloric and hydrochloric acid affect the excitation conditions in the plasma itself. Another well-known effect produced by acids is their influence on the duration of the nebulisation period required to gain a steady state signal.

Clogging of the injector tube by carbon or salt deposits is observed after prolonged spraying of organic samples, such as oils or organic solvents, or samples with high salt content. Organic solvents, nebulised pneumatically, lead to a smaller aerosol size because of lower surface tension and viscosity. Hence, the solvent and analyte input in the plasma is increased and a signal enhancement may be observed. However, in some cases the solvent load may be too high, thus affecting the plasma stability and decreasing the excitation temperature and the electron density.

Due to the high gas temperature of the ICP, long residence times, and inert gas atmosphere, chemical interference from the formation of thermally stable compounds or radicals are rarely observed for ICP sources, with low power ICPs being the only exception. However, this interference is common in atomisation sources with low gas temperatures, for example the DCP, MIP, or flame.

Easily ionisable elements, such as alkali and alkaline earth metal elements, can alter the emission intensity and may cause an enhancement or a depression. This problem is more serious with DCPs, MIPs, and CMPs, while less important with ICPs. Several mechanisms have been suggested to explain these changes, for example lateral diffusion, changes in thermal conductivity, an altered volatilisation rate, ambipolar diffusion, or shifts in the ionisation equilibrium and the collisional processes.

#### 12.4.4

#### Quantitative and Qualitative Analysis

Today, atomic emission spectroscopy always makes use of relative quantitation, i. e. unknown samples are quantitatively analysed after calibration with samples of known composition. The most common approach to calibration is internal standardisation. The underlying assumption, introduced by Gerlach in 1925, is that the ratio of the analyte mass to the mass of the internal standard, matching the analyte in its chemical properties, emission wavelength, energy of the line, and ionisation

potential, is constant, despite any fluctuations in the system. Internal standards thus compensate for instrumental fluctuations and improve the accuracy and precision of the determination.

Because many elements have several strong emission lines, AES can be regarded as a multivariate technique per se. Traditionally, for quantitative analysis in atomic emission spectroscopy, a single strong spectral line is chosen, based upon the criteria of line sensitivity and freedom of spectral interferences. Many univariate attempts have been made to compensate spectral interferences by standard addition, matrix matching, or interelement correction factors. However, all univariate methods suffer from serious limitations in a complex and line-rich matrix.

On the other hand, atomic emission spectra are inherently well suited for multivariate analysis due to the fact that the intensity data can be easily recorded at multiple wavelengths. The only prerequisite is that the calibration set encompasses all likely constituents encountered in the real sample matrix. Calibration data are therefore acquired by a suitable experimental design. Not surprisingly, many of the present analytical schemes are based on multivariate calibration techniques such as multiple linear regression (MLR), principal components regression (PCR), and partial least squares regression (PLS), which have emerged as attractive alternatives.

Generally, AES systems are calibrated with multi-element standard samples. In the case of sparks, arcs, glow discharges, and laser ablation, solid samples are required, which are rarely available in large enough numbers to provide a satisfactory calibration. Hence, in solid sample analysis secondary standards are usually prepared.

For conventional analysis by ICP or DCP, liquid samples are used, which are either easily prepared or commercially available. Interference problems are reduced to a minimum if the calibration solutions are matched to the samples with respect to their content of acids and easily ionisable elements (see above). Calibration curves obtained with sparks, arcs, and laser ablation systems are usually curved so that 8–15 calibration samples or more are needed to define a suitable calibration. In the case of liquid analysis by DCP and ICP, fewer calibration samples can be used due to the better linearity and dynamic range and absence of self-absorption effects. With the introduction of liquids, the spray chamber is the major source of flicker noise due to aerosol formation and transport. While shot noise can easily be compensated by longer integration times, the flicker noise is of multiplicative nature so that any element can be used as an internal standard provided that a true simultaneous measurement of the analyte and internal standard line intensity is possible.

To find optimal conditions for a given analysis, the principal parameters can be varied in a rational way. In the case of an ICP, to which the further discussion will be limited, this concerns the flow rate of aerosol carrier gas, the RF power input, the observation height above the induction coil, and the sample uptake rate. Numerous simple optimisation schemes have been described in the literature, especially for ICP analysis. In addition, sophisticated and complex diagnostics have been suggested in the past to characterise the performance of ICP-AES systems,

**Table 12.3** Diagnostics to characterise ICP-AES performance (adapted from [48]).

<b>Figures of Merit</b>	<b>Diagnostics</b>	<b>Spectral Line</b>	<b>Measurement</b>
Selectivity	Resolution	Ba(II) 230.424	Line profile
Repeatability	RSD of signal	Mg(I) 285.213	RSD
Long term stability	Warm-up time	Ar(I) 404.442 Ba(II) 455.403 Zn(II) 206.423	Intensity as function of time
	Stability	Ar(I) 404.442 Ba(II) 455.403 Zn(II) 206.423	RSD
Robustness	Mg(II)/Mg(I)	Mg(I) 285.213 Mg(II) 280.270	Signal-to-background ratio
Limit of detection	Signal-to-background ratio RSD	Ni(II) 231.604 Background at 230 nm	Signal-to-background ratio RSD with optimised exposure time

most of them requiring additional instrumentation. However, with commercial instruments a simple approach based on several lines has been proposed by Mermet and other authors [48]. Table 12.3 gives an overview of which diagnostic can be used to monitor the instrument's performance: The spectral resolution is measured in the UV region where most analytical lines are found. Warm-up time and long term stability are determined via the temporal behaviour of three lines. Due to the all-solid-state RF generators, warm-up times are today usually about 15 min. The Mg(II)/Mg(I) ratio can be utilised to characterise the robustness of the plasma and the sensitivity of the method due to changes in the matrix. In the case of a plasma, this corresponds to a constant excitation temperature and electron density as well as a similar spatial distribution of the species along the plasma axis. High RF power together with a low carrier gas flow and moderate solvent loading and larger inner diameter of the injector usually result in robust conditions which are characterised by Mg(II)/Mg(I) ratios above ten, while, for example, a ratio of four indicates a high sensitivity to matrix effects. Lower power favours a better signal to background ratio and improved detection limits.

For a long time qualitative analysis was mainly carried out with DCP systems, while the sequential or direct reading ICP systems were too time- and sample-consuming for a general survey analysis. With the improved simultaneous observation of multiple emission lines via echelle spectrometer, a general qualitative analysis of unknown samples becomes easily possible under robust plasma conditions.

## 12.4.5

### Advantages and Limitations

#### 12.4.5.1 Absolute and Relative Sensitivity

In the analysis of simple solutions with known composition, for ICP-AES short term precision between 0.2–3 % relative standard deviation for analytes with concentrations ten times the detection limits may be achieved, while over several hours a 5 % RSD can be expected. This precision in combination with its robustness make ICP-AES superior to ICP-MS for the determination of minor and major components. With ICP-AES most elements (about 73) can be determined routinely at the  $10 \mu\text{g L}^{-1}$  level or better in solution with radial viewing. In favourable cases and/or axial viewing, detection limits  $< 1 \mu\text{g L}^{-1}$  can be achieved. For a single emission line, a linear range of four orders of magnitude may be easily attained and as many as six orders of magnitude can be observed in favourable cases. The linear range can be extended by multivariate calibration, as different emission lines with different sensitivities can be utilised for trace, minor, and major concentrations. While the speed of ICP-AES analysis will depend on whether simultaneous or sequential instruments are used for detection, generally this can vary between 2 and 6 samples per minute. Today, ICP-AES systems can be operated unattended overnight, due to the modern automated designs and safety inherent in the use of inert argon gas.

#### 12.4.5.2 Hyphenated Techniques

Amongst the wide range of sample introduction methods available for atomic emission spectroscopy, chromatographic methods are most popular as they transform a complex mixture into a time-resolved separated analyte stream [49].

**Gas chromatography and atomic emission spectroscopy (GC-AES)** The combination of gas chromatography and plasma emission spectroscopy provides a specific and selective detection system for a large variety of analytes, e. g. metallic elements, hydrogen, carbon, nitrogen, phosphorus, oxygen, sulfur, and the halogens. Compared to the Ar ICP, the hyphenation of a GC with a normal pressure helium microwave-induced plasma (MIP) is extensively used, due to its superior performance in the determination of all elements that are particularly relevant in organic analysis (C, H, N, O, S, P and halogens) and its significantly lower operation cost. In a first approximation, the emission intensity and mass response factor from an element in the plasma can be assumed to be independent of the structure of the organic parent compound. This is ideal for GC detection, since it significantly simplifies calibration. GC-MIP-AES is a universal, element selective detector providing detection limits in the low pg range. It is thus an ideal complement to GC-MS, particularly for screening purposes. The introduction of gaseous samples into a plasma offers several advantages over liquid introduction, as the transport efficiency approaches 100 % in contrast to pneumatic nebulisation where 95 % of the sample is discarded. Sample introduction is achieved via a heated transfer line. In the

case of hyphenated GC-ICP-AES, the carrier gas from the GC (normally He) is mixed with the Ar flow used to sustain the plasma and directly introduced into the plasma. The high sensitivity of ICP-AES detection, however, is partially offset by the large dilution of the GC effluent. Generally, the scope of analysis in GC-ICP-AES is limited, e.g. to the determination of metal-organic species. These constitute a small group of compounds with similar chemical properties that are converted into volatile species, which, additionally, allows a substantial preconcentration and removal of interferences.

**Liquid chromatography and atomic emission spectroscopy (LC-AES)** Liquid chromatography (LC) is the most popular separation method for ionic, polar, nonpolar, and neutral compounds of intermediate to high molecular weight, low volatility and low thermal stability. The LC effluent with a flow rate of up to  $1 \text{ mL min}^{-1}$  is connected directly to the nebuliser. The often reported poor detection limits for LC-ICP-AES combinations are due to the ineffective conversion of the effluent into an aerosol. This can be improved by utilising an efficient nebuliser such as the direct injection nebuliser (DIN). While aqueous mobile phases are easily handled, organic phases are a greater challenge because of the increased spectral background and changes in the plasma characteristics. A simple solution is the use of a microbore LC with column diameters of  $\leq 1 \text{ mm}$  and lower mobile phase flow rates. Carbon deposition on the torch can be prevented with a cooled spray chamber or addition of 1–4% oxygen to the Ar plasma support gas. Microwave plasmas are difficult to use for LC detection: Due to the low plasma enthalpy which is insufficient to desolvate and vaporise liquid aerosols effectively, they cannot tolerate the introduction of liquid phases at the usual LC flow rates. Again, the DIN or a thermospray interface can improve the coupling but this adds significantly to the complexity of the system.

**Capillary electrophoresis and atomic emission spectroscopy (CE-AES)** Capillary electrophoresis (CE) is a rapidly emerging tool for many routine clinical and pharmaceutical applications. Due to the high separation efficiency of the CE, this combination allows the speciation of elements even in rather complex matrices such as human serum. A challenge for this hyphenation is the interface compatible with the low flow rate of CE, which can be as little as a few  $\text{nL min}^{-1}$ , compared with a typical sample introduction rate of  $1 \text{ mL min}^{-1}$  into the ICP. Most interfaces reported in the literature contact the CE via a suitable Pt contact in a sheath buffer flow, which is mixed with the CE effluent, e.g. in a PEEK tee. As the total flow is significantly increased by the make-up flow, a conventional nebuliser can be used for sample introduction.

**Flow injection analysis and atomic emission spectroscopy (FIA-AES)** Flow injection analysis (FIA) is a method in which small sample volumes, typically about 10–200  $\mu\text{L}$ , are injected into a continuously flowing carrier stream. Corresponding transient signals can then be monitored each time a sample is introduced into the atomiser. The primary advantage of FIA as a means of sample introduction

is that relatively high salt concentration in the sample can be tolerated, while viscosity effects and other interference are minimised. Further, FIA allows one to include several operations such as on-line dilution, standard addition, on-line preconcentration and separation, which improve the sample throughput and ease of operation. For these reasons, many commercial ICP-AES systems can optionally be interfaced to highly automated FIA systems for unattended sample preparation and measurement.

## 12.5 Summary

Although a brief survey of the current literature shows that the number of studies employing AAS is declining compared to the use of ICP-AES and ICP-MS, AAS remains one of the workhorses of elemental analysis. This clearly indicates that AAS has become a mature analytical technique, both in instrumentation and analytical methodology. The differences in performance for different elements makes AAS and ICP-AES not alternatives, but complementary analytical techniques. Table 12.4 illustrates this conclusion by a simplified comparison of the main analytical features of ICP-AES and -MS, and flame and graphite furnace AAS, respectively. The operating cost for ICP-AES is still significantly higher than for AAS because of the considerable argon consumption during operation. Despite the generally very high performance of ICP-MS which makes it a preferred analytical tool

**Table 12.4** Simplified comparison of ICP-AES, ICP-MS, flame and GF-AAS.

	<b>ICP-AES</b>	<b>ICP-MS</b>	<b>Flame AAS</b>	<b>GF-AAS</b>
Detection limits	Very good for most elements, ppb	Excellent for most elements, ppt	Very good for some elements, ppb	Excellent for some elements, ppt
Sample throughput	5–30 elements per min and sample	All elements per 2–6 min and sample	20 s per element and sample	5 min per element and sample
Linear dynamic range	$10^5$	$10^5$	$10^3$	$10^2$
Precision				
short term	0.2–3 %	1–3 %	0.1–1 %	1–5 %
long term	< 5 %	< 5 %		
Dissolved solids	2–25 %	0.1–3 %	0.5–3 %	>20 %
No of elements detectable	> 75	> 73	> 68	> 50
Sample usage	High	Low	Very high	Very low
Unattended operation	Yes	Yes	No	Yes
Operating cost	High	High	Low	Medium
Capital cost	High	Very high	Low	Medium/high

where available and where economically feasible, ICP-AES is a highly useful technique as it offers excellent detection limits, particularly for those elements which are traditionally difficult to determine with ICP-MS due to interferences from elements such as Ca, Fe, and As.

In atomic emission spectroscopy flames, sparks, and MIPs will have their niche for dedicated applications, however the ICP stays the most versatile plasma for multi-element determination. The advances in instrumentation and the analytical methodology make quantitative analysis with ICP-AES rather straightforward once the matrix is understood and background correction and spectral overlap correction protocols are implemented. Modern spectrometer software automatically provides aids to overcome spectral and chemical interference as well as multivariate calibration methods. In this way, ICP-AES has matured in robustness and automation to the point where high throughput analysis can be performed on a routine basis.

## References

- 1 G. R. Bunsen, *Philos. Mag.*, **20**, 1860, 89–98.
- 2 W. Grotrian: *Graphische Darstellung der Spektren von Atomen mit ein, zwei und drei Valenzelektronen*, Springer, Berlin 1928.
- 3 C. E. Harvey: *Spectrochemical Procedures*, Applied Research Laboratories, Glendale, CA 1950, Ch. 4.
- 4 A. Walsh, *Spectrochim. Acta*, **7**, 1955, 108–117.
- 5 C.Th. J. Alkemade, J. M. W. Milatz, *Appl. Sci. Res. B*, **4**, 1955, 289–299.
- 6 C.Th. J. Alkemade, J. M. W. Milatz, *J. Opt. Chem. Soc. Am.*, **45**, 1955, 583–584.
- 7 *Atomic Absorption Spectrometry*, ed. S. J. Haswell, Elsevier, Amsterdam 1991.
- 8 B. Welz, M. Sperling: *Atomabsorptionspektrometrie*, 4th edition, Wiley-VCH, Weinheim 1997.
- 9 H. Becker-Ross, S. Florek, U. Heitmann et al., *Fresenius' J. Anal. Chem.*, **355**, 1996, 300–303
- 10 J. M. Harnly, *J. Anal. At. Spectrom.*, **14**, 1999, 137–146.
- 11 H. Falk, *Prog. Anal. Spectrosc.*, **3**, 1980, 181–208.
- 12 K. Niemax, A. Zybin, C. Schnürer-Patschan et al., *Anal. Chem.*, **68**, 1996, 351A–356A.
- 13 A. Zybin, C. Schnürer-Patschan, M. A. Bolshov et al., *Trends Anal. Chem.*, **17**, 1998, 513–520.
- 14 B. L'vov, *Spectrochim. Acta*, **17**, 1961, 761–770.
- 15 R. G. Godden, D. R. Thomerson, *Analyst*, **105**, 1988, 1137–1156.
- 16 W. R. Hatch, W. L. Ott, *Anal. Chem.*, **40**, 1968, 2085–2087.
- 17 B. Welz, M. Melcher, H. W. Sinemus et al., *At. Spectrosc.*, **5**, 1984, 37–42.
- 18 H. T. Delves, *Analyst (London)*, **95**, 1970, 431–480.
- 19 Z. Grobenski, R. Lehmann, R. Tamm et al., *Mikrochim. Acta I*, **1982**, 115–125.
- 20 L. Ebdon, M. R. Cave, *Analyst (London)*, **107**, 1982, 172–187.
- 21 D. S. Gough, *Spectrochim. Acta B*, **54**, 1999, 2067–2072.
- 22 R. A. Newstead, W. J. Price, P. J. Whiteside, *Prog. Anal. At. Spectrosc.*, **1**, 1978, 267–298.
- 23 M. Prügger, R. Torge, *Ger. Pat.*, 1,964,469, filed December 23, 1969.
- 24 H. Koizumi, K. Yasuda, *Anal. Chem.*, **47**, 1975, 1679–1682.
- 25 S. B. Smith, G. M. Hieftje, *Appl. Spectrosc.*, **37**, 1983, 419–424.
- 26 W. Snelleman, *Spectrochim. Acta B*, **23**, 1968, 403–411.
- 27 A. T. Zander, T. C. O'Haver, P. N. Keliher, *Anal. Chem.*, **48**, 1978, 1166–1175.
- 28 D. M. Templeton, F. Ariese, R. Cornelis et al., *Pure Appl. Chem.*, **72**, 2000, 1453–1470.
- 29 R. Lobinski, *Appl. Spectrosc.*, **51**, 1997, 260A–278A.
- 30 B. Kolb, G. Kemmner, F. H. Schleser et al., *Fresenius' J. Anal. Chem.*, **221**, 1966, 166–175.
- 31 J. C. Van Loon, B. Radziuk, *Can. J. Spectrosc.*, **21**, 1976, 46–50.
- 32 O. F. X. Donard, in *5th Colloquium Atomspektroskopische Spurenanalytik*, Bodenseewerk, ed. B. Welz, Perkin-Elmer, Überlingen 1989, p. 395.
- 33 C. Bendicho, M. T. C. de Loos-Vollebregt, *J. Anal. At. Spectrom.*, **6**, 1991, 353–374.

- 34** L. H. J. Lajunen: *Spectrochemical Analysis by Atomic Absorption and Emission*, Royal Society of Chemistry, Cambridge 1992.
- 35** A. Montaser, D. W. Golightly: *Inductively Coupled Plasmas in Analytical Atomic Spectrometry*, VCH, New York 1992.
- 36** G. L. Moore: *Introduction to Inductively Coupled Plasma Atomic Emission Spectrometry*, Elsevier, Amsterdam 1989.
- 37** P. W. J. M. Boumans: *Inductively Coupled Plasma Emission Spectroscopy, Part I and II*, John Wiley & Sons, New York 1987.
- 38** M. Thompson, J. N. Walsh: *A Handbook of Inductively Coupled Plasma Spectrometry*, Blackie, Glasgow 1993.
- 39** M. S. Cresser: *Flame Spectrometry in Environmental Chemical Analysis*, Royal Society of Chemistry, Cambridge 1994.
- 40** A. Montaser, *Appl. Spectrosc.*, **52**, 1998, 406A–426A.
- 41** *Laser-Induced Plasmas and Applications*, eds. L. J. Radziemski, D. A. Cremers, Marcel Dekker, New York 1989.
- 42** *Glow Discharge Optical Emission Spectrometry*, eds. R. Payling, D. G. Jones, A. Bengston, John Wiley & Sons, New York 1997.
- 43** H. Becker-Ross, S. V. Florek, *Spectrochim. Acta, Part B*, **52**, 1997, 1367–1375.
- 44** J. Sneddon, Sample Introduction in Atomic Spectroscopy in *Advances in Atomic Spectroscopy*. Vol. 1, ed. J. Sneddon, JAI, Greenwich 1992, p. 81–124.
- 45** S. A. Darke, J. F. Tyson, *Microchem. J.*, **50**, 1994, 310–36.
- 46** W. P. Carey, *Trends Anal. Chem.*, **13**, 1994, 210–218.
- 47** D. Günther, S. E. Jackson, H. P. Longrich, *Spectrochim. Acta, Part B*, **54**, 1999, 381–409.
- 48** J. M. Mermet, E. Poussel, *Appl. Spectrosc.*, **49**, 1995, 12A–18A.
- 49** *Element-specific Chromatographic Detection by Atomic Emission Spectroscopy*, ed. P. Uden, American Chemical Society, Washington 1991.

## **Section VI**

### **Methods 5: Surface Analysis Techniques**

## 13

### Surface Analysis Techniques

A. Macková, S. A. Morton, C. G. H. Walker, and K. Volka

#### 13.1

##### Introduction [1, 2]

Surface analysis uses different techniques to probe the surface leading to a *response*, an *analytical signal* serving as a source of *analytical information*. The probe/response combinations used in surface analysis include electrons, ions, photons, neutrals, heat, and electric field. Practically all combinations may form the basis of techniques used in surface analysis and so their list is rather long and should by no means be considered to be complete. This is also due to fact that very subtle variations of a technique sometimes become known by their own name and acronym. Some of these acronyms are listed in the Appendix, Section 13.6.

There are several ways to classify the surface analysis techniques.

According to the probe used we have

1. *Photon Probe Techniques*, divided further according to the fundamental process used:
  - Scattering techniques (Raman spectroscopy),
  - Absorption techniques (infrared spectroscopy, EXAFS, SEXAFS, NEXAFS),
  - Emission techniques (UPS, XPS, LAMMS).
2. *Electron Probe Techniques*, based on:
  - Elastic scattering processes (TEM, REM, LEEM, BSE, THEED, LEED, RHEED)
  - Inelastic processes (REELS, TEELS, EPXMA, AES, SEM)
3. *Ion Probe Techniques*, based on
  - Elastic scattering processes (RBS, MEIS, ISS, ERD)
  - Inelastic processes (NRA, CPAA, SIMS, SNMS)
4. *Field Probe techniques* (STM)

The IUPAC Compendium of Analytical Nomenclature, Definitive Rules 1997 recommends the following scheme:

1. The electron, photoelectron and related spectroscopies
  - The photoelectron emission spectroscopies (UPS/UPES, XPS/XEPS DSPES, SRPES, SECSA, PED, ARPS/ARPES)

- Electron impact spectroscopies (HREELS/HEELS, EELS, EELFS/EXELFS, IS, ETS)
  - Electron-induced photon emission spectroscopies (IPS, BIS, BS)
  - Appearance potential spectroscopies (SXAPS, AEAPS, DAPS, TCS, XEAPS, EAPFS, IETS)
  - Auger electron spectroscopies (EAES, SAM, ARAES, SPAES, IAES, AEES)
  - The electron coincidence spectroscopies
2. The photon spectroscopies resulting from the use of electromagnetic radiation (TXRF)
  3. Neutron and ion scattering
    - Ion scattering (ISS, RBS)
    - Inelastic neutron scattering (INS)
    - Ion neutralisation spectroscopy (INS)
  4. Mass spectroscopy
    - Secondary ion mass spectrometry (SIMS)
    - Fast-atom bombardment mass spectroscopy (FAB MS)
    - Field-ion mass spectroscopy (FIMS)
  5. Other spectroscopic techniques
    - Metastable desorption spectroscopy (MDS)
    - Inverse photoelectron spectroscopy (IPES/BIS)
  6. Desorption and related techniques
    - Thermal desorption spectroscopy (TPD)
    - Temperature programmed reaction spectroscopy (TPRS)
  7. Spectroscopy/diffraction hybrids
    - Photoelectron diffraction (XPD)
    - Extended X-ray absorption fine structure (EXAFS)
    - Surface extended X-ray absorption fine structure (SEXAPS)
    - Near-edge X-ray absorption fine structure (NEXAFS/XANES)

For practical purposes a discrimination between the methods can be made according to information obtained on:

- Surface elemental composition
- Chemical bonding and molecular composition
- Surface electronic structure

In this chapter an attempt will be made to present the fundamentals of some of the spectroscopic methods used for the characterization of surfaces. As shown the spectroscopic methods represent a very important part of the arsenal used for characterization of surfaces, but in many cases it is difficult to separate the spectroscopic principals of a particular method from those of closely related techniques. Also usage of the term spectroscopy is sometime confusing. A broader definition of spectroscopy will be accepted here embracing not only the interaction of matter with electromagnetic radiation/photons, but also the interaction with particles (electrons, ions, molecules). Diffraction, desorption, microscopic, and imaging methods have been excluded from the discussion, but we are not quite rigorous in some cases where these methods are very closely connected to related spectroscopic methods.

### 13.2

#### Definition of the Surface [2-4]

Surface is a poorly defined term. The IUPAC recommendation is to distinguish three terms: surface in general, physical surface and experimental surface.

*Surface (general)* is the “outer portion” of a sample of undefined depth. This term is to be used in general discussions of the outside regions of the sample.

*Physical surface* is the outermost atomic layer of a sample (this is the layer which would be in direct contact with the vacuum, if the sample were placed in a vacuum).

*Experimental surface* is that portion of the sample with which there is significant interaction with the particles or radiation used for excitation. It is the volume of sample required for analysis, or the volume corresponding to the escape of emitted radiation or particles, whichever is larger.

A typical problem of surface analysis is the study of a material deposited on or adhered to a substrate. Coverage of a substrate by one atomic or molecular layer of a species is called a *monolayer*. The term *multilayer* designates that more than one layer of a species covers the substrate. In contrast to the monolayer, in this case not all elementary units of the layer are in contact with the surface layer of the substrate. Surface coverage for both monolayer and multilayer coverage is defined as the ratio of the amount of substance covering the surface to the monolayer capacity. Coverage equals unity for one complete monolayer on the substrate. The *film* is a material which has been deposited or adhered to a substrate and has a uniform thickness within 20 % of its average thickness, which is less than 10 µm.

A major problem of all surface methods is their sensitivity. Among the surface techniques only a limited number of atoms must be detected. Contained in a 1 cm<sup>3</sup> bulk sample is ca. 10<sup>22</sup> molecules, in one 1 cm<sup>2</sup> of the surface only ca. 10<sup>15</sup>, and when following a component present at the 1 % level, a technique sensitive to ca. 10<sup>13</sup> atoms is needed. A *surface sensitive technique* is more sensitive to the atoms located near the surface than to the atoms in the bulk. A *surface specific technique* gives signals due to atoms of the physical surface only. The mass fraction of the component in the experimental surface divided by its total amount in the volume of interest is often called *surface concentration*. It can be given in terms of atoms (particles) (ppm) or in terms of mass (µg g<sup>-1</sup>).

### 13.3

#### Selection of method [5]

There are many criteria according to which the method can be selected. A discussion of the decision steps has been given in detail elsewhere. A survey of the method is given in the reference data table along with some characteristics (Tab. 13.1). This table allows one to select the method according to the information needed and its parameters. Some tentative figures are also given allowing an estimate of the price and availability of a suitable laboratory to be made.

Table 13.1 Reference data table.

Technique	Sample	Conditions	Surface, specificity			Surface, resolution			Time needed for analysis	
			Form/Type	Size	Information Depth	Detectability	Depth	Lateral	Prep.	Meas.
AES	s	1 cm <sup>2</sup>	UHV	3 nm	0.1 at.%	3 nm	100 nm	1 h	3 h	10 min
APECS	s	5 mm	UHV	0.5 nm	0.5 ML	0.2	0.5 mm	1 h	5 h	2 h
APFIM	s	50 nm	UHV	0.1 $\mu$ m	10 at.%	0.2 nm	1 nm	8 h	8 h	
ARUPS	cr	> 1 mm	UHV	1 nm	0.1 ML	0.5 nm	1 nm	1 h	1 h	
ATR	s(flat), ]	mm-cm	>10 $\mu$ m	ML				5 min	5 min	1 h
CPAA	s	1 cm <sup>3</sup>	HV	bulk	1 ng g <sup>-1</sup>			5 min	10-100 h	10 min
DAPS	s	5 mm	UHV	0.5 nm	0.05 ML	2 nm	1-100 $\mu$ m	1 h	30 min	1 h
Ellipsometry	s(flat)]/l	0.2-1		10 nm	< 1 ML	1 $\mu$ m	10-100 $\mu$ m	mins	10 s-10 min	h
EMS	s	5 mm	UHV	0.5 nm	0.1 ML	2 nm	1-100 $\mu$ m	1 h	10 h	1 h
EPMA	s, powder	10 nm-1 cm	V	2 $\mu$ m	0.1 at.%	1 $\mu$ m	1 $\mu$ m	15 min	5 min - 5h	5 min - 1 h
ERD	s	0.5 cm <sup>2</sup>	HV	1 $\mu$ m	0.1 at.%	20 nm	1 mm	1 min	10 min	30 min
ESD	s	5 mm	UHV	0.5 nm	0.01 ML	0.5 nm	1-100 $\mu$ m	1 h	30 min	1 h
ESDIAD	s	5 mm	UHV	0.5 nm	0.01 ML	0.5 nm	1-100 $\mu$ m	1 h	5 h	1 h
EWCRDS	s	cm			0.01 ML					
GDOES	s (flat)	> 12 mm	V	100 $\mu$ m	10 <sup>14</sup> at.cm <sup>-1</sup>	2 nm	2 nm	2 min	15 min	5 min
GEXRF	th	> 10 cm <sup>2</sup>		1-100 nm	10 <sup>11</sup> at.cm <sup>-2</sup>	0.1 nm	5 cm	30 min	10 min-3 h	1 h
GIKRF	s	> 0.5 cm <sup>2</sup>		3 nm-1 $\mu$ m	10 <sup>12</sup> at.cm <sup>-3</sup>	0.3-100 nm	1 cm	0	2 h	1 h-1 day
HREELS	cr	1 mm	UHV	0.2 nm	< 1 ML	1 nm	1-5 mm	days	days	weeks
IETS	s/th	5 mm		0.5 nm	0.01 ML	0.5 nm	5 mm	1 h	30 min	1 h
IPES	s	> 1 mm	UHV	0.5 nm	0.1 ML	0.5 nm	1 mm	1 h	5 h	1 h
ISS	s	1 cm <sup>2</sup>	UHV	1-2 ML	0.001 ML	1 ML	150 $\mu$ m	30 min	10 min	15 min
LEIS	s	1 cm <sup>2</sup>	UHV	0.01 nm	0.01-0.1 at.%	0.1 nm	1 min	10 min	10 min	
LMMS	s	mm <sup>2</sup>	V	10-50 nm	10 <sup>7</sup> at.		3 $\mu$ m	10 min	10 min	4 h
NDP	s	0.5 cm <sup>2</sup>	HV	bulk	10 <sup>15</sup> at.cm <sup>-2</sup>	10-20 nm		5 min	0.5-1 h	10 min
NEXAFS	s	5 mm	UHV	0.5 nm	0.01 ML	0.5 nm	1 mm	1 h	30 min	1 h
NRA	s	3 mm	HV	0.1-1 $\mu$ m	0.1-100 ppm	5-100 nm	1 mm	0	10 min	15 min
PAES	c	>1 mm	UHV	0.2 nm	0.1 at.%	0.1 nm	100 nm	1 h	2 h	2 h
PAS	s, l	0.2-1 cm		10 nm	1 ML		10 $\mu$ m	10 min	10 min	10 min

<b>PEEM</b>	s	5 min	UHV	5 nm	0.1 ML	0.5 nm	30 nm	30 min	> 1 h	5 min – 1 h
<b>PIES</b>	s	> 1 mm	UHV	0.2 nm	0.1 ML	0.2 nm	0.05 nm	2 h	2 h	2 h
<b>PIGE</b>	s, pellet	> mg	HV	50 µm	>10 ppm		10 µm	0–2 h	>10 min	5 min
<b>PIXE</b>	s, powder	1 mm	HV	50 µm	0.12 ppm	10 µm	1 µm	2 h	10 min	3 min
<b>RBS</b>	s	0.25 cm <sup>2</sup>	UHV	2–10 µm	0.1 at.%	25 nm	0.5 nm	1 min	10 min	5 min
<b>REELS</b>	c	5 mm	UHV	0.5 nm	0.01 ML	2 nm	1–100 µm	1 h	30 min	1 h
<b>SEM</b>	s, powder	1 nm <sup>-1</sup> cm	V	0.2 nm–10 µm	0.1 at.-%	0.2 nm	0.2 nm	15 min	5 min – 5 h	5 min – 1 h
<b>SEMPA</b>	s, powder	10 nm <sup>-1</sup> cm	V	2 µm	0.1 at.-%	1 µm	1 µm	15 min	15 min – 5 h	5 min – 1 h
<b>SERS</b>	th	µm–mm		1 µm		1 µL		5 µm	10 min	10 min
<b>SFG</b>	transparent s, l	0.1–1 mm <sup>2</sup>		1 nm–1 µm	0.1 ML	0.3 nm	11 µm	30 min	2 h	30 min
<b>SHG</b>	transparent s, l	1 mm <sup>2</sup>		10 nm–1 µm	0.1 ML	0.3 nm	10 µm	30 min	2 h	30 min
<b>SIMP</b>	s	0.25 cm <sup>2</sup>	V				0.1 nm	1 min	10 min	15 min
<b>SIMS/dyn</b>	s	0.01–2.5	UHV	10 nm–100 µm	ppb–ppm	10 nm–5 µm	0.1–5 µm	20 min	5 min–20 h	2 h
<b>SIMS/static</b>	s, powder	> 0.5 mm	UHV	1 nm	10 <sup>9</sup> atm cm <sup>-2</sup>		0.5 µm	0	10 min	10 min
<b>SNMS</b>	s	0.25 cm <sup>2</sup>	UHV	> 100 µm	0.1 ng g <sup>-1</sup>	0.5		20 min	5 min–2 h	2 h
<b>SPEELS</b>	c	5 mm	UHV	0.5 nm	0.01 ML	2 nm	1–100 µm	1 h	5 h	1 h
<b>SPIPES</b>	c	> 1 mm	UHV	0.5 nm	0.1 ML	0.5 nm	1 nm	1 h	5 h	1 h
<b>SPUPS</b>	c	5 mm	UHV	0.5 nm	0.5 ML	0.5 nm	1 nm	1 h	> 1 h	1 h
<b>SPXPS</b>	c	5 mm	UHV	0.5 nm	0.5 ML	0.5 nm	1 nm	1 h	> 1 h	1 h
<b>STS</b>	s	1 mm	UHV	0.5 nm	0.001 ML	0.5 nm	0.1 nm	1 h	5 min	1 h
<b>UPS</b>	c	5 mm	UHV	0.5 nm	0.01 ML	2 nm	1 nm	1 h	30 min	1 h
<b>XAFS</b>	s	5 mm		1–5 nm	0.01 ML	1–5 nm	1 nm	1 h	30 min	1 h
<b>XPS</b>	s	5 mm	UHV	10 nm	0.1 at.-%	0.2 nm	0.01–1 nm	30 min	> 1 h	5 min – 1 h
<b>XPD</b>	cr	5 mm	UHV	5 nm	0.1 at.-%	0.2 nm	0.01–1 nm	1 h	> 2 h	> 1 h
<b>XRF</b>	s, l, th	8–500 µm		30 nm–8 µm	ppm	2%	0.2 nm	5 min	3–60 s	5 min
<b>XSW</b>	cr	5 mm		1 nm–8 µm	ppm	0.2 nm–1 µm	0.1 nm	2 h	3 h	3 h

<sup>a</sup> Data for techniques in the normal fonts are taken from ref. [5] and have been compiled from a questionnaire action, data for techniques given in italics are only an estimate of the authors of this chapter.

<sup>b</sup> Diameter or area.

<sup>c</sup> Abbreviations: s solid, l liquid, cr crystal, c (solid) conductor, V vacuum, HV high vacuum (ca  $10^{-3}$ – $10^{-5}$  Pa), UHV ultra high vacuum, ML monolayer, th thin film.

Table 13.1 continued.

Technique	Type of information								Cost, ECU /b	Number of facilities /c	Type of laboratory /d	User skill needed/d
	Elemental composition	Molecular composition	Spot, line or map analysis	Depth profile	Film/layer thickness	Dielectric constant	Phase changes	Density				
AES									500	500	M	S
<i>APECS</i>									*****	*	L	S
APFIM									1000	50	M	S
ARUPS									***	***	M	S
ATR									*	****	M	S
CPAA									500-1000	500	M	T
DAPS									***	**	M	S
Ellipsometry									40	10000	S	T
EMS									****	**	L	S
EPMA									*	****	S	T
ERD									100	300	L	T
ESD									***	1000	M	S
ESDIAD									****	**	L	S
EWCRD <b>S</b>									****	*		
GDOES									100	500	S	T
GEXRF									600-6000	2	M	S
GIXRF										10	M	S
HREELS									1000	500	M	S
IETS									**	**	S	T
IPES									****	**	M	S
ISS									70	500	M	T
LEIS									200	300	M	S
LMMS									600	300	S/M	S
NDP									1000	50	L	S
NEXAFS									****	**	L	S
NRA									200	300	M	S
PAES									*****	*	L	S
PAS									60	200	M	T
PEEM									****	***	M	S
PIES									****	**	M	S
PIGE									500	50	M	S
PIXE									500	300	M	S

Technique	Type of information								Cost, ECU /b	Number of facilities /c	Type of laboratory /d	User skill needed/e
	Elemental composition	Molecular composition	Spot, line or map analysis	Depth profile	Film/layer thickness	Dielectric constant	Phase changes	Density				
RBS									500	500	M	S
<i>REELS</i>									**	***	M	S
<i>SEM</i>									*	*****	S	T
<i>SEMPA</i>									***	***	M	S
<i>SERS</i>									**	***	M	S
SFG									600	50	M	S
SHG									600	50	M	S
<i>SIMP</i>									500	400	M	S
<i>SIMS/dyn</i>									100-2000	500	M	S
<i>SIMS/static</i>									150-400	100	M	S
<i>SNMS</i>									100-2000	500	M	S
<i>SPEELS</i>									*	**	L	S
<i>SPIPES</i>									*****	*	L	S
<i>SPUPS</i>									*****	**	L	S
<i>SPXPS</i>									*****	**	L	S
<i>STS</i>									***	***	M	S
<i>TXRF</i>									10-200	200	M	T
<i>UPS</i>									***	1000	M	S
<i>XAFS</i>									****	**	L	S
<i>XPD</i>									***	***	M	S
<i>XPS</i>									400	400	M	S
<i>XPS</i>									**	****	M	S
XRF									20	5000	M	T
XSW									*****	*	L	S

<sup>a</sup> Data for techniques in the normal fonts are taken from the ref. [5] and have been compiled from a questionnaire action, data given in italics are only an estimate by the authors of this chapter.

<sup>b</sup> Estimated cost per sample: from \* cheap (10 ECU) to \*\*\*\*\* very expensive (2000 ECU).

<sup>c</sup> Estimated number of facilities: \* < 10, \*\* 10–100, \*\*\* 100–1,000, \*\*\*\* 1,000–10,000, \*\*\*\*\* > 10,000.

<sup>d</sup> S small (company quality control, field laboratory), M medium (university, company), L research campus of multinational company, major university, government run national laboratories.

<sup>e</sup> S specialist, doctoral level or equivalent, T technician, bachelors level or equivalent.

At present the most popular techniques for chemical surface characterization are X-ray photoelectron spectroscopy (XPS), Auger electron spectroscopy (AES), secondary ion mass spectrometry (SIMS) and also infrared (IR) techniques, which bring different and complementary information.

The critical point of the surface analysis is to prevent any changes to the surface before or during the experiment, because of this most methods do not allow one to carry out the technique *in situ*, as ultra high vacuum (UHV) is needed.

UHV is required for most surface analysis techniques for several reasons:

- to have sufficient mean free path of the probe and detected particles (electron, ions, atoms)
- to eliminate the signal from the interaction of the probe particle with the molecules in the gas phase
- to preserve a reproducibly clean surface during all measurements.

Even though the first two requirements allow work at pressures better than  $10^{-4}$  Torr, contamination of the surfaces occurs in less than 1 s at this pressure. This means that for maintenance of a clean surface pressures lower than  $10^{-9}$  Torr are needed. These pressures are now routinely obtainable.

Another problem is connected with sputtering and heating of the surface. Surfaces in UHV are initially covered in “crud” that is associated with prior exposure to the atmosphere. This normally consists of several monolayers of oxide and adsorbed hydrocarbons that need to be cleaned away by argon ion bombardment to permit analysis of the sample by a surface sensitive technique. This process of sputter cleaning can change the surface composition and/or structure and is not always successful at removing all contamination.

Interaction of the highly energetic particles with the sample may also result in heating of the targeted parts (especially for thermally nonconductive samples) and additional cooling may be required to minimise this effect.

For some methods erosion of the surface is inherent. This is typical for dynamic SIMS, where the sputtered particles are analysed.

## 13.4 Individual Techniques

### 13.4.1 Angle Resolved Ultraviolet Photoelectron Spectroscopy [6, 7]

**Acronyms:** ARUPS (angle resolved ultraviolet photoemission spectroscopy)  
ARPES (angle resolved photoelectron spectroscopy)

#### 13.4.1.1 Introduction

Samples are exposed to monochromatic ultraviolet radiation (typically 10–100 eV) and the energies and emission angles of the ejected photoelectrons are measured to reveal information on the valence band electronic structure.

#### 13.4.1.2 Instrumentation

The measurement is carried out in an UHV chamber. Ultraviolet photons from a source such as a He lamp (21.2 or 40.8 eV) are shone at the sample to eject photoelectrons. The emitted electrons are collected by an electron energy analyser, such as a hemispherical mirror analyser that has a narrow angular acceptance to produce a spectrum of the number of electrons emitted with a given kinetic energy and at a given angle. Varying the emission angle by moving the sample or the analyser enables spectra to be acquired across a range of emission angles. Such datasets allow the momentum vectors of the emitted electrons to be determined to produce “band maps” of the electronic structure of the valence bands. By using a synchrotron source instead of a He lamp the momentum of the emitted electrons can be varied by changing the photon energy, enabling different regions of the band structure to be explored for a given range of emission angles.

#### 13.4.1.3 Sample

Samples must be single crystal metallic or semiconducting UHV compatible materials.

#### 13.4.1.4 Analytical Information

“Band maps” of the electronic structure of the top few atomic layers.

#### 13.4.1.5 Performance Criteria

Spatial, angular and energy resolutions are strongly dependent on the electron energy analyser and photon source used. However, spatial resolution may be as good as 10 µm, energy resolution as good as 5 meV, and angular resolution as good as 10 mrad.

Typically concentrations of a few atomic percent at the surface can be detected, depending strongly on the cross-section of the particular elements present. Sensitivity decreases rapidly with depth below the surface and is often negligible below a depth of approximately five atomic layers.

High surface sensitivity makes the technique vulnerable to contamination, necessitating the use of UHV procedures. The low energy of the emitted electrons makes the technique vulnerable to the presence of stray magnetic fields and so magnetic shielding may be required.

The spectrum is influenced by the particular crystal structure of the sample’s top few atomic layers, which may not be completely representative of the bulk material.

The technique is only applicable to single crystal materials and is generally not suitable for insulating materials.

#### 13.4.1.6 Applications

ARUPS is used to probe the three-dimensional band structure of the electronic states near the Fermi level that are responsible for determining a material's electronic properties and also to study the nature of the bonding between the atoms in the sample or between the sample and adsorbate molecules on its surface.

#### 13.4.1.7 Other Techniques

UPS (Ultraviolet photoelectron spectroscopy), is similar to ARUPS but spectra are collected at a fixed angle to determine the sample's overall valence band density of states (DOS). UPS is not restricted to single crystal samples. SPUPS (Spin polarised UPS) allows the density of states to be determined independently for the spin-up and spin-down electrons of a magnetic material by using a polarisation sensitive detector.

### 13.4.2

#### Appearance Potential Spectroscopy [8]

*Acronyms:* APS (appearance potential spectroscopy)

DAPS (disappearance potential spectroscopy)

AEAPS (Auger electron appearance potential spectroscopy)

SXAPS (soft X-ray appearance potential spectroscopy)

XAPS (X-ray appearance potential spectroscopy)

##### 13.4.2.1 Introduction

The energy of an incident ionising radiation (usually electrons) is gradually increased such that the energy passes over the ionisation threshold of a core level of an atom in the surface being studied. This is the basis of the appearance potential spectroscopies. In the case of DAPS, the onset of ionisation is detected by a reduction in the intensity of the elastically scattered beam. For AEAPS, the Auger electron current is measured as the incident beam energy is increased. For SXAPS, it is the appearance of X-ray emission, which is detected. If the incident radiation is X-rays, then the methods are more generally known as X-ray absorption fine structure (EXAFS) and related techniques.

##### 13.4.2.2 Instrumentation

The measurement is carried out in an UHV chamber. Electrons from an electron gun in the energy range 50–2000 eV are directed onto the sample. The incident electron energy is gradually increased. In the case of DAPS, the elastically scattered primary electrons are detected using a retarding field analyser (RFA). As the energy

of the incident beam passes through an ionisation edge, the number of elastically scattered electrons drops slightly.

In the case of AEAPS, it is not necessary to detect individual Auger peaks, as the total secondary electron yield can be measured instead. The electron cascade within the material can act as an electron multiplier increasing the AEAPS signal. Hence an RFA could be used or an electron detector of a type used in a scanning electron microscope.

For SXAPS, the instrumentation is very simple. A filament is used as a source of electrons and is mounted close to the sample. The electrons from the filament are accelerated towards the sample. A screening mesh in front of the detector allows X-rays to pass into the detector, but not electrons. The X-rays cause photoelectrons to be emitted from the wall of the detector and these photoelectrons are collected on a thin wire. The detector has a superficial similarity to a Geiger-Muller tube. UHV is not needed for the instrumentation (this is especially true for SXAPS), but a clean surface is necessary for reliable data.

#### 13.4.2.3 Sample

Conducting samples, which survive well in UHV are normally studied. Insulating or biological samples will usually degrade in the beam.

#### 13.4.2.4 Analytical Information

The elemental composition within the surface may be determined, but quantification is difficult. In addition, information regarding the empty density of states can be revealed. It therefore supplies complementary information to inverse photoelectron spectroscopy (IPES) and scanning tunnelling spectroscopy (STS).

#### 13.4.2.5 Performance Criteria

Typically a content of ~5 at.% in the surface region can be determined or alternatively ~20 % of one monolayer covering the surface. These estimates are very much dependent on the material as there are large variations in sensitivity depending on the density of empty states within the sample.

The change in the elastically scattered yield when the primary beam energy passes through an ionisation threshold is typically 0.1 %. Hence, electronic differentiation is used to enhance the weak signal. AEAPS is approximately 10 times more sensitive than DAPS. SXAPS is approximately 10,000 times less sensitive than DAPS and hence is the least used despite its simple instrumentation.

#### 13.4.2.6 Applications

APS is used to determine the empty density of states and elemental composition of conducting materials. Currently a little used technique.

#### 13.4.2.7 Other Techniques

TCS (Total (or target) current spectroscopy) is similar to DAPS, but it is a very low energy technique (0–15 eV) and all the secondary electrons originate from the valence band.

#### 13.4.3

#### Atom Probe Field Ion Microscopy [5, 8]

*Acronyms:* APFIM (atom probe field ion microscopy)

##### 13.4.3.1 Introduction

APFIM is an extension of field ion microscopy (FIM). In FIM, an atomically sharp metallic tip is kept in an atmosphere of gas and a high electric field is then applied in the region of the sharp tip. Gas atoms on the tip are emitted from it and impinge on a phosphor screen. The very small area of gas emission from the tip can be viewed on the screen giving images of the tip at atomic resolution. With APFIM, a mass spectrometer is added to the instrumental set-up. This provides the ability to identify which atoms are being emitted from the surface. A sudden pulse is applied to the tip and this can cause a layer of atoms to be removed from it. The atoms emitted enter a drift tube and the time of arrival of the atoms at the detector enables their mass to be determined. This produces atomic resolution images in three-dimensions of the material comprising the tip.

##### 13.4.3.2 Instrumentation

A UHV chamber containing the sample in the form of a sharp tip is required. A time of flight mass spectrometer to identify the type of atoms emitted from the surface is also needed.

##### 13.4.3.3 Analytical Information

APFIM provides information concerning the three-dimensional arrangement of elements within the sample at atomic resolution.

##### 13.4.3.4 Performance Criteria

The sample should be in the form of a sharp tip and be electrically conducting. The form of the sample is less convenient than for the scanning probe methods, but APFIM does provide extra elemental information.

##### 13.4.3.5 Applications

APFIM is used where the elemental composition of the material at the very highest spatial resolution is needed.

### 13.4.4

#### Attenuated Total Reflection Spectroscopy [9–11]

*Acronyms:* ATR (attenuated total reflection)  
 MIR (multiple internal reflection)  
 FMIR (frustrated multiple internal reflections)

##### 13.4.4.1 Introduction

The attenuation of a beam of radiation passing through an optical element from a high refractive index material, under the condition of total internal reflection, is measured. The sample must be in good optical contact with the surface of the optical element at which total internal reflection occurs.

Ranges of operation: from ultraviolet to infrared, but mid-infrared typical.

##### 13.4.4.2 Instrumentation

Attenuated total reflection spectroscopy is realized on standard spectrometers using an attachment introduced into the sampling area. Different geometric arrangements are used to direct the radiation through the optical element and onto the detector. The primary difference is in the shape of the optical element. Single (usually denoted as ATR) or multiple reflections (typically 8–20 for MIR or FMIR) can be achieved. Typical materials (crystalline and amorphous) for the optical element are: As<sub>2</sub>Se<sub>3</sub>, AgCl, CdTe, diamond, Ge, KRS 5 (thallous bromide iodide), quartz, Si, ZnSe, and glass. The choice of material depends on the frequency range of operation.

##### 13.4.4.3 Analytical Information

The ATR spectrum, (i. e. the dependence of the reflectance on the wavenumber), for a sample resembles the transmission spectrum, but two features exclude a direct comparison:

1. The depth of penetration is directly proportional to the wavelength; this means that the absorption bands at shorter wavenumber are intensified in the ATR spectra.
2. The maximum shifts and intensity distortions can occur due to optical dispersion. These differences are more pronounced for smaller band separations and stronger bands.

A Kramers–Kronig analysis allows one to separate the absorption index and refractive index spectra. Different algorithms for this analysis are available.

##### 13.4.4.4 Performance Criteria

The penetration depth is a complex function of the absorption and refractive indexes of the sample and ATR element, wavelength, and angle of incidence of radiation.

The angular dependence of the penetration depth allows depth profiling, but due to superposition of the contributions from different depths an analysis can be difficult.

#### 13.4.4.5 Applications

This method is not suitable for powders (particularly if they are hard). Study of the surfaces of compact samples is very sensitive to the quality of the optical contact reached between the sample and the ATR attachment. Good contact can be easily obtained when analysing surfaces of elastomeric materials. The optical contact is usually poor for rough and rigid samples.

By using the MIR or FMIR techniques a longer effective pathlength can be obtained through multiple reflections.

On the other hand, the ATR technique is very useful in cases when the ATR attachment can be used as an integral part of the surface experiment. If covered by an optically transparent thin-layer electrode (e.g. Pt), electrode phenomena can be studied. Monolayers, Langmuir–Blodgett can be transferred onto the attachment or *in situ* experiments can be done with the ATR attachment in optical contact with the hydrophobic part of the Langmuir–Blodgett layer.

#### 13.4.5

#### Auger Electron Spectroscopy [5, 6, 8, 12, 13]

**Acronyms:** AES (Auger electron spectroscopy)

EEAES (electron excited Auger electron spectroscopy)

XXAES (X-ray excited Auger electron spectroscopy)

SPAES (spin polarised Auger electron spectroscopy)

##### 13.4.5.1 Introduction

An incident exciting beam (normally electrons) is directed at a surface. The atoms in the surface enter an excited state and can relax by the emission of an Auger electron, which has a characteristic energy. The energy spectrum of Auger electrons (20–2000 eV) emitted following the primary ionisation of a core energy level can reveal the chemical composition of the surface layers.

##### 13.4.5.2 Instrumentation

The measurement is carried out in an UHV chamber. Fixed energy electrons from an electron gun in the energy range 100 eV–10 keV are directed on to the sample (beam diameter 0.1–1 mm). The electrons from this primary beam excite electrons from the surface (known as secondary electrons) and some of the primary electrons ‘bounce’ from the nuclei of the surface atoms to create backscattered primary electrons. The primary beam of electrons can also cause atoms in the surface to emit Auger electrons, which have energies characteristic of the element that emitted them. Some of the electrons emitted from the surface pass through an aperture

and into an electron energy analyser, which selects electrons over a narrow range of energies, and these electrons are then detected. A spectrum is obtained as the first or second derivative of the secondary electron current by changing the voltages on the electron energy analyser such that the energy of electrons which pass through the analyser is gradually changed.

#### 13.4.5.3 Sample

Conducting samples which survive well in UHV are normally studied. Insulating or biological samples degrade in the beam.

#### 13.4.5.4 Analytical Information

The first or second derivative of secondary electron current, with respect to the analyser energy is measured (Fig. 13.1). The secondary electron current can also be measured by electron counting techniques. The resultant electron spectrum reveals a series of peaks at different electron energies. The energy of the peaks is characteristic of the element that produced the electrons and thus the elements comprising the top few monolayers of the surface can be determined.

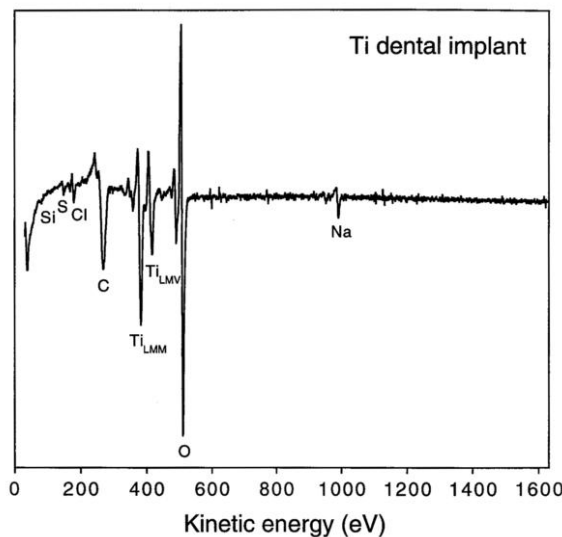


**Fig. 13.1** Auger electron survey spectrum from a titanium dental implant surface, showing that the surface consists of a titanium surface oxide, with a carbon contamination overlayer and some trace impurities (3 keV primary electrons, 250 nA primary beam current) (reproduced from [5] with permission).

#### 13.4.5.5 Performance Criteria

Energy resolution is normally in the range 0.5–2 eV.

Typically a content of ~0.5 at.% in the surface region can be determined or alternatively ~2% of one monolayer covering the surface. This depends on the intensity of Auger emission for the element concerned. Typically, Auger electron

emission is high for low atomic number elements and gradually drops as the atomic number increases.

Auger electrons are not emitted by hydrogen and helium.

#### 13.4.5.6 Applications

This method is a workhorse technique for surface science experiments in UHV. Typically it is used to determine surface, cleanliness prior to the main experiment. The usual contaminants are carbon and oxygen. It is also used in metallurgy, microelectronics and corrosion science.

#### 13.4.5.7 Other Techniques

If the primary beam consists of ions, then the technique is known as ion excited AES or IAES. This offers no major advantages in sensitivity, but simultaneous Auger emission and depth profiling can be carried out. By varying the take-off angle of the detected electrons, some information regarding the depth profile of the elements under study can be obtained. This technique is known as ARAES (angle resolved AES). Due to the longer path length, ARXPS (angle resolved X-ray photoelectron spectroscopy) is a better method in this regard. Spin polarised AES is possible using a Mott detector as with other spin polarised techniques. This can provide information regarding the spin resolved density of states for different elements (see also SPUPS, spin polarised ultraviolet photoelectron spectroscopy). The low detection rate of the Mott detector makes data collection for SPAES very slow.

#### 13.4.6

#### Auger Photoelectron Coincidence Spectroscopy [14–16]

*Acronyms:* APECS (Auger photoelectron coincidence spectroscopy)

##### 13.4.6.1 Introduction

In coincidence spectroscopy two or three particles originating from a single event are detected simultaneously. In APECS an X-ray beam is shone at a sample to excite photoelectrons from core levels, leaving behind excited core hole states. These decay virtually immediately by Auger emission of an electron. Simultaneous detection of the photoelectron/Auger electron pair allows all other electrons not directly involved in that event to be eliminated. This produces spectra that are completely free of background signal from scattered secondary electrons and eliminates overlapping peaks from closely related decay events.

#### 13.4.6.2 Instrumentation

An electron energy analyser such as a cylindrical mirror analyser (CMA) is used to detect photoelectrons emitted at a kinetic energy precisely corresponding to the core level of interest. A second CMA is used to sweep continuously through the energy range of the corresponding Auger peak. Only those Auger electrons whose detection coincides exactly with the simultaneous detection of a photoelectron by the first CMA are counted. This eliminates all electrons not directly involved in the particular photoemission process of interest; including secondary electrons or Auger electrons that have been generated by photoemission from other core levels with very similar energies. This produces Auger spectra that are free of backgrounds and other, superimposed, peaks, allowing the true Auger peak shape to be determined. The process can also be reversed, scanning the first (photoelectron) CMA whilst keeping the second CMA at a fixed (Auger) energy to produce true, background free, photoelectron peaks instead.

#### 13.4.6.3 Sample

UHV compatible conductors that are stable over an extended period of UHV and X-ray exposure.

#### 13.4.6.4 Analytical Information

True peak shapes for Auger electron spectroscopy (AES) or X-ray photoelectron spectroscopy (XPS) that are free from the backgrounds, overlapping peaks and satellite features that are present in conventional AES or XPS are obtained.

#### 13.4.6.5 Performance Criteria

The requirement that only events where both emitted electrons are detected significantly reduces the count rate compared to standard XPS or AES as the probability of both electrons entering the correct analysers is very low. Count rates are between one count per minute and one count per second.

The energy resolution of 0.5–1 eV is significantly worse than in conventional AES or XPS as emphasis must be placed on maximizing the achievable count rate at the expense of overall resolution. Spatial resolution is around 0.5 mm. Typical energy range is 50–2000 eV. APECS is sensitive to all elements except H and He.

The requirement that both electrons must be ejected from the sample without undergoing scattering, combined with the geometrical effects resulting from the angle between the two detectors, means that APECS is significantly more surface sensitive than either XPS or AES alone, by about a factor of two. Hence, sensitivity is negligible below about five atomic layers.

UHV is required for this technique. High surface sensitivity combined with long acquisition times means that it is limited to samples that will remain stable and clean in vacuum for many hours under the X-ray beam.

#### 13.4.6.6 Applications

APECS is used in studies where determining the true shape of the XPS or Auger peaks free from background subtraction errors or overlapping features is important, such as for compiling standard reference spectra, instrument calibration, and verification of theoretical models of photoelectron and Auger emission.

#### 13.4.6.7 Other Techniques

PAES (positron annihilation Auger electron spectroscopy) is another technique for producing true AES peak shapes that are free of the secondary electron background. PAES is identical to conventional Auger electron spectroscopy except that the sample excitation is done with a low energy beam of positrons rather than a higher energy beam of electrons.

#### 13.4.7

#### Charge Particle Activation Analysis [5, 17]

*Acronyms:* CPAA (charge particle activation analysis)

HIAA (high energy ion activation analysis)

##### 13.4.7.1 Introduction

CPAA is an analytical method for determining the elemental composition concentration of trace elements in the near surface region. The activated region in CPAA is prescribed both by the penetration range (it is defined as the thickness of appropriate material which stops the charged particle) and the charged particle beam diameter. Activation analysis is a highly sensitive, non-destructive technique for the detection of trace amounts of elements in a variety of matrices. The sample to be analysed is activated by irradiation with an ion beam of a suitable type and energy. Artificial radioisotopes are created by nuclear reactions with nuclides present in the sample. The half-life of the radionuclides produced and the type and energy of the emitted radiation are used to identify the elements present.

##### 13.4.7.2 Instrumentation

For CPAA, protons and deuterons have to be accelerated to energies between a few MeV and 20–30 MeV and twice as high for helium-3 or helium-4 particles. An isochronous cyclotron, designed as a variable energy accelerator, covers this energy range. The energy of the beam should be well defined (an accuracy of 0.1 MeV) and reproducible. An important consideration is the beam uniformity for even irradiation of the beam spot area. If the beam energy is higher than that required for sample activation, the energy can be reduced by energy loss in a filter foil of a carefully chosen thickness.

#### 13.4.7.3 Sample

CPAA has no special limitations on the type of samples that can be studied. The sample should have a size of the order of cm in the usual case of solid samples. The simplest measurement is possible for solid samples with good thermal conductivity, not powdered and available as a foil or sheet with the thickness slightly larger than the range of the charged particles in the material (it means that charged particles should be stopped in the sample). However, CPAA also offers a number of possibilities for the determination of trace elements in biological materials.

The main disadvantages of CPAA are its complexity and cost, its lower suitability for liquid samples, and heating of the sample during irradiation. Special precautions have to be taken for samples that are not massive and are poor thermal conductors. Samples may need to be mounted on a cooled background to prevent overheating during irradiation. Even then, the temperature of the sample surface may rise by many hundreds of °C with beam currents of the order of 10 µA. A conducting surface layer or foil may be needed when irradiating insulating materials to prevent overheating and consequent sample damage.

#### 13.4.7.4 Analytical Information

Qualitative analysis is based on the identification of the created radioisotopes, mainly using high-resolution gamma-ray spectroscopy. In CPAA a related method is mostly used, whereby a sample and a standard are irradiated and the activity from the analysed element is measured in both the sample and the standard. The concentration in the sample can then, in principle, be calculated from the concentration in the standard and the ratio of the activities measured in the sample and the standard.

#### 13.4.7.5 Performance Criteria

For optimum analytical sensitivity it is desirable to produce the maximum amount of activity in the sample to determine and measure that activity with the maximum efficiency. The measurement of activities with short half-lives should be carried out as soon as possible after the irradiation. It follows from the basic equation of activation analysis that 50 % of the maximum activity is obtained after irradiation time equal to one half-life and more than 90 % after four half-lives.

Detection limits down to  $1 \text{ ng g}^{-1}$  can be reached for certain isotopes. The choice of ion type and energy provide versatility for optimising sensitivity and selectivity to suit particular problems. Proton energies from 5 to 20 MeV are needed to obtain a sufficiently high cross-section for good sensitivity in CPAA. CPAA has excellent sensitivity especially for light elements, such as B, C, N and O. CPAA is unique amongst activation techniques its ability to determine of H and He contents at levels below  $1 \mu\text{g g}^{-1}$ .

CPAA can also be performed after radiochemical separations of products to improve detection limits.

Sample heating when a high beam current is used may lead to changes or damage of the sample. Cross-sections are generally lower than those for neutron activation analysis (NAA). Counting times of 10 to 120 h are necessary to achieve high sensitivity and this reduces the number of samples that can be analysed. Ionisation energy loss prevents the irradiation of large volumes and so the ion range limits the produced activity.

#### 13.4.7.6 Application

Activation analysis is primarily a technique used for detection of impurities in bulk materials.

CPAA offers a number of interesting possibilities for the determination of trace elements in biological materials. It allows the determination of those elements that are difficult or impossible to determine by neutron activation, such as Al, Si, V, Cr, Ni, Cd, Sn, Tl, and Pb.

It makes CPAA a powerful technique when a sufficiently powerful accelerator is available.

#### 13.4.7.7 Other Techniques

NAA (neutron activation analysis) is similar to CPAA but uses thermal neutrons, (typically from a nuclear reactor), to activate the sample rather than charged particles. In general, the detection limits of NAA are in the range  $10^{-8}$ – $10^{-14}$  g.

There is no intrinsic depth sensitivity in NAA due to activation of the whole sample. Neutron losses in the sample are negligible.

#### 13.4.8

#### Diffuse Reflection Spectroscopy [10, 11]

**Acronyms:** DRIFTS (diffuse-reflectance (or reflection) infrared Fourier transform spectroscopy)

##### 13.4.8.1 Introduction

The diffusely scattered radiation from a sample is collected, refocused and detected. Typical range of operation is from the ultraviolet to the infrared.

##### 13.4.8.2 Instrumentation

Special reflectometers or emission photometers are constructed for measurement of diffuse reflectance, but, by using a suitable attachment, the measurement can be realized in principle using any spectrometer. The main requirement is an integrating sphere (Ulbricht sphere) or mirrors covering a large solid angle (particularly in the infrared region). Separation of the specular and diffuse reflection components is critical for the quality of diffuse reflection spectra that rely on spatial filtering

(irradiation normal to the surface or out-of-plane configuration) or mechanical beam stops (“blocker”).

#### 13.4.8.3 Analytical Information

It is not usually possible to measure the absolute reflectance of a sample and so, instead, the relative reflectance is measured as the ratio of the reflectance of the sample to the reflectance of a reference non-absorbing material. Powdered samples are usually diluted with a non-absorbing particulate matrix such as KBr. This helps meet the prerequisites of the Kubelka–Munk model. KBr is then also used as a reference medium.

If the scattering coefficient is independent of wavelength, the information obtained is similar to that obtained from transmission measurements. Under this condition a linear dependence between the Kubelka–Munk function and the concentration should be found. For low absorption, the sensitivity of diffuse reflectance is greater than that of transmittance, while strong absorption bands are less pronounced in the diffuse reflection. The scattering coefficient increases with diminishing particle size, while the depth of penetration of the radiation diminishes. The mean layer thickness penetrated within the sample becomes smaller and so the absorbed fraction is reduced. This fact is particularly useful for investigating adsorbed species on finely dispersed samples. Restrahlen bands can sometimes complicate the spectrum and their elimination is very difficult. The origin of these bands lies in the total reflection that occurs when the refractive index of air is higher than the refractive index of the sample.

#### 13.4.8.4 Performance Criteria

The quality of the spectra depends critically on the sample material (its crystal form, refractive index, and absorbance), particle shape and size, packing density, texture of the macroscopic surface as well as on the experimental arrangement (angles of incidence and observation, prevention of the specular fraction from reaching the detector). Presence of the specular component results in strong compression of the spectrum. This compression also occurs in the case of strong absorption in the sample, when the specular component can be the main contribution to the detected signal. The usual method of overcoming band suppression is a dilution of the sample as mentioned.

In general, the reproducibility of the measurements is often limited.

#### 13.4.8.5 Applications

Diffuse reflection spectroscopy is particularly useful for measuring the spectra of adsorbed molecules, chemically modified surfaces, and catalysts. All spectral ranges from the UV to the infrared are used. Different information can be obtained in different spectral ranges. Adsorption under the influence of Van der Waals forces generally changes the electronic spectrum of the substrate only slightly,

but significant changes are observed in the case of chemisorption. Acid–base reactions, charge-transfer complexes, redox reactions, reversible cleavage reactions and photochemical reactions of the adsorbed substance can all be studied.

#### 13.4.9

#### Elastic Recoil Detection Analysis [5, 35, 37]

**Acronyms:** ERDA or ERD (elastic recoil detection (analysis))  
RS (recoil spectrometry)

##### 13.4.9.1 Introduction

ERDA is one of the most useful ion-beam analysis techniques for depth profiling of light elements.

A beam of energetic ions is directed at the sample. When the mass of the incident ion is bigger than the mass of the target atoms in the sample a forward scattering geometry can be used to detect the recoiling light atoms which emerge after collisions with the heavier incident ions. Atoms recoiled from the surface appear at different energies for the different elements.

##### 13.4.9.2 Instrumentation

The basic experimental equipment is the same as in Rutherford backscattering spectrometry (RBS), but it is usual to use the glancing geometry with very small incident angles.

ERDA relies on the ability to discriminate between forward-scattered incident ions and recoiling light target atoms. In a typical experimental arrangement Mylar foil is placed in front of the detector to block out the scattered incident ions but allow the lighter recoiling target atoms to pass through to the detector. A 10 µm thick Mylar foil completely stops 2.6 MeV He<sup>+</sup> ions but recoiled protons go through with a low energy loss. In cases where the system parameters are calibrated, ERDA is standardless, and the analysis is independent of the sputtering effects.

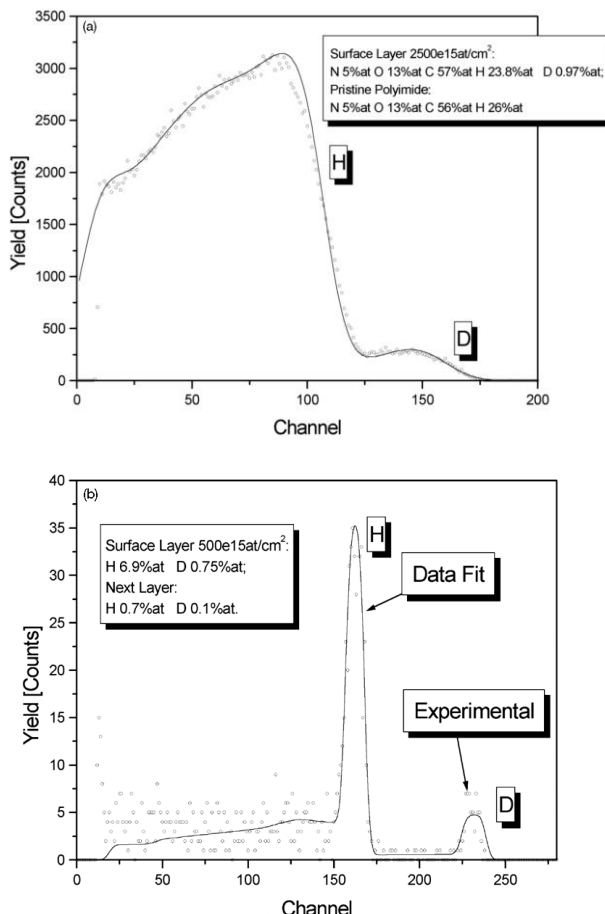
##### 13.4.9.3 Sample

The sample could be a multilayer system or bulk material. The lateral and interlayer homogeneity is important to obtain an undeformed spectrum for quantitative analysis.

##### 13.4.9.4 Analytical Information

The spectra of the forward recoiled sample atoms are detected (Fig. 13.2). In contrast to RBS where light masses produce a signal at low energies with a low ion yield the detected energy and yield of the ERDA signals for the different masses depend strongly on the stopping power and thickness of the range foil. Each ele-

**Fig. 13.2** The forward recoiled spectrum of  $^1\text{H}$  and  $^2\text{H}$  from  $^4\text{He}^+$  ions incident with energy 2.18 MeV on a thin deuterated polyimide film (a) and with energy 2.75 MeV on D-plasma treated  $\text{LiNbO}_3$  (b).



ment in the spectrum has its own depth scale with a unique energy-to-depth transformation because of the difference in stopping powers for the different recoiled atoms. The observed recoiling peaks are broadened due to energy straggling in the stopping foil. The depth scale can be calculated using the energy loss method, as in RBS.

#### 13.4.9.5 Performance Criteria

The sensitivity of ERDA depends on the experimental arrangement and the system-dependent background levels. Typically, 0.1 at.% of  $^1\text{H}$  is observable and from 0.1 to 1 at.% of heavier atoms. Simple ERDA analyses are performed using surface barrier detectors with a stopping foil and have a depth resolution of typically 20 to 60 nm. Accessible depths depend on the projectile, its energy and sample composition: for example 2.8 MeV  $\text{He}^+$  ions have a range of around 2.75 mm

in silicon. In a simple arrangement with MeV  $\alpha$ -particles it is possible to profile only H to depths up to 1 mm in common materials (e.g. Si). With higher mass projectiles heavier elements like N, O and F can also be analysed by ERDA technique.

Absolute measurement of light atom contents by ERDA is best achieved by using standards. The stopping foil must be uniformly thick, free of pin-holes, and its thickness must be greater than or equal to the projectile penetration range in the foil and less than the recoil range in the foil. The stopping foil method is not suitable for analyses of heavier elements using heavy projectiles (see TOF-ERDA below).

#### 13.4.9.6 Applications

Since ERDA is complementary to RBS analysis, this method should be a part of every MeV ion-beam analysis system. When it is employed on small Van de Graaf accelerators, ERDA can be used for determining concentration depth profiles or areal densities of hydrogen and of deuterium. Using larger Van de Graaf accelerators with the ability to accelerate heavy ions, this technique can be used for concentration depth profiling of heavier elements up to fluorine.

#### 13.4.9.7 Other Techniques

The TOF ERDA (time-of-flight ERDA) technique is used to distinguish between a large number of different particles that are recoiled simultaneously. The technique is based on the simultaneous measurement of the energy and velocity of the detected particles. From these two values the mass of the particle can be calculated. The velocity is determined by measuring the time elapsed between the detection of a particle in two sequential detectors that are placed at a fixed distance from each other. The full TOF measurement also requires a two-dimensional multichannel analyser, which is not commonly found in every ion beam laboratory.

Another possible geometry for ERDA is the transmission mode. In this case the sample must be thinner than the range of the recoiled atom to be profiled, (its penetration depth in that material). The main advantage of transmission ERDA is an increased sensitivity (by up to two orders of magnitude) in comparison to conventional reflection-geometry ERDA.

ERCS (elastic recoil coincidence spectrometry) is a variation of transmission ERDA. Two detectors are used, one to detect the scattered incident particle and the other to detect the recoiled target atom. This technique is very suited to the study of polymers, which can be easily made as thin self-supporting films.

#### 13.4.10

#### Electron Momentum Spectroscopy [18]

**Acronyms:** EMS electron momentum spectroscopy)  
(e, 2e) spectroscopy.

#### 13.4.10.1 Introduction

Electron momentum spectroscopy measures the electronic structure of materials whereby an incoming electron with known energy and momentum scatters from an electron in a solid, transferring some of its energy, so that this electron is also ejected from the solid. If the energy and momentum of both the ejected and scattered electrons are measured in coincidence then it is possible to calculate, using the elemental laws of energy and momentum conservation, the energy and momentum of the ejected electron before the collision.

#### 13.4.10.2 Instrumentation

In some experiments, the primary electrons have energies of about 50 keV. The two electrons after the collision have energies of 25 keV and are decelerated after emerging from the sample. They pass through electron energy analysers to ensure that each electron has precisely the right energy. If there are simultaneous events on both detectors, the event is counted. Such high-energy electrons result in poor surface sensitivity. In other coincidence experiments, much lower energy (10–100 eV) electrons are used and this results in much higher surface sensitivity.

#### 13.4.10.3 Sample

Metals, insulators, semiconductors, gases.

#### 13.4.10.4 Analytical Information

By using high-energy primary electrons this technique provides information concerning the energy and momentum of electrons within the sample. By using low energy electrons, the technique can provide information on the spin–orbit coupling and exchange coupling in magnetic materials.

#### 13.4.10.5 Performance Criteria

The technique is sensitive to the surface for low energy primary electrons.

High voltages are needed. High vacuum or UHV is required if lower energy electrons are used.

#### 13.4.10.6 Applications

EMS is used to determine electron momenta and energies within solids and (for the low primary energy electrons) to shed light on the role of exchange coupling and spin–orbit coupling in the dynamic interaction of low energy electrons in the valence band of solids.

**13.4.11****Electron Probe Microanalysis [1]**

**Acronyms:** EPMA (electron probe microanalysis)

EDX (energy dispersive X-ray)

EMPA (electron microprobe analysis)

EPXMA (electron probe X-ray microanalysis)

**13.4.11.1 Introduction**

EPMA is a general term for methods using bombardment of a solid specimen by electrons, which generate a variety of signals, e.g. X-rays. An electron beam is made to strike a surface using an electron gun from a scanning electron microscope. The X-rays generated by the electrons striking the surface contain elemental composition information from the sample surface down to a depth of ~2 µm. The energy range of operation of the incident electron beam lies from 1 keV to 20 keV.

**13.4.11.2 Instrumentation**

Electrons from a primary beam are made to strike a surface and the resulting X-ray emission from that surface is detected. The X-rays are detected using a solid state lithium drifted silicon detector called a Si(Li) detector. X-rays that strike the detector generate electron–hole pairs, and the larger the energy of the X-ray, the more electron–hole pairs that are generated. The electron–hole pairs are prevented from re-combining by application of a large electric field within the Si(Li) detector. The electrons and holes travel to opposite ends of the detector where they generate an electric pulse. The larger the pulse, the higher the energy of the X-ray. Hence, an X-ray spectrum can be acquired in one go, with each pulse being assigned to a different bin in a histogram. This can be done with the aid of a multichannel analyser.

**13.4.11.3 Sample**

Conducting samples are usually studied. Some samples degrade under electron bombardment.

**13.4.11.4 Analytical Information**

The Si(Li) detector is capable of detecting X-rays down to ~200 eV which implies that all elements from beryllium upwards can be detected. The sensitivity rises as the X-ray energy increases. This is due to the fluorescence yield, which increases with atomic number.

The elements composing the top ~2 µm of the surface are determined from analysing the X-ray spectrum. The beam can be scanned across the surface to create images of each element in the scanned area (see SEM: scanning electron microscopy).

#### 13.4.11.5 Performance Criteria

Spatial resolution is normally in the region of  $\sim 2 \mu\text{m}$ . Energy resolution varies with X-ray energy but typically varies from 50 eV at a X-ray energy of 1.5 keV to 200 eV at an X-ray energy of 6 keV.

The electron beam spreads out as the primary electrons strike the surface. This means that the spatial resolution is limited by how much the beam spreads within the material ( $\sim 2 \mu\text{m}$ ). The probability of X-ray emission reduces with atomic number, so elements with low atomic number are difficult to detect and helium and hydrogen have never been detected using EPMA. The depth of penetration of the electron beam into the material is  $\sim 2 \mu\text{m}$ . This means that EPMA is not a truly surface sensitive technique but is more sensitive to the bulk.

#### 13.4.11.6 Applications

EPMA is used in metallurgy, microelectronics and corrosion science.

### 13.4.12

#### Electron Stimulated Desorption [7, 8]

*Acronyms:* ESD (electron stimulated desorption)

##### 13.4.12.1 Introduction

Low energy electrons are directed at the surface and can cause an atom or molecule on the surface to be desorbed. Electron stimulated desorption usually occurs by electronic energy transfer and not by direct momentum transfer. Other processes include conversion of one binding energy state to another and desorption of atomic and molecular species which may be charged (positive or negative) or neutral (ground state or excited). This technique also has a more specialised form called electron stimulated desorption ion angular distributions or ESDIAD (see below). Incident electron energy is typically less than 500 eV for ESD.

##### 13.4.12.2 Instrumentation

An electron beam strikes the surface of a single crystal at glancing incidence, and a small fraction of the ions ejected from the surface are collected using a mass spectrometer. The detection of positively charged ions is generally favored over negatively charged ions since a voltage can suppress interference from the primary electrons in the detection system. A quadrupole system cannot measure total desorption cross-sections. For this purpose, a series of concentric grids can be used similar to a low energy electron diffraction (LEED) system.

**13.4.12.3 Sample**

Samples that can be studied include metals, highly ionic oxides, alkali-metal halide solids and semiconductors among others, usually with an adsorbed layer of gas or other atom/molecule.

**13.4.12.4 Analytical Information**

The incident electron energy is varied and the ejected ion current is measured. The experiments can be carried out at different temperatures. The resultant spectra provide information on intermolecular forces and the bonding length of defect surface structure. By comparison with computer models thermal dynamics of adsorbed species can be obtained. Desorption of an adsorbed molecular species can occur by the breaking of an intramolecular bond or the breaking of a molecule–surface bond.

**13.4.12.5 Performance Criteria**

The desorption cross-section varies considerably depending on substrate and adsorbed species. As such the performance varies considerably on the system being studied. Different desorbing species can be selected using a mass spectrometer. This technique requires a good vacuum. Most of the desorption may originate from minority states and desorption cross-sections vary enormously from species to species. The cross-sections for metallic adsorbates (e.g. Cs on W, or Th on W) are low. The information provided by ESD is semi-quantitative.

**13.4.12.6 Applications**

Used for the study of adsorbate on metals or semiconductors.

**13.4.13****Electron Stimulated Desorption Ion Angular Distributions [7, 8]**

*Acronyms:* ESDIAD (electron stimulated desorption ion angular distributions)

**13.4.13.1 Introduction**

Low energy electrons are directed at the surface and can cause an atom or molecule on the surface to be desorbed. By measuring the intensity of the desorbed species as a function of take-off angle information regarding how the molecule is oriented on the surface can be determined (i.e. bond directionality). Electron stimulated desorption ESD usually occurs by electronic energy transfer and not by direct momentum transfer.

Range of emitted ions: 0 to 10 eV

#### 13.4.13.2 Instrumentation

An electron beam strikes the surface of a single crystal at glancing incidence, and a small fraction of the ions ejected from the surface are collected by a channeltron mounted on a motor-driven, computer-controlled goniometer. The detector can traverse a spherical surface and map out ESD ion intensity as a function of angle. Digital data are displayed in three-dimensional form, and digital background subtraction can be utilized to enhance the appearance of ESDIAD patterns.

An alternative approach is to arrange for the particles that are ejected to encounter a four-grid electrostatic lens array. All positive ion and neutral ESD species pass through the grid system, striking the first of two micro-channel plates (MCP) which produce about one million electrons for each positive ion (or excited-state neutral). This electron pulse is accelerated into a resistive anode, causing an expanding ring of charge, centred at the pulse arrival point, to propagate across the thin conductive film. The position analysis computer translates it into a three-dimensional image.

#### 13.4.13.3 Sample

Samples that can be studied include metals, highly ionic oxides, alkali-metal halide solids and semiconductors among others.

#### 13.4.13.4 Analytical Information

A map of ion intensity versus the direction of take-off is acquired. By comparison with model structures a number of characteristics can be determined such as the bonding geometry of surface species from adsorbate on single-crystal surfaces, intermolecular forces, bonding length and orientations of defect surface structure. This leads to an understanding of the thermal dynamics of adsorbed species.

#### 13.4.13.5 Performance Criteria

The performance criteria are similar to ESD. Different desorbing species can be selected using a mass spectrometer. This technique requires single crystals and a good vacuum. Most of the desorption may originate from minority states and desorption cross-sections vary enormously from species to species. The information provided is semi-quantitative.

#### 13.4.13.6 Applications

Used for the study of adsorption site symmetry of molecules on single crystal surfaces such as in the production and observation of synthetic catalytic intermediate species at high coverage. There are overlaps with techniques such as LEED (low energy electron diffraction) and SEXAFS (surface X-ray absorption fine structure).

## 13.4.14

**Ellipsometry [5, 10, 11, 19]**

*Acronyms:* no acronym used.

**13.4.14.1 Introduction**

Ellipsometry involves measurement of the change of polarization that occurs when polarized radiation is reflected from a specular surface. Ellipsometry is an extension of the reflection technique in which the polarization of the reflected radiation rather than just its intensity is measured. Ranges of operation: from ultra-violet to infrared, UV/Visible is typical.

**13.4.14.2 Instrumentation**

The basic optical components of an ellipsometer are: a source (L), a polarizer (P), an analyser (A) and a detector (D). Some additional components, like compensators (C, e.g. quarter-wavelength plate) and modulators (M, e.g. photoelastic modulator) are added in some configurations. Typical configurations are PCSA or PSCA, where S is the sample.

There are several principles used for measurement: null method, photometric method, and interferometry, the first two being the most important.

In null ellipsometry information about the optical system is obtained from the azimuths of P, C, A, the relative phase retardation of the compensator  $\delta_C$  and, in the case of measurements on surfaces, the angle of incidence that reduces the dc or an ac-component of the detected radiation flux to zero. Photometric ellipsometry is based on measurement of the variation of the detected radiation flux as a function of one or more of the above parameters (azimuth angle, phase retardation, or angle of incidence).

**13.4.14.3 Sample**

Mirror-like surfaces are required.

**13.4.14.4 Analytical Information**

The three-medium problem is the simplest surface problem to be solved: one unknown thin film on a substrate immersed in an ambient. The optical properties of each medium are defined by wavelength dependent refractive indices  $n_i$  and real absorption coefficients  $k_i$ . As the properties of the ambient and substrate are usually known or measured before the formation of the surface thin film, the goal of the ellipsometric measurement is to determine the unknowns  $n_2$ ,  $k_2$  and  $d$  the thickness of the thin film.

#### 13.4.14.5 Performance Criteria

The surface sensitivity depends on the ability to resolve small angular differences. For null ellipsometry, the angular resolution is mechanically limited to  $0.01\text{--}0.02^\circ$ , which implies sensitivity to film thickness of about 0.01 nm, corresponding to about 1/20 of a monolayer. In photometric instruments or in the instruments in which the null is established electronically the precision is improved to 0.001 nm, which means that very small fractions of a monolayer can be detected.

While UV/Visible ellipsometry is often applied at a single wavelength only, Fourier spectroscopy based infrared ellipsometry covers a broad range of wavelengths. Using infrared ellipsometry the thickness of a film of a few monolayers on metal can be detected with about 1 nm uncertainty.

#### 13.4.14.6 Applications

The adsorption of molecular species on surfaces, oxidation of semiconductor and metal surfaces in contact with gaseous or liquid ambients, and electrode/electrolyte interface have all been studied by ellipsometry. Layers such as Langmuir–Blodgett films, liquid crystals, proteins and coatings on metal or dielectric substrates can be studied. There are many applications in biology and medicine, including the interaction of blood with foreign surfaces, antigen-antibody immunological reactions in thin films, real-time adsorption kinetics of proteins, etc.

### 13.4.15

#### Extended Energy Loss Fine Structure [8]

*Acronyms:* EXELFS (extended energy loss fine structure)  
EELFS (electron energy loss fine structure)

##### 13.4.15.1 Introduction

EXELFS is generally carried out in a conventional transmission electron microscope. The electron beam loses energy through various mechanisms, but includes characteristic energy losses by the excitation of an electron from a core state. This results in a sudden rise in the number of loss events at a certain energy below that of the primary beam energy, corresponding to an absorption edge of an element contained within the sample. The excited core electron has a certain probability of being backscattered to the emitting atom. This can in turn affect the initial probability of ionisation by the incident beam. This gives rise to oscillations in the ionisation probability with electron energy loss (better known as EXAFS (X-ray absorption fine structure) oscillations). Hence, information regarding the local structure around the atom whose absorption edge is acquired can be obtained. A much higher spatial resolution can be obtained with EXELFS than with EXAFS.

Range of operation: Incident electron energy is typically hundreds of keV.

#### 13.4.15.2 Instrumentation

A conventional transmission electron microscope is required as well as an electron energy analyser to measure the electron energy loss spectra. It is often preferable to keep the energy of the detected electrons constant and to sweep the energy of incident electrons instead to improve signal to noise and energy resolution.

#### 13.4.15.3 Analytical Information

EXELFS spectra provide information regarding the local environment surrounding the atom whose absorption edge is studied. The specific local information includes the atom type of neighbouring atomic shells, the distance of those shells from the central (absorbing) atom and the static or dynamic disorder. The latter is given by the Debye–Waller value. The two electron final state can make the interpretation of EXELFS spectra more complicated than that of EXAFS. Normally, EXELFS would be regarded as a bulk sensitive technique. However, by the use of grazing incidence electrons, it is possible to probe the near surface region.

#### 13.4.15.4 Performance Criteria

Primary electron energy is 100–500 keV.

The sample should be able to withstand the intense incident electron beam. As in EXAFS, it can be difficult to distinguish elements in the shells surrounding the central atom if they are close in atomic number and it can also be difficult to distinguish static from dynamic disorder.

#### 13.4.15.5 Applications

EXELFS is used in many applications where local state information is required such as materials analysis (for example the structure of amorphous materials). It can be used where the amount of material is too small for conventional EXAFS experiments, or where a high spatial resolution of the local structure is required.

#### 13.4.15.6 Other Techniques

PEELS (parallel electron energy loss spectroscopy) is a method whereby electron energy loss spectra can be acquired in a transmission electron microscope with great rapidity. This is accomplished by the use of a multi-element solid-state detector. Typically, PEELS is used to determine the composition of the sample under study and does not have sufficient energy resolution to provide EXELFS data. Improvements in detector technology may change this.

#### 13.4.16

#### **Evanescence Wave Cavity Ring-down Spectroscopy [11, 20, 21]**

*Acronyms:* EWC-RDS (evanescence wave cavity ring-down spectroscopy)

#### 13.4.16.1 Introduction

EWC RDS is based upon the measurement of the rate of attenuation of a radiation pulse during intra-cavity total internal reflection.

#### 13.4.16.2 Instrumentation

A laser beam is focused on a cavity formed by two mirrors and a Pellin–Broca prism and the time behaviour of the radiation intensity inside the cavity is monitored by the small fraction of radiation that is transmitted through the second mirror to a detector. Another arrangement uses a properly shaped monolithic, totally internally reflecting polygonal minicavity (from square to octagonal, with at least one convex facet to induce stability). Photon tunneling through the piezoelectrically driven prism introduces radiation into the cavity and extracts a small portion for monitoring. The time needed for attenuation of the pulse to  $1/e$  of the original intensity is denoted as the base ring-down time.

#### 13.4.16.3 Performance Criteria

This technique is critically dependent on the quality of the mirrors and cavity, respectively. Super polishing to  $<0.05$  nm root-mean-square of surface roughness is essential. Under such conditions the arrangement with Pellin–Broca prism exhibits a base ring-down time of about 1  $\mu$ s and yields a minimum detectable absorbance change of about 32 ppm. A ring-down time of about 800 ns is found for a 1 cm square mini-cavity.

#### 13.4.16.4 Applications

Sub-monolayer detection of adsorption phenomena is possible (e. g. 0.04 monolayer of I<sub>2</sub> on fused silica).

### 13.4.17

#### Glow Discharge Optical Emission Spectrometry [5, 22–24]

*Acronyms:* GDOES (glow discharge optical emission spectrometry)

#### 13.4.17.1 Introduction

This destructive method enables the rapid simultaneous determination of a variety of elements including non-metals and the in-depth profiling analysis of conductive samples. The optical emission is obtained by means of a diode-type discharge tube, the Grimm lamp, which is operated under low-pressure argon flow ( $\sim 300$  Pa). Atoms sputtered from the sample are excited in the glow discharge plasma by collisions with ions and electrons. The emitted characteristic radiation is in the visible and UV range.

#### 13.4.17.2 Instrumentation

A GDOES device consists of two main parts: a Grimm lamp and an optical spectrometer, which is usually a polychromator. First the lamp is evacuated and then filled with the working gas (usually argon). The discharge is initiated by applying a voltage of typically 500–1000 V. Ar<sup>+</sup> ions are created as projectiles, which bombard the surface of the sample. The sputtered sample atoms diffuse into the plasma. The sputter rate depends on the sample material and the discharge parameters. Some sample atoms are excited by collisions with electrons and the emitted light is analysed with an optical spectrometer. Heavy projectiles in the energy range 30 eV–100 keV are generally recommended for the excitation, but also high-energy 50 keV–3 MeV Ar ions have been applied. The usual sputter rates are in the range 5–200 nm s<sup>-1</sup>. The simplicity and speed is a big advantage of GDOES. A total time of 1 min is required to obtain a calibrated depth profile of 40–50 elements in routine analysis.

#### 13.4.17.3 Sample

A flat solid sample is needed, the size should be of the order of centimeters.

#### 13.4.17.4 Analytical Information

The intensities of emission lines of selected elements are recorded continuously by a computer during measurement. Using calibration curves obtained by means of calibration standards under identical discharge conditions, concentration depth profiles of the chosen elements in the analysed sample are determined from the recorded emission line intensity.

#### 13.4.17.5 Performance Criteria

Owing to the well-known high sensitivity of optical emission spectrometry, detection limits reach from  $\sim 10^{-5}$  g g<sup>-1</sup> for metals and C, S, P, B to  $\sim 10^{-3}$  g g<sup>-1</sup> for elements such as H, O, N, considering instantaneous analysis. For quantitative analysis using calibration standards, accuracy 0.2–1 at.%, has been reported for thin layer analysis. For the bulk analysis one has to expect inferior accuracy in the 5–10% range, also for the general case of instantaneous in-depth analysis.

The simplicity and speed of GDOES have made it a powerful tool for rapid and accurate in-depth profiling, especially of iron and steel thin films, and selvage routine analysis. In routine analysis a calibrated depth profile of 40–50 elements can be obtained in 1 min. Using an integration time of 0.1 s, this could result in a depth resolution of  $\sim 0.5$  nm. The disadvantage of GDOES is the need for calibration standards, which are not available for all elements and concentration ranges.

#### 13.4.17.6 Application

The field of application for GDOES is very broad and includes surface treatment studies of samples prepared by different techniques such as galvanization, nitriding, carbonitriding, carburization, diffusion, chemical and thermochemical treatments, thermic treatments, PVD and CVD coating, electrodeposition, painting, and semiconductor multilayer growth.

#### 13.4.17.7 Other Techniques

GDMS (glow discharge mass spectrometry) is a similar technique to GDOES but GDMS uses a mass spectrometer instead of an optical emission spectrometer.

The optical radiation, which is emitted from sputtered particles, is measured in a technique called either SCANIIR (surface composition by analysis of neutral and ion impact radiation) IBSCA (ion beam spectrochemical analysis) BLE (bombardment-induced light emission). Heavy particles in the energy range 30 eV–100 keV are recommended for the excitation in BLE. Similar to SNMS (secondary neutral mass spectrometry) see Section 13.4.39.7, strong matrix effects occur in GDOES, they are attributed to the varying de-excitation processes.

LAMMA, or LAMMS, or LMMS (laser microprobe mass analysis or spectroscopy), is based on laser ablation. A high frequency laser beam scans the area of the sample in a minimum step size, time-of-flight mass spectra of each scan are evaluated with respect to several ion signals and transformed into two-dimensional distribution plots.

### 13.4.18

#### High Resolution Electron Energy Loss Spectroscopy [5, 8]

*Acronyms:* HREELS, HEELS (high resolution electron energy loss spectroscopy) (sometimes abbreviated also to EELS).

#### 13.4.18.1 Introduction

A highly monochromated primary electron beam (energy 1–50 eV) impinges on a sample. Many electrons are elastically scattered directly from the surface whereas others undergo inelastic scattering by exciting a vibrational state of atoms in the surface layers. The scattered electrons reflected back from the surface are collected and their energies are analysed.

#### 13.4.18.2 Instrumentation

The electron beam from an electron gun is passed through a monochromator which results in a highly monochromatic electron beam with an energy spread < 10 meV at a typical primary beam energy between 1 and 10 eV. The electrons are often made to strike the surface at grazing angles of incidence. The reflected electrons pass through an electron energy analyser before being detected.

#### 13.4.18.3 Sample

Samples should have flat surfaces and should preferably be conducting.

#### 13.4.18.4 Analytical Information

The source of information is a dependence of electron current on electron energy loss.

There are three important scattering mechanisms in HREELS: dipole scattering, impact scattering and negative ion resonance scattering.

For dipole scattering, the electron is scattered a long distance from the sample ( $\sim 10$  nm) and generates surface phonons. Only vibrational modes, which are perpendicular to the surface are normally excited in dipole scattering and the low energy losses result in only a small angle of deflection from the original direction.

For impact scattering, electrons scatter at much shorter range ( $\sim 0.3$  nm) and over a much wider angle than dipole scattering. Impact scattering has a much lower probability than dipole scattering and can be distinguished from dipole scattering by moving the analyser away from the specular direction.

#### 13.4.18.5 Performance Criteria

HREELS probes vibrational features from  $\sim 0$  to  $>4000\text{ cm}^{-1}$  with resolution of  $< 1\text{ meV}$  ( $8\text{ cm}^{-1}$ ). It has a much more limited resolution in comparison with the infrared based methods.

The method is sensitive to all elements but only in the top few atomic layers for metals or to fractions of a monolayer (much less than 1%) for bands with large dipole moment changes. It can be possible to detect vibrational ( $<0.5\text{ eV}$ ) and electronic losses (1–50 eV) in the same instrument.

It is possible to monitor vibrational modes below  $1000\text{ cm}^{-1}$  where RAIRS (reflection absorption infrared spectroscopy) has problems with sufficient intensity of the IR source.

HREELS has poor spatial resolution (1–5 mm) and it requires an UHV chamber with very good magnetic shielding. Stray charges may build up in the spectrometer, which then requires frequent baking. HREELS is difficult to quantify. It is best for small, non-magnetic single crystals. HREELS is not very sensitive to insulating materials, as surface charging makes the analyses difficult. It has poor sensitivity for rough surfaces and is difficult to use with depth profiling.

HREELS equipment is expensive (minimum \$ 80,000) and there are a small number of commercial suppliers. HREELS instruments are very complex and bulky and it is difficult to optimise the electron optics for the primary beam.

#### 13.4.18.6 Applications

HREELS is used to investigate vibrational scattering mechanisms on surfaces. It helps to provide molecular orientation information for molecules on surfaces as well as bond strengths, adsorption geometry and surface acoustic and optical phonon information.

#### 13.4.18.7 Other Techniques

REELS, ELS (reflection electron energy loss spectroscopy) and EELFS, EXELFS (extended electron energy loss fine structure) work with a higher fixed energy of the primary electrons (50–200 eV and 10–80 keV, respectively) and higher energy losses of the scattered primary electrons ranging from 0.005 eV to several hundred and from 200–4000 eV, respectively.

REELS provides information concerning higher energy loss mechanisms than HREELS such as plasmons, interband transitions and characteristic energy losses. EXELFS is a technique used in TEM (transmission electron microscopes). It provides information similar to EXAFS (X-ray absorption fine structure), (i.e. data regarding the immediate neighbourhood of atoms of certain elements in the sample). EXELFS is bulk sensitive.

TEELS (transmission electron energy loss spectroscopy) is another technique that is used in a TEM. The electron energy loss is much higher than in EXELFS and characteristic energy losses can be observed. This provides information concerning the elemental composition of the sample. The spectra are detected using a multi-element solid-state semiconductor detector, which results in spectra being acquired in parallel. Hence the name: PEELS (parallel electron energy loss spectroscopy).

#### 13.4.19

#### Inelastic Electron Tunneling Spectroscopy [25, 26]

*Acronyms:* IETS (inelastic electron tunneling spectroscopy)

#### 13.4.19.1 Introduction

Electrons (0–1 eV) are caused to tunnel between two conducting substrates through an insulating layer which has a film of material deposited on it. Electrons can tunnel through the insulating layer and attached film without losing any energy (i.e. an elastic process) or some energy may be lost (i.e. an inelastic process). Hence the technique is sensitive to the empty states within the film.

Range of applied voltage: –1.5 to 1.5 V

**13.4.19.2 Instrumentation**

The current–voltage ( $I$ – $V$ ) characteristic of the metal–insulator–film–metal (M–I–x–M) junction is measured. AC modulation of the voltage can be used with lock-in amplifiers to obtain a plot of the  $d^2I/dV^2$  against  $\Delta V$  (i.e. against electron energy). Liquid helium temperatures are typically required for IETS experiments.

**13.4.19.3 Sample**

The sample is a film placed on a thin insulating substrate and then sandwiched between two metallic plates. Molecules adsorbed on an oxide or oxide-supported metal can be studied in this way.

**13.4.19.4 Analytical Information**

Vibrational modes of the molecules in the film are displayed as sharp peaks on the plot of  $d^2I/dV^2$  against  $\Delta V$ . Even though both Raman and infrared active modes are also active in IETS, only modes perpendicular to the surface are observed (as is also the case in reflection spectroscopy based techniques).

**13.4.19.5 Performance Criteria**

Resolution of the order  $10\text{ cm}^{-1}$  is reached.

**13.4.19.6 Applications**

IETS is applied to the study of films such as monolayers, self-organised. Adsorption experiments are limited by the low temperature required for the experiment.

**13.4.20****Inverse Photoelectron Spectroscopy [27, 28]**

*Acronyms:* IPS, IPES (inverse photoelectron spectroscopy)

BIS (Bremsstrahlung isochromat spectroscopy)

ARIPES (angle resolved inverse photoemission spectroscopy)

KRIPES ( $k$ -resolved inverse photoemission spectroscopy)

SPIPES (spin polarised inverse photoelectron spectroscopy)

**13.4.20.1 Introduction**

A beam of low energy electrons with a fixed energy (5–50 eV) and momentum is shone at the sample where they couple with the unoccupied bands above the Fermi energy. The electrons lose energy by emitting a photon and dropping down into another unoccupied band at a lower energy. The initial energy of the electron is known; hence by measuring the energy of the photon that is emitted the remain-

ing energy of the final state can be determined, to produce a spectrum that is representative of the unoccupied density of states above the Fermi level.

#### 13.4.20.2 Instrumentation

This technique requires UHV conditions. An electron gun is used to direct a beam of low energy electrons onto the sample. The electrons couple with unoccupied states above the Fermi level from which they decay into lower unoccupied states by the emission of a photon. This photon hits a diffraction grating and is diffracted, (at an angle that is dependent on its energy), onto a position (and hence energy) sensitive photon detector such as a CCD. Since the initial energy of the electron is known, and the energy of the photon has been measured, the energy of the final unoccupied band can then be determined. Hence a spectrum that is representative of the unoccupied density of states above the Fermi level can be produced. Alternatively, photons of a fixed energy can be measured whilst the energy of the electron beam is scanned to produce the spectrum, a mode known as Bremsstrahlung isochromat spectroscopy (BIS).

By varying the angle of incidence of the electrons their momentum ( $k$ ) can be varied to produce “band maps” of the unoccupied states as a function of momentum that are analogous to those of the occupied states produced in angle-resolved ultraviolet photoelectron spectroscopy (ARUPS). This is known as  $k$ -resolved inverse photoemission spectroscopy (KRIES) or angle resolved inverse photoemission spectroscopy (ARIPES).

If a spin-polarised electron gun is used then separate spectra of the unoccupied “spin-up” and “spin-down” density of states can be produced that are analogous to the “spin-up” and “spin-down” spectra of the occupied states produced by spin-resolved ultraviolet photoemission spectroscopy (SRUPS). This is also known as spin polarised inverse photoelectron spectroscopy (SIPES).

#### 13.4.20.3 Sample

UHV compatible conductors for IPES/BIS.

Single crystal UHV compatible conductors for ARIPES/KRIES.

Magnetic UHV compatible conductors for SIPES.

Due to the low count rates obtained in all variations of IPES the sample must be stable under intense electron beams in UHV for prolonged periods.

#### 13.4.20.4 Analytical Information

This technique determines the density of unoccupied states above the Fermi level. Hence IPES is complementary to ultraviolet photoelectron spectroscopy (UPS), which measures the density of occupied states below the Fermi level. As in UPS, angle or spin resolved variants of the technique can be used to perform band mapping of single crystals or to produce spin-resolved spectra of magnetic samples.

#### 13.4.20.5 Performance Criteria

The inverse photoemission process is much less efficient than the photoemission process (by some five orders of magnitude). This can be offset somewhat because electron beams can generally be made more intense than X-ray beams. However, count rates are still much lower, and acquisition times much longer than in UPS.

The energy range of IPES is typically 5–50 eV, the energy resolution is generally about 0.2 eV and the spatial resolution is generally about 1 mm. Surface sensitivity is similar to UPS, i.e. limited primarily to the top 5 atomic layers.

UHV is required for this technique. High surface sensitivity combined with long acquisition times means that IPES is limited to samples that will remain stable and clean in vacuum for many hours under the electron beam.

The low energies of the electrons involved means that the technique can be vulnerable to stray magnetic fields and magnetic shielding may be required. Spectra can be influenced by the particular crystal structure of the sample's top few atomic layers, which may not be completely representative of the bulk material. IPES is generally not suitable for insulating materials.

#### 13.4.20.6 Applications

The empty states immediately above the Fermi level play a vital role in surface chemistry, optical properties, and the electrical conduction of semiconductors and so IPES and its variants can reveal vital information about these properties that is complementary to the information on the occupied density of states obtained from UPS.

### 13.4.21

#### Ion Neutralisation Spectroscopy [2]

*Acronyms:* INS (ion neutralisation spectroscopy)

##### 13.4.21.1 Introduction

An incident beam of helium ions impinges on a surface. The incident ion neutralises upon interaction with the surface and an electron is emitted from the surface. Determination of the energy spectrum of the emitted electrons provides information regarding the electronic density of states of the surface.

##### 13.4.21.2 Instrumentation

UHV is required for this technique. The helium source should be free of impurities to ensure UHV and a high pumping speed is needed in order to pump away the helium after it has interacted with the surface. The helium ions are created by collision with an electron beam and focused onto the sample surface. The incident ion energy is usually in the range of 5 to 10 eV. The energy distribution of electrons

emitted from the surface as result of the ion impacts is measured using an electron energy analyser.

#### 13.4.21.3 Sample

Metal, semiconductor or insulator.

#### 13.4.21.4 Analytical Information

INS is believed to be dominated by an Auger neutralisation process. This process occurs when an electron from the conduction band of the surface tunnels into the potential well of the incident ion. The electron then falls into a deeper well and gives its excess energy to another conduction band electron, which then leaves the solid and may be detected. The emitted electron is an Auger electron and contains information concerning the density of states of the electrons in the near surface region. Other processes are also possible, but it is believed that the Auger de-excitation mechanism dominates. The presence of adsorbed atoms on the surface changes the electronic states of the surface region, which gives marked changes in the emitted electron energy spectrum.

#### 13.4.21.5 Performance Criteria

INS is highly surface sensitive. Interpretation is difficult due to the presence of more than one de-excitation mechanism.

#### 13.4.21.6 Applications

Applied to materials where the understanding of the electronic structure of the surface is poor such as molecular films on metallic or semiconducting substrates.

#### 13.4.21.7 Other Techniques

INS is very similar to MIES (metastable impact electron spectroscopy) or PIES (penning ionisation electron spectroscopy) except that in INS ions are used instead of metastable atoms.

### 13.4.22

#### Ion Probe Microanalysis [29, 35, 37]

*Acronyms:* IPMA, SIMP (scanning ion microprobe)  
PMP (proton microprobe)  
SPMP (scanning proton microprobe)

#### 13.4.22.1 Introduction

Ion probe microanalysis is a technique in which the sample is bombarded by a well focused beam of primary ions (diameter less than 10 µm) and the secondary ions ejected from the sample are detected in a mass spectrometer.

When a beam of charged particles passes through a thin specimen, the beam transmitted in the forward direction includes some particles that scattered elastically off atomic nuclei or lost energy due to interaction with electrons (inelastically scattered) as well as those particles that were left unscattered. An image formed with this forward-transmitted beam is referred to as a bright field image.

#### 13.4.22.2 Instrumentation

A fully equipped proton microprobe chamber should include microscopes for transmission and reflective viewing of the specimen, a Si(Li) detector for detection of X-rays, surface barrier detectors for backward and forward scattering, and a detector for gamma-rays. It is important for microprobe work that the ion source produces a beam of the maximum possible brightness and that this brightness is maintained during transmission of the beam through the accelerator and associated beam optics. Charged particle beams are focused by means of magnetic or electrostatic lenses. The focal length of such lenses depends on the energy of the particles. The achievement of good spatial resolution requires a good basic ion optics design, high precision in fabrication, careful alignment and careful elimination of sources of interference.

#### 13.4.22.3 Sample

Ion probe microanalysis is suited to high sensitivity multi-element analysis of both thick and thin specimens. Solid state samples are required. It is not possible to perform elemental analysis for an extended structure of irregular shape except by repeated measurements with a fixed beam at many selected points.

#### 13.4.22.4 Analytical Information

In order to measure the distribution of elements along a line or map elemental distribution over an area, the focussed beam spot must be scanned and the detector signal recorded as a function of the displacement of the beam from its normal position. When a beam of ions scans an area of a specimen, the emitted radiation carries information in three degrees of freedom: the two scanning dimensions and the energy.

Scanning ion microprobe and scanning proton microprobe are very useful techniques for *in situ* element or isotope distribution analysis. With protons or heavy ions, the mean free path between ionising events is generally much shorter than the specimen thickness and hence multiple inelastic scattering occurs. The energy loss spectrum is then a measure of specimen thickness. If the specimen thickness exceeds the range of the slow heavy ions in an IMP (ion microprobe) then trans-

mission signals are not available. However, in a PMP (proton microprobe), where the typical energy is 3 MeV, the proton range may be some hundreds of microns and the mean free path between inelastic collisions will be less than 100 nm.

#### 13.4.22.5 Performance Criteria

With bright field transmission imaging in which the unscattered transmitted beam is running directly into a detector, it may be necessary to restrict the beam current to about  $10^4$  particles s $^{-1}$ . PMP gives 1  $\mu\text{m}$  spatial resolution for microanalysis with 100 pA beams of protons or alpha particles. Each image is collected over 20 min.

Sample discolouration may occur and is usually due to ionisation, (whereas overheating causes physical deformation). It affects only sensitive specimens under intense bombardment. The sensitivity depends inversely on the beam diameter. Some effects must be taken into account, such as the charging of insulating components, and the sputter removal of some components, which prevents repeat investigations. Image contrast may also arise from chemical or topographic rather than isotopic differences.

#### 13.4.22.6 Application

Metallurgy-metals provide an ideal specimen for microbeam analysis, their high thermal conductivity minimizes thermal damage and their high electrical conductivity removes any possibility of specimen charging giving rise to a beam deflection.

It is possible to extract a microbeam from the vacuum system to use external beam measurement for specimens that cannot be placed in the vacuum, but the beam will suffer considerable scattering from the air or gas as well as from any exit foil. Nevertheless such an external microbeam can be very useful for low-resolution studies, for example in archaeology or biological sciences.

The technique has successfully been applied to the examination of nuclear membranes and the processes of etching of latent tracks in polymers.

#### 13.4.22.7 Other Techniques

IPM can be used simultaneously with RBS (Rutherford backscattering spectrometry), NRA (nuclear reaction analysis), PIXE (particle induced X-ray emission) or PIGE (particle induced gamma ray emission). More specialized examples include the field ion microscope (FIM), which gives better than atomic resolution in the study of high melting point materials.

**13.4.23****Low-energy Ion Scattering Spectrometry [30, 31]**

*Acronyms:* LEIS (low-energy ion scattering spectrometry)

**13.4.23.1 Introduction**

LEIS is a typical surface specific method, which detects particles scattered only from the uppermost surface layer of the solid. The scattering of low energy ions of inert gases from the surface of a sample is measured. At low energies (< 5 keV) the ions are neutralised, if they penetrate below the top two or three monolayers, so only a few monolayers of the solid participate in the ion scattering process. In this way LEIS differs from RBS, in which the neutralisation processes are negligible.

**13.4.23.2 Instrumentation**

LEIS uses a low energy ion beam of ions formed from inert gases in an ion source to interact with the sample surface. The beam energy is typically less than 10 keV. LEIS is a surface sensitive technique and it should be performed under clean high vacuum conditions. In most research systems  $10^{-8}$  Pa in the target chamber is a minimum requirement.

Any inert gas ions from the beam penetrating below the surface are neutralized. LEIS uses electrostatic energy analysers and only the charged particles are detected. Electrostatic analysers are suited to low energy analysis, they are simple to operate, and they provide good energy resolution.

**13.4.23.3 Sample**

The sample should be solid, with a size of around 1 cm. The requirements are the same as for RBS measurements and the sample must be cleaned due to atmospheric and other surface contaminants, to obtain a pure surface composition measurement.

**13.4.23.4 Analytical Information**

LEIS measurements result in an energy spectrum of the backscattered ions from the sample surface. The energy of scattered ions provides information on the mass of the surface atoms, which is directly related to their chemical identity. The cross-section, solid angle and transmission factor (the analyser acts as an energy filter, with transmission characteristics that depend on the mode of operation) are used for these calculations.

#### 13.4.23.5 Performance Criteria

In order to optimise the mass resolution of LEIS it is advisable to use a projectile with a mass close to that of the target atom and to employ the largest possible scattering angle. Under these conditions it is possible to detect low levels of contaminants on the surface. For high atomic mass impurities, the ultimate sensitivity is  $5 \times 10^{-4}$  monolayers using  $\text{He}^+$  ions and  $1 \times 10^{-4}$  monolayers using  $\text{Ar}^+$  ions, while the detection limit for O is between  $10^{-2}$  and  $10^{-1}$  monolayers. The ultimate accuracy of quantitative elemental composition analysis is 5–10% when applying a suitable calibration procedure.

The use of LEIS for the determination of ordered atomic positions at the surface atomic layer is based on its extreme surface selectivity. When changing the scattering geometry by rotating the crystal, different atoms in the first atomic layer may become shadowed by other atoms, which result in changed intensities of the respective LEIS signals.

The limited mass resolution is the major problem in LEIS. This method is insensitive for the detection of low levels of C on surfaces. The detection sensitivity is also a function of the state of the surface. A highly contaminated (O or CO) or insulating surface produces an energy spectrum of scattered ions with a relatively high background.

The preferential neutralization of inert gas ions, which penetrate below the surface atom layer, is responsible for the extreme surface sensitivity of LEIS. This is an advantage of LEIS. The weakness is introduced by the uncertainty in ion yield that results from surface scattering.

#### 13.4.23.6 Application

The main characteristic of LEIS is its high selectivity for the outermost layer of a solid owing to the large scattering cross-section. For practical analysis, it is necessary to clean the solid surface in UHV prior to analysis to remove contamination and adsorbed layers. LEIS is frequently used for segregation, adsorption and reaction studies on well-defined surfaces which were carefully prepared within the UHV system rather than for the analysis of thin unknown layers. LEIS is a powerful tool in studies of chemistry, crystallography and electronic structure in the monolayer range on a solid surface.

#### 13.4.23.7 Other Technique

In general LEIS is based on the same principle as RBS, HEIS and MEIS, but it uses a low energy ion beam. HEIS (high energy ion scattering) and MEIS (medium energy ion scattering) work with high or medium energy projectiles respectively. The energy range of the initial projectiles is chosen with respect to the measured sample characteristics (especially the elements present) and taking into account what information is needed about the sample.

## 13.4.24

**Near Edge X-ray Absorption Spectroscopy [5]**

*Acronyms:* NEXAFS (near edge X-ray absorption spectroscopy)

**13.4.24.1 Introduction**

A monochromatic X-ray beam is directed onto a sample, which typically has a molecular film on the surface. The wavelength of this beam is ramped through an absorption edge of one of the elements that constitutes part of the film. As a monochromatic beam of X-rays at various wavelengths is needed, synchrotron radiation is used as the X-ray source for NEXAFS. Data are acquired from a region near to the absorption edge (~50 eV wide).

**13.4.24.2 Instrumentation**

Synchrotron radiation of high intensity and polarity (> 90 %) is required. The X-rays must pass through a monochromator before striking the sample. The sample is usually placed in a low vacuum chamber for experiments in the soft X-ray energy range. The NEXAFS signal can be detected through a number of routes; often the total electron yield from the sample is measured and this signal is divided by the total photon flux striking the sample to normalize out any variations that might result simply from changes in the flux of synchrotron radiation.

**13.4.24.3 Sample**

The sample is usually no smaller than ~2 mm across and must be able to withstand the intense X-ray beam from the synchrotron.

**13.4.24.4 Analytical Information**

NEXAFS spectra are frequently dominated by intramolecular resonances of  $\pi$  or  $\sigma$  symmetry. The energy, intensity and polarization dependence of these resonances can be used to determine the orientation and intramolecular bond lengths of the molecule on the surface. NEXAFS probes the element specific empty electronic states and has local electronic and bonding structure sensitivity. The orientation of the molecules can be determined using angular resolved spectra and analysis of the  $\pi^*$  resonances.

**13.4.24.5 Performance Criteria**

The primary X-ray energy is typically 1000–4000 eV. NEXAFS is sensitive to ~1 % of a single monolayer. Samples need to be able to survive intense doses of X-ray radiation.

#### 13.4.24.6 Applications

NEXAFS is used to determine the orientation of and bonding structure of adsorbates on a surface. For instance, it is used for the analysis of self organizing monolayers.

#### 13.4.24.7 Other Techniques

Extended X-ray absorption fine structure (EXAFS) is similar to NEXAFS but makes use of a wider energy region around the adsorption peak to determine information about the type of atoms surrounding the atom of interest and their distances from it.

### 13.4.25

#### Neutron Depth Profiling [32–34]

*Acronyms:* NDP: neutron depth profiling.

##### 13.4.25.1 Introduction

NDP is a prompt nuclear analysis technique, which employs a nuclear reaction that results in emission of charged particles with a specific kinetic energy. It is one of the most powerful non-destructive techniques for depth profiling of some light elements especially for  $^{10}\text{B}$  and  $^6\text{Li}$ , which have very high thermal neutron capture cross-sections of 3837 and 940 barn respectively.

##### 13.4.25.2 Instrumentation

The samples are kept in a vacuum chamber and are irradiated with thermal neutrons produced by the nuclear reactor.

TOF-NDP (time of flight NDP) is a variation of the traditional NDP. It uses time-of-flight techniques with superior resolution compared to conventional energy measurements conducted with surface barrier detectors.

##### 13.4.25.3 Sample

The solid state sample is preferred. Depending on the nuclear reaction used and the type of the analysed material, the sample surface region down to a depth of several micrometers can be analysed.

##### 13.4.25.4 Analytical Information

If the thermal neutron capture takes place beneath the sample surface, the energy loss of charged particle stopping in the sample can be used to obtain information about the Li or B concentration profile (Fig. 13.3). The amount of energy loss is related to the distance that the charged particle has travelled within the specimen.

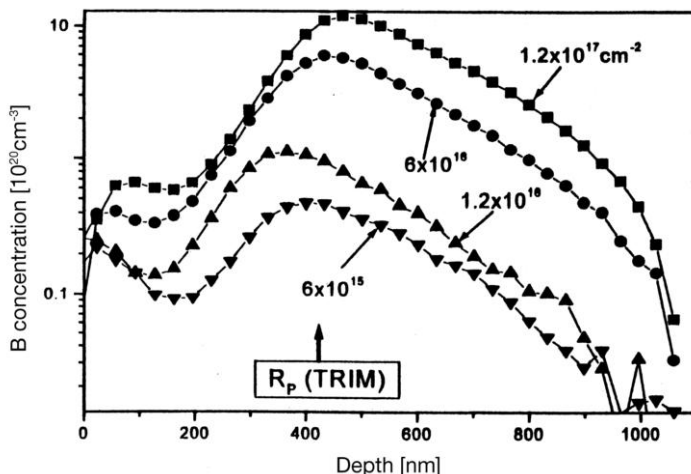


**Fig. 13.3** Concentration depth profiles of boron atoms implanted at 100 keV into polyimid for different boron fluences (in atoms  $\text{cm}^{-2}$ ).  $R_p$  (TRIM) is a projection of the ion path length on the original ion direction as simulated by TRIM code.

#### 13.4.25.5 Performance Criteria

In each of the reactions of  $^{10}\text{B}(n,\alpha)^7\text{Li}$  and  $^6\text{Li}(n,\alpha)^3\text{H}$ , two charged particles are emitted. These particles carry a characteristic energy given by the exoergic reaction. The coincidence method, (where both of the particles that are produced by a single event are detected), can be used for very thin samples. It leads to an improvement in the lithium or boron detection limit of several orders of magnitude. The element depth distribution can be reconstructed with a resolution of 10–20 nm. NDP is extensively used for the determination and depth profiling of the following elements (typical detection limit in  $10^{15}$  atom  $\text{cm}^{-2}$  is given in parentheses):  $^3\text{He}$  ( $10^{-3}$ ),  $^6\text{Li}$  ( $10^{-3}$ ),  $^{10}\text{B}$  ( $10^{-2}$ ),  $^{14}\text{N}$  (1),  $^{35}\text{Cl}$  (10).

#### 13.4.25.6 Application

The NDP method is an excellent tool for studying numerous problems in solid-state physics (diffusion, sputtering), materials science (corrosion), life science and especially in microelectronics, where the tight control of boron distribution and transport is vital to semiconductor device fabrication.

#### 13.4.26

#### Particle Induced Gamma Ray Emission [5, 35, 36]

**Acronyms:** PIGE or PIGME (particle induced gamma ray emission)

#### 13.4.26.1 Introduction

PIGE or PIGME is a versatile non-destructive technique which is complementary to other ion beam techniques (especially particle induced X-ray emission, PIXE). It is the most common application of nuclear analysis.

#### 13.4.26.2 Instrumentation

The high-energy proton beam from an accelerator is used to irradiate the sample. PIGE is mostly based on the nuclear reaction induced by MeV protons where nuclear  $\gamma$ -rays are produced.

In most cases a high purity germanium (HPGe) detector or scintillation detectors with multichannel acquisition systems are used for detection of  $\gamma$ -rays. A typical detector solid angle is 0.1 to 0.5 sr, the sample to detector distance is typically a few cm. The lower the incident ion energy the fewer resonances are involved in ion–gamma reactions and non-uniform angular distributions are more likely to be observed. The choice of sample geometry affects the depth of ion penetration and hence the thickness of the layer that can be analysed. For metals and other good thermal conductors it is possible to use a beam current of the order of 1  $\mu\text{A}$  without special cooling arrangements. Typical current is 100 nA.

The energy scale, including non-linearity, can be calibrated using radioactive sources.

#### 13.4.26.3 Sample

PIGE has similar requirements as PIXE, but the  $\gamma$ -ray absorption in the sample is negligible.

#### 13.4.26.4 Analytical Information

The PIGE method is typically less sensitive than the related methods utilizing X-ray detection (PIXE). The  $\gamma$ -ray peaks are generally well isolated and the energy is high enough that no correction for absorption is necessary. The energy and intensity of the  $\gamma$ -ray lines produced indicate the elements that are present and their amounts respectively. Sophisticated peak search and fitting routines are widely used for computer analysis of complex  $\gamma$ -ray spectra. The effect of multiple scattering causes the continuum to be higher at the low energy side of a peak than on the high energy one. The background elimination in the analysis should be taken into account.

#### 13.4.26.5 Performance Criteria

For protons with energies from 1 to 3 MeV, the best sensitivities are found for Li, B, F, Na and Al and these elements can be determined simultaneously in many cases. For example a precision of better than 1% can be obtained for F and Na determination with a measuring time of a few minutes. At proton energies above 3 MeV,

the  $\gamma$ -ray emission from medium and heavy elements begins to compete with the light elements. The highest cross-sections are for light isotopes (Atomic number < 30), which can be determined with good sensitivity ( $1 \mu\text{g g}^{-1}$  or less).

Many reactions have narrow resonances, which are suitable for depth profiling.

The main improvement in the use of PIGE in the last decade has been the introduction of external beams. The external beams offer several advantages, such as the ability to measure organic samples (even volatile ones) or large specimens (e.g. paintings) that cannot be placed within the normal analysis chamber.

#### 13.4.26.6 Applications

The most notable application of heavy ion induced gamma ray emission has been in the profiling of hydrogen using beams of  $^7\text{Li}$  or  $^{11}\text{B}$ .

#### 13.4.27

##### Particle Induced X-ray Emission [5, 31, 37–39]

*Acronyms:* PIXE (particle induced X-ray emission)

#### 13.4.27.1 Introduction

PIXE is a method using X-ray emission for elemental analysis. A high energetic proton beam excites emission of characteristic X-rays from the sample atoms due to inner-shell ionisation. PIXE is not a true nuclear technique, since the ionisation of the atoms by the ion beam and the subsequent emission of characteristic X-rays are purely atomic electromagnetic (rather than nuclear) processes. Methods and data for using K and L lines of X-rays, produced by ion beams (mostly proton beams) are well established and thick or thin samples can be analysed with an absolute precision of 10% or better.

The main advantages of PIXE are its good sensitivity, multi-element capability and speed of analysis.

#### 13.4.27.2 Instrumentation

Ions, in particular protons from a particle accelerator, in the energy range 1–4 MeV, are used with beam spots 1  $\mu\text{m}$ –10 mm in diameter.  $\alpha$ -Particles from some radioactive sources ( $^{241}\text{Am}$ ) can also be used for excitation. The energy of emitted photons is measured by a wavelength dispersive Bragg spectrometer or by an energy-dispersive spectrometer with semiconductor Si(Li) or Ge(Li) detectors.

### 13.4.27.3 Sample

PIXE is able to investigate solid samples with sizes of the order of a cm and thicknesses on the scale of micrometers. However, PIXE can also be used for unusual samples like liquids and gases. Due to low absorption of X-rays in the sample it is better to investigate thin samples, the composition of which can be determined with better accuracy.

### 13.4.27.4 Spectrum

A typical PIXE spectrum of a sample from environmental research is shown in Fig. 13.4.

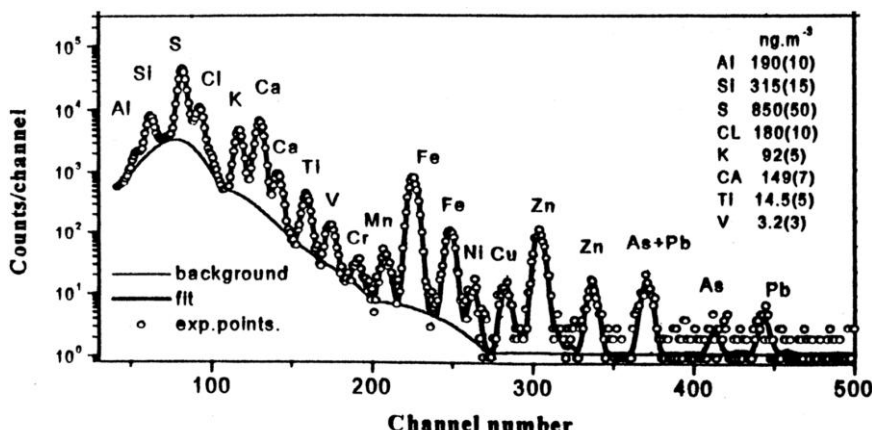


Fig. 13.4 PIXE spectrum of fine aerosol fraction collected on Nucleopore filter at a suburban station. Composition shown in right-hand corner.

### 13.4.27.5 Analytical Information

The energy dependence of the emitted X-rays is a monotonically increasing function of atomic number (Moseley law). So, the position of the peaks in the spectrum is characteristic of individual elements.

Intensities of the characteristic X-ray lines can be converted into concentration data. X-ray yield depends on the number of atoms in the sample, the ionisation cross-section, the detector solid angle, intensity of the ion beam etc. and so the determination of an absolute concentration of an element in an unknown matrix represents a complicated problem. In practice, the evaluation of the sample composition involves the comparison of X-ray yields from the unknown sample with that from known standards.

It is necessary in PIXE to take into account some correction factors for thickness evaluation due to X-ray absorption in the sample. In some samples (esp. in alloys) the influence of secondary X-ray emission should also be considered.

#### 13.4.27.6 Performance Criteria

PIXE should achieve sensitivities in the range  $0.1\text{--}1 \mu\text{g g}^{-1}$ , but this depends on the target and measurement arrangement. PIXE has a very low detection limit  $10^{-8}\text{--}10^{-10} \text{ g}$  in standard practice.

This method is not used for elemental depth profiling, because of its low depth resolution. The depth accessibility for  $\sim\text{MeV}$  ions is a few  $\mu\text{m}$ . In PIXE strong matrix effects are encountered. The major advantage of the use of ions in PIXE is a reduction in the background in comparison to that obtained when electrons are used (electron microprobe induced X-ray emission, EDX). The optimal depth range for useful results appears to be between 0.1 and 10  $\mu\text{m}$ .

PIXE enables the determination of composition for all elements with  $Z$ , atomic number, higher than 5. An examination of PIXE spectra shows that the characteristic X-ray peaks are superimposed on a background, which forms a limiting factor in sensitivity. It is possible to obtain limited depth profile information using ion induced X-ray emission. The depth resolution is angle and ion energy dependent and is not as good as for other techniques.

#### 13.4.27.7 Application

PIXE is the preferred method for such applications as the analysis of 15 to 20 elements in a thin sample such as air filters, or for automated analysis of large numbers of geological or archaeological samples, due to its short measurement time. The low absolute detection limit and good sensitivity for elements such as S, P, Cl, K and Ca, Fe make PIXE of great importance in biological and medical applications.

Particle induced X-rays can be generated with a microbeam (of order 10  $\mu\text{m}$ ) to perform high sensitivity-lateral mapping of trace elements distributions. Such a beam can also be brought into air for analysis of biological and vacuum-degradable samples.

#### 13.4.27.8 Other Techniques

The detection limit for PIXE is much lower than for electron induced X-rays. X-ray induced fluorescence (XRF) is the main alternative to PIXE. However, electrons or  $\gamma$ -photons can stimulate X-ray fluorescence too. If large samples that cannot be placed in the usual vacuum chamber are involved, (such as archaeological samples or artefacts that might have dimensions of metres), then XRF may be the preferred method; but for small samples or microprobe applications PIXE is more advantageous. TRXRFA (total reflection X-ray fluorescence analysis) offers low detection limit. From experiment it was concluded that this technique is useful only at glancing geometry (small incidence and exit angles with respect to the surface plane).

### 13.4.28

#### Penning Ionisation Electron Spectroscopy [8]

*Acronyms:* PIES (Penning ionisation electron spectroscopy)

SPI (surface Penning ionisation)

SPIES (surface Penning ionisation spectroscopy)

MIES (metastable impact electron spectroscopy)

MAES (metastable atom electron spectroscopy)

##### 13.4.28.1 Introduction

A low energy beam of metastable excited gas atoms is directed at the sample. The interaction with the surface de-excites the atoms and ejects an electron from the surface. This electron is collected by an electron energy analyser to reveal information about the surface electronic structure and bonding geometry.

##### 13.4.28.2 Instrumentation

This technique requires vacuum conditions. A low energy ( $<0.4$  eV) beam of noble gas atoms such as helium or neon is excited into a metastable energy state and directed at the surface of a sample. Immediately upon contact with the surface the atom de-excites and transfers its energy to a surface atom, which ejects an electron, a process known as Penning Ionisation. The emitted electrons are collected by an electron energy analyser such as a hemispherical mirror analyser to produce a spectrum showing the number of electrons emitted with a given kinetic energy. Such spectra are representative of, although not identical to, the sample's valence band electronic density of states.

Since the de-excitation energies of the metastable atoms are generally in the range 10–30 eV the spectra are very similar to those obtained in ultraviolet photo-electron spectroscopy (UPS). However, PIES is much more surface sensitive, essentially limited to the topmost atomic layer. Furthermore, orbitals that protrude further out from the surface interact more strongly with the impinging gas atoms and so give a stronger PIES signal, allowing PIES to reveal information about surface molecular orientation.

##### 13.4.28.3 Sample

Vacuum compatible solids. PIES is particularly useful for studying molecular adsorbate overlayer geometry on metallic single crystals.

##### 13.4.28.4 Analytical Information

PIES reveals information about the valence band electronic density of states of the topmost atomic layer. It also reveals information about the molecular orientation of this layer.

Comparison with UPS spectra allows particular UPS features to be assigned to particular molecular orbitals based on the strength of their PIES interaction.

#### 13.4.28.5 Performance Criteria

The energy resolution is strongly dependent on the particular type of electron energy analyser and beam source used, however it may be as good 10 meV. Spatial resolution is determined by the electron energy analyser and may be a few tens of micrometers.

The excitation energy can be changed (analogous to the use of different photon energies in UPS) by choosing different excited states of different noble gas atoms for the metastable ion beam.

The technique is sensitive to the composition and molecular orientation of the topmost atomic layer of the sample.

The elemental sensitivity of PIES is similar to that of UPS i.e. a few atomic percent at the surface.

High surface sensitivity makes the technique vulnerable to contamination, necessitating the use of UHV procedures. The low energy of the emitted electrons makes the technique vulnerable to the presence of stray magnetic fields and so magnetic shielding is normally required.

Analysis of the spectra can be complicated by the presence of multiple decay channels for the excited gas atom interacting with the surface, resulting in additional satellite peaks in the spectrum.

#### 13.4.28.6 Applications

The high surface specificity, the sensitivity to surface molecular geometry, and the negligible surface damage that the very low energy beams produce make the technique particularly suitable for studying molecular adsorption on metallic single crystals. Particularly in cases where the adsorbate bonding may be very weak and would be disrupted by more aggressive surface probes.

#### 13.4.28.7 Other Techniques

Ion neutralisation spectroscopy (INS) is very similar to PIES but makes use of ions, rather than metastable excited gas atoms.

### 13.4.29

#### Photoacoustic Spectroscopy [40]

*Acronyms:* PAS (photoacoustic spectroscopy)

#### 13.4.29.1 Introduction

PAS is a technique based on the so-called optoacoustic effect. When a short pulse of electromagnetic radiation interacts with condensed matter, the absorbed energy is converted into heat by fast nonradiative relaxation processes. Subsequently, the thermal expansion of the instantaneously heated medium causes an acoustic pulse, which is detected.

#### 13.4.29.2 Instrumentation

A PAS spectrometer consists of a source of intensity modulated electromagnetic radiation, a monochromator if necessary, a photoacoustic cell, and the electronics for detecting and storing the photoacoustic signal. The photoacoustic cell is the section containing the sample and the microphone, with its preamplifier, or a piezoelectric detector in intimate contact with the sample. In the infrared range a Michelson scanning interferometer is used. The moving mirror is additionally sinusoidally driven to obtain a modulation of the output radiation.

#### 13.4.29.3 Analytical Information

Analytical information is gained from the dependence of the relative acoustic signal on wavelength, which represents the absorption spectra of the compound. By changing the modulation frequency absorption information from different depths of the studied material can be obtained. For materials with low thermal diffusivity this layer can be about 0.1 µm at a chopping frequency of 10–100 kHz, but 10–100 µm for a frequency of 5 Hz.

#### 13.4.29.4 Performance Criteria

Temperature changes of  $10^{-7}$  to  $10^{-6}$  °C can be detected with a piezoelectric detector in intimate contact with the sample, detection with a microphone is 10–100 times less sensitive. As only absorbed radiation contributes to the detected signal absorption spectra of highly scattering materials, such as powders, amorphous solids, gels, and colloids, can be obtained. A wide range of electromagnetic radiation can be used with the same detection system, the only limitation being sufficient energy of the source (min.  $10 \mu\text{W cm}^{-2}$ ) and sufficient transparency of the other optical components of the measuring system across the full energy range of interest. Hence, spectra from the UV to infrared range can be measured with the same equipment. Photoacoustic spectroscopy is not considered suitable for fast measurements and it is limited by the speed of sound, the slow microphone ( $<20 \mu\text{s}$ ) or the piezoelectric response time ( $<0.1 \mu\text{s}$ ).

#### 13.4.29.5 Application

Spectra of adsorbed or chemisorbed species on non-absorbing or highly reflecting substrates can be measured. PAS is a simple and highly sensitive method for identification of compounds separated by thin layer chromatography or for study of catalysts.

### 13.4.30

#### Photoemission Electron Microscopy [41–44]

*Acronyms:* PEEM (photoemission electron microscopy)

**13.4.30.1 Introduction**

X-rays are shone onto a sample to eject photoelectrons. These are collected and focused onto a phosphor screen to produce a magnified, real time, high-resolution image of the distribution of elements and/or magnetic domains over the sample surface.

**13.4.30.2 Instrumentation**

This technique generally requires UHV. An X-ray beam from an anode or synchrotron source is used to excite photoelectrons from the sample. These pass through a series of electrostatic lens which focus them to form a magnified real time image of photoelectron distribution on a phosphor screen in a manner that is analogous to optical microscopes but which is element specific. This image can either be viewed directly by eye or with a CCD camera interfaced to image analysis software.

The tunable photon energies available at a synchrotron source can be used to significantly enhance the elemental contrast available in PEEM by choosing a photon energy that corresponds to an absorption edge of a particular element of interest, thus greatly increasing the number of photoelectrons emitted from those areas that specifically contain that element.

By using circularly polarized X-rays from a synchrotron source the intensity of photoemission becomes dependent on the magnetisation of the sample. This can be used to provide element specific magnetic contrast for imaging magnetic domains whose behaviour can then be studied in real time.

Topographical features of the sample produce distortions in the image and this effect can be used to provide additional topographical contrast.

**13.4.30.3 Sample**

UHV compatible, solid samples. Samples must be reasonably flat to avoid excessive topographic distortions.

**13.4.30.4 Analytical Information**

PEEM provides high-resolution real time images of elemental or magnetic domain distribution with topographic sensitivity.

**13.4.30.5 Performance Criteria**

Energy range 50–2000 eV.

Spatial resolution as good as 30 nm.

Magnification up to x10,000.

Element specific magnetic contrast capability for imaging magnetic domains.

Real time element specific imaging.

PEEM is sensitive to all elements except hydrogen and helium.

Atomic sensitivities of a few percent of a monolayer at the surface.

When used for element specific magnetic imaging PEEM is sensitive to all three components of the magnetisation.

The technique can be used to study both ferromagnetic and anti-ferromagnetic domains, depending on the polarisation of the X-rays.

Sensitivity decreases rapidly with depth and is generally negligible below about 10 atomic layers depending on energy.

Its surface sensitivity makes the technique vulnerable to surface contamination so it is generally done under UHV conditions.

Magnetic imaging is limited to use at synchrotron radiation facilities because of the requirement for circularly polarized X-ray beams.

Electrostatic electron focusing is susceptible to the presence of stray magnetic fields and so magnetic shielding may be necessary.

#### 13.4.30.6 Applications

PEEM is particularly useful for imaging semiconductor microstructures, doing microparticle analysis, studying real time processes such as surface diffusion, or for magnetic domain imaging in data-storage applications. It is also useful in other applications where real time high-resolution imaging of elemental or magnetic domain distribution is required.

#### 13.4.31

##### **Positron Annihilation Auger Electron Spectroscopy [45–48]**

*Acronyms:* PAES: positron annihilation Auger electron spectroscopy.

#### 13.4.31.1 Introduction

A beam of low energy positrons is shone onto the sample. Some of the positrons annihilate core electrons of the surface atoms, leaving them in an excited state, which decays by Auger emission of an electron. The energies of the Auger electrons are characteristic of the atoms involved and so measurement of the electron energies reveals information about the elemental composition of the sample surface.

Typical emitted electron energy range is 50–2000 eV.

#### 13.4.31.2 Instrumentation

This technique requires UHV conditions. A beam of low energy positrons is directed at the sample. Some of these positrons annihilate core electrons bound to atoms in the surface to leave behind a vacant “core hole”. The atom relaxes by the emission of an Auger electron which is detected in the same way as in AES. Auger electrons can also be detected using a time of flight system with the timing signal generated by the detection of the gamma ray associated with the annihilation event.

This technique is identical to Auger electron spectroscopy (AES) with the exception that positron annihilation is used to excite the core hole rather than a beam of high-energy electrons. The use of a positron beam has a number of distinct advantages. An electron beam that is energetic enough to excite core holes for AES will also produce a huge background signal of backscattered and secondary electrons which is many times larger than the Auger signal of interest and must be removed during data analysis. This background is completely absent in PAES resulting in true peak shapes that are free of distortions caused by background subtraction.

The electron beam used in AES delivers a large energy dose and a high electric charge density to the surface of the sample that can cause extensive damage to some materials. The energy dose in PAES is some five orders of magnitude lower than in AES and has charge densities 1000 times lower, eliminating any damage or charging.

The position beam comes from radioactive emission (e.g.  $^{22}\text{Na}$ ) or a high intensity dedicated positron beam source.

#### 13.4.31.3 Sample

UHV compatible materials. PAES may be used on insulators or delicate samples, such as weakly physisorbed molecules that cannot be studied easily with conventional AES.

#### 13.4.31.4 Analytical Information

Elemental composition of the topmost atomic layer with peak shapes that are free of data manipulation artefacts.

#### 13.4.31.5 Performance Criteria

This technique is extremely surface sensitive. Virtually all positron annihilation occurs in the very topmost atomic layer.

Contents of 1% of the surface layer can be detected, depending on the intensity of Auger emission for the element concerned. Typically, Auger electron emission is high for low atomic number elements and gradually drops as the atomic number increases.

PAES is sensitive to all elements except hydrogen and helium.

Its extreme surface sensitivity makes this technique vulnerable to the presence of contamination.

Access to low energy positron beams is extremely limited and so PEAS is only available at a few facilities.

Peak overlaps can make some element identification difficult.

#### 13.4.31.6 Applications

PAES can be used to study weakly adsorbed molecules and insulators that cannot be studied easily by AES.

PAES is also used where the composition of the very topmost layer is important, such as in catalysis.

PAES is particularly useful in studies where determining the true shape and relative magnitude of the Auger peak free from background subtraction errors is important, such as for the compilation of Auger reference standards, instrument calibration, and verification of theoretical models of Auger emission.

#### 13.4.31.7 Other Techniques

Auger photoelectron coincidence spectroscopy (APECS) is another technique that is used to produce background-free Auger spectra.

### 13.4.32

#### Raman Spectroscopy [5, 10]

*Acronyms:* no acronym used.

##### 13.4.32.1 Introduction

By irradiation of the sample with monochromatic radiation a small proportion of the radiation is re-emitted (scattered) with the wavelengths differing by frequencies corresponding to the vibrational modes of the sample. Frequencies smaller (Stokes process) or higher (anti-Stokes process) than the excitation frequency are observed. The strength of the effect is determined by the derivative of the molecular polarisability of the sample with respect to the vibrational coordinates.

##### 13.4.32.2 Instrumentation

Dispersive Raman spectrometers are used with excitation in the visible range (typically He–Ne or Ar<sup>+</sup> lasers are used), Fourier transform Raman spectrometers are used with excitation in the near infrared range (Nd:YAG laser). For both ranges, microscopic techniques working with a laser beam diameter of micrometer size, are commercially available.

##### 13.4.32.3 Sample

Raman spectroscopy is not particularly surface sensitive but a surface enhanced Raman scattering (SERS) effect is observed on some metals (copper, gold, silver, nickel etc). On an appropriately prepared (roughened) surface or on metal colloids the surface coverage of molecules can be measured by Raman spectroscopy with high sensitivity.

#### 13.4.32.4 Analytical Information

The Raman spectrum, represented as the dependence of the relative intensity of the detected signal on wavenumber (Fig. 13.5) provides information on the sample's composition, structure, and vibrational modes that is complementary to the infrared spectrum.

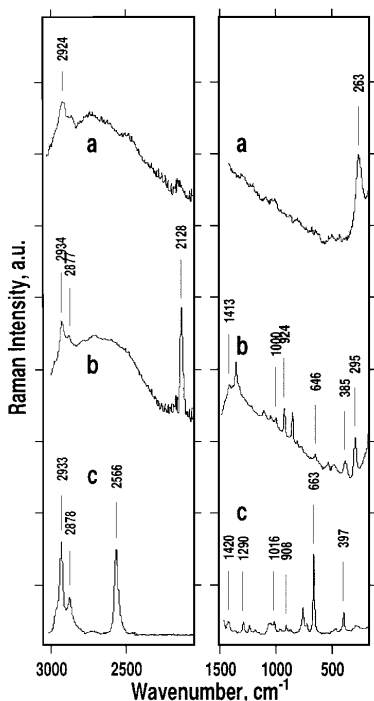


**Fig. 13.5** FT Raman spectra of a layer of 2-mercaptoethanol on polished (a) and rough (b) gold substrate compared with the spectrum of pure 2-mercaptoethanol (c)

#### 13.4.32.5 Performance Criteria

The Raman effect is a very weak effect in comparison with inherently accompanying Rayleigh scattering (which can be eliminated by using good quality monochromatisation or filtering), and with fluorescence of the sample or any accompanying impurities. The last effect can be eliminated using near infrared radiation for excitation of the Raman spectra.

SERS effect allows an enhancement of the signal of the order of  $10^3$ – $10^6$ . It means that even subnanomolar amounts of the component in the irradiated area can be detected.

#### 13.4.32.6 Application

Used in the study of catalysis and electrochemistry.

**13.4.33****Reflection-absorption Spectroscopy [5, 10, 11]**

*Acronyms:* IRRAS, IRAS (infrared reflection-absorption spectroscopy)

RAIRS (reflection-absorption infrared spectroscopy)

FT RAIRS (Fourier transform reflection-absorption infrared spectroscopy)

GIS (grazing incidence spectroscopy)

**13.4.33.1 Introduction**

Measurement of sample layers of thickness ranging from many times the wavelength down to fractions of a monolayer placed on a mirror. Absorption by the sample reduces the mirror's reflectance.

Range of operation of incident radiation: typically mid-infrared.

**13.4.33.2 Instrumentation**

In a typical set-up (constructed as an accessory to be mounted in the sample compartment of a commercial FT spectrometer), infrared radiation is focused on the sample surface at a defined angle. The reflected beam is focused onto a detector. Irradiation with a polarized IR beam is often used.

Reflection-absorption spectra of fairly thick surface films (i. e., thickness between 0.2 and 20  $\mu\text{m}$ ) are easily achieved using standard accessories for specular reflectance spectrometry with incidence angles from 15 to 75°. Incidence angles much less than 15° are difficult to attain with conventional optics since it becomes difficult to separate the incident and reflected rays. A so-called grazing angle accessory is needed to attain angles of incidence above 75°. Grazing incidence geometry leads to an increase in the path length in comparison with the transmission experiment, an increase in the irradiated area proportional to the secant of the angle of incidence, and an enhancement in the electric field vector of the IR photon perpendicular to the surface. Near grazing incidence the contribution of the incoming wave interferes constructively with the 180°-phase shifted reflected wave. In total, a sensitivity increase of the order of a factor of 20 in comparison with the transmission methods is to be expected on a highly reflective sample, such as a metal single crystal surface.

In the extreme case of grazing incidence, the component of the electric field perpendicular to the plane of incidence is very small.

**13.4.33.3 Sample**

Mirror-like surfaces are required.

#### 13.4.33.4 Analytical Information

RAIRS results in a spectrum that is similar to that of a transmission measurement. For grazing incidence geometry, only molecular vibrations giving rise to a dynamic dipole perpendicular to the surface are infrared active; this is termed the surface selection rule for surface vibrational spectroscopy.

#### 13.4.33.5 Performance Criteria

Grazing incidence allows one to measure monomolecular or sub-monomolecular layers. For a thickness of about 1 nm, band absorbances of the order of  $10^{-3}$ – $10^{-4}$  are measured with an  $85^\circ$  angle of incidence. The overall size of the sampled area achieved with the given geometrical arrangement is critical for sensitivity.

An outstanding gain in sensitivity, allowing one to identify and quantify surface layers of some nanometers thickness, can be observed for strong oscillators due to the Berreman effect.

#### 13.4.33.6 Limitations

Strong dispersion associated with intense absorption bands can cause significant changes in the absorption peak position and shape: for example  $1\text{--}4\text{ cm}^{-1}$  for moderately absorbing species (benzene, acetone) and  $\sim 22\text{ cm}^{-1}$  for strongly absorbing species (copper oxide on copper).

With layers of a thickness comparable to that of the measured wavelengths, the increase of the absorption with the thickness can be corrupted by a modulation connected with the regularly varying standing wave formed. With a thickness below one-quarter wavelength, the response decays not only with the thickness but, additionally, with the field amplitude approaching the node. Thus zero sensitivity is to be expected at the very surface of the metal substrate.

For a number of practical reasons, low frequency modes ( $< 600\text{ cm}^{-1}$ ) are not generally observable. This means that it is not usually possible to see the vibration of the metal–adsorbate bond and attention is instead concentrated on the intrinsic vibrations of the adsorbate species in the range  $600\text{--}3600\text{ cm}^{-1}$ .

#### 13.4.33.7 Applications

RAIRS is used for characterization of adsorbates on metal surfaces, their transformations and kinetics (for example CO on metallic surfaces), catalytic reactions, characterisation of semiconductor structures, high-temperature oxidation of metals (use of so-called Berreman effect), electrode/electrolyte interface, Langmuir–Blodgett and other ultrathin organic films.

#### 13.4.33.8 Other techniques

Modulation spectroscopy uses a periodic (sinusoidal) variation of a parameter influencing the reflectivity of the sample, such as wavelength, angle of incidence, electric field (electroreflectance), temperature (thermoreflectance), surface charge density (piezoreflectance), magnetic field strength (magnetoreflectance). This technique allows the effect of an external perturbation on the sample to be studied and also enhances otherwise weak details on a large background.

If a photoelastic modulator is used to generate alternately parallel and perpendicular polarized radiation, the ac signal detected will be due to the difference in the absorption of radiation of each polarization. The effect of the background can be eliminated in this way. In the infrared region, this type of experiment is denoted as polarization modulation, PM FTIRAS.

#### 13.4.34

#### Reflection Electron Energy Loss Spectroscopy [7]

*Acronyms:* REELS: reflection electron energy loss spectroscopy (sometimes abbreviated also to EELS).

##### 13.4.34.1 Introduction

A primary electron beam (energy typically 100–2000 eV) impinges on a sample. The electrons bounce off the surface and many electrons are elastically scattered from the surface. Other electrons undergo inelastic scattering by exciting a plasmon or interband transition in the surface layers. The energies of the reflected electrons are analysed to produce an energy loss spectrum. This loss spectrum consists of a series of loss peaks at different energies and intensities. The technique is normally available on instrumentation designed primarily for Auger electron spectroscopy (AES), (or X-ray photoelectron spectroscopy (XPS) where an electron gun has been fitted) and thus provides useful extra information on the sample surface under study.

##### 13.4.34.2 Instrumentation

The electron beam from a simple electron gun is directed at the sample surface. The beam normally has an energy spread ~1–2 eV at a typical primary beam energy of between 100–2000 eV. The reflected electrons pass through an electron energy analyser before being detected.

##### 13.4.34.3 Sample

Samples should have reasonably flat surfaces and preferably be conducting.

#### 13.4.34.4 Analytical Information

The source of information is dependent on electron current, primary beam energy and electron energy loss. The plasmon losses are typically of the order of ~10 eV and can provide information on the permittivity of the material under study. EELS is thus complementary to optical reflectivity techniques. Interband transitions can be compared with theoretical models of the electronic structure of the material.

#### 13.4.34.5 Performance Criteria

The method is sensitive to energy losses of greater than ~1 eV. Hence it cannot detect vibrational losses as in high resolution electron energy loss spectroscopy (HREELS). The detection volume is limited to the top few atomic layers for metals.

REELS requires an UHV chamber with magnetic shielding; stray charges may build up in the spectrometer which then requires frequent baking. REELS is difficult to quantify. It is best for small, non-magnetic single crystals and has poor sensitivity for rough surfaces. It is not very sensitive for insulating materials as surface charging makes their analysis difficult. REELS equipment is relatively low cost in comparison to HREELS.

#### 13.4.34.6 Applications

EELS spectra can be used to estimate permittivity of the material under investigation.

#### 13.4.34.7 Other Techniques

Scanning low energy electron loss microscopy (SLEELM) can provide a map of electron energy loss peaks across a surface.

Extended electron energy loss fine structure (EELFS, EXELFS) works with higher fixed energy of primary electrons (10–80 keV, respectively) and higher energy losses of the scattered primary electrons ranging from 200–4000 eV, respectively. EXELFS is a technique used in transmission electron microscopes (TEM). It provides information similar to X-ray absorption fine structure (EXAFS) i.e. data regarding the immediate neighbourhood of atoms of certain elements in the sample. EXELFS is bulk sensitive. Transmission electron energy loss spectroscopy (TEELS) is another technique that is used in a TEM. The electron energy loss is much higher than in EXELFS and characteristic energy losses can be observed. This provides information concerning the elemental composition of the sample. The spectra are detected using a multi-element solid-state semiconductor detector, which results in a spectrum being acquired in parallel. Hence the name PEELS.

### 13.4.35

#### Resonant Nuclear Reaction Analysis [5, 35, 37]

*Acronyms:* RNRA (resonant nuclear reaction analysis)  
NRA (nuclear reaction analysis)

##### 13.4.35.1 Introduction

As a result of ion beam irradiation of a material two distinct phases exist during which the emission of particles (NRA) and gamma rays (see PIGE) or X-rays (see PIXE) take place. Nuclear reactions are isotope specific (the nuclear reaction takes place on the specific isotope only) with no direct relationship between the mass of the target nucleus and the energy of the emitted particles. The detection of small amounts of isotopes is very easy, especially in the case of a sharp nuclear resonance cross section for the reaction, which is used in RNRA. NRA is induced by protons, deuterons or alpha particles with an energy from 100 keV up to several MeV. NRA in combination with RNRA has become very popular for depth profiling of light elements. RNRA uses the resonant cross section dependence on the initial ion beam energy, which can be many times higher than the non-resonant one. Since RNRA is not only depth sensitive, but selects particular target isotopes, this technique opens the way to detailed isotope-sensitive studies.

##### 13.4.35.2 Instrumentation

The equipment required for ion–ion analysis is typically a vacuum chamber, a solid-state detector, and an accelerator, which produces the ions (protons, alpha particles and deuterons) with energies 0.5–2 MeV. Energies above 3 MeV make the (d, p) reaction useful for the study of metals. The samples are irradiated by the ion beam and the products of the resonance reaction can be monitored by measuring the emitted charged particles and/or subsequent  $\alpha$ -radiation of the resulting nucleus. Magnetic analysers should be used to separate reaction products from scattered ions and to achieve better energy resolution. In general, the probing ion beam hits the sample at normal incidence. If the ion energy used is equal to the resonant energy, the resonance reaction takes place on the nuclei located at the surface. If the beam energy is higher than the resonant energy the resonance occurs at depth due to the energy losses of the initial ions. By measuring the yield for constant cumulated charge and varying the beam energy in small steps, the yield as a function of ion beam energy can be interpreted as the amount of the element at various depths, i. e. it provides the concentration depth profile. Of course, the finite resonance width, the beam energy spread of the accelerator, and the energy straggling of the ion beam projectiles in the target have to be considered in the analysis. Incident ion energies from 0.5 to 2 MeV are most useful for minimising interference from reactions on heavy isotopes.

#### 13.4.35.3 Sample

The sample should be a solid material, usually the trace elements or impurities in the bulk material are investigated.

#### 13.4.35.4 Analytical Information

The spectrum of charged products of the nuclear reaction is measured. The yield of nuclear reaction products is directly dependent on the cross section (which defines the probability of a specific type of interaction) and the density of target atoms in the sample.

High peak cross-sections at resonances give high sensitivity of RNRA. Energy loss by the incident ion can be used to determine depth profiles by resonance scanning. Energy loss by both incident and product ions may be used for depth profiling of particular isotopes in a manner analogous to Rutherford backscattering spectrometry (RBS). The advantage of RNRA is that there is no natural background from the high Z components of the target in comparison with methods using back-scattering, where the ions backscattered from the heavy elements in the sample produce a background in the spectra and hence decrease the sensitivity for the light elements.

#### 13.4.35.5 Performance Criteria

The nuclear reaction methods are suitable for the determination of several isotopes from  $^1\text{H}$  to  $^{32}\text{S}$ . The most frequently used reactions are  $(\text{p},\alpha)$ ,  $(\text{d},\text{p})$  and  $(\text{d},\alpha)$  providing useful alternative methods for the determination of isotopes such as  $^2\text{D}$ ,  $^{12}\text{C}$  and  $^{16}\text{O}$  compared with RBS or elastic recoil detection analysis (ERDA). Alpha induced reactions have a limited use. Some  $^6\text{Li}$  induced reactions have been tested and the  $(^{11}\text{B}, \alpha)$  reaction has been used for hydrogen determination and profiling. Cross-sections of 10 to 100 mb sr $^{-1}$  are observed for proton and deuteron induced reactions with light isotopes such as D, Li, Be and B. Detection limits of the order of 10  $\mu\text{g g}^{-1}$  or even less are then possible with measuring times of the order of tens of minutes. Isotopes up to  $^{32}\text{S}$  can be determined in heavier matrices at mg g $^{-1}$  levels depending on the maximum beam current that the sample can withstand.

The use of glancing incidence or emergence for heavy incident ions or produced ions respectively can give typical depth resolutions at the surface of 10 to 100 nm.

The maximum analysis depth is usually limited to 1  $\mu\text{m}$ . The composition of the target usually cannot be estimated from one measurement.

#### 13.4.35.6 Application

This method is particularly useful for the determination of light elements (isotopes) in the sample. Some elements cannot be detected by other methods (for example RBS). NRA is a complementary method to RBS, PIXE, and PIGE.

### 13.4.35.7 Other Techniques

See CPAA (charge particle activation analysis).

### 13.4.36

#### Rutherford Backscattering Spectrometry [5, 35, 37, 49]

*Acronyms:* RBS: Rutherford backscattering spectrometry. Other acronyms can be found to distinguish the ion beam energy used: HEIS: high energy ion scattering, MEIS: medium energy ion scattering or generally ISS: ion scattering spectrometry. The physical principles are the same.

##### 13.4.36.1 Introduction

RBS is the most commonly used non-destructive nuclear method for elemental depth analysis of nm to  $\mu\text{m}$  thin films. It involves measurement of the number and energy distribution of energetic ions (usually protons or  $\text{He}^+$ ) elastically back-scattered within the near-surface region of solid targets. From such measurements it is possible to determine, with some limitations, both the atomic mass and the content of elemental target constituents as a function of depth below the surface.

##### 13.4.36.2 Instrumentation

An ion beam with an energy of the order of 100 keV to several MeV is provided by an accelerator and impinges on a sample located in a vacuum chamber (vacuum of the order  $10^{-3}$ – $10^{-5}$  Pa). Samples are mounted, several per load, on the table of a goniometer which allows three degrees of freedom, two for the sample position and one for the angle, so as to enable sample changing and manipulation without breaking the vacuum. Surface barrier detectors are primarily used for ion detection.

##### 13.4.36.3 Sample

The sample could be a multilayer system or bulk material. The lateral and inter-layer homogeneity is important to obtain an undeformed spectrum for quantitative analysis.

##### 13.4.36.4 Analytical Information

Two main phenomena provide the analytical information: (i) the energy transfer and (ii) the kinematics in elastic collisions between atomic nuclei and ions. The Rutherford scattering cross-section is a function of atomic number, target mass and scattering angle and depends on the initial projectile energy. From the number of detected scattered particles, the content of a particular element in the target can be determined. Finally, the incident particle loses energy in penetrating the solid, both along the incident path prior to scattering and along the exit path. The mea-

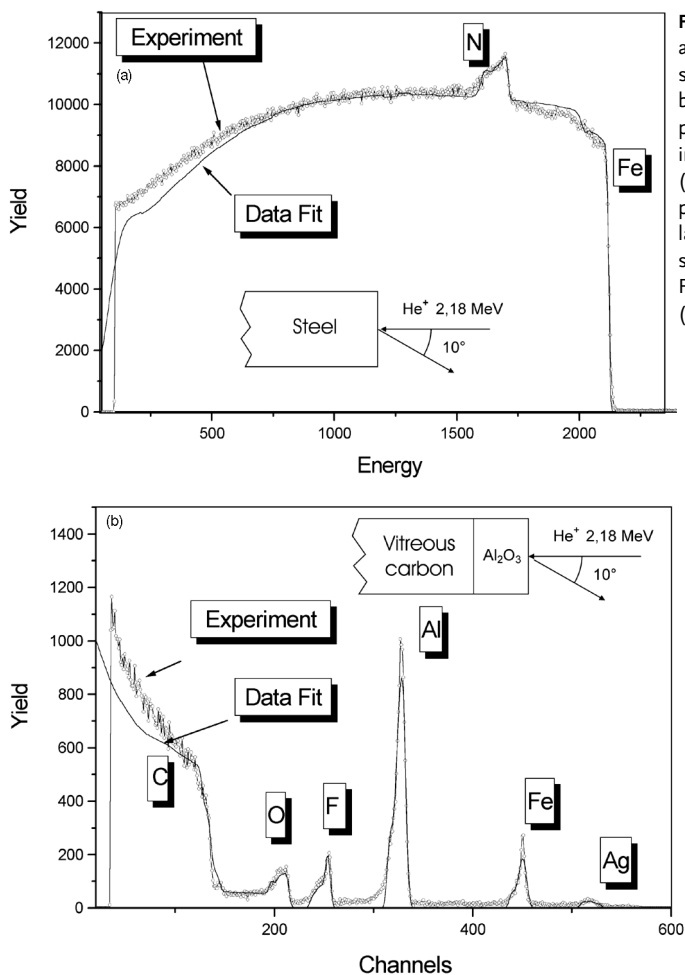


**Fig. 13.6** Measured and simulated RBS spectra (incident beam 2.18 MeV alpha particles) of nitrogen implanted into steel (energy scale, a) and plasma oxidized Al layer on carbon substrate with Ag, F, Fe as impurities (channels, b).

sured energy loss can be transformed into a depth measurement using the known stopping cross-section (ion stopping in the material). Thus, energy differences in the energy spectra can be used to identify scattering depths and hence provide a depth profile of target constituents. An example of an RBS spectrum is shown in Fig. 13.6.

#### 13.4.36.5 Performance Criteria

The sensitivity of RBS for the detection of trace impurities in bulk samples depends strongly on the sample composition and the experimental conditions. For impurities heavier than the substrate, the signal of which lies in the background-free region, it is possible to measure infinitesimal amounts of impurities simply by increasing the integrated charge. The near surface depth resolution

can be improved by selecting a glancing incident or exit geometry; this improvement results from the increased path length through the surface region. Impurities, which are lighter than the substrate, are usually detected with poor sensitivity and several atomic percent are needed for their detection.

The major strengths of RBS are absolute composition measurement of layered structures or trace impurity concentration through a precise knowledge of the cross-section. RBS is not usually employed for the analysis of samples of totally unknown composition or for the depth profiling of sample containing a multitude of unknown elements. A problem arises if the material contains several elements with overlapping signals in the RBS spectra, or if the sample is inhomogeneous, resulting in deformed spectra.

#### 13.4.36.6 Applications

Principal applications include bulk composition analysis and major element profiling, minor element identification, and study of multilayered systems including depth profiling. Thin film analysis is used for studies of solid-state reactions, inter-diffusion, stoichiometry, film thickness, uniformity and impurity content. Investigated systems are prepared by various techniques for example by conventional and reactive evaporation, rf and dc magnetron sputtering, laser ablation, ion beam assisted deposition, sol–gel techniques, ion implantation or plasma surface treatment. The investigated materials are used for optics, microelectronics, hard and protective coatings, diffusion studies, magneto-optic recording media etc.

#### 13.4.36.7 Other Techniques

Non-Rutherford backscattering spectrometry (Non-RBS or n-RBS) measurement improves the detection sensitivity of light impurities, the light elements have a resonant cross-section for light highly-energetic projectiles (e.g. protons), which could be many times higher than for RBS. The measurement at resonant energy is sensitive to the light elements e.g. C (proton energy 1742 keV), N, and O.

Channeling-RBS is a method for the investigation of adventitious atoms in the interstitial space of monocrystals. Channeling is the steering of a beam of energetic ions into open spaces (channels) between close-packed rows or planes of atoms in a crystal. A goniometer is a crucial part of the channeling equipment. Channeling is used to study many surface properties, such as surface reconstruction or relaxation of the outermost layer of atoms.

#### 13.4.37

#### Scanning Electron Microscopy [5]

*Acronyms:* SEM: scanning electron microscopy, SEMPA: scanning electron microscopy with polarisation analysis, EDX: energy dispersive X-ray analysis, EPMA: electron probe microanalysis, SAM: scanning Auger microscopy.

### 13.4.37.1 Introduction

A tightly focussed beam of high energy electrons (typically 10 keV) is rastered back and forth across the surface of the sample. The impact of the high energy electrons ejects low energy secondary electrons from the sample which are collected by a detector to produce a real time magnified image of the sample.

### 13.4.37.2 Instrumentation

This technique requires vacuum conditions. A tightly focused beam of high energy electrons (2–100 keV or higher) is rastered across the surface of the sample. This generates a number of effects including emission of low energy secondary and Auger electrons from the surface, generation of X-rays from within the sample and the backscattering of the primary electrons. The analysis of these different forms of emission reveals complementary information about the sample. The output from an electron or X-ray detector within the instrument is sent to a display that is synchronised to the raster frequency of the beam to produce a real time magnified image of the sample. The magnification is changed by keeping the size of the image constant whilst increasing or decreasing the size of the area of the sample being scanned by the electron beam. Hence electron microscopy does not require the use of multiple sets of focusing optics for different magnifications as would be the case in optical microscopy.

The emission of secondary electrons is very sensitive to surface topography and so the collection of these electrons allows a topographic image of the sample to be obtained that has a much greater depth of field and a much higher ultimate magnification than would be possible with conventional optical microscopy techniques. Secondary electron microscopy also has a high surface sensitivity of a few tens of Angstroms.

When secondary electrons are emitted from a magnetic material they become polarised and so by using a polarisation sensitive detector such as a Mott detector to collect the secondary electrons an image can be obtained that has magnetic contrast, allowing magnetic domain structures to be studied. This technique is known as scanning electron microscopy with polarization analysis (SEMPA).

Images with elemental contrast can be obtained by detecting the high energy backscattered electrons, whose intensity is a function of the atomic number of the elements in the sample. These electrons also have a greater penetration depth than secondary electrons and so can be used for studying buried structures.

Quantitative information about the elemental distribution and concentration can be obtained by analysing the energies of the X-rays emitted, which are characteristic of the elements involved. This is known as energy dispersive X-ray analysis (EDX) or electron probe microanalysis (EPMA). It is essentially a bulk technique that reveals composition down to a depth of several microns.

Quantitative information regarding the surface (~1 nm depth) elemental distribution and concentration can be obtained by analysing the energies of the Auger electrons emitted, which are also characteristic of the elements involved. This is known as scanning Auger microscopy or SAM. The instrumentation involved in

detecting the Auger electrons is the same as in Auger electron spectroscopy (AES) and the reader should refer to that technique to learn more. Ultra high vacuum is required for SAM.

#### 13.4.37.3 Sample

Vacuum compatible conducting solids. Non-conductors such as biological samples are generally coated with a thin layer of gold to render them conductive. Biological or insulating samples may also degrade under electron bombardment.

#### 13.4.37.4 Analytical Information

Secondary electron mode: real time magnified topographic contrast images.

Back-scattering mode: real time magnified elemental contrast images.

EDX mode: quantitative analysis of elemental composition and distribution at particular points of interest in the secondary or back-scattered images as well as magnified elemental contrast images.

SEMPA: magnified magnetic contrast images of domain structures.

SAM: quantitative analysis of surface ( $\sim 1$  nm depth) elemental composition and distribution at particular points of interest in the secondary or back-scattered images as well as magnified elemental contrast images.

#### 13.4.37.5 Performance Criteria

Magnifications ranging from 3x to 500,000x are possible depending on the instrument. Spatial resolution may be as good as 20 Å.

One of the major strengths of SEM is that the depth of field is very large (generally 10–60 % of the width of the field), ranging from 1 μm at high magnifications up to several mm at low magnifications. This is much larger (by some 300 times) than the depth of field obtainable in conventional optical microscopy at equivalent magnifications. Hence SEM allows realistic looking images of highly three-dimensional samples, such as biological structures, to be obtained.

Depth sensitivity depends on the analysis mode and energy range used. SEM with low energy secondary electrons can result in a surface sensitivity of 20 Å, whilst EDX reveals information about the top few microns of the sample. Depth sensitivity for back-scattered electrons is greatly dependent upon the electron beam energy and the elemental composition of the sample but is generally hundreds of nanometers.

Elemental sensitivity in EDX mode is 0.1 % depending on the elements in question with an accuracy of 1–3 % achievable. The elemental sensitivity for the SAM mode is ~1 % with an accuracy of ~5 % achievable.

EDX is not sensitive to elements lighter than carbon in the periodic table and has only limited sensitivity for elements lighter than sodium. SAM is not sensitive to H or He, but has better sensitivity to lower atomic number elements.

EDX is not able to produce the sort of information on chemical states than can be obtained in X-ray photoelectron spectroscopy (XPS) as the achievable resolution is only some 3 eV. SAM can produce some information regarding chemical state.

Quantitative EDX and SAM are most effective on flat polished samples.

Count rates in EDX are generally much lower than in backscattering or secondary electron mode and so it is often used for quantitative analysis of particular points of interest within a backscattered or secondary electron image, although EDX images can also be acquired if necessary. The same is true of SAM.

Mott scattering is a very inefficient means of electron detection and so magnetic contrast SEMPA images will require much longer acquisition times.

Exposure to intense electron beams may cause damage to the sample.

#### 13.4.37.6 Applications

SEM is one of the most widely used analytical techniques across all fields of science, technology and industry. Applications include imaging of highly three-dimensional biological structures, imaging and microanalysis of semiconductor structures, magnetic domain imaging for data storage applications, and imaging of fracture surfaces in component failure analysis.

#### 13.4.38

##### Scanning Tunneling Spectroscopy [50]

*Acronyms:* STS (scanning tunneling spectroscopy)

#### 13.4.38.1 Introduction

Scanning tunneling spectroscopy is a technique which is carried out using a scanning tunneling microscope (STM). The STM is one of a family of scanned probe techniques that can provide atomic level (or near atomic level) resolution. A sharp conducting tip is brought within a tenth of a nm from a surface such that an electric current can flow by quantum tunneling between the tip and sample. By rastering the tip across the surface a map of the surface defined by the tunneling current can be acquired. In the case of STS, the voltage ( $V$ ) at each point can be varied and the corresponding variation in the current ( $I$ ) measured. The resulting  $I-V$  curve is characteristic of the electronic structure at the particular tip position. Hence images of the electronic structure can be acquired at atomic resolution.

#### 13.4.38.2 Instrumentation

A scanning tunneling microscope is the principal piece of equipment. The microscope should be placed in an UHV chamber in order to ensure clean surfaces. A lock-in-amplifier can be used to acquire  $dI/dV$  or  $dI/dz$  (where  $z$  is the height of the tip above the surface) curves. The experiments are often carried out at cryogenic temperatures.

#### 13.4.38.3 Sample

Samples should have reasonably flat surfaces and preferably be metallic or semi-conducting. However, it has been shown that very thin films of insulators can also be analysed.

#### 13.4.38.4 Analytical Information

The electrons tunnel from filled states to empty states. The filled states can be in the tip or in the sample. Hence by varying the sample tip voltage both filled and empty states in the sample can be probed. A good understanding of the electronic structure of the tip is necessary to understand the data. The data is often displayed in the form  $(dI/dV)/(I/V)$  which is known as the normalized conductance which approximates the density of states of the sample.

#### 13.4.38.5 Performance Criteria

The technique is sensitive to surface contamination. The nature of the tip can affect both the spatial resolution and the  $I/V$  curves of the acquired STS data.

#### 13.4.38.6 Applications

STS spectra are used to acquire information regarding the electronic structure at atomic resolution.

#### 13.4.38.7 Other Techniques

Other scanned probe techniques such as atomic force microscopy may provide a type of spectroscopy by measuring the force on the tip as a function of distance, but are little used. The scanning near-field optical microscopy (SNOM) method can also provide standard far-field optical spectroscopy techniques but at an almost atomic resolution.

### 13.4.39

#### Secondary Ion Mass Spectrometry [5, 51]

*Acronyms:* SIMS (secondary ion mass spectrometry)

#### 13.4.39.1 Introduction

In SIMS, a beam of ions (with an energy of a few keV) is used to sputter the surface of a solid sample. The resulting secondary positively or negatively charged ions are analysed in a mass spectrometer. There are two modes of SIMS application differing primarily in the ion current and energy used. In the *static mode* an extremely low primary ion current density  $1 \text{ nA cm}^{-2}$  with a low primary ion energy  $0.5\text{--}2 \text{ keV}$  is used, resulting in a negligible sputtering rate of  $0.1 \text{ nmol h}^{-1}$ .

The *dynamic mode* uses a higher ion current density and the sputtering rate is typically  $1 \text{ } \mu\text{mol h}^{-1}$ . So, in the static mode the outermost surface layer may exist for hours before being completely removed in contrast to the dynamic mode where the surface layers are stepwise removed and depth profile analysis is possible.

#### 13.4.39.2 Instrumentation

The primary ions, generated by plasma discharge ( $\text{O}_2^+$ ,  $\text{O}^-$ ,  $\text{Ar}^+$ ), by thermionic surface emission ( $\text{Cs}^+$ ,  $\text{Li}^+$ ) or by liquid metal field emission ( $\text{Ga}^+$ ,  $\text{In}^+$ ), are accelerated (2–50 kV) and focused onto the sample. The secondary ions are transferred by ion optics into a mass spectrometer.

Three types of instrumentation exist for dynamic SIMS: non-imaging ion probes, direct-imaging ion microanalysers and scanning ion microprobes-microscopes. Non-imaging ion probes are often an accessory of Auger electron spectroscopy (AES), electron spectroscopy for chemical applications (ESCA), or electron microscopy systems and allow a point analysis. Imaging equipment allows a point-to-point analysis of the surface with a primary beam of size 10–300  $\mu\text{m}$  (microanalysers) or below 10  $\mu\text{m}$  (microprobes-microscopes).

SIMS requires clean ultra-high vacuum conditions to avoid contamination and reaction with residual gas components and normally has a relatively large analysed area.

#### 13.4.39.3 Sample

The secondary ion yield is sensitive to surface roughness and contamination which may change the relation between ion yield and element concentration.

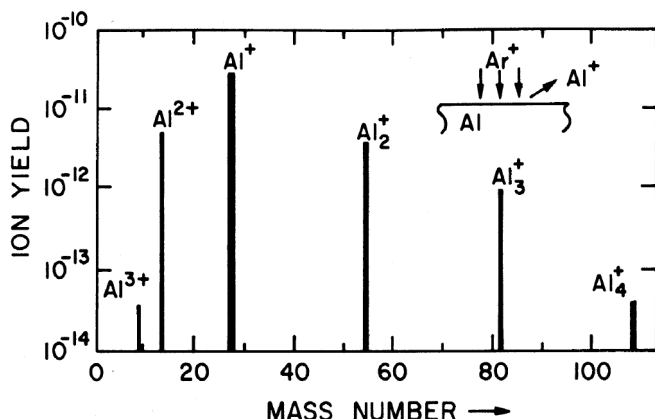
#### 13.4.39.4 Analytical Information

Analytical information is extracted from the mass spectrum, i. e. from the dependence of intensity (total counts) on the mass-to-charge ratio. The spectra of both positive and negative secondary ions are complex exhibiting not only singly and multiply charged atomic ions but all ionised clusters of target atoms (Fig. 13.7). All elements including hydrogen can be detected. In static mode the conditions are optimised to detect large molecular ions free from the ions formed in some recombination processes.

Elemental micro-mapping combined with depth profiling provides a three-dimensional analysis of the elemental structure.

Quantitative analysis is not easy due to extremely large variations in secondary-ion yield (due to the matrix effects, the target matrix affects the secondary ion yields markedly), up to five orders of magnitude, and the lack of simple quantitative algorithms. The best accuracy for quantitative SIMS analysis can be achieved by calibration using suitable standards.

**Fig. 13.7** Secondary ion cluster spectrum from Ar bombardment of Al.



#### 13.4.39.5 Performance Criteria

High mass resolution is necessary to avoid peak interferences in SIMS. However, relative intensity is strongly reduced with the increasing mass resolution due to narrower entrance slits in the mass spectrometer. Lateral resolution of  $0.3 \mu\text{m}$  or less is possible but the sensitivity is reduced in proportion to the resolution. The excellent mass resolution of less than 1 ppm and wide dynamic range is available for many elements.

SIMS is a method with a very low detection limit, typically  $10^{-7} \text{ g g}^{-1}$  range.

The main limitation in trace analysis arises from interferences in the SIMS spectra due to detected clusters, hydrocarbons, oxides and hydrides. SIMS is an excellent and powerful analytical destructive technique, but it is based upon processes that are not yet sufficiently understood.

#### 13.4.39.6 Application

SIMS applications cover a wide range of fields from pure research to industrial material control.

#### 13.4.39.7 Other Techniques

Secondary neutral mass spectrometry (SNMS) makes use of the sputtered neutral particles by using post-sputter ionisation. This is accomplished by laser (laser beam SNMS or SALI-surface analysis by laser ionisation) or by electron beams (e-beam SNMS), by collisions of electrons generated by hf discharge (electron gas SNMS), by excitation in various forms of plasma or discharge cell or by surface ionisation. A major difference from a conventional SIMS lies in the insertion of an ionising plasma chamber in front of the mass spectrometer. The grids placed before the plasma environment for post-ionisation act as an electrical diaphragm between the sample and the chamber, which prevents ions entering or leaving the chamber. Thus only neutral species enter the ionising chamber, and species ionised within

the chamber cannot reach the sample. Ionisation of neutral species within the chamber is achieved by a low pressure high-frequency plasma.

Neutral atom yields are high, especially for low energy incident ions. Since the ionisation probability of secondary particles obtained directly from the sputtering process is low, the yield of secondary ions can be enhanced by post-ionisation. The matrix effects occurring in SIMS are expected to be considerably smaller in SNMS and therefore quantification of the spectra to determine elemental composition may be much more accurate.

In fast-atom bombardment mass spectrometry (FAB) primary neutral atoms of energies 3–10 keV are used to sputter clusters and molecular ions from the sample.

#### 13.4.40

### Spectroscopy of Surface Electromagnetic Waves [52]

*Acronyms:* SEW (surface electromagnetic waves spectroscopy)

#### 13.4.40.1 Introduction

A thin dielectric film deposited on a metal increases SEW attenuation which becomes stronger as eigenfrequencies of the film vibrations are approached.

#### 13.4.40.2 Instrumentation

Modulated radiation from a tunable IR laser falls onto a prism at the condition of attenuated total reflection. Arising evanescent radiation can excite SEW on a metal surface at a suitable distance from the prism base. SEW propagates along the metal surface and can be attenuated by a thin dielectric film deposited on this metal. By means of a similar prism placed at a certain distance from the first one the SEW is transformed into normal radiation and detected by a pyroelectric detector.

#### 13.4.40.3 Performance Criteria

The SEW excitation efficiency is affected by both the angle of incidence in the prism and the gap height, the last being different for the coupler and decoupler prism. The size of the gap depends on the metal and the conditions of its evaporation. An absorption spectrum is obtained by a differential method in which the ratio of intensities is measured for a SEW on the metal surface with a film and without a film at various distances between the prisms.

#### 13.4.40.4 Applications

Very thin films of organic and inorganic substances on metal surfaces can be measured down to monolayers.

#### 13.4.41

### Spin Polarised Electron Energy Loss Spectroscopy [53, 54]

*Acronyms:* SPEELS: spin polarised electron energy loss spectroscopy.

#### 13.4.41.1 Introduction

A polarised electron beam is made to strike a surface using an electron gun with a spin polarised electron source. The electrons reflected from the surface are energy analysed and then their spin polarisation is determined. This provides information regarding spin dependent scattering within the sample.

Range of operation: Primary beam energy from 10 to 1000 eV.

#### 13.4.41.2 Instrumentation

Electrons from a polarised primary electron beam are directed on to a surface and the spin state of the electrons that are reflected from the surface is determined. Typically, a polarised electron source consists of a GaAs crystal upon which polarised light is projected. The emerging photoelectrons from the GaAs crystal have up to 50 % polarisation. The electrons that are detected are first passed through an electron energy analyser and then through a Mott detector to determine the spin state of the electrons.

#### 13.4.41.3 Sample

Conducting samples with interesting magnetic properties are usually studied.

#### 13.4.41.4 Analytical Information

Information regarding magnetic coupling and exchange-excitation processes can be determined. If the polarisation of the spin of the electron has changed between entering the sample in the primary beam and the detected scattered electron, then a ‘spin-flip’ exchange process must have occurred. This can reveal information on exchange processes occurring within the material.

#### 13.4.41.5 Performance Criteria

Primary polarisation 20–25 %.

Emission current 10–20 µA.

Target current 100–500 nA.

Primary energy 10–1000 eV.

Energy resolution 0.25 eV.

Scattering angle 90°.

The Mott detector for determining the spin state of electrons has a very low efficiency, which results in long collection times for SPEELS spectra.

#### 13.4.41.6 Applications

SPEELS is used for pure research into magnetic materials such as transition metal oxides.

#### 13.4.41.7 Other Techniques

Spin polarised ultraviolet photoelectron spectroscopy (SPUPS) can also reveal information about the electron polarisation of magnetic samples.

#### 13.4.42

#### Spin Polarised Ultraviolet Photoelectron Spectroscopy [54, 55]

**Acronyms:** SPUPS: spin polarised ultraviolet photoelectron spectroscopy, SPXPS: spin polarised X-ray photoelectron spectroscopy.

##### 13.4.42.1 Introduction

Magnetic samples are exposed to ultraviolet radiation and the energies and spin orientation of the emitted photoelectrons are measured to reveal information about the spin resolved valence band electronic structure of the material. Range of operation typically 10–200 eV. This technique is similar to ultraviolet photoelectron spectroscopy but SPUPS is also sensitive to the polarisation of the electrons as well as their energy.

##### 13.4.42.2 Instrumentation

The measurement is carried out in an UHV chamber. Monochromatic ultraviolet photons from a synchrotron source are shone at a magnetised sample to eject photoelectrons. The emitted electrons are collected by an electron energy analyser such as a hemispherical mirror analyser (HMA) to determine their energy. They then pass through this analyser to a Mott detector where they are accelerated up to 20,000–100,000 V before colliding with a gold foil. The electrons scatter off the foil and are detected by pairs of channeltrons arranged along perpendicular axes. The direction in which a given electron is scattered is partially dependent upon its spin orientation (an effect known as Mott Scattering); hence the combination of energy and spin data provided by the HMA and the Mott detector can be used to construct separate ultraviolet photoelectron spectroscopy (UPS) spectra for the “spin up” and “spin down” electrons. These spectra are representative of, although not identical to, the sample’s spin resolved valence band electronic density of states.

#### 13.4.42.3 Sample

Magnetic UHV compatible materials.

#### 13.4.42.4 Analytical Information

Spin resolved valence band and shallow core level electronic structure of the top few atomic layers.

#### 13.4.42.5 Performance Criteria

The Mott scattering process is extremely inefficient resulting in count rates for SPUPS that are 4–5 orders of magnitude less than in equivalent UPS spectra. The low count-rate means that the technique is generally restricted to use with extremely intense photon sources such as synchrotrons and also generally results in lower resolutions than are achievable in conventional UPS. The spatial resolution is normally of the order of 100 µm and the energy resolution is normally of the order of 0.1 eV.

Typically contents of a few atomic percent at the surface can be detected, depending strongly on the cross-section of the particular elements present. Sensitivity decreases rapidly with depth below the surface and is often negligible below a depth of approximately five atomic layers. Electron polarisations of a few percent can be measured.

Low count rates mean that acquiring a single spectrum can take an hour or more. High surface sensitivity makes the technique vulnerable to contamination, necessitating the use of UHV procedures. The low energy of the emitted electrons combined with the stated objectives of studying magnetic effects makes the technique very vulnerable to the presence of stray magnetic fields and so magnetic shielding is normally required. It is normally necessary to collect multiple spectra with the sample magnetised in alternate directions to properly determine the spin resolved band structure; hence the technique is normally restricted to samples with a strong remnant magnetisation that can be flipped by an electromagnet inside the chamber. Spectra can be strongly influenced by the particular crystal structure and by the quality of the sample's top few atomic layers, which may not be completely representative of the bulk material, making careful sample preparation and characterisation essential.

#### 13.4.42.6 Applications

SPUPS is used to probe the spin resolved electronic states near the Fermi level of magnetic materials. These states are responsible for determining a material's electronic and magnetic properties.

#### 13.4.43

### Sum-Frequency Generation Vibrational Spectroscopy [5, 56]

*Acronyms:* SFG: sum-frequency generation.

#### 13.4.43.1 Introduction

SFG is a second-order non-linear optical process in which two laser beams overlap in a medium and generate the sum-frequency. As a second order process it is allowed on surfaces or interfaces, where the inversion symmetry is broken. In a typical experiment, one beam of infrared and the other of visible wavelength are mixed allowing SFG vibrational spectroscopy.

#### 13.4.43.2 Instrumentation

A typical experimental set-up consists of a pulse Nd:YAG laser which is used to pump an optical parametric/difference frequency generation system to produce tunable infrared radiation with a wavelength up to 9  $\mu\text{m}$ . The infrared beam is then overlapped with a frequency-doubled output beam from the laser (532 nm) at the sample surface. A photo-multiplier is used for detection. Sum frequency vibrational spectra are generated by scanning the IR frequencies through the energy range of vibrational excitations.

#### 13.4.43.3 Analytical Information

Information about molecular orientation and conformation at a surface, and sometimes even surface structure, is gained from the dependence of the SFG signal on wavenumber.

#### 13.4.43.4 Performance Criteria

Typically, a spot of several hundred micrometers of the sample is irradiated by the infrared and visible pulse energies at 100  $\mu\text{J}$  and 1 mJ, respectively. A gain of about 100 photons  $\text{pulse}^{-1}$  is observed, but the maximum signal one can get is limited only by the local maximum input intensity that the interface can tolerate without damage.

The strength of the resonant SFG response depends upon several factors: the surface density of the molecule of interest, the line width of the transition, the IR transition moment and the Raman transition strength. The last two factors restrict the technique to the study of vibrational modes, which are both infrared and Raman active.

Some of the disadvantages include low detected signal levels and difficulties in determining a quantitative relationship between the peak intensities and the number of sampled molecules.

#### 13.4.43.5 Applications

Although solid/solid interfaces can be studied, SFG represents a most powerful analytical tool for liquid interfaces. A wide range of systems has been studied including neat liquid/vapour, liquid mixture/vapour, neat liquid/solid, and neat liquid/liquid interfaces, and also surfactants at liquid/air, liquid/solid, and/or liquid/liquid interfaces, and electrochemistry at solid/liquid interfaces.

#### 13.4.43.6 Other Methods

Second harmonic generation (SHG) spectroscopy is based on the same principles (two photons of frequency  $\nu$  are converted to one photon of frequency  $2\nu$ ). SFG has appeared to be the more successful and versatile technique to date.

### 13.4.44

#### Surface Plasmon Resonance Spectroscopy [11, 57, 58]

*Acronyms:* SPR spectroscopy (surface plasmon resonance spectroscopy)

##### 13.4.44.1 Introduction

The surface resonance phenomenon in a thin metallic film is measured by attenuated total reflection as a function of either incident angle (using monochromatic light) or excitation wavelength (at a constant value of the incident angle).

Ranges of operation: from visible to infrared, typically visible.

##### 13.4.44.2 Instrumentation

A SPR spectrometer has the following four principal components: a source of radiation, an optical coupling element, a thin metallic film and a detector. Thin layers of SPR active metals are most often produced by vacuum evaporation or sputtering.

Two arrangements of ATR optical prism couplers are used: the Kretschmann-type arrangement with a metallic film deposited directly onto the coupling prism and the Otto-type arrangement with a metallic film separated from the coupling prism by air or other dielectric material of a thickness of about one wavelength of the radiation used in the experiments. The Kretschmann configuration is more convenient and is used in most applications.

SPR sensing platforms are combined with transducing layer(s) to enable the use of SPR for chemical sensing and biosensing.

##### 13.4.44.3 Analytical Information

SPR is a general spectroscopic method for sensing refractive index changes near the surface of a metal film. The dependence of reflectance on the incident angle or excitation wavelength is defined as a SPR spectrum. The corresponding curve

is characterized by position, width, and depth of the resonance dip in reflectance as a function of incident angle or wavelength. These features depend on the nature of the metal and thickness of its film. The position of the reflectivity minimum is the quantity that is most sensitive to the refractive index of the adjacent medium, and therefore it is usually used for the purpose of sensing. By fixing the wavelength or the angle of incidence at an appropriate constant value, the resonance can be positioned at any particular value of the incident angle or wavelength, respectively. The thickness, reflection and absorption indexes and optical parameters of the thin layer under study may be determined from SPR reflectivity spectra.

#### 13.4.44.4 Performance Criteria

Amplitude-based SPR sensing devices typically attain a refractive index resolution in the  $10^{-6}$ – $10^{-5}$  range. Angular and spectral interrogation-based systems provide even better resolution, allowing the measurement of refractive index changes as small as  $10^{-7}$ . This corresponds to a detection limit for an adsorbed protein layer of less than  $1 \text{ pg mm}^{-2}$ .

#### 13.4.44.5 Applications

SPR is used in sensors and biosensors, but this method can also be used for the study of adsorption or chemical reactions in thin films as well as for the study of molecular interactions, conformational changes etc.

### 13.4.45

#### Total Reflection X-ray Fluorescence Spectroscopy [5, 59]

*Acronyms:* TXRF or TRXRF: total reflection X-ray fluorescence.

##### 13.4.45.1 Introduction

An X-ray beam hits a flat sample at a highly grazing angle so that total external reflection occurs. As a result the X-rays only penetrate the top few atomic layers, where they cause X-ray fluorescence emission. Thus this technique combines high surface sensitivity with the high atomic sensitivity of the (otherwise normally bulk sensitive) fluorescence technique.

Typical energy range of incident radiation 1–20 keV.

##### 13.4.45.2 Instrumentation

A narrow beam of X-rays is directed at a flat sample at grazing incidence, typically less than 10 mrad, so that total external reflection of the X-rays occurs. As a result the X-rays only penetrate the top few atomic layers, where they excite X-ray fluorescence. The emitted photons are then detected with a Si(Li) detector. Fluorescence detection is extremely sensitive to very low content (1 part in  $10^8$  for transition

metals and 1 part in  $10^{10}$  for low atomic mass elements) but is normally a bulk sensitive technique; TXRF allows it to be used in a surface specific manner. TXRF is used particularly in semiconductor wafer processing for quantitative analysis of surface contamination present at very low concentrations. A map of contamination over the whole wafer can be obtained by rotating the sample in the beam.

UHV is not required and the technique can even be used to study liquids, however, the emphasis on detecting low levels of surface contamination means that either UHV or clean room conditions will normally be used. This technique may be used in conjunction with a high intensity synchrotron source or with the X-ray standing wave (XSW) technique to boost sensitivity still further.

#### 13.4.45.3 Sample

The sample need not be conducting but must be very flat due to the grazing incidence of the beam, and TXRF is often used on silicon wafers.

#### 13.4.45.4 Analytical Information

Quantitative element specific and surface specific measurement of extremely low atomic concentrations on flat surfaces.

#### 13.4.45.5 Performance Criteria

Angle of incidence is generally 1–10 mrad.

Energy range 1–20 keV.

Beam size is a few mm<sup>2</sup>.

Beam spot size on the sample is a few mm across perpendicular to the beam axis but the full width of the sample along the beam axis as the grazing incidence angle that is required spreads out the beam spot considerably. Thus by rotating the sample the whole area of a wafer can be mapped in a few minutes.

This technique is not restricted to UHV, and it can be used in atmosphere or in clean room conditions.

Increased sensitivity can be obtained by using a powerful synchrotron source or by using TXRF in conjunction with the X-ray standing wave (XSW) technique. When X-rays are incident on a material that contains distinct boundaries between different layers, standing waves of X-rays will form. The standing waves are used to obtain a depth profile of the fluorescence signal for different angles of incidence or exit. The acronyms GIXFR (grazing incidence X-ray fluorescence) and GIXFR (grazing-exit X-ray fluorescence) are used for these methods.

The spatial resolution of TXRF is generally only several mm.

The analysis area is several cm<sup>2</sup>.

Atomic contents of 1 part in  $10^8$  for transition metals or 1 part in  $10^{10}$  for low atomic mass elements are possible.

Depth sensitivity is 50 Å.

TXRF can detect all elements with atomic masses from sulfur to uranium.

#### 13.4.45.6 Applications

Non-destructive, non-UHV, measurement of very low concentrations of impurities on the surfaces of flat samples, particularly Si wafers.

#### 13.4.46

#### Transmission Spectroscopy [5]

*Acronyms:* no acronym used, but usually this method is denoted as absorption spectroscopy.

##### 13.4.46.1 Introduction

The ratio of the radiant power after and before the transmission of the electromagnetic radiation through the absorbing layer, i. e. transmittance, is measured.

Range of operation: mid- and far infrared.

##### 13.4.46.2 Instrumentation

Conventional dispersive or Fourier transform spectrometers are used. Transmission spectroscopy of surfaces employs the same basic experimental geometry as that used for bulk samples.

##### 13.4.46.3 Performance Criteria

The transparency of the substrate and the ability to compare the combined transmissivity of the substrate and its deposited surface layer with that of the substrate without this layer is crucial. A film thickness of the order of one micrometer is typical.

For characterization of surfaces or adsorbed molecules on fine powders a mixture of the sample with KBr powder pressed into a disk is used. The so-called scattered transmission method is based on the measurement of the transmittance of a very thin layer of pulverised material. This method takes advantage of the fact that, with increasing wavelength, the scattering media, which are composed of very small particles, become more transparent and it is possible to record good absorption spectra with scattered transmission, especially in the mid-infrared region. Disks are usually prepared by pressing the powdered sample into a wafer between 0.1 and 0.25 mm thick. Good results can be obtained for solids with a high surface area.

##### 13.4.46.4 Applications

Adsorption and heterogeneous catalysis have been studied by this method.

#### 13.4.47

### **Ultraviolet Photoelectron Spectroscopy [5, 6–8]**

**Acronyms:** UPES, UVPES, UPS, UVPS: ultraviolet photoelectron spectroscopy. The use of the term *photoemission spectroscopy* (PES) is discouraged.

#### 13.4.47.1 **Introduction**

Samples are exposed to monochromatic ultraviolet radiation (typically in the range 10–100 eV) and the energies of the emitted photoelectrons are measured to reveal information on the valence band electronic structure of the sample.

#### 13.4.47.2 **Instrumentation**

The measurement is carried out in an UHV chamber. Ultraviolet photons from a He lamp (21.2 or 40.8 eV) are shone at the sample to eject photoelectrons. The emitted electrons are collected by an electron energy analyser, such as a hemispherical mirror analyser, to produce a spectrum showing the number of electrons emitted with a given kinetic energy. Such spectra are representative of, although not identical to, the sample's valence band electronic density of states (DOS).

By using a synchrotron source instead of a He lamp to provide the ultraviolet photons a photon energy can be selected that preferentially favours emission from a particular element by exploiting variations in photoemission cross-section. The partial density of states contribution from each individual element can then be determined.

#### 13.4.47.3 **Sample**

Samples are normally metallic or semiconducting UHV compatible materials.

#### 13.4.47.4 **Analytical Information**

The valence band electronic structure of the top few atomic layers can be determined from the variation in photoelectron intensity as a function of electron kinetic energy and incident photon energy.

#### 13.4.47.5 **Performance Criteria**

Spatial and energy resolutions are strongly dependent on the particular type of electron energy analyser and photon source used. However the spatial resolution may be as good as 10 µm and the energy resolution may be as good as 5 meV.

Typically content of a few atomic percent at the surface can be detected, depending strongly on the cross-section of the particular elements present. Sensitivity decreases rapidly with depth below the surface and is often negligible below a depth of approximately five atomic layers.

High surface sensitivity makes the technique vulnerable to contamination, necessitating the use of UHV procedures. The low energy of the emitted electrons makes the technique vulnerable to the presence of stray magnetic fields and so magnetic shielding is normally required. The spectrum can be influenced by the particular crystal structure of the sample's top few atomic layers, which may not be completely representative of the bulk material. This technique is generally not suitable for insulating materials.

#### 13.4.47.6 Applications

UPS is used to probe the electronic states near the Fermi level that are responsible for determining a material's electronic properties and to study the nature of the bonding between the atoms in the sample or between the sample and adsorbate molecules on its surface.

#### 13.4.47.7 Other Techniques

Measurement of the photoelectron intensity from single crystal samples as a function of both their kinetic energy and emission angle allows the total momentum of the photoelectrons to be determined, enabling "band-maps" of the electronic density of states of the material to be produced. See angle resolved ultraviolet photo-electron spectroscopy (ARUPS).

By combining the electron energy analyser with a polarization sensitive Mott Detector separate spin-up and spin-down valence band density of states spectra can be produced for magnetic samples. This technique is known as spin polarised ultra-violet photoelectron spectroscopy (SPUPS).

### 13.4.48

#### X-ray Absorption Fine Structure [8]

**Acronyms:** XAFS: X-ray absorption fine structure, EXAFS: extended X-ray absorption fine structure, XANES: X-ray absorption near edge spectroscopy, (XAFS includes both EXAFS and XANES).

##### 13.4.48.1 Introduction

A monochromatic X-ray beam is directed onto a sample. The wavelength of the beam is ramped through an absorption edge of an element, which is a constituent of the sample, whilst the extent of the X-ray absorption is measured to produce an absorption spectrum. As a monochromatic beam of X-rays at various wavelengths is needed, synchrotron radiation is used as the X-ray source for XAFS.

For XANES, a narrow energy range ( $< 50$  eV) close to the absorption edge is studied. However, for extended X-ray absorption spectroscopy (EXAFS) the spectrum is acquired at energies much further from the absorption edge. Information

regarding the local structure around the atom whose absorption edge is acquired can be obtained.

Range of operation: Incident photon energies in the range from 1 to 20 keV.

#### 13.4.48.2 Instrumentation

A synchrotron radiation source is required. Normally, EXAFS and XANES are bulk sensitive techniques. However, by measuring the total electron current emitted from the sample, both methods can be made relatively surface sensitive. The detection of the electron current is called total electron yield (TEY). The sample is normally placed inside a “cell” containing noble gas atoms (Ar and He). These gases prevent the electrons from combining with atoms in the air, which might otherwise affect the acquisition of the data. The intensity of the incident synchrotron radiation may vary and so its flux is continuously measured by passing the light through another cell prior to striking the sample. The ratio of the TEY to the incident flux provides the spectral data.

#### 13.4.48.3 Analytical Information

EXAFS spectra provide information regarding the local environment surrounding the atom whose absorption edge is being studied. The specific local information includes the atom type of neighbouring atomic shells, the distance of those shells from the central (absorbing) atom and the static or dynamic disorder. The latter is given by the Debye–Waller value.

XANES spectra provide local structure information and the oxidation state. In the XANES region, electrons that are excited from the core level (usually the K level) jump into unfilled bound states, nearly bound states (resonances) or continuum states. Due to multiple electron scattering, XANES spectra are harder to interpret than EXAFS spectra.

#### 13.4.48.4 Performance Criteria

The sample should be able to withstand the intense X-ray beam from the synchrotron. For the TEY technique, the sample should be conducting. XAFS study of low atomic number elements  $Z < 11$  provides less information. It can be difficult to distinguish elements in the shells surrounding the central atom if they are close in atomic number. It can be difficult to distinguish static from dynamic disorder.

#### 13.4.48.5 Applications

EXAFS is used in many applications where local state information is required such as materials analysis, protein crystallography, or the structure of liquids and amorphous materials. XANES can also be used to determine the oxidation state of an element in a sample.

#### 13.4.48.6 Other Techniques

Surface EXAFS (SEXAFS) uses Auger or photo-electrons to detect the EXAFS signal. This ensures that this technique has a much higher surface sensitivity than EXAFS acquired using the total electron yield method. SEXAFS requires ultra-high vacuum and the detection instrumentation normally associated with Auger electron spectroscopy (AES) or X-ray photoelectron spectroscopy (XPS) techniques.

#### 13.4.49

#### X-ray Photoelectron Diffraction [60–66]

*Acronyms:* XPD (X-ray photoelectron diffraction)

PED or PhD (photoelectron diffraction)

PH or PEH (photoelectron holography)

##### 13.4.49.1 Introduction

Crystalline samples are exposed to monochromatic X-ray radiation resulting in the ejection of energetic photoelectrons from core levels. These electrons are diffracted as they pass through the crystal lattice producing a pattern of varying photoemission intensity as a function of azimuthal and polar emission angle that reveals element specific crystallographic information about the near surface region.

Range of operation of incident radiation typically 1000–2000 eV.

##### 13.4.49.2 Instrumentation

Experiment is carried out in an UHV chamber. Monochromatic X-ray photons, typically from Al-K<sub>α</sub> (1486.6 eV) or Mg-K<sub>α</sub> (1253.6 eV) radiation are shone at a crystalline sample to eject photoelectrons from core levels. The emitted electrons undergo diffraction and interference as they pass through the crystal lattice and are collected by an electron energy analyser such a hemispherical mirror analyser (HMA) that has fine angular and energy discrimination capability. The angular distribution of electrons from a given core level is determined by varying the azimuthal and polar angle of the sample to produce a map of the photoelectron intensity as a function of emission angle for a given core level. This diffraction pattern is element specific and is influenced by the neighbouring atoms and so it provides extensive information about the crystallographic structure of the near surface region that is complementary to that obtained in low energy electron diffraction (LEED) or scanning tunneling microscopy (STM). The diffraction pattern can also be thought of as a photoelectron hologram of the surface atomic structure of the sample, hence the alternate name of photoelectron holography (PH or PEH).

By using a synchrotron source to provide the X-rays the diffraction pattern for a particular core level can be studied as a function of electron kinetic energy instead of angle; which has the advantage of keeping the experimental geometry constant to remove effects such as changing depth sensitivity at different emission angles, as well as providing additional crystallographic information.

#### 13.4.49.3 Sample

The sample must be a single crystal semiconductor or metal and its surface should be smooth and flat so that the electron emission angle can be accurately determined. High surface sensitivity makes the technique vulnerable to contamination, necessitating the use of UHV procedures. However this surface sensitivity combined with the element specific crystallographic information that XPD provides makes the technique ideal for studying the structure of adsorbed molecular layers on single crystal substrates.

#### 13.4.49.4 Analytical Information

Element specific crystallographic information about the near surface region.

#### 13.4.49.5 Performance Criteria

Angular and energy resolutions are strongly dependent on the particular type of electron energy analyser and photon source used. However, energy resolution may be as good as 0.1 eV and angular resolution as good as 10 mrad. The high energy resolution achievable with XPD means that it is sensitive enough to detect the small chemical shifts in the kinetic energy of the photoelectrons that result from variations in the chemical environment of a particular element. Hence crystallographic data can be acquired using XPD that is not just element specific but chemical state specific too.

Typically content of a few percent at the surface can be detected, depending strongly on the photoemission cross-section of the particular elements present. Sensitivity decreases rapidly with depth below the surface and is often negligible below a depth of approximately 5–10 nm, depending on electron energy. All elements can be detected directly with the exception of hydrogen and helium.

The composition of the surface as probed by XPD may not be completely representative of the bulk material due to surface segregation or relaxation of the lattice. However the surface specific crystallographic information provided by XPD means that it is a particularly useful technique for studying such surface reconstructions.

#### 13.4.49.6 Applications

XPD is used to probe the element specific, or chemical state specific, crystallographic structure and near neighbour atomic arrangement of atoms in the near surface region of a crystalline material or of adsorbate molecules on its surface.

#### 13.4.50

#### X-ray Photoelectron Spectroscopy [5, 6, 8, 12, 13]

*Acronyms:* XPS or XPES: X-ray photoelectron spectroscopy, ESCA: electron spectroscopy for chemical applications (originally analysis), PESIS: photoelectron spectroscopy of inner shell, ARXPS: angle resolved X-ray photoelectron spectroscopy,

SRPES: synchrotron radiation photoelectron spectroscopy. For photon energies less than 300 eV also SXPS: soft X-ray photoelectron spectroscopy.

#### 13.4.50.1 Introduction

Samples are exposed to monochromatic X-ray radiation (typically with an energy range of 1–2 keV but energies up to 10 keV may be used) and the characteristic energies of the emitted photoelectrons are measured to reveal information about the elemental composition, elemental distribution, and chemical bonding characteristics of the near surface region.

#### 13.4.50.2 Instrumentation

The measurement is carried out in an UHV chamber. Monochromatic X-ray photons, typically from an Al-K<sub>α</sub> (1486.6 eV) or Mg-K<sub>α</sub> (1253.6 eV) X-ray source, are shone at the sample to eject photoelectrons. These electrons have energies ranging from 0 eV up to almost the same energy as the incident photons but most are emitted at a few discrete energies that are characteristic of the elements present in the sample. The photoelectrons are collected by an electron energy analyser such as a hemispherical mirror analyser (HMA) to produce a spectrum of the number of electrons vs. their kinetic energy. Analysis of this spectrum provides quantitative information about the composition of the near surface region of the sample.

Although XPS generally only reveals information about a particular point on the sample surface that is typically 100 μm to 1 mm across, a number of different approaches can be used to generate image maps of the elemental distribution over a wider area. By using a microfocused X-ray source images with a resolution of some 10 μm may be obtained by scanning the sample under the beam or scanning the beam across the sample surface. Alternatively images may be produced by scanning the area of analyser sensitivity across the surface using electrostatic electron deflector plates. This method is more straightforward and cheaper to implement but has significantly poorer resolution (100 μm). Many modern electron energy analysers have imaging optics and detectors, which collect XPS spectra from many discrete points simultaneously to produce an image of elemental distribution. This method produces the highest resolution spatial images with a resolution of better than 10 μm.

Tilting the sample so that the analyser collects electrons that are emitted at a more grazing angle increases the surface sensitivity of the technique. By acquiring spectra at several different angles, which have different surface sensitivities, quantitative information about the depth distribution of the elements in the top few nanometers of the sample can be extracted, this is known as angle resolved XPS (ARXPS).

The energy resolution of XPS may be as good as 0.2 eV, which is sensitive enough to detect the small chemical shifts in the kinetic energy of the photoelectrons that result from variations in the chemical environment of a particular element. By analysing the shape of an XPS peak the relative contribution from different chem-

ical states can be determined, revealing important information about the sample chemistry and atomic bonding.

By using a synchrotron source to provide the X-rays a photon energy can be selected that preferentially enhances emission from a particular peak by exploiting variations in photoemission cross-section as a function of photon energy to increase sensitivity to the given element.

#### 13.4.50.3 Sample

Samples are generally metallic or semiconducting UHV compatible materials. However insulating samples such as polymers can also be studied if a low energy “flood gun” electron source is used to supply electrons to the surface of the sample, replacing those ejected by photoemission and preventing net sample charging that would otherwise distort the position and shape of the XPS peaks.

#### 13.4.50.4 Analytical Information

XPS reveals quantitative information about the elemental composition of the top 10 nm or so of the sample (Fig. 13.8). Using higher energy X-rays from a source such as a Ti-K $\alpha$  (2040 eV) gun, or a high energy synchrotron, can increase the kinetic energy of the photoelectrons and hence the analysis depth.

Images of the elemental distribution across a wider area of the sample surface can be obtained either by using an imaging electron energy analyser or by scanning the position of the sample, the X-ray beam, or the analysis spot.

Quantitative elemental depth profiles can be obtained by collecting XPS spectra at different emission angles, which have differing depth sensitivities, and analysing

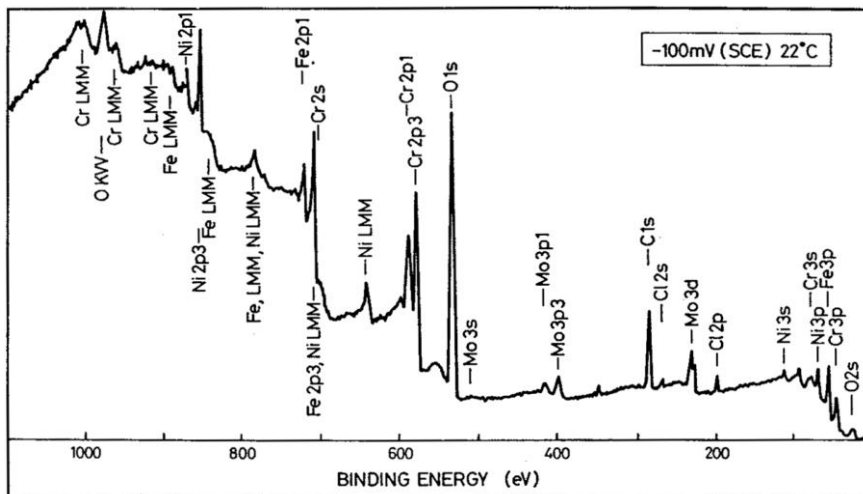


**Fig. 13.8** XPS survey spectrum recorded after polarisation of the steel 20Cr18Ni6.1Mo0.2N to  $-100$  mV (SCE) at  $22^\circ\text{C}$  in  $0.1$  M HCl +  $0.4$  M NaCl (reproduced from [5] with permission).

the resulting changes in the peak intensities from the different elements in the sample (angle resolved XPS).

Small chemical shifts in the XPS peaks can be used to discriminate between contributions coming from the different chemical states of a particular element. This reveals important quantitative information about the nature of the chemical and bonding environment for each element in the sample. This is particularly important in the study of polymers where the material's properties are determined by small changes in the bonding of the carbon atoms.

#### 13.4.50.5 Performance Criteria

Spatial and energy resolutions are strongly dependent on the particular type of electron energy analyser and X-ray source used. However spatial resolution may be as good as 10 µm, depth resolution may be as good as 0.2 nm and the energy resolution may be as good as 0.2 eV.

Typically content of one percent or less at the surface can be detected, depending strongly on the photoemission cross-section of the particular elements present. Using various corrections to the signal intensities the accuracy of the surface concentration measurement can be as good as  $\pm 10\%$ . Sensitivity decreases rapidly with depth below the surface and is often negligible below a depth of approximately 5–10 nm, depending on electron energy. All elements can be detected directly with the exception of hydrogen and helium.

High surface sensitivity makes the technique vulnerable to contamination, necessitating the use of UHV procedures. Spectra taken on crystalline samples can be influenced by diffraction effects, which can lead to variations in the peak intensity at different emission angles (see X-ray photoelectron diffraction, XPD). The composition of the surface as probed by XPS may not be completely representative of the bulk material due to surface segregation, degradation or contamination.

Some samples such as polymers may be damaged by exposure to the intense X-ray beam.

An electron flood gun must be used to avoid charging distortions when studying insulators.

#### 13.4.50.6 Applications

XPS is one of the most widely used surface and materials analysis techniques in both academia and industry. Applications include semiconductor wafer defect analysis, identification of surface contamination in industrial processes, adhesion chemistry analysis, analysis of fracture or failure surfaces, and analysis of the strength and type of carbon bonding in polymers.

#### 13.4.50.7 Other Techniques

Auger electron spectroscopy, (AES), requires very similar equipment to XPS and the two techniques are frequently integrated into the same analytical system to provide complementary information about a sample.

Ultraviolet photoelectron spectroscopy (UPS) is a very similar technique to XPS that makes use of much lower energy photons to emphasise variations in the low energy valence band electronic structure.

X-ray photoelectron diffraction (XPD) is closely related to XPS but exploits the variations in XPS peak intensity that occur at different emission angles in crystalline samples to reveal element specific crystallographic information.

#### 13.4.51

#### X-ray Standing Wave [67–71]

*Acronyms:* XSW: X-ray standing wave, NIXSW: normal incidence X-ray standing wave.

##### 13.4.51.1 Introduction

When single crystal samples are exposed to a narrow beam of monochromatic X-rays the regular arrangement of the atoms leads to diffraction of these X-rays at certain critical angles, a condition known as Bragg reflection. The incoming and outgoing X-rays then interfere to form a standing wave that permeates the material and even extends beyond it. The resulting periodic spatial variations in the amplitude of the X-rays within the lattice means that the X-ray absorption signal from a given element becomes very sensitive to its relative position in that lattice. Thus XSW provides a sensitive, element-specific, probe of crystal structure or of the bonding site of an absorbed molecule on a surface. Energy range is typically 2–80 keV

##### 13.4.51.2 Instrumentation

A narrow beam of monochromatic X-ray photons from a synchrotron is shone onto a single crystal sample at an angle that satisfies the Bragg condition for that material in order to establish an X-ray standing wave throughout the sample. The X-ray absorption signal from the element of interest is then monitored by a technique such as Auger electron spectroscopy (AES), X-ray photoelectron spectroscopy (XPS) or X-ray fluorescence (XRF) as the relative position of the standing wave is gradually shifted through the lattice by changing the reflection angle or photon energy slightly. The relative position of the standing wave with respect to the crystal lattice can be calculated from theory for any given combination of angle and photon energy and so, by studying how the absorption signal of a particular element changes as the wave moves through the lattice, the position of that element's atoms within that lattice can be established precisely. As the standing wave extends some distance beyond the surface of the sample the technique is particularly useful

for studying the bonding of absorbed molecules. Although UHV conditions are not a requirement for XSW the emphasis on using XSW to study molecular absorption means that UHV is frequently used to avoid contamination problems. This technique normally requires a synchrotron X-ray source so that the standing wave conditions can be altered by changing the photon energy rather than the experimental geometry. Synchrotrons also have the additional advantages of producing a highly collimated X-ray beam that is extremely bright and so can be used for studying dilute systems.

#### 13.4.51.3 Sample

Single crystal materials, buried interfaces and adsorbates on single crystal surfaces.

#### 13.4.51.4 Analytical Information

Element specific and/or chemical species specific crystallographic and bonding information.

#### 13.4.51.5 Performance Criteria

When XPS is used to detect the element of interest in the XSW experiment the energy resolution may be as good as 0.2 eV and so XSW can be used to probe the bonding of a particular chemical species within the lattice or on the sample surface by making use of small chemical shifts in the XPS peaks. XSW is very good at distinguishing between adsorption occurring at slightly different sites within the lattice that would otherwise appear very similar in complementary techniques such as surface extended X-ray absorption fine structure (SEXAFS).

An X-ray beam with energy 2–5 keV is required, and energies may be as high as 80 keV for some applications.

Minimum spot size for the X-ray beam is generally 0.5–1 mm.

The requirement for highly collimated intense X-ray beams with variable photon energy often restricts the technique to use at synchrotron sources. Although for certain applications a laboratory X-ray source may be sufficient.

XSW has the advantage of not being inherently restricted to use in UHV conditions and it can be used to study buried interfaces.

The depth sensitivity of XSW is dependent on the technique used to detect the X-ray absorption. If AES or XPS is used then the technique is surface sensitive with negligible sensitivity below 5–10 atomic layers, whereas using fluorescence detection results in bulk sensitivity. Typically concentrations of a few atomic percent of a monolayer at the surface can be detected. The use of XPS for element detection can also make the XSW technique chemical species specific.

Very high angular resolution is required for this experiment as the width of the “rocking curve” of angles over which the standing wave condition is satisfied can be mere seconds of arc. Though it may be more than a degree in some configura-

tions where the beam hits the sample at close to normal incidence (normal incidence X-ray standing wave) NIXSW.

XSW was initially restricted to very high quality single crystals such as semiconductors due to its extreme sensitivity to the degree of crystal perfection, although the recent development of NIXSW techniques that have wider angular rocking curves, (and are hence less sensitive to crystal perfection), have now made it applicable to conventional single crystal metallic samples.

XSW does not give a direct measurement of the position of a given atom, rather it gives the atom's position relative to the bulk unit cell of the lattice. XSW of adsorbates yields poor results in systems where extensive reconstruction of the surface has occurred, as it cannot determine where adsorbate atoms are relative to this re-constructed surface, only relative to the unreconstructed bulk lattice.

The quality of XSW data is very sensitive to the angular spread and photon energy resolution of the X-ray beam, which normally makes it necessary to use a synchrotron source.

#### 13.4.51.6 Applications

Element specific crystallography of single crystals. Study of the site specific and/or chemical state specific bonding of adsorbates to single crystal surfaces. Structure of buried interfaces. Applications, where UHV specific techniques are not applicable.

### 13.5

#### Further Information

Information on some other techniques or acronyms, software for surface science studies, surface science databases, research centers and institutes, user groups and bulletin boards, academic research groups, teaching resources for surface science, conferences, commercial services and suppliers, sources of practical information, and also, a collection of links to lecture courses and tutorials covering a broad range of surface science can be found on web sites, e.g.:  
<http://www.uksa.org> and <http://www.chem.qmw.ac.uk/surfaces/>.

#### Acknowledgements

The authors would like to thank Graham Beamson, RUSTI, Daresbury Laboratory, Warrington, UK for the permission to use data from the Scienta X-ray Photoelectron Spectrometer and to Jiri Homola, Institute of Radioengineering and Electronics, Academy of Sciences of the Czech Republic and University of Washington, Department of Electrical Engineering, Seattle, USA, and to V. Hnatowicz, Nuclear Physics Institute, Academy of Sciences of the Czech Republic for cooperation on some parts of this chapter.

**13.6****Appendix: List of Acronyms Related to Surface Analysis**

(Reference to the sections 13.6.X of this chapter are given)

- (e, 2e) Spectroscopy, 10  
AEAPS Auger Electron Appearance Potential Spectroscopy, 2  
AEES Nuclear Auger Electron (Emission) Spectroscopy\*  
AES Auger electron spectroscopy, 5  
APECs Auger Photoelectron Coincidence Spectroscopy, 6  
APFIM Atom Probe Field Ion Microscopy, 3  
APS Appearance Potential Spectroscopy, 2  
ARAES Angle Resolved Auger Electron Spectroscopy, 5  
ARIPES, Angle Resolved Inverse Photoemission Spectroscopy, 20  
ARPES Angle Resolved Photoelectron Spectroscopy, 1  
ARPS. viz ARPES, 1  
ARUPS Angle Resolved Ultraviolet Photoemission Spectroscopy, 1, 20  
ARXPS Angle Resolved X-ray Photoelectron Spectroscopy, 50  
ATR attenuated total reflection, 4  
BIS, Bremsstrahlung Isochromat Spectroscopy, 20  
BLE Bombardment-induced Light Emission, 17  
BS Momentum-resolved Bremsstrahlung Spectroscopy\*  
BSE Back-Scattered Electron Imaging\*  
CMA Cylindrical Mirror Analyser  
CPAA Charge Particle Activation Analysis, 4  
DAPS Disappearance Potential Spectroscopy, 2  
DRIFTS, Diffuse-Reflectance (or Reflection) Infrared Fourier Transform Spectroscopy, 8  
DSPES Gamma-ray (or Dept-selective) Photoelectron Spectroscopy\*  
EAES Electron-excited Auger Electron Spectroscopy. viz AES, 5  
EAPFS Extended (Electron) Appearance Potential Fine Structure Analysis\*  
EDX Energy Dispersive X-ray Analysis, 11, 37  
EEAES Electron Excited Auger Electron Spectroscopy, 5  
EELFS Extended Electron Energy Loss Fine Structure, 15, 34  
EELS Electron Energy Loss Spectroscopy, 34  
ELS Energy Loss Spectroscopy. viz REELS, 18  
EMPA Electron Micro Probe Analysis. viz EPMA, 11  
EMS Electron Momentum Spectroscopy, 10  
EPMA Electron Probe Micro Analysis, 11, 37  
ERCS Elastic Recoil Coincidence Spectrometry, 9  
ERDA or ERD Elastic Recoil Detection (Analysis), 9  
ESCA Electron Spectroscopy for Chemical Applications (originally Analysis), 50  
ESD Electron Stimulated Desorption, 12  
ESDIAD Electron Stimulated Desorption Ion Angular Distributions, 13  
ETS Electron Transmission Spectroscopy\*

- EWCARDS Evanescent Wave Cavity Ring-down Spectroscopy, 16  
EXAFS Extended X-ray Absorption Fine Structure, 24, 34, 48  
EXELFS Extended Electron Energy Loss Fine Structure. viz EELFS, 15, 34  
FAB MS Fast-Atom Bombardment Mass Spectrometry, 39  
FIM Field Ion Microscopy, 22  
FIMS Field-Ion Mass Spectroscopy. viz APFIM, 3  
FMIR frustrated multiple internal reflections, 4  
GDMS Glow Discharge Mass Spectrometry, 17  
GDOES Glow Discharge Optical Emission Spectrometry, 17  
GIS Grazing Incidence Spectroscopy, 33  
HEIS High Energy Ion Scattering, 23  
HIAA High Energy Ion Activation Analysis, 7  
HMA Hemispherical Mirror Analyser  
HREELS or HEELS High Resolution Electron Energy Loss Spectroscopy, 18, 34  
IAA Ion Activation Analysis\*  
IBSCA Ion Beam Spectrochemical Analysis, 17  
IEAES Ion Excited Auger Electron Spectroscopy\*  
IETS Inelastic Electron Tunneling Spectroscopy, 19  
INS Inelastic Neutron Scattering\*  
INS Ion Neutralisation Spectroscopy, 21  
Ion Excited AES. viz AES, 5  
IPES. viz IPS, 20  
IPMA Ion Probe Microanalysis, 22  
IPS Inverse Photoelectron Spectroscopy, 20  
IRAS. viz IRRAS, 33  
IRRAS Infrared Reflection-Absorption Spectroscopy, 33  
IS Ionisation Spectroscopy\*  
ISS Ion Scattering Spectrometry, 36  
KRIPIES, k-Resolved Inverse Photoemission Spectroscopy, 20  
LAMMA Laser Microprobe Mass Analysis or Spectroscopy, 17  
LAMMS. viz LAMMA, 17  
LEED Low-Energy Electron Diffraction\*  
LEEM Low-energy Electron Microscopy\*  
LEIS Low-energy Ion Scattering Spectrometry, 23  
LMMS. viz LAMMA, 17  
MAES Metastable Atom Electron Spectroscopy, 28  
MCP Micro-Channel Plates  
MDS Metastable Desorption Spectroscopy\*  
MEIS Medium Energy Ion Scattering, 23  
MIES Metastable Impact Electron Spectroscopy, 28  
MIR Multiple Internal Reflection, 4  
NDP Neutron Depth Profiling, 25  
NEXAFS Near Edge X-ray Absorption Spectroscopy, 24  
NIXSW Normal Incidence X-ray Standing Wave, 51  
NRA Nuclear Reaction Analysis, 35

- PAES Positron Annihilation Auger Electron Spectroscopy, 31  
PAS Photoacoustic Spectroscopy, 29  
PED or PhD Photoelectron Diffraction, 49  
PEELS Parallel Electron Energy Loss Spectroscopy, 18, 34  
PEEM Photoemission Electron Microscopy, 30  
PEH Photoelectron Holography, 49  
PESIS Photoelectron Spectroscopy of Inner Shell, 50  
PIES Penning Ionisation Electron Spectroscopy, 28  
PIGE Particle Induced Gamma Ray Emission, 26  
PIGME. viz PIGE, 26  
PIXE Particle Induced X-ray Emission, 27  
PMP Proton Microprobe, 22  
RAIS Reflection-Absorption Infrared Spectroscopy, 33  
RBS Rutherford Backscattering Spectrometry, 36  
REELS Reflection Electron Energy Loss Spectroscopy, 18, 34  
REM Reflection Electron Microscopy\*  
RHEED Reflection High-Energy Electron Diffraction\*  
RNRA, Resonant Nuclear Reaction Analysis, 35  
RS Recoil Spectrometry. viz ERDA, 9  
SALI Surface Analysis by Laser Ionisation, 39  
SAM Scanning Auger Microscopy, 37  
SCANIIR Surface Composition by Analysis of Neutral and Ion Impact Radiation, 17  
SECSA Scanning Electron Spectroscopy for Chemical Analysis\*  
SEM Scanning Electron Microscopy, 37  
SEMPA Scanning Electron Microscopy with Polarisation Analysis, 37  
SERS Surface Enhanced Raman Scattering, 32  
SEW Surface Electromagnetic Waves Spectroscopy, 40  
SEXAFS Surface EXAFS, 49  
SEXAPS Soft X-ray Appearance Potential Spectroscopy\*  
SFG Sum-Frequency Generation, 43  
SHG Second Harmonic Generation (SHG) Spectroscopy, 43  
SIMP Scanning Ion Microprobe, 22  
SIMS Secondary Ion Mass Spectrometry, 39  
SLEEM Scanning Low Energy Electron Loss Microscopy, 34  
SNMS Secondary Neutral Mass Spectrometry, 39  
SPAES Spin Polarized Auger Electron Spectroscopy, 5  
SPEELS Spin Polarised Electron Energy Loss Spectroscopy, 41  
SPI Surface Penning Ionisation, 28  
SPIES Surface Penning Ionisation Spectroscopy, 28  
SIPES, Spin Resolved Inverse Photoelectron Spectroscopy, 20  
SPMP Scanning Proton Microprobe, 22  
SPR Surface Plasmon Resonance Spectroscopy, 44  
SPUPS Spin Polarised Ultraviolet Photoelectron Spectroscopy, 42  
SPXPS Spin Polarised X-ray Photoelectron Spectroscopy, 42

- SRPES Synchrotron Radiation Photoelectron Spectroscopy, 50
- SRUPS Spin-Resolved Ultraviolet Photoemission Spectroscopy, 20
- STM Scanning Tunneling Microscopy, 38
- STS Scanning Tunneling Spectroscopy, 38
- SXAPS Soft X-ray Appearance Potential Spectroscopy, 2
- SXPS Soft X-ray Photoelectron Spectroscopy, 50
- TEELS Transmission Electron Energy Loss Spectroscopy, 18, 34
- TEM Transmission Electron Microscopy, 18
- THEED Transmission High-Energy Electron Diffraction\*
- TOF ERDA Time-of-Flight Elastic Recoil Detection Analysis, 9
- TOF-NDP Time-of-Flight Neutron Depth Profiling, 25
- TPD Thermal Desorption Spectroscopy\*
- TPRS Temperature Programmed Reaction Spectroscopy\*
- UHV ultra high vacuum
- UPS Ultraviolet Photoelectron Spectroscopy, 20, 47
- UVPES. viz UPS, 47
- UVPS. viz UPS, 47
- XAFS X-ray Absorption Fine Structure, 48
- XANES X-ray Absorption Near Edge Spectroscopy, 48
- XAPS X-ray Appearance Potential Spectroscopy, 2
- XEAES X-ray Excited Auger Electron Spectroscopy, 5
- XEAPS X-ray Excited Electron Appearance Potential Spectroscopy\*
- XPD Photoelectron Diffraction, 49
- XPES. viz XPS, 50
- XPS X-ray Photoelectron Spectroscopy, 50
- XRF X-ray Induced Fluorescence, 27
- XSW X-ray Standing Wave, 51

Usage of acronyms is very typical for surface analysis methods. Synonyms or different acronyms are used often for very subtle clones of the techniques so this list cannot be regarded as complete. A system for generation of acronyms for the names of the individual techniques is given by IUPAC recommendation [2]. Techniques marked with an asterisk are not discussed in detail in this chapter.

## References

- 1 Kellner, R., Mermel, J.-M., Otto, M. et al., *Analytical Chemistry*, Wiley-VCH, Weinheim 1998.
- 2 *IUPAC Compendium of Analytical Nomenclature, Definitive Rules 1997*, Blackwell Science, Oxford 1998.
- 3 Attard, G., Barnes, C., *Surfaces*, Oxford Science Publications, Oxford 1998.
- 4 Nix, R., *An Introduction to Surface Chemistry*, <http://www.chem.qmw.ac.uk/surfaces/scc/>.
- 5 Brune, D., Hellborg, R., Whitlow, H. et al., *Surface Analysis*, Wiley-VCH, Weinheim 1997.
- 6 Prutton, M., *Surface Physics*, Oxford University Press, Oxford 1984.
- 7 Zangwill, A., *Physics at Surfaces*, Cambridge University Press, Cambridge 1990.
- 8 Woodruff, D. P., Delchar, T. A., *Modern Techniques of Surface Science*, Cambridge University Press, Cambridge 1994.
- 9 Urban, M. W., *Attenuated Total Reflectance Spectroscopy of Polymers*, American Chemical Society, Washington 1996.
- 10 Schrader, B., *Infrared and Raman Spectroscopy*, VCH, Weinheim 1995.
- 11 Volka, K., Homola, J., Gauglitz, G. et al., *Critical Assessment of Spectrochemical Procedures for Surface/Interface Analysis-XXVI. Molecular Analysis Using Measurement of Attenuation of Electromagnetic Radiation (540/27/98)*, IUPAC, Analytical Chemical Division, Commission on Spectrochemical and other Optical Procedures for Analysis, in preparation.
- 12 Walls, J. M., *Methods of Surface Analysis, Techniques and Applications*, Cambridge University Press, Cambridge 1990.
- 13 *Practical Surface Analysis, Vol. 1, Auger and X-ray Photoelectron Spectroscopy*, eds. Briggs D., Seah M. P. Wiley, Chichester 1990.
- 14 Jensen, E., Bartynski, R. A., Hulbert, S. L. et al., *Rev. Sci. Instrum.*, **1992**, *63*, 3013–3026.
- 15 Bartynski, R. A., Jensen, E., Hulbert, S. L. et al., *Progr. Surf. Sci.*, **1996**, *53*, 155–162.
- 16 Arena, D. A., Bartynski, R. A., Hulbert, S. L., *Rev. Sci. Instrum.*, **2000**, *71*, 1781–1787.
- 17 Fink, D., Biersack, J. P., Stumpff, Chr. et al., *Nucl. Instrum. Methods, Sect. B*, **1986**, *15*, 740–743.
- 18 <http://www.rspheysse.anu.edu.au/ampl/research/ems/index.html>.
- 19 Ayyam, R. M. A., Bashara, N. M., *Ellipsometry and Polarized Light*, North-Holland, Amsterdam 1977.
- 20 Pipino, A., Hudgens, J. W., Huie, R. E., *Chem. Phys. Lett.*, **1997**, *280*, 104.
- 21 Pipino, A., Hudgens, J. W., Huie, R. E., *Rev. Sci. Instrum.*, **1997**, *68*, 2978.
- 22 Payling, R., *Mater. Forum*, **1994**, *18*, 195–213.
- 23 Ohashi, Y., Yamamoto, Y., Tsuivoyama, K. et al., *Surf. Interface Anal.*, **1979**, *1*, 53–57.
- 24 Knudson, A. R., Nagel, D. J., Comas, J. et al., *Nucl. Instrum. Methods*, **1978**, *149*, 507–10.
- 25 Lewis, D. M., Spencer, J. E. D., Fiels, B. O., *Spectrochim. Acta, Part A*, **1988**, *44*, 247–261.
- 26 [http://www.wsu.edu/~hipps/pdf\\_files/ietsrev.pdf](http://www.wsu.edu/~hipps/pdf_files/ietsrev.pdf).
- 27 Smith, N. V., *Rep. Progr. Phys.*, **1988**, *51*, 1227–1294.
- 28 <http://www.phys.ntnu.no/~sraen/dif4903/elspec.pdf>.

- 29** <http://rses.anu.edu.au/rses/Probe SHRIMP.html>.
- 30** Werner, H. W., Garten, R. P. H., *Rep. Prog. Phys.*, **1984**, *47*, 221–344.
- 31** *Ion Beams for Materials Analysis*, eds. Bird, J. R., Williams J. S., Academic Press, Australia, 1989.
- 32** <http://www.ncnr.nist.gov/instruments/cndp/>.
- 33** <http://www.osp.cornell.edu/vpr/ward/NDP.html>.
- 34** Downing, R. G., Lamaze, G. P., Langland, J. K et al., *NIST J. Res.*, **1993**, *98*, 109.
- 35** Bird, J. R., *Nucl. Instrum. Methods, Sect. B*, **1990**, *45*, 516–518.
- 36** Borderie, B., Barrandon, J. N., Delanay, B. et al., *Nucl. Instrum. Methods*, **1979**, *163*, 441–451
- 37** *Handbook of Modern Ion Beam Materials Analysis*, eds. Tesmer, J. R., Nastasi, M., Material Research Society, Pittsburgh, 1995.
- 38** Cahill, T. A. , *Annu. Rev. Nucl. Part. Sci.*, **1980**, *30*, 211–252.
- 39** Bosch F., ElGoresy, A., Herth, W. et al., *Nucl. Sci. Appl.*, **1980**, *1*, 1.
- 40** Rosencwaig, A., *Photoacoustics and Photoacoustic Spectroscopy*, Wiley, New York, 1980.
- 41** Swiech, W., Fecher, G. H., Ziethen, C. et al., *J. Electron. Spectrosc. Relat. Phenom.*, **1997**, *84*, 171–188.
- 42** Anders, S., Padmore, H. A., Duarte, R. M. et al., *Rev. Sci. Instrum.* **1999**, *70*, 3973–3981.
- 43** <http://www.src.wisc.edu/mephisto/default.htm>.
- 44** <http://xraysweb.lbl.gov/peem2/PEEM2-02.html>.
- 45** Lei, C., Mehl, D., Koymen, A. R., Gotwald, F. et al., *Rev. Sci. Instrum.*, **1989**, *60*, 3656–3660.
- 46** Jensen, K. O., Weiss, A., *Phys. Rev. B*, **1990**, *41*, 3928–3936.
- 47** Yang, S., Zhou, H. Q., Jung, E. et al., *Rev. Sci. Instrum.*, **1997**, *68*, 3893–3897.
- 48** <http://www.uta.edu/physics/research/weiss/paes-mech.html>.
- 49** Ziegler, J. F., Biersack, J. P., Littmark, U., *The Stopping and Ranges of Ions in Solids*, Pergamon Press, New York 1985.
- 50** *Scanning Probe Microscopy: Analytical Methods (Nanoscience and Technology)*, ed. R. Wiesendanger, Springer, Heidelberg 1998.
- 51** *Practical Surface Analysis*, Vol. 2, Ion and Neutral Spectroscopy, eds. Briggs D., M. P. Seah M. P., Wiley, Chichester, 1992.
- 52** Agranovich, V. M., Mills, D. L., *Surface Polaritons*, North-Holland, Amsterdam, 1982.
- 53** <http://www.anphy.uni-duesseldorf.de/els/els.htm>.
- 54** Kessler, J., *Polarized Electrons*, Springer-Verlag, Berlin 1985.
- 55** Johnson, P. D., *Rep. Progr. Phys.*, **1997**, *60*, 1217–1304.
- 56** <http://srs.dl.ac.uk/XUV-VUV/pes.html>.
- 57** Miranda, P. B., Shen, Y. R., *J. Phys. Chem. B*, **1999**, *103*, 3292–3307.
- 58** Kambhampati, D. V., Knoll, W., *Curr. Opin. Colloid Interface Sci.*, **1999**, *4*, 273–280.
- 59** Frutos, A. G., Corn, R. M., *Anal. Chem.* **1998**, *44*A.
- 60** Egelhoff, Jr., W. F., *Phys. Rev. B*, **1984**, *30*, 1052–1055.
- 61** Woodruff, D. P., Bradshaw A. M., *Rep. Progr. Phys.* **1994**, *57*, 1029–1080.
- 62** Fadley, C. S., Chen, Y.; Couch, R. E. et al., *Progr. Surf. Sci.*, **1997**, *54*, 341–386.
- 63** Fadley, C. S., van Hove, M. A., Hussain, Z. et al., *Surf. Rev. Lett.*, **1997**, *4*, 421–440.
- 64** <http://electron.lbl.gov/ped/ped.html>.
- 65** <http://www.phys.warwick.ac.uk/~sppw/phd.html>.
- 66** <http://w3.rz-berlin.mpg.de/mp/SurfaceStructure/PhotoelectronDiffraction.html>.
- 67** Stoev, K. N., Sakurai, K., *Spectrochim. Acta, Part B*, **1999**, *54*, 41–82.
- 68** Bedzyk, M. J., Materlik, G., *Phys. Rev. B*, **1985**, *31*, 4110.
- 69** Woodruff, D. P., Seymour, D. L., McConville, C. F. et al., *Phys. Rev. Lett.*, **1987**, *58*, 1460–1462.
- 70** Woodruff, D. P., Symour, D. L., McConville, C. F. et al., *Surf. Sci.*, **1988**, *195*, 237–254.
- 72** <http://www.phys.warwick.ac.uk/~sppw/nixsw.html>.
- 73** Griffiths, P. R., de Haseth, J. A., *Fourier Transform Infrared Spectrometry*, Wiley, New York, 1986.

## **Section VII**

### **Applications 1: Bioanalysis**

## 14

### Bioanalysis

Willem M. Albers, Arto Annila, Nicholas J. Goddard, Gabor Patonay, and Erkki Soini

#### 14.1

##### General Introduction

###### 14.1.1

###### Spectroscopy in the Biosensor and Genomics Age

Bioanalysis is presently in a new breakthrough stage, in which much recently developed technology and knowledge is revolutionising the way bioanalysis is practised. Microarray platforms have become commercially available during the last ten years and microfluidics and micro-electrophoresis systems will also be making their entry on the market very soon. Due to advances in microsystems in the 1990s (MST and MEMS), the realisation of complete systems for chemical analysis and synthesis within chips or within compact analysers is gradually becoming a reality. Such systems may be directly linked to or integrated into desktop or laptop computers (e.g. as a disk drive). It can thus be expected that within a few years the appearance of a bioanalytical laboratory will be very different. Large, costly facilities and hand labour will be largely replaced by miniaturised, autonomous, high-throughput analysis systems. It has been particularly the *Human Genome Project* that has accelerated the advances in this miniaturisation process, but the methods are now also crossing over to other bioanalysis areas.

The 1990s also witnessed the rapid commercialisation of biosensor technology. Although a large part of the biosensor literature lies in the field of electroanalysis, much work is concerned with new optical detection techniques, suitable for coverage in a handbook dedicated to spectroscopy. Advances in quite a number of science disciplines, most notably materials science, have contributed to the development of biosensors, but the major force was the successful marriage between electronics and biotechnology. Presently, there are many new programmes that modify and integrate biosensors, producing devices that have better sensitivity, specificity, stability and decreased manufacturing costs and are cast in array format, enabling fast "multidetection". Biosensors can play an important role in applications where rapid detection and continuous use are important. Presently, the ad-

vances in biosensors are quickly crossing over to (or merging with) other bioanalysis areas. It can be expected that during the first five years of the new millennium genomics and proteomics techniques will be effectively combined with biosensors and this will particularly revolutionise the practice of clinical diagnostics and drug discovery.

In many cases, however, novel technology is still rooted in conventional chemical analysis concepts, in which spectroscopy still holds a firm lead. In many cases the stages of protein analysis still comprise sample handling, separation, detection and (to an ever increasing degree) data processing and interpretation. For detection, spectroscopic techniques hold the advantage of rapidity, high information content and high sensitivity for quite a number of tasks to be performed in the multifarious bioanalysis field. The scope of the present chapter, therefore, lies predominantly in describing the basic methods and chemistry that are likely to preserve their significance also in the future analytical device technologies.

#### 14.1.2

#### **Genomics, Proteomics and Drug Discovery**

The field of *genomics* aims at characterising all the genes of an organism, starting from the DNA sequence to its structure and polymorphism. The most ambitious enterprise within genomics has been the Human Genome Project, which is dedicated to the sequencing of the 3 billion base pairs of the whole human genome. This endeavour required new, advanced tools for DNA replication, sequencing and analysis. Although the techniques for DNA analysis are still being further developed, the Human Genome Project actually ran 4 years ahead of schedule, when the first working draft of the human genome was completed in June 2000. Also the genomes of some other relevant organisms have been completely mapped. As a logical consequence of the results in genomics, the year 2000 witnessed the birth of the *proteomics* field [1]. The term 'proteomics' was coined in 1995 and refers to experimental tools for locating, isolating and characterising all proteins that are produced by a genome [2]. Both genomics and proteomics rely heavily on gel electrophoresis (GE), capillary electrophoresis (CE) and, more recently, capillary array electrophoresis (CAE) [3, 4].

The term 'functional genomics' is presently used for the elucidation of the function of genes (regulation, interactions and products) [5, 6]. Functional genomics relies on much the same methods as employed in proteomics. From a spectroscopic point of view the most interesting methods for detection of DNA involve fluorescence detection [7], particularly laser-induced fluorescence (LIF) in the visible and near-infrared (VIS/NIR) region (400–1100 nm). Apart from fluorescence detection for DNA, other spectroscopic methods have gained importance in genomics, particularly mass spectroscopy [8].

Presently, attention has also been moving to 'functional proteomics' in which specific functions of proteins are mapped. Functional proteomics is evolving fast and various novel tools have been developed for the study of protein–protein inter-

actions, quantification and comparisons of protein expression, and advanced protein function mapping [9]. Also annotated proteomic databases have been set up. All these advances will have a large impact on diagnostic and therapeutic product development and the identification of important biomarkers and novel drug targets. Functional proteomics and drug discovery are closely related fields. Drug discovery is mainly concerned with the screening of small organic compounds against a range of receptors relevant in disease control, but also involves the screening of peptides, either produced by organisms or by combinatorial chemistry methods. Completely new approaches for screening very large numbers of chemicals have been devised in the 1980s and 1990s [10].

#### 14.1.3

##### **Biosensor Technologies**

Biosensors are chemical sensors that utilise a biomolecule for the determination of an analyte by intimate coupling of the biomolecule to a suitable detection device (optical, electrochemical, piezoelectric, calorimetric) [11, 12]. Frequently, additional filters are used to provide some initial selection of analytes, to shield the sensing device from fouling and to protect the sensor as a whole from mechanical damage. An ideal biosensor should provide a real-time readout of the concentration of an analyte in its natural environment and follow the changes in concentrations reversibly. This ideal has been realised to date only for some types of catalytic sensors (based on enzymatic action). For many other types of devices, however, this is not yet realised, such as for biosensors that rely on affinity interactions, for which the term “single-use biosensor” or “dosimeter” is more appropriate. The minimum requirement for a device to be called a biosensor is that the device should provide a quick readout of the concentration without the need for adding reagents [13].

Biosensors comprise a rapidly growing technology field that continuously reshapes bioanalysis, particularly diagnostics and functional proteomics, but also various other chemical monitoring fields (environmental monitoring, drug discovery, process industry, food analysis). The first biosensor system was already commercialised in the early 1970s by Yellow Springs Instrument Co. (YSI) and was used for the determination of glucose in blood, urine and bioprocesses. In the 1980s relatively little commercial activity was yet observed, but new sensor types were developed at a rapid pace in many research laboratories. There were many successful demonstrations of biosensors based on electrochemical, optical, microcalorimetric and piezoelectric transducers. In the 1990s a number of new sensor technologies moved successfully from the research laboratory into the marketplace.

Advances in optical biosensors have contributed significantly to the speed of bioanalysis by supplying real-time monitoring of binding reactions, without the need for labelling of biomolecules (real-time BioInteraction Analysis or BIA). Some of the methods in biosensor technology are based on optical phenomena and can therefore be placed in a spectroscopic context (see Section 14.2.7). Optical biosensors have traditionally been used in a number of proteomics subfields, such

as antibody screening and epitope mapping, in which the dissociation and association rates and affinity constants can be directly determined.

*In vivo* monitoring, particularly of glucose for the care of diabetics, still receives much attention in R&D worldwide. This is not surprising, since home glucose monitoring forms the largest single-analyte market. This market is still expanding: a growth from \$2.6 billion in 1997 to an estimated \$5.9 billion in 2002 has been projected. Although various electrochemical sensors for *in vivo* monitoring have been developed, non-invasive monitoring by direct spectroscopic methods is still receiving attention. More than 20 firms and institutes have notified that they are working on such systems, and a few have released equipment for direct measurement of blood glucose, although these instruments are still bulky and expensive. The reliability of the glucose measurements is, however, still under critical evaluation.

#### 14.1.4

#### Biomolecular Structure Determination

The elucidation of three-dimensional biomolecular structure is still heavily dominated by X-ray crystallography, but for the analysis of biomolecular structure in aqueous solution NMR spectroscopy has become the method of choice, particularly when dynamic molecular information is also needed. Therefore, a rather large part of this chapter will be dedicated to biomolecular NMR, focussing on the analysis of proteins (see Section 14.3). Apart from the determination of primary and tertiary structure, the determination of the secondary structure of proteins is still important in bioanalysis. Secondary structure features (mainly  $\alpha$ -helix and  $\beta$ -sheet content) are still dominated by IR spectroscopy and circular dichroism techniques (see Section 14.2.8). Secondary structural features of proteins and conformational stability will probably grow in significance through the advent of diseases like transmissible spongiform encephalopathy (TSE), which are caused by conformational changes in Prion proteins. Furthermore, due to the increase in the production and use of chiral compounds in the pharmaceutical sector, the demand for analysis by circular dichroism has also seen a steady growth.

#### 14.1.5

#### Bioinformatics

Scientists become more and more dependent on extensive data banks to access structural information on proteins and nucleic acids. With the constant growth of these public databases, there has emerged a large need for robust analytical data handling software that is able to partly elucidate the significance of the data. For instance, geneticists use special software to analyse the hybridisation patterns obtained from DNA chips. Bioinformatics is the branch of science that enables scientists, researchers and physicians to manage large amounts of data via powerful computational tools, with which the large amounts of data can be classified and organised [14, 15]. The application areas of bioinformatics lie in drug de-

sign, gene research, and advanced medical procedures. Computational approaches have been applied to biology and medicine, databases and search tools, to genome and proteome analysis, and mapping of the human brain.

An important factor in the progress of bioinformatics has been the constant increase in computer speed and memory capacity of desktop computers and the increasing sophistication of data processing techniques. The computation power of common personal computers has increased within 12 years approximately 100-fold in processor speed, 250-fold in RAM memory space and 500-fold or more in hard disk space, while the price has nearly halved. This enables acquisition, transformation, visualisation and interpretation of large amounts of data at a fraction of the cost compared to 12 years ago. Presently, bioanalytical databases are also growing quickly in size and many databases are directly accessible via the Internet. One of the first chemical databases to be placed on the Internet was the Brookhaven protein data bank, which contains very valuable three-dimensional structural data of proteins. The primary resource for proteomics is the ExPASy (*Expert Protein Analysis System*) database, which is dedicated to the analysis of protein sequences and structures and contains a rapidly growing index of 2D-gel electrophoresis maps. Some primary biomolecular database resources compiled from spectroscopic data are given in Tab. 14.1.

## 14.2 Optical Spectroscopy in Bioanalysis

### 14.2.1 Introduction

Applications of optical spectroscopy have advanced rapidly in bioanalysis and can be considered as a primary tool for detection in DNA analysis and immunoassays as well as in medicinal and pharmaceutical analysis where rapid data acquisition, sensitivity and reproducibility are crucial. It is especially fluorescence spectroscopy that has flourished in bioanalysis, where a plethora of interesting approaches are competing in the scientific and commercial sector. Besides synthetic dyes, the intrinsic fluorescence of enzymes [16, 17] and fluorescent proteins (see Section 14.2.2.7) is increasingly used, because some of these biomolecules have highly optimised photochemical properties. The following paragraphs intend to give an overview of the most important trends and emerging techniques in optical bioanalysis methods, the emphasis being on the underlying synthetic and bioconjugation issues.

**Table 14.1** Overview of some major biomolecular databases on the internet.

<b>Database name</b>	<b>Site</b>	<b>Provider</b>	<b>Contents</b>	<b>Charge</b>
Map of the human genome	<a href="http://www.ncbi.nlm.nih.gov/genemap99/">http://www.ncbi.nlm.nih.gov/genemap99/</a>	National Center for Biotechnology Information (NCBI), a division of the National Library of Medicine (NLM) at the National Institutes of Health (NIH).	One of the starting links for retrieving human genome sequence data and data of other genomes.	Free access via the internet
Brookhaven Protein Data Bank	<a href="http://www.rcsb.org/pdb/">http://www.rcsb.org/pdb/</a>	Research Collaboratory for Structural Bioinformatics (RCSB), non-profit consortium, CA, USA	World-wide repository for the processing and distribution of 3-D biological macromolecular structure data, X-ray crystallographic and NMR data.	Freely downloadable structure files. Display of structures via free programs of other vendors (e.g. Chimera, Rasmol, WebLab Viewer)
Cambridge Crystallographic Database	<a href="http://www.ccdc.cam.ac.uk/index.html">http://www.ccdc.cam.ac.uk/index.html</a>	Cambridge Crystallographic Data Centre, Cambridge, UK	Computerised database containing comprehensive data for organic and metal-organic compounds studied by X-ray and neutron diffraction	Paid subscription on database and programs for search and display
ExPASy	<a href="http://www.expasy.ch/">http://www.expasy.ch/</a>	Swiss Institute of Bioinformatics (SIB), Geneva, Switzerland	Major proteomics database comprising interpreted 2DE gels of various organisms (Liver, plasma, HepG2, HepG2SP, RBC, lymphoma, CSF, macrophage-CL, ery-throleukemia-CL, platelet, yeast, E.coli, colorectal, kidney, muscle, macrophage-like-CL, Pancreatic Islets, Epididymus, dictyostelium).	Freely downloadable database and program for searching and displaying ( Melanie Viewer)
Argonne Protein Mapping Group	<a href="http://www.anl.gov/BIO/PMG/">http://www.anl.gov/BIO/PMG/</a>	Argonne National Laboratory, Center for Mechanistic Biology and Biotechnology, University of Chicago	2DE proteome database of Mouse liver, human breast cell lines, and Pyrococcus furiosus	Free access via the internet

Danish Centre for Human Genome Research	<a href="http://biobase.dk/cgi-bin/cells/">http://biobase.dk/cgi-bin/cells/</a>	Danish Centre for Human Genome Research, University of Aarhus	2DE proteome database of human (primary keratinocytes, epithelial, hematopoietic, mesenchymal, hematopoietic, tumors, urothelium, amnion fluid, serum, urine, protasomes, ribosomes, phosphorylations) and mouse (epithelial and new born) proteomes	Free access via the internet
HOMSTRAD (HOMologous STRucture Align-ment Database)	<a href="http://www.cryst.bioc.cam.ac.uk/~homstrad/">http://www.cryst.bioc.cam.ac.uk/~homstrad/</a>	Crystallography and Bioinformatics Department of Biochemistry University of Cambridge	HOMSTRAD is a derived database of structure-based alignments for homologous protein families. Known protein structure (from the PDB database) are clustered into homologous families (i.e., common ancestry), and the sequences of representative members of each family can be aligned on the basis of their 3D structures using various programs.	Freely downloadable structure files and display programs
LIPIDAT	<a href="http://www.lipidat.chemistry.ohio-state.edu/">http://www.lipidat.chemistry.ohio-state.edu/</a>	Ohio State University, Ohio, USA	relational database of thermodynamic and associated information on lipid mesophase and crystal polynorphic transitions. There are 19,957 records in the database. The database includes lipid molecular structures.	Free access via the internet
CarbBank, CCSD and CCRC	<a href="http://bssv01.lancs.ac.uk/gig/pages/gag/carbbank.htm">http://bssv01.lancs.ac.uk/gig/pages/gag/carbbank.htm</a> <a href="http://www.ccrc.uga.edu/">http://www.ccrc.uga.edu/</a>	Georgia State University, Athens, Georgia, USA	The CCSD is a database containing complex carbohydrate structures and associated text. The information is derived from scientific publications and submissions by authors. CarbBank is the computer program to allow access to the information in the CCSD database files. CCRC is the web version of the database.	Free access after registration

### 14.2.2

## VIS/NIR Fluorescence Spectroscopy in DNA Sequencing and Immunoassay

### 14.2.2.1 Introduction

Fluorescence and absorption techniques are of prime importance in bioscience today. Most of the recently developed separation techniques, including gel electrophoresis (GE), capillary electrophoresis (CE) and high-performance liquid chromatography (HPLC) as well as gene probes and immunoassays, rely on detection in the visible and near-infrared (VIS/NIR) region through the use of fluorescent or absorbing probes [7, 18–21]. Fluorescent probes are highly versatile and can be used in very many types of assays. An overview of the use of fluorescent probes in bioanalytical applications is presented in Tab. 14.2.

The large majority of fluorescent probes absorb in the near-UV region (300–400 nm) and emit in the visible light region (400–700 nm), but the utilisation of the far-red (700–900 nm) and particularly the near-infrared region (900–2000 nm) is more advantageous and profitable. Optical light sources and detectors in this spectral region become continuously cheaper through their large-scale use in the telecommunications field. Recently developed photodiodes and diode lasers have been applied in quite novel techniques for biomolecule detection. The near-IR region is also promising due to the lower interference from the environment and the low scattering in turbid media, which makes biomedical sensing applications, in particular, very attractive. For fiber optic sensing the near-infrared is also favourable, because of the lower losses in quartz fibers around 1400 nm. Another advantage provided by VIS/NIR spectroscopic detection is that relatively low energy transitions are used which do not readily affect the structural integrity of the biological analytes or media. Thus, recent advances in spectroscopic methods utilising VIS/NIR fluorophores and chromophores in biomolecular analysis of nucleic acids and immunological assays will be the larger focus of this section.

The development of new absorbing or fluorescent probe molecules for the near-IR region is a relatively new field. The main problem with near-IR chromophores lies in the broadness of the absorption peaks, the small Stokes' shifts and the low quantum yields observed with the more conventional dyes. Recently, novel chromophores have been designed and synthesised with much more favourable properties and many types of probes are commercially available. These dyes generally comprise xanthenes, rhodamines, polymethines and phthalocyanines (Pc). There are also important applications of rare earth elements, such as europium, osmium and ruthenium in time-resolved fluorescence. With visible probes that absorb and fluoresce in the 400–700 nm region there is the danger of high background absorption or fluorescence of the bio-matrix. Thus, background absorbance and fluorescence needs to be eliminated, which may be problematic and time consuming. Probes in the 700–1100 nm region provide an advantage over visible fluorophores and chromophores due to a significantly reduced interference from the bio-matrix and thus increase the detection sensitivity. Also scattering in the NIR region is greatly reduced in comparison to the visible region due to the

Table 14.2 Fluorescent probes and their applications [compiled from Ref. 21 with permission].

<b>Application area</b>	<b>Subfield or technology</b>	<b>Typical dyes or assay system used</b>	<b>Description</b>	<b>References</b>
Ion indicator dyes	pH	Near-neutral pH: fluorescein diacetate, carboxyfluorescein and its esters, 5-sulfophluorescein diacetate, BCECF and its Acidic pH: di- and trifluorofluoresceins (Oregon Green) and dichlorofluorescein, 9-amino-6-chloro-2-methoxyacridine, 8-hydroxypyrene-1,3,6-trisulfonic acid (HPTS)  LysSensor probes	Physiological detection of pH is presently performed with various new fluorescent dyes. BCECF and its membrane-permeant ester have become the most widely used fluorescent indicators for estimating intracellular pH. Studies related to: role of intracellular pH in diverse physiological and pathological processes, cell proliferation, apoptosis, muscle contraction, malignancy, multidrug resistance, ion transport and homeostasis, endocytosis and Alzheimer's disease.	22
$\text{Na}^+$ and $\text{K}^+$		Crown ethers conjugated to the benzofuranyl fluorophore (SBFI) and PBF1, sodium green, CoroNa Red,	Detection of physiological concentrations of $\text{Na}^+$ and $\text{K}^+$ in the presence of other monovalent cations. Applications are: <ul style="list-style-type: none"> <li>• Estimation of <math>\text{Na}^+</math> gradients in isolated mitochondria,</li> <li>• Measurement of intracellular <math>\text{Na}^+</math> levels or <math>\text{Na}^+</math> efflux in cells from a variety of tissues: Blood (platelets, monocytes and lymphocytes), Brain (astrocytes, neurons, and presynaptic terminals), Muscle (perfused heart, cardiomyocytes and smooth muscle), secretory epithelium cells,</li> </ul>	23

Table 14.2 (continuing)

Application area	Subfield or technology	Typical dyes or assay system used	Description	References
$\text{Ca}^{2+}$ , $\text{Mg}^{2+}$ , $\text{Al}^{3+}$	Calcein, fura-2, BTC, various derivatives of Calcium Green, fluo-3 AM and fluo-4 AM and some of their dextran conjugates EGTA, APTRA and BAPTA Aequorin (bioluminescent indicator for $\text{Ca}^{2+}$ ) Calcein, Mag-fura-2, Magnesium Green and others	Measurement of intracellular and extracellular, $\text{Ca}^{2+}$ concentrations (fluorescence microscopy, flow cytometry and fluorescence spectroscopy). Conjugates with dextrans are used to confine the indicator to the cytosol. Major applications to the study of calcium regulation and transport.	• Correlation of changes in intracellular $\text{Na}^+$ with $\text{Ca}^{2+}$ concentrations, intracellular pH and membrane potential has been used in combination with other fluorescent indicators.	23 24

Zinc and other metal ions	<p>Newport Green DCF and PDX, Fura-Zin, FluoZin and TSQ indicators (<math>Zn^{2+}</math>).</p> <p>Calcine, Phen Green FL and SK (Fe<math>^{2+}</math>, Cu<math>^{2+}</math>, Cu<math>^+</math>, Hg<math>^{2+}</math>, Pb<math>^{2+}</math>, Cd<math>^{2+}</math> and Ni<math>^{2+}</math>.)</p> <p>2,3-Diaminonaphthalene (selenium)</p>	<p>Zinc is an important divalent cation in biological systems, influencing DNA synthesis, microtubule polymerization, gene expression, apoptosis, immune system function and the activity of enzymes such as carbonic anhydrase and matrix metalloproteinases (MMP). <math>Zn^{2+}</math> is functionally active in synaptic transmission and is a contributory factor in neurological disorders including epilepsy and Alzheimer's disease.</p>
$F^-$ , $Cl^-$ , $Br^-$ , $I^-$	Calcine, 6-methoxyquinolinium derivatives (SPQ), MQAE, MEQ and cell-permeant DiH-MEQ, lucigenin,	<p>Measurement of intracellular <math>Cl^-</math> has renewed relevance to research on cystic fibrosis, and can be performed with a variety of probes. Conventional applications of <math>Cl^-</math> detection are:</p> <ul style="list-style-type: none"> <li>• Membrane chloride transport (e.g. sodium-dependent transport, Renal brush-border, GABA<sub>A</sub> receptor),</li> <li>• Intracellular chloride activity <ul style="list-style-type: none"> <li>• Quenching of Al<math>^{3+}</math>-calcein complex fluorescence has been used as the basis of method for fluoride determination with a detection limit of 0.2 ng mL<math>^{-1}</math>.</li> <li>• Detection of <math>Cl^-</math>, <math>Br^-</math> and <math>I^-</math> are also much performed via chemiluminescence.</li> </ul> </li> </ul>

Table 14.2 (continuing)

Application area	Subfield or technology	Typical dyes or assay system used	Description	References
CN <sup>-</sup>		o-Phthaldialdehyde and naphthalene-2,3-dicarboxaldehyde	Determination of cyanide in blood, urine and other samples via reaction of fluorophore in presence of primary amine.	27
Sulfide		5,5'-Dithiobis-(2-nitrobenzoic acid) (DTNB or Ellman's reagent), monobromobimane,	Sulfide has been determined for histochemical studies, probing of dynamic changes of red cell membrane thiol groups, subcellular location of cathepsin D, and studies related to glucose-6-phosphate dehydrogenase, glutathione, glutathione transferase, 6-mercaptopurine e.o.	28
Phosphate and pyrophosphate	DCPIP, NBT, Amplex Red/resorufin		Detection of free phosphate in solution through the formation of the fluorescent products (e.g. resorufin via malate phosphorylase, glucose oxidase and HRP resorufin)	29
Nitric oxides	4-Amino-5-methylamino-2',7'-difluorofluorescein (DAF), 2,3-Diaminonaphthalene and N-methyl-4-hydrazino-7-nitrobenzofuran		Role of nitric oxide in signal transduction has been recently realised, yielding new fluorimetric assays for NO <sup>2-</sup> and NO.	30

Gasses	Oxygen, peroxide, etc.	fluorophores that generate or detect reactive oxygen species, such as including singlet oxygen, superoxide, hydroxyl radical, peroxides. E.g.: mero-cyanine 540, Rose Bengal acetate; xanthene dyes e.o. detection of peroxide via HRP.	Various applications in bioscience: oxydation/peroxydation of lipids, fatty acids and cholesterol, NADH, NADPH, dopamines, ascorbic acid, histidine, triptophan, tyrosine, cysteine, glutathione, proteins and nucleic acids. Relevance to research of Alzheimers disease.	31
General biomolecule detection	Functional group labeling and detection with single dye molecules.	Nearly all known fluorescent dye conjugates of drugs, haptens, proteins, immunoglobulins, and nucleic acid: coumarin's, fluorescein's cyanines, rhodamines. Specialised dyes: BODIPY & Alexa Fluor, various extended cyanine dyes	Main application in diagnostics, laboratory assays, immunoassays, histochemistry, immunohistochemistry, flow cytometry and cellular diagnostics.	7, 18-21
Labeling and detection with fluorescent proteins or other fluorescent biomolecules	Phycobiliproteins, green fluorescent proteins	Diagnostic assay use, histochemical staining, imaging of live organisms and their functions.	32	
Functional group labeling and detection with fluorescent latex particles	Fluorescent dye loaded micro- and nanoparticles.	Diagnostic assay use (particularly in immunochromatography tests) and flow cytometry.	33	
Enzyme-labeled fluorescence (ELF)	Various phosphate-labeled fluorescent dyes, ELF 97	Uses phosphatase-based signal amplification. Applicable to: immunohistochemical and cytological staining. mRNA <i>in situ</i> hybridization, detection of endogenous phosphatase activity, and blot analyses.	34	

Table 14.2 (continuing)

Application area	Subfield or technology	Typical dyes or assay system used	Description	References
Tyramide signal amplification (TSA) Technology	Various tyramide-labeled dyes	Utilizes the catalytic activity of horse-radish peroxidase (HRP) to generate high-density labeling of target (also <i>in situ</i> ). Involves coupling of tyramide-fluorescent dye conjugate to protein tyrosine sidechains via peroxidase-mediated formation of an O,O'-dityrosine adduct. Applied to: immunohistochemical staining and <i>in situ</i> hybridization.		35
Protein detection	Protein quantitation in solution in gels, in CE and 2DE, and on blots	SYTO, SYBR, fluorescamine and o-phthalaldialdehyde, novel dyes: BODIPY, NanoOrange, CBQCA and SYPRO protein gel stains	In addition to the conventional dyes for protein staining (Coomassie Blue, colloidal gold), many novel fluorescent stains have been developed that allow highly sensitive protein quantitation in solution and in gels, particularly the SYPRO protein gel stains.	36
Peptide analysis, sequencing and synthesis	All fluorescent dye labels with reactive groups for amine, dansyl chloride, dansyl chloride.	Fluorescent isothiocyanates.	N-Terminal amino acid analysis, peptide sequencing, peptide synthesis, labeling peptides in solution, solid-phase synthesis of labeled peptides	37

Detection of cytoskeletal proteins (actin, tubulin).	Fluoresceine, Alexa Fluor, BODIPY and other conjugates of actin, tubulin and phallotoxins	Study of <i>in vivo</i> cytoskeleton dynamics. Labels of phalloidin and phallacidin are used for selectively labeling F-actin. Tubulin conjugates are used for observation of cell cycle-dependent microtubule dynamics, mitotic spindle morphogenesis and visualisation of tubulin transport in neurons.
Nucleic acid analysis	Nucleic acid labelling, detection and quantitation with single fluorescent dye molecules	<p>Cyanine dyes and phenanthridine dyes, ethidium bromide and propidium iodide DAPI, "Hoechst dyes", acridine orange, 7-AAD and hydroxystilbamine.</p> <p>New dyes have been developed for nucleic acid detection in solution and staining in gels</p> <p>Cell membrane-impermeant dyes, incl. stains for dead cells (SYTOX Dyes), high affinity stains (the cyanine dimers TOTO, YOYO etc.), and counterstains (cyanine monomers, YO-PRO, TO-PRO e.o.).</p> <p>SYTO cyanine cell-permeant nucleic acid dye</p> <p>Dyes for ultrasensitive solution quantitation (PicoGreen for dsDNA, OligoGreen for ssDNA and RiboGreen for RNA),</p>

Table 14.2 (continuing)

Application area	Subfield or technology	Typical dyes or assay system used	Description	References
			The three classes of “classic” nucleic acid stains are: Intercalating dyes (ethidium bromide and propidium iodide), Minor-groove binders, (DAPI and the “Hoechst dyes”), Miscellaneous nucleic acid stains with special properties (acridine orange, 7-AAD and hydroxystilbamidine).	39
	Hybridization detection incl. FISH (fluorescence in situ hybridization)	ChromaTide nucleotides	Fluorophore- and hapten-labeled nucleotides for enzymatic incorporation into DNA or RNA probes for FISH (fluorescence in situ hybridization), for DNA arrays and microarrays and for other hybridization techniques	40
		SYBR Green	Real-time quantitative nucleic acid gel stain used in PCR	41
	Universal Linkage System (ULS)		Platinum-based chemistry for producing bright, fluorophore-labeled hybridization probes	42
	Enzyme-Labeled Fluorescence (ELF)		Phosphatase-based signal amplification assay also applicable to nucleic acid labeling (see description under proteins)	43

	Tyramide Signal Amplification (TSA) Technology	HRP-based assay with tyramide-fluorescent dye conjugate also applicable to nucleic acid labeling (see description under proteins)	44
Membrane and lipid research	General lipid and cell membrane labeling	Lipid and fatty acid derivatives of BODIPY, nitrobenzoxadiazole (NBD), pyrene, perylene, 9-anthroyloxy and dansyl fluorophores, cis-parinaric acid.	45
		Fluorescence labeled lipids and fatty acids are generally used to: investigate lipid traffic, e.g. fluorescence recovery after photobleaching (FRAP) and other techniques examine lipid-lipid and lipid-protein interactions via FRET measurements characterize lipid domains by fluorescence correlation spectroscopy (FCS) characterize lipid domains by near-field scanning optical microscopy. detect phospholipase activity investigate the cellular uptake of lipids investigate lipid metabolism and signalling study membrane fusion (pyrene eximer formation) and structural dynamics Detect lipid peroxidation	
Membrane potential-sensitive probes	Various styryl dyes (ANEP, RH) and Indo-, thia- and oxa-carbocyanines, merocyanines, bisoxonols and rhodamines.	Dynamic optical detection and imaging of membrane potential changes.	46

Table 14.2 (continuing)

<b>Application area</b>	<b>Subfield or technology</b>	<b>Typical dyes or assay system used</b>	<b>Description</b>	<b>References</b>
Detection of enzymatic action	Glycosidases, glucuronidases etc.	A large variety of $\beta$ -galactosidase, $\beta$ -glucuronidase, amylase, neuraminidase, sialidase, chitinase, cellulase substrates	Endogenous glycosidase activity is frequently used to characterize strains of microorganisms and to selectively label organelles of mammalian cells. Defects in glycosidase activity are characteristic of several diseases. $\beta$ -D-glucuronide activity is used primarily for contamination detection of E-coli. $\beta$ -amylase levels in various fluids of the human body are of clinical importance. Plant and microbial $\beta$ -amylases are important industrial enzymes. Cellulase enzymes are relevant in food, fuel, animal feed and clothing applications	47
	Proteases and peptidases	7-Aminocoumarins, rhodamine 110, fluorescein casein	Peptidases and proteases play essential roles in protein activation, cell regulation and signaling, in the generation of amino acids for protein synthesis or utilization in other metabolic pathways.	48
	Metabolism of phosphates and Polyphosphates, ATP e.o.	• phosphatases	Phosphatase substrates (classic chromogenic substrates: BCIP and NBT. Novel fluorescent substrates: Fluorescein diphosphate, Dimethyl-acridine phosphate, methylumbelliferyl phosphates, ELF 97 e.o.); bioluminescent determination of ATP;	49

Oxidoreductases	Fluorogenic reagents for H <sub>2</sub> O <sub>2</sub> in conjunction with peroxidases (HRP) and catalase. (Amplex Red/resorufin etc.). Electrochemical and chemiluminescent approaches are also much used Nitroreductase/Nitrate reductase	Systems are used in a wide variety of bioassays by linking various oxidases to HRP via hydrogen peroxide. Determination of glucose, cholesterol, choline glutamate, xantine, uric acid, galactose etc.	50
Miscellaneous enzymes	Various probes for microsomal dealkylase, lipase, acetylcholinesterase, acetyltransferase and carbonic anhydrase		51
Carbohydrate analysis	Lectins	Fluorescent Concanavalin A, wheat germ agglutinin (WGA) fluorescein conjugates, lectins from <i>Griffonia simplicifolia</i> , <i>Phaseolus vulgaris</i> , <i>Araucaria hypogaea</i> , <i>Helix pomatia</i> , <i>Glycine max</i> , Cholera Toxin Subunits A and B	52 Lectins and other carbohydrate-binding proteins bind to specific configurations of sugar molecules can serve to identify cell types or cellular components, making them versatile primary detection reagents in histochemical applications and flow cytometry. Fluorescent derivatives of carbohydrate-binding proteins have been used to detect cell-surface and intracellular glycoconjugates by microscopy and flow cytometry, to localize glycoproteins in gels and on protein blots, to precipitate glycoproteins in solution and to cause agglutination of specific cell types.

Table 14.2 (continuing)

<b>Application area</b>	<b>Subfield or technology</b>	<b>Typical dyes or assay system used</b>	<b>Description</b>	<b>References</b>
Cellular biochemistry	Probes for mitochondria	Rhodamines and rosamines, Carbocyanines, stryryl dyes, lipophilic acridine orange, lucigenin, MitoTracker and MitoFluor Probes	Mitochondria-selective reagents for assessment of mitochondrial activity, localization and abundance, monitoring effects of pharmacological agents, such as anaesthetics that alter mitochondrial function. Important role in apoptosis	53
	Probes for the endoplasmic reticulum and Golgi apparatus	The flattened membranous sacs of the endoplasmic reticulum (ER) and the Golgi apparatus can be stained with a variety of lipophilic probes and then distinguished on the basis of their morphology.  Probes for the Golgi apparatus are fluorescently labeled ceramides and sphingolipids, which tend to associate preferentially with the trans-Golgi.	The endoplasmic reticulum (ER) and Golgi apparatus are responsible for the proper sorting of lipids and proteins in cells. Cell-permeant probes for these organelles are lipids or chemicals that affect protein movement. Enzymes in the ER are involved in synthesis of cholesterol and membranes and in the detoxification of hydrophobic drugs through the cytochrome P-450 system. Several enzymes in the Golgi glycosylate lipids and proteins, resulting in some fluorescent lectins being useful markers for this organelle.	54

Calcium regulation	Cyclic adenosine 5'-diphosphate ribose (cADP-ribose), 3-deaza-cADP-ribose, Ryanodine derivatives, BODIPY FL thapsigargin etc.	Studies of calcium release. Calmodulin mediates many of the regulatory functions of calcium ions. Fluorescently labeled calmodulin is used to study the <i>in vivo</i> behavior of the protein (e.g. in the mammalian mitotic spindle). <i>In vitro</i> , fluorescently labeled calmodulin has been used for:
		<ul style="list-style-type: none"><li>• Following the binding of protein kinase substrates by calmodulin</li><li>• Studying the interactions of myogenic basic helix-loop-helix transcription factors with calmodulin</li><li>• Investigating the molecular mechanisms for calmodulin trapping by calcium/calmodulin-dependent protein kinase I,</li><li>• Characterizing inhibitors of calmodulin activation of MLCK-catalyzed phosphorylation of the smooth-muscle regulatory chain</li></ul>

Table 14.2 (continuing)

<b>Application area</b>	<b>Subfield or technology</b>	<b>Typical dyes or assay system used</b>	<b>Description</b>	<b>References</b>
Blood coagulation	Fluorescent heparin conjugates	Study of heparin binding to thrombin, low-density lipoproteins, lipoprotein lipase, circulatory serine proteases, proteinase inhibitors, heparin-binding growth factors, blood vessel-associated proteins (fibronectin and laminin) and binding to cells and tissues. Study of anticoagulant activity and the modulation of the structure, function and metabolism of many proteins and enzymes.		56
Protein kinases, protein phosphatases and nucleotide-binding proteins	Bisindolylmaleimides, fluorescent polymyxin B analogs, hypericin and hypocrellins, blue-fluorescent N-methylanthraniloyl (MANT) analog of cGMP, fluorescent forskolin	Studies on protein kinase inhibitors and activators, cyclic nucleotides, adenylylate cyclase, etc.		57

Receptor binding	<p>Various acetylcholine receptors (probes to <math>\alpha</math>-bungarotoxin probes, fluorescent derivatives of pirenzepine), adrenergic receptors (derivatives of prazosin and CGP 12177), GABA<sub>A</sub> receptor (muscarinic conjugates), neurokinin receptors (conjugates of substance P), neuropeptide C receptors, angiotensin II receptor, opioid receptors (naloxone and naltrexone probes)...</p> <p><math>\text{Ca}^{2+}</math> channels: <math>\alpha</math>-conotoxin probes, fluorescent dihydropyridines and verapamil ryandine etc.</p> <p>Probes for the <math>\text{Na}^+</math> channel and the <math>\text{Na}^+/\text{H}^+</math> antiporter: amiloride analogs</p> <p><math>\text{Na}^+/\text{K}^+</math>-ATPase: ouabain probes</p> <p>Probes for <math>\text{K}^+</math> channels and carriers: glibenclamide conjugates for the ATP-dependent <math>\text{K}^+</math> channel, apamin probes for small-conductance <math>\text{Ca}^{2+}</math>-activated <math>\text{K}^+</math> channels,</p> <p>Probes for <math>\text{Cl}^-</math> channels and carriers: ivermectin probes for glutamate-gated <math>\text{Cl}^-</math> channels, stilbene disulfonates: (anion-transport Inhibitors),</p>	<p>Fluorescent receptor ligands can provide a sensitive means of identifying and localizing some of the most pivotal molecules in cell biology. Many types of fluorescently labelled and unlabeled ligands exist for various cellular receptors, ion channels and ion carriers. Many of these site-selective fluorescent probes may be used on live or fixed cells, as well as in cell-free extracts. Many new dyes provide extremely sensitive detection, which enables measurement of low-abundance receptors. Various methods for further amplifying detection of these receptors have been reported.</p> <p>A variety of probes for <math>\text{Ca}^{2+}</math>, <math>\text{Na}^+</math>, <math>\text{K}^+</math> and <math>\text{Cl}^-</math> ion channels and carriers have been described. Ion flux that affects the cell membrane potential, can be indicated with potential-sensitive probes.</p>
------------------	--	---

Table 14.2 (continuing)

<b>Application area</b>	<b>Subfield or technology</b>	<b>Typical dyes or assay system used</b>	<b>Description</b>	<b>References</b>
Phagocytosis	Dichlorodihydrofluorescein diacetate, OxyBURST technology	Monitoring of the oxidative “burst” produced by activation of an NADPH oxidase in a chain of events starting with the binding of surface-bound IgG immune complexes interact with Fc receptors.		59
Apoptosis	Various fluorescence based kits, e.g. those using annexin V conjugates Caspase protease activity	Apoptosis is a genetically controlled cell death. Various approaches are used in studying apoptosis, and to distinguish live cells from early and late apoptotic cells and from necrotic cells. Apoptosis assays may be based on:	<ul style="list-style-type: none"> <li>• Nucleic acid stains,</li> <li>• Annexin V conjugates</li> <li>• Protease activity</li> <li>• Mitochondrial stains</li> <li>• Free radicals</li> <li>• Ion indicators</li> <li>• Esterase activity</li> <li>• ATP:ADP ratio</li> </ul>	60

**Table 14.3** Comparison of noise levels in the NIR in visible regions.

<b>Noise source</b>	<b>NIR region</b>	<b>Visible region</b>
Detector	low	high
Scatter (Rayleigh/Raman)	reduced	6 × greater at 250 nm than 820 nm
Autofluorescence	mostly absent	autofluorescence of biomolecules

wavelength dependence of Raman scattering. These benefits are shown in Tab. 14.3.

Excitation in the visible part of the electromagnetic spectrum (400–700 nm) can be accomplished with the 488 nm argon, 546 nm mercury-arc, 633 nm HeNe, and 647 nm Kr laser lines. Longer wavelength electronic transitions can be induced by the near-infrared gallium–aluminum–arsenide (GaAlAs) laser diode with an output at 785 nm. The advantages of using laser diodes instead of argon lasers are listed in Tab. 14.4. Fluorescence detection in the NIR region utilising avalanche photodiodes (APD) instead of conventional photo multiplier tubes (PMT) provides additional benefits as shown in Tab. 14.5. In addition, APDs not only offer greater quantum efficiency but also show lower power consumption in comparison to PMTs. The complementary advantages of diode laser excitation and APD signal transduction are especially applicable to bioanalytical techniques.

**Table 14.4** Comparison of diode lasers and argon ion lasers as excitation sources.

<b>Parameter</b>	<b>Laser diode</b>	<b>Argon laser</b>
Wavelength (nm)	785	488
Lifespan (h)	100 000	3000
Power output (W)	0.02	~ 5
Power output	0.15	1800
Replacement (\$)	10	5000

**Table 14.5** Comparison of avalanche photodiodes and photomultiplier tubes as signal transducers.

<b>Parameter</b>	<b>APD</b>	<b>PMT</b>
Quantum efficiency at 820 (%)	80	0.3
Internal amplification	low	high
Size	mm	cm
Power Consumption	very low	low
Lifetime (h)	100 000	10 000
Replacement cost (\$)	50	500

### 14.2.2.2 Chemistry of VIS/NIR Dyes

The chemistry of VIS/NIR-absorbing dyes is well established in a variety of bioanalysis applications including DNA analysis and immunological assays [7]. Numerous approaches have been applied to the development of dyes for these specific fields. The major tools for designing new dyes are (1) to apply structure–color correlation rules or (2) to approximate the absorption range of the target dye by quantum chemical calculation. A bathochromic or hypsochromic shift can be affected by simple structural modifications, applying general guidelines of the structure–color correlation. These comprise: (1) increasing the overall electron density, (2) increasing the strength of the donor and acceptor groups in the dye, (3) increasing the conjugation length (longer oscillator), e.g. by polymerisation and (4) increasing the “dimensionality” of the molecule. Semiempirical quantum chemical methods are still quite often used to assess the absorption wavelengths of candidate dyes prior to synthesis. Older methods were based on the Pariser–Parr–Pople molecular orbital (PPP MO) method [61] or XNDO/S method [62]. Presently, INDO methods in conjunction with more extensive configuration interaction schemes are frequently used [63]. These methods are nowadays applicable to quite large molecules and even on a desktop computer quite large structures (up to 500 atoms) can be readily evaluated. DFT methods, however, yield very much improved accuracy of calculations, particularly when metals are also involved [64], but are only applicable to smaller molecules.

In addition to the desired absorption maxima, other factors must be considered to tailor the chromophore for its desired function. Such customisation leads to incorporation of proper functionalities for covalent coupling to biomolecules and organic or water solubility. Furthermore, the fluorescence maximum in the desired region, the quantum yield ( $\varphi_f$ ), and the fluorescence lifetime ( $\tau$ ) should also be taken into consideration in the design of dye molecules. These alterations can generally be achieved by structural modification of known chromophore structures. For example, the quantum yield of a fluorophore can be estimated by comparison with existing fluorophores with known quantum yields. This estimation can be achieved simply by comparing the wavelength-integrated intensity of the unknown to that of the standard using the following equation where  $Q$  is the quantum yield,  $I$  is the integrated intensity, OD is the optical density, and  $n$  is the refractive index.

$$Q = Q_R \frac{I}{I_R} \frac{\text{OD}_R}{\text{OD}} \frac{n^2}{n_R^2} \quad (1)$$

#### Visible-absorbing dyes

##### *Rhodamines and fluoresceins*

The most commonly used visible fluorophores are the rhodamine and fluorescein analogues. These dyes can be derivatized with either an isothiocyanato group (–NCS) or an *N*-hydroxysuccinimidyl (NHS) ester functionality for covalent labelling at the amino group of proteins or amino-functionalised nucleotides (Fig. 14.1). A number of dyes containing reactive groups are commercially available and they are as a rule inexpensive.

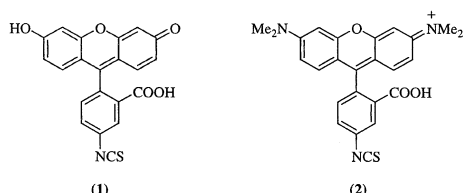


**Fig. 14.1** Structure of isothiocyanato-functionalized fluorescein (**1**) and tetra-methylrhodamine (**2**).

Fluorescein is a hydroxylated xanthene (fluorone) with intense green fluorescence. This well-known dye has been used as a tracer in underground streams and water supplies, as well as a marker for sea-rescue proceedings [65]. The biolabel FITC, fluorescein isothiocyanate (**1**, Fig. 14.1), was first introduced for use as an antibody label for rapid identification of pathogens in 1958 by Riggs et al. [66]. Since then, this dye has been an established marking tool in DNA synthesisers, crime-scene analysis, and immunoassay. Other visible dyes, exemplified by tetra-methylrhodamine isothiocyanate (**2**, Fig. 14.1), are similar in structure to fluorescein except they possess amino moieties ( $-NR_2$ ) in place of the peripheral hydroxy/oxo groups. These cationic xanthene dyes exhibit many of the desirable properties for biological labeling such as a high fluorescence quantum yield and good water solubility [67].

Recently, fluorescein and tetraethylrhodamine derivatives were utilized in the evaluation of biotin-dye conjugates for use in an HPLC assay to assess relative binding of biotin derivatives with avidin (Av) and streptavidin (SAv) [68]. These derivatives are targeted for radiotherapy of cancer in which the biotin derivative carries a radionucleide to cancer cells. These biotin-dye conjugates incorporated a 4,7,10-trioxatridecane-1,13-diamino linker as a 17 Å spacer to assess the changes in rates of association and dissociation with Av or SAv.

#### *Thiazole orange*

Thiazole orange (TO, Fig. 14.2) is a cyanine dye that shows a relatively large emission enhancement upon intercalation with double-stranded DNA (dsDNA) and a moderate DNA binding affinity ( $K_d = 10^{-5}$  M). These specific features make thiazole orange derivatives ideal candidates for fluorescent DNA-binding probes. Thompson et al. synthesized a carboxylic acid-functionalized thiazole orange **9** and conjugated it to the amino-terminal zinc finger of the glucocorticoid receptor DNA binding domain (GR-DBD) for DNA sequence specificity binding studies [69]. Photooxidation of the thiazole orange intercalation complex cleaves DNA, which provides a convenient assay for determining the preferred binding site, a 5'-TGTCT-3' sequence.

Synthesis of TOTO dimers is illustrated in Fig. 14.3. The initially formed iodooalkyl derivatives **12** were treated with *N,N,N',N'*-tetramethyl-1,3-diaminopropane in anhydrous MeOH to furnish the symmetrical dimers **13**. As shown by Jacobsen

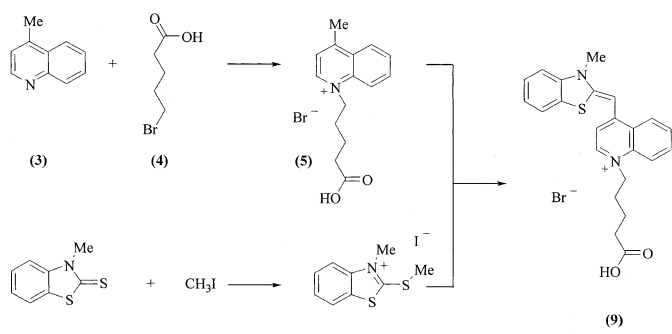


**Fig. 14.2** Synthetic route to carboxylic acid functionalised thiazole orange **9**

and his co-workers, these bis-cyanines **13** interact with dsDNA in a sequence-selective manner via noncovalent bis-intercalation [70]. Upon complex formation with the 5'-CTAG-3' sequence of dsDNA, these chromophores exhibit an enhanced fluorescence emission several thousand orders of magnitude greater than the free TOTO dimers.

The final TOTO chromophores were evaluated as sequence-selective bis-intercalators via fluorescence and  $^1\text{H}$ - $^1\text{H}$  NOESY NMR spectroscopy. The TOTO chromophores were found to form a complex with dsDNA, where each separate chromophoric unit is sandwiched between two base pairs in a (5'-CpT-3'): (5'-ApG-3') site while the linker lies in the minor groove. Fluorescence dsDNA binding studies provided a correlation between the linker length of the TOTO dimers and the binding strength. The results indicated that the fluorescence quantum yield of the dimers increases with the length of the linker upon binding to the CTAG sequence. However, this effect does not correlate with the binding selectivity.

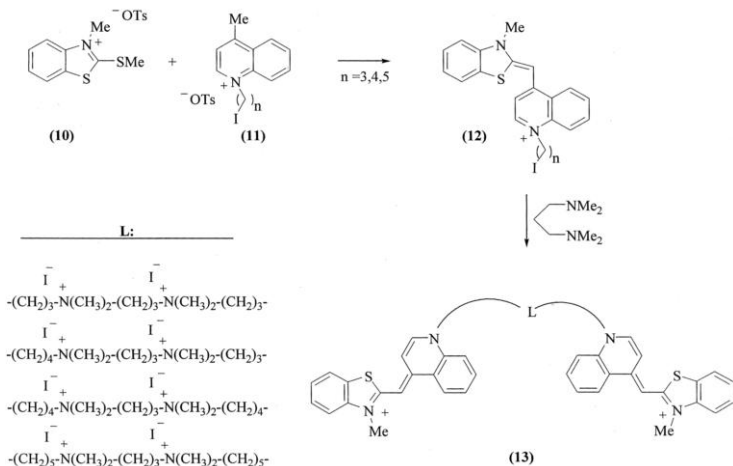


**Fig. 14.3** Synthetic pathways to TOTO dimers **13**.

### Cy<sup>TM</sup> Dyes

The Cy<sup>TM</sup> dyes were developed by Waggoner and his group at Carnegie Mellon University in Pittsburgh, PA. The dyes, with reactive moieties such as a carboxylic acid group or an *N*-hydroxysuccinimidyl (NHS) ester (**16**, **17**, Fig. 14.4), are commercially available from Molecular Probes (Eugene, OR, USA) and Amersham Life Science (Pittsburgh, PA, USA). The dyes contain one or more peripheral sulfonate groups to improve their aqueous solubility. Bio-conjugates, such as Cy5-dUTP (a pentamethine derivative), are commercially available or can be readily prepared. The Cy3<sup>TM</sup> series consist of indolium trimethine cyanine dyes that absorb in the 535–555 nm range, which is compatible with the 546 nm mercury-arc line. Emission of this series of cyanines occurs in the 570–605 nm range. The Cy5<sup>TM</sup> dyes are vinyl analogues of the Cy3<sup>TM</sup> dyes and give a bathochromic shift with absorption in the 620–650 nm region and emission in the 665–725 nm region. This absorption in the orange part of the electromagnetic spectrum allows the pentamethines to be excited via the 633 nm HeNe or 647 nm Kr laser lines. Both series have large extinction coefficients in the range of 130,000 to 250,000 M cm<sup>-1</sup>.

Recently, the active *N*-hydroxysuccinimidyl (NHS) esters of Cy3 and Cy3NOS (**17**, Fig. 14.4) were used to label oligonucleotides by Randolph *et al.* [71]. While Cy3 contains a bis-sulfonate functionality for improved water-solubility, Cy3NOS is mono-sulfonated. The reaction of **14** and **15** produced the carboxy-substituted dye **16**, which was further treated with *N,N*'-disuccinimidyl carbonate in a mixture of DMF/pyridine to give the nonsymmetric *N*-hydroxysuccinimidyl substituted Cy<sup>TM</sup> dyes **17**. Dyes **17** were then covalently linked via a short or long tether at the C-5 position of deoxyuridine to multiply-label DNA. The correlation study between the labeling density and the sensitivity of the DNA fluorescent probe demonstrated that labeling at every 6th base pair with Cy3 showed the optimal fluorescence.

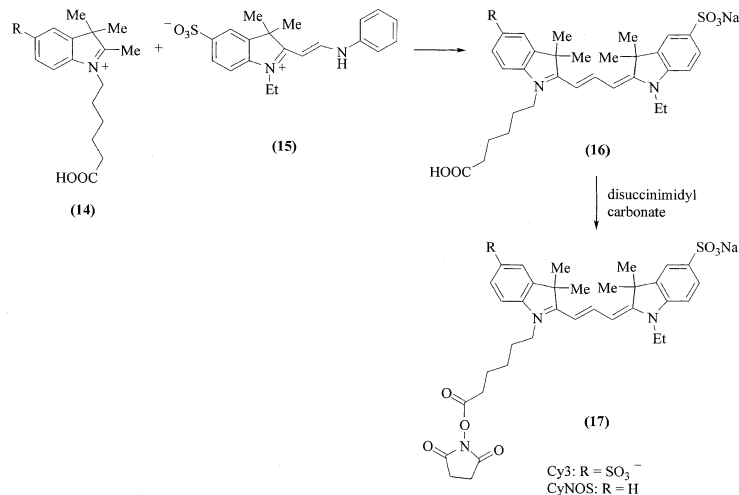


Fig. 14.4 Synthetic route to nonsymmetric dyes Cy3 and Cy3NOS.

### NIR-absorbing dyes

The recent availability of inexpensive semiconductor laser diodes such as gallium-aluminum-arsenide (GaAlAs) with an emission wavelength at 785 nm has led to an increase in the use of NIR fluorophores for bioanalytical applications. As mentioned earlier, the use of a NIR fluorophore can lower the background interference from the biological sample. The IRD™ dyes are commercially available from LI-COR Inc. They are indolium heptamethine cyanine dyes whose absorption coincides with the output of the GaAlAs laser diode. These dyes contain isothiocyanate or phosphoramidite functionalities for labeling amino residues of antibodies or synthetically modified nucleotides, respectively. The general commercial availability of functionalized NIR absorbing chromophores is partially limited and the dyes are rather expensive due to the laborious purification procedures. The most commonly used NIR chromophores belong to the cyanine-type dyes including carbocyanines, squaryliums, and phthalocyanines (Pc), and naphthalocyanines (NPc).

### Carbocyanine dyes

The classical synthetic route to symmetrical indolium heptamethine cyanine dyes by the Strekowski approach [72] is represented in Fig. 14.5. Introduction of an isothiocyanato (-NCS) functionality into the dye is accomplished by facile nucleophilic displacement of the meso-chloro substituent in the intermediate product 22. This method provides amino-reactive cyanines with absorption in the 770–800 nm region.

A similar approach also supplies heptamethine cyanine dyes with altered spectroscopic properties for more specific applications. For example, Flanagan et al. incorporated fluorine and heavy atoms such as I, Br, and Cl into polymethine dyes, as shown in Fig. 14.6, to alter the fluorescence lifetime of the dye without disturbing the other spectroscopic properties [73]. The fluorine or heavy-atom modified

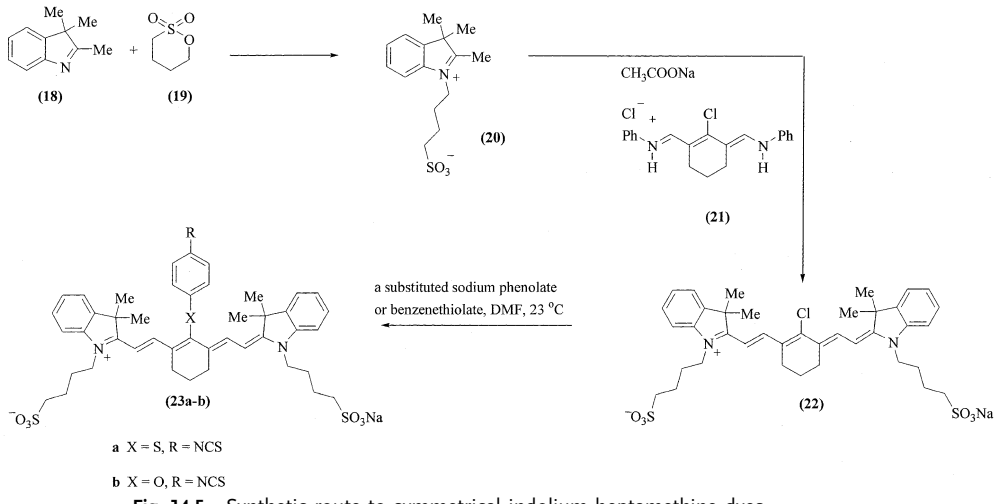
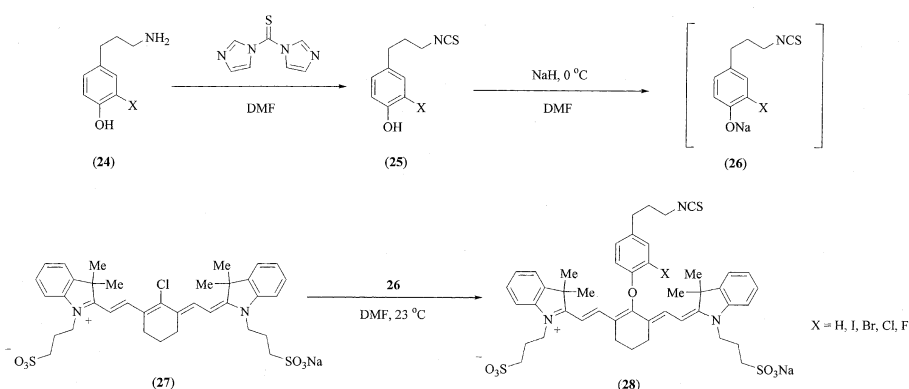
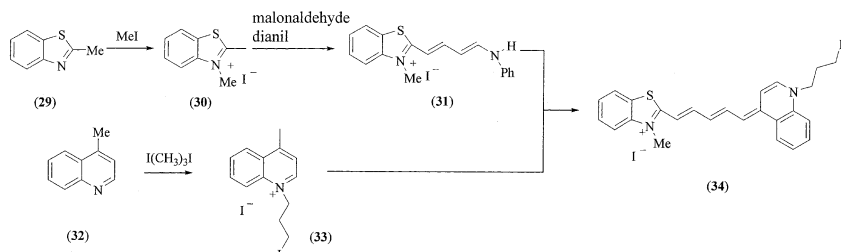


Fig. 14.5 Synthetic route to symmetrical indolium heptamethine dyes.



**Fig. 14.6** Synthetic route to near-infrared heavy atom modified isothiocyanate dyes.



**Fig. 14.7** Synthesis of thiazole green 34 (TAG) used for low-level detection of DNA restriction fragment by CE.

isothiocyanato phenol **25** was obtained from the reaction of the appropriate substituted tyramine **24** with 1,1-thiocarbonyldimidazole in DMF. The sodium phenolate of **24** was further treated with meso-chloro dye **27** to afford the final dye **28**.

Thiazole green represents another class of carbocyanines, which was recently utilized in the low-level detection of DNA restriction fragments by Soper et al. [74]. This dye is comprised of a quinolinium and a thiazolium nucleus joined by a pentamethine chain. The synthetic route to the thiazole green **34** is shown in Fig. 14.7. 2-Methylbenzothiazole **29** was allowed to react with methyl iodide to give the *N*-methyl derivative **30** which was further treated with malonaldehyde-dianil hydrochloride to afford the intermediate product **31**. The intermediate product **31** was then allowed to react with *N*-(3-iodopropyl)lepidinium iodide **33**, which had been obtained from the reaction of lepidine with 1,3-diiodopropane, to finally afford the asymmetrical thiazole green **34**.

Recently, Chairs analyzed the oxazolium pentamethine cyanine dye **35** (DODC, Fig. 14.8) in DNA binding studies utilizing his competitive dialysis method [75]. The nucleic acid structures included single-stranded, duplex, triplex, and tetraplex forms. The comparative assay demonstrated that DODC binds to triplex DNA more selectively than any of the tetraplex forms included in the assay. In addition, the

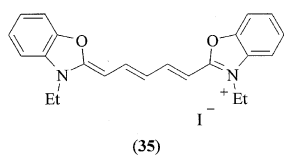


**Fig. 14.8** Structure of 3,3'-diethyloxadadicarbocyanine (DODC) studied by Ren *et al.* [75].

absorbance spectrum of DODC is red-shifted and a signal centered at 610 nm is observed in the CD spectrum upon binding.

A new class of long-wavelength ( $> 1000$  nm) NIR dyes suitable for bio-conjugation **37** (Fig. 14.9) has been developed by Strekowski *et al.* [76]. These long wavelength NIR chromophores provide biolabels with increased sensitivity and detection limits. The isothiocyanato-substituted benz[*c,d*]indolium heptamethine cyanine dyes **37** were obtained by nucleophilic displacement of the meso-chlorine atom of the commercially available dye IR-1048 (**36**). This nucleophilic displacement is suggested to proceed through an  $S_{RN}1$  pathway that includes a cationic radical dye intermediate [77].

#### Squaraine and croconine dyes

Squaraine dyes and the structurally related croconine dyes have also been described with intense absorptions in the NIR region ( $\epsilon > 200,000 \text{ M.cm}^{-1}$ ) [78]. In the synthetic field there is presently much activity to find squaraine dyes with very high absorption wavelengths. For instance, Meier and Petermann described novel NIR dyes with absorption wavelengths in excess of 900 nm by coupling ferrocenes to the squaraine moiety [79] and squaraine and croconine chromoinophores compatible with lipophilic matrices have been described by Citterio *et al.* [80]. Presently, a variety of squaraine dyes and croconine dyes are commercially available from H.W. Sands Corporation (Jupiter, Florida, USA).

Of the squaraine dyes *N*-succinimidyl ester-derivatized indolium-squaraine dyes have been specifically developed for conjugation to biomolecules, because this class of dyes has been shown to exhibit high photostability, a long fluorescence lifetime and spectral properties (absorption, emission, and fluorescence lifetime) which are

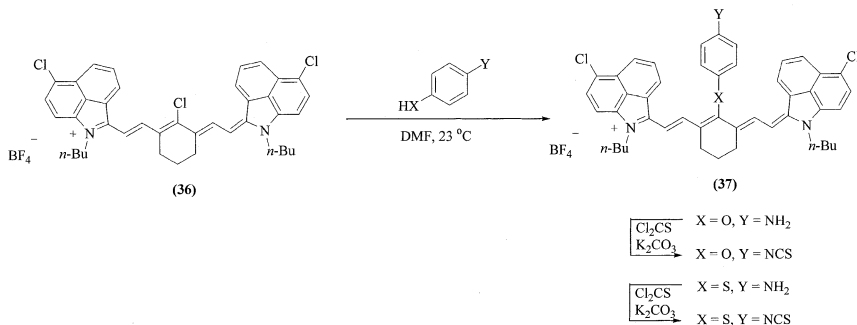


**Fig. 14.9** Isocyanato-derivatised long-wavelength NIR dyes synthesised by Strekowski *et al.* [77].

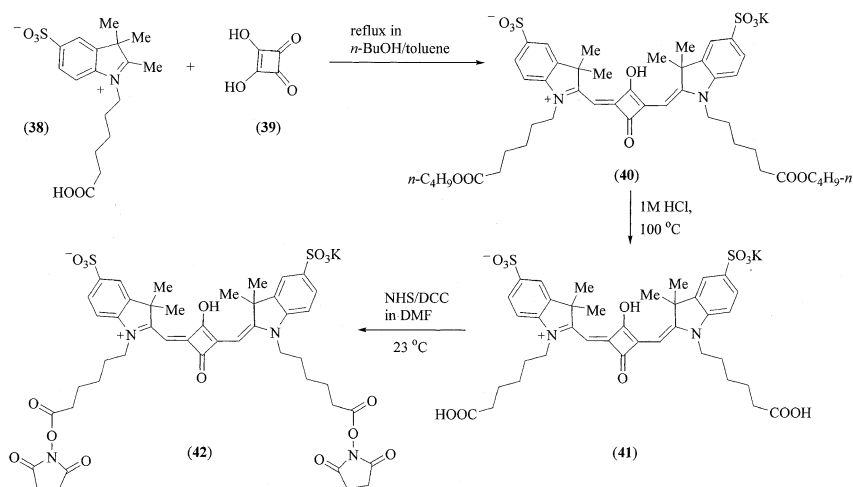


**Fig. 14.10** Synthetic route to Sq635 squaraine dye **42** containing *N*-succinimidyl ester moieties [81].

independent of pH at physiological conditions (pH 6–9) [81]. The water-soluble squaraine dyes exhibit a four- to five-fold fluorescence quantum yield enhancement when covalently bound to proteins [82]. Recently, Oswald et al. described the synthesis of indolium Sq635 (**42**, Fig. 14.10) and the benz[e]indolium Sq660 NHS esters for use in a fluorescence resonance energy transfer (FRET) immunoassay [83]. In the competitive immunoassay, the donor Sq635-HSA has spectral overlap with the acceptor Sq660-anti-HSA which results in a high  $R_o$  of 70 and leads to detection limits of  $10^{-7}$  M.

#### *Phthalocyanins and naphthalocyanins*

The NIR absorbing phthalocyanines (Pcs) and naphthalocyanines (Npcs, Fig. 14.11) are planar chromophores comprising four 1,3-diiminoisoindolenine subunits with an 18-electron cavity. These cyanines can exist as the metal-free (Pc and NPc) or metal-complexed form (MPc and MNpc). The absorbance, emission, fluorescence lifetime, and other photophysical properties are strongly influenced by the central metal ion. Specifically, metal complexation with transition metals provides a selective method to alter the quantum yield ( $\phi_f$ ) and the fluorescence lifetime ( $\tau$ ) of the photoexcited triplet state, which allows MPcs and MNpcs to be strong candidates for use in the photodynamic therapy (PDT) of cancer [84]. These dyes are obtained by cyclotetramerization of the appropriate precursors including di-imino-isoindoline, phthalic anhydride, phthalimide, or benzene dicarbonitrile [85]. The metal-free Pcs or NPcs can then be altered to give the metal-functionalized dye via an insertion reaction with appropriate metal salt. However, most synthetic chemists rely on the direct method to obtain the metal-ion Pcs and NPcs which involves heating the precursors with the appropriate metal salt in a high

boiling solvent such as quinoline, *o*-dichlorobenzene, or tetrahydronaphthalene. Although the photophysical properties can be fine-tuned by the central metal substituent, other structural modifications of these dyes are difficult to accomplish in comparison to carbocyanines or squaraines due to the formation of numerous isomeric products. In addition, these molecules are extremely insoluble, especially in the aqueous solutions that are used in bioconjugation protocols. On the other hand, phthalocyanines and naphthalocyanines are extremely stable to strong bases and acids, heat, and direct exposure to light.

In order to overcome the limited solubility of MNPcs, Brasseur et al. recently synthesized and evaluated the PDT (photodynamic therapy) activity of bis(alkylsiloxy) complexes of naphthalocyanines (45, Fig. 14.11) [86, 87]. It has been established that axial substitution of the central metal ion diminishes the tendency of these dyes to form H-aggregates in solution and the diaxial substituted SiNPs follow this trend with an enhanced stability to photooxidation in comparison to Al- and Zn-NPcs [88, 89]. In the synthesis of 45, benz[*f*]diimino-isoindolenine 43 undergoes cyclotetramerization with silicon tetrachloride to yield the intermediate dichloride. The axial ligands of the dichloro-intermediate are then hydrolyzed to furnish silicon(IV) 2,3-naphthalocyanine dihydroxide 44. The bis(alkylsiloxy) ligands are then introduced via substitution of the axial dihydroxide moieties with the appropriate chlorosilane derivatives to provide the photosensitizing SiNPs 45. The photodynamic properties of bis-substituted SiNPs were evaluated against the EMT-6 tumor in Balb/c mice. Although the bis(alkylsiloxy) SiNPs showed some phototoxicity *in vitro*, they gave excellent results *in vivo*, especially the derivative 45d.

#### 14.2.2.3 Bioanalytical Applications of NIR and Visible Fluorescent Dyes

##### DNA sequencing

As mentioned above, the Human Genome Project, which was initiated in the late 1980s, has spurred the development of technology necessary to facilitate the formidable task of sequencing and decoding the human genome. The dideoxy

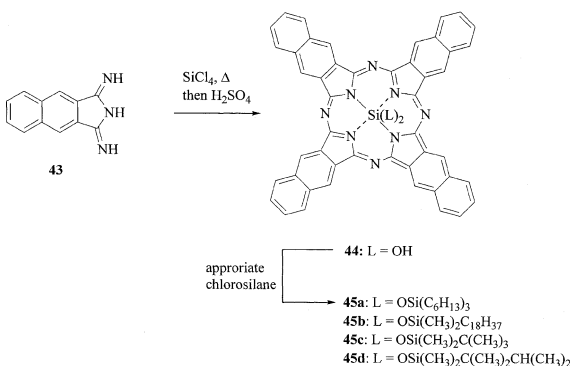


**Fig. 14.11** Synthesis of bis (alkylsiloxy)SiNPs [86, 87].

chain termination method of DNA sequencing, developed by Sanger and coworkers in 1977 is the primary method used in DNA sequencing [90]. Generally, DNA sequencing involves three stages of fragmentation, beginning with the chromosome and ending up with segments of DNA four to five hundred base pairs in length (Fig. 14.12) [91–94]. The starting point of the Sanger method is the M13 vector containing the foreign DNA insert. A short strand of DNA complementary to a portion of the M13 vector is synthesized. This strand of DNA, referred to as a primer, will bind to the complementary portion of the M13 vector. The M13 vector and the primer are placed in a solution containing the enzyme DNA polymerase. DNA polymerase will catalyze the synthesis of DNA from the 3' end of the primer. The newly synthesized DNA will be complementary to the sequence of the foreign or inserted DNA. DNA synthesis, catalyzed by DNA polymerase, requires the presence of all of the deoxynucleotide bases. The Sanger method utilizes modified bases, called dideoxynucleotides, which lack the 3'-hydroxy on the sugar residue that normal nucleotides have. When DNA polymerase incorporates a dideoxynucleotide into a growing strand of DNA, the strand terminates immediately thereafter. Chain termination occurs because the dideoxy nucleotide lacks the 3'-hydroxy

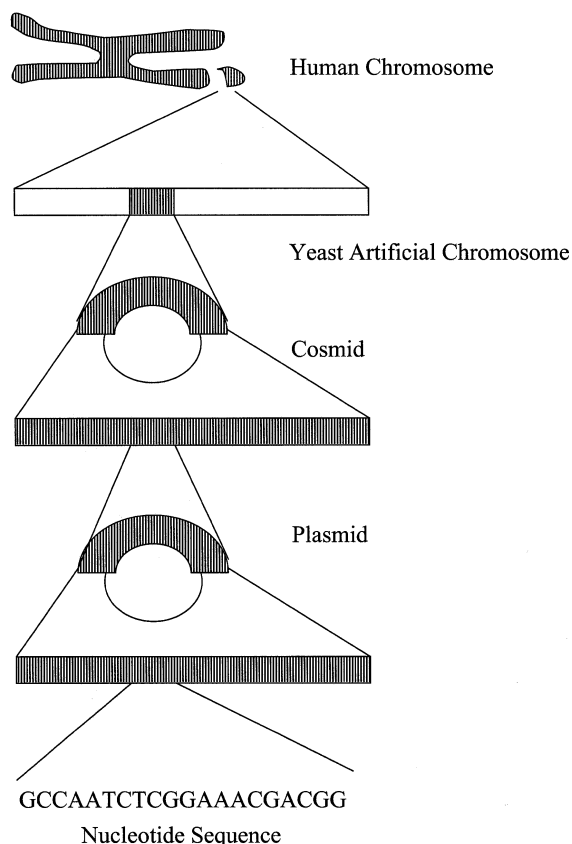


**Fig. 14.12** Schematic illustration of the fragmentation steps in the sequencing of DNA.

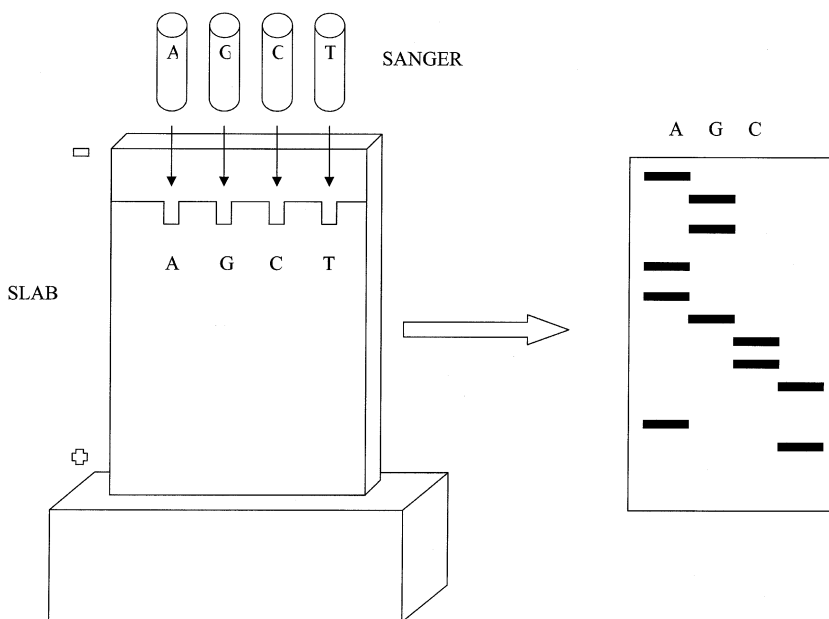


**Fig. 14.13** The Sanger method for DNA sequencing.

functionality necessary to form the phosphodiester linkage with the next nucleotide. Four reactions are carried out in the Sanger method. In each case, a mixture of the primer, inserted DNA or template, all four deoxynucleotides, and one of the four dideoxynucleotides are allowed to react. Consider the reaction mixture containing the primer, template, DNA polymerase, the four deoxynucleotides, and dideoxycytidine. The newly synthesized DNA will be complementary to the template DNA. However, DNA polymerase will occasionally incorporate dideoxycytidine into the growing chain, resulting in termination of the growing chain. Dideoxycytidine is incorporated into the growing chain only when deoxyguanosine is the complementary base present in the template DNA. If the reaction was carried out properly, the products of the reaction are DNA fragments of varying lengths, which are complementary to the template DNA. All fragments terminated with the incorporation of dideoxycytidine, corresponding to the point when DNA polymerase encountered deoxyguanosine in the template DNA. The only difference in the other three reactions is that a different dideoxynucleotide is used in each. The reaction products are then separated via gel electrophoresis. In the past, isotopic labels were used to visualize components present in the mixture. The sequence is then read directly from the gel (Fig. 14.13). The sequence of the template may then be determined, since it is complementary.

One of the initial goals of the Human Genome Project was the development of technology that could increase the rate at which DNA could be sequenced. Traditionally, isotopic labeling was used for the detection of DNA fragments. Sequencing using isotopic labels was a very time consuming process. A great deal of

human skill was needed for the interpretation of band patterns. Also, it was necessary to transcribe the data once they had been compiled. Furthermore, radioisotopes pose health problems and are costly. As sequencing technology progressed, the reading of audioradiographs became a limiting step in the process. The use of laser induced fluorescence (LIF) detection offered an alternative to radiolabeling. LIF detection offered the possibility of real time, automated detection. Sequence information could be stored directly by computer, eliminating possible data transcription errors. The exposure time necessary when using radiolabels is eliminated with LIF detection since detection is real-time. Furthermore, software may be written for the interpretation of data, eliminating the need for skilled personnel to read the data. DNA sequencing with LIF detection offers substantial advantages over isotopic labeling, with respect to speed and safety. Consequently, LIF detection is now the most common method of detection used for DNA sequencing.

While DNA sequencing by slab gel electrophoresis has been the primary method used in the past, sequencing by capillary gel electrophoresis is fast becoming the dominant technique. Sequencing rates in slab gel electrophoresis can be increased by operating the gels at high voltages. However, this produces excessive heat. Gel-filled capillaries allow for the use of high electric field strengths. Due to the high surface to volume ratio associated with capillaries, heat is dissipated rapidly, allowing for high separation voltages. Resolution of capillary based systems is generally better than slab gels and read lengths are up to 25 times longer when using gel-filled capillaries [95]. In order to match the throughput of DNA sequencing by capillary gel electrophoresis to that of slab gels, multiple capillary instruments must be used. The first capillary array instrument was developed by Mathies and coworkers [96, 97], and an integrated capillary array electrophoresis (CAE) system for the simultaneous processing of 96 samples in 48 electrophoresis channels has been devised [98]. Dovichi has also designed capillary-based instruments for DNA sequencing [95, 99, 100].

### DNA sequencing with visible fluorophores

The use of fluorescent labels with DNA sequencing was first demonstrated in 1986 [101–103]. Ansorge and coworkers developed a DNA sequencing method that used a primer labeled with rhodamine [103]. The products of the sequencing reactions were separated on four different lanes. Excitation was accomplished from a single laser and detection was achieved through the use of photodiodes. Smith and coworkers developed a DNA sequencing method which used a primer labeled with four different fluorescent tags [101]. The sequencing products were then combined and separated on a single lane. The sequence analysis was based on the different spectral characteristics of the chosen dyes. An advantage of using four dyes is that the separation occurs in one lane. Consequently, the throughput of the method is improved four times. The use of fluorescent detection schemes in DNA sequencing also allows for longer read lengths with respect to isotopic labelling. When radioactive labels were used, the separation had to be stopped when the fastest moving fragment reached the end of the plate. As a result, resolution was poor

for the longer fragments since they did not travel as far in the gel. To accommodate this loss of resolution, smaller lengths of DNA were used. With fluorescence detection, the excitation source is fixed at the end of the capillary or gel. All fragments must traverse the length of the gel or column in order to be detected. Consequently, the resolution of the larger fragments is much better, allowing for longer read lengths with respect to isotopic labelling.

Karger and coworkers developed a capillary gel electrophoretic method for sequencing that uses primers labeled with four dyes; FAM, JOE, ROX, and TAMRA (Fig. 14.14) [104]. The dyes used by Karger are commercially available fluorescein and rhodamine derivatives (see earlier section on visible absorbing dyes). Gel-filled capillaries have been shown to have distinct advantages over conventional slab gels. They allow for the use of higher applied voltages since capillaries dissipate heat more efficiently than slab gels, resulting in rapid, high resolution separations [95, 105–106, 107, 108]. The instrument design uses two lasers, an argon ion laser at 488 nm and a helium-neon laser at 514 nm, and two detection windows (Fig. 14.15). Detection limits for the dye labelled primers are in the low picomolar range (0.7–3.5 pM). Dovichi and coworkers describe a similar method which utilizes the same four dye-labeled primer [95], however, a filter wheel design is used for detection (Fig. 14.16).

In an effort to simplify detection schemes, two dye sequencing methods have also been developed [99, 100] (Fig. 14.17). TAMRA and ROX were used to label the primers. In one Sanger reaction, TAMRA labeled primer was extended in the presence of ddATP and ddCTP. The concentrations of ddATP and ddCTP used in the reaction were adjusted to give a 3:1 peak height ratio. Consequently, the termination fragments are distinguishable on the basis of peak height. Similarly, ROX labeled primer was extended in the presence of ddGTP and ddTTP.

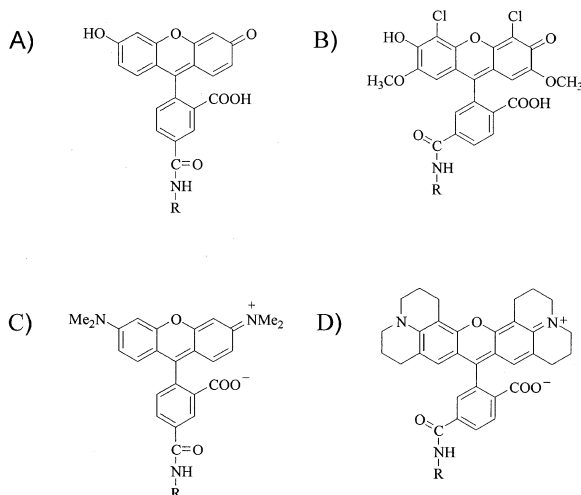


**Fig. 14.14** Structures of the four visible dyes used in DNA sequencing: A) FAM, B) JOE, C) TAMRA and D) ROX. R denotes a linker between the chromophore and the nucleotide primer.

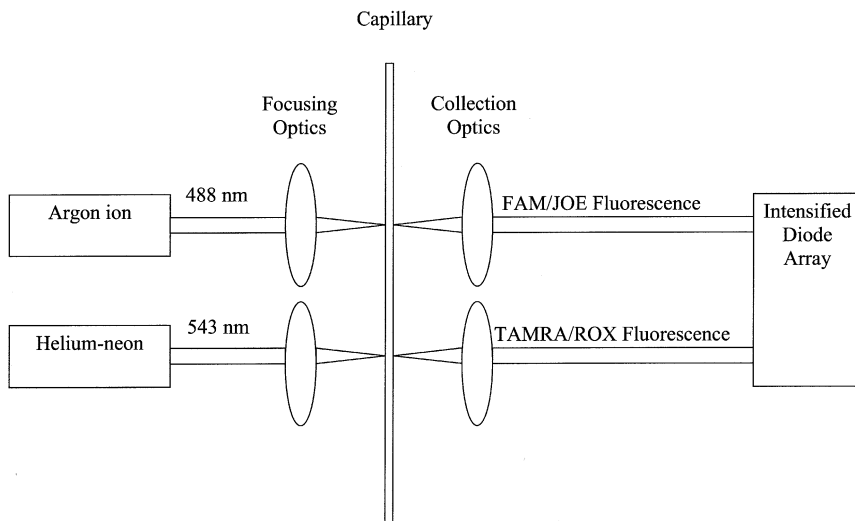


**Fig. 14.15** Schematic of two-laser, two-detection window, four-dye DNA sequencing instrumentation developed by Karger and co-workers. Adapted from ref. 104.

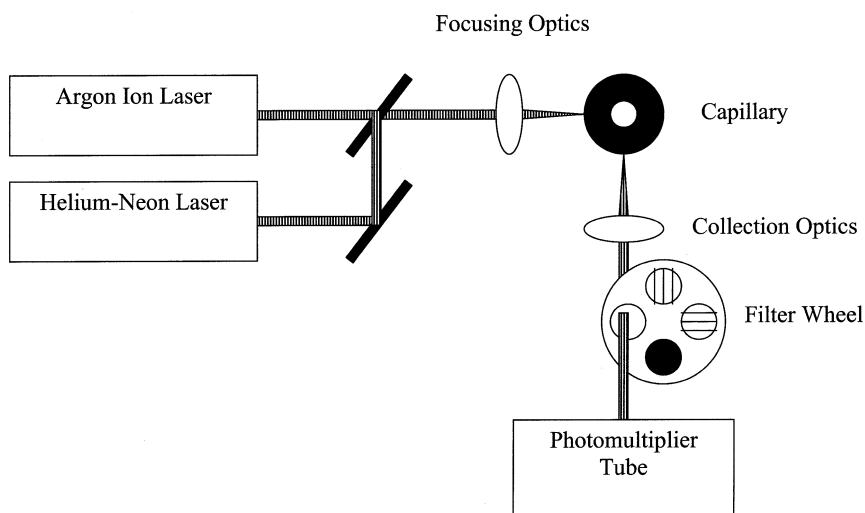


**Fig. 14.16** Schematic of two-laser, filter wheel, four-dye DNA sequencing instrumentation developed by Dovichi. Adapted from ref. 93.

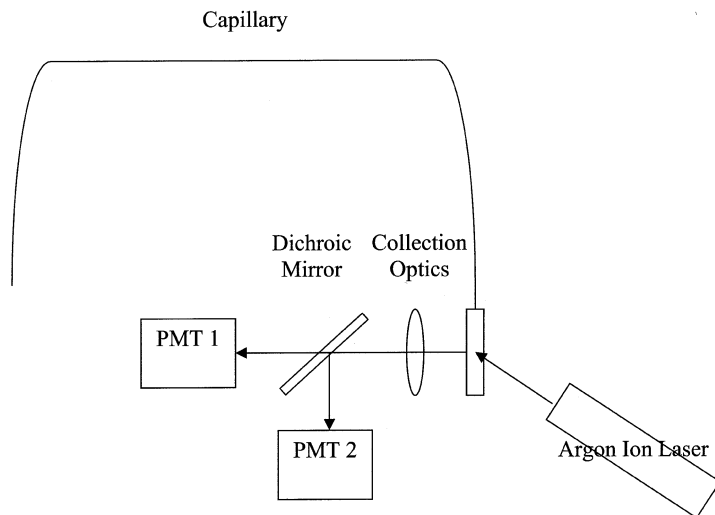


**Fig. 14.17** Schematic of one-laser, dual detector, two-dye DNA sequencing instrumentation.  
Adapted from ref. 99 and 100.

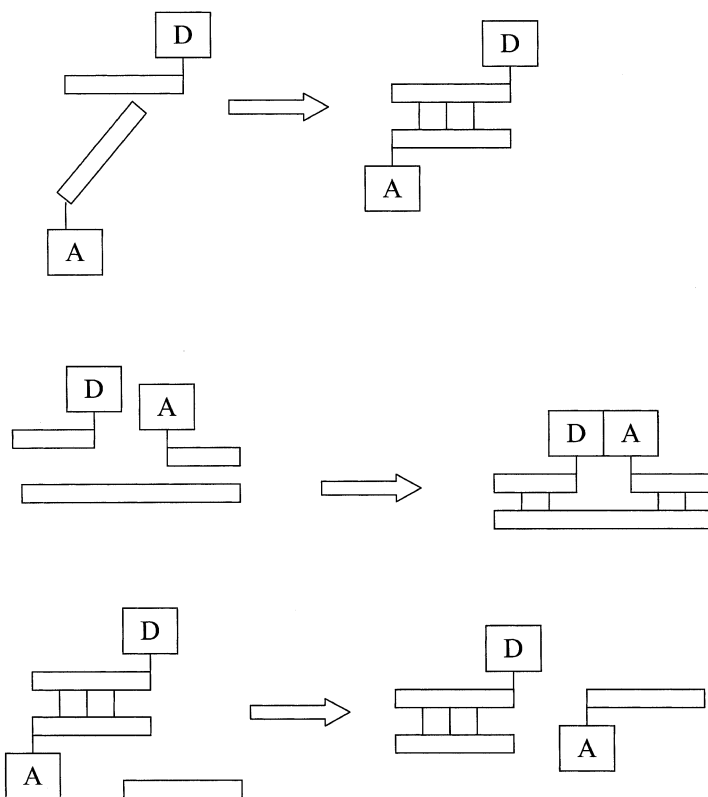


**Fig. 14.18** Examples of various energy transfer schemes. D is the donor and A is the acceptor.

Again, the concentrations of the dideoxynucleotides were adjusted to give a 3:1 peak height ratio.

When using multiple dyes for DNA sequencing, it is advantageous for the dyes to have comparable emission intensities upon excitation at a common wavelength, so that the emission intensity of each dye is comparable. Furthermore, the dyes should display distinct emission spectra so that they are discernible from each other. This is difficult to accomplish. However, the use of fluorescence energy transfer allows for simultaneous optimization of both of these requirements. The use of donor-acceptor pairs allows for the equalization of emission intensity at a common excitation wavelength. The use of energy transfer fluorescent dye labeled primers offers improved sensitivity with respect to single dye labeled primers [90, 101, 109, 110]. Examples of energy transfer schemes are shown in Fig. 14.18.

Mathies and coworkers have performed work on energy transfer using FAM, a fluorescein derivative, as the donor, and FAM, JOE, TAMRA, and ROX as the acceptors (Fig. 14.19) [111]. The acceptor dyes exhibit fairly distinct emission maxima at 525, 555, 580, and 605 nm, respectively, and all energy transfer fluorescent dye

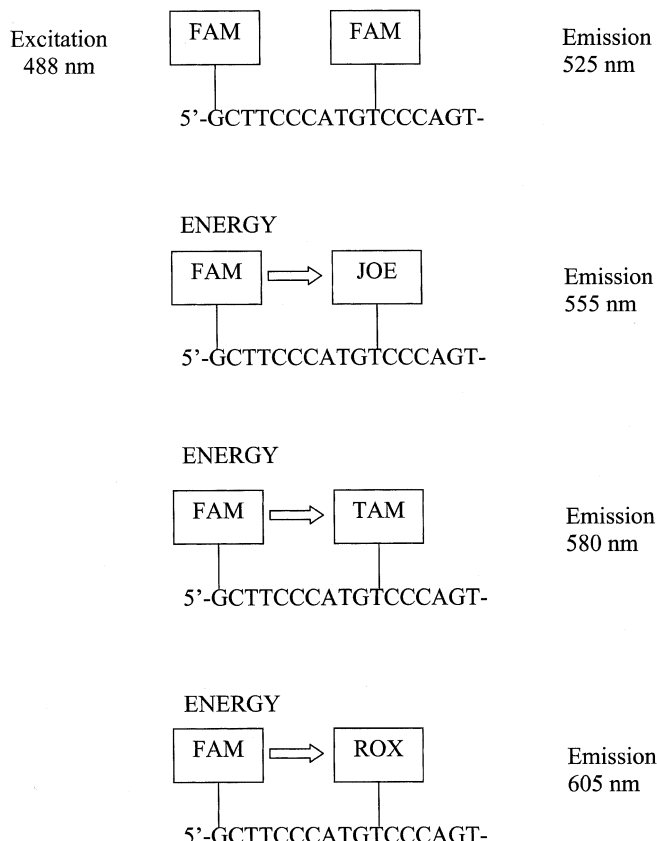


Fig. 14.19 Energy transfer scheme utilised by Mathies and coworkers.

labeled primers exhibited a strong absorbance at the 488 nm line of the argon ion laser. The group systematically adjusted the distance between the donor and acceptor pair in order to arrive at the optimal characteristics for the desired application. While fluorescein and rhodamine derivatives are the most common visible dyes used for DNA sequencing, other groups are using cyanine dyes [71], as well as DNA-intercalating dyes such as thiazole orange, to label DNA [69, 70].

Further work done by Mathies and coworkers utilized a cyanine dye energy transfer system [112]. The cyanine donor was attached at the 5' end of the primer. Fluorescein or rhodamine derivatives were used as the acceptor and were located 10 bases away from the donor. The 488 nm line of an argon ion laser was used for excitation. The fluorescence intensity of the energy transfer dyes was 1.4 to 24 times stronger than when the individual acceptor chromophores were excited at the 488 nm line. The cyanine dye used as the donor showed improved photostability and higher extinction coefficients, with respect to FAM. The cyanine dye exhibited a large absorption cross section but a low quantum yield. This increased the Stoke's shift of the acceptor dyes and minimized cross-talk between the detection channels. The system design illustrates that dyes with high absorption cross sections but low quantum yields may be used for improved energy transfer systems, thereby greatly expanding the repertoire of available donor dyes.

### DNA sequencing with NIR fluorophores

While the use of visible fluorescent dyes for DNA sequencing offers multiple advantages over traditional methods of detection, these dyes absorb and fluoresce in a region of the spectrum that is prone to autofluorescence from the sample matrix, gel, or from impurities. The result of these interferences is an overall increase in noise, resulting in a loss of sensitivity. Recently, near-infrared fluorophores have been used as labels in DNA sequencing in an effort to increase sensitivity [113–115]. The NIR portion of the spectrum is generally defined as the region between 700 and 1200 nm. NIR dyes have good molar extinction coefficients ( $\sim 150,000\text{--}250,000 \text{ M cm}^{-1}$ ) and quantum yields in the range 0.05 to 0.5. Since biological molecules do not possess intrinsic fluorescence in this spectral region, NIR dyes are well suited for bioanalytical applications [116–126]. Furthermore, the autofluorescence exhibited by gels, glass, and solvents is nonexistent in the NIR region. In addition, scatter noise (Rayleigh and Raman) is reduced with NIR dyes, since noise intensity is related to the wavelength of detection by  $1/4$ . As a result of the decreased noise levels associated with the use of NIR dyes, detection is not limited by noise levels, but rather by detector performance. Consequently, laser induced fluorescence detection methods using NIR fluorophores, are potentially more sensitive than detection schemes that employ visible fluorophores.

Some of the major disadvantages associated with visible LIF detection are the cost and complexity associated with the necessary equipment. LIF detection in the NIR region requires the use of solid-state components. Semiconductor diode lasers have proven to be optimal excitation sources for NIR fluorophores. Diode lasers are inexpensive, compact, have long operating lifetimes, can be operated in

continuous or pulsed mode, and provide satisfactory power [127]. Another attractive feature is that diode lasers are available at a variety of wavelengths (635, 750, 780, 810, and 830 nm).

Photomultiplier tubes are the most common signal transducers used in visible LIF detection. PMTs are ideal for work in the visible region of the spectrum. However, their quantum efficiencies deteriorate rapidly at longer wavelengths. Even red-sensitive PMTs only possess quantum efficiencies of 0.01 at 800 nm [127]. For these reasons PMTs are poor choices for signal transducers when working in the NIR region. However, photodiodes are an excellent choice as signal transducers when working in the NIR region, since silicon based semiconductor materials have here high quantum efficiencies, typically 80 % [127]. In most cases avalanche photodiodes are used since they posses internal amplification, unlike conventional photodiodes.

Soper and coworkers have developed instrumentation for highly sensitive DNA sequencing by capillary gel electrophoresis using NIR LIF detection [115]. The nucleotide sequence was determined using a single lane/single dye technique. An M13 sequencing primer was labelled at the 5' end with a tricarbocyanine dye with an isothiocyanate functionality. The molar concentrations of the dideoxynucleotides were varied such that the molar ratios were 4:2:1:0 (A:C:G:T). Base identification was based on peak intensity. A comparison was done with the NIR LIF system versus visible LIF. The 488 nm line of an argon ion laser was used as the excitation source. An M13 sequencing primer was labelled with the visible fluorescent dye TAMRA. The noise generated by the gel matrix was 20 times larger with the argon ion laser than it was with the Ti:Saphire laser. The quantum yield of the visible dye was 0.9 vs. 0.07 for the NIR dye. Despite the lower quantum yield of the NIR dye, the detection limit for the NIR dye labeled primer was 34 zmol, as opposed to 1.5 amol for the visible dye labeled primer. The significant improvement in the detection limit of the NIR dye, roughly two orders of magnitude, was attributed to the minimal background interference at the wavelength of detection.

Patonay and coworkers have done work with NIR LIF detection for DNA sequencing on slab gels [114]. Four heptamethine cyanine dyes were used in the study, although the four line, one dye method was employed for sequencing. A modified thymine base with a terminal amino linker was incorporated into the primer. All dyes possessed an isothiocyanate functionality which allowed for conjugation. Reverse phase HPLC was used to remove excess dye. Sequencing was carried out on a Li-Cor model 4000 DNA sequencer (Figs. 14.20 and 14.21). 500 bases were read with a 1 % error rate. Individual bands consisting of 0.1 fmol were routinely detected.

While spectral discrimination is the most common method of base calling used, temporal discrimination offers several advantages: (1) The lifetime of the fluorophore is independent of concentration, (2) fluorescence lifetime values may be determined with more accuracy than fluorescence intensity, (3) temporal measurements are not hindered by broad emission profiles, and (4) a single detection channel may be used. Soper has developed a method using heavy atom modified NIR dyes for base calling in DNA sequencing using temporal discrimination [74]. One

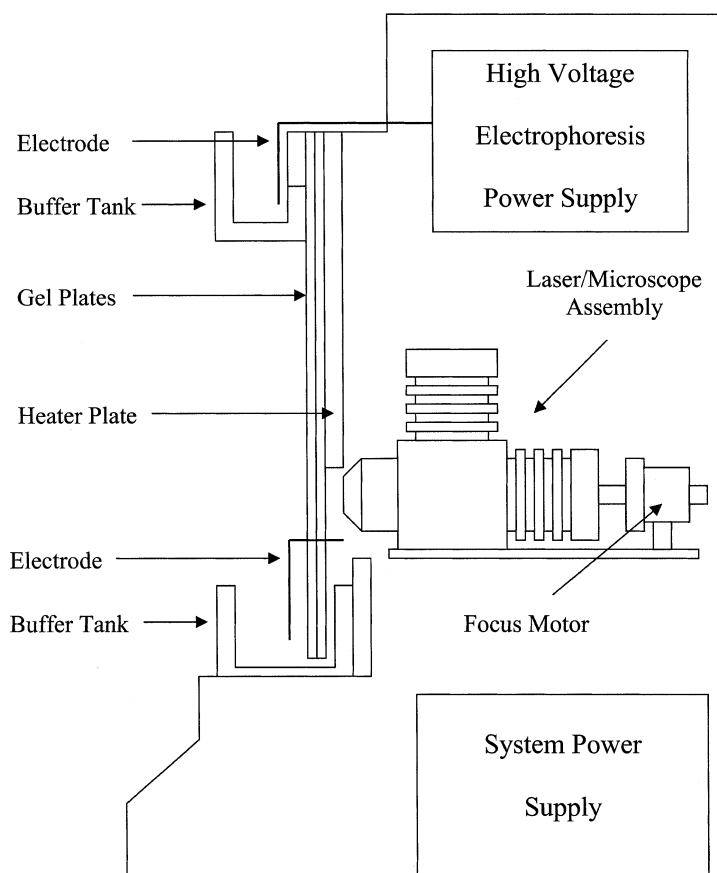


**Fig. 14.20** The LI-COR DNA sequencer. Adapted from ref. 113.

of the major problems associated with lifetime determinations is the complexity of the apparatus required to carry out the measurements. Many problems associated with lifetime determinations for DNA sequencing are alleviated by using NIR fluorescence. Soper et al. attained very high precision due to the lack of interfering photons associated with the NIR region. In order to obtain fluorophores with distinct decay times, the photophysical properties of tricarbocyanine dyes were modified by the incorporation of a heavy atom. This resulted in a change in the fluorophores' singlet state photophysics (quantum yield and lifetime), due to increased inter-system crossing [128–130]. The emission and absorption maxima of the fluorophores were unchanged by the heavy atom modification. The electrophoretic mobility remained unchanged, negating the need for post-run corrections for mobility discrepancies often encountered in multiple dye approaches. The dyes developed by Soper could serve as ideal labels for DNA sequencing applications since only one excitation source is required and detection may be accomplished on a single channel.

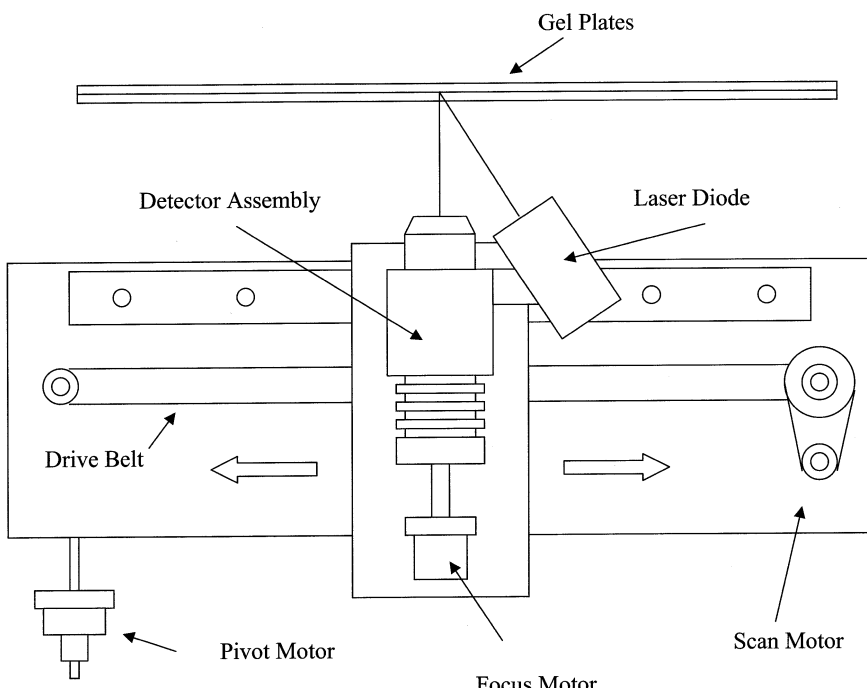


**Fig. 14.21** Top view of the LI-COR DNA sequencer. Adapted from ref. 113.

### Immunochemistry

Immunoassays are an analytical technique based on the highly specific interaction between an antibody and an antigen. Due to their ability to measure trace amounts of analyte in complex matrices, immunoassays are widely used in clinical, pharmaceutical, and environmental chemistry. Berson and Yalow were the first to use antibodies as an analytical tool, reporting picogram detection of insulin [131]. Immunoassays are the primary method used in diagnosing diseases such as acquired immunodeficiency syndrome (AIDS) [132], cysticercosis [133], and schistosomiasis [134, 135]. Due to their widespread use, growth in the field has been tremendous over the past decades.

One of the advantages of the immunoassay technique is the wide variety of formats available. Generally speaking, immunoassays are carried out using either competitive or non-competitive formats. Competitive assays may be carried out by labelling either the antibody or the antigen, depending on what the analyte is. If the analyte is an antibody, then antigen is coated on a support surface. Labelled antibody is then added. Finally, unlabeled antibody from the sample is added. The labelled and unlabeled antibody bind competitively on a limited number of sites, i.e., the coated antigen. The amount of antibody present is determined by the change in signal (Fig. 14.22). Alternatively, if the analyte is an antigen, then

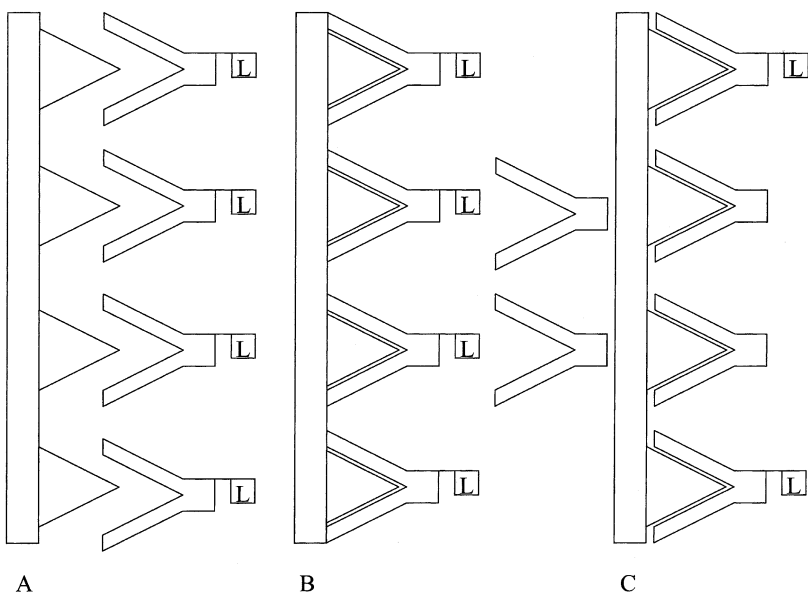


**Fig. 14.22** Illustration of a competitive immunoassay procedure where the analyte is an antibody. A) Antigen is coated onto a solid support and labelled antibody is introduced. B) Analyte is introduced, which competes with labelled antibody for binding sites. C) The amount of label is quantified.

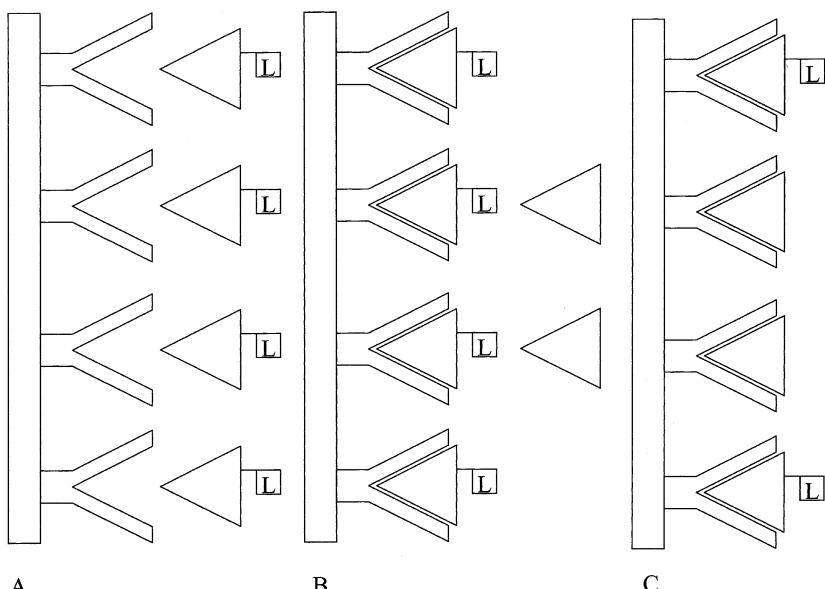


**Fig. 14.23** Illustration of a competitive immunoassay procedure where the analyte is antigen. A) Antibody is coated onto a solid support and labelled antigen is introduced. B) Analyte is introduced, which competes with labelled antigen for binding sites. C) The amount of label is quantified.

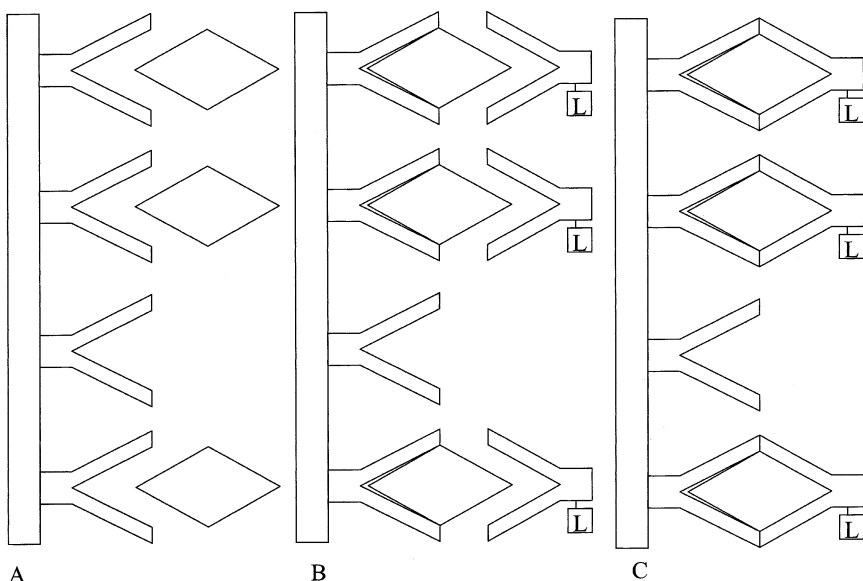


**Fig. 14.24** Illustration of a non-competitive ('sandwich') immunoassay format. A) Antibody is coated onto a solid support (the 'capture' antibody) and antigen from the sample is introduced. B) A second labelled antibody (the detection antibody) is introduced. C) The amount of labelled antibody is quantified.

antibodies are fixed to a solid support. Labelled antigen is then added. Finally, unlabeled antigen from the sample is added. The labelled and unlabeled antigen compete for the binding sites on the antibody. The amount of antigen present in the sample is determined by signal change. Signal intensity decreases with increasing analyte concentration (Fig. 14.23).

Non-competitive assays operate on a different principle. The basic principle involves the binding of a limited amount of one reagent to an excess of the second reagent. Most often, the solid support is saturated with antigen. Excess antigen is removed during a washing step. The sample antibody is then added. In the final step, a second labelled antibody, specific for the primary antibody, is added. Unlike competitive assays, signal intensity increases with analyte concentration in non-competitive assays (Fig. 14.24).

In the early stages of immunoassay technology, radiolabels were employed as tracers. Isotopic labels were popular due to their high sensitivity, selectivity, and unobtrusive nature. The use of radioactive labels does have drawbacks, such as health and safety issues, short shelf life, cost, long exposure times, and disposal problems. Due to these drawbacks, there has been considerable growth in the development of nonisotopic labels for use in immunoassays. Consequently, radioactive labels are now rarely used in immunoassays. Several criteria needed to be met in order for nonisotopic labels to become a viable alternative to radioactive labels: 1. Noniso-

pic labels needs to match radioisotopes in terms of sensitivity; 2. the label needs to be easily coupled to the antibody or antigen; 3. the label should be nontoxic and amenable to automation; and 4. the label should not affect the antibody-antigen interaction [136].

Enzyme-linked immunosorbent assay (ELISA) is perhaps the most popular immunoassay format, due to its versatility and high sensitivity. In ELISA a solid support is coated with antibody and antigen is then added. Hereafter, a second antibody covalently bound to an enzyme is added. Following an appropriate incubation period and washing steps, enzyme substrate is added, resulting in the appearance of a colored or fluorescent product. A major advantage of this method is that with a high turnover number associated with the enzyme a very high sensitivity can be reached. A single enzyme may produce as many as 1000 product molecules. Horseradish peroxidase (HRP) and alkaline phosphatase are common enzyme labels. There are, however, disadvantages associated with the use of enzyme labels. The large size of the enzyme can affect the antibody-antigen interaction and the assays are quite sensitive to temperature and pH. Finally, the enzyme may cause non-specific binding.

### Immunochemistry with visible fluorophores

The use of fluorescent labels is a superior alternative to enzyme labels. While some enzyme labels do produce fluorescent products, most produce colored substrate products, necessitating the use of absorbance detection. Due to the high background noise associated with absorbance detection, the method is inherently less sensitive than fluorescence detection. Fluorescent labels are generally smaller than enzyme labels and therefore are less likely to interfere in antibody-antigen interactions or promote nonspecific binding. Fluorescein and rhodamine derivatives are commonly used in fluorescence immunoassays. A typical conjugation reaction involves a dye functionalized with an isothiocyanate group that is reactive toward primary amines at basic pH. Factors that affect the sensitivity of fluorescence immunoassays are autofluorescence from matrix components (such as bilirubin), scattering of excitation light, fluorescence quenching, and photobleaching processes. The instrumentation used to measure fluorescence is also a key component in method sensitivity. The use of a suitable fluorophore is critical in the development of sensitive assays.

An ideal fluorophore should have the following characteristics: a high molar absorptivity and a high quantum yield, a large Stokes' shift in order to minimize light scatter, quick efficient coupling reactions, good solubility under physiological conditions, low non-covalent affinity for biomolecules in order to minimize nonspecific interactions, photostability, and small label size relative to the molecule to which it is to be attached. Variations of the basic fluorescence immunoassay format may be used in order to tailor photophysical properties to a specific application or to overcome some of the disadvantages associated with fluorescence detection. Examples of these variations include fluorescence polarization, time-resolved fluorescence and fluorescence energy transfer.

There is presently still much research on novel visible fluorescent labels for immunoassay. Examples are fluorinated fluoresceins [137], BODIPY dyes [138] and Alexa Fluor dyes [139]. The BODIPY fluorophores were designed as replacements for fluorescein, tetramethylrhodamine and Texas Red. The Alexa Fluor series of dyes, which presently span the whole visible and part of the near-infrared region, have several advantages, such as a high absorbance at wavelengths of maximal output of common excitation sources, efficient fluorescence and high photostability of the bioconjugates. Additionally, Alexa Fluor dyes are well soluble in water, which simplifies bioconjugation and lowers the danger of precipitation and aggregation of the conjugates. The spectra are also not affected by pH between 4 and 10.

### Immunochemistry with NIR fluorophores

The use of near-infrared fluorophores as labels in fluorescence immunoassays provides several advantages over visible fluorophores. When using visible dyes, sensitivity is ultimately limited by interference resulting from light scatter, quenching effects, and matrix autofluorescence. Furthermore, visible lasers have the disadvantages of high cost, relatively short operational lifetimes, size, maintenance cost, and limited wavelength range [140]. Near-infrared fluorescence immunoassays have the ability to overcome many of the limitations imposed by visible LIF detection schemes. Detection in the NIR region of the spectrum requires the use of solid-state components. Laser diodes, characterised by long operating lifetimes, low cost, and small size, are ideal as excitation sources. Furthermore, the emission of available laser diodes is compatible with several classes of polymethine cyanine dyes. Avalanche photodiodes are used for detection in the near-infrared region. Avalanche photodiodes have long operating lifetimes, are inexpensive, have internal amplification, and have high quantum efficiencies in the near-infrared region. All of the advantages associated with detection in the near-infrared region allow for rugged, compact, and sensitive instrumentation.

Boyer and coworkers were the first to develop instrumentation for near-infrared fluorescence immunoassays [117]. Williams and coworkers also developed instrumentation for detection of near-infrared fluorescence in solid-phase immunoassays [118]. The instrument consists of a semiconductor laser coupled with a fiber-optic cable, a silicon photodiode for detection, a sample stage coupled to a motor drive, and a data acquisition device. The instrument could detect 500 pM concentrations of human immunoglobulin G (IgG) on a nitrocellulose matrix. The assay was performed in roughly two hours. The detection limits obtained on this instrument were comparable to that obtainable with ELISA. The assay developed by Williams suffers from excessive scatter generated from the membrane, nonspecific binding, and incompatibility with conventional microtiter plate immunoassay formats [140]. Patonay and coworkers developed a NIR fluorescence immunoassay apparatus that overcame many of these limitations. Baars and Patonay have evaluated a novel NIR dye NN382 (Fig. 14.25) for the ultrasensitive detection of peptides with capillary electrophoresis [141]. A solid-phase, NIR fluorescence immunoassay system was

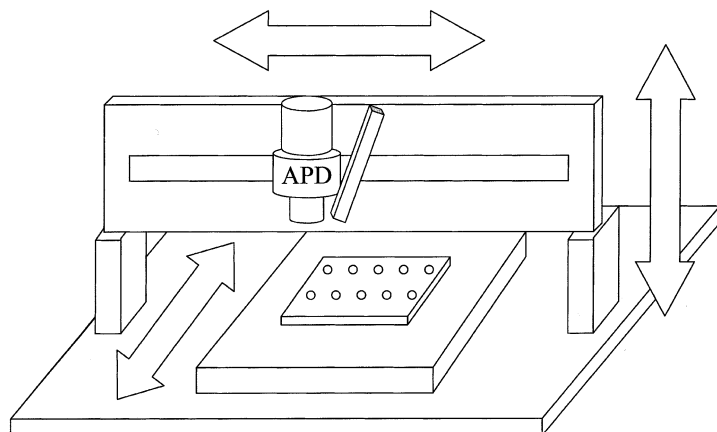


**Fig. 14.25**  
Schematic  
illustration  
of near-infrared  
fluorescence  
immuno-  
assay  
instrumen-  
tation.

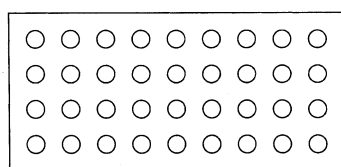
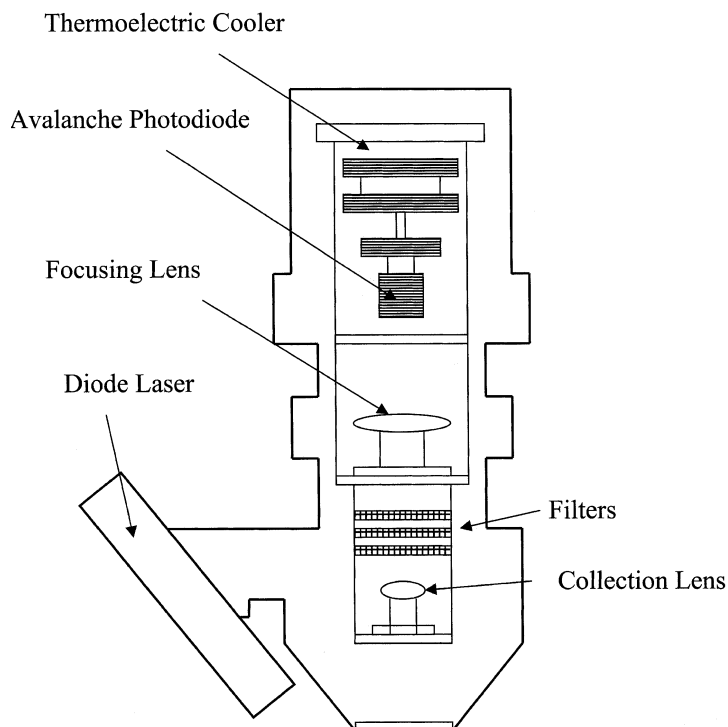


**Fig. 14.26** Schematic illustration  
of the avalanche photodiode  
detector used in the NIR fluo-  
rescence immunoassay instrumen-  
tation.

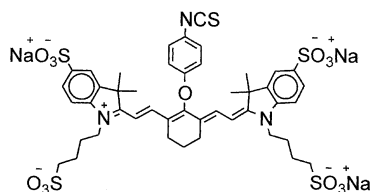


**Fig. 14.27** Structure of NIR dye NN382.

developed by coupling a Li-Cor 4200 fluorescence microscope with an orthogonal scanner as illustrated in Figs. 14.26 and 14.27.

Recently several novel NIR fluorescence probes have been reported. Heptamethine cyanine dyes have previously been used for DNA sequencing, metal ion detection, protein labeling, and pH and hydrophobicity determinations [142]. The novel dye NN382 has a high molar adsorptivity (180,000) and a good quantum yield for the dye-protein conjugate (0.59) [143, 144]. The isothiocyanate functionality present on the dye is reactive toward the primary amine groups of the antibody under basic conditions. The sulfonate groups present on the dye increase its aqueous solubility and minimize nonspecific binding to the polystyrene matrix. Numerous microtiter plates were evaluated for background scatter and the one which produced the least noise was chosen for the experiments. It was necessary to optimize the conditions, i.e., temperature, pH, molar ratio, and reaction time, for conjugation of NN382 to goat anti-human IgG. Deviations from the optimal derivatisaton conditions result in deterioration of assay sensitivity. The assay developed was able to detect 20 pM human IgG, resulting in roughly an order of magnitude improvement in sensitivity as compared to traditional labels. Additionally, the assay was less time-consuming than ELISA.

#### NIR fluorophore-based immuno and DNA-probes

It is presently attractive to utilise NIR fluorescent dyes in optical fiber sensors, allowing for miniaturization, small analyte volumes, and the ability to carry out the analysis in remote locations, while retaining the advantages of NIR detection, such as the lower background interference. Danesvar et al. developed a NIR fiber optic immunosensor (Fig. 14.28), which was applied to the detection of human IgG [145], legionella pneumophila serogroup 1 (LPS1) [146] and the pesticide bromacil [147]. Generally, similar or slightly higher detection limits could be obtained compared to that of an ELISA assay. Fiber optic NIR-fluorescence probes have recently also been used for the assessment of heterogeneity of immobilised antibodies in a fiber optic sensor [148]. The homogeneity of antibody preparations and site-directed immobilisation of the antibodies via the Fc domain clearly yielded a lower heterogeneity.

Although NIR-fluorescence markers are now widespread in bioanalysis, further improvements are still needed to raise the power and lower the cost of the current techniques for applications in high-throughput and *in vivo* experiments. An array

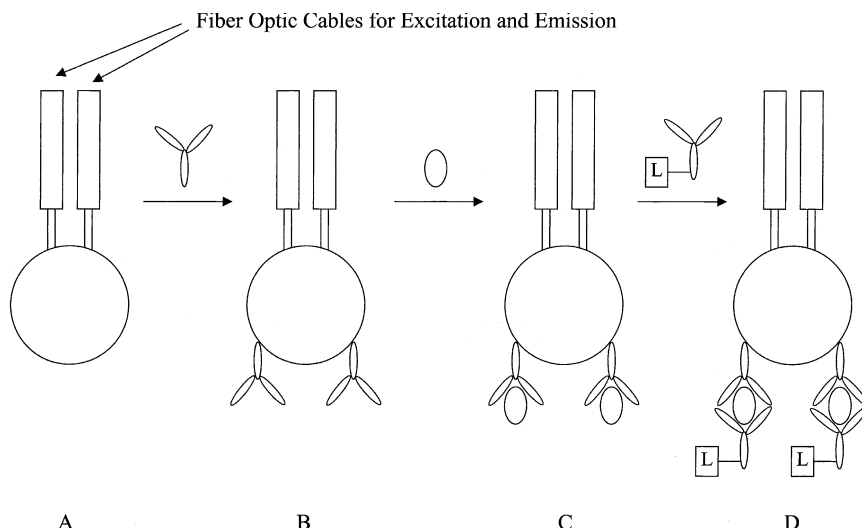


**Fig. 14.28** Schematic illustration of the NIR-fluorescence immunoprobe as described by Danesvar et al. A) Fiber optic cables are used for remote excitation and emission collection from a sensitive terminal prepared from polymethyl-

methacrylate or polystyrene. B) A primary antibody is coated onto the surface of the terminal. C) Antigen from the sample is introduced. D) The labelled secondary antibody is quantified.

immunosensor based on NIR fluorescence has been described by Ligler and co-workers [149]. The system consisted of a diode laser at 635 nm and a cooled CCD detector. Samples were introduced by a fluidics system and the analysis was based on a sandwich assay using the Cy5 dye. With this set-up three different analytes could be detected simultaneously.

Another field of work is directed to DNA analysis with NIR fluorophores. Pilevar et al. have recently described a fiber optic sensor for DNA hybridisation, in which the dye IRD 41 (of LI-COR Inc., Lincoln, NE, USA) was used for the real-time hybridisation of RNA of Helicobacter Pylori at picomolar concentrations [150]. Recently optical nanosensing in which nanometer-scale probes are used for intra-cellular measurements has also been pioneered [151].

#### 14.2.2.4 Fluorescence Polarisation Methods

Fluorescence polarisation spectroscopy is still very much used to probe the rotational dynamics of single molecules, either on surfaces or in solution [152]. In bioanalytical assays the fluorescence emission intensity is measured as a function of rotational speed. When a solution of fluorophores is excited with polarised light, the fluorophores selectively absorb those photons that are parallel to the transition moment of the fluorophore, resulting in photoselective excitation. The fluorophore molecules rotate to varying extents during the fluorophore lifetime. If the fluores-

cence emission is polarised, then small, rapidly rotating fluorophores will give small signals and fluorophores that rotate at slower rates will give large signals. Hence, fluorescence emission intensity is a function of rotational speed, which is correlated to size. In a fluorescence polarisation immunoassay, a labelled antigen is excited with polarised light. When the antibody binds to the antigen, the rotation of the complex is much slower than that of the labelled antigen and the emission intensity increases. It is important that the labelled antigen is small so that its signal may be differentiated from the signal of the immunocomplex. Although fluorescence polarization assays have a limited dynamic range, they are useful for identification or quantification of small molecules. With state-of-the-art optical microscopes and novel fluorescent probes attached to specific protein domains it has also recently become possible to quantify angular rotations in individual protein molecules that mediate specific functions [153].

There have been several new developments in fluorescence polarization immunoassay (FPIA). Lackowicz and Terpetschnig reviewed the use of long-lifetime metal–ligand complexes in fluorescence polarization assays [154, 155]. New complexes with Re(I) and Ru(II) were described for the highly sensitive detection of high-molecular weight analytes by FPIA. Laser-induced fluorescence polarisation detection has been used by Yatscoff and coworkers in capillary electrophoresis detection (CE-LIFP) [156]. For the analyte cyclosporin picomolar detection limits were attained.

#### 14.2.2.5 Time-resolved Fluorescence

One of the factors, which significantly decreases sensitivity in fluorescence immunoassays, is the background fluorescence exhibited by the sample matrix. This ‘autofluorescence’ decreases exponentially as a function of time. Therefore, it is favourable to use fluorophores with a very long lifetime and use time-resolved fluorescence detection (TR-FIA). In TR-FIA the excitation source is pulsed and the detection is gated such that the detector does not become ‘active’ until the autofluorescence emission has decayed. This gives a very effective elimination of the fluorescence background. Rare earth metals (e.g. europium) complexed to organic ligands have been much used as labels, due to the very long lifetime of their excited state [157–160]. Additionally, these complexes display a high quantum yield, a large Stokes’ shift and very narrow emission lines.

The lanthanide chelates have found general application in fluorometric immunoassays and also form the basis of one of the more popular immunoassay platforms: the DELFIA system by Perkin-Elmer/Wallac. To date a large number of lanthanide chelates have been synthesised and investigated as labels in TR-FIA [160]. In a first generation of reagents, the lanthanides still had to be extracted into a stable soluble complex to give an optimal signal, but by now assays have also been designed in which the extraction step can be omitted. This enables more simplified TR-FIA assays and also gives the possibility of homogeneous assays and micro-imaging applications. Already a number of studies have employed

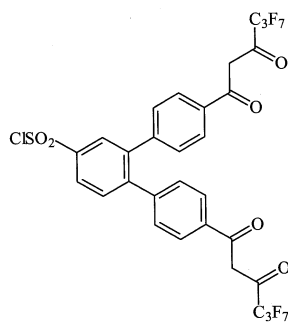


**Fig. 14.29** Structure of the novel label 4,4'-bis (1'', 1'', 1'', 2'', 2'', 3'', 3'', heptafluoro-4'', 6''-hexanedion-6''-yl)-chlorosulfo-o-terphenyl (BHHCT) for TR-FIA [161]. The compound can be covalently bound to proteins and functions as a tetradendate ligand for complexation of  $\text{Eu}^{3+}$ .

the novel label BHHCT (Fig. 14.29) for TR-FIA. This dye enabled much lower detection limits in a number of assays: e.g.  $3.6 \text{ pg ml}^{-1}$  for an assay of IgE [161] and  $46 \text{ fg ml}^{-1}$  for  $\alpha$ -fetoprotein (AFP) [162]. More recently, various other reports have appeared on improvements of TR-FIA immunoassays. Zuber et al. developed a mathematical model for the kinetics of a homogeneous immunometric assay with TR-FIA [163]. Europium chelates have been used for the determination of prostate-specific antigen on individual microparticles [164]. A dual-label TR-FIA method has been reported for the simultaneous detection of phenytoin and phenobarbital [165] and for the simultaneous determination of pregnancy-associated plasma protein A and the free  $\beta$ -subunit of human chorionic gonadotropin (hCG) [166].

#### 14.2.2.6 Fluorescence Excitation Transfer

Fluorescence excitation transfer (or fluorescence resonance energy transfer), FRET, is a non-radiative process of energy transfer from one fluorophore (the donor) to another fluorophore (the acceptor), in which excitation of the donor gives rise to a fluorescence signal at the emission wavelength of the acceptor. The process of energy transfer is efficient when the emission spectrum of the donor significantly overlaps with the excitation spectrum of the acceptor [167]. Additionally, the process depends strongly on the distance between the donor and acceptor. FRET is dependent on the inverse sixth power of the intermolecular separation. Thus, fluorescence excitation transfer may be used for enhancement of the Stokes' shift and in bioassays where the distance between two binding partners should be reported.

The first obvious use of FRET is in sandwich immunoassay. A first report along this line was presented by Ullman et al. in 1976 [168]. Wei et al. investigated 10 combinatorial pairs of conventional fluorescent dyes and assessed the optimal conditions for energy transfer [169]. Oswald et al. described a fluorescence resonance energy transfer immunoassay for human serum albumin (HSA) based on the indolium dye Sq635 (Fig. 14.10) and the benz[e]indolium dye Sq660 [83]. A detection limit of  $10^{-7} \text{ M}$  of HSA was reported.

FRET has been also used to obtain fluorescent particles in which the Stokes' shift can be significantly enlarged and to some degree controlled [170]. This is the main principle behind the TransFluoSpheres of Molecular Probes Inc (Eugene, Oregon, USA). In these microparticles more than two dyes can be used, which form a fluorescence energy transfer chain. The TransFluoSpheres are used as immunofluorescent reagents, as retrograde neuronal tracers, microinjectable cell tracers and standardization reagents for flow cytometry and microscopy (see ref. 33).

#### 14.2.2.7 Bioanalytical Applications of Fluorescent Proteins

##### **Phycobiliproteins**

Phycobiliproteins are stable and highly soluble fluorescent proteins derived from cyanobacteria and eukaryotic algae. They contain covalently linked tetrapyrroles that play a role in harvesting light in the photosynthetic reaction center. The biological process involves fluorescence resonance energy transfer from the tetrapyrrole to a pair of chlorophyll molecules [171, 172]. Because of their role in light collection, phycobiliproteins have optimized their absorption and fluorescence and reduced quenching caused either by internal energy transfer or by external factors such as changes in pH or ionic composition. For bioanalytical applications a number of phycobiliproteins are used: B-phycoerythrin (B-PE), R-phycoerythrin (R-PE) and allophycocyanin (APC). These are dyes that enable highly sensitive assay applications with the possibility for multiparameter detection. Quantum yields as high as 0.98 and extinction coefficients as high as 2,400,000 have been reported. These compounds are able to give five to ten times greater fluorescence signals than that of conventional fluorescein conjugates. The fluorescence properties of B-PE, R-PE and APC are compared in Tab. 14.6.

Bioanalytical applications of phycobiliproteins (and also green fluorescent proteins, see next paragraph) predominantly lie in flow cytometry and immunoassay [173, 174]. In particular, flow cytometers capable of collecting data from three or four chromophores are presently being developed, and polychromatic flow cytometry (PFC) will soon be a major tool for explorations in cell biology and immunology. The much enlarged amount of information enables characterisation of rare cell populations, allows identification and characterization of novel cell subsets, and identification of functionally homogeneous subsets of cells within the immune system. Recently, Baumgarth et al. have investigated multicolor cytometric systems for up

**Table 14.6** Fluorescence data of phycobiliproteins.

<b>Phycobiliprotein</b>	<b>Molecular weight</b>	$\lambda_{Max}$ (nm)	$\varepsilon$ ( $cm^{-1}M^{-1}$ )	$\lambda_{Max}$ (nm)	<b>Fluorescence quantum yield</b>
B-Phycoerythrin	240 000	546,565	2,410,000	575	0.98
R-Phycoerythrin	240 000	480,546,565	1,960,000	578	0.82
Allophycocyanin	104 000	650	700,000	660	0.68

**Table 14.7** Fluorescence data of green fluorescent proteins (from Ref. 177).

<b>Protein abbreviation/ species/colour</b>	<b>Molecular weight</b>	<b><math>\lambda_{\text{max}} \text{ (nm)}</math></b>	<b><math>\lambda_{\text{em}} \text{ (nm)}</math></b>	<b><math>\varepsilon \text{ (cm}^{-1}\text{M}^{-1}\text{)}</math></b>	<b>Fluorescence quantum yield</b>
GFP/ <i>Aequorea victoria</i> (jellyfish)/green	27 000	397	509	27 600	0.80
amFP486/ <i>Anemonia majano</i> /green	25 400	458	486	40 000	0.24
zFP506/ <i>Zoanthus</i> sp./ Yellow-green	26 100	496	506	35 600	0.63
dsRed/ <i>Discosoma</i> / Orange-Red	28 000	558	583	75 000	0.70
dsFP483/ <i>Discosoma striata</i> /blue-green	26 400	443	483	23 900	0.46
cFP484/ <i>Clavularia</i> / green	30 400	456	484	35 300	0.48

to 11 distinct fluorescent signals and two scattered light parameters for characterizing single cells also using phycobiliproteins [175].

### Green fluorescent proteins

Green fluorescent proteins from the jellyfish *Aequorea victoria* (GFP) and various other marine organisms like the *Anthozoa* species present in coral reefs provide interesting fluorescent proteins, which are increasingly used in bioassay work today. They are investigated as markers of gene expression and for protein localisation (Tab. 14.7) [176, 177]. Many of these proteins are presently commercially available from CLONTECH Laboratories Inc. (Palo Alto, CA, USA). Presently the orange-red fluorescent protein “DsRed” (trade name by CLONTECH) from the corallimorpharian *Discosoma* genus has received much interest, because its fluorescence in the red enables better suppression of autofluorescence and can be very well used in FRET experiments [178]. (DsRed is an excellent acceptor for excitation by the yellow fluorescent variants of GFP as a donor dye.) The fluorophore in green fluorescent proteins is formed from a tripeptide (Gln-Tyr-Gly) sequence in the wild type GFP by autocatalysis. It has been proposed by Gross et al. that a continued oxidation may lead to a further extension of the conjugated side chain leading to the chromophore in the DsRed protein molecule (Fig. 14.30) [179].

#### 14.2.3

### Bioanalytical Applications of Multi-photon Fluorescence Excitation (MPE)

#### 14.2.3.1 Introduction

As an interesting alternative to normal fluorescence excitation, multiphoton excitation (MPE, see next paragraph) has recently appeared as a viable method in various bioanalytical applications [180, 181]. Two-photon excitation (2PE) has been used

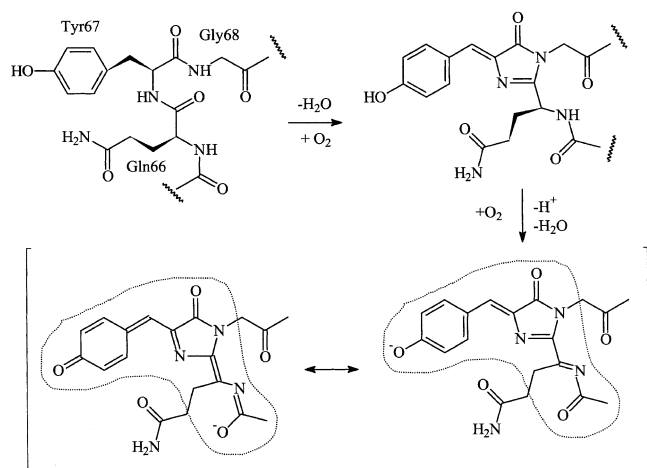


**Fig. 14.30** Proposed mechanism of formation of the red fluorescent chromophore from amino acid side chains in DsRed.

most frequently, but there are also many examples of three-photon excitation (3PE) to be found in the literature. The low-background and small excitation volumes attainable with MPE suggest that multi-photon excitation is best suited for applications requiring small volumes (femtoliters or lower). Thus, MPE is presently regarded as a superior detection method in capillary electrophoresis enabling also multi-parameter measurements. As the detection limit of the direct integration measurement may reach down to a single molecule, 2PE is also applied successfully in bioaffinity assays. Additionally, due to the high transparency of tissues and other biological media in the far-red and near IR, MPE is a unique tool for three-dimensional imaging of tissues and cells. In these paragraphs the general bioconjugate chemistry and some recent bioanalytical applications are briefly introduced.

#### 14.2.3.2 MPE Fluorescence Dyes

Various investigations on the multiphoton excitation of biological molecules, such as the aromatic amino acids (tryptophan, tyrosine and phenylalanine), FAD, NADH, serotonin and melatonin [182–185], have appeared in the literature. There are also many synthetic dyes that have peak two-photon cross sections large enough to be useful as probes in bioassays [186]. Albota et al. recently designed novel compounds with increased MPE fluorescence [187]. The concept was to construct donor–acceptor–donor (D–A–D) or acceptor–donor–acceptor (A–D–A) dyes of sufficient length, in which the excitation causes a symmetric charge transfer from the ends of the molecule towards the center or vice versa. Excitation usually effects a charge displacement from the donor end of the molecule towards the acceptor end. Three important features of the molecules were studied: 1. the nature of the molecule (A–D–A or D–A–D), 2. the conjugation length and 3. the strength of the donor or acceptor groups. By varying these parameters the two-photon excitation could be

maximised through increasing the 2PE cross section,  $\delta(\omega)$ , which is related to the imaginary part of the second hyperpolarizability,  $\text{Im } \gamma(-\omega; \omega, \omega, -\omega)$  according to:

$$\delta(\omega) = \frac{8\pi^2 \eta \omega^2}{n^2 c^2} L^4 \text{Im } \gamma(-\omega; \omega, \omega, -\omega) \quad (2)$$

Since the second hyperpolarizability is involved in the equation, symmetrical molecules of the D–A–D type and A–D–A type are suitable, but also donor-substituted porphyrins, in which charge transfer may occur in two dimensions. Table 14.8 briefly summarises MPE cross sections of some reported dyes. Some of the special dyes synthesised for very large MPE effects are presented in Fig. 14.31. As can be observed from the data, there is a reasonably good correlation between the observed and calculated excitation and cross section data. The increase in length gave the most substantial increase in the 2PE cross section and in excitation wavelength.

**Table 14.8** Comparison of MPE cross sections of conventional and engineered chromophores.

Compound	$\lambda_{\text{max}} \text{ (nm)}$	$\lambda_{\text{2PE}} \text{ (nm)}$	$\delta_{\text{2PE}} \text{ (10}^{-50} \text{ cm}^4 \cdot \text{s/photon)}$
rhodamine B		840	210
fluorescein (pH=11)		782	38
compound 1		514	12
compound 2	374	605	210
compound 3	408	730	995
compound 4	428	730	900
compound 5	456	775	1250
compound 6	472	835	1940

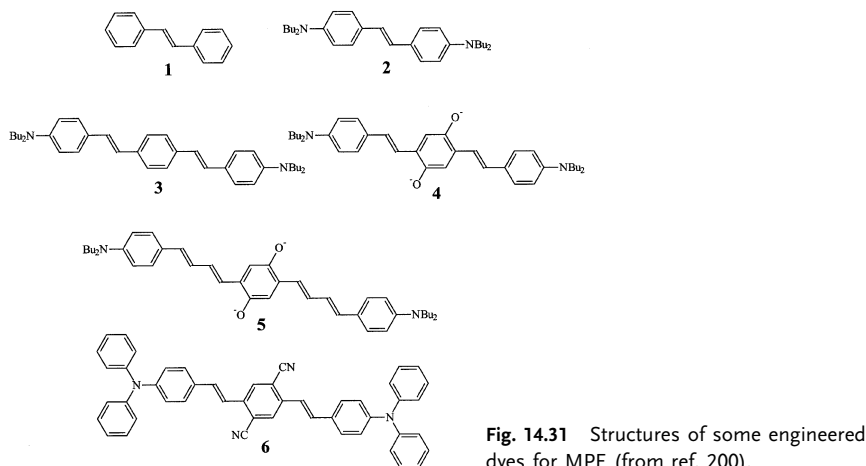


**Fig. 14.31** Structures of some engineered dyes for MPE (from ref. 200).

#### 14.2.3.3 Two-photon Excitation Immunoassays

Recently, 2PE has been applied in a variety of immunological and DNA hybridisation assays with promising results. The experiments of Soini and coworkers have shown that homogenous single step bioaffinity assays can be performed with good sensitivity and dynamic range by using two-photon fluorescence excitation [188]. The assay concept is a very promising alternative when there is a need to reduce sample volumes, because the signal is obtained from a very small focal volume, in which the signal strength is independent of the sample volume (Fig. 14.32). The sensitivity is two orders of magnitude larger in solution measurements compared to conventional fluorometric techniques. The main advantage is that the technique allows for single-step, non-separation assays, working for both immuno-metric and competitive binding assays (homogeneous immunoassay). Other advantages are that the sample cuvette does not contribute to the background signal, and that kinetic reaction monitoring and multiparametric measurements are possible.

The usefulness of two-photon fluorescence excitation in homogeneous bioaffinity assays has been verified by using microbeads as the solid phase [188]. Biochemically activated 3  $\mu\text{m}$  polystyrene microbeads were used as solid phase to bind the analyte  $\alpha$ -fetoprotein (AFP) (Fig. 14.33). Each microbead acts as a local concentrator of the analyte. When a fluorescent biospecific reagent molecule either attaches directly to the analyte forming a sandwich-type  $\text{Ab}-\text{Ag}-\text{Ab}^*$ -complex on the microbead surface (immunometric measurement) or competes in binding to the surface of the microbead (competitive measurement), the amount of analyte molecules bound to the microbeads becomes measurable by observing the two-photon fluorescence signal from individual microbeads. In such an assay the analyte and the reagent solution, comprised of microbeads and a fluorescent tracer, can be dispensed simultaneously into a single reaction volume. The signal from the microbeads is measured after incubation directly from same reaction volume.

Due to the concentrating effect on the microbeads, the signal from the tracer bound to each microbead for the full dose of the analyte is several orders of magnitude stronger than the signal background from the free tracer. In fact, the signal of the free tracer at the zero dose level determines the lowest limit of the working range. The working range and sensitivity depend on the assay parameters such as affinity, microbead capacity, number of microbeads in an assay and tracer concentration. Theoretically, a linear working range of up to four orders of magnitude can be reached.

#### 14.2.3.4 MPE in Gel and Capillary Electrophoresis

As discussed in Section 14.2.1, normal (one-photon) fluorescence spectroscopy (1PE) has been the method of choice in capillary electrophoresis (CE) and gel electrophoresis (GE) with visible and NIR fluorescent dyes. MPE fluorescence, however, is also quite suitable for detection in CE and GE. For instance, Song et al. fractionated coumarine dyes with capillary electrophoresis, and detected the dyes at attomole concentrations by 2PE fluorescence [189]. Generally, detection limits are comparable to those attainable by normal fluorescence. However, MPE is particu-

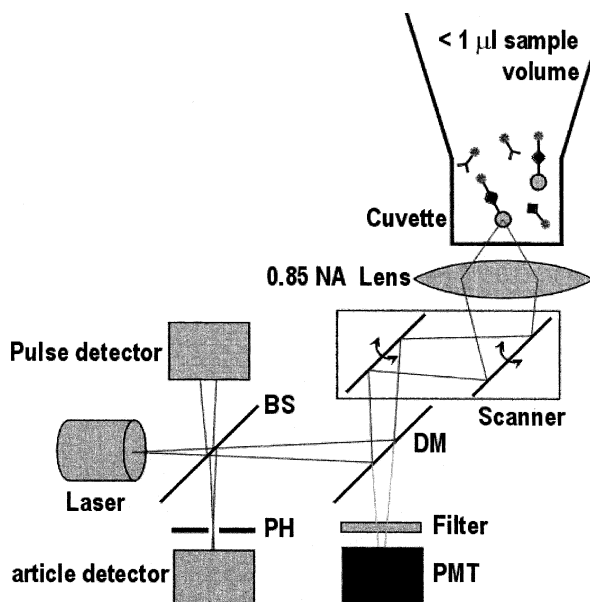


**Fig. 14.32** The optical scheme of a typical 2PE set-up; BS is a beam splitter, DM is a dichroic mirror, PH is a pinhole and PMT is a photomultiplier tube.

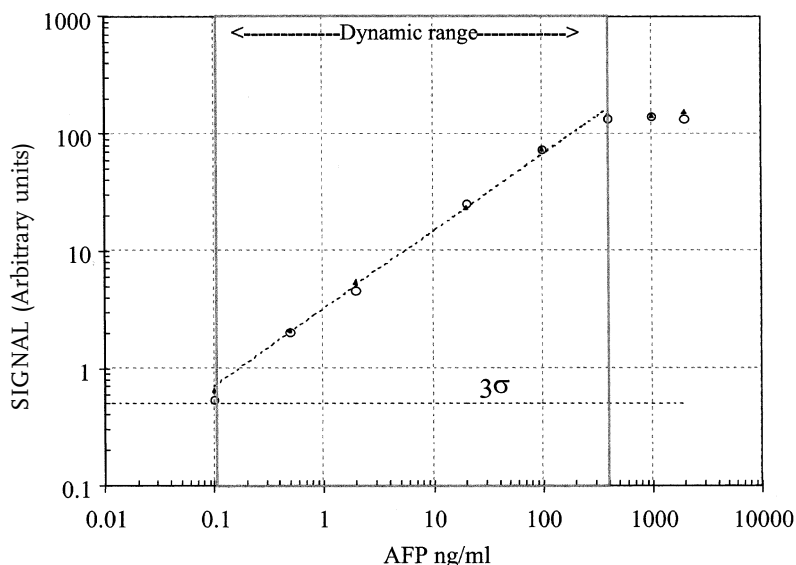


**Fig. 14.33** Two standard curves for an AFP assay with microbeads with two different measurement volumes, 25 μl (◆) and 2 μl (○). The curves show that both volumes give practically same result.

larly useful in situations where multiparameter measurements are required and where the compounds to be detected have similar spectroscopic properties, but differ in their MPE cross sections. MPE is also useful when the analytes have very different spectral properties, but where the MPE gives possibilities for excitation with a single light source. 2PE and 3PE fluorescence of FAD, NADH, serotonin, melatonin and similar compounds in CE has been extensively studied by Shear and coworkers [180, 184, 190]. All these analytes had substantial MPE cross sections in the wavelength range between 710 and 750 nm. The detection limits of the CE/MPE detection scheme ranged from 350 zmols for FAD to 27 amols for serotonin [190].

#### 14.2.3.5 MPE in Tissue Imaging

As remarked in Section 14.2.2.1, the high transparency of biological tissues in the near-IR region and the low photon energy allow high intensities to be used without the risk of photobleaching and photodamage of the specimens. Additionally, with the use of highly focussing optics, as used in confocal microscopy, very small volumes in biological tissues can be sampled with MPE fluorescence, achieving unprecedented 3-D resolution. Thus, microscopic specimens can be raster-scanned, keeping the focal point within a plane perpendicular to the laser beam ( $x-y$  direction) and collecting fluorescence and background photons from a tightly confined spatial region as a function of the  $x$  and  $y$  positions. Additionally, the specimen (or objective) can be adjusted in micrometer steps in the  $z$  direction at different planes within the sample.

An interesting demonstration of such imaging capabilities was given by Kleinfield et al., who introduced MPE laser scanning microscopy to the imaging of cortical blood flow at the level of individual capillary blood vessels in the rat neocortex through openings created in the crania [191]. 2PE fluorescence was excited with a 830 nm laser beam, attaining a depth resolution down to 600  $\mu\text{m}$ . This is several hundred micrometers deeper than can be attained with conventional confocal microscopy. Fig. 14.34a represents a horizontal view in the vicinity of a capillary reconstructed from a set of scans in the  $x-y$  direction. These scans were acquired at between 310 and 410  $\mu\text{m}$  depth in 1  $\mu\text{m}$  steps. The inset shows the intensity profile along the cross-section for a scan that passed through the central axis of the selected capillary. The vessel cross-section ('caliber') was estimated from the number of pixels with intensity above the background level. Figure 14.34b gives successive planar images through a small vessel, acquired with a 16 ms interval. The change in position of unstained objects, interpreted as red blood cells, is indicated by the series of arrows. The velocity of the red blood cell was estimated to be 0.11  $\text{mm s}^{-1}$ .

#### 14.2.3.6 Future Prospects of MPE Fluorescence Spectroscopy

As can be concluded from the previous examples, MPE fluorescence is useful, but must at the present stage still be considered as a complementary tool to existing, more straightforward bioanalytical techniques. There are still many instances in

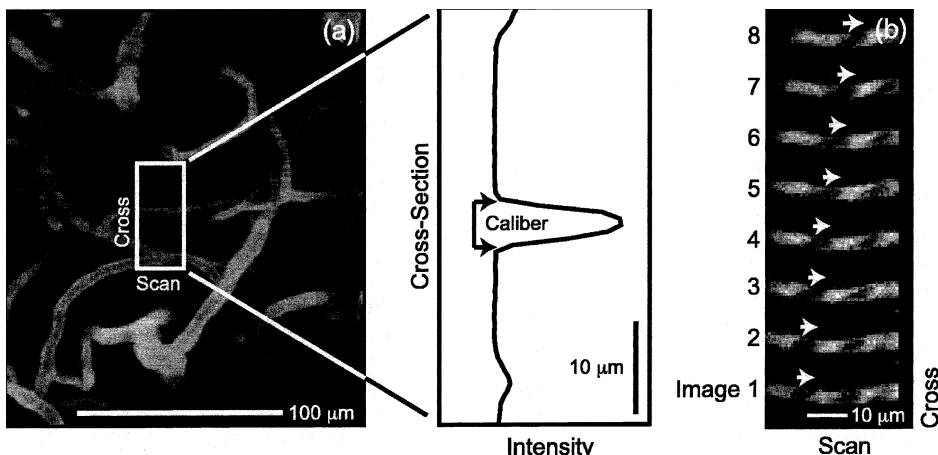


**Fig. 14.34** MPE fluorescence images of structures in the rat neocortex (reproduces from ref. 191, with permission): (a) Image of single microvessels, whose caliber was determined from the measured cross section in a planar image (a, inset), (b) successive, rapidly acquired planar images of the microvessel, revealing the movement of dark objects (non-fluorescent red blood cells) in the microvessel containing serum spiked with a fluorescent label.

which single-photon excitaton or single photon confocal scanning microscopy yields equivalent or even better results with more economic equipment [181]. Presently, the high cost of Ti:Sapphire lasers presents a substantial barrier to the construction of cheap devices, but novel diode lasers may contribute in the near future to reducing the cost. MPE fluorescence offers presently the greatest advantages in the characterization of biological samples and tissues. Additionally, there are interesting new perspectives in immunoassays based on MPE, because it enables fast single-step, separation-free immunoassays and DNA hybridisation assays in very small volumes [188]. Recently 2PE fluorescence polarization measurements have also been presented in optically dense specimens [192]. As indicated, the method may also be very useful for high throughput screening of drugs. Monitoring of the release of products (e.g. various cytokines, tumor necrosis factor, Fasligand etc.) can be made in a one-step assay without coated tubes and separation procedures. The method is applicable also for whole blood samples because the laser illumination is far beyond the absorption of hemoglobin. Thus, MPE as introduced in this section, has the potential to become a new generic platform for *in vitro* diagnostics when less expensive pulsed laser light sources also become a reality.

## 14.2.4

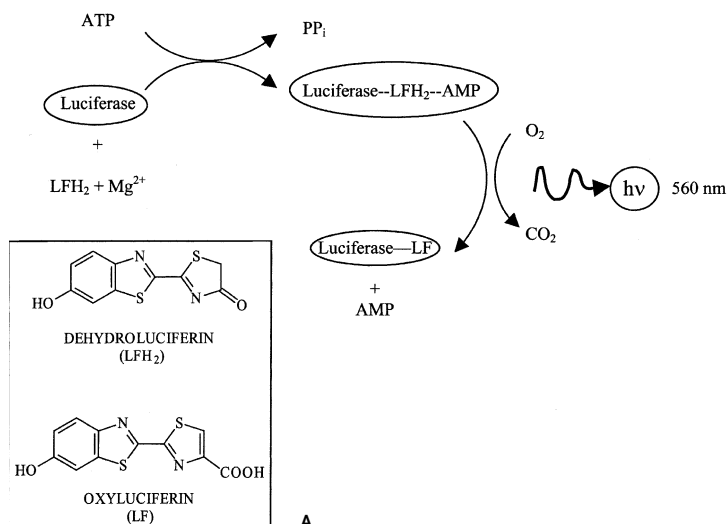
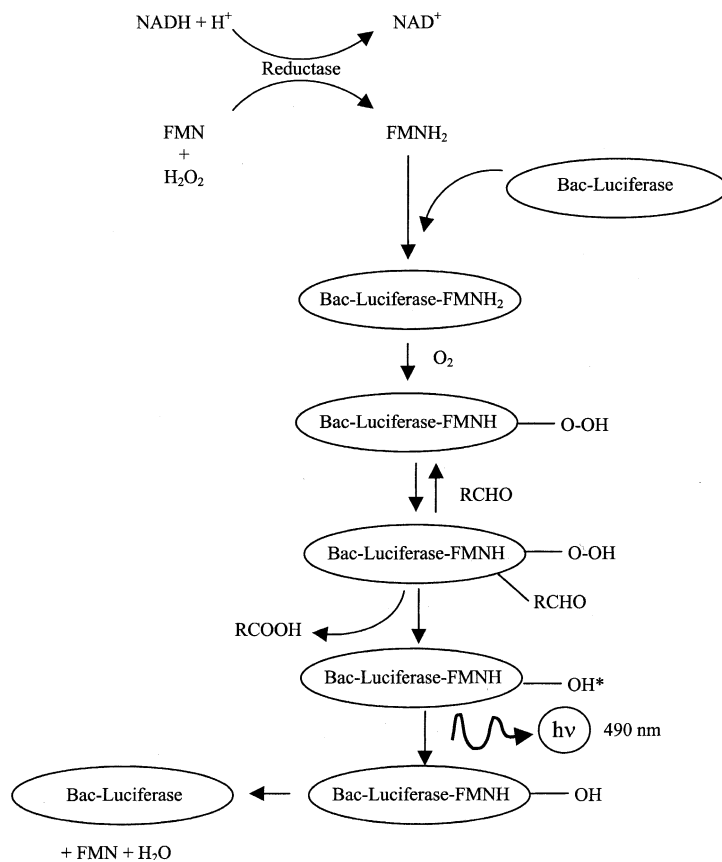
**Bioluminescence, Chemiluminescence and Electrochemiluminescence**

Luminescence phenomena are used in many bioanalytical assays. A first overview of BL and CL reagents and bioanalytical techniques was described in 1978 in a volume of Methods in Enzymology, edited by Marlene DeLuca [193], and hereafter there have been various new developments, both in new reagents and in instrumental design, which have placed these techniques at the forefront of bioanalysis [194, 195]. At present, electrochemically generated chemiluminescence (ECL) is gaining the larger interest for realizing highly sensitive bioassays, particularly immunoassays [196, 197].

A classical bioluminescent system is the luciferase system from the firefly *photinus pyralis*. This system has been widely used for the determination of ATP and analytes that are involved in the conversion of ATP. In the firefly luciferase reaction, ATP and the reduced form of the dye compound luciferin is converted to AMP and an oxidized and decarboxylated form of luciferin in the presence of magnesium and the luciferase enzyme (Fig. 14.35A). This reaction produces light with a quantum efficiency of almost 100 %. Classic applications of the luciferine/luciferase reaction are, for instance, the determination of ATP in mitochondria. Enzymatic reactions can be coupled via ATP to other enzymatic reactions (e.g. kinases), which broadens the application potential of the luciferase system to a large variety of analytes. Magnesium activity can also be determined very sensitively, because the reaction depends greatly on magnesium. A second class of bioluminescent reactions comprises the bacterial luciferases, which are part of the electron-transport pathway from reduced substrates to oxygen via flavins. Thus, these bioluminescent reactions can be coupled to enzymes that convert flavins like NADH and FADH<sub>2</sub>. Most bacterial luciferases convert the reduced form of flavinmononucleotide (FMNH<sub>2</sub>) to its oxidised form (FMN) producing light very efficiently (Fig. 14.35B).

The classical CL reaction is that of luminol with hydrogen peroxide catalyzed by horseradish peroxidase (HRP). Such reactions are frequently coupled to hydrogen peroxide-producing enzymatic reactons, e.g. the oxidase enzymes [198], providing a sensitive alternative to HRP-based absorbance or fluorescence detection (Fig. 14.35C). New CL reagents have recently been developed, including novel luminol and isoluminol derivatives [199, 200], acridinium ester labelling reagents, [201–203] and 1,2-dioxetane derivatives [204, 205]. Recently a regenerable immunosensor has been described by Marquette and Blum for the detection of the herbicide 2,4-dichlorophenoxyacetic acid (2,4-D), based on the luminol/HRP system [206]. A CL-based fiberoptic sensor in a flow injection analysis (FIA) configuration with a competitive immunodetection scheme was used in this system.

In ECL the luminescence is produced as the result of an electrochemical reaction. A reactive species is produced electrochemically at an electrode and diffuses into the bulk solution and reacts with chemicals in the vicinity of the electrode. There are various mechanisms by which ECL can be initiated: (1) by electrochemical initiation of a conventional CL reaction (e.g. of luminol), (2) by electrochemical modification of an analyte molecule into a species which can take part in a CL re-

**A****B**

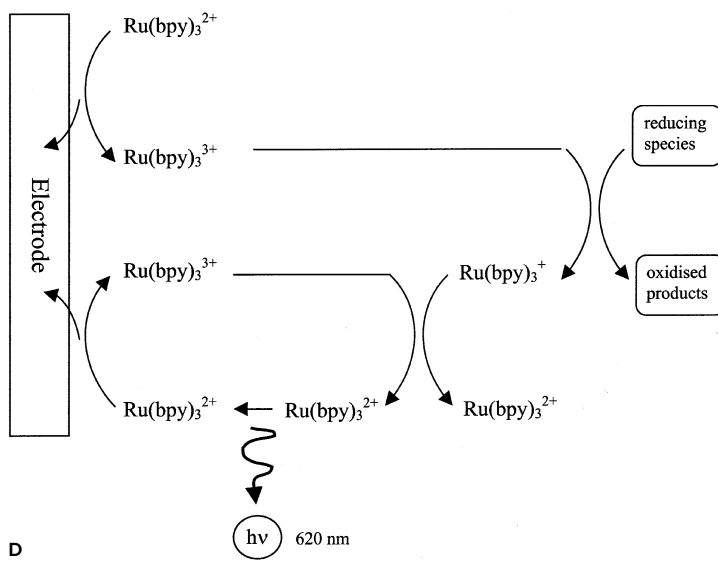
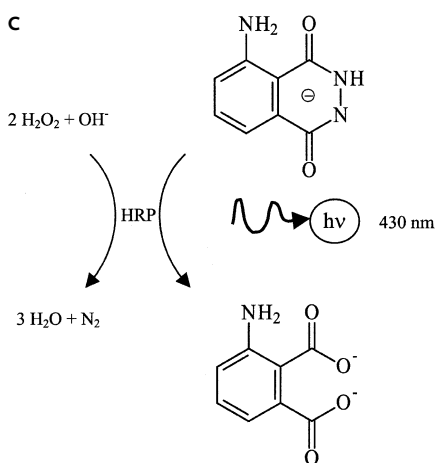


**Fig. 14.35** Examples of various luminescent reactions. (A) The firefly Luciferase reaction. (B) The bacterial luciferase reaction.

(C) The luminol reaction with horseradish peroxidase catalyst. (D) The electroluminescence of  $\text{Ru}(\text{bpy})_3$ .

action, (3) by high energy transfer of electrons to or from electrochemically generated organic radicals (e.g. radical ion recombinations between polycyclic aromatic hydrocarbons), (4) through high energy electron transfer reactions between inorganic ions (e.g. between transition metal complexes) and (5) through emissions from certain oxide-covered valve metal electrodes (i.e. cathodic luminescence). Electrochemiluminescence has initially relied much on the luminol reaction, but presently the majority of analytical techniques are based on ruthenium trisbipyridyl ( $\text{Ru}(\text{bpy})_3$ ) complexes, which has the great advantage that the luminescent reagent can be regenerated at the electrode. This results in an enhanced detection sensitivity (Fig. 14.35D). The advantages of ECL detection over CL and BL are that the luminescence reaction (initiation, rate and course) can be electronically controlled and even modulated, while the light is produced very close to the electrode. This gives major advantages in sensitivity. Additionally, ECL is more compatible with flow injection analysis techniques and additional information can be obtained about the reaction via electrochemistry. As a disadvantage can be mentioned that sensing applications are still difficult to realise due to the need to add reagents to the assay system.

Immunoassays presently form probably the most active area of exploitation of CL, ECL and BL, as evidenced by the extensive commercialization of luminescent immunoassay analyzers and test kits. Among these, acridinium ester-based CL assays for alkaline phosphatase and amplified CL assays using peroxidase labels have become the most widespread [207, 208]. Besides immunoassays CL and BL have been used in nucleic acid assays [209–211] and in cellular studies concerning, for instance, phagocytosis [212]. ECL immunoassays based on ruthenium trisbipyridyl labels are now becoming popular in clinical immunoassay analyzers [213].

Recently the incorporation of bacterial luciferase genes ("Lux genes") into bacteria (e.g., recombinant *E. coli*) has also been successfully exploited. The group of Karp and co-workers in Finland has pioneered this area and recently reported a BL-based biosensor for the specific detection of the tetracycline group of antibiotics using a bioluminescent *Escherichia coli* K-12 strain [214]. The *E. coli* contained a 'sensor' plasmid, containing five genes from the bacterial luciferase operon of *Photobacterium luminescens*, which yielded a tetracycline-dependent light production.

#### 14.2.5

#### Bioanalytical Applications of NIR Absorption Spectroscopy

Near-infrared absorption spectroscopy is increasingly used in agriculture, food science, medicine, life sciences, pharmaceuticals, textiles, general chemicals, polymers, process monitoring, food quality control and in clinical *in vivo* measurements [215, 216]. The increase in popularity is largely due to the availability of miniaturised NIR-spectrometers by a variety of vendors (e.g. Ocean Optics Inc.). The most promising applications of NIR-absorbance spectroscopy clearly lie in process control, because of the relatively low complexity of the sample in chemical and biochemical processes, e.g. compared to biological tissues. Also in food quality control

NIR-IR has been successfully used, as exemplified by the analysis of fat in raw milk [217].

NIR-spectroscopy has also been prospected for use in *in vivo* monitoring of important tissue and blood metabolites, such as glucose, creatinine, lactate, urea, cholesterol, oxygen and hemoglobin [326]. NIR spectroscopy can be easily applied to the measurement of tissues due to the great transparency of skin for near-IR radiation. The most interesting analyte for *in vivo* monitoring is, unquestionably, glucose. There is still a huge need for the reliable diagnosis of diabetes mellitus, and self-monitoring of blood glucose in people with diabetes with a non-invasive method would give substantial advantages over the present finger-prick methods. For *in vivo* glucose monitoring promising systems have been designed, which rely heavily on multivariate calibration methods [218, 219]. Unfortunately, the present NIR absorbance methods, as based on multivariate calibration, are still quite unreliable. This has been recently demonstrated by Arnold and coworkers [220]. Essentially, the unreliability is due to the small signals produced by glucose relative to other signals and the complexity of the tissue matrix. Presently, *in vivo* glucose monitoring is surfacing more rapidly in the patent literature as in the scientific literature.

#### 14.2.6

#### Bulk Optical Sensing Techniques

Within the rapidly growing field of chemical sensor and biosensors, optical sensing strategies are still very much at the center of interest, as evidenced from the untiring quest for new principles of transduction and the commercialisation of optical sensing instruments [221]. A chemical sensor generally comprises the integration of a chemical recognition element with a particular detection system. In the case of a biosensor, a biomolecule is used as the recognition element. Chemical sensor systems should be capable of providing continuous, specific quantitation without the need for addition of external reagents [222]. A variety of approaches for the generation of an optical signal from a selective biological binding event have been evaluated. Although most of the earlier developed systems relied on absorption or fluorescence detection, research has now shifted much towards the detection of refractive index changes. The next section will be dedicated mainly to the evanescent wave-based techniques, while this section briefly introduces the methods based on bulk absorbance and fluorescence transduction.

The receptors that can be used in optical sensors can be either synthetic or from a biological source, while there are also many approaches to chemically or genetically engineered biological receptors for use in sensors [223]. Presently, combinatorial chemistry and molecular imprinting are at the forefront of receptor research, particularly for the more complicated analytes, such as drugs and chemical warfare agents. Cation receptors were the first prototypes of designed receptors, based on the rules of supramolecular chemistry [224]. Cation receptors based on calixarenes have been used, e.g. for the direct measurement of sodium in blood [225]. The design of anion receptors has also been the subject of intensive research due to the

fundamental role that anions play in biochemical processes [226]. Anion sensing, however, is yet a degree more complex than cation sensing and has, as a consequence, been slower in its development. Anions are much larger and their shapes are more variable, while they exist only in a limited pH range. Thus, a potential anion receptor must be designed to satisfy the particular anion's unique characteristics of size, shape and pH dependence.

In ion-selective electrodes a signal is generated by the permselective exchange of ions into a hydrophobic membrane phase. For optical transduction the ion-receptor complexation has to be coupled to a complementary chemical process in an absorbing or fluorescent dye compound. Such sensing matrices are used frequently in conjunction with fiber optics for the construction of sensor systems. A first way to achieve optical transduction is to include a lipophilic acidochromic dye (chromoionophore) into the membrane phase together with the receptor. The complexation of the metal ion by the ligand will expel a proton, which changes the absorbance or fluorescence spectrum. The advantage is that no synthetic modification of the receptor or dye is needed. Originally, lipophilic Nile Blue (phenoxazine) derivatives were much used, but also acridine, fluoresceine and various other synthesised chromoionophores have been described with signal-transducing properties [227–230]. Chromoionophores that are compatible with lipophilic matrices and have absorptions in the NIR region have also been described [80]. Many cation receptors and chromoionophores are commercially available. For instance, the ETH series of chromoionophores is available from Fluka AG, which has also issued a practical guide for making optical sensing matrices.

That these sensors have practical significance is illustrated by the publications of Hisamoto et al. and Wang et al., which have described the measurement of common ions directly in serum [228, 229]. Alternatively, the complexation of the metal ion may influence the partition of the lipophilic dye in the membrane phase, which can affect the fluorescence yield of the dye. Recently this principle has been demonstrated with potential sensitive dyes by Wolfbeis and Mohr [231, 232]. This approach is also applicable to the sensing of neutral species and anions, as exemplified by sensor matrices for 2-phenetylamine [233] and nitrate [234].

In a second approach, the dye is made an integral part of the receptor, such that absorbance and/or fluorescence parameters are directly modified by the complexation reaction. This is a more developed form of indicator chemistry and is in supramolecular terminology defined as "semiochemistry" [224, 235]. Receptor molecules modified with photosensitive groups may display very large changes in their photophysical properties upon the binding of analytes, and this can enable very sensitive detection. For instance, Chapoteau et al. reported already in 1992 a colorimetric method for the determination of lithium in blood serum, not requiring any sample pretreatment or solvent-extraction steps [236]. The chromogenic ionophore exhibited exceptionally high selectivity for lithium over sodium ( $>> 4000:1$ ). Many ion receptors, and also receptors for small organic compounds have been reported in the literature, based on azophenol [236, 237], spirobenzopyran [238], antracene [239] or coumarine [240]. Presently, calixarenes with covalently linked chromogenic or fluorogenic groups are still at the center of interest [241]. Although already in

1992 Shinkai et al. and Diamond et al. had reported on different azophenol-modified calixarenes for quantitation of lithium [242, 243], more complex structures have recently been produced, of which the usefulness in bulk optodes and in realistic sample matrices still needs to be assessed. Modified calixarenes have been produced for sensing of anions [244] and small organic molecules, such as dopamine [245] and 2-phenethylamine [233], while chiral recognition by calixarene derivatives has also been studied [246]. Furthermore, calixarenes have been produced in which fluorescence can be switched on upon binding of the analyte, a principle that may afford extremely sensitive sensors [247]. Recently, a variety of new squarilium dyes with signal transducing properties have been reported in the literature. Akkaya et al. have reported on squarine dyes with phenylboronic acid groups for the detection of carbohydrates [248] and similar dyes with sensitivity for zinc ions [249] and calcium ions [250].

Imprinted polymers have lately shifted into the center of interest, particularly in the quest for sensors for analytes more complex than ions [251]. The principle of molecular imprinting is basically simple: a well-optimised mixture of monomers with various functional groups is polymerised in the presence of the analyte (the 'template'). Hereafter, the analyte is eluted from the polymer matrix, which leaves complementary binding sites in the polymer for the analyte. This polymer can then be used in an analytical system or sensor. Artificial enzymes can also be produced by molecular imprinting, in which a transition state analogue of a chemical reaction is used as the template molecule [252].

There are already some reports of the combination of fluorescence with imprinted polymers [253]. If the functional monomers are fluorescent and are designed to have specific chemical interactions with the analyte it is possible to directly monitor the binding via changes in fluorescence of the polymer [254, 255]. For reasons of background and sensitivity, the activation of fluorescence by the binding of analyte to an imprinted polymer would be the most preferred situation. Turkewitsch et al. described a first example of this novel design for template-selective recognition sites in imprinted polymers with the analyte cyclic AMP [254]. The polymer included a fluorescent dye, a dimethylaminostyryl-pyridinium derivative, as an integral part of the recognition cavity, thus serving as both the receptor and transducing element for the fluorescence detection of cAMP in aqueous media. The imprinted polymer displayed quenching of fluorescence in the presence of cyclic AMP in aqueous solution, whereas almost no effect was observed in the presence of cyclic GMP. The affinity constant of the polymer for cyclic AMP was about  $10^5 \text{ M}^{-1}$ .

#### 14.2.7

#### **Evanescence Wave Spectroscopy and Sensors**

##### 14.2.7.1 **Introduction**

To perform spectroscopy on biomolecules at a surface, it would be favourable to confine the measurement to a thin layer at the surface, in the region where the molecules are immobilised. Typically, this region would range from 5 nm for

small proteins to 50 nm for large protein assemblies such as ribosomes. Methods based on evanescent waves permit such spectroscopy by guiding light parallel to the surface of the optical substrate upon which the biomolecules are immobilised. According to the Fresnel equations, light is internally reflected at interfaces between high and low refractive index at angles larger than a critical angle. The electrical field, however, penetrates into a thin layer of the medium with a lower refractive index to some degree and with a strong exponential decay at increasing distances from the surface (the *evanescent wave*). Before discussing the various applications the theory of evanescent waves will be briefly reviewed.

#### 14.2.7.2 Theory of Total Internal Reflection

##### Reflection and refraction

At a dielectric interface, we can have both reflection and transmission, as shown in Fig. 14.36 [256]. The following conditions must be satisfied:

$$\theta_3 = \theta_1$$

$$\frac{\sin \theta_2}{\sin \theta_1} = \frac{n_1}{n_2} = \left( \frac{\epsilon_1}{\epsilon_2} \right)^{1/2} \quad (3)$$

Where  $n$  is the refractive index,  $\epsilon$  the permittivity and  $\mu$  the permeability of the dielectric media. The incident, reflected and refracted rays are coplanar (located in the  $x$ - $z$  plane, the plane of incidence, in Fig. 14.36). Transverse electric (TE), perpendicular ( $\perp$ ) or s-polarised light has its electric vector perpendicular to the plane of incidence ( $x$ - $z$  plane) in Fig. 14.36, while transverse magnetic (TM), parallel ( $\parallel$ ) or p-polarised light has its magnetic vector perpendicular to the plane of incidence.

##### The Fresnel equations

The Fresnel equations describe the reflection and transmission coefficients at the interface of two optical media. The polarisation of the incident light affects the magnitude of these coefficients. It is possible to derive expressions for the intensities of the reflected and refracted rays. These differ for the TE and TM polarisations as follows:

$$R_{\text{TE}} = \frac{\sin^2(\theta_2 - \theta_1)}{\sin^2(\theta_2 + \theta_1)} = \frac{(n_1 \cos \theta_1 - \sqrt{n_2^2 - n_1^2 \sin^2 \theta_1})^2}{(n_1 \cos \theta_1 + \sqrt{n_2^2 - n_1^2 \sin^2 \theta_1})^2} \quad (4)$$

$$T_{\text{TE}} = \frac{\sin 2\theta_1 \sin 2\theta_2}{\sin^2(\theta_2 + \theta_1)} = \frac{4n_1 \cos \theta_1 \sqrt{n_2^2 - n_1^2 \sin^2 \theta_1}}{(n_1 \cos \theta_1 + \sqrt{n_2^2 - n_1^2 \sin^2 \theta_1})^2} \quad (5)$$

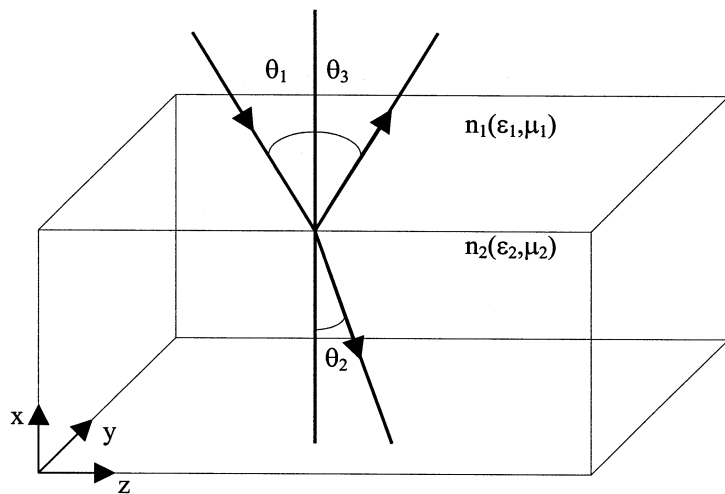


**Fig. 14.36** Reflection and refraction of light at the interface between two dielectric media having different refractive indices.

$$R_{TM} = \frac{\tan^2(\theta_1 - \theta_2)}{\tan^2(\theta_1 + \theta_2)} = \frac{(n_2^2 \cos \theta_1 - n_1 \sqrt{n_2^2 - n_1^2 \sin^2 \theta_1})^2}{(n_2^2 \cos \theta_1 + n_1 \sqrt{n_2^2 - n_1^2 \sin^2 \theta_1})^2} \quad (6)$$

$$T_{TM} = \frac{\sin 2\theta_1 \sin 2\theta_2}{\sin^2(\theta_1 + \theta_2) \cos^2(\theta_1 - \theta_2)} = \frac{4n_1 n_2 \cos \theta_1 \sqrt{n_2^2 - n_1^2 \sin^2 \theta_1}}{(n_2^2 \cos \theta_1 + n_1 \sqrt{n_2^2 - n_1^2 \sin^2 \theta_1})^2} \quad (7)$$

These expressions are only valid for non-normal incidence ( $\theta_1 > 0$ ). For the special case of normal incidence, these expressions become:

$$R = \left( \frac{n_1 - n_2}{n_1 + n_2} \right)^2 \quad (8a)$$

$$T = \frac{4n_1 n_2}{(n_1 + n_2)^2} \quad (8b)$$

Note that the polarisation has no effect at normal incidence, as it is not possible to distinguish a particular plane of incidence.

#### Total internal reflection (TIR)

If we have the condition  $\theta_2 = \pi/2$ , then the transmission coefficients for both TE and TM polarised light go to zero, because the term  $\sin 2\theta_2$  becomes zero. Thus, the transmission coefficient is zero when  $\theta_2 = \pi/2$ . In this case,

$$\sin \theta_c = \frac{n_2}{n_1} \quad (9)$$

And the angle of incidence at which this condition is true is called the critical angle. Since the sine function can only produce values from  $-1$  to  $+1$  for real angles, we can see that for this condition to be satisfied  $n_2 < n_1$ . In other words, total internal reflection can only occur when light travels from a high index to a lower index medium. For angles of incidence greater than or equal to the critical angle, total internal reflection occurs regardless of the polarisation.

### Evanescent waves

When the angle of incidence at a high-low refractive index boundary is greater than the critical angle, light is totally internally reflected. It can be shown that, although there is no energy transmitted across the interface, an electromagnetic wave, the evanescent wave, is present on the other side of the boundary. This wave propagates parallel to the interface and decays away exponentially with distance from the boundary. The penetration depth of the evanescent wave is given by:

$$d = \frac{\lambda}{2\pi\sqrt{n_1^2 \sin^2 \theta_1 - n_2^2}} \quad (10)$$

Where  $\gamma$  is the vacuum wavelength of the light. The penetration depth is the distance over which the intensity of the evanescent field decays to  $1/e$  of its original intensity. This means that, except near the critical angle, the penetration of the evanescent wave into the optically rarer medium is no more than a wavelength. As an example, if we take an SF10 prism ( $n=1.732$ ) in contact with water ( $n=1.333$ ) at a wavelength of 633 nm (HeNe laser), then the critical angle is 50.32 degrees. If our angle of incidence is 60 degrees, the penetration depth is approximately 146 nm.

While the evanescent field does not propagate into the rarer medium, it does propagate parallel to the interface and can interact with the lower index medium. Thus, if the lower index medium is absorbing, fluorescent or scattering, some of the light will be absorbed and the reflectivity will be reduced from unity. In the case of fluorescent or scattering media, fluorescence emission or scattered light from the evanescent field will be observed.

### Optical absorption

The attenuation factor  $a$  links the imaginary part  $K$  of the complex refractive index to the loss per unit length:

$$I_x = I_0 e^{-ax} \quad \text{or} \quad \ln \frac{I_x}{I_0} = -ax \quad (11)$$

Where  $I_0$  is the initial intensity and  $I_x$  is the intensity after the light has propagated a distance  $x$  through the absorbing medium, and

$$\alpha = \frac{4\pi K}{\lambda} \quad (12)$$

But the Lambert-Beer law states that

$$\log \frac{I_0}{I_x} = \epsilon c x \quad (13)$$

Where  $\epsilon$  is the molar extinction coefficient ( $\text{m}^2 \text{ mol}^{-1}$ ) and  $c$  the concentration ( $\text{mol m}^{-3}$ ). Combining Eq. (11), (12) and (13) yields:

$$K = \frac{\epsilon c \lambda \ln 10}{4\pi} \quad (14a)$$

Thus, we can calculate the imaginary part of the complex refractive index of a dielectric medium if we know the extinction coefficient and concentration of the absorbing species. If the lower index medium in a total internal reflection configuration has a complex refractive index, that is it is lossy, then the reflection coefficient is reduced from unity, even for angles of incidence above the critical angle.

### Attenuated total internal reflection (ATR)

The small decrease in reflectivity observed when light is reflected by TIR at the interface between non-absorbing and absorbing media is termed attenuated total internal reflection. If the light is scanned over a range of wavelengths, then an absorption spectrum can be generated. Figure 14.37 illustrates the effect of the ima-

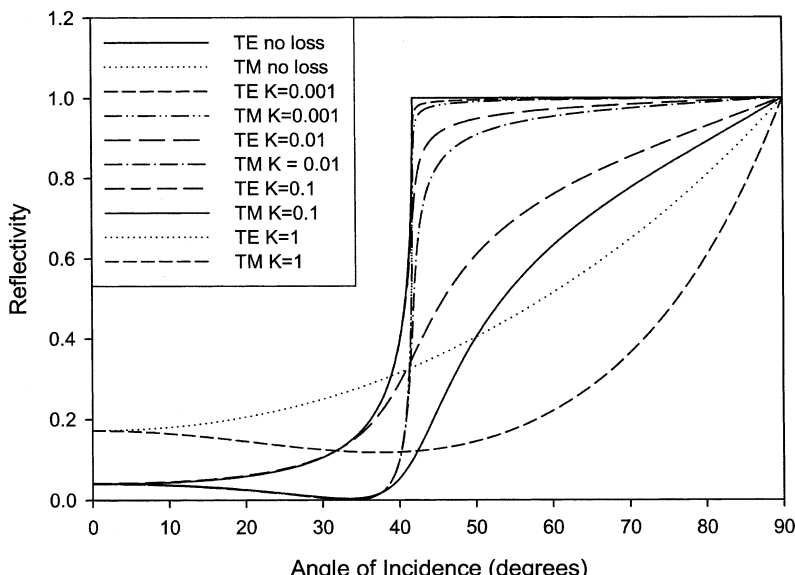


**Fig. 14.37** Reflectivities calculated for angles of incidence between 0 and 90 degrees for internal reflection at the interface between dielectric media having refractive index 1.5 and  $1.0 + iK$ .

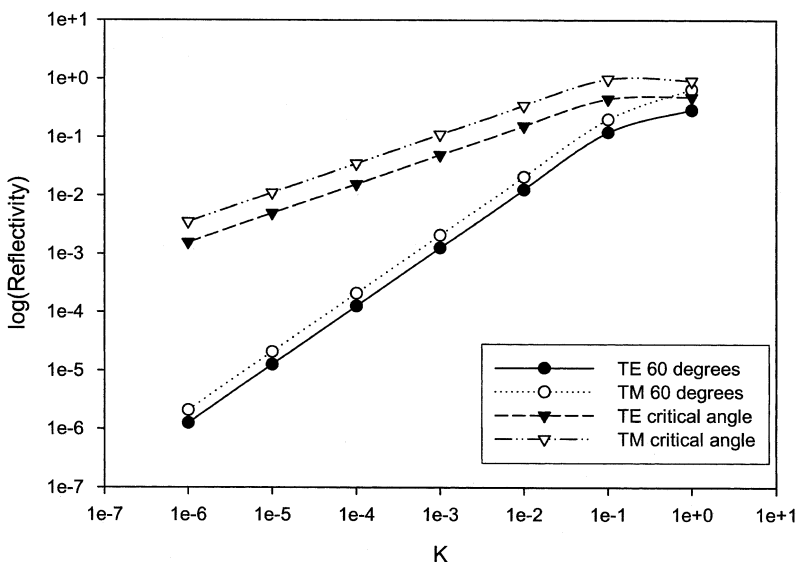


**Fig. 14.38** Log(reflectivity) for internal reflection at the interface between dielectric media having refractive index 1.5 and  $1.0 + iK$  for two angles of incidence, 60 degrees and the critical angle (41.8 degrees).

inary part of the refractive index on the reflectivity in a simple TIR configuration. When the imaginary part of the complex refractive index is quite small (0.001), the reflectivity curves only deviate significantly from the curves for the no-loss situation around the critical angle. At higher loss values, the curves deviate strongly from the no-loss values.

Figure 14.38 shows log(reflectivity) for internal reflection at the interface between dielectric media having refractive index 1.5 and  $1.0 + iK$  for two angles of incidence, 60 degrees and the critical angle (41.8 degrees). It can be seen that the TM polarisation gives slightly higher sensitivity, and that operating at the critical angle for  $K \approx 0.1$  also gives higher sensitivity. Above these values of  $K$ , the reflectivity is a non-linear function of  $K$ .

### Effective path length and sensitivity

We can use the preceding calculations to determine an effective path length for a material having a given value of  $K$ . This is calculated as a fraction of the path length of the material in a conventional spectrophotometer. Since Eq. (14) can be written as:

$$\varepsilon c = \frac{4\pi K}{\lambda \ln 10} \quad (14b)$$

In addition, we can use the reflectivity of the ATR configuration to calculate an effective absorbance or optical density:

$$A = \log \frac{I_0}{I} = -\log R \quad (15)$$

The ratio of the sensitivities for the ATR and conventional systems allows us to calculate an effective path length:

$$r_s = \frac{-\log R}{\epsilon cl} = \frac{-\gamma \ln 10 \log R}{4\pi Kl} = \frac{-\gamma \ln R}{4\pi Kl} \quad (16)$$

For example, if we use ATR at the interface between dielectric media having refractive index 1.5 and  $1.0 + 0.00001i$ , we can calculate that  $\epsilon c = 86.24 \text{ m}^{-1}$  or  $0.8624 \text{ cm}^{-1}$ . Operating at the critical angle for such a system, using TM polarisation, we obtain a value for  $R$  of 0.97487, which gives a value of 0.011055 for  $-\log(R)$ . This shows that the sensitivity of the ATR configuration is approximately 1/78 (0.011055/0.8624) of that of a conventional spectrophotometer, or the effective path length is 1/78 cm compared to a conventional 1 cm cuvette.

Although the effective path length is considerably shorter for a simple ATR configuration, the volume of material sensed is very small, since the penetration depth into the sensed material is generally very small. If we assume a circular input beam of radius  $r$  for both the conventional and ATR configurations, then the input beam will form an elliptical spot at the interface between the two media whose area will be given by:

$$A = \frac{\pi r^2}{\cos \theta_1} \quad (17)$$

The volume of material sensed will be given by the product of the area of the spot and the penetration depth  $d$ :

$$V = \frac{\pi r^2 \lambda}{2\pi \cos \theta_1 \sqrt{n_1^2 \sin^2 \theta_1 - n_2^2}} \quad (18)$$

And for the conventional cuvette the volume sensed will be given by:

$$V = \pi r^2 l \quad (19)$$

Where  $l$  is the path length of the cuvette. The ratio of these two volumes is:

$$r_V = \frac{\lambda}{2\pi l \cos \theta_1 \sqrt{n_1^2 \sin^2 \theta_1 - n_2^2}} \quad (20)$$

One obvious way to increase the sensitivity of ATR systems is to increase the number of reflections. This can be achieved by using a thin transparent slab and coupling the light in and out through the end faces of the slab. Many different configurations have been devised utilising this method, including schemes where the light enters and exits by the same face and single- and double-sided slabs. If the reflectivity for a single total internal reflection is  $R$ , then for  $n$  reflections the total reflectivity is  $R^n$ . ATR slab waveguides in IR-transparent materials such as silicon, germanium, zinc selenide and KRS-5 are commercially available for FTIR instruments.

### Waveguides

We can utilise the phenomenon of TIR to construct a waveguide. If we have a slab of transparent dielectric of a higher refractive index than its surroundings, light can be waveguided in the slab. Even a simple microscope slide can act as a slab waveguide if light can be coupled into it in such a way as to exceed the critical angle on reflection at the boundaries of the slab. Figure 14.39 shows a simple ray model of the propagation of light along the waveguide at a characteristic angle of incidence by successive reflections. To minimise losses, TIR is used as the reflection mechanism.

It might appear that  $\theta$  can adopt any angle, but this is not the case. Consider an observer moving along the  $z$ -axis who sees only the transverse ( $x$ -direction) motion. For a self-consistent picture, this observer must see the ray having the same phase every time the ray reaches him. If this were not the case, over a large number of reflections the phase shifts would cancel out, giving an intensity of zero. For this not to occur, the total phase shift over a complete cycle from  $x = 0$  to  $2a$  and back to 0 must again be an integral multiple of  $2\pi$ . This is termed the transverse resonance condition.

If  $2a$  is large compared to the wavelength of the light, then there will be a large number of angles  $\theta$  that satisfy the transverse resonance condition. As the thick-

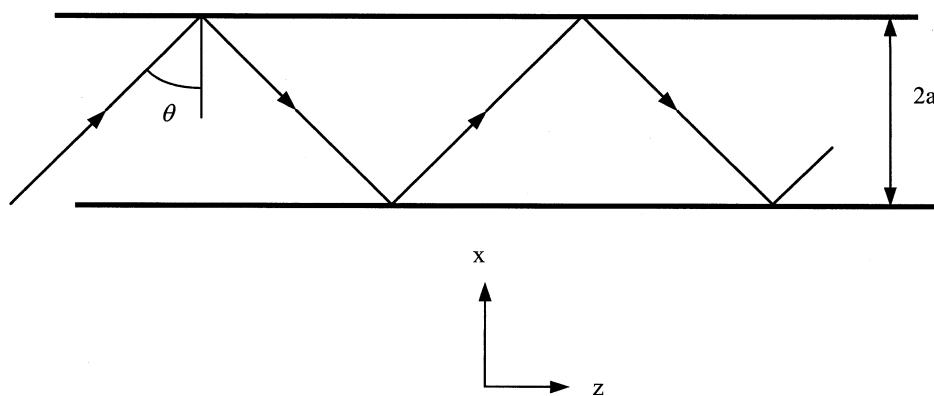


**Fig. 14.39** A simple model of a slab waveguide showing the propagation of light in a zig-zag path.

ness of the waveguide is reduced, the number of possible solutions decreases until, in the limit, there is only one angle at which the light can propagate. Each discrete angle of propagation is termed a mode, and below a critical thickness (the cut-off thickness) no waveguide modes can be supported. Waveguides are termed monomodal if they can only support one mode or multimodal if they can support more than one mode. Since a thin, monomodal, waveguide will support the largest number of internal reflections, we find the sensitivity of monomodal waveguides to be higher than multimodal waveguides. Since the thickness of a monomodal waveguide is typically less than a wavelength, these waveguides are too fragile to be used without a thick substrate for support. This reduces the sensitivity, as only one side of the waveguide is exposed to the sample to be analysed.

A guided mode in a waveguide also produces an evanescent field in the lower-index layers outside the waveguide. In essence, some of the light is travelling outside the high-index waveguiding layer. The effective refractive index ( $N$ ) of the waveguide depends on the bulk refractive indices of the waveguide and cladding, and the relative proportions of the light in the waveguide and the cladding layers. This means that the effective index is always between the waveguide and cladding indices.

The other implication of this is that if the refractive index of the cladding layer changes, the effective index of the waveguide changes, which can be detected by a change in phase. Thus, waveguides are sensitive to changes in refractive index as well as absorption outside the waveguide layer. To maximise this sensitivity, we need to increase the amount of light in the evanescent field. To do this, we require a large difference between the waveguide and cladding refractive indices and the waveguide should be thin enough to support only a single mode. Because of the nature of the equations that determine the supported modes of a waveguide, exact analytical solutions are not possible and numerical solutions are required. Figure 14.40 shows the sensitivity of a planar waveguide to changes in the external bulk refractive index as a function of waveguide thickness, Figure 14.41 shows the sensitivity of the waveguide to changes in thickness of an adsorbed layer on the surface as a function of waveguide thickness and Fig. 14.42 shows the sensitivity of the waveguide to losses in the cover layer.

These graphs clearly show that there is an optimum waveguide thickness that maximises sensitivity to refractive index change for a particular mode, that these optimum thicknesses are different for TE and TM modes, that TM modes are generally more sensitive than TE modes and that the zero order modes are the most sensitive. The general form of all three graphs is the same, as they are effectively measuring the fraction of the light present in the evanescent field that is interacting with the material being sensed.

The calculations in the preceding section have been performed for a simple planar slab waveguide of infinite extent but finite thickness sandwiched between semi-infinite substrate and cover layers. Other waveguide configurations are possible, most notably the cylindrically symmetrical case of a high refractive index rod surrounded by a lower index cladding. This is the fiber-optic configuration used widely in telecommunications.

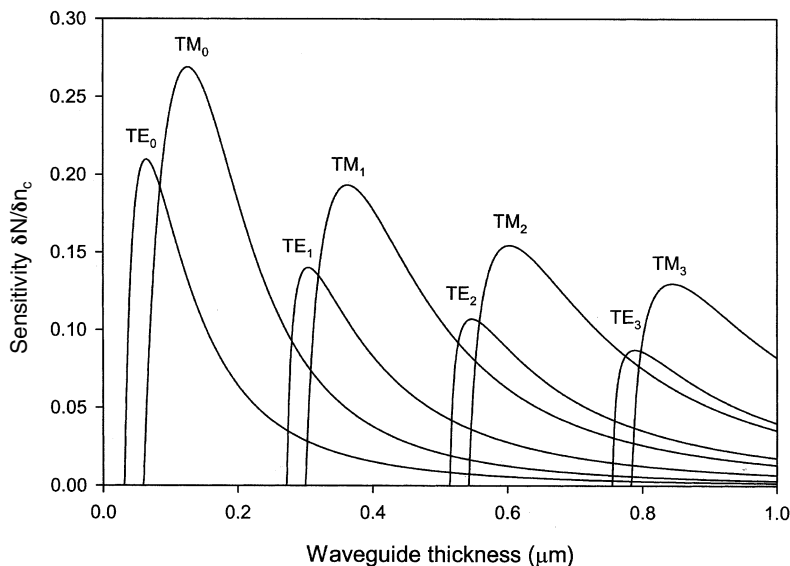


**Fig. 14.40** Graph of the sensitivity (ratio of the TM modes. Substrate index 1.46, waveguide change of waveguide effective index to change index 2.00 and cover layer index 1.333 calculated for illumination at 660 nm. of waveguide thickness for the first four TE and

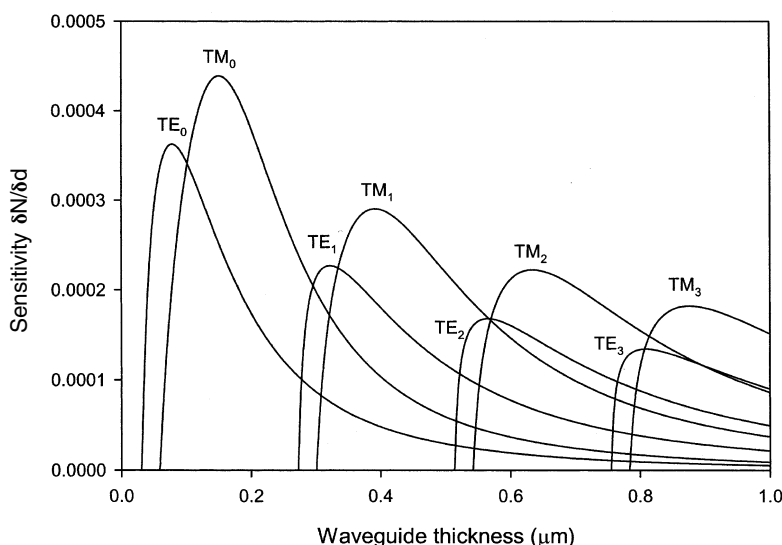


**Fig. 14.41** Graph of the sensitivity (ratio of the first four TE and TM modes. Substrate index 1.46, waveguide index 2.00, adlayer index 1.45 in thickness of a thin adlayer) of the waveguide and cover layer index 1.333 calculated for illumination at 660 nm. as a function of waveguide thickness for the

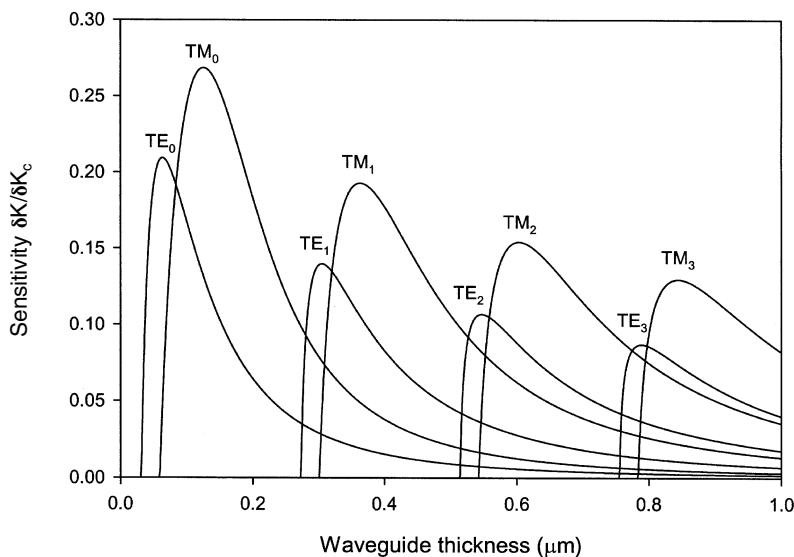


**Fig. 14.42** Graph of the sensitivity (ratio of the thickness for the first four TE and TM modes. change of the imaginary part of waveguide effective index to change in the imaginary index Substrate index 1.46, waveguide index 2.00, cover layer index 1.333 calculated for illumination at 660 nm.

#### 14.2.7.2 Measurement Configurations

There are various possible configurations, which utilise evanescent waves for biomolecular sensing and spectroscopy [221, 257]. Waveguides (either planar or in an optical fiber) can be used as prism couplers, grating couplers, mode couplers (interferometers), and in surface plasmon resonance (SPR), reflectometric interference and frustrated total internal reflection (FTR) experiments. Grating couplers use a grating fabricated in either the substrate or waveguide to couple light in and out of the waveguide. As the surface refractive index changes, the coupling angle changes, giving a change in angular position of the out-coupled light on an appropriate detector. In this mode, grating couplers work very much like SPR and resonant mirror (RM) sensors. They can also be used purely as a means of coupling light in and out of the waveguide to permit detection of absorption or fluorescence changes. Interferometers (such as Mach-Zender or Michelson devices) use a separate reference channel that does not undergo the chemical binding stage to act as a phase reference. A periodic change in intensity at the output is observed, caused by interference between the sensing and reference channels as the refractive index on the sensing channel changes. A problem with interferometers is that the output can be ambiguous, as a large change in refractive index can take the output through more than one cycle. These devices are generally very sensitive.

Ellipsometric sensors make use of the phase changes between the TM and TE modes propagating in a waveguide. If equal intensities of TE and TM are excited at the input, the polarisation state of the output will depend on the relative phase shift between TE and TM at the output. Since the sensitivity of the waveguide is different for TE and TM modes, a change in refractive index on the waveguide surface will result in a change in polarisation at the output. Like interferometric sensors, the output is cyclic and can result in ambiguous outputs. The sensitivity is very high.

In frustrated total internal reflection (FTR) experiments a leaky high index waveguide, which permits in- and out-coupling at well-defined coupling angles, is used. The coupling angle depends strongly on the cover layer refractive index. They can also be used to monitor absorption, as the reflectivity is a strong function of the loss in the cover layer.

### Fiber optics

Optical fibers are cylindrical waveguides consisting of a high index core surrounded by a low index cladding layer. Because of their low losses, fiber optics are widely used in the telecommunications industry, although the properties of telecommunications fiber optics make them poor sensors. Specially designed fiber optics can be used as biosensors, using a thin or no cladding layer on a monomode fiber core to permit interaction of the evanescent field with the material to be sensed [25]. Conventional fiber optics have also been widely used for sensing applications, but in the majority of cases they have been used as a convenient means of delivering and collecting light for conventional spectroscopies.

### End-fire coupling

End-fire coupling, as its name implies, is carried out by focusing a laser beam into a diffraction-limited spot centered on the waveguiding layer. Although end-fire coupling is conceptually very simple, it is not easy to perform in practice. One example where end-fire coupling has been successfully used in biological sensing applications is the difference interferometer [258–259, 260, 261]. If we consider Fig. 14.41, we can see that there are waveguide thicknesses at which the difference in sensitivity between the TE and TM modes is at a maximum. If linearly polarized light is launched at  $45^\circ$  to the plane of the waveguide, equal intensities of the appropriate TE and TM modes will be launched. Since end-fire coupling will generally excite more than one mode, the waveguide thickness is chosen such that only monomode operation will be possible at the excitation wavelength, and that the difference in sensitivity between the TE and TM mode is maximized. As the surface refractive index changes, the retardation of the TE and TM modes will change by different amounts, changing the relative phase of the TE and TM modes, and hence the polarization state of the out-coupled light. When the TE and TM components are in phase, the outcoupled light will be polarized in the same direction as the in-coupled light. As the phase difference between TE and TM increases, the

out-coupled light will become elliptically polarized, reaching circular polarization when the phase difference reaches  $\pi/2$ . At a phase difference of  $\pi$ , the light will be linearly polarized again, but at  $90^\circ$  to the polarization of the in-coupled light. As the phase difference increases further, the light will again become circularly polarized at  $3\pi/2$ , but with the opposite handedness, while at  $2\pi$  the cycle will be complete and the out-coupled light will be polarized identically to the in-coupled light. This cycle can be followed using an appropriate arrangement of beam splitters, polarizers and detectors, returning the TE-TM phase difference after processing the detector outputs. Since the phase difference is a cyclical function of surface refractive index, this device does not give an unambiguous measurement of surface refractive index. It can track slow changes in refractive index, but can only track the index successfully if the index change causes a smaller than  $\pm\pi$  phase change between successive samples of the output. Because the path lengths employed in this type of sensor can be quite large ( $\sim 10$  mm), the sensitivity is quite high. Effenhauser et al. [262] were able to detect  $10^{-11}$  M concentrations of human IgG using anti-human IgG antibodies with a difference interferometer configuration and a thin titanium dioxide waveguide. In studies with a bidiffractive grating coupler system, Kubitchko et al. have used nanoparticles to enhance the sensitivity for the detection of analytes like the thyroid-stimulating hormone (TSH) [306]. Without amplification the detection limit was 430 pM and with amplification by a latex-conjugated sandwich antibody the detection limit dropped to 0.11 pM, which is the clinically interesting range (0.3–667 pM TSH).

### **Grating couplers**

A grating structure at the substrate-waveguide or waveguide-cover layer interface can be used to couple light into the waveguide [263]. A major advantage of this method is that the waveguide can be fabricated on a simple planar substrate and coupling can take place through the bottom of the substrate. Careful design of the waveguide and grating can permit the use of TM-polarised light at the Brewster angle, which eliminates reflection at the bottom surface of the substrate.

Dubendorfer et al. [264] employed a chirped grating coupler design, where the grating period varies continuously along the width of the coupling area. This means that light will only couple into the waveguide at the location where the grating equation is satisfied. Thus, the position in space of the out-coupled beam is a simple function of the surface refractive index. They were able to detect refractive index changes of  $5 \times 10^{-6}$ , corresponding to changes in surface loading of 5 pg mm<sup>-2</sup>.

### **Resonant mirror (RM)**

The RM device consists of a high-index substrate ( $\sim 1$  mm thick lead glass,  $n_d = 1.72825$ ), a thin low-index spacer (about 1000 nm of magnesium fluoride or silica) and a very thin monomode waveguiding layer (about 100 nm of titanium oxide, zirconium oxide, hafnium oxide or silicon nitride). It can be used to monitor re-

fractive index and absorbing or fluorescent species within the evanescent field above the waveguide surface [265]. Light incident above the critical angle on the substrate/spacer interface is coupled into the waveguiding layer via the evanescent field in the spacer layer when the propagation constants in the substrate and waveguide match. For monochromatic light, this occurs over a very narrow range of angles, typically spanning less than 10 arc minutes. The device has been termed the resonant mirror because it contains a resonant cavity (the waveguide) and it acts as a nearly perfect reflector for light incident above the critical angle. Since the waveguiding layer acts as a resonant cavity, the light reflected from the RM device undergoes a full  $2\pi$  phase change as we scan across the resonance. To detect the resonance position, a phase reference must be provided, which is substantially constant in phase. This could be provided by splitting off part of the input beam and recombining it with the light from the sensor, but this is instrumentally difficult, and means that the object and reference beams travel by widely separated paths. Ideally, the two beams should travel by identical paths, so that phase-shifting effects (such as temperature changes) are common to both beams. This can be accomplished in the RM sensor by using the TE mode as reference for the TM resonance and vice versa. This is only feasible because the resonance positions for TE and TM are widely separated.

The resonance positions may be determined in two ways:

1. In angle, using monochromatic input light covering a range of input angles (angular scan mode) [265].
2. In wavelength, using broadband input light at a fixed input angle (wavelength scan mode) [266].

To determine the resonance angles or wavelengths, at which light couples into the waveguiding layer, linearly polarised light at  $45^\circ$  to the plane of the waveguiding layer is applied to the device, exciting equal intensities in the TE and TM modes. The output light from the device is passed to a crossed analyser, which only passes light that has undergone a  $\pi$  phase change in the sensor device. In the angular measurement mode, the input light is a converging monochromatic wedge beam, covering a sufficiently wide range of input angles to permit the resonance angle (for the fixed wavelength) to be determined for the required range of surface refractive indices. In the wavelength measurement mode, the input light is a well-collimated beam of white light, covering a sufficiently wide range of wavelengths to permit the resonance wavelength (at the fixed input angle) to be determined.

Buckle et al. [267] used the RM to monitor antigen/antibody and enzyme/substrate/inhibitor interactions using several methods for immobilization of the biomolecules at the sensor surface. Sensitivities in the nM range were reported. Watts et al. [268] used the RM sensor to monitor the binding of microbial cells to antibodies immobilized on the surface of the sensor. They detected the binding of *Staphylococcus Aureus* (Cowan-1 strain) to human immunoglobulin G (hIgG), covalently immobilized on the sensor surface via aminopropylsilane, at concentrations between  $8 \times 10^6$  and  $8 \times 10^7$  cells  $\text{cm}^{-3}$ . By employing a sandwich assay using a

hIgG-gold particle conjugate, detection limits were reduced by a factor of 1000. It appeared feasible to detect between  $4 \times 10^3$  and  $1.6 \times 10^6$  cells  $\text{cm}^{-3}$  in spiked milk samples.

A range of instruments based on the RM is commercially available (the IASys system of Labsystems/Affinity Sensors), using the angular scan mode to determine the resonance angles. These instruments can only measure refractive index changes.

#### 14.2.7.4 Surface Plasmon Resonance (SPR)

Surface plasmon waves are excited in thin metal films when appropriate coupling conditions are met. The surface plasmon wave is an oscillation of the free electrons in the metal under the influence of the electric field of the light [257]. For sensor applications, the Kretschmann configuration [269–270, 271] is most often used, where a thin metal layer (usually 50 nm gold) is deposited on a glass prism, and light is coupled into the metal film at the coupling angle. This configuration is shown in Fig. 14.43. Only TM polarized light shows this behaviour, where the mode is localised at the metal-cover layer interface. TE polarized light does not show this behaviour. Since the metal film is very lossy (it has a large imaginary component of the complex refractive index), the reflected light is very strongly attenuated at the coupling angle. The coupling angle is a very strong function of the cover layer refractive index. Thus, as material binds to the metal layer there is a change in the angle at which the drop in reflectivity occurs. This is the basic sensing mechanism for SPR biosensors, as shown in Fig. 14.44.

Instrumentation for SPR sensors generally comprises a monochromatic light source (a filtered incandescent lamp, LED or laser) followed by a cylindrical lens to provide illumination over a wide range of angles. A CCD detector is then used to monitor to position of the dip in intensity (angle measurement mode),

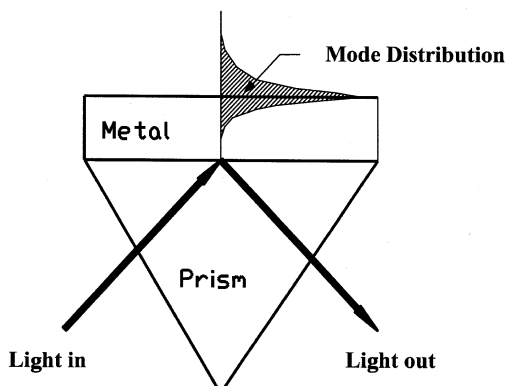


**Fig. 14.43** The Kretschmann configuration for excitation of SPR in a thin metal layer.

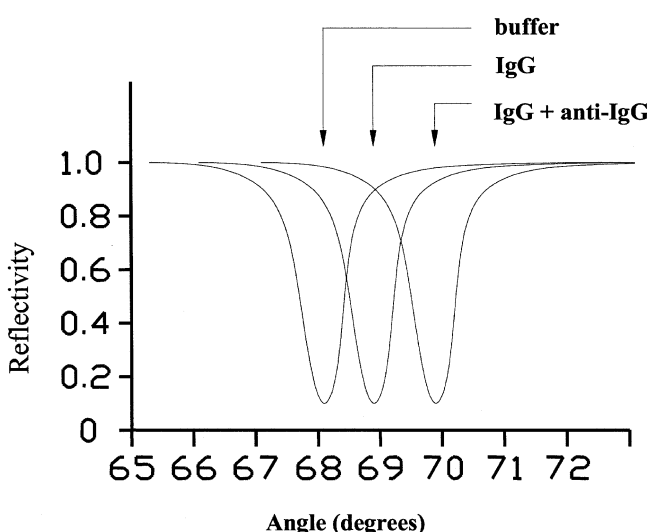


**Fig. 14.44** Illustration of the shift in resonance angle at various stages in the adsorption of biomolecules to the metal surface.

which indicates the coupling angle. Alternatively, a collimated beam of white light may be used at a fixed angle of incidence, and the wavelength position of the dip determined (wavelength measurement mode). Systems of this kind have no moving parts, and thus can follow very rapid changes in the angular position of the reflectivity dip. The metals most often used are gold or silver, but copper can also be used. These metals all have the high conductivity needed to give a relatively narrow dip in reflectivity, making the task of following small changes in the position of the dip easier.

### Commercial SPR biosensors

Commercial systems using SPR sensing methods have become available from a number of suppliers. These systems range from large multichannel laboratory bench instruments to simple single-channel integrated devices in an integrated-circuit style package. Since its commercialisation SPR has been used for the detection of a large variety of biomolecules. Reviews on the applicability of SPR detection have appeared rather regularly, discussing biomolecular interactions of proteins, nucleic acids, lipids and carbohydrates [272–277]. SPR has also shown some usefulness in the study of conformation changes of adsorbed proteins. For instance, Boussaad et al. have used multiwavelength SPR to study conformational and electronic changes induced by the electron-transfer reaction in cytochrome c [278], and Sota et al. studied the acid-induced denaturation of an immobilized protein [279]. DNA hybridization has also been studied by SPR [280]. Through many studies much new knowledge has been acquired on the kinetics of antigen–antibody reactions at surfaces [281].

The BiaCore system was the first commercialised SPR instrument based on the Kretschmann configuration. The BiaCore is a multi-channel instrument that has been extensively used for biological assay work, and in the monitoring of both thermodynamic (dissociation constants) and kinetic (on and off rates) parameters of a wide range of biomolecular interactions. A full overview of the work done with the BiaCore can be obtained from the manufacturer's website [282]. Recent applications include the determination of streptomycin residues in whole milk [283], bovine insulin-like growth factor (IGF)-binding protein-2 [284], global conformational transitions in human phenylalanine hydroxylase [285], peptides from the GH loop of foot-and-mouth disease virus [286], gentamicin residues [287], penicillin residues in milk [288], HIV-1 protease inhibitor interactions [289] and acylated proteins [290]. A competitive instrument to the BiaCore, the "IBIS" series of biosensors, has also been developed in the Netherlands at the Twente Technical University and is based on the conversion of angle data into a time interval by the use of a vibrating mirror system [291, 292].

The Spreeta<sup>TM</sup> device manufactured by Texas Instruments is a complete miniaturised SPR sensor containing an infra-red LED emitting at 830 nm, a cast polymer prism with a gold SPR layer, a 256 element linear CMOS image sensor and a 4 Kbit serial EEPROM memory [293]. It is packaged as a single unit of dimensions 41.40 by 28.92 by 13.49 mm with a standard 16 pin 0.3 in dual-in-line connector. Melendez et al. have reported a resolution of  $10^{-5}$  refractive index units using this device [194]. Elkind et al. describe the use of the Spreeta device as a refractive index sensor for a direct assay for human creatine kinase MB (CK-MB, a marker for heart attacks) using adsorbed anti-CK-MB antibodies, obtaining a change in index of  $\sim 4 \times 10^{-4}$  for binding of 100 ng ml<sup>-1</sup> of CK-MB [295]. They were also able to assay trinitrotoluene (TNT) using a competitive assay format by immobilising a trinitrobenzene-bovine serum albumin adduct to the sensor surface, then reacting the TNT sample with anti-TNT antibodies and passing the resultant solution over the sensor surface. If high concentrations of TNT were present in the sample, then most of the antibody binding sites were occupied, resulting in a reduced rate of binding of the antibody to the trinitrobenzene-BSA coated sensor surface. With this assay it was possible to detect 7 ng ml<sup>-1</sup> of TNT. Sesay and Cullen have used the Spreeta sensor to monitor endocrine disrupting chemicals (EDC) in aqueous samples [296]. Estrone-3-glucuronide (E3G) was used as a model EDC, and a competitive assay format was developed. Ovalbumin-E3G conjugate was immobilised by adsorption onto the sensor surface, while the sample to be assayed was pre-incubated with a known concentration of anti-E3G antibody. The pre-incubated sample was passed over the treated sensor surface for a fixed time, followed by washing with phosphate-buffered saline solution to remove any non-specifically bound material. The SPR peak shift was then determined and used to derive the concentration of E3G in the original sample by reference to a calibration curve. The sensor surface could be regenerated using a strong domestic detergent (Persil biological liquid) to remove all the biological material. The detection range was 10–150 ng ml<sup>-1</sup>.

### Fiber and waveguide SPR

Fiber optic devices are attractive in many applications because they can be physically very small, provide remote operation and electrical isolation from the associated instrumentation. For these reasons, many designs for fiber-optic SPR sensors have been developed. They all rely on phase matching between the optical mode in the fiber and the surface plasmon wave. Since the control over the coupling angle is lost in a fiber, wavelength scanning is often employed. Slavik et al. [297] have shown that a wavelength-scanned fiber-optic SPR sensor can detect very low concentrations of proteins. They used a single-mode optical fiber with a cut-off wavelength of 724 nm which was polished down to remove all but 500 nm of the cladding. The resulting device was coated with 65 nm of gold to support surface plasmons and then 19 nm of tantalum pentoxide to adjust the sensor's operating range to refractive indices between 1.329 and 1.353. This device was capable of detecting  $40 \text{ ng ml}^{-1}$  of human immunoglobulin G (IgG) using anti-human IgG antibodies immobilised on the sensor surface by cross-linking with glutaraldehyde.

Similar behaviour is observed when a thin metal layer is coated on a planar waveguide. Harris et al. [298] have developed the theory of waveguide-coupled SPR sensors. Brecht and Gauglitz have compared the performance of a waveguide-coupled SPR sensor against a grating coupled waveguide, a channel waveguide interferometer and a thin-film reflectance sensor for the detection of pesticides using a competitive assay format with anti-triazine antibodies [299]. Instead of using a full spectrum scan, the intensity at a fixed wavelength was monitored. The limit of detection for triazine was found to be  $0.15 \text{ ng cm}^{-3}$ .

### Sensitivity and applications of SPR-based biosensor instruments

In a recent review by Homola et al., the analytical characteristics of various SPR instrumentation configurations for SPR have been compared with respect to the type of coupling (prism or grating) and the mode of measurement (angular, wavelength and intensity read-out) [300, 301]. In principle, the prism-coupler (Kretschmann) configuration was assessed as being capable of yielding the highest sensitivity (in terms of refractive index change) in comparison with a grating coupler based set-up, particularly when the method of interrogation was based on intensity measurements. Lekkala and Sadowski have used the Kretschmann configuration in conjunction with lock-in amplifiers for the highly sensitive detection of intensity changes at near-resonance conditions [302]. The system was used for the optimisation of antibody orientation on various lipid-modified surfaces [303].

Although the intrinsic sensitivity of SPR measurements (without any amplification schemes) had been initially assessed to be of the order of  $1 \text{ nM}$  or  $150 \text{ ug l}^{-1}$  for IgG [304], lower detection limits for small analytes have been reported [305, 306]. In most studies equilibrium dissociation constants ranged from nanomolar to micromolar, with a few studies in the picomolar range [307, 308]. The resolution of SPR measurements has to some extent been improved by using well-designed reference surfaces and sophisticated data processing techniques [309]. SPR has

been combined with other techniques, such as mass spectrometry [310] and AFM + electrochemistry [311]. Particularly the combination of multichannel SPR with MALDI-TOF can be regarded as a powerful tool for proteomics research (see Section 14.4.6).

In general, SPR-based biosensors have detection limits around 50 pM or 100 pg cm<sup>-2</sup>. This is not always sufficient for the detection of low molecular weight analytes where concentrations fall below picomolar [312]. In such cases amplification of the signal by sandwich assay formats is presently the only solution. Already in 1988 Mandenius and Mosbach had used quartz particles to amplify ellipsometric measurements of biospecific interactions [313]. Similar labels, which have a large effect on the refractive index near the surface, will be suitable for use with SPR. For instance, Lyon et al. have described the use of colloidal Au nanoparticles to enhance the SPR response, through strong optical coupling between the film and the particle, achieving detection limits for human IgG down to 6.7 pM using a sandwich immunoassay format [314]. Besides a large shift in incident angle, the collodial gold gives a broadening of the plasmon resonance peak and an increase in minimum reflectance.

#### 14.2.7.5 Reflectometric Interference Spectroscopy (RIfS)

Reflectometric measurements are technically easy to perform and can yield useful information about thin films and their interfaces. The partial reflection of incident light from two interfaces of a thin film with a thickness of about 1 μm can function as a Fabry-Perot interferometer with low reflectance. In the situation depicted in Fig. 14.45a, the reflected light will show an interference pattern as a function of wavelength, according to:

$$R = R_1 + R_2 + 2\sqrt{R_1 R_2} \cos\left(\frac{4\pi n d}{\lambda}\right) \quad (21)$$

where  $R$  is the reflectance,  $\lambda$  the wavelength,  $n$  the effective refractive index and  $d$  the effective thickness of the optical layer.

An increase in optical thickness of the thin film, caused by e.g. ligand adsorption, will shift the interference spectrum to a higher wavelength and widen the distance between the minima and maxima in the interference spectra as illustrated in Fig. 14.45b. This is the principle behind reflectometric interference spectroscopy, or RIfS [315]. Due to the high sensitivity of the detection (ppm levels of phase shifts can be measured [316]), the RIfS device has been successfully used for the study of various biological interactions at surfaces, such as mouse anti-atrazine/atrazine [317] and DNA-ligand interactions [318]. The principle of RIfS also allows the construction of low-cost devices.

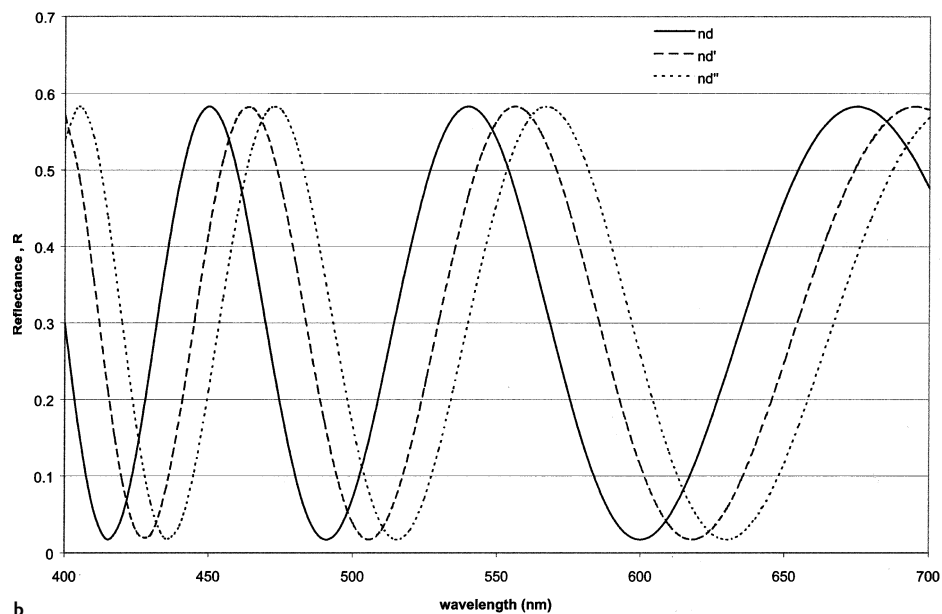
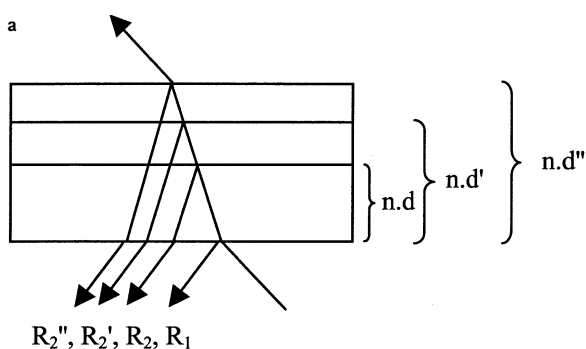


**Fig. 14.45** The principle of interference reflectometry at a thin film of increasing optical thickness: (a) The thin optical layer with several reflections from increasing optical thicknesses

$nd$ ,  $nd'$  and  $nd''$ . (b) Calculated interference curves with:  $R_1=0.2$ ,  $R_2=0.1$ ,  $n=1.35$  and

$nd=1000$  nm,  $nd'=1030$  nm and  $nd''=1050$  nm.

#### 14.2.7.6 Total Internal Reflection Fluorescence (TIRF) and Surface Enhanced Fluorescence

In assays based on fluorescence labels there is generally a low degree of discrimination of the signal from molecules in the bulk solution from molecules bound to the surface (e.g. of a sensor). Surface enhanced fluorescence can be used to partly discriminate the signal from surface bound species from those in the bulk solution. This can be done either by using normal evanescent waves or using amplification of evanescent waves through a thin metal layer via SPR. Additionally it is possible to excite plasma oscillations in metal nanoparticles, which causes a strongly enhanced near-field at the particle surface. Molecules located in this near-field feel a higher light field strength, which results in enhanced light-induced molecular responses. The dipole momentum of the excited molecules interacts with the metal. Surface-enhanced fluorescence of molecules adsorbed on silver island films is already a well-known phenomenon, and is also related to other surface enhanced optical phenomena, such as Raman scattering [319, 320]. Time resolved surface enhanced fluorescence of molecules positioned close to submicroscopic metal particles has also been investigated by Ausseneegg et al. [321]. Measurement of picosecond time-resolved fluorescence indicated a significant shortening of the lifetime of the excited molecular state.

Recently, Schalkhammer et al. have discussed the relevance of surface enhanced fluorescence in immunosensing applications (surface-enhanced fluoroimmunoassay, SE-FIA) [322]. The enhancement mechanism was explained by an electrodynamic model and the interaction between metal particle and fluorophore for the excitation and emission process was discussed. It was shown that the discrimination power increased with decreasing quantum efficiency of the fluorophore. This suggested that in SE-FIA a low-quantum efficiency fluorophore needs to be used, as was shown by experiments with model compounds.

Due to the surface sensitivity surface enhanced fluorescence has become particularly popular in the characterisation of thin molecular films, such as Langmuir-Blodgett films and self-assembled biomembranes. Two surface enhanced spectroscopic techniques (surface enhanced IR absorption, SEIRA, and surface enhanced fluorescence, SEF) were recently applied to the study of biomembrane systems by the group of Reiner Salzer [323]. With SEIRA, specific fingerprints of biomolecules could be obtained with a tenfold IR intensity enhancement. With SEF signal enhancement factors greater than 100 were obtained. The enhancement factor was very dependent on the properties and structure of the metal clusters used. With the two techniques biomembranes formed from vesicles with embedded nicotinic acetylcholine receptors were spectroscopically characterized.

### 14.2.8

#### Infrared and Raman Spectroscopy in Bioanalysis

##### 14.2.8.1 FTIR, FTIR Microscopy and ATR-FTIR

Fourier transform infrared spectrometry has very much revolutionized the investigation of peptides and proteins, and is used in various clinical chemistry applications [324–326]. FTIR is most frequently used in protein chemistry to determine the secondary structure content [327–330], to assess conformational changes in proteins [331–333] and to study protein unfolding [334, 335]. FTIR has been used to characterise basic structural motifs of model peptides, such as  $\alpha$ -helices and  $\beta$ -turns [336–338]. Hydration of proteins has also been extensively studied, particularly with relevance to the determination of the structural integrity of lyophilized protein preparations [339]. A relatively new trend is the characterisation of the secondary structures of peptide fragments of proteins in different solvents [340–343]. FTIR studies of proteins and peptides are usually concerned with the amide groups and their deuterium substituted analogues. The carboxyl groups are also commonly analyzed by FTIR studies [344].

Although technically less easy to perform, FTIR spectroscopy is also an ideal tool for studying membranes and membrane-associated proteins, because of the possibility of examining samples in different physical states. Secondary structure and conformational changes have been described for ATPases, photosystem II reaction center proteins and bacteriorhodopsin, as well as proteins in the membrane of gastric carcinoma cells and erythrocytes [345–350]. The orientation in lipid bilayers can be studied with polarized FTIR, which yields insight into the orientation of toxins, ion channels and proteins in cell membranes [351–355]. FTIR has also been extensively applied to the study of protein adsorption to solid surfaces [357]. These studies often involve the use of attenuated total reflectance (ATR) accessories [357]. Thus, studies have been performed on the adsorption of IgG and F(ab')<sub>2</sub> to siliceous surfaces [358], serum albumin to organotrichlorosilane-derivatised surfaces [359] and proteins on alkylmercaptan-derivatised surfaces [360]. FTIR microscopes have given new possibilities for the study of proteins in their native environment, such as in serum, whole blood, bone, brain tissue and many other matrices [361–363].

The application of FTIR directly to clinical studies and diagnosis has been very much debated. Methods for *in vivo* monitoring of glucose have until now been more presented in the patent literature than in the scientific literature. IR spectroscopy methods, however, have been described for the *in vivo* monitoring of glucose, hemoglobin, urea, albumin, phosphocreatine, and nitric oxide [326].

##### 14.2.8.2 Raman Spectroscopy

Raman spectroscopy is increasingly being applied not only to the analysis of proteins and peptides [364–366], but also to the analysis of polymers [367], viruses [368] and skin lesions [369]. Generally higher concentrations of samples are required as with FTIR, although resonance enhancement techniques can alleviate

this problem. Although Raman spectroscopy is much used for protein structure elucidation, FTIR and circular dichroism (CD) are still more commonly employed. This is mainly due to better instrument availability and less problems with sample preparation. A recent technical improvement of Raman spectroscopy is the use of near-infrared excitation. Today such spectrometers are all well available. As standard FTIR is concerned with main-chain vibrations, Raman spectroscopy focusses more on side-chain vibrations. Tryptophan and tyrosine are the most frequently investigated side chains, but cysteine and histidine side chain resonances are also much studied [370–376]. Raman spectroscopy is frequently applied to the study of heme vibrations in porphyrin-containing proteins due to the possibility to use resonance enhancement [377].

#### 14.2.8.3 Surface Enhanced Raman Spectroscopy (SERS)

Since its discovery in 1974, surface enhanced Raman spectroscopy, or surface enhanced Raman scattering (SERS), has been an important method for examining surface adsorption of organic molecules [378, 379]. For instance, SERS has been employed in studies of adsorption of small peptides to silver [380]. Recent investigations have focussed on the study of photosynthetic membranes and cytochromes [381, 382]. Rather novel applications include elucidation of virus structure and proteins adsorbed onto vaccine adjuvants [383] and gene diagnostics [384]. SERS has recently also been applied in non-resonant conditions to observe colorless, single biomolecules [385]. SERS has been combined with scanning probe techniques to obtain Raman imaging of DNA-molecules at a 100 nm resolution [386]. The combination of a confocal microscope and careful surface treatments extends the application of SERS to the study of adsorbates on a wider range of surfaces [387], while the applicability of SERS has recently been expanded to the study of interfacial materials by overlayer deposition [388]. In the latter technique, materials that do not display Raman enhancement themselves, are deposited as an ultrathin overlayer on Raman-active surfaces, expanding the application of SERS to metallic, semiconductor and insulator films. A novel spectroelectrochemical cell for surface Raman spectroscopy has also been developed, which has been used for studies on cytochrome P450 [389].

#### 14.2.9

##### Circular Dichroism

Circular dichroism (CD) is a form of light absorption spectroscopy that measures the difference in absorbance of right- and left-circularly polarized light (rather than the absorbance of isotropic light) by a sample in solution. CD is related to optical rotary dispersion (ORD), which is the variation of optical rotation as a function of wavelength. CD spectra recorded between 180 and 260 nm enable fast routine determination of secondary structural types in proteins, i.e. the  $\alpha$ -helix, parallel and antiparallel  $\beta$ -sheet and  $\beta$ -turn content. The use of CD spectroscopy in bioanalysis is expected to grow, due to the expanding markets for chiral compounds [390]. Con-

temporary CD instrumentation allows levels of accuracy for the determination of 97 % for  $\alpha$ -helices, 75 % for  $\beta$ -sheet, 50 % for  $\beta$ -turns and 89 % for the other structure types. The most common application of CD is the study of conformation changes (secondary and tertiary structure). As such the technique lends itself well to the study of folding and unfolding induced by temperature, pH and chaotropic ions [391, 392]. Model synthetic peptides have been examined by CD to explore the physical basis of the formation of  $\alpha$ -helix and  $\beta$ -sheet formations [933, 394]. CD is increasingly used to examine tertiary structural features of proteins through aromatic amino acid mutant proteins [395, 396]. The use of CD in membrane and surface adsorption studies has been, unfortunately, limited by differential light scattering and absorption flattening [397].

Vibrational circular dichroism (VCD) was developed as a supplementary technique in the 1970s, and is the IR counterpart of CD [398]. VCD measures the differential absorption of left and right circularly polarized IR light by chiral molecules. Since there are more spectral lines in the IR region than in the UV and each can have a chiral response, a more elaborate stereochemical and structural analysis is possible than on the basis of CD. Researchers have started to use VCD for conformational studies of all classes of chiral molecules, especially carbohydrates [399].

## 14.3 NMR Spectroscopy of Proteins

### 14.3.1 Introduction

Nuclear magnetic resonance spectroscopy is likely the most versatile method for the study of biomolecules. The power of NMR originates from the fact that practically every atom with a magnetic nucleus gives rise to an individual signal in the NMR spectrum that carries spatial and temporal information of the local chemical environment of that atom. Solution conditions in high resolution NMR experiments mimic the natural biological environment and results relate to functional assays.

Proteins, owing to their many biological functions, display versatile phenomena to investigate. In addition there are spectroscopic reasons in favor of proteins. Proteins, as a class of molecules, give particularly well-dispersed NMR spectra because of rich local diversity in their physical-chemical structures. Proteins can also be obtained, using the methods of molecular biology, in large quantities enriched uniformly or selectively with  $^{13}\text{C}$  and  $^{15}\text{N}$  as well as deuterated or specifically reprotoinated to make use of a large repertoire of heteronuclear NMR experiments. These are the main reasons why NMR spectroscopy of proteins is highly developed.

Progress in spectroscopy, instrumentation, computational methods, data analysis and sample production has resulted in astonishingly versatile and powerful methods well-documented in the original papers, recent reviews (e.g. [400–406]) and

textbooks on NMR spectroscopy (e.g. [407, 408]). The most important recent innovations in the field of NMR include the introduction of weakly aligned systems [409] and the transverse relaxation optimized spectroscopy [410]. These discoveries have significantly expanded the realm of high resolution NMR spectroscopy by including new directional and range-independent information and by significantly enlarging the set of molecules amenable to NMR. Many of the NMR methods that were originally developed for proteins have been amended to be suitable for studies of other classes of molecules, in particular nucleic acids and carbohydrates.

### 14.3.2

#### Protein Sample

##### 14.3.2.1 Solubility and Stability

Successful NMR spectroscopy begins from successful sample preparation [411]. Usually it is very difficult to compensate for a poorly “behaving” molecule by spectroscopic means. Indeed the preparation of a highly soluble labeled protein sample is often the limiting factor, not the spectroscopy, in the studies of proteins and their complexes by NMR. Problems with samples manifest themselves typically as low signal-to-noise ratio (SNR) or fast transverse relaxation i.e. broad lines or multiple signals. These can be signs of poor solubility, oligomerization, aggregation, conformational isomerism or perhaps paramagnetic ion impurities, all deleterious for carrying out detailed NMR studies. However, low-quality spectra may also be indicative of an interesting phenomenon perhaps worthy of an investigation itself.

The signal-to-noise ratio of NMR has increased many folds over the decades due to the progress in instrumentation and methodology. Nevertheless, NMR remains a comparatively insensitive method, owing to the minute nuclear magnetic moments, compared with many forms of optical spectroscopy. Therefore fairly large amounts of material are required for experiments. Even though compounds on a nanogram scale can be detected using special NMR probes, detailed structural studies, e.g. determination of three-dimensional structures, need at least a few hundred micromolar protein solutions in few hundred microliter volumes. Proteins, that are obtained by overexpression in bacterial or eukaryote hosts and subsequently purified by affinity, ion-exchange or gel-filtration etc., come in large quantities and are usually sufficiently pure for NMR spectroscopy. Small molecule impurities are easy to detect and often indifferent for heteronuclear NMR spectroscopy, unless occurring in much higher concentrations than the solute of interest or unless they happen to possess a particular activity in the system of interest.

The high solubility of a biomolecule required for NMR cannot be taken for granted. The spectral characteristics might be compromised, even without an apparent aggregation, seen as weak signals or broad lines. Often it is not obvious if or how unspecific binding or aggregation or oligomerization, that lead to increase in rotational correlation times, can be avoided. Temperature, pH and ionic strength are among the easiest parameters to vary in search of appropriate solvent conditions. Knowledge of the properties of a protein, such as isoelectric

point (pI), acquired during the production and purification may provide valuable clues about the conditions and additives, i.e. co-solvents that may improve the spectral appearance. Some of the commonly used co-solvents include surfactants such as CHAPS, octylglucoside, SDS, alcohol such as trifluoroethanol, zwitter-ionic compounds such as glycine and also sometimes denaturants such as urea and DMSO. Ligands or inhibitors of enzymes or cofactors of proteins may improve the spectral appearance. Chimeric constructs have also been used to improve the behavior [412]. Nevertheless, it is difficult to take into account all aspects that have an influence on the spectral appearance and suitable conditions are often found after trial and error.

The presence of more than one conformation may give rise to multiple signals or broadened lines due to exchange and may significantly reduce SNR, complicating assignment and interpretation of the spectra. The solvent conditioning may alter the equilibrium towards a single conformation. Provided that there is some evidence or even hypothesis of conformational heterogeneity, e.g. proline *cis-trans* isomerism or flexibility in the catalytic site due to the lack of ligand or hinge motions in a multi-domain structure, it may help to understand and eventually to solve the problem of conformational isomerism by protein engineering [413]. Of course, it should be kept in mind not to change the solvent conditions or to engineer the protein to render the original biological question meaningless. Functional assays help to judge the appropriateness of the solvent conditioning or protein engineering. NMR itself, e.g. when used to follow reaction kinetics, can be used to assess functional properties.

A stable sample is a necessity for extensive studies such as the determination of three-dimensional structure, which require several weeks of measurement time. Bacterial growth, due to non-sterile conditions, in the sample tube can be largely eliminated by using sodium azide ( $\text{NaN}_3$ ) at 0.02 % (w/v). Proteins are also subject to degradation by proteolytic enzymes that may be present in the sample in minute amounts after the purification. Application of a “cocktail” of inhibitors against the common proteases largely eliminates the enzymatic breakdown. Exposed cystein residues not paired in disulfide bonds may, with time, form intermolecular disulfide bonds, generating dimers or higher oligomers depending on the number of exposed cysteins. Dithiotreitol (DTT) in a stoichiometric excess to cysteins can be used to keep *all* cysteins in the reduced state. Alternatively the unpaired cysteins could often be mutated to serines to avoid the problem of unnatural pairing. Deamidation of asparagine (Asp) over time is a potential problem in certain sequences but can be avoided by engineering the corresponding sequence.

In practice, it is difficult to take into account or rationalize all aspects that influence the sample solubility and stability. Fortunately, the protein stability and solvent conditions are easy to monitor, in particular by heteronuclear correlation spectroscopy. Amide resonances are sensitive reporters of changes in the protein structure or in the solvent conditions. Mass spectroscopy that requires very little material is a very practical method of monitoring the protein sample. Once optimal conditions are found experiments should be conducted promptly.

### 14.3.2.2 Isotope Labeling

The purpose of isotope labeling is to produce the molecule of interest enriched with the isotopes of preferable nuclear magnetic properties in order to extract more information or to facilitate the interpretation of the information and, more frequently, to make the study feasible in the first place. In many applications it is advantageous to increase the proportions of  $^{13}\text{C}$  and  $^{15}\text{N}$  that are both spin- $\frac{1}{2}$  nuclei, from their natural abundance 1.1 % and 0.4 % respectively, as high as possible, to nearly 100 %, for the detection. The labels facilitate assignment by multidimensional heteronuclear correlation spectroscopy. In other applications selective labeling provides the means to simplify the interpretation, e.g. to distinguish intermolecular correlations from intramolecular signals or segmental labeling [414, 415] e.g. to reduce the number of signals.

In large systems perdeuteration is the efficient way to slow the transverse relaxation [416–419] and specific reprotonation serves to maintain crucial information [420]. The labels allow measurements of dihedral via scalar couplings [421] and projection angles via cross correlation rates [422] as well as internuclear directions via residual dipolar couplings [421]. Furthermore site-specific spin labels, i.e. paramagnetic electrons, can be used to extract long-range distance information [423]. Today isotope labeling is an integral part of biomolecular NMR spectroscopy [402].

#### $^{13}\text{C}$ and $^{15}\text{N}$ labeling

Uniform  $^{13}\text{C}$  and  $^{15}\text{N}$  labeling provides improved signal dispersion and editing by multidimensional experiments or filtering by isotope or spin-state as well as various routes for coherence transfer and ways to measure scalar and dipolar couplings. Solvent suppression in heteronuclear correlation experiments is also much easier than in homonuclear correlation experiments.

Uniformly labeled proteins are customarily obtained via overexpression in bacteria grown in a culture medium having enriched metabolites as the sole sources of carbon and nitrogen. For bacterial expression  $^{13}\text{C}$ -glucose (or  $^{13}\text{C}$ -acetate) and  $^{15}\text{N}$ -ammonium sulfate or chloride are commercially available and commonly used. The use of the minimal medium easily leads to reduction in growth and to a reduced yield compared to the use of a rich medium. The choice of a host strain and vector, and at times also the codon usage, have to be optimized to reach a yield that is sufficient, given the current price of  $^{13}\text{C}$ -glucose. The  $^{15}\text{N}$ -compounds are inexpensive and thus can be used for testing much of the performance of the protein. More recently, rich growth media with isotope labels have become commercially available to facilitate the uniform enrichment. To make proteins with post-translational modifications, expression in eukaryote hosts, primarily in yeast, reaches sufficient expression levels [424].

For studies of protein complexes intermolecular correlations can be distinguished from intramolecular correlations by filtered heteronuclear experiments, provided that one of the components is labeled selectively and differently from the other. This approach is also useful for large protein complexes to acquire simplified spectra to alleviate the assignment. For the same end, segments of a poly-

peptide chain can selectively be labeled by  $^{13}\text{C}$  and  $^{15}\text{N}$  using inteins, splicing enzymes [415]. The inteins also provide the way to obtain cyclic peptides with labels that are significantly more inexpensive than labeled amino acids from the solid state peptide synthesis. DNA and RNA molecules are nowadays obtained with labels from cell-free synthesis using uniformly labeled ribonucleotide triphosphates (NTP) [425–428].

### Deuteration

Perdeuteration has become an indispensable means for circumventing problems of transverse relaxation ( $T_2$ ) inherent to large biomolecules and their complexes [419]. Protons, due to their large nuclear magnetic moment, are the main cause of dipolar relaxation of protons themselves as well as the directly bound heteronucleus. The relaxation problem can largely be reduced by uniform deuteration. Perdeuterated proteins are obtained by growing host microorganisms in deuterium oxide ( $\text{D}_2\text{O}$ ) often concurrently with  $^{15}\text{N}$  and/or  $^{13}\text{C}$  labeling. The expression levels in  $\text{D}_2\text{O}$  are usually comparable to that in  $\text{H}_2\text{O}$  but the growth is compromised. When the labeled protein is dissolved in  $\text{H}_2\text{O}$  the amide deuterons exchange for protons which serve as the main source of magnetization for coherence transfer in heteronuclear correlation experiments and also for the direct detection of the signal during the acquisition. The high degree of labeling is advantageous in reducing the transverse relaxation of the aliphatic carbons and amide protons in transverse relaxation optimized spectroscopy (TROSY) at high magnetic fields [410, 429]. Obviously perdeuteration reduces significantly the distance information available via interproton nuclear Overhauser enhancements (NOE). A compromise between the favorable relaxation properties and the extent of NOE data may be found by adjusting the degree of deuteration with the  $\text{D}_2\text{O}$  content in the culture medium. A suitable degree of random fractional deuteration is often above 50 %.

Alternatively, an important portion of the conformational restrictive NOEs can be recovered by relabeling for protonated methyl rotors of aliphatic residues [420]. This is accomplished using either selectively labeled amino acids that are more readily incorporated during the expression than *de novo* synthesized amino acids or more affordably by using selectively protonated non-glucose carbon sources. It depends on the metabolism of a particular metabolite how the protons become incorporated in specific positions in the amino acids. The methyl group of pyruvate is a precursor for the methyls of alanine, valine, leucine and  $\gamma$ -rotor of isoleucine. More recently, protonated methyl rotors of valine, leucine and isoleucine have been derived using  $\alpha$ -ketoglutarate. It has been demonstrated that these labeling strategies are sufficient to obtain short-range distance data for determination of three-dimensional structures when the reduced distance information from highly perdeutrated proteins is compensated partly by using the directional restraints and hydrogen bond restraints. More sophisticated labeling strategies are designed to reprotonate  $\text{C}^\alpha$  to be used as the sole source of magnetization for experiments in  $\text{D}_2\text{O}$ .

### 14.3.2.3 Dilute Liquid Crystals

Perhaps surprisingly, biomolecules as large as proteins tumble in water so stochastic that it is difficult to observe any degree of molecular alignment [430]. It is only proteins with prosthetic groups of high magnetic anisotropic susceptibility, such as globins with heme-groups, that acquire a noticeable degree of alignment in isotropic milieu [431]. In general it is when molecules are first dissolved in a dilute liquid crystal that they assume a minute but measurable degree of molecular alignment [409]. The molecular alignment arises from the interaction between the molecule of interest and the liquid crystal particles. The steric hindrance, i.e. the shape of the molecule, determines the size and direction of the alignment [432]. The surface charges on the biomolecule, the charge texture on the liquid crystalline particle and the ions or co-solvents in the solution may make a contribution to the size and direction of alignment.

The molecular alignment manifests itself as residual dipolar couplings (RDC) and chemical shift anisotropy (CSA) that carry information about directions and molecular shape. The preferred degree of molecular alignment is small, of the order of  $10^{-3}$ , to retain essentially all the characteristics of high-resolution NMR spectra. Otherwise full span dipolar couplings and CSAs would render the spectrum of a complex molecule hopelessly uninterpretable. RDCs reveal the directions of internuclear vectors and frequency shifts the directions of the components of CSA tensors [433]. The information content is highly complementary to the torsion angles available from three-bond scalar couplings and to the interproton distances available from nuclear Overhauser enhancements when determining the three-dimensional structure. Furthermore, the anisotropy data implicitly contain information about the molecular shape via simulations [432]. The directional dependence of dipolar couplings and chemical shifts is easy to interpret and to compare with values computed from known three-dimensional structures. In this way structures and conformational changes and the formation of quaternary structures are easy to examine and to analyze without extensive structure determination.

A number of aqueous liquid crystalline media suitable for inducing a weak alignment of biomolecules are known [405]. It should be understood that the choice for a particular liquid crystalline system depends on the properties of the biomolecule, liquid crystalline particles and temperature, ionic strength and eventual co-solvents. Some of the critical factors affecting the formation of the liquid crystal and the size and direction of the solute alignment may be difficult to anticipate beforehand and preliminary experiments are often required to find a suitable system. Furthermore, the set of aqueous liquid crystals for aligning biomolecules is likely to continue to expand as the search for novel media is currently in progress.

#### Liquid crystal composed of organic compounds

Certain amphiphatic molecules arrange themselves in discoidal bilayered structures known as bicelles. The bicelles have highly anisotropic magnetic susceptibility and thus the property to align themselves in the magnetic field with the plane normal perpendicular to the field [434]. This results in a uniaxial medium suitable for

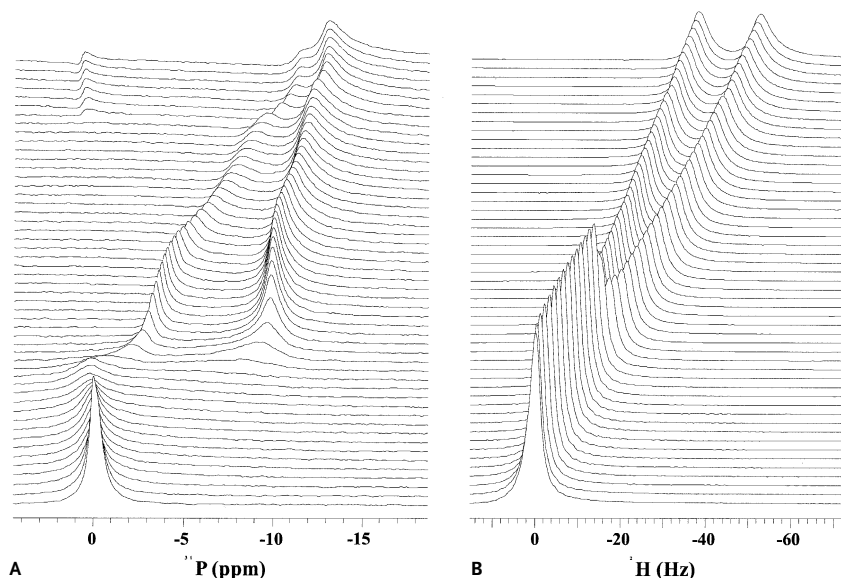


**Fig. 14.46** Deuterium (A) and phosphorus (B) spectra as a function of temperature of a liquid crystal composed of DHPC:DMPC (1:3) dispersed in water (5 % w/v). The liquid crystalline phase emerges near 30 °C and isotropic phase reappears above 50 °C.

aligning solute molecules. Bicelles can be prepared, for example, from a mixture of (3:1) dry dimyristolphosphatidylcholine and dihexanoylphosphatidylcholine dissolved in water to a concentration above 3 % (w/v) [435]. The long-chain lipid is thought to make the bilayer and the short-chain lipid confines and protects the perimeter of the disc. The solubilization is best carried out at low temperature near 0 °C where the viscosity is low and components mix properly. The liquid crystalline phase is stable in the temperature range from approximately 30 to 50 °C depending slightly on the exact composition of the medium. The correctly prepared phase should be uniform and transparent. The presence of the liquid crystalline phase is easy to confirm by measuring the deuterium quadrupolar splitting of  $\text{D}_2\text{O}$  or from the shifted phosphorus signals of the phosphatidylcoline head groups (Fig. 14.46).

The size of the alignment can be tuned by varying the concentration of the liquid crystal, however, above the critical concentration required for the liquid crystalline phase to form [435]. The tuning is a convenient way to adjust the range residual dipolar couplings and chemical shift anisotropy optimal for the measurements. Provided that the alignment is induced, not exclusively by the molecular shape, but also by the electric interactions between the surfaces of the solute and liquid crystal particle the ionic strength of the solution will influence both the size and the direction of the alignment. This phenomenon can be exploited by “doping” the bicelles with a small amount of charge. In this way it is possible to create several non-redundant alignments and to collect non-redundant data for the structure determination.

Liquid crystal phases can also be prepared by dissolving various polyethylene glycols, referred to as  $C_mE_n$  compounds such as  $C_{12}E_5$ , in water above 3% (w/v) [436]. A small amount of short chain alcohol such as hexanol helps to form the phase by stabilizing the exposed edges of the lamellae. The liquid crystalline phase is found in the temperature range from 30 to 40 °C. However, the actual composition of polyethylene glycol or their mixtures or any of their derivatives may noticeably alter the phase diagram and transition temperatures. The phase transitions to and from the liquid crystalline phase, again depending on the composition, show hysteresis as a function of temperature. Another lamellar phase can be prepared from cetylpyridinium bromide/hexanol/sodium bromide [437]. The liquid crystalline phase is stable and robust, tolerating different buffer conditions, temperature ranges and concentrations.

### **Liquid crystals prepared from biological material**

Many particles of biological origin are also suitable for making lyotropic liquid crystals. For example filamentous phages most notably Pf1, fd, and tobacco mosaic virus (TMV) readily align their long axis along the magnetic field [438–440]. The full degree of alignment of Pf1 is obtained already at modest field strengths e.g. at the field of a 300 MHz NMR spectrometer. The liquid crystalline phase is stable over a wide range of temperatures, above 5 °C, and it does not depend on the concentration as the phage particles align individually, unlike bicelles and lamellae where a critical concentration has to be exceeded. It is in the nature of the phages to carry high charge on their surfaces. Consequently electric interactions often play a role in the alignment, in addition to the molecular shape. The presence of electric contributions can often be deduced by varying the salt concentration. The Pf1 particles are negatively charged and therefore suitable for work with DNA which is also negatively charged. On the other hand an attractive Coulombic interaction may lead to an exchange dominated alignment [441]. Likewise, when using particles of biological origin more specific interactions may come into play and express themselves already at very dilute concentrations of liquid crystalline particles as very large dipolar couplings. The low pI ~ 4 of Pf1 implies that particle aggregation becomes a problem in acidic conditions. The bacterial phages can be produced in an infected bacterial culture and harvested after cell lysis and purified by precipitation and finally in a salt-gradient by an ultracentrifuge.

Fragments of purple membranes (PM) of *Halobacterium salinarum* align in the magnetic field [442]. The amount of the alignment can be tuned by varying the concentration of purple membranes and the solute alignment is also affected by salt that screens electric interactions between the negatively charged membranes and solutes. At tens of mM concentrations of monovalent ions, however, the PM membranes undergo transition to a gel where the membrane patches can no longer be oriented with the magnetic field. An order of magnitude lower concentrations of divalent salt are required for a similar phase transition to gel.

### Oriented matrices

A cross-linked polyacrylamide gel customarily used in electrophoresis can be compressed or strained to bring about an oriented medium suitable for weakly aligning biomolecules [443]. The oriented matrix is robust, i.e. insensitive to the solvent conditions such as pH, temperature and co-solvents, which makes it a suitable medium for the study of e.g. denatured proteins. Furthermore, the matrix is expected to be insensitive to the surface charge of the biomolecule. The director of the medium is determined by the direction of the strain, not by the magnetic field, which opens possibilities for acquiring data of a sample in different orientations with respect to the magnetic field. The main disadvantage of the polymeric systems is that the solute molecule has to be included in the solution prior to the polymerization or driven to the matrix by electrophoresis or diffusion. Alternatively, the matrix can be dried and made to reswell by solution containing the solute of interest.

Oriented matrices can also be prepared from a liquid crystal composed of membranes and bacterial phages by polymerization to the acrylamide gel. The resulting “frozen” medium is no longer a liquid crystal but an oriented matrix whose director is independent of the magnetic field.

#### 14.3.3

### Proton NMR Experiments

The large magnetic moment of a proton, a spin- $\frac{1}{2}$  particle, and its high natural abundance are the reasons for the historical predominance of  $^1\text{H}$  NMR spectroscopy. There are numerous homonuclear  $^1\text{H}$  experiments, however, certain of them have proven to be most applicable to biomolecular NMR spectroscopy and are mentioned here. The emphasis is on the principles of the experiments, their processing and information content. The reader is encouraged to consult textbooks [407, 408] for a proper description of the experiments using the appropriate nomenclature, which is not possible to introduce here. Furthermore, the operation of an NMR spectrometer and procedures for setting experiments, including calibrations, are usually found in text books or spectrometer manuals and are not discussed here.

In general all the present-day pulse sequences employ pulse field gradients (PFG) for selection of desired coherences and/or for removal of artifacts. Furthermore, phase sensitive experiments are preferred over their magnitude mode counterparts due to the superior resolution and the possibilities for analyzing the multiplet patterns for coupling constants. For the quadrature detection, the states-TPPI protocol [444] is often the most advantageous to displace artifacts to the edges of spectra. For small proteins and peptides and for many other biomolecules the basic proton correlation experiments are the most practical and require no isotope labeling. Many of the elements of the basic proton correlation experiments are also embedded in many heteronuclear experiments.

#### 14.3.3.1 One-dimensional NMR Experiment

Customarily studies of a biomolecule by NMR spectroscopy will begin by recording a one-dimensional (1D) proton spectrum. The 1D spectrum allows consideration of the signal-to-noise ratio (SNR) for further studies. Signals must be easily visible above the noise from a spectrum acquired by averaging 32 scans or preferably less for two-dimensional correlation experiments to be feasible (Fig. 14.47). For equimolar concentrations larger proteins have lower apparent SNR because they have larger line widths than smaller proteins and peptides.

1D spectra of peptides and small proteins usually permit one to judge from the line widths whether aggregation or exchange processes are likely to compromise the performance. For larger proteins in particular it may be difficult to find sufficiently isolated signals in the 1D spectrum to measure line widths. Furthermore, the proton line widths of a large protein may not be adequate to evaluate the feasibility of further experiments. The feasibility of NMR studies for larger proteins is better judged on the basis of heteronuclear experiments and at least a  $^{15}\text{N}$ -labeled sample is required.

The overall dispersion of the signals seen in 1D is an important attribute of the structural characteristics of a protein. Well-structured proteins display signals over large spectral regions whereas resonances of unstructured or unfolded proteins lump together and have values similar to that found in short (random coil) pep-

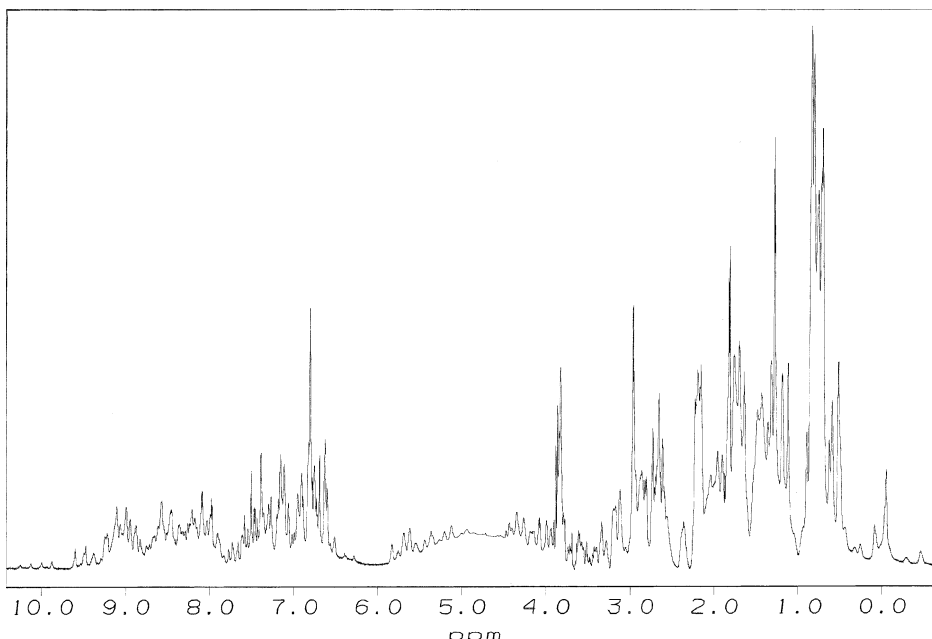


**Fig. 14.47** One-dimensional spectrum of a 3-mM human SH3 domain of Tec protein dissolved in  $\text{H}_2\text{O}/\text{D}_2\text{O}$  (90/10 v/v) recorded at 25 °C and pH 6 with an 500 MHz NMR spectrometer. Water signal was filtered post acquisition. Courtesy of Hanna Avikainen.

tides. In particular, the chemical shift dispersion in amide, alpha and methyl proton resonance regions is indicative of the structure. 1D can be used to monitor the effects of variables such as pH, temperature, ionic strength or co-solvents on the SNR and the dispersion of signals. However, when using non-deuterated co-solvents the solvent signal suppression may become problematic.

Owing to the high concentration of water it is necessary to record the 1D proton spectrum using solvent suppression. The same applies to other non-deuterated solvents. There are various ways to reduce the solvent lines to a level comparable to the signals of the solute in order to utilize the full dynamic range of detection of the NMR spectrometer. Saturation of the water line by selective radiation during the recycle delay is a simple, effective and robust method. Therefore the presaturation method is commonly used. The main disadvantage of the method is that the solute signals near the solvent signals are also easily saturated, thus complicating the assignment. Even a partial saturation will compromise the quantitative spectroscopy. The exchangeable protons, such as amide protons, are also subject to the saturation transfer that diminishes their signal intensity.

More selective schemes for the solvent suppression employ selective pulses, spin-lock purge pulses and field-gradient pulses. Some of these methods aim to saturate the water signal in milliseconds rather than during the recycle delay, while others are designed to maintain the water magnetization in equilibrium. To destroy the water magnetization selective pulses are used to generate orthogonal components for the solvent and solute magnetizations and subsequently to destroy the solvent signal by RF-inhomogeneity or to dephase the solvent coherence by pulsed-field gradients. To place the water magnetization along the  $z$ -axis during the acquisition, selective pulses or binomial sequences are employed for selective excitation, and pulsed-field gradients are used to destroy any residual transverse magnetization caused by pulse imperfections [445]. In this way radiation damping is largely avoided and also noticeable gains in the signal intensity of the exchangeable protons are obtained.

Post-acquisition methods are used to improve the *appearance* of the spectrum. Filtering the low-frequency components by convolution is one of the most widely used methods to suppress the residual solvent signal [446]. The filtered data set is constructed by subtracting the data “smeared” by the filter function from the original FID (Fig. 14.47). If the solvent signal is away from the carrier frequency, i.e. high-frequency components are to be removed, then the original data are initially digitally frequency shifted to zero by multiplication by an exponential function and subsequently filtered and finally restored to the original position by multiplication by the complex conjugate of the exponential function.

A flat baseline is obviously an important merit of a spectrum of any dimensionality. There are various reasons for a poor baseline. The baseline will have an offset and curvature if the signal phase at the beginning of the acquisition period or the indirect dimension is not a multiple of  $90^\circ$  and if the sampling delay is not adjusted to zero, i.e.  $t_0 = 1$ , or to the inverse of twice of the spectral width, i.e.  $t_0 = 1/(2sw)$ . The Hahn echo can be used to adjust the initial sampling delay for the acquisition dimension. For the indirect dimensions in two- or higher dimensional

spectra the phase evolution during e.g. off-resonance pulses and mixing periods must be taken into account to set the initial sampling delay correctly. The baseline distortions may also result from corrupted data points at the beginning of the acquisition period. These can be corrected by reconstruction of the initial points by a backward linear prediction. A receiver gain that is too high compared with the dynamic range of the analog–digital converter will result in signals with “wiggles”. Also a finite rise time of audio filters may cause a baseline roll. In modern spectrometers this is circumvented by oversampling, i.e. sampling the signal with the maximal frequency of the analog-to-digital converter (ADC), and reconstructing the signal mathematically afterwards for processing.

#### 14.3.3.2 Correlation Experiments

The principle purpose of correlation experiments is to establish a one-to-one mapping from the signal to its source i.e. to the particular atomic nucleus in the molecule. This assignment task involves identification of the members in the coupling network, referred to as the spin system. In addition, correlation experiments, as such or with modifications, are suitable for measurements of scalar and dipolar couplings. Correlation in the two dimensions is the most natural dimensionality because the spin–spin interactions are pair wise. Three-dimensional or experiments of higher dimensionality are constructed from concatenated two-dimensional experiments. Homonuclear three-dimensional experiments, such as TOCSY–NOESY, are not considered here because in many cases the multidimensional heteronuclear experiments are superior.

For all homonuclear experiments there are certain common guidelines to follow. When preparing a correlation experiment it is the expected line shapes and widths that determine the lengths of acquisition and indirect dimension and the processing. Narrow in-phase lines allow a considerable degree of freedom for the setting experiments whereas broad antiphase lines are the most difficult. The repetition rate of the acquisition for signal averaging should be adjusted properly to reach optimal SNR or to obtain quantitative spectra.

#### COSY-type experiments

Correlated spectroscopy (COSY) was among the first two-dimensional (2D) NMR experiment realized [447, 448] and it is still among the most useful NMR experiments. COSY generates cross peaks in the 2D spectrum at the intersection of resonances of coupled spins (Fig. 14.48). In proteins cross peaks are observed for geminal, i.e. over two bonds, and vicinal, i.e. over three bonds, protons and in small peptides also couplings over four bonds may be detected. Thus the COSY spectrum allows the identification of spin systems for the assignment. However, apart from peptides, the overlap and degeneracy in chemical shifts is likely to prevent one from obtaining entire spin systems exclusively from the COSY spectrum; additional experiments are required.

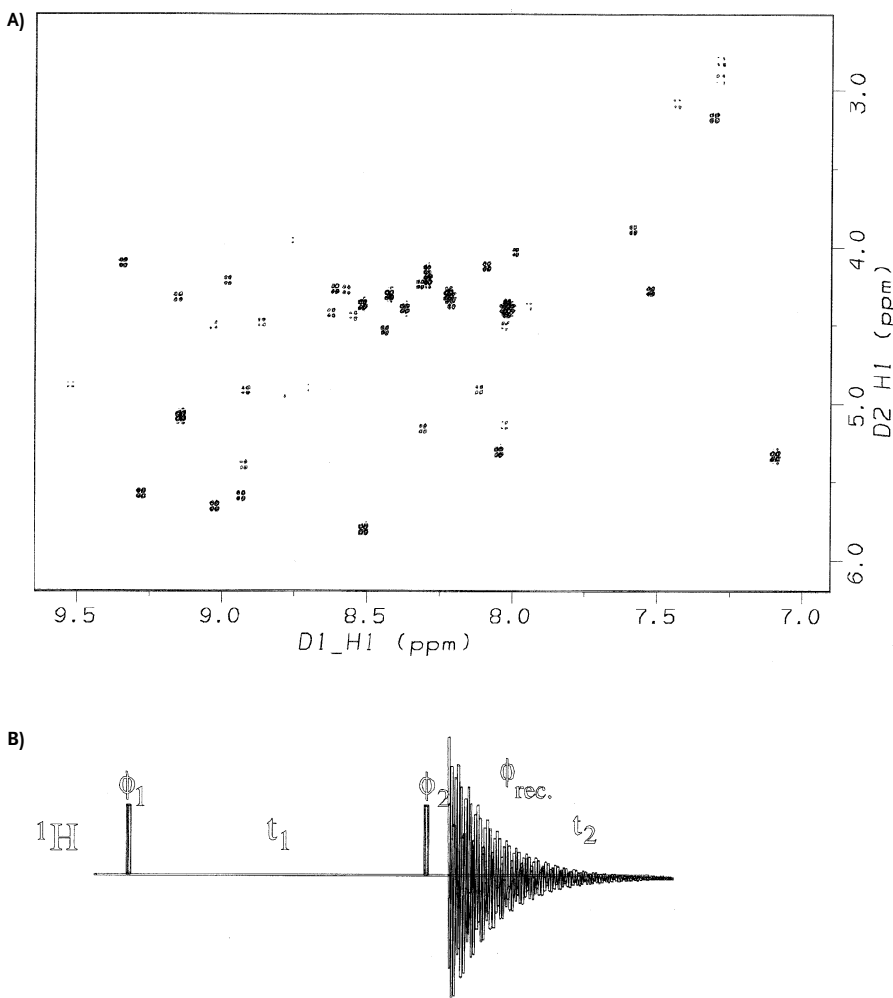


**Fig. 14.48** COSY spectrum of a 1-mM SH3 sample in  $\text{H}_2\text{O}/\text{D}_2\text{O}$  (90/10 v/v) recorded at 30 °C with a 500 MHz NMR spectrometer using the phase sensitive COSY experiment  
(A) spectrum (B) pulse sequence.

The COSY spectrum also provides information about the coupling constants in the fine structures of cross peaks. The value of the three-bond scalar coupling is related to the torsion via the Karplus equation [449] and knowledge of the couplings together with NOEs provides stereospecific assignment. The coupling can be determined from the frequency separation of the antiphase absorptive doublet. For two coupled spins i.e. without passive coupling partner such as the  $^3J_{\text{HNH}\alpha}$  of residues other than glycines (that have two  $\text{H}_\alpha$ ) the lobes of the cross-peak are separated by the coupling constant along the directly observed direction. However,

as the linewidth increases comparable to the coupling constant, or even larger, the positive and negative lobes of the antiphase line began to cancel each other more and more, thereby increasing the apparent separation of the multiplet components. This aberration from the true coupling value has to be taken into account when measuring coupling constants. Analyses of the antiphase lines for extracting the true separation of the multiplet components require that the spectrum has been processed to maintain Lorentzian line shapes. In practice when the line width is twice as large as the coupling constant or more it is difficult to obtain an accurate value. Therefore, scalar coupling constants are preferably measured by heteronuclear experiments. Due to the self-cancellation of the broad antiphase lines the sensitivity of the experiment also decreases with increasing molecular weight. Otherwise for peptides and small proteins COSY is among the most sensitive of experiments.

The COSY pulse sequence is very simple, consisting of the recycle delay, the first  $90^\circ$  pulse succeeded by the incremental delay  $t_1$ , the other  $90^\circ$  pulse followed by the acquisition period  $t_2$  (Fig. 14.48B). The phases of the pulses and the receiver are cycled according to CYCLOPS and axial peaks are suppressed by inverting the phases of the first pulse and receiver. The residual axial peaks are moved to edges of the spectrum by the States-TPPI protocol. A product operator analysis shows that the cross-peak has an antiphase lineshape and that the diagonal peak differs by  $90^\circ$  and thus cannot be phased simultaneously for absorption. The nature of the antiphase lines requires that the data in the indirect dimension  $t_1$  are collected sufficiently long, at least longer than  $1/(4J)$ , otherwise the signal intensity is reduced due to self-cancellation of the antiphase lines. For the measurement of couplings the acquisition dimension  $t_2$  can well be longer than  $1/(2J)$  as the recycle delay can be shortened correspondingly. The COSY spectra are customarily processed for resolution using sine bell weight functions. The analysis of coupling constants requires that the  $F_2$  slices have been adequately zero-filled, e.g. to about 0.5 Hz per point.

There are a number of variant COSY experiments and extensions to COSY. One of the main goals of the descendants has been to remove the dispersive tails of the diagonal peaks that may obscure the near-diagonal cross-peaks. The double-quantum filtered (2QF) COSY experiment [450] yields a spectrum with absorptive anti-phase lines for the diagonal peaks of the coupled spins and the attenuated diagonal resonance of the uncoupled spins. The drawback of 2QF-COSY over COSY is the two-fold decrease in sensitivity. Also the total acquisition time for a concentrated sample may become long because of the longer phase cycle. The P-COSY experiment is designed for the same purpose as 2QF-COSY but offers greater sensitivity.

E-COSY is an abbreviation for methods to generate coupling patterns with, exclusively, the active components. The fine structure of the E-COSY cross-peak is a superposition of two-quantum and three-quantum COSY peaks so that the two components that stem from the passive couplings cancel each other to leave a simplified coupling pattern. The active coupling can be measured directly from the antiphase separation on either of the multiplets as usual and the passive couplings can be measured from the displacements of the two antiphase multiplets. Importantly, the method will not be subject to the errors due to finite linewidths. Further-

more, the E-COSY experiment serves to determine the relative sign of the passive couplings. The same principle is used in heteronuclear experiments. The pre-TOCSY-COSY experiment aims to recover resonances attenuated by the solvent presaturation. The mixing sequence prior to the first 90° pulse serves to transfer magnetization to H<sub>α</sub> that is near to the irradiated water line.

Relayed COSY [451] is a straightforward extension to COSY. An additional coherence transfer delay is inserted in the pulse sequence before the acquisition period in order to relay coherence from the second spin to a third spin. This will result in a spectrum with the cross peak between the first and the third spin even if they are not directly coupled but only via the second spin. The chemical shifts are monitored before the coherence transfer steps, i.e. t<sub>1</sub>, and after, i.e. t<sub>2</sub>. The mixing time for the second coherence transfer depends, of course, on the couplings, for proteins the delay from 20 to 40 ms is usually a good compromise between transfer efficiency and relaxation losses. There is no new information compared to COSY, however, in the case of degenerate shifts, R-COSY provides means of assessing whether the spins belong to the same spin system. The acquisition and processing of R-COSY is similar to COSY.

### Multiple quantum spectroscopy

Multiple quantum spectroscopy offers complementary information to COSY to elucidate scalar coupling networks [452]. The multiple quantum transitions are observed indirectly during t<sub>1</sub>. The two-quantum (2Q) experiment is commonly used to circumvent problems in COSY due to diagonal peaks, self-cancellation of signals and solvent suppression.

The idea is to generate the 2Q coherence that evolves with the frequency sum of the chemical shifts Ω<sub>1</sub> + Ω<sub>2</sub> of two coupled spins I<sub>1</sub> and I<sub>2</sub>. The active coupling J<sub>12</sub> will not evolve during t<sub>1</sub>. During the acquisition cross-peaks appear along F<sub>2</sub> at frequencies of Ω<sub>1</sub> and Ω<sub>2</sub> with the absorptive antiphase splittings corresponding to J<sub>12</sub> and along F<sub>1</sub> at a frequency of Ω<sub>1</sub> + Ω<sub>2</sub> with absorptive in-phase lineshape and a dispersive antiphase component that add constructively. These cross-peaks are referred to as direct peaks. In addition three-spin coherences that originate from the J<sub>12</sub> and J<sub>13</sub> couplings and from the J<sub>13</sub> and J<sub>23</sub> couplings become observable and result in cross-peaks along F<sub>2</sub> at frequencies of Ω<sub>3</sub> and along F<sub>1</sub> at frequencies of Ω<sub>1</sub> + Ω<sub>2</sub>. These cross-peaks with double antiphase dispersive nature along F<sub>2</sub> and with dispersive antiphase and absorptive in-phase components along F<sub>1</sub> are referred to as remote peaks. In general the direct and remote peaks can be distinguished from each other by the opposite line shape along F<sub>2</sub>. Considering the lineshapes, the acquisition and processing parameters along t<sub>2</sub> are similar to those used in COSY, whereas along the indirect dimension t<sub>1</sub> it is not necessary to collect data extensively and cosine apodization is appropriate.

### Total correlation spectroscopy

Total correlation spectroscopy (TOCSY) also known as homonuclear Hartmann–Hahn (HOHAHA) experiment provides all relayed connectivities within a spin system [453, 454]. The primary intention in TOCSY as in other relayed experiments is to establish connectivities in less crowded spectral regions to facilitate the assignment of spin systems.

The key idea in TOCSY is to transfer in-phase magnetization from spin to spin throughout the spin system by an isotropic mixing sequence rather than to rely on transferring antiphase coherence during free precession periods. During the mixing sequence the system is governed by the strong coupling Hamiltonian. The intensity of a cross-peak will depend on the topology of the spin system, i.e. the ways the spins are coupled, the various coupling constants and the properties of the mixing sequence. There are several mixing sequences. The DIPSI-2 sequence [455] is better than WALTZ-16 [456] or MLEV-17 when relaxation is neglected (Fig. 14.49). The actual performance of a mixing sequence over the others depends on the implementation and the accuracy of the calibrations.

Dipolar couplings during the mixing period may give rise to the rotating-frame Overhauser effect (ROE). Attenuation of the in-phase TOCSY peaks due to the ROE peaks of opposite sign can be particularly important for larger proteins but can be largely eliminated by interrupting the mixing train so that laboratory-frame nuclear Overhauser enhancements with opposite sign to ROEs can develop to cancel each other. These sequences are referred to as clean (TOCSY). Furthermore, adiabatic mixing sequences (WURST-8) [456] have low sensitivity to RF field inhomogeneity and miscalibration of the field strength. The sensitivity enhanced TOCSY pulse sequence retains two orthogonal components of magnetization for post-acquisition reconstruction of the spectrum to achieve a gain of  $v_2$  in the SNR.

The evolution during the indirect dimension and acquisition are not constrained by the scalar couplings because the peaks in TOCSY are mostly in-phase and only resolution should be considered when setting the acquisition and indirect dimensions and weight functions in processing. It is seldom worthwhile to collect  $t_1$  longer than  $1.5T_2$  where  $T_2$  is the transverse relaxation time. The length of the isotropic mixing sequence is subject to two opposing conditions. On the one hand a long mixing sequence is preferred to obtain a correlation between the spins at the opposite ends of the network and on the other hand all correlations are preferably observed. These constraints are difficult to meet simultaneously and therefore usually two or more TOCSY spectra with mixing times from 30 to 120 ms, depending on the relaxation, are collected. The interpretation of TOCSY is subject primarily to two concerns. Since the experiment provides correlations along the network of spins it may remain uncertain which nucleus in the spin system gives rise to which signal in particular when chemical shifts are not unambiguous. The other concern is that cross-peaks may not always be observed due to the intensity variation of the signal as a function of the mixing time. Furthermore, if TOCSY is used to estimate coupling constants it must be kept in mind that the signal intensity depends on *all* couplings in the spin system. Short mixing times transfer mostly via a single scalar coupling and are more reliable for coupling constant measurements.

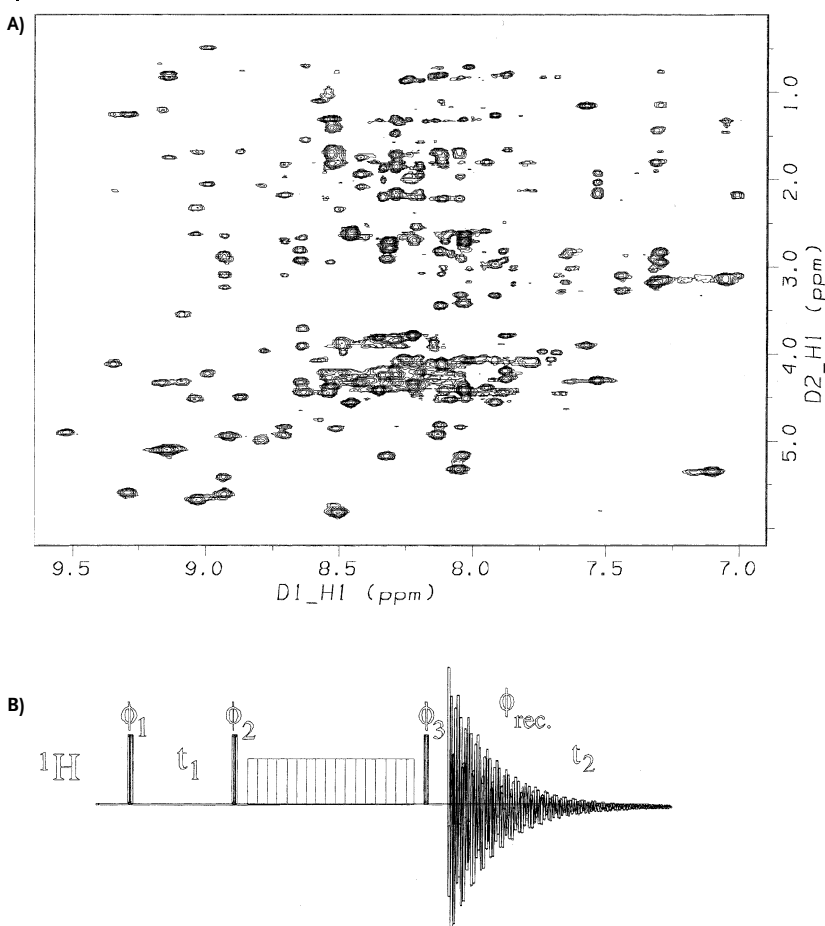


**Fig. 14.49** (A) TOCSY spectrum of a 1-mM SH3 sample in  $\text{H}_2\text{O}/\text{D}_2\text{O}$  (90/10 v/v) recorded at 30 °C with a 500 MHz NMR spectrometer using the DIPSI-2 mixing sequence (B).

#### 14.3.3.3 Cross-relaxation Experiments

The elucidation of the scalar coupling network by the correlation experiments is, apart from small molecules, not sufficient for the unambiguous, sequential and stereo-specific assignment. The complementary information of spatially adjacent protons is obtained via cross-relaxation experiments, the laboratory-frame nuclear Overhauser enhancement spectroscopy (NOESY) and the rotating-frame nuclear Overhauser effect spectroscopy (ROESY). These experiments provide also the distance restraints for the structure determination and help to recognize exchange processes.

### NOESY

The NOESY experiment is composed of the frequency labeling part, i.e.  $t_1$  flanked by two  $90^\circ$  pulses, ensued by the magnetization transfer via dipolar couplings during the mixing period  $\tau_m$  before the read pulse for the acquisition  $t_2$  (Fig. 14.50). During the mixing period relaxation processes govern the longitudinal magnetization. The autorelaxation results in the diagonal peak and the cross-relaxation results in the cross-peaks in the NOESY spectrum. Both peaks are absorptive in-phase in both dimensions. The phase cycling will remove higher coherences than zero. Consequently, in addition to the longitudinal magnetization the cross peak may have an undesirable zero-quantum contribution. The zero-quantum peak is antiphase in both dimensions, just as a COSY peak, but dispersive with respect to the NOE peaks. The intensity of the zero-quantum peak depends on the chemical shift difference of the spins in question and the mixing time. Furthermore, the transverse zero-quantum term relaxes during the mixing period faster than the desirable longitudinal magnetization. Therefore, the zero-quantum artifacts are usually observed when the mixing time is short but can further be suppressed by varying the length of the mixing time, a procedure known as  $z$ -filtration. However, for short mixing times it may be difficult to vary the mixing time sufficiently without introducing problems in the interpretation due to the averaging.

When setting the NOESY experiment it is worthwhile to make sure that the baseline is flat and the total measuring time will yield adequate SNR. The recycle delay should be  $3T_1$ , where  $T_1$  is the longitudinal relaxation time, otherwise the intensity of the cross-peaks can be affected by the steady-state conditions. The length of the mixing time is subject to contradictory demands. A long mixing time, of the order of  $T_1$ , will give high intensities for the cross-peaks and have small zero-quantum artifacts. On the other hand multiple magnetization transfers, referred to as spin-diffusion, will affect the intensity and obscure the interpretation. Therefore, a compromise depending on the size of the protein has to be made or a series of NOE spectra must be collected for more precise calibration of intensities to distances. For large proteins the dipolar relaxation is effective and short mixing times are appropriate whereas for small proteins or peptides longer mixing times are required. Furthermore, the cross-relaxation rate constant depends on the rotational correlation time and changes its sign at short correlation times, thereby making the observation of NOEs for small molecules difficult unless there is a freedom to change temperature so as to affect the rotational correlation time. For proper integration of the cross-peaks during processing, window functions for the resolution enhancement are to be applied with caution because signals differing in their line-widths will then not retain relative intensities. Otherwise the in-phase absorptive peaks allow considerable freedom for choosing lengths acquisition and indirect dimensions and their apodization.

Chemical exchange, not too slow compared with the mixing time, can result in cross-peaks in the NOESY spectrum. The chemical exchange peaks are hard to distinguish from the NOE peaks but they have a different sign from the ROE peaks. Furthermore, coupled exchange and spin-diffusion can result in complicated spectra.

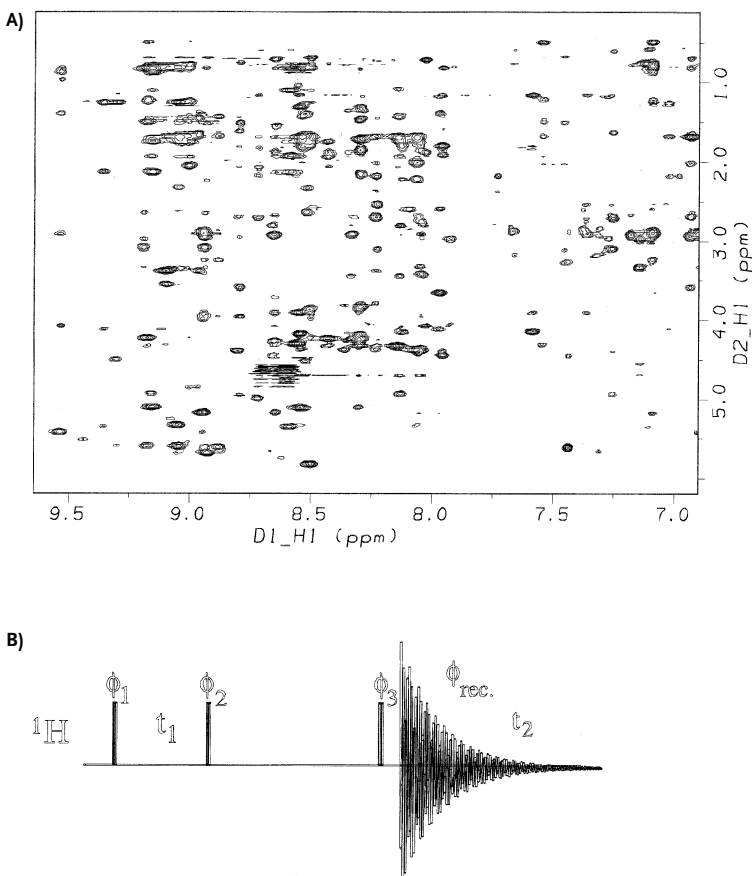


**Fig. 14.50** (A) NOESY spectrum of a 1-mM SH3 sample in  $H_2O/D_2O$  (90/10 v/v) recorded at 30 °C with a 500 MHz NMR spectrometer using the NOESY sequence (B).

### ROESY

The ROESY experiment [454, 458] follows the cross-relaxation in the rotating-frame that is established by locking the spins with a train of RF-pulses. During the spin-lock any components of magnetization orthogonal to the RF-field are dephased by the inhomogeneity of the RF-field. The longitudinal magnetization is governed by rotating-frame relaxation rates. The rotating-frame cross-relaxation rate constant is positive for all correlation times, which makes ROESY particularly suitable for studies of small peptides. The ROESY cross-peaks depend, in addition, on the resonance offset from the carrier. The offset dependence appears as a phase error along  $F_1$  and  $F_2$  which can be removed during processing. However, the intensity of cross-peaks for the off-resonance spins will have an opposing NOE contribution in addition to ROE. The offset dependence has to be taken into account in quantitative analysis of the cross-peak intensities. The ROE mixing time is usually kept

shorter than the corresponding NOE mixing time because the ROE build-up is twice as fast as the NOE build-up. The in-phase absorptive cross-peaks and diagonal peaks but of opposing sign to each other allow considerable freedom in setting the parameters for the acquisition and indirectly detected dimensions and their processing.

The ROE experiment is potentially subject to artifacts rising from isotropic mixing. The TOCSY transfer will reduce the intensity of the ROE cross-peak and obscure the quantification. In particular consequent TOCSY and ROE transfers have the same sign as the authentic ROE peaks and may easily be misinterpreted. Therefore, as long as the long spin-lock is not sufficiently strong to match the Hartmann–Hahn condition there is only need to watch for artifacts for those spins that have closely similar chemical shifts or shifts that are placed on opposite sides with respect to the carrier. Eventual artifact related problems can be noticed by taking spectra with different carrier positions and varying the strength of the spin-lock.

In contrast to the NOE experiment the cross-peaks of the ROE experiment are of opposite sign with respect to the chemical-exchange peaks. This is a particularly valuable property in studies of complex formation where peaks arise both from cross-relaxation and chemical exchange. Furthermore, the assignment of stereospecific restraints to the methylene protons that are often subject to spin-diffusion can be facilitated by the ROESY measurement. The ROE cross-peaks that stem from the relayed transfer have opposite sign with respect to the direct transfer and thus the methylene ROE signals do not tend to equal values.

#### 14.3.4

#### **Heteronuclear NMR Experiments**

Heteronuclear NMR experiments have many virtues over the homonuclear  $^1\text{H}$  experiments when labeled samples are available for the measurements. It is for the high molecular weight proteins and protein complexes that the heteronuclear experiments are imperative. Heteronuclear methods compared with homonuclear experiments provide improved resolution via increased dimensionality and editing and filtering possibilities and various ways for coherence transfer and for measurement of scalar and dipolar couplings to increase the information content. It is in the nature of amino acids in folded proteins to contain distinguishable nuclei that are coupled to each other with various strengths of couplings that lay the foundation for the rich repertoire of heteronuclear experiments. Furthermore, relaxation measurements of  $^{15}\text{N}$  and also  $^{13}\text{C}$  are much more amenable to interpretation than those of protons. Today heteronuclear experiments are indispensable for biomolecular NMR spectroscopy.

##### 14.3.4.1 **Basic Heteronuclear Correlation Experiments**

Many heteronuclear multidimensional correlation experiments appear superficially complicated but actually comprise simple building blocks for coherence transfer and for recording chemical shift and/or coupling evolution. These basic elements

are simple and robust. The usual protocol begins by transferring proton magnetization to the heteronucleus i.e.  $^{15}\text{N}$  or  $^{13}\text{C}$ , which is subject to further actions and finally the coherence is returned to the proton for detection. This indirect detection scheme is superior in sensitivity to direct methods because of the proton's large gyromagnetic ratio and favorable relaxation properties. The most frequently used experiments are the heteronuclear multiple quantum coherence (HMQC) [459] and heteronuclear single quantum coherence (HSQC) experiments [460]. More recently it was discovered that significant gains in SNR for large proteins at high magnetic fields are obtained by selecting particular multiple components for the detection to result in transverse relaxation optimized spectroscopy (TROSY) [410].

### **HMQC**

The HMQC experiment begins by a coherence transfer from proton to the heteronucleus during a delay matched to  $2\tau = 1/(2J)$ ,  $J_{\text{HN}} = 94 \text{ Hz}$  and  $J_{\text{HC}\alpha} = 140 \text{ Hz}$ , to result in a multiple-quantum (MQ) coherence that evolves during  $t_1$ . The heteronuclear coupling is not active under MQ during  $t_1$  but the  $^1\text{H}$  chemical shift evolution must be refocused by a  $180^\circ$  proton pulse. The MQ coherence is transferred to the proton for detection. Before the acquisition antiphase dispersive components can be purged by a  $90^\circ$  proton pulse. During the acquisition  $t_2$  heteronuclear decoupling is employed. Homonuclear scalar couplings during the coherence transfer periods will cause a phase error along  $F_1$ . The size of the error is fairly small but it depends on the size of the coupling and cannot be simply compensated. The HMQC experiment is very simple with only a few pulses and it is therefore a favored building block in more complicated experiments.

### **HSQC**

The HSQC experiment (Fig.14.51) is based on the INEPT (insensitive nuclei enhanced by polarization transfer) sequence which converts proton magnetization to the antiphase single-quantum (SQ) coherence that evolves during  $t_1$  [460]. The scalar coupling evolution is refocused by a  $180^\circ$  proton pulse or decoupled. Homonuclear scalar couplings do not contribute to the lineshape along  $F_1$ . The reverse transfer from the heteronucleus to proton is analogous. Homonuclear scalar couplings during the coherence transfer periods will affect the amplitude of the peak and cause an antiphase dispersive contribution along  $F_1$  which can be purged by a  $90^\circ$  proton pulse just before the acquisition. During the acquisition the  $t_2$  heteronucleus is decoupled.

The decoupled HSQC experiment employs the refocused INEPT sequence to generate an in-phase SQ coherence that is desirable e.g. for measurements of heteronuclear relaxation rates. The transfer function of the refocused INEPT depends on the proton multiplicity. i.e. the number of protons bound to the heteronucleus. This can be used to edit the spectrum or, when an overall maximal transfer efficiency is required,  $2\tau = 1/(3J)$  makes a good compromise. The constant time

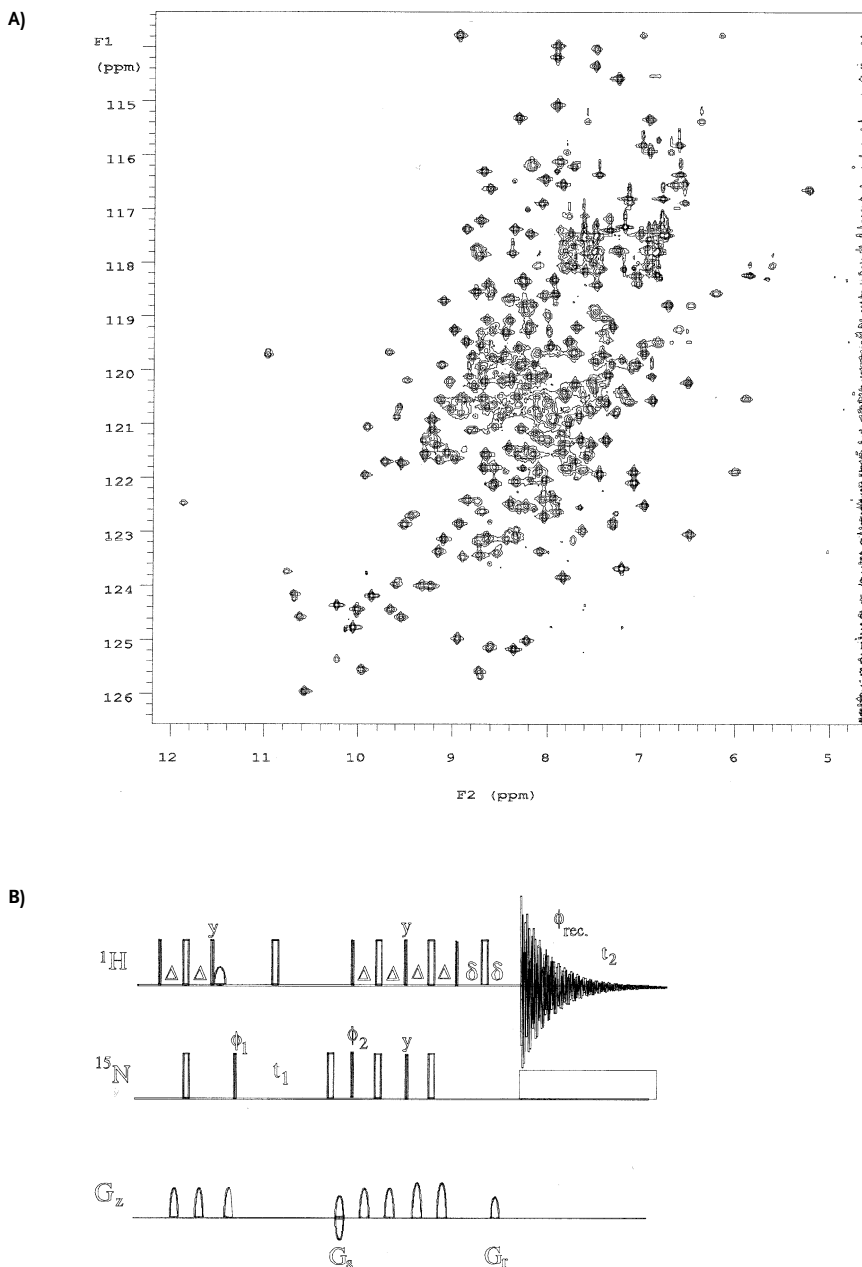


**Fig. 14.51** (A) HSQC spectrum of a 1-mM cellulase sample in  $\text{H}_2\text{O}/\text{D}_2\text{O}$  (90/10 v/v) recorded at 40 °C with an 800 MHz NMR

spectrometer using the gradient selected sensitivity enhanced HSQC sequence (B). Courtesy of Outi Salminen.

(CT) HSQC has an evolution period  $t_1 = T$  fixed in length. This brings in two advantages. The homonuclear couplings do not modulate the signal during  $t_1$  and consequently there is no homonuclear multiplet structure along  $F_1$ . This is particularly useful for fully  $^{13}\text{C}$ -enriched samples to remove the  $^{13}\text{C}$ – $^{13}\text{C}$  couplings of aliphatic carbons that cannot be selectively decoupled. The other advantage is the narrow lines. The linewidth along the indirect dimension does not depend on the transverse relaxation rate but is mainly determined by the window function used for processing. The transverse relaxation rate appears only as a constant factor that scales the intensity. The optimum trade-off between intensity and resolution depends on each particular case.

### TROSY

At high magnetic field strengths the chemical shift anisotropy (CSA) interaction of  $^{15}\text{N}$  is a comparable source of relaxation as the dipole–dipole (DD) interaction. The same is true for the amide proton CSA and DD. Therefore the four multiplet components of the amide spin pair have different relaxation rates, depending on whether the DD and CSA mechanism interfere constructively or destructively. When other sources of relaxation such as those due to remote protons are negligible the differential relaxation effect on the multiplet components is large and also, in practice, attainable at high magnetic fields for large perdeuterated proteins. It is the most slowly relaxing multiplet component that is of particular interest and it is possible to filter away the other multiplet components for spectral simplification. This is the essence of the transverse relaxation optimized spectroscopy (TROSY) [410, 462]. The resulting spectrum is superior to an HSQC experiment under the aforementioned conditions.

The pulse sequence resembles superficially that of the sensitivity enhanced HSQC [462]. Obviously neither proton during  $t_1$  nor  $^{15}\text{N}$  during the acquisition  $t_2$  should be decoupled to maintain the multiplet components. It is the latter part of the pulse sequence used for the reverse transfer from  $^{15}\text{N}$  to  $^1\text{H}$  including the gradient selection that chooses the most slowly relaxing multiplet component for the detection (Fig. 14.52).

The intensity of the TROSY component can be further boosted by sensitivity enhancement and more importantly by taking advantage of the  $^{15}\text{N}$  steady state magnetization [462]. The TROSY principle has been implemented in many heteronuclear correlation experiments such as those used for the main chain assignment and measurement of scalar and dipolar couplings that exploit coherence transfer between the amide nuclei before the acquisition. The TROSY principle works also for the CH pairs in aromatic rings and side chain  $\text{NH}_2$  groups [463]. TROSY has significantly increased the molecular size limit of proteins and their complexes feasible for NMR studies [464, 465].

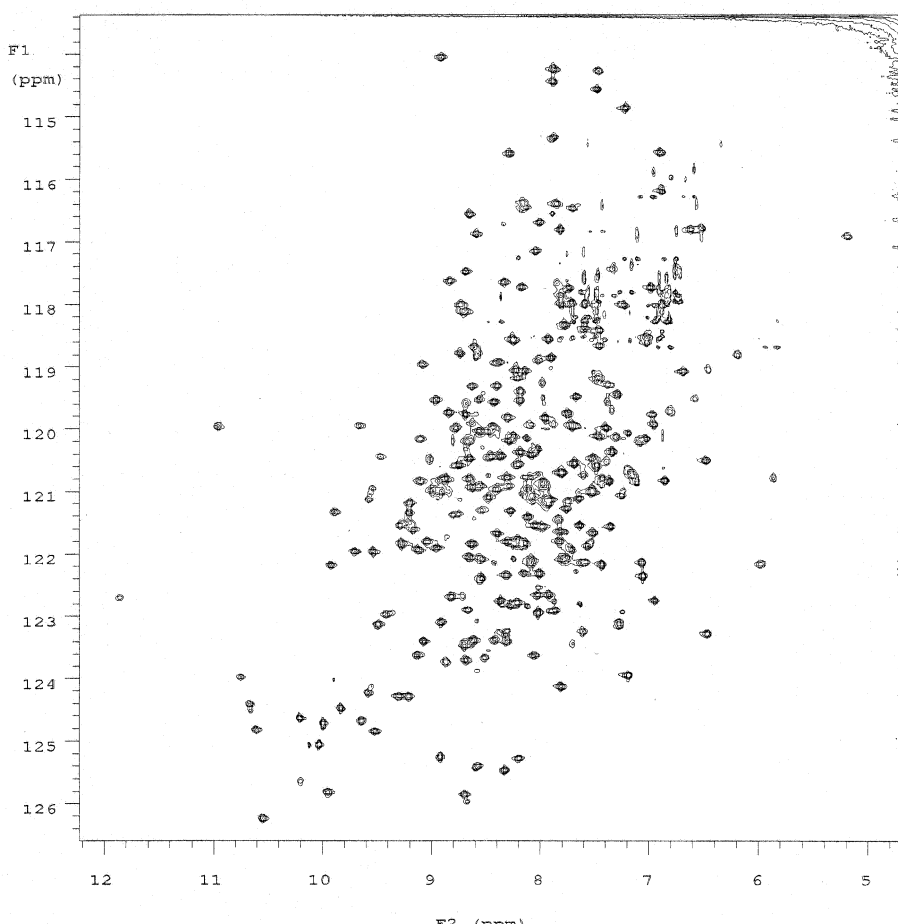


**Fig. 14.52** TROSY spectrum of a 1-mM cellulase sample in  $\text{H}_2\text{O}/\text{D}_2\text{O}$  (90/10 v/v) recorded at 40 °C with an 800 MHz NMR spectrometer using the gradient selected TROSY sequence.

#### 14.3.4.2 Edited and Filtered Experiments

The basic heteronuclear experiments are easy to combine with the two-dimensional homonuclear experiments to produce three- or four-dimensional edited spectra. In this terminology editing means selection of the protons that are attached to the heteronucleus. The main purpose of these experiments is to reduce the signal overlap of the homonuclear two-dimensional experiments.

Combinations of NOESY with HSQC (or HMQC) and TOCSY with HSQC are among the most useful edited three-dimensional experiments (D. Marion, P. C. Driscoll, L. E. Kay, P. T. Wingfield, A. Bax, A. M. Gronenborn, G. M. Clore. *Biochemistry* 28, 6150–6156 (1989). E. R. P. Zuiderweg, S. W. Fesik *Biochemistry* 28, 2387–2391 (1989)). For example the NOESY-HSQC (Fig. 14.53) begins with the NOESY sequence and is followed directly by the HSQC sequence. It is important

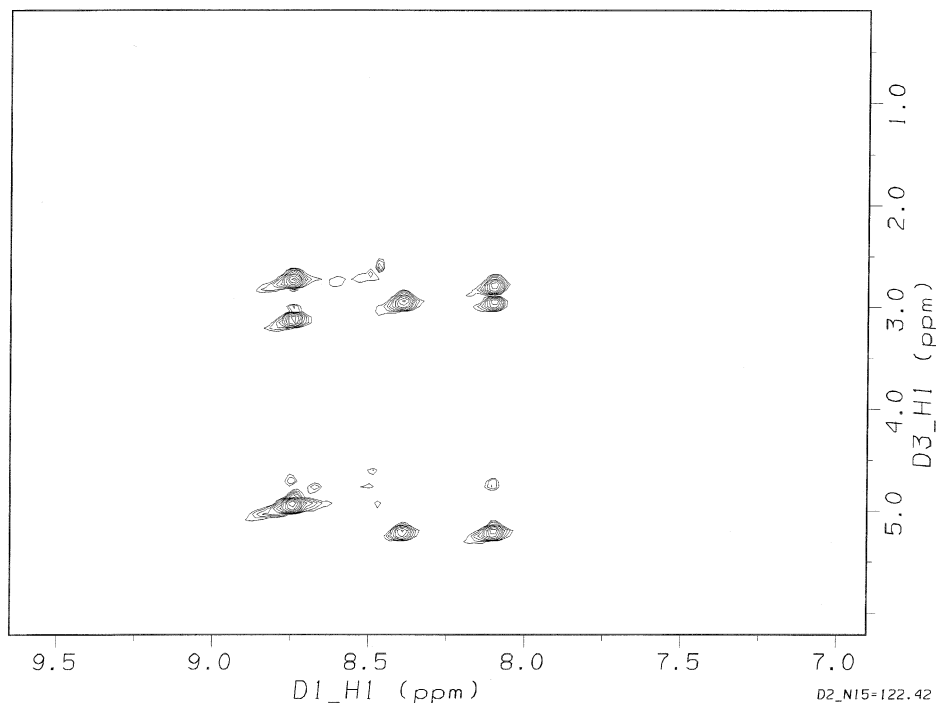


**Fig. 14.53** Plane  $^1\text{H}$ - $^1\text{H}$  of  $^1\text{H}$ - $^{15}\text{N}$ -NOESY-HSQC spectrum of a 3-mM SH3 sample in  $\text{H}_2\text{O}/\text{D}_2\text{O}$  (90/10 v/v) (A) and a plane  $^1\text{H}$ - $^1\text{H}$  of  $^1\text{H}$ - $^{15}\text{N}$ -TOCSY-HSQC (A) and  $^1\text{H}$ - $^{15}\text{N}$ -NOESY-HSQC (B) recorded at 25 °C with a 500 MHz NMR.

to acquire enough data points (typically 128 and 2048) along the proton dimensions ( $t_1$ ) and ( $t_3$ ) whereas fewer increments (typically 32) along the  $^{15}\text{N}$  editing dimension ( $t_2$ ) will suffice. The F1–F3 plane at each F2 displays the homonuclear correlations, just as in the two-dimensional spectrum but edited with respect to the heteronucleus. It will take about three days to acquire a spectrum with good SNR.

Clearly the homonuclear and the heteronuclear experiments could be combined in the reverse order i.e. HSQC-NOESY and HSQC-TOCSY. The main advantage in these schemes relates to  $^{15}\text{N}$ -edited experiments in which the narrower amide proton spectral width is sampled during  $t_1$  and the full proton spectral width is collected during  $t_3$ . On the other hand water suppression is more effective when HSQC follows NOESY. Also the sensitivity enhancement can be incorporated into the NOESY-HSQC experiment. For the TOCSY-HSQC or HSQC-TOCSY it does not matter because both the TOCSY and HSQC sequences can be implemented with the sensitivity enhancement. It should be mentioned that the TOCSY type of transfer is more effective between  $^{13}\text{C}$  nuclei than between protons and therefore the HCCH-TOCSY experiment is preferred when a doubly labeled sample is available.

Even if the heteronuclear editing provides a big advantage over the two-dimensional homonuclear experiments, this is not sufficient when two protons with a

mutual correlation have degenerate chemical shifts. This can be of importance, in particular, in NOESY that contains a large number of cross-peaks. The four-dimensional HMQC-NOESY-HMQC experiment provides editing in two dimensions to alleviate the overlap problem. The NOESY part is flanked by two HMQC sequences. Obviously the two HMQC parts can be chosen to edit with respect to the same or different heteronucleus i.e.  $^{15}\text{N}$  or  $^{13}\text{C}$ . The total acquisition times tend to be long, several days to achieve sufficient resolution along the indirect dimensions.

For studies of intermolecular interactions, filtered experiments are valuable. The essence of filtered experiments is to distinguish protons on the basis of the heteronucleus to which they are bound. In the terminology, filtering means rejection of the protons that are bound to the heteronucleus. Therefore, provided that the heteronuclei in the subunits that make the quaternary complex are labeled differently i.e. either the target protein or the ligand is labeled, it is possible to employ filtering experiments to distinguish e.g. intermolecular proton NOEs from intramolecular NOEs. While for the heteronuclear edited experiments it is sufficient to have only a modest degree of labeling, it is mandatory for the filtered experiments to have a very high degree of labeling, i.e.  $\geq 98\%$ . The most robust filters are the double spin-echo type. However, it should be kept in mind that none of the filter sequences will work properly if the labeling degree is not close to 100 %. Leakage of signal will lead to misinterpretation.

#### 14.3.4.3 Triple Resonance Experiments

The assignment of signals is, of course, a prerequisite for any detailed interpretation of NMR spectra. The advent of triple resonance experiments [466] for double labeled and, more recently, for perdeuterated proteins has been very important in resolving the assignment problem. The fundamental principle of all triple resonance experiments is a directional relay of the magnetization from nucleus to nucleus via the scalar coupling network concurrent with a multi-dimensional detection of the resonance frequencies. In this way it is possible to correlate several nuclei with enough dispersion to avoid degeneracy, even for large proteins. Today many of the triple resonance experiments are well established (see e.g. [400, 404 and 467]). The principles of how to use them are described below whereas a more thorough discussion can be found in the reviews. In addition the triple resonance experiments are the skeletons for experiments designed to measure scalar and dipolar couplings.

The assignment of resonances to the chemical structure commences from the main chain atoms HN, N, CA, CO and CB. The experiments, i.e. the pulse sequences for this purpose, appear superficially complex but are in fact built from concatenated parts of heteronuclear polarization transfers. The magnetization is often derived from the amide proton and also from the amide nitrogen when using transverse relaxation optimized spectroscopy. Subsequently the polarization is relayed to amide nitrogen and further to carbons. Three-dimensional spectra are produced by acquiring the frequencies of the amide proton directly and recording

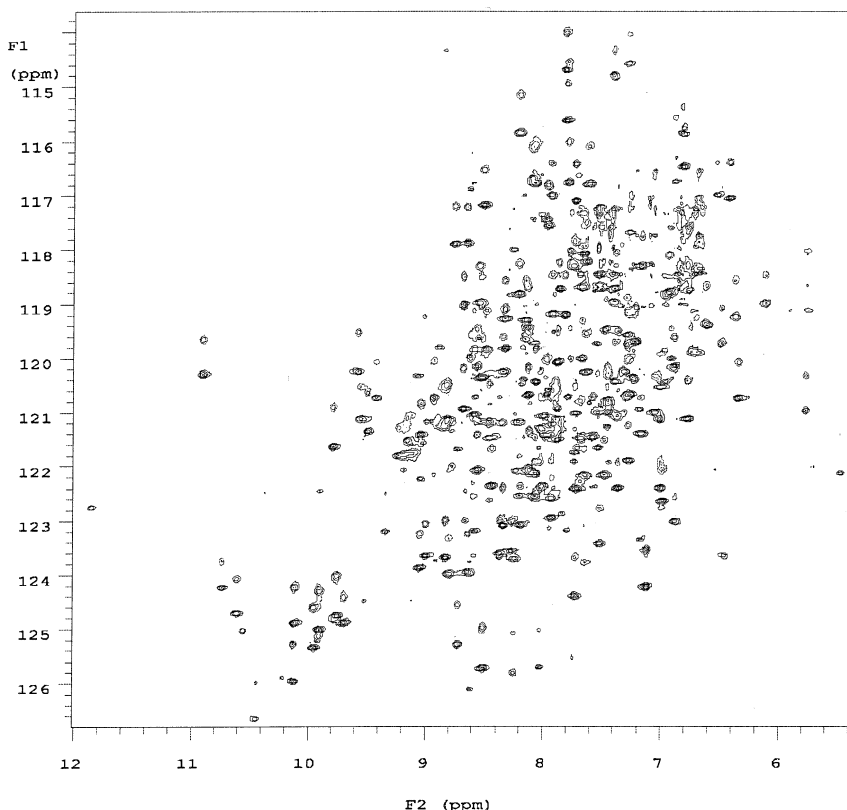


**Fig. 14.54 A** (continuing on page 121).

indirectly the frequencies of amide nitrogen and either aliphatic carbon or carboxyl carbon (or both in four-dimensional experiments).

It is the coupling network that dictates the possibilities to select correlations to be observed. The key idea is to produce a mutually complementary pair of spectra, e.g. HNCA and HN(CO)CA. The former displays both intra- and inter-residue correlations and the latter exclusively the inter-correlations. Alternatively, an exclusive inter-HNCA can be recorded. The pair of spectra displaying for each amide nuclei resonances both intra- and inter-carbon resonances allow one to trace the polypeptide backbone from one residue to another. The sequential walk is interrupted at prolines and at times potentially due to exchange broadening.

The other commonly used pair of experiments involves also resonances of CB i.e. HNCACB and HN(CO)CACB. Of course, these experiments are less sensitive since the total intensity is divided among CA and CB, but the knowledge of CB shifts will ascertain the type of residue with more confidence than with CA only. The third pair of experiments is the HNCO and HN(CA)CO. The principle is the same as above but now the carbonyl carbons are used instead. The former experiment is among the most sensitive triple resonance experiment whereas the latter is among the least sensitive, making this pair unbalanced. Certain modifica-

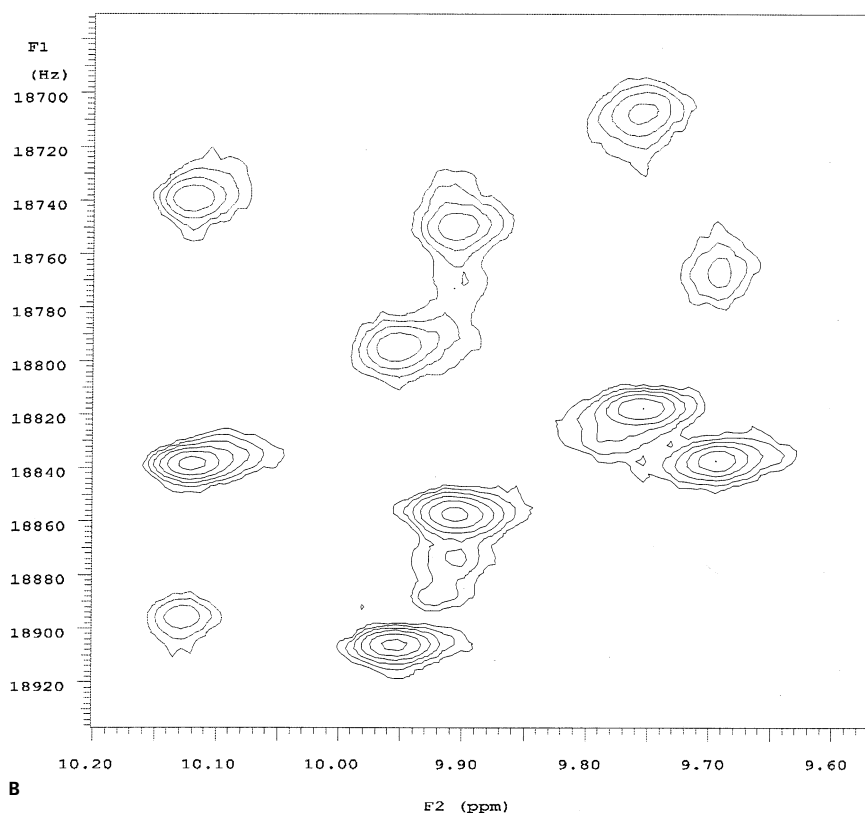


**Fig. 14.54** (A) Spin-state edit  $^{15}\text{N}$ - $^1\text{H}$  correlation spectra of a 1-mM cellulase sample in  $\text{H}_2\text{O}/\text{D}_2\text{O}$  (90/10 v/v) recorded at 40 °C in a dilute liquid crystal composed of filamentous phages with a 600 MHz NMR spectrometer using the gradient selected TROSY sequence modified to select various spin states. The displacement of the multiplets contain in addition to the 94 Hz scalar coupling residual dipolar contributions (B).

tions to the latter experiment improve the performance, however, at the cost of non-uniform performance for the various amino acid residues.

Today there are many variants of the basic sequences. The most important modifications are the transverse relaxation optimized experiments suitable for perdeuterated proteins, the sensitivity enhanced versions and the constant time (CT) implementations for improved resolution. Furthermore there are many experiments based on the basic sequences designed to measure scalar and residual dipolar couplings, often also implemented with spin-state selection as exemplified in Fig. 14.54.

The assignment of side chain resonances is a more laborious undertaking. The proton detected versions of the aforementioned experiments such as HN(CA)HA and HN(CACB)HAHB reveal the protons at the stem of the side chain. Customarily carbons and aliphatic protons are obtained by CC(CO)NH, HC(C-CO)NH, HCCH-COSY and -TOCSY experiments. Furthermore there are special experiments to correlate nuclei in the aromatic and polar side chains.

## 14.4

### Bioanalytical Mass Spectroscopy

#### 14.4.1

#### Introduction

Mass spectroscopy (MS) has flourished in various bioanalytical applications for the last 20 years mainly due to the increased demand for fast and sensitive analysis of proteins and nucleic acids separated on gels (2DE) and in capillary electrophoresis (CE). Mass spectrometric analysis requires no fluorescence or radioactive labeling and the mass spectra offer a far more complete analysis. This section will give a summarized impression of the field as it is developing today. Since there are a multitude of modifications and expansions to MS, there is still not very much clarity as to which technique will become 'standard' in proteomics and genomics research. At the moment electrospray (ESI) MS and matrix-assisted laser desorption (MALDI) MS are competing techniques, while various combined forms of MS and tandem MS (MS/MS) have also recently been explored to further increase the resolution of MS spectra of biomolecules and enable multiplexing, higher throughput etc.

Although ESI and MALDI overlap in their scope of application, MALDI-TOF mass spectrometry has been used by most research groups due to the high duty cycle of the TOF spectrometer (acquisition of a spectrum within one second), which has made it more amenable to high-throughput analysis. The MALDI technique also allows the analysis of the highest mass-to-charge ratios ( $m/z$  up to 300 kD). Arguably MALDI-TOF, as it is useful for the analysis of solid phases and bioarrays, will remain the technique of choice for bioarrays. ESI-MS, however, is also gaining momentum, because of the better compatibility of ESI with microchips, which is a major innovation force in proteomics today [468]. Various successful demonstration experiments with microchips have recently been reported for performing on-chip sample preparations, such as solid phase extraction, tryptic digestion, pre-separation and pre-concentration. The combination of microchips with ESI-MS seems to be one of the most promising developments today for proteomics research.

#### 14.4.2

#### MALDI-TOF

Matrix-assisted laser desorption ionization (MALDI) was first described by Karas and Hillenkamp in 1988 [469]. At that time it was a revolutionary method for the ionisation and analysis of large biomolecules. Now many more MS methods have been devised, but the analysis of complete protein masses is still only possible by MALDI [470]. With MALDI, a 'matrix' (crystals of small organic molecules) with a small amount of analyte is ionised by a short laser pulse at a wavelength close to the adsorption band of the matrix molecules. This produces predominantly singly charged molecular ions, which are detected by the TOF spectrometer. The ana-

lyte ions are generally produced by a gas-phase proton-transfer from the matrix to the analyte. The advantages of the method are that it is a fast process (ionisation in milliseconds) and that it yields an absolute intrinsic *m/z* ratio of the biomolecule. MALDI thus also enables the analysis of complex mixtures. As matrices, generally carboxylic acid or hydroxyl-containing aromatic compounds are used, which can form stable carbanions in the gas phase. For proteins, matrices like nicotinic acid, cinnamic acid or 2,5-dihydroxybenzoic acid have been much used. For nucleic acid analysis 3-hydroxypicolic acid has been favoured most, but also 4-nitrophenol and 8-hydroxyquinoline have been recently proposed as efficient matrices [520]. The effectiveness of mass spectrometry is evident in its capability to identify a variety of biomolecules up to 300 kDa. Presently, MALDI-TOF MS is mostly used for the analysis of solid phases, due to the solid matrix. Due to the laser excitation source, however, the area interrogated can be very small. The method thus has a strong potential not only for the reading of DNA-arrays, but also for peptide mapping from microbeads [471].

#### 14.4.3

##### **Electrospray Methods (ESI-MS)**

Of the mild ionization techniques electrospray ionization (ESI) has been one of the first to be used for organic compounds, but was introduced for the analysis of biomolecules only recently by Fenn et al. [472]. With ESI-MS, liquid is sprayed into a mass spectrometer with the aid of a very high electric field from a needle-type injector (e.g. a gold-coated capillary). This is a soft ionization technique suitable for the characterisation of biomolecules ranging from several hundred to several thousand in molecular weight. For proteomics research, however, the staggering number of proteins to be analysed from a single organism still places large demands on the sample preparation, and this is the main driving force behind the combination of ESI-MS with microfluidic chips [468, 473]. The first demonstration system of a microchip-ESI interface was described by Karger et al. and consisted of a microfabricated multiple-channel glass chip fabricated by standard photolithographic, wet chemical etching, and thermal bonding procedures (Fig. 14.55) [474]. With this device, separations of model proteins were investigated (myoglobin, recombinant human growth hormone, ubiquitin and endorphin). A high voltage was applied individually from each buffer reservoir to spray the samples sequentially from each channel into the mass spectrometer. To maintain a stable electrospray a liquid flow of 100–200 nL min<sup>-1</sup> was used. The detection limit of the microchip MS experiment for myoglobin was below  $6 \times 10^{-8}$  M. Samples in 75 % methanol and aqueous samples could be successfully analyzed with good sensitivity.

Although the interface of a TOF spectrometer with ESI has been traditionally difficult, orthogonal injection has recently proven to be a good method to enable the ESI method to be coupled with a TOF spectrometer [475]. This also gives possibilities of studying biomolecular complexes. ESI has also recently been coupled to ion mobility spectrometry, which enables a higher resolution in comparison with

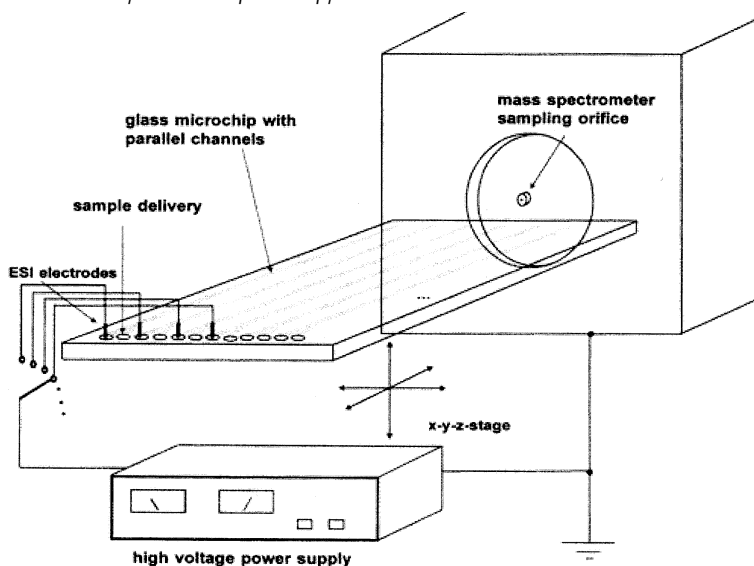


Fig. 14.55 A microchip interface to ESI-MS. (Karger et al 1997, Ref. 474).

normal ESI-MS, as exemplified with the tryptic digest of hemoglobin [476]. Smith et al. have also elaborated on the use of ESI with a Fourier transform ion cyclotron resonance (FTICR) detector [477]. The combination of the multiple charging phenomena of ESI with the superior mass resolution of FTICR gives a superior performance for the analysis of small peptides.

#### 14.4.4 Tandem-MS

Various forms of tandem mass spectroscopy (MS/MS) have also been used in the analysis of biomolecules. Such instruments consist of an ionisation source (ESI or MALDI or other) attached to a first mass analyser followed by a gas-phase collision cell. This collision cell further fragments the selected ions and feeds these ions to a second mass detector. The final mass spectrum represents a 'ladder' of fragment ions. In the case of peptides the collision cell usually cleaves the peptides at the amide bond. The ladder of resulting peptides reveals the sequence directly [496]. Thus, tandem MS instruments, such as the triple quadrupole and ion-trap instruments have been routinely applied in LC-MS/MS or ESI-MS/MS for peptide sequencing and protein identification via database searching. New configurations, which have been moving into this area include the hybrid Q-TOF [498], the MALDI-TOF-TOF [499] and the Fourier transform ion cyclotron resonance instruments [500].

## 14.4.5

**TOF-SIMS**

Secondary ion mass spectroscopy (SIMS) is a surface analysis technique based on the bombardment of the surface with a highly focused ion beam. The ions are usually  $\text{Cs}^+$  or  $\text{Ga}^+$ . The bombardment disrupts the uppermost layer of the substrate, giving rise to the emission of surface elements and intact molecules characteristic of the composition in the uppermost layer of the surface. SIMS is routinely used for depth profiling of elements in various inorganic materials and is usually a rather destructive method [478]. However, when limiting the ion dose per surface area below a certain limit more intact molecules of a larger mass can be emitted from the surface ("static SIMS"). SIMS is generally used in conjunction with a time-of-flight (TOF) mass selector, which gives, in principle, possibilities for the detection of very large molecular masses, as with MALDI-TOF.

Static SIMS has usually been applied to the analysis of small organic molecules on surfaces. One of the first investigations comprised the self-assembly of biotinylated compounds on gold and the variation of the density of biotin for optimal binding to avidin [479]. Some other examples are self-assembled layers of alkylmercaptans on silver and gold [480, 481] and  $\pi$ -extended viologens and alkylmercaptans on gold [482]. Metal surfaces generally give the best yield of intact organic ions. For instance, in the self-assembly of alkylmercaptans and other compounds on gold, various aspects of the chemisorption process have been elucidated with SIMS [480, 481]. Additionally, SIMS has been used in the study of protein adsorption. For instance Davies et al. studied the adsorption of proteins to steel, glass, polypropylene, and silicone surfaces [483] and Pradier studied protein adsorption to stainless steel [484]. Protein immobilization onto self-assembled films on gold has also recently been studied [485].

Although inorganic surfaces have been traditionally studied most by SIMS, presently the technique is also applied to polymeric substrates. For instance, Volooj et al. have studied the adsorption of cationic detergents on keratin fibers [486]. Keller et al. reported the TOF-SIMS analysis of small molecules, such as peptides, Nile Blue and cholesterol, on surfaces using Nafion 117 as a matrix for controlled formation of molecular ions [487, 488]. This already points to new possibilities for ionization with SIMS for the analysis of larger fragments. To date, however, only masses up to 1760 MU (for insulin) have been reported [489].

An interesting capability of TOF-SIMS, however, is to image the presence of molecules at micrometer spatial resolution via characteristic fragments [491]. For instance, Galla et al. have imaged the pulmonary surfactant protein C in mono-, bi- and multilayers of lipids with TOF-SIMS [492]. In a recent report Belu et al. described TOF-SIMS imaging of (recombinant)  $^{15}\text{N}$ -labelled streptavidin micro-patterned by light activation on PET substrates [493]. SIMS spectra of normal streptavidin and  $^{15}\text{N}$ -labelled streptavidin were compared. The positive ion SIMS-spectra yielded characteristic peaks for streptavidin at  $m/z$  70 (from proline and arginine) and  $m/z$  130 (from tryptophan), while  $^{15}\text{N}$ -labelled streptavidin gave corresponding peaks at  $m/z$  71 and  $m/z$  131. The negative SIMS spectra gave peaks at  $m/z$  26

(CN<sup>-</sup>) and  $m/z$  42 (CNO) for streptavidin and  $m/z$  27 and  $m/z$  43 for the <sup>15</sup>N-labelled streptavidin. The anion at  $m/z$  27 ( $\text{C}^{15}\text{N}^-$ ) enabled the most unambiguous imaging of the streptavidin on the protein microarray.

#### 14.4.6

##### MS in Protein Analysis

The task of a proteome analysis is quite formidable, as it may be necessary to identify thousands of proteins from a single organism. Besides the application of mild ionisation techniques, the use of new computational methods for correlating mass spectrometric data with information in protein sequence databases has led to the capability for 'mass fingerprinting', in which large numbers of proteins can be rapidly identified [493–496]. This type of analysis is generally referred to as 'descriptive proteomics'. As opposed to the genome, the proteome is not a static system. Various clinical studies need to assess the protein expression of one organism with that of another to establish the mechanism by which genetic mutations, infections or drugs modify the functions of the organism. Therefore, more and more emphasis is placed on 'dynamic proteomics', the capability to study the proteome's time-dependent changes, as well as 'quantitative proteomics' instead of mere descriptive proteomics.

The classic technique for separation of proteins, before identification by MS, has been (and still is in many laboratories) 2-dimensional electrophoresis (2DE), a technique that has been known since 1975 [497]. In 2DE proteins are mapped in one direction by net charge (using isoelectric focussing, IEF) and in a second, perpendicular direction by size (using sodium dodecyl sulfate polyacrylamide gel electrophoresis, SDS-PAGE). 2DE allows analytical scale separation of up to 10,000 individual proteins as well as micropreparative scale separation of proteins for further analysis. The identification of the proteins separated on the gel generally starts with the isolation of the protein spots from the gel slab and their enzymatic digestion to smaller fragments. Hereafter MS can be used in two ways for the final identification: either directly by ESI-MS or MALDI-TOF-MS, or indirectly by chromatographic separation of the fragments followed by tandem mass spectroscopy (MS/MS). At the Swiss Institute of Bioinformatics highly automated methods for the mapping of proteins on gels have been used, in which the proteins are first digested in the gel and then transferred to a PVDF membrane. This membrane is then directly scanned by MALDI-TOF-MS [493]. The identification is hereafter performed with specialised software, to create a 2-dimensional map that contains the fingerprint data as well as the identification results. These results are accessible via the ExPASy server (See Table 14.1).

There have been recent reports of new MS configurations for proteomics research, particularly new MS/MS systems. One such development is the combination of MALDI with a Q-TOF mass spectrometer, which enables, besides an enhanced resolution and sensitivity, interesting opportunities for automation [498]. MALDI TOF-TOF has been described by Medzihradski et al. and has the same benefits as MALDI-Q-TOF but is also capable of collisional-induced dissociation (CID) and very fast scan rates [499]. The most recent addition to the repertoire is the

Fourier transform ion cyclotron resonance spectrometer, with a mass accuracy better than 1 ppm. Such instruments have been used in the characterisation of hundreds of intact molecules in a single analysis of proteins from *E. coli* [500].

Despite the development of new MS methods and instrumentation, the scanning and interpretation of proteins of 2DE gels has many limitations in the study of the proteome. Proteins of low abundance, high lipophilicity and low solubility (e.g. membrane proteins), and proteins that have an extremely low or high isoelectric point or have extremely low or high masses are not easily assessed with 2DE. Also, protein complexes cannot be studied with 2DE. In all cases the sample presentation to the spectrometer is the bottleneck in obtaining high-quality spectroscopic data, sometimes necessitating multi-step procedures. For instance, researchers have used multidimensional chromatographic sample preparation systems, such as two-dimensional HPLC [501] and solid-phase microextraction, multistep elution, CE and MS/MS [502] for protein mapping. Methods have been developed to either replace the SDS-PAGE dimension or the IEF dimension by a liquid chromatographic (LC) method prior to MS analysis [503, 504]. Aebersold and coworkers described a completely chromatographic system coupled to tandem MS spectroscopy (LC/LC-MS/MS) for the analysis of low abundance proteins in yeast [505], while Link et al. described a similar LC/LC-MS/MS system in which protein mixtures from the sample were first digested and the resulting peptides were separated by 2-dimensional LC (cation exchange LC in one dimension and reverse phase LC in the other dimension) [506].

In addition to scanning gels and sampling proteins from HPLC and CE runs, the possibility of sampling proteins separated on microfluidic cartridges has been explored. Multistep procedures can be performed very efficiently on microchips and thus combinations of microchips, particularly with ESI-MS, are in the center of interest. A first example is offered by the work of Marko-Varga and coworkers, who used three microfabricated components in an automated set-up for proteomics analysis [507]: a microchip digestion unit, a piezoelectric dispenser and a silicon microvial array (Fig. 14.56.). The microchip digestion unit was anisotropically etched in 110-silicon and contained 30 parallel trenches, 250 µm deep, 50 µm wide and 1.2 mm long, in which trypsin or chymotrypsin was immobilized [508]. The unit enabled on-line protein digestion. The microdispenser was processed from silicon by a pn-etch stop process and furnished with a piezoceramic actuator and moreover functioned as a normal ink-jet printer head. This actuator provided a convenient technique to spot the protein digests in nanovials on silicon substrate plates, which could then be analysed by MALDI-TOF. To obtain highly homogeneous sample-matrix layers in the nanovials, a 'seed-layer' method was used [509].

Researchers have recently explored the possibility of combining the BiaCore instrument with MS, in which analytes immobilized on the sensor chip were analyzed with MALDI-TOF directly from the area of the flow cells (Fig. 14.57a) [310, 510, 511]. Detection limits in the low-femtomol range could be realised from studies with a model sandwich assay system, and the presence of antibody/antigen species retained during the interaction analysis could be confirmed (human myoglo-

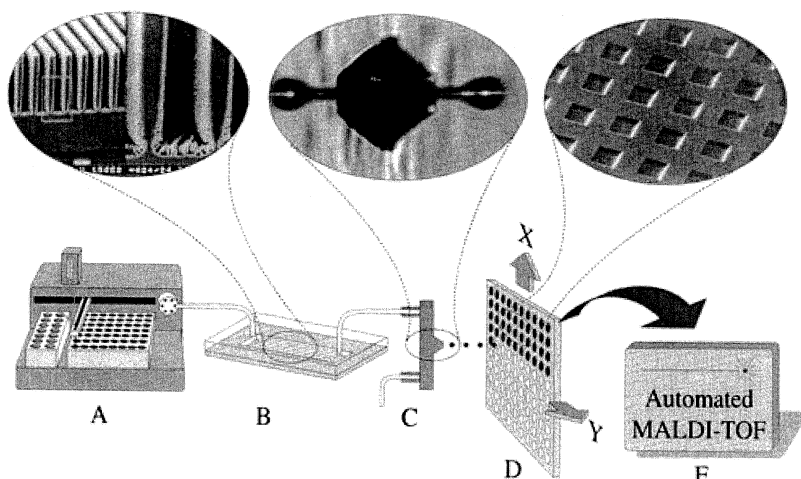


**Fig. 14.56** The integrated microanalytical workstation, with the inserts showing micro-machined parts of the system. The system comprises: (A) automated sample pretreatment and injection, (B) ■-chip IMER (photo insert shows a SEM picture of the lamella structure

with the porous layer), (C) a microdispenser used to deposit sample into nanovials (D) shallow nanovials ( $300 \times 300 \times 20 \text{ }\mu\text{m}$ ) on the MALDI target plate; and (E) automated MALDI-TOF MS analysis.  
(reproduced from ref. 507 with permission)

bin at  $m/z = 17,200$  Da and anti-human myoglobin at  $m/z = 144500$  Da, Fig. 14.57b). Although there are as yet no reports of coupling the BiaCore with ESI-MS, the general compatibility of the flow regimes in the BiaCore and that of ESI-MS could be a reason to attempt combination of these techniques into an on-line instrument in the near future.

Apart from proteome analysis there are various other types of analysis on proteins that have been performed with MS. These include analysis of binding constants and epitope analysis. ESI-MS has been used for the analysis of binding constants for various complexes formed in solution, ranging from small organic host-guest complexes to large biological complexes [512]. Kempen and Brodbelt recently described an improvement in the methodology by the use of an added second host or guest with known affinity  $K$  [513]. Closely related to the determination of binding constants is the investigation of enzyme kinetics with MALDI-TOF MS, which has recently been explored by Houston et al. [514]. They assessed the kinetics of a tyrosin phosphatase by using the formation of a covalent phosphoenzyme intermediate and following the appearance of this complex in real-time. Another field of work, which has also appeared rather recently, is the identification of epitopes directly by MALDI-MS [515]. Epitopes could be identified directly by comparing the MS spectrum of the complex directly with that of an unreacted control sample.

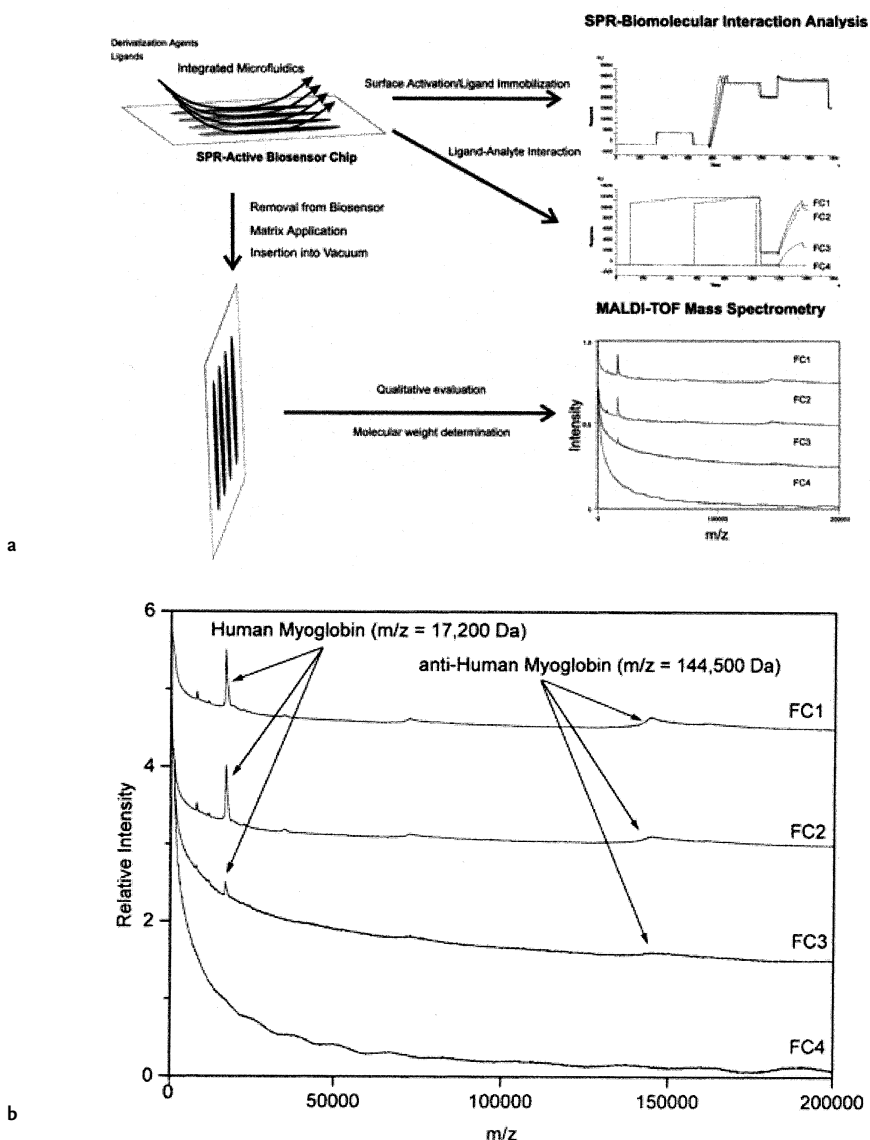


**Fig. 14.57** General scheme of the chip-based SPR-BIA/MS as reported by Nelson et al. [510]. (a) The microfluidics of the BiaCore are capable of delivering nanoliters of solution through flow cells either serially or in parallel (each flow cell has the dimension of  $0.5\text{ mm} \times 2.0\text{ mm}$ ). The real-time monitoring capabilities of SPR is used for determination of the kinetic parameters of the interaction, while MALDI-TOF analysis of the flow cells directly from the surface of the sensor chip was used to evaluate analytes retained during the SPR experiments. (b) MALDI TOF mass spectra of analytes retained during the SPR analysis of the myoglobin/anti-myoglobin system. (reproduced from Anal. Chem. with permission)

## 14.4.7

**MS in Nucleic Acid Analysis**

In nucleic acid analysis considerable progress has recently been reported for methods based on MS. Although ESI-MS can also be used in nucleic acid analysis, MALDI-TOF-MS has been used by most research groups. Various reviews on the use of MALDI-TOF for nucleic acid analysis have appeared, which focus on DNA characterization [516, 517], DNA sequencing [518] and DNA sizing [519].

The genomics and proteomics tasks for MS are mainly sizing and sequencing of DNA and the identification of genetic changes and polymorphisms and the applications are now also moving fast into the clinical diagnostics arena (e.g. early cancer detection) [520]. In determining the size of DNA strains MALDI-TOF has already replaced conventional gel electrophoresis, because with MALDI-TOF a mass accuracy of better than 1% can be obtained for DNA up to 2200 bases in length. Such an accuracy can only be surpassed by full sequencing. The sensitivity of MALDI-TOF is also superior to gel electrophoresis: below femtomol sensitivities are easily attained. MALDI-TOF MS is now also rapidly replacing the conventional Sanger DNA sequencing methods. The relevance of MALDI-TOF MS in single nucleotide polymorphism studies (SNP genotyping) is also increasing rapidly [521]. Enzymatic DNA sequencing coupled with MALDI-TOF MS has been shown to be effective for discovering previously unknown types of SNPs, either via DNA (mini)sequencing, direct mass analysis or via peptide nucleic acid hybridization probes (PNSs). Single-stranded DNA (ssDNA) has been sequenced by MALDI-TOF MS by using either digestion of the nucleotides or 'in-source' fragmentation. Only a little work has been reported on the sequencing of double-stranded DNA (dsDNA). The direct sequencing of DNA has recently been accelerated by the use of exonuclease III from *E. coli* and a much improved sample clean-up procedure [522].

**14.5  
Conclusions**

From the numerous developments in the areas described above it will be clear that many types of conventional analysis with large, expensive laboratory instruments will still be needed for elucidation of the complex structure and specific functions of biomolecules (IR, NMR and MS). Besides elaborate spectroscopic measurements for structure and sequence determination, the need for dynamic studies in real samples by *in situ*, *in vivo* and real-time measurements is also expanding. Although many new techniques will make the more conventional fluorescent labels obsolete, it can be expected that specialised fluorescence probes, particularly those with signal generation capability, will be needed in the future for fast diagnostics products. In this arena novel dyes with an increased Stokes' shift and an emission in the near-IR remain in the center of interest, as well as novel dyes

for two-photon excitation. Novel fluorescent particles are also increasingly used in fast diagnostics tests.

Spectroscopy has, unfortunately, also shown some of its limitations. For instance, the near-IR absorbance spectroscopy for the detection of glucose *in vivo*, has not significantly advanced. Also the commercialisation of biosensors in the (bio)chemical process industry has been slowing down due to difficulties with long-term stability and calibration. In clinical diagnostics, only a few optical biosensor devices have been able to meet the demands on sensitivity and selectivity and labelling of reagents will still be required to obtain reliable measurements below nanomolar concentrations in real samples. Some devices, however, are based on labels that can be confined within the sensor, and these may operate reversibly or can be regenerated for continuous use. Otherwise disposable devices are still likely to be used for a long time in the diagnostics area. For instance, electrophoretic separations can presently also be performed on injection-moulded plastic substrates [523].

As seen in some of the examples given above, spectroscopic methods are very much combined with other techniques to provide more information more quickly. Optical sensors using injection-molded microfluidics systems have already been on the market for 10 years (the BiaCore), but presently the combination of spectrometers or optical sensors with microfluidics, capillary electrophoresis and DNA arrays is still very much in the center of interest. For instance, an optical biosensor can be combined with mass spectroscopy, allowing very rapid sequential determination of the binding constants, charge, size and sequence of a target protein [511].

Micromechanical systems will probably also enter the arena of bioanalysis within a few years ("BioMEMS"), which opens up unique possibilities for sample processing (and also detection) at the micro-scale ( $\mu$ -TAS) [524, 525]. New advances in *silicon processing* have already resulted in novel, proven concepts for miniaturised sample handling and readout in diagnostics, genomics and proteomics applications [526, 527]. The efforts towards miniaturisation are mainly due to the favourable effect of miniaturisation on the sample throughput [528]. Processing in silicon has the great advantage that the electronics can be placed with the analysis system on the same chip. The throughput of analysis systems is further enhanced through sensor arrays and by including more sophisticated fluid handling systems, which may be particularly useful in proteomics and genomics and in drug discovery [529].

## References

- 1 M. J. Dutt, K. H. Lee, *Curr. Opin. Biotechnol.*, **2000**, *11*, 176.
- 2 V. Wasinger, S. Cordwell, A. Cerpa-Poljak et al., *Electrophoresis*, **1995**, *16*, 1090.
- 3 L. Koutny, D. Schmalzing, O. Salas-Solano et al., *Anal. Chem.*, **2000**, *72*, 3388.
- 4 I. Kheterpal, R. A. Mathies, *Anal. Chem.*, **1999**, *71*, 31A.
- 5 *Proteome Research: New Frontiers in Functional Genomics*, eds. M. R. Wilkins, K. L. Williams, R. D. Appel, D. F. Hochstrasser, Springer Verlag, Berlin 1997.
- 6 *Proteome and Protein Analysis*, eds. R. M. Kamp, D. Kyriakidis, T. Choli-Papadopoulou, Springer Verlag, Berlin 1999.
- 7 *Topics in Fluorescence Spectroscopy. 4: Probe Design and Chemical Sensing*, ed. J. R. Lakowicz, Plenum Press, New York 1994.
- 8 J. S. Andersen, M. Mann, *FEBS Lett.*, **2000**, *480*, 25.
- 9 R. E. Banks, M. J. Dunn, D. F. Hochstrasser et al., *The Lancet*, **2000**, *356*, 1749.
- 10 P. Hensly, D. G. Myszka, *Curr. Opin. Biotechnol.*, **2000**, *11*, 9.
- 11 *Biosensors. Fundamentals and Applications*, ed. A. P. F. Turner, I. Karube, G. Wilson, Oxford University Press, Oxford 1987.
- 12 *Handbook of Biosensors and Electronic Noses*, ed. E. Kress-Rogers, CRC Press, Boca Raton, FL 1996.
- 13 F. W. Scheller, U. Wollenberger, A. Warsinke et al., *Curr. Opin. Biotechnol.*, **2001**, *12*, 35.
- 14 H. H. Rashidi and L. K. Buehler, *Bioinformatics Basics, Applications in Biological Science and Medicine*, CRC Press, Boca Raton, FL 1999.
- 15 *Bioinformatics: Sequence, Structure, and Databanks: A Practical Approach*, ed. D. Higgins, W. Taylor Oxford University Press, Oxford 2000.
- 16 J. Galbán, Y. Andreu, J. F. Sierra et al., *Luminescence*, **2001**, *16*, 199–210.
- 17 S. D'Auria, J. R. Lakowicz, *Curr. Opin. Biotechnol.*, **2001**, *12*, 99.
- 18 *Applied Fluorescence in Chemistry, Biology and Medicine*, ed. W. Rettig, B. Strehmel, S. Schrader et al., Springer Verlag, Berlin 1998.
- 19 ACS Symp. Ser., **1993**, *538*.
- 20 *Fluorescent and Luminescent Probes for Biological Activity*, ed. W. T. Mason, Academic Press, New York 1999.
- 21 R. P. Haugland, *Handbook of Fluorescent Probes and Research Chemicals*, 7th edition, Molecular Probes Inc., Eugene, OR 1999.
- 22 M. M. Martin, L. Lindqvist, *J Lumin.*, **1975**, *10*, 381; B. Khodorov, O. Valkina, V. Turovetsky, *FEBS Lett.*, **1994**, *341*, 125; J. A. Thomas, R. N. Buchsbaum, A. Zimniak et al. *Biochemistry*, **1979**, *18*, 2210–2218; A. M. Paradiso, R. Y. Tsien, T. E. Machen, *Proc. Natl. Acad. Sci.*, **1984**, *81*, 7436; W-C. Sun et al., *J Org. Chem.*, **1997**, *62*, 6469; M. Nedergaard, S. Desai, W. Pulsinelli, *Anal. Biochem.*, **1990**, *187*, 109; C. S. Huang, S. J. Kopacz, C. P. Lee, *Biochim. Biophys. Acta*, **1983**, *722*, 107–115; C. C. Overly, K. D. Lee, E. Berthiaume et al., *Proc. Natl. Acad. Sci. USA*, **1995**, *92*, 3156.

- 23** A. Minta, R. Y. Tsien, *J. Biol. Chem.*, **1989**, *264*, 19449–19457; K. Meuwis, N. Boens, F. C. De Schryver et al., *Bioophys. J.*, **1995**, *68*, 2469–2473; H. Szmacinski, J. R. Lakowicz, M. L. Johnson, *Methods Enzymol.*, **1994**, *240*, 723–748; S. Jayaraman, Y. Song, L. Vetrivel et al., *J. Clin. Invest.*, **2001**, *107*, 317–324.
- 24** *Calcium Signaling Protocols*, ed. D. Lambert, Humana Press, Totowa, NJ, USA 1999; *A Practical Guide to the Study of Calcium in Living Cells*, ed. R. Nuccitelli, Academic Press, New York 1994, 342 pp.; D. A. Williams, K. E. Fogarty, R. Y. Tsien et al., *Nature*, **1985**, *318*, 558–561; H. Iatridou, E. Foukaraki, M. A. Kuhn et al., *Cell Calcium*, **1994**, *15*, 190–198; S. Girard, A. Luckhoff, J. Lechleiter et al., *Biophys. J.*, **1992**, *61*, 509–517; A. Takahashi, P. Camacho, J. D. Lechleiter et al., *Physiol. Rev.*, **1999**, *79*, 1089–1125; R. Y. Tsien, *Biochemistry*, **1980**, *19*, 2396–2404; Y. Ohmiya, T. Hirano, *Chem. Biol.*, **1996**, *3*, 337–347; E. Murphy, C. C. Freudenrich, L. A. Levy et al., *Proc. Natl. Acad. Sci. USA*, **1989**, *86*, 2981–2984; J. P. van der Wolk, M. Klose, J. G. de Wit JG et al., *J. Biol. Chem.*, **1995**, *270*, 18975–18982.
- 25** L. M. Canzoniero, D. M. Turetsky, D. W. Choi, *J. Neurosci.*, **1999**, *19*, RC31; C. J. Frederickson, E. J. Kasarskis, D. Ringo et al., *J. Neurosci. Methods*, **1987**, *20*, 91–103; M. A. Kuhn et al., *Proc. SPIE-Int. Soc. Opt. Eng.*, **1995**, 2388, 238.
- 26** O. S. Wolfbeis, E. Urbano, *J. Heterocycl. Chem.*, **1982**, *19*, 841; A. S. Verkman, M. C. Sellers, A. C. Chao et al., *Anal. Biochem.*, **1989**, *178*, 355–361; J. Biwersi, A. S. Verkman, *Biochemistry*, **1991**, *30*, 7879–7883; J. Biwersi, B. Tulk, A. S. Verkman, *Anal. Biochem.*, **1994**, *219*, 139–143; H. B. Li, F. Chen, *Fresenius' J. Anal. Chem.*, **2000**, *368*, 501–504.
- 27** A. Sano, M. Takezawa, S. Takitani, *Anal. Sci.*, **1986**, *2*, 491.
- 28** H. Deakin, M. G. Ord, L. A. Stocken, *Biochem. J.*, **1963**, *89*, 296; N. S. Kosower, E. M. Kosower, G. L. Newton et al., *Proc. Natl. Acad. Sci. USA*, **1979**, *76*, 3382–3386.
- 29** R. H. Upson, R. P. Haugland, M. N. Malekzadeh et al., *Anal. Biochem.*, **1996**, *243*, 41–45.
- 30** H. Kojima et al., *Angew. Chem. Int. Ed. Engl.*, **1999**, *38*(21), 3209; T. P. Misko, R. J. Schilling, D. Salvemini et al., *Anal. Biochem.*, **1993**, *214*, 11–16; A. Buldt, U. Karst, *Anal. Chem.*, **1999**, *71*, 3003–3007.
- 31** M. Krieg, *Biochim. Biophys. Acta*, **1992**, *1105*, 333–335; G. Bottiroli, A. C. Croce, P. Balzarini et al., *Photochem. Photobiol.*, **1997**, *66*, 374–383; D. C. Neckers, O. M. Valdes-Aguilera, *Adv. Photochem.*, **1993**, *18*, 315; S. Miranda, C. Opazo, L. F. Larrondo et al., *Prog. Neurobiol.*, **2000**, *62*, 633–648.
- 32** R. Y. Tsien, *Nature Biotechnol.*, **1999**, *17*, 956; G. S. Baird, D. A. Zacharias, R. Y. Tsien, *Proc. Natl. Acad. Sci. USA*, **2000**, *97*, 11984.
- 33** (a) D. A. Armbruster, R. H. Schwarzhoff, E. C. Hubster et al., *Clin. Chem.*, **1993**, *39*(10), 2137–46; (b) J. Szollosi, S. Damjanovich, L. Matyus, *Cytometry*, **1998**, *34*(4), 159–179; (c) Y. Z. Zhang, C. Kemper, A. Bakke et al., *Cytometry*, **1998**, *33*, 244–248; (d) D. L. Luchtel, J. C. Boykin, S. L. Bernard et al., *Biotechnol. Histochem.*, **1998**, *73*, 291–309; J. M. Brinkley, R. P. Haugland, V. Singer, *1994 US Pat.*, 5,326,692.
- 34** Z. Diwu, D. H. Klaubert, R. P. Haugland, *Proc. SPIE-Int. Soc. Opt. Eng.*, **1999**, *3602*, 265; K. D. Larison, R. BreMiller, K. S. Wells et al., *J. Histochem. Cytochem.*, **1995**, *43*, 77–83.
- 35** J. F. Breininger, D. G. Baskin, *J. Histochem. Cytochem.*, **2000**, *48*, 1593–1599; M. N. Bobrow, T. D. Harris, K. J. Shaughnessy et al., *J. Immunol. Methods*, **1989**, *125*, 279–285; R. P. van Gijlswijk, H. J. Zijlmans, J. Wiegant et al., *J. Histochem. Cytochem.*, **1997**, *45*, 375–382.
- 36** O. H. Lowry et al., *J. Biol. Chem.*, **1951**, *193*, 265; S. Fazekas de St Groth, R. Webster, A. Datyner, *Biochim. Biophys. Acta*, **1963**, *71*, 377; M. M. Bradford, *Anal. Biochem.*, **1976**, *72*, 248–254; S. Udenfriend, S. Stein, P. Bohlen et al.,

- Science*, **1972**, *178*, 871–872; C. C. Goodno, H. E. Swaisgood, G. L. Cattignani, *Anal. Biochem.*, **1981**, *115*, 203–211; P. K. Smith, R. I. Krohn, G. T. Hermanson et al., *Anal. Biochem.*, **1985**, *150*, 76–85; L. J. Jones et al., *FASEB J.*, **1996**, *10*, A1512, abstract #2954; Y. Liu, R. S. Foote, S. C. Jacobson et al., *Anal. Chem.*, **2000**, *72*, 4608–4613; W. F. Patton, *Electrophoresis*, **2000**, *21*, 1123–1144; W. F. Patton, *Biotechniques*, **2000**, *28*, 944–948; J. X. Yan, R. A. Harry, C. Spibey et al., *Electrophoresis*, **2000**, *21*, 3657–3665.
- 37** H. Rinderknecht, *Experientia*, **1960**, *16*, 430; L. C. Felton, C. R. McMillion, *Anal. Biochem.*, **1961**, *2*, 178; G. Weber, *Biochem. J.*, **1952**, *51*, 155; N. Seiler, *Methods Biochem. Anal.*, **1970**, *18*, 259–337; J. K. Lin, J. Y. Chang, *Anal. Chem.*, **1975**, *47*, 1634–1638; K. Muramoto, H. Kamiya, H. Kawauchi, *Anal. Biochem.*, **1984**, *141*, 446–450; S. W. Jin, G. X. Chen, Z. Palacz et al., *FEBS Lett.*, **1986**, *198*, 150–154; L. L. Maggiora, C. W. Smith, Z. Y. Zhang, *J. Med. Chem.*, **1992**, *35*, 3727–3730; H. Maeda, H. Kawauchi, *Biochem. Biophys. Res. Commun.*, **1968**, *31*, 188–192.
- 38** D. L. Taylor, Y. L. Wang, *Proc. Natl. Acad. Sci. USA*, **1978**, *75*, 857–861; K. Barber, R. R. Mala, M. P. Lambert et al., *Neurosci. Lett.*, **1996**, *207*, 17–20; D. Szczesna, S. S. Lehrer, *J. Muscle Res. Cell Motil.*, **1993**, *14*, 594–597.
- 39** J. B. Le Pecq, M. Le Bret, J. Barbet et al., *Proc. Natl. Acad. Sci. USA*, **1975**, *72*, 2915–2919; A. R. Morgan, J. S. Lee, D. E. Pulleyblank et al., *Nucleic Acids Res.*, **1979**, *7*, 547–569; G. K. McMaster, G. G. Carmichael, *Proc. Natl. Acad. Sci. USA*, *74*, 4835–4838 (1977); W. Schnedl, A. V. Mikelsaar, M. Breitenbach et al., *Hum. Genet.*, **1977**, *36*, 167–172; B. Weisblum, E. Haenssler, *Chromosoma*, **1974**, *46*, 255–260; H. A. Crissman, Z. Darzynkiewicz, J. A. Steinkamp et al., *Methods Cell Biol.*, **1990**, *33*, 305–314; I. Saiki, C. D. Bucana, J. Y. Tsao et al., *J. Natl. Cancer Inst.*, **1986**, *77*, 1235–1240; W. Muller, D. M. Crothers, *J. Mol. Biol.*, **1968**, *35*, 251–290; B. Festy, M. Daune, *Biochemistry*, **1973**, *12*, 4827–4834; T. L. Netzel et al., *J. Phys. Chem.*, **1995**, *99*, 17936; M. Poot, L. L. Gibson, V. L. Singer, *Cytometry*, **1997**, *27*, 358–364; L. M. Popa, S. Winter, G. Lober, *Biochem. Mol. Biol. Int.*, **1994**, *34*, 1189–1196; W. Beisker, E. M. Weller-Mewe, M. Nusse, *Cytometry*, **1999**, *37*, 221–229; E. S. Mansfield, J. M. Worley, S. E. McKenzie et al., *Mol. Cell Probes*, **1995**, *9*, 145–156; S. J. Ahn, J. Costa, J. R. Emanuel, *Nucleic Acids Res.*, **1996**, *24*, 2623–2625; L. Reyderman, S. Stavchansky, *J. Chromatogr. A*, **1996**, *755*, 271–280; L. J. Jones, S. T. Yue, C. Y. Cheung et al., *Anal. Biochem.*, **1998**, *265*, 368–374; M. Fujita, S. Tomita, Y. Ueda et al., *Mol. Pathol.*, **1998**, *51*, 342; F. Karlsen, H. B. Steen, J. M. Nesland, *J. Virol. Methods*, **1995**, *55*, 153–156; D. M. Schmidt, J. D. Ernst, *Anal. Biochem.*, **1995**, *232*, 144–146; Y. Hamaguchi et al., *Environ. Health*, **1997**, *60*, 14.
- 40** E. Schrock, S. du Manoir, T. Veldman et al., *Science*, **1996**, *273*, 494–497; B. Forghani, G. J. Yu, J. W. Hurst, *J. Clin. Microbiol.*, **1991**, *29*, 583–591.
- 41** C. Schneeberger, P. Speiser, F. Kury et al., *PCR Methods Appl.*, **1995**, *4*, 234–238; J. Huang, F. J. DeGraves, D. Gao et al., *Biotechniques*, **2001**, *30*, 150–157.
- 42** J. C. Wiegant, R. P. van Gijlswijk, R. J. Heetebrrij et al., *Cytogenet. Cell Genet.*, **1999**, *87*, 47–52; H. J. Tanke, J. Wiegant, R. P. van Gijlswijk, *Eur. J. Hum. Genet.*, **1999**, *7*, 2–11; J. C. Alers, J. Rochat, P. J. Krijtenburg et al., *Genes Chromosomes Cancer*, **1999**, *25*, 301–305.
- 43** V. B. Paragas, Y. Z. Zhang, R. P. Haugland et al., *J. Histochem. Cytochem.*, **1997**, *45*, 345–357.
- 44** E. J. Speel, A. H. Hopman, P. J. Komminoth, *Histochem. Cytochem.*, **1999**, *47*, 281–288.
- 45** R. D. Kaiser, E. London, *Biochim. Biophys. Acta*, **1998**, *1375*, 13–22; J. A. Monti, S. T. Christian, W. A. Shaw et al., *Life Sci.*, **1977**, *21*, 345–355; A. Chattopadhyay, E. London, *Biochim. Biophys. Acta*, **1988**, *938*, 24–34; H. J. Galla, E. Sackmann, *J. Am. Chem. Soc.*, **1975**, *97*, 4114–4120; Y. Barenholz, T. Cohen, E. Haas et al., *J. Biol. Chem.*, **1996**, *271*, 3085–3090; A. S. Waggoner,

- L. Stryer, *Proc. Natl. Acad. Sci. USA*, **1970**, *67*, 579–589; P. Luan, M. Glaser, *Biochemistry*, **1994**, *33*, 4483–4489; L. A. Sklar, B. S. Hudson, R. D. Simoni, *Proc. Natl. Acad. Sci. USA*, **1975**, *72*, 1649–1653.
- 46** P. J. Sims, A. S. Waggoner, C. H. Wang et al., *Biochemistry*, **1974**, *13*, 3315–3330; J. A. London, D. Zecevic, L. B. Cohen, *J. Neurosci.*, **1987**, *7*, 649–661; E. Fluhler, V. G. Burnham, L. M. Loew, *Biochemistry*, **1985**, *24*, 5749–5755; S > T. Smiley, M. Reers, C. Mottola-Harts-horn et al., *Proc. Natl. Acad. Sci. USA*, **1991**, *88*, 3671–3675; L. M. Loew, *Methods Cell Biol.*, **1993**, *38*, 195–209; P. Schaffer, H. Ahammer, W. Muller et al., *Pflugers Arch.*, **1994**, *426*, 548–551; Y. Tsau, P. Wenner, M. J. O'Donovan et al., *J. Neurosci. Methods*, **1996**, *70*, 121–129; A. Grinvald, R. D. Frostig, E. Lieke et al., *Physiol. Rev.*, **1988**, *68*, 1285–1366; M. Zochowski, M. Wachowiak, C. X. Falk et al., *Biol. Bull.*, **2000**, *198*, 1–21.
- 47** V. A. Rakhamanova, R. C. MacDonald, *Anal. Biochem.*, **1998**, *257*, 234–237; D. E. Jones, Jr., D. M. Cui, D. M. Miller, *Oncogene*, **1995**, *10*, 2323–2330; A. G. Rao, P. Flynn, *Biotechniques*, **1990**, *8*, 37; D. C. Young, S. D. Kingsley, K. A. Ryan et al., *Anal. Biochem.*, **1993**, *215*, 24–30; M. Zhou, C. Zhang, R. H. Upson et al., *Anal. Biochem.*, **1998**, *260*, 257–259; A. Tronsmo, G. E. Harman, *Anal. Biochem.*, **1993**, *208*, 74–79.
- 48** R. Lotterberg, U. Christensen, C. M. Jackson et al., *Methods Enzymol. C*, **1981**, *80*, 341–361; B. G. Rosser, S. P. Powers, G. J. Gores, *J. Biol. Chem.*, **1993**, *268*, 23593–23600; S. P. Leytus, L. L. Melhado, W. F. Mangel, *Biochem. J.*, **1983**, *209*, 299–307; S. S. Twining, *Anal. Biochem.*, **1984**, *143*, 30–34.
- 49** B. Rotman, J. A. Zderic, M. Edelstein, *Proc. Natl. Acad. Sci. USA*, **1963**, *50*, 1; F. Leiraa, J. M. Vieitesa, M. R. Vieytesb et al., *Toxicon*, **2000**, *38*, 1833–1844; S. Avrameas, *J. Immunol. Methods*, **1992**, *150*, 23–32; K. R. Gee, W. C. Sun, M. K. Bhalgat et al., *Anal. Biochem.*, **1999**, *273*, 41–48; R. D. Petty, L. A. Sutherland, E. M. Hunter, I. A. Cree, *J. Biolumin. Chemilumin.*, **1995**, *10*, 29–34.
- 50** M. Zhou, Z. Diwu, N. Panchuk-Voloshina, *Anal. Biochem.*, **1997**, *253*, 162–168; D. M. Amundson, M. Zhou, *J. Biochem. Biophys. Methods*, **1999**, *38*, 43–52; M. Zhou, N. Panchuk-Voloshina, *Anal. Biochem.*, **1997**, *253*, 169–174; K. E. McElroy, P. J. Bouchard, M. R. Harpel et al., *Anal. Biochem.*, **2000**, *284*, 382–387; M. Zhou, C. Zhang, R. P. Haugland, *Proc. SPIE-Int. Soc. Opt. Eng.*, **2000**, *3926*, 166.
- 51** D. W. Rosenberg, H. Roque, A. Kappas, *Anal. Biochem.*, **1990**, *191*, 354–358; E. Solito, C. Raguenes-Nicol, C. de Coupade et al., *Br. J. Pharmacol.*, **1998**, *124*, 1675–1683; H. S. Hendrickson, E. K. Hendrickson, I. D. Johnson et al., *Anal. Biochem.*, **1999**, *276*, 27–35; H. S. Hendrickson, P. N. Rauk, *Anal. Biochem.*, **1981**, *116*, 553–558; H. S. She, D. E. Garsetti, M. R. Steiner, *Biochem. J.*, **1994**, *298*, 23–29; M. Zhou, C. Zhang, R. P. Haugland, *Proc. SPIE-Int. Soc. Opt. Eng.*, **2000**, *3926*, 166; H. S. Hendrickson, K. J. Kotz, E. K. Hendrickson, *Anal. Biochem.*, **1990**, *185*, 80–83; R. C. Trievet, F. Y. Li, R. Mar-morstein, *Anal. Biochem.*, **2000**, *287*, 319–328; D. E. Hruby, E. M. Wilson, *Methods Enzymol.*, **1992**, *216*, 369–376; C. K. Lefevre, V. L. Singer, H. C. Kang et al., *J. Histochem. Cytochem.*, **1999**, *47*, 545–550.
- 52** R. M. Guasch, C. Guerri, J. E. O'Conor, *Exp. Cell Res.*, **1993**, *207*, 136–141; R. Renthal, A. Steinemann, L. Stryer, *Exp. Eye Res.*, **1973**, *17*, 511–515; M. W. Miller, J. A. Hanover, *J. Biol. Chem.*, **1994**, *269*, 9289–9297; N. Ito, S. Imai, S. Haga et al., *Histochem. Cell Biol.*, **1996**, *106*, 331–339; I. Virtanen, *Histochemistry*, **1990**, *94*, 397–401; A. K. Kenworthy, N. Petranova, M. Edidin, *Mol. Biol. Cell*, **2000**, *11*, 1645–1655; G. Sahagun, S. A. Moore, Z. Fabry, *Am. J. Pathol.*, **1989**, *134*, 1227–1232.
- 53** L. B. Chen, *Methods Cell Biol.*, **1989**, *29*, 103–123; J. Habicht, K. Brune, *Exp. Cell Res.*, **1980**, *125*, 514–518; J. Bereiter-Hahn, *J. Int. Rev. Cytol.*, **1990**, *122*, 1–63; M. Septinus, W. Seiffert, H. W. Zimmermann, *Histochemistry*, **1983**, *79*, 443–456; M. Septinus, T. Berthold, A. Naujok et al., *Histochemistry*, **1985**,

- 82, 51–66; S. J. Rembush, M. A. Trush, *Free Radical Biol. Med.*, **1994**, *17*, 117–126; M. Poot, Y. Z. Zhang, J. A. Kramer et al., *J. Histochem. Cytochem.*, **1996**, *44*, 1363–1372; A. J. Pereira, B. Dalby, R. J. Stewart et al., *J. Cell Biol.*, **1997**, *136*, 1081–1090; J. Sakanoue, K. Ichikawa, Y. Nomura et al., *J. Biochem. (Tokyo)*, **1997**, *121*, 29–37.
- 54** R. E. Pagano, O. C. Martin, *Cell Biology: A Laboratory Handbook*, 2nd edition, academic press, New York, ed. J. E. Celis, 1998, Vol. 2, 507–512; M. Terasaki, J. Song, J. R. Wong et al., *Cell*, **1984**, *38*, 101–108; L. Cole, D. Davies, G. J. Hyde et al., *J. Microsc.*, **2000**, *197*, 239–249; M. Terasaki, L. A. Jaffe, *J. Cell Biol.*, **1991**, *114*, 929–940; L. Cole, D. Davies, G. J. Hyde et al., *Fungal Genet. Biol.*, **2000**, *29*, 95–106.
- 55** A. H. Guse, C. P. da Silva, I. Berg et al., *Nature*, **1999**, *398*, 70–73; Y. Cui, A. Galione, D. A. Terrar, *Biochem. J.*, **1999**, *342*, 269–273; L. Wong, R. Aarhus, H. C. Lee et al., *Biochim. Biophys. Acta*, **1999**, *1472*, 555–564; X. Zhang, J. Wen, K. R. Bidasee et al., *Biochem. J.*, **1999**, *340*, 519–527; B. Abrenica, J. S. Gilchrist, *Cell Calcium*, **2000**, *28*, 127–136; D. A. Malencik, T. S. Huang, S. R. Anderson, *Biochem. Biophys. Res. Commun.*, **1982**, *108*, 266–272; J. Baudier, E. Bergeret, N. Bertacchi et al., *Biochemistry*, **1995**, *34*, 7834–7846; J. A. Putkey, M. N. Waxham, *J. Biol. Chem.*, **1996**, *271*, 29619–29623; K. Torok, D. J. Cowley, B. D. Brandmeier et al., *Biochemistry*, **1998**, *37*, 6188–6198.
- 56** A. Ogamo, K. Matsuzaki, H. Uchiyama et al., *Carbohydr. Res.*, **1982**, *105*, 69–85; M. Sobel, D. F. Soler, J. C. Kermode et al., *J. Biol. Chem.*, **1992**, *267*, 8857–8862; L. Berry, A. Stafford, J. Fredenburgh et al., *J. Biol. Chem.*, **1998**, *273*, 34730–34736; K. L. Bentley, R. J. Klebe, R. E. Hurst et al., *J. Biol. Chem.*, **1985**, *260*, 7250–7256.
- 57** C. S. Chen, M. Poenie, *J. Biol. Chem.*, **1993**, *268*, 15812–15822; B. A. Newton, *J. Gen. Microbiol.*, **1955**, *12*, 226; I. Takahashi, S. Nakanishi, E. Kobayashi, *Biochem. Biophys. Res. Commun.*, **1989**, *165*, 1207–1212; T. Hiratsuka, *J. Biol. Chem.*, **1982**, *257*, 13354–13358.
- 58** M. J. Anderson, M. W. Cohen, *J. Physiol.*, **1974**, *237*, 385–400; N. H. Salzman, F. R. Maxfield, *Subcellular Biochemistry*, Vol. 19: *Endocytic Components: Identification and Characterization*, 1993, Kluwer Academic Publ, Dordrecht 95–123; Y. Wang, Q. Gu, F. Mao et al., *J. Neurosci.*, **1994**, *14*, 4147–4158; J. L. Reid, J. Vincent, *Cardiology*, **1986**, *73*, 164–174; H. Heithier, D. Hallmann, F. Boege et al., *Biochemistry*, **1994**, *33*, 9126–9134; H. Wang, K. M. Standifer, D. M. Sherry, *Vis. Neurosci.*, **2000**, *17*, 11–21; M. R. Tota, S. Daniel, A. Sirotina et al., *Biochemistry*, **1994**, *33*, 13079–13086; B. Walker, J. Gray, D. M. Burns et al., *J. Peptides*, **1995**, *16*, 255–261; H. Haller, C. Lindschau, B. Erdmann et al., *Circ. Res.*, **1996**, *79*, 765–772; V. M. Kolb, A. Koman, L. Terenius, *Life Sci.*, **1983**, *33 Suppl. 1*, 423–426; O. T. Jones, D. L. Kunze, K. J. Angelides, *Science*, **1989**, *244*, 1189–1193; D. Schild, H. Geiling, J. Bischofberger, *J. Neurosci. Methods*, **1995**, *59*, 183–190; T. R. Kleyman, E. J. Crago, Jr., *J. Membr. Biol.*, **1988**, *105*, 1–21; P. A. Fortes, *Biochemistry*, **1977**, *16*, 531–540; B. Lohrke, M. Derno, B. Kruger et al., *Pflugers Arch.*, **1997**, *434*, 712–720; G. Fricker, H. Gutmann, A. Droulle et al., *Pharm. Res.*, **1999**, *16*, 1570–1575.
- 59** D. A. Bass, J. W. Parce, L. R. Dechatelet et al., *J. Immunol.*, **1983**, *130*, 1910–1917; T. C. Ryan, G. J. Weil, P. E. Newburger et al., *J. Immunol. Methods*, **1990**, *130*, 223–233.
- 60** J. P. Aubry, A. Blaecke, S. Lecoanet-Henchoz et al., *Cytometry*, **1999**, *37*, 197–204; N. A. Thornberry, Y. Lazebnik, *Science*, **1998**, *281*, 1312–1316.
- 61** M. Matsuoka, Synthetic Design of Infrared Absorbing Dyes, in *Infrared Absorbing Dyes*, eds. A. R. Katritzky and G. J. Sabongi, Plenum Press, New York 1990.
- 62** R. Zahradník, *Fortschr. Chem. Forsch.*, **1968**, *10*, 158.
- 63** R. J. Beunker, S. D. Peyerimhoff, *Theoret. Chim. Acta*, **1974**, *35*, 33.

- 64** Density-functional Theory of Atoms and Molecules, eds. R. G. Parr and W. Yang, Oxford University Press, New York 1989.
- 65** F. J. Green, *The SigmaAldrich Handbook of Stains, Dyes and Indicators*, Aldrich Chemical Company Inc., Milwaukee, WI, 1990, p. 374.
- 66** J. L. Riggs, R. J. Seaward, J. H. Burkhalter et al., *Am. J. Pathol.*, **1958**, *34*, 1081.
- 67** E. Terpetschnig, O. S. Wolfbeis, Luminescent Probes for NIR Sensing Applications, in *Near Infrared Dyes for High Technology Applications*, eds. S. Daehne, U. Resch-Genger, O. S. Wolfbeis, NATO ASI Series, Kluwer, Dordrecht, The Netherlands 1998, 161–182.
- 68** D. S. Wilbur, P. M. Pathare, D. K. Hamlin et al., *Bioconjugate Chem.*, **2000**, *11*, 584.
- 69** M. Thompson, N. W. Woodbury, *Biochemistry*, **2000**, *39*, 4327.
- 70** D. Staerk, A. A. Hamed, E. B. Pederson et al., *Bioconjugate Chem.*, **1997**, *8*, 869.
- 71** J. B. Randolph, A. S. Waggoner, *Nucleic Acids Res.*, **1997**, *14*, 2923.
- 72** M. Lipowska, G. Patonay, L. Strekowski, *Synth. Commun.*, **1993**, *23*, 3087.
- 73** C. V. Owens, Y. Y. Davidson, S. Kar et al., *Anal. Chem.*, **1997**, *69*, 1256.
- 74** J. H. Flanagan, C. V. Owens, S. E. Romero et al., *Anal. Chem.*, **1998**, *79*, 2676.
- 75** J. Ren, J. B. Chaires, *J. Am. Chem. Soc.*, **2000**, *122*, 424.
- 76** L. Strekowski, unpublished results
- 77** L. Strekowski, M. Lipowska, G. Patonay *J. Org. Chem.*, **1992**, *57*, 4578.
- 78** D. Keil, H. Hartmann, C. Reichardt. *Liebigs Ann. Chem.*, **1993**, 935.
- 79** H. Meier, R. Petermann *Tetrahedron Lett.*, **2000**, *41*, 5475.
- 80** D. Citterio, L. Jenny, S. Rásónyi, *Sens. Actuators B*, **1997**, *202*, 38–39.
- 81** E. Terpetschnig, H. Szmacinski, A. Ozinskas et al., *Anal. Biochem.*, **1994**, *217*, 197.
- 82** B. Oswald, L. Patsenker, J. Duschl et al., *Bioconjugate Chem.*, **1999**, *10*, 925.
- 83** B. Oswald, F. Lehmann, L. Simon et al., *Anal. Biochem.*, **2000**, *280*, 272.
- 84** H. Ali, J. E. van Lier, *Chem. Rev.*, **1999**, *99*, 2379.
- 85** N. B. McKeown, Phthalocyanine Synthesis, in *Phthalocyanine Materials: Synthesis, Structure and Function*, eds. B. Dunn, J. W. Goody, A. R. West, Cambridge University Press, Cambridge, 1998, p. 331.
- 86** N. Brasseur, T. L. Nguyen, R. Langlois et al., *J. Med. Chem.*, **1994**, *37*, 415.
- 87** N. Brasseur, R. Ouellet, K. Lewis et al., *Photochem. Photobiol.*, **1995**, *62*, 1058.
- 88** B. L. Wheeler, G. Nagasubramanian, A. J. Bard et al., *J. Am. Chem. Soc.*, **1984**, *106*, 7404.
- 89** W. E. Ford, M. A. J. Rodgers, L. A. Schechtman et al., *Inorg. Chem.*, **1992**, *31*, 3371.
- 90** F. Sanger, S. Nicklen, A. R. Coulson, *Proc. Natl. Acad. Sci. USA*, **1977**, *74*, 5463.
- 91** National Research Council USA, *Sequencing the Human Genome*, National Academy Press, Washington, DC, 1998.
- 92** US Department of Energy, Office of Energy Research, Office of Health and Environmental Research, *Human Genome 199192 Program Report*, DOE/ER0544P, US Government Printing Office, Washington, DC, 1998.
- 93** N. J. Dovichi, Capillary Gel Electrophoresis for Large Scale DNA Sequencing: Separation and Detection, in *Handbook of Capillary Electrophoresis*, ed. J. P. Landers, CRC press, Boca Raton, FL, 1997, p. 545.
- 94** K. Murray, *J. Mass Spectrom.*, **1996**, *31*, 1203.
- 95** H. Swerdlow, J. Z. Zhang, D. Y. Chen et al., *Anal. Chem.*, **1991**, *63*, 2835.
- 96** R. A. Mathies, X. C. Huang, *Nature*, **1992**, *359*, 167.
- 97** X. C. Huang, M. A. Quesada, R. A. Mathies, *Anal. Chem.*, **1992**, *64*, 2149.
- 98** P. C. Simpson D. Roach, A. T. Wooley et al. *Proc. Natl. Acad. Sci.*, **1998**, *95*, 2256.
- 99** H. R. Starke, J. Y. Yan, J. Z. Zhang et al., *Nucleic Acids Res.*, **1994**, *22*, 3997.
- 100** H. Lu, E. Arriaga, D. Y. Chen et al., *J. Chromatogr. A*, **1994**, *680*, 497.
- 101** M. L. Smith, J. Z. Sanders, R. J. Kaiser et al., *Nature*, **1986**, *321*, 674.

- 102** J. M. Prober, G. L. Trainor, R. J. Dam et al., *Science*, **1987**, *238*, 336.
- 103** W. Ansorge, B. S. Sproat, J. Stegemann et al., *J. Biochem. Biophys. Methods*, **1986**, *13*, 315.
- 104** S. Carson, A. S. Cohen, A. Belenkii et al., *Anal. Chem.*, **1993**, *65*, 3219.
- 105** L. M. Smith, *Nature*, **1991**, *349*, 812.
- 106** A. S. Cohen, D. R. Najarian, B. L. Karger, *J. Chromatogr.*, **1990**, *516*, 46.
- 107** A. E. Karger, J. J. Harris, R. F. Gesteland, *Nucleic Acids Res.*, **1991**, *19*, 4955.
- 108** H. Swerdlow, R. Gesteland, *Nucleic Acids Res.*, **1990**, *18*, 1415.
- 109** Y. Wang, J. Ju, B. A. Carpenter et al., *Anal. Chem.*, **1995**, *67*, 1197.
- 110** Y. Wang, J. M. Wallin, J. Ju et al., *Electrophoresis*, **1996**, *17*, 1485.
- 111** S. C. Hung, R. A. Mathies, A. N. Glazier, *Anal. Biochem.*, **1997**, *252*, 78.
- 112** S. C. Hung, J. Ju, R. A. Mathies et al., *Anal. Biochem.*, **1996**, *243*, 1527.
- 113** L. MiddendoRF, J. Amen, R. Bruce et al., Near-Infrared Fluorescence Instrumentation for DNA analysis, in *Near Infrared Dyes for High Technology Applications*, eds. S. Daehne, U. Resch-Genger, O.S. Wolfbeis, NATO ASI Series, Kluwer, Dordrecht, 1998, p. 141.
- 114** D. B. Shealy, M. Lipowska, J. Lipowski et al., *Anal. Chem.*, **1995**, *67*, 247.
- 115** D. C. Williams, S. A. Soper, *Anal. Chem.*, **1995**, *67*, 3427.
- 116** T. Imasaka, H. Nakagawa, T. Okazaki et al., *Anal. Chem.*, **1990**, *62*, 2404.
- 117** A. E. Boyer, M. Lipowska, J. Zen et al., *Anal. Lett.*, **1992**, *25*, 415.
- 118** R. J. Williams, N. Narayanan, G. A. Casey et al., *Anal. Chem.*, **1994**, *66*, 3102.
- 119** K. Sauda, T. Imasaka, N. Ishibashi, *Anal. Chem.*, **1986**, *58*, 2649.
- 120** K. Sauda, T. Imasaka, N. Ishibashi, *Anal. Chim. Acta*, **1986**, *187*, 353.
- 121** A. J. G. Mank, H. Lingeman, C. Gooyer, *Trends Anal. Chem.*, **1992**, *11*, 210.
- 122** R. J. Williams, M. Lipowska, G. Patonay et al., *Anal. Chem.*, **1993**, *65*, 601.
- 123** D. Andrews-WilberForce, G. Patonay, *Spectrochim. Acta, Part A*, **1990**, *46*, 1153.
- 124** T. Fuchigami, T. Imasaka, M. Shiga, *Anal. Chim. Acta*, **1993**, *282*, 209.
- 125** T. Higashijima, T. Fuchigami, T. Imasaka et al., *Anal. Chem.*, **1992**, *64*, 711.
- 126** J. H. Flanagan, B. L. Legendre, Jr., R. P. Hammer et al., *Anal. Chem.*, **1995**, *67*, 341.
- 127** S. McWhorter, S. A. Soper, *Electrophoresis*, **2000**, *21*, 1267.
- 128** S. P. McGlynn, T. Azumi, M. Kinoshita, *Molecular Spectroscopy of the Triplet State*, Prentice Hall, Englewood Cliffs, NJ 1969.
- 129** G. Kavarnos, G. Cole, P. Scribe et al., *J. Am. Chem. Soc.*, **1971**, *93*, 1032.
- 130** S. R. Davidson, R. Bonneau, J. Joussot-Dubien et al., *Chem. Phys. Lett.*, **1980**, *74*, 318.
- 131** S. A. Berson, R. S. Yalow, *J. Clin. Invest.*, **1959**, *38*, 1996.
- 132** V. C. W. Tsang, K. Hancock, M. Wilson, Enzyme-linked Immunotransfer Blot Technique for Human T-lymphotropic Virus Type III/Lymphadenopathy Associated Virus (HTLVIII/LAV) Antibodies, in *Immunology Series no. 15. Procedural Guide*, Centers for Disease Control, Atlanta, GA, 1986.
- 133** V. C. W. Tsang, J. A. Brand, A. E. Boyer, *J. Infect. Diseases*, **1989**, *159*, 50.
- 134** V. C. W. Tsang, K. Hancock, A. L. Beatty et al., *J. Immunol.*, **1984**, *132*, 2607.
- 135** K. Hancock, V. C. W. Tsang, *J. Immunol. Methods*, **1986**, *92*, 167.
- 136** A. R. Swamy, Ph.D. Thesis, Georgia State University, Atlanta, GA, 1999.
- 137** W.-C. Sun, K. R. Gee, D. H. Klaubert et al., *J. Org. Chem.*, **1997**, *62*, 6469.
- 138** J. Karolin et al., *J. Am. Chem. Soc.*, **1994**, *116*, 7801.
- 139** N. Panchuk-Voloshina, R. P. Haugland, J. Bishop-Stewart et al., *J. Histochem. Cytochem.*, **1999**, *47*, 1179–1188.
- 140** A. R. Swamy, J. C. Mason, H. Lee et al., Near-Infrared Absorption/Luminescence Measurements, in *Encyclopedia of Analytical Chemistry*, Wiley, London 2000.
- 141** M. J. Baars, G. Patonay, *Anal. Chem.*, **1999**, *71*, 667.
- 142** G. A. Casay, D. B. Sheally, G. Patonay, *Top. Fluoresc. Spectrosc.*, **1994**, *4*, 183.
- 143** N. Narayanan, G. Patonay, *J. Org. Chem.*, **1995**, *60*, 2391.

- 144** N. Narayanan, L. Strekowski, M. Lipowska et al., *J. Org. Chem.*, **1997**, *62*, 9387.
- 145** M. I. Danesvar, G. A. Casay, G. Patonay et al., *J. Fluoresc.*, **1996**, *6*, 69.
- 146** M. I. Danesvar, J. M. Peralta, G. A. Casay et al., *J. Immunol. Methods*, **1999**, *226*, 119.
- 147** I. Wengatz, F. Szurdoki, A. R. Swamy et al., *Proc. SPIE-Int. Soc. Opt. Eng.*, **1995**, *2388*, 408.
- 148** R. A. Vijayendran, D. E. Leckband., *Anal. Chem.*, **2001**, *73*, 471
- 149** C. A. Rowe, S. B. Scruggs, M. J. Feldstein et al., *Anal. Chem.*, **1999**, *71*, 433.
- 150** S. Pilevar, C. C. Davis, F. Protugal. *Anal. Chem.*, **1998**, *70*, 2031.
- 151** B. M. Cullum, T. Vo-Dinh, *TIBTECH*, **2000**, *18*, 388.
- 152** T. Ha, T. A. Laurence, D. S. Chemla et al., *J. Phys Chem. B*, **1999**, *103*, 6839.
- 153** J. N. Forkey, M. E. Quinlan, Y. E. Goldman. *Prog. Biophys. Mol. Biol.* **2000**, *74*, 1.
- 154** E. Terpertschnig, H. Szmacinski, J. R. Lakowicz, *Anal. Biochem.*, **1995**, *227*, 140.
- 155** E. Terpertschnig, H. Szmacinski, J. R. Lakowicz. *Methds Enzymol.*, **1997**, *278*, 295.
- 156** L. Ye, X. Chris Le, J. Z. Xing et al., *J. Chromatogr B*, **1998**, *714*, 59.
- 157** K. Pettersson, H. Siitari, I. Hemmilä et al., *Clin. Chem.*, **1983**, *29*, 60.
- 158** I. Hemmilä, Time-resolved Fluorometry: Advantages and Potentials, in *High Throughput Screening*, ed. J. P. Devlin, Marcel Dekker, New York 1997.
- 159** I. Hemmilä, V.-M. Mukkala, H. Takalo. *J. Alloys Compd.*, **1997**, *249*, 158.
- 160** H. Karsilayan, I. Hemmilä, H. Takalo et al., *Bioconjugate Chem.*, **1997**, *8*, 71.
- 161** J. Yuan, G. Wang, H. Kimura et al., *Anal. Biochem.*, **1997**, *154*, 283.
- 162** J. Yuan, K. Matsumoto, H. Kimura. *Anal. Chem.*, **1998**, *70*, 596
- 163** E. Zuber, L. Rosso, B. Darbouret et al., *J. Immunoassay*, **1997**, *18*, 21.
- 164** T. Lövgren, P. Heinonen, P. Lehtinen et al., *Clin. Chem.*, **1997**, *43*, 1937.
- 165** W.-B. Chang, B.-L. Zhang, Y.-Z. Li et al., *Microchem. J.*, **1997**, *55*, 287.
- 166** Q. Qin, M. Christiansen, T. Lövgren et al., *Immunol. Methods*, **1997**, *205*, 169.
- 167** L. Stryer, R. P. Haugland, *Proc. Natl. Acad. Sci. USA*, **1967**, *58*, 719.
- 168** E. F. Ullman, M. Schwartzberg, K. E. Rubenstein, *J. Biol. Chem.*, **1976**, *251*, 4172.
- 169** A.-P. Wei, J. N. Herron, D. A. Christensen, *ACS Symp. Ser.*, **1992**, *511*, 105.
- 170** J. M. Brinkley and R. P. Haugland, US Pat., *5 326 692*, 1994.
- 171** V.T. Oi, A.N. Glazer, L. Stryer. *J. Cell Biol.*, **1982**, *93*, 981.
- 172** R. MacColl, *J. Fluoresc.*, **1991**, *1*, 135.
- 173** G. Sohn, C. Sautter, *J. Histochem. Cytochem.*, **1991**, *39*, 921.
- 174** N. Nakamura, T. Matsunaga, *Anal Lett.*, **1991**, *24*, 1075.
- 175** N. Baumgarth, M. Roederer, *J. Immunol. Methods*, **2000**, *243*, 77–97.
- 176** *Green Fluorescent Proteins*, eds. K. F. Sullivan and S. A. Kay, Academic Press, New York 1999.
- 177** M. V. Matz, A. F. Fradkov, Y. A. Labas et al., *Nature Biotechnol.*, **1999**, *17*, 969.
- 178** D. Yarbrough, R. M. Wachter, K. Kallio et al., *Proc. Natl. Acad. Sci. USA*, **2001**, *98*, 462.
- 179** L. A. Gross, G. S. Baird, R. C. Hoffman et al., *Proc. Natl. Acad. Sci. USA*, **2000**, *97*, 11990.
- 180** C. Xu, W. Zipfel, J. B. Shear, R. M. Williams et al., *Proc. Natl. Acad. Sci. USA*, **1996**, *93*(20), 10763–10768.
- 181** J. B. Shear, *Anal. Chem.*, **1999**, *71*, 598A.
- 182** A. A. Rehms, P. R. Callis, *Chem. Phys. Lett.*, **1993**, *208*, 276.
- 183** B. Kierdaszuk, I. Gryczynski, A. Modrak-Wojcik et al., *Photochem. Photobiol.*, **1995**, *61*, 319.
- 184** S. Maiti, J. B. Shear, R. M. Williams et al., *Science*, **1997**, *275*, 530.
- 185** M. L. Gostkowski, J. B. McDoniel et al., *J. Am. Chem. Soc.*, **1998**, *120*, 18.
- 186** C. Xu, W. W. Webb, *J. Opt. Chem. Am. B*, **1996**, *13*, 481.
- 187** M. Albotă, D. Beljonne, J.-L. Bredas et al., *Science*, **1998**, *281*, 1653.
- 188** P. E. Hänninen, A. Soini, N. J. Meltola et al., *Nature Biotechnol.*, **2000**, *18*, 548.
- 189** J. M. Song, T. Inoue, H. Kawazumi et al., *J. Chromatogr. A*, **1997**, *765*, 315.
- 190** S. Maiti, J. B. Shear, W. W. Webb, *Bioophys. J.*, **1996**, *70*, A210.

- 191** D. Kleinfeld, P. P. Mitra, F. Helmchen et al., *Proc. Natl. Acad. Sci. USA*, **1998**, 95, 15741.
- 192** G. A. Baker, S. Pandey, F. V. Bright, *Anal. Chem.*, **2000**, 72, 5748.
- 193** M. A. DeLuca (ed.) *Methods Enzymol.*, **1978**, 57.
- 194** L. J. Kricka, *Anal. Chem.* **1999**, 71, 293R.
- 195** *Bioluminescence and Chemiluminescence: Molecular Reporting with Photons*, eds. W. Hastings, L. J. Kricka, P. E. Stanley, Wiley, Chichester 1997.
- 196** A. W. Knight, G. M. Greenway, *Analyst*, **1994**, 119, 879.
- 197** A. W. Knight, *Trends Anal. Chem.*, **1999**, 18, 47.
- 198** W. R. Seitz, in ref. 193, Ch. 38, p. 445.
- 199** H.-S. Zhuang, Q.-E. Wang, F. Zhang et al., *Chin. J. Chem.*, **1997**, 15, 123–129.
- 200** H. Yoshida, K. Todoroki, K. Zaitsu et al. *Daigaku Chuo Bunseki Senta Hokoku*, **1996**, 14, 20–26; *Chem. Abstr.*, **1997**, 126, 327211.
- 201** O. Suzuki, G. Masuda, N. Shiohata et al., *Eur. Pat.*, 812823, 1997; *Chem. Abs.*, **1998**, 128, 72655.
- 202** U. Piran, J. J. Quinn, *PCT Int. Appl.*, WO 9834109, 1998; *Chem. Abs.*, **1998**, 129, 158856.
- 203** H. Akhavan-Tafti, Z. Arghavani, R. Desilva, *PCT Int. Appl.*, WO 9726245, 1997; *Chem. Abs.*, **1997**, 127, 176354.
- 204** M. Matsumoto, N. Watanabe, H. Kobayashi et al., *Jpn. Pat.*, 09157271, 1997; *Chem. Abs.*, **1997**, 127, 50626.
- 205** I. Bronstein, B. Edwards, A. Sparks et al., *PCT Int. Appl.*, WO 9714954, 1997; *Chem. Abs.*, **1997**, 127, 25442.
- 206** C. A. Marquette, L. J. Blum, *Talanta*, **2000**, 51, 395.
- 207** P. Luppa, C. Bruckner, I. Schwab et al., *Clin. Chem.*, **1997**, 43, 2345.
- 208** R. John, R. Henley, N. Oversby, *Ann. Clin. Biochem.*, **1997**, 34, 396.
- 209** M. Verhaegen, T. K. Christopoulos, *Anal. Chem.*, **1998**, 70, 4120.
- 210** I. Alexandre, N. Zammattéo, P. Moris et al., *J. Virol. Methods*, **1997**, 66, 113.
- 211** M. Ronaghi, M. Uhlen, P. Nyren, *Science*, **1998**, 281, 363.
- 212** D. Crocian, R. Olinescu, G. R. Turcu, *Rom. J. Biophys.*, **1997**, 7, 87.
- 213** K. Erler, *Wien. Klin. Wochenschr.*, **1998**, 110(Suppl. 3), 5–10.
- 214** M. T. Korpela, J. S. Kurittu, J. T. Karvinen et al., *Anal. Chem.*, **1998**, 70, 4457.
- 215** I. Murray, I. A. Cowe, *Making Light Work: Advances in Near Infrared Spectroscopy*, Wiley-VCH, Weinheim 1992.
- 216** *Near-Infrared Applications in Biotechnology (Practical Spectroscopy Vol. 25)*, ed. R. Raghavachari, Marcel Dekker, New York 2000.
- 217** S. Sasic, Y. Ozaki, *Anal. Chem.*, **2001**, 73, 64.
- 218** C. Fischbacher, K. U. Jagemann, K. Danzer et al., *Fresenius' J. Anal. Chem.*, **1997**, 359, 78.
- 219** H. J. Kim, Y. A. Woo, S. H. Chang et al., *Anal. Sci. Technol.*, **1998**, 11, 47.
- 220** M. A. Arnold, J. J. Burmeister, G. W. Small, *Anal. Chem.*, **1998**, 70, 1773.
- 221** G. Gauglitz, *Sens. Update*, **1996**, 1, 1.
- 222** D. R. Thévenot, K. Toth, R. A. Durst et al., *Pure Appl. Chem.*, **1999**, 71, 2333–2348.
- 223** F. W. Scheller, U. Wollenberger, A. Warsinke et al., *Curr. Opin. Biotechnol.*, **2001**, 12, 35.
- 224** J.-M. Lehn, *Supramolecular Chemistry*, VCH, Weinheim 1995.
- 225** R. Forster, D. Diamond, *Anal. Chem.*, **1992**, 64, 1721.
- 226** F. P. Schmidtchen, M. Berger, *Chem. Rev.*, **1997**, 97, 1609.
- 227** S. O'Neill, S. Conway, J. Twellmeyer et al., *Anal. Chim. Acta*, **1999**, 398, 1.
- 228** E. Wang, L. Zhu, L. Ma et al., *Anal. Chim. Acta*, **1997**, 357, 85.
- 229** H. Hisamoto, N. Miyashita, K. Watanabe et al., *Sens. Actuators B*, **1995**, 29, 378.
- 230** K. Suzuki, H. Ohzora, K. Tohda et al., *Anal. Chim. Acta*, **1990**, 237, 155.
- 231** O. S. Wolfbeis, *Sens. Actuators B*, **1995**, 29, 140.
- 232** G. J. Mohr, I. Murkovic, F. Lehmannet al., *Sens. Actuators B*, **1997**, 39, 239.
- 233** Y. Kawabata, T. Yamashiro, Y. Kitazaki et al., *Sens. Actuators B*, **1995**, 29, 135.
- 234** G. J. Mohr, O. S. Wolfbeis, *Anal. Chim. Acta*, **1995**, 316, 239.
- 235** A. W. Czarnik (ed.), *ACS Symp. Ser.*, **1993**, 538.
- 236** E. Chapoteau, B. P. Czech, W. Zazulak et al., *Clin. Chem.*, **1992**, 38, 1654.
- 237** K. R. A. L. Sandanayake, I. O. Sutherland, *Tetrahedron Lett.*, **1993**, 34, 3165.

- 238** K. Kimura, T. Yamashita, M. Yokoyama, *J. Chem. Soc., Perkin Trans.*, **1992**, *92*, 613.
- 239** F. Fages, J.-P. Desvergne, K. Kampke et al., *J. Am. Chem. Soc.*, **1993**, *115*, 3658.
- 240** J. Bourson, J. Pouget, B. Valeur, *J. Phys. Chem.*, **1993**, *87*, 4552.
- 241** D. Diamond, K. Nolan, *Anal. Chem.*, **2001**, *73*, 22A.
- 242** K. Iwamoto, K. Araki, H. Fujishima et al., *J. Chem. Soc., Perkin Trans. 1*, **1992**, *92*, 1885.
- 243** S. J. Harris, G. Barrett, M. A. McKervey et al., *J. Chem. Soc., Chem. Commun.*, **1992**, *92*, 1287.
- 244** P. A. Gale, Z. Chen, M. G. B. Drew et al., *Polyhedron* **1998**, *17*, 405.
- 245** K. Odashima, K. Yagi, K. Tohda et al., *Bioorg. Med. Chem. Lett.*, **1999**, *9*, 2375.
- 246** T. Grady, S. J. Harris, M. R. Smyth et al., *Anal. Chem.*, **1996**, *68*, 3775.
- 247** I. Aoki, T. Sakaki, S. Tsutsui et al., *Tetrahedron Lett.*, **1992**, *33*, 89.
- 248** B. Kukrer, E. U. Akkaya, *Tetrahedron Lett.*, **1999**, *40*, 9125.
- 249** G. Dilek, E. U. Akkaya, *Tetrahedron Lett.*, **2000**, *41*, 3721.
- 250** E. U. Akkaya, S. Turkyilmaz, *Tetrahedron Lett.*, **1997**, *38*, 4513.
- 251** G. Wulff, *Angew. Chem. Int. Ed. Engl.*, **1995**, *34*, 1812–1832.
- 252** J.-M. Kim, K.-D. Ahn, G. Wulff, *Macromol. Chem. Phys.*, **2001**, *2105*–1108.
- 253** O. S. Wolfbeis, E. Terpetschnig, S. Pilletsy et al., in *Applied Fluorescence in Chemistry, Biology and Medicine*, ed. W. Rettig, Springer Verlag, Heidelberg 1999, 277–295
- 254** P. Turkewitsch, B. Wandelt, G. D. Darling et al., *Anal. Chem.*, **1998**, *70*, 2025–2030.
- 255** D. L. Rathbone, D. Su, Y. Wang et al., *Tetrahedron Lett.*, **2000**, *41*, 123–126.
- 256** E. Hecht, *Optics*, 3rd edition, Addison Wesley, London 1997.
- 257** T. Vo-Dinh, L. Allain, in *Biomedical Photonics*, ad. T. Va-Dinh, CRC Press, Boca Raton, **2003**, 20-1–20-40.
- 258** C. Fattinger, H. Koller, D. Schlatter et al., *Biosens. Bioelectron.*, **1993**, *8*, 99.
- 259** W. Huber, R. Barner, C. Fattinger et al., *Sens. Actuator, B.*, **1992**, *6*, 122.
- 260** C. Stamm, W. Lukosz, *Sens. Actuator, B*, **1993**, *11*, 177.
- 261** C. Stamm, W. Lukosz, *Sens. Actuator, B*, **1994**, *18*, 183.
- 262** D. Schlatter, R. Barner, C. Fattinger et al., *Biosens. Bioelectron.*, **1993**, *8*, 109.
- 263** D. Clerc, W. Lukosz, *Sens. Actuator, B*, **1994**, *19*, 581.
- 264** J. Dubendorfer, R.E. Kunz, *Appl. Opt.*, **1998**, *37*, 1890.
- 265** R. Cush, J.M. Cronin, W.J. Stewart et al., *Biosens. Bioelectron.*, **1993**, *8*, 347
- 266** N. J. Goddard, D. Pollard-Knight, C.H. Maule, *Analyst*, **1994**, *119*, 583
- 267** P.E. Buckle, R.J. Davies, T. Kinning et al., *Biosens. Bioelectron.*, **1993**, *8*, 355.
- 268** H.J. Watts, C.R. Lowe, D.V. Pollard-Knight, *Anal. Chem.*, **1994**, *66*, 2465
- 269** E. Kretschmann, H. Raether, *Z. Naturforsch. A*, **1968**, *23*, 2135
- 270** A. Otto, *Z. Phys.*, **1968**, *216*, 398.
- 271** B. Liedberg, C. Nylander, I. Lundström, *Sens. Actuators*, **1993**, *4*, 299.
- 272** A. Szabo, L. Stoltz, R. Granzow, *Curr. Opin. Struct. Biol.*, **1995**, *5*, 699.
- 273** M. Raghavan, P. J. Björkman, *Structure*, **1995**, *3*, 331.
- 274** P. A. van der Merwe, A. N. Barclay, *Curr. Opin. Immunol.*, **1996**, *8*, 257.
- 275** D. G. Myszka, *Curr. Opin. Biotechnol.*, **1997**, *8*, 50.
- 276** P. Schuck, *Annu. Rev. Biophys. Biomol. Struct.*, **1997**, *26*, 541.
- 277** M. Fivash, E. M. Towler, R. J. Fisher, *Curr. Opin. Biotechnol.*, **1998**, *9*, 97.
- 278** S. Boussaad, J. Pean, N. J. Tao, *J. Anal. Chem.*, **2000**, *72*, 222.
- 279** H. Sota, Y. Hasegawa, *Anal. Chem.*, **1998**, *70*, 2019.
- 280** E. Kai, S. Sawata, K. Ikebukuro et al., *Anal. Chem.*, **1999**, *71*, 796–800.
- 281** D. G. Myszka, X. He, M. Dembo et al., *Biophys. J.*, **1998**, *75*, 583.
- 282** <http://www.biacore.com/customer/references.phtml>
- 283** G.A. Baxter, J.P. Ferguson, M.C. O'Connor et al., *J. Agric. Food Chem.*, **2001**, *49*, 3204.
- 284** F.E. Carrick, B.E. Forbes, J.C. Wallace, *J. Biol. Chem.*, **2001**, *276*, 27120
- 285** T. Flatmark, A.J. Stokka, S.V. Berge, *Anal. Biochem.*, **2001**, *294*, 95
- 286** P. Gomes, E. Giralt, D. Andreu, *Mol. Immunol.*, **2000**, *37*, 975
- 287** W. Haasnoot, R. Verheijen, *Food Agric. Immunol.*, **2001**, *13*, 131.

- 288** V. Gaudin, J. Fontaine, P. Maris, *Anal. Chim. Acta*, **2001**, *436*, 191.
- 289** P.O. Markgren, M.T. Lindgren, K. Gertow et al., *Anal. Biochem.*, **2001**, *291*, 207.
- 290** M.O. Roy, M. Pugniere, M. Jullien et al., *J. Mol. Recognit.*, **2001**, *14*, 72.
- 291** R. P. H. Kooyman, A. T. M. Lenferink et al., *Anal. Chem.*, **1991**, *63*, 83.
- 292** <http://www.ibis-spr.nl/homeframe.htm>
- 293** <http://www.ti.com/spreeta>
- 294** J. Méléndez, R. Carr, D. Bartholew et al., *Sens. Actuators, B*, **1997**, *38(1-3)*, 375.
- 295** J.L. Elkind, D.I. Stimpson, A. A. Strong et al., *Sens. Actuators, B*, **1999**, *54*, 182.
- 296** A.M. Sesay, D.C. Cullen, *Environ. Monitoring Assess.*, **2001**, *70*, 83.
- 297** R. Slavik, J. Homola, J. Ctyroky et al., *Sens. Actuators, B*, **2001**, *74(1-3)*, 106.
- 298** R.D. Harris, J.S. Wilkinson, *Sens. Actuators, B*, **1995**, *29(1-3)*, 261.
- 299** A. Brecht, G. Gauglitz, *Anal. Chim. Acta*, **1997**, *347(1-2)*, 219.
- 300** J. Homola, S. S. Yee, G. Gauglitz, *Sens. Actuators, B*, **1999**, *54*, 3.
- 301** J. Homola, I. Koudela, S. S. Yee, *Sens. Actuators, B*, **1999**, *54*, 16.
- 302** J. O. Lekkala, J. W. Sadowski, Surface Plasmon Immunosensors, in *Chemical Sensor Technology*, ed. M. Aizawa, Kodansha Ltd, Tokyo 1994, Vol. 5, p. 199.
- 303** I. Vikholm, T. Viitala, W. M. Albers et al., *Biochim. Biophys. Acta*, **1999**, *1421*, 39.
- 304** M. J. Eddowes, *Biosensors*, **1987/1988**, *3*, 1.
- 305** T. A. Morton, D. G. Myszka, *Methods Enzymol.*, **1998**, *295*, 268.
- 306** Kubritchko, J. Spinke, T. Bruckner et al., *Anal. Biochem.*, **1997**, *253*, 112.
- 307** D. G. Myszka, *J. Mol. Recognit.*, **2000**, *12*, 390.
- 308** J. E. Pearson, J. W. Kane, I. Petrak-Kalloti et al., *J. Immunol. Methods*, **1998**, *221*, 87.
- 309** D. G. Myszka, *J. Mol. Recognit.*, **1999**, *12*, 279.
- 310** C. Williams, T. A. Addona, *TIBTECH*, **2000**, *18*, 45.
- 311** A. Badia, S. Arnold, V. Scheumann et al., *Sens. Actuators, B*, **1999**, *54*, 145.
- 312** W. M. Albers, I. Vikholm, T. Viitala et al., in *Handbook of Surfaces and Interfaces of Materials*, ed. H. S. Nalwa Academic Press, New York 2001, Vol. 5, Ch. 1.
- 313** C. F. Mandenius, K. Mosbach, *Anal. Biochem.*, **1988**, *170*, 68.
- 314** L. A. Lyon, M. D. Musick, M. J. Natan, *Anal. Chem.*, **1998**, *70*, 5177.
- 315** G. Gauglitz, W. Nahm, *Fresenius' J. Anal. Chem.*, **1991**, *341*, 279.
- 316** A. Brecht, G. Gauglitz, *Fresenius' J. Anal. Chem.*, **1994**, *349*, 360.
- 317** A. Brecht, J. Piehler, G. Lang et al., *Anal. Chim. Acta*, **1995**, *311(3)*, 289–299.
- 318** J. Piehler, A. Brecht, G. Gauglitz et al., *Anal. Biochem.*, **1997**, *249*, 94.
- 319** D. A. Weitz, S. Garoff, J. I. Gersten et al., *J. Electron Spectrosc. Relat. Phenom.*, **1983**, *29*, 363.
- 320** S. A. Maskevich, G. A. Gachko, A. A. Maskevich et al., *Proc. SPIE-Int. Soc. Opt. Eng.*, **1995**, *2370*, 131.
- 321** F. R. Aussenegg, A. Leitner, M. E. Lippitsch, *Rev. Roum. Phys.*, **1988**, *33*, 349.
- 322** T. Schalkhammer, F. R. Aussenegg, A. Leitner et al., *Proc. SPIE-Int. Soc. Opt. Eng.*, **1997**, *2976*, 129.
- 323** G. Steiner, C. Kuhne, B. Leupolt et al., *Proc. SPIE-Int. Soc. Opt. Eng.*, **1998**, *3256*, 106.
- 324** B. C. Smith, *Fundamentals of Fourier Infrared Spectroscopy*, CRC Press, Boca Raton 1996.
- 325** M. L. McKelvy, T. R. Britt, B. L. Davis et al., *Anal. Chem.*, **1998**, *70*, 119R.
- 326** L. M. Ng, R. Simmons, *Anal. Chem.*, **1999**, *71*, 343R.
- 327** L.-J. Jiang, W.-Y. Sun, M.-H. Shu et al., *Spectrosc. Lett.*, **1998**, *31*, 347.
- 328** H. R. Constantino, J. D. Andya, S. J. Shire et al., *Pharm. Sci.*, **1997**, *3*, 121.
- 329** A. Stevens, D. Michael, T. J. Schleich, *Mol. Biol. Biophys.*, **1998**, *1*, 221.
- 330** A. A. Tulub, *Biofizika*, **1997**, *42*, 1208
- 331** M. Trinquier-Dinet, M.-T. Boisdon, J. Perie et al., *Spectrochim. Acta, Part A*, **1998**, *54*, 367.

- 332** Y.-Y. Sun., Y.-C. Liu., M.-H. Ma et al., *Gaojing Xuexiao Huaxue Xuebao*, **1998**, 19, 135.
- 333** B. Caughey, G. J. Raymond, R. A. Bessen., *J. Biol. Chem.*, **1998**, 273, 32230.
- 334** H. Zhang, Y. Ishikawa, Y. Yamamoto et al., *FEBS Lett.*, **1998**, 426, 347.
- 335** N. B From, B. E. Bowler, *Biochemistry*, **1998**, 37, 1623.
- 336** E. Vass, E. Lang, J. Samu et al., *J. Mol. Struct.*, **1998**, 440, 59.
- 337** K. Taga, M. G. Sowa, J. Wang et al., *Vib. Spectrosc.*, **1997**, 14, 143.
- 338** D. K.Graff, B. Pastrana-Rios, S. Y. Venyaminov et al., *J. Am. Chem. Soc.*, **1997**, 119, 11282.
- 339** J. F. Carpenter, S. J. Prestrelski, A. Dong, *Eur. J. Pharm. Biopharm.*, **1998**, 45, 231.
- 340** R. A.Shaw, G. W. Buchko, G. Wang et al., *Biochemistry*, **1997**, 36, 14531.
- 341** W. C.Wigley, S. Vijayakumar, J. D. Jones et al., *Biochemistry*, **1998**, 37, 844.
- 342** J. Corbin, N. Méthot, H. H. Wang et al., *J. Biol. Chem.*, **1998**, 273, 771.
- 343** S. Nishimura, H. Kandori, A. Maeda, *Biochemistry*, **1998**, 37, 15816.
- 344** S. Kim, B. A. Barry, *Biophys. J.*, **1998**, 74, 2588.
- 345** F. Tanfani, G. Lapathitis, E. Bertoli et al., *Biochim. Biophys. Acta*, **1998**, 1369, 109.
- 346** J. De Las Rivas, J. Barber, *Biochemistry*, **1997**, 36, 8897.
- 347** H. Shi, L. Xiong, K.-Y. Yang et al. *J. Mol. Struct.*, **1998**, 446, 137.
- 348** H. Kandori, N. Kinoshita, Y. Shichida, *J. Phys. Chem. B*, **1998**, 102, 7899.
- 349** J.-J. Wang, C.-W. Chi, S.-Y. Lin et al., *Anticancer Res.*, **1997**, 17, 3473.
- 350** Q. Zhou, S. Sun, S.Zhang et al., *Guangpuxue Yu Guangpu Fenxi*, **1998**, 18, 162.
- 351** A. Menikh, M. T. Salch, J. Gariépy et al., *Biochemistry*, **1997**, 36, 15865.
- 352** H. Kandori, *J. Am. Chem. Soc.*, **1998**, 120, 4546.
- 353** J. Le Coutre, H. R. Kaback, C. K. N. Patel et al., *Proc. Natl. Acad. Sci. USA*, **1998**, 95, 6114.
- 354** M. K. Bahng, N. J. Cho, J. S. Park et al., *Langmuir*, **1998**, 14, 463.
- 355** H. S. Kim, J. D. Hartgerink, M. R. Ghadiri, *J. Am. Chem. Soc.*, **1998**, 120, 4417.
- 356** P. Tengvall, I. Lundstrom, B. Liedberg, *Biomaterials*, **1998**, 19, 407.
- 357** K. Oberg, A. L. Fink, *Anal. Biochem.*, **1998**, 256, 92.
- 358** J. Buijs, W. Norde, J. W. Th. Lichtenbelt, *Langmuir*, **1996**, 12, 1605.
- 359** S. Ge, K. Kojio, A. Takahara et al., *J. Biomater. Sci. Polym. Ed.*, **1998**, 9, 131.
- 360** M. Lestelius, B. Liedberg, P. Tengvall, *Langmuir*, **1997**, 13, 5900.
- 361** Y. Gotshal, R. Simhi, B.-A. Sela et al., *Sens. Actuators, B*, **1997**, 42, 157.
- 362** S. M. Levine, D. L. Wetzel, *Free Radical Biol. Med.*, **1998**, 25, 33.
- 363** D. L. Wetzel, D. N. Slatkin, S. M. Levine, *Cell. Mol. Biol.*, **1998**, 44, 15.
- 364** Y. Yoshimura, *Kagaku to Kogyo*, **1997**, 71, 548.
- 365** L. A. Lyon, C. D. Keating, A. P. Fox, A. P. et al., *Anal. Chem.*, **1998**, 70, 341R.
- 366** G. Xue, *Prog. Polym. Sci.*, **1997**, 22, 313.
- 367** R. Callender, H. Deng, R. Gilmanshin, *J. Raman Spectrosc.*, **1998**, 29, 15.
- 368** S. A.Overman, G. J. Thomas, *J. Raman Spectrosc.*, **1998**, 29, 23.
- 369** S. Fendel, B. Schrader, *Fresenius' J. Anal. Chem.*, **1998**, 360, 609.
- 370** N. Okishio, R. Fukuda, M. Nagai et al., *J. Raman Spectrosc.*, **1998**, 29, 31.
- 371** S. Hashimoto, M. Sasaki, H. Takeuchi, *J. Am. Chem. Soc.*, **1998**, 120, 443.
- 372** T. Miura, T. Satoh, A. Hori-I, et al., *J. Raman Spectrosc.*, **1998**, 29, 41.
- 373** M. Unno, J. F. Christian, J. S. Olson et al., *J. Am. Chem. Soc.*, **1998**, 120, 2670.
- 374** X. Zhao, D. Wang, T. G. Spiro, *J. Am. Chem. Soc.*, **1998**, 120, 8517.
- 375** X. Zhao, D. Wang, T. G. Spiro, *Inorg. Chem.*, **1998**, 37, 5414.
- 376** T. Miura, T. Satoh, A. Hori-I et al., *J. Raman Spectrosc.*, **1998**, 29, 41.
- 377** J.-S. Wang., *Huaxue*, **1997**, 55, 65.
- 378** M. Fleischmann, P. J. Hendra, A. J. McQuilan, *Chem. Phys Lett.*, **1974**, 26, 163.
- 379** D. J. Jeanmaire and R. P. Van Duyne, *J. Electronanal. Chem.*, **1977**, 84.1
- 380** T. M. Herne, A. M. Ahern, R. A. Garrett, *J. Am. Chem. Soc.*, **1991**, 113, 846.

- 381** E. Y. Kryukov, A. V. Feofanov, A. A. Moskalenko et al., *Asian J. Spectrosc.*, **1997**, *1*, 65.
- 382** S. Lecomte, H. Wackerbarth, P. Hildebrandt et al., *J. Raman Spectrosc.*, **1998**, *29*, 687.
- 383** M. Jang, I. Cho, P. Callahan, *J. Biochem. Mol. Biol.*, **1997**, *30*, 352.
- 384** T. Vo-Dinh, L. Allain, D. L. Stokes, *J. Raman Spectrosc.*, **2002**, *33*, 511.
- 385** K. Kneipp, H. Kneipp, G. Deinum et al., *Appl. Spectrosc.*, **1998**, *52*, 175.
- 386** V. Decker, D. Zeisel, R. Zenobi et al., *Anal. Chem.*, **1998**, *70*, 2646.
- 387** Z. Q. Tian, J. S. Gao, X. Q. Li et al., *J. Raman Spectrosc.*, **1998**, *29*, 703.
- 388** M. J. Weaver, S. Zou, H. Y. H. Chan, *Anal. Chem.*, **2000**, *72*, 38A.
- 389** G. Niaura, A. K. Gaigalast, V. L. Vilker, *J. Raman Spectrosc.*, **1997**, *28*, 1009.
- 390** E. Zubritsky, *Anal. Chem.*, **1999**, *71*, 545A.
- 391** Y.-W. Yang, C.-C. Teng, *Int. J. Biol. Macromol.*, **1998**, *22*, 81.
- 392** D. N. Georgieva, S. Stoeva, S.A. Ali et al., *Spectrochim. Acta, Part A*, **1998**, *54*, 765
- 393** S. Padmanabhan, M. A. Jiménez, D. V. Laurents et al., *Biochemistry*, **1998**, *37*, 17318.
- 394** S. E. Blondelle, B. Forood, R. A. Houghten et al., *Biochemistry*, **1997**, *36*, 8393.
- 395** M. M. Juban, M. M. Javadpour, M. D. Barkley, *Methods Mol. Biol.*, **1997**, *78*, 73.
- 396** S. M. Kelly, N. C. Price, *Biochim. Biophys. Acta*, **1997**, *1338*, 161.
- 397** H. Hermel, in *Particle Surface Characterization Methods*, eds. R. H. Mueller, W. Mehnert, G. E. Hildebrand, Medpharm Scientific Publishers, Stuttgart 1997, p. 159.
- 398** L. A. Nafie, T. A. Keiderling, P. J. Stephens, *J. Am. Chem. Soc.*, **1976**, *98*(10), 2715.
- 399** P. K. Bose, P. L. Polavarapu, *J. Am. Chem. Soc.*, **1999**, *121*, 6094.
- 400** G. M. Clore, A. M. Gronenborn, *Curr. Opin. Chem. Biol.*, **1998**, *2*(5), 564.
- 401** A. E. Ferentz, G. Wagner, *Q. Rev. Biophys.*, **2000**, *33*(1), 29.
- 402** K. H. Gardner, L. E. Kay, *Annu. Rev. Biophys. Biomol. Struct.*, **1998**, *27*, 357.
- 403** L. E. Kay, *Biochem Cell Biol.*, **1998**, *76*(2-3), 145.
- 404** K. Pervushin, *Q. Rev. Biophys.*, **2000**, *33*(2), 161.
- 405** J. H. Prestegard, H. M. al-Hashimi, J. R. Tolman, *Q. Rev. Biophys.*, **2000**, *33*, 371.
- 406** G. Wider, *Biotechniques*, **2000**, *29*, 1278 and 1292.
- 407** J. Cavanagh, W. J. Fairbrother, A. G. Palmer et al., *Protein NMR Spectroscopy: Principles and Practice*, Academic Press, New York 1996.
- 408** F. J. M. Van de Ven, *Multidimensional NMR in Liquids: Basic Principles and Experimental Methods*, VCH, Weinheim 1995.
- 409** N. Tjandra, A. Bax, *Science*, **1997**, *278*, 1111.
- 410** K. Pervushin, R. Riek, G. Wider, K. Wüthrich *Proc. Natl. Acad. Sci. USA*, **1997**, *94*, 12366.
- 411** S. Bagby, K. I. Tong, M. Ikura, *Methods Enzymol.*, **2001**, *339*, 20.
- 412** P. Zhou, A. A. Lugovskoy, G. Wagner, *J. Biomol. NMR*, **2001**, *20*, 11.
- 413** S. Bagby, K. I. Tong, D. Liu et al., *J. Biomol. NMR*, **1997**, *10*, 279.
- 414** T. Yamazaki, T. Otomo, N. Oda et al., *J. Am. Chem. Soc.*, **1998**, *120*, 5591.
- 415** T. Otomo, N. Ito, Y. Kyogoku et al., *Biochemistry*, **1999**, *38*, 16040.
- 416** D. M. LeMaster, F. M. Richards, *Biochemistry*, **1988**, *27*, 142.
- 417** D. A. Torchia, S. W. Sparks, A. Bax, *J. Am. Chem. Soc.*, **1988**, *110*, 2320.
- 418** M. Sattler, S. W. Fesik, *Structure*, **1996**, *4*, 245.
- 419** L. E. Kay, K. H. Gardner, *Curr. Opin. Struct. Biol.*, **1997**, *7*, 722.
- 420** N. K. Goto, K. H. Gardner, G. A. Mueller et al., *J. Biomol. NMR*, **1999**, *13*, 369.
- 421** A. Bax, G. Kontaxis, N. Tjandra, *Methods Enzymol.*, **2001**, *339*, 127.
- 422** H. Schwalbe, T. Carluomagno, M. Henning, *Methods Enzymol.*, **2001**, *338*, 35.
- 423** J. L. Battiste, G. Wagner, *Biochemistry*, **2000**, *39*, 5355.
- 424** H. Denton, M. Smith, H. Husi et al., *Protein Expr. Purif.*, **1998**, *14*, 97.
- 425** D. P. Zimmer, D. M. Crothers, *Proc. Natl. Acad. Sci. USA*, **1995**, *92*, 3091.

- 426** R. T. Batey, N. Cloutier, H. Mao, *Nucleic Acids Res.*, **1996**, *24*, 4836.
- 427** E. P. Nikonowicz, *Methods Enzymol.*, **2001**, *338*, 320.
- 428** M. H. Werner, V. Gupta, L. J. Lambert et al., *Methods Enzymol.*, **2001**, *338*, 283.
- 429** M. Salzmann, K. Pervushin, G. Wider et al., *Proc. Natl. Acad. Sci. USA*, **1998**, *95*, 13585.
- 430** N. Tjandra, S. Grzesiek, A. Bax, *J. Am. Chem. Soc.*, **1996**, *118*, 6264.
- 431** J. R. Tolman, J. M. Flanagan, M. A. Kennedy et al., *Proc. Natl. Acad. Sci. USA*, **1995**, *92*, 9279.
- 432** M. Zweckstetter, A. Bax, *J. Am. Chem. Soc.*, **2000**, *122*, 3791.
- 433** J. A. Losonczi, M. Andrec, M. W. Fischer MW et al., *J. Magn. Reson.*, **1999**, *138*, 334.
- 434** C. R. Sanders, J. H. Prestegard, *Bioophys. J.*, **1990**, *58*, 447.
- 435** A. Bax, N. Tjandra, *J. Biomol. NMR*, **1997**, *10*, 289–92.
- 436** M. Rückert, G. Otting, *J. Am. Chem. Soc.*, **2000**, *122*, 7793.
- 437** L. G. Barrientos, C. Dolan, A. M. Gronenborn, *J. Biomol. NMR*, **2000**, *16*, 329.
- 438** M. R. Hansen, L. Mueller, A. Pardi, *Nat. Struct. Biol.*, **1998**, *5*, 1065.
- 439** M. R. Hansen, P. Hanson, A. Pardi, *Methods Enzymol.*, **2000**, *317*, 220.
- 440** G. M. Clore, M. R. Starich, A. M. Gronenborn, *J. Am. Chem. Soc.*, **1998**, *120*, 10571.
- 441** D. D. Ojennus, R. M. Mitton-Fry, D. S. Wuttke, *J. Biomol NMR* **14**, 175–179, (1999).
- 442** J. Sass, F. Cordier, A. Hoffmann et al., *J. Am. Chem. Soc.*, **1999**, *121*, 2047.
- 443** R. Tycko, F. J. Blanco, Y. Ishii, *J. Am. Chem. Soc.*, **2000**, *122*, 9340.
- 444** D. Marion, M. Ikura, R. Tschudin et al., *J. Magn. Reson.*, **1989**, *85*, 393.
- 445** M. Pirotto, V. Saudek, V. Sklenar, *J. Biomol. NMR*, **1992**, *2*, 661.
- 446** D. Marion, M. Ikura, A. Bax, *J. Magn. Reson.*, **1989**, *84*, 425.
- 447** J. Jeener, Lecture, Ampère Summer School, Basko Polje, Yugoslavia, 1971.
- 448** W. P. Aue, E. Bartholdi, R. R. Ernst, *J. Chem. Phys.*, **1976**, *64*, 2229.
- 449** M. Karplus, *J. Phys. Chem.*, **1959**, *30*, 11.
- 450** U. Piantini, O. W. Sorensen, R. R. Ernst, *J. Am. Chem. Soc.*, **1982**, *104*, 6800.
- 451** G. Eich, G. Bodenhausen, R. R. Ernst, *J. Am. Chem. Soc.*, **1982**, *104*, 3731.
- 452** C. Dalvit, M. Rance, P. E. Wright, *J. Magn. Reson.*, **1986**, *69*, 356.
- 453** L. Braunschweiler, R. R. Ernst, *J. Magn. Reson.*, **1983**, *53*, 521.
- 454** A. Bax, D. G. Davis, *J. Magn. Reson.*, **1985**, *63*, 207.
- 455** M. Rance, *J. Magn. Reson.*, **1987**, *74*, 557.
- 456** A. J. Shaka, J. Keeler, R. Freeman, *J. Magn. Reson.*, **53**, 313–340 (1983).
- 457** E. Kupce, P. Schmidt, M. Rance et al., *J. Magn. Reson.*, **1998**, *135*, 361.
- 458** A. A. Bothner-By, R. L. Stephens, J.-M. Lee et al., *J. Am. Chem. Soc.*, **1984**, *106*, 811.
- 459** L. Müller, *J. Am. Chem. Soc.*, **1979**, *101*, 4481.
- 460** G. Bodenhausen, D. J. Ruben, *Chem. Phys. Lett.*, **1980**, *69*, 185.
- 461** M. Salzmann, G. Wider, K. Pervushin et al., *J. Biomol. NMR*, **1999**, *15*, 181.
- 462** J. Cavanagh, M. Rance *Annu. Rep. NMR Spectrosc.*, **27**, 1–58, (1993).
- 463** K. Pervushin, D. Braun, C. Fernandez et al., *J. Biomol. NMR*, **2000**, *17*, 195.
- 464** R. Riek, G. Wider, K. Pervushin et al., *Proc. Natl. Acad. Sci. USA*, **1999**, *96*, 4918.
- 465** R. Riek, K. Pervushin, K. Wuthrich, *Trends Biochem. Sci.*, **2000**, *25*, 462.
- 466** M. Ikura, L. E. Kay, A. Bax, *Biochemistry*, **1990**, *29*, 4659.
- 467** G. M. Clore, A. M. Gronenborn, *Methods Enzymol.*, **1994**, *239*, 349; G. M. Clore, A. M. Gronenborn, *Trends Biotechnol.*, **1998**, *16*, 22.
- 468** R. D. Oleschuk, D. J. Harrison, *Trends Anal. Chem.*, **2000**, *19*, 379.
- 469** M. Karas, F. Hillenkamp, *Anal. Chem.*, **1988**, *60*, 2299–2301.
- 470** F. Hillenkamp, M. Karas, *Int. J. Mass Spectrom.*, **2000**, *200*, 71.
- 471** A. Douchette, D. Craft, L. Li, *Anal. Chem.*, **2000**, *72*, 3355.
- 472** J. B. Fenn, M. Mann, C. K. Meng et al., *Science*, **1989**, *246*, 64–71.
- 473** C. Henry, *Anal. Chem.*, **1997**, *69*, 359A.

- 474** Q. Xue, F. Foret, Y. M. Dunayevskiy et al., *Anal. Chem.*, **1997**, *69*, 426.
- 475** I. V. Chernushevich, W. Ens, K. G. Standing, *Anal. Chem.*, **1999**, *71*, 452A.
- 476** R. Guevremont, D. A. Barnett, R. W. Purves et al., *Anal. Chem.*, **2000**, *72*, 4577.
- 477** R. D. Smith, *Int. J. Mass Spectrom.*, **2000**, *200*, 509.
- 478** R. Falcone, D. Mello, A. Passaro et al., *Surf. Interface Anal.*, **2000**, *30*, 251.
- 479** B. Hagenhoff, M. Deimel, A. Bennighoven, *Proceedings of the 9th International Conference on SIMS*, Wiley, Chichester 1994, 792–795.
- 480** M. J. Tarlov, J. G. Newman, *Langmuir*, **1992**, *8*, 1398–1405.
- 481** B. Hagenhoff, A. Benninghoven, J. Spinke et al., *Langmuir*, **1993**, *9*, 1622–1624.
- 482** W. M. Albers, J. Likonen, J. Peltonen et al., *Thin Solid Films*, **1998**, *330*, 114.
- 483** J. Davies, C. S. Nunnerley, A. J. Paul, *Colloids Surf. B*, **1996**, *6*, 181.
- 484** C. M. Pradier, P. Bertrand, M. N. Bellon-Fontaine et al., *Surf. Interface Anal.*, **2000**, *30*, 45.
- 485** N. Patel, M. C. Davies, C. Martyn et al., *Langmuir*, **1997**, *13*, 6485.
- 486** S. Volooj, C. M. Carr, R. Mitchell and J. C. Vickerman, *Surf. Interface Anal.*, **2000**, *29*, 422.
- 487** B. A. Keller, P. Hug, *Proceedings of the 12th International Conference on Secondary Ion Mass Spectroscopy*, Brussels, 1999, p. 885. (Publ. in Sims XII, A. Benninghoven, P. Bertrand, H. N Migeon, M. W. Werner (Eds), Elsevier Science, Amsterdam, 2000).
- 488** B. A. Keller, P. Hug, *Proceedings of the 12th International Conference on Secondary Ion Mass Spectroscopy*, Brussels, 1999, p. 749. (Publ. in Sims XII, A. Benning Noven, P. Bertrand, H. N Migeon, M. W. Werner (Eds), Elsevier Science, Amsterdam, 2000).
- 489** K. J. Wu, R. W. Odom, *Anal. Chem.*, **1996**, *68*, 873–882.
- 490** G. Gillen, J. Bennet, M. J. Tarlov et al., *Anal. Chem.*, **1994**, *66*, 2170–2174.
- 491** H.-J. Galla, N. Bourdos, A. von Nahmen et al., *Thin Solid Films*, **1998**, *362*, 327–329.
- 492** A. M. Belu, Z. Yang, R. Aslami et al., *Anal. Chem.*, **2001**, *73*, 143–150.
- 493** P.-A. Binz, M. Müller, D. Walther et al., *Anal. Chem.*, **1999**, *71*, 4981.
- 494** V. Egelhofer, K. Bussov, C. Luebbert et al., *Anal. Chem.*, **2000**, *72*, 2741.
- 495** M. J. Chalmers, S. J. Gaskell, *Curr. Opin. Biotechnol.*, **2000**, *11*, 384.
- 496** S. P. Gygi, R. Aebersold, *Curr. Opin. Chem. Biol.*, **2000**, *4*, 489.
- 497** P. O'Farrell, *J. Biol. Chem.*, **1975**, *250*, 4007–4021.
- 498** A. Shevchenko, A. Loboda, A. Shevchenko et al., *Anal. Chem.*, **2000**, *72*, 2132.
- 499** K. F. Medzihradsky et al., *Anal. Chem.*, **2000**, *72*, 552.
- 500** L. Pesa-Tolic et al., *J. Am. Chem. Soc.*, **1999**, *121*, 7949.
- 501** G. I. Opteck, S. M. Ramirez, J. W. Jorgenson et al., *Anal. Biochem.*, **1998**, *258*, 349.
- 502** W. Tong, A. Link, J. K. Eng et al., *Anal. Chem.*, **1999**, *71*, 2270.
- 503** J. A. Loo et al., *Electrophoresis*, **1999**, *20*, 743.
- 504** Y. Oda et al., *Proc. Natl. Acad. Sci. USA*, **1999**, *96*, 6591.
- 505** S. P. Gygi, G. L. Corthals, Y. Zhang et al., *Proc. Natl. Acad. Sci. USA*, **2000**, *97*, 9390.
- 506** A. J. Link, J. Eng, D. M. Schieltz et al., *Nature Biotechnol.*, **1999**, *17*, 676.
- 507** T. Laurell, J. Nilsson, G. Marko-Varga, *J. Chromatogr. B*, **2001**, *752*, 217.
- 508** J. Drott, L. Rosengren, K. Lindström et al., *Mikrochim. Acta*, **1999**, *131*, 115.
- 509** P. ÖnneRFjord, S. Ekström, J. Bergqvist, J. Nilsson, T. Laurell and G. Marko-Varga, *Rapid Commun. Mass Spectrom.*, **1999**, *13*, 315.
- 510** R. W. Nelson, J. R. Krone, O. Jansson, *Anal. Chem.*, **1997**, *69*, 4363.
- 511** R. W. Nelson, D. Nedelkov, K. A. Tubbs, *Anal. Chem.*, **2000**, *72*, 404A.
- 512** M. Przybylski, M. O. Glocker, *Angew. Chem. Int. Ed. Engl.*, **1996**, *35*, 806.
- 513** E. C. Kempen, J. S. Brodbelt, *Anal. Chem.*, **2000**, *72*, 5411.
- 514** C. T. Houston, W. P. Taylor, T. S. Widlanski et al., *Anal. Chem.*, **2000**, *72*, 3311.
- 515** J. G. Kiselar, K. M. Downard, *Anal. Chem.*, **1999**, *71*, 1792.

- 516** P. William, C. Chou, D. M. Schielta, in *Automation Technologies for Genome Characterization*, ed. T. J. Beugelsdijk, Wiley, New York 1997, p. 227.
- 517** P. Crain, J. A. McCloskey, *Curr. Opin. Biotechnol.*, **1998**, *9*, 25.
- 518** C. R. Cantor, K. Tang, J. H. Graber et al., *Nucleosides Nucleotides*, **1997**, *20*, 591.
- 519** D. M. Lubman, J. Bai, Y. Liu et al., in B. S Larsen and C. N McEwen (Eds), *Mass Spectrometry of Biological Materials*, eds. B.S. Larsen, C. N. McEwen, 2nd edition, Marcel Dekker, New York 1998, p. 405.
- 520** B. Guo, *Anal. Chem.*, **1999**, *71*, 333R.
- 521** T. J. Griffin, L. M. Smith, *TIBTECH*, **2000**, *18*, 77.
- 522** U. Puapaiboon, J. Jai-nhuknan, J. A. Cowan, *Anal. Chem.*, **2000**, *72*, 3338.
- 523** R. M. McCormick, R. J. Nelson, M. G. Alonso-Amigo et al., *Anal. Chem.*, **1997**, *69*, 2626.
- 524** D. Figgeys, D. Pinto, *Anal. Chem.*, **2000**, *72*, 330A.
- 525** J. P. Kutter, *Trends Anal. Chem.*, **2000**, *19*, 352.
- 526** A. G. Hadd, D. E. Raymond, J. W. Halliwell et al., *Anal. Chem.*, **1997**, *69*, 3407.
- 527** L. Martynova, L. E. Locascio, M. Gaitan et al., *Anal. Chem.*, **1997**, *69*, 4783.
- 528** G. H. W. Sanders, A. Manz, *Trends Anal. Chem.*, **2000**, *19*, 364.
- 529** D. G. Myszka, R. L. Rich, *Pharmaceutical Science & Technology Today*, **2000**, *3*, 310.

## **Section VIII**

### **Applications 2: Environmental Analysis**

## **Introduction**

*Damia Barcelo*

The two chapters that were selected for this topic one on GC-ion trap mass spectrometry, by Sablier and Fujii and the other by Schröder on LC-MS in environmental analysis give an excellent contribution to the application of GC-MS and LC-MS to environmental analysis. Both chapters include many practical aspects and examples in the environmental field and also cover the historical perspective of the techniques and show the perspective on ionisation and scanning modes. Advances achieved in GC-ion trap by the use of external ion sources and GC/MS/MS possibilities are discussed. The LC-MS chapter provides an overview of the first applications of LC/MS interfacing systems, such as moving belt, direct liquid introduction (DLI) and particle beam (PB), and then on the more recent soft ionisation techniques, like thermospray and atmospheric pressure ionisation interfacing systems.

Perhaps the most interesting aspect is the number of applications reported. There are many applications in the environmental field, especially of LC-MS, such as the analysis of dyes, explosives, polycyclic aromatic hydrocarbons (PAH), surfactants, toxins, pesticides (including herbicides, fungicides etc.), quaternary amines, toluidines and thiocyanate compounds, carbamates, organophosphorus compounds, phenoxy carboxylic acids, phenylureas, thioureas and sulfonylureas, triazines, estrogenic compounds, haloacetic acids and disinfection byproducts, organoarsenic compounds, sulfonic acids and antifouling pesticides. The advantage of using a particular ionisation method, for instance atmospheric pressure ionisation versus electrospray, are discussed for each class of compounds. In this respect we think that these two chapters will give a useful picture of the application of mass spectrometry to the environmental chemistry field. Finally, I would like to thank the authors of these two chapters for their time and effort in preparing their contributions. Without their engagement the application of mass spectrometry to environmental analysis would certainly have not been possible.

# 15

## LC-MS in Environmental Analysis

*H. Fr. Schröder*

### 15.1

#### Introduction

##### 15.1.1

#### Historical Survey of the Development of LC-MS

The history of the development of liquid chromatography-mass spectrometry (LC-MS) from its beginnings in the early 1970s till the 1990s has been briefly outlined by Niessen [1]. The main reason for its rapid progress was the lack of a substance-specific detector system for the analysis of non-volatile polar, thermolabile compounds; these not being amenable to gas chromatography coupled with mass spectrometric detection (GC-MS). This had been a considerable disadvantage in any analytical research that had involved handling complex mixtures composed of either nonpolar and polar or just polar compounds.

The initial step, the introduction of liquids and liquid mixtures through a narrow capillary into a high vacuum system, was first undertaken by Talroze et al. [2] about 30 years ago. This step developed into an approach that combined a high resolution liquid chromatographic technique and the universal detector mass spectrometer ((HP)LC-MS). The following three different interfacing strategies resulted from this first analytical research approach for handling complex mixtures of polar, non-volatile compounds [3–5]:

(1) Atmospheric-pressure chemical ionisation was favoured by Horning et al. [3], whereas (2) Scott et al. [4] applied a moving-wire system which became transformed and finally resulted in the moving-belt interface. (3) The research of Arpino and his co-workers [5] led further in the direction initiated by Talroze [2], which after all had brought about the direct liquid introduction interface.

The first two commercially available LC-MS interfaces were the moving-belt interface and the direct liquid introduction interface. These hyphenated techniques promoted pharmacological research at several stages of drug development. The polar pharmaceutical compounds that were under research in pharmacological experiments, their polar by-products from chemical synthesis or even the very polar

metabolites of pharmaceuticals could be substance-specifically analysed in underivatized forms. Since compounds are degraded under such pharmacological experimental conditions, that is, in body fluids, renal excretions or faeces of test animals and test subjects, such compounds for research purposes are often more polar than the precursor compounds. GC separation prior to determination necessitated the derivatization of polar compounds in order to identify the volatile derivatives by MS or other detector systems. This procedure may however discriminate against compounds which do not react with the derivatization agents. LC-MS as an alternative separation and detection technique to GC-MS allows analysis without any discriminating derivatization step prior to ionisation and determination. So identification and peak purity assessment that had been impossible with unspecific detector systems applied previously, such as ultraviolet (UV), refractive index (RI) or fluorescence detection, then became realizable with the on-line combination of LC and MS.

"The history of LC-MS is characterised by many attempts to solve the difficult problems faced; only a few of these attempts resulted in successful LC-MS interfaces, which also became commercially available, [1]. Niessen sketched the development of LC-MS from the late 1970s till the early 1990s by scanning the number of papers published annually according to the LC interfaces: moving belt (MBI), direct liquid introduction (DLI), particle beam (PBI), fast atom bombardment (FAB) or continuous flow FAB (CF-FAB), thermospray (TSP), electrospray (ESI), and atmospheric-pressure chemical ionisation (APCI). A tremendous increase in the overall LC-MS publications was observed from the mid-1990s. At the same time, atmospheric pressure ionisation interfaces (API) such as APCI or ESI came much into favor. After 30 years of investigation and development of the on-line combination of liquid chromatography and mass spectrometry (LC-MS), both these techniques, APCI and ESI, became routine laboratory methods.

### 15.1.2

#### First applications of LC-MS

Today, attention focuses on three application areas: LC-MS is mainly applied in the pharmaceutical industry but also plays an important role in environmental analysis and natural-product analyses, i.e. in biochemical and biotechnological research. In addition, there is large-scale use of LC-MS in industrial research, where the analysis and elucidation of compound mixtures of personal care products, detergents and cleaning agents, etc., i.e. unknown mixtures of polar and nonpolar compounds, produced by competitors are of great interest. In all these applications in which polar compounds are involved, LC-MS has become the method of choice.

In environmental analysis, the LC-MS technique proved a very convenient and robust analytical technique for determining and identifying polar pollutants, predominantly in aqueous matrices, such as groundwater, all types of surface waters, wastewaters, leachates and eluates of soil samples. Aqueous eluates and organic extracts of fruits and vegetables containing either polar precursor compounds or their metabolites were examined in order to detect, identify and quantify the

polar compounds. Now, the comprehensive literature covering general aspects of LC-MS in environmental chemistry [6–11] or different aspects of the environmental application of LC-MS [12–25] is available in article-, chapter-, and book-form.

Over the last few years several general reviews in the field of environmental analysis have been published describing the use of mass spectrometry in general as a basic analytical technique for the determination of contaminants in environmental matrices [7, 8, 26, 27]. Recently, reviews have dealt with the topics of compound classes or interfacing techniques. Polar organic pollutants such as pesticides and herbicides were the most extensively reviewed environmental compounds. Brief descriptions of the state of the art of various mass spectral techniques are given and their various applications are outlined. LC-MS application reviews in environmental analysis have been reported by several authors. The papers of, e.g., Barceló [20], Clench et al. [28], Moder et al. [27], Ferrer et al. [29], Slobodnik et al. [22], Stan et al. [30] deal with the identification and quantification of pesticides in the environment. Polar pesticides and their metabolites were presented in an overview published by Slobodnik et al. [31] and the overview of Barceló et al. [32] reported sample handling strategies and analysis of pesticides in environmental waters. Besides overviews of triazine herbicides and their metabolites [33, 34] the determinations of phenoxyacetic acid [35] and quaternary ammonium [36] herbicides by LC-MS were reported. Even an interlaboratory study for the validation of liquid chromatography-mass spectrometry methods in the pesticide analysis of chlorinated herbicides, carbamates and benzidines by LC-MS with different MS instruments and interfaces, such as PBI and TSP, was published [37]. TSP, PBI, APCI and ESI applications were discussed for the analyses of pesticides, surfactants, dye-stuffs and PAHs in environmental matrices [28].

The reviews of Berger et al. [38], Schröder [23] and Schröder et al. [21] dealt with structure elucidation and quantification by LC-MS and MS<sup>n</sup>, while Kiewiet et al. [39], DiCoccia [40] and Marcomini et al. [41] reported how surfactants and their degradation products in an aquatic environment were tracked down. Dyes were the topics of reviews published by Hites [42] and Riu et al. [43]. Reemtsma reported about the application of API techniques in water analysis [44, 45], Clench et al. [28] described applications of LC-MS for a minor part of environmental contaminants, whereas the overview of Barceló [24] succeeded in covering the topic for the whole spectrum of contaminants.

The objective of this contribution is to present a comprehensive, up-to-date overview of the increasingly widespread use of LC-MS in environmental analysis to determine polar contaminants such as aromatic sulfonates, complexing agents, drugs and diagnostic agents, dyes, explosives, haloacetic acids, PAHs, pesticides, phenols, organoarsenic compounds, surfactants, toxins and xenoestrogens. LC-MS analytical methods for determining the anthropogenic precursor compounds as well as their biodegradation or physicochemical degradation products in the environment will be reported. Published results are compiled within tables and will therefore provide a convenient overview of the interfaces used and the compounds analysed.

This survey will include reports about applications with interfaces which have been used during the last decade when the role of LC-MS analysis extended so

that LC-MS has now become, besides GC-MS, the most important analytical technique in environmental organic analytical chemistry. The results which are reviewed here were generated with the following interfaces: direct liquid introduction (DLI), particle beam (PBI), fast atom bombardment (FAB) and continuous flow FAB (CF-FAB), thermospray (TSP) and the most used actual atmospheric pressure interfaces (API), the electrospray, also designated as “ion spray” (ESI), and the atmospheric-pressure chemical ionisation (APCI) interface.

Besides the history of LC-MS that Niessen [1] rendered he gave an excellent description of these types of interfaces and their different principles of operation. Moreover, he extensively discussed LC-MS interfacing strategies as combined with these different types of interfaces.

At the outset of the LC-MS evolution, the main problem was how to determine the small quantities of analytes dissolved in large quantities of eluents. In order to determine the small quantities of analytes contained in the column effluents, the analytes must be brought into a system operating under high vacuum conditions. In addition, chromatographic integrity and mass spectrometric sensitivity must be maintained:

Therefore three principal strategies for handling the effluents of the LC-columns were under research: 1. Removal of solvent by vaporization and subsequent ionisation of the analytes first led to the moving-belt interface which, later, was followed by the development of particle beam ionisation. 2. Direct ionisation was the basic principle of the continuous flow-FAB interface, whereas 3. nebulization of the column effluent was the basic principle of DLI, TSP, APCI or ESI ionisation [1].

All these interfaces were applied for the determination of medium to strong polar environmental contaminants in water and aqueous eluates or suspensions. Their relevance for the examination of environmental samples varied. During the last years of the previous decade, ESI and APCI have seen a spectacular rise, while TSP, that had been employed as the “work-horse” under routine conditions in the late 1980s and early 1990s was used less and less, and DLI ionisation was almost completely abandoned.

Particle beam ionisation, however, for a short time, became the interface of preference, since its spectra are similar to those electron impact (EI) spectra listed in the NIST-library, and so sustain any identification of unknown compounds. Its sensitivity, though, was quite unsatisfactory.

## 15.2

### Applications of LC-MS Interfaces in Environmental Analyses

With a certain delay, various types of interfaces that had been developed and applied in pharmacological and pharmaceutical research during the past three decades came to be used in environmental analytical applications. The following survey of “LC-MS in environmental analysis” will start with a description of the moving belt interface (MBI), followed by other interface types - DLI, PBI, FAB, TSP,

and will finish with the applications and results obtained with the API interfaces APCI and ESI.

MBI was already phased out more than 10 years ago, so that applications with the help of MBI, reported on during the late 1980s, will be described here just for the sake of completeness. DLI and FAB or CF-FAB, which were there from the very beginning of the LC-MS evolution, and were applied on a large scale in the early 1990s, are hardly used nowadays [1], as the literature discloses.

#### 15.2.1.

##### **Moving Belt Interface (MBI)**

As mentioned before, the first steps in substance-specific environmental LC-MS analysis were undertaken by interfacing LC and MS with the help of the moving wire system which was later modified into the moving belt technique. For a couple of years, the MBI technique, which, different from the interfaces used later and now, provided electron impact-like mass spectra, was used. First, this LC-MS interface type that had been used in pharmaceutical and pharmacological research concerned with the analysis of drugs and their metabolites was also successfully applied for the analysis of all kinds of anthropogenic chemicals or natural products, as well as for all kinds of pollutants, low volatile nonpolar pollutants and polar pollutants (e.g. benzidines, nitrosamines, anilines, nitroaromatics, dinitroaromatics, hydrazines, amides, phenylenediamines, organophosphites, acrylates, pyridines, phthalates, nitrophenols, pesticides, halogenated pyridines and alkyl tins [46]) present in the environment.

So different types of pesticides, i.e., carbamates [47, 48], chloro-phenoxyacetic acids [49], phenyl- and sulfonylureas [50–54], halogenated triazines [46], as well as non-ionic surfactants [55], polycyclic aromatic hydrocarbons (PAH) [56–58] and polar pharmaceutical compounds [59] were determined. This technique first used a steel wire which later was substituted by a Kapton® ribbon. However, it was soon replaced by the particle-beam interface, because the complex mechanical device led to considerable difficulties with the endless, continuously moving belt.

#### 15.2.2

##### **Direct Liquid Introduction (DLI)**

During the short time of their application in the early 1980s, DLI interfaces were often applied for substance-specific analysis [60] of various types of pesticides and herbicides (triazines, carbamates, organophosphorus compounds) [61–67], chlorinated phenoxyacetic acids, phenylureas, analides (alachlor, propachlor and aldi-carb) [63].

Because of its unsatisfactory sensitivity, a result of the low flow rate and the clogging of the diaphragms separating the eluting analytes from the high vacuum of the ion source, the application of the DLI interface technique was successively reduced. Because of all the disadvantages observed with its application, the DLI approach was soon replaced by the application of the more robust TSP interface,

permitting high flow rates without any split into the mass spectrometer. Such high flow rates, combined with TSP ionisation (DLI:TSP flow rates = 0.1 : 2.0 mL min<sup>-1</sup>), improved sensitivity as a result of the high concentrations of analytes contained in the column effluents.

As a result of new interfacing techniques that arose during the mid-80s, techniques more advantageous in LC-MS analyses, the number of contributions which presented DLI data decreased tremendously in the 1990s and today these data are no longer being cited.

### 15.2.3

#### **Particle Beam Interface (PBI)**

Particle beam interfacing of LC-MS was designed for the analysis of less volatile compounds using the advantage of the ability to record positive (PCI) and negative (NCI) chemical ionisation and electron impact (EI) mass spectral data on the analytes examined [60]. This ability to collect spectra which can be used for library matching or structural elucidation of unknown compounds with the help of the EI fragmentation pattern available from EI-GC-MS analysis was examined to produce library-searchable EI spectra which were then compared with NIST-library data [68]. Several pesticides were used for optimization [68, 69] resulting in spectra that could be compared favourably with EI spectra from pure samples. But calibration curves for quantification purposes were found to be generally non-linear under the conditions applied [68].

A commercially available PBI interface was the product of results Willoughby and Browner obtained from monodisperse aerosol generation interface, also known by its acronym MAGIC-LC-MS [70]. But the impact on LC-MS analyses was reduced because of unsatisfactory detection limits associated with the use of a broad spectrum of analytes. This drawback could not be compensated by the advantage that the production of library-searchable EI spectra represented.

The considerable and increasing number of applications where this interface operated in parallel to the TSP interface was the beginning of a fruitful development in LC-MS analysis. The method in general was reviewed in several papers and was also partly compared to results obtained by other interface types [6, 29, 32, 71]. In the field of environmental analysis, that is, predominantly in the detection, identification and quantification as well as in the confirmation after UV-DAD [72] of pesticides, herbicides and their biochemical or physicochemical degradation products, PBI-MS was applied. These results can be found in the literature together with a few results on surfactants and dyes.

The spectrum of pesticides examined contained all different types of pesticides. So, besides the biogenic pesticide rotenone in water after SPE [73] acidic pesticides in water [74, 75] or soil [76] as well as non-acidic compounds were under research. Cappiello et al. identified and quantified [77] 13 acidic and 32 basic-neutral pesticides in water samples. With the application of large-volume injections for the analyses of these compounds [75, 78] an improvement in sensitivity was observed which made trace analysis possible. The variation of the ionisation mode, EI,

PICI or NICI, could also improve the determination efficiency. Application of NICI improved the detection efficiency of chlorinated compounds in off-line [79] or on-line determinations [80] and of triazines, anilides and organo-phosphorus pesticides [81].

One of the most intensively examined type of pesticides handled under PBI conditions were the chlorinated phenoxy acids and their esters which were determined in water [82–86] and soil samples [83, 86]. Even results of an interlaboratory comparison study of 10 chlorinated phenoxy acids using PBI or TSP ionisation were published by Jones et al. [37] [87]. Statistically significant differences were observed between the interfaces and under these conditions PBI was found to have a better precision than TSP [87]. Betowski et al. [88] observed thermal degradation induced by residence time in the ion source and the influence of ion source temperature in the ionisation of the chlorinated phenoxy acid derivatives 2,4-D and MCPA. Several authors successfully examined a large number of different carbamate pesticides [67, 89, 90] and their transformation products by PBI-LC-MS [89, 90], by PBI-FIA-MS (flow injection analysis) [67] or by supercritical fluid chromatography (SFC) PBI-interfaced to MS [91].

Application of PBI to phenylurea pesticides [74, 92–94] and their chlorinated compounds such as diuron, linuron and monuron [95] in environmental samples allowed their determination in surface and drinking waters in underivatized form. An improvement in sensitivity for the determination of phenylurea and isocyanates was obtained with a post-column alcohol addition [96].

For triazines and their polar hydroxy metabolites PBI-MS was also very effective. These pesticides could be determined in drinking and surface water [97] and in humic soil extracts after SFE [98] with good results. Soil samples were also under research for acidic and non-acidic herbicides [76] which also were determined by PBI-MS, e.g., imazamethabenz-methyl in three different soil extracts [99]. Diquat and paraquat as quaternary ammonium pesticides were observed in drinking water after SPE (Dowex resin) with a recovery of >75% by PBI-MS [100].

For the determination of several different groups of polar pesticides [101, 102] the application of LC-MS in combination with PBI-MS was very useful. The application of this technique because of its EI-like fragmentation pattern was helpful in the identification of biochemical, physicochemical and chemical degradation products, as confirmed with the analysis of the biodegradation of 3-chloro-*p*-toluidine-HCl in soils [103] or with the photodegradation products of alachlor, aldicarb and methiocarb. 4 alachlor-, 8 aldicarb- and 4 methiocarb degradation products were observed [104]. Petrier et al. applied PBI-MS to monitor the degradation of pentachlorophenol and atrazine under ultrasonification [105] and the results of degradation of bromacil in a water matrix by UV photolysis were published [106] while the degradation products of bromacil ozonation were reported by Acher et al. and Hapeman et al. [106, 107].

The non-atmospheric pressure ionisation interfaces (non-API) PBI and TSP besides the API interfaces ESI and APCI were applied for the analysis of the *N*-methylcarbamate pesticides (methomyl, aldicarb, aldicarb sulfoxide, aldicarb sul-

fone, carbaryl, methiocarb, carbofuran, and 3-hydroxycarbofuran). The PBI interface provided the worst results [108] of all other interfaces under research.

Simultaneously with the use of PBI for the analysis of pesticides and agrochemicals, both dispersed in large quantities in the environment [109], this interface type was also applied to perform the determination of a broad spectrum of pollutants generated by degradation processes, mobilized from waste disposals and contained in the leachates [110] and finally found in the aquatic environment. The analysis of 500 L samples of drinking water made the pollution of these waters with alkylphenol ethoxylates (APEOs) and alkylphenol carboxylates (APECs) obvious [111]. As polar constituents of wastewater samples non-ionic surfactants of NPEO type and their acidic metabolites, plasticizers, and plastic additives could be confirmed by the application of PBI-LC-MS [112].

The precursors of the potential carcinogenic aromatic amines, azo and diazo dyes were also under research by PBI. So 14 commercially available azo and diazo dyes were characterised and analysed by PBI, TSP and ESI-LC-MS. While PBI gives molar mass information and various fragments, TSP and ESI result only in molecular ions with little fragmentation and therefore little structural information [113].

The eight triphenylmethane dyes, malachite green, leucomalachite green, gentian violet, leucogentian violet, brilliant green, pentamethyl gentian violet, *N,N'*-tetramethyl gentian violet, and *N,N*,*N*',*N*'-tetramethyl gentian violet, were characterised by PBI-LC-MS while in parallel the six cationic dyes were reduced in the ion source to form the corresponding leuco compounds [114]. Maguire published a study of the Yamaska River in Canada from the period 1985–1987, that proved the occurrence of 15 dyes in water, suspended solids, and sediment downstream of textile mills [115]. PBI-LC-MS was used by Voyksner et al. [116] to identify reduction products of azo and diazo dyes.

PBI-LC-MS could also be applied for the simultaneous detection and quantification of the nonpolar, lipophilic PAHs and their more polar metabolites. So PBI-LC-MS was used to identify and quantify PAHs [28, 117, 118] and nitro-PAHs [119]. Flow-injection detection limits at the pg level could be obtained under NICI conditions. A broad range of organic pollutants besides PAHs, such as aromatic sulfonic acids and chlorinated phenoxy acid herbicides in soil and water were determined quantitatively and could be confirmed by PBI LC-MS [86, 117]. The method was specific for PAHs with molar masses > 170 Da [86] (> 178 Da [117]). PAHs were ionised as molecular ions, as base peak and doubly-charged molecular ions. The capacity of PBI for providing library-searchable EI spectra was confirmed. PBI besides moving-belt and APCI (operated as heated pneumatic nebulizer interface). LC-MS interfaces were compared for qualitative and quantitative analyses of PAHs. While PBI ionisation resulted in the detection of 7 PAHs, the APCI interface showed good results and made it possible to detect all 16 target PAHs plus coronene in coal tar. MBI was inefficient for more volatile compounds [120]. Pace et al. [121] applied PBI in order to study PAHs with molar masses within the range 300–450 Da in soils. Spectra varied with the ion distribution ratio of the single- to the doubly-charged molecular ion, dependent on the molec-

ular weight, source temperature and concentration. Doerge et al. [118] reported PBI-LC-MS work to detect and quantify PAHs and oxygenated metabolites in sediment and water samples from the the Exxon Valdez oil spill in Alaska with ng detection limits. The PAH spectra were identical with EI library spectra and oxygenated PAH spectra contained molar mass information and diagnostic fragment ions.

Biological degradation of PAHs was brought about in water samples and precursor compounds and metabolites were analysed by PBI. Naphthalene, 1-methyl- and 2-methylnaphthalene, acenaphthene and acenaphthylene were studied [122]. The limitations of the data in the GC-MS library for comparison with the PB LC-MS results were emphasized and the disadvantages of the PBI method were discussed.

PBI was evaluated for packed-column SFC-MS [91]. Fundamental studies on the effects of various operational parameters were reported and the sensitivity of the system was evaluated.

After these first tentative attempts at combining LC with MS, some respectable results could be achieved, however, technical problems, e.g., the service life of the belts (which were exposed to considerable differences of temperature and pressure with the MBI interface) or the quite poor sensitivity of the DLI or PBI interfaces, led to substitution of these interfaces. In thir place, MBI, DLI or PBI have gained firm acceptance among the various approaches to LC-MS. But even the advantage of the PBI interface, its capability to produce library searchable spectra, could not prevent its disappearance. The disadvantages of MBI, DLI or PBI, which are quite evident in comparison with those types of interfaces that will be presented in the following, were simply too grave to let them survive in routine application under the conditions of ultra-trace analysis.

#### 15.2.4

#### **Fast Atom Bombardment (FAB) and Continuous Flow FAB (CF-FAB)**

While the removal of solvent by vaporization and its subsequent ionisation was the principle of MBI that came to be followed up later by PBI in the FAB process, a quite different ionisation technique, direct ionisation of compounds from a target, is the principle of the FAB technique.

Besides analysis for pharmaceutical, biochemical and biological research operating with FAB or CF-FAB, environmental applications were reported between the late 1980s and early 1990s. Their application reached its peak in about 1992 [1].

Some reviews were published dealing with this type of interface and its application in environmental analysis [24, 42, 123]. Qualitative and quantitative analysis of polar pollutants by FAB or CF-FAB was performed with extracts of aqueous matrices, such as wastewater, surface water, seawater, raw and drinking water [124–129], for all types of surfactants (non-ionics, anionics, cationics and amphoteric) in urban wastewaters, receiving waters (rivers and costal receiving areas), and groundwater [124–148], for metabolites of surfactants [130, 149–153], and brominated surfactants [137, 154].

Some of these results are worth mentioning because of their importance to FAB studies, particularly of surfactants. Results of flow injection analysis (FIA) by CF-FAB and by ESI-MS and MS/MS were compared for MS-quantification of cationic dodecyl-, tetradecyl- and hexadecyltrimethyl-ammonium surfactants and their deuterated analogues dissolved in water [155]. FIA-ESI, however, was the method with greater specificity. Linear alkylbenzenesulfonates (LAS) in filtered river water and sewage samples could be determined qualitatively and quantitatively by CF-FAB-MS and MS/MS by Borgerding et al. with a detection limit of 1 ng abs [135]. Simultaneously the differentiation between linear and branched AS homologues was enabled by scanning the parent ions of  $m/z$  183 or  $m/z$  197. LC-MS with a frit-FAB interface was applied in order to analyse non-ionic surfactants. The mass spectra contained  $[M+H]^+$  ions together with a series of fragment ions of  $\Delta m/z$  44, which are characteristic of ethoxylated alcohols. This interpretation was supported by MS/MS measurements [132]. Unlike in this work, significant fragmentation will occur if mixtures of polyethoxylated and polypropoxylated surfactants are analysed by SFC MS [156].

With FAB, TOF, MALDI, ESI-MS, field desorption (FD) MS and GC-MS technique the analytical capabilities for non-ionic gemini surfactants were compared [157]. Parees et al. reported on the analysis of a series of oligomeric ethoxylated surfactants of this type which showed an improved surface activity. Even an antibacterial lipopeptide biosurfactant, lichenysin A, cultured and isolated, was analysed by FAB-MS and FAB-MS/MS, ESI-MS and various other methods [158]. The compound was characterised and the lipid moiety contained a mixture of 14 linear and branched  $\beta$ -hydroxy fatty acids from C<sub>12</sub> to C<sub>17</sub>.

Beside these bipolar, surface active compounds a broad spectrum of polar compounds, sulfonated azo dyes [159, 160], sulfonates [161], additives in commercial dyes [145], benzo[a]pyrene conjugates [162, 163], DNA adducts [164], ozonation products of surfactants [165, 166], explosives [167] and so forth applying FAB or CF-FAB were qualitatively determined or even quantified with success. Grange et al. [159] used accurate mass measurements for identification and confirmation of e.g. sulfonated azo dyes [159].

However, FAB ionisation was most frequently applied for the detection of pesticides due to both the broad dispersion of these substances throughout the environment combined with a need for information about these compounds of concern and the improved detection limits of this method. So the whole spectrum of polar pesticides belongs to this group of compounds which again were often over-proportional under comprehensive research [138]. CF-FAB-MS was applied to the detection of glyphosate [168], and CF-FAB-MS and electrospray ionisation were compared by recording herbicide spectra on the same magnetic sector instrument and the same LC system [169]. Both techniques provide accurate high-resolution measurements. Non-volatile and thermally labile components, e.g., pesticides in natural or purified drinking water, were investigated by Bruchet et al. [170] who applied FAB-MS/MS and TSP-LC-MS/MS. A series of sulfonyl urea herbicides, with phenyl, norbornene, pyridine or pyrimidine ring substituents [54, 171], were characterised by CF-FAB-MS. These methods here permitted characterization of the

molecular weights in spite of their high thermolability and their low volatility [172]. In the same manner, simultaneous determination of phenylurea and carbamate herbicides diuron, linuron, siduron, methyldymron, chlorpropham, and swep in water was performed by Okura et al. [173], and Tondeur et al. studied quaternary ammonium pesticides, e.g., paraquat, diquat and dibenzoquat [174].

In a LC-MS study [175] applying FAB besides TSP, APCI, ESI, plasma desorption (PD) ionisation a series of N- and P-containing pesticides were studied. Collision-induced dissociation (CID) spectra were recorded. Pesticide residues could readily be identified, confirmed and quantified. The results for several different polar pesticides were compared with APCI and ESI and were presented [176].

The metabolism of compounds predominantly results in more polar compounds than the precursor molecules, so for the follow-up of pesticides in the environment in the late 1980s and early 1990s FAB and CF-FAB-MS at this stage of MS development met the need. CF-FAB-MS was applied by Reiser et al. [171] to unknown sulfonylurea herbicide metabolites using packed capillary columns. New and unusual heterocyclic ring-opened metabolites and hydrolysis products were identified and metabolic pathways proposed. The metabolism of cycloate, a thiocarbamate herbicide, was investigated [177].

The analysis of dyes as constituents in environmental samples was reported by different groups. The fragmentation of carbocyanine dyes was studied by FAB-MS/MS and ESI-MS by Melnyk et al. [178], whereas Soubayrol et al. [179] discussed the use of FAB-MS and ESI-MS in the analysis of alizarin dyes from ancient materials. The degradation of four sulfonated azo dyes by lignin peroxidase labeled with  $^{18}\text{O}$  was studied and the sulfonated products were analysed by FAB-MS and ESI-MS [180]. Wastewaters were under research for dyes by FAB, so trace level dyestuffs components in mixtures of process sewage containing chlorinated diphenyl sulfides and dyestuffs were identified or confirmed by accurate mass measurements [159]. Food and cosmetic dyes (Acid Blue 9, Acid Violet 17, Quinoline Yellow, Acid Red 51, Acid Red 87 and Acid Red 92) were determined qualitatively and quantitatively by CF-FAB-MS in colored municipal wastewater samples. Results of balances in the sewage treatment process indicating a resistance to degradation and sorption were presented [181]. Evaluation of various separation techniques by Brumley et al. led to the application of micellar electrokinetic chromatography (MEKC) and capillary LC in the analyses of environmental matrices for seven selected synthetic dyes [182]. Recovery data for spiked water and soil matrices were obtained. Capillary LC detection was performed using CF-FAB-MS, which allowed confirmation.

The polar metabolites of PAHs were important analytes and were studied with FAB in MS and MS/MS mode [24, 183, 184]. Quantitative determinations by FAB-MS required that the sample ions were completely separated from the background ions of glycerol [185]. A CF-FAB-MS method was developed by Teffera [186] for analysis of conjugates of benzo[a]pyrene (BAP) in the negative ion mode. The PAH-DNA acetylaminofluorene adduct could be determined with detection limits improved by up to 3 orders of magnitude in the low pmol and low fmol ranges [187]. Tsuruda et al. [188] analysed all the major peaks from isolated perfused liver metabolism of  $^{14}\text{C}$ -labelled naphthalene by FAB-MS/MS. The results were

compared with *in vivo* urinary acidic metabolites. CF-FAB-MS and -MS/MS were used to investigate the detection and structural characterization of amino-PAH-DNA nucleoside adducts in ng and pg concentrations [189] and the adducts of deoxyguanosine with a series of PAHs and amino-PAHs [190]. The complementary nature of positive and negative product ions was discussed [189].

Explosives were also examined by FAB-MS and MS/MS. The spectra of cyclic nitramine and nitroguanidine were compared with results obtained by ESI-MS and MS/MS. While FAB resulted in fragmentation (loss of H<sub>2</sub>O, NO<sub>2</sub> and NO) ESI CID spectra were simple [167].

Despite an improvement in recording conditions by the use of the array detector to collect time-resolved data, which resulted in spectra with significantly enhanced sensitivity if compared with normal FAB [191], both techniques, FAB and CF-FAB-MS, however, suffered from the background generated by the essential FAB matrix. Though application of the continuous flow technique in combination with FAB improved the signal-to-noise (S/N) ratio, the improvement of detection limits was not sufficiently satisfactory. What is quite advantageous and more marked than in other interface types is, because of soft ionisation, the possibility of determining molecular mass by FAB and the identification after fragmentation by MS/MS.

### 15.3

#### LC-MS Interfaces Applied in Environmental Analysis During the Last Decade

##### 15.3.1

##### Achievements and Obstacles

Right from the outset of the 1990s, a selection of those interfaces that could be adapted to a routine LC-MS analysis was observable. This trend had been initiated by pharmacological and pharmaceutical research, although it had the TSP interface at its disposal, which was a well-adapted and reliable type of interface that had shown its full capacity in manifold appliances. The sample material, being available only in very limited quantities for such research, and improved separation techniques, as, for example, capillary electrophoresis (CE) or capillary zone electrophoresis (CZE) necessitated different types of interfaces that could be operated with considerably smaller amounts of sample than the TSP interface, which reached its optimized sensitivity with flow rates of about 2 mL min<sup>-1</sup>. Such a desirably lower sample demand is guaranteed by atmospheric pressure ionisation (API) interfaces, atmospheric pressure chemical ionisation (APCI) and electrospray ionisation (ESI) interface.

The limitations in the flows here were determined by the LC or CE-technique applied for on-line separation prior to MS detection.

As the abbreviation "API" implies, ionisation takes place under atmospheric pressure conditions. Therefore the API techniques APCI and ESI can handle samples eluting from an LC column or bypassing the analytical column when FIA is applied, and in this feature are quite different from the TSP ionisation technique

as the name implies and as reported on in the literature [1, 22]. Nevertheless the qualitative results obtained by means of TSP, APCI or ESI interfaces, which were used predominantly in environmental analysis during the last decade, may be identical or may be quite different. Three different results form the worst case.

Fig. 15.1a–c exemplify a mode of presentation for mass spectra of a mixture of non-ionic polyethylene glycol (PEG) surfactant homologues obtained by TSP, APCI and ESI in the positive FIA-MS mode. The equidistant ions in the spectra that are equally spaced by  $\Delta m/z$  44 u ( $-\text{CH}_2\text{--CH}_2\text{--O}-$ ) are caused by different polyethyleneglycol chain lengths of the alkylpolyethyleneglycol ether homologues (alkylethoxylates; AEO). A comparison between the signal patterns of these FIA spectra showed that for all three spectra the patterns were similar, i.e., the results of the ionisation were comparable.

The analysis of another non-ionic surfactant mixture of alkylpolypropyleneglycol ether type (alkylpropoxylates; APO) was performed in the same manner, FIA-MS(+), and resulted in the FIA-MS spectra shown in Fig. 15.2a–c. Differing in their ethoxy chain links, now polypropylene glycol (PPG) chain links instead of PEG units, the signals were also equidistant in the FIA-MS spectra yet they now differed by  $\Delta m/z$  58 u equivalent to ( $-\text{CH}(\text{CH}_3)\text{--CH}_2\text{--O}-$ ). The differences in the results obtained with the different interfaces were tremendous. TSP (a) provided a distribution of homologues in the form of ammonium adduct ions ( $[\text{M}+\text{NH}_4]^+$ ) and molecular ions ( $[\text{M}+\text{H}]^+$ ), APCI (b) ionisation showed a predominance of ammonium adduct ions, whereas under ESI ionisation the sensitivity was low and resulted in background ions without relevance to the expected compounds.

The third quite impressive example was obtained from a study with alkylether-sulfates recorded as TSP, APCI and ESI-LC-MS total ion currents or in the form of select mass traces. The correspondences or the differences in the ionisation results observed or pointed out before for the analyses of alkylpolyether surfactants, respectively, were recorded under positive ionisation, the adequate ionisation mode

**Fig. 15.1, 15.2, 15.3 on pages 165–167**

**Fig. 15.1. a–c:** Overview spectra of non-ionic polyethylene glycol (PEG) surfactant mixture (AEOs with general formula:  $\text{C}_n\text{H}_{2n+1}\text{O}-(\text{CH}_2-\text{CH}_2\text{--O})_x\text{--H}$  ( $n = 13$ ;  $x = 1\text{--}17$ )) recorded in flow injection mode (FIA) bypassing the analytical

column and ionised in the positive mode by means of the different interface types: (a) TSP-FIA-MS(+) ( $[\text{M}+\text{NH}_4]^+$ ), (b) APCI-FIA-MS(+) ( $[\text{M}+\text{NH}_4]^+$  and  $[\text{M}+\text{H}]^+$ ) and (c) ESI-FIA-MS(+) ( $[\text{M}+\text{NH}_4]^+$  and  $[\text{M}+\text{H}]^+$ ).

**Fig. 15.2. a–c:** Overview spectra of non-ionic polypropylene glycol (PPG) surfactant mixture (APOs with general formula:  $\text{C}_n\text{H}_{2n+1}\text{O}-(\text{CH}(\text{CH}_3)\text{--CH}_2\text{--O})_x\text{--H}$  ( $n = 7$ ;  $x = 1\text{--}10$ ) recorded in flow injection mode (FIA) bypassing

the analytical column and ionised in the positive mode by means of the different interface types: (a) TSP-FIA-MS(+) ( $[\text{M}+\text{NH}_4]^+$ ), (b) APCI-FIA-MS(+) ( $[\text{M}+\text{NH}_4]^+$  and  $[\text{M}+\text{H}]^+$ ) and (c) ESI-FIA-MS(+) (no ions observable).

**Fig. 15.3. a–j:** LC-MS total ion current traces (RIC) and selected mass traces of  $[\text{C}_{12}\text{--O}(\text{EO})_3\text{--SO}_3]^-$  ions or  $[\text{C}_{14}\text{--O}(\text{EO})_3\text{--SO}_3]^-$  ions of alkylpolyethersulfate blend recorded by

means of the different interface types and ionisation modes: TSP(-) (a,b), APCI(+) (c,d), APCI(-) (e,f), ESI(+) (g,h) and ESI(-) (i,j). Gradient elution separated on RP-C<sub>18</sub> column.

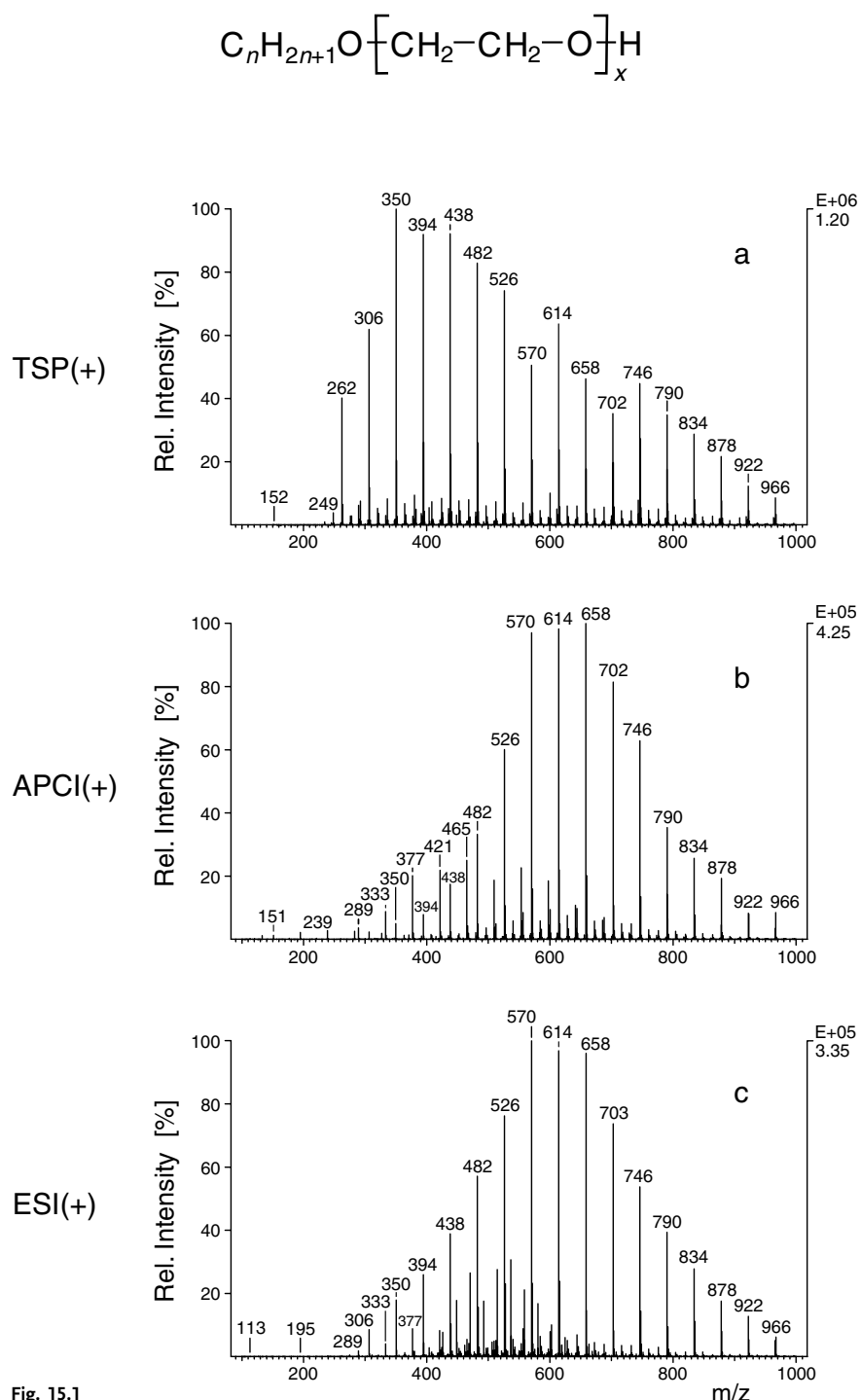


Fig. 15.1

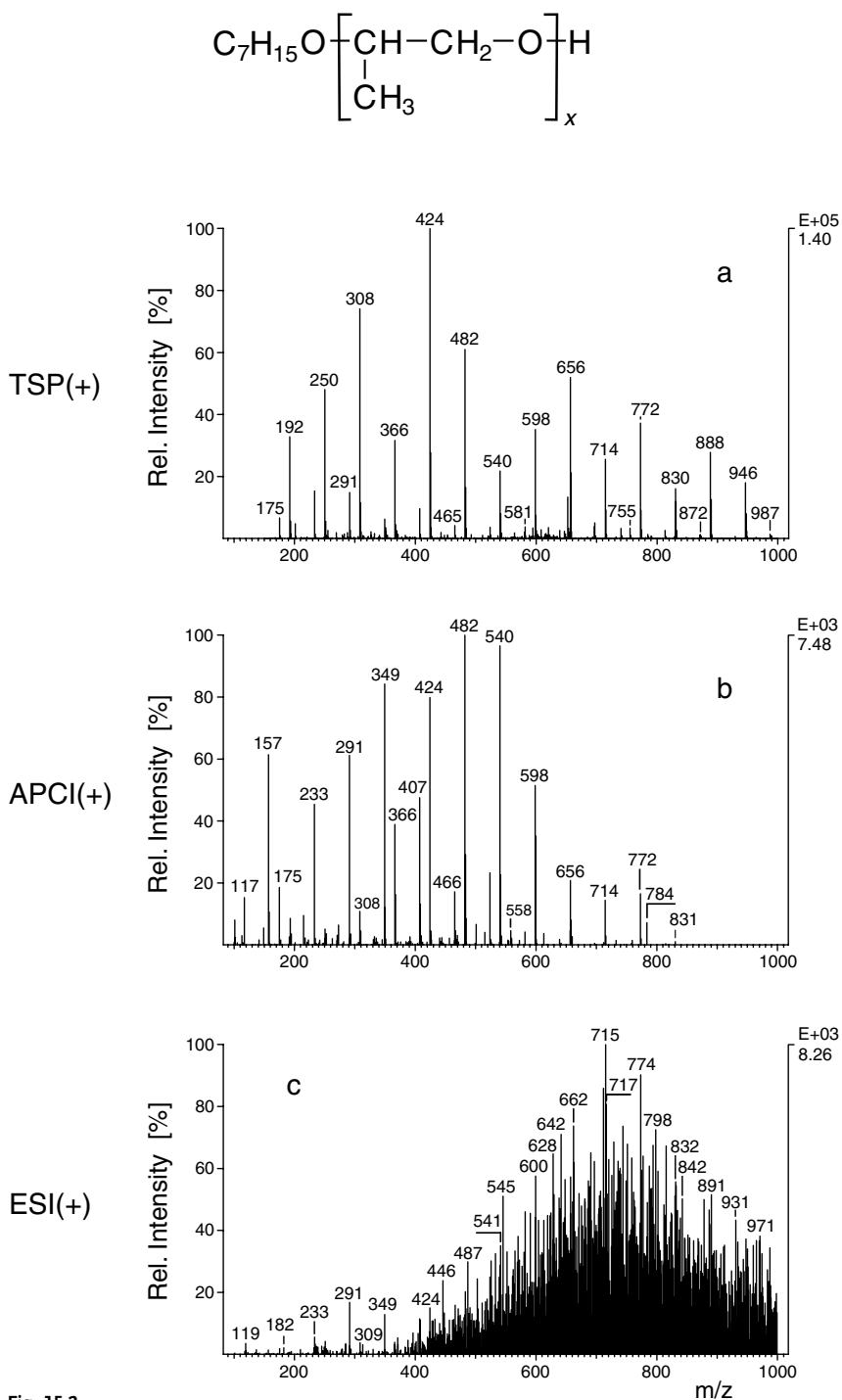


Fig. 15.2

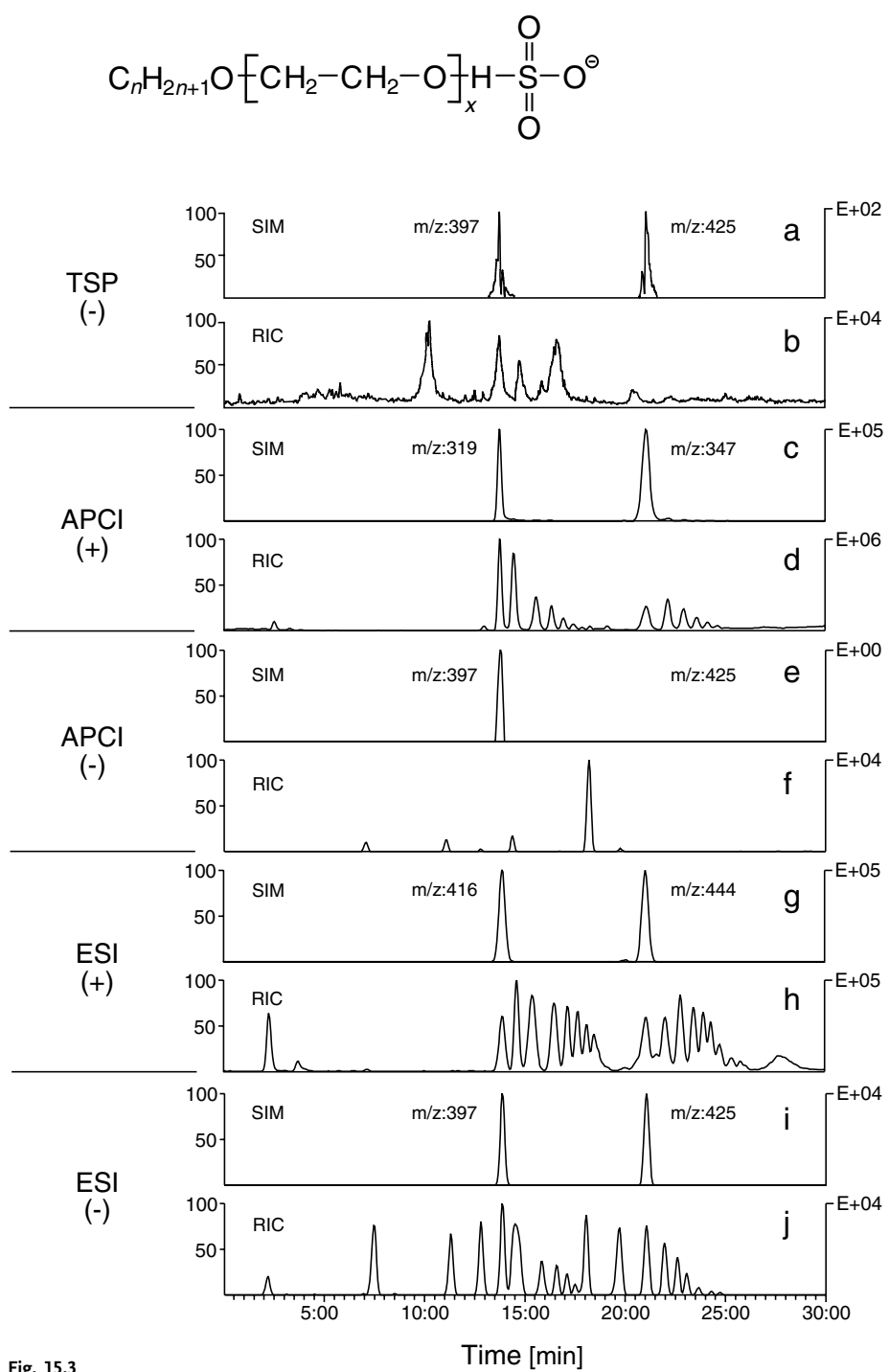


Fig. 15.3

for this type of compounds. In order to illustrate the differences observed in the ionisation process when using TSP, APCI or ESI interfaces and recording either in positive or negative mode, a mixture of C<sub>12</sub>- and C<sub>14</sub>- homologues of alkylether-sulfates ( $C_nH_{2n+1}-O-(CH_2-CH_2-O)_x-SO_3H$ ;  $n = 12, 14$ ) was separated by LC, ionised by TSP(-) (Fig. 15.3a,b) [23], APCI(+) (Fig. 15.3c,d), APCI(-) (Fig. 15.3e,f), ESI(+) (Fig. 15.3g,h) and ESI(-) (Fig. 15.3i,j) [21] and detected by MS. Again the results demonstrate a considerable variation in the ionisation efficiencies of different interface types operated either in positive or negative mode. Within a comparison of the results of all interfaces, only the LC-ESI-MS(-) total current trace (Fig. 15.3j) presented the entire spectrum of the separated AES homologues on the grounds of their alkyl chain lengths and in accordance with PEG chain lengths. The signals in the mass traces  $m/z$  397 (C<sub>12</sub>-AES) or 425 (C<sub>14</sub>-AES) (Fig. 15.3i) belong to the  $[C_{12}-O-(EO)_3-SO_3]^-$  ion or  $[C_{14}-O-(EO)_3-SO_3]^-$  ion, respectively.

The intensities of ions obtained under TSP-conditions (Fig. 15.3a,b) were weak [23] whereas APCI(+-TIC (Fig. 15.3c,d) looked fine but ionisation had resulted in  $[M-SO_3]^+$  ions ( $[C_nH_{2n+1}-O-(CH_2-CH_2-O)_x-H]^+$ ). APCI(-) ionisation was impossible (Fig. 15.3e,f) and ESI(+) (Fig. 15.3g,h) ionised the AES homologues  $C_nH_{2n+1}-O-(CH_2-CH_2-O)_x-SO_3H$  with  $x \geq 3$ .

On the one hand, these results presented the correspondence in an impressive manner; on the other hand, they showed the differences in the analytical results obtained by TSP, APCI or ESI interfaces. TSP as the work-horse for routine analysis could be used to examine medium-polar and strongly polar compounds, while APCI ionisation led to successful ionisation of medium-polar or even lipophilic pollutants such as PAHs. The ESI interface (Fig. 15.2c), though inappropriate for ionisation of polypropylene glycolethers, enabled researchers to cope with the strongly polar ionic AES compounds in an excellent manner.

### 15.3.2

#### Soft Ionisation Interfaces (TSP, APCI and ESI)

One of the most serious drawbacks that has been observed in the ionisation process with TSP, APCI, ESI interfaces, and also with FAB, is the soft ionisation of the analytes which mostly leads to molecular ions or molecular adduct ions. Though molecular mass information is provided, there is little or no structural information at all observable with PBI or electron impact (EI) MS. This soft ionisation is clearly disadvantageous for any identification of environmental contaminants, since it generates either considerably less or no fragments at all, and hence is unable to confirm the presence of such compounds of environmental concern. With the commercial availability of tandem devices, tandem mass spectrometry (MS/MS) helped to overcome these identification obstacles via collision-induced dissociation (CID) in MS/MS mode or via ion trap in MS<sup>n</sup> mode. Today, even bench-top machines provide the possibility of MS<sup>n</sup>. However, when TSP began to become the method of choice in environmental analysis and became commercially available, MS/MS technology was still quite expensive. Users of TSP ionisation with spectrometers not amenable for MS/MS had the possibility to record

spectra in discharge-on- or, alternatively, in filament-on-mode to induce or support the generation of fragment ions. The fragmentation observed under these conditions, however, was quite divergent and less extensive than in the EI mode and often identification could not be achieved because the fragmentation was not reproducible. API ionisation methods installed on conventional mass spectrometers and applied for analysis in the early 1990s allowed one to perform fragmentation recording mass spectra under so-called in-source-CID (also termed pre-analyser CID or cone voltage fragmentation (CVF)) conditions by applying an appropriate voltage difference between two regions of the API source. The method was followed up to solve the identification problem, since for small molecules no structure elucidation could be achieved [192–195]. Many analyses could be performed in this way, though the results were not at all satisfactory. This method was sometimes denoted as “poor-man’s MS/MS” [196].

Although in-source-CID is a useful technique, the method has distinct limitations, which should be pointed out here. To demonstrate the capabilities of in-source-CID as applied to environmental samples, a separation and fragmentation of a mixture of nonylphenolethoxylate homologues (NPEO) contained in SPE extracts was performed and the results were compared to MS/MS product ion spectra recorded by triple quad MS. A SPE extract was submitted to APCI-MS(+) under in-source-CID-conditions or to APCI-MS/MS(+) after normal-phase-C<sub>18</sub>-LC. While under in-source-CID conditions all NPEO homologue ions were fragmented, under MS/MS CID conditions the [M+NH<sub>4</sub>]<sup>+</sup> ion at *m/z* 634 was selected to pass into the collision cell to be fragmented. The separation in both cases resulted in a single peak in the ion current trace (TIC) containing the whole mixture of NPEO homologues. Product ion spectra were recorded by adjusting different capillary voltages or tube lens voltages and by variation of the collision energy, respectively.

Figures 15.4a–c present in-source-CID spectra. While under “normal” LC-APCI-MS conditions no fragmentation could be observed (Fig. 15.4a), the complex mixture of precursor and product ions is observable (Fig. 15.4b), since with in-source-CID all ions that are present in the ion source are subjected to CID. The choice of more elevated potentials, however, led to a complete fragmentation with less expressiveness for identification (cf. Fig. 15.4c). CID, however, performed in a collision cell of an MS/MS instrument or in an ion trap, first leads to a selection of a particular precursor ion with improved signal-to-noise (S/N) ratios and fragmentation takes place in a more controlled way, as shown in Fig. 15.5a–c. Due to the collision energy imposed, abundant variations of precursor ions or product ions can be observed yet the characteristic fragment ions can be recognized.

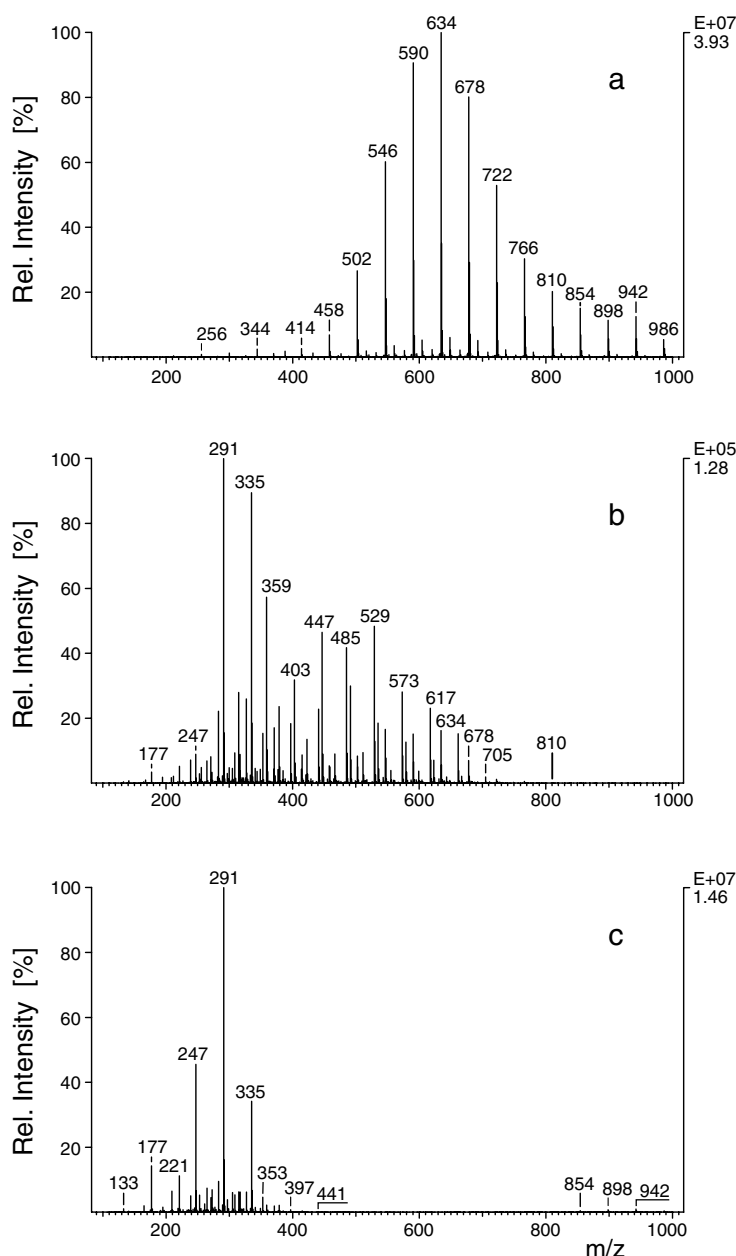


**Fig. 15.4. a–c:** LC-MS/MS spectra of nonylphenolpolyglycoether blend (NPEO) recorded in "in-source CID mode". Spectra were recorded for comparison of in-source CID results and results obtained with conventional MS/MS (cf.

Fig. 15.5). An alkylphenolpolyglycoether blend (APEO) was submitted to "in-source CID" under variation of capillary: tube lens voltages.  
 (a) capillary : tube lens: 20 V / 60 V,  
 (b) 110 V / 150 V and (c) 190 V / 190 V.

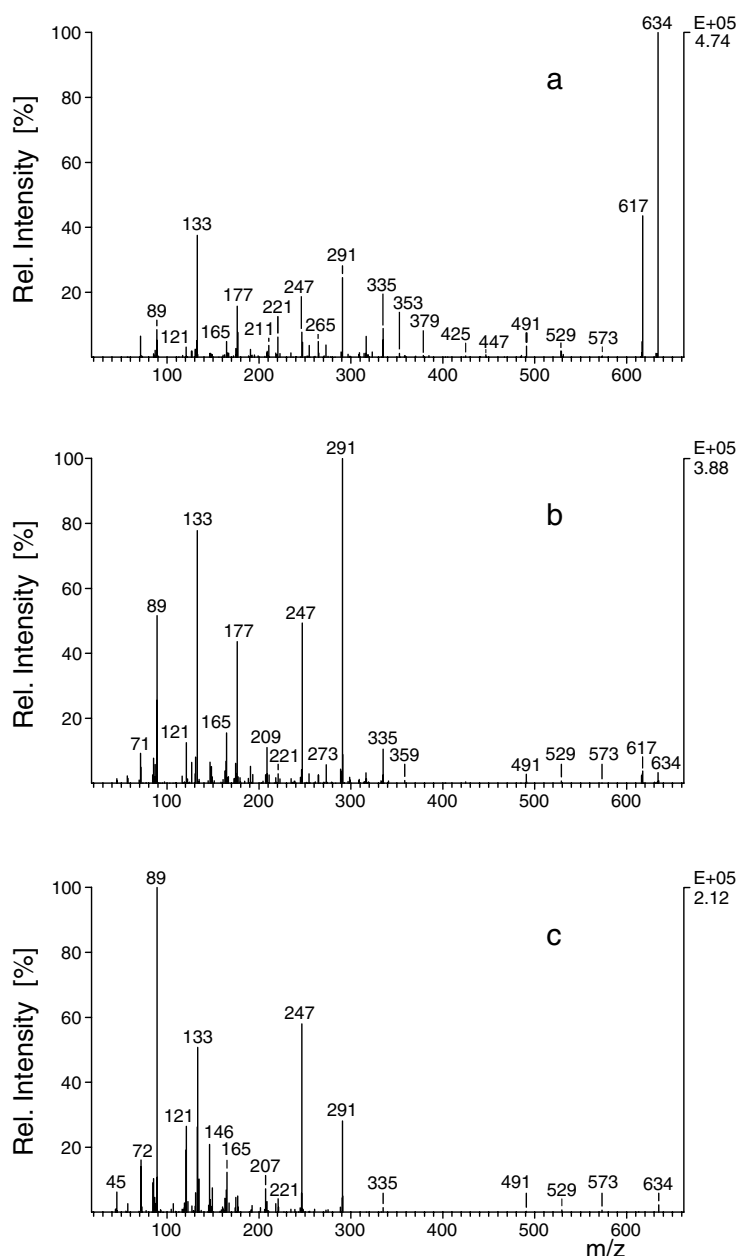


**Fig. 15.5. a–c:** LC-MS/MS(+) of nonylphenol-polyglycoether blend (NPEO) recorded by CID of selected  $[M+NH_4]^+$  parent ion  $m/z$  634 in collision chamber of TSQ in MS/MS mode. Collision gas: argon. Due to the collision energy imposed: (a) -25 eV, (b) -35 eV and (c) -50 eV, the precursor ions and product ions varied in abundance.

### 15.3.3

#### The Applications of Soft Ionising Interfaces

##### 15.3.3.1 Applications Using Thermospray Ionization Interface (TSP)

During the second half of the 1980s, the TSP interface, which had first been introduced in 1983 [197], became the most widely-used technique for coupling LC and MS. The main disadvantage of DLI, its low sensitivity, had soon led to its replacement by the TSP interface, before, in the mid-1990s, the commercial breakthrough of API technology took place.

The option of high flow rates, combined with TSP ionisation, helped to improve the sensitivity because of the quantitative transfer of analytes in the column effluents into the mass spectrometer. High flow rates under reversed-phase conditions (RP) as well as normal-phase separations (NP) were amenable to this interface type. Thermospray ionisation takes place by means of a solvent-mediated chemical ionisation (CI) process, where a filament or discharge electrode is employed, or by an ionisation process which is enabled, and supported by a volatile buffer such as, for example, ammonium acetate, that is added to the eluent to improve positive ionisation.

While the number of reviews and papers reporting on TSP ionisation in environmental application had increased in the 1980s, the 1990s, with the development and commercial availability of interfaces using atmospheric pressure ionisation techniques, brought about a decrease in TSP publications. During this period TSP reviews covered applications in environmental analysis [6] in general or in the whole spectrum of polar pollutants [6, 198], while others reported on specific types of compounds or compound classes such as pesticides [22, 32, 199]. In addition strategies for the rapid characterization of organic pollutants in solid wastes and contaminated soils using LC-MS with TSP and other types of interfaces (PBI, ESI, and APCI) in combination with flow injection analysis and MS and MS/MS detection [71] were presented. Liu et al. [43] reported, in an overview, on current methodologies for determining sulfonated azo dyes in environmental waters elaborated by TSP, APCI, and ESI (ion spray) using LC-MS. TSP analyses of azo dyes were reviewed by Yinon et al. [200]. The unequivocal identification of isomers, oligomers and homologues of surfactants and their biodegradation intermediates in environmental samples at trace levels by LC-MS were also reviewed, with particular attention to thermospray (TSP) [23, 40] and ESI [40]. But the most comprehensive research work was done on pesticides, herbicides and fungicides, determined by TSP-FIA or LC-MS and MS/MS [22, 32, 199]. In accordance with the widespread use of these compounds in agriculture, papers dealing with the application of TSP ionisation were found in the literature.

Table 15.1 reflects the applications of TSP used as the interface to couple MS with different liquid chromatographic separation techniques in environmental analytical applications. A list from the literature is presented for different groups of compounds.

**Table 15.1** Environmental applications in LC-MS performed by thermospray interface (TSP).

<b>Topic</b>	<b>References</b>
<b>Reviews</b>	
General reviews	6, 198
Compound class specific reviews	
– Dyes	43, 200
– Pesticides	22, 32, 199
– Surfactants	23, 40
<b>Compound classes</b>	
– Dyes	28, 43, 113, 200–202
– Explosives	198, 203–206
– Polycyclic aromatic hydrocarbons	28, 207–209
– Surfactants	23, 28, 40, 210–234
– Toxins	235
<b>Pesticides (including herbicides, fungicides etc.)</b>	
– Anilides, quaternary amines, toluidines and thiocyanate compounds	175, 239–245, 248, 264, 501
– Carbamates	32, 108, 175, 239, 242, 244–257
– Organophosphorus compounds	166, 175, 176, 239, 242, 244, 247, 256, 259, 261–263, 287, 523
– Phenoxycarboxylic acids	176, 244, 264–269, 501
– Phenylureas, thioureas and sulfonylureas	175, 176, 239, 240, 242, 244, 246–248, 254–256, 270–272
– Triazines	94, 175, 176, 239, 240, 242, 244–247, 256, 266, 273–284
– Miscellaneous	266, 287–290
– Comparison of TSP interfaces with different types of interfaces	32, 40, 71, 94, 108, 113, 166, 175, 176, 199, 200, 205, 240, 257, 271, 275, 276, 311, 501, 503, 509, 523

### Dyes

Dyes, and especially azo dyes, compounds of environmental concern because of their carcinogenic potential, were studied with TSP-LC-MS [28, 201]. An overview presented current methodologies for determining sulfonated azo dyes in environmental waters using TSP [200]. Results obtained by LC-MS and capillary zone electrophoresis (CZE) MS, coupled with TSP-, APCI-, and ESI interface were discussed [43].

A standard commercial TSP interface was modified to increase the sensitivity to sulfonated azo dyes and to permit their analysis. The sensitivity could be increased in order to determine sub- $\mu\text{g}$  amounts of the dyes. A by-product of AZO 4 (2,2'-di-hydroxy-4-sulfonyl-6-nitro-1,1'-azobisisnaphthalene) which could not previously be identified by LC-MS, was then confirmed to be a structural isomer of AZO 4 [202].

Fourteen commercial azo and diazo dyes were characterised and analysed by three different LC-MS interfaces: the TSP-, PBI- and ESI interfaces. TSP-LC-MS mainly resulted in  $[\text{M}+\text{H}]^+$  ions with little fragmentation [111]. Aqueous solutions of the monosulfonated azo dyes with concentrations between 50 and 200 ppm were analysed by LC-MS coupled with TSP-, ESI- and APCI interfaces. TSP was

not as successful as ESI or APCI which gave more structural information. Loss of  $[Na]^+$  ( $\Delta m/z$  23 u) in the fragmentation proved to be common in all dyes.

### Explosives

TSP-LC-MS with explosives was one of the topics Arpino [198] presented when he reviewed the applications of TSP interfacing. General operating principles, optimisation strategies and possible ionisation mechanisms were presented.

TSP-LC-MS/MS was applied to qualitative analyses of explosives such as ethylene glycol dinitrate,  $\beta$ -cyclotetramethylene tetranitramine ( $\beta$ -HMX), cyclotrimethylene trinitramine (RDX), diethyleneglycol dinitrate, glycerol trinitrate, 2,6-dinitrotoluene (2,6-DNT), 2,4,6-trinitrotoluene (TNT), 2,4-dinitrotoluene (2,4-DNT), 3,4-dinitrotoluene (3,4-DNT) and pentaerythritol tetranitrate (PETN). Detection limits with excellent selectivity were in the pg range, discharge-on mode improved the sensitivity by a factor of 25 for dinitrotoluenes [203]. Nitroaromatic and nitramine explosives in water were quantitatively examined by HPLC with photodiode array detection (UV-DAD) and compared with TSP-LC-MS and LC-MS/MS (SIM and selected reaction monitoring (SRM)) in negative ion mode. MS quantitation limits were 10–100 ng L<sup>-1</sup>, presenting underestimated concentrations in SIM and SRM mode [204].

TSP-LC-MS in the negative mode was used to identify and quantify the explosives TNT, RDX and hexyl, as well as their degradation products and other pollutants, in groundwater samples of an ammunition hazardous waste site after SPE applying LiChrolut® EN. 31 compounds could be identified, such as nitramines and their by-products, TNT and partially nitrated toluenes, 1,3,5-trinitrobenzene and partially nitrated benzenes, aminonitrotoluenes, nitroanilines, hexyl and nitrophenols [205].

TSP-LC-MS and LC/NMR analyses were applied to characterise the phototransformation products of 2,4,6-trinitrotoluene generated by sunlight. Combined information from both analytical techniques allowed structural characterization of several acidic nitroaromatic compounds and some not commercially available photo-transformation products of TNT [206].

### Polycyclic aromatic hydrocarbons (PAH)

While PAHs with more than 3 rings are strong lipophilic compounds amenable to normal phase LC, their physicochemical or chemical degradation products are more or less polar compounds which enable the application of RP-LC in combination with TSP interfacing. Clench et al. [28] gave brief descriptions of the state of the art of TSP and some other mass spectral techniques in the analysis of PAHs, in addition to other pollutants of environmental concern. Benzo[a]pyrene (BaP) and its metabolites in air, 1,6-, 3,6- and 6,12-dione derivatives, were studied by TSP or APCI-LC-MS, after they had been extracted from particles. TSP ionisation in the negative mode yielded predominantly  $[M]^-$ ,  $[M-H_2O]^-$  or  $[M+CH_3COO]^-$ . TSP calibration graphs for BaP were linear at 10–1000, with detection limits of 1–20 ng

[207]. Negative ion spectra provided the richest information when spectra of hydroxylated metabolites (1–4 OH groups) include  $[M-H]^-$  ions, and fragments attributed to progressive dehydration were recorded [208]. The fragmentation of conjugated metabolites was found to be greater than predicted.

Primary and secondary photolysis products of pyrene, 1-hydroxypyrene or 1,6- and 1,8-pyrenequinones, respectively, in water and in Brij 35 micellar media were analysed and quantified by TSP-LC-MS [209].

### **Surfactants**

LC-MS methodologies applying TSP interfacing for unequivocal identification of isomers, oligomers and homologues of surfactants and their biodegradation intermediates in environmental samples at trace levels have been reviewed [28] very extensively [23, 40].

Trace amounts of alcohol ethoxylates (AOE) in diluted aqueous environmental samples were determined by TSP-LC-MS in sewage treatment plant (STP) effluents and river water which were spiked with a mixture of AEOs.  $[M+H]^+$  and  $[M+NH_4]^+$  ions were observed and highly branched AEOs could be distinguished from isomeric linear AEOs. The method could be validated [210]. Sum parameter analyses for the determination of different types of surfactants and their primary degradation products, methylene blue active (MBAS) and bismuth active substances (BiAS), were compared with substance-specific methods applying TSP combined with FIA, LC-MS and MS/MS. With MS methods, surfactants and metabolites could be determined quantitatively, while MBAS and BiAS methods failed [211]. Alkyl polyglucosides were followed in the biological wastewater treatment process (WWTP) and could be recognized as easily degradable [212], whereas fluorine-containing surfactants, non-ionics and anionics, were found to be very stable against biochemical and physicochemical treatment [213, 214]. Non-ionic fluorinated compounds with a hydrophilic moiety consisting of PEG chains could be biodegraded to shortened PEG chains carboxylated in the terminal position [213].

TSP methods were used for the determination of polar organic pollutants concentrated by SPE or liquid–liquid extraction [215]. TSP-FIA and LC-MS and -MS/MS methods were described for the qualitative and quantitative analysis of hardly eliminable or non-biodegradable polar compounds, such as surfactants in inflows and effluents from municipal biological wastewater treatment plants [215–224]. Non-ionic surfactants and their metabolites (primary degradation products) as well as anionic surfactants of linear alkylbenzenesulfonate type dominated the effluents. Parent and product ion scans or neutral loss scans in the TSP-MS/MS mode were applied to identify surfactants from WWTP [225] and in surface water samples from the river Elbe [226] and its tributaries [226–228]. Surfactants were observed even in drinking water after a soil filtration process and activated carbon treatment. Pattern recognition by TSP-FIA-MS and MS/MS was applied for confirmation [224, 229–231].

By LC-MS, retention time shifts which occurred because of surface-active compound adsorption on the analytical column could be confirmed. TSP was used

to monitor polar pollutants, predominantly several types of surfactants, in textile [232] and municipal wastewaters [233]. Results of biochemical [232, 233] and physicochemical [232] treatment for elimination were reported and precursor compounds and degradation products generated under these treatment steps were identified by CID. The treatment of recalcitrant wastewater constituents of the surfactant type by ozone ( $O_3$ ) or  $O_3$  combined with UV ( $O_3/UV$ ) [231, 234] or by hydrogen peroxide/UV [234] was examined and compounds arising were studied by MS/MS for identification [231, 234] and by biotoxicity testing (*Vibrio fisheri* and *Daphnia magna*) [231].

### Toxins

Only soft ionizing interfaces such as TSP [235], FAB [236–238] and API interfacing techniques (cf. 15.3.3.2 ESI, toxins) were able to handle thermolabile, polar seafood toxins that were classified, e.g., as amnesic shellfish-poisoning toxin, paralytic shellfish-poisoning toxin and as diarrhetic shellfish-poisoning toxin, according to the toxic results observed after ingestion.

### Pesticides (including herbicides, fungicides etc.)

Of all the organic pollutants measured by LC-MS in aqueous environmental matrices, e.g., drinking water, surface and groundwater, pesticides with the application of TSP ionisation became the most studied compound group. With the phasing-out of most chlorine-containing pesticides because of their persistence and their bio-accumulation potential the new generation of pesticides were designed to be more polar and therefore more biodegradable.

#### *Anilides, quaternary amines, toluidines and thiocyanate compounds*

Anilide-, N-substituted amine-, quaternary amine-, toluidine- and thiocyanate pesticides were not so often used and therefore papers reporting on these pollutants in the environment are quite rare.

A comprehensive paper by Volmer et al. [175] reported on these compounds and other types of pesticides. Residues of 19 amine- and anilide-pesticide derivatives (alachlor, allidochlor, bentazone, butachlor, carboxin, dimethachlor, oxicarboxin, metalaxyl, metazachlor, monalide, pendimetalin, pentanochlor, prochloraz, propachlor, propanil, tebutam, trifluralin) were readily identified, confirmed and quantified by TSP LC-MS and different ionisation techniques (APCI, ESI, FAB and PD) at  $< 100 \text{ ng L}^{-1}$  after  $C_{18}$ -SPE [175]. For propioanilide,  $C_{18}$  Empore<sup>®</sup> extraction from river water and spiked seawater was applied prior to detection [239]. In real environmental water samples from estuaries, metolachlor and the anilide alachlor could be confirmed by both LC-MS techniques, ESI and TSP [240]. The chemical and photochemical stability of metolachlor (2-chlor-6'-ethyl-N-(2-methoxy-1-methyl-ethyl)acet-o-toluidide) in organic-free water and lake water was determined by TSP-LC-MS. Sunlight degradation was found to be faster than chemical degrada-

tion, however, near-surface half-lives were determined with 22 d in summer and 205 d in winter. Photoproducts and four chemical dechlorination products were observed [241].

The effects of various additives on the sensitivity and selectivity of TSP-LC-MS of thiocyanates and anilines were studied to optimize ionisation conditions. Trialkylammonium formates were found to increase the selectivity and sensitivity of the TSP process [242]. TSP-LC-MS was also used for the characterization of the quaternary amine pesticides paraquat, difenzoquat, diquat, mepiquat and chlormequat from water and soil samples. Base peaks were  $[M+H]^+$  and  $[M-CH_3+H]^+$  [243]. Difenzoquat, a difficult-to-determine quaternary ammonium pesticide was analysed using a post-column ion-pair extraction system [244].

### *Carbamates*

Carbamates applied as insecticides were often observed in environmental samples because of their widespread use. They could be identified, confirmed and quantified after sample concentration by C<sub>18</sub> SPE by SIM-TSP at < 100 ng L<sup>-1</sup> according to the CEC drinking water limit. The interfacing techniques APCI, ESI, FAB and PD supported the elucidation of fragmentation mechanisms in TSP mass spectra [175]. TSP ionisation was evaluated for the LC-MS determination of 128 pesticides (containing 22 carbamates and 2 thiocarbamates besides 16 triazines-, 4 pyrimidine-, 3 triazole-, 2 pyridine-, 3 morpholine-, 1 N-substituted amide-, 12 aniline- and 1 di-nitroaniline, 24 organophosphorus, 15 phenylurea and 1 thiourea, 5 carboxylic, 8 phenoxy acid, 5 carboxylic ester and 4 quaternary ammonium pesticides) having a wide range of polarities. Detection limit, linearity and reproducibility data are given. Possibilities for the confirmatory analysis of carbamates were reported [245].

Besides those of other polar pesticides, mass spectra of carbamates were obtained from several surface and drinking water samples after on-line concentration on a precolumn prior to TSP-LC-MS [246].  $[M+H]^+$  or  $[M+NH_4]^+$  of the pesticides were observed as base peaks [244] [247]. In negative mode, fragments such as  $[M-CO NHCH_3]^-$  were observed for carbamates [244]. A multi-residue TSP-LC-MS method was described for carbamates and thiocarbamate pesticides in water samples after C<sub>18</sub>-SPE [248]. After concentration on C<sub>18</sub> Empore® disks carbamates from river water and spiked seawater samples at concentration levels of 0.25, 25 and 1000 µg L<sup>-1</sup> were determined by LC-UV and confirmed by TSP-LC-MS (detection limits: 2–20 µg L<sup>-1</sup>) [239]. The results obtained for the analysis of the N-methylcarbamate pesticides methomyl, aldicarb, aldicarb sulfoxide, aldicarb sulfone, carbaryl, methiocarb, carbofuran, and 3-hydroxycarbofuran by LC-MS in combination with the non-API interfaces TSP and PBI were compared with the results of API interfacing (ESI and APCI) [108]. The TSP interface performed well, and TSP in the SIM mode resulted in detection limits of a few ng, offering a viable method for confirmation at the regulatory level of about 0.1 ppm. The main problem with TSP interfacing was signal stability [108]. With emphasis on N-methylcarbamates the performances of on-line MS detection coupled to SPE and LC were

reviewed when TSP interfaces besides PBI or ESI ionisation were applied [32]. Automated on-line SPE followed by LC techniques for monitoring carbamates and their transformation products in traces in well waters were investigated TSP-LC-MS with time-scheduled SIM could be used for confirmation [249]. Pollution by carbamate pesticides and metabolites was sporadic and exceeded the limit of  $0.5 \mu\text{g L}^{-1}$  for total pesticides allowed by the EEC Drinking Water Directive. The main toxic metabolites of carbamates, 3-hydroxycarbofuran and methiocarb sulfoxide [249], should be included in future monitoring programs. Comparing the results of TSP and ESI ionisation in SIM modes for the quantitative determination of 10 carbamate pesticides, quite different in polarity, made obvious that ESI was 10–150 times better than using TSP ionisation [250].

The effects of coeluting carbamate pesticides carbofuran, propoxur and pirimicarb combined with ion formation suppression under TSP-LC-MS conditions were discussed applying multivariate curve resolution and ranking analysis [251].

The use of different eluents in LC-RP separations was examined to optimize LC separation and determination of carbamates besides other pesticides by TSP-LC-MS [244]. The effects of additives on LC separation and of the vaporizer temperature on ion formation in TSP-FIA-MS analysis were studied for *N*-methylcarbamate [252], carbamates [242] and (thio)carbamates [242] pesticides. A strong reduction in abundance of the characteristic ions  $[\text{M}+\text{H}-\text{CH}_3\text{NCO}]^+$  and  $[\text{M}-\text{H}-\text{CH}_3\text{NCO}]^-$  for methiocarb and its sulfoxide were found because of thermal degradation at  $90^\circ\text{C}$  which made quantitation difficult [252]. The addition of trialkylammonium formates increased selectivity and sensitivity, detection limits being  $< 20 \text{ ng}$  in full scan mode [242].

An interlaboratory examination quantifying 16 carbamate pesticides from four classes was performed applying three commercially available TSP interface types. In contrast to several literature reports very similar spectra were obtained, however, thermally labile carbamates gave varying results [253]. In an interlaboratory study with nine participating laboratories a TSP LC-MS method was evaluated to determine three *N*-methylcarbamates, three *N*-methylcarbamoyloximes, two substituted urea pesticides and one carbamic acid ester. Data confirmed that interlaboratory variation was greater than that within labs [254]. The multiresidue method for determining 19 thermally labile and non-volatile carbamate pesticides in fruits and vegetables published by Liu et al. [255] involved a single extraction step followed by TSP-LC-MS(+/−) (SIM). Limits of detection in apples, beans, lettuce, peppers, potatoes and tomatoes were observed with 0.025–1 ppm and recoveries ranged from 69–110% [255].

The carbamate pesticides aldicarb, carbaryl and their degradation products, all under research in photochemical degradation studies, were characterised by TSP-LC-MS and MS/MS. A tentative photodegradation pathway for the different pesticides in water was postulated [256].

The degradation of the carbamates carbofuran and methiocarb in estuarine waters was compared with that of aqueous samples exposed to UV light in the laboratory. TSP- and ESI-LC-MS were used for product monitoring and identification of degradation products. The predominant degradation pathways observed here,

however, were hydrolytic and microbial degradation [257]. Tap water was analysed for thiobencarb degradation products as a result of chlorination. Several compounds were determined [258].

#### *Organophosphorus compounds*

Besides TSP-spectra from organophosphorus and different groups of polar pesticides, APCI, ESI, FAB and PBI spectra were presented. CID allowed the identification of pesticide residues and the confirmation and quantification of these compounds by TSP at concentrations  $< 100 \text{ ng L}^{-1}$  [175]. Barceló et al. [239] extracted river water and spiked seawater samples by C<sub>18</sub> Empore® disks to concentrate organophosphorus pesticides prior to identification and quantification while Bagheri et al. [247] for the same purpose used on-line SPE for phosphorus pesticides and TSP-LC-MS.

After aircraft spraying, levels of temephos and its degradation products, i.e., temephos sulfoxide and isomers, were determined by TSP-LC-MS in extracts of water samples with detection limits of 1–2 ng and mean recoveries of 80%. Temephos sulfoxide and its isomers were measured [259]. To improve the determination of TSP-LC-MS for polar organophosphorus pesticides, trialkylammonium formates were found to increase selectivity and sensitivity with detection limits of  $< 20 \text{ ng}$  even in full scan mode [242]. The use of different eluents in RP separations was examined for an optimized separation and determination of organophosphorus pesticides and their biodegradation products by TSP-LC-MS [244]. Different adduct ions were formed ( $[\text{M}+\text{NH}_4]^+$  or  $[\text{M}]^-$  and  $[\text{M}-\text{R}]^-$  ( $\text{R} = \text{Me}$  or  $\text{Et}$ )) depending on the eluent used. Under normal phase (NP) conditions eluents enhanced the response in some cases and provided more structural information [244]. Ion chromatography (IC) coupled with TSP-MS/MS was compared with an ESI interfaced IC for the determination of ionic compounds in agricultural chemicals. The solid-phase suppressor applied allowed methyl phosphate and methyl sulfate determination [260]. Lacorte et al. described a TSP-LC-MS method for quantitative determination of 10 organophosphorus pesticides and their photolytic transformation products in river waters [261] and in estuarine waters [262]. For quantification  $[\text{M}+\text{H}]^+$  and  $[\text{M}+\text{NH}_4]^+$  or  $[\text{M}+\text{CH}_3\text{CN}]^+$  were used in the positive mode, while  $[\text{M}-\text{H}]^-$  and  $[\text{M}+\text{HCOO}]^-$  were used under negative ionisation. The limit of detection was found to be  $0.01\text{--}0.1 \mu\text{g L}^{-1}$ . TSP-LC-MS was used also for the characterization of the organophosphorus pesticides fenitrothion and parathion-methyl and their degradation products after photolysis [256]. TSP-LC-MS in the positive mode was also applied to study the anaerobic aquatic metabolism of the <sup>14</sup>C-pyrimidinyl-tebu-pirimphos. S-ethyl isomers as metabolites were identified [263].

#### *Phenoxycarboxylic acids*

Isolation and trace enrichment in off-line and on-line modes were described together with TSP-LC-MS determination of the spiked phenoxy acetic acid herbicides 2,4-dichlorophenoxy acetic acid (2,4-D), 4-chloro-2-methylphenoxy acetic acid

(MCPA), and 2-(4-chloro-2-methylphenoxy)propionic acid (MCPP) in estuarine waters [264]. Chlorinated phenoxy acids were identified in Rhine water after ion-pair LC on-line with TSP-LC-MS detection [265]. Liquid–liquid extraction was applied to concentrate chlorinated phenoxy acids, triazines and amphoteric pesticides from water samples prior to TSP-LC-MS [266]. FIA-TSP-MS/MS was used as a fully automated screening method for phenoxy acid herbicides in water samples at the low  $\mu\text{g L}^{-1}$  levels without sample concentration [267]. The optimization of RP-separation combined with TSP-LC-MS for phenoxy acid analysis in negative mode was studied [244]. Samples with eight chlorophenoxy carboxylic acid herbicides were analysed by Geerdink et al. [268]. Selectivity of measurement was studied using 2,4,5-trichlorophenoxyacetic acid (2,4,5-T), and triclopyr, which differs in just one mass unit. Screening of surface water samples spiked at the  $1 \mu\text{g L}^{-1}$  level was easily achieved without analyte concentration and a minimum of sample clean-up [268]. An interlaboratory comparison of TSP and PBI-LC-MS for the analysis of 10 chlorinated phenoxy acid herbicides was evaluated in seven laboratories by TSP and PBI. Sample extracts were analysed for 2,4-D, 2,4-DB, MCPA, MCPP, 2,4,5-T, dinoseb, dalapon, 2,4,5-TP, dicamba, 2,4-DB and 2,4,5-TP. Statistically significant differences were found between interfaces. PBI generally had better precision than TSP, however, for the quantitative analysis of low levels, TSP in the negative ion mode should be preferred [87]. The anaerobic degradation of the herbicide picloram, a 4-amino-3,5,6-trichloropyridine-2-carboxylic acid, in anoxic freshwater sediments was examined by Ramanand et al. An intermediate and its recalcitrant metabolite were separated and analysed by NMR and TSP-LC-MS [269].

#### *Phenylureas, thioureas and sulfonylureas*

Volmer et al. studied phenylureas and sulfonylureas by TSP-LC-MS after sample concentration by C<sub>18</sub> SPE [175]. 15 phenylurea- and 1 thiourea pesticides besides 112 polar pesticides from other pesticide classes were examined by TSP ionisation, detection limits and TSP mass spectra of these polar compounds were presented [245]. Besides other polar pesticides, the phenylurea pesticides isoproturon and diuron were on-line concentrated on a precolumn from several surface and drinking water samples and then determined by TSP-LC-MS [247]. A multi-residue TSP-LC-MS method was published by Moore et al. for the determination of the urea pesticides chlortoluron, diuron, isoproturon, and linuron in water samples after C<sub>18</sub>-SPE [248]. C<sub>18</sub> Empore® disks were applied to concentrate phenylureas from river water and spiked seawater samples prior to TSP-LC-MS. Detection limits of 2–20  $\mu\text{g L}^{-1}$  and recoveries between 80 and 125% were observed [239]. TSP-LC-MS (SIM) in the positive mode allowed determination of the urea pesticides chlorbromuron, diuron, linuron, metobromuron, monuron, neburon in apples, beans, lettuce, peppers, potatoes and tomatoes with detection limits of 0.025–1 ppm [255]. 20 other polar pesticides, linuron, which was under suspicion of being a dietary oncogenic risk (US Natl. Res. Council) was determined by TSP-LC-MS a single rapid procedure in vegetables with detection limits of 0.05–0.10 ppm [270]. TSP-LC-MS and ESI were used in a multi-residue method for determination of the sul-

fonlylurea herbicides chlorsulfuron and the methyl esters of sulfometuron, metsulfuron, tribenuron, bensulfuron, chlorimuron and primisulfuron. Both TSP and the ESI interface provide mass spectra with three structure-significant ions necessary for unambiguous identification in environmental samples [271]. The validation of the enzyme immunoassay for the herbicide triasulfuron in soil and water samples was performed by means of TSP-LC-MS. Immunoassay results compare favourably with LC-MS ( $r=0.88$ , in soil) but have a lower detection limit of 0.05 ppb (water) and 0.10 ppb (soil) [272]. Phenylurea pesticides were examined by TSP-LC-MS after on-line SPE [246] while in parallel the use of different eluents [244] or the effects of additives to LC separation [242] were studied. Compounds could be recorded as base peak in positive ion mode as  $[M+NH_4]^+$  adduct ions [244]. When TSP-LC-MS was applied in order to characterise the phenylureas (chlortoluron, isoproturon, diuron, linuron and diflubenzuron) in estuarine waters  $[M+H]^+$  was generally the base peak [240]. Compared with a parallel applied ESI ionisation TSP results were not satisfactory.

In an interlaboratory study with nine participating laboratories a TSP-LC-MS method was evaluated in order to determine diuron and linuron. Depending on the compounds, the intralaboratory precisions range from 6.5–33 with a relative standard deviation (RSD) of 1% [254]. After linuron had been submitted to photochemical degradation, TSP-LC-MS and MS/MS was used to characterise the degradation products. A tentative photodegradation pathway for the different pesticides in water was postulated by Durand et al. [256].

### *Triazines*

Triazine derivatives and their de-alkylated or hydroxylated degradation products were studied by LC-UV or TSP-FIA-MS/MS after isolation and trace enrichment by liquid–liquid extraction [266], SPE cartridge extraction [246] [273] or by C<sub>18</sub> Empore® extraction disks [239]. Optimization of SPE procedures influenced the quality of the FIA MS/MS spectra [273]. Recoveries for the atrazine metabolites were found to be only 3–17% if Empore disks were applied [239]. Comprehensive research was published by Volmer et al. who determined 13 [175] or 16 [245] triazines and N-heterocyclic pesticides, which were readily identified, confirmed and quantified by TSP according to the CEC drinking water limit at < 100 ng L<sup>-1</sup> by time-scheduled SIM. Several surface and drinking water samples were analysed in the SIM mode and low levels of simazine and atrazine with detection limits of 2–90 ng L<sup>-1</sup> in the course of an on-line low-level screening of polar pesticides in drinking and surface waters [247]. Triazines and other pollutants in river water samples were also determined at low- to sub- $\mu$ g L<sup>-1</sup> levels in a full automated SPE-LC-MS using TSP or PBI ionisation [94]. The analysis of 12 triazines and 11 of their biodegradation products was achieved by multiple reaction monitoring in the FIA-MS/MS mode [274]. Detection limits for triazines and hydroxylated degradation products were 0.5–0.15  $\mu$ g L<sup>-1</sup> and 0.2–0.45  $\mu$ g L<sup>-1</sup> water, respectively [274]. The occurrence of hydroxylated degradation products of atrazine in the stream water from Goodwater Creek watershed was determined by TSP-LC-MS and ESI-

LC-MS/MS. The proportions of the different degradation products were observed with 100% for hydroxy-atrazine, 25% for deethylhydroxy-atrazine and 6% for deisopropylhydroxy-atrazine, with concentration ranges of  $\mu\text{g L}^{-1}$  [275]. A SPE method was described for the preconcentration of atrazine and its metabolites from water samples by RP-C<sub>18</sub> or on a benzenesulfonic acid cation exchange support prior to TSP-LC-MS [276]. The qualitative and quantitative analysis of triazines and their metabolites in environmental samples by selecting different eluents in LC-RP separations [244] or various operating modes in TSP-LC-MS/MS was examined [277]. Studies of degradation products in polluted soil samples and after aquatic photodegradation were also carried out [277]. Chlorotriazines and their hydroxylated metabolites recorded in TSP-MS(+) mode resulted in [M+H]<sup>+</sup> base peaks despite the presence of ammonium acetate. The same results were observed when TSP-LC-MS was applied to the characterization of the triazines atrazine, simazine, ametryne, cyanazine, deethylatrazine and desopropylatrazine and triazine metabolites in estuarine waters after TSP ionisation [240]. The effects of various mobile phase additives on the sensitivity and selectivity of TSP-LC-MS for the determination of 55 polar pesticides were studied to optimize conditions [242]. With the addition of trialkylammonium formates selectivity and sensitivity could be increased [242].

TSP was also used for the characterization of triazines and their degradation products after physicochemical and chemical degradation experiments. Cyanazine was monitored after photolysis [256] whereas atrazine and simazine and their degradation products were determined by TSP-MS and -MS/MS after ozonolysis [278]. The main degradation pathways observed were dealkylation, deamination, dehalogenation and hydroxylation [256, 278]. The photodegradation pathways of atrazine by dealkylation reactions were also observed by Schmitt et al. [279] applying capillary electrophoresis in combination with TSP-MS and MS/MS. LC-MS/MS was applied to screen and characterise chlorotriazines and hydroxytriazines as degradation products after ozonolysis in aqueous solutions with the help of product and parent ion scans [280]. The kinetics and mechanism of the chemical oxidation of prometryn and prometryne, terbutryne, ametryne and desmetryne by NaOCl [281], or HClO and ClO<sub>2</sub> [282], respectively, were studied. Intermediates formed after NaOCl treatment in the sequence R-S-CH<sub>3</sub> (R = prometryn), R-SO-CH<sub>3</sub>, R-SO<sub>2</sub>-CH<sub>3</sub>, R-O-SO<sub>2</sub>-CH<sub>3</sub>, were identified by TSP-LC-MS after SPE and confirmed by synthesis [281]. All triazines reacted in the same way, reactions with HClO occurring much faster than with ClO<sub>2</sub> giving the sulfoxide, sulfone and the sulfone hydrolysis product. Reactions with ClO<sub>2</sub> gave only the sulfoxide. A general pathway for the oxidation of these triazines was proposed [282]. TSP-LC-MS was used to confirm three highly polar metabolites of the triazine herbicide hexazinone in SPE-extracts of soil and vegetation, using SIM of the protonated molecular ions [283]. A SFE method using CO<sub>2</sub> containing different modifiers was described for the extraction of atrazine and its polar metabolites from sediments, followed by identification and quantification by TSP-LC-MS [284]. Extraction mixtures which contained strong nucleophiles (MeOH; H<sub>2</sub>O; triethylamine) caused significant or total degradation of atrazine.

### Miscellaneous

TSP ionisation was also applied for the analyses of fungicides. After the isolation and trace enrichment of captan, captafol, carbendazim, chlorothalonil, ethirimol, folpet, metalaxyl and vinclozolin on C<sub>18</sub> Empore® disks from drinking, river and estuarine water samples TSP-LC-MS analysis was performed but only carbendazim, ethirimol and metalaxyl could be analysed by LC-MS [285].

Surface water was analysed for about 300 pesticides and organic compounds [286]. When LC-MS/MS was applied the fungicide dichloran and bacterial transformation products from a chemostat system could be observed. Some more non-common pesticides were examined under application of TSP-LC-MS. So 2 C<sub>18</sub> and 2 XAD resin cartridges were used to examine the recoveries of thermally labile pesticides from water. Compounds under research were benazolin, bromofenoxim, ethofumesate, fenamiphos and phenmedipham. Recoveries were highest (>85%) with C<sub>18</sub> with detection limits of 1–10 ng (TSP full scan) and 60–800 pg (SIM) [287]. TSP-LC-MS was applied for determination and identification of the insecticide imidacloprid which was present as residue in vegetables at 0.01–0.60 mg kg concentrations [288]. TSP-LC-MS was used to confirm positive LC-UV results (>0.05 ppm) of the insecticide hydramethylnon from extracts of pasture grass samples [289].

After a comprehensive extraction procedure the triazolopyrimidine herbicide metosulam could be determined in soil samples by LC-UV and TSP-LC-MS with excellent agreement between the methods [290].

#### 15.3.3.2 Atmospheric Pressure Ionization Interfaces (API)

##### Applications using atmospheric pressure chemical ionization interface (APCI)

In parallel with the routine application of TSP the improvement in the handling of the atmospheric pressure ionisation (API) techniques for coupling LC with MS in environmental analysis proceeded. During the last decade of the last century, the dissemination of this interfacing technique grew tremendously with the up-coming demand for low detection limits in the analysis of polar organic pollutants of concern present in the environment in very low concentration ranges.

Two different types of API interfaces came into routine use for coupling LC and MS, the atmospheric pressure chemical ionisation (APCI) interface and the electrospray (ESI) or ion-spray interface. Both interfaces ionise outside the mass spectrometer at ambient pressure before the ions enter the high-vacuum mass analyser region. To enter into the high vacuum region of the MS the ions generated at ambient pressure have to pass a very small orifice. This process and the different techniques applied from the different commercially available interfaces were extensively described by Slobodnik et al. [22] when they applied this interfacing technique to the analysis of polar pesticides. This ionisation process is supported by nebulisation which is performed pneumatically in the APCI process or, for ESI, by means of a strong electrical field, while ion-spray uses both nebulisation techniques. Ion spray ionisation can be termed a combination of both, pneumatic neb-

ulisation and in parallel nebulisation by means of an electrical field. The formation of the spray and the ionisation of the compounds were described extensively [22].

The main distinctions between both interface types were the flow rates and the molecular weight ranges that could be handled. In the start of API, it was possible to have high flow rates ( $2 \text{ mL min}^{-1}$ ) compared to the small flows ( $20 \mu\text{L min}^{-1}$ ) amenable to ESI interfacing. The application of heat and pneumatic nebulisation for APCI ionisation allowed the handling of the  $0.1\text{--}2.0 \text{ mL}$  LC-elutents of RP separations. With the invention of ion spray the disadvantage of low flow rates combined with ESI disappeared because flow rates could be increased. The most important advantage of ESI, however, is its capacity for handling very polar organics with molecular weights of 100 up to  $> 100,000 \text{ Da}$ , with which this interface also grew to be the work-horse of analytical protein chemists.

The application of MS/MS or in-source-CID for identification of pollutants brought problems, since no product ion libraries were available. Product ion spectra either had to be interpreted for compound identification or standard comparison had to be performed provided that standards were available. To overcome this disadvantage, analysts prepared their own libraries suitable for the instrument generated on or for instruments of the same type. Attempts at generating mass spectral libraries for polar compounds determined by API methods were reported and the results obtained with their application in real environmental samples were discussed [291, 292]. The generation of IT-MS<sup>n</sup> product ion spectra and their use for identification provided the most promising results so far. The preparation of a universally applicable product ion library for the identification of polar compounds, i.e. of a library which could work with various equipments for identification, still remains wishful thinking.

A series of surveys and reviews [28, 44, 45, 293] dealt with the simultaneous determination of a broad range of polar compounds in environmental samples by API interfaces. Possibilities and limitations of structure elucidation by LC-ion trap multiple mass spectrometry (LC-ITMS<sup>n</sup>) were the topic overview [38]. As shown later, pesticide residue analysis was the most frequent application of LC-MS in water sample analysis, as the number of review articles on the subject of pesticide analysis and their degradation products demonstrates [20, 22, 29, 30, 32, 199, 294]. The analysis of dyes by means of API interfacing techniques was reviewed by three groups [43, 161, 200], while the LC-MS analysis of surfactants, as compounds of environmental concern, was comprehensively reviewed [21].

In Tab. 15.2 the applications of APCI used as interface to couple MS in environmental analytical applications are listed, specified for different groups of compounds.

### Drugs and diagnostic agents

The use of APCI for the analysis of drugs or their metabolites in environmental samples is not yet as common as for ESI applications (cf. 15.3.3.2 ESI, drugs). Predominantly aqueous samples, e.g., effluents of STPs or wastewaters from pharmaceutical industry were studied. Surface and groundwater samples were also under

**Table 15.2** Environmental applications in LC-MS performed by atmospheric pressure chemical ionization interface (APCI).

<b>Topic</b>	<b>References</b>
<b>Reviews</b>	
General reviews	28, 44, 45, 293
Compound class specific reviews	
– Dyes	43, 161
– Pesticides	20, 22, 29, 30, 32, 199
– Surfactants	21, 24, 39–41
<b>Compound class applications</b>	
– Drugs and diagnostic agents	292, 295, 296
– Dyes	28, 43, 161, 201, 297
– Estrogenic compounds	298–301
– Explosives	205, 291, 302
– Haloacetic acids	303
– Polycyclic aromatic hydrocarbons	28, 207, 304–314, 394
– Phenols	315–320, 323
– Sulfonic acids	297
– Surfactants	226, 326–328, 330–346, 479
– <b>Pesticides (including herbicides, fungicides etc.)</b>	
– Anilides, quaternary amines, toluidines and thiocyanate compounds	175, 260, 320, 323, 347–352, 385
– Carbamates	108, 175, 320, 325, 353–360
– Organophosphorus compounds	175, 320–322, 324, 353, 354, 360–368, 370–372, 385
– Phenoxy carboxylic acids	176, 320, 325, 348, 361
– Phenylureas, thioureas and sulfonylureas	175, 320, 322, 325, 350, 351, 353, 354, 358, 361, 373–385
– Triazines	175, 260, 320, 323–325, 350, 351, 353, 354, 361, 362, 368, 374–377, 382, 385–387, 389, 390
– Phenolic compounds	320–325
– Antifouling pesticides	324, 368, 377, 378
– Miscellaneous	324, 358, 384, 391–394
– <b>Comparison of ESI interfaces with different types of interfaces</b>	6, 20–22, 28, 29, 32, 43, 71, 108, 155, 161, 175, 176, 185, 199, 205, 291, 297–300, 311, 317, 320, 322, 325–327, 334, 340, 346, 347, 351, 353, 355, 357, 358, 361, 373, 374, 381, 385, 389, 390, 394

research, because drugs and their degradation behavior in the environment have attracted the attention of environmental chemists and the public. With the exception of wastewaters from pharmaceutical industry the water samples contained low concentrations of compounds of concern. Pre-concentration was necessary prior to RP-LC. Methods for the determination of drug residues in water samples by means of APCI-LC-MS or -CE-MS were elaborated and applied to river water samples. Pharmaceuticals such as naproxen, bezafibrate, diclofenac, ibuprofen or their degradation product clofibrat acid were determined (cf. 15.3.3.2 ESI, drugs) [295]. As drugs were observed in municipal wastewaters or in industrial effluents, APCI and ESI-FIA- and LC-MS and MS/MS besides GC-MS were applied to follow

polar and nonpolar organic pollutants (e.g. drugs, their precursor compounds from synthesis and biochemical degradation products generated during wastewater treatment process). An extraction and concentration scheme, MS and MS/MS spectra of pharmaceuticals were presented [296]. Baumann et al. [292] also elaborated a library of APCI and ESI product ion mass spectra of steroids, morphine and drugs of abuse based on wideband excitation in an ion trap mass spectrometer. The spectra were applied to compare results with results obtained from urine, forensic and blood samples.

### Dyes

The number of applications dealing with the analysis of dyes for APCI-interfaced MS analysis is small despite azo dyes being compounds of environmental concern because of the carcinogenic potential of their degradation products [297]. ESI was used predominantly [161] because an increased tendency of fragmentation under APCI was observed [201] and therefore a more widespread analytical dissemination could be observed by applying ESI for the determination of these very polar compounds (cf. 15.3.3.2 ESI, dyes). An overview covering the extraction and pre-concentration of dyes from water using SPE was presented together with the current LC-MS methodologies which were coupled with APCI, ESI and TSP to the MS for determining sulfonated azo dyes in environmental waters. Capillary zone electrophoresis (CZE) coupled with MS was also discussed [43]. The application of APCI, ESI, PBI or TSP interfaced to LC-MS was discussed when determinations of dyes in environmental matrices were reported [28] and results from the analysis of sulfonic compounds and sulfonated azo dyes using APCI and ESI-LC-MS were reported. Non-volatile TBA ion pairing agents which were removed on-line prior to MS analysis improved separation [297].

### Estrogenic compounds

With increasing sensitivity and decreasing detection limits estrogenic compounds, present in very low concentrations in environmental samples, have become an emerging area of concern. For the determination of metabolites of natural and synthetic estrogens LC-MS is the method of choice, whereas for the analyses of the precursors GC-MS without derivatization or after silylation of the analytes should be favoured. The analysis of 17 $\beta$ -estradiol in the aquatic environment was examined extensively using APCI or ESI-LC-MS (cf. 15.3.3.2 ESI, estrogens) [298]. The estrogens estrone, 17 $\beta$ -estradiol, estriol and 17 $\alpha$ -ethinylestradiol were analysed in raw and treated wastewaters after C<sub>18</sub> SPE [299, 300] and the number of compounds analysed was extended to a total of 10 estrogens and progesterons [301]. APCI(+) ionisation and ESI were applied after RP separation but MRM (multiple reaction monitoring) detection was essential to improve selectivity.

### **Explosives**

Contaminated sites from ammunition production during World War II are often heavily polluted by explosives and their metabolites. Both, precursor nitro compounds and metabolite amino compounds are mobile in the ground and may reach drinking and groundwaters. The API interfaces APCI and ESI were used to compare and to confirm TSP-LC-MS(-) results for the identification of pollutants in ammunition hazardous waste sites (cf. 15.3.3.2 ESI, explosives). 31 compounds could be identified in water samples after SPE using LiChrolut® EN. The precursor compound TNT and partially nitrated toluenes, 1,3,5-trinitrobenzene, nitramines and their by-products were found (cf. 15.3.3.1 TSP, explosives) [205]. 1,3,5-trinitro-1,3,5-triazacyclohexane (RDX) and the nitroso-RDX metabolites were determined by APCI-LC-MS in groundwater samples after SPE (Sep-Pak Porapak RDX). The advantage of APCI was to provide a 20-fold greater signal for nitroaromatics than ESI, whilst ESI produces a 5-fold increase in response for nitramines [302]. As the determination and identification of pollutants emitted from ammunition production and disposal became more and more important a list of compounds examined and available as EI-MS or API-MS (ESI and APCI) spectra, e.g. explosives and pesticide residues, in environmental samples was published by Schreiber et al. [291]. The limits of the application of these libraries for identification were elucidated and discussed.

### **Haloacetic acids**

In the disinfection process of drinking water, besides other chlorinated compounds, halogenated carboxylic acids arise. For quality control of drinking water the determination of these contaminants was established using LC-MS with a preference for ESI (cf. 15.3.3.2 ESI, haloacetic acids). An application of APCI-MS for haloacetic acid analysis was reported after CE separation in a non-aqueous medium [303].

### **Polycyclic aromatic hydrocarbons (PAH)**

PAHs, contaminants of public concern because of the carcinogenic potential of benzo[a]pyrene and some of their homologues preferentially, were determined by LC with fluorescence detection. The chemical or biochemical degradation products, however, being more polar and hardly detectable because of missing knowledge about their characteristic, highly specific excitation and emission wavelengths were determined by APCI-LC-MS and MS/MS.

Basic research work was performed to establish a method for the determination of PAHs and their hydroxylated degradation products, standard mixtures of hydroxy PAHs were determined qualitatively and quantitatively by APCI and ESI-LC-MS. Under S/N = 3:1 conditions detection limits of 0.3–50 µg mL<sup>-1</sup> were obtained in APCI mode whereas ESI ionisation was less sensitive (cf. 15.3.3.2 ESI, PAH) [304]. The whole spectrum of PAHs determined according to EPA protocol were analysed in solid waste by APCI-LC-MS(+) and HPLC with fluorescence detection after liquid–liquid extraction, however, determination was disturbed by methylated PAH [305]. A capillary column SFC was interfaced by APCI to an

MS detector and PAH analysis was performed with a heated pneumatic nebulizer. CO<sub>2</sub> was used as the mobile phase to determine benz[a]anthracene, constituents of a pond sediment contaminated with coke oven residues and of a standard mixture of PAHs. Detection limits observed were 40 pg for the [M+H]<sup>+</sup> ion of chrysene (S/N=2) [306]. APCI-LC-MS/MS was performed to identify and to differentiate isomeric PAHs in coal tar [28, 307]. Fragment ion spectra were presented and peak area ratios were found to be a reliable indicator for isomeric differentiation [307]. In a short overview the state of the art of various mass spectrometric techniques applied to environmental analysis of PAHs in natural matrices was given and the application of different types of interfaces, APCI, ESI, PBI and TSP, was compared and described [28]. Thirty one oxidized PAH derivatives containing up to five condensed aromatic rings and carrying different functional groups (e.g. carboxyl, dicarboxylic anhydride, lactone, hydroxyl and carbonyl) were characterised by APCI-LC-MS/MS in the positive and negative mode applying in-source CID with four different fragmentor voltages. APCI-LC-MS allowed the investigation of PAHs at trace levels [308]. After ozone treatment of 29 PAHs the compounds and their degradation products, benzo[a]pyrene-4,5-dione and 4-oxa-benzo[d,e,f]-chrysen-5-one were characterised from retention by comparison to reference standards and APCI-LC-MS data [309]. APCI-LC-MS and GC-MS were applied to determine and to identify polar products from the ozonolysis of benzo[a]pyrene. Atmospheric degradation by ozone was simulated and BAP ozonolysis products determined as mainly quinones and carboxylic acids resulting from oxidative ring opening reactions [310]. Benzo[a]pyrene and its degradation products (metabolites or physicochemical) in air were studied [207] by APCI- and TSP-LC-MS. APCI ionisation yielded mostly [M]<sup>-</sup> and [M-H]<sup>-</sup> ions (TSP: [M]<sup>-</sup>, [M-H<sub>2</sub>O]<sup>-</sup> or [M+CH<sub>3</sub>COO]<sup>-</sup>). The 1,6-, 3,6- and 6,12-dione derivatives from oxidative BAP degradation were detected adsorbed on air particulates [311]. APCI-LC-MS was also applied to characterise PAHs with high-molecular masses (> 300 Da) in air filters and in biological material (zebra mussels) after extraction with dichloromethane and MeOH. Mass spectra and ion chromatograms showed similar profiles for the different samples. Results suggest that these PAHs contained in coal tar and air particulates were accumulated in tissues of zebra mussel [312]. The determination of PAHs by ELISA kits for the determination of PAHs among the organic analytes in various industrial effluents were examined and confirmed by APCI-LC-MS. Unequivocal identification of ELISA positive target analytes was obtained. The advantages and limitations of the three RAPID-magnetic particle-based ELISA kits were reported [313]. Heteroatoms (N, S, O, P) substituted were analysed in samples of a pond sediment contaminated by coke-oven residues by APCI-LC-MS/MS. The S-containing heterocyclic compounds were identified by SRM and quantified [314].

### Phenols

Many phenolic compounds were applied as pesticides because of their toxicity, especially against insects. For the follow-up of these compounds in waters GC-MS was the method of choice, but some LC-MS methods were also established

for analysis [315–319]. Molecular ions were observed under negative APCI or ESI ionisation after RP-LC and SPE. APCI was found to be more effective than ESI [317]. The endocrine disruptor compounds, the Bisphenol A, nonyl- and octylphenols, as industrial chemicals with high production rates or as metabolites of non-ionic surfactants had also been analysed by LC-MS, however, detection limits were poor compared to GC-MS. In a study with automated on-line SPE-APCI-MS was observed to be more sensitive for nitrophenolic pesticides (e.g. dinoseb, 4-nitrophenol and dinoterb) than the application of PBI. Limits of detection were reported [320]. The degradation of pentachlorophenol (PCP) in natural waters was studied by LC-DAD and confirmed by APCI-LC-MS both after Lichrolut EN SPE. A half-life of PCP in ground water, in estuarine and river waters of < 2 h was reported [321]. A test mixture of 17 pesticides also containing the nitrophenol pesticide trifluralin was used to develop a quantitative on-line SPE-LC-MS and MS/MS method using APCI or ESI interfaces [322]. While trifluralin was not detected by ESI, detection limits ( $S/N=3$ ) with APCI were observed with  $3.0$  or  $0.2 \mu\text{g L}^{-1}$  in full scan or SIM mode, respectively. In a monitoring study of priority pesticides and other organic pollutants in river waters from Portugal using GC-MS and APCI-LC-MS [323, 324] besides other pesticides the phenolic compounds 2,4,6-trichlorophenol, pentachlorophenol, 2,4-dichlorophenol and the 2-, 3- or 4-mono chlorophenols were determined in the negative ionisation mode [324]. Baglio et al. [325], however, observed that APCI was not as effective in the ionisation of 2-methyl-4,6-dinitrophenol as pneumatically assisted ESI (ion spray) when they studied standard solutions of the pesticide mixtures.

### **Surfactants**

From the application of surfactants in household, handicraft and industry a large quantity of these compounds have been discharged with wastewaters and despite biological treatment considerable quantities of them have reached the environment. Therefore surfactants continue to be an environmental concern. Knowledge of the endocrine disrupter potential of some surfactant metabolites had heightened public interest about the fate of these pollutants.

Only the application of LC-MS analysis can be conceived of as reliable surfactant analysis. To elaborate determination methods for the analysis of the anionic surfactant mixture of alkyl ethoxysulfates (AES) APCI and ESI-MS(+/−) studies combined with in-source MS/MS examinations were performed and results were compared (cf. Fig. 15.4 and 15.5 and 15.3.3.2 ESI, surfactants). APCI fragment ion spectra revealed the alkyl chain length and the number of ethoxylate moieties therefore APCI was found to be the method of choice [326]. To confirm determination methods applied in surfactant analyses an inter-laboratory comparison study of LC-MS techniques and enzyme-linked immunosorbent assay for the determination of surfactants in wastewaters was performed in seven laboratories. The quantitative determination of the non-ionic NPEOs, AEOs, coconut diethanol amides (CDEAs) and the anionic LAS, NPEO-sulfates and the secondary alkane sulfonates (SAS) was performed under APCI or ESI-interfacing conditions in positive or negative

mode [327] using LC and/or FIA-MS or MS/MS. The stability of SPE concentrated analytes spiked into wastewater effluents and groundwater samples was studied using the non-ionic surfactant mixtures of NPEOs, AEOs and CDEAs and the anionic mixture of LAS.  $C_{18}$  SPE cartridges were stored at 4 °C or -20 °C, water samples were kept cold (4 °C) before the compounds were analysed. Stability in a water matrix, even when preservation agents had been used, was very poor, samples pre-concentrated on SPE cartridges immediately after sampling were stable for up to 1 month at 4 °C, and for longer at -20 °C (cf. 15.3.3.2 ESI, surfactants) [328].

Qualitative determination methods for so-called gemini surfactants (2 anionic and 1 cationic), a new type of compound with highly improved surface activity, were reported. Results of APCI or ESI-FIA-MS or LC-MS and MS/MS with mass and fragment ion spectra were presented [329] and fragmentation pathways were proposed. Synthetically produced surfactant mixtures may contain undesirable by-products, hardly degradable in the environment and relevant in the drinking water works. Billian et al. described the detection and identification of the synthetic by-product n-decyl-isomaltoside contained in a technical surfactant mixture of APGs. APCI-LC-MS and MS/MS in negative mode in parallel with the use of NMR spectroscopy allowed identification [330].

The analyses of environmental samples confirmed the ubiquitous presence of surfactants in surface and sea water as a result of the surfactants discharged with STP effluents. Analysis of River Elbe (Germany) water samples by GC-MS and APCI-LC-MS and MS/MS confirmed qualitatively the presence of nonpolar and polar organic pollutants of AEO, NPEO, CDEA and aromatic sulfonic acid type, respectively [226]. After  $C_{18}$  and/or SAX SPE anionic and non-ionic surfactants were qualitatively and quantitatively analysed in surface water samples by APCI-LC-MS in the negative or positive mode, respectively. Alkylphenol ethoxylates (APEOs) could be confirmed in river water at levels of 5.6 µg L<sup>-1</sup> [331].

A concentration and detection method for the non-ionic surfactants of APEO type dissolved in river water samples using XAD-16 and APCI-LC-MS and MS/MS, respectively, was developed. Octylphenol ethoxylates (OPEOs) oligomers containing 5–14 ethoxylate groups were confirmed in the Meguro river (Japan) and treated wastewater from a discharge canal [332]. NPEOs and LAS were observed and quantified in sea water and sediment samples from the German Bight of the North Sea or Waddensea marinas and estuaries applying APCI or ESI-FIA and LC-MS and MS/MS in the positive or negative mode, respectively [333].

AEOs spiked into raw wastewaters were applied to elaborate an APCI or ESI-LC-MS method to determine non-ionic surfactants after SPE. Ionisation efficiencies of both interface types were compared and the more effective APCI technique then was applied for quantification [334]. Recoveries observed with standard determination methods for surfactants and MS detection techniques for different types of surfactants (e.g. alkylether carboxylates, sulfosuccinates, fatty acid polyglycol amines, quaternary carboxoalkyl ammonium compounds, modified AEOs, EO/PO compounds, APGs, alkyl polyglucamides, betaine and sulfobetaine) in spiked wastewater samples were compared by applying APCI and/or ESI(+/-). Poor recoveries were obtained by standard methods but good results by MS [335]. APCI and

ESI-FIA-MS/MS and LC-MS/MS analyses were performed to characterise polar pollutants in the wastewaters of Thessaloniki (Greece) STP after C<sub>18</sub> or LiChrolut EN-SPE. LC-MS(+), MS/MS spectra of sequentially eluted non-ionics as dominating pollutants in inflow and effluent, (AEOs and NPEOs) and their degradation products (PEGs) and their chromatograms were presented [336]. In municipal wastewaters organic pollutants were analysed by APCI and ESI in FIA and LC-MS(+-) mode confirming the predominance of surfactants [337, 338]. Results of quantification were reported. The application of FIA-MS screening vs. time consuming LC-MS techniques was discussed. Complex wastewater samples were analysed by Preiss et al. [339] by means of APCI and ESI-MS coupled on-line with <sup>1</sup>H-NMR. The identification of compounds was reported and advantages and disadvantages of the techniques used were discussed. A mixture of homologs of NPEOs in the inflow and effluent of a STP were analysed by a novel rapid screening method, combined precursor ion scanning and multiple reaction monitoring, using APCI MS/MS and ESI MS/MS (cf. 15.3.3.2 ESI, surfactants). NPEO concentrations as low as 50 ppt could be detected [340]. Industrial wastewaters (e.g. petrochemical, textile, pulp mill and ammunition plant effluents) were monitored by GC-MS and APCI-LC-MS. Polyethoxylated aliphatic and aromatic non-ionic surfactant compounds and their degradation products were observed by APCI-MS and characteristic ions were listed [341]. The biodegradation of AEOs treated by wastewater biocoenoses of different STPs resulted in multiple different biodegradation pathways monitored and elucidated by APCI-FIA-MS and MS/MS. NPEOs and NPEO-sulfates were degraded aerobically and anaerobically and the metabolites were determined and identification was performed by triple quad and ion trap MS/MS [342]. To improve the elimination efficiencies in a conventional and 3 bio-membrane, assisted wastewater treatment plants operated in parallel were studied by APCI- and ESI-FIA and LC-MS(+-) and MS/MS, respectively. Qualitative, semi-quantitative and quantitative results on AEOs, NPEOs and LASs were reported. Diagnostic scans were applied for confirmation [343]. The elimination for surfactants and drugs spiked into a conventional and into a biomembrane-assisted STP was monitored by APCI-FIA and LC-MS and MS/MS. NPEOs and OPEOs were observed and followed by a semiquantitative pattern recognition approach [344].

Halogenated APEOs already observed in a FAB study by Rivera et al. [154] in drinking water samples were quantitatively analysed and identified in drinking, surface and wastewater as well as in river sediments and STP sludges by APCI-LC-MS(+-) (cf. 15.3.3.2 ESI, surfactants) under optimized conditions [345]. Despite the polarity and therefore improved solubility of surfactants in water the content of surfactants in STP sludges cannot be neglected. Methanol/dichloromethane extraction by means of ultrasonification was used to extract anionic and nonionic surfactants and their degradation products. APCI or ESI-LC-MS was applied but for determination of the less polar AEO, NPEO and CDEA APCI-LC-MS(+) was used [346].

### Pesticides (including herbicides, fungicides etc.)

Of all the organic pollutants measured in environmental matrices, pesticides still continue to be the most studied. They are the focus of drinking water, surface and groundwater. With every new generation of pesticides coming on the market, compounds become more polar and, in parallel, less persistent in the environment and during separation and detection in the laboratory. LC-MS and MS/MS as method of choice for the analysis of polars provided molecular weight and structural information not always sufficient for identification. The new trend toward the application of an ion trap with the possibility of MS<sup>n</sup> offer significant improvement over “conventional” MS/MS.

#### *Anilides, quaternary amines, toluidines and thiocyanate compounds.*

APCI- and ESI-LC-MS in the ion-pair LC-mode was used to characterised the quaternary ammonium herbicides diquat, paraquat, difenzoquat, mepiquat and chlorimequat in spiked tap water samples after SPE (Sep-Pak silica). Detection limits down to 0.1–4 µg L<sup>-1</sup> were obtained and reproducibility results were reported [347].

A simultaneous MS method was developed for the determination of acidic and neutral rice herbicides and their degradation products in trace quantities in estuarine waters (Ebro delta). Positive APCI was applied for the determination of molinate and 3,4-dichloroaniline, the major degradation products of propanil whereas negative ionisation was applied to acid compounds. 8-Hydroxybentazone and 4-chloro-2-methylphenoxyacetic acid were successively observed in the samples [348]. After LC-UV-DAD APCI-LC-MS in the more sensitive negative mode was used to confirm propanil and its major degradation product, 3,4-dichloroaniline, in surface water and soil samples after pesticide application to dry rice fields. Propanil was found to be rapidly degradable to 3,4-dichloroaniline [349]. APCI-LC-MS was used to analyse surface water samples for organonitrogen pesticides e.g. metolachlor and triazines. Detection limits after dichloromethane extraction or after SPE (Carbopack B), were < 3 ng L<sup>-1</sup> applying APCI-LC-MS and < 4 ng L<sup>-1</sup> if GC/NPD was used [260].

An APCI-LC-MS method was developed and described for the quantitative determination of the anilide pesticides alachlor and metazachlor in ground water samples. After optimization of instrumental conditions detection limits of 0.001–0.005 µg L<sup>-1</sup> (50–300 pg injected) could be obtained. Recovery, precision and linearity data were reported [350]. The pesticide bentazone was one of the most frequently found compounds determined by APCI-LC-MS in shallow groundwater samples from twosandy and two clay catchment areas [351].

Stability studies of SPE-adsorbed anilides and N-substituted amines (bentazone, molinate and metolachlor) were performed by means of APCI-LC-MS. From river water samples containing the pesticides and their degradation products, the pesticides had been extracted prior to APCI-LC-MS [320]. The SPE adsorbed compounds were stored on SPE cartridges (styrene-divinylbenzene) for up to 3 months at ambient temperature, +4 °C and –20 °C. After 3 month storage at –20 °C on the polymeric cartridges recoveries were > 90% [320].

When metolachlor was submitted to a degradation process by *Cunninghamella elegans* [352] APCI-LC-MS was used to track the metabolic process over a period of 96 h. After incubation had stopped six metabolites were concentrated and separated prior to identification. Predominantly an O-demethylation of the N-alkyl side chain of metolachlor and benzylic hydroxylation of the arylalkyl side chain was observed [352].

#### *Carbamates.*

For trace analysis of carbamate pesticides and other pesticide compounds Hogenboom et al. [353] developed a substance specific APCI-LC-MS/MS method using short columns. Detection limits of  $0.03\text{--}5 \mu\text{g L}^{-1}$  in full-scan and  $2\text{--}750 \text{ ng L}^{-1}$  in SIM mode were reported. The pesticides could be successfully identified from a search against a pesticide MS/MS library. In a comprehensive TSP study with a series of N- and P-containing pesticides (amines, anilides, carbamates, phosphonates, phenylureas, sulfonylureas and triazines) APCI spectra and CID spectra were obtained and APCI was useful for solving fragmentation mechanisms observed in TSP mass spectra [175]. Doerge et al. [354] examined different classes of pesticides (triazines, carbamates, phenylureas, organophosphates) quantitatively by APCI-MS. With this method they observed that sensitivity was less affected by differences in analyte structure than using TSP or PB-LC-MS. In the analysis of N-methylcarbamate pesticides (methomyl, aldicarb, aldicarb sulfoxide, aldicarb sulfone, carbaryl, methiocarb, carbofuran, and 3-hydroxycarbofuran) [108] all the API interfaces performed better than the TSP and PBI [320] interfaces. Comparing APCI with ESI (ion spray) applications, APCI resulted in a better sensitivity, linearity and covered more carbamates. Molecular weight information and abundant fragment ions were provided while ion spray gave comparable performance but mainly protonated molecular ions and less fragmentation. Comparable results were obtained by Fernández et al. with carbamate residues in fruits and vegetables. Detection limits observed were 10 to 100 times lower than EU maximum residue levels (cf. 15.3.3.2 ESI, carbamates) [355]. An automated on-line extraction and pre-concentration based on high-performance immunoaffinity chromatography combined with RP-HPLC and APCI-MS detection were described for the determination of the fungicide carbendazim. For a quick determination an ELISA method was applied with the result that both analytical methods, APCI-LC-MS and ELISA, correlated well [356].

River water samples were under research by APCI and ESI-LC-MS to analyse seven N-methylcarbamate pesticides quantitatively. The effects of varying APCI and ESI conditions were investigated, confirming that APCI resulted in less effective sensitivity [357].

The contamination of fruits and vegetables with pesticides became a problem with the increased application of pesticides because of an intensified agriculture. So the comparison of APCI and ESI-LC-MS for the determination of 10 pesticides of carbamate type (pirimicarb, carbofuran, 3-hydroxycarbofuran, aldicarb, and its metabolites, the sulfoxide and the sulfone), besides others in fruits, met the

need and proved that the application of APCI was more efficient than ESI. A positive-negative mode switch in the MS run allowed the determination of eight pesticides in matrix-matched standards [358]. APCI-LC-MS was applied to validate an ELISA method using anti-rabbit immunoglobulin G antibodies for the determination of traces of carbaryl in vegetable and fruit extracts. An illustrative mass chromatogram presenting the degradation of carbaryl to 1-naphthol [359] confirmed that APCI interfacing allowed the detection of pesticides at very low levels. The increased application of pesticides in agriculture led to an accumulation of these pollutants in the food chain with the result that pesticides were observed in body fluids. Itoh et al. [360] elaborated a method for the determination of carbamates by APCI in biological fluids (e.g. serum or urine). They described this method as a very rapid method which requires only an extremely simple pretreatment process. While ESI-LC-MS was used to analyse acidic polar pesticides in water APCI-LC-MS was applied to determine carbamates. Under these conditions the specific fragment ions  $[M+H-CONCH_3]^+$  [325] could be observed.

#### *Organophosphorus compounds.*

For trace analysis of organophosphorus pesticides Hogenboom et al. [353] developed a substance specific APCI-LC-MS/MS method using short columns. An on-line SPE-APCI-LC-MS(+/−) and MS/MS method was described [322] for the analysis of a test mixture of 17 pesticides containing the organophosphorus compounds dimethoate, fenamiphos, coumaphos, fenchlorphos, chlorpyriphos and bromophos-ethyl at low  $\text{ng L}^{-1}$  levels applying samples of 100 mL for concentration. Under CID conditions APCI and ESI-MS/MS resulted in similar product-ion spectra obtained from protonated molecular ions. A pesticide MS/MS library could be applied successfully for identification [322, 353]. Automated on-line SPE followed by LC-MS interfaced by APCI or PBI was applied to fenitrothion, malathion, parathion-ethyl and vamidothion. The study demonstrated the higher sensitivity of APCI compared to PBI [320, 361]. A comprehensive study by Volmer et al. of pesticides by applying different types of interfaces (TSP, ESI and APCI) confirmed that the application of APCI was very useful for solving fragmentation mechanisms observed in TSP-MS spectra obtained from the organophosphorus pesticides butonate, dichlorovos and trichlorfon [175]. A modified method was described for quantitative monitoring of various phosphorus pesticides (parathion-methyl, fenitrothion, diazinon and chlorpyrifos) in river water [362], (coumaphos, azinophos-ethyl, azinophos-methyl, triazophos, parathion, fenthion malathion fenitrothion, parathion-methyl, disulfoton, dimethoate, omethoate, mevinphos, trichlorfon) and in ground water [324]. For (*E*)- and (*Z*)-mevinphos, dichlorvos, azinphos-methyl, azinphos-ethyl, parathion-methyl, parathion-ethyl, malathion, fenitrothion, chlorfenvinphos, fenthion and diazinon [363] fully automated on-line SPE and LC-UV-DAD or APCI-LC-MS(+/−) were performed. The effects of temperature and extraction voltage on the mass spectra obtained in an APCI-LC-MS examination analyzing the organophosphorus pesticides acephate, azinphos-ethyl, fenitrothion, fensulfothion, fenthion, metamidofos, paraoxon-methyl, parathion-methyl, trichlor-

fon, vamidothion and vamidothion sulfoxide in groundwater samples were studied. Calibration and detection limit data were provided but recoveries were poor [364]. A robust method was developed for the determination of 56 different insecticides and fungicides of predominantly organophosphorus type in groundwater samples for a pilot survey study in Almeria (Spain). Pesticides were analysed using different GC techniques besides APCI-LC-MS. A subsequent interlaboratory study using all methodologies showed good agreement between the techniques [365]. The analyses of fenamiphos and diazinon as potential ground water contaminants by APCI-MS proved that under APCI ionisation sensitivity influenced by differences in analyte structure was less affected than observed with TSP or PBI-LC-MS [354].

Fenthion, temephos and their degradation products were determined by HPLC-DAD and APCI-LC-MS in rice field water samples after SPE (Empore C<sub>18</sub>). Four fenthion transformation products could be identified in the positive or negative modes whereas the degradation of temephos resulted in six products. For both pesticides the oxo-analogue products predominate [366]. After rice fields had been treated with fenitrothion, crop waters were sampled and analysed by ELISA, LC-DAD and MS coupled by APCI interface. Fenitrothion, fenitrooxon, 3-methyl-4-nitrophenol and the s-Me isomer of fenitrothion were identified by LC-MS [367].

Biodegradation of fenitrothion, ethyl-parathion, methyl-parathion in natural waters was observed and examined by APCI-LC-MS. Various degradation products could be identified unequivocally. All transformation products were observed to be more stable than the parent compound except in ground water [321]. Physicochemical and biochemical degradation was observed after SPE adsorption if storage conditions were not optimised. First attempts to study the stability of different pesticides of organophosphorus type and concentrated on the SPE materials Hypersphere-1, IST Envirolut and LiChrolut were reported. APCI-LC-MS analysis was used for confirmation. Complete recoveries were obtained after storage at -20 °C for 1 month for water spiked at 10 µg L<sup>-1</sup>. Degradation occurred after storage temperatures of 4 °C and at room temperature [368]. The results were compared to stabilities in acidified and non-acidified ground water [369]. A monitoring procedure for 21 organophosphorus pesticides in biological fluids using APCI-LC-MS [370] was elaborated. Propaphos, isoxathion, iprofenos, malathion, fenitrothion and chlorpyrifos were determined by APCI in serum or urine. Itoh et al. [360] described a method amenable to these matrices which required only an extremely simple pretreatment process despite complex matrices.

The organophosphorus herbicide butamifos and its 4-nitrophenyl derivative were submitted to photodegradation. Products were analysed by APCI-LC-MS. MS peaks obtained from the precursors and their degradation products were tabulated and a mechanism of degradation was proposed [371]. The ozone degradation pathway of pirimiphos methyl in industrial water was examined [372] by ion-trap EI or PICI in GC-MS, or in APCI and ESI-LC-MS mode. APCI and ESP mass chromatograms of the pirimiphos methyl oxidation products and fragmentation data were reported and an ozonolysis degradation pathway was proposed (cf. 15.3.3.2 ESI, organophosphorus compound).

**Phenoxy carboxylic acids.** The application of APCI in the determination of the polar acidic phenoxycarboxylic acids led to unsatisfactory results. Nevertheless this method was applied by Santos et al. [348] for the determination of the 2,4-D, MCPA and MCPP herbicides and their degradation products in trace quantities in estuarine waters of drainage of the Ebro delta. Response for the very polar acidic compounds preferentially ionised by ESI in the negative mode with excellent sensitivity [176, 325] in the APCI mode, however, was reduced (cf. 15.3.3.2 ESI, organophosphorus compounds) [348]. Results obtained by APCI or PBI, however, proved an increased sensitivity of APCI compared to PBI [320].

*Phenylureas, thioureas and sulfonylureas.*

The capabilities of a modern API source as a universal LC-MS coupling tool were checked by performing pesticide analysis of the polar urea pesticides metoxuron, monuron, monolinuron, chlortoluron, metobromuron, metabenzthiazuron, isoproturon, diuron, linuron in the low pmol range (limits: 10–100 pg) [373].

An on-line SPE-APCI-LC-MS and MS/MS method was described by Slobodnik et al. [322] for the analysis of a test mixture of 17 pesticides containing monuron, diuron and neburon at low  $\text{ng L}^{-1}$  levels applying samples of 100 mL for concentration.

APCI-LC-MS [325] was applied to determine phenylurea herbicides in water samples with detection limits all in the low pg range, whereas ESI-LC-MS was used to analyse the acidic polar pesticides. Under APCI conditions the specific fragment ion of phenylureas  $m/z$  72 corresponding to  $[\text{O}=\text{C}=\text{N}^+(\text{CH}_3)_2]$  could be observed [325]. Fragmentation pathways were presented. In a TSP-LC-MS study covering 15 phenylurea and thiourea pesticides APCI-LC-MS/MS was used to elucidate fragmentation behavior observed under TSP conditions [175].

The urea pesticides diuron, fluormeturon, neburon and linuron cited as potential groundwater contaminants from US EPA in the National Pesticide Survey were quantitatively determined by APCI-LC-MS(+) [354]. APCI-LC-MS was also used to test for 46 pesticide compounds in shallow groundwater samples from two sandy and two clay catchment areas. Of the neutral polars observed, isoproturon belonged to the most frequently found compound [351]. Spliid et al. described an APCI-LC-MS method for the determination of isoproturon and different types of pesticides and their degradation products in ground water samples. Detection limits, recovery and linearity data were reported [350].

Surface water samples from Southeastern regions of France and from the St. Lawrence River in Canada were monitored by APCI-LC-MS and MS/MS in the positive mode. Diuron and isoproturon were confirmed by MS/MS. Results obtained by LC-MS and ion trap LC-MS/MS were found to be comparable [374]. A substance-specific robust APCI-LC-MS/MS method using short columns for trace analysis of phenylureas was elaborated and validated. Despite the low quantity of sample applied (15 mL) detection limits of  $< 5 \mu\text{g L}^{-1}$  in full-scan and  $< 750 \text{ ng L}^{-1}$  in SIM mode, respectively, could be achieved. Product ion spectra were obtained from  $[\text{M}+\text{H}]^+$  parent ions and by means of a pesticide MS/MS library

the majority of the pesticides were successfully identified [353]. When natural waters [375, 376] were analysed by a rapid target analytical technique for quantitative determination of microcontaminants in water by applying on-line single-short-column separation coupled with ion trap APCI-LC-MS and -MS/MS phenylurea herbicides and triazine derivatives were under research. Results obtained from concentration of 4 mL water samples containing eight phenylureas were poor compared to results obtained from triazine determination [376]. Isoproturon and fluorometuron were monitored in environmental waters. Besides these urea pesticides a series of organo-phosphorus, triazine, chlorophenoxy acid, phenolic and thiocarbamates pesticides were also analysed from 200 mL water samples by on-line SPE-APCI-LC-MS and PBI-MS [361]. The analytical capabilities of the different ionisation techniques with the analyses of urea pesticides were discussed and the behavior under different ionisation conditions was documented [320].

Four selected antifouling booster biocides, to which diuron belongs, were determined by APCI-LC-MS after enrichment by C<sub>18</sub>-SPE from marine waters. Detection limits of 0.01–0.18 µg L<sup>-1</sup> [377] or < 5 ng L<sup>-1</sup> were obtained with recoveries > 91% [378]. The other antifouling biocides also quantified were Kathon 5287, TCMTB and TCMS pyridine. To validate pesticide analysis methods phenylurea pesticides were determined quantitatively by APCI-LC-MS in an interlaboratory testing performed with aqueous real-life samples (drinking water, surface water and groundwater) containing pesticides ranging from 0.02–0.8 µg L<sup>-1</sup> [379]. A coupled column system (LC-LC) was used and detection was performed either with UV or by APCI-MS which allowed direct quantification down to 0.01 µg L<sup>-1</sup> and in parallel confirmation of the results.

Yarita et al. developed an APCI-LC-MS(+/−) method to analyse diuron and linuron and their respective degradation products, 1-(3,4-dichlorophenyl)urea and 1-(3,4-dichlorophenyl)-3-methylurea before the method was then applied to follow biodegradation of diuron in sewage sludge over a period of 28 d [380].

The determination of sulfonylurea degradation products of chlorsulfuron, met-sulfuron-methyl, thifensulfuron-methyl and tribenuron-methyl in soil by LC-UV detection was studied with standards and real environmental samples. Compounds observed were confirmed by APCI- and ESI-LC-MS/MS. SRM was applied to identify five degradation products by LC-MS/MS(+/−). Calibration graphs were linear from 0.05–1 µg mL<sup>-1</sup> with detection limits of 10–50 µg kg<sup>-1</sup> [381]. Attempts were made to couple an immunoaffinity concentration step with APCI-LC-MS determination for the analysis of phenylureas and triazines in water and sediment samples. Calibration graphs were linear at 0.01–0.2 µg L<sup>-1</sup> groundwater, with typical detection limits of 1–5 ng L<sup>-1</sup> [382]. An anti-isoproturon immunosorbent immobilized on 500 mg silica was used to concentrate and to purify phenylurea herbicides (chlortoluron, isoproturon, diuron, linuron and diflubenzuron) from aqueous samples prior to quantitative LC-UV-DAD determination and APCI-LC-MS confirmation. With the application of 50 mL of water detection limits < 1 µg L<sup>-1</sup> in SIM mode were obtained [383]. The comparison of APCI and ESI-LC-MS for the determination of the fluorine-containing phenylurea pesticide diflubenzuron and 10 pesticides of carbamate type in fruits [358] was reported. This compound was

also determined in plums, strawberries and blackcurrant-based fruit drinks [384] with recoveries of 76%.

**Phenolic compounds.** In Portuguese rivers tri-, di and mono-chlorophenols were determined by APCI-LC-MS in negative mode in parallel with other pesticides. SPE was performed with Oasis cartridges [323].

**Triazines.** The optimization of sensitivity in the quantitative determination of polar pesticides was the purpose of comparing the atmospheric pressure interfaces APCI and ESI in the field of pesticide analysis. Optimized detection limits were observed to be dependent on eluent flow-rates used in the analysis. Triazines were less sensitive to variations in flow-rates under both ionisation techniques (cf. 15.3.3.2 ESI, triazines) [385]. APCI was used for solving fragmentation mechanisms observed by TSP-LC-MS/MS of triazines and other pesticides [175]. APCI-LC-MS was applied to determine triazines whereas ESI-LC-MS was used to analyse the acidic and more polar pesticides in water. MS<sup>n</sup> results from triazine derivatives resulting in a cleavage of lateral chains followed by ring opening were presented [325]. To improve specificity and selectivity a substance-specific APCI-LC-MS/MS method for trace analysis of the triazine derivatives propazine and terbutylazine was developed. Product ion spectra obtained by CID from [M+H]<sup>+</sup> ions from the majority of the pesticides could be successfully identified from a search against a pesticide MS/MS library compiled in-house [353]. APCI-LC-MS methods were elaborated and described for the determination of triazine pesticides and their degradation products in ground water [350, 354]. Detection limits were obtained with 0.001–0.005 µg L<sup>-1</sup>, corresponding to 50–300 pg injected. Recovery, precision and linearity data were reported [350]. Natural waters were analysed for a series of triazine derivatives by ion trap APCI-LC-MS and MS/MS. A rapid target analytical technique for quantitative determination of microcontaminants in water by on-line single-short-column separation was developed and applied and detection limits of 0.1–1 µg L<sup>-1</sup> could be obtained [376]. Typical MRM chromatograms were reported when herbicides were examined applying the same technique [386]. In Portuguese rivers priority pesticides of triazine type besides phenols were determined by APCI-LC-MS. SPE was performed with Oasis cartridges. “Hot spots” were located [323]. The results obtained by APCI-LC-MS and GC-NPD were compared for the quantification of seven different triazines and their degradation products in surface water samples. Detection limits after dichloromethane extraction or after SPE (Carbopack B), were 0.6–3 ng L<sup>-1</sup> applying APCI-LC-MS and 0.4–4 ng L<sup>-1</sup> by GC/NPD, respectively, with in parallel good recoveries [260].

The problems of stability of SPE concentrated pesticides were studied also with triazines as targets [320, 368, 369]. Polymeric SPE materials Hysphere-1, IST Envirolut and LiChrolut were examined using APCI-LC-MS analysis for confirmation. Complete recoveries could be confirmed by APCI-LC-MS analysis after storage at –20 °C for 1 month for water samples spiked at 10 µg L<sup>-1</sup> [368, 369]. APCI-LC-MS was used to confirm LC-UV-DAD monitoring results of pesticides in water from the Ebro delta. In parallel stability of pesticides which had been adsorbed and stored on SPE cartridges (styrene-divinylbenzene) for up to 3 months was judged [320]. To handle large sample quantities with the increasing number of analyses

automated SPE off and on-line coupled to LC systems came into use. Triazines besides other pesticides were concentrated by automated on-line SPE prior to determination by APCI or PBI-LC-MS [320]. Fully automated on-line SPE combined with LC and coupled with UV-DAD or APCI-MS was used in pesticide analysis. A modified SAMOS method was developed and described for quantitative monitoring of the triazine pesticides desethylatrazine, atrazine, terbutylazine, simazine and propazine besides phosphorus pesticides in river waters [362]. To establish robust determination methods, the triazine derivatives atrazine, simazine and their degradation products desethylatrazin, hydroxyatrazine and hydroxysimazine were spiked into tap and surface water samples. These samples were used to confirm suitability for FIA coupled with APCI to fulfil criteria recommended in the Netherlands for GC-MS analysis of pesticides. The APCI-FIA-MS/MS results obtained were quite promising because the polar desethylatrazine could be confirmed by FIA-MS but was not observed by GC-MS [387]. Samples from 95 Missouri streams and 46 Midwestern state streams were analysed for atrazine and its biodegradation products using APCI-LC-MS after cation exchange and SPE [388]. Several polar degradation products were quantified and confirmed by APCI LC-MS/MS. Maximum concentrations for the streams were reported, proving that ca. 60% of the atrazine load was atrazine metabolites. Detection limits were 0.04–0.1 µg L<sup>-1</sup> [388]. In Europe and Canada these compounds were observed in environmental water samples when 48 target pesticides belonging to 8 different classes along with their degradation products were monitored in surface waters. API methods were applied for analysis of samples from Southeastern regions of France and from the St. Lawrence River in Canada. Triazine derivatives, as all the other neutral compounds, were determined by APCI-LC-MS in the positive mode, whereas ESI in negative mode was applied to the acidic compounds and sulfonylureas [374]. Priority pesticides (e.g. atrazine, simazine, terbutylazine, Irgarol, deisopropylatrazine and deethylatrazine and other types of pesticides) and other organic pollutants were monitored by APCI-LC-MS in 43 river water samples from Portugal and concentrations were reported [324]. For confirmation of results obtained from analyses of triazines and phenylureas in water and sediment samples operated in coupling with an immunoaffinity column, LC-MS-APCI was used [382].

Since triazines are very mobile in the aquatic environment, the presence of these pesticide types in groundwater samples could be confirmed. Pollution was observed when neutral pesticides contained in shallow groundwater samples from two sandy and two clay catchment areas were analysed in APCI mode [351]. The most frequently (> 300 samples) determined compound was atrazine with its degradation products.

For the biodegradation of atrazine and <sup>14</sup>C-labeled atrazine by *Rhizobium sp.* strain APCI-LC-MS was used for qualitative follow-up, for quantification, however, ESI with simazine as an internal standard was applied. Metabolisation but no mineralization could be observed [389]. APCI and ESI-MS were applied to determine humic substances and dissolved organic matter (DOM) together with the fungicide anilazine (2,4-dichlor-6-(2-chloranilino)-1,3,5-triazine) which was

bound to DOM. With anilazine bound residues, a high release was found of the main metabolite, the dihydroxy-anilazine [390].

*Antifouling pesticides.*

Different antifouling pesticides of triazine type were determined in Portuguese rivers by APCI-LC-MS(+) after SPE for concentration, which was performed with Oasis cartridges [323].

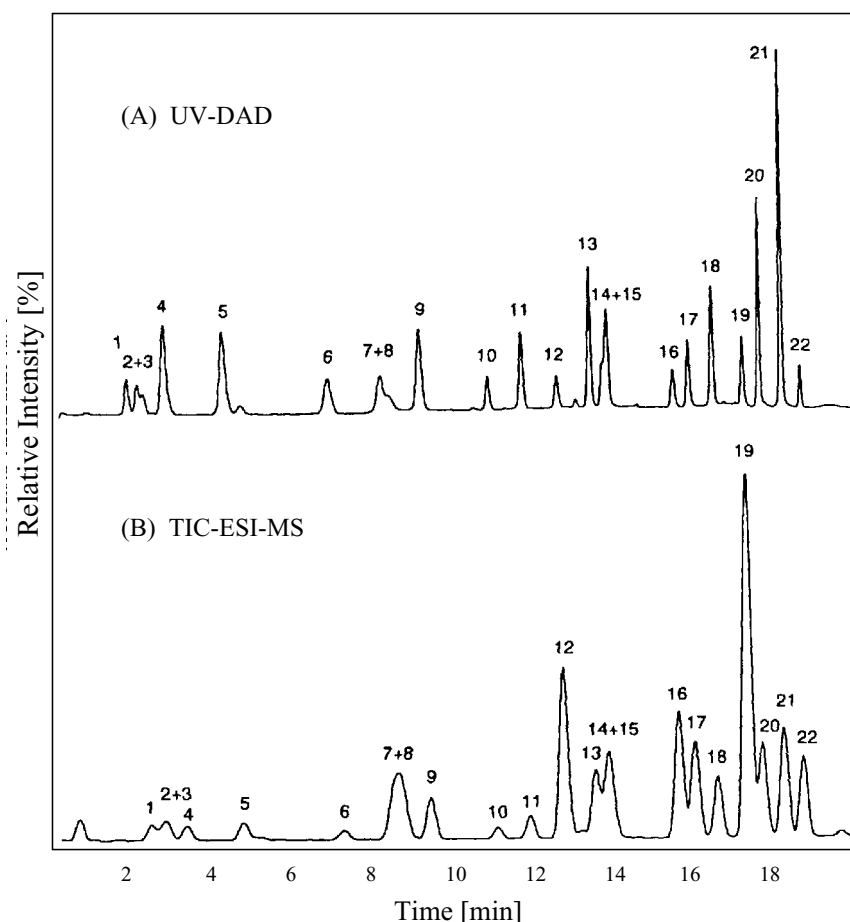


**Fig. 15.6** Electropherogram of 22 aromatic sulfonate compounds (standard) with (A) UV-DAD detection and (B) ESI-MS(-) detection. Reproduced with permission from [395] © Elsevier, 1990.

### *Miscellaneous.*

From the large group of pesticides, the triazole herbicide amitrole could be analysed in water samples via an automated SPE-APCI-LC-MS/MS procedure after a precolumn derivatization using 9-fluorenylmethoxy-carbonyl chloride. Recoveries in drinking water and surface water of >95% or 75%, respectively, could be achieved [391]. Degradation experiments in an aqueous medium combined with APCI-LC-MS proved that the total photodegradation of imidacloprid in water under natural sunlight in a pilot plant could be achieved in the presence of TiO<sub>2</sub> as catalyst. Levels of imidacloprid and the degradation product 6-chloronicotinic acid were monitored, five compounds were volatile and were detected by GC/MS [392].

APCI and ESI-LC-MS were compared to determine, besides other substances, acaricidic clofentezine and fungiciddic thiabendazole in fruits. Detection limits observed were equivalent to 0.002–0.033 mg per kg of crop [358]. APCI ionisation was found to be more efficient than ESI. When clofentezine was also determined in plums, strawberries and blackcurrant-based fruit drinks [384] mean overall recoveries of 70% from spiked extracts were observed. An efficient APCI-LC-MS/MS method was developed for the quantitative determination and identification of intact daminozide in apples and apple leaves [393]. APCI mass and MS/MS spectra of daminozide were presented. Recoveries for daminozide in apples and apple leaves were 98–102% and 112–116% and detection limits were observed with 0.008 and 0.02 mg kg<sup>-1</sup> for apples and leaves, respectively.

The tin-containing pesticide fenbutatin oxide [394] in tomatoes, cucumbers and bananas was determined by APCI-LC-MS. Mean recoveries in SIM mode, recording seven ions of the isotopic cluster at *m/z* 515.2–521.2, were observed with 88% (tomatoes) and 80% (cucumbers and bananas). Detection limits were 0.06–0.12 ng μL<sup>-1</sup>.

### **Applications using electrospray ionization interface (ESI)**

As demonstrated (cf. Fig. 15.1 and 15.2) with the results of ionisation observed in the spectra of the non-ionic surfactant mixtures of AEOs or APOs or for ionisation of the anionic surfactant mixture of AES (cf. Fig. 15.3), if APCI or ESI interfaces were applied, both API interface types presented considerable differences in the ionisation processes. These differences were in both the type of ions and the efficiency of ionisation, i.e., either high molecular or low molecular compounds were favoured in ionisation and no ionisation takes places with the one interface whereas the other interface type ionises the compounds with high sensitivity. Obviously ESI is the interface which handles the very polar, partly charged compounds with low as well as high molecular weights in the best way, while the APCI interface can be used successfully for the more lipophilic compounds contained in water samples, e.g. phenol compounds. With the improved flexibility of ESI handling low and high flow rates of eluents ESI-CEz-MS became a powerful tool to separate complex mixtures with an improved separation efficiency never previously observable with any kind of LC (see Fig. 15.6) [395].

**Table 15.3** Environmental applications in LC-MS performed by elektrospray interface (ESI).

<b>Topic</b>	<b>References</b>
<b>Reviews</b>	
General reviews	28, 44, 45
Compound class specific reviews	
– Dyes	43, 161, 200
– Pesticides	22, 29, 30, 32, 199
– Surfactants	21, 24, 39–41
– Sulfonates	161
– Toxines	396
<b>Compound classes</b>	
– Complexing agents	397–399
– Drugs and diagnostic agents	292, 295, 296, 400–416
– Dyes	28, 43, 297, 416, 417, 421–429
– Estrogenic compound	298–301, 430
– Explosives	205, 291, 302, 431, 432
– Haloacetic acids and disinfection byproducts	433–439
– Organoarsenic compounds	428
– Polycyclic aromatic hydrocarbons	28, 304, 442, 443
– Phenols	315–319, 346, 444
– Sulfonic acids	161, 297, 445–449
– Surfactants	21, 28, 40, 155, 212, 226, 326–329, 333, 334, 336, 339, 340, 343, 345, 346, 422, 450–482
– Toxins	396, 410, 483–488
– <b>Pesticides (including herbicides, fungicides etc.)</b>	
– Anilides, quaternary amines, toluidines and thiocyanate compounds	175, 240, 347, 385, 489–506
– Carbamates	108, 175, 257, 355, 357, 358, 424, 500, 502, 503, 506–515, 519, 537
– Organophosphorus compounds	155, 175, 322, 353, 385, 397, 500, 510, 515–523, 537
– Phenoxy carboxylic acids	325, 351, 374, 500–502, 524–532
– Phenylureas, thioureas and sulfonylureas	175, 240, 271, 325, 358, 373, 374, 381, 385, 500, 502, 503, 506, 508, 511, 512, 525, 527, 533–537, 539–554
– Triazines	175, 240, 275, 276, 325, 385, 389, 390, 424, 500, 502, 506, 510, 511, 513, 519, 536, 537, 546, 553, 555–562
– Antifouling pesticides	563
– Phenolic pesticides	317, 322, 325, 351, 527
– Miscellaneous	358, 502, 540, 564–576
– <b>Comparison of ESI interfaces with different types of interfaces</b>	21, 28, 29, 32, 40, 43, 108, 113, 155, 161, 175, 176, 185, 199, 200, 205, 240, 257, 271, 275, 276, 291, 297–300, 317, 322, 325–327, 334, 340, 347, 351, 353, 355, 357, 358, 373, 374, 381, 385, 389, 390, 501, 503, 509, 523, 533

These effects observable while comparing APCI and ESI led the users to apply preferentially ESI rather than APCI ionisation, with the result that more papers dealing with ESI applications were published.

The overviews and reviews dealing with the applications of the ESI interface in environmental matrices in general have been mentioned with the applications of the APCI interface because of the overlap which exists between both interface types [28, 44, 45]. Pesticide residue analysis again was the most frequent application of ESI-LC-MS in the analysis of water samples [22, 29, 30, 32, 199] with the result that there was a tremendous increase in papers published within the last few years. Several reviews reporting ESI-MS results obtained with dyes [43, 161, 200], surfactants [21, 24, 39–41], sulfonates [161] or toxins [396] were published in the literature.

Table 15.3 reflects the applications of ESI used as the interface to couple MS with manifold liquid chromatographic separation techniques (LC, SFC, IC, CE, CZE, FAI (high-field asymmetric wave form ion mobility spectrometry)) in environmental analytical applications. The literature for different groups of compounds is presented.

### Complexing agents

Many complexing agents are hardly degradable and therefore can be observed in environmental waters. Since the complexing agents such as ethylenediamino tetra-acetic acid (EDTA), nitrotriacetic acid or aminophosphonic acids are extremely polar compounds, they were determined preferentially by ESI-LC-MS. IC interfaced by ESI to the MS allowed the determination of EDTA in  $\mu\text{g L}^{-1}$  quantities without any pre-concentration [397]. Metal complexes of EDTA were very stable and could be observed after ESI-LC-MS as  $[\text{M+metal}]^+$  ions in positive ionisation mode [398]. ESI CE-MS was applied to separate and to quantify the stable Ni-EDTA complexes [399].

### Drugs and diagnostic agents

ESI was the most common interface for monitoring drugs and their metabolites in the aquatic environment. Industrial effluents from pharmaceutical industries, STP effluents, groundwater and surface water samples were studied. Low concentrations of pollutants of concern made pre-concentration necessary before compounds were detected and identified by ESI-LC-MS and MS/MS [400–404].

Environmental water samples were examined by ESI-LC-MS/MS to analyse the antibiotic penicillin, sulfonamide, nitroimidazole, nitrofuran, 2,4-diaminopyrimidine and macrolide compounds and chloramphenicol. SRM and MRM techniques were applied [401]. To elaborate a method for determining drugs by (ion spray) ESI-LC-MS and MS/MS 22 Different neutral and weakly basic drugs (e.g. antiphlogistics,  $\beta$ blockers,  $\beta_2$ -sympathomimetics, lipid regulators, antiepileptic agents, psychiatric drugs and vasodilators) were spiked into wastewater, river water and drinking water samples. The determination of phenazone, carbamazepine, cyclophosphamide, ifosfamide and pentoxifylline was affected by organic matrix compounds which made application of ESI-LC-MS/MS essential. MS/MS detection limits of five neutral drugs were down to  $10 \text{ ng L}^{-1}$  [402]. Methods for the determination of drug residues in water by means of API-LC-MS or API-CE-MS applying ESI

or APCI interfaces were elaborated and drugs such as paracetamol, clofibrate acid, penicillin V, naproxen, bezafibrate, carbamazepine, diclofenac, ibuprofen and mefenamic acid could be separated and determined. The method was then applied to river water samples, where naproxen, bezafibrate, diclofenac, ibuprofen and clofibrate acid were determined in  $\text{ng L}^{-1}$  concentrations [295]. ESI-LC-MS and MS/MS were used to analyse and confirm 18 antibiotics in water samples after SPE (Lichrolut EN and C<sub>18</sub>) or after lyophilization. The group of antibiotics analysed included penicillins, tetracyclines (TETs), sulfonamides and macrolide antibiotics. Quantification limits were 50  $\text{ng L}^{-1}$  for TETs and 20  $\text{ng L}^{-1}$  for all other antibiotics examined [404]. ESI-LC-MS, MS/MS and HPLC/UV were applied to determine 13 sulfonamide drugs in environmental water samples after LiChrolut EN SPE. Detection limits ranged from 0.2–3.7  $\mu\text{g L}^{-1}$  for all sulfonamides while recoveries were 50–90%. Sulfamethoxazole and sulfadiazine were detected at 30–2000 and 10–100  $\text{ng L}^{-1}$ , respectively [400]. Five tetracycline antibiotic derivatives in ground and waste water were analysed by ESI-LC-MS(+) after C<sub>18</sub> or polymeric (Oasis) phase SPE. CID spectra were presented [405].

The qualitative and quantitative analysis of iodine containing X-ray contrast media and their metabolites in environmental waters of the city of Berlin (Germany), in raw and treated sewage, in surface waters, bank filtrate and raw drinking water, was performed by ESI-LC-MS and MS/MS in positive mode [406, 407]. Concentrations observed were 1.6–20.7  $\mu\text{g L}^{-1}$  [403].

An ESI-LC-MS and MS/MS method for the determination of neutral drugs e.g. caffeine, propyphenazone, 4-aminoantipyrin, diazepam, glibenclamide, nifedipine, omeprazole, oxyphenbutazone and phenylbutazone in groundwater, surface and wastewater was presented. Concentration levels of these compounds in 14 STP effluents and 11 German rivers were reported [408]. Salicylic acid, ketoprofen, naproxen, diclofenac, ibuprofen and genfibrozil were determined by ESI-LC-MS after SPE in water samples taken from several Spanish rivers and STP effluents. Results were compared with results from toxicity testing [409]. Sixty different pharmaceuticals covering analgesics, antipyretics, antiphlogistics, antirheumatics, lipid reducing compounds, antiepileptics, vasodilatators, tranquilizers,  $\beta$ -blockers, anti-neoplastic drugs, iodated X-ray contrast media and antibiotics were determined by GC-MS or ESI-LC-MS/MS and maximum contractions were reported [410]. Sixteen aromatic sulfonamides were monitored in the effluents of municipal STPs applying ESI-LC-MS and MS/MS in positive mode. Concentrations observed in secondary effluents or surface waters ranged from 5 to 1700  $\text{ng L}^{-1}$  [411]. The very polar phenylsulfonamides and their metabolites, both relevant for water works, were determined by ESI-LC-MS(-) and by GC-MS after derivatization. Real environmental samples and samples from a testfilter were analysed [412]. ESI-FIA- and LC-MS and MS/MS besides GC-MS were applied to follow polar and nonpolar organic pollutants in wastewater treatment process. Total ion and mass chromatograms as well as MS/MS spectra of pharmaceuticals were presented. Substance-specific scans in the MS/MS mode were used for identification (cf. APCI) [296].

The extent of exposure to cyclophosphamide and ifosfamide in 24 workers in two hospitals was monitored in air and from wipe and pad samples as well as from

gloves and urine using ESI-LC-MS (ion spray) and MS/MS. Because of incorrect use of the vertical laminar airflow hoods an increased contamination was observed [413].

Different drugs were submitted to aerobic biodegradation and results were monitored in FIA-ESI-MS mode [414]. The degradation of the pharmaceutical compound 4-fluorocinnamic acid in wastewater treatment process over a period of 149 h was followed by ESI-LC-TOFMS in the negative mode to recognize precursor compound and biodegradation products. The tentative biodegradation pathway was presented [415]. An ESI-LC-TOFMS in positive and negative mode was applied to perform “exact mass” measurements of aromatic sulfonamides and sulfonates in spiked samples and anaerobically treated textile wastewater [416].

A library of ESI and APCI product ion mass spectra of a number of steroids, morphine and drugs of abuse based on wideband excitation in an ion trap mass spectrometer was assembled and was applied to real environmental samples [292].

### Dyes

Dyes are used for manifold applications, predominantly in the textile industries but the food industry is also uses some of these compounds. The strongly polar compounds can be ionised by ESI interface in negative mode without fragmentation [201]. Ion chromatography (IC) coupled with MS-LC separation in the ion-pairing mode by addition of volatile amines allowed the separation and determination of the very strongly polar metabolites of dyes [416, 417]. The determination of sulfonated azo dyes in water and wastewater [43] or dye stuffs, PAHs, surfactants and pesticides in environmental matrices [28] were the topics of papers which compared the results of application of the different interface types, ESI, TSP and APCI [43] or ESI, APCI, TSP and PBI [28], respectively. In very early applications of ESI-LC-MS Bruins et al. [418, 419] reported on the analysis of dyes. The behavior of these compounds in the wastewater treatment process was elucidated by several groups [200], biodegradation processes were observed and followed [201, 420, 421] and even on-line ESI-LC-MS coupled with NMR was performed for identification [422]. Substance specific scans, loss of SO<sub>3</sub>, in CID mode helped to improve the confirmation [201, 420].

SPE followed by CZE/UV and optimized capillary zone electrophoresis (CZE) with ESI-MS detection was used to determine monosulfonated (Mordant Yellow 8) and a series of disulfonated azo dyes (Acid Red 1, 13, 14 and 73, Mordant Red 9, Acid Yellow 23 and Acid Blue 113) quantitatively in spiked (3 mg l<sup>-1</sup> of each compound) groundwater samples and industrial effluents [423]. Azo dyes besides pesticides and herbicides were determined by ion trap MS interfaced by a commercial ESI to the LC-device. By adjusting the repeller voltage (in-source CID) and doing MS/MS in the ion trap for [M+H]<sup>+</sup> ions CID spectra were obtained. With online ESI-LC-ITMS, detection limits of 0.1–1.0 ng could be easily achieved. IT-MS/MS and ESI-CID data were provided and compared [424]. ESI was used for coupling CZE and MS or LC and MS to analyse SPE concentrated sulfonated azo dyes and LAS in industrial effluents. CZE-MS offered higher separation power and

was less affected by matrix components than LC-MS. Detection limits for sulfonated azo dyes in SIM mode were observed with 100–800 µg L<sup>-1</sup> for CZE-MS [425]. Capillary electrophoresis (CE) with UV-DAD detection or MS interfaced by ESI in negative mode were applied for the identification of five reactive vinylsulfone dyes and their hydrolysis products in spent dyebaths and raw and treated wastewaters after C<sub>18</sub> SPE. Concentrations of the different dyes and hydrolysis products in sewage effluents ranged from 23 to 42 µg L<sup>-1</sup> [426]. Anthraquinone dyes (e.g. Disperse Blue 3) was characterised besides other pollutants in the effluents of a textile company by ESI-LC-MS and -MS<sup>n</sup> in positive ion mode and in addition using the in-line data obtained from LC/NMR [422]. Sulfophthalimide, sulfophthalimide, sulfophthalamic acid and sulfophthalic acid as metabolites of sulfophthalocyanine textile dyes were determined qualitatively and quantitatively by ion pairing ESI-LC-MS and MS/MS resulting in quantification limits of 2–10 µg L<sup>-1</sup> [417]. Eighteen polysulfonated anionic dyes and their degradation products were analysed by HPLC-UV and ESI-LC-MS(-) in the form of [M-xA]<sup>x-</sup> (A = H or Na) using volatile ion-pairing reagents. MS spectra were presented and structures were proposed according to the MS spectra obtained [427]. Aromatic sulfonic acids and sulfonated azo dyes were analysed by ESI-LC-MS. For improvement of LC separation non-volatile TBA ion pairing agents were used and then removed on-line prior to ESI-MS analysis [297]. The coupling of ion-exchange and ion-pairing chromatography by ESI with tandem mass spectrometry (MS/MS) was studied by Siu et al. who performed LC separations of a mixture of six permitted food dyes [428].

Quaternized cellulose is used as a sorbent to remove azo dyes from wastewater samples. For cellulose recycling purposes reductive degradation was performed and products of Orange II and Remazol Red F3B were determined by ESI-LC-MS and MS spectra of azo dyes and reduction products were reported [429]. As major oxidative degradation products of the azo dye Uniblue A four reaction products were identified under UV irradiation (254 nm)/ peroxydisulfate treatment. Possible reaction pathways were discussed [421].

### Estrogenic compounds

The metabolic degradation products of natural and synthetic estrogens, present as glucuronides or sulfates, are strongly polar compounds in order to make their renal elimination possible. Therefore LC-MS is the method of choice to determine these compounds in underivatized form. For the analyses of the the precursor compounds, however, GC-MS is amenable and widely used because of the high sensitivity observed (cf. 15.3.3.2 APCI, estrogens). Comprehensive studies with ESI and APCI methods were performed [298], raw and treated wastewaters were examined quantitatively [300, 301].

The most prominent ions under ESI(+) ionisation observed in natural water extracts were [M+Na]<sup>+</sup> adduct ions [298]. Estrogens and progestogens of natural and anthropogenic origin from environmental samples were analysed using different SPE materials prior to ESI-LC-MS. For the determination of estrogens MS was op-

erated in negative mode while progestogens were determined in positive ion mode.  $[M-H]^-$  or  $[M+Na]^+$  ions were obtained [430].

### Explosives

World War II wastes, such as explosives may cause considerable problems because of the mobility of their metabolites generated under anaerobic conditions, the anilines, which are under suspicion as carcinogens. Results of ESI and APCI were taken to compare TSP-LC-MS(-) results in the negative mode for the explosives TNT, RDX and hexyl and their degradation products in groundwater samples from ammunition hazardous waste sites. Applying SPE (LiChrolut® EN) 31 compounds could be identified, such as nitramines and their by-products, TNT and partially nitrated toluenes, 1,3,5-trinitrobenzene (cf. 15.3.3.1 TSP, explosives) [205]. Cyclic nitramine explosives were examined in real and spiked soil samples to recognize degradation pathways. Mononitroso, dinitroso and trinitroso metabolites and ring cleavage products were determined by ESI-LC-MS in negative mode, resulting in  $[M-H]^-$  ions [431]. The explosive 1,3,5-trinitro-1,3,5-triazacyclohexane (RDX) and its nitroso-RDX metabolites were analysed by ESI and APCI-LC-MS in groundwater samples after SPE (Sep-Pak Porapak RDX) (cf. 15.3.3.2 APCI, explosives). APCI provided a 20-fold greater signal for nitroaromatics than ESI. Detection limits of 0.03–0.14 mg L<sup>-1</sup> and recoveries of 71–130% were found [302]. EI-MS or ESI-MS spectra of explosive residues contained in a drainage water extract of an ammunition plant were published and the list of compounds examined was reported. The comparability and the limitations of the application of these libraries for identification were discussed [291]. A two-step (anaerobic/aerobic) composting was performed in a reactor system containing 2,4,6-trinitrotoluene-contaminated soil. Three new TNT metabolites, 4-acetyl amino-2-hydroxyl amino-6-nitrotoluene, 4-formamido-2-amino-6-nitrotoluene and 4-acetyl amino-2-amino-6-nitrotoluene, were observed as  $[M+H]^+$  ions, which arised first under anaerobic conditions and then were degraded aerobically to > 99% [432].

### Haloacetic acids and disinfection byproducts

The main source of haloacetic acids in the environment is free chlorine or bromine. In the disinfection process of drinking water chlorine is applied, which may result in the generation of halogenated carboxylic acids besides a broad spectrum of volatile halogenated compounds amenable for electron capture detection (GC-ECD) or GC-MS. The application of ESI-LC-MS meanwhile has been established for quality control of drinking water to determine these contaminants substance-specifically [433, 434]. A method for the quantitative determination of nine chlorinated and brominated haloacetic acids at ppt-levels was elaborated and put into practice with a flow injection ESI-FAIMS/MS (high field asymmetric waveform ion mobility) device [435]. Another method applying ESI-LC-MS after SPE (Li-Chrolut EN, HR-P, Isolute ENV+ and Oasis HLB) for the quantitative determination of several mono- up to tri-halogenated acetic acids containing chlоро or bromo

substituents or a mixture of both in tap water, drinking and swimming pool water was presented [436]. The problem of separating haloacetic acids from matrix compounds present in the extracts and of determining them was solved by applying three different approaches: FAIMS [435, 437, 438, 439], MS after generation of organic complexes with high *m/z* ratios by coupling the analytes with perfluoroheptanoic acid or by application of high resolution MS using TOF instruments, all MS interfaced by ESI. New disinfection byproducts generated by applying ozone with either chlorine or chloramine determined by ESI-LC-MS were reported [440].

### **Organotin compounds**

The coupling of ion-exchange (IEC) and ion-pairing chromatography using ESI coupled with MS/MS allowed the determination of several environmentally important organotin compounds in complex mixtures. An arsenobetaine could be confirmed by MS/MS after IEC [428]. Arsenc species were determined by ESI-LC-MS applying post column methanol addition [441].

### **Polycyclic aromatic hydrocarbons (PAH)**

The results of PAH analysis with different types of interfaces (e.g. ESI, APCI, PBI and TSP - were reported by Clench et al. reviewing the state of the art of various mass spectral techniques [28]. For more polar PAHs pneumatically assisted ESI-LC-MS was used to determine mixtures of hydroxy polycyclic aromatic hydrocarbons. The abundance of ions dependent on flow rates was shown. ESI ionization was found to be less sensitive compared to APCI ionisation [304]. PAH analysis with ESI-LC-MS combined with RP-LC with post-column addition of silver nitrate was applied for the determination of 10 PAHs in river water. PAHs resulted in  $[M]^+$  and  $[M+Ag]^+$ . The detection limits of different PAHs in spiked samples ranged from 0.001 to 0.03  $\mu\text{g L}^{-1}$  [442].

The gas-phase reactions of PAHs with OH and  $\text{NO}_3$  radicals generated in situ via photolysis of methyl nitrite were followed by ESI-MS. Naphthalene and  $d_8$ -labeled naphthalene were used as PAH components [443].

### **Phenols**

The determination of phenols was preferentially performed using GC-MS with analytes in underivatized or derivatized form, but LC-MS methods were also developed. API methods for the analysis of phenols in aqueous matrices were applied [315, 316, 317]. APCI-LC-MS was found to be more sensitive than ESI application despite the possibility of improving ESI-sensitivity by a post-column addition of diethylamine [317]. Detection limits were observed with 0.02–20 ng injected onto the column. The determination of alkylphenols and bisphenol A as compounds with endocrine disruptor potential was also performed by ESI-LC-MS from aqueous [318, 319] and sediment samples with detection limits in the low  $\mu\text{g L}^{-1}$  range [346].

With the use of ESI-CE-MS a total of 11 priority phenols could be easily separated and quantitatively determined [444].

### Sulfonic acids

Aromatic sulfonic acids are hardly degradable and, because of their polarity, very mobile during the drinking water treatment process resulting in the need for a reliable determination method. Twenty two aromatic sulfonates were extracted using four different SPE phases before the compounds were separated, confirming the excellent performance and separation power of ESI-CE-MS (cf. Fig. 15.6) [395]. Twenty aromatic sulfonic acids and their metabolites observed in industrial wastewaters were determined by ESI-LC-MS(-) and MS/MS using volatile amines for ion-pairing purposes in LC separation [445]. Several sulfonic acids such as *p*-toluenesulfonic acid, naphthalene-2,6-disulfonic acid and 2-aminonaphthalene-1,5-disulfonic acid were used as markers for studying processes in the leachate plume and in the groundwater downstream of a landfill. ESI-LC-MS(-) mass chromatograms and spectra were shown and the feasibility of ESI in the monitoring was discussed [446]. Benzene and naphthalenesulfonates in leachates and plumes of landfills were determined by ESI-LC-MS(-) after ion-pairing LC [447]. A sensitive ESI-LC-MS method for the determination of poly(naphthalenesulfonate) (PNS) contaminants in water after ion-pairing SPE extraction using ammonium acetate was elaborated and validated by naphthalenesulfonate-formaldehyde condensates. Environmental relevance of these compounds was confirmed by the analyses of grab samples of waste, river and ground water, containing PNS type compounds levels between 53 ng L<sup>-1</sup> and 32 µg L<sup>-1</sup> [448]. Naphthalenesulfonate-formaldehyde condensates were analysed by ESI-LC-MS(-) after ion-pairing LC [449], supporting the results reported by Crescenzi et al. [448]. Aromatic sulfonates known as hardly degradable pollutants in the aquatic environment were determined in landfill leachates and groundwater by ESI-LC-MS in negative mode [450]. Eighteen monomeric aromatic sulfonates which were contained in heavily loaded industrial wastewaters from textile industry were examined by ESI-LC-MS(-) before and after anaerobic and aerobic degradation. Six selected compounds were quantified in SRM mode [451]. Quadrupole mass spectrometers in positive and negative ESI-LC-TOFMS mode were applied to perform “exact mass” measurements of aromatic sulfonates and sulfonamides in spiked samples and anaerobically treated textile wastewater [416].

### Surfactants

Several review papers have reported on the application of ESI in the analysis of surfactants. Di Corcia reviewed LC-MS methods for the unequivocal identification of isomers, oligomers and homologues of the technical blends of surfactants and their biodegradation intermediates in environmental samples at trace levels with particular attention to ESI and TSP applications [40]. Clench et al. [28] described the applications of LC-MS in environmental analysis using the interfaces PBI, TSP, APCI and ESI in use or just coming into use in the early 1990s.

Reports obtained from ESI interfaced LC-MS on non-ionic surfactants as medium polar compounds compared to the strong polar anionics predominantly covered the AEOs, NPEOs and some up-coming surfactants.

When APCI and ESI-LC-MS were compared in their ionisation efficiency for AEOs spiked into raw wastewater the more effective APCI technique was preferentially applied because low detection limits could be obtained (cf. 15.3.3.2 APCI, surfactants) [334]. Non-ionic polyethoxylate surfactants such as aliphatic alkylethoxylates (AEOs) and nonylphenol polyethoxylates (NPEOs) in water were determined by ESI-LC-MS after SPE using GCB. Recoveries were 85–97% and concentrations in municipal wastewaters were observed at ppt levels [452]. Surface water from the river Elbe (Germany) was qualitatively analysed, particularly for polar organic pollutants, using ESI and APCI-LC-MS and MS/MS. For identification, diagnostic scans in the MS/MS mode or neutral loss (NL) mode were performed, which confirmed non-ionic and anionic surfactants (cf. 15.3.3.2 APCI, surfactants) [226]. A mixture of 2-butyl branched AEOs, each containing an average of five ethoxy units was biodegraded prior to analysis by ESI-LC-MS. MS and MS/MS spectra and mass chromatograms of neutral and acidic metabolized branched surfactants were reported proving that the ethoxylate chain was shortened or oxidized resulting in highly polar intermediates [453]. ESI-FIA-MS/MS(+), LC-MS and MS/MS analyses were performed to characterise non-ionic surfactants in the wastewater extracts of Thessaloniki (Greece) STP after SPE using C<sub>18</sub> or LiChrolut EN. MS and MS/MS spectra of non-ionics as dominating pollutants (AEOs and NPEOs) in inflow and effluent samples were presented (cf. 15.3.3.2 APCI, surfactants) [336].

ESI-LC-MS and MS/MS were used to identify the components of three non-ionic surfactant mixtures, NPEOs, secondary alcohol ethoxylates (SAE) and primary AEOs [454] used in wool scouring [455] and to monitor intermediates in the photocatalytic degradation of SAEs over a suspension of TiO<sub>2</sub> particles. Typical spectra at various stages of degradation were obtained, indicating the initial preferential cleavage of ethoxyl groups over OH radical reactions with the aliphatic alkyl chains resulting in cleavage at the secondary carbon in the molecules [454]. The photocatalytic decomposition products were the same as observed in the MS under CID conditions [455]. A robust LC-determination of NPEOs and octylphenol ethoxylates (OPEOs) in sewage plant effluents by fluorescence detection was confirmed by ESI-LC-MS(+) using 1-(4-methoxyphenyl)hexan-1-ol as internal standard. The limit was 5 µg L<sup>-1</sup> applying 100 mL of effluent, which was extracted by GCB-SPE. Use of MS/MS in neutral loss (NL) mode allowed an increased selectivity in detection [456]. NPEOs, OPEOs and AEOs of different alkyl chain length were routinely determined by ESI-LC-MS(+) in wastewater and sludges, treated in different ways, in gradient elution mode [457]. Nonylphenols (NPs) and NPEOs extracted from wastewater treatment plant influent and effluent and surface water sediment were determined by ESI-LC-MS in negative or positive ionisation mode, respectively, using stable isotope-labeled standards [458]. The short and long EO-chain APEOs, besides halogenated NPEOs and nonylphenolpolyether carboxylates (NPECs), in estuarine water and sediment samples after high-temperature sonicated extraction were determined by ESI-LC-MS in positive or negative mode. Limitations of the

method were discussed [459]. A method for the determination of NPEO homologues by ESI-LC-MS in positive mode in river water samples was described by Taino et al. [460]. ESI-LC-MS and MS/MS were used to characterise recalcitrant intermediate species generated from biotransformation of the branched alkyl chain of industrial blends of NPEOs. After a biodegradation period of 2 weeks, species oxidized in both side-chains, alkyl (CAPEO) and PEG (APEC) chain, could be confirmed. Less abundant metabolites having only the alkyl chain carboxylated (CAPEs) were also formed and before degradation proceeded in a slow transformation to alkyl and polyether chain carboxylated compounds (CAPECs) [461]. A novel rapid screening method, combined precursor ion scanning and multiple reaction monitoring, using ESI MS/MS or APCI MS/MS (cf. 15.3.3.2 ESI, surfactants) was elaborated to monitor homologue mixtures of NPEOs contained in the inflows and effluents of STPs. The method proved to be more selective and specific than current methods for NPEO profiling [340].

ESI-LC-MS and MS/MS were applied to elucidate the metabolism of 4-NPs, the metabolites of NPEOs. The metabolites observed were identified as 4-hydroxy- and 4-(dihydroxy)-NPs, glucosylated at the phenolic OH group and further glucosylated or glucuronidated [462]. Anionic and non-ionic surfactants (e.g. LAS and short and long chain NPEOs, respectively) were characterised in the effluents of a textile company by ESI-LC-MS and MS<sup>n</sup> using an ion trap in positive ion mode. The combination of MS<sup>n</sup> and stop-flow-LC/NMR in-line data allowed identification to a great extent [339, 422]. Halogenated APEOs and their metabolites were quantitatively analysed and identified in drinking, surface and wastewater as well as in river sediments and STP sludges by ESI or APCI-LC-MS(+/−) under optimized conditions [345]. Brominated and chlorinated compounds of NPEOs and OPEOs were confirmed. Quantitative determination of NPEO surfactant homologues in marine sediment using normal-phase ESI-LC-MS was performed resulting in detection limits of 2–10 ng g<sup>−1</sup> with linear calibration graphs from 0.5–500 ng [463]. Pope noe et al. [464] described an ESI (ion spray) LC-MS method for the quantitative analysis of the anionic surfactants, alkyl sulfates (AS) and alkyl ethoxysulfates (AES) in natural waters. The method was validated with spiked samples, using 36 AES homologue species. Linear calibration curves and recoveries > 90%, except for highly spiked effluents, (75%), were observed. Comparing ESI and APCI for the analysis of AES APCI in positive mode at low cone voltages proved to be the method of choice because its fragment ion spectra revealed the alkyl chain length and the number of ethoxylate moieties [326]. This was, in contradiction, reported after a comparison of API techniques in positive or negative mode as presented in Fig. 15.3 [21]. The analysis of selected AES homologues was performed by ESI-FIA-MS/MS(−) or ESI-LC-MS(−), homologue distributions in industrial blends were presented [329]. Solid-phase micro-extraction (SPME) was used for concentration of LAS homologues (C<sub>10</sub>–C<sub>13</sub>) from municipal wastewaters. Homologues were then determined with high selectivity and sensitivity by ESI-LC-MS under in-source-CID conditions [465]. SPME was also applied for the concentration of water-soluble components of sludges and sediments before the pollutants (e.g. phthalates, fatty acids, nonionic surfactants, chlorinated phenols and carbohydrate

derivatives) were detected by ESI-LC-MS [466]. LAS in wastewater inflows and effluents and coastal waters (Cadiz, Spain) were determined by automated SPE followed by ESI-LC-MS(-) and ESI-CE-MS(-) and results were compared to CE-UV. LAS in concentrations  $> 990 \mu\text{g L}^{-1}$ ,  $> 136 \mu\text{g L}^{-1}$  or  $> 739 \mu\text{g L}^{-1}$  were observed in inflows, effluents and coastal waters [467]. LAS together with dialkyltetralinsulfonates (DATS) in aqueous environmental samples could be detected and quantified by LC-FL and subsequently were confirmed by ESI-LC-MS. Compounds were extracted by graphitized carbon black (GCB) [468]. The long-chain intermediates from the biodegradation of LAS in the marine environment were monitored by ESI-LC-MS(-) after SPE ( $\text{C}_{18}$  followed by SAX). The metabolite pattern observed indicated an (-oxidation resulting in  $\text{C}_{11}$ -chain molecules in seawater samples and  $\text{C}_{13}$ -chain molecules in interstitial waters [469]. Carboxylic degradation products, the so-called sulphophenyl carboxylates (SPCs), of LAS in coastal waters were concentrated by SPE and analysed by ESI-LC-MS(-). Total ion chromatograms (TICs) and SIM traces were presented. Fragment ions obtained by source CID were tabulated. Recoveries of 51–96% were observed, with a general improvement parallel to increasing alkyl chain length [470]. Testfilter experiments with LAS resulted in SPCs determined by ESI-LC-MS(-) applying an ion suppressor module to improve sensitivity [394]. The quantitative determination of LAS in sea water and sediment samples from the German Bight of the North Sea or Waddensea marinas and estuaries applying ESI-FIA and LC-MS and MS/MS in the negative mode were performed. Concentrations observed for LAS compounds were  $< 39\text{--}106 \text{ ng g}^{-1}$  dry matter and  $< 30 \text{ ng L}^{-1}$  in water samples from estuaries [333].

Elimination efficiencies for surfactants as predominantly observed pollutants in a conventional and in parallel three bio-membrane assisted wastewater treatment plants were studied. ESI-FIA and LC-MS and MS/MS in negative mode were used to qualify and quantify LAS. Diagnostic scans were applied for confirmation [343]. The elimination efficiency of LAS in a wet air oxidation reactor by chemical treatment of a wastewater was monitored by ESI-FIA-MS(-) applying a pattern recognition [471].

The determination of perfluorinated anionic surfactants, perfluorinated alkane-sulfonates and perfluorocarboxylates, in surface water samples after an accidental release of perfluorosurfactant contaminated fire-fighting foam was performed qualitatively and quantitatively by ESI-LC-MS and MS/MS. The ESI-LC-MS and MS/MS(-) TICs of the determination of perfluoroctanesulfonate (PFOS), perfluorohexanesulfonate (PFHxS), perfluoroctanoic acid (PFOA), perfluoroheptanoic acid (PFHpA), perfluorododecanoic acid in water samples were presented [472]. Anionic and non-ionic surfactants and their degradation products were determined qualitatively and quantitatively by ESI-LC-MS in sewage sludge samples. Ultrasonification was applied for extraction while ESI interface in negative mode was used for more polar compounds (e.g. NPECs). APCI (cf. APCI) was used predominantly in positive mode to ionise the AEOs, NPEOs and PEGs [346]. Already in 1990 organic ammonium, sulfate and sulfonate surfactant compounds were determined by Conboy et al. after ion chromatography by ESI-IC-MS in positive mode. MS and MS/MS spectra were provided (see Fig. 15.7) [473]. The qualitative and quantita-

tive analysis of the cationic surfactants ditallow-dimethylammonium chloride (DTDMAC), diethylester dimethylammonium chloride and diesterquat by microbore LC-MS under ESI ionisation was examined using LAS as ion-pairing reagent. STP inflows and effluents and river water samples were studied. Cationic surfactant concentrations of 0.4 up to 140 µg L<sup>-1</sup> were found in river and sewage waters [474]. After SFE using CO<sub>2</sub>, DTDMAC was determined by HPLC-UV or HPLC-fluorescence and confirmed by ESI-LC-MS(+) in anaerobically stabilized sewage sludges to study their presence in the phasing-out period. It became obvious that DTDMAC levels in sludge had dropped by 94% from 1991–1994 due to the producers' voluntary ban on its use in Europe [475]. An industrial blend of C<sub>12</sub> and C<sub>14</sub>-N-methylglucamides and their biodegradation under aerobic conditions was examined by ESI-LC-MS to determine precursor and metabolite compounds in municipal sewage plant inflow and effluent samples. Degradation involved ω-oxidation of the alkyl chain followed by a ω-oxidation. The C<sub>4</sub> glucamic acid could be observed as a degradation intermediate, but higher homologues were not found, probably due to rapid breakdown [476]. To determine non-ionic surfactants of alkyl polyglucoside type (APGs) in wastewater effluents an ESI-LC-MS method was elaborated [477, 478]. Despite the fact that monitoring also covered potentially arising metabolites as observed in an APG degradation study monitored under TSP ionisation conditions [212] no metabolites were detected here. The qualitative determination of so-called gemini surfactants with highly improved surface activity by APCI or ESI-FIA-MS and LC-MS and MS/MS was reported. Mass spectra, fragment ion spectra and fragmentation pathways were presented [479]. Results of LC techniques and enzyme-linked immunosorbent assays for the determination of surfactants in wastewaters were obtained in an interlaboratory comparison study performed in seven laboratories. The non-ionic NPEOs, AEOs, coconut diethanol amides and the anionic LAS, NPEO-sulfates and secondary alkane sulfonates (SAS) were quantitatively determined by ESI and APCI-LC-MS and MS/MS (cf. 15.3.3.2 APCI, surfactants) [327]. In parallel to stability studies of pesticides the stability of surfactant compounds contained in water matrices or adsorbed on SPE phases was examined using ESI or APCI-LC-MS. NPEOs, alcohol ethoxylates (AEOs), coconut diethanol amides (CDEAs) and LAS were examined. After storage at 4 °C or 20 °C the compounds were analysed with SIM detection limits at 0.05–0.70 µg L<sup>-1</sup> (cf. 15.3.3.2 APCI, surfactants) [328]. Advantages and drawbacks of the application of added non-ionic, anionic and cationic surfactant mixtures to nitroaromatic spiked sediments for an improved extraction of these nitroaromatic compounds were discussed after results of ESI-LC-MS of fractions from SFE were compared [480]. Polar Fenton oxidation products of surfactants (lauryl sulfate) were analysed by ion spray (ESI) MS. ESI-LC-MS provided information on the oxidation mechanism which resulted in mainly hydroxyl and epoxide group or aldehyde compounds [481]. MS spectra were presented [482].

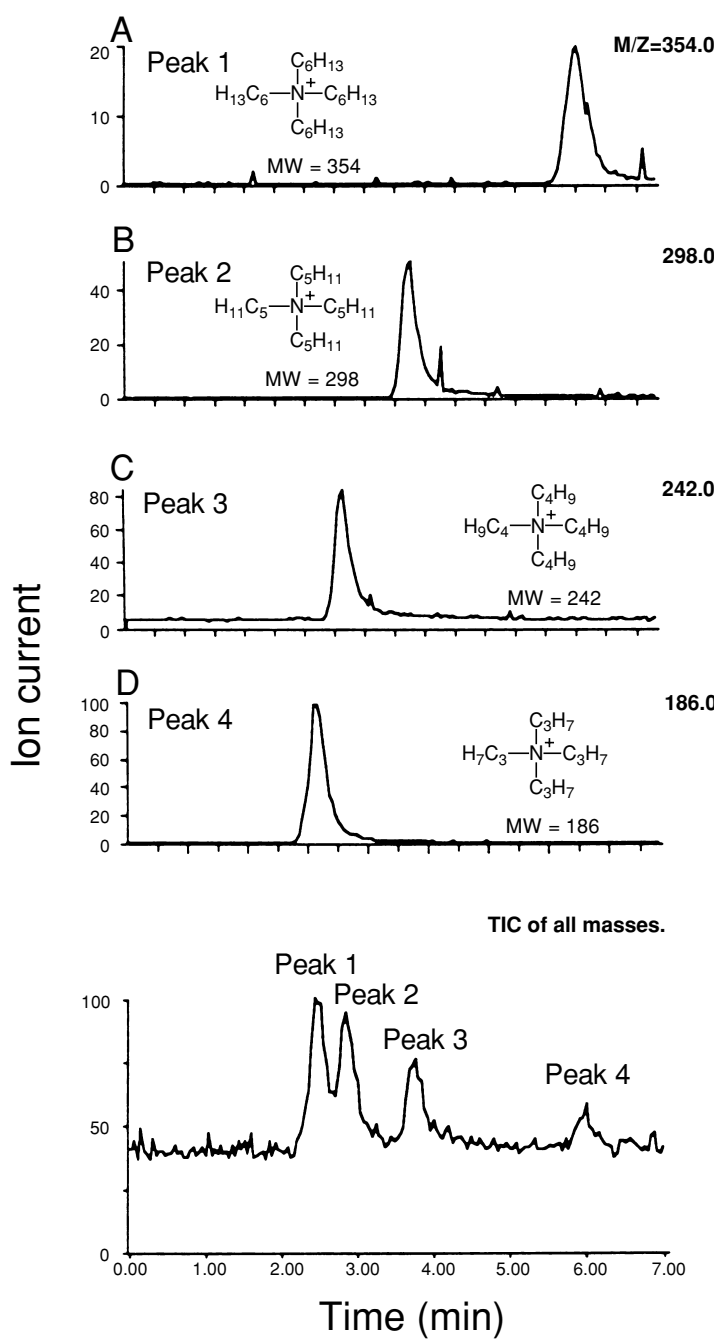


**Fig. 15.7** One of the first published ion chromatography application interfaced by ESI with MS. ESI-IC-MS(+) total ion current trace (TIC) and selected mass traces of an industrial blend of quaternary ammonium compounds. Reproduced with permission from [473] © American Chemical Society, 1990.

### Toxins

No reports were found of the analyses of free biogenic toxins in the environment, i.e. in surface or seawaters, but on the seafood toxins contained in shellfish and other seafood many papers are available since the invention of the soft ionizing interfaces. A review paper from Quilliam [396] reported the different types of toxins. Domoic acid is an amnesic shellfish-poisoning toxin originating from blue mussels which could be contained in shellfish. Its quantitative determination was studied by ESI-LC-MS(+) and MS<sup>n</sup>. MRM results were presented which allowed an unambiguous identification and quantitation combined with a minimum of sample cleanup [483]. ESI-LC-MS was used to handle thermolabile, polar seafood toxins such as domoic acid and isodomoic acids. LC eluent compositions were optimized for detection [410]. Even the very lipophilic shellfish toxins such as okadaic acid could be studied by ESI-LC-MS in positive mode, resulting in  $[M+Na]^+$  and  $[M+NH_4]^+$  adduct ions [484]. ESI or an ion spray interfacing technique operated in MS and MS/MS mode were found to be useful tools to determine and identify the shellfish toxins ciguatoxin and maitotoxin [485]. Cyanobacterial hepatotoxins in drinking water were analysed by CE-MS [486] and new pectenotoxins could be identified by LC-MS and MS/MS [487]. ESI-LC-MS(+) with micro-LC was applied to study SPE conditions of microcystins [488].

### Pesticides (incl. herbicides, fungicides etc.)

#### *Anilides, quaternary amines, toluidines and thiocyanate compounds.*

The quaternary ammonium herbicides paraquat and diquat were first separated by CZE and then detected by ESI on a laboratory-built TOF instrument by means of volatile buffers. Depending on the buffer the ESI-TOF mass spectra of paraquat and diquat under these conditions showed singly and doubly charged molecular ions [489]. Moyano et al. also applied ESI-CZE-MS(+) to the determination of the herbicides mepiquat, chlormequat, diquat, paraquat and difenoquat in water. MS/MS provided the structural information essential for the confirmation of identity [490]. For product quality check-up of formulations of the herbicide chlormequat ESI-CZE-MS was used, allowing the determination of contaminants contained in the formulation [491]. The quaternary ammonium pesticides paraquat; diquat, difenoquat, chlormequat and mepiquat were analysed by ESI-LC-MS(+). Prior to analysis ion-pairing extraction was applied to concentrate compounds prior to analysis on different SPE materials (e.g. C<sub>8</sub>, C<sub>18</sub>, and PS-VDB) [492]. Separation of chlormequat on ODS1 combined with optimised ESI-LC-MS(+) allowed direct quantification on an ion trap instrument at levels lower than those required for residue analysis in foods and also in drinking water [493]. The determination of diquat and paraquat in water samples was performed by ion-pairing ESI-LC-MS using labeled diquat-d<sub>4</sub> dibromide or paraquat-d<sub>8</sub> dichloride and trifluoroacetic acid for ion-pairing purposes. The ions observed were  $[M^{2+}-H]^+$  and  $[M^{2+}+OOCCF_3]^+$  for diquat and paraquat, respectively. Detection limits

were  $< 0.2 \mu\text{g L}^{-1}$  [494]. The addition of heptafluorobutyric acid (HFBA) as ion pairing agent allowed the determination of paraquat and diquat in water without sample preparation by ESI-LC-MS(+). Detection limits for paraquat and diquat were observed with 5 and  $1 \mu\text{g L}^{-1}$  [495]. ESI-FIA and ESI-CZE-MS(+) resulted in quantitation limits ( $S/N=3$ ) of  $200 \mu\text{g L}^{-1}$  for paraquat and diquat. [496]. Ion-pairing LC was applied to analyse the quaternary ammonium herbicides diquat, paraquat, difenzoquat, mepiquat and chlormequat by ESI and APCI-LC-MS(+). Detection limits down to  $0.1\text{--}4 \mu\text{g l}^{-1}$  were obtained [347]. From solid samples chlormequat and mepiquat residues in grain were quantitatively determined by ESI-LC-MS and MS/MS after extraction with MeOH-H<sub>2</sub>O-acetic acid (75:24:1, v/v/v) prior to an SPE and elution step. Detection limits were observed with 2 and  $6 \mu\text{g kg}^{-1}$  for mepiquat and chlormequat [497].

Anilide pesticides were analysed by Ferrer et al. [498] who reported an ESI-LC-MS(-) method for the determination of the oxanilic and sulfonic acid derivatives of acetochlor, alachlor and metolachlor after C<sub>18</sub> SPE or liquid/liquid extraction using dichloromethane from surface and groundwater samples. Quantitation limits of  $0.01 \mu\text{g L}^{-1}$  combined with recoveries of 88% for both oxanilic and sulfonic acid derivatives were obtained (cf. triazines) [240]. An ESI (ion spray) LC-MS/MS method was developed for the qualitative and quantitative analysis of the very polar sulfonic acid metabolites of acetochlor, alachlor, metolachlor and dimethenamid observed in groundwater at trace levels. MS/MS spectra were reported and calibration graphs were linear at  $0.25\text{--}10 \text{ ng injected on-column}$  [499]. Anilides and N-substituted amine pesticides in natural waters after SPE (Carbograph 4) were simultaneously determined qualitatively and quantitatively using ESI-LC-MS [500]. An automated SPE procedure combined with ESI-LC-MS(-) (ion spray) was used for the detection and quantification of the acidic herbicides benazolin, bentazone and 6- and 8-hydroxybentazone in environmental waters. Good fragmentation was observed under ESI conditions providing more information than TSP-LC-MS. SIM detection limits of  $0.01\text{--}0.03 \mu\text{g L}^{-1}$  were observed, dependent on the extraction voltages [501]. Bentazone and alachlor were examined when an on-line dual-precolumn-based trace enrichment step applying the SPE materials (PLRS-S, Hyshere-l, LiChrolut EN and Isolute ENV +) and two different pHs was studied (cf. 13.3.3.2 APCI, triazines) [502]. ESI [503], FAB and APCI-LC-MS and MS/MS [175] were used for the multiresidue determination of a broad range of pesticides and to explain fragmentation mechanisms observed in a TSP study of anilides [175]. The methods were validated for selectivity, linear dynamic range, detection limit, precision and ruggedness. Biodegradation of alachlor in river water over a period of 28 d was performed. ESI-LC-MS besides GC/MS after derivatization were applied to follow the disappearance of alachlor. Several degradation products could be confirmed by comparison with synthetic standards [504]. ESI-LC-MS and MS/MS were performed on an orthogonal-acceleration (oa) TOF to characterise the photodegradation products of alachlor in water after on-line SPE. MS and product ion MS spectra of precursor and degradation products were presented and structures proposed for the observed product ions were shown [505] or degradation was followed by applying ESI-LC-MS and MS/MS. Effective monitoring of the de-

gradation process was possible and unknowns could be identified using MS/MS [506].

**Carbamates.** A fast, sensitive and selective method for the concentration and analysis of 9 N-methylcarbamate pesticides was reported by Volmer et al. [507]. Three different SPME fibres combined with short-column ESI-LC-MS(+) and MS/MS were applied. The detection limits observed were 0.3–1.9 µg L<sup>-1</sup>. Signal intensities increasing by a factor of 2–7 were observed [508] using non-volatile buffers in the separation process prior to ESI-MS. After LC removal of the non-volatile buffers was essential. The results obtained by ESI and APCI-LC-MS and MS/MS for the analysis of the eight N-methylcarbamate pesticides and their degradation products were compared with results obtain with the application of TSP or PBI (cf. 15.3.3.1 TSP, carbamates) [108]. ESI-LC-MS and TSP-LC-MS were used for quantitative determination of 10 different carbamate pesticides which showed a broad variety in polarity. ESI-SIM detection limits were typically 10–60 pg which was 10–150 times better than using TSP-MS (cf. 15.3.3.1 TSP, carbamates) [509]. Interfacing a commercial ESI source to an ITMS allowed the determination of carbamates as well as triazines and azo dyes. Identification could be performed either by IT-MS/MS or by ESI-CID [424].

The determination of carbamates by ESI-MS in environmental waters was reported in various papers. In one study the simultaneous determination of 26 non-acidic and 13 acidic pesticides in natural waters was performed. Recoveries observed were > 80% except for carbendazim, butocarboxim, aldicarb and molinate which were all better than 67% [500]. Forty five different pesticides of thiocarbamate, carbamate and carbamoyloxime type e.g. molinate or mercaptodimethur, carbaryl, ethifencarb, primicarb, propoxur, carbofuran, butocarboxim, aldicarb, carbetamide, methomyl, or oxamyl, aldicarbsulfone and butoxycarboxim besides other types were analysed SPE (Carbograph 4) by ESI-LC-MS(+) (cf. 15.3.3.2 ESI, triazines) [510]. For the multiresidue determination of carbamates and thiocarbamates in environmental samples parallel to a broad range of N- and P-containing pesticides ESI [503], FAB, PD and APCI-LC-MS and MS/MS interfacing techniques besides TSP [175] were used. Carbofuran and promecarb traces in water were determined quantitatively by means of ESI-LC-MS(+) (ion spray). TIC traces and mass spectra were presented. Detection limits of < 25 pg were observed [511]. Seven N-methylcarbamate [357] and 12 carbamate pesticides [512] were quantitatively analysed by ESI-LC-MS in river water or surface water from a lake, a groundwater well, a cistern, a farm pond and from drinking water samples, respectively. Compared to APCI-LC-MS ESI was found to be more sensitive [357]. Applying SPME coupled to ESI-LC-MS the carbamate pesticides aminocarb, asulam, barban, chlorpropham, methomyl, oxamyl, promecarb, propham and carbofuran in leachates of soil samples could be determined by applying positive ionisation. [513].

For the analysis of 10 carbamates in fruits and vegetables a comparison of ESI and APCI-LC-MS switching from positive to negative ionisation was performed (cf. APCI; carbamates). APCI was more efficient than ESI. Detection limits were equivalent to 0.002–0.033 mg per kg of crop [358]. Nevertheless, DiCorcia applied ESI-LC-MS(+) to analyse 12 N-methylcarbamate insecticides in 10 types of fruits

and vegetables. Recoveries were > 80% for all matrices with detection limits of a few hundred pg per g sample [514]. For the routine quantification of phenoxy carb, pyrimicarb and other types of pesticides e.g., carbendazim, thiophanate methyl, phosmet, thiabendazole in apples and pears ESI-LC-MS was applied, showing limits of detection and quantitation of 0.01–0.02 and 0.02–0.05 mg kg<sup>-1</sup>, respectively [515]. Thirteen carbamate pesticides were monitored by a newly established ESI and APCI-LC-MS procedure in oranges, grapes, onions and tomatoes after concentration by solid-phase dispersion (MSPD). Quantitative results were reported for both interface types (cf. 15.3.3.2 APCI, carbamates) [355].

The degradation of the carbamates carbofuran and methiocarb in estuarine waters was monitored by TSP- and ESI-LC-MS in positive and negative mode. TSP- and ESI-LC-MS in positive and negative mode were used for product monitoring and identification of hydrolytic and microbial degradation products (cf. 15.3.3.1 TSP, carbamates) [257]. When carbofuran, together with diuron, isoproturon, atrazine and alachlor, dissolved in surface waters at low levels was treated by UV light the physicochemical degradation products were analysed and characterised by applying ESI-LC-MS and MS/MS (cf. 16.3.3.2 ESI, phenylurea) [506].

#### *Organophosphorus compounds.*

An ESI-LC-MS(+) and MS/MS method was elaborated for the detection and characterization of phosphorothioate and -dithioate herbicides in environmental matrices. Compounds studied were diazinon, chlorpyrifos-methyl, chlorpyrifos, azinphos-ethyl, azinphos-methyl and phosmet. MS and MS/MS spectra were reported which confirmed that low-energy CID of [M+H]<sup>+</sup> enabled identification by characteristic fragmentation patterns of the phosphorodithioates [516]. ESI-LC-MS was used to elucidate fragmentation behavior observed in a TSP-LC-MS study of the phosphorus pesticides butenoate, dichlorvos and trichlorfon [175]. A test mixture of 17 pesticides containing the organophosphorus compounds dimethoate, fenamiphos, coumaphos, fenchlorphos, chlorpyriphos and bromophos-ethyl at low ng L<sup>-1</sup> levels were analysed by on-line SPE-ESI-LC-MS and MS/MS. A pesticide MS/MS library was successfully applied for identification [322, 353]. An ESI-LC-MS procedure was elaborated for the analysis of the polar and/or thermally labile organophosphorus pesticides trichlorfon, dichlorvos, dimethoate, oxydemeton-methyl, cis- and trans-mevinphos, demeton-S-methyl, fenamiphos, fenitrothion, fenthion and diazinon in groundwater [517] and surface water samples [518]. A variety of SPE materials (Amberchrom, LiChrolut EN, cyclohexyl, SDB, C18 and Isolute ENV) was examined. In contrast to TSP-LC-MS no thermal degradation was observed for trichlorfon [518]. Under these conditions transformation products such as fenthion sulfoxide were also observed. Detection limits in SIM mode were observed with 0.01–0.20 µg L<sup>-1</sup> [517] or 0.001 µg L<sup>-1</sup> [518], respectively.

A study with environmental samples was performed analyzing 26 non-acidic (e.g. organophosphorus, carbamate, triazine, anilide, N-substituted amine and phenylurea type) and 13 acidic (urea and phenoxy acid type) target pesticides simultaneously by ESI-LC-MS with recoveries of about 80% [500]. Drinking, ground and

river water samples containing the phosphorus compounds omethoate, demeton sulfoxide, demeton sulfone, monocrotophos, trichlorphon, dimethoate, azino-phos-methyl, malathion, ethoprophos, diazinon, phoxim, primiphos-methyl were concentrated by SPE using Carbograph 4 prior to ESI-LC-MS [510]. Several phosphorus target pesticides could be monitored using on-line SPE and ESI-LC-MS(+) detection. Results were confirmed by MS/MS [519]. The analysis of groundwaters spiked with fenamiphos was performed by ESI-LC-MS. The stability of samples adsorbed by Lichrolut-EN or styrene divinylbenzene cartridges and stored at –20 °C, 4 °C and ambient temperature for 80 d was studied [520]. ESI-IC-MS was successfully applied for glyphosate determination [397]. An automated SPE-LC-MS and MS/MS method interfaced by ESI was described for determination of the very polar phosphorus pesticides glyphosate, glufosinate and the glyphosate biodegradation product aminomethylphosphonic acid in drinking and surface waters [397, 521]. The detection in negative mode was selective, reliable and applicable to wastewater, drinking and surface water. Detection and quantitation limits were 0.03 and 0.05 µg L<sup>-1</sup>, respectively with recoveries of 96% [521]. Samples were analysed by ESI-LC-MS at 1 µg L<sup>-1</sup> levels and the background was reduced by about 2 orders of magnitude and salt adduction could be prevented [397]. For the routine quantification of the phosphorus pesticides dimethoate, thiophanate methyl, phosmet and other types of pesticides e.g. phenoxy carb, pyrimicarb, carbendazim, thiabendazole in apples and pears an ESI-LC-MS method was elaborated. Limits of detection and quantitation were 0.01–0.02 and 0.02–0.05 mg kg<sup>-1</sup>, respectively [515]. A novel metabolite of profenofos could be identified by ESI-LC-MS. Spectra of the metabolite which was identified as the glucosyl-sulfate conjugate of 4-bromo-2-chlorophenol were presented [522]. Ionic compounds contained in agricultural chemicals were determined by ESI-ion chromatography-MS and TSP-ion chromatography-MS/MS applying a solid-phase chemical suppressor. The method was tested on a standard solution. ESI spectra give intense [M-H]<sup>-</sup> peaks for methyl phosphate and methyl sulfate [523]. To follow the physico-chemical degradation products of pirimiphos methyl after ozone treatment, different MS methods, ion-trap EI or PICI-GC/MS, or ESI or APCI interfaced LC-MS, were applied. Illustrative ESI and APCI mass chromatograms of the pirimiphos methyl oxidation products and fragmentation data were reported and an ozonolysis degradation pathway was proposed (cf. 15.3.3.2 APCI, organophosphorus compounds) [155].

#### *Phenoxy carboxylic acids.*

In many contributions reporting on acidic pesticides in environmental samples ESI applied as ion spray was predominantly performed to analyse these pollutants. APCI, however, was not as effective as ESI as studies with standard solutions of the pesticide mixtures made obvious [325] when phenoxy acid compounds were determined using both types of interface. MSn quantitative results were used for confirmation. Mass detection after CZE-MS interfaced by ESI was successfully applied to analyse drinking water spiked with chlorinated acid herbicides. Selected-ion elec-

tropherograms of the 16 analytes provided detection limits ( $S/N = 3$ ) at  $8\text{--}250 \mu\text{g L}^{-1}$  [524]. To improve the ionisation efficiency the analysis of different types of so-called post-emergence herbicides of 2-(4-aryloxyphenoxy) propionic acid type (fluazifop, haloxyfop, fenoxaprop and quizalofop) in spiked groundwater and drinking water samples by ESI-LC-MS (ion spray) was studied [525]. Separation of enantiomers was performed on a chiral phase under CE conditions combined with ESI-MS in negative ionisation mode.  $[\text{M}-\text{H}]^-$  ions for the pesticide compounds mecoprop, dichlorprop and fenoprop [526].

Eighteen acidic herbicides such as phenoxy acids, sulfonylureas and phenols or their biodegradation products in groundwater samples were quantified by ESI-LC-MS(-) and confirmed by MS/MS. Recoveries of phenoxy acid derivatives were  $>80\%$ . [527]. Di Corcia et al. quantified 13 acidic pesticides of phenoxy acid and urea type and 26 non-acidic (base and neutral) pesticides of carbamate, triazine, anilide, N-substituted amine and organophosphorus type in natural waters after Carbograph 4 SPE. Recoveries observed for acidic compounds were better than 80% [500]. SPE applying GCB was also used successfully to concentrate and to determine acidic pesticides in aqueous samples by ESI-LC-MS [528, 529]. Screening examinations applying four different SPE materials (PLRS-S, Hysphere-1, LiChrolut EN and Isolute ENV +) were performed for concentration of a wide range of polar and acidic pesticides (e.g. 2,4,5-T and MCPA) in river water prior to analysis applying ESI-LC-MS(-) (cf. 15.3.3.2 ESI, triazines) and confirmation by MS/MS detection [502]. A protocol for the automated SPE in combination with ESI-LC-MS(-) for the quantitative determination of the phenoxy acid derivatives 2,4-D, MCPA, MCPP and MCPB in environmental waters was established [501]. A broad spectrum of pesticides contained in shallow groundwater samples from 2 sandy and 2 clay catchment areas were analysed using ESI-LC-MS or APCI-LC-MS. MCPA was observed as the predominant acidic pesticide compound when  $> 300$  samples were analysed [351]. Phenoxyalkanoic pesticide compounds were among the target compounds in surface water samples from Southeastern regions of France and from the St. Lawrence River in Canada. ESI-LC-MS results confirmed by MS/MS in the negative mode and ion trap LC-MS/MS were found to be comparable [374].

The metabolism of MCPA in water and soil samples was followed by ESI-LC-MS(-) and MS/MS. The main metabolite of MCPA, 4-chloro-2-methylphenol was determined with a detection limit of  $40 \text{ ng L}^{-1}$  for ground and surface water samples [530].

To optimize analytical results in the separation process TBA was used as the ion pairing agent in the quantitative analyses of phenoxy acid derivatives such as MCPA, 2,4-D, mecoprop, dichlorprop, 2,4,5-T, MCPB, 2,4-DB and 2,4,5-TP in drinking and surface water samples [529]. Under the same conditions, ion-pairing with TBA fluoride [531] or ammonium acetate [532], the arylphenoxypropionic herbicides fluazifop, fenoxaprop, quizalofop, haloxyfop and diclofop and some of their Me, Et and Bu-esters were determined in surface, ground water or drinking water [531] or in soil [532] by ESI-LC-MS in SIM mode. Recoveries and detection limits were reported.

### *Phenylureas, thioureas and sulfonylureas.*

Three different types of urea pesticides were used on a large scale: phenylureas, thioureas and sulfonylureas. Therefore these and their degradation products will be observed in the environment. For optimization ESI and FAB ionisation results in combination with LC-MS were compared on the same magnetic sector instrument. The mass spectra of several herbicides (e.g. bensulfuron methyl, bromacil and degradation products) were compared for each technique and high resolution results were obtained [533]. Different types of so-called post-emergence herbicides (sulfonylureas, imidazolines and 2-(4-aryloxyphenoxy) propionic acids) were studied by ESI-LC-MS (ion spray) after Carbograph 4-SPE. Recoveries were reported to be > 85%. Fragmentation and signal intensities, dependent on orifice plate voltage, were examined [525]. For improvement of LC separations in the analysis of phenylurea pesticides non-volatile buffers were applied which were removed prior to ESI-MS by a postcolumn removal technique [508]. To achieve good LC separations an eight component mixture of sulfonylurea crop protection chemicals were analysed on a capillary electrophoresis (CE) system adapted to an ESI-MS system (ion spray) [534]. CZE-UV results from the determination of 12 sulfonylurea herbicides in water were confirmed by ESI-LC-MS in positive mode combined with in-source CID [535]. Phenylurea herbicides in water samples could be determined with detection limits in the low pg range using both API-techniques, ESI and APCI, in MS and MS<sup>n</sup> (15.3.3.2 APCI, phenylureas) [325]. For a high throughput combined with a substance-specific determination of the polar urea pesticides metoxuron, monuron, monolinuron, chlortoluron, metabromuron, metabenzthiazuron, isoproturon, diuron, linuron, ESI-FIA-MS without prior chromatographic separation was performed successfully (cf. 15.3.3.2 APCI, phenylureas) [373]. ESI-LC-MS in parallel to TSP-LC-MS in SIM mode was used in a multiresidue method for the determination of the sulfonylurea herbicides chlorsulfuron and the methyl esters of sulfometuron, metsulfuron, tribenuron, bensulfuron, chlorimuron and primisulfuron. Mass spectra with three structure-significant ions essential for unambiguous identification in environmental samples were obtained with both interfaces, ESI as well as TSP (cf. 15.3.3.1 TSP, phenylureas) [271]. From both interface types characteristic advantages and drawbacks (cf. 15.3.3.2 ESI, triazines) could be reported if they were applied to the analysis of phenylurea pesticides in estuarine waters [240]. The optimization of SPE and ESI-LC-MS and MS/MS conditions for ultratrace analysis of polar pesticides like urea pesticides 3,4-dichlorophenylurea (DPU) and 3,4-dichlorophenylmethylurea (DPUM) in water were described. Detection limits were in the range of 0.2 to 2 ng L<sup>-1</sup>. The applicability was demonstrated by the analyses of surface and estuarine water [536]. For a study of a wide range of polar and acidic pesticides in river water by LC-UV/DAD and ESI-LC-MS and MS/MS detection, an on-line dual-precolumn-based trace enrichment step resulted in reliable results if MS/MS was used for determination and confirmation [502]. In a study the simultaneous determination of 13 (6) acidic and 26 (10) pesticides in natural waters (in waters of the Calabria region, Italy [537]) after SPE (Carbograph 4) using ESI-LC-MS was performed. Confirmation was obtained by MS applying different extraction voltages for fragmentation purposes (cf. 15.3.3.2

ESI, triazines) [537]. Recoveries observed were > 80% except for carbendazim, butocarboxim, aldicarb and molinate, all better than 67% [500]. An aoTOF-MS interfaced by ESI was used to screen and identify unknown compounds and pesticides in water samples by MS and MS/MS. Structures for compounds observed besides pesticides were proposed [538]. Traces of the phenylurea pesticides linuron and monolinuron in water were determined quantitatively. Calibration graphs obtained after Supelclean ENVI-18 SPE were linear with detection limits < 25 pg [511]. Large numbers of phenylurea herbicide analyses led to the elaboration of on-line preconcentration techniques coupled to ESI-LC-MS. The procedure was demonstrated and validated with several pesticides using 10 ml of sample, resulting in detection limits of about 10 ng L<sup>-1</sup> [539]. ESI-LC-MS and MS/MS were applied to quantify and to confirm 16 different herbicides of sulfonylurea [527] type in surface water samples. Surface water samples were extracted by SPE (Spe-ed RP-102). As confirmation criteria RT, molecular ion and two fragment ions besides ion abundance ratios were defined. Quantitation at 0.1 and 1.0 ppb level was demonstrated [540].

Diuron and isoproturon were analysed by ESI-LC-MS(+) and MS/MS in surface water samples from Southeastern regions of France and from the St. Lawrence River in Canada. Confirmation was performed by MS/MS [374]. The determination of one thiourea and four urea pesticides in environmental waters was carried out by ESI-LC-MS(+) and MS/MS (cf. 15.3.3.2 ESI, carbamates) [512]. The seven sulfonylurea herbicides thifensulfuron methyl, metsulfuron methyl, triasulfuron, chlorsulfuron, rimsulfuron, tribenuron methyl and bensulfuron methyl in environmental waters were quantitatively analysed by ESI-LC-MS(+) after SPE. Recoveries under SIM were reported [541]. Phenylurea herbicides and their degradation products in water were examined by ESI-LC-MS(+) resulting in a separation of 22 compounds within a 50 min run. Detection limits were in ng L<sup>-1</sup> ranges. The effect of the LC mobile phase on the MS response was studied [542]. In water and food phenylureas and sulfonylureas could be determined quantitatively by ESI-LC-MS and MS/MS at low pg and fg levels. The ESI approach proved to have better sensitivity and precision than existing TSP-LC-MS methods [503]. ESI-LC-MS(-) and MS/MS were applied for the determination of the mothproofing agents sulcofuron and flucofuron in environmental waters [543, 544]. Product ion mass spectra of mitins and MRM chromatograms were reported. Absolute detection limits in MRM mode for sulcofuron and flucofuron were reported [543]. Results of C<sub>18</sub> SPE and LLE were comparable [544]. The reactions of <sup>14</sup>C-labelled isoproturon and some of its metabolites, including [<sup>14</sup>C]-4-isopropylaniline, in aqueous solutions with humic monomer catechol was followed by ESI-LC-MS(+/-). It was observed that aniline-derived pesticides covalently bound in soil may not be fully undegradable, nor fully immobile [545].

A hot phosphate-buffered water extraction system (buffer, water at 90 °C or soxhlet with methanol) followed by subsequent C<sub>18</sub>-SPE coupled on-line to ESI-LC-MS was used for the analysis of monolinuron, metabenzthiazuron, linuron and neburone in naturally aged agricultural soil. [546]. The comparison of ESI and APCI-LC-MS for the determination of diflubenzuron in fruits, proved that APCI was more efficient than ESI. The application of positive-negative mode switching MS al-

lowed detection limits equivalent to 0.002–0.033 mg per kg crop [358]. A novel screening method elaborated for the automated detection and identification of isotopically labelled pesticide compounds using ESI-LC-MS(+) and MS/MS on an ion trap and isotope pattern recognition software. Identification of degradation products could be achieved and metabolic pathways were elucidated [547]. The sulfonylurea pesticide triasulfuron was determined in soil samples by ESI-LC-MS(+) after MeOH–phosphate buffer extraction and SPE (Supelclean LC-Si) clean up with overall recoveries of > 83% [548] while chlorsulfuron, metsulfuron-methyl, thifensulfuron-methyl and triasulfuron in soil could be quantified by ESI-LC-MS after acidic extraction with recoveries > 80% [549]. The same sulfonylurea herbicides and in addition tribenuron-methyl were analysed in soil water. Quantification was performed, based on the integrated abundance of  $[M-H]^-$  ions. SRM was used for confirmation [550]. The sulfonylurea herbicides nicosulfuron, thifensulfuron methyl, metsulfuron methyl, sulfometuron methyl, chlorsulfuron, bensulfuron methyl, tribenuron methyl and chlorimuron methyl were quantitatively determined in soil extracts by ESI-LC-MS(+) and MS/MS in SRM mode, proving a 400-fold increase in quantification [551]. ESI-LC-MS in positive and negative mode was applied to monitor biodegradability of thifensulfuron methyl [552] and tribenuron-methyl in soil [381]. Five and four ions of soil-induced degradation products were identified as metabolites [552] or [381] (cf. 15.3.3.2 APCI, ureas), respectively. Diuron and atrazine or diuron and isoproturon dissolved in water were submitted to photolysis by UV light performed under conditions selected to be close to those found in the environment. To follow the photolysis products SPE-LC using two short columns (cf. 15.3.3.2 ESI, triazines) on-line coupled with ESI-MS [553] or ESI-LC-MS and MS/MS [506] was applied, respectively. Two degradation products of isoproturon could be confirmed [506]. The chemical degradation of chlortoluron observable during the water disinfection process with HOCl/ClO<sup>-</sup> was elucidated by ESI-LC-MS and MS<sup>n</sup>. The product ion spectra of chloro-hydroxylated and hydroxylated by-products resulted in a quite complex fragmentation pattern. A fragmentation scheme was proposed [554].

#### *Triazines.*

ESI-LC-MS was used to characterise and differentiate the triazine herbicides atrazine, terbutylazine, propazine and prometryn. In source CID spectra were reported. Low-energy CID of  $[M+H]^+$  ions confirmed the characteristic fragmentation patterns and permitted distinction of isomeric triazines [555]. Results obtained from ESI-LC-MS and APCI-LC-MS and MS/MS for the analysis of polar triazine pesticides in water confirmed a better performance of APCI compared to ESI (cf. 15.3.3.2 APCI, triazines) [325].

To optimize the whole analytical procedure, extraction and detection SPE and ESI-LC-MS and MS/MS were studied with polar pesticides like atrazine and some of their transformation products such as deisopropylatrazine, hydroxyatrazine and deethylatrazine. Detection limits in surface and estuarine water were in the range 0.2 to 8 ng L<sup>-1</sup>. [536]. The application of ESI and APCI developed as tech-

niques to solve the interpretation of fragmentation mechanisms was performed in parallel in a comprehensive TSP study of triazine pesticides with *N*-heterocyclic, phenylureas, sulfonylureas, thioureas, anilides, carbamates, thiocarbamates, and organophosphorus compounds [175]. The dependence of detection limits on the eluent flow-rate and signal response of different types of pesticides such as triazines was studied by ESI and APCI. Dramatic losses in sensitivity for the hydrophobic pesticide compounds were observed with increasing flow rates, triazines were less sensitive with both ionisation techniques (cf. 15.3.3.2 APCI, triazines) [385]. Ion-trap MS (IT-MS) was also applied for analysis using a commercial ESI interface. Environmental contaminants such as pesticides of triazine and carbamate type and azo dyes were analysed and identified by IT-MS<sup>n</sup> or ESI-CID (cf. 15.3.3.2 ESI, dyes). Detection limits were reported by Lin et al. [424]. While LC-MS interfaced by ESI had been developed as a common routine method for the determination of triazine pesticides the analytical approach using SFC-MS interfaced by ESI was reported. Compared to TSP-LC-MS applied in parallel, the ESI-SFC-MS method using SPE by RP-C<sub>18</sub> or by SAX for concentration was one order of magnitude more sensitive than TSP but was suitable only for the less polar chlorotriazines [276]. Even micellar electrokinetic chromatography (MEKC) was combined with ESI-MS(+) for the analysis of a mixture of the triazine herbicides atrazine, propazine, ametryn and prometryn using sodium dodecylsulfate for electrophoresis [556].

In real environmental water samples traces of atrazine and hydroxyatrazine were determined quantitatively after SPE (Supelclean ENVI-18) by means of ESI-LC-MS(+). Calibration graphs were linear at 0.025–10 ng on-column combined with detection limits < 25 pg [511]. The six major very polar degradation products of atrazine, amino and hydroxyatrazines, were determined in spiked river, drinking and groundwaters samples by ESI-LC-MS in SIM mode after SPE (Carbograph 4) in ng L<sup>-1</sup> ranges [557]. Under trace level analysis conditions using ESI-LC-MS detection, limits for atrazine and hydroxyatrazin of 10 and 30 pg, respectively, were observed [558]. Samples of drinking, ground and river waters were spiked with a mixture of 45 different pesticides e.g. the triazine derivatives cyanazine, simazine, atrazine and terbutylazine before SPE (Carbograph 4) and ESI-LC-MS(+) was performed (cf. 15.3.3.2 ESI, carbamates) [510].

In a study covering a wide range of polar and acidic pesticides deethylatrazine and atrazine besides anilide, phenoxy acid, phenylurea, carbamates and other types of specific pesticides in river water were determined by ESI-LC-MS and MS/MS. Recoveries, depending on preconcentration steps, obtained with different SPE materials (PLRS-S, Hyshere-1, LiChrolut EN and Isolute ENV +) and at different pH values were reported [502]. Sixteen of the most widely used pesticides in Southern Italy were monitored in surface water samples taken in the Calabria region. Triazines were determined quantitatively by LC-UV and ESI-LC-MS(+) and were confirmed by MS [537]. In another study the simultaneous determination of 26 non-acidic (base and neutral: e.g. triazine, carbamate, anilide, *N*-substituted amine, urea and organophosphorus type) and 13 acidic (sulfuron and phenoxy acid type) pesticides in natural waters was performed using ESI-LC-MS. Recoveries

were reported (cf. 15.3.3.2 ESI, carbamates) [500]. Triazines (e.g., simazine, atrazine, terbutylazine) besides other pesticides in soils were extracted by a hot phosphate-buffered water extraction with subsequent C<sub>18</sub>-SPE prior to ESI-LC-MS analysis. In this way 35 target pesticides could be monitored and results were confirmed by MS/MS [519, 546]. An ESI interfaced LC-MS (oaTOF) was used for the identification of polar organic microcontaminants in surface waters (the river Rhine) performing accurate mass determination. The triazine derivatives propazine and terbutylazine could be identified by their positively recorded ion masses and the losses of propene and butene, respectively [559]. ESI-LC-MS/MS was applied to monitor and confirm the hydroxylated degradation products of atrazine in the stream water from Goodwater Creek watershed samples collected over a period of 2 years [275]. When ESI and TSP were compared with respect to their feasibility for the analysis of pesticides such as atrazine, simazine, ametryne, cyanazine, deethylatrazine and desopropylatrazine and triazine metabolites or chlortoluron, isoproturon, diuron, linuron and diflubenzuron in estuarine waters, TSP was found to offer greater sensitivity for triazines than for phenylurea herbicides, whereas ESP was more sensitive for phenylurea herbicides [240].

SPME coupled to ESI-LC-MS was used to determine the triazine pesticides simazine, atrazine, propazine and prometryn in leachates obtained from soil samples. SPME compared with other extraction methods showed less interference from the matrix compound [513].

Bonding studies to examine the strength of adsorbance of the fungicide anilazine to humic substances and dissolved organic matter (DOM) were performed applying ESI and APCI ionisation. If anilazine bound residues could be observed, a high release of the main metabolite, the dihydroxy-anilazine, was found [390]. Several degradation studies were performed which were accompanied by ESI-LC-MS and MS/MS in order to monitor results. The physicochemical degradation applying UV radiation to atrazine contained in surface water at low levels was examined [506]. The applicability of SPE-LC using two short columns and/or single-short-column LC combined on-line with ESI-MS was demonstrated for the photolysis of the pesticide atrazine dissolved in water under conditions selected to be close to those found in the environment [553]. Applying ESI-LC-MS allowed one to follow the rapid metabolism of atrazine by an enzyme from *Pseudomonas* strain ADP resulting in carbon dioxide, ammonia and chloride. The precursor compound and the active enzyme could be identified [560]. A *Rhizobium* sp. strain was applied to biodegrade atrazine and <sup>14</sup>C-labeled atrazine. The metabolic process was quantitatively followed by ESI-LC-MS using simazine as an internal standard. Hydroxy-atrazine was the only metabolite which was detected after 8 d [389]. Atrazine degradation products generated by Fenton's reagent (Fe<sup>2+</sup> and H<sub>2</sub>O<sub>2</sub>) were analysed by ESI-LC-MS combined with an in-line radioisotope detector. The <sup>14</sup>C-labeling procedure made it obvious that a derivatization of the more polar atrazine products is necessary [561]. For a reductive dechlorination of atrazine, fine-grained zero-valent Fe was applied and degradation was followed by ESI-LC-MS and MS/MS. The dechlorinated product 2-ethylamino-4-isopropylamino-1,3,5-triazine was charac-

terised. Detection limits observed were 0.15 ng mL<sup>-1</sup> for triazines and 6.2 ng mL<sup>-1</sup> for the degradation product [562].

#### *Antifouling pesticides*

Organotin compounds have been observed in manifold surface water samples because of their widespread use in antifouling paintings and in agricultural chemicals. Their determination could be performed by ESI-LC-MS after SPE. Compared to LC-ICP-MS (inductive coupled plasma) ESI-LC-MS showed a decreased sensitivity [563].

#### *Miscellaneous*

An ESI-LC-MS and MS/MS method was described for the quantitative determination of tebufenozide in water samples. The in-source CID spectra were reported. The detection and quantification limits were 0.001 and 0.005 ppb, respectively [564]. To avoid signal suppression in the determination of tebufenozide and hydroxy-tebufenozide in wheat hay a method for postcolumn introduction of an internal standard was elaborated for ESI-LC-MS applications [565]. The insecticide avermectin B1 was determined in oranges using ESI-LC-MS(+). Different fragmentor voltages were applied and fragmentation patterns observed were tentatively identified [566]. The degradation products from the aerobic and anaerobic incubation of emamectin benzoate in microbially active soil were characterised by ESI-LC-MS and MS/MS proving that emamectin benzoate is biodegradable in soil [567]. ESI-LC-MS and APCI-LC-MS were applied for the determination of clofentezine besides others pesticides in fruits. APCI was found to be more efficient than ESI [358].

Traces of imidazolinone herbicides in natural waters (river, ground and drinking water) could be determined by ESI-LC-MS. The product-ion mass spectrum of the [M+H]<sup>+</sup> ion of imazethapyr was presented. [568]. The imidazolinone herbicides imazapyr, *m*-imazamethabenz, *p*-imazamethabenz, *m,p*-imazamethabenz-methyl, imazethapyr and imazaquin were determined in water and soil. Detection limits of 4–7 ng L<sup>-1</sup> in groundwater, 9–13 ng L<sup>-1</sup> in river water and 0.1–0.05 ng g<sup>-1</sup> in soil were observed [569]. For the examination of the extraction efficiency of the same imidazolinone herbicides contained in soil samples ESI-LC-MS was used. Detection limits were < 14 ng g<sup>-1</sup> (S/N = 3) [570]. Mean recoveries for imazethapyr were 92% [571]. In the same way six imidazolinone herbicides in five different soil types were analysed. Extraction profiles were reported. Recoveries of 95–105% were obtained [572]. Stout et al. described an ESI-LC-MS and MS/MS method for the determination of the six imidazolinone herbicides imazapyr, imazamethabenz, imazmethapyr, imazamethabenz-methyl, imazethapyr and imazaquin in tap, lake and well water samples which made sample clean-up obsolete [573]. The advantages of ESI-LC-MS and MS/MS for pesticide and herbicide residue analysis with respect to the determination of imidazolinones in H<sub>2</sub>O, and imazethapyr and its metabolites in plants were discussed from a historic, scientific

and economic viewpoint [574]. A microwave-assisted extraction (MAE) of the herbicide imidazolinone and its 1-hydroxyethyl as well as glucosyl(1-hydroxyethyl) metabolite was elaborated using ESI-LC-MS. Recoveries observed were about 100% for all compounds. Compared with conventional extraction procedures sample throughput could be increased six-fold [575]. Sixteen different herbicides of imidazolinone, sulfonylurea and sulfonamide type in surface water were determined quantitatively and confirmed by ESI-LC-MS. Confirmation was performed by MS/MS, reaching quantitation levels of 0.1 and 1.0 ppb [540].

To concentrate the fungicide carbendazim extracted from spiked water, environmental water and soil extracts immunoaffinity extraction was performed coupled to RP-LC-ESI-MS. Quantitation limits were 100 ppb and 25 ppt in soil and lake water, respectively [576]

#### 15.4 Conclusions

In the past two decades, LC-MS has become a generally accepted analytical technique in many fields of analyses. In the environmental analysis of organic pollutants besides GC-MS LC-MS has gained importance for the determination and identification of polar organic compounds (cf. Tab. 15.1–15.3), though the role of the application to the analysis of inorganics should not be forgotten [577–581].

However, its full significance was not recognized until after LC-MS had become established as a hyphenated research technique. This method revealed its special potential when, in order to determine the degree of pollution in aquatic matrices, sum parameter analyses, such as chemical oxygen demand (COD) or total organic carbon (TOC), came to be replaced by substance-specific LC-MS methods which afforded identification of polar contaminants. The importance of LC-MS analysis comes to light especially if we take into account that, apart from all those anthropogenic polar substances released into the environment that can be determined in a reliable way only since the eighties, still far more biogenic polar compounds exist in the environment. The significance of these substances in the environment may of course be relativized, since only a small number of them are of any ecotoxicological relevance. However, those polar substances that hardly degrade in the environment, are extremely mobile in aquatic systems, and make their way to drinking water treatment plants, are not to be neglected in their number. Although they could be removed from drinking water to a great extent, yet the substances applied for hygienisation can, in combination with dissolved organic matter, lead to new undesirable polar drinking water byproducts.

Previously, GC-MS analysis could do no more than help, dependent on the origin of the water, to account for between 5 and a maximum of 25% of the carbon water contained in the shape of defined chemical compounds – and this was achieved only after prior expensive derivatisation of a part of the non-volatile pollutants. With the introduction of LC-MS analysis, the number of identified polar substances has increased considerably, but the potential of the method could not be

fully exploited, since the transferability and dissemination of mass spectral data and libraries of product ion spectra to another instrument, different in type, is quite restricted. The availability of standards for identification is limited, too, and is a question of costs. The use of the expensive high-resolution instruments such as magnetic instruments, time-of-flight (TOF) or Fourier transform ion cyclotron resonance (FTICR) mass spectrometers in combination with MS/MS, or the possibility of MS<sup>n</sup> studies on cheaper ion trap instruments will improve the capacity for identifying especially metabolites or physicochemical degradation products.

It should not go unmentioned, as also documented in the applications reviewed before, that no interface is able to ionise each compound with the same selectivity and sensitivity. Moreover nearly every type of interface has its advantages in the analysis of polar compounds and only the application of several interfaces provides the maximum of desired information.

Nevertheless LC-MS with the most common API interfaces applied has undoubtedly become the most powerful tool for those environmental chemists who are working with samples taken from aquatic systems. Chemists working in this research area had already recognized this perspective in the late 1970s [2–5], other users, however, realised it only about 10 years later [128, 129, 152–154, 215, 582]. Today, this technique sees essential improvements and the perspective it opens up now is its combination with other powerful techniques, e.g. NMR [339, 422]. This combination has already led to some profound results and more amazing results can be expected in future with the combination of new analytical techniques.

## References

- 1 Niessen, W.M.A.: Developments in Interface Technology for Combined Liquid Chromatography, Capillary Electrophoresis, Supercritical Fluid Chromatography-Mass Spectrometry, in *Applications of LC-MS in Environmental Chemistry; J. Chromatogr. Library*, Vol. 59, ed. D. Barceló, D. Elsevier, Amsterdam **1996**, p. 1.
- 2 Talroze, V.L., Skurat, V.E., Gorodetskii, I.G. et al., *Russian J. Phys. Chem.* **1972**, 46, 456.
- 3 Horning, E.C., Carroll, D.I., Dzidic, I. et al., *J. Chromatogr.* **1974**, 99, 13.
- 4 Scott, R.P.W., Scott, C.G., Munroe, M. et al., *J. Chromatogr.* **1974**, 99, 395.
- 5 Arpino, P.J., Baldwin, M.A., McLafferty, F.W. *Biomed. Mass Spectrom.* **1974**, 1, 80.
- 6 Clement, R.E., Eiceman, G.A., Koester, C.J. *Anal. Chem.* **1995**, 67, 221R.
- 7 Gordon, D.B., Lord, G.A., Jones, D.S. *Rapid Commun. Mass Spectrom.* **1994**, 8, 544.
- 8 Clement, R.E., Yang, P.W., Koester, C.J. *Anal. Chem.* **1999**, 71, 257R.
- 9 Clement, R.E., Eiceman, G.A., Koester, C.J. *Anal. Chem.* **1993**, 65, 85R.
- 10 Clement, R.E., Langhorst, M.L., Eiceman, G.A. *Anal. Chem.* **1991**, 63, 270R.
- 11 Clement, R.E., Yang, P.W., Eiceman, G.A. *Anal. Chem.* **1997**, 69, 251R.
- 12 *Application of LC-MS in Environmental Chemistry; J. Chromatogr. Library*, Vol. 59, ed. D. Barceló, Elsevier, Amsterdam **1996**, p.564.
- 13 Stan, H.J., Heberer, Th.: in *Analysis of Pesticides in Ground, Surface Water*, ed. H.J. Stan, (Ed.), Springer, Berlin **1995**, p.143.
- 14 Lin, H.-Y., Voyksner, R.D.: Practical Aspects of Ion Trap Mass Spectrometry, in *CRC Series Modern Mass Spectrometry* Vol. 111, Chemical Environmental, Biomedical Applications, eds.R.E. March, J.F.J. Todd, CRC, Boca Raton, FL **1995**, ch. 14.
- 15 Yergey, A.L., Edmonds, Ch.G., Lewis I.A.S. et al.: *Liquid Chromatography/Mass Spectrometry Techniques, Applications*, Plenum Press, New York, **1990**, p. 1.
- 16 Carpioli, R.M.: *Continous-Flow Fast Atom Bombardment Mass Spectrometry*, Wiley, Chichester **1990**, p.1.
- 17 Rosen, J.D.: *Applications of New Mass Spectrometry Techniques in Pesticide Chemistry*, Wiley, New York **1987**, p. 1.
- 18 Brown, M. *ACS Symp. Ser.*, **1990**, 420, 1.
- 19 Niessen, W.M.A.: Liquid Chromatography – Mass spectrometry, in *Chromatographic Science Series*, Vol. 79, Marcel Dekker, New York **1998**, p. 648.
- 20 Barceló, D.: Sample handling, analysis of pesticides, their transformation products in water matrices by liquid chromatographic techniques, in *Techniques, Instrumentation in Analytical Chemistry*, Vol. 21; Sample Handling, Trace Analysis of Pollutants - Techniques, Applications, Quality Assurance, ed. Barceló, D., Elsevier, Amsterdam **2000**, p.155.
- 21 Schröder, H.Fr., Ventura, F: Applications of liquid chromatography-mass spectrometry in environmental chem-

- istry; Characterization, determination of surfactants, their metabolites in water samples by modern mass spectrometric techniques, in *Techniques, Instrumentation, in Analytical Chemistry*, Vol. 21; Sample Handling, Trace Analysis of Pollutants - Techniques, Applications, Quality Assurance, ed. Barceló, D., Elsevier, Amsterdam **2000**, p. 828.
- 22** Slobodnik, J., Brinkman, U.A.Th. LC/MS interfacing systems in environmental analysis: Applications to polar pesticides, in *Analytical Chemistry*, Vol. 21, Sample Handling, Trace Analysis of Pollutants - Techniques, Applications, Quality Assurance, ed. Barceló, D., Elsevier, Amsterdam **2000**, p. 935.
- 23** Schröder, H.Fr.: Separation, Identification, Quantification of Surfactants, their Metabolites, in Waste Water, Surface Water, Drinking Water by LC-TSP-MS, FIA-TSP-MS, MS-MS, in *Applications of LC-MS in Environmental Chemistry*, ed. Barceló, D., Elsevier, Amsterdam **1996**, p. 263.
- 24** Barceló, D. *Anal. Chim. Acta* **1992**, 263, 1.
- 25** Barceló, D. *Analyst* **1991**, 116, 681.
- 26** Lopez-Avila, V. *J. AOAC Int.* **1999**, 82, 217.
- 27** Moder, M., Popp, P.: in *Applications of Solid Phase Microextraction*, ed. Pawliszyn, J., Royal Society of Chemistry, Cambridge **1999**, p. 311.
- 28** Clench, M.R., Scullion, S., Brown, R., et al., *Spectrosc. Eur.* **1994**, 6, 16, 21.
- 29** Ferrer, I., Barceló, D. *Analisis* **1998**, 26, M118.
- 30** Stan, H.-J., Fuhrmann, B.: Schriftenreihe Biologische Abwasserreinigung zum Kolloquium im Sonderforschungsbereich 193 der DFG an der Technischen Universität Berlin, Biologische Behandlung Industrieller und Gewerblicher Abwässer, Anwendung der LC-MS in der Wasseranalytik, **2001**, Vol. 11, p. 3.
- 31** Slobodnik, J., van Baar, B.L.M., Brinkman, U.A.Th. *J. Chromatogr. A* **1995**, 703, 81.
- 32** Barceló, D., Hennion, M.-C., *Anal. Chim. Acta* **1995**, 318, 1.
- 33** Dean, J.R., Wade, G., Barnabas, I.J. *J. Chromatogr. A* **1996**, 733, 295.
- 34** Pacakova, V., Stulik, K., Jiskra, J. *J. Chromatogr. A* **1996**, 754, 17.
- 35** Cserhati, T., Forgacs, E. *J. Chromatogr. B* **1998**, 717, 157.
- 36** Pico, Y., Font, G., Molto, J.C. et al., *J. Chromatogr. A* **2000**, 885, 251.
- 37** Jones, T.L., Betowski, L.D., Lopez-Avila, V. *Trends Anal. Chem.* **1994**, 13, 333.
- 38** Berger, U., Kölliker, S., Oehme, M. *Chimia* **1999**, 53, 492.
- 39** Kiewiet, A.T., de Voogt, P. *J. Chromatogr. A* **1996**, 733, 185.
- 40** DiCorcia, A. *J. Chromatogr. A* **1998**, 794, 165.
- 41** Marcomini, A., Zanette, M. *J. Chromatogr. A* **1996**, 733, 193.
- 42** Hites, R.A. *Int. J. Mass Spectrom. Ion Processes* **1992**, 118/119, 369.
- 43** Riu, J., Schonsee, I., Barceló, D. et al., *Trends Anal. Chem.* **1997**, 16, 405.
- 44** Reemtsma, T. *Trends Anal. Chem.* **2001**, 20, 500.
- 45** Reemtsma, T. *Trends Anal. Chem.* **2001**, 20, 533.
- 46** Krost, K.J., *Appl. Spectrosc.* **1993**, 47, 821.
- 47** Wright, L.H. *J. Chromatogr. Sci.* **1982**, 20, 1.
- 48** Stamp, J.J., Siegmund, E.G., Cairns, T. et al., *Anal. Chem.* **1986**, 58, 873.
- 49** Games, D.E., Lant, M.S., Winwood, S.A. et al., *Biomed. Mass Spectrom.* **1982**, 9, 215.
- 50** Cairns, T., Siegmund, E.G., Doose, G.M. *Biomed. Mass Spectrom.* **1983**, 10, 24.
- 51** Cairns, T., Siegmund, E.G., Stamp, J.J. *Rapid Commun. Mass Spectrom.* **1987**, 1, 90.
- 52** Barefoot, A.C., Reiser, R.W. *J. Chromatogr.* **1987**, 398, 217.
- 53** Barefoot, A.C., Reiser, R.W. *Biomed. Environ. Mass Spectrom.* **1989**, 18, 77.
- 54** Barefoot, A.C., Reiser, R.W., Cousins, S.A. *J. Chromatogr.* **1989**, 474, 39.
- 55** Levsen, K., Wagner-Redeker, W., Schäfer, K.H. et al., *J. Chromatogr.* **1985**, 323, 135.
- 56** Krost, K.J. *Anal. Chem.* **1985**, 57, 763.

- 57** Sim, P.G., Boyd, R.K., Gershey, R.M. et al., *Biomed. Environ. Mass Spectrom.* **1987**, *14*, 375.
- 58** Perreault, H., Ramaley, L., Sim, P.G. et al., *Rapid Commun. Mass Spectrom.* **1991**, *5*, 604.
- 59** Games, D.E., Rontree, J.A., Fowlis, I.A. *J. High Res. Chromatogr.* **1994**, *17*, 68.
- 60** Garcia, J.F., Barceló, D. *J. High Res. Chromatogr.* **1993**, *16*, 633.
- 61** Parker, C.E., Haney, C.A., Harvan, D.J. et al., *J. Chromatogr.* **1982**, *242*, 77.
- 62** Voyksner, R.D., Bursey, J.T. *Anal. Chem.* **1984**, *56*, 1582.
- 63** Voyksner, R.D., Bursey, J.T., Pellizzari, E.D. *J. Chromatogr.* **1984**, *312*, 221.
- 64** Parker, C.E., Haney, C.A., Hass, J.R. *J. Chromatogr.* **1982**, *237*, 233.
- 65** Parker, C.E., Yamaguchi, K., Harvan, D.J. et al., *J. Chromatogr.* **1983**, *319*, 273.
- 66** Shalaby, L.M. *Biomed. Mass Spectrom.* **1985**, *12*, 261.
- 67** Honing, M., Barceló, D., Jager, M.E. et al., *J. Chromatogr. A* **1995**, *712*, 21.
- 68** Kleintop, B.L., Eades, D.M., Yost, R.A. *Anal. Chem.* **1993**, *65*, 1295.
- 69** Bellar, T.A., Budde, W.L., Kryak, D.D. *J. Am. Soc. Mass Spectrom.* **1994**, *5*, 908.
- 70** Willoughby, R.C., Browner, R.F. *Anal. Chem.* **1984**, *56*, 2626.
- 71** de la Guardia, M., Garrigues, S. *Trends Anal. Chem.* **1998**, *17*, 263.
- 72** Aguilar, C., Borrull, F., Marce, R.M. *Chromatographia* **1996**, *43*, 592.
- 73** Ho, J.S., Budde, W.L. *Anal. Chem.* **1994**, *66*, 3716.
- 74** Cappiello, A., Famiglini, G., Palma et al., *Environ. Sci. Technol.* **1995**, *29*, 2295.
- 75** Cappiello, A., Famiglini, G., Berloni, A. *J. Chromatogr. A* **1997**, *768*, 215.
- 76** Jimenez, J.J., Bernal, J.L., Del Nozal, M.J. et al., *J. Assoc. Off. Anal. Chem.* **2000**, *83*, 756.
- 77** Cappiello, A., Famiglini, G., Bruner, F. *Anal. Chem.* **1994**, *66*, 1416.
- 78** Rezai, M.A., Famiglini, G., Cappiello, A. *J. Chromatogr. A* **1996**, *742*, 69.
- 79** Aguilar, C., Borrull, F., Marce, R.M. *J. Chromatogr. A* **1998**, *805*, 127.
- 80** Slobodnik, J., Hogenboom, A.C., Louter, A.J.H. et al., *J. Chromatogr. A* **1996**, *730*, 353.
- 81** Louter, A.J.H., Hogenboom, A.C., Slobodnik, J. et al., *Analyst* **1997**, *122*, 1497.
- 82** Bruner, F., Berloni, A., Palma, P. *Chromatographia* **1996**, *43*, 279.
- 83** Kim, I.S., Sasinos, F.I., Stephens, R.D. et al., *Anal. Chem.* **1991**, *63*, 819.
- 84** Mattina, M.J.I. *J. Chromatogr.* **1991**, *542*, 385.
- 85** Cappiello, A., Famiglini, G. *Anal. Chem.* **1995**, *67*, 412.
- 86** Brown, M.A., Stephens, R.D., Kim, I.S. *Trends Anal. Chem.* **1991**, *10*, 330.
- 87** Jones, T.L., Betowski, L.D., Lesnik, B. et al., *Environ. Sci. Technol.* **1991**, *25*, 1880.
- 88** Betowski, L.D., Pace, C.M., Roby, M.R. *J. Am. Soc. Mass Spectrom.* **1992**, *3*, 823.
- 89** Slobodnik, J., Hoekstra-Oussoren, S.J.F., Jager, M.E. et al., *Analyst* **1996**, *121*, 1327.
- 90** Slobodnik, J., Jager, M.E., Hoekstra-Oussoren et al., *J. Mass Spectrom.* **1997**, *32*, 43.
- 91** Jedrzejewski, P.T., Taylor, L.T. *J. Chromatogr. A* **1995**, *703*, 489.
- 92** Bagheri, H., Slobodnik, J., Marce Recasens, R.M. et al., *Chromatographia* **1993**, *37*, 159.
- 93** Minnaard, W.A., Slobodnik, J., Vreuls et al., *J. Chromatogr. A* **1995**, *696*, 333.
- 94** Slobodnik, J., Louter, A.J.H., Vreuls, J.J. et al., *J. Chromatogr. A* **1997**, *768*, 239.
- 95** Mattina, M.J.I. *J. Chromatogr.* **1991**, *549*, 237.
- 96** White, J., Brown, R.H., Clench, M.R. *Rapid Commun. Mass Spectrom.* **1997**, *11*, 618.
- 97** Prosen, H., Zupancic-Kralj, L., Marsel, J. *J. Chromatogr. A* **1995**, *704*, 121.
- 98** Schutz, S., Hummel, H.E., Duhr, A. et al., *J. Chromatogr. A* **1994**, *683*, 141.
- 99** Atienza, J., Jimenez, J.J., Herguedas, A. et al., *J. Chromatogr. A* **1996**, *721*, 113.
- 100** Kambhampati, I., Roinestad, K.S., Hartman, T.G. et al., *J. Chromatogr. A* **1994**, *688*, 67.
- 101** Marcé, R.M., Prosen, H., Crespo, C. et al., *J. Chromatogr. A* **1995**, *696*, 63.
- 102** Dijkstra, R.J., Van Baar, B.L.M., Kientz, C.E. et al., *Rapid Commun. Mass Spectrom.* **1998**, *12*, 5.

- 103** Primus, T.M., Tawara, J.N., Johnston, J.J. et al., *Environ. Sci. Technol.* **1997**, *31*, 346.
- 104** Bagheri, H., Slobodnik, J., Brinkman, U.A.Th. *Anal. Lett.* **2000**, *33*, 249.
- 105** Petrier, C., David, B., Laguian, S. *Chemosphere* **1996**, *32*, 1709.
- 106** Acher, A.J., Hapeman, C.J., Shelton, D.R. et al., *J. Agric. Food Chem.* **1994**, *42*, 2040.
- 107** Hapeman, C.J., Anderson, B.G., Torrents, A. et al., *J. Agric. Food Chem.* **1997**, *45*, 1006.
- 108** Pleasance, S., Anacleto, J.F., Bailey, M.R. et al., *J. Am. Soc. Mass Spectrom.* **1992**, *3*, 378.
- 109** Mattina, M.J.I.: in *Applications of LC-MS in Environmental Chemistry*, ed. D. Barceló, Elsevier, Amsterdam **1996**, p.325.
- 110** Hsu, J., D. Barceló (Ed.), in *Applications of LC-MS in Environmental Chemistry*, ed. D. Barceló, Elsevier, Amsterdam **1996**, p. 345.
- 111** Clark, L.B., Rosen, R.T., Hartman, T.G. et al., *Int. J. Environ. Anal. Chem.* **1991**, *45*, 169.
- 112** Clark, L.B., Rosen, R.T., Hartman, T.G. et al., *Int. J. Environ. Anal. Chem.* **1992**, *47*, 167.
- 113** Straub, R., Voyksner, R.D., Keever, J.T. *J. Chromatogr.* **1992**, *627*, 173.
- 114** Turnipseed, S.B., Roybal, J.E., Rupp, H.S. et al., *J. Chromatogr. B* **1995**, *670*, 55.
- 115** Maguire, R.J. *Water Sci. Technol.* **1992**, *25*, 265.
- 116** Voyksner, R.D., Straub, R.F., Keever, J.T. et al., *Environ. Sci. Technol.* **1993**, *27*, 1665.
- 117** Singh, R.P., Brindle, I.D., Jones, T.R.B. et al., *J. Am. Soc. Mass Spectrom.* **1993**, *4*, 898.
- 118** Doerge, D.R., Clayton, J., Fu, P.P. et al., *Biol. Mass Spectrom.* **1993**, *22*, 654.
- 119** Bonfanti, L., Careri, M., Mangia, A. et al., *J. Chromatogr. A* **1996**, *728*, 359.
- 120** Anacleto, J.F., Ramaley, L., Benoit, F.M. et al., *Anal. Chem.* **1995**, *67*, 4145.
- 121** Pace, C.M., Betowski, L.D. *J. Am. Soc. Mass Spectrom.* **1995**, *6*, 597.
- 122** Gremm, T.J., Frimmel, F.H. *Chromatographia* **1994**, *38*, 781.
- 123** Ventura, F.: Characterization of surfactants in water by desorption ionization methods, in *Environmental Analysis: Techniques, Applications, Quality Assurance*, Vol. 13, ed. D. Barceló, Elsevier, Amsterdam **1993**, p.481.
- 124** Rivera, J., Fraisse, D., Ventura, F. et al., *Fresenius' J. Anal. Chem.* **1987**, *328*, 577.
- 125** Rivera, J., Fraisse, D., Ventura, F. et al., *Biomed. Environ. Mass Spectrom.* **1988**, *16*, 403.
- 126** Rivera, J., Caixach, J., Espadaler, I. et al., *Water Supply* **1989**, *7*, 97.
- 127** Crathorne, B., Fielding, M., Steel, C.P. et al. *Environ. Sci. Technol.* **1984**, *18*, 797.
- 128** Watts, C.D., Crathorne, B., Fielding, M. Et al., in *Org. Micropollut. Aquat. Environ.*, eds. A. Bjørseth, G. Angeletti, Comm. Eur. Communities, EUR 8518, Reidel, Dordrecht **1984**, p. 120.
- 129** *Org. Micropollut. Aquat. Environ.*, eds. Rivera, J., Ventura, F., Caixach, J. et al., Comm. Eur. Communities, EUR 10388, Reidel, Dordrecht **1986**, p.77.
- 130** Ventura, F., Fraisse, D., Caixach, J. et al., *Anal. Chem.* **1991**, *63*, 2095.
- 131** Rivera, J., Ventura, F., Caixach, J. et al., *Int. J. Environ. Anal. Chem.* **1987**, *29*, 15.
- 132** Rockwood, A.L., Higuchi, T. *Tenside Surfact. Deterg.* **1992**, *29*, 6.
- 133** Takeuchi, T., Watanabe, S., Kondo, N. et al., *Chromatographia* **1988**, *25*, 523.
- 134** Lawrence, D.L. *J. Am. Soc. Mass Spectrom.* **1992**, *3*, 575.
- 135** Borgerding, A.J., Hites, R.A. *Anal. Chem.* **1992**, *64*, 1449.
- 136** Ventura, F., Caixach, J., Figueras, A. et al., *Water Res.* **1989**, *23*, 1191.
- 137** Ventura, F., Figueras, A., Caixach, J. et al., *Water Res.* **1988**, *22*, 1211.
- 138** Rivera, J., Caixach, J., Ventura, F. et al., *Chemosphere* **1985**, *14*, 395.
- 139** Schneider, E., Levsen, K., Daehling, P. et al., *Fresenius' J. Anal. Chem.* **1983**, *316*, 488.
- 140** Fernandez, P. Valls, J.M. Bayona, J. Albaigés *Environ. Sci. Technol.* **1991**, *25*, 547.
- 141** Valls, M., Bayona, J.M., Albaigés, J. *Int. J. Environ. Anal. Chem.* **1990**, *39*, 329.

- 142** Field, J.A., Barber, L.B., Thurman, E.M. et al., *Environ. Sci. Technol.* **1992**, 26, 1140.
- 143** Simms, J.R., Keough, T., Ward, S.R. et al., *Anal. Chem.* **1988**, 60, 2613.
- 144** Gilliam, J.M., Landis, P.W., Occolowitz, J.L. *Anal. Chem.* **1983**, 55, 1531.
- 145** Ventura, F., Figueras, A., Caixach, J. et al., *Org. Mass Spectrom.* **1988**, 23, 558.
- 146** Siegel, M.M., Tsao, R., Oppenheimer, S. et al., *Anal. Chem.* **1990**, 62, 322.
- 147** Schneider, E., Levsen, K., Boerboom, A.J.H. et al., *Anal. Chem.* **1984**, 56, 1987.
- 148** Shiraiishi, H., Otsuki, A., Fuwa, K. *Bull. Soc. Chem. Jpn.* **1992**, 55, 1410.
- 149** Ventura, F., Caixach, J., Romero, J. et al., *Water Sci. Technol.* **1992**, 25, 257.
- 150** Gilliam, J.M., Landis, P.W., Occolowitz, J.L. *Anal. Chem.* **1984**, 56, 2285.
- 151** Goad, L.J., Prescott, C.M., Rose, M.E. *Org. Mass. Spectrom.* **1984**, 19, 101.
- 152** Schneider, E., Levsen, K. in *Org. Micropollut. Aquat. Environ.*, eds. A. Bjørseth, G. Angeletti, Comm. Eur. Communities, EUR 10388, Reidel, Dordrecht **1986**, p. 14.
- 153** Schneider, E., Levsen, K. *Fresenius' J. Anal. Chem.* **1987**, 326, 43.
- 154** Rivera, J., Ventura, F., Caixach, J. et al., in *Org. Micropollut. Aquat. Environ.*, eds. A. Bjørseth, G. Angeletti, Comm. Eur. Communities, EUR 11350, Reidel, Dordrecht **1988**, p. 329.
- 155** Coran, S.A., Bambagiotti-Alberti, M., Giannellini, V. et al., *Rapid Commun. Mass Spectrom.* **1998**, 12, 281.
- 156** Kalinoski, H.T., Hargiss, L.O. *J. Am. Soc. Mass Spectrom.* **1992**, 3, 150.
- 157** Parees, D.M., Hanton, S.D., Cornelio Clark, P.A. et al., *J. Am. Soc. Mass Spectrom.* **1998**, 9, 282.
- 158** Yakimov, M.M., Timmis, K.N., Wray, V. et al., *Appl. Environ. Microbiol.* **1995**, 61, 1706.
- 159** Grange, A.H., Donnelly, J.R., Brumley, W.C. et al., *Anal. Chem.* **1994**, 66, 4416.
- 160** Ventura, F., Caixach, J., Figueras, A. et al., *Fresenius' J. Anal. Chem.* **1989**, 335, 222.
- 161** Reemtsma, T. *J. Chromatogr. A* **1996**, 733, 473.
- 162** Yang, Y., Egestad, B., Jernström, B. et al., *Rapid Commun. Mass Spectrom.* **1991**, 5, 499.
- 163** Teffera, Y., Baird, W.M., Smith, D.L. *J. Chromatogr.* **1992**, 577, 69.
- 164** Enya, T., Kawanishi, M., Suzuki, H. et al., *Chem. Res. Toxicol.* **1998**, 11, 1460.
- 165** Corless, C., Reynolds, G., Graham, N. et al., *Water. Res.* **1989**, 23, 1367.
- 166** Calvosa, L., Monteverdi, A., Rindone, B. et al., *Water. Res.* **1991**, 25, 985.
- 167** Borrett, V., Dagley, I.J., Kony, M. et al., *Eur. Mass Spectrom.* **1995**, 1, 59.
- 168** *Applications of New Mass Spectrometry Techniques in Pesticide Chemistry*, eds. Fujiwara, H., Wratten, S.J., Rosen, J.D., Wiley, New York **1987**. p.128.
- 169** Kotrebai, M., Tyson, J.F., Block, E. et al., *J. Chromatogr. A* **2000**, 866, 51.
- 170** Bruchet, A., Legrand, M.F., Arpino, P. et al., *J. Chromatogr. Biomed. Appl.* **1991**, 562, 469.
- 171** Reiser, R.W., Barefoot, A.C., Dietrich, R.F. et al., *J. Chromatogr.* **1991**, 554, 91.
- 172** Bourgeois, G., Benicha, M., Azmani et al., *Analisis* **1995**, 23, 23.
- 173** Ohkura, T., Takechi, T., Deguchi, S. et al., *Jpn. J. Toxicol. Environ. Health* **1994**, 40, 266.
- 174** Tondeur, Y., Sovocool, G.W., Mitchum, R.K. et al., *Biomed. Environ. Mass Spectrom.* **1987**, 18, 733.
- 175** Volmer, D., Levsen, K. *J. Am. Soc. Mass Spectrom.* **1994**, 5, 655.
- 176** Schröder, H. *Fr. Environm. Monitoring, Assessment* **1997**, 44, 503.
- 177** Onisko, B.C., Barnes, J.P., Staub, R.E. et al., *Biol. Mass Spectrom.* **1994**, 23, 626.
- 178** Melnyk, M.C., Carlson, R.E., Busch, K.L. et al., *J. Mass Spectrom.* **1998**, 33, 75.
- 179** Soubayrol, P., Dana, G., Bolbach, G. et al., *Analisis* **1996**, 24, M34.
- 180** Chivukula, M., Spadaro, J.T., Renganathan, V. *Biochemistry* **1995**, 34, 7765.
- 181** Borgerding, A.J., Hites, R.A. *Environ. Sci. Technol.* **1994**, 28, 1278.
- 182** Brumley, W.C., Brownrigg, C.M., Grange, A.H. *J. Chromatogr. A* **1994**, 680, 635.
- 183** Day, B.W., Skipper, P.L., Zaia, J. et al., *Chem. Res. Toxicol.* **1994**, 7, 829.

- 184** Wolf, S.M., Vouros, P. *Chem. Res. Toxicol.* **1994**, *7*, 82.
- 185** Kostainen, R., Tuominen, J., Luukkanen, L. et al., *Rapid Commun. Mass Spectrom.* **1997**, *11*, 283.
- 186** Teffera, Y. *Diss. Abstr. Int. B* **1992**, *53*, 240B.
- 187** Wolf, S.M., Vouros, P., Norwood, C. et al., *Anal. Chem.* **1995**, *67*, 891.
- 188** Tsuruda, L.S., Lame, M.W., Jones, A.D. *Drug Metab. Dispos.* **1995**, *23*, 129.
- 189** Wolf, S.M., Annan, R.S., Vouros, P. et al., *Biol. Mass Spectrom.* **1992**, *21*, 647.
- 190** Wolf, S.M., Vouros, P., Norwood, C. et al., *J. Am. Soc. Mass Spectrom.* **1992**, *3*, 757.
- 191** Tyler, A.N., Romo, L.K., Frey, M.H. et al., *J. Am. Soc. Mass Spectrom.* **1992**, *3*, 637.
- 192** Voyksner, R.D., Pack, T. *Rapid Commun. Mass Spectrom.* **1991**, *5*, 263.
- 193** Perkins, J.R., Parker, C.E., Tomer, K.B. *J. Am. Soc. Mass. Spectrom.* **1992**, *3*, 139.
- 194** Lane, S.J., Brindled, K.A., Taylor, N. et al., *Rapid Commun. Mass Spectrom.* **1993**, *7*, 953.
- 195** Bitsch, F., Shackleton, C.H.L., Ma, W. et al., *Rapid Commun. Mass Spectrom.* **1993**, *7*, 891.
- 196** Niessen, W.M.A. *J. Chromatogr. A* **1998**, *794*, 407.
- 197** Blakley, C.R., Vestal, M.L. *Anal. Chem.* **1983**, *55*, 750.
- 198** Arpino, P. *Mass Spectrom. Rev.* **1992**, *11*, 3.
- 199** Barceló, D., Honing, M., Chiron, S., in *Applications of LC-MS in Environmental Chemistry*, ed. D. Barceló, Elsevier, Amsterdam **1996**, p. 219.
- 200** Yinon, J., Betowski, L.D., Voyksner, R.D., in *Applications of LC-MS in Environmental Chemistry*, ed. D. Barceló, Elsevier, Amsterdam **1996**, p.187.
- 201** Rafols, C., Barceló, D. *J. Chromatogr. A* **1997**, *777*, 177.
- 202** Groepelin, A., Linder, M.W., Schellenberg, K. et al., *Rapid Commun. Mass Spectrom.* **1991**, *5*, 203.
- 203** Verweij, A.M.A., De Bruyn, P.C.A.M., Choufoer, C. et al., *Forensic Sci. Int.* **1993**, *60*, 7.
- 204** Gates, P.M., Furlong, E.T., Dorsey, T.F. et al., *Trends Anal. Chem.* **1996**, *15*, 319.
- 205** Astratov, M., Preiss, A., Levsen, K. et al., *Int. J. Mass Spectrom. Ion Processes* **1997**, *167/168*, 481.
- 206** Godejohann, M., Astratov, M., Preiss, A. et al., *Anal. Chem.* **1998**, *70*, 4104.
- 207** Koeber, R., Bayona, J.M., Niessner, R. *Environ. Sci. Technol.* **1999**, *33*, 1552.
- 208** Greaves, J., Bieri, R.H. *Int. J. Environ. Anal. Chem.* **1991**, *43*, 63.
- 209** Sigman, M.E., Schuler, P.F., Ghosh, M.M. et al., *Environ. Sci. Technol.* **1998**, *32*, 3980.
- 210** Evans, K.A., Dubey, S.T., Kravetz, L. et al. *Anal. Chem.* **1994**, *66*, 699.
- 211** Schröder, H. Fr. *Vom Wasser* **1992**, *79*, 193.
- 212** Schröder, H. Fr. Proceedings of the 4th World Surfactant Congress, eds. Comité Espanol de la Detergencia (C.E.D.), Royal Society of Chemistry, Cambridge **1996**, Vol. 3, pp. 121–135.
- 213** Schröder, H. Fr. *Vom Wasser*, **1992**, *78*, 211.
- 214** Schröder, H. Fr. *Vom Wasser* **1991**, *77*, 277.
- 215** Schröder, H. Fr. *Vom Wasser* **1989**, *73*, 111.
- 216** Clark, L.B., Rosen, R.T., Hartman, T.G. et al., *Res. J. Water Pollut. Control Fed.* **1991**, *63*, 104.
- 217** Schröder, H. Fr. *J. Chromatogr.* **1993**, *647*, 219.
- 218** Schröder, H. Fr. *Water Sci. Technol.* **1991**, *23*, 339.
- 219** Schröder, H. Fr. *Korr. Abwasser* **1992**, *39*, 387.
- 220** Paxéus, N., Schröder, H. Fr. *Water Sci. Technol.* **1996**, *33*, 9.
- 221** Schröder, H. Fr. *Water Sci. Technol.* **1998**, *38*, 151.
- 222** Schröder, H. Fr. *Vom Wasser* **1993**, *80*, 323.
- 223** Schröder, H. Fr. *Vom Wasser* **1993**, *81*, 299.
- 224** Schröder, H. Fr. *Water Sci. Technol.* **1992**, *25*, 241.
- 225** Schröder, H. Fr. *Water Sci. Technol.* **1996**, *34*, 21.
- 226** Schröder, H. Fr. *J. Chromatogr. A* **1997**, *777*, 127.
- 227** Schröder, H. Fr. *J. Chromatogr. A* **1995**, *712*, 123.
- 228** Schröder, H. Fr. *Fresenius' J. Anal. Chem.* **1995**, *353*, 93.

- 229** Schröder, H. *Fr. J. Chromatogr.* **1991**, *554*, 251.
- 230** Schröder, H. *Fr. J. Chromatogr.* **1993**, *643*, 145.
- 231** Schröder, H. *Fr. Water Sci. Technol.* **1996**, *33*, 331.
- 232** Schröder, H. *Fr. Trends Anal. Chem.* **1996**, *15*, 349.
- 233** Schröder, H. Fr., in *DVGW-Schriftenreihe zum 7. BMFT-Statusseminar "Neue Technologien in der Trinkwasserversorgung"* Nr. 108, Eschborn **1990**, p. 121.
- 234** Schröder, H. *Fr. Vom Wasser* **1994**, *83*, 187.
- 235** Wils, E.R.J., Hulst, A.G. *Rapid Commun. Mass Spectrom.* **1993**, *7*, 413.
- 236** Mirocha, C.J., Cheong, W., Mirza, U. et al., *Rapid Commun. Mass Spectrom.* **1992**, *6*, 128.
- 237** Maruyama, J., Noguchi, T., Matsunaga, S. et al., *Agric. Biol. Chem.* **1984**, *48*, 2783.
- 238** White, K.D., Sphon, J.A., Hall, S. *Anal. Chem.* **1986**, *58*, 562.
- 239** Barceló, D., Durand, G., Bouvot, V. et al., *Environ. Sci. Technol.* **1993**, *27*, 271.
- 240** Molina, C., Durand, G., Barceló, D. *J. Chromatogr. A* **1995**, *712*, 113.
- 241** Kochany, J., Maguire, R.J. *J. Agric. Food Chem.* **1994**, *42*, 406.
- 242** Vreeken, R.J., Van Dongen, W.D., Ghijssen, R.T. et al., *Int. J. Environ. Anal. Chem.* **1994**, *54*, 119.
- 243** Barceló, D., Durand, G., Vreeken, R.J. *J. Chromatogr.* **1993**, *647*, 271.
- 244** Barceló, D., Durand, G., Vreeken, R.J. et al., *J. Chromatogr.* **1991**, *553*, 311.
- 245** Volmer, D., Levsen, K., Wünsch, G. *J. Chromatogr. A* **1994**, *660*, 231.
- 246** Chiron, S., Dupas, S., Scribe, P. et al., *J. Chromatogr. A* **1994**, *665*, 295.
- 247** Bagheri, H., Brouwer, E.R., Ghijssen, R.T. et al., *J. Chromatogr.* **1993**, *647*, 121.
- 248** Moore, K.M., Jones, S.R., James, C. *Water Res.* **1995**, *29*, 1225.
- 249** Chiron, S., Valverde, A., Fernandez-Alba, A. et al., *J. Assoc. Off. Anal. Chem.* **1995**, *78*, 1346.
- 250** Liska, I., Slobodnik, J. *J. Chromatogr. A* **1996**, *733*, 235.
- 251** Salau, J.S., Honing, M., Tauler, R. et al., *J. Chromatogr. A* **1998**, *795*, 3.
- 252** Honing, M., Barceló, D., van Baar, B.L.M. et al., *J. Am. Soc. Mass Spectrom.* **1994**, *5*, 913.
- 253** Volmer, D., Levsen, K., Honing, M. et al., *J. Am. Soc. Mass Spectrom.* **1995**, *6*, 656.
- 254** Lopez-Avila, V., Jones, T.L. *J. Assoc. Off. Anal. Chem.* **1993**, *76*, 1329.
- 255** Liu, C.-H., Mattern, G.C., Yu, X. et al., *J. Agric. Food Chem.* **1991**, *39*, 718.
- 256** Durand, G., de Bertrand, N., Barceló, D. *J. Chromatogr.* **1991**, *554*, 233.
- 257** Chiron, S., Torres, J.A., Fernandez-Alba, A. et al., *Int. J. Environ. Anal. Chem.* **1996**, *65*, 37.
- 258** Kodama, S., Yamamoto, A., Matsunaga, A. *J. Agric. Food Chem.* **1997**, *45*, 990.
- 259** Lacorte, S., Ehresmann, N., Barceló, D. *Environ. Sci. Technol.* **1996**, *30*, 917.
- 260** Sabik, H., Jeannot, R. *J. Chromatogr. A* **1998**, *18*, 197.
- 261** Lacorte, S., Barceló, D. *J. Chromatogr. A* **1995**, *712*, 103.
- 262** Lacorte, S., Lartiges, S.B., Garrigues, P. et al., *Environ. Sci. Technol.* **1995**, *29*, 431.
- 263** Halarnkar, P.P., Leimkuehler, W.M., Green, D.L. et al., *J. Agric. Food Chem.* **1997**, *45*, 2349.
- 264** Chiron, S., Martinez, E., Barceló, D. *J. Chromatogr. A* **1994**, *665*, 283.
- 265** Vreeken, R.J., Ghijssen, R.T., Frei, R.W. et al., *J. Chromatogr. A* **1993**, *654*, 65.
- 266** Barceló, D., Durand, G., Albaiges, J., in *Org. Micropollut. Aquat. Environ.*, eds. A. Bjørseth, G. Angeletti, Comm. Eur. Communities, EUR 13152, Reidel, Dordrecht **1991**, p.132.
- 267** Geerdink, R.B., Kienhuis, P.G.M., Brinkman, U.A.Th. *J. Chromatogr.* **1993**, *647*, 329.
- 268** Geerdink, R.B., Kienhuis, P.G.M., Brinkman, U.A.Th. *Chromatographia* **1994**, *39*, 311.
- 269** Ramanand, K., Nagarajan, A., Suflita, J.M. *Appl. Environ. Microbiol.* **1993**, *59*, 2251.
- 270** Mattern, G.C., Liu, C.-H., Louis, J.B. et al., *J. Agric. Food Chem.* **1991**, *39*, 700.
- 271** Volmer, D., Wilkes, J.G., Levsen, K. *Rapid Commun. Mass Spectrom.* **1995**, *9*, 767.

- 272** Brady, J.F., Turner, J., Skinner, D.H. *J. Agric. Food Chem.* **1995**, *43*, 2542.
- 273** Geerdink, R.B., Attema, A., Niessen, W.M.A. et al., *LC/GC Int.* **1998**, *11*, 361.
- 274** Geerdink, R.B., Berg, P.J., Kienhuis, P.G.M. et al., *Int. J. Environ. Anal. Chem.* **1996**, *64*, 265.
- 275** Lerch, R.N., Donald, W.W., Li, Y.-X. et al., *Environ. Sci. Technol.* **1995**, *29*, 2759.
- 276** Nelieu, S., Stobiecki, M., Sadoun, F. et al., *Analusis* **1994**, *22*, 70.
- 277** Abian, J., Durand, G., Barceló, D. *J. Agric. Food Chem.* **1993**, *41*, 1264.
- 278** Meesters, R.J.W., Forge F., Schröder, H. *Fr. Vom Wasser* **1995**, *84*, 287.
- 279** Schmitt, P., Freitag, D., Sanlaville, Y. et al., *J. Chromatogr. A* **1995**, *709*, 215.
- 280** Nelieu, S., Stobiecki, M., Kerhoas, L. et al., *Rapid Commun. Mass Spectrom.* **1994**, *8*, 945.
- 281** Mascolo, G., Lopez, A., Foldenyi, R. et al., *Environ. Sci. Technol.* **1995**, *29*, 2987.
- 282** Mascolo, G., Lopez, A., Passino, R. et al., *Water Res.* **1994**, *28*, 2499.
- 283** Fischer, J.B., Michael, J.L. *J. Chromatogr. A* **1995**, *704*, 131.
- 284** Papilloud, S., Haerdi, W., Chiron, S. et al., *Environ. Sci. Technol.* **1996**, *30*, 1822.
- 285** Salau, J.S., Alonso, R., Batllo, G. et al., *Anal. Chim. Acta* **1994**, *293*, 109.
- 286** Schrap, S.M., van den Heuvel, H., van der Meulen, J. et al., *Chemosphere* **2000**, *40*, 1389.
- 287** Eisert, R., Levsen, K., Wunsch, G. *Int. J. Environ. Anal. Chem.* **1995**, *58*, 103.
- 288** Fernandez-Alba, A.R., Valverde, A., Aguera, A. et al., *J. Chromatogr. A* **1996**, *721*, 97.
- 289** Stout, S.J., Peterson, R.P., daCunha, A.R. et al., *J. Assoc. Off. Anal. Chem.* **1995**, *78*, 862.
- 290** Maycock, R., Hastings, M., Portwood, D. *Int. J. Environ. Anal. Chem.* **1995**, *58*, 93.
- 291** Schreiber, A., Efer, J., Engewald, W. *J. Chromatogr. A* **2000**, *869*, 411.
- 292** Baumann, C., Cintora, M.A., Eichler, M. et al., *Rapid Commun. Mass Spectrom.* **2000**, *14*, 349.
- 293** Kienhuis, P.G.M., Geerdink, R.B., *Trends Anal. Chem.* **2000**, *19*, 460.
- 294** Aguera, A., Fernandez-Alba, A.R. *Analisis* **1998**, *26*, M123.
- 295** Ahrer, W., Scherwenk, E., Buchberger, W. *J. Chromatogr. A* **2001**, *910*, 69.
- 296** Schröder, H. *Fr. Waste Management* **1999**, *19*, 111.
- 297** Sacher, G., Nussbaum, R., Rissler, K. et al., *Chromatographia* **2001**, *54*, 65.
- 298** Ma, Y.-C., Kim, H.-Y. *J. Am. Soc. Mass Spectrom.* **1997**, *8*, 1010.
- 299** Lagana, A., Bacaloni, A., Fago, G. et al., *Rapid Commun. Mass Spectrom.* **2000**, *14*, 401.
- 300** Baronti, C., Curini, R., d'Ascenzo, G. et al., *Environ. Sci. Technol.* **2000**, *34*, 5059.
- 301** de Alda, M.J.L., Barceló, D. *J. Chromatogr. A* **2000**, *892*, 391.
- 302** Cassada, D.A., Monson, S.J., Snow, D. et al., *J. Chromatogr. A* **1999**, *844*, 87.
- 303** Ahrer, W., Buchberger, W. *Fresenius J. Anal. Chem.* **1999**, *365*, 604.
- 304** Galceran, M.T., Moyano, E. *J. Chromatogr. A* **1996**, *731*, 75.
- 305** Schröder, H. *Fr. Proceedings of the IWA Conference, Critical F12Technologies to the World in 21st Century: Pollution Control, Reclamation in Process Industries*, Beijing, P.R.China, **2000**, p.125.
- 306** Thomas, D., Sim, P.G., Benoit, F.M. *Rapid Commun. Mass Spectrom.* **1994**, *8*, 105.
- 307** Mansoori, B.A. *Rapid Commun. Mass Spectrom.* **1998**, *12*, 712.
- 308** Letzel, T., Poschl, U., Rosenberg, E. et al., *Rapid Commun. Mass Spectrom.* **1999**, *13*, 2456.
- 309** Letzel, T., Rosenberg, E., Wissiack, R. et al., *J. Chromatogr. A* **1999**, *855*, 501.
- 310** Koeber, R., Bayona, J.M., Niessner, R. *Int. J. Environ. Anal. Chem.* **1997**, *66*, 313.
- 311** Koeber, R., Niessner, R., Bayona, J.M. *Fresenius' J. Anal. Chem.* **1997**, *359*, 267.
- 312** Marvin, C.H., Smith, R.W., Bryant, D.W. et al., *J. Chromatogr. A* **1999**, *863*, 13.
- 313** Charles, L., Pepin, D. *J. Chromatogr. A* **1998**, *804*, 105.
- 314** Thomas, D., Crain, S.M., Sim, P.G. et al., *J. Mass Spectrom.* **1995**, *30*, 1034.
- 315** Puig, D., Silgoner, I., Grasserbauer, M. et al., *Anal. Chem.* **1997**, *69*, 2756.

- 316** Wissiack, R., Rosenberg, E., Grasserbauer, M. *J. Chromatogr. A* **2000**, 896, 159.
- 317** Jauregui, O., Moyano, E., Galceran, M.T. *J. Chromatogr. A* **1997**, 787, 79.
- 318** Pedersen, S.N., Lindholst, C. *J. Chromatogr. A* **1999**, 864, 17.
- 319** Motoyama, A., Suzuki, A., Shirota, O. et al., *Rapid Commun. Mass Spectrom.* **1999**, 13, 2204.
- 320** Aguilar, C., Ferrer, I., Borrull, F. et al., *Anal. Chim. Acta* **1999**, 386, 237.
- 321** Castillo, M., Domingues, R., Alpendurada, M.F. et al., *Anal. Chim. Acta* **1997**, 353, 133.
- 322** Slobodnik, J., Hogenboom, A.C., Vreuls, J.J. et al., *J. Chromatogr. A* **1996**, 741, 59.
- 323** Azevedo, D.A., Lacorte, S., Viana, P. et al., *Chromatographia* **2001**, 53, 113.
- 324** de Almeida Azevedo, D., Lacorte, S., Vinhas, T. et al., *J. Chromatogr. A* **2000**, 879, 13.
- 325** Baglio, D., Kotzias, D., Larsen, B.R. *J. Chromatogr. A* **1999**, 854, 207.
- 326** Jewett, B.N., Ramaley, L., Kwak, J.C.T. *J. Am. Soc. Mass Spectrom.* **1999**, 10, 529.
- 327** Castillo, M., Riu, J., Ventura, F. et al., *J. Chromatogr. A* **2000**, 889, 195.
- 328** Petrovic, M., Barceló, D. *Fresenius J. Anal. Chem.* **2000**, 368, 676.
- 329** Bachus, H., Stan, H.-J. *Schriftenreihe Biologische Abwasserreinigung zum Kolloquium im Sonderforschungsbereich 193 der DFG an der Technischen Universität Berlin, Biologische Behandlung industrieller und gewerblicher Abwässer, Anwendung der LC-MS in der Wasseranalytik*, **2001**, Vol. 11, p. 248.
- 330** Billian, P., Hock, W., Doetzer, R. et al., *Anal. Chem.* **2000**, 72, 4973.
- 331** Scullion, S.D., Clench, M.R., Cooke, M. et al., *J. Chromatogr. A* **1996**, 733, 207.
- 332** Yamagishi, T., Hashimoto, S., Kanai, M. et al., *Bunseki Kagaku* **1997**, 46, 537.
- 333** Bester, K., Theobald, N., Schröder, H.-Fr. *Chemosphere* **2001**, 45, 817.
- 334** Cretier, G., Podevin, C., Rocca, J.-L. *Analisis* **1999**, 27, 758.
- 335** Li, H.-Q., Schröder, H. Fr. *Water. Sci. Technol.* **2000**, 42, 391.
- 336** Schröder, H. Fr., Fytianos, K. *Chromatographia* **1999**, 50, 583.
- 337** Efer, J., Schreiber, A., Ceglarek, U., Engewald, W. *Schriftenreihe Biologische Abwasserreinigung zum Kolloquium im Sonderforschungsbereich 193 der DFG an der Technischen Universität Berlin, Biologische Behandlung industrieller und gewerblicher Abwässer, Anwendung der LC-MS in der Wasseranalytik*, **1999**, Vol. 11, p. 125.
- 338** Efer, J., Ceglarek, U., Anspach, T. et al., *Wasser Abwasser* **1996**, 138, 577.
- 339** Preiss, A., Levensen, K. *Schriftenreihe Biologische Abwasserreinigung zum Kolloquium im Sonderforschungsbereich 193 der DFG an der Technischen Universität Berlin, Biologische Behandlung industrieller und gewerblicher Abwässer, Anwendung der LC-MS in der Wasseranalytik*, **1999**, Vol. 11, p. 169.
- 340** Plomley, J.B., Crozier, P.W., Taguchi, V.Y. *J. Chromatogr. A* **1999**, 854, 245.
- 341** Castillo, M., Barceló, D., in *Techniques, Instrumentation in Analytical Chemistry*, Vol. 21, Sample Handling, Trace Analysis of Pollutants - Techniques, Applications, Quality Assurance, ed. Barceló, D., Elsevier, Amsterdam **2000**, p.537.
- 342** Schröder, H.Fr. *J. Chromatogr. A*, **2001**, 926, 127.
- 343** Li, H.-Q., Jiku, F., Schröder, H. Fr. *J. Chromatogr. A* **2000**, 889, 155.
- 344** Schröder, H.Fr. *Water Sci. Technol.*, **2002**, 46, 57.
- 345** Petrovic, M., Diaz, A., Ventura, F. et al., *Anal. Chem.* **2001**, 73, 5886.
- 346** Petrovic, M., Barceló, D. *Anal. Chem.* **2000**, 72, 4560.
- 347** Castro, R., Moyano, E., Galceran, M.T. *J. Chromatogr. A* **1999**, 830, 145.
- 348** Santos, T.C.R., Rocha, J.C., Barceló, D. *J. Chromatogr. A* **2000**, 879, 3.
- 349** Santos, T.C.R., Rocha, J.C., Alonso, R.M. et al., *Environ. Sci. Technol.* **1998**, 32, 3479.
- 350** Spliid, N.H., Koppen, B. *J. Chromatogr. A* **1996**, 736, 105.
- 351** Spliid, N.H., Koppen, B. *Chemosphere* **1998**, 37, 1307.
- 352** Pothuluri, J.V., Evans, F.E., Doerge, D.R. et al., *Arch. Environ. Contam. Toxicol.* **1997**, 32, 117.

- 353** Hogenboom, A.C., Slobodnik, J., Vreuls, J.J. et al., *Chromatographia* **1996**, *42*, 506.
- 354** Doerge, D.R., Bajic, S. *Rapid Commun. Mass Spectrom.* **1992**, *6*, 663.
- 355** Fernandez, M., Pico, Y., Manes, J. J. *Chromatogr. A* **2000**, *871*, 43.
- 356** Thomas, D.H., Lopez-Avila, V., Betowski, L.D. et al., *J. Chromatogr. A* **1996**, *724*, 207.
- 357** Takino, M., Yamagami, T., Daishima, S. *Bunseki Kagaku* **1997**, *46*, 555.
- 358** Barnes, K.A., Fussell, R.J., Startin, J.R. et al., *Rapid Commun. Mass Spectrom.* **1997**, *11*, 117.
- 359** Nunes, G.S., Marco, M.P., Ribeiro, M.L. et al., *J. Chromatogr. A* **1998**, *823*, 109.
- 360** Itoh, H., Kawasaki, S., Tadano, J. J. *Chromatogr. A* **1996**, *754*, 61.
- 361** Aguilar, C., Ferrer, I., Borrull, F., Marce et al., *J. Chromatogr. A* **1998**, *794*, 147.
- 362** Lacorte, S., Vreuls, J.J., Salau et al., *J. Chromatogr. A* **1998**, *795*, 71.
- 363** Lacorte, S., Barceló, D. *Anal. Chem.* **1996**, *68*, 2464.
- 364** Lacorte, S., Molina, C., Barceló, D. *J. Chromatogr. A* **1998**, *795*, 13.
- 365** Fernandez-Alba, A.R., Aguera, A., Contreras, M. et al., *J. Chromatogr. A* **1998**, *823*, 35.
- 366** Lacorte, S., Jeanty, G., Marty, J.-L. et al., *J. Chromatogr. A* **1997**, *777*, 99.
- 367** Oubina, A., Ferrer, I., Gascon, J. et al., *Environ. Sci. Technol.* **1996**, *30*, 3551.
- 368** Ferrer, I., Barceló, D. *J. Chromatogr. A* **1999**, *854*, 197.
- 369** Ferrer, I., Barceló, D. *J. Chromatogr. A* **1997**, *778*, 161.
- 370** Kawasaki, S., Ueda, H., Itoh, H. et al., *J. Chromatogr.* **1992**, *595*, 193.
- 371** Katagi, T. *J. Agric. Food Chem.* **1993**, *41*, 496.
- 372** Chiron, S., Rodriguez, A., Fernandez-Alba, A. *J. Chromatogr. A* **1998**, *823*, 97.
- 373** Dobberstein, P., Münster, H. *J. Chromatogr. A* **1995**, *712*, 3.
- 374** Jeannot, R., Sabik, H., Sauvard, E. et al., *J. Chromatogr. A* **2000**, *879*, 51.
- 375** Hogenboom, A.C., Speksnijder, P., Vreeken, R.J. et al., *J. Chromatogr. A* **1997**, *777*, 81.
- 376** Hogenboom, A.C., Niessen, W.M.A., Brinkman, U.A.Th. *J. Chromatogr. A* **1998**, *794*, 201.
- 377** Ferrer, I., Ballesteros, B., Marco, M.P. et al., *Environ. Sci. Technol.* **1997**, *31*, 3530.
- 378** Thomas, K.V. *J. Chromatogr. A* **1998**, *825*, 29.
- 379** van der Heeft, E., Dijkman, E., Baumann, R.A. et al., *J. Chromatogr. A* **2000**, *879*, 39.
- 380** Yarita, T., Sugino, K., Ihara, T. et al., *Anal. Commun.* **1998**, *35*, 91.
- 381** Bossi, R., Vejrup, K., Jacobsen, C.S. *J. Chromatogr. A* **1999**, *855*, 575.
- 382** Ferrer, I., Hennion, M.-C., Barceló, D. *Anal. Chem.* **1997**, *69*, 4508.
- 383** Ferrer, I., Pichon, V., Hennion, M.-C. et al., *J. Chromatogr. A* **1997**, *777*, 91.
- 384** Barnes, K.A., Fussell, R.J., Startin, J.R. et al., *Rapid Commun. Mass Spectrom.* **1995**, *9*, 1441.
- 385** Asperger, A., Efer, J., Koal, T. et al., *J. Chromatogr. A* **2001**, *937*, 65.
- 386** Hogenboom, A.C., Brinkman, U.A.Th., Niessen, W.M.A. *LC.GC Int.* **1997**, *10*, 669.
- 387** Geerdink, R.B., Niessen, W.M.A., Brinkman, U.A.Th. *J. Chromatogr. A* **2001**, *910*, 291.
- 388** Lerch, R.N., Blanchard, P.E., Thurman, E.M. *Environ. Sci. Technol.* **1998**, *32*, 40.
- 389** Bouquard, C., Ouazzani, J., Prome, J.-C. et al., *Appl. Environ. Microbiol.* **1997**, *63*, 862.
- 390** Klaus, U., Pfeifer, T., Spiteller, M. *Environ. Sci. Technol.* **2000**, *34*, 3514.
- 391** Bobeldijk, I., Broess, K., Speksnijder, P. et al., *J. Chromatogr. A* **2001**, *938*, 15.
- 392** Aguera, A., Almansa, E., Malato, S. et al., *Analisis* **1998**, *26*, 245.
- 393** Mol, H.G.J., van Dam, R.C.J., Vreeken, R.J. et al., *J. Chromatogr. A* **1999**, *833*, 53.
- 394** Barnes, K.A., Fussell, R.J., Startin, J.R. et al., *Rapid Commun. Mass Spectrom.* **1997**, *11*, 159.
- 395** Loos, R., Alonso, M.C., Barceló, D. *J. Chromatogr. A* **2000**, *890*, 225.
- 396** Quilliam, M.A., in *Applications of LC-MS in Environmental Chemistry*, ed. D. Barceló, Elsevier, Amsterdam **1996**, p. 414.

- 397** Bauer, K.-H., Knepper, T.P., Maes, A. et al., *J. Chromatogr. A* **1999**, 837, 117.
- 398** Baron, D., Hering, J.G. *J. Environ. Qual.* **1998**, 27, 844.
- 399** Sheppard, R.L., Henion, J. *Electrophoresis* **1997**, 18, 287.
- 400** Hartig, C., Storm, T., Jekel, M. *J. Chromatogr. A* **1999**, 854, 163.
- 401** Lange, F.T., Sacher, F., Metzinger, M., Wenz, M. *Schriftenreihe Biologische Abwasserreinigung zum Kolloquium im Sonderforschungsbereich 193 der DFG an der Technischen Universität Berlin, Biologische Behandlung industrieller und gewerblicher Abwässer, Anwendung der LC-MS in der Wasseranalytik*, **2001**, Vol. 11, p. 193.
- 402** Ternes, T.A., Hirsch, R., Mueller, J. et al., *Fresenius J. Anal. Chem.* **1998**, 362, 329.
- 403** Putschew, A., Jekel, M. *Schriftenreihe Biologische Abwasserreinigung zum Kolloquium im Sonderforschungsbereich 193 der DFG an der Technischen Universität Berlin, Biologische Behandlung industrieller und gewerblicher Abwässer, Anwendung der LC-MS in der Wasseranalytik*, **2001**, Vol. 11, p. 213.
- 404** Hirsch, R., Ternes, T.A., Haberer, K. et al., *J. Chromatogr. A* **1998**, 815, 213.
- 405** Zhu, J., Snow, D.D., Cassada, D.A. et al., *J. Chromatogr. A* **2001**, 928, 177.
- 406** Putschew, A., Wischnack, S., Jekel, M. *Sci. Total Environ.* **2000**, 255, 129.
- 407** Hirsch, R., Ternes, T.A., Lindart, A. et al., *Fresenius J. Anal. Chem.* **2000**, 366, 835.
- 408** Ternes, T., Bonerz, M., Schmidt, T. *J. Chromatogr. A* **2001**, 938, 175.
- 409** la Farré, M., Ferrer, I., Ginebreda, A. et al., *J. Chromatogr. A* **2001**, 938, 187.
- 410** Sacher, F., Lange, F.T., Brauch, H.-J. et al., *J. Chromatogr. A* **2001**, 938, 199.
- 411** Hartig, C., Jekel, M. *Schriftenreihe Biologische Abwasserreinigung zum Kolloquium im Sonderforschungsbereich 193 der DFG an der Technischen Universität Berlin, Biologische Behandlung industrieller und gewerblicher Abwässer, Anwendung der LC-MS in der Wasseranalytik*, **1999**, Vol. 11, p. 93.
- 412** Knepper, T.P., Kirschköfer, F., Licher, I. et al., *Environ. Sci. Technol.* **1999**, 33, 945.
- 413** Minoia, C., Turci, R., Sottani, C. et al., *Rapid Commun. Mass Spectrom.* **1998**, 12, 1485.
- 414** Möhle, E., Kempter, C., Kern, A. et al., *Acta Hydrochim. Hydrobiol.* **1999**, 27, 430.
- 415** New, A.P., Freitas dos Santos, L.M., Biundo, G. L. et al. *J. Chromatogr. A* **2000**, 889, 177.
- 416** Storm, T., Hartig, C., Reemstma, T. et al., *Anal. Chem.* **2001**, 73, 589.
- 417** Reemstma, T. *J. Chromatogr. A* **2001**, 919, 289.
- 418** Bruins, A.P., Covey, T.H., Henion, J.D. *Anal. Chem.* **1987**, 59, 2642.
- 419** Bruins, A.P., Weidolf, L.O.G., Henion, J.D. et al., *Anal. Chem.* **1987**, 59, 2647.
- 420** Edlund, P.O., Lee, E.D., Henion, J.D. et al., *Biomed. Environ. Mass Spectrom.* **1989**, 18, 233.
- 421** McCallum, J.E.B., Madison, S.A., Alkan, S. et al., *Environ. Sci. Technol.* **2000**, 34, 5157.
- 422** Preiss, A., Sanger, U., Karfisch, N. et al., *Anal. Chem.* **2000**, 72, 992.
- 423** Riu, J., Schonsee, I., Barceló, D. *J. Mass Spectrom.* **1998**, 33, 653.
- 424** Lin, H.-Y., Voyksner, R.D. *Anal. Chem.* **1993**, 65, 451.
- 425** Barceló, D., Riu, J. *Biomed. Chromatogr.* **2000**, 14, 14.
- 426** Poiger, T., Richardson, S.D., Baumhamer, G.L. *J. Chromatogr. A* **2000**, 886, 271.
- 427** Holcapek, M., Jandera, P., Zderadicka, P. *J. Chromatogr. A* **2001**, 926, 175.
- 428** Siu, K.W.M., Guevremont, R., Le Blanc, J.C.Y. et al., *J. Chromatogr.* **1991**, 554, 27.
- 429** Laszlo, J.A. *Environ. Sci. Technol.* **1997**, 31, 3647.
- 430** de Alda, M.J.L., Barceló, D. *J. Chromatogr. A* **2001**, 938, 145.
- 431** Groom, C.A., Beaudet, S., Halasz, A. et al., *J. Chromatogr. A* **2001**, 909, 53.
- 432** Bruns-Nagel, D., Drzyzga, O., Steinbach, K. et al., *Environ. Sci. Technol.* **1998**, 32, 1676.
- 433** Hashimoto, S., Otsuki, A. *HRC-J. High Resolut. Chromatogr.* **1998**, 21, 55.
- 434** Takino, M., Daishima, S., Yamaguchi, K. *Analyst* **2000**, 125, 1097.
- 435** Ells, B., Barnett, D.A., Purves, R.W. et al., *Anal. Chem.* **2000**, 72, 4555.

- 436** Loos, R., Barceló, D. *J. Chromatogr. A* **2001**, *938*, 45.
- 437** Ells, B., Barnett, D.A., Froese, K. et al., *Anal. Chem.* **1999**, *71*, 4747.
- 438** Magnuson, M.L., Kelty, C.A. *Anal. Chem.* **2000**, *72*, 2308.
- 439** Debre, O., Budde, W.L., Song, X. *J. Am. Soc. Mass. Spectrom.* **2000**, *11*, 809.
- 440** Richardson, S.D., Thruston, A.D., Jr., Caughran, T.V. et al., *Proc.-Water Qual. Technol. Conf.* **1998** 2223.
- 441** Shimizu, N., Inoue, Y., Daishima, S. et al., *Anal. Sci.* **1999**, *15*, 685.
- 442** Takino, M., Daishima, S., Yamaguchi, K. et al., *J. Chromatogr. A* **2001**, *928*, 53.
- 443** Sasaki, J., Aschmann, S.M., Kwok, E.S.C. et al., *Environ. Sci. Technol.* **1997**, *31*, 3173.
- 444** Tsai, C.Y., Her, G.R. *J. Chromatogr. A* **1996**, *743*, 315.
- 445** Storm, T., Reemtsma, T., Jekel, M. *J. Chromatogr. A* **1999**, *854*, 175.
- 446** Suter, M.J.F., Riediker, S., Zipper, C. et al., *Analusis* **1997**, *25*, M23.
- 447** Riediker, S., Suter, M.J.F., Giger, W. *Water Res.* **2000**, *34*, 2069.
- 448** Crescenzi, C., Di Corcia, A., Marcomini, A. et al., *J. Chromatogr. A* **2001**, *923*, 97.
- 449** Wolf, C., Storm, T., Lange, F.T. et al., *Anal. Chem.* **2000**, *72*, 5466.
- 450** Suter, M.J. - F., Riediker, S., Schwoerer, V.G. *Schriftenreihe Biologische Abwasserreinigung zum Kolloquium im Sonderforschungsbereich 193 der DFG an der Technischen Universität Berlin, Biologische Behandlung industrieller und gewerblicher Abwässer, Anwendung der LC-MS in der Wasseranalytik*, **1999**, Vol. 11, p. 41.
- 451** Storm, T., Reemtsma, T., Jekel, M. *Schriftenreihe Biologische Abwasserreinigung zum Kolloquium im Sonderforschungsbereich 193 der DFG an der Technischen Universität Berlin, Biologische Behandlung industrieller und gewerblicher Abwässer, Anwendung der LC-MS in der Wasseranalytik*, **1999**, Vol. 11, p. 57.
- 452** Crescenzi, C., DiCorcia, A., Samperi, R. et al., *Anal. Chem.* **1995**, *67*, 1797.
- 453** DiCorcia, A., Crescenzi, C., Marcomini, A. et al., *Environ. Sci. Technol.* **1998**, *32*, 711.
- 454** Sherrard, K.B., Marriott, P.J., Amiet, R.G. et al., *Environ. Sci. Technol.* **1995**, *29*, 2235.
- 455** Sherrard, K.B., Marriott, P.J., McCormick, M.J. et al., *Anal. Chem.* **1994**, *66*, 3394.
- 456** Mackay, L.G., Croft, M.Y., Selby, D.S. et al., *J. Assoc. Off. Anal. Chem.* **1997**, *80*, 401.
- 457** Cohen, A., Klint, K., Bøwadt, S. et al., *J. Chromatogr. A* **2001**, *927*, 103.
- 458** Ferguson, P.L., Iden, C.R., Brownawell, B.J. *J. Chromatogr. A* **2001**, *938*, 79.
- 459** Ferguson, P.L., Iden, C.R., Brownawell, B.J. *Anal. Chem.* **2000**, *72*, 4322.
- 460** Takino, M., Daishima, S., Yamaguchi, K. *J. Chromatogr. A* **2000**, *904*, 65.
- 461** DiCorcia, A., Costantino, A., Crescenzi, C. et al., *Environ. Sci. Technol.* **1998**, *32*, 2401.
- 462** Bokern, M., Nimtz, M., Harms, H.H. *J. Agric. Food Chem.* **1996**, *44*, 1123.
- 463** Shang, D.Y., Ikonomou, M.G., MacDonald, R.W. *J. Chromatogr. A* **1999**, *849*, 467.
- 464** Popeno, D.D., Morris, S.J., III, Horn, P.S. et al., *Anal. Chem.* **1994**, *66*, 1620.
- 465** Ceglarek, U., Efer, J., Schreiber, A. et al., *Fresenius J. Anal. Chem.* **1999**, *365*, 674.
- 466** Moder, M., Popp, P., Pawliszyn, J. *J. Microcol. Sep.* **1998**, *10*, 225.
- 467** Riu, J., Eichhorn, P., Guerrero, J.A. et al., *J. Chromatogr. A* **2000**, *889*, 221.
- 468** Crescenzi, C., DiCorcia, A., Marchiori, E. et al., *Water Res.* **1996**, *30*, 722.
- 469** González-Mazo, E., Honing, M., Barceló, D. et al., *Environ. Sci. Technol.* **1997**, *31*, 504.
- 470** Riu, J., González-Mazo, E., Gómez-Parra, A. et al., *Chromatographia* **1999**, *50*, 275.
- 471** Mantzavinos, D., Burrows, D.M.P., Willey, R. et al., *Water Res.* **2001**, *35*, 3337.
- 472** Moody, C.A., Kwan, W.C., Martin, J.W. et al., *Anal. Chem.* **2001**, *73*, 2200.
- 473** Conboy, J.J., Henion, J.D., Martin, M.W. et al., *Anal. Chem.* **1990**, *62*, 800.
- 474** Radke, M., Behrends, T., Foerster, J. et al., *Anal. Chem.* **1999**, *71*, 5362.
- 475** Fernandez, P., Alder, A.C., Suter, M.J.-F. et al., *Anal. Chem.* **1996**, *68*, 921.

- 476** Eichhorn, P., Knepper, T.P. *J. Mass Spectrom.* **2000**, *35*, 468.
- 477** Eichhorn, P., Knepper, T.P. *J. Chromatogr. A* **1999**, *854*, 221.
- 478** Eichhorn, P., Knepper, T.P. *Schriftenreihe Biologische Abwasserreinigung zum Kolloquium im Sonderforschungsbereich 193 der DFG an der Technischen Universität Berlin, Biologische Behandlung industrieller und gewerblicher Abwässer, Anwendung der LC-MS in der Wasseranalytik*, **1999**, Vol. 11, p. 156.
- 479** Schröder, H.Fr. *Schriftenreihe Biologische Abwasserreinigung zum Kolloquium im Sonderforschungsbereich 193 der DFG an der Technischen Universität Berlin, Biologische Behandlung industrieller und gewerblicher Abwässer, Anwendung der LC-MS in der Wasseranalytik*, **2001**, Vol. 11, p. 223.
- 480** Porschmann, J., Blasberg, L., Mackenzie, K. et al., *J. Chromatogr. A* **1998**, *816*, 221.
- 481** Cuzzola, A., Raffaelli, A., Saba, A. et al., *Rapid Commun. Mass Spectrom.* **1999**, *13*, 2140.
- 482** Cuzzola, A., Raffaelli, A., Saba, A. et al., *Rapid Commun. Mass Spectrom.* **2000**, *14*, 834.
- 483** Furey, A., Lehane, M., Gillman, M. et al., *J. Chromatogr. A* **2001**, *938*, 167.
- 484** Quilliam, M.A. *J. Assoc. Off. Anal. Chem. Int.* **1995**, *78*, 555.
- 485** Lewis, R.J., Holmes, M.J., Alewood, P.F. et al., *Nat. Toxins*, **1994**, *2*, 56.
- 486** Siren, H., Jussila, M., Liu, H. et al., *J. Chromatogr. A* **1999**, *839*, 203.
- 487** James, K.J., Bishop, A.G., Draisici, R. et al., *J. Chromatogr. A* **1999**, *844*, 53.
- 488** Rivasseau, C., Hennion, M.-C. *Anal. Chim. Acta* **1999**, *399*, 75.
- 489** Hiracka, K., Saito, S., Katsuragawa, J. et al., *Rapid Commun. Mass Spectrom.* **1998**, *12*, 1170.
- 490** Moyano, E., Games, D.E., Galceran, M.T. *Rapid Commun. Mass Spectrom.* **1996**, *10*, 1379.
- 491** Wycherley, D., Rose, M.E., Giles, K. et al., *J. Chromatogr. A* **1996**, *734*, 339.
- 492** Castro, R., Moyano, E., Galceran, M.T. *J. Chromatogr. A* **2000**, *869*, 441.
- 493** Evans, C.S., Startin, J.R., Goodall, D.M. et al., *J. Chromatogr. A* **2000**, *897*, 399.
- 494** Taguchi, V.Y., Jenkins, S.W.D., Crozier, P.W. et al., *J. Am. Soc. Mass Spectrom.* **1998**, *9*, 830.
- 495** Marr, J.C., King, J.B., *Rapid Commun. Mass Spectrom.* **1997**, *11*, 479.
- 496** Song, X., Budde, W.L. *J. Am. Soc. Mass Spectrom.* **1996**, *7*, 981.
- 497** Juhler, R.K., Vahl, M. *J. Assoc. Off. Anal. Chem.* **1999**, *82*, 331.
- 498** Ferrer, I., Thurman, E.M., Barceló, D. *Anal. Chem.* **1997**, *69*, 4547.
- 499** Vargo, J.D. *Anal. Chem.* **1998**, *70*, 2699.
- 500** DiCorcia, A., Nazzari, M., Rao, R. et al., *J. Chromatogr. A* **2000**, *878*, 87.
- 501** Chiron, S., Papilloud, S., Haerdi, W. et al., *Anal. Chem.* **1995**, *67*, 1637.
- 502** Hogenboom, A.C., Hofman, M.P., Jolly, D.A. et al., *J. Chromatogr. A* **2000**, *885*, 377.
- 503** Volmer, D.A., Vollmer, D.L., Wilkes, J.G. *LC.GC* **1996**, *14*, 216.
- 504** Mangiapane, S., Benfenati, E., Grasso, P. et al., *Environ. Sci. Technol.* **1997**, *31*, 3637.
- 505** Hogenboom, A.C., Niessen, W.M.A., Brinkman, U.A.Th. *Rapid Commun. Mass Spectrom.* **2000**, *14*, 1914.
- 506** Hogenboom, A.C., Niessen, W.M.A., Brinkman, U.A.Th. *J. Chromatogr. A* **1999**, *841*, 33.
- 507** Volmer, D.A., Hui, J.P.M. *Arch. Environ. Contam. Toxicol.* **1998**, *35*, 1.
- 508** Gardner, M.S., Voyksner, R.D., Haney, C.A. *Anal. Chem.* **2000**, *72*, 4659.
- 509** Honing, M., Riu, J., Barceló, D. et al., *J. Chromatogr. A* **1996**, *733*, 283.
- 510** Crescenzi, C., DiCorcia, A., Guerriero, E. et al., *Environ. Sci. Technol.* **1997**, *31*, 479.
- 511** Giraud, D., Ventura, A., Camel, V. et al., *J. Chromatogr. A* **1997**, *777*, 115.
- 512** Wang, N., Budde, W.L. *Anal. Chem.* **2001**, *73*, 997.
- 513** Moder, M., Popp, P., Eisert, R. et al., *Fresenius J. Anal. Chem.* **1999**, *363*, 680.
- 514** DiCorcia, A., Crescenzi, C., Lagana, A. et al., *J. Agric. Food Chem.* **1996**, *44*, 1930.
- 515** Lacassie, E., Dreyfuss, M.-F., Daguet, J.L. et al., *J. Chromatogr. A* **1999**, *830*, 135.
- 516** Banoub, J., Gentil, E., Kiceniuk, J. *Int. J. Environ. Anal. Chem.* **1995**, *61*, 143.

- 517** Molina, C., Grasso, P., Benfenati, E. et al., *J. Chromatogr. A* **1996**, *737*, 47.
- 518** Molina, C., Honing, M., Barceló, D. *Anal. Chem.* **1994**, *66*, 4444.
- 519** Hernandez, F., Sancho, J.V., Pozo, O. et al., *J. Chromatogr. A* **2001**, *939*, 1.
- 520** Molina, C., Grasso, P., Benfenati, E. et al., *Int. J. Environ. Anal. Chem.* **1996**, *65*, 69.
- 521** Vreeken, R.J., Speksnijder, P., Bobeldijk-Pastorova, I. et al., *J. Chromatogr. A* **1998**, *794*, 187.
- 522** Capps, T.M., Barringer, V.M., Eberle, W.J. et al., *J. Agric. Food Chem.* **1996**, *44*, 2408.
- 523** Mohsin, S.B. *Anal. Chem.* **1999**, *71*, 3603.
- 524** Song, X., Budde, W.L. *J. Chromatogr. A* **1998**, *829*, 327.
- 525** D'Ascenzo, G., Gentili, A., Marchese, S. et al., *Environ. Sci. Technol.* **1998**, *32*, 1340.
- 526** Otsuka, K., Smith, C.J., Grainger, J. et al., *J. Chromatogr. A* **1998**, *817*, 75.
- 527** Koppen, B., Spliid, N.H. *J. Chromatogr. A* **1998**, *803*, 157.
- 528** D'Ascenzo, G., Gentili, A., Marchese, S. et al., *Chromatographia* **1998**, *48*, 497.
- 529** Crescenzi, C., Di Corcia, A., Marchese, S. et al., *Anal. Chem.* **1995**, *67*, 1968.
- 530** Pozo, O., Pitarch, E., Sancho, J.V. et al., *J. Chromatogr. A* **2001**, *923*, 75.
- 531** D'Ascenzo, G., Gentili, A., Marchese, S. et al., *J. Chromatogr. A* **1998**, *813*, 285.
- 532** Lagana, A., Fago, G., Marino, A. et al., *Anal. Chim. Acta* **1998**, *375*, 107.
- 533** Reiser, R.W., Fogiel, A.J. *Rapid Commun. Mass Spectrom.* **1994**, *8*, 252.
- 534** Garcia, F., Henion, J.D. *J. Chromatogr.* **1992**, *606*, 237.
- 535** Kryniotsky, A.J., *J. Assoc. Off. Anal. Chem.* **1997**, *80*, 392.
- 536** Steen, R.J.C.A., Hogenboom, A.C., Leonards, P.E.G. et al., *J. Chromatogr. A* **1999**, *857*, 157.
- 537** Curini, R., Gentili, A., Marchese, S. et al., *Chromatographia* **2001**, *53*, 244.
- 538** Bobeldijk, I., Vissers, J.P.C., Kearney, G. et al., *J. Chromatogr. A* **2001**, *929*, 63.
- 539** Baltussen, E., Snijders, H., Janssen, H.-G. et al., *J. Chromatogr. A* **1998**, *802*, 285.
- 540** Rodriguez, M., Orescan, D.B. *Anal. Chem.* **1998**, *70*, 2710.
- 541** DiCoccia, A., Crescenzi, C., Samperi, R. et al., *Anal. Chem.* **1997**, *69*, 2819.
- 542** DiCoccia, A., Costantino, A., Crescenzi, C. et al., *J. Chromatogr. A* **1999**, *852*, 465.
- 543** Hancock, P.M., White, S.J.G., Catlow, D.A. et al., *Rapid Commun. Mass Spectrom.* **1997**, *11*, 195.
- 544** Hancock, P.M., Walsh, M., White, S.J.G. et al., *Analyst* **1998**, *123*, 1669.
- 545** Scheunert, I., Reuter, S. *Environ. Pollut.* **2000**, *108*, 61.
- 546** Crescenzi, C., Di Corcia, A., Nazzari, M. et al., *Anal. Chem.* **2000**, *72*, 3050.
- 547** Drexler, D.M., Tiller, P.R., Wilbert, S.M. et al., *Rapid Commun. Mass Spectrom.* **1998**, *12*, 1501.
- 548** Gennari, M., Ferraris, L., Negre, M. et al., *J. Assoc. Off. Anal. Chem.* **2000**, *83*, 1076.
- 549** Marek, L.J., Koskinen, W.C. *J. Agric. Food Chem.* **1996**, *44*, 3878.
- 550** Bossi, R., Koppen, B., Spliid, N.H. et al., *J. Assoc. Off. Anal. Chem.* **1998**, *81*, 775.
- 551** Li, L.Y.T., Campbell, D.A., Bennett, P.K. et al., *Anal. Chem.* **1996**, *68*, 3397.
- 552** Brown, H.M., Joshi, M.M., Van, A.T. et al., *J. Agric. Food Chem.* **1997**, *45*, 955.
- 553** Hogenboom, A.C., Steen, R.J.C.A., Niessen, W.M.A. et al., *Chromatographia* **1998**, *48*, 475.
- 554** Zambonin, C.G., Losito, I., Palmisano, F. *Rapid Commun. Mass Spectrom.* **2000**, *14*, 824.
- 555** Banoub, J., Gentil, E., Kiceniuk, J. *Int. J. Environ. Anal. Chem.* **1995**, *61*, 11.
- 556** Nelson, W.M., Tang, Q., Harrata, A.K. et al., *J. Chromatogr. A* **1996**, *749*, 219.
- 557** DiCoccia, A., Crescenzi, C., Guerriero, E. et al., *Environ. Sci. Technol.* **1997**, *31*, 1658.
- 558** Cai, Z., Cerny, R.L., Spalding, R.F. *J. Chromatogr. A* **1996**, *753*, 243.
- 559** Hogenboom, A.C., Niessen, W.M.A., Little, D. et al., *Rapid Commun. Mass Spectrom.* **1999**, *13*, 125.
- 560** Boundy-Mills, K.L., de Souza, M.L., Mandelbaum, R.T. et al., *Appl. Environ. Microbiol.* **1997**, *63*, 916.
- 561** Arnold, S.M., Talaat, R.E., Hickey, W.J. et al., *J. Mass Spectrom.* **1995**, *30*, 452.

- 562** Monson, S.J., Ma, L., Cassada, D.A. et al., *Anal. Chim. Acta* **1998**, *373*, 153.
- 563** González-Toledo, E., Companó, R., Dolors Prat, M. et al., *J. Chromatogr. A* **2002**, *946*, 1.
- 564** Banoub, J.H., Martin, R.C., Hodder, H. et al., *Analusis* **1997**, *25*, M15.
- 565** Choi, B.K., Gusev, A.I., Hercules, D.M. *Anal. Chem.* **1999**, *71*, 4107.
- 566** Valenzuela, A.I., Redondo, M.J., Pico, Y. et al., *J. Chromatogr. A* **2000**, *871*, 57.
- 567** Chukwudebe, A.C., Atkins, R.H., Wisslocki, P.G. *J. Agric. Food Chem.* **1997**, *45*, 4137.
- 568** D'Ascenzo, G., Gentili, A., Marchese, S. et al., *J. Chromatogr. A* **1998**, *800*, 109.
- 569** Lagana, A., Fago, G., Marino, A. *Anal. Chem.* **1998**, *70*, 121.
- 570** D'Ascenzo, G., Gentili, A., Marchese, S. et al., *Analusis* **1998**, *26*, 251.
- 571** Stout, S.J., DaCunha, A.R., Safarpour, M.M. *J. Assoc. Off. Anal. Chem.* **1997**, *80*, 426.
- 572** Kryni茨基, A.J., Stout, S.J., Nejad, H. et al., *J. Assoc. Off. Anal. Chem.* **1999**, *82*, 956.
- 573** Stout, S.J., daCunha, A.R., Picard, G.L. et al., *J. Agric. Food Chem.* **1996**, *44*, 2182.
- 574** Stout, S.J., daCunha, A.R., Picard, G.L. et al., *J. Assoc. Off. Anal. Chem.* **1998**, *81*, 685.
- 575** Stout, S.J., daCunha, A.R., Picard, G.L. et al., *J. Agric. Food Chem.* **1996**, *44*, 3548.
- 576** Bean, K.A., Henion, J.D. *J. Chromatogr. A* **1997**, *791*, 119.
- 577** Ahrer, W., Buchberger, W. *J. Chromatogr. A* **1999**, *854*, 275.
- 578** Koester, C.J., Beller, H.R., Halden, R.U. *Environ. Sci. Technol.* **2000**, *34*, 1862.
- 579** Charles, L., Pepin, D., Casetta, B. *Anal. Chem.* **1996**, *68*, 2554.
- 580** Buchberger, W., Ahrer, W. *J. Chromatogr. A* **1999**, *850*, 99.
- 581** Magnuson, M.L., Urbansky, E.T., Kelty, C.A. *Anal. Chem.* **2000**, *72*, 25.
- 582** Rivera, J., Ventura, F., Caixach, J. et al., in *Organic Micropollutants in the Aquatic Environment*, Vienna **1985**, p. 77.

## 16

# Gas Chromatography/Ion Trap Mass Spectrometry (GC/ITMS) for Environmental Analysis

*Michel Sablier and Toshihiro Fujii*

### 16.1

#### Introduction

The development of the concept of linking analytical instrumentation is motivated by the need for chemists to unequivocally detect, characterize, and quantify compounds in unknown mixtures. Mass spectrometry has long been recognized as a valuable analytical tool because of its superior reproducibility, repeatability, specificity, and limits of detection. The coupling of the “universal” detection power of mass spectrometry (MS) with the relatively inexpensive and versatile separation capabilities of gas chromatography (GC), together with the technological advances that have been achieved over the past 30 years, has led to widespread use of GC/MS instrumentation, some 80% of which is represented by GC/MS quadrupole-based systems.

Quadrupole ion trap mass spectrometry is a recent development in mass spectrometry that appears to be particularly well suited for high-sensitivity chromatographic applications. An ion trap, or Paul trap, is an extraordinary device that functions both as an ion store and as a mass spectrometer. The development of GC/MS using an ion trap mass spectrometer has recently culminated in the realization of low-cost instruments capable of classical modes of ionization associated with MS/MS, ranking ion traps in the domain of both high-specificity mass spectrometers and benchtop mass spectrometers. Advances in ion trap technology for GC/MS, such as improved trapping efficiency and resolution, have led to numerous applications in many areas of analytical chemistry. The ion storage capability of ion traps provides a sensitivity advantage over that of traditional quadrupole mass spectrometers and has spurred rapid growth of the GC/MS ion trap market, with probably over 5000 ion trap units sold worldwide.

Although ion trap mass spectrometry is a relatively new technique, the use of ion traps for GC coupling has been widespread, with the main driving force residing in the ability to obtain full-scan mass spectra with a very high sensitiv-

ity, often one order of magnitude larger than with traditional quadrupole mass spectrometers.

Many aspects of ion traps are reported in the literature [1–3], and these features are not covered here. Additionally, Chapter 10 of this Handbook covers the general principles and applications of mass spectrometry. Rather, this chapter focuses on the use of GC/ion trap mass spectrometry (ITMS) in environmental analysis, describing the principles of operation, giving examples of applications of ion traps in the environmental field, and highlighting recent developments in this area.

## 16.2

### Practical Aspects of CC/ITMS

#### 16.2.1

##### **Historical survey**

The first commercial GC ion trap mass spectrometer, the ITD700<sup>®</sup>, was launched by Finnigan in 1984. It was capable of acquiring full-scan and selected ion electron ionization (EI) mass spectra over a mass range of 650 u for samples eluting from a GC column coupled to an ion trap via a heated open-split interface. The ITD800<sup>®</sup> ion trap detector was then introduced as an upgraded version of the ITD700<sup>®</sup> and included chemical ionization (CI) capabilities and automatic ionization control routine procedures. ITMS<sup>®</sup>, the next ion trap mass spectrometer marketed by Finnigan, was a multipurpose research instrument providing MS/MS custom scan procedures through its scan editor software. The ITS40<sup>®</sup> ion trap, also marketed by Finnigan, was introduced as a benchtop GC/MS system especially designed for routine analysis. With the introduction of MS/MS technology, offering the potential of performing selected-ion monitoring analysis on an instrument priced competitively with current benchtop GC/MS linear quadrupole instruments, there is little doubt that ion trap technology is becoming of increasing interest to manufacturers of mass spectrometers (cf. Appendix for a list of manufacturers and representative products).

#### 16.2.2

##### **Principles of Operation**

GC/MS coupling has been the driving force behind the commercial development of the quadrupole ion trap, as evidenced by its ability to obtain full-scan mass spectra with a high sensitivity. The introduction of ion trap mass spectrometers occurred during a period of growth in the application of mass spectrometry to analysis of compounds of environmental interest, with commercial systems consisting mainly of a capillary column GC combined with a conventional quadrupole analyzer. The problem of introducing a capillary column effluent into a low-pressure device with a limited pumping speed was, in fact, solved about 20 years ago from ex-

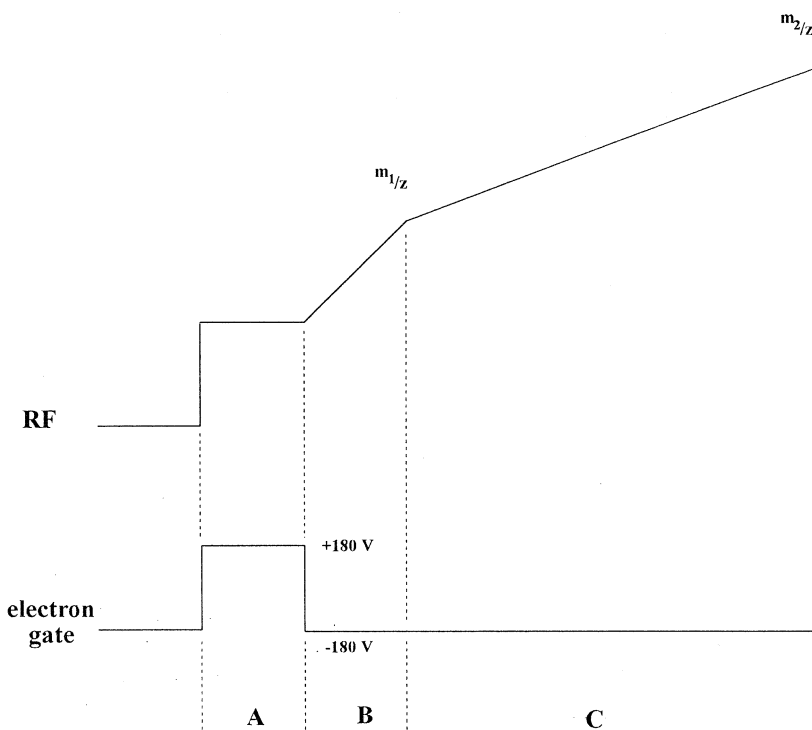


**Fig. 16.1** Scan function of the ion trap for obtaining a mass spectrum. The scan function consists of an ionization period A, where the electron gate is biased at a positive potential

(cf. text), a period B for ejection of the background ions, and an analytical ramp C, where ions are acquired from mass  $m_1$  to mass  $m_2$ .

pertise gained with coupling such columns to quadrupolar instruments. The main advance was the development of the mass-selective instability mode of mass analysis, which revolutionized the use of the ion trap as a mass analyzer. In this mode of operation, a radiofrequency RF voltage is applied to the central ring electrode of the ion trap, while the two end-cap electrodes are held at ground potential [4]. By definition, each ion confined within the ion trap is associated with a value of the  $q_z$  parameter on the  $q_z$  axis of the stability diagram correlated with a particular mass-to-charge  $m/z$  ratio. To record a mass spectrum, the RF voltage is increased with time so that ions of successively greater  $m/z$  ratio are ejected through holes in one of the end-cap electrodes as they develop unstable trajectories, ions are then detected with a classical electron multiplier. The scanning sequence of the ion trap consists of three steps performed repeatedly: (1) ionization and storage of ions above a chosen  $m/z$  ratio, (2) ejection of background ions below the  $m/z$  range of interest, and (3) ejection and detection of ions in order of increasing  $m/z$  ratio (Fig. 16.1). Full-scan mass spectra covering the desired range of analysis are then recorded. The execution of a single scan program is called a microscan.

During a GC/MS acquisition, the data for each microscan are summed, and the analytical spectrum obtained from the data system results from the averaging of this sum. The ion trap is operated with helium buffer gas to provide adequate cooling of the ions generated; the operating pressure (ca. 1 mTorr) is usually provided by the carrier gas flow through the GC column, avoiding the necessity for an additional helium gas cylinder.

### 16.2.3

#### **Ionization and Scanning Modes**

##### **16.2.3.1 Electron Ionization**

The most common configuration for GC/ITMS in its first stage of development was a single capillary GC column coupled to an ion trap. Electron ionization (EI) in the trap is achieved by passing a current of several tens of microamperes through a filament. Injection of the electrons from the filament is controlled by a gate lens biased at a positive potential during the ionization period and a negative potential during the analytical ramp. In routine use, the validity of ion trap for its sensitivity as an analytical tool must be correlated to a reliable spectra library searching procedure for rapid identification of unknowns in a chromatogram. However, in the ion trap, the affectors of spectral characteristics depend on ion chemistry and instrumental design. Specific compounds can undergo ion–molecule reactions under EI conditions, and a large amount of ions can result in space-charge effects; these factors are related to sample concentration and are a limitation for rapid and efficient identification of unknowns.

The number of ions that are created and trapped at a given sample pressure is controlled by the ionization time and the filament emission current. A longer ionization period leads to a greater number of trapped ions, and consequently a poorer resolution for preponderant ions of low  $m/z$  compared to high  $m/z$  ions as the ions are scanned out from the ion trap, since the total number of ions is decreased during the analytical ramp. In contrast, with quadrupole mass analyzers, space-charge effects are more noticeable because all of the ions above a particular  $m/z$  ratio are trapped at the same time. It is noteworthy that, in most commercial instruments, recognizing space-charge effects in GC/ITMS data is complicated by the acquisition of centroided peaks for reconstructed mass spectra which tends to hinder the characterization of changes in resolution, peak shape, and mass assignment. These space-charge effects, which impair the performance of GC/ITMS, have been addressed by using modified control routines to reduce the number of ions generated. For this purpose, automatic gain control (AGC) has been introduced to reduce space-charge effects by limiting the number of ions generated at different points during the elution of a sample during a chromatographic run. When AGC returns a large total ion current, the ionization time for subsequent microscans is reduced (conversely, the ionization time for the following microscans is increased when the measured total ion current is low). Along a chromatographic peak, the total ion current changes with the concentration profile during elution, AGC responds to the change by decreasing the ionization time at the top of the

peak, where the concentration of the sample is highest, and increasing the ionization time along the sides of the eluting peak, where the concentration of the sample is lower. To summarize, AGC minimizes space-charge effects when the sample pressure is high, and acts to enhance the sensitivity when the sample pressure is low. In addition, reduction of the ionization time limits the extent of perturbing ion–molecule reactions between newly generated ions and neutral precursors. A compromise between AGC settings and filament emission current usually gives optimized sensitivity [5].

EI spectra covering the full-scan mass range are normally acquired with a segmented EI scan program. The EI scan program of commercial ion traps normally produces a complete mass spectrum by combining the spectra obtained from four scan segments and includes: (1) a variable ionization time, (2) a rapid RF ramping for ejection of low mass ions, and (3) an RF analytical ramp for the defined segment (Fig. 16.2). The main purpose of the segmented scan program is to reduce self-chemical ionization and ion–molecule processes by shortening the residence time of the ions in the ion trap between ionization and detection. Moreover, the segmented scan program allows adjustment of the ionization settings of each segment (ionization time, RF level). For GC/MS experiments, the scan repetition rate (number of scans acquired each second) can be increased by reducing the number of scan segments and/or reducing the mass range of analysis. A larger scan repetition rate is obtained if a single scan segment is used.

A supplementary RF voltage, the axial modulation, is applied during the scan program to improve the resolution by increasing the efficiency with which the ions are resonantly ejected from the ion trap during the RF analytical ramp.

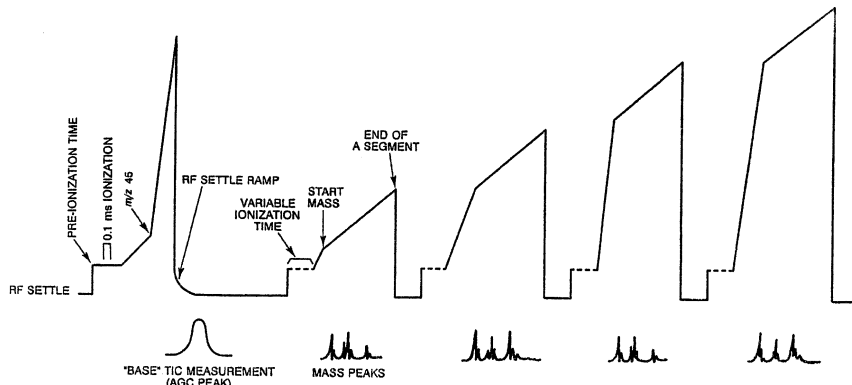


**Fig. 16.2** Representative four-segment scan function for acquiring EI mass spectra. Each AGC scan function consists of a pre-ionization

AGC settings, and a rapid rf scan to get a rough measurement of the total ionic current. All segments include the steps described in the text. (Reprinted with permission from [5])

### 16.2.3.2 Chemical ionization

Chemical ionization (CI), a less energetic ionization method than EI, is often used in conjunction with EI to aid in identifying the molecular weights of samples. CI has the advantage of allowing better control of transferred internal energy (through the choice of reagent gases), which favors the formation of protonated molecules through proton transfer or radical cations through charge exchange processes. The flexibility of being able to switch from EI to CI in the same experiment has contributed to the growing interest in ion trap analyzers. In addition, the CI potentialities of ion traps have played a major role in establishing ion traps as promising devices for analytical applications. CI operation of the ion trap was reported in 1987, only 3 years after its commercial introduction [6]. The first drawbacks encountered under CI conditions, space-charge effects and ion–molecule reactions, were circumvented by using modified routine sequences similar to the AGC procedure described below.

The reagent gas and sample pressures employed for CI operation of ion traps are intermediate between those used in conventional mass spectrometers and those used in ion cyclotron resonance (ICR) spectrometers. CI in an ion trap is effected by using  $10^{-6}$  to  $10^{-4}$  Torr of reagent gas compared to the 1 Torr range of pressure used in conventional ion sources. If the sample to reagent gas ratio is drastically decreased, even down to 1:10 to limit the space-charge effects, this feature precludes however effective limitation of sample electron ionization processes. As a consequence, fragments resulting from EI can contribute significantly to the resulting CI mass spectrum. What is accomplished under classical CI conditions by using a high pressure ion source is achieved in the ion trap by using long reaction times. Ion traps are generally operated in the mass-selective instability mode. During the timing sequence, the ion trap is first held at a low RF voltage to eliminate residual ions (Fig. 16.3). After the ionization period, the RF voltage is raised to an RF value in accordance with the  $m/z$  ratio of the stored reagent ions. At this value, lower mass ions show unstable trajectories, while higher mass ions are inefficiently trapped. This first reaction period allows an effective population of reagent ions to be established through ion–molecule processes, typically  $\text{CH}_5^+$  and  $\text{C}_2\text{H}_5^+$  under methane CI conditions (pressure in the  $1,0 \cdot 10^{-5}$  Torr range and reaction time of about 15 ms). The nature of the reagent population can be controlled through the length of the first reaction period; for example, shortening this period induces an increase in the  $\text{CH}_5^+$  ion population at the expense of  $\text{C}_2\text{H}_5^+$  ions under methane CI conditions. This controls the ongoing ion–molecule reactions between reagent ions and sample molecules, and reduces EI interferences, since trapping is inefficient for high-mass ions. The desired reagent ion population is subjected to a fast RF voltage ramp to achieve the sample reaction period RF level. Ion–molecule reactions between the sample molecules and reagent ions take place during this interval, typically 50 to 100 ms, in which the RF value settles, allowing efficient trapping of the resulting product ions. This value of 50 to 100 ms should be compared to the  $10^{-4}$  s ion residence time in conventional high pressure ion sources. The RF voltage is subsequently scanned for mass analysis. The entire sequence is repeated and the acquired microscan spectra are added and averaged to obtain the analytical spectrum.

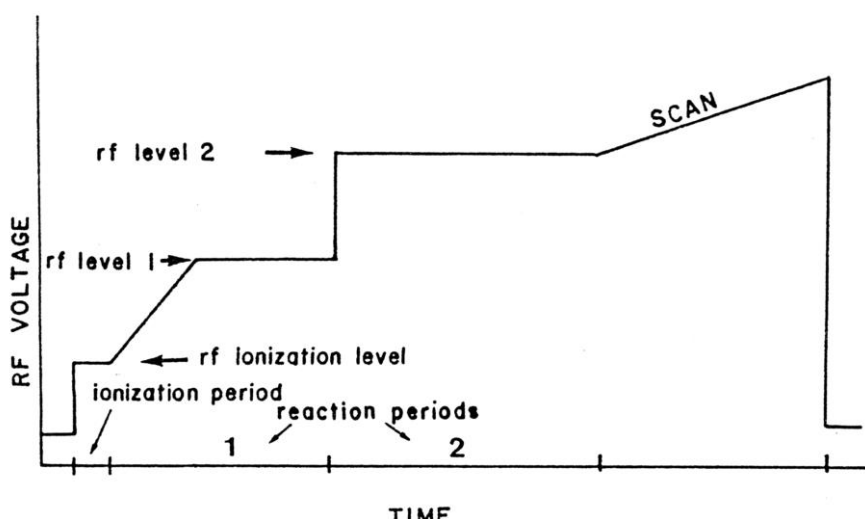


**Fig. 16.3** Timing sequence for acquiring a mass spectrum under CI ion trap conditions. A low RF voltage is first applied to clear the ion trap of residual ions; the RF voltage is then allowed to settle at RF level 1 and RF level 2 to allow reagent ion formation and the CI process respectively; and the RF analytical ramp is scanned for data acquisition. (Reprinted with permission from [6]).

Experimental variables do, however appear to be critical in obtaining reproducible CI spectra with ion traps, this is a feature common to all mass spectrometer instruments. But improper selection of RF voltages, time intervals, or operating pressures can yield unexpected results, and could be at the origin of some criticisms concerning this mode of ionization in ion trap mass spectrometry. Obviously, and as a matter of fact, under methane CI conditions, ion traps present characteristic properties such as a smaller  $m/z$  ratio for the  $\text{CH}_5^+/\text{C}_2\text{H}_5^+$  ions, and a reduced yield of adduct ions  $[\text{M}+29]^+$ ,  $[\text{M}+41]^+$ . The lack of effective stabilizing conditions for the removal of internal energy has been proposed to account for the absence of such adducts [6].

Among the parameters influencing the CI ion trap conditions, reaction time, temperature and pressure are of most importance. For example, the time allowed for the reagent ions to react with the sample molecules (reaction period 2) has been shown to alter the appearance of CI spectra and could certainly explain the main differences noted in comparing ion trap mass spectrometry with linear quadrupole mass spectrometry. However, prolonging the reaction time increases the total number of sample ions; this feature can be used to enhance weak signal ions within the confines of sampling time limitation to avoid space-charge effects. The ratio of the helium buffer gas pressure to the CI reagent gas pressure is typically in the range 100:1. Collisional deactivation by helium has a dramatic effect on the CI mass spectrum in limiting subsequent fragmentations from the protonated molecules generated under the CI process. Thus, there are several major differences between con-

ditions employed in CI ion trap operations and those used with conventional mass spectrometers.

Accumulation of a large concentration of reagent ions, which accounts for the large population of sample ions, is the main characteristic of the ion trap under CI conditions. Optimum conditions for CI experiments are controlled through a pre-scan procedure to determine the appropriate ionization and reaction times: automatic reaction control (ARC), analogous to AGC used in EI experiments. During chromatographic elution of a sample, ARC acts to accommodate these parameters to provide a full mass spectral scan in accordance with the concentration profile. The two major types of ion–molecule reactions, that take place are charge transfer and proton transfer. The exothermicity of these ion–molecule reactions is such that there exists a risk that EI-like ions will appear in the CI mass spectrum; for example, under methane CI conditions and in the presence of reagent gas ions generated during the first reaction period, the radical ion  $\text{CH}_4^+$  is likely to undergo high-energy charge transfer reactions while the protonated ion–molecule reaction product  $\text{CH}_5^+$  undergoes mainly low-energy proton transfer reactions. Particular attention has been paid to these features of ion traps in the development of modified ARC procedures now available in commercial instruments. These new ARC-CI functions are based on extended control over the composition of the reagent ion population.

#### 16.2.3.3 Full Scan Versus Selected-Ion Monitoring

The selected-ion monitoring (SIM) scanning mode is used to increase sensitivity by collecting continuously the ion current for a single  $m/z$  ratio. For beam-type mass spectrometers, the SIM mode is usually more sensitive than the full scan mode because of the likely signal-to-background ratio (S/B) enhancement provided by this continuous single mass monitoring mode. However, in ion traps, the S/B gain obtained by switching from full scan mass spectrum acquisition to SIM is lower than with quadrupole analyzers where continuous scanning for one mass is carried out. Indeed, reducing the acquisition range to record a single mass shortens one part of the scan program, affecting only the number of microscans, inducing only a relatively modest increase in S/B. This major drawback for GC/MS is counterbalanced by the improved quantitation obtained with the SIM acquisition procedure, since the GC peak profile is more accurately reproduced due to the increase in the scan repetition rate.

#### 16.2.4

#### Advances in GC/ITMS

Although the ion trap is considered by many analysts to be the most or one of the most sensitive instruments for GC/EI MS and positive ion GC/CI MS, new techniques to improve instrument performance are being developed. We briefly describe here new scanning sequences, the fitting of external ion sources, and applications of GC/MS/MS procedures.

### 16.2.4.1 Methods for Improving Performances: Increasing the Signal-to-Background Ratio

One advantage of the ion trap is its large dynamic range. However, a high level of background ions may prevent the detection of dilute analytes. The problem to solve is to increase S/B by employing shorter ionization times to lower the background ions and avoid space-charge effects. Some researchers have proposed using SIM methods to selectively eject background ions prior to mass analysis to reduce background interferences and to enhance sensitivity.

Since ions are physically trapped according to their secular frequency, single frequency resonance ejection methods have been used to remove ions of a particular  $m/z$  ratio by applying an additional potential to the end-cap electrodes at the fundamental axial secular frequency of the ion to be ejected. Broadband excitation and combination of RF voltages and resonant ejection frequencies have been employed for this purpose. Nonlinear relationships between the ionization time and the resulting ion signal have led to the conclusion that single frequency resonance ejection methods are more suited to the elimination of a single ion species due to the step-by-step procedure of these ejection techniques [7].

Multiple-frequency resonance ejection methods have been developed to eject specifically one or more ion species simultaneously. Digital waveform generators have been used for this purpose and have been shown to provide greater control over the excitation processes [7]. Most of these methods are derived from ICR mass spectrometry.

Commercial introduction of ion isolation/ejection techniques to reduce background interferences by the use of waveform generators coupled to digital function generators and personal computer systems has greatly contributed to customization of GC/ITMS instruments. These instruments are now providing with an extended simplicity numerous methods for the utilization of customized sequences for specific analytical applications.

### 16.2.4.2 External Ion Sources

Although ions can be generated by EI and CI of compounds introduced directly into an ion trap, it might be desirable to apply other methods of ionization. Moreover, the use of an external ion source may solve the problem of self-CI during GC/EI-ITMS analyses. Such considerations have been the basis of studies on the injection of externally generated ions into an ion trap [8].

In the external ion source configuration of ion traps, a dual EI/CI ion source is directly coupled to the ion trap through a focusing lens system. The externally generated ions are accelerated from the ion source, focused through a lens system and injected into the ion trap. A simple gated electronic lens system is used to correlate the injection step to the ionization period of the classical scanning sequence. Ion injection into ion traps is facilitated by the presence of helium bath gas at a relatively high pressure ( $1.0 \times 10^{-3}$  Torr), which removes kinetic energy of the entering ions and permits efficient trapping.

External ion sources have been developed principally to address the perturbing effect of self-CI processes that form  $[M+1]^+$  adduct ions during EI process. Such reactions result in an increased  $[M+1]^+/M^+$  ratio or in the appearance of artifact peaks due to adduct formation, both of which lead to ambiguity in identification of samples, especially for samples containing isotopes. Self-CI effects are easily observed at relatively low partial pressure of samples for compounds having a high gas-phase acidity, or possessing proton-donor or proton-acceptor functions. The proposed solution lies in reducing the density of neutral compounds (analytes or contaminants) that are involved in the ion-molecule reactions leading to these adducts.

Besides reducing ion-molecule reaction processes, injection of externally generated ions offers the possibility of conducting negative ion chemical ionization (NICI) experiments. NICI is not efficient in the usual configuration of ion traps because of the lack of thermal electrons due to the presence of the RF storage field. Consequently, under EI conditions, positive ions are estimated to be formed  $10^3$  times more efficiently in ion traps than negative ion. In addition, nascent negative ions are subjected to recombination reactions with the predominant positive ions to form neutral species. The negative ion mode of operation is useful for the analysis of compounds bearing electronegative functional groups such as halogenated pesticides. Consequently to use the NICI mode, the appropriate species must be formed in an external ion source and subsequently injected into the ion trap.

The major drawbacks to using an external ion source was related to the complexity of operation in switching from EI to CI in contrast to the usual configuration, and the requirement for an additional vacuum system. Nevertheless, external ion source GC/ITMS is undergoing commercial development, and manufacturers currently provide external ion source designs for the new generations of ion-trap mass spectrometers.

#### 16.2.4.3 GC/MS/MS

In general, SIM procedures can be useful for enhancing sensitivity for target analytes in clean matrices, but at the expense of mass spectral information. In addition, as the sample matrix becomes more complex, it becomes more difficult to obtain the necessary sensitivity to distinguish the analyte signal from any interfering chemical background signal. Therefore, when only SIM procedures are used, low detection limits are rarely attainable in complex matrices.

For improved sensitivity and selectivity, GC/MS/MS in the ion trap meets the criteria for obtaining low detection limits. MS/MS enhances selectivity by separating the target compound from the chemical background (due to the matrix), and, in essence, the matrix is virtually eliminated. The result is a better signal/background ratio (and lower detection limits). Collision induced dissociation (CID) of isolated ion species in an ion trap has thus become a powerful technique.

In comparison to linear quadrupole instruments, the CID process in an ion trap is more complex since the selected ionic species are resonantly excited at their se-

cular frequency of motion. This frequency is subject to some slight changes when the ions move away from the center of the trap and when the number of ions confined within the trap changes. In addition, a large set of parameters needs to be adjusted (ionization time, RF level for ionization, RF and/or DC voltages for excitation, isolation times, RF level for CID, excitation frequency, excitation voltage) and, finally, tuning procedures are time consuming. Application of CID for GC coupling, for which elution peak width might not exceed a few seconds, has only been made possible by the development of sophisticated set of programs. Multi-frequency irradiation methods are usually employed to perform CID with high efficiency and short periods of irradiation. However, compared to beam-type mass spectrometers, ion traps offer three main advantages when used in the MS/MS mode. First, the ion trap operates in the pulsed mode, and allows accumulation of ions mass selectively over time in such a way that a rather constant target ion number can be selected over varying concentration profiles. Second, the CID process in the ion trap involves a large number of collisions between the mass selected ion and light helium buffer gas atoms. Under these conditions, the energy transferred per collision is very low ; as a result, only the lowest dissociation pathways are attained, which simplifies the CID spectra. Third, it is possible to totally dissociate the mass-selected ion and, confine within the ion trap nearly all of the fragment ions (this accounts for the high efficiency of dissociation generally reported in the literature; efficiency of dissociation is defined as 100 times the ratio of the sum of the product ion signal intensities to the parent ion signal intensity). The ion isolation CID sequence can be repeated one or several times to provide  $(MS)^3$  and  $(MS)^n$  sequences, a process known as multiple-stage mass-selective operation. Clearly, the development of benchtop GC/MS/MS ion traps over the past few years has expanded the use of MS/MS for analytical purposes.

### 16.3

#### Examples of Applications of GC/ITMS

##### 16.3.1

##### Requirements for Environmental Analysis

In environmental analysis, strict criteria are highly desirable. The detection of identified pollutants and toxic material must be certain, and original analysis should be supported by a confirmatory procedure. Moreover, recording a mass spectrum in the low parts per million (ppm) to parts per trillion (ppt) concentration range is much more complex than recording a mass spectrum of a reference standard. Although confirmatory procedures are well-documented for a variety of analytical methods in the regulatory arena, including mass spectrometry techniques after the elaboration of good laboratory practices, confirmatory procedures for ion trap mass spectrometry are not so clearly defined. However, the examples of the following section show that ion traps have the outlined criteria of reliability, practicality, accuracy, limit of detection, and specificity.

Of fundamental importance are the instrumental tune-up and calibration tests. Originally, decafluorotriphenylphosphine (DFTPP; bis(perfluorophenyl)-phenyl phosphine) was recommended as one of the most appropriate reference compounds, although perfluorobutylamine (PFTBA; FC 43) has a large popularity among the mass spectrometrists. A second test compound, 4-bromo-fluorobenzene (BFB) was introduced in 1984 for the tuning procedure in methods for the analysis of volatile organic compounds (VOCs). In both cases, relative peak abundance measurements in the ion trap from repetitive injections of small quantities of DFTPP and BFB through a capillary GC column have been shown to be good, with relative standard deviation of 3 to 26% [9].

Good mass spectra quality indices must be provided. These indices consist of criteria defining the characteristics for an acceptable mass spectrum including: the absence of ions in excess of the values expected for the molecular ion (except adduct ions under CI conditions), the absence of non-logical neutral losses, molecular and fragment ions within the theoretical range of variation for the isotopic abundances relative to the parent ions. Comparison with standard MS spectra from the reference NIST (National Institute of Standards and Technology) library usually provides good results, even at low levels of concentration during GC injection into the ion trap.

The ability to detect a residue at a level one order of magnitude below the regulatory level is normally required. Careful attention must be paid to extrapolating spectral data of standard reference spectra, which can be misleading with respect to the true level of detection available in the real sample.

Coupling GC to mass spectrometry implies criteria directly related to the GC separation, and retention time criteria are of paramount importance to the mass spectrometric identification. One advantage of combining capillary column technology with mass spectrometry is that only a small quantity of sample is required for full mass analysis. However, scan repetition rate must be restricted to the values specified in the protocol employed and retention time correlation must be bracketed in a window within 15 scans of the reference standard. EI spectra have been widely used for identification due to their “fingerprinting” capabilities allowing identification through comparison with published data and library references or through the fragmentation patterns of the sample. One of the main strengths of GC/ITMS lies in the ability of ion traps to reliably produce full mass spectra at low concentration levels. For confirmatory purposes, as processed usually in mass spectrometry, selected-ion monitoring procedures can be satisfactory only if conducted on more than three ions of structural significance and observed in the expected relative abundance ratio with respect to the precursor molecular ion. Monitoring a smaller number of ions can lead to misleading identification of residues, and this approach is generally used for screening purposes only.

The following sections report successful use of GC/ITMS for the detection and characterization of compounds of environmental concerns (see Tab. 16.1).

**Table 16.1** Compounds of environmental concern characterized by GC/ITMS and reported sensitivities.

Compound	Reported Sensitivity	Reference
Benzene, carbon tetrachloride, 1,2-dichloroethane, trichloroethene, 1,4-dichlorobenzene, 1,1-dichloroethene, 1,1,1-trichloroethane, vinyl chloride	0.1–10 $\mu\text{g L}^{-1}$ <sup>a</sup>	10
Acetone, acrolein, acrylonitrile, allyl chloride	1 $\mu\text{g L}^{-1}$ <sup>a</sup>	11
2,3,7,8-Tetrachlorodibenzodioxin	100 fg $\mu\text{L}^{-1}$ <sup>b</sup>	16
(Tri-n-butylmethyl)tin	1.3 pg <sup>c</sup>	18
(Di-n-butylmethyl)tin	1.9 pg <sup>c</sup>	18
Tebufelone	0.27 ng <sup>d</sup>	19
Diazepam	2 ng	20

*a* Corresponding to 0.5 to 50 ng of each compound in a sample of 5 mL of water; purge-and-trap extraction technique; fluorobenzene as internal standard at 1  $\mu\text{g L}^{-1}$ .

*b* Reported as a current detection limit.

*c* Under CI acetonitrile ionization conditions; presented as minimal detection amounts of Sn for S/B = 3.

*d* GC/MS/MS analysis; daughter ion spectrum of the *m/z* 248 fragment ion.

### 16.3.2

#### Determination of Volatile Organic Compounds in Drinking Water; EPA Methods

The monitoring of volatile organic compounds (VOCs) in drinking water has led to their regulation in drinking water in several countries, especially in the United States where the Environmental Protection Agency (EPA) has set such regulations since 1979. Distinct approaches have emerged, focusing on either identifying one or more listed analytes or targeting a specific analyte for which a methodology is optimized. These regulations have established maximum VOC contaminant levels. In the early 1990s, a combination of a capillary GC column and a benchtop ion trap was used to evaluate EPA Methods 524.2 [10, 11]. A standard purge-and-trap extraction system was used, and AGC and full mass range scanning of the ion trap were employed for complete identification of compounds. Optimum purge-and-trap GC/MS conditions for the detection of eight regulated (benzene, carbon tetrachloride, 1,2-dichloroethane, trichloroethene, 1,4-dichlorobenzene, 1,1-dichloroethene, 1,1,1-trichloroethane, vinyl chloride) and 51 unregulated volatile compounds in drinking water were determined. At the 2  $\mu\text{g L}^{-1}$  level with a 5 mL water sample, the grand mean measurement accuracy for 54 compounds was 95% of the true value, with a mean relative standard deviation of 4% [10]. At the 0.2  $\mu\text{g L}^{-1}$  level, the grand mean measurement accuracy for 52 compounds was 95%, with a mean relative standard deviation of 3% [10]. At this level, the failure to detect chloromethane and dichlorodifluoromethane was attributed to their high vapor pressure and poor retention. Extension of the method to 28 additional compounds gave reliable results for a maximum contaminant level of 1  $\mu\text{g L}^{-1}$  or lower [11]. Standardization and quality control proposals for VOCs in drinking water and ambient air,

and for less volatile compounds were subsequently summarized [12]. During these investigations, the ITD operating in the full scan mode of acquisition was demonstrated to be a good compromise between minimum analysis time and complete separation of compounds of different origin in the same mixture. This is in accordance with cost-effectiveness in analytical laboratories, which requires the optimization of the number of samples that can be processed in a given work period without loss of quality of analysis.

### 16.3.3

#### Detection of Dioxins and Furans

Polychlorodibenzodioxins (PCDDs) and polychlorodibenzofurans (PCDFs) are of great environmental concern, and their determination by GC/ITMS is a good example of the application of GC/ITMS in analytical chemistry. These compounds are determined mainly in complex mixtures, where they may be present at trace level. Because of their suspected toxicity and their persistence in the environment, PCDDs and PCDFs are classified as priority pollutants. The methods of detection specified by environmental agencies usually call for monitoring the total concentration of all the congeners of these compounds, with a particular emphasis on the overall isomers of the most potent 2,3,7,8-tetrachloro-substituted congeners of PCDD (2,3,7,8-T<sub>4</sub>CDD).

High-resolution gas chromatography (HRGC) coupled with high-resolution mass spectrometry (HRMS) is currently prescribed by most regulatory agencies. However, such determinations are costly due to the time required for extensive sample preparation, the use of <sup>13</sup>C-labeled internal standards, and expensive high-resolution mass spectrometers. The main problem in detecting dioxins lies in the likely presence of interferents, such as the matrix itself or PCDFs, and the overlap of isotopic clusters during the analysis requiring HRMS and resolving power of several tens of thousands. Tandem mass spectrometry (MS/MS) has been proposed to circumvent the costly use of HRMS, with detection limits approaching those obtained under HRMS conditions; however, neither technique can completely remove all interferences, making the two techniques complementary [13]. Recently, a rapid screening technique for the detection and quantitation of 2,3,7,8-TCDD using GC/ITMS operated in the MS/MS mode has been reported [14]. Although the sensitivity of the ion trap MS/MS technique appeared to be fairly good and comparable to that of tandem quadrupole mass spectrometry, the scanning functions available at that time in ITMS were a limiting factor in the development of GC/ITMS for the quantitation of dioxins. Software advances since then have overcome this limitation. Commercial software is now available for deconvoluting mass spectra obtained from coeluting compounds and for conducting MS/MS experiments using multiple-reaction monitoring with several daughter ions, which is required for the analysis of tetra- to octa-PCDDs/PCDFs during a single chromatographic run. Since then, the CID procedure has been used to optimize both molecular ion isolation and directed fragmentation of the PCDDs and PCDFs with an ion trap [15]. The multifrequency irradiation mode of excitation

was found to be the best compromise in terms of conversion efficiencies for the parent ion to the [M–COCl] daughter ion and for compatibility of irradiation duration on a gas chromatographic time scale.

A comparative study of three mass spectrometric methods for the determination of tetra- to octa-chlorodibenzo-*p*-dioxins/furans using HRMS, triple-stage quadrupole mass spectrometry, and ion trap mass spectrometry has been recently published [16]. The following aspects of the determination of PCDDs/PCDFs were examined : (1) tuning procedures, (2) calibration curve preparation, (3) 2,3,7,8-T<sub>4</sub>CDD detection limits, (4) examples of ion signals from 2,3,7,8-T<sub>4</sub>CDD obtained at 50 times the HRMS detection limit, (5) relative response factors, (6) ionization cross sections, and (7) comparison of signal ions due to hexachloro-*p*-dibenzodioxin (H<sub>6</sub>CDD) congeners from real samples. The current 2,3,7,8-T<sub>4</sub>CDD detection limits of the three methods (coupled to GC) are 10 fg L<sup>-1</sup> by HRMS, 150 fg L<sup>-1</sup> by triple-stage quadrupole, and 100 fg L<sup>-1</sup> by ion trap. Examples of the ion signals obtained with each technique for a low concentration of 2,3,7,8-T<sub>4</sub>CDD are shown in Fig. 16.4, where the signal-to-background ratios for HRMS and the ion trap are seen to be comparable. For HRMS and triple-stage quadrupole mass spectrometry, the approved methods called for the observation of two *m/z* ratios, whereas for the ion trap, there is no approved method and additional ion species were monitored to increase sensitivity and selectivity. These investigations permit one to state that, while the HRMS detection limit for T<sub>4</sub>CDD is lower than that of triple stage quadrupoles and ion traps, there is evidence that all interferences are not eliminated by using HRMS alone. Consequently, there is a need for instruments that can achieve high specificity by MS/MS operation and ion traps are ideally suited for this purpose.

#### 16.3.4

##### Other Examples

The advantages and disadvantages of the ion trap approach to multi-residue pesticide analysis have been assessed for the purpose of conducting routine analysis for the determination of pesticide residues in food [17]. The driving force behind this approach is to reduce analytical costs. Chemical ionization is currently used in GC/MS analysis of trace levels of pesticides to reduce interferences of matrix components and to provide higher specificity through the production of protonated molecular ions for the residues of interest. The precision and accuracy of ion trap for trace level detection of pesticides is within acceptance ranges (relative standard deviation of less than 10% with a correlation coefficient of 0.995 or greater). The ion trap has been found to be sensitive for the detection of nitrogen-containing compounds. The use of a single ion area measurement is acceptable for trace level quantification. Finally, the ion trap can be used in multi-residue pesticide analysis as a replacement detection system capable of automatic confirmation and quantification in a shortened analytical step [17].

A growing concern about the presence of organotin in the environment has created a need for faster, more sensitive and more accurate analytical methods for its

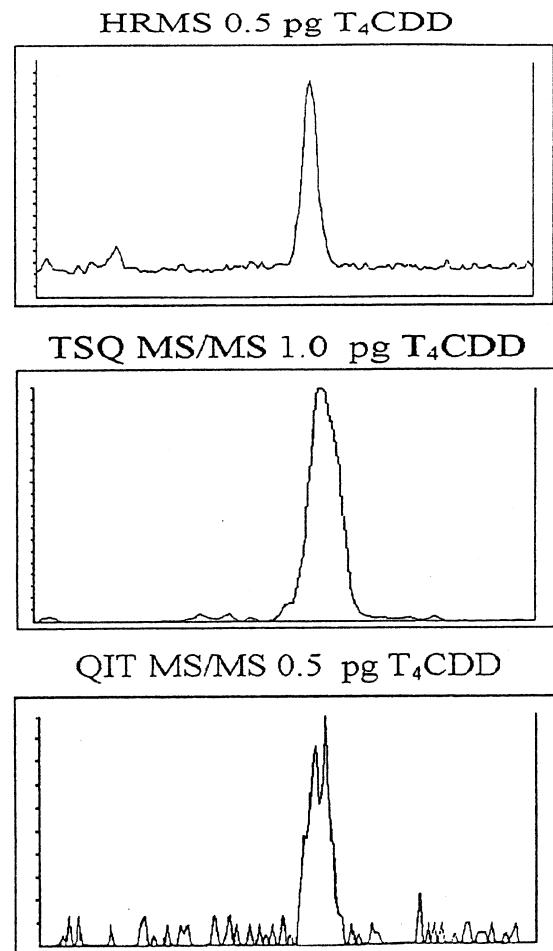


**Fig. 16.4** Ion signals obtained for low concentrations of 2,3,7,8-T<sub>4</sub>CDD: (top) HRMS, 0.5 pg injected in 1  $\mu$ L (signal obtained at 50 times the detection limit), sum of  $m/z$  320 [M]<sup>+</sup> and 322 [M + 2]<sup>++</sup>; (middle) triple-stage quadrupole MS, 1.0 pg injected in 1  $\mu$ L, sum of  $m/z$  257 and 259[M - CO<sup>37</sup>Cl]<sup>+</sup>; and (bottom) ion trap, 0.5 pg in 1  $\mu$ L, sum of  $m/z$  257, 259, 194, and 196. [M]<sup>+</sup>, and [M+2]<sup>++</sup> are the molecular ion with <sup>35</sup>Cl atoms only and the molecular ion with a single <sup>37</sup>Cl atom respectively;  $m/z$  257, 259 and 194, 196 correspond to loss of COCl<sup>+</sup> and 2COCl<sup>+</sup>, respectively. (Reprinted with permission from [16].)

detection in environmental samples. GC/ITMS has been shown to be a powerful technique for determining trace and ultratrace quantities of tributyltin and its degradation products in water after hydride derivatization and Grignard methylation, which provides lower detection limits under EI conditions [18]. The wide linear dynamic range and picogram sensitivity of the ion trap operating in the EI mode make this GC/MS configuration suitable for routine trace and ultratrace analysis of organotin.

The performance of GC/ITMS for the analysis of a model drug, tebufelone, has been studied to evaluate the selectivity, linear range, accuracy, and precision of this method for sampling drugs in biological matrices [19]. Compared to GC linear quadrupole mass spectrometry, the SIM mode of operation of the ion trap provided a higher degree of selectivity for the analysis of tebufelone spiked rabbit plasma samples, and gave linear standard curves over three orders of magnitude of concentration, with an associated detection limit of  $100 \text{ pg mL}^{-1}$ .

Diazepam has been used as a test compound for a comparative study of GC/ITMS versus a GC linear benchtop quadrupole mass spectrometer in both the full mass scanning mode and the SIM mode [20]. A major concern involved evaluating whether GC/ITMS provides mass spectra in a concentration-dependent way and whether this technique yields mass spectra that can be searched against conventional mass spectral data libraries. In the full scan mode, the ion trap had a signal/background ratio of 1400 for a 2 ng injection of diazepam, with an ion ratio precision varying from 5 to 13%. In the SIM mode, the ion trap had an average signal/background ratio of 14,000, with an ion ratio precision of 6 to 15% [20]. Overall, compared to quadrupole mass spectrometry, GC/ITMS in the full scan mode provided an equivalent precision in ion ratio at a greater signal/background ratio, but was 5 to 10-fold less accurate in the SIM mode.

## 16.4 Future Prospects in GC/Chemical Ionization-ITMS

### 16.4.1 Chemical Ionization in Environmental Analysis

CI techniques are used favorably to generate molecular ion species for the unequivocal identification of compounds. Determining the molecular weights of the compounds under investigation is an important step in the analytical process. One of the main advantages of CI is that the degree of fragmentation, and therefore the amount of energy deposited into the analyte, can be controlled by the choice of reagent gas and provides direct information on the molecular weight of the analytes under these soft ionization conditions. This is certainly why CI mass spectrometry has become a powerful analytical technique in various disciplines, including pharmacology, medicinal chemistry, forensic science, petroleum exploration, and environmental analytical chemistry. Moreover, listings of the molecular weights of the majority of drugs, toxic substances, and their related metabolites are now accessible. In addition, CI is characterized by the relative facility with which switching from one reagent gas to another allows one to perform confirmatory experiments to reveal the presence of specific ions, whatever their polarity, by the interchange of the reactant gas, methane for ammonia for example. However, due to the limited extent of fragmentation, CI must generally be coupled to MS/MS procedures to ensure complete and accurate characterization.

Fundamental investigations of the ionization mechanism for CI have been extensive, but novel GC/MS applications are still being developed. The criteria for developing a CI reagent are its availability in a highly pure state, its relative inertness toward many substrate molecules, and, consequently, its ability to give only limited reactive ions confined to the low mass region of the acquired mass spectrum. Among the potential positive ion reagents useful for CI, examples with acetonitrile and pentafluorobenzyl alcohol as CI reagents are reported here (Section 16.4.2).

As stated earlier, the CI process takes place during the reaction period of the CI scan mode of the ion trap. Since the duration of this period is long compared to the short residence time of ions in a classical high-pressure CI ion source, a gain in specificity can be expected when this mode of ionization is used in ion traps. This feature has recently permitted the development of ion attachment mass spectrometry in the ion trap with sodium ion as a reagent ion (Section 16.4.3.2).

#### 16.4.2

#### Examples of Unusual Reagents for Chemical Ionization

Acetonitrile has been reported to be an effective reactant for the positive ion CI of long-chain hydrocarbons, as well as in localizing the unsaturated hydrocarbon double-bond position [21]. More recently, a rapid method has been presented for determining the location of double bonds in polyunsaturated fatty acid methyl esters by ITMS [22]. EI is known to cause double bond migration in fatty acid methyl esters, resulting in ambiguous spectra, and CI with the usual reagent gases does not yield useful fragments. Methods based on derivatization to induce fragmentation from charged or radical sites remote from the double bonds have the disadvantage of requiring an additional chemical modification step prior to analysis. CI-based methods with vinylamine, and vinyl methyl ether as reagent gases are limited to special cases and to determining the locations of a minimum number of double bonds. The acetonitrile mass spectrum under ion trap CI conditions includes major ions at  $m/z$  40 (loss of H) and  $m/z$  54 (identified as the 1-(methyleneimino)-1-ethenylum ion), inducing adduct formation with the fatty acid methyl ester at M+40 and M+54, respectively. The  $[M+54]^+$  adduct ion observed in the CI mass spectrum is a superposition of isomers corresponding to reaction across each double bond and is indicative of the degree of unsaturation. Tandem mass spectrometry conducted on the isolated  $[M+54]^+$  ion results in diagnostic ions that include the hydrocarbon end, and ions that include the methyl ester end. Locations of double bonds have been demonstrated for fatty acid methyl esters with up to six double bonds when considering these ions together [22].

A significant contribution to the measurement of hydroxy carbonyls in air has been recently demonstrated by using pentafluorobenzyl alcohol as a chemical ionization reagent monitoring the intensity of the products  $[M+H]^+$  and  $[M+181]^+$  ions [23]. Hydroxy carbonyls and other carbonyls are first derivatized with (pentafluorobenzyl) hydroxylamine, and then silylated with bis(trimethylsilyl)trifluoroacetamide to improve resolution and sensitivity in the chromatograms. Pentafluorobenzyl alcohol CI-mass spectra are straightforward for the identification of glycolalde-

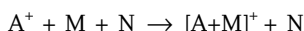
hyde and hydroxyacetone in the presence of coeluting interferences by monitoring both the  $[M+H]^+$  and the  $[M+181]^+$  ion signals, which are severely enhanced compare to pure methane-Cl. The first measurements of hydroxyacetone and 3-hydroxy-2-butanone in ambient air have been reported, and ultratrace concentrations (pptv levels) of methyl vinyl ketone, methacrolein, methylglyoxal, glycolaldehyde, and hydroxyacetone have been measured [23]. Extension of the method to the measurement of water-soluble carbonyls, for which no or little ambient air data exist, is straightforward.

### 16.4.3

#### **Ion Attachment Mass Spectrometry**

##### 16.4.3.1 Principle

Thermal alkali-metal ion association reactions are described by the following simplified expression:



Where A denotes a positively charged alkali metal ion, M is a neutral species, and N acts as a third-body. The binding energy of the molecule M, considered as a Lewis base, to the alkali metal cation  $A^+$  is defined by the enthalpy change for the preceding reaction. Deriving primarily from electrostatic forces, the binding energy of the reagent alkali metal ion  $A^+$  to the molecule M must be high enough to permit a significant number of adducts to be formed at the partial pressure used in the experiments. Cationized molecular adducts are generally stable and, apart from their intrinsic interest as a chemical process, association reactions would therefore be potentially useful for determining the molecular weights of the neutral species M by monitoring the  $m/z$  ion ratio of the  $[A+M]^+$  adduct. Such use of alkali metal cations as reagent species for CI mass spectrometry has been investigated previously [24, 25]. The relative binding energies of a large number of molecules have been measured and correlated with theoretical calculations. These results indicate that the ion binding energies of a wide range of alkali metal ion complexes are high enough to be detectable at low concentrations as long as the attachment process is kinetically efficient. Consequently, the chemical ionization process of alkali metal ion association reactions (ion attachment mass spectrometry, IAMS) offers a unique and interesting potential in analytical chemistry [26]. Currently IAMS is available commercially in a complete form (Anelva Co.).

Alkali metal ions are generated by thermionic emission externally to the ion source and injected into a chamber containing a reagent gas with a trace amount of sample [24]. The ions bind to the sample according to the termolecular process described above. Typically, molecules that have intrinsically high alkali metal ion chemical ionization sensitivities are molecules that are polar or polarizable species. Binding energies are usually in the  $50\text{ kcal mol}^{-1}$  range, or less, for effective binding. Then, it has been demonstrated that trace amounts of alkenes can be detected in the presence of alkanes [24]. More recently, ion attachment mass spectrometry has been developed for continuous measurement of perfluoro compounds (PFCs)

of environmental concern in semiconductor manufacturing [27]. Five greenhouse gases,  $\text{CF}_4$ ,  $\text{CHF}_3$ ,  $\text{C}_2\text{F}_6$ ,  $\text{SF}_6$ , and  $\text{c-C}_4\text{F}_8$ , were studied with the intention of developing improved methods for PFC analysis at the trace level (ppb range). The results demonstrate the feasibility of real-time measurements for PFC trace monitoring by generating only adduct ions from  $\text{Li}^+$  ion attachment process.

#### 16.4.3.2 Sodium Ion Attachment Reactions with GC/ITMS

The first direct demonstration of the applicability of alkali ion attachment reactions using a sodium cation emitter as a novel and sensitive technique of ionization for ion trap mass spectrometry was made with an ion trap mass spectrometer equipped with an external ion source to generate the reagent  $\text{Na}^+$  ions [28]. The combination of alkali metal ion attachment with an ion trap may well represent a noticeable improvement in the selectivity and sensitivity of current GC ion trap technology, and may enlarge the scope of use of this type of mass spectrometer.

Sodium adduct formation has been applied to the detection and characterization of derivatives of explosives, and the detection of phthalate samples. A signal-to-background ratio of ca. 10 : 1 was obtained with a mixture of dimethyl, diethyl, and di-n-octyl phthalates injected into a GC column at the 100 pg level. The major peaks in all of the spectra corresponded to the molecular adducts  $[\text{M}+\text{Na}]^+$ , giving straightforward data on the molecular weights of the samples. For detection of explosives, sodium ion attachment reactions offer the advantages of direct determination of molecular weights with a very low level of fragmentation. This simplifies the interpretation of the mass spectra and offers the possibility of distinguishing between pre-ionization decomposition and ion fragmentation. Two nitramine derivatives, 1,3,5-trinitro-1,3,5-triazacyclohexane (RDX) and 1,3,5,7-tetranitro-1,3,5,7-tetraazacyclooctane (HMX), could be deduced from the  $m/z$  121 adduct observed under solid probe introduction conditions associated with the  $\text{Na}^+$  ion attachment reaction. Analysis of pentaerythrityl tetranitrate (PETN) permits unequivocal identification of decomposition products as well as the molecular adduct.

Sodium ion attachment reactions have been investigated for commercial GC ion trap mass spectrometers [29]. The alkali metal ion method was shown to be particularly suitable for ion traps by simply replacing the electron filament with a sodium emitter, and inverting the gate lens potential to allow the injection of positive ions. Figure 16.5 compares the relative response in the EI and sodium ion attachment modes of ionization under the same chromatographic separation conditions for a mixture of 10 organic compounds bearing different functional groups. The optimized conditions for both cases lead to the conclusion that the sensitivity for the mixture components is satisfactorily large under sodium ion attachment mass spectrometry. With the detection of solely molecular adducts, it is unlikely that any confusion in assignment of the molecular weights of the detected species would result. It appears that the detection may be sensitive to the structure of the analyte in the formation of the molecular adducts since the  $\text{Na}^+$  affinity favors bind-

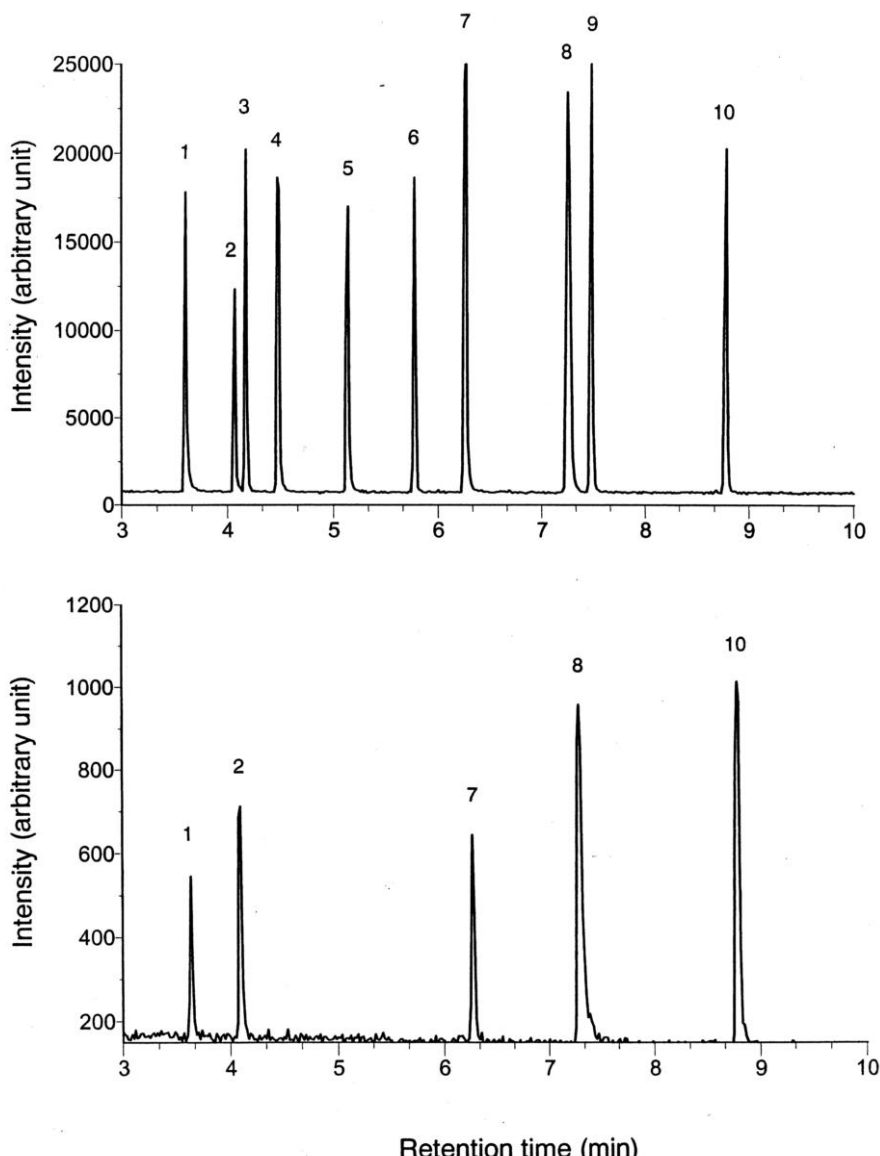


**Fig. 16.5** Reconstructed total ion current (RTIC) chromatograms of a test mixture of 10 compounds, each at a concentration of  $0.1 \text{ g L}^{-1}$  ( $1 \mu\text{L}$  injected; split 1:40). Conditions: (top) EI and (bottom)  $\text{Na}^+$  ionization conditions.

ing to certain compounds under the ion trap conditions as shown by the disappearance of peaks corresponding to 1-decene, *o*-dichlorobenzene, thioanisole, iodoocane and *n*-undecane under the  $\text{Na}^+$  ionization conditions. EI and sodium ion attachment ionization modes in the ion trap gave a similar signal/background ratio for functionalized compounds in the test mixture (Fig. 16.5). Methyl caprate, which was chosen as a model compound to define some of the figures of merit for the technique, provided a detection limit in the  $10^{-4}$  g L<sup>-1</sup> range.

Ion trap mass spectrometers demonstrate complete applicability to these alkali metal ion attachment reactions due to their *in-time* confinement capability, which provides a high efficiency for alkali ion attachment reactions compared to conditions in a classical quadrupole ion source. This method should be of general interest to those needing to solve problems involving organic pollutants, samples diluted in a matrix, pyrolytic products and samples that are of environmental concern, in situations where classical chemical ionization techniques are not always satisfactory due to their structure-dependent responses. One of the main advantages of sodium ion attachment reactions for such analysis is that the ionization conditions are not pressure dependent, unlike conventional CI ionization processes.

## 16.5 Conclusion

It was recently recognized that “the quadrupole ion trap has undergone a renaissance from a novel ion storage device to a conventional mass analyzer used for GC/MS” [7]. Clearly, the coupling of gas chromatography to ion traps has been a driving force for the development of commercial instruments, but recent advances in software capabilities have greatly contributed to the customization of operating procedures for analytical purposes. Consequently, gas chromatography/ion trap mass spectrometry (GC/ITMS) has become increasingly important for both qualitative and quantitative analysis of a wide range of organic compounds, and a large number of applications are being found for ion trap mass spectrometry in analytical chemistry.

The development of ion trap systems, first targeted to compete with GC benchtop quadrupole mass spectrometers, has led to sophisticated high performance instruments that are simple to operate and accessible to a wider range of users. The reasonable cost of current commercial GC/ITMS instruments, with additional CI and MS/MS capabilities, opens up the possibilities for environmental analysis to a broader range of laboratories. New analytical methods appear to be very promising for the future of the ion trap, taking advantage of what are the ion trap’s unique abilities, namely, ion storage and mass selectivity.

**16.6****Appendix: List of Main Manufacturers and Representative Products for GC/ITMS**

- Thermoquest (San Jose, CA; <http://www.thermo.com>),  
Finnigan PolarisQ Benchtop ion trap GC/MS
- Varian Inc. (Palo Alto, CA; <http://www.varianinc.com>),  
Saturn 2000 ion trap GC/MS
- Hitachi Ltd. (Tokyo, Japan; <http://www.hitachi-hitech.com>), 3DQ ion trap GC/  
MS, until recently, Hitachi Ltd. and Teledyne Tech. were developing the 3DQ  
quadrupole ion trap mass spectrometer.

## References

- 1 March, R.E.; Hugues, R.J.; Todd, J.F.J. *Quadrupole Storage Mass Spectrometry*. Wiley Interscience, New York 1989.
- 2 *Practical Aspects of Ion Trap Mass Spectrometry*, eds. March, R.E.; Todd, J.F.J. CRC Press, Boca Raton, FL 1995, Vol. 1–3.
- 3 Todd, J.F.J. *Mass Spectrom. Rev.* 1991, 10, 3.
- 4 Stafford, G.C.; Kelley, P.E.; Syka, J.E.P. et al. *Int. J. Mass Spectrom. Ion Processes* 1984, 60, 85.
- 5 Huston, C.K. *J. Chromatogr.* 1992, 606, 203.
- 6 Brodbelt, J.S.; Louris, J.N.; Cooks, R.G. *Anal. Chem.* 1987, 59, 1278.
- 7 Yates, N.A.; Booth, M.M.; Stephenson, J.L.; Yost, R.A., in *Practical Aspects of Ion Trap Mass Spectrometry*, vol. III, chap. 6, eds. R.E. March and J.F.J. Todd, CRC Press, Boca Raton, FL 1995.
- 8 Louris, J.N.; Amy, J.W.; Ridley, T.Y. et al. *Int. J. Mass Spectrom. Ion Processes* 1989, 88, 97.
- 9 Eichelberger, J.W.; Budde, W.L. *Biomed. Environ. Mass Spectrom.* 1987, 14, 357.
- 10 Eichelberger, J.W.; Bellar, T.A.; Donnelly, J.P.; Budde, W.L. *J. Chromatogr. Sci.* 1990, 28, 460.
- 11 Munch, J.W.; Eichelberger, J.W. *J. Chromatogr. Sci.* 1992, 30, 471.
- 12 Budde, W.L. in *Practical Aspects of Ion Trap Mass Spectrometry*, vol. III, chap. 12, eds. R.E. March and J.F.J. Todd, CRC Press, Boca Raton, FL 1995.
- 13 Reiner, E.J.; Schellenberg, D.H.; Taguchi, V.Y. et al. *Chemosphere* 1990, 10, 1385.
- 14 Plomley, J.B.; Koester, C.J.; March, R.E. *Org. Mass Spectrom.* 1994, 29, 372.
- 15 Plomley, J.B.; March, R.E.; Mercer, R.S. *Anal. Chem.* 1996, 68, 2345.
- 16 March, R.E.; Splendore, M.; Reiner, E.J. et al. *Int. J. Mass Spectrom.* 2000, 197, 283.
- 17 Cairns, T.; Chiu, K.S.; Navarro, D. et al., in *Practical Aspects of Ion Trap Mass Spectrometry*, vol. III, chap. 13, eds. R.E. March and J.F.J. Todd, CRC Press, Boca Raton, FL 1995.
- 18 Plzak, Z.; Polanska, M.; Suchanek, M. *J. Chromatogr. A* 1995, 699, 241.
- 19 Wehmeyer, K.; Knight, P.M.; Parry, R.C. *J. Chromatogr. B* 1996, 676, 53.
- 20 Fitzgerald, R.L.; O'Neal, C.L.; Hart, B.J. et al., *J. Anal. Toxicol.* 1997, 21, 445.
- 21 Monetti, G.; Pieraccini, G.; Favretto, D. et al. *J. Mass Spectrom.* 1998, 33, 1148.
- 22 Van Pelt, C.; Brenna, J.T. *Anal. Chem.* 1999, 71, 1981.
- 23 Spaulding, R.S.; Frazey, P.; Roa, X. et al. *Anal. Chem.* 1999, 71, 3420.
- 24 Hodges, R.V.; Beauchamp, J.L. *Anal. Chem.* 1976, 48, 825.
- 25 Fujii, T.; Ogura, M.; Jimba, H. *Anal. Chem.* 1989, 61, 1026.
- 26 Fujii, T. *Mass Spectrom. Rev.* 2000, 19, 111.
- 27 Fujii, T.; Arulmozhiraja, S.; Nakamura, M.; Shiokawa, Y. *Anal. Chem.* 2001, 73, 2937.
- 28 Faye, T.; Brunot, A.; Sablier, M. et al. *Rapid Commun. Mass Spectrom.* 2000, 14, 1066.
- 29 Sablier, M.; Fujii, T.; Rolando, C. *Proceedings of the 48<sup>th</sup> ASMS Conference on Mass Spectrometry*, Long Beach CA, 2000 June 11–15.

## **Section IX**

### **Application 3: Process Control**

## **Introduction**

*John Green*

The quality of life currently enjoyed by a large proportion of the world's population is ever more dependent upon the multitude of various materials we are able to produce and use. Fabrics, plastics, prepared and preserved foodstuffs and pharmaceuticals exemplify broad categories of products that are used everyday by millions. All these commodities are the result of manufacturing and conversion processes that are controlled for quality, consistency and economic viability.

Processes can usually be categorised as either continuous or batch operations. A continuous process accepts a continuous supply of feedstocks and produces product continuously. A batch process accepts a charge of feedstocks that is converted to product and subsequently removed from the process equipment for storage and sale. Process control is important to both these types of operation.

Process control is commonly included as a part of process engineering and has been dealt with in many engineering textbooks. An introduction to the fundamental concepts can be found in several references [1–4].

In a more general sense process control encompasses those procedures used to ensure that products are manufactured according to a previously agreed specification with a guarantee of purity and a fitness for purpose whilst the process used operates efficiently. Process control in its simplest form can involve inspection of the final product of a process which, if satisfactory, leads to a decision to continue operating the process in a similar manner whilst, if the product is unsatisfactory, the process must be altered to bring the product back to the agreed specification. Operating a process out of control results in waste or at least involves a need for reprocessing, reduces the economic viability of the operation and can have a serious environmental impact.

A schematic illustrating basic process control is presented in Fig. 1. The process is shown as a simple conversion of feedstocks to products. Measurements can be made on either the feedstocks or the products and the results are used by the process control system to modify the processing conditions, if necessary. In cases where the feedstocks are the major source of variation then the measurements are used in a feed forward mode to change the process. Crude oil refining is a case where this type of control is desirable because the feedstock varies with the

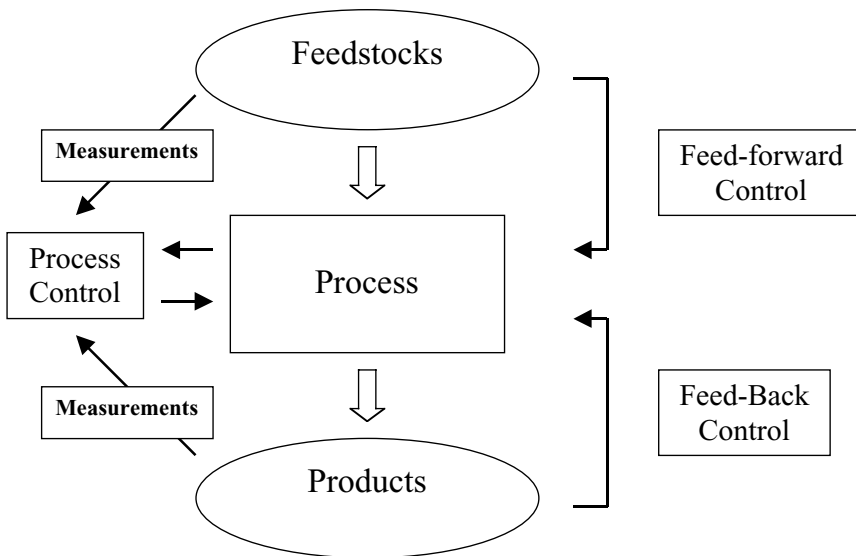


**Fig. 1** A schematic view of process control.

origin of the material. In cases where the feedstock is essentially invariant, for instance air separation plants, and the product is to be produced to stringent specifications then feed back control is often more useful. In other cases a combination of these can be the most effective scheme.

In practice, many processes which are used to produce today's complex materials to exacting specifications are very complex and involve multiple stages each of which needs to be in control and each of which has an impact on the following stages and the final product. The processes are commonly subject to external influences such as a change in the feedstock characteristic (for example the industrial production of hydrogen and the drying of harvested grain with different moisture and protein contents) or changes in the temperature or humidity of the ambient conditions. There are also internal influences, such as changes to the equipment being used, causing changes in flow rates, or the progressive deactivation of a catalyst used in the process. Good process control is designed to cope with these changes and either indicates the process changes that are needed to rectify the problems or initiates the necessary changes automatically.

Process control is achieved by taking account of a selection of inputs, which involve some form of process measurement, and comparing these to a known set of acceptable values. Modifications to the process conditions are made accordingly. Process control can be manual or automatic. Manual operation involves manufacturing personnel taking note of the measurements or alarms activated by measurements and acting accordingly. Automatic operation utilises the measurement signals by feeding them into an electronic or computerised system that compares measured values with a database of values representative of acceptable or optimised operation and then initiates automatic corrective action on the basis of an established model.

The inputs or incoming signals to a process control scheme can be from a variety of measurement sources. In general these can either be measurements of the process conditions or measurements of the process materials involved in the operation. Temperature, pressure and flow are the most common process conditions used. As process control becomes more demanding then chemical and physical measurements of the materials being processed or produced can be used. These include for example colour, density and chemical composition. This is the important link to chemical measurements and the spectroscopic applications, which are the subject of this section of this handbook.

### Concepts of Process Analysis

Process analysis is the general term applied to analytical techniques used to provide information for controlling processes. Such methods can provide a wide range of information relating to the physical and chemical properties of the material being examined and also the properties and characteristics of the products that will result as a consequence of the process conditions being used. This information, when used effectively, can provide a significant input into process control schemes which impact upon the quality, consistency and usefulness of the product as well as the efficiency of the operation.

Process analysis can be achieved in different ways including traditional laboratory methods carried out in a central laboratory, using methods in localised 'at-plant' laboratories or automated on-line methods. The terms at-line and in-line are also used to describe different approaches to the application of the analytical methods. In large manufacturing processes, which can be exemplified by integrated petrochemical complexes or, to a slightly lesser degree, large food manufacturing operations, transporting samples to central laboratories and waiting for results brings with it unacceptable delays. Using techniques located near the process operations and arranged so that relatively non-specialised staff can carry out the tests provides immediate results on-demand that can be acted upon quickly. Even better, if the implementation costs can be justified, is to install equipment directly on the operating process so that measurements are made in real time. Coupling such on-line measurements to appropriate control mechanisms results in tight control of the process to provide product that is consistent and on specification.

Methods of monitoring processes as they proceed changes the out-dated philosophy of quality control as an 'end of pipe' activity to a quality assurance philosophy where a process being continuously monitored and kept within prescribed conditions will be assured of producing acceptable product. The out-dated 'end of pipe' quality control examination could lead to products being discarded, sold at a loss, or recycled for reprocessing. In contrast, continuous process control can identify deviations from acceptable operating conditions before off-specification product is produced and process changes can be made to bring the process back to optimum operating conditions. Even within specification limits process analysis and

control can improve the consistency of a product, which is an advantage to customers with stringent processing criteria.

Data generated from process analysis techniques are commonly displayed on control charts and the term statistical process control (SPC) is often used to describe the use of such data visualisation [5]. As the amount of data available increases, due both to different measurements and greater frequency of measurements, then combinations of different data provide improved methods of monitoring the processes concerned. The procedures and concepts of multivariate SPC incorporating principal component analysis (PCA) and partial least squares (PLS) analysis then become important [6]. The different SPC approaches are all aimed at providing better process control and improved process understanding.

Processes and processing equipment or plant are now commonly used for producing a range of materials including different grades of one product or entirely different materials. Process control and the associated primary measurements have their contributions to make to this type of operational regime. Changing the grade of a material produced can involve a reduction in production rate and the production of unusable material during the period of change. Ensuring that the change can be made as rapidly and efficiently as possible can have important economic consequences. In cases where equipment is used for different products cleaning procedures must be effective to ensure good manufacturing practice, here again the effective application of process analysis can be beneficial.

Continuous processes during normal, in-control operation, operate in a state of equilibrium and fluctuations should be at a minimum, however, there are significant periods of operation where non-normal conditions are experienced. Such conditions include start-up after for example a maintenance shutdown, abnormally high or low production requirements and catalyst regeneration or replenishment operations. It is here that process control using well-designed process analysis techniques can be particularly beneficial by reducing the time that the plant is not operating according to the requirements. With batch processes each period of operation, feed-stock charging, reaction and completion are to some extent different conditions and can need different process control and associated analysis protocols.

Processes for producing chemicals, materials and goods are complex and varied and to ensure the correct product is produced effectively process control procedures are vital but underlying these procedures process analysis techniques, including spectroscopies can be used as an important source of primary data.

### Practical Considerations for Process Analysis

Consideration must be given to the sample for which results are sought, the requirements of the analysis, the available equipment, its capability and suitability and the feasibility of linking to a control system that can bring about the necessary changes to the process.

Samples may be solid, liquid, gaseous or multiphase, at high or low temperatures, under non-ambient pressures, with variable flow rates and as a result of

their composition may be corrosive or abrasive. All these factors affect the feasibility of applying process analysis techniques.

Analytical requirements vary according to the process control that is required. Chemical composition may be needed at percentage levels or trace levels with single components or complete analyses being required. Physical characteristics of the sample may be important as with many polymer-processing operations. The accuracy and precision needed will depend upon the application of the results. The speed of response is also important, for example in some process applications of leak detection of explosive materials analysis is required every few seconds whereas in processes that change slowly a rapid response would be unnecessary as process modifications could not be made in such a short time.

The analytical equipment that is chosen needs to be capable of satisfying the requirements. It often needs to be robust to withstand the chemical environment. Cost is an important factor, which is linked to whether equipment may be multiplexed so as to carry out a number of similar analyses. Operationally, simple, reliable and long-term calibration is important, the capability of automatic fault diagnosis can be an advantage and the benefits of a non-invasive technique are considerable.

If analytical equipment can be identified to do the required task then the links to process control must be considered, for the analytical results to be of value appropriate changes to the process must be possible.

### Spectroscopy and Process Analysis

Spectroscopy is only one of the general methods of analysis used to monitor processes. Chromatography, electrochemical techniques and a broad range of physical measurements are commonly used [7] but are obviously beyond the scope of both this section and indeed this Handbook. The role of spectroscopy in process analysis has recently been reviewed [8].

Process analysis can be carried out in a traditional analytical laboratory with samples being transported from the process of interest to the laboratory. This is still a commonly used procedure but has serious drawbacks, notably the delays that inevitably result. These delays can mean that the process is producing off-specification material for a considerable time before the fact is realised. This is especially important if large volume or high value materials are being produced. An alternative is to locate the laboratory close to the process operations [9] and avoid the serious delays involved in transporting samples and waiting for analytical results. Automating the analysis so that process operators can use the equipment quickly and efficiently helps to reduce delays even further. On-line or in-line analysis where no extraction of sample is required is the preferred procedure although the technology costs involved sometimes dictate that this is not economically viable. In other situations, especially where safety considerations are involved, rapid analyses can be essential and automated on-line analysis with a minimum delay in obtaining the result is the only acceptable procedure.

Using spectroscopic techniques for process control can present special requirements. A laboratory environment being used for process analysis is technically no different from the use of such equipment as described elsewhere in this Handbook. Operational considerations may dictate that the equipment is available at specific times to accept the process samples according to a prescribed schedule but this is an organisational matter for the laboratory and manufacturing management. The use of spectroscopy in on-line and in-line environments is usually very different. Process conditions commonly experienced include chemical vapours, dust and vibration, whilst some equipment may be open to the elements, located in zoned areas and used by operations staff unaccustomed to such equipment. The siting of equipment is therefore important. Siting options include a controlled cabinet, an analyzer house or a designated part of the process area or control room.

The interface between the sample and the spectrometer is vital wherever a spectrometer is sited. The sample can be piped into the spectrometer or, in some cases; the radiation used by the spectrometer can be transmitted to a convenient sample or probe location point using optical fibres or other light-pipe devices. The sample presented to the spectrometer must be representative of the material from which the measurement is required and the interaction between the radiation of the spectrometer and the sample must be suitable for the measurement to be made (sufficient power and suitably clean interface).

Sample lines can be a serious cause of malfunction of process analysis techniques, which will subsequently adversely affect the process control procedures. Long sample lines or those having high pressure drops will cause delays in the sample transport and therefore the analysis will relate to process conditions already passed. Sample lines can become blocked as a result of entrained material or as a result of insufficient heat tracing causing condensation or solidification. Consequently results will either be unavailable or will be erroneous. Practical sampling procedures and sample pretreatments have been briefly summarised and discussed [10].

Consideration needs to be given to the sample interface and the measurement technique used. Some techniques relate to the whole sample whereas others are very much surface measurements. For example, microwave spectroscopy and infrared transmission measurements provide values on the bulk sample whereas X-ray fluorescence and Raman spectroscopy are very much surface techniques, only penetrating the sample to a limited degree.

### **Common Spectroscopies for Process Analysis & Control**

The spectroscopic techniques most commonly used for process analysis involve the use of infrared or UV/visible radiation. Mass spectroscopy has a considerable number of varied applications especially in the area of gas analysis. NMR technology is being increasingly used for a range of applications. Atomic spectroscopies, used extensively from a laboratory base for process control, are finding applications in automatic on-line measurement where the sampling systems can be suitably

adapted. Details of these spectroscopies in process analysis and control and their applications are specifically dealt with in the following parts of this section of the Handbook.

### **Specialised Spectroscopies and Emerging Techniques**

There are a number of spectroscopies that are not commonly used for process analysis but do have specialised applications. Other techniques are emerging as possible methods for the future. Some of these techniques and their applications are discussed briefly below.

#### **Microwave spectroscopy**

Although the most well known use of microwave spectroscopy is in the fundamental studies of the rotational structure of free molecules and as a method of determining dipole moments the technique is finding applications in the area of process analysis. Its use for process samples depends upon the analyte having different permittivity characteristics to that of the sample as a whole and so the technique is admirably suited to the determination of water or moisture in solids and liquids.

Microwave spectroscopy has found applications in the food processing industry as well as in the polymer and chemicals manufacturing industries. Water, fat and protein determinations have been demonstrated together with reported applications for the measurement of polymerisation rates and the water content of organic and mineral acids. Determinations have also been reported of the percentage solids in lime slurry and, in another application, the water, phenol and diphenol oxide content of a reaction mixture [11]. A varied range of solid and liquid samples has been examined including a range of meat and dairy products, pet foods, doughs and coal. The technique is applicable to the bulk properties of a sample and is therefore not restricted to that section of the sample in proximity to the cell windows as is sometimes the case in some optical and X-ray fluorescence spectroscopies. The equipment is suitable for use in the form of a bench-top instrument or as an in-pipe installation.

It has been suggested that developments in microwave spectrometers could provide sensors for particular chemical compounds with high specificity and sensitivity [12]. Indeed microwave spectroscopy has been used to specifically monitor ethylene oxide concentrations in medical sterilisation units [13].

#### **REMPI Spectroscopy**

The use of resonance enhanced multiphoton ionisation (REMPI) spectroscopy linked to time of flight mass spectroscopy has been demonstrated in on-line monitoring of combustion by-products in industrial flue gases [14] and in a research project dedicated to the analysis of coffee roasting processes [15]. REMPI is a highly

selective and sensitive technique and depends upon selective ionisation of target species in a flowing gas stream. In the examples cited this is of course a hyphenated technique.

#### **Ion Mobility Spectrometry**

Ion mobility spectrometry (IMS) is a form of mass analysis and is most commonly associated with military use for the portable detection of nerve gases and the detection of explosives and drugs at international borders and airports. Applications in process analysis are being found in the analysis of gas streams. It is particularly suited to trace analysis (ppb) of easily ionisable species. The sample is drawn over a semi-permeable membrane through which the compounds of interest pass into an ionisation chamber. Typically a nickel 63 source provides a means for ionization, the ions then pass down a drift tube to the detector, small ions arriving before larger ions. Examples of continuous analysis of ammonia, and organic amines are described in application notes provide by Molecular Analytics [16]. Other companies providing IMS equipment have concentrated more on the military and security applications.

#### **Acoustic Emission Spectroscopy and Ultrasound Techniques**

Acoustic emission spectroscopy has been applied to process analysis to detect physical rather than chemical changes. However its use appears less widespread than it maybe deserves. Detection of the movement of particles or bubbles in reactors can, when coupled with process knowledge, provide a means of monitoring the extent of process changes. Applications include the monitoring of granulation, fluidisation, agglomeration, milling and drying procedures. A reported application is in the detection of particle entrainment during a solvent removal process, which shows that the process has reached completion. A primary benefit realised from such a solvent removal application is the rapid turnaround of processing equipment that can be achieved. However a secondary benefit is an improved process, as further processing causes the removed solvent, which is subsequently recycled, to become contaminated with the entraining material. Eventually this results in the solvent being unsuitable for recycling or the product of the primary process becoming impure and out of specification. A number of application notes are available from Process Analysis and Automation [17]. Acoustic techniques have been used to monitor crystallisation processes [18].

Active ultrasound uses a source of sound radiation, which is applied to a process sample, with a detector placed such that modification to the signal can be detected and related to changes in the sample. Signal attenuation, velocity measurements and wavelength selective absorption provide the means of probing the sample. This approach promises to provide both chemical and physical information but as yet has not been used extensively. A number of on-line polymer-related studies have been reported in which polymer flow behaviour, viscosity, blend characterisation, and foaming-process monitoring have been examined [19].

## Inferential Analysis

Inferential analysis [20, 21] is not a spectroscopy but could have a bearing upon the use of all process analysis techniques. It is a term being used to describe measurements that are not made but are inferred from other properties of the process under scrutiny. These methods rely upon process models being available for the process concerned. The value of this approach, quite apart from the fact that no expensive equipment is needed, is that it can give an indication of a measurement when it is impossible to extract a sample without it undergoing change or where inserting a probe is impractical. Inferential methods can also be useful to provide values between the frequency of the installed measurement devices or indeed when the measurement devices are off-line for maintenance purposes. The quality of an intermediate or a product, can in some instances be inferred from the values of temperature, pressure and flow rates in the area of the process under consideration.

## Summary

Process control, achieved in part as a result of good process measurements, can provide a number of operational benefits including:

- Operating cost improvements
- Increased rate of production
- Reduced energy use
- Reduced laboratory costs
- Reduced production of off-specification material
- Less re-working of material
- Less waste production and disposal
- Reduced environmental impact
- Improved health and safety as a result of reduced exposure to chemicals
- Continuous control of product quality
- Improved process understanding

Effective process control needs reliable, robust, often rapid inputs from measurement techniques. Spectroscopy can provide such inputs if the right technique is selected, the sample interface is well designed and the data analysis is carried out effectively.

## References

- 1 Coulson and Richardson's *Chemical Engineering*, Volume 3, eds. J. F. Richardson, D. G. Peacock, Pergamon Press, 1994, Vol. 3, pp. 560–731.
- 2 K. Dutton, S. Thompson, B. Barraclough, *The Art of Control Engineering*, Addison Wesley Longman, London 1997.
- 3 F. G. Shinsky, *Process Control Systems, Application, Design and Tuning*, 3rd Edition, McGraw Hill, New York, 1988.
- 4 Chem. Eng., 1999, 106 (8), 76.
- 5 J. S. Oakland, R. F. Followell, *Statistical Process Control*, 2nd Edition, Heinemann Newnes, 1990.
- 6 M. H. Kaspar, W. H. Ray, *AIChE J.*, 1992, 38, 1593.
- 7 K. J. Clevett, *Process Analyzer Technology*, Wiley, New York 1986.
- 8 *Spectroscopy in Process Analysis*, ed J. Chalmers, Sheffield Academic Press, 2000.
- 9 T. Lynch, *CAST*, 1999, June/July, 4.
- 10 J. R. P. Clarke, *Process Control Quality*, 1992, 4 (1), 1.
- 11 Epsilon Industrial Inc., 2215 Garnd Avenue, Parkway, Austin, Texas 78728; [www.epsilon-gms.com](http://www.epsilon-gms.com)
- 12 H. D. Rudolph, *Microwave Spectroscopy – Instrumentation and Applications*, in *Encyclopedia of Analytical Science*, ed. A. Townshend, Academic Press, New York 1995, Vol. 6, p. 3271.
- 13 Z. Zhu, I. P. Matthews, W. Dickinson, *Rev. Sci. Instrum.*, 1997, 68(7) 2883.
- 14 R. Zimmermann, H. J. Heger, A. Kettrup et al., *Rapid Commun. Mass Spectrom.*, 1997, 11, 1095.
- 15 R. Zimmermann, H. J. Heger, R. Dorfner et al., *SPIE*, 1997, 3108, 10.
- 16 Molecular Analytics, 25 Loveton Circle, PO Box 1123, Sparks, MD 21152-1123; [www.ionpro.com](http://www.ionpro.com)
- 17 Process Analysis & Automation, Fernhill Road, Farnborough, Hampshire, GU14 9RX, UK; [www.paa.co.uk](http://www.paa.co.uk)
- 18 J. G. Bouchard, M. J. Beesley, J. A. Sal-keld, J. A., *Process Control Quality*, 1993, 4(4), 261.
- 19 L. Piche, R. Gendron, A. Hamel et al., *Plastics Eng.*, 1999, October, 39.
- 20 M. Tham, Department of Chemical & Process Engneering, University of Newcastle upon Tyne, UK; <http://lorient.ncl.ac.uk/ming/infer/infer.htm>
- 21 J. V. Kresta, T. E. Marlin, J. F. McGregor, *Comput. Chem. Eng.*, 1994, 18 (7), 597.

## 17

# Optical Spectroscopy

John Green

### 17.1 Introduction

Optical spectroscopy can be defined in terms of the electromagnetic spectrum and includes those regions from the vacuum UV to the mid- or far-IR. The wavelengths associated with the different spectroscopies are shown in Fig. 17.1 together with an expanded view of the optical spectroscopy region including the different wavelength units commonly used.

The commonest form of optical spectroscopy measurement involves simple absorption governed by the well-known Beer–Lambert law. However, reflection, light scattering, fluorescence and chemiluminescence methods are also employed in applications relating to process control.

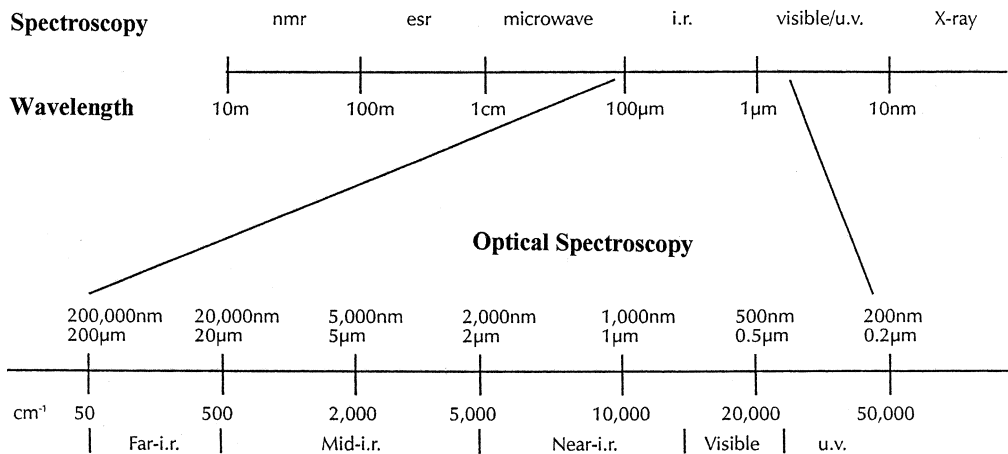


**Fig. 17.1** The electromagnetic spectrum showing the wavelength units commonly associated with the different spectroscopies used in chemical analysis. The wavelength range relat-

ing to the optical spectroscopies is expanded in the diagram. Adapted from a diagram supplied by Clairet Scientific [1].

The interaction of radiation of the UV, visible and IR regions of the electromagnetic spectrum with molecules causes different perturbations to occur in the molecules concerned. UV and visible light generally cause electronic transitions whilst interaction with IR radiation results in vibration modes being excited. Simple absorption measurements involve the differential measurement of the radiation on passing through the sample. Reflection measurements use the same general principle but the detector is positioned to measure reflected radiation. Scattering of radiation results from some interactions and the resulting shift in radiation frequency is a measure of the species present in the sample. Raman spectroscopy makes use of this phenomenon. Fluorescence measurements monitor the radiation emitted from a species within the sample that has previously been excited by the radiation source. Chemiluminescence is the measurement of emitted light from a species, usually as a result of the interaction with a second chemical. The chemical interaction produces a product in an electronically excited state that, on relaxation, emits chemiluminescence radiation.

Instruments vary widely in their design depending upon the purpose for which they are built. Common features include a source of radiation, a means of bringing the radiation and the sample of interest together in a cell or probe, and a detector. In applications to process measurement perhaps the most distinctive feature is the sample interface. The source of radiation used and the detectors are similar and often identical to laboratory-based instrumentation. Almost all of today's instruments include data acquisition and control electronics together with a user interface in a computerized form. To obtain the optimum performance from analytical and control systems, links to distributed control systems for feed-back and feed-forward control are vital.

Optical spectroscopies are appropriate for many process analysis applications because they can provide a rapid analysis of process stream composition in an industrially robust form requiring little regular maintenance. On-line implementation means that extracting manual samples is avoided and results obtained using computerized data handling methods can be linked to automatic control schemes. Recently a review of spectroscopy in process analysis has been published which contains descriptions and describes applications of optical spectroscopies [2].

The optical spectroscopies having established or potential process analysis applications described in this section include:

- Mid-infrared
- Non-dispersive infrared analysers
- Near-infrared
- Ultraviolet/visible
- Raman spectroscopy
- Fluorescence techniques
- Chemiluminescence
- Laser techniques
- Optical sensors

The emphasis will be on the applications of these techniques rather than a detailed description of the techniques themselves that are covered in other sections of the Handbook.

## 17.2 Mid-infrared

By far the most common use of mid-infrared radiation for process analysis is in the non-dispersive infrared analysers that are discussed below. The widespread use of FTIR spectrometers in the mid-IR has yet to be fully realized in process analytical applications. The requirements for the optical components and the wavelength stability of the instruments available have, until recently, detracted from the use of this region of the spectrum in on-line process analysis. Optical fibers that provide such a benefit to the applications of NIR (see below) are not available for the mid-IR in robust forms or forms that are capable of transmitting over more than a few tens of metres. Improvements and developments to sample cells, particularly designs of attenuated total reflectance (ATR) cells, for use with mid-IR are being made and will influence the application of the technique. An impressive list of applications including both FTIR and the NDIR approaches has been compiled [2, 3].

## 17.3 Non-dispersive Infrared Analysers

In terms of the number of optical spectroscopic instruments used in process analysis non-dispersive infrared is perhaps the most common and has an established record of success. The mid-infrared section of the spectrum provides a region rich in chemical information having absorptions specific to individual chemical species where interferences can be avoided.

These NDIR instruments are mainly used for gas samples although multiple reflection cells are available in a variety of materials that are applicable for the analysis of liquids. Filters are chosen according to the analyte to be determined and the other components of the matrix. Carbon dioxide, carbon monoxide, ethylene, nitrogen oxides and sulfur dioxide are typical analytes.

There is not an extensive recent scientific literature devoted to these methods but many of the instrument suppliers provide technical details and specifications in their literature and websites [4, 5].

A variety of designs are commercially available and include combinations of single and dual beam and single and multiple wavelength.

The instruments, see Fig. 17.2, comprise a sample cell through which the radiation is passed together with a reference cell to compensate for radiation source drift and output. Contamination of the cell walls can be compensated for using selected dual beam instruments in which one wavelength is used for the measurement and a second wavelength, not absorbed by the sample is a measure of contamination.

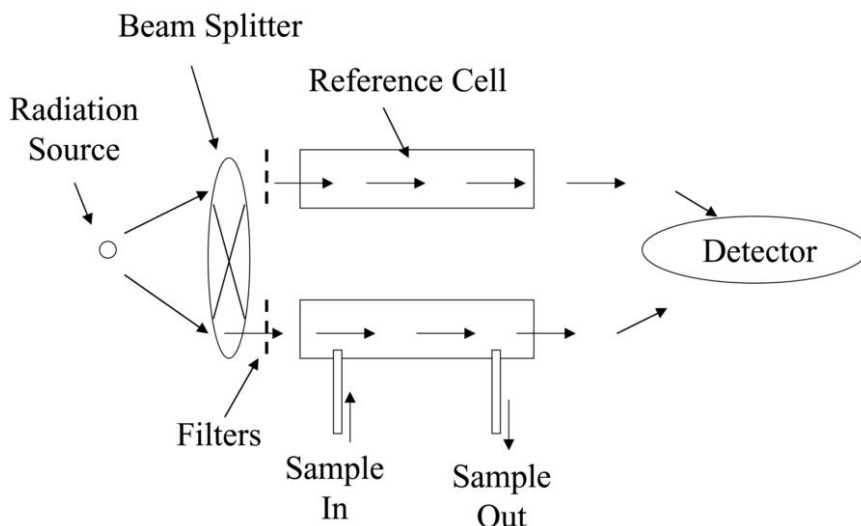


**Fig. 17.2** Typical arrangement of components of a dual beam NDIR process analyser.

Narrow bandpass filters can improve the selectivity of such analysers and can be a means of using the instruments for multiple components. Using a filter chamber filled with an interfering sample component can increase the utility of such instruments.

#### 17.4 Near-infrared Spectroscopy

Whilst infrared spectroscopies all involve vibrational mode excitation of molecules different regions of the infrared interact in different ways with the species present. Mid-infrared cause fundamental vibrations to occur whereas near-infrared results in the excitation of overtone and combination modes of vibration. These modes are so-called forbidden transitions and they result in the weak absorptions that give NIR spectroscopy some of its unique properties.

Although near-infrared radiation was discovered by Herschel in 1800, NIR spectroscopy has only recently become an established technique for process analysis [6, 7]. The increasing success and widespread application of NIR spectroscopy in this area is a result of several advantageous features and technical developments.

Cell path lengths need to be longer for NIR than for mid-IR or UV/visible spectroscopy because the absorptions are weaker. This has two advantages, firstly the process stream often contains particulates that can block narrower cells and secondly the pressure drops of longer pathlength cells are considerably reduced.

NIR radiation can be transmitted down readily available, relatively cheap optical fibers thus allowing spectrometers to be located remotely from the process streams they are monitoring, away from potentially hazardous areas. Optical fibers also provide a convenient means of multiplexing a single spectrometer to several streams, thus reducing the overall cost of the analyses. Optical fibers, optical switching and sample probes have been crucial to the development of NIR spectroscopy for process analytical applications [8, 9].

The improved use and availability of chemometrics allows the overlapping spectra of multicomponent mixtures that are characteristic of NIR absorptions to be analysed successfully and the components quantified. A series of calibration samples of known composition are analysed to establish a calibration model, which is subsequently used to determine the composition of unknown samples. The same approach can be used to correlate NIR spectra with non-compositional properties of samples so the technique is regularly used to determine and estimate operational and quality properties of process streams, for example octane numbers, distillation points and viscosity.

As a consequence of the above factors NIR spectroscopy is now applied to a wide range of process applications in the oil refining, petrochemical, polymer, pharmaceutical, food, environmental and agricultural industries.

Instrumentation for NIR process analysis can be of several forms. Perhaps most simply, but less commonly, fixed filter photometers may be used to pass several chosen wavelengths of light through a sample extracted from a process stream. Interference filters located on a rotating disc allow light of certain frequencies to pass through the sample. The absorption measurements achieved allow sample composition and properties to be estimated as a result of previous calibrations. More commonly, scanning spectrometers, Fourier transform, photodiode array and spectrometers utilizing an acousto-optic tunable filter are used, allowing a continuous spectrum of a chosen sample to be obtained for subsequent analysis using chemometrics and previously determined calibration routines.

NIR radiation, at least those wavelengths suitable for probing the overtone bands, is not absorbed by silica optical fibers and so the spectrometer can be remotely linked to the sample. In hazardous areas such as many petrochemical applications this allows the spectrometer to be located in a safe area without having to transport the sample from the chemical plant. Furthermore it is possible to switch the NIR radiation between fibers so that one source can be used sequentially to excite and analyse several sample points. Both these advantages, resulting from the transparency of silica to NIR radiation can reduce the cost of such applications considerably.

Various probes are available for introducing the radiation to the sample. Transmission probes can be either of an insertion or flow-through type. Reflectance probes utilise a reflective surface to return the radiation to the detector. Internal reflectance probes employ attenuated total reflectance at a sample surface to obtain an absorption value.

A typical arrangement is shown in Fig. 17.3 illustrating a single spectrometer multiplexed to three process stream transmission cells by optical fibers. Spectral

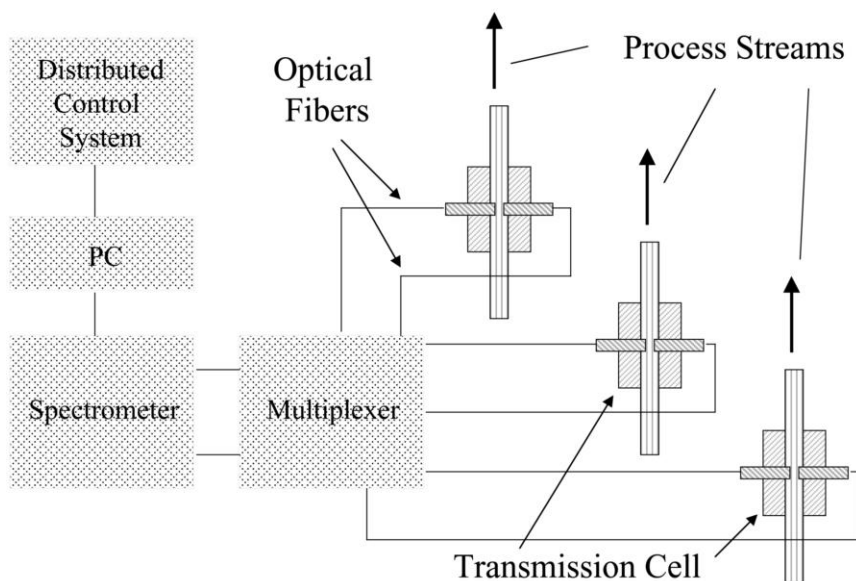


**Fig. 17.3** Schematic of typical multiplexed NIR process analysis arrangement showing spectrometer, multiplexer, optical fibers and trans-

mission cells together with the connections to the PC and distributed control system.

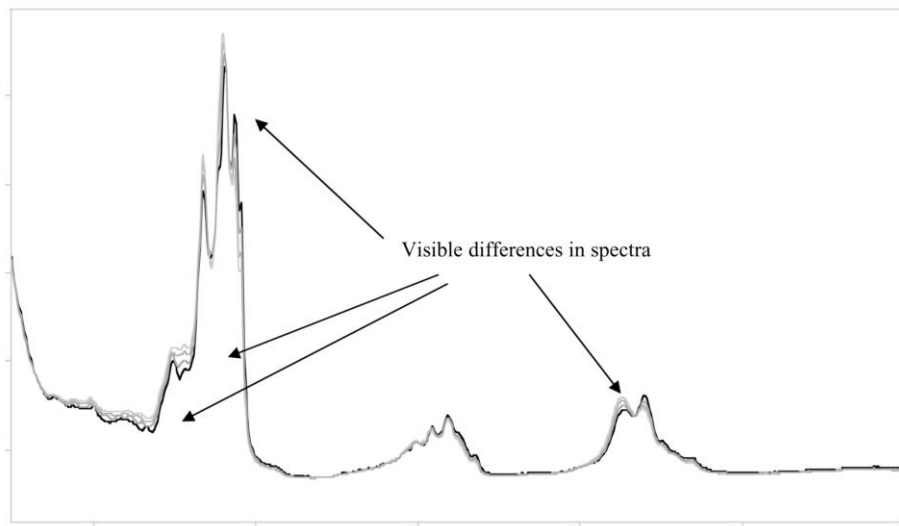


**Fig. 17.4** Superimposed NIR spectra of pentane, hexane, heptane and octane.

data are then analysed by the computer and transmitted to the distributed control system.

Because NIR absorptions are typically broad, individual components of mixtures overlap very considerably. This is illustrated in Fig. 17.4 that shows the superimposed spectra of pentane, hexane, heptane and octane. In order to obtain quantitative information from such spectra prior calibration using PLS calibration routines is required. When the individual components have significant differences in their spectra calibration is not difficult and several samples prepared to cover the expected range of samples concentrations will serve to provide a calibration. In cases where the sample to be analysed contains similar components (e.g. hydrocarbons) then more samples will be required to build an appropriate calibration. Transferring calibrations from one instrument to another is possible, sometimes without any mathematical transformation routine. This is especially true if the spectrometers concerned are of the same design and manufacture.

Various probes are available for introducing the radiation to the sample. Transmission probes can be either of an insertion or flow-through type. Reflectance probes utilise a reflective surface to return the radiation to the detector. Internal reflectance probes employ attenuated total reflectance at a sample surface to obtain an absorption value.

The applications of NIR spectroscopy to process analysis and control are far too numerous to comprehensively cover in a text of this type. A regular review of literature in this area is given in NIR News [10]. Examples in Tab. 17.1 illustrate the breadth of NIR applications to process analysis. Table 17.2 summarises the use of NIR in process analysis.

**Table 17.1** Examples of the application of NIR spectroscopy to on-line process analysis

<b>Industrial Sector</b>	<b>Example Reference from Recent Literature</b>
Petrochemicals	Feed-forward control of a steam cracker for production of ethylene and propylene 11
	Fast on-line analysis of process alkane gas mixtures by NIR spectroscopy 12
Pharmaceuticals	On-line measurement of moisture and particle size in the fluidized-bed processing with NIR spectroscopy 13
	Automated system for the on-line monitoring of powder blending processes using NIR spectroscopy 14
Polymers	On-line NIR sensing of CO <sub>2</sub> concentration for polymer extrusion foaming processes 15
Environment	
Food	In-line measurement of tempered cocoa butter and chocolate by means of NIR spectroscopy 16
Agriculture	On-line cane analysis by NIR spectroscopy 17

**Table 17.2** Near-IR spectroscopy for process analysis

Molecular parameter used in measurement:	Interaction with sample:
Overtone and combination bands of molecular vibrations	Liquids, transmission depth Solids, surface reflectance correlation to bulk property
<b>Typical information sought:</b>	Gases, transmission path length
Quantitative information on sample components	<b>Limits of determination:</b>
<b>Measurement environment:</b>	Absorbing materials, percentages to, at very best, 10 ppm levels
Liquids, gases and solids can be investigated	<b>Time needed for analysis:</b>
<b>Equipment:</b>	Calibration, hours/days depending on sample availability and optical differences in sample components Sample preparation, not generally applicable to on-line analysis. Measurement, seconds/minutes Evaluation, seconds using predetermined calibration routines.
Near-IR spectrometer Sample cells and probes Optical fiber connections (optional) Fiber multiplexer	<b>Cost:</b> Large on-line installation: 250–500 K GBP Laboratory spectrometer: 30–50 K GBP
<b>Type of laboratory:</b>	<b>Sample requirement:</b>
Optimal use as an on-line technique. Can be used in QC/QA laboratory after initial development work	Liquids, mm/cm pathlength Gases, adequate pathlength depending on pressure, e.g. 10 cm Solids, surface exposure to radiation
<b>Skill needed:</b>	Specialist to arrange/develop analysis Competent technical skill to operate.
<b>Techniques yielding similar information:</b>	Optical spectroscopies

## 17.5 Ultraviolet/Visible Spectroscopy

UV and visible photometers are commonly used for a range of process stream components. Hydrogen sulfide and sulfur dioxide are common examples. The approach is similar to the use of NDIR measurements and several manufacturers supply equipment based on this principle [4, 5]. The source of radiation is split into two beams (sample and reference) and passed alternately through filters. The ‘sample’ filter allows light to pass that is absorbed by the analyte of interest the ‘reference’ filter provides a beam that is not absorbed by the analyte. The

ratio of the absorptions is a measure of the analyte concentration. The choice of filters is crucial if potential interferences are to be avoided. Equipment design allows such analyzers to be used at elevated temperatures and pressures and depending upon the analyte concerned ppm values are achieved.

Alternatively the whole UV/Visible spectrum may be recorded and by using appropriate calibration and chemometric techniques it is often possible to determine severely overlapping peaks.

In a similar way to NIR, UV/Visible can be used in absorption and reflection modes. Spectra that are due to electronic transitions are generally broad, as in the NIR, because several vibrational levels will be populated by the primary electronic transition.

The applications of UV/Visible spectroscopy depend upon the analyte of interest having absorptions in the relevant region of the spectrum. For organic compounds aromatic unsaturation provides an excellent absorption chromophore. Thus UV spectroscopy has been used to determine antioxidant levels in polymers [18] during the process of extrusion, the aromatic contents of petroleum [19], the purity of organic products, effluent control of fluorine in the nuclear processing industry [4], determination of methylhydroquinone inhibitor in the storage of acrylonitrile [4], aromatics in process water to minimize environmental impact and as a means of assessing the chemical oxygen demand.

Colour is an important quality control property in many industries including the water and petrochemical industries, each uses visible spectrometry methods to assess quality according to comparisons with different standards. ASTM and Saybolt colour measurements are reported using process UV photometers [4].

UV/Visible spectroscopy is also used as the detection means for a number of process analyses following wet-chemical sample treatment with a selected reagent. Systems are available for the analysis of ammonium, nitrate, nitrite and phosphate in a range of aqueous process streams following appropriate clean-up and reagent colour development [20].

## 17.6

### Raman Spectroscopy

The Raman effect was first predicted and then demonstrated early in the 20th century. Until recently it has been a specialist tool with niche applications very much confined to laboratory environments. Recent developments and improvements in laser light sources, detector technology, optical fibers and optical filters have led to an increase in its use. This is now having its impact upon process analysis as robust equipment becomes available and the potential advantages of the technique become widely appreciated.

Raman spectroscopy is a scattering technique in that it utilizes the scattered radiation when light impinges on a sample. Most incident light is scattered elastically, having the same wavelength as the original light (Raleigh scattering) but a very small proportion is scattered inelastically having a frequency shifted from

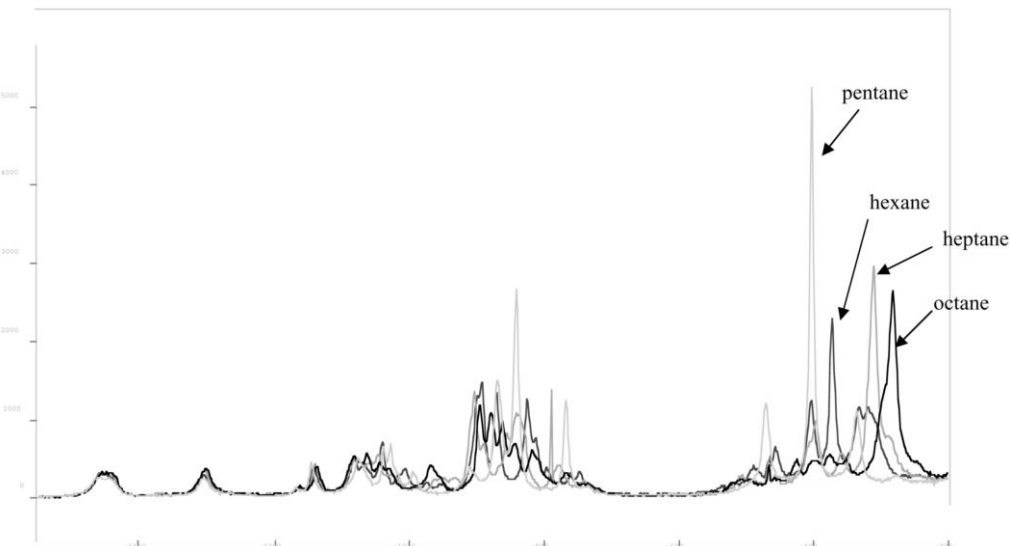


Fig. 17.5 Superimposed Raman spectra of pentane, hexane, heptane and octane

that of the original frequency. The shift is caused by interaction with the sample molecules and relates directly to their molecular vibrations. Raman spectroscopy gives information akin to and complementary to mid-infrared spectroscopy.

Raman is particularly sensitive to unsaturation in symmetrical environments and is therefore an appropriate method for many aromatic species. Generally it is the sensitivity to large changes in polarizability that provides strong Raman signals. Infrared in contrast responds more sensitively to vibrations with large changes in dipole moments. With simple molecules Raman and IR are completely complementary, with for example oxygen, nitrogen and hydrogen Raman gives a signal whilst for IR these molecules are inactive. However the spectral characteristics of Raman resemble mid-IR in that sharp features are dominant in contrast to the NIR where bands are broad, diffuse and largely overlapping for different chemicals.

Raman spectroscopy has a number of benefits for process analysis applications. For appropriate samples Raman spectra are rich in information content. Figure 17.5 shows the superimposed Raman spectra of pentane, hexane, heptane and octane which can be compared with the corresponding NIR spectra in Fig. 17.4. The spectra and resultant information are similar to those obtained from mid-IR.

The wavelength of the incident exciting radiation can however be in the NIR, visible or UV regions of the spectra thus making the use of optical fibers possible. Optical fibers bring their own advantages including multiplexing capabilities and remote location of spectrometer and sample points. Options for the sample interface include a window, or site glass, into the process providing an essentially non-invasive method or an insertion probe incorporating a ruggedised bundle of fibers. Both the exciting radiation and the scattered radiation can enter and exit the sam-

ple through the same window and use the same fiber optic cable. In practice the arrangements may not be quite as simple if only because of the precautions that need to be taken as a result of using laser light in operational areas [21, 22]. Using either window or probe the sample interface is therefore a flow-past device, as compared to the flow through devices common with absorption and transmission measurements. This can be very important for viscous polymers or liquids and for multiphase streams that may otherwise block the flow path.

The choice of Raman instrumentation for process analysis is dependent upon the particular application. Laser light sources of different wavelengths: 532 nm, 633 nm 785 nm and 1064 nm being commonly used with 785 nm being perhaps the most common. The light source chosen will depend upon the sample composition, the sensitivity needed, the existence of potential fluorescing materials and the availability of a suitable detector. Most spectrometers used for process applications are dispersive with charge coupled device (CCD) detectors although in some applications where fluorescence presents problems the use of Fourier transform (FT) instruments is advantageous. Depending upon the probes used, optical filtering may be required. With the fiber bundle probes optical filtering is not used and silica artifacts are minimized by the fiber end geometries. With the site glass interfaces optical filtering is incorporated into the optics to remove the Raman signal originating from the silica and also to remove the Raleigh scattered light, otherwise the Raman signals from the sample would be obscured. Holographic filters have become the commonly used choice in process applications. Whilst CCD detectors are most common the use of charge induction device (CID) detectors is reported to offer some advantages [23]. Array detectors offer an alternative means of multiplexing the system by using different locations on the CCD chip to provide the signal from different sample points.

A schematic diagram showing the main components of a typical process analysis arrangement for Raman spectroscopy is shown in Fig. 17.6.

Fluorescence is commonly regarded as a major problem in the use of Raman spectroscopy and indeed fluorescence of species in the samples of interest can mask the Raman signal of the analyte molecules. However it is often possible to choose a laser wavelength that avoids the problem or to use techniques such as shifted excitation Raman difference spectroscopy [24] or subtracted shifted Raman spectroscopy [25].

Quantification of Raman spectra requires the use of internal standardization and this can sometimes be achieved using an essentially invariant feature of the sample. For example in the analysis of styrene in a polymerization reaction the styrene phenyl peak was used [26].

Applications of Raman for process analysis have been reported in the open literature and in the patent literature which is clearly a sign that some of the applications are regarded as commercially sensitive.

Distillation column monitoring was one of the first reports of using on-line Raman spectroscopy in real time for process analysis. This application used FT Raman coupled to a remote sample cell with optical fibers [27] to determine the 'bottoms' product of a solvent recovery column. The system was linked to a control

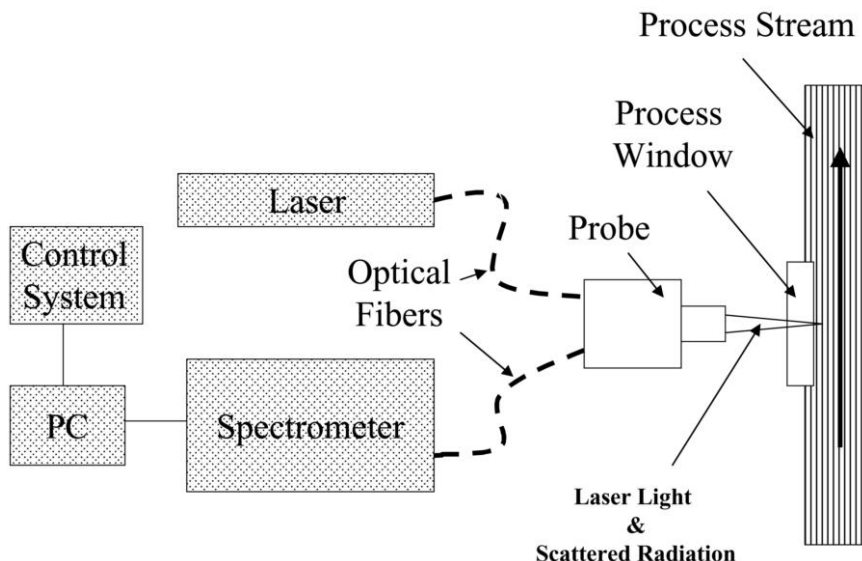


**Fig. 17.6** Schematic diagram of a typical arrangement using Raman spectroscopy for process analysis.

strategy using statistical process control with defined upper and lower action limits.

The monitoring of the calcination process in the production of the rutile-structured titanium dioxide from the anatase structure is recorded as a notable success [28]. A fiber optic probe appropriately positioned in the calcination kiln monitors the composition of the powder undergoing processing. The Raman bands of the two forms of titanium dioxide are quite distinct and as a result the operating conditions of the kiln (fuel and air-flows) can be adjusted to give optimum production.

The production of phosphorus trichloride from phosphorus and chlorine is an important step in the manufacture of a number of agrochemical products. Raman spectroscopy has been used to monitor the reaction and control the raw material feed rates. This maximises production of phosphorus trichloride, minimizes the formation of phosphorus pentachloride and ensures safe operation when plant shut-down periods are needed. Remote analysis is achieved using optical fibers to provide a safer operation and a more rapid analysis than was previously possible [29, 30].

Hydrocarbon streams have also been investigated and Raman-using systems have been patented. The monitoring of emulsion polymerizations by Raman spectroscopy is also proposed. Pharmaceutical process applications of Raman spectroscopy include the monitoring of the active ingredient in a product without sample preparation. The identification of gemstones and the determination of the synthetic/natural origins are well known.

Gas analysis can be achieved using Raman spectroscopy and is of particular value when the gases and vapours concerned are infrared inactive. In a pharmaceutical application oxygen can be detected in the headspace of sealed vials [31]. Anaesthetic compounds have been determined using the laser cavity as a cell [32]. A trace hydrogen sensor using Raman scattering has been reported [33]. Gas–liquid equilibria for a cyclohexane–toluene mixture have been investigated using sequential Raman measurements of the gas and liquid phases [34].

A variety of commercial polymerisation reactions have been followed using on-line Raman spectroscopy in which the progressive disappearance of the unsaturation provides a measurement of the extent of reaction. Emulsion co-polymerisation of methyl methacrylate, butyl acrylate and styrene has been followed in this way [28].

A number of model *in situ* and on-site applications of low resolution, and therefore low cost, Raman spectroscopy have been reported including the quantitative monitoring of synthetic rubber and polystyrene emulsion polymerisations, detection of illicit drugs and explosives and detection of cyanide in wastewater using a surface enhanced Raman system [26].

It has been noted elsewhere that Raman and infrared techniques provide complementary information and therefore it is not surprising that these different approaches are commonly considered for the same application. In some cases it has been concluded that either Raman or infrared techniques can be used to obtain the information required. Comparisons of the techniques for aromatic hydrocarbon determinations have been reported from laboratory studies [35, 36].

Developments in SERS and SERRS have yet to make an impact upon process analysis but some potential means of using these enhanced sensitivity methods have been proposed.

Table 17.3 summarizes the use of Raman in process analysis.

## 17.7 Laser Diode Techniques

Laser diodes are providing analytical capabilities in the area of process analysis, particularly for the analysis of gases. A range of diodes is available covering the NIR wavelength range of 0.6 to 2  $\mu\text{m}$ , suitable for detecting overtone and combination bands. Individual diodes have very narrow wavelength outputs and can only be tuned over a narrow range of several nm. The high spectral resolution of diode laser sources provides the specificity of the technique as the radiation is tuned selectively to correspond to the absorption features of the analyte molecule. Oxygen, carbon monoxide, hydrogen chloride, hydrogen fluoride and ammonia are amongst the gases that can be analysed using this approach. The monitoring of ammonia in stack gas has also been achieved using laser diode techniques with a reported detection limit of 2 ppm at 100 Torr with a 1 m path length [37]. Commercial equipment is available for these applications [38]. Laser diode methods for monitoring atmospheric gases have been reviewed [39]. In a later paper this was extended to on-line process monitoring [40].

**Table 17.3** Raman spectroscopy for process analysis

Molecular parameter used in measurement:	Interaction with sample:
Molecular bond vibrations from scattered radiation	Laser radiation focused within sample meaning different depths can be probed for appropriate samples
<b>Typical information sought:</b>	Information obtained from $\mu\text{m}$ depths of field
Quantitative information on sample components. Supplementary molecular structural information available if needed.	<b>Limits of determination:</b> Raman active materials, percentages to ppm levels. Lower detection levels with surface enhanced methods but not generally used for process analysis.
<b>Measurement environment:</b>	<b>Time needed for analysis:</b> Calibration, depends on analyte and availability of distinct Raman absorption differences in sample components Sample preparation, not generally applicable to on-line analysis. Measurement, seconds/minutes Evaluation, seconds using predetermined calibration routines.
Liquids, gases and solids can be investigated	
<b>Equipment:</b>	
Laser source Raman spectrometer Sample probes Raleigh scattering filters Optical fiber connections (optional) Fiber multiplexer (optional)	
<b>Type of laboratory:</b>	<b>Cost:</b> Large on-line installation: 250–500 K GBP Laboratory spectrometer: 50–80 K GBP Lower cost spectrometers becoming available
Optimal use for process analysis as an on-line technique. Can be used in QC/QA/research laboratory	
<b>Skill needed:</b>	<b>Sample requirement:</b> Access to sample through non-contaminated optically transparent window. Use of probe incorporating optical fibers.
Specialist to arrange/develop analysis Competent technical skill to operate.	
<b>Techniques yielding similar information:</b>	
Other optical spectroscopies Raman is a complementary technique to mid-IR	

The application of NIR laser diode spectroscopy to the on-line analysis of atmospheric pressure chemical vapour decomposition has been reported. In the process of depositing a thin layer of tin on a glass surface the monitoring of methane in the presence of oxygen, water and dichloromethyl tin dichloride in the reactor is important. Laser diode spectroscopy has been used at high sensitivity (detection limit of 0.01 %) and at high frequency (5 Hz) for this purpose [40].

The methods are robust withstanding temperatures of several hundred degrees and elevated pressures [38].

## 17.8 Fluorescence

Fluorescence spectroscopy has similar applications to UV/Visible spectroscopy as it originates from radiation emission from an excited electronic state of the species to be analysed. The most common application in process terms is the determination of hydrocarbons in water. A range of hydrocarbons including fuels, oils, aromatic chemicals and PAHs [41] has been determined in industrial, process and potable waters. An on-site laser probe for the detection of petroleum products in water and soil has been described although it is not known whether such systems are in regular use for this application [42]. Although not the most common method for determining sulfur dioxide commercial equipment has been available based upon fluorescence methods. A reported specialized use of fluorescence in process control involved investigations of the residence time of polymeric materials in extruders in which a fluorescence additive at a low concentration was traced as it passed through the extruder entrained within the polymer [43]. There are also considerable prospects for the use of on-line fluorescence measurements linked to control in the food industry and an application to sugar samples has been described [44].

## 17.9 Chemiluminescence

Chemiluminescence principles are used in commercial analyzers for the determination of nitric oxide for process control purposes [45]. The nitric oxide is reacted with oxygen to produce nitrogen dioxide in an electronically excited state; this then decays with the emission of light. Detection of the emitted light with a photomultiplier tube provides a measure of the original concentration of the nitric oxide. By suitably treating process samples containing both nitrogen dioxide and nitric oxide both species can be determined. In as much as optical means are used to detect the chemiluminescence this is another use of optical spectroscopy in process analysis.

### 17.10 Optical Sensors

Sensors based upon optical spectroscopy principles have been developed for the process measurement of pH and dissolved oxygen as well as the physical characteristics of turbidity. The pH and oxygen sensors rely upon sol-gel immobilized reagents that respond to changes in the process stream in which they are immersed. Evanescent wave absorption is used to detect pH related colour changes and fluorescent quenching of an oxygen sensitive ruthenium compound provides a means of detecting dissolved oxygen. The determination of hydrocarbons in water has been reported using evanescent wave absorption into a hydrophobic coating on an optical fiber that serves to concentrate the analyte [46, 47]. Commercialisation of such devices is still in its infancy but a colour and turbidity monitor is available from Siemens Environmental Systems [48].

### 17.11 Cavity Ringdown Spectroscopy

This technique has yet to find an established place in process analysis although the prospects look interesting. The fundamentals of the technique have been described [49] and the use for gas analysis discussed by several authors [50, 51]. Furthermore the development to applications involving condensed systems using a form of evanescent wave has been described [52].

The story of the application of optical spectroscopy to process analysis is not complete, there are developments and improvements being made such that, in the future, chapters will be added as the capabilities are extended to enable us to gain a better appreciation of our manufacturing processes.

## References

In the area of process analysis useful information is often contained within the literature and on the websites of commercial companies supplying equipment. Consequently, the references below contain some such details as examples of the equipment and information available. In this respect the details are not intended to be comprehensive. The inclusion or otherwise of specific companies does not imply endorsement or otherwise of the products described in the websites.

- 1 Clairet Scientific, 17 Scirocco Close, Moulton Park Industrial Estate, Northampton, NN3 6AP. [www.clairet.co.uk](http://www.clairet.co.uk)
- 2 *Spectroscopy in Process Analysis*, ed. Chalmers, J. M., Sheffield Academic Press, 2000.
- 3 Coates, J. P., Shelley, P. H., in *Encyclopedia of Analytical Chemistry*, ed. Meyers, R. A., Wiley, New York 2000, p.8217.
- 4 Teledyne Analytical Instruments, 16830, Chestnut Street, City of Industry, California 91748, USA. [www.teledyne-ai.com](http://www.teledyne-ai.com)
- 5 Servomex, Servomex Group Ltd, Jarvis Brook, Crowborough, East Sussex, UK. [www.servomex.co.uk](http://www.servomex.co.uk)
- 6 Goldman, D. S., in *Encyclopedia of Analytical Chemistry*, ed. Meyers, R. A., Wiley, New York 2000, Vol. 9, p.8256.
- 7 McClure, W. F., *Anal. Chem.*, 66(1), 1994, 43A.
- 8 Workman, J., *NIR News*, 6(4), 1995, 8.
- 9 Workman, J., *NIR News*, 6(6), 1995, 7.
- 10 [www.nirpublications.com](http://www.nirpublications.com)
- 11 Ganorieau, J. P., Riberi, E., Loublier, M. et al., *Entrophie*, 34 (210), 1998, 23.
- 12 Boelens, H. F. M., Kok, W. T., De Noord, O. et al., *Appl. Spectrosc.*, 54(3), 2000, 406.
- 13 Goebel, S. G., Steffens K-J., *Pharm. Ind.*, 60(10), 1998, 889.
- 14 Sekulic, S. S., Wakeman, J., Doherty, P. et al., *J. Pharm. Biomed. Anal.*, 17(8), 1998, 1285.
- 15 Nagata, T., Ohshima, M., *Polym. Eng. Sci.*, 40(8), 2000, 1843.
- 16 Bolliger, S., Zeng, Y., Windhab, E. J., *J. Am. Oil Chem. Soc.*, 76(6), 1999, 659.
- 17 Staunton, S. P., Lethbridge, P. J., Grimley et al., *Proceedings of the 21st Conference of the Australian Society of Sugar Cane Technology*, 1999, p. 20.
- 18 Herman, H., Hope, P., *Polymer Process Engineering* 97, ed. Coates, P. D., Institute of Materials, London 1997.
- 19 NovaChem BV van Rensselaerweg 4, 6956 AV Spankeren/Dieren, The Netherlands. [www.novachembv.com](http://www.novachembv.com)
- 20 Bran+Luebbe GmbH, PO Box 1360, D-22803 Norderstedt. [www.bran-luebbe.de](http://www.bran-luebbe.de)
- 21 Carleton, F. B., Weinberg, F. J., *Proc. R. Soc. London, Ser. A*, 447, 1994, 513.
- 22 Adler, J., Carleton, F. B., Weinberg, F. J., *Proc. R. Soc. London, Ser. A*, 440, 1993, 443.
- 23 Bonner-Denton, M., Gilmore, D. A., *SPIE*, 2388, 1995, 121.
- 24 Shreve, A. P., Cherepy, N. J., Mathies, R. A., *Appl. Spectrosc.*, 46, 1992, 707.

- 25** Bell, S. E. J., Bourguignon, E. S. O., Dennis, A., *Analyst*, **123**, **1998**, 1729.
- 26** Clarke, R. H., Londhe, S., Premasiri, W. R. et al., *J. Raman Spectrosc.*, **30**, **1999**, 827.
- 27** Martin, M. Z., Garrison, A. A., Roberts, M. J. et al., *Process Control Quality*, **5**, **1993**, 187.
- 28** Everall, N., King, B., Clegg, I., *Chem. Br.*, **36**(7), **2000**, 40.
- 29** Jobin Y., *Application Note, Raman Applications in the Agri-Chemical Industry*, Instruments SA, Jobin Yvon/Spex Division, 16–18 rue du Canal, 91165 Longjumeau.
- 30** Gervasio, G. J., Pelletier, M. J., *At-Process.*, **3**, **1997**, 7.
- 31** Gilbert et al., *SPIE*, **2248**, **1994**, 391.
- 32** Gregoris et al., *SPIE*, **1336**, **1990**, 247.
- 33** Alder-Golden, S. M., et al., *Appl. Opt.*, **31**(6), **1992**, 831.
- 34** Kaiser et al., *Ber. Bunsen-Ges., Phys. Chem.*, **96**, **1992**, 976.
- 35** Gresham, C. A., Gilmore, D. A., Bonner Denton, M., *Appl. Spectrosc.*, **53**(10), **1999**, 1177.
- 36** Cooper, J. B., Wise, K. L., Welch, W. T. et al., *Appl. Spectrosc.*, **51**(11), **1997**, 1613.
- 37** Martin, P. A., Feher, M., *NIR News*, **7**(3), **1996**, 10.
- 38** Norsk Elektro Optikk A/s PO box 384, N-1471, Skarer, Norway. [www.neo.no](http://www.neo.no)
- 39** Feher, M., Martin, P. A., *Spectrochim. Acta, Part A*, **51**, **1995**, 1579.
- 40** Holdsworth, R. J., Martin, P. A., Raisbeck, D. et al., *Topical Issues in Glass*, **3**, **1999**.
- 41** Turner Designs, <http://oilinwatermonitors.com>
- 42** Schade, W., Bublitz, J., *Environ. Sci. Technol.*, **30**, **1996**, 1451.
- 43** Senoussi, A., Hope, P. S., Hilliard, L. A. et al., *Annual Meeting of the Polymer Processing Society*, Manchester, 1993.
- 44** Christensen, J., Norgaard, L., Carsten, L., *Spectrosc. Eur.*, **11**(5), **1999**, 20.
- 45** Eco Physics, 3915 Research Park Drive, Ann Arbor, Michigan 48108–1600. <http://ic.net/~ecophys>
- 46** Burck, J., Roth, S., Kramer, K. et al., *J. Hazardous Mater.*, **83**, **2001**, 11.
- 47** Forschungszentrum Karlsruhe, Institute for Instrumental Analysis. [www.ifia.fzk.de/home\\_en.htm](http://www.ifia.fzk.de/home_en.htm)
- 48** <http://www.siemens.co.uk/env-sys/>
- 49** Paul, J. B., *Anal Chem.*, **1997**, 287A.
- 50** Wen-Bin, Y., *Ultra Sensitive Trace Gas Detection using Cavity Ringdown Spectroscopy*, IFPAC January 21–24, 2001, Amelia Island, FL, USA; [www.Meeco.com](http://www.Meeco.com); [www.tigeroptics.com](http://www.tigeroptics.com);
- 51** Crosson, E et al, *Cavity Ringdown Spectroscopy: Developing a Simple and Rugged Trace Isotope Analyzer*, IFPAC January 21–24, 2001 Amelia Island, FL, USA; Informed Diagnostics Inc, Sunnyvale, CA
- 52** Pipino, A. C. R., *Phys. Rev. Lett.*, **83**(15), **1999**, 3093.

# **18**

## **NMR**

*Loring A. Weisenberger*

### **18.1**

#### **Introduction**

Nuclear magnetic resonance (NMR) offers process control a wide variety of information. NMR has gained the reputation of being very expensive in terms of capital, maintenance and personnel and is therefore generally regarded as being limited to the research laboratory. However, depending on the information sought, a NMR analyzer for process control is easier to apply and thus less expensive than many of the common process instruments. Details on the theory and execution of modern NMR techniques are located elsewhere in this book and are not duplicated in this chapter. An excellent review by Maciel [1] on the application of NMR to process control and quality control is available. More recently, Nordon et al. [2] offer a review of the past as well as a look to the future for process NMR spectrometry.

### **18.2**

#### **Motivations for Using NMR in Process Control**

The driving force behind the desire to apply NMR spectroscopy to process control lies in its inherent quantitative nature and its ability to differentiate between chemical structures. In common with many spectroscopic techniques, NMR can be simply explained as a means of applying energy to a sample, measuring the energy absorbed and relating this to some property of the sample. For Fourier transform NMR, the input energy is in the form of a radio frequency (RF) pulse. The output energy is a RF pulse, at the same frequency, that decays with time and originates from the nuclei in the sample. The difference reveals information about the sample. The magnet serves to produce energy levels in the nuclei that will respond to the RF pulse.

The quantitative nature of NMR comes from the response of the nuclei in the sample. The amplitude of the response from any nucleus being excited is the same as the amplitude of the response from all other individual nuclei excited

under the same conditions. Therefore, the contribution to the overall signal from any single nucleus is a simple fraction of all those excited. In words more commonly associated with optical spectroscopy the extinction coefficient for all excited nuclei are the same. This leads to the inherently simple quantitative nature of NMR spectroscopy.

Differentiating between chemical structures comes from a second effect. The exact frequency at which a nucleus absorbs energy is determined by the electrons surrounding, and therefore shielding, the nucleus from the external magnetic field. This shielding is therefore a function of the associated chemical structure. Different chemical structures shift the frequency at which different nuclei respond. Fortunately, this frequency difference is consistent for similar chemical structures and is known as the chemical shift. Chemical shifts are referenced to a peak in the spectrum of an agreed standard compound. The chemical shift relative to the reference chemical shift indicates what types of chemical structures are in the sample. The chemical shifts, relative to tetramethyl silane (TMS), of various chemical structures are well known and documented for many nuclei and especially for  $^1\text{H}$  and  $^{13}\text{C}$  NMR spectroscopy. Other nuclei use different chemical shift reference compounds. NMR signals have both amplitude and frequency. Together these two characteristics allow the determination of the chemical structures to be determined and a quantitative estimate of the sample components to be made. The actual experiment is a little more complicated than described here. In practice the time response of the nuclei must be considered and the magnetic coupling between nuclei can further complicate the spectrum. Both coupling and relaxation times can however be used to gain additional information about the sample. The utilization of relaxation rates as a means of analyzing process samples is considered later in this section.

When a spectrum is collected and the chemical structures of the individual components are known, a simple computation allows the compounds in the sample to be quantified. In general, organic compounds give a number of peaks in their NMR spectra. However, in order to quantify the components of a sample only one peak from each compound is normally, needed. Each identified peak is integrated and divided by the number of nuclei associated with the chemical structure that it represents, e.g. for a methyl group with three protons the peak area is divided by three, for a methylene group with two protons the number is two and so forth. Each normalized area is divided by the sum of all of the normalized areas of all of the relevant peaks. This provides a mole fraction for the compounds. The weight fraction for that compound is determined when the normalized areas are multiplied by their respective molecular weights and divided by the sum of the weights for all of the relevant peaks. The quantitative determination of a complex mixture of chemicals is only limited by the resolution between peaks and the ability to assign a chemical structure or compound to a peak or set of peaks. Furthermore, even when detailed chemical structures are not available, useful process information can be obtained from NMR spectra by considering more generalized structures such as aliphatics and aromatics which give signals in specific regions of the spectrum.

In comparison to optical spectroscopies calibration of NMR has a fundamental simplicity because the concept of an extinction coefficient is not required. For optical techniques different chemical structures in a given molecule respond differently in amplitude to the excitation. A correction factor or extinction coefficient is used to correct the amplitude in order to correctly quantify the sample. The extinction coefficients are determined by running a series of samples with differing amounts of the compounds, measuring the response amplitude at a given frequency and generating a calibration curve. Such calibrations are required for FTIR, NIR or UV but not for NMR. In the case of very complex mixtures, optical techniques require training sets for complex mathematical algorithms. These training sets are generated by varying operating parameters, measuring the response of the optical technique and analyzing the sample by independent techniques. NMR does not require training sets since complex mathematical algorithms are not generally applied. One NMR spectrum acquired under the proper conditions can provide a detailed analysis of a complex mixture in a straightforward algebraic fashion. On the other hand, chemometrics used with NMR data on highly complex systems such as fuels will prove to be a powerful combination. The simple relationship between the NMR signal and quantity of material will simplify the application of chemometrics to systems which yield highly complex NMR spectra with severely overlapping peaks.

Similarly, chromatographic techniques require calibrations of retention times and response factors. Calibrations are usually accomplished in advance by injecting known mixtures into the system and measuring retention times and response factors. Chromatographic techniques are notoriously time consuming, of the order of several minutes even with a short column. The faster the chromatogram is acquired, generally the poorer the resolution and the greater the artifacts such as tailing. Gas chromatography also suffers from temperature problems. If the inlet or column temperature is too high, the sample might decompose. If the inlet or column temperature is too low, a higher molecular weight compound may not vaporize and will eventually foul the inlet or column. NMR does not suffer from these kinds of constraints. Usually a single pulse with an acquisition time of less than 10 s is all that is required for good data. The temperature of the sample compartment, be it a flow probe or static cell can be regulated to the sample temperature.

As stated, the quantitation from a NMR spectrum is relative only to those components measured, but in many cases, absolute quantitation is required. Absolute quantitation is the determination of the amount of a substance with regard to all of the substances present. It is usually expressed as the amount of a substance per unit volume or weight of the sample but can also be expressed as a percentage. NMR provides a convenient means for demonstrating the difference between relative and absolute measurements. Assume a solvent system is composed of water, acetone and acetonitrile in a 5:3:2 ratio by weight.  $^{13}\text{C}$  NMR would only detect the acetone and acetonitrile. And the relative result would be 60% acetone and 40% acetonitrile i.e. it only represents the carbon-containing solvents. However,  $^1\text{H}$  NMR would detect all three solvents. The result would reflect the exact ratio of the three solvents. The absolute result is equivalent to the relative result in

this case. The  $^{13}\text{C}$  spectrum could be made into an absolute quantitation method simply by calibrating the NMR signal against a known amount of either solvent. Some kind of calibration is required for most (but not all) uses of absolute quantitation. For process NMR, this usually involves measuring the absolute response against *at least* two standards. Generally, the amplitude (area) calibration is linear against concentration. Also, it only needs to be calibrated for one compound since all others are relative to that compound. For single unknown samples, an internal standard compound can be weighed into a known amount of sample to provide direct calibration. In the above example, one might choose  $^{13}\text{C}$  NMR over  $^1\text{H}$  NMR when the acetone or acetonitrile are much less than water. By eliminating the water signal, the dynamic range for the compounds of interest is increased.

Conceptually, from an engineering perspective, NMR for process control is quite simple. The sample is brought to the instrument from the process via a side stream. The sample flows through a quartz, sapphire or zirconia tube positioned in the magnetic field and returns to the process via another side stream. The design of the sample system depends upon the conditions of the process sample, including temperature, pressure and flow rate. The data are acquired and transferred to the process control room without operator intervention. The sample handling system can include a manifold so that one analyzer can monitor and provide process control information for more than one position in the process. Generally, the unwanted deposits on windows or elsewhere in the instrument associated with the optical techniques are not a problem. No waste is generated as is the case with LC or titrations. No column compatibility or fouling issues are present that are normally associated with GC. No one has to collect samples.

For on-line applications the effects of sample flow on the NMR signal must be considered. First, the flow rate must be slow enough to allow the magnetization to come to equilibrium. That means the time in the magnet must be in the range from one to five times the spin-lattice relaxation time,  $T_1$ . Whilst this can be a long time, the advantage to the flowing system is that the time inside the RF coil is short so that the RF pulse rate can be faster than the normal five times  $T_1$  since each pulse will excite a new set of molecules. The second issue is that the nuclei excited by the RF pulse must be in the coil long enough for their signal to be detected by the coil. The third issue is that the flow introduces some errors which cause  $T_2$  to be shorter than in a static sample leading to broader peaks. In the case of broadline NMR that has little effect. In the case of high resolution NMR, it can have a detrimental effect, depending on the analysis.

Another driving force behind using NMR for process control is the non-destructive nature of the technique. In some cases, the material is packed into a suitable container, usually a tube or vial, analyzed and then returned to the bulk, or if the material flows, it can be piped through the instrument. For other methods the sample is analyzed neat or in a solvent. In both cases the sample can usually be recovered with minimal effort. No waste is generated.

NMR provides several alternative approaches to a problem. If one nucleus does not prove effective, then an alternative may work. If one pulse sequence does not provide the best information, another may prove more effective. If one option is too

expensive, a less expensive version might work. If the molecular dynamics is not in the correct range, try a higher or lower temperature. If the frequency domain does not provide enough resolution, the time domain might. In any event, some of these choices are obvious and can be made prior to proceeding. Others require some experimentation and analysis. This versatility is demonstrated in the two basic methods of NMR for process control. Broadline NMR is a time domain technique and FT-NMR, also called (Fourier transform) high resolution NMR, is a frequency domain technique. While based on the same general principles, the information available from either technique is very different.

### 18.3 Broadline NMR

The least expensive process NMR option is a small 10–20 MHz (0.2–0.4 T) magnet with a desktop computer containing most of the necessary electronics for a complete pulsed NMR experiment. This is commonly referred to as broadline NMR. With a low field strength, the linewidth of any peak is large compared to the chemical shift scale. Separating peaks into meaningful chemical shifts and the appropriate chemical structures is not attempted. The time domain is used exclusively to provide information on the sample.

Physically, the magnet is small,  $20 \times 20 \times 20 \text{ cm}^3$ . The temperature control unit can be considerably larger, depending on the temperature range and control desired. The RF electronics are usually contained within a personal computer. A RF pulse is used to excite the sample and the response of the sample is recorded as a function of time.

The response signals from the nuclei decay exponentially with time. Many factors affect this decay, including field homogeneity and the motions of the molecules. When considering only the pure relaxation processes, the relaxation is characterized by the spin–spin relaxation time,  $T_2$ . When external factors such as magnetic field inhomogeneity are considered, the apparent spin–spin relaxation time is referred to as  $T_2^*$ . Since homogeneity will influence all molecules in the same way, only the molecular motions are considered here. The resolution between molecular species is a function of the difference between the characteristic times of the molecules. Typically,  $T_2^*$  is directly related to the “shape” of the free induction decay (FID). In the case of a single component, the  $T_2^*$  is related to the time response by the following equation:

$$M(t) = M_0 \exp(-t/T_2^*) \quad (1)$$

where  $M(t)$  is the magnetization at time  $t$  and  $M_0$  is the initial magnetization. In the case of a multi-component system the response is the simple sum of all of the components as a function of time.

$$M_{\text{total}}(t) = \sum M_{n0} \exp(-t/T_2^* n), \quad n = 1 \text{ to the number of components} \quad (2)$$

where  $M_{\text{total}}(t)$  is the total magnetization at time  $t$  and  $n$  is the component index. With the appropriate curve fitting software, all of the variables can be determined with several iterations. The limitation to this method is the differences between the  $T_2^*$ 's. In general if the ratio of the  $T_2^*$ 's is not greater than two, the fitting algorithms will have difficulty accurately discerning the variables for each component. If the  $T_2^*$ 's can be determined independently, then the restriction is relaxed. Each species may also have a Gaussian component which can be accounted for in a similar fashion to the previous equations.

In general, when the components and their  $T_2^*$ 's have been previously determined, the initial magnetization for each component can be calculated. Knowing the initial magnetization for each of the components allows the mole fraction of each component to be determined as its initial magnetization divided by the total initial magnetization.

The drawback to this approach is relating the time domain information to a chemical species or physical phenomena. Many broadline systems are used in an empirical fashion in which the results are correlated with a process control parameter or measured physical property. However, this approach alone does not indicate which chemical species is being measured. The signals could be due to water or fat content, bound water versus free water in a slurry or different phases of a polymer, crystalline, amorphous or interfacial regions. To ensure that these correlations are due to specific chemical species broadline NMR data must be related to some other primary analytical technique such as high resolution NMR.

An even more simplistic approach is used when doing spin counting which is simply “counting” all of the nuclei (spins) contributing to the signal. In spin counting, a broadline system is calibrated using a known volume of a standard solution. Immediately after the RF pulse, the initial response of the sample is recorded. This is mathematically compared to the initial response of the standard. The result is a correlation of the number of protons in the given volume. The technique requires precise temperature and pressure control. An example is measuring the total hydrogen content of a petroleum fraction and comparing that to an equal weight of a standard such as n-octane.

Other NMR parameters, such as the spin-lattice relaxation time,  $T_1$ , and spin-lattice relaxation time in the rotating frame,  $T_{1p}$ , are used in a similar fashion although the equations are different. Each uses a unique pulse sequence to probe a specific dynamic property of the molecule.  $T_1$ 's are related to the short range, high frequency motions of a molecule whereas,  $T_{1p}$ 's are related to longer range motions in the kHz region. Chemical compounds with similar  $T_2^*$ 's might have vastly different  $T_1$ 's or  $T_{1p}$ 's and therefore alternative methods are available for determining the different components in a solution. Diffusion times add yet another option to the range of motions that can provide differences between compounds. Diffusion times are measured by altering the static magnetic field such that the position of a molecule in the sample is encoded in the signal. As the molecule moves throughout the volume, the encoding changes the signal. More diffusion results in faster decay of the signal. Thus, the diffusion weighted analysis favors

slow moving and generally larger molecules. The magnetic field is altered using linear magnetic field gradients added to the probe or the magnet.

Broadline NMR made its mark in the food industry [3–12] with substantial work done in Europe [13–16]. Originally, Chapman and others [17] applied wideline NMR to the determination of solid fat in oil. By heating a fat in oil sample, the fat is melted and the total intensity of the FID is measured. Then a second measurement is taken at a lower temperature where the fat has solidified. The ratio of the two measurements indicates the solid fat content. This method is quick and more precise than other methods such as differential scanning calorimetry (DSC).

More simplistically, several methods exist to determine the amount of water or oil in foodstuffs. One is the spin counting method described previously. The absolute signal amplitude of the FID is simply measured as a function of the weight of the material. When measured against a carefully calibrated set of standards, the amount of material is determined. The drawback to this method is that it only works well when only one measurable component is present and the other components are not detected by the NMR instrument.

Guillou and Tellier [18] used a 20 MHz wideline instrument to measure ethanol in alcoholic beverages. A Carr–Purcell–Mieboom–Gill [19] pulse sequence is used to encode the scalar coupling of the methyl and methylene in ethanol. By examining the difference between the modulated and unmodulated echoes at time  $t=1/(2J)$  it is possible to determine the volume percent of ethanol in an aqueous solution. The proportion is given by the equation

$$\Delta(1/(2J)) \propto (5d_a/m)t_v \quad (3)$$

Where the right-hand side of the proportionality represents the hydrogen content of ethanol per unit volume, where  $d_a$  is the density of pure ethanol,  $t_v$  is the percentage of alcohol,  $m$  is the molecular mass and  $J$  is the scalar coupling of the methylene and methyl protons. The correlation is very good in the 0–70% (v/v) range. With no sample preparation, they measured several wines. Based on the differing characteristics of the wines, they were able to show also that glucose does not interfere with the ethanol measurements.

Engelbart and others [20] provided a detailed molecular description of the curing process of towpreg materials and its relationship to changes in the NMR signal in a broadline system. Figure 18.1 shows how these materials, which are carbon fibers coated by “towing” them through epoxy resin, exhibit a change in  $T_2$  of four orders of magnitude as the material cures. By monitoring the  $T_2$  of the material, the degree of cure is monitored and the optimum temperature program can be chosen. Additionally, Fig. 18.2 shows that the degree of cure can be monitored successfully while strips of towpreg are pulled through the NMR magnet and probe. Fig. 18.3 shows the set-up of the fibers being pulled through the magnet and probe. By using four strips of towpreg, cured between 10 and 40%, they found good agreement between DSC measurements and the on-line NMR system.

NMR work on polyethylene (PE) is extensive, not surprisingly because its production exceeds all other plastics by an order of magnitude. The physical properties vary with composition. Most producers use high resolution NMR to characterize

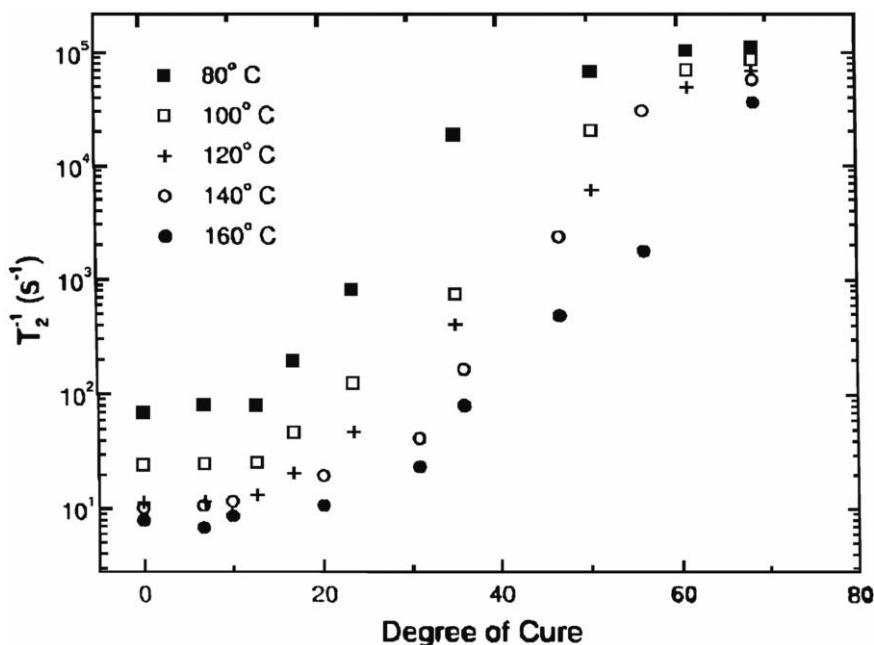


Fig. 18.1 Laboratory correlation between degree of cure and spin-spin relaxation time. Reprinted with permission from [20].

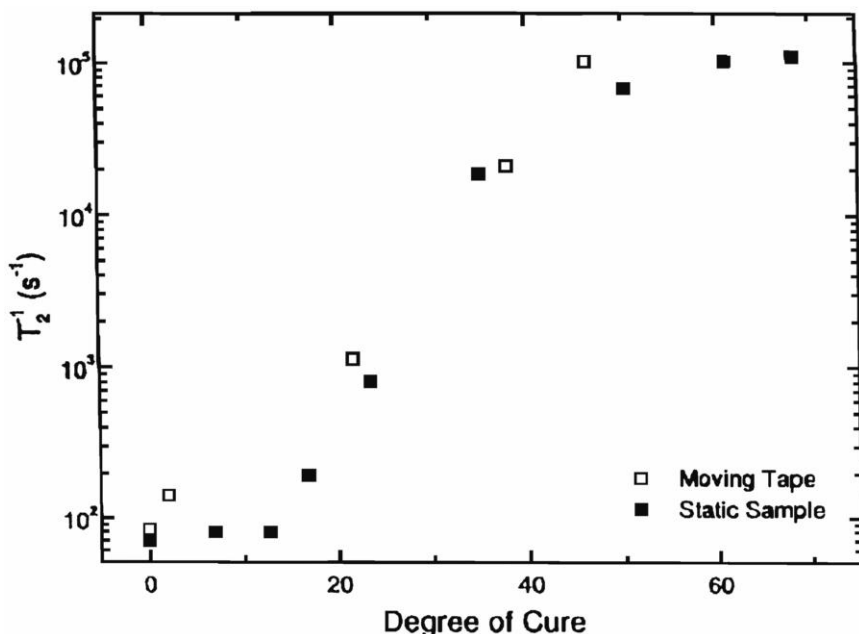
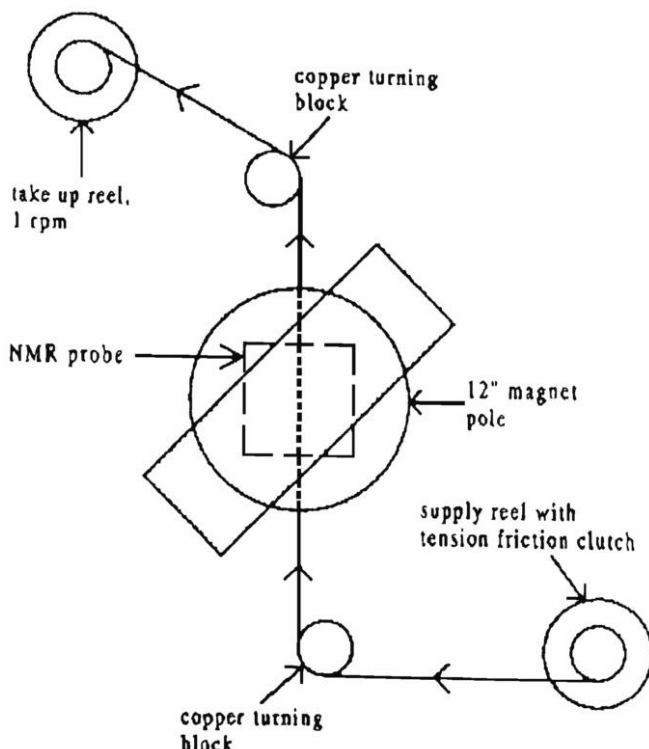


Fig. 18.2 On-line simulation: Correlation between degree of cure and spin-spin relaxation time for both static and moving towpreg. Reprinted with permission from [20].



**Fig. 18.3** Laboratory set-up for NMR dynamic measurements.  
Reprinted with permission from [20].

the chain branching of their different grades of PE. The process of obtaining NMR spectra is slow and difficult, depending on the solvents and conditions used and on the grade of the polymer. However, most of the PE producers use NMR for quality control of their product lines and many use it for process control and monitoring of their reactors, albeit with a large time delay. Many are also using this information for blending different grades of PE to provide the desired properties of a particular product line.

With this much interest in polyethylene, many attempts have been made to use low frequency NMR in either the time domain or frequency domain to monitor and control the production more rapidly. Auburn International (now part of Oxford Instruments) developed a widely adopted system based on the time domain spectrometers [21]. In this case, sample preparation is no longer an issue since the system accepts either powder or pellets and no solvent is used. The Auburn systems determine crystalline and amorphous ratios, viscosity, melt index and molecular weight. For other types of polymers, the list of advertised measurements include tacticity, rubber content, copolymer analysis, and various rheological properties. These values are determined by correlating several routine but laborious methods with the decay of the NMR signal under various pulse sequences. The man-hours

saved by using this technique are an added value to the fact that the information is returned quickly enough to control the process.

The manufacturers of these kinds of instruments all have a long list of applications. Most of the applications are similar and many are pre-packaged as specific analyzers so that they simply unpack, set up and data is acquired within an hour or so after the magnet temperature equilibrates. The instrument vendors for broadline systems are Bruker Instruments [22], Oxford Instruments [23], Praxis [24], Process Control Technology (PCT) [25] and Resonance Instruments [26]. Determination of oil and/or water content dominates the applications. Oil and water analyses are established for seeds and soil in the agriculture industry, catalysts and detergents in the chemicals industry, capsules, tablets and powders in the pharmaceutical and cosmetic industries as well as a wide variety of foodstuffs.

Although the determination of oil and water dominates the use of NMR spectroscopy there is a wide range of other imaginative applications. In the polymer industry, in addition to the PE characteristics discussed previously, many other properties are analyzed using broadline NMR systems. The details of these applications are generally available from the manufacturers of broadline NMR systems mentioned in the previous paragraph. For fibers, the amount of added spin finish on the outside layer of the polymer is determined based on the distinct NMR signals resulting from differences in the mobility of components in the finish and the polymer. In a similar analysis, plasticizer content can be determined in bulk polymer or final product samples, utilizing the higher mobility of the lower molecular weight plasticizer to distinguish it from the polymer. The composition of blended materials can be determined to give the rubber or filler content. Polymer blend compatibility can also be assessed by utilizing the different relaxation rates of the various blend components. Like the towpreg example described previously, the extent of polymerization and the degree of crosslinking are other properties that can be monitored as a result of the changes in NMR relaxation rates as the mobility of the polymer changes.

The food industry continues to provide some interesting and unusual applications of process control beyond water and oil measurements, such as the study of a cooking process [27] or of a freezing process. Catalysis is another area with unique applications. The characteristics of a catalyst that can be measured by broadline NMR include activity and selectivity.

Many analyses easily cross industry lines. The chemical and pharmaceutical industries are interested in the analyses that determine the coating weight of a coated particle such as with a time-released drug. Like the spin finish on fibers, the coating has a different relaxation rate than the encapsulated material. Fluorine analysis is another unique application of NMR technology since the signal derives from the fluorine nuclei rather than hydrogens. The materials for which this technique for process analysis and control might be used include toothpaste, fluoropolymers and fluorochemicals.

Droplet size analysis is of particular interest to both the food industry, for margarine, and to the cosmetic industry, for various make-up emulsions. Droplet size is also a good example of the use of magnetic field gradients to encode spatial in-

**Table 18.1** Broadline NMR.

Characterized parameter:	Surface specificity		
Energy of radio frequency absorption	Information depth: Bulk		Detectability: > 1 %
Type of information:	Resolution		
Composition or property based on specific nuclei relaxation	Depth:	Lateral:	Other: Not used for spatially resolved analysis
Measurement environment: Difficulties	Time needed for analysis:		
Strong magnetic field	Preparation	Measurement	Evaluation
RF excitation	0.5 to 5 min	0.5 to 5 min	1 to 5 min
Air or nitrogen			
Equipment:	Cost [ECU]:		No. of facilities:
Broadline NMR analyzer	\$ 40–80,000		Common
Type of laboratory: User skill needed:	Sample		
Small	Unskilled	Form type Solid, liquid or slurry	Size: 0.5 to 150 ml
Techniques yielding similar information			
FTIR, GC-MS			

formation into the NMR analysis. By applying a magnetic field gradient, the rate that a mobile molecule moves through a sample is monitored. With the appropriate model, the size and distribution of the sizes of the domains are determined. The complement to this analysis is the determination of particle size for pigments or fillers in liquids such as paint. In this case, the signal does not generally originate from the component of interest. Instead the matrix provides the NMR signal necessary to determine the average particle size. This is similar to the way NMR is used to determine the pore sizes and their distribution in catalysts or in rocks for oil recovery.

The use of broadline NMR in process control is summarized in Tab. 18.1.

#### 18.4 FT-NMR

As the field strength of the magnets increases, the resolution in the frequency domain increases. Peaks representing different chemical structures are resolved. A direct correlation exists between the chemical shift of a peak and the chemical species that it represents. The relative mole and weight fractions of an identified chemical are easily calculated.

At the lower end of the magnet strengths, around 40–60 MHz (0.9–1.4 T), the systems are made using small permanent magnets typically measuring  $30 \times 30 \times 30$  cm $^3$ . Depending on the design, the fringe field of the magnet is usually contained inside the magnet enclosure. The electronics are considerably larger and more complex than the broadline systems possibly occupying a couple of 50 cm racks 1 m tall. The electronics are generally more robust than for the broadband NMR analyzer. The RF, temperature control and shim power supply are all housed in the rack with the magnet on top. Plenty of space and fans are added for cooling the electronics in a hostile industrial environment. The hardware is often driven by a personal computer that is separate from the other electronics. These systems are ideal for placing on-line or near the process. They are easily fitted to an industry standard protective enclosure while the computer can be located in the control room. There is little maintenance beyond the initial installation. A sample delivery system is simply a pipe running from the process stream to the instrument with a tube running through the magnet made of a more specialized non-magnetic material such as glass, quartz, sapphire or zirconia. The choice of which flow tube is used is determined by the harshness of the sample, pressure, temperature and cost. The sample is returned to the process without alteration. In general, after the analysis is initially established, these systems are run automatically as an analyzer with the required information being transmitted to the process control panel. Alternatively, they can also be used as small bench-top analyzers in a QA/QC laboratory.

The use of low field FT-NMR in process control is summarized in Table 18.2.

On the high resolution side of magnet strengths, the systems range from 100 MHz up to 900 MHz (2.3–21 T). The magnets are made of superconducting wire that is cooled to  $-269$  °C by liquid helium. The dewar of liquid helium is blanketed with liquid nitrogen to reduce the boil-off rate of the liquid helium. These designs provide high field magnets without the large cost of the electricity required by electromagnets. The maintenance costs are higher since liquid nitrogen must be replaced weekly or bi-weekly and liquid helium must be topped quarterly or semi-annually but this is more than offset by the electrical savings.

These systems also occupy a lot of space. The fringe field of a magnet is the magnetic field outside the physical magnet itself. The stronger the magnetic field, the larger the fringe field will be. This can be dangerous since ferromagnetic objects are easily pulled towards the field, creating uncontrollable projectiles. Untrained or poorly supervised personnel may inadvertently wheel a gas cylinder past the magnet with catastrophic effects, possibly to both the magnet and the personnel. It is also dangerous because persons with pacemakers or metal plates can be adversely affected by any strong magnetic field. The extent of the fringe field for a superconducting magnet is typically measured in meters, so that a safety zone around the magnet is necessary. Furthermore, the electronics should be outside this zone as well, thereby occupying additional space. Some systems now come with shielded magnets that have substantially reduced fringe fields. Nevertheless, it is difficult to imagine a superconducting system anywhere near the process line. Although in some extreme cases where the costs are justified, superconducting systems could be used on-line [1].

**Table 18.2** Low field FT-NMR.

Characterized parameter:	Surface specificity:		
Energy of radio frequency absorption	Information depth: Bulk	Detectability: > 1 %	
Type of information:	Resolution:		
Composition based on specific nuclei	Depth: Not normally used for spatially resolved analysis	Lateral:	Other:
Measurement environment: Difficulties	Time needed for analysis:		
Strong magnetic field	Preparation 0.5 to 5 min	Measurement 0.5 to 5 min	Evaluation 1 to 5 min
RF excitation			
Air or Nitrogen			
Equipment:	Cost [ECU]:		No. of facilities:
Low field FT-NMR Spectrometer	\$ 80–120,000		Less common
Type of laboratory: User skill needed:	Sample		
Small	Unskilled	Form type Solid, liquid or slurry	Size: 0.5 to 5 ml
Techniques yielding similar information:			
FTIR, GC-MS			

Both types of FT-NMR system can contribute to process control whether on-line or in the laboratory. The smaller systems are ideal for monitoring solutions or mixtures with a detection limit of about 1 %. This involves the integration of peaks from the materials of interest in the sample. In some cases, the important parameter is the exact chemical shift of a particular peak. As conditions in a process change, the position of a sensitive peak will shift in a predictable manner. Changes in the chemical shift of a peak can be related to changes in pH or complex formation. In some cases, the appearance or disappearance of a peak can be used to monitor the progression of a reaction.

Haw and others [28] demonstrated the utility of low field frequency domain NMR for determining the amount of oxygenates in gasoline. By using LC pumps, they blended methyl *tert*-butyl ether (MTBE) and/or ethanol with gasoline and monitored the process using a 42 MHz NMR system with a flow probe. Figure 18.4 shows only minor degradation in the signal of ethyl benzene when the flow is increased from static to  $6 \text{ ml min}^{-1}$ . From the NMR spectrum, they calculated the amount and type of added oxygenate. A  $^1\text{H}$  NMR spectrum (Fig. 18.5) of a typical gasoline shows features including the aromatic (8–6 ppm), olefinic (6.5–5 ppm) and aliphatic protons (3–0 ppm). It also demonstrates that with a sample flow of  $2 \text{ ml min}^{-1}$  the MTBE (3.2 ppm) can be monitored up to 20 % v/v. In a more demanding analysis, ethanol can be measured from 2 % v/v in the presence of MTBE (Fig. 18.6).

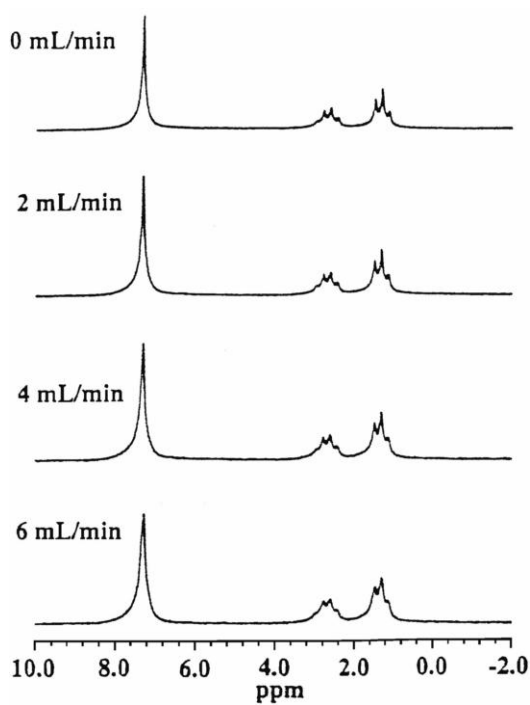


**Fig. 18.4** The 42 MHz proton spectra of ethyl benzene flowing at various rates. The spectra were not sensitive to flow rates in the range shown. Reprinted with permission from [28].

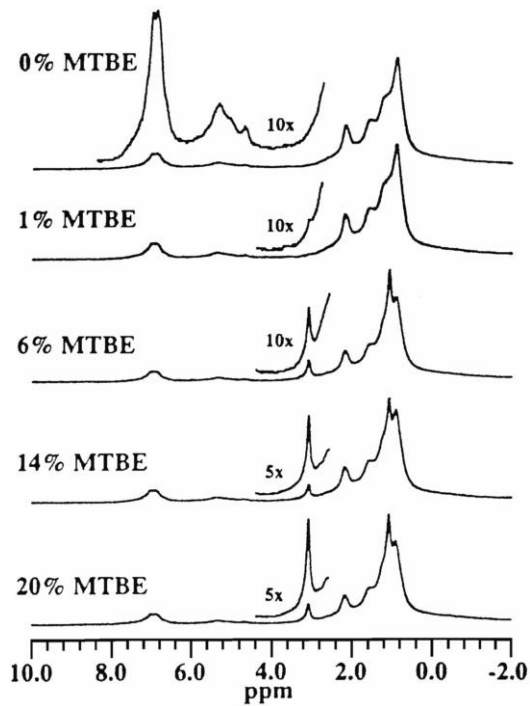
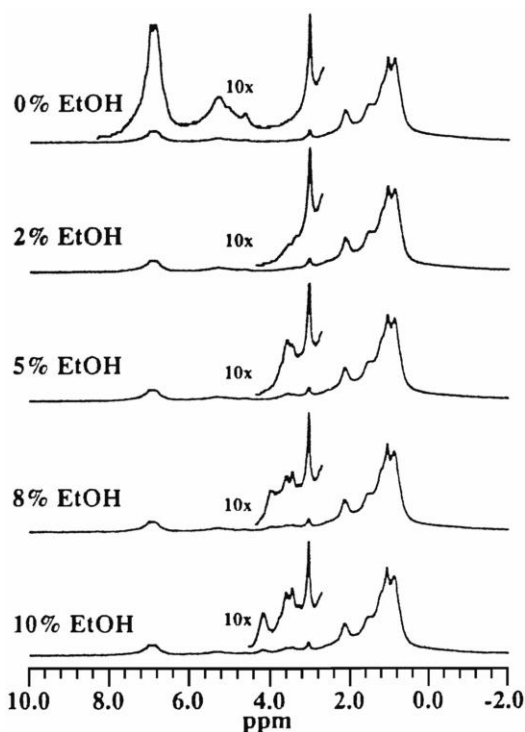


**Fig. 18.5** The 42 MHz proton spectra of various blends of MTBE and regular, unleaded gasoline. The highlighted areas show signals from MTBE or the aromatic and olefinic protons of gasoline. All spectra were acquired with 12 scans on samples flowing at  $2.00 \text{ ml min}^{-1}$ . Reprinted with permission from [28].

**Fig. 18.6** The 42 MHz proton spectra of various blends of ethanol in 10% MTBE in gasoline. All spectra were acquired with 12 scans on samples flowing at  $2.00 \text{ ml min}^{-1}$ . The concentration dependence of the hydroxyl proton chemical shift is apparent in the expanded plots. Reprinted with permission from [28].



Edwards and Giannetto [29] (Process NMR Associates [30]) have reported the application of an on-line NMR system to monitor the sulfuric acid alkylation process at a refinery. This is an excellent example of using the full capabilities of a low-field frequency-domain NMR analysis. Figure 18.7 shows the full spectrum which includes the acid/water peak at about 10 ppm and the hydrocarbons from about 8 to 0 ppm. In this example, the weight percent of the acid/water fraction is determined against the hydrocarbon fraction by simply measuring the area beneath each peak. This ratio is an indication of the quality of the emulsion. Similarly, the alkane to alkene ratio is determined and used to monitor feed compositions. This is more clearly demonstrated in Fig. 18.8 where the olefins are in the region from 6 to 4 ppm. In a more complex analysis, but demonstrating the versatility of the NMR measurements, the acid strength is determined from the position of the acid/water peak. The position is entered into a third order equation that is related to the acid strength. All of this information is acquired from a single measurement in less than 2 min and returned to the controller for optimizing the process. The previous method for determining the acid strength was a titration, where the emulsion was separated into acid and hydrocarbon fraction. Samples for the titration method were taken every 4 h. The titration method was slow, labor intensive and hazardous since samples had to be collected from the alkylation unit, separated into fractions and poured into the apparatus. The NMR system simply

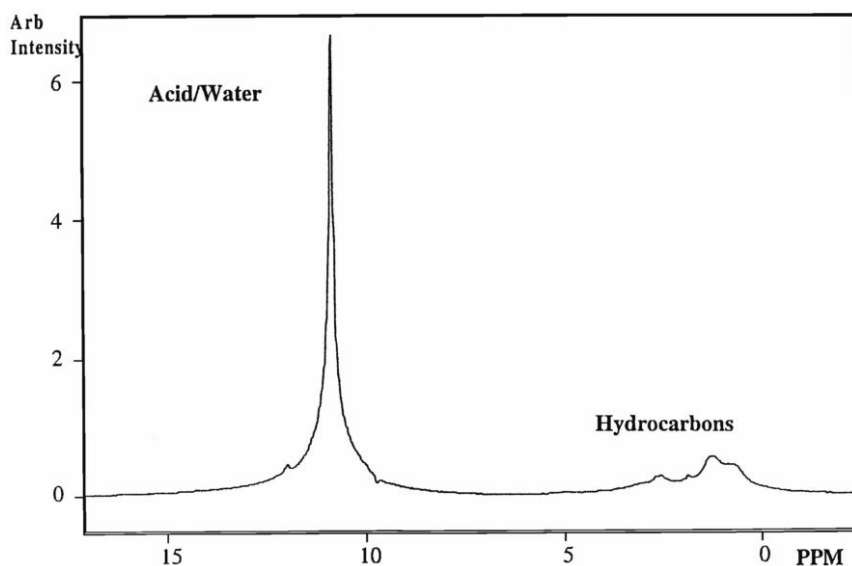


**Fig. 18.7** On-Line  $^1\text{H}$  NMR spectrum of the intact  $\text{H}_2\text{SO}_4$ /hydrocarbon emulsion. Reprinted with permission from [29].

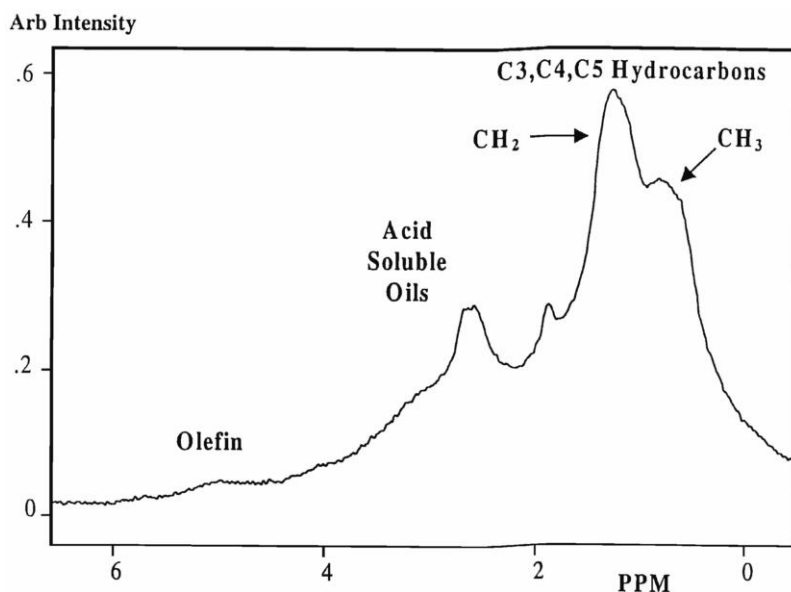


**Fig. 18.8**  $^1\text{H}$  NMR spectrum of the hydrocarbon region of the intact emulsion. Reprinted with permission from [29].

takes a sample via a side stream to the instrument and returns the sample to the unit with another pipe.

The Foxboro Company [31] purchased the process NMR division of Elbit ATI in 1997 and turned a process/portable NMR system into a series of analyzers for the petroleum refining industry. By using a variety of modeling and chemometric algorithms, the Foxboro NMR analyzers convert NMR data into traditional refining measurements including API gravity, viscosity, and reed vapor pressure (RVP). These analyzers touch on nearly every aspect of the refining process from crude oil blending through distillation, fluid catalytic cracking and sulfuric acid alkylation to product blending.

One of the most complex examples of using NMR for process control is its application to transforming growth factor- $\beta_3$ . Blommers and Cerletti [32] developed a methodology using high resolution NMR. The 2D NOE spectrum of the TGF- $\beta_3$  serves as a fingerprint to monitor and control batch-to-batch variations of the material. The NMR spectrum for a given batch is compared to the TGF- $\beta_3$  as well as the reference spectra for fully reduced TGF- $\beta_3$  and for a mutant version. This is a challenging application since the differences between the 25 kDa structures lie in the placement and number of disulfide bonds and hence the three-dimensional structure.

In addition to Process NMR Associates and Foxboro, Anasazi [33] and Hitachi [34] both produce low field FT-NMR systems although the instruments are designed for laboratory use rather than as process analyzers. High field FT-NMR systems are produced by three manufacturers, Bruker Instruments [35], JOEL [36] and Varian [37].

The use of high field FT-NMR in process control is summarized in Tab. 18.3.

**Table 18.3** High field FT-NMR.

Characterized parameter:	Surface specificity:		
Energy of radio frequency absorption	Information depth: Bulk	Detectability: 10 ppm	
Type of information:	Resolution:		
Composition based on specific nuclei	Depth: 100 $\mu\text{m}$ Lateral: 10 $\mu\text{m}$ Other:		
Measurement environment: Difficulties	Time needed for analysis:		
Strong magnetic field RF excitation Air or nitrogen	Preparation 0.5 to 5 min	Measurement 0.5 to 24 h	Evaluation 1 to 5 min
Equipment:	Cost [ECU]:		No. of facilities:
FT-NMR Spectrometer	\$ 200 K–\$ 4 MM		Common
Type of laboratory: User skill needed:	Sample		
Large	Experienced technician or professional	Form type Solid, liquid or slurry	Size: Large 0.5 to 5 ml
Techniques yielding similar information:			
FTIR, GC-MS			

### 18.5 Conclusion

With the ever-increasing demands for efficiency and quality in production, analyzers and controllers of all types will slowly gain acceptance in many industries. NMR offers a wide variety of options for on-line analysis as well as at-line plant laboratory analysis. Information generated by NMR analyzers can be immediately fed back into the process, providing more accurate and rapid control. Implementation is relatively easy. Installation requires a fast loop from the process, possible sample conditioning and running the communications lines to the control room. Some software development is required to convert the NMR measurements into meaningful data for the operators or control units. Such procedures are no different than for most on-line analyzers. The benefits of NMR analyzers depend upon their capability of providing quantitative chemical information without complex models or calibrations. As the NMR analyzer becomes more valued, the cost will seem less of an obstacle.

## References

- 1 Maciel, G., *NATO ASI Ser., Ser. C*, 1994, 447, 225–75.
- 2 Nordon, A., McGill, C., Littlejohn, D., *Analyst*, 2001, 126, 260–72.
- 3 Wiggall, P., Ince, A., Walker, E., *J. Food Technol.*, 1970, 5(4), 353–62.
- 4 Wetstrom, R., *J. Am. Oil Chem. Soc.*, 1971, 48(1), 15–17.
- 5 Tessier, A., Linard, A., Delaveau, P. et al., *Z. Lebensm.-Uters. Forsch.*, 1983, 176(1), 12–15.
- 6 Sleeter, R., *J. Am. Oil Chem. Soc.*, 1983, 60(2), 343–9.
- 7 Schmidt, S., *Adv. Exp. Med Biol.*, 1991, 302, 599–613.
- 8 Rutledge, D., *J. Chim. Phys. Phys.-Chim. Biol.*, 1992, 89(2), 273–85.
- 9 Simoneau, C., McCarthy, M., Reid, D. et al., *Trends Food Sci. Technol.*, 1992, 3(8–9), 208–11.
- 10 Davenel, A., Marchal, P., *Dev. Food Sci.*, 1994, 36, 35–42.
- 11 McDonald, P., *Food Process*, ed. Gaonkar, A., Elsevier, Amsterdam 1995, 23–36.
- 12 Sun, X., Moreira, R., *J. Food Process. Preserv.*, 1996, 20(2), 157–67.
- 13 Sambuc, E., *Rev. Fr. Corps Gras*, 1974, 21(12), 689–98.
- 14 Ribaillier, D., *Inf. Technol.*, 1980, 67, 19–28.
- 15 Rutledge, D., Khaloui, M., Ducauze, C., *Rev. Fr. Corps Gras*, 1988, 35(4), 157–62.
- 16 Bezecna, L., Tenkl, L., Konradova, M., Slechtilska, S., *Czech. Rostl. Vyroba*, 1991, 37(1), 75–80.
- 17 Chapman, D., Richards, R. E., York, R. W., *JOACS*, 1960, 37, 243–6.
- 18 Guillou, M., Tellier, C., *Anal. Chem.*, 1988, 60, 2182–2185.
- 19 Meiboom, S., Gill, D., *Rev. Sci Instrum.*, 1958, 29, 688–691.
- 20 Engelbart, R., Conradi, M., Stoddard, R., *43rd Int. SAMPE Symp.*, 1998, 43, 928–36.
- 21 Roy, A., Marino, S., *Am. Lab.*, 1999, 31(21), p. 32–33.
- 22 Bruker Analytik GmbH, Rheinstetten, Germany.
- 23 Oxford Instruments Analytical, Buckinghamshire, UK.
- 24 Praxis, San Antonio, TX, USA.
- 25 Process Control Technologies, Fort Collins, CO, USA.
- 26 Resonance Instruments Ltd., Witney, UK.
- 27 Stapley, A., Goncalves, J., Gladden, L. et al., *IChemE Res. Event–Eur. Conf. Young Res. Chem. Eng.*, 1995, 2, 1064–6.
- 28 Skloss, T., Kim, A., Haw, J., *Anal. Chem.*, 1994, 66, 536–42.
- 29 Edwards, J., Giammateo, P., *Proc. Annu. ISA Anal. Div. Symp.*, 1998, 31, 73–77.
- 30 Process NMR Associates, Danbury, CT, USA.
- 31 The Foxboro Company, Foxboro, MA, USA.
- 32 Blommers, M., Cerletti, N., *Pharm. Sci.*, 1997, 3(1), 29–36.
- 33 Anasazi Instruments, Inc., Indianapolis, IN, USA.
- 34 Hitachi Instruments, Inc., San Jose, CA, USA.
- 35 Bruker Analytik GmbH, Rheinstetten, Germany.
- 36 JOEL Ltd, Akishima, Japan.
- 37 Varian, Inc., Palo Alto, CA, USA.

## 19

### Process Mass Spectrometry

*Christian Hassell*

#### 19.1

##### Introduction

Process mass spectrometry (MS) is a very powerful technique for process monitoring and control, providing a unique combination of speed, selectivity, dynamic range, accuracy, precision and flexibility. The technique has become a standard for gas-phase analysis in several industrial applications, including steel manufacturing, fermentation off-gas analysis, and the production of ethylene oxide and ammonia. Among its attributes:

- Speed: of the order of 1 s per analyte per sample stream, thus permitting true real-time analysis.
- Sensitivity: low pp ( $10^{-6}$ ) detection limits are routine for many applications, and low ppb ( $10^{-9}$ ) or even ppt ( $10^{-12}$ ) levels are achievable for certain applications.
- Wide dynamic range: MS detection limits are not dependent on pathlength, as with most optical techniques, thus the same MS analyzer can be used for measurements from ppb to nominal 100 %.
- Easily multipointed: most commercial systems are supplied with multiple sample valves, accommodating up to 64 or more sample streams.
- Cost: although the system hardware is quite expensive, the ability to multipoint often results in lower cost per sample point.
- Flexibility: new analytes are easily added to the sample analysis matrix.
- Ideal for process diagnostics/information rich: mass spectral interpretation is relatively straightforward, especially in conjunction with spectral libraries.

On the other hand, MS has its limitations, and each of the above attributes has its caveats, as will be described later in this chapter. Among its limitations are:

- Most commercially available instrumentation is limited to the analysis of gas-phase sample streams, although membrane technology is sometimes employed for the analysis of volatile organics in certain liquid streams.

- Overlap of fragmentation patterns can be severe for some applications, making analysis of some stream components very difficult.

As with any process analyzer, thorough application review is the key to matching the process analysis need to the most appropriate measurement technology.

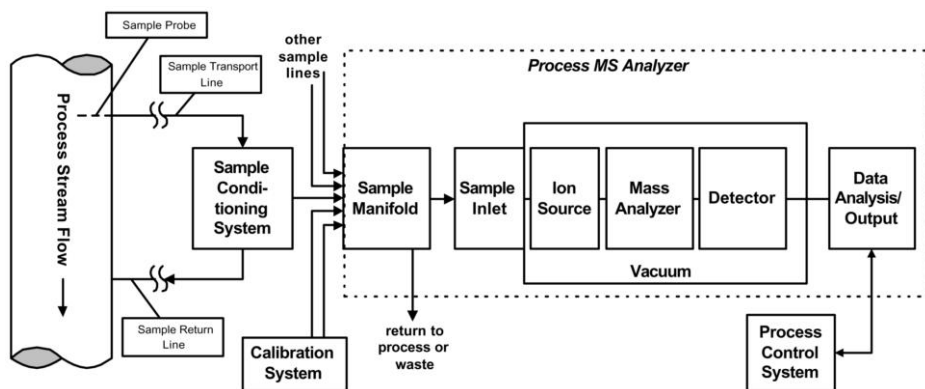
Wide acceptance of process mass spectrometry has been hindered by a perception that it is too complicated and delicate. This perception may have its roots in many undergraduate chemistry laboratories, where it is quite common to have hands-on experience with optical spectrometers and gas chromatographs, whereas MS is often introduced as the large complex instrumentation in the basement, run by a sort of “priesthood” of specialists. (This same situation may be one of the barriers to acceptance of nuclear magnetic resonance for process monitoring.) While it is true that process MS involves moving parts and somewhat delicate source materials, such items have been ruggedized in current commercial instrumentation to a degree that MS reliability and ease of use are equivalent to, or in some cases better than, other common process analysis technologies.

This chapter seeks to clarify the current state of process MS instrumentation and dispel some of the common misperceptions. It is aimed at the chemist or engineer who needs a practical solution to solve a process problem. As such, it is biased toward practical instrumentation that is commercially available. Review articles [1] are available that describe the latest instrumental developments that utilize more exotic mass analyzers and novel ionization sources.

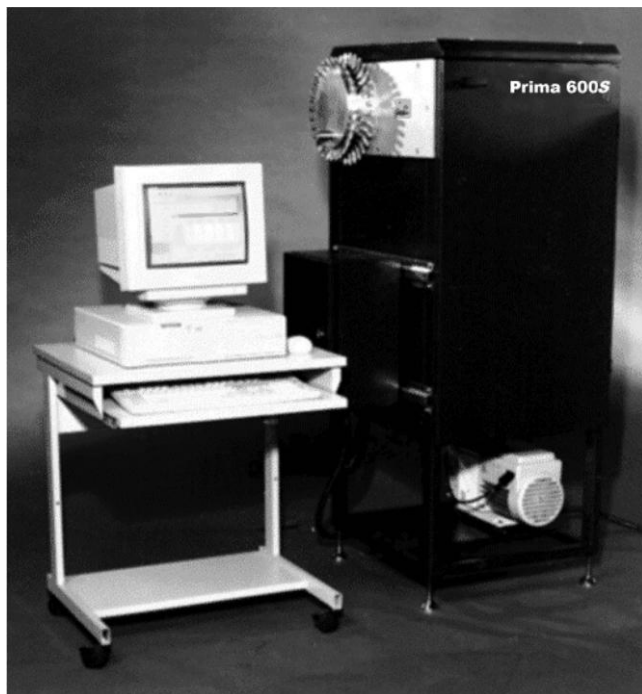
## 19.2 Hardware Technology

Figure 19.1 is a block diagram of a typical process analyzer system, consisting of a sample collection and conditioning system, sample manifold, sample inlet, ion source, mass analyzer, detector, and a data analysis and output system that interfaces with the process control system. The dashed line indicates the parts of the overall system that are considered to comprise the analyzer itself (i.e., what is normally included when one purchases a process MS). Figure 19.2 is a photograph of a commercial process MS that incorporates these components. Aspects of these various components are described below, with emphasis on how they are applied in a process mass spectrometer.

Some issues are common to all components in the analyzer system, including consideration of materials of construction and heating/cooling requirements. Many options also exist for installing a process MS in toxic, corrosive or explosive environments. For example, a general purpose analyzer can be placed in an analyzer house or shelter that is temperature-controlled and designed to protect from such hostile environments. Alternatively, the components within the dashed line of Fig. 19.1 can be placed within a cabinet that is purged with an inert atmosphere and that includes an integral temperature control system, thereby eliminating the need for a separate shelter.



**Fig. 19.1** Block diagram of a process mass spectrometer analyzer system.



**Fig. 19.2** A commercial process mass spectrometer. Note rotary valve on the upper part of the analyzer, facing the computer. (Photograph used with permission of ThermoOnix Inc.).

### 19.2.1

#### Sample Collection and Conditioning

Although a thorough treatment of sample collection and conditioning is beyond the scope of this chapter, a few aspects merit mention. Because mass spectrometers are often used to monitor multiple sample points throughout a process, they are usually positioned in a central location to which samples are transported from distant sample points. Often it is possible to transport samples several hundred meters, but the system design must ensure representative samples by considering temperature, flow and pressure changes throughout the run. Particulates should be excluded with filters to approximately  $0.5\text{ }\mu\text{m}$ ; several stages of filtering are often employed along the sample system to reduce ploggage of the final smallest filter. Generally, most sample line problems can be avoided by keeping all sample lines as short as possible, keeping them flowing continuously, and ensuring that lines are heated if condensation is possible. Figure 19.1 illustrates a common method of ensuring representative sampling and rapid continuous flow of sample. With this method, known as a fast-loop sampling system, the sample is rapidly transported to and from the sample conditioning system, with a small bypass fraction drawn into the sample manifold.

A sample manifold is usually used at the mass spectrometer to connect several sample lines and calibration gases to the analyzer. Many designs are available, usually incorporating either solenoid or rotary valves; a rotary valve can be seen on the side of the analyzer in Fig. 19.2. Most modern manifold designs permit all samples not being analyzed to flow continuously via a bypass (this bypass loop is commonly referred to as the *slow-loop*), thus permitting better representative sampling while preventing condensation that might occur in a line that is not actively being transported. Several proprietary manifold designs are very good at minimizing cross-contamination between samples, while achieving rapid stream switching and reducing design complexity in sample conditioning systems.

Water, in the form of vapor or droplets, is a common element of many sample streams. Too much water vapor can either overwhelm the mass spectrometer, or present a significant sample transport problem if condensation should occur in the sample line. It is possible to remove water vapor with driers, but one must ensure that other analytes of interest are not being removed as well. Fine water droplets can be removed with coalescing filters, and in some cases large water droplets can be excluded by simply designing the sample line with several right-angle bends.

### 19.2.2

#### Sample Inlet

Several different techniques can be employed to introduce the sample into the mass spectrometer. These inlets must transition the sample from the higher pressure of the sample line to the vacuum required for the mass spectral analysis, yet this transition must occur without affecting the concentrations of the analytes of

interest. Specialized inlets are occasionally used for liquid sample analysis, and it is also possible to vaporize or sparge liquid streams for analysis; however, this discussion will only focus on the far more common application to gas stream analysis.

#### 19.2.2.1 Direct Capillary Inlets

These are used on most commercial process mass spectrometers. Often a 1 m long capillary of 10–100 µm inner diameter is sufficient to provide the necessary pressure drop. Deactivated fused silica is the most common capillary material, since it is reasonably inert and does not exhibit significant memory effects with most sample streams. Heating the capillary further reduces memory effects and pluggage due to condensation. Capillaries can also be made of other materials such as stainless steel or nickel if silica is problematic. Molecular leaks (pinhole orifices) are sometimes used, either in conjunction with or in place of the capillary. Porous frits, either of sintered glass or metal, are sometimes used to avoid pluggage problems with a capillary or molecular leak, but these can often exhibit greater memory effects.

#### 19.2.2.2 Membrane Inlets

These are used for many sample introduction systems. They are useful precisely because they violate the normal requirement that the sample introduced into the MS be representative of the sample stream, in that they exclude certain portions of the sample in order to reduce interferences or to preconcentrate the sample to increase the sensitivity. Membranes are sometimes used to directly sample volatile organics in liquid streams (e.g., VOCs in wastewater), permitting the analyte to permeate to the low pressure side of the membrane for direct introduction into the MS ion source without requiring vaporization or sparging of the liquid. Membrane inlets are also frequently used for ambient air monitoring for volatile organics, achieving a degree of preconcentration of analytes while minimizing the introduction of normal air gases. Calibration of membrane inlet systems can be more difficult than direct inlet systems, and standard membrane materials can be problematic for analysis of very polar compounds, but resources [2] are available to assist in the selection of the best membrane material and design of the system.

#### 19.2.2.3 Gas Chromatography (GC)

This is sometimes employed as a process MS inlet. Process GC–MS presents more fault and routine maintenance issues, and the delay associated with a chromatographic separation often negates the significant speed advantage of process MS. However, few analytical techniques are as powerful as GC–MS, especially for pilot plants and processes with very complex matrices or with frequent production of unknown byproducts. Commercial process GC–MS instrumentation is available, and is being ruggedized and made more rapid with further advances in the area of “fast-GC”.

### 19.2.3 Ionization

Ionization is the process by which the analyte of interest gains a charge, thus allowing it to interact with the electromagnetic fields of the mass analyzer. Electron impact (EI) ionization is used almost universally in process MS due to its stability and relative simplicity. In EI, sample molecules pass through an energetic beam of electrons emitted from a hot filament. This beam imparts a charge on the molecule, and frequently fragments the molecule into smaller charged particles. The profile of fragments for a given compound is very reproducible between instruments, and is known as a fragmentation pattern or cracking pattern. The electron beam energy is usually set to 70 eV, which provides very stable production of ions, even with minor variations in electron beam energies. Lower energies are occasionally used to achieve less fragmentation, which can be useful if the fragmentation patterns of stream components are very similar; however, this approach should be used with caution, since ion production can be erratic and the resultant component quantitation more variable. Use of 70 eV EI also permits comparison of unknown spectra with various EI-MS libraries, which are usually composed of 70 eV spectra.

Various filament materials are available for process MS. Tungsten is rugged and inexpensive, but not suitable for applications requiring accurate CO and CO<sub>2</sub> measurements due to outgassing and hydrocarbon reactions on the reactive W surface. Tungsten has a higher work function and thus operates at a higher temperature, which can help to heat the source to reduce adsorption and contamination. Rhenium is not commonly used for process MS, although it is useful for hydrocarbon measurement applications due to the reduced formation of CO and CO<sub>2</sub>. Thoriated iridium filaments have a low work function and hence produce large quantities of electrons at relatively low temperatures, which can contribute to filament lifetime; these are also very good for hydrocarbon and CO and CO<sub>2</sub> measurement applications. Choice of filament material is largely application-dependent, but thoriated iridium filaments usually offer the best balance of ruggedness and freedom from interference.

EI sources are available in either closed or open designs. In a closed design, the sample is introduced into a confined region that contains the ionizing electron beam. This confinement results in a higher concentration of sample (due to the limited conductance of the design) and higher degree of ionization, resulting in greater sensitivity. The disadvantage to this closed design is that the increased residence time of the gas components can result in greater source contamination, requiring more frequent cleaning. The open design permits better pumping and clearing of the source region, but this in turn causes a reduction in sensitivity. In either case, materials of construction for the source can affect the degree of contamination, especially in the case of polar molecules interacting with relatively active stainless steel surfaces. Either type can be heated with an auxiliary heater to reduce contamination from streams that contain high concentrations of hydrocarbons or polar ("sticky") molecules; if the analysis requirements are suited to tungsten filaments, the higher work function of W often provides sufficient radiant heating of the source to reduce contamination.

In addition to ion production and fragmentation, ion sources contain a number of ion lens elements that focus and accelerate the ion beam for injection into the mass analyzer. Contamination from the sample can alter the electrostatic fields of these lens elements, resulting in changes in performance that require more frequent recalibration or cleaning of the source elements. A careful assessment of the application at hand will lead to the best source design, often leading to analyzers that require routine maintenance only on an annual basis. For example, in the analysis of high concentrations of polar organics, a heated open source with Pt components might be warranted. For analysis of trace nonpolar compounds in ambient air, an unheated closed source would result in excellent sensitivity with minimal risk of source contamination.

Electron impact ionization is rugged, reliable and provides excellent precision and accuracy for most applications. However, the fragmentation of the parent molecules in the analysis stream can sometimes lead to spectra that are severely overlapped or even indistinguishable. For example, in certain hydrohalocarbon production processes, single halogens and hydrogens are easily cleaved from the parent molecules, resulting in virtually identical mass spectra. In such cases, it would be advantageous to utilize a softer ionization technique (i.e., one that predominantly produces charged parent molecules, with minimal fragmentation), such as chemical ionization (CI); indeed, both EI and CI mass spectra are often required for confirmation of compound identification in laboratory mass spectrometry. In the case of the hydrohalocarbons, the parent molecules would be easily distinguished with CI. However, in practice, CI is very difficult to utilize on-line, since the technique requires additional reagent gases, and is not as stable or rugged as EI. Softer ionization, either with CI or other techniques such as electrospray, glow discharge or field ionization, is an area of current research that promises to extend the utility of mass spectrometry for a number of difficult applications.

#### 19.2.4

##### Mass Analyzers

After the sample molecules have received a charge, and possibly undergone fragmentation, the charged particles are injected into the mass analyzer, sometimes referred to as the mass filter, which separates these particles according to their mass. In actuality, this separation is carried out on the basis of the mass-to-charge ratio ( $m/z$ ) of the particles. Many different types of mass analyzer designs are available, but magnetic sectors and quadrupoles are the most common choices for most process applications.

###### 19.2.4.1 Sector Mass Analyzers

These employ either an electric or a magnetic field to separate the charged particles that are injected from the ion source. The field bends the ions into a circular trajectory, with the heavier particles (higher  $m/z$ ) undergoing less of a bend than the lighter particles (lower  $m/z$ ). A static field can be used, with several detectors

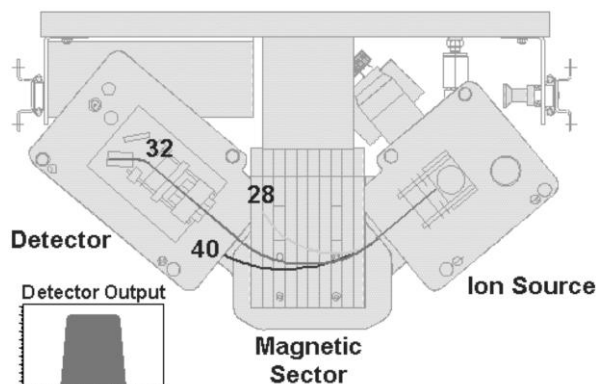


**Fig. 19.3** Magnetic sector mass analyzer, with  $m/z$  32 impinging on the detector; note flat-topped peak profile. (Used with permission of ThermoOnix Inc.)

placed in the path of the individual trajectories; this design offers good stability at the expense of flexibility, since a new detector would need to be installed if a new species needed to be monitored. A more common approach is to use a single detector and scan the field such that each trajectory falls on the detector as the field is swept; this offers a greater degree of flexibility, and modern electronics permit stability on a par with the static field design. Although either electric or magnetic fields can be utilized for sector MS, magnetic sector instruments are usually preferred for process MS because of their better long-term stability compared to electric sector instruments. Figure 19.3 illustrates a magnetic sector analyzer.

#### 19.2.4.2 Quadrupole Mass Analyzers

These consist of four parallel rods with the ends arranged in a square pattern as shown in Fig. 19.4. The rods at opposite corners of the square are electrically connected. An rf signal is applied to one set, and an equivalent but inverted rf signal is applied to the opposite set. Likewise, opposing positive and negative DC offset voltages are applied to the rod sets. This combination creates a resonance condition that permits particles with a specific  $m/z$  to travel down the length of the rods, while all other  $m/z$  particles are annihilated by collision with one of the rods or some other surface. By scanning the DC offset, different  $m/z$  particles will resonate to reach the detector, thus resulting in a mass spectrum. Although the small diameter quadrupole rods in residual gas analyzers are sufficient for some process monitoring applications, better stability for more complex processes is usually achieved with larger diameter rods designed for process mass analyzers.

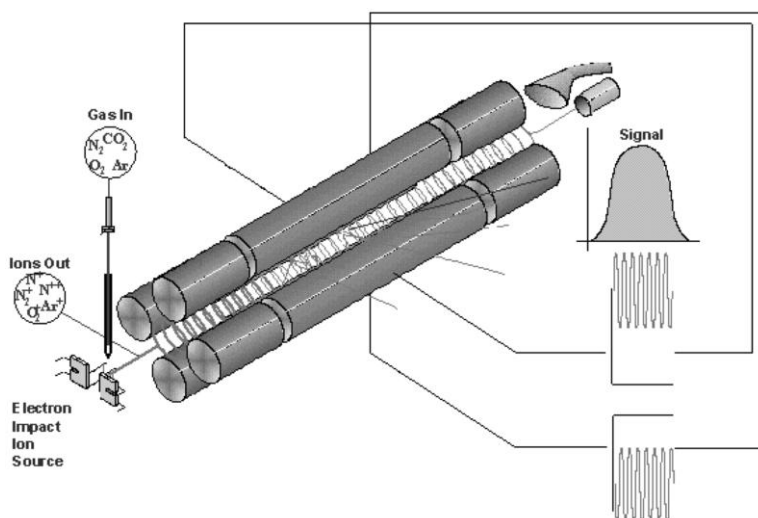


**Fig. 19.4** Quadrupole mass analyzer, with  $m/z$  32 impinging on detector; note gaussian peak profile. (Used with permission of ThermoOnix Inc.)

#### 19.2.4.3 Choice of Analyzer

The choice between magnetic sector and quadrupole mass analyzers depends upon the application. Magnetic sectors are inherently more stable for a number of reasons. The resulting peak shape has a flat top, which is less susceptible to small fluctuations in mass alignment. In contrast, the peak shape is gaussian with a quadrupole, which results in greater signal drift with only slight mass alignment fluctuations. This stability is particularly important in the case of overlapping fragmentation patterns, since matrix deconvolution algorithms can propagate significant error into the final result if stability is poor. Furthermore, with a magnetic sector, ion injection into the magnet field is typically at 1000 eV, compared to 3–5 eV ion injection into a quadrupole. In operation, both systems will experience a degree of contamination that will slightly change the electrostatics of the order of 0.1–0.5 eV within the analyzer; this effect is relatively insignificant to the 1000 eV of the magnetic sector, but is much more significant to the lower-energy quadrupole, requiring more frequent cleaning and more frequent calibration to compensate. This can be particularly important for contamination-prone processes, such as with high concentrations of hydrocarbons, halogenated compounds or sulfur compounds.

Quadrupoles are generally faster, less expensive, more compact and have higher mass ranges for analysis (up to 600  $m/z$ , compared with 200  $m/z$  for a magnetic sector). This last aspect makes them particularly well suited for analysis of trace VOCs in ambient air. Although the gaussian peak shape is more prone to drift, this is often not a problem for sample streams that do not contain components with overlapping fragmentation patterns. Likewise, a quadrupole may be ideal

for applications that do not involve significant amounts of contamination-inducing components, such as with air monitoring or many fermentation processes.

Other mass analyzer designs, such as time-of-flight, ion trap and ion cyclotron resonance, hold promise for higher resolution, faster analysis speed and increased mass range, but these designs are currently seldom used in on-line applications due to their complexity, higher cost and increased requirements for operator expertise. Other novel designs are on the horizon that utilize further advances in miniaturization, signal processing, and more stable electronics. As with all process analysis technologies, developments in laboratory instrumentation are often eventually transferred to process analyzers.

#### 19.2.5

##### **Detectors**

Most process analyzers utilize either a Faraday cup or a secondary electron multiplier (SEM) for detection. The Faraday cup is the simpler and more rugged and stable of the two, but is generally useful for detection of species at higher concentrations (100 ppm to 100 %). The SEM is much more sensitive, capable of measurements in the ppb range. It is quite common to configure a process MS with both detectors, along with a set of electrostatic lenses to switch the mass-filtered ion beam between the two detectors. This results in a single process analyzer that is capable of quantitation from 1 ppb to 100 %!

#### 19.2.6

##### **Vacuum System**

As shown in Fig. 19.1, the ion source, mass analyzer and detector are incorporated into a vacuum system. This vacuum must be sufficient (i.e., the mean free path must be sufficiently long) to prevent collisions between particles prior to analysis. A roughing pump is first used to provide vacuum for the sample inlet, as well as to provide the backing pumping for the turbomolecular pump, which provides the vacuum needed (between  $10^{-5}$  and  $10^{-7}$  Torr) for the ion source and mass filter. Specialized pumps and oils are available for corrosive processes. The fact that process MS requires vacuum pumps is often cited as a reason for avoiding the technique, but modern pumps are sufficiently rugged that they are rarely a cause of analyzer failure. Ion, getter and diffusion pumps are not routinely used for process monitoring, although getter pumps may become more common as process MS instrumentation is miniaturized.

#### 19.2.7

##### **Data Analysis and Output**

Figure 19.5 is an EI mass spectrum of a typical sample stream that might be associated with a fermentation process; for simplicity, only nitrogen, oxygen, argon and carbon dioxide will be considered. In the case of a particular  $m/z$  to which only one

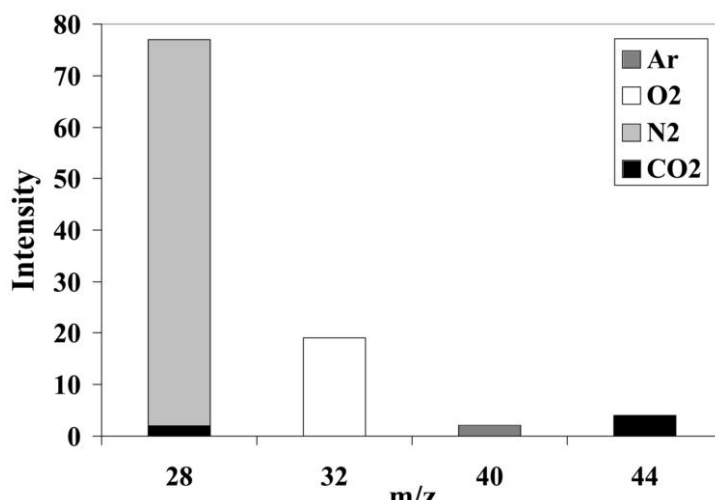


**Fig. 19.5** Mass spectrum of air, showing only relevant mass-to-charge (*m/z*) ratios.

compound contributes a fragment (e.g., for mass 32, only oxygen contributes a fragment), signal intensity (*i*) is simply a product of the sensitivity factor (*s*) and the concentration (*c*) of that one compound:

$$i = sc$$

In the case of oxygen, quantitation is then simply a matter of monitoring the intensity at *m/z* 32 and dividing by the sensitivity factor.

The situation is more complex when two or more compounds contribute ion fragments to the same *m/z*. In our fermentation example, *m/z* 28 is predominantly due to nitrogen, but carbon dioxide has a minor fragment at that same *m/z* (due to cleavage of an oxygen atom from the molecule), and thus contributes to the total signal at *m/z* 28, as seen at the bottom of this peak in Fig. 19.5. Carbon dioxide has a major fragment at *m/z* 44, to which no other compounds in the sample contribute fragments. Since fragmentation patterns are very consistent, one could measure the intensity at *m/z* 44, determine the concentration of carbon dioxide, and then calculate the relative contribution of carbon dioxide to *m/z* 28, thus correcting for the potential error in nitrogen quantitation due to the presence of carbon dioxide. In practice, this correction is performed in real-time via matrix deconvolution using least squares techniques, according to the simplified matrix:

$$C = S^T I$$

in which *C* is the concentration vector, *S* is the sensitivity  $\times$  fragmentation matrix, and *I* is the intensity vector. In practice, other factors are included in the deconvolution, such as detector gain weightings.

Resulting concentrations are often reported as relative concentrations, with all specified gases totalized to 100%, rather than as absolute concentrations. This

further enhances the stability of the measurements, since small changes in flow and pressure in the sample line are effectively normalized out. However, this can lead to measurement error if unknown or unexpected compounds are present in significant quantity. Close review with process engineers will usually assist in determining which mode is most appropriate for a given process.

Modern deconvolution algorithms and fast computers permit deconvolution of very complex matrices, and minor components can be measured in the presence of components that at first glance might seem to overlap too much to permit quantitation. However, instrument noise eventually places a limit on how well this will work in practice. A common rule of thumb is that a minor component cannot be deconvolved and accurately measured if the major component contributes more than 30 times the signal of the minor component for a given  $m/z$ . With this rough rule, one can use library spectra and historical or modeled stream composition information to determine if MS is a feasible solution for the application. One caution with using library spectra: these often do not include the contribution of minor elemental isotopes that result in trace peaks in the spectrum, and thus do not indicate the degree to which these trace peaks of major components will interfere with minor components. For example, formaldehyde has a major peak at  $m/z$  29, but nitrogen also has a fragment here due to the  $^{14}\text{N}^{15}\text{N}$  dimer; although minor, in air this dimer contributes much more to  $m/z$  29 than do ppm levels of formaldehyde, and thus prevents the measurement of formaldehyde at trace levels in air.

Modern process MS analyzers are controlled by microcontrollers and PC computers. Many incorporate internal processors that permit stand-alone operation, with a PC only required for initial configuration. The processor then handles all measurement and quantitation, as well as data interfacing, fault diagnosis and alarming, and calibration. Process mass spectrometers can be directly interfaced to plant distributed control systems, programmable loop controllers, or other process control systems.

#### 19.2.8

#### **Calibration System**

As might be deduced from the above discussion of data analysis, accurate quantitation requires accurate determination of fragmentation patterns and sensitivity factors for calibration. Several options are described below for calibrating a process MS, but all have some common issues. It is common for calibration software to permit one to calibrate the MS to one gas, and then establish the sensitivity of all other components relative to that first gas. For example, one might establish the absolute sensitivity factor of nitrogen, and then establish the relative sensitivity factors for oxygen (relative to nitrogen). Drift mechanisms within MS are such that they can usually be corrected by calibrating nitrogen alone more frequently, and only occasionally re-establishing the relative sensitivities of oxygen. Since instrument drift can be caused by a number of factors, some of which might not have an equal effect on all gases, this relative sensitivity calibration scheme should be checked for each application. However, most commercial process MS vendors

can provide recommendations on the frequency of calibration for common applications. In many cases, it is necessary to perform a complete recalibration only on a monthly basis. A complete recalibration should also be performed following any maintenance on the analyzer, especially if the ion source has been cleaned or the filaments replaced.

#### 19.2.9 **Gas Cylinders**

Gas cylinders are commonly used for process MS calibration because of their relative simplicity and economy. Cylinders should be prepared gravimetrically, ideally by a supplier experienced in the preparation of accurate trace gas mixtures. Caution must be exercised in relying completely on gas cylinder suppliers' certificates of analysis, and it is frequently advisable to validate cylinders via another primary technique such as GC, although one should first scrutinize how that primary technique is itself calibrated. Stability of the gas mixture must be checked. PTFE-linings and electropolished cylinder interiors are often used to slow degradation.

In practice, fragmentation patterns are determined with a series of binary mixtures of a specific analyte and an inert balance gas (frequently Ar, He or N<sub>2</sub>) that does not produce fragment ions that overlap with the analyte of interest. Background signals (due to trace leaks or minor filament outgassing) can be corrected by calibrating with an additional cylinder containing only the balance gas. Finally, it is common to have an additional cylinder of a representative gas mixture for fine tuning of sensitivities and correction of errors due to differences in gas viscosities.

#### 19.2.10 **Permeation Devices**

Permeation devices have long been used for calibrating process analyzers, and they are an excellent alternative to gas cylinders, particularly if the analyte is unstable in a cylinder at low concentrations. These devices make use of the fact that most liquid compounds permeate through polymers at a constant rate for a particular temperature and gas flow rate. In practice, a known amount of liquid of a particular compound is sealed within a polymer tube (often PTFE) of known dimensions, which in turn is placed within a thermostatted container. A carrier gas, often dry air or nitrogen, is then swept at a constant rate through the container, thus transporting a constant amount of the compound of interest to the analyzer. Permeation devices can be gravimetrically calibrated to a high degree of accuracy, and in turn provide a very accurate means of calibrating process analyzers. Permeation rates are low, making these devices particularly useful for calibration at trace levels; this also means that the polymer tubes need to be refilled usually only a few times a year.

**19.2.11****Sample Loops**

Sample loop calibrators are commonly used for low concentration analytes that are difficult to prepare or are unstable in gas bottles. They are also extremely flexible, in that new compounds can be calibrated upon acquisition of a sample of the pure compound in liquid form. Sample loops are basically small heated known-volume vessels into which a small amount of liquid standard is injected. The sample vaporizes, and the entire volume is then pumped past the inlet, into which a small amount of the vapor is drawn for calibration. Drawbacks of sample loops include the lack of automation for unattended calibration, and inaccuracies inherent in making manual injections of nanoliter-scale liquid volumes. For ambient air monitoring of toxic compounds, one should bear in mind the safety implications of handling syringes that contain potentially hazardous analytes.

**19.2.12****Maintenance Requirements**

Maintenance requirements for process mass spectrometry are generally less than with process gas chromatography, which process MS often replaces. In general, one should check pump oil levels and color on at least a weekly basis. The degree of oil darkening is often an indicator of aging, but even in the absence of color change, the oil should be replaced semi-annually. In certain processes, ion source filaments often remain in service for over a year, but it is generally recommended that active filaments be replaced on the same schedule as the pump oil. Ion sources may need to be cleaned with some regularity in certain processes. Filters for samples and cooling air should be monitored and changed as required. Most commercial process MS analyzers incorporate sophisticated diagnostics capabilities to alert when there is a problem requiring correction or maintenance.

**19.2.13****Modes of Operation**

Process mass spectrometers are used predominantly for continuous quantitation of compounds that are included in the initial configuration. In the interest of speed, only the  $m/z$ s that are required for the analysis are measured. However, one of the most powerful aspects of process MS is the ability to do qualitative analysis on process streams. This is particularly useful for pilot plant operation, or for diagnosing process upsets in scaled-up processes. Several commercial vendors provide instruments that can operate routinely in quantitative mode, then occasionally perform a full mass scan to be archived for future scrutiny if a problem is subsequently detected downstream of the MS sample point. These full mass scans can be compared with library spectra to identify new byproducts. Some systems incorporate rather sophisticated pattern recognition and deconvolution algorithms that can achieve a degree of semiquantitation with no a priori knowledge of sample compo-

nents or concentration. While this can be an extremely powerful application of MS, such automated compound identifications are best confirmed by someone with some training in mass spectral interpretation.

### 19.3 Applications

Process MS is commonly used for gas analysis in many manufacturing processes, including:

- Fermentation off-gas
- Steel manufacturing (blast furnace gases, etc.)
- Ethylene oxide
- Ethylene cracking
- Ammonia
- Partial oxidation of hydrocarbons

In addition, MS has also proven to be an excellent choice for ambient air monitoring in such processes as:

- Vinyl chloride monomer
- Ethylene oxide
- Acrylonitrile–butadiene–styrene (ABS) polymer processing
- Solvent monitoring (toluene, benzene, acetone, dimethylacetamide, etc.)

Due to its speed and flexibility, process MS is very useful for pilot plant studies, and for troubleshooting process upsets [3]. In many cases, a “roving” MS can be installed temporarily to gather as much process development information as possible, or to solve a vexing upset problem. Subsequently, it may be determined that a simpler, single-component analyzer is sufficient to control the process, but this determination is now based upon comprehensive real-time empirical data rather than on process models alone. Many process analyzer professionals spend much time retrofitting analyzers into new processes that were designed with inadequate or inappropriate monitoring capabilities. Pilot plant installations of powerful analyzers such as mass spectrometers can avoid such retrofits and thus greatly speed time-to-market of new products.

Development of new applications can be a complex exercise for any process analyzer technology, including MS. One must consider what stream component information is required to control or monitor the process, including analysis accuracy and precision, as well as how rapidly such information is required. One should determine the concentration ranges expected in both normal and upset conditions; a process analyzer is frequently of greatest value in helping to recover rapidly from upsets, so one must take care that it will operate accurately at those times. Additionally, data regarding sample stream temperature, pressure, and flow are required to design an appropriate sample conditioning system. The range of ambient conditions will dictate the design of the analyzer housing or shelter. Finally, one

should compare the analyzer maintenance requirements to the expertise and availability of local maintenance personnel. In many cases, more than one analyzer technology may appear to be suitable, which can lead to emotions and vendor loyalties playing a disproportionate role in the final analyzer decision. However, the best solution usually appears if one reiterates through the above process, involving both process engineers and line operators in the information gathering.

### 19.3.1

#### **Example Application: Fermentation Off-gas Analysis**

Fermentation processes are commonly monitored with mass spectrometry, and serve as an excellent application to demonstrate the accuracy, flexibility, and economical benefits of the technique. Fermentation processes are common in pharmaceuticals, brewing and ethanol production processes, and are an active area of industrial research as a possible alternative to classical petrochemical processes. Fermentations are usually performed in agitated tanks, known as fermentors, that contain the organism of interest and various nutrients; gases are sparged into the fermentor to provide the required level of oxygen. Although fermentations can be monitored with several other techniques, mass spectrometry offers the advantage that it can measure major air gases ( $N_2$ ,  $O_2$ , Ar,  $CO_2$ ), as well as trace volatile organic species (ethanol, toluene, acetic acid, etc.) that are present in the headspace of the fermentor. In addition, MS is ideal for fermentation process development and scale-up, since one instrument can be multipointed to several fermentors, with each requiring different measurement methods. Thus, although the initial analyzer expense can be quite substantial, the resultant cost per analysis per sample point frequently makes MS more economical than installing individual discrete (i.e., single-component) analyzers on each fermentor. Often the economics are such that two MSs can be installed in such a way that each monitors half of the total number of fermentors (thereby effectively halving the measurement cycle time); in the event of an analyzer failure, the remaining functioning unit can then switch to monitoring all fermentors while repairs are made.

With most aerobic fermentations, it is important to accurately measure the respiratory quotient (RQ), which is the ratio of  $CO_2$  evolution to  $O_2$  uptake. Although RQ can be determined using discrete oxygen and carbon dioxide monitors (paramagnetic and infrared analyzers, respectively), such an approach could lead to errors due to differing drift characteristics of the separate monitors. With MS, both gases can be measured on the same instrument, thus increasing both accuracy and precision. (This same benefit is important for many other processes such as partial oxidation of hydrocarbons, in which a single analyzer can be used to monitor both oxygen and the hydrocarbon, thus increasing efficiency and safety.) In addition, the MS can also measure  $N_2$  and Ar, which are not usually consumed in the fermentation process, and these measurements can then be used to calculate total flow in and out of the fermentor; in practice, however, it is common to use flow meters for such measurements, and have the MS running in a relative concentration mode.

As stated above, volatile organic species can be measured in the headspace with MS. The liquid-phase concentration of these same components can then be inferred using Henry's Law. This assumes that the fermentation media is well mixed, and that none of the volatile species is present in the fermentor gas inlet. Although thermodynamic properties can be used to calibrate for these liquid phase concentrations, it is generally best to inject a known amount of the compound of interest into the media, measure the liquid phase concentration with a laboratory technique such as gas chromatography, and calibrate the MS measurements against these liquid measurements. Camelbeeck et al. [4] have demonstrated that headspace component measurements are not affected by changes in the rate of mixing by aeration and/or agitation.

The flexibility of MS can further be utilized to monitor for microorganism mutation in certain situations. For example, in one proprietary process, the microorganism is known to be prone to a mutation in which the resulting mutant produces a small amount of hydrogen during glucose metabolism. The MS can be configured to monitor for hydrogen occasionally, and thus alert to this condition well before the reduced product yield is detected.

Table 19.1 contains composition information for a typical aerobic fermentation off-gas stream, along with the precision that is achievable with a magnetic sector process MS. Table 19.2 contains the fragmentation pattern matrix for this same sample stream; note that this is similar to the example presented above in the discussion of data analysis, but this particular stream now contains ethanol. This more complicated stream presents further challenges to deconvolution due to more severe fragmentation pattern overlap: ethanol interferes with the direct

**Table 19.1** Fermentation off-gas composition, with precision obtained with process MS.

Analyte	Mol %	Precision (% absolute)
Nitrogen	79	0.006
Oxygen	16	0.004
Argon	1	0.001
Carbon dioxide	4	0.004
Ethanol	0.06	0.001

**Table 19.2** Fragmentation pattern matrix for fermentation off-gas.

Mass ( <i>m/z</i> )	Nitrogen	Oxygen	Argon	Carbon dioxide	Ethanol
28	100			5	
31		0.015			100
32		100			
40			100		
44				100	
45				1.2	45.2

**Table 19.3** Recommended calibration gases for aerobic fermentation process, with ethanol.

<b>Component</b>	<b>Cylinder 1</b>	<b>Cylinder 2</b>	<b>Cylinder 3</b>	<b>Cylinder 4</b>	<b>Cylinder 5</b>
Nitrogen	78.08			79	
Oxygen	20.95			16	
Argon	0.934			1	
Carbon dioxide	0.033	5		4	
Ethanol			0.08	0.06	
Helium	99.999	balance	balance		

simple measurement of oxygen, carbon dioxide interferes with nitrogen, and ethanol and carbon dioxide interfere with each other. Note, however, from the precision values shown in Tab. 19.1 that the deconvolution algorithm adequately accounts for these overlapping fragmentation patterns.

Table 19.3 describes the set of gas standards that would be used for this fermentation monitoring application. Gas cylinders are the recommended calibration method for this application because accurate and stable mixtures can be procured from many gas suppliers. As described above in the calibration section, initially a complete calibration must be performed with all calibration gases, to be repeated monthly, with a weekly or daily subset calibration with nitrogen alone to correct for most normal instrument drift. Frequency of calibration is very application

**Table 19.4** Process mass spectrometry.

<b>Characterized parameter:</b>	<b>Surface specificity:</b>				
Mass-to-charge ratio (Molecular mass of ions)	Information depth: n/a	Detectability: ppb to 100 %			
<b>Type of information:</b>	<b>Resolution:</b>				
Molecular composition (quantitative, qualitative)	Depth: Not used for spatially resolved analysis.	Lateral: Other:			
<b>Measurement environment: Difficulties</b>	<b>Time needed for analysis:</b>				
Vacuum	Fragmentation pattern overlap	Total: 5 s/analyte/stream (excluding sample transport time)			
<b>Equipment:</b>	<b>Cost [ECU]:</b>	<b>No. of facilities:</b>			
Magnetic sector or Quadrupole Mass Spectrometer, Electron Impact ionization	60,000–150,000	Fairly common			
<b>Type of laboratory:</b>	<b>User skill needed:</b>	<b>Sample</b>			
n/a	Unskilled	Form Type: Gas, occasionally for dissolved VOCs with use of membrane inlet			
<b>Techniques yielding similar information:</b>					
FTIR, GC, IMS					

dependent, and the above schedule may be adjusted as dictated by the required accuracy and precision for process control. In this example, Cylinder 1 is pure He, used to establish background levels for all analytes. Cylinder 2 is essentially dry air, used to establish sensitivities for nitrogen, oxygen and argon. Cylinders 3 and 4 are used to establish the fragmentation patterns and sensitivities for carbon dioxide and ethanol, respectively. (Although ethanol has the major peak at  $m/z$  31, the minor peak here from a major component, oxygen, usually dictates that  $m/z$  45 is required for the analysis of ethanol.) Finally, Cylinder 5 contains a mixture that closely resembles the stream composition, and this is used to fine-tune the sensitivities of all gases and correct for viscosity differences. Cylinder 5 also constitutes what is commonly known as a check blend: if operators have reason to suspect that the analyzer is reporting incorrect values, they can switch to monitor this check blend for validation of the instrument.

#### 19.4 Summary

As will have become tediously apparent to the reader of this chapter, any potential installation of process MS application requires a thorough review of the process, including the key information that is needed to control it. This is true for any process analysis technology. As described above, process MS offers several options for each part of the overall system, and therein lies much of the unique flexibility of the technique. Again, a thorough process application review will narrow the choices for components. In addition, several process MS vendors and consultants are very experienced at designing systems to meet the needs of the process.

Table 19.4 summarises the main relevant characteristics of process mass spectrometry.

Process MS is a reliable technique that can provide rapid and precise multicomponent analysis on process streams. The ability to monitor multiple sample points with a single analyzer makes MS very economical for many applications, even with the high cost of the analyzer itself. Maintenance requirements on modern MS analyzers are on a par with or lower than most other analyzer technologies. In addition to permanent installations for routine process control, these attributes also make process mass spectrometry extremely useful for process development and troubleshooting.

## References

- 1 J. Workman, D. J. Veltkamp, S. Doherty et al., *Anal. Chem.*, **1999**, *71*, R121–R180.
- 2 M. A. Lapack, J. C. Tou, C. G. Enke, *Anal. Chem.*, **1991**, *63*, 875A.
- 3 M. A. DesJardin, S. J. Doherty, J. R. Gilbert et al., *Process Control Qual.*, **1995**, *6*, 219.
- 4 J. P. Camelbeeck, D. M. Comberbach, M. Orval et al., *Biotechnol. Tech.*, **1991**, *5*, 443.

## 20

# Elemental Analysis

*J. S. Crighton*

### 20.1

#### Applications of Atomic Spectrometry in Process Analysis

Elemental analysis in general, and atomic spectrometry in particular, play a key role in all aspects of process development, optimisation and control. The most obvious aspects of this contribution are in the control of the composition of the product itself. For example, in the cement industry, X-ray fluorescence (XRF) has long been used to measure the elemental composition of kiln feed (particularly Ca, Si, Fe and Al concentrations), since this can affect the efficiency of operation of the kiln as well as the quality of the clinker produced [1, 2]. Similarly, in the metallurgical industry, XRF has been used alongside atomic emission spectrometry (AES), particularly utilising arc/spark sample introduction systems, to control alloy composition during the production process (see e.g. [3–12]). In other cases, atomic spectrometry may be used on a quality control basis to control the content of specific additives in the final products. For example, inductively coupled plasma atomic emission spectrometry (ICPAES) is often used to measure Ca, Mg, P and Zn in lubricating oils as a means of checking that the correct concentrations of additives have been added to the products [13]. Other applications, which are perhaps less obviously directly related to process control, can still play an equally important role in terms of overall operation of the process and some of these are described briefly below.

Detailed description of all aspects of the application of atomic spectrometry to analysis of the huge variety of sample matrices associated with industrial processes is clearly outside the scope of this chapter and so only a brief overview is given of each application area. For detailed discussion of the application of atomic spectrometry in industrial analysis, the reader should refer to the annual reviews of this topic published in *Atomic Spectrometry Updates* in conjunction with *J. Anal. At. Spectrom.*, [3–12]. In Section 20.2, specific applications of atomic spectrometry to on-line/at-line analysis are discussed in more detail.

### 20.1.1

#### Catalyst Control

In order to achieve optimum performance from any catalytic process, it is essential that the concentrations of active components and any associated promoters are maintained within relatively narrow boundaries. For homogeneous catalysis processes, it is relatively easy to take samples and analyse using ICPAES or XRF in order to ensure that optimum concentrations are maintained and this application also lends itself well to on-line or at-line approaches (see Section 20.2). For heterogeneous catalysts however, the taking of regular samples is generally much more difficult and the contribution of atomic spectrometry may be restricted to process development at the pilot plant stage or analysis of post-mortem samples. Again, ICPAES or XRF may be used for analysis of heterogeneous catalysts, depending on the support matrix and active elements which require to be determined. ICPAES suffers from the obvious disadvantage that samples normally require to be digested prior to analysis but XRF generally has poorer limits of detection and can suffer from particle size effects and other matrix effects arising for example from the presence of coke or corrosion metals in used catalysts. Atomic spectrometry can also be used as a means of agreeing settlement prices (based on precious metal concentrations) between catalyst suppliers and users, although due to the high values involved, the analytical precision required (often agreement within 1 % for analyses carried out by each party), can necessitate use of more labour intensive, time consuming analytical approaches (e.g. fire assay).

Performance of heterogeneous catalysts can be adversely affected by the presence of poisons in feedstocks, even at very low (e.g.  $\text{ng g}^{-1}$ ) concentrations since these can become more concentrated on the catalysts. Similarly, low concentrations of catalyst elements can migrate into downstream parts of the process, where they can cause problems with downstream catalysts. For example, low ( $\text{ng g}^{-1}$ ) concentrations of iodine in acetic acid (originating from the catalyst), can cause poisoning of the vinyl acetate catalyst. For precious metals, even very low concentrations migrating into the products can have a significant economic impact on the process by the time they are multiplied up by high flow rates and extended operating times. Although ICPAES can be used for some of these applications, limits of detection can often be inadequate and more sensitive analytical techniques such as inductively coupled plasma – mass spectrometry (ICP-MS) must be used. For the determination of poisons on heterogeneous catalysts, the nature of the potential poisons is generally unknown and it can be difficult to choose a sample digestion approach which can be guaranteed to retain all possible elements. In these cases, laser ablation ICP-MS can be extremely useful in view of the low limits of detection which can be achieved and broad elemental coverage without the necessity of digesting the sample (and danger of losing elements through precipitation or volatilisation).

Although in most cases it is sufficient to determine total concentrations of elements in the samples, in a few instances, it is necessary also to determine the chemical species present. ICP based techniques lend themselves well to these requirements since they can be readily combined with chromatographic techniques

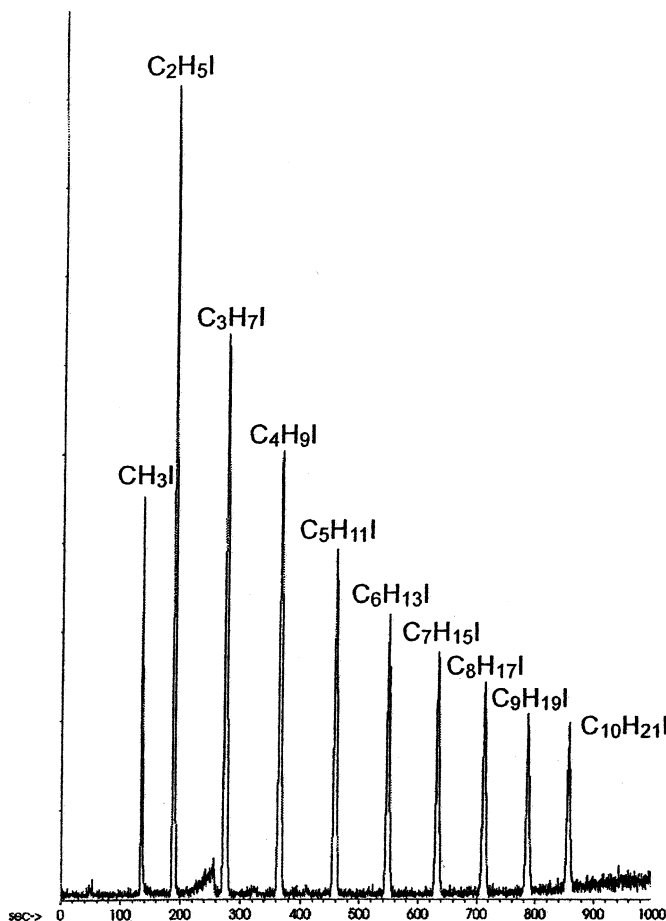


Fig. 20.1 a

**Fig. 20.1** (a) GC-ICPMS trace of standard obtained from an intermediate stream within a containing 350 ppb alkyl iodides in acetic Acid mixed acid/anhydride carbonylation process. and (b) similar trace (to Figure 20.1 (a))

(see [3–12]). For example, Fig. 20.1(b) shows a chromatogram obtained from an intermediate stream within a mixed acid/anhydride carbonylation process, analysed using capillary gas chromatography coupled with ICP-MS (the corresponding chromatogram obtained from a standard containing 350 ng g<sup>-1</sup> of mixed alkyl iodides in acetic acid is shown in Fig. 20.1(a) for comparison). The ICP-MS was used to monitor mass 127, providing a completely iodine specific detection for the GC system, thus allowing measurement of organo-iodine compounds in the process sample down to ng g<sup>-1</sup> levels. A full knowledge of the iodo compounds present at various stages of the process can allow the process to be optimised to ensure low concentrations of residual iodine in the products.

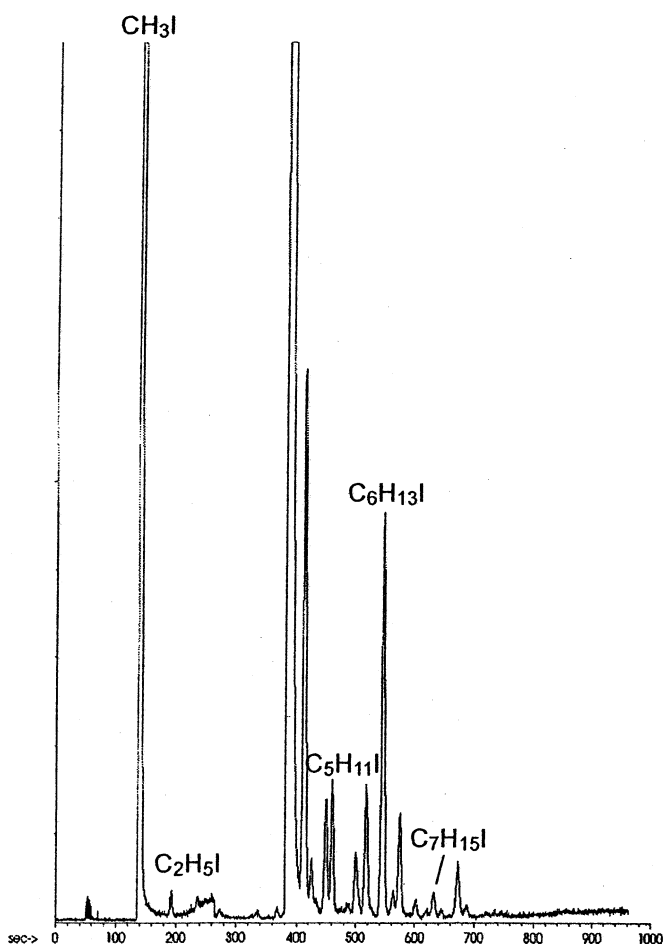


Fig. 20.1 b

## 20.1.2

**Corrosion Monitoring**

Corrosion of component parts of the process plant can be readily monitored by measuring the concentrations of associated “corrosion metals” (e.g. Fe, Ni, Cr, Mn, Mo) in downstream process streams or products. In view of its rapid, multi-element capability, ICPAES lends itself well to these applications, although ICP-MS with its inherently lower detection limits, can permit measurement of lower rates of corrosion and of minor alloy components which can aid in identifying which plant component is corroding.

In many cases, the alloy composition of the major plant components will be known and the one responsible for the corrosion can often therefore be identified from the ratios of the concentrations of the “corrosion metals” measured in the downstream process streams or products. In cases where the alloy compositions are not known, however, obtaining this information can be difficult, since it is often impossible to analyse the material without destructive sampling and accessibility restrictions may prohibit analysis using portable analytical equipment. In these instances, a technique which has regularly been used within the BP Group is the XRF “Rubbing” technique. This technique, which was developed at the BP Research Centre in Sunbury involves gently abrading/polishing the surface of the alloy of interest with a flexible polymer disk impregnated on one side with 15 µm diamond particles (661X; 3M, St Paul, MN, USA). During this process, approximately 1 mg of sample is transferred onto the surface of the disk. Since it is only the tips of the diamond particles which abrade the alloy surface, the metal transferred onto the rubbing disk is in the form of very small particles of less than 1 µm. Thus, in XRF terms, the sample is in the form of a “thin film” resulting in no absorption and/or enhancement effects. This therefore gives rise to universal, linear calibrations for the elements of interest, which are independent of alloy type. The resulting rubbing disks can be analysed by wavelength dispersive (WD) or energy dispersive (ED) XRF using relative element response factors (determined either empirically or calculated using fundamental parameters) and results normalised to 100 %. The results are thus independent of the weight of sample transferred to the rubbing disk and analysis can be accomplished with few or no calibration standards. The method can be used for any alloy type and gives results which are typically within 5 % relative (95 % confidence) for elements in the concentration range 0.1 to 100 % (lower concentrations can be measured by analysing the disks using laser ablation ICP-MS [14].

Figure 20.2 shows results obtained for a number of elements in a variety of alloy types including aluminum, copper, iron, nickel and titanium based alloys using an

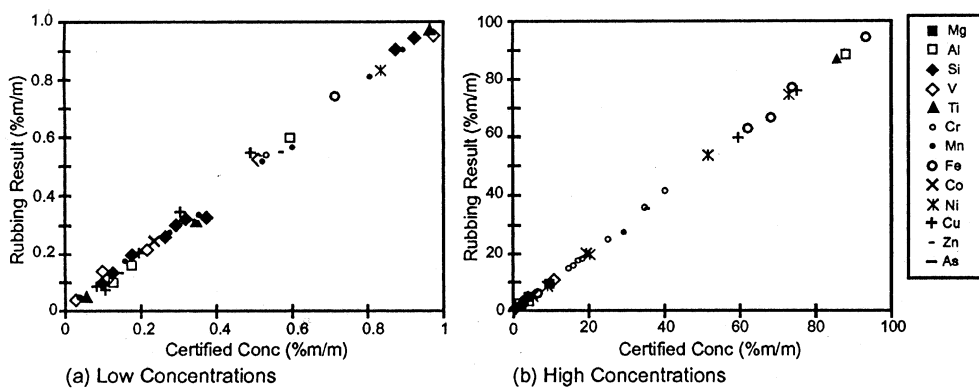


Fig. 20.2 XRF “rubblings” results obtained for aluminum, copper, iron, nickel and titanium based alloys: (a) Low concentrations; (b) high concentrations.

EDXRF spectrometer with calibration based on element response factors calculated using fundamental parameters (no standards). The advantages of the technique are that it is fast, simple, essentially non-destructive and can be used to sample an item of almost any shape or size, in almost any location without requiring any special tools or equipment. The sampling can even be carried out by plant personnel and posted to a remote laboratory for analysis. The only real precaution required is that since only 1 mg of material is transferred to the rubbing disk, the sample surface should be clean and representative of the component as a whole. This can usually be accomplished by cleaning the components with solvent and then abrasive paper prior to sampling, although in cases of severe corrosion, it may be necessary to remove surface contamination with a scurfing tool prior to final clean-up and sampling. The method has even been used for analysis of welds in order to check that correct welding rods had been used by contractors.

### 20.1.3

#### **Reducing Environmental Impact**

With the increasing public awareness regarding the environmental impact of industrial processes and products, there is increasing pressure on companies to ensure not only compliance with any existing legislation but also that all possible steps are taken to minimise any risks of adverse effects. Again, atomic spectrometry plays a pivotal role in this assurance process. This can range from ensuring low concentrations of harmful components in the products produced to ensuring that any potentially hazardous components in waste streams and products are eliminated or minimised and that any residual hazardous waste is treated and/or disposed of in a responsible manner.

The pressure to reduce environmental damage generally results in an ever increasing drive to measure harmful components at lower and lower levels and this can put pressure on analytical techniques used to make the measurements. For example, EDXRF and WDXRF are widely used throughout the industry for determination of sulfur in petroleum products. However, the continuous tightening of legislation and lowering of specification levels for sulfur in road transport fuels over recent years has resulted in some international standard methods and some instrumentation being inadequate for use at the lower sulfur specification levels. A report detailing which methods are adequate for the European fuel specifications for 2005 ( $50 \text{ mg kg}^{-1}$  S max.) and beyond has recently been published [15].

For measurement of heavy metals and other harmful trace elements in effluents and solid waste, standard methods are available which generally utilise digestion and/or concentration followed by analysis using atomic absorption spectrometry (AAS), ICPAES, or increasingly ICP-MS. A comprehensive range of such methods has been produced by the US Environmental Protection Agency [16]. For a more detailed discussion of the use of atomic spectrometry in environmental analysis, the reader is referred to the comprehensive annual reviews of this topic produced as *Atomic Spectrometry Updates* [17–26].

## 20.1.4

**Troubleshooting Process Problems**

Many process problems fall into one of the categories already described above. However, often problems can be associated with formation of deposits of unknown origin and composition in various parts of the plant. For a completely unknown deposit, XRF is generally more suitable than solution techniques such as ICPAES or AAS since only small amounts of material are often available and it can be very difficult to decide on a digestion approach if the nature of the material is unknown. Qualitative analysis of deposits using XRF is generally straightforward but obtaining quantitative results can be difficult since, by the very nature of the sample, appropriate calibration standards are not available. One approach to this problem which has been used at the BP Research Centre for many years is the XRF 'SMEAR' technique [27]. In this approach, the sample (down to 10 mg) is ground and mixed with zirconium oxide and a small amount of the mixture (about 1 mg) is slurried with a few drops of ethanol and smeared on the outside of the polymer film window of an X-ray cell. This results in production of a thin film sample which can be analysed by XRF with virtually no absorption/enhancement effects using universal calibrations produced using simple oxide standards. By ratioing the net element intensities to that of zirconium, effects of sample thickness (weight) and film distribution/homogeneity can be compensated. Accuracy/precision of the 'SMEAR' technique has been shown to be  $\pm 10\%$  relative and the technique can be used to measure element concentrations in the range 0.1 % m/m to 100 % m/m.

Another approach to semi-quantitative analysis of unknown samples such as deposits is to produce theoretical calibrations based on fundamental parameters. The problem with this approach is that it relies on carrying out a complete analysis of the sample in order to correctly calculate corrections for matrix effects. Unfortunately, many deposits contain high concentrations of light elements such as carbon which cannot be reliably determined using XRF. Unless this information is obtained in another way (e.g. using an alternative analytical technique such as microanalysis), concentrations calculated using fundamental parameters can be seriously in error (for example, many programmes will assume that all of the elements which can be measured represents 100 % of the sample, even although in reality they may only comprise 10 % of the sample with the rest being carbon). Another problem with some fundamental parameter approaches is that they assume that the sample is a bulk sample and no thickness corrections are applied. Again, this can lead to serious errors if only a very small amount of sample is available. Some XRF instruments utilising fundamental parameter approaches can get round these problems by using measurements of scattered X-ray tube lines to gain information about the concentration of low mass elements which cannot be measured directly and this information can be fed into the fundamental parameter calculations.

Figure 20.3 shows results obtained with a Spectro X-Lab EDXRF spectrometer utilising this approach for samples with light element concentrations (loss on ignition) up 57 % m/m. Accuracy for the major elements is generally similar to that

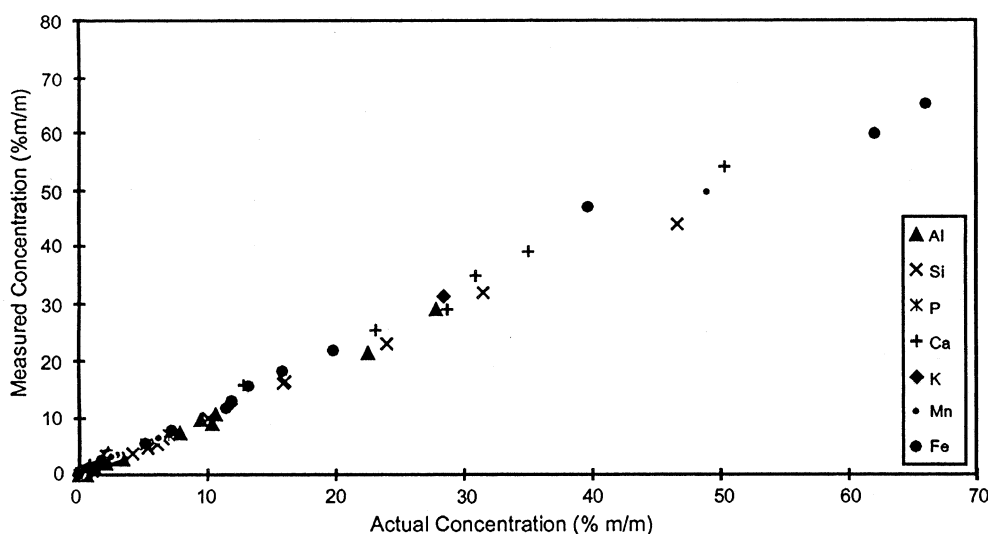


**Fig. 20.3** EDXRF results for a wide variety of reference materials with loss on ignition up to 57% m/m obtained using fundamental parameter calculations with correction for unmeasured light elements using scattered radiation.

obtained using the 'SMEAR' approach, but the X-Lab method has the advantages that it can measure down to much lower concentrations ( $\text{mg kg}^{-1}$  levels) and is less operator dependent (obtaining the correct film thickness for the 'SMEAR' technique and producing well dispersed films without agglomeration is somewhat of an art which must be perfected by the operator). Utilising one of these approaches for semi-quantitative analysis using XRF, the nature of most deposits comprising inorganic components can normally be established, particularly when used in conjunction with X-ray diffraction (XRD).

## 20.2 On-stream/at-line Analysis

At the present time, most elemental analysis for process control is still based on laboratory analysis as described above. With currently available analytical technology, in many cases, this is the only viable approach. However, where measurements can be carried out on-stream or at-plant, the benefits can be substantial. With traditional laboratory based analysis, sampling frequency is limited and labour costs can be substantial if continuous round-the-clock process monitoring is required. On-stream analyses can provide the capability of closed loop control of the process allowing optimum operating conditions to be maintained, minimising costs and resulting in a more stable product with fewer off-specification products produced. On-stream analysers can also be used to control product blending to

specification limits with less ‘give-away’ from production of over specified product. However, one must bear in mind that typical costs for a fully installed on-line system, complete with sample conditioning and safety systems are about an order of magnitude higher than that of a similar at-plant system. These additional costs can only be justified where a very high sampling frequency is required and where the closed loop control loop can make major improvements to the operation of the process. In many cases, particularly with continuous processes, the high frequency sampling may only be justified during the period where process conditions are changing rapidly (e.g. start-ups or shut-downs). During steady-state operations, the benefits of the high sampling frequency may be marginal. In these cases, an at-plant approach may be more appropriate from a cost-benefit point of view. In this section, on-stream applications of atomic spectrometry for process analysis/control are discussed, however, virtually all of the approaches described could equally be applied on an at-stream basis.

### 20.2.1

#### X-ray Fluorescence (XRF)

For on-stream elemental analysis, by far the most suitable and widely used technique is XRF. The technique is particularly suitable for on-stream applications since it is robust, non-destructive, uses no hazardous reagents, requires minimal maintenance and can be easily mounted in an inherently safe enclosure. The technique is capable of simultaneous measurement of elements from Al to U in the concentration range from ppm levels up to high percentages and in many cases can achieve precisions of 1% RSD or better. Analysis times vary depending on the particular application and type of equipment used but a typical cycle time would be a few minutes, thus lending itself to closed loop control systems requiring a high sampling frequency.

Figure 20.4 shows a schematic diagram of a typical on-stream XRF analyser. The figure shows a flow cell for on-stream liquid analyses, but this could equally well be a specialised cell designed for powder/slurry analysis, a conveyer belt containing solid material, or even a continuous flowing solid material such as a roll of paper (further details of these specialist applications are given in Sections 20.2.1.3 and 20.2.1.4). The flowing sample is irradiated with a source of X-rays (normally either an X-ray tube or a radioisotope source) and the fluorescent X-rays produced in the sample are measured using a detector appropriate to the particular application involved.

For efficiency of excitation, the energy of the X-ray source should be close to, but higher than the absorption edge for the element(s) to be measured. Traditionally radioisotopes were used as the source of X-rays for on-stream XRF analysers. Table 20.1 shows typical isotope sources used and the range of elements which they can be used for. These sources have the advantages that they are small, have good stability and require no external power. However, as shown in Tab. 20.1, the sources decay at vastly different rates. Some, such as  $^{109}\text{Cd}$  and  $^{55}\text{Fe}$  will decay and require replacement every few years (during which time performance will be degrad-

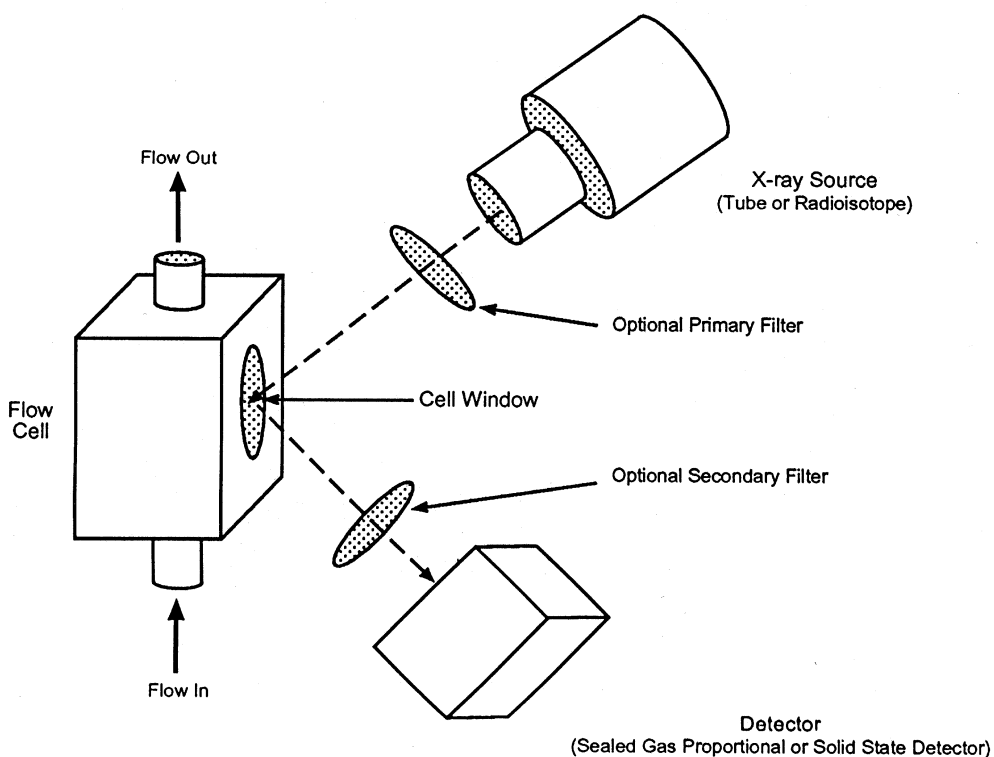


**Fig. 20.4** Schematic diagram of on-stream EDXRF analyser.

ing all the time), whereas others such as  $^{241}\text{Am}$  have half lives measured in several hundred years which can present disposal problems. Furthermore, the flux produced by radioisotope sources is generally too low for use with high resolution (WDXRF) detectors and the excitation efficiency is not high for all elements. A further complication is that the X-ray source cannot be switched off, which can hamper maintenance operations and can present a potential safety hazard. For these reasons, most modern systems now use an X-ray tube as the source. Excitation efficiency of the X-ray tube is generally higher than with radioisotope sources and can be optimised through use of an appropriate tube anode material, operating vol-

**Table 20.1** Common isotope sources for XRF analysis.

Source	$^{55}\text{Fe}$	$^{241}\text{Am}$	$^{109}\text{Cd}$	$^{244}\text{Cm}$
Half Life (years)	2.7	433	1.3	17.8
Energy Range (kV)	1.5 to 5.0	8.5 to 40	5.0 to 18	4.5 to 11.5
Analytes (K lines)	Si to V	Zn to Nd	Cr to Mo	Ti to Se
(L lines)	Nb to Ce		Tb to U	La to Pb

tage and filter material. The flux from the X-ray tube can also be high enough to permit use of WDXRF detectors or secondary targets for optimal excitation of the analyte elements in the sample. Unlike radioisotope sources, X-ray tubes can be switched off when not in use, simplifying maintenance operations. The major disadvantage of the tubes is that they need an external high voltage source and occasionally, in the case of high power tubes, cooling water.

For on-stream/at-plant applications, the detectors which are used are generally of the energy dispersive (EDXRF) type. In the normal range of operation ( $< 20$  keV), these have poorer resolution than wavelength dispersive (WDXRF) detectors but have the advantages that they can measure multiple elements simultaneously and so are generally lower cost than an equivalent WDXRF system (effectively requiring separate crystal and detector for each element to be determined). The smaller collection angle for a WDXRF system, compared to EDXRF also generally necessitates a higher power source, thus again adding to the cost differential. The EDXRF detectors used in XRF spectrometers fall into two distinct categories. The lowest cost systems are based on sealed gas proportional detectors. In addition to the low cost, these have the advantage that they can be operated at room temperature. The disadvantage is that the resolution of these detectors is very poor (typically between 10 and 20% of the X-ray photon energy measured). Thus, for all but the simplest applications/matrices, peak overlap can be a severe problem. The second type of EDXRF detector is based on solid state devices (usually lithium drifted silicon or germanium). These detectors have much better resolution than the sealed gas proportional detectors, but in the normal operation range ( $< 20$  keV) they are not as good as WDXRF detectors. The main disadvantage of the solid state detectors is that they must be cooled down (with liquid nitrogen or Peltier cooling), in order to operate. Typical resolution for a Peltier cooled Si(Li) detector is around 195 eV. Figure 20.5 shows a typical EDXRF spectrum of a process solution containing high levels of corrosion metals compared with the single peak which would be observed for Fe and Ni if a sealed gas proportional detector had been used (inset). One method of compensating for the poor resolution of the sealed gas proportional detectors is the use of filters. These can either be used to remove contributions from interfering lines, to reduce background, or can even be used to perform “non-dispersive” XRF using “balanced filters”. In the latter approach, two filters are used sequentially, one which absorbs the analyte line well and the other which does not. The difference between the two measurements gives information on the analyte element of interest.

One aspect of XRF analysis in general, and on-stream XRF in particular, which is often poorly understood is that of sampling depth. There is a general tendency for people to think of X-rays as being a very penetrating form of radiation and to infer that the XRF system is carrying out an analysis of the entire sample which is presented to it. While in some cases, this is a good assumption, in others XRF is only measuring the concentration of analyte in a very shallow region of the sample near the cell window. Table 20.2 shows the “critical depths” (i.e. depth below which greater than 99% of the fluorescent X-rays would be absorbed before they reached the sample surface (cell window)) for a selection of materials as a function of X-ray

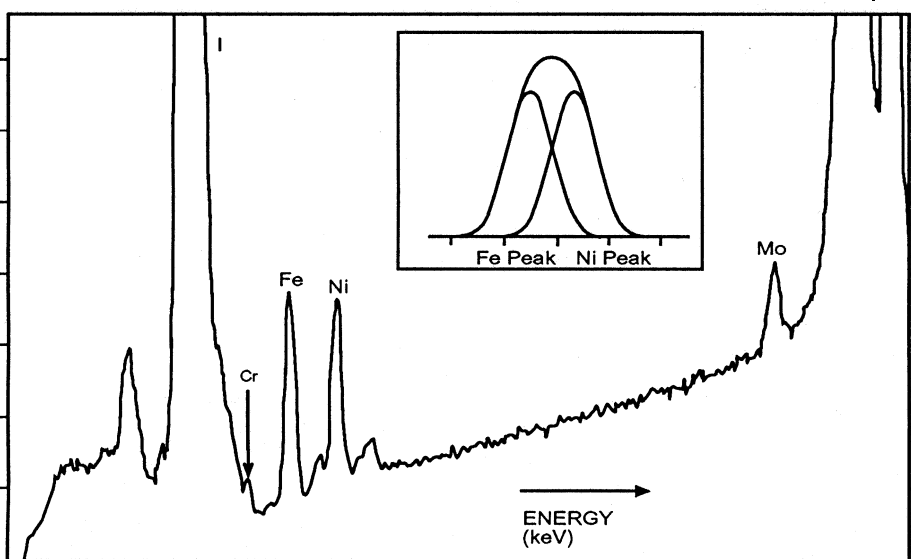


**Fig. 20.5** EDXRF spectrum of a reactor sample containing corrosion metals obtained using a Si(Li) detector and (inset) a typical spectrum obtained using a sealed gas proportional counter showing unresolved Fe and Ni peaks.

line energy (analyte element). From this, we can see that, whereas if we were to measure a heavy element such as Pd ( $K_{\alpha}$  line) in a hydrocarbon matrix such as gasoline, the sampling depth would be over 9 cm, if we were to measure sulfur in the same matrix, the sampling depth would be less than 0.3 mm. Furthermore, if we were to attempt to measure sulfur in a relatively heavy matrix such as steel, the analytical measurement would be restricted to a depth of less than 3  $\mu\text{m}$  from

**Table 20.2** XRF critical depths<sup>a</sup> for a selection of sample types.

Element	Line	Energy (keV)	Critical Depth (cm)			
			Gasoline	Water	Quartz	Iron
Na	K	1.04	0.0022	0.0008	0.0004	0.00005
S	K	2.31	0.021	0.0068	0.0009	0.0003
Sn	L	3.44	0.074	0.023	0.0028	0.0010
Ca	K	3.69	0.091	0.028	0.0034	0.0012
Fe	K	6.40	0.48	0.14	0.016	0.0051
Zn	K	8.63	1.2	0.36	0.039	0.0014
Au	L	9.67	1.6	0.50	0.055	0.0020
PB	L	10.50	2.0	0.63	0.068	0.0024
Mo	K	17.40	6.8	2.6	0.31	0.010
Pd	K	21.10	9.2	4.0	0.51	0.017

<sup>a</sup> depth is defined as depth below which more than 99% of the fluorescent radiation would be absorbed before it reached the detector (for a conventional XRF geometry with take-off angle approximately equal to 45°).

the sample surface. It is therefore clear that for any successful XRF measurement (on-stream or at-line), we must ensure that the sample depth which is sampled is representative of the sample as a whole.

Limits of detection depend very much on the analyte element, the matrix, the excitation conditions, the detector, the presence of any special filters and the measurement time. Under optimal conditions, limits of detection down to single ppm levels can be achieved using counting times of a few minutes.

#### 20.2.1.1 Liquid Process Streams

The main limitation associated with on-line analysis of liquid process streams using XRF is that the stream must be contained within a window material. This material must be strong and robust enough to withstand extended exposure to the temperature and pressure of the stream, be resistant to chemical attack or abrasion and yet be sufficiently transparent to the fluorescent X-rays to enable measurements to be made down to low enough concentrations to allow accurate measurements to be made. There are very few materials which will satisfy these requirements and in practice, the only suitable materials are beryllium or polymer films of thickness between about 10 and 50  $\mu\text{m}$ . The choice of material and thickness for the window of the flow cell represents a trade-off between analytical sensitivity and maximum temperature, pressure and chemical/mechanical resistance. Figure 20.6 shows the transmission of various window materials as a function of X-ray energy (analyte element). It is clear, that for measurement of light elements such as sulfur, the window material should be as thin as possible (subject to temperature and pressure limitations). Normally where the sample is not corrosive, beryllium windows are used since these are generally more robust and less liable to stretching and distortion than polymer films and require less frequent replacement. For corrosive streams, the beryllium windows can be protected with a thin plastic coating, but for abrasive

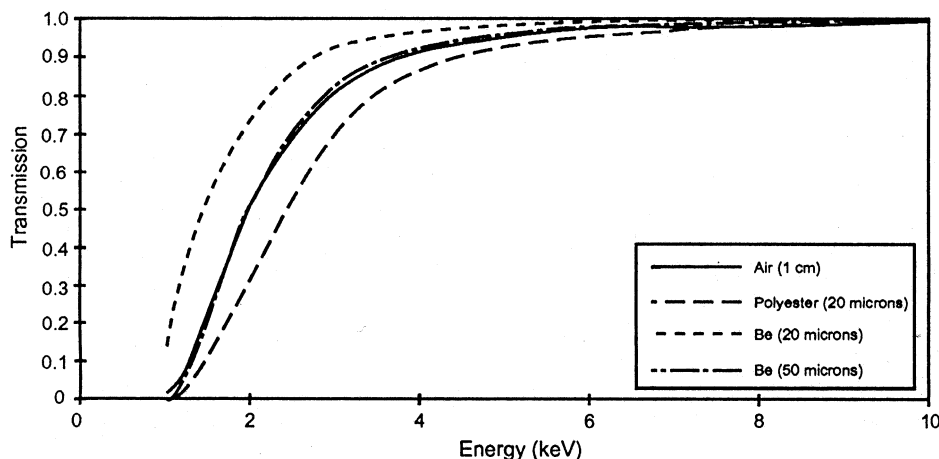


Fig. 20.6 Transmission of various window materials for XRF flow cells.

or very corrosive materials, this is not robust enough and a replaceable polymer film must be used inside the beryllium window. For acidic streams, any of the commonly used polymer films (e.g. polyester, polyimide or polypropylene) can be used, but for caustic streams, polypropylene films are generally best. None of the films are particularly resilient for use with strongly alkaline streams and so in some instances, the flow cell may need to be bypassed during caustic flush cycles to avoid window rupture. The limitation on stream temperature and pressure is normally due to the plastic window material. For polymer film windows, the limits of temperature and pressure are generally in the range 30 to 90 °C and 5 to 10 psi depending on the polymer used and the film thickness. For beryllium windows however, temperature and pressure can be up to 90 °C and 30 psi depending on the window thickness. In extreme cases, very robust windows made of polyvinylidene fluoride (PVDF) can be used for applications with streams at up to 200 °C and 800 psi, but in these cases, the absorption of the X-rays by the window can be so large that only X-ray transmission measurements (rather than XRF) can be made and measurements are restricted to high concentrations of analytes (e.g. measurement of percent levels of sulfur in crude oil and fuel oil pipelines).

Figure 20.6 also shows the absorption of X-rays as a function of energy (analyte element) for air. It is clear that for light elements absorption of fluorescent X-rays due to air in the optical path can be significant. For this reason, the optics used for these measurements should be as closely coupled as possible. Furthermore, the optical path should be purged with helium or argon-free nitrogen (argon significantly interferes with sulfur measurements when sealed proportional detectors are used). For on-stream applications, nitrogen is generally preferred on cost grounds.

As discussed in Section 20.2.1, for measurement of light elements, the sampling depth can be as low as a few microns. Thus any deposition on the sample window can significantly affect the measured results. For this reason, windows normally require regular cleaning and/or replacement. The frequency of cleaning/replacement will depend very much on the particular sample streams being measured but could typically be every few weeks. Furthermore, the presence of any particulate matter can cause severely erroneous and erratic results in cases where sampling depth is limited. In order to reduce susceptibility to such problems, many liquid streams require a sample conditioning system to be installed upstream of the analyser to remove particulates and water (in the case of hydrocarbon streams). Since XRF results are also influenced by sample density, the sample conditioning system may also require facilities for temperature and pressure regulation. This obviously adds to the cost of an on-stream system compared to an equivalent at-plant or laboratory based system.

Commercial on-stream XRF analysers for liquid process streams are produced by a number of manufacturers (see Appendix). These can either be configured for monitoring single or multiple streams. In most cases, the X-ray monitoring head (source and detector) moves sequentially from one flow cell to another for sequential monitoring. Solid reference samples are normally also incorporated in one or more of the positions monitored by the measurement head and used to calibrate and correct for instrumental drift. In many instances, however, plumbing multiple

streams to the same location may be impractical and, in these cases, installing multiple single stream monitors may be more appropriate. The commercial units available are generally mounted in fully interlocked and X-ray shielded NEMA 12, 4X or cast aluminum cabinets which can be equipped with a variety of CENELEC and NFPA purge systems for use in potentially explosive environments. Most systems incorporate leak sensors in the base of the cabinet which will completely shut down the unit in the event of a cell window rupture or other leak. In addition, a combustible gas monitor can be incorporated to monitor the purge gas from the enclosure.

Use of on-stream XRF analysis for monitoring liquid process streams has been reported for a number of applications including measurement of Fe, Cu, Co, Ni and Mo from five different points in a solution purification process of a cobalt refinery [28]; analysis of Cu, As and S in copper electrolyte purification solutions [29]; control of a solvent extraction process for La and Nd [30, 31]; continuous monitoring of catalyst elements (Mn, Co and Br) in terephthalic acid process solutions [32]; and measurement of various elements (particularly sulfur) in petroleum product and refinery streams [33, 34].

The latter application area has seen a great deal of effort and development expended over the past few years in view of the increasing global concern regarding the impact of the burning of fossil fuels on the environment. Sulfur concentration is one of the critical components responsible for damaging emissions to the environment, since it is a major contributor to the formation of acid rain. Oil companies are currently making enormous efforts to modify refinery processes to produce a range of low sulfur products (particularly road transport fuels), ahead of ever more stringent government specification limits. In order to understand and control the processes involved, on-stream X-ray analysis systems can be used to measure the sulfur concentrations in various process streams including the crude oil feed and the various streams used in the blending of gasoline and diesel road transport fuels. Sulfur concentrations of crude oil feedstocks are generally very high (percent concentrations), so these can be measured using X-ray transmission systems capable of withstanding pressures up to 800 psi and temperatures of 100 °C. For the streams used in the production of road transport fuels however, measurements must be made at ever decreasing levels. For example, within the European Union, the current specifications (2000), for sulfur in road transport fuels are maximum 350 mg kg<sup>-1</sup> for diesel and 150 mg kg<sup>-1</sup> for gasoline. The proposed limits for 2005 are currently maximum 50 mg kg<sup>-1</sup> sulfur for both gasoline and diesel. Although on-line XRF systems are available which claim to be able to achieve precisions of better than 1 mg kg<sup>-1</sup> standard deviation at 20 mg kg<sup>-1</sup> sulfur concentration, in reality, the reproducibility is likely to be much higher than this once all sources of error are included (e.g. calibration errors, drift etc.). In a recent Europe-wide round-robin including over 30 laboratories for example, reproducibilities for sulfur measurements at the 50 mg kg<sup>-1</sup> level were found to be 17 mg kg<sup>-1</sup> and 24 mg kg<sup>-1</sup> for diesel and gasoline respectively, even using the latest generation of laboratory based EDXRF spectrometers specifically optimised for sulfur determination. The EDXRF technique was not considered suitable for use at sulfur

concentrations below 50 mg kg<sup>-1</sup> [15]. Thus it seems likely that, as sulfur concentration specifications continue to reduce, on-stream XRF analysers may be replaced with techniques which are inherently more suited to low level measurements (e.g. UV fluorescence) for this application area.

#### 20.2.1.2 Trace Analysis and Corrosion Monitoring

With conventional on-line XRF systems such as those described above, limits of detection are restricted to, at best, ppm concentrations and often much higher levels. However, many applications, such as corrosion monitoring in pure water streams, require that metals are measured at much lower concentrations (down to ppb levels). These metal contaminants can be present either in the form of particulate matter or as fully dissolved components of the stream. Generally, measurement of metals at these levels requires the use of techniques such as ICPAES, AAS or, for very low concentrations, ICP-MS. However, these techniques are not well suited to on-line applications and in the case of particulate matter require that the samples are digested with acids prior to analysis. This therefore restricts the monitoring process to time consuming and labour intensive laboratory based analyses, resulting in a relatively poor sampling frequency. An elegant solution to this problem has been described by Connolly and Walker [35]. They have developed an on-line XRF system specifically designed for measurement of corrosion metals and other trace elements down to sub-ppb levels in water streams (although the approach could equally be applied to other flowing process streams). The system, which is now available commercially (see Appendix), utilises one or two flow cells equipped with holders capable of holding either conventional membrane filters for particulate analyses or ion exchange filters for dissolved metals. With a two-cell system, the stream can be passed first through the membrane filter for particulate removal/analysis and then through the cell equipped with an ion exchange filter for dissolved metal analysis. Metals on the filters are continuously monitored using an XRF system equipped with either an X-ray tube or radioisotope source and a sealed gas proportional detector or solid state Si(Li) detector. The systems also incorporate a Coriolis based flow sensor and software to permit the total mass of analyte metals on the filter to be plotted as a function of total flow through the cell(s). The gradient of this plot effectively gives the concentration of the metal of interest in the stream.

The detection limits for concentration of elements in the stream are a function of flow rate through the cell and sampling time. However as an example, the absolute detection limit in terms of the smallest amount of analyte on the filter which can be detected is of the order of 5 µg. Thus for a flow rate of 0.4 L min<sup>-1</sup> and a sampling time of 20 min, the limit of detection in terms of concentration in the solution stream is 0.6 ppb. Even lower limits could be achieved with higher flow rates and/or sampling time, although obviously the latter would result in a poorer sampling frequency. The systems can cope with sample flow rates of between 0.2 and 0.4 L min<sup>-1</sup> with temperatures in the range 5 to 32 °C and pressures up to 35 psi. Since the filter samples are essentially thin films (from an XRF calibration

point of view), calibrations are linear over the normal operation range and can be accomplished using simple thin film standards for particulates analyses or can be easily prepared by passing laboratory prepared solution standards through the ion exchange filters. Care should be taken with the latter approach, however, to ensure that flow rates used are compatible with the kinetics of the absorption process. A new standard test method for on-line measurement of low level particulate and dissolved metals in water by X-ray fluorescence based on the above approach has recently been approved [36].

#### 20.2.1.3 Analysis of Slurries and Powders

Flow cells for on-stream XRF analysis of slurries are generally similar to those for liquid streams (Section 20.2.1.1), although the abrasive nature of some slurries can place additional constraints on the window material and more frequent replacement of the windows may be required. Furthermore, since in general, solid materials absorb X-rays more strongly than liquid streams, detection limits are usually not as good for solid materials as for liquid streams and are rarely better than 50 to 200 ppm. Also, to avoid settling of particles during the measurement process, flow rates for slurry samples must be maintained relatively high (typically 20 to 45 L min<sup>-1</sup>).

For analysis of powder samples, a variety of approaches have been adopted. Fig. 20.7 shows some typical examples. The gravity sampler is generally similar to the flow cells used for liquid streams but can include a vibrating sample packing device for reproducible packing density. A novel variation of this approach which has been developed for on-stream cement analysis utilises a highly polished metal closure over the viewing port which retains the sample during the packing process, producing a smooth flat surface which can then be analysed directly during the measurement phase without requiring use of a window between the sample and the measuring head [2]. Other approaches which do not require use of a window material include the reciprocating arm sampler and the rotating disc powder sampler (Fig. 20.7). In the former approach, a moving arm extends into the product chute and collects a powder sample which is automatically compacted into a pellet and then moved under the measuring head for analysis. With the rotating disc sampler, the measuring head is placed over a turntable that rotates into the sample chute to collect the sample. The latter approach can allow larger particles to be analysed but is less likely to give precise and accurate results. This results from one of the main problems associated with any analysis of powder or slurry samples using XRF: particle size effects. These effects can occur when the penetration depth of the X-rays is similar to or smaller than the particle size of the sample to be measured. In this case the XRF intensity observed becomes a function of the size and composition of the individual particles rather than of the concentration of the analyte element in the sample as a whole. In these cases, the XRF intensity observed will even depend on the chemical form of the analyte as well as its concentration, even after application of interelement corrections (this effect is often referred to as the “heterogeneity” or “mineralogical” effect [37]). This effect is particularly severe in cases where

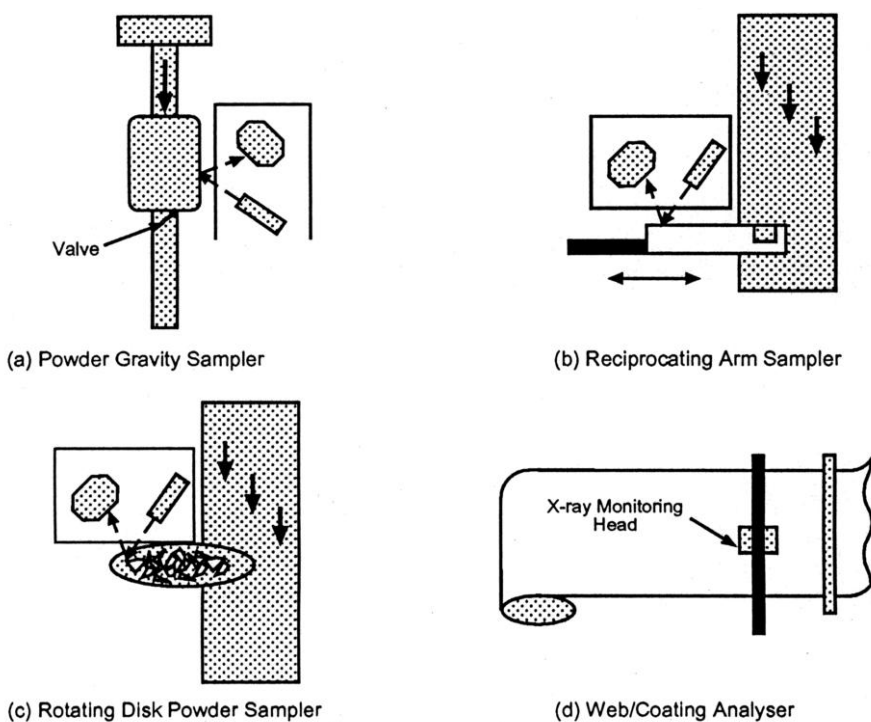
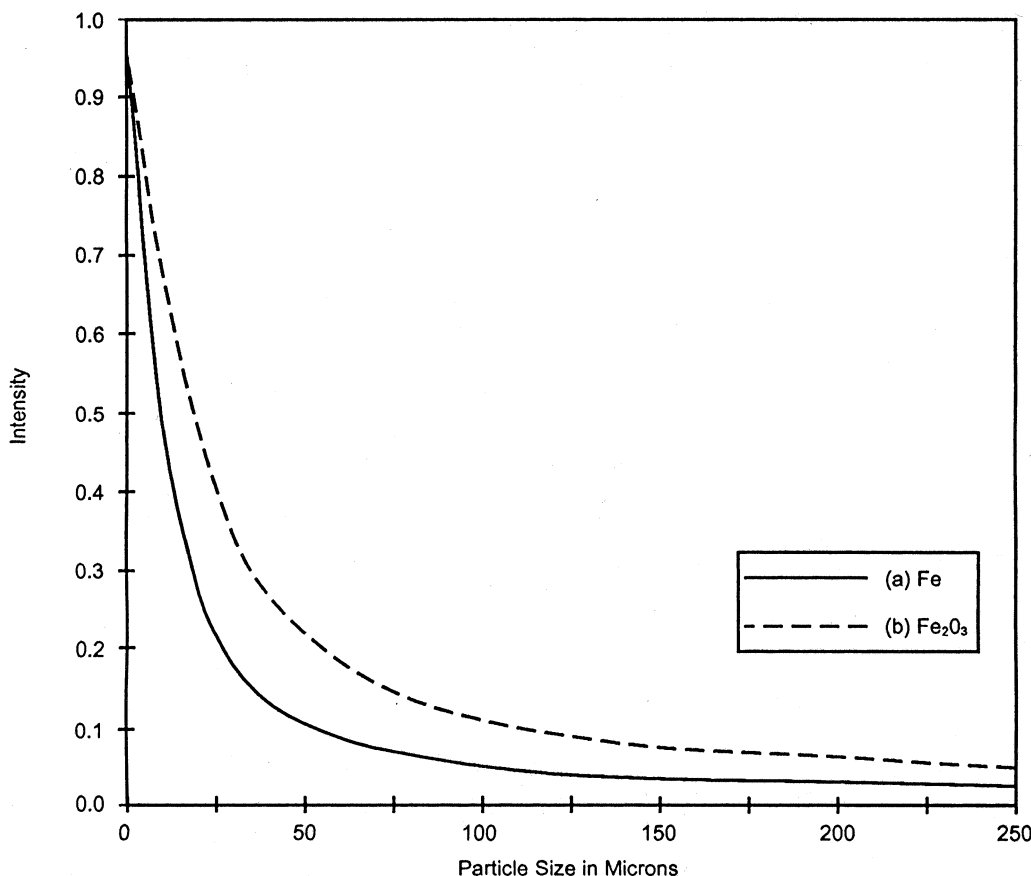


Fig. 20.7 Configurations for on-stream XRF analysis of solids.

strongly absorbing materials are mixed with a light matrix. Figure 20.8 shows how the XRF intensity would vary as a function of particle size for iron in petroleum coke. Curves are shown for iron present in metallic form (e.g. steel particles) and if it were present as the oxide (e.g. rust particles). It is clear that for particle sizes even as small as a few microns, completely different results would be obtained depending on which form of iron particles were present in the sample, even for exactly the same overall iron concentration. Since penetration depth is a function of the energy of the fluorescent X-rays (Tab. 20.2), this problem is generally worse for light element measurements.

Although one must be aware of the potential problems posed by particle size effects in slurry and powder analysis, in many cases, the range of particle size and particle composition for a process stream is sufficiently constant that reliable measurements can be made using on-line XRF systems. Successful applications which have been reported include: an on-stream XRF measuring system for ore slurry analysis [38]; a system for direct XRF analysis of pulverised coal streams [39]; and on-stream analysis of cement using XRF [2, 40]. The latter is available as a commercial on-stream cement analyser which it is claimed can measure lime saturation factors (a function of Ca, Si, Al and Fe concentrations) with a relative standard deviation of better than 1% in 100 s measurement time. Obtaining such results with a sampling frequency of over 10 measurements per hour can allow effi-



**Fig. 20.8** Plot showing variation in XRF intensity for iron in coke as a function of particle size: (a) Iron present as metallic iron particles; (b) iron present as iron oxide (rust) particles.

cient control of the raw mix chemical composition, permitting optimum operation of the kiln and ensuring the quality of the finished product.

#### 20.2.1.4 Direct Analysis

Commercial systems are available which permit direct analysis of solid material on a conveyor belt (see Appendix). Typically the XRF monitoring system comprises a low power X-ray tube and sealed gas proportional detector monitoring head which is mounted about 100 to 300 mm above the conveyor belt, in some cases using shock absorbing mountings. A material height limiter/regulator is often installed upstream of the measuring head to control the material surface to probe distance. Systems of this type are commonly employed in the mineral industry and can cope with tonnage up to 2000 t h<sup>-1</sup> using a conveyor system with width up to 1500 mm.

A system of this type has been described for automatic sorting of waste glass [41]. In the latter system, the XRF spectrum of a glass fragment is measured using the monitoring head mounted above the conveyor belt and the spectrum is compared with a library of stored spectra for known types of glass. Once identified, the system automatically diverts the glass fragment to a container of like composition using rams. In this way, it is claimed that a substantially continuous stream of glass fragments on the conveyor belt can be sorted according to glass type (composition).

A similar approach can also be used for web/coating applications. The monitoring can be carried out either on a discrete strip on the web, or by using a computer controlled scanning pattern over the width of the web. This approach can be used either to determine composition or sample/coating thickness. Typical applications are: silicone on release paper; coatings on steel or other metals; polycarbonate coatings on fibers/textiles, silver emulsion on photo film and so forth. For relatively straightforward applications, simpler systems based on X-ray transmission can be used to measure sample/coating thickness or density [42]. Such a system could typically comprise a radioisotope source and simple, low cost NaI detector mounted at the opposite side of the sample. The intensity ( $I$ ) of the transmitted X-rays is given by:

$$I = I_0 e^{-\mu \rho l}$$

where,  $I_0$  is the incident X-ray intensity,  $\mu$  is the mass attenuation coefficient,  $\rho$  is the sample density, and  $l$  is the thickness of the sample along the X-ray path. If the mass attenuation coefficient is known (or effectively determined from calibration samples), then the measurement of  $I$  effectively gives a measurement of the areal density ( $\rho l$ ). Thus, if the density of the sample is known (or constant), the measurement gives a direct measure of the thickness of the sample. Conversely, if the thickness is known (or constant), the measurement of transmitted intensity gives a measure of the sample density. The range of thickness which can be measured depends on the absorption properties of the material being measured and the energy of the X-ray source, but is typically in the micron range. In some cases, the method can be extended for use with layer materials and when a conventional XRF geometry probe is used, attenuation of the XRF line from an element in the substrate can be used to measure the thickness of a coating above the substrate.

A particularly novel application of on-line XRF using direct analysis has been described by Creasy [43]. The author described development of a wavelength dispersive X-ray spectrometer, specifically designed to analyse the composition of molten metal in an electron beam furnace (effectively similar to an extremely large electron microscope!). Specially designed twin wavelength monitor systems were used to permit simultaneous measurements of the analyte element and a proportion of the Bremsstrahlung which was used to compensate for variation of beam current in the furnace. The monitor systems were protected from the furnace environment by water cooling and through the use of thin foil windows. A flow of argon was maintained from the spectrometer to the furnace to help reduce condensation.

sation on the windows. It was found that the system was stable for an entire melt (which could last over 10 h) and that in the course of the actual melting, the system could be used for control purposes, providing instant feedback to the operators. Attempts at using EDXRF for this application were unsuccessful since the very high electron flux from the furnace destroyed the Si(Li) detectors.

### 20.2.2

#### Atomic Emission Spectrometry

##### 20.2.2.1 Plasma Spectrometry

Plasma spectrometry, particularly ICPAES and ICP-MS, is widely used for laboratory based elemental analysis of process samples in view of its inherent sensitivity, relative ease of use and rapid multi-element capability (see Section 20.1). However, these techniques are inherently unsuitable for on-stream applications since the sample introduction systems are not robust and are prone to blockage and drift problems caused by changes in sample physical properties, temperature or degradation of pump tubing. Furthermore, conventional plasma based systems (ICP or microwave plasmas) cannot cope with particulates larger than a few microns and can rarely tolerate significant flow rates of volatile solvents or gaseous samples. The systems also generally require large quantities of expensive gases (Ar or He), are not well suited to operation in a hostile environment (e.g. large temperature fluctuations or vibration) and due to the very high temperature of the source (up to 10,000 K), are difficult to make inherently safe for use in potentially explosive atmospheres. Nevertheless, some authors have reported successful application of specially modified plasma based systems to on-stream analysis for particular applications.

#### Liquid streams

Frederici et al. [44] have modified a charge injection device (CID) based ICPAES spectrometer for on-line continuous process monitoring of aqueous industrial waste streams. As discussed in Section 20.2.2.1, the weak point of ICPAES instruments in terms of on-stream analysis is usually the sample introduction system. The authors modified the sample introduction system to facilitate low maintenance and continuous unattended operation. The normal peristaltic pump was replaced by dual metering pumps to eliminate the need for frequent tube replacement and the autosampler was replaced by a valving system to permit switching between the waste streams to be monitored and rinse/calibration and quality control check streams. A separate stream containing internal standards was mixed with the sample/calibration streams on-line resulting in an approximate 20 % dilution. Internal standards were carefully chosen to compensate for changes in the composition of the waste streams (particularly pH) and multiple wavelengths were monitored for each analyte to check for any potential spectral interference. The normal Meinhard nebuliser was replaced by a Burgener high solids nebuliser to improve the tolerance of the system to the presence of particulates in the waste streams and to reduce the incidence of blockages, (although large particles still had to be removed

from the streams using an up-stream filter). Axial viewing of the plasma was selected to provide better limits of detection, which were in the range 0.0008 to 0.031 mg L<sup>-1</sup> for the 15 elements measured. The observed limits of detection were typically about three orders of magnitude lower than the prescribed action levels for this application. The system was found to perform well for most elements although some memory problems were experienced with mercury. Results obtained were compared with those obtained using the traditional laboratory approach (including sample digestion) and were found to give good agreement for a sample resembling tap water. However, the system is unlikely to perform well for more complex waste streams, which normally contain a significant proportion of particulate matter and which would definitely require digestion prior to analysis.

### Gaseous effluents

An ICPAES system has also been designed for analysis of high temperature and high pressure fossil fuel process streams, such as those encountered in coal combustors and gasifiers [45]. Such streams can vary enormously in composition and particle loading on a timescale of seconds and any sampling systems must maintain the sample stream at high temperature (typically 650 °C) and flow rates above 2 L min<sup>-1</sup> in order to prevent condensation or loss of particulate matter in the sample transport system. Conventional ICP excitation sources, typically operating with argon as plasma gas and with rf power between 1 and 1.5 kW will not tolerate such high flow rates of gases containing combustion products and particulates. The authors therefore used an argon/helium plasma operating at very high power (5 kW), together with a specially designed torch with ceramic injector and heated sample transfer line to cope with the high temperature gaseous process stream. Elements in the sample stream were measured using a battery of 0.1 m monochromators, viewing the plasma through a bundle of fiber optics. Calibration was affected using an ultrasonic nebuliser equipped with a heater and condenser for aerosol desolvation. Once calibrated, the system was claimed to be stable for 8 h or longer.

One of the problems with the above approach is that due to the very high power required, a very large, bulky rf generator must be used. Trassy and Diemiaszonek [46] have modified a conventional 1.6 kW argon ICP system for analysis of the gaseous effluents from incineration and other industrial plants. Injection of air into the central channel of an ICP causes the channel to increase in width from its normal value of 2–3 mm to 8–10 mm. This results in a corresponding reduction in the depth of the toroidal region of the plasma, resulting in a reduced rf coupling efficiency. The authors found that this could be compensated using a larger diameter torch (23 mm cf. 19 mm for a conventional torch). Using a 1.5 mm diameter alumina injector, the authors were able to maintain a stable plasma at 1.6 kW rf power with flow rates of up to 0.7 L min<sup>-1</sup> of air introduced to the plasma via the injector tube. This flow rate is however, still much too low to allow isokinetic sampling of a gaseous effluent stream and so a two-stage sampling device was used (Fig. 20.9). Sample gas from the flue was sampled at high flow rate using a diaphragm pump (protected from particulates using a filter). This gas stream was sub-sampled

(either before or after the particulate filter) for injection into the ICP using a two-headed peristaltic pump. The two pump heads were exactly out of phase to reduce modulation of the flow (reduced from 80% with single pump head to 10% for the double head arrangement as described.). Thermal conductivity of the plasma was found to vary substantially with water vapor loading and so the gaseous effluents and aerosol produced from the ultrasonic nebuliser used for calibration were passed through a desolvation system. Limits of detection obtained by the authors for various metals are shown in Tab. 20.3. These are typically well below the threshold limit values for flue gases of industrial plants which are typically in the  $0.050$  to  $1.0 \text{ mg m}^{-3}$  range [47]. Precision was found to be around 2 to 4 % RSD using a 2 s integration time, although some memory problems were experienced with mercury.

The main problems associated with systems such as those described above which require sample streams to be transported to the plasma is that unless the stream is maintained at a high temperature, condensation can occur in the pipework and/or injector tube; and unless a very high sample flow rate is maintained

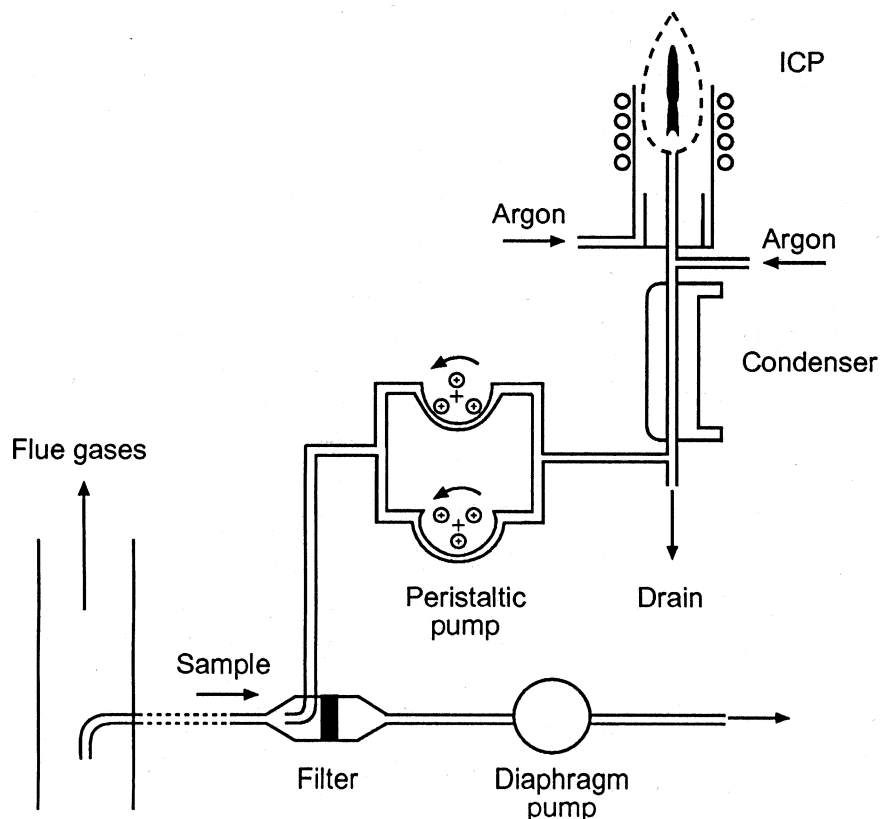


**Fig. 20.9** Two-stage sampling system used by Trassy and Diemiaszonek [46] for on-line analysis of gaseous effluents using ICPAES.

**Table 20.3** Detection limits<sup>a</sup> for on-line analysis of gaseous effluents by ICPAES.

<b>Element</b>	<b>Line (nm)</b>	<b>Detection Limit (<math>\mu\text{g}/\text{m}^{-3}</math>)</b>
Al	308.215	0.5
As	193.696	25
Ca	317.933	0.3
Cd	228.502	0.5
Co	228.616	0.5
Cr	267.716	0.2
Cu	324.754	0.3
Fe	259.940	0.3
Hg	253.652	5
K	766.491	2
Li	670.784	1
Mg	279.079	3
Mn	257.610	0.05
Na	589.592	5
Ni	231.604	3
Pb	220.351	6
Ti	334.941	0.1
Zn	213.856	1

<sup>a</sup> Limits of detection quoted are based on 3 standard deviations in air, according to Trassy and Diemiaszonek [46].

( $> 2 \text{ L min}^{-1}$ ), particulate matter is unlikely to be transported representatively into the plasma. Both of these problems could potentially be eliminated if the plasma could be mounted directly in the off-gas stream itself. Woskov et al. [48] have described a continuous, real time, microwave plasma element sensor which may be suitable for this application. A schematic diagram of the device is shown in Fig. 20.10. The device comprises a tapered, shorted, microwave waveguide made of refractory material which is mounted in the hot flue gas stream. A passageway in the waveguide allows flue gas to flow freely through the waveguide and a microwave plasma initiated in this region of the waveguide excites contaminant atoms present in the flue gas. Atomic emission from the contaminant elements excited in this way is measured using a spectrometer viewing the plasma through a robust fiber optic such as unclad quartz which is capable of withstanding long term exposure to the hot environment of the flue gas. Calibration of the device may be affected by ablating an alloy plate mounted below the gas inlet to the waveguide, using a laser system. In addition to eliminating the problems of condensation and particulate drop-out associated with sample transport systems such as those described above, the in-stream microwave sensor should also eliminate the memory problems often encountered with mercury measurements.

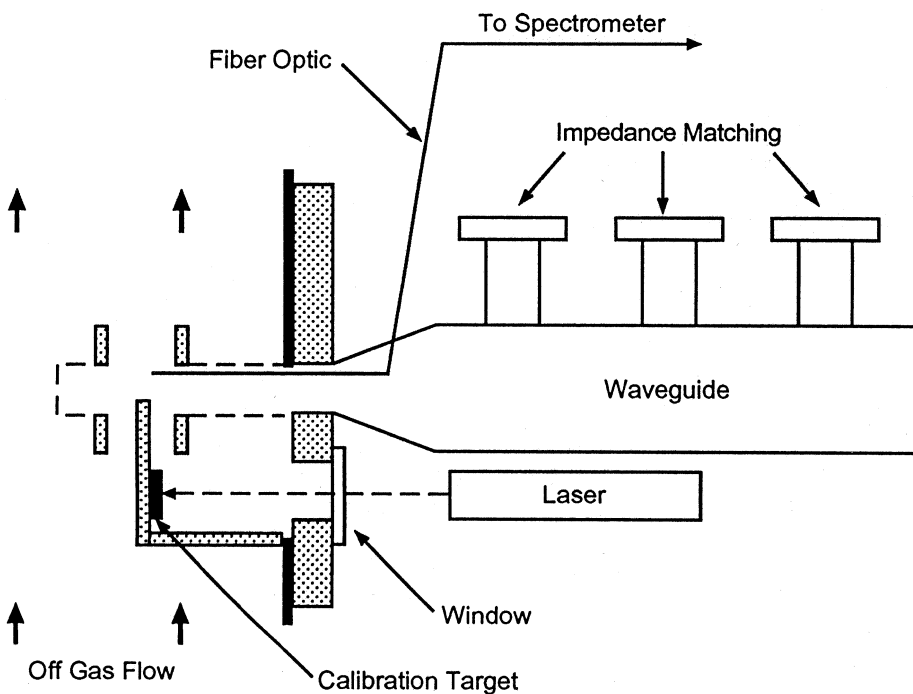
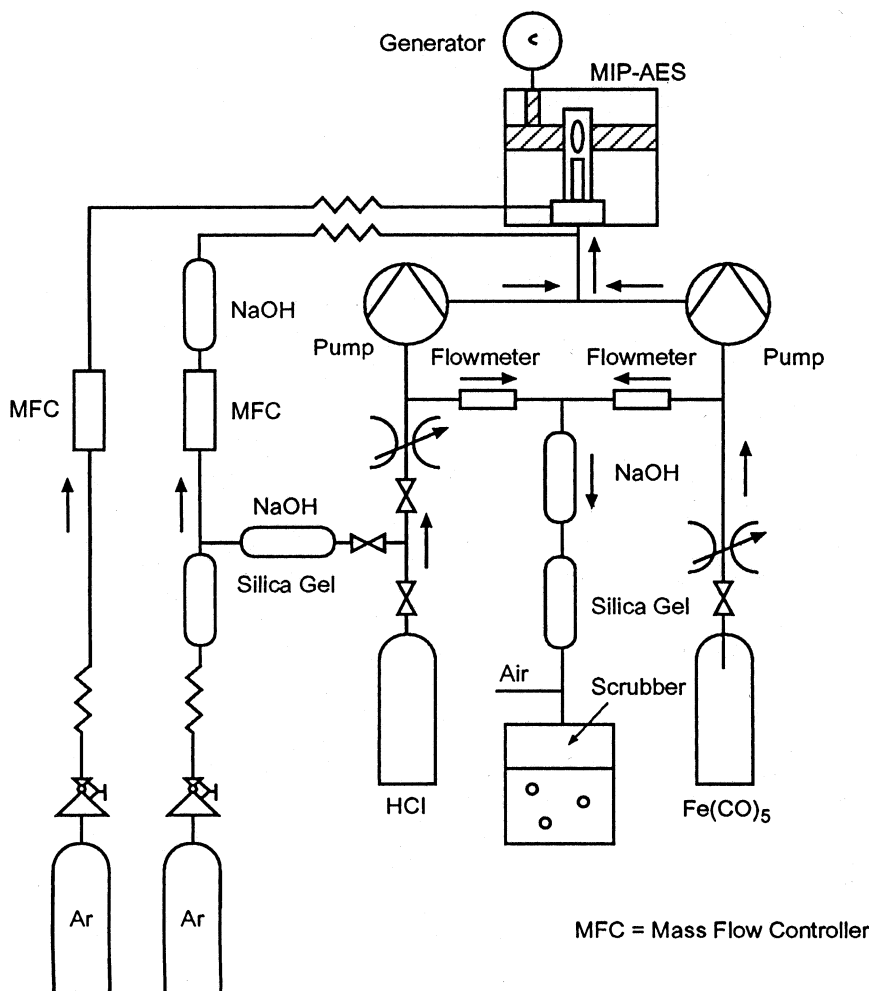


Fig. 20.10 Continuous real time microwave plasma element sensor for flue gas monitoring [48].

### Reactive gases

In the semiconductor industry, there is an increasing requirement to measure elemental contamination in reactive gases down to extremely low (sub ppb) concentrations since these can have a major influence on the quality of the devices produced. In particular, devices produced using chemical vapor deposition and reactive ion etching are particularly sensitive to impurities in the process gases used. The elemental contaminants can be present in the gases as particulates or vapors or a combination of both forms [49]. A direct analytical system is therefore preferred which will allow determination of the total contaminant concentrations independent of their chemical and physical forms. Calibration of direct plasma based systems for analysis of gases is more difficult than for solutions since the former generally involves carefully adding a controlled flow rate of a known concentration of volatile analyte contained in a carrier stream into a carefully controlled flow of the gas stream to be analysed. The volatile analyte stream can be obtained using a gaseous form of the analyte (if available), using diffusion tubes, or by passing the carrier gas stream through a liquid analyte for which the vapor pressure is accurately known. All of these approaches have been used, but unfortunately, for many analytes it is very difficult to obtain compounds suitable for use in this way to calibrate the system. A further complication is that for corrosive gases (e.g. HCl), any valves used to control the gas flow rates are likely to be a significant source of contamination. A solution to this problem which was proposed by

Schram [50], used a bypass-backflush balancing system in which peristaltic pumps were used instead of valves to control the gas flow rates for introduction of HCl gas into an ICPAES instrument. The author obtained a limit of detection of around  $2 \text{ ng g}^{-1}$  for Fe in gaseous HCl. A similar system has also been used for analysis of gaseous HCl using a microwave induced plasma (MIP) [51]. A typical example of the bypass-backflush system used by these authors to introduce the HCl gas to the MIP and to calibrate the system by standard additions with iron pentacarbonyl is shown in Fig. 20.11. This system permits continuous sampling of a gaseous HCl stream and achieves a limit of detection of  $0.25 \mu\text{g L}^{-1}$  of Fe in argon with a reproducibility of 6%. The use of peristaltic pumps permitted gas flow rates to be changed without moving any valves. This was important since it was found that the iron



**Fig. 20.11** Bypass-backflush balancing system For direct sampling of reactive gas (HCl) for plasma emission spectrometry [51].

emission intensity dropped for about 10 min before reaching a steady state when the hydrogen chloride cylinder was opened (due to corrosion of the valve). A similar approach has been used together with a modified electrothermal atomisation atomic absorption spectrometer (ETA-AAS) for determination of Fe, Ni and Cu in HCl, Cl<sub>2</sub> and BCl<sub>3</sub> [49]. The ETA-AAS approach afforded limits of detection which were similar to those obtained using plasma emission spectrometry but had the advantage that solution standards could be used to perform the standard additions calibrations.

In order to minimise the amounts of toxic gases used, Barnes and co-workers have advocated the use of a sealed ICP source for the analysis of arsine [52,53], silane [54], HCl [55] and Cl<sub>2</sub> [56]. However limits of detection obtained with this system were relatively high compared with the alternative approaches described above and long stabilisation times were often required in order to obtain stable plasma conditions. For example, under flowing conditions, the limit of detection for Sn in HCl was found to be around 300 ng g<sup>-1</sup>, and the authors found that it was necessary to add chlorine gas to the plasma in equal volumes to the HCl to prevent deposition of tin. The limit of detection reported by the authors for arsenic in silane was equally unimpressive (200 ppb v/v) and compares unfavourably with the limit of detection of 0.5 ppb (v/v) reported by Hutton et al. for direct analysis of silane using ICP-MS [57]. The latter authors also reported a detection limit of 0.65 ppb (v/v) for iodine in the same application with precisions between 2 and 5 % RSD.

#### 20.2.2.2 Laser Based Techniques

Conventional plasma spectrometry (e.g. ICPAES, ICP-MS) can also be used for direct analysis of solid samples by using a laser to ablate the surface of the sample to be analysed, and transporting the ablated material to the plasma using a flow of gas (e.g. argon) contained in a transfer tube. This approach has been successfully used for analysis of a wide variety of materials using laboratory based instruments. However, the approach is not well suited to process analysis (particularly on-line analysis), since in addition to the problems associated with the plasma source itself (high cost, high temperature, requirement for large amounts of expensive gases, e.g. Ar or He), the sample transport system also introduces a number of additional problems associated with sample deposition/condensation, memory effects and non-representative sample transport.

A more suitable approach for on-line analysis is to view atomic emission directly from the small plasma formed above the sample surface when the sample is ablated using the laser. This approach, which is shown schematically in Fig. 20.12 has been applied to analyses of a variety of materials (e.g. [58–74]) and is known under a variety of names such as laser induced plasma spectrometry (LIPS), laser induced breakdown spectrometry (LIBS) and laser spark emission spectrometry (LASS). The laser used is typically a Nd:YAG laser operating either at its fundamental, doubled or quadrupled frequency, although excimer and CO<sub>2</sub> lasers have also been used. The important parameter of the laser is that it must be capable

of producing focused pulses with power density of at least  $10^9 \text{ W cm}^{-2}$ . Spot sizes for the focused laser are usually between 0.1 and 1 mm diameter and a common configuration may use a Nd:YAG laser capable of delivering 250 mJ in 7 ns at a rate of 10 Hz.. The spectrometer used often incorporates a diode array or CCD detector so that multiple wavelengths can be monitored simultaneously and so that full peak shapes can be observed to check for broadening or self-absorption effects which are more common in LIPS than in cases where the plasma is independent of the ablation event (e.g. LA-ICPAES). This latter problem is particularly prevalent during the early stages of plasma formation when temperature and electron density are high and recombination events give rise to broad continua emission (high backgrounds). For this reason, the LIPS system must incorporate a rapid time-gated detection system as illustrated in Fig. 20.12. A typical experiment may involve a delay time of 0.5  $\mu\text{s}$  to 1 ms and an integration time of 1 to 50  $\mu\text{s}$  depending on the laser conditions, sample material and concentration of analyte element to be measured. Figure 20.13 shows how the signal to noise ratio changes with delay time for a typical ablation of a glass sample (taken from [69]).

With any laser ablation process, the interaction of the laser with the sample, and hence the amount of material ablated can vary significantly, depending on the sample matrix, color and condition of the surface and the thickness of any coating. This normally necessitates use of an internal standard approach to the analysis, where the intensity of the analyte element is ratioed to the line from another element in the sample whose concentration is known. One potential problem with this approach however, is that one element may be preferentially ablated in preference

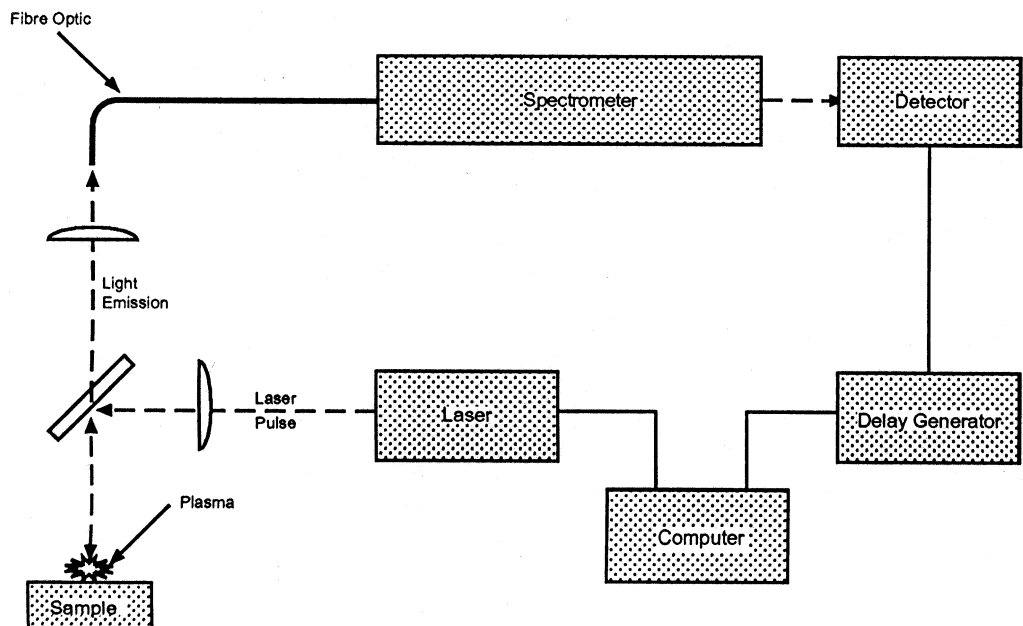
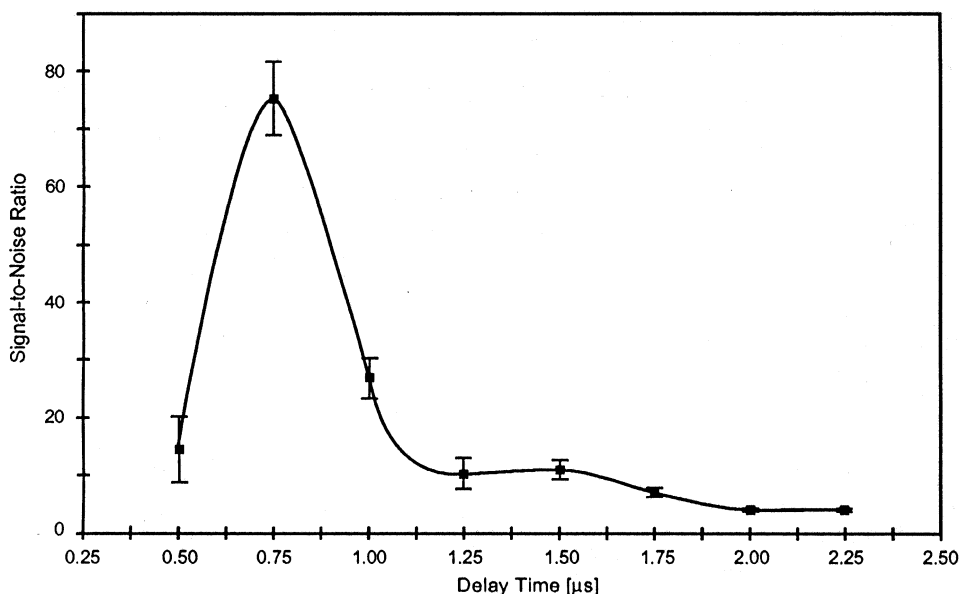


Fig. 20.12 Schematic diagram of typical laser induced plasma spectrometry (LIPS) system.



**Fig. 20.13** Example of effect of delay time on signal-to-noise ratio for laser induced plasma spectroscopic (LIPS) analysis. (Example shows Si: 288.158 nm in molten glass with 0.1 micro-

nanosecond gate width and Q-switched Nd:YAG laser with 75 mJ laser pulse energy. Reprinted from [69] with permission from Elsevier Science.

to the other (e.g. it may be present in a more volatile form in the sample matrix). In some cases, this can necessitate that the entire sample is ablated. For example, in the LIPS analysis of coal ash deposits collected on copper substrates, Ottesen [70] found that consistent results could only be obtained after several successive laser shots had ablated most of the outer material and copper lines from the underlying substrate began to appear in the emission spectra (indicating total ablation of the remaining thin coating deposit).

A particular problem associated with LIPS which does not occur in systems with separate ablation and excitation plasmas (e.g. LA-ICPAES) is that not only can the amount of sample ablated vary from laser shot-to shot, but the plasma temperature itself can also vary [69]. Figure 20.14 (taken from [69]) shows how the plasma electron temperature can vary from shot-to shot for a homogeneous glass sample. In such cases, unless both analyte lines and their associated internal standard lines originate from excited electronic states of similar energies, the internal standard approach will not work. A potential solution to this problem has been described by Panne et al [69] in which results were normalised using Saha–Boltzmann equilibrium relationships calculated using electronic excitation temperatures and densities obtained from measurements of several atom and ion line ratios. This approach was found to reduce errors associated with plasma temperature variations in the LIPS analysis of major elements in glass samples, resulting in improved

measurement precision and highly linear calibrations for Si, Ca and Al in more than 20 different glass samples.

Despite the problems discussed above, LIPS has been successfully applied in a number of process analysis applications. In some cases, the LIPS system has been used off-line as in the application described by Ottesen in which air cooled metallic substrates were used to collect fly ash deposits from a pulverised coal combustion for subsequent analysis off-line [70]. Calibration standards were prepared by spraying aqueous solutions onto heated substrates using an air brush and the method was found to work well provided that the deposits were sufficiently thin to permit complete ablation. Other workers have proposed on-line LIPS systems for process control. An example is the apparatus proposed by Sabsabi [71] for in situ analysis of pre-selected components of homogeneous solid compositions. In particular, the author proposed that the system could be used for measurement of the concentration of active ingredients (e.g. drugs) in pharmaceutical products such as tablets, by monitoring an element present in the active component (e.g. P, Na or S). In the example quoted, phosphorus was measured using a carbon line as internal standard.

One of the advantages of a laser based technique is that it affords the possibility of making spatially resolved measurements with a spatial resolution typically around 0.1 mm. In addition, since each laser pulse typically removes about 1 to 2  $\mu\text{m}$ , repeated ablation/analysis at the same spot allows information to be obtained regard-

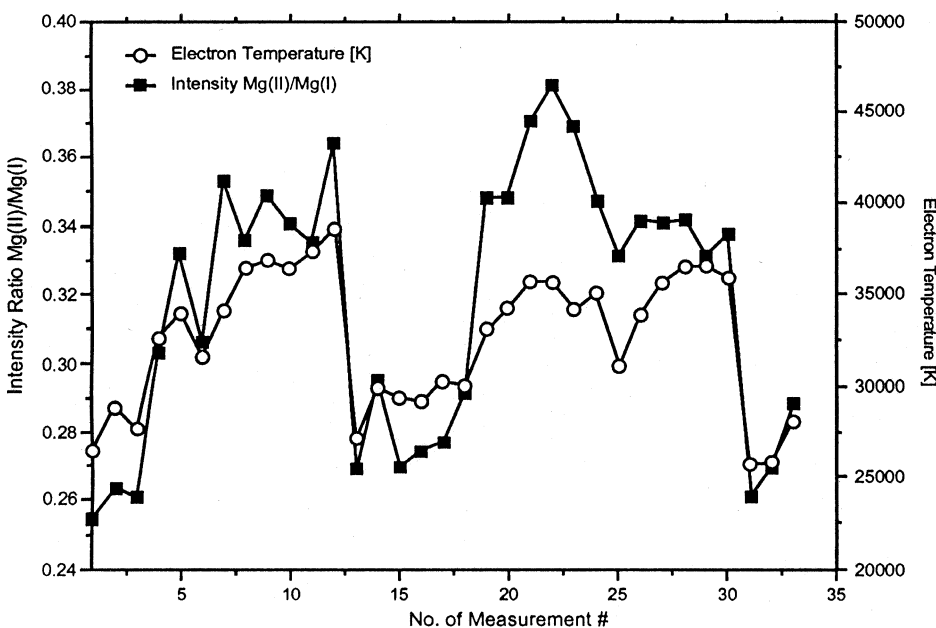
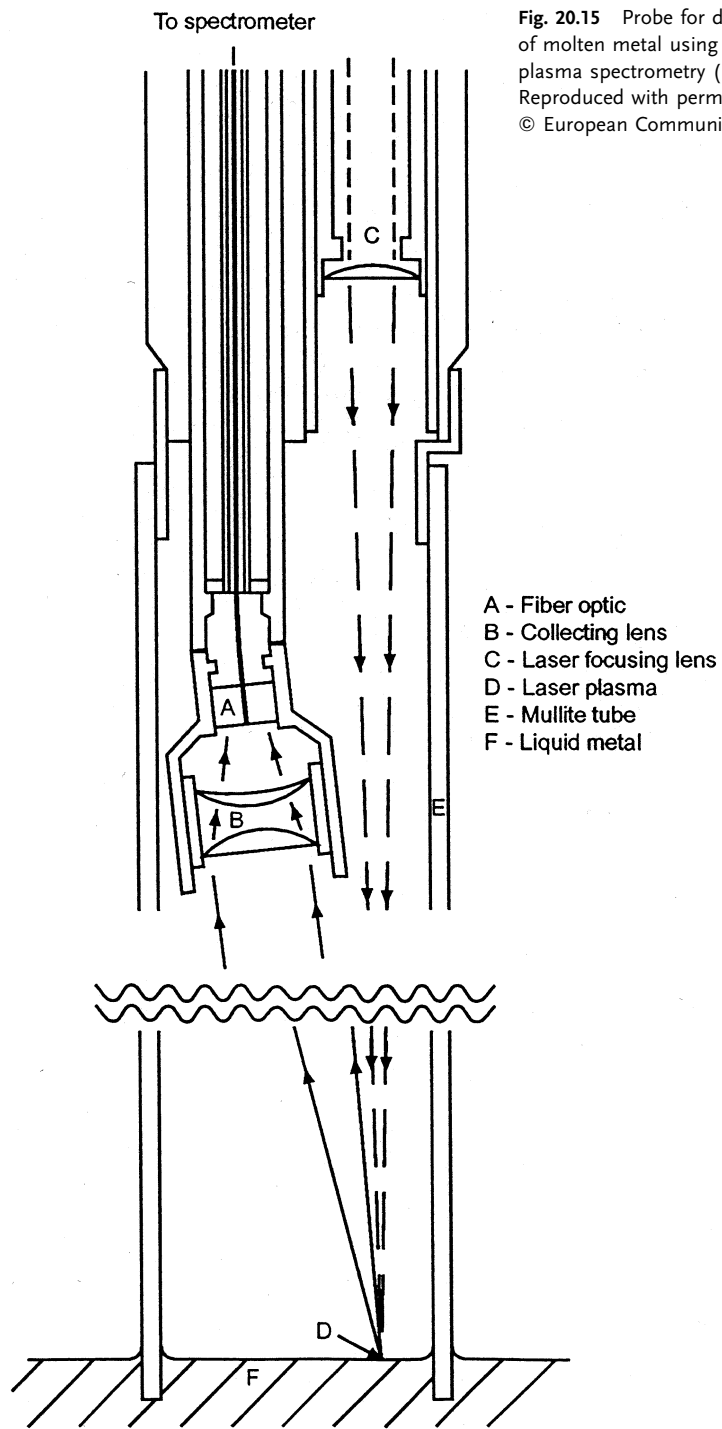


Fig. 20.14 Variation in  $\text{Mg}(\text{II})/\text{Mg}(\text{I})$  line intensity ratio and electronic excitation temperature for LIPS analysis of homogeneous glass sample NIST SRM 1830. Reprinted from [69] with permission from Elsevier Science.



**Fig. 20.15** Probe for direct analysis of molten metal using laser induced plasma spectrometry (LIPS).  
Reproduced with permission from [74],  
© European Communities.

ing concentration distributions as a function of depth from the surface (i.e. elemental depth profiles). Hakkanen and Korppi-Tommola [72] have demonstrated that these features of LIPS can be useful for measurement of the weight and composition of paper coatings. Lines originating from the major elements present in the coating pigments (Al, Si and Ca) were used to measure coating weight with corrections for plasma temperature accomplished using Mg ion-atom line ratios. In addition, the ratios of carbon line intensity to that of carbon plus silicon provided a measure of organic binder content. Using the latter approach, a good correlation with known coating composition was obtained and the authors were able to demonstrate an enhancement in organic binder content in the top few microns of the coatings studied. One problem identified by the authors however, was that the results obtained for kaolin based coatings were influenced by the particle size of the filler. The method could therefore only be applied in cases where the particle size distribution of the filler materials was known and constant.

In addition to its use with solid samples, LIPS can also be applied to analysis of liquids. Panne et al [73] have used the technique for *in situ*, on-line process analysis of major constituents in glass melts during a vitrification process for fly and bottom ashes resulting from waste incineration. The system used employed a vertical, single axis observation geometry in which the laser was directed through a pierced 45° mirror then focused onto the sample surface using a single lens. Light emission from the plasma was collimated using the same lens and directed into a fiber optic bundle using the mirror. The use of the fiber optic bundle permitted the spectrometer to be located remotely from the hot melt. The single axis geometry permitted the glass melt to be observed through a small (30 mm) opening in the oven, thereby minimising thermal losses during the melting process. Changes in plasma temperature and electron density were corrected using Saha–Boltzman equilibrium relationships calculated using measurements of several atom and ion line ratios. Good agreement was obtained between LIPS results and those obtained using conventional analytical techniques for concentration ratios of Si, Al and Ca.

As with all techniques for on-line production control analysis, very often as much effort must be expended to make the equipment robust enough to operate in a hostile environment as in the basics of the analytical technique itself. Jowitt and Whiteside [74] have described development of such a system for laser analysis of liquid steels. The laser, spectrometer and associated accessories were built into a specially designed mobile unit to allow easy access to and from the furnaces to be studied. The laser was mounted on a lift mast which allowed the laser unit to be placed above the furnace. Special measures had to be taken to protect the laser and optical components from heat and to reduce the effects of vibration on the optical alignment. Analysis was accomplished using a probe consisting of a single refractory tube which entered the molten metal (Fig. 20.15). A flow of argon was used to protect the lenses from dust and fumes and this flowed down through the probe and out through the molten metal, holding the surface of the metal at the focus of the laser focusing lens. The lens unit had to be mounted 1.8 m away from the molten metal surface to prevent optical effects due to lens heating and damage

to the fiber optic caused by the intensity of the infrared radiation focused on its tip. The system was successfully applied for monitoring silicon (ratioed to iron) in a blast furnace. However, use of a fiber optic restricts the system to measurements above 200 nm and therefore prohibits measurement of important elements in the steel making process such as carbon, sulfur and phosphorus (whose main emission lines lie in this spectral region). The authors have carried out some preliminary measurements on solid samples using a modified probe incorporating a direct spectral path in place of the fiber optic but this has yet to be incorporated in a system for direct, on-line analysis of molten metal.

### 20.3 Conclusions

As discussed above, atomic spectrometry plays a key role in the development, optimisation and efficient operation of most industrial processes. At the present time most of these applications are carried out using laboratory based analyses. In some cases the benefits of on-line analysis can be substantial, affording a much higher sampling frequency, permitting tighter control of the process. Some progress has

**Table 20.4** X-ray fluorescence (XRF).

Characterized parameter:	Surface specificity:			
Energy/wavelength of X-ray emission	Information depth: Microns to centimeters	Detectability: ppm to percent		
Type of information:	Resolution:			
Elemental composition	Depth:	Lateral:	Other: Not normally used for spatially resolved analysis but can be down to sub mm	
Measurement environment: Difficulties	Time needed for analysis:			
X-ray tube or radioisotope excitation Air, vacuum, nitrogen or helium optical path	Matrix/particle size effects	Prep. 0.5 to 5 min	Measurement 1 to 5 min	Evaluation 1 to 5 min
Equipment:	Cost [ECU]:		No. of facilities:	
Energy Dispersive (ED) or Wavelength Dispersive (WD) XRF spectrometer	15,000–150,000		Very common	
Type of laboratory:	User skill needed:	Sample:		
Small	Unskilled	Form type Solid, liquid or slurry	Size: 1 cm to several m	
Techniques yielding similar information				
ICPAES, AAS, LIPS				

**Table 20.5** Plasma emission spectrometry (ICPAES or MIPAES).

Characterized parameter:	Surface specificity		
Atomic emission lines	Information depth:	Detectability:	ppb to percent
<b>Type of information:</b>		<b>Resolution</b>	
Elemental composition		Depth:	Lateral:
		Not normally used for spatially resolved analysis	
<b>Measurement environment:</b>		<b>Time needed for analysis:</b>	
High temperature plasma	Spectral interferences	Preparation Up to 1 h	Measurement 1 to 5 min
	Sample introduction		Evaluation 1 to 5 min
<b>Equipment:</b>		<b>Cost [ECU]:</b>	<b>No. of facilities:</b>
Inductively coupled plasma or microwave induced plasma, High resolution uv/vis spectrometer		30,000–100,000	Very common
<b>Type of laboratory:</b>		<b>Sample:</b>	
Small medium	Moderate	Form type Liquid or gas Solids after digestion	Size: ml
<b>Techniques yielding similar information:</b>			
ICPMS, AAS, LIPS, XRF			

been made in developing atomic spectrometric techniques for on-stream or at-line analysis, particularly using XRF, which is inherently well suited to these applications in view of its stability and robustness. However, all of the techniques employed can suffer from severe limitations which restrict their use to specific niche applications. Furthermore, a high cost and substantial development time is often associated with making the systems robust enough for operation in hostile and potentially hazardous environments, and in many cases, this is not completely successful. Thus, with currently available technology, although on-line elemental analysis can provide substantial benefits for a few applications, there seems little prospect of this leading to a substantially reduced requirement for laboratory based analysis in the near future.

Tables 20.4 to 20.8 summarize the use of atomic spectrometry in process control.

**Table 20.6** Laser induced plasma spectrometry (LIPS (or LIBS)).

<b>Characterized parameter:</b>	<b>Surface specificity:</b>		
Atomic emission lines	Information depth: 1 to 2 microns	Detectability: ppb to percent	
<b>Type of information:</b>		<b>Resolution:</b>	
Elemental composition	Depth: 1 to 2 microns	Lateral: 0.1–1 mm	Other:
<b>Measurement environment:</b> Difficulties		<b>Time needed for analysis:</b>	
Laser induced plasma	Spectral interferences Changes in plasma temp.	Prep. None	Measurement 1 to 5 min      Evaluation 1 to 5 min
<b>Equipment:</b>		<b>Cost [ECU]:</b>	<b>No. of facilities:</b>
Laser, high resolution uv/vis spectrometer, time gated detection system		50,000–100,000	Limited
<b>Type of laboratory:</b>	<b>User skill needed:</b>	<b>Sample:</b>	
Large	Moderate to high	Form type Solid	Size: >1 mm
<b>Techniques yielding similar information:</b>			
Laser ablation ICPMS or ICPAES, XRF			

**Table 20.7** Inductively coupled plasma mass spectrometry (ICPMS).

Characterized parameter:	Surface specificity:		
Atomic mass of ions	Information depth:	Detectability: ppt to percent	
<b>Type of information:</b>	<b>Resolution:</b>		
Elemental composition	Depth:	Lateral:	Other: Not normally used for spatially resolved analysis but can be down to 10 microns if used with laser ablation
<b>Measurement environment:</b>	<b>Difficulties:</b>		
High temperature plasma	Spectral interferences Sample introduction	Prep. Up to 1 h	Measurement 1 to 5 min      Evaluation 1 to 5 min
<b>Equipment:</b>	<b>Cost [ECU]:</b>		
Inductively Coupled Plasma, quadrupole or sector mass spectrometer	100,000–250,000		
<b>Time needed for analysis:</b>			
<b>Type of laboratory:</b>	<b>User skill needed:</b>		
Medium Large	Moderate	Form type Liquid or gas Solid (with laser ablation) or after digestion)	Size: ml
<b>Sample:</b>			
<b>Techniques yielding similar information:</b>			
ICPAES, AAS, LIPS, XRF			

**Table 20.8** Atomic absorption spectrometry (AAS).

<b>Characterized parameter:</b>	<b>Surface specificity:</b>			
Absorption of atomic lines	Information depth:	Detectability: ppb to percent		
<b>Type of information:</b>	<b>Resolution:</b>			
Elemental composition	Depth:	Lateral:	Other: Not normally used for spatially resolved analysis	
<b>Measurement environment:</b>	<b>Difficulties:</b>		<b>Time needed for analysis:</b>	
Flame or graphite furnace	Matrix effects Sample introduction	Prep. Up to 1 h	Measurement 1 to 5 min	Evaluation 1 min
<b>Equipment:</b>	<b>Cost [ECU]:</b>		<b>No. of facilities:</b>	
Atomic absorption spectrometer	10,000–30,000		Very common	
<b>Type of laboratory:</b>	<b>User skill needed:</b>		<b>Sample:</b>	
Small	Low	Form type Liquid or gas Solids after digestion	Size: ml	
<b>Techniques yielding similar information:</b>				
ICPAES, ICPMS, AAS, XRF				

### Acknowledgements

The author gratefully acknowledges information provided by Hobré Instruments, Oxford Instruments and Spectro Analytical Instruments which greatly assisted in the production of the section of this chapter relating to on-line XRF analysis. The author would also like to thank Carole Hampton of the BP Information Centre, Sunbury for obtaining copies of most of the references quoted in the text.

## Appendix: Suppliers of On-line XRF Equipment

### General On-line XRF

Kevex Spectrace  
1275 Hammerwood Ave.  
Sunnyvale  
CA 94089  
USA  
[www.spectrace.com](http://www.spectrace.com)

Metorex International OY  
Nihtisillankuja 5  
PO Box 85  
FIN-02631 ESPOO  
Finland  
[www.metorex.fi/default.htm](http://www.metorex.fi/default.htm)

Spectro Analytical Instruments  
Boschstr. 10  
47533 Kleve  
Germany  
[www.spectro-ai.com](http://www.spectro-ai.com)

### Trace Analysis/Corrosion Monitoring

Detora Analytical Inc.  
PO Box 2747  
Alliance  
Ohio 44601-0747  
USA  
[www.detora.com/default.htm](http://www.detora.com/default.htm)

### On-line Cement Analysis

Oxford Instruments  
Wyndyk furlong  
Abingdon Business Park  
Abingdon  
Oxon OX14 1UJ  
UK  
[www.oxinst.com/analytical/](http://www.oxinst.com/analytical/)

## References

- 1 R. Duer, *World Cement*, **1999**, 63–65.
- 2 S. T. Pedersen, M.S. Finney, *World Cement*, **1998**, 29, 30–37.
- 3 J. Marshall, J. Carroll, J. S. Crighton, *J. Anal. Atom. Spectrom.*, **1990**, 5, 323R–360R.
- 4 J. Marshall, J. Carroll, J. S. Crighton, *J. Anal. Atom. Spectrom.*, **1991**, 6, 283R–321R.
- 5 J. Marshall, J. Carroll, J. S. Crighton et al., *J. Anal. Atom. Spectrom.*, **1992**, 7, 349R–388R.
- 6 J. Marshall, J. Carroll, J. S. Crighton et al., *J. Anal. Atom. Spectrom.*, **1993**, 8, 337R–375R.
- 7 J. Marshall, J. Carroll, J. S. Crighton, et al., *J. Anal. Atom. Spectrom.*, **1994**, 9, 319R–353R.
- 8 J. Marshall, J. Carroll, J. S. Crighton, *J. Anal. Atom. Spectrom.*, **1995**, 10, 359R–402R.
- 9 J. S. Crighton, J. Carroll, B. Fairman et al., *J. Anal. Atom. Spectrom.*, **1996**, 11, 461R–508R.
- 10 J. S. Crighton, B. Fairman, J. Haines et al., *J. Anal. Atom. Spectrom.*, **1997**, 12, 509R–542R.
- 11 B. Fairman, M. W. Hinds, S. M. Nelms et al., *J. Anal. Atom. Spectrom.*, **1998**, 13, 233R–267R.
- 12 B. Fairman, M. W. Hinds, S. M. Nelms et al., *J. Anal. Atom. Spectrom.*, **1999**, 14, 1937–1969.
- 13 Method number IP 437/98, Standard Methods for Analysis and Testing of Petroleum and Related Products, Institute of Petroleum, London, 2000.
- 14 A. Raith, R. C. Hutton, I. D. Abell et al., *J. Anal. Atom. Spectrom.*, **1995**, 10, 591–594.
- 15 *Sulphur Methods for EN228 and EN590 Fuel Specifications*, CEN/TC19 WG27 Report on Round Robin Exercise, May 2000.
- 16 *Methods for the Determination of Metals in Environmental Samples*, US Environmental Protection Agency, Cincinnati, 1991 (see also [www.epa.gov/epa-home/index/key.htm](http://www.epa.gov/epa-home/index/key.htm)).
- 17 M. S. Cresser, J. Armstrong, J. Dean et al., *J. Anal. Atom. Spectrom.*, **1991**, 6, 1R–68R.
- 18 M. S. Cresser, J. Armstrong, J. Dean et al., *J. Anal. Atom. Spectrom.*, **1992**, 7, 1R–66R.
- 19 M. S. Cresser, J. Armstrong, J. Cook et al., *J. Anal. Atom. Spectrom.*, **1993**, 8, 1R–78R.
- 20 M. S. Cresser, J. Armstrong, J. Cook et al., *J. Anal. Atom. Spectrom.*, **1994**, 9, 25R–85R.
- 21 M. S. Cresser, J. Armstrong, J. Cook et al., *J. Anal. Atom. Spectrom.*, **1995**, 10, 9R–60R.
- 22 M. S. Cresser, L. M. Garden, J. Armstrong et al., *J. Anal. Atom. Spectrom.*, **1996**, 11, 19R–86R.
- 23 J. Dean, L. M. Garden, J. Armstrong et al., *J. Anal. Atom. Spectrom.*, **1997**, 12, 19R–87R.
- 24 J. R. Dean, O. Butler, A. Fisher et al., *J. Anal. Atom. Spectrom.*, **1998**, 13, 1R–56R.
- 25 M. R. Cave, O. Butler, J. M. Cook et al., *J. Anal. Atom. Spectrom.*, **1999**, 14, 279–352.
- 26 M. R. Cave, O. Butler, J. M. Cook et al., *J. Anal. Atom. Spectrom.*, **2000**, 15, 181–235.

- 27** G. E. Purdue, R. W. Williams, *X-ray Spectrom.*, **1985**, *14*, 102–108.
- 28** M. Hietela, D. J. Kalnicky, *Adv. X-ray Anal.*, **1989**, *32*, 49–57.
- 29** R. A. Davidson, E. B. Walker, C. R. Barrow et al., *Appl. Spectrosc.*, **1994**, *48*, 796–800.
- 30** M. Casarci, F. Bellisario, G. M. Gasparini et al., *Value Adding Solvent Extr. [Pap ISEC '96]*, **1996**, *2*, 1121–1126.
- 31** Li Wenli, G. P. Ascenzo, R. Curini et al., *Anal. Chem.*, **1998**, *362*, 253–260.
- 32** Kevex Spectrace Application Note ([http://www.spectrace.com/Applications/analysis%g\\_terephthalic%cid.htm](http://www.spectrace.com/Applications/analysis%g_terephthalic%cid.htm))
- 33** R. J. Fredericks, R. R. Comtois, W. Holtman, *Proc. Annu. Symp. Instrum. Process Ind.*, **1995**, *50*, 33–38.
- 34** S. Yamashita, T. Shimizu, *Adv. Instrum. Control*, **1996**, *51*, 23–32.
- 35** D. Connolly, C. Walker, *Ultrapure Water*, **1998**, *15*, 53–58.
- 36** ASTM Method No. D6502-99, American Society for Testing and Materials, Philadelphia, **1999**.
- 37** R. Tertian, F. Claisse, *Principles of Quantitative X-ray Fluorescence Analysis*, Heyden, London 1982, Ch. 17.
- 38** B. Holynska, M. Lankosz, J. Ostachowicz et al., *Adv. X-ray Anal.*, **1989**, *32*, 45–47.
- 39** D. J. Connolly, R. W. Dye, M. J. Mravich et al., *US Pat.*, **5,818,899**, Oct. 6 1998.
- 40** R. E. Collins, R. J. Blue, M.C. Mound, *ZKG Int.*, **1995**, *48*, 540–549
- 41** R. Dejaiffe, J. E. Willis, A. L. Heilveil, *PCT Int. Appl.*, WO96 23212 (Cl.G01N23/223), 1 Aug. 1996, *US Appl.*, **379696**, 26 Jan 1995.
- 42** W. D. Drotning, *Anal. Instrum.*, **1988**, *17*, 385–397.
- 43** L. E. Creasy, *Adv. X-ray Anal.*, **1994**, *37*, 729–733.
- 44** C. Frederici, S. Doorns, D. Villanueva et al., *At-Process*, **1998**, *3*, 125–131.
- 45** R. R. Romanosky, A. S. Visconti, S. S. Miller et al., *Prepr. Pap. Am. Soc., Div. Fuel Chem.*, **1993**, *38*, 272–278.
- 46** C. C. Trassy, R. C. Diemiaszonek, *J. Anal. Atom. Spectrom.*, **1995**, *10*, 661–669.
- 47** Council directive 94/67/CE on the Incineration of Hazardous Wastes, *Off. J. Eur. Comm.*, 31 December 1994, L365, 34.
- 48** P. P. Woskov, D. L. Smatlak, D. R. Cohner et al., *US Pat.*, **5,479,254**, 26 Dec 1995.
- 49** B. Baaske, C. Högel, S. Kirschner et al., *Spectochim. Acta, Part B*, **1997**, *52*, 1459–1467.
- 50** J. Schram, *Fresenius' J. Anal. Chem.*, **1992**, *343*, 727–732.
- 51** S. Kirschner, A. Gollock, U. Telgheder, *J. Anal. Atom. Spectrom.*, **1994**, *9*, 971–974.
- 52** T. Jacksier, R. Barnes, *J. Anal. Atom. Spectrom.*, **1992**, *7*, 839–844.
- 53** T. Jacksier, R. Barnes, *Spectrochim. Acta, Part B*, **1993**, *48*, 941–945.
- 54** M. J. Jajl, R. Barnes, *J. Anal. Atom. Spectrom.*, **1992**, *7*, 833–838.
- 55** T. Jacksier, R. Barnes, *J. Anal. Atom. Spectrom.*, **1994**, *9*, 1299–1303.
- 56** T. Jacksier, R. Barnes, *Spectrochim. Acta, Part B*, **1994**, *49*, 797–809.
- 57** R. C. Hutton, M. Bridenne, E. Coffre et al., *J. Anal. Atom. Spectrom.*, **1990**, *5*, 463–466
- 58** I. Ahmad, B. J. Goddard, *J. Fiz. Malays.*, **1993**, *14*, 43–54.
- 59** K. Song, Y. I. Lee, J. Sneddon, *Appl. Spectrosc. Rev.*, **1997**, *32*, 183–235.
- 60** D. A. Rusak, B. C. Castle, B. W. Smith et al., *CRC Crit. Rev. Anal. Chem.*, **1997**, *27*, 257–290.
- 61** V. Majidi, M. R. Joseph, *CRC Crit. Rev. Anal. Chem.*, **1992**, *23*, 143–162.
- 62** L. Moenke-Blankenburg, *Laser Microanalysis*, Wiley, New York 1989.
- 63** L. J. Radziemski, D. A. Cremers, *Laser Induced Plasmas and Applications*, Marcel Dekker, New York 1989.
- 64** L. J. Radziemski, *Microchem. J.*, **1994**, *50*, 218–234.
- 65** C. Haisch, J. Lierman, U. Panne et al., *Anal. Chim. Acta*, **1997**, *346*, 23–35.
- 66** C. Haisch, R. Niessner, O. I. Matveev et al., *Fresenius' J. Anal. Chem.*, **1996**, *356*, 21–26.
- 67** R. Wisbrun, I. Schechter, R. Niessner et al., *Anal. Chem.*, **1994**, *66*, 2964–2975.
- 68** R. E. Neuhauser, U. Panne, R. Niessner et al., *Anal. Chim. Acta*, **1997**, *346*, 37–48.

- 69** U. Panne, M. Clara, C. Haisch et al., *Spectrochim. Acta, Part B*, **1998**, *53*, 1957–1968.
- 70** D. K. Ottesen, *Symp. (Int.) Combust. [Proc.]*, **1992**, *24*, 1579–1585.
- 71** M. Sabsabi., J. F. Bussiere, *PCT Int. Appl.*, WO98 20325 (G01N 21/71, 33/15), 14 May 1998.
- 72** H. J. Häkkänen, J. E. I. Korppi-Tommola, *Anal. Chem.*, **1998**, *70*, 4724–4729.
- 73** U. Panne, M. Clara, C. Haisch et al., *Spectrochim. Acta Part B*, **1998**, *53*, 1969–1981.
- 74** R. Jowitt, I. Whiteside, *Laser Analysis of Liquid Steels*, Comm. Eur. Communities (Rep. Eor. 13932), 1997.

## **Section X**

### **Hyphenated Techniques**

## **Introduction**

*John C. Fetzer*

This chapter covers the use of spectrometers as detectors for chromatographic separations. Modern separation methods can often give a chromatogram that is composed of a large number of individually resolved peaks. The use of spectrometers in this fashion yields molecular information about each peak. This can greatly aid in peak identification and quantitation. The identification of peaks can also give the analyst information on contaminants in a product, the occurrence of side-reactions in a synthesis, the distribution of isomers, and the answers to many other specific questions.

Full-spectrum UV absorbance and fluorescence detection, and mass, infrared, nuclear magnetic resonance, and atomic spectrometries are the more common methods used. The basic aspects and limitations of these types of spectrometric detection are described.

UV absorbance and fluorescence detection are only of moderate use as liquid chromatography detectors for organic compounds because most of these do not have very characteristic spectra and many do not even fluoresce. These indistinct spectra are marked by one or two broad bands. For a few classes, however, this is not the case. The polycyclic aromatic hydrocarbons (PAHs), for example, have spectra that contain several sharp bands in a distinct pattern for each PAH. For this class of compounds, these detectors are much more sensitive and give more information on the peak identities than any other type of detector.

Mass spectrometry can be used for peak identification, with fragmentation patterns showing the presence of specific chemical groups. Infrared and NMR detection are useful for this because they also give information about the chemical functionality of the peaks detected. This can be used either to determine the structure of unknown peaks or to monitor specific chemical structures such as methyl groups, a carbonyl group, or an ether linkage.

Atomic detectors monitor the presence of specific atoms that are contained in the components of each eluting peak. This can be extremely useful when the analytes contain less common elements such as the halogens or metals. Simultaneous monitoring of several elements, even of the very common elements carbon, hydrogen, sulfur, oxygen, and sulfur, can also help identify the component molecules.

Several applications of each technique are given to show the capabilities and utilities of each. The discussion will also focus on the complementary nature of the information each detector provides in comparison to some of the others.

## **21**

# **Hyphenated Techniques for Chromatographic Detection**

*John C. Fetzer*

### **21.1**

#### **Introduction**

In all of the many forms of chromatography, detection is an inherently important final step. The type of detection can aid in the analysis by gathering information that can be used to identify the peaks seen. There can be many peaks that elute from the column of a gas, liquid, or supercritical-fluid chromatograph. Certain detectors are in fact spectrometers that examine each peak for specific information on its identity. This chapter deals with this use of spectrometers as the tail-end detector in chromatography. Other separation techniques, such as field-flow fractionation or capillary electrophoresis, differ in their separation mechanisms, but as far as coupling to spectrometers behave like one of these three types of chromatography.

If the analysis is the separation of many common complex mixtures, then many peaks can be either partially or fully resolved. The simplest and least expensive, and therefore the commonest, chromatographic detectors only yield a response for a peak, with little diagnostic power to identify it other than the retention time. The flame-ionization detector in GC and the refractive index or single-wavelength UV absorbance and fluorescence detectors in HPLC or SFC are good examples of simple, widely-used detectors of this type. This is not a limitation for routine analyses, such as those used for product quality control or process monitoring. For complex mixtures or for the situation where a problem has been identified and its causes need to be determined, chromatography with simple detectors is woefully insufficient. The hyphenated techniques, however, are ideal tools in many of these situations.

The hyphenated techniques provide a synergy where the combination far outperforms either technique alone. The spectroscopist often only thinks of the chromatograph as a novel, albeit very useful, sample inlet device. Only moderate thought is given to optimizing the separation in the way a chromatographer might do. Concurrently, many chromatographers think of the detector as only a device to identify peaks, with little concern about resolution, matrix effects, and other factors that are the spectroscopists' major concerns. They do not approach the detection in the way

a spectroscopist might. In reality, the strengths of one part compensate for the weaknesses of the other. Chromatograms are inherently complicated, but spectral information can readily simplify this by identifying some (if not all) of the peaks. The spectrometers, on the other hand, often cannot identify very similar compounds, such as isomers, and suffer greatly from matrix effects. The chromatographic retention time, coupled to the spectrometric data, often surmounts these. Additionally, the separation by its fundamental nature reduces the matrix effects because the components are separated and elute individually, making the spectrometric detection more valid.

The use of spectrometers as detectors has become very prevalent in the past decade. More and more of the hyphenated techniques reviewed here have moved from the realm of unique devices found only in an academic or government research facility. Many are now available as off-the-shelf instrument packages readily available from several possible instrument companies. In some cases, these have become very commonplace detectors because they have been commercially available for a decade or more. These are the cases when a mass spectrometer or atomic emission spectrometer is used as a gas chromatography detector or when the mass spectrometer or UV absorbance spectrometer are used as a liquid chromatography detector.

These more common separation–detection combinations have had wide usage for many years and will, therefore, be covered here in what can only be considered as a cursory fashion in relation to all of the work done with them. From the myriad of references to the operation of these detectors and their use, only a few examples have been chosen to illustrate the power of each detector when coupled to a chromatograph.

The reader will be referred to much more extensive review articles or books for details on their wide range of applications. The annual review issue of the journal *Analytical Chemistry* is a good starting point. In these review issues, alternating years cover techniques and applications. The first are a series of reviews focusing on the variety of analytical techniques, principally the various types of chromatography and spectrometry. The second is divided into a series of articles on areas such as pharmaceuticals, polymer analysis, petroleum and other fossil fuels, and environmental analyses. These issues usually appear as the mid-June volume of the journal.

The area of hyphenated techniques is so active that any researcher who wishes to stay abreast of the use of new applications and techniques must read the literature constantly. Each new issue of any of the major analytical chemistry journals contains one or two or more articles in this field. Conversely, by the nature of hyphenated techniques, an article on one particular technique can appear in many possible places. For example, an article on an HPLC separation with full spectrum UV absorbance detection of polycyclic aromatic hydrocarbons (PAHs) could appear in any of the journals that deal with analytical chemistry, chromatography, spectrometry, the chemistry of the PAHs, or materials containing PAHs. This author's own publications list shows several examples of papers appearing in each type of journal, even though each could have appeared in a different one than the one it did.

This leads to the need for table-of-contents and electronic search services to keep up.

In this chapter the various spectrometric detectors will be reviewed. These will be arranged by spectrometer type, as the use of certain detectors is not limited to only one certain mode of chromatography. For each detector, however, the individual problems inherent to coupling with each mode of chromatography will be covered. For example, the issue of how to remove the mobile-phase solvents in LC-MS will be part of the discussion of that technique in the MS section. This will be a separate segment from the problems inherent to GC-MS or SFC-MS.

These techniques generate such a wealth of data that their advent at the same time as the development of computer systems that are of high-capability and capacity, fast, reliable, and inexpensive, cannot be mere coincidence. The use of data systems with the instrumentation systems for hyphenated techniques, however, is beyond the scope of this review and will only be mentioned when it is part of an inherent advantage or disadvantage of a particular technique.

## 21.2

### Electronic Spectral Detection

UV absorbance and fluorescence are useful types of spectrometry for many classes of molecules. They measure changes in the energy levels of the molecular electrons. The wavelengths of light used correspond to energies that send electrons from a ground to an excited state. This usually involves the  $\pi$  bonding or lone pair electrons in the molecule, but higher energy (lower wavelength) transitions involving  $\sigma$  bonding electrons can also be seen. As a rule of thumb, the lower the wavelength, the greater the variety of molecules that will absorb.

UV absorbance spectrometry measures the energy absorbed when the electrons go from the ground to an excited state, while fluorescence measures the full process of that energy change and the one that results when the excited state energy is lost through photon emission. Fetzer and Biggs reviewed the use of these types of detectors for environmental analyses [1]. The specific advantages of full-spectrum UV and fluorescence detection were highlighted by many examples relating to detection of the polycyclic aromatic hydrocarbons (PAHs).

The photodiode-array based UV absorbance detector, usually abbreviated as either the PDA or DAD, but in this chapter as DAD, has been used in a wide range of applications since it was introduced commercially almost two decades ago. It allows collection of the complete UV absorbance spectrum of the HPLC column eluent. The general principles and operation of the DAD have been reviewed by Huber and George in a book on DADs and their application [2]. This book is also a good primer on the use of the DAD in fields such as clinical, pharmaceutical, environmental, polymer, and biotechnology analyses.

In this detector, a beam from a “white light” source is passed through the flow cell. Any wavelength that is absorbed by a compound flowing through the cell is attenuated following normal Beer–Lambert law behavior. The resulting light is dif-

fracted and focused on a row of optically sensitive semiconductor devices (the photo-diode array). Each photo-diode corresponds to a small spectral range and the light intensity on it affects its electronic output. With the collection of the UV spectra of the column eluent, peak identification and quantitation can both be accomplished at the same time. The simple substitution of a high-pressure flow cell for the one routinely used in HPLC makes the DAD amenable for SFC detection. There are no specific issues that arise in SFC-DAD that differ from those described for HPLC.

Certain compound classes, such as the PAHs, are ideal for this type of detection. The UV spectra of the PAHs are very intense and contain many bands that aid in definitive identification. Seemingly small differences in isomeric structure can lead to great differences in the pattern of band locations and intensities. As an example, the spectra of two isomeric PAHs are shown. The difference in the spectra arises from the different arrangements of the  $\pi$  electrons in the different ring structures of the PAH isomers. Figures 21.1 and 21.2 show the UV absorbance spectra for two similar PAHs, each one having only one or two rings more on the core structure of the bottom one in Fig. 21.1, dibenzo[cd,lm]perylene. The second pair consists of isomeric PAHs. Although the two spectra are similar, there are significant differences that characterize each. For other compound classes the differences between isomers and even very structurally different species, will be much less pronounced. This is because the presence of sulfur, oxygen, nitrogen, and other heteroatoms makes the electronic distributions less distinct and individualistic.

A DAD in static mode, when used as a stand-alone spectrometer, has slightly less sensitivity than a conventional scanning-monochromator spectrometer based on grating optics. The DAD can collect usable spectra at around 0.001 absorbance units (AU) full scale. For certain compounds with a number of intense and narrow bands, such as the PAHs, this may be even lower because the pattern of bands is so distinct. Since the spectra of many compounds have only one or two broad bands, the higher value would be the typical limit. In the dynamic mode used with HPLC, the limit for useful diagnostic spectra is around 0.01 AU, with 0.002 AU to 0.004 AU being the limit for most PAHs.

Other molecular structure factors, such as the presence of methyl or other alkyl substitution also have an effect on DAD spectra. A single alkyl-group attachment shifts the absorbance spectrum of the parent compound upwards by 1–2 nm. Although additional alkyl substitution shifts the spectrum even higher, the shift is not strictly additive. The presence of a fused saturated ring usually causes an upward shift of 5–10 nm. These small shifts in spectral location require that the DAD have corresponding resolution to see these changes.

Interestingly, when perdeuterated (every hydrogen atom totally substituted by deuterium) compounds are used as internal standards for MS detection, their presence can also be seen in the HPLC-DAD spectra. These compounds appear as blue-shifted spectra relative to those of the unsubstituted versions. For example, perdeutero-perylene has a downward shift of about 2 nm in its spectrum relative to the unsubstituted perylene, its absorbance maximum is at 432 nm compared with 435 nm for normal perylene. This is due to the electronic nature of deuterium

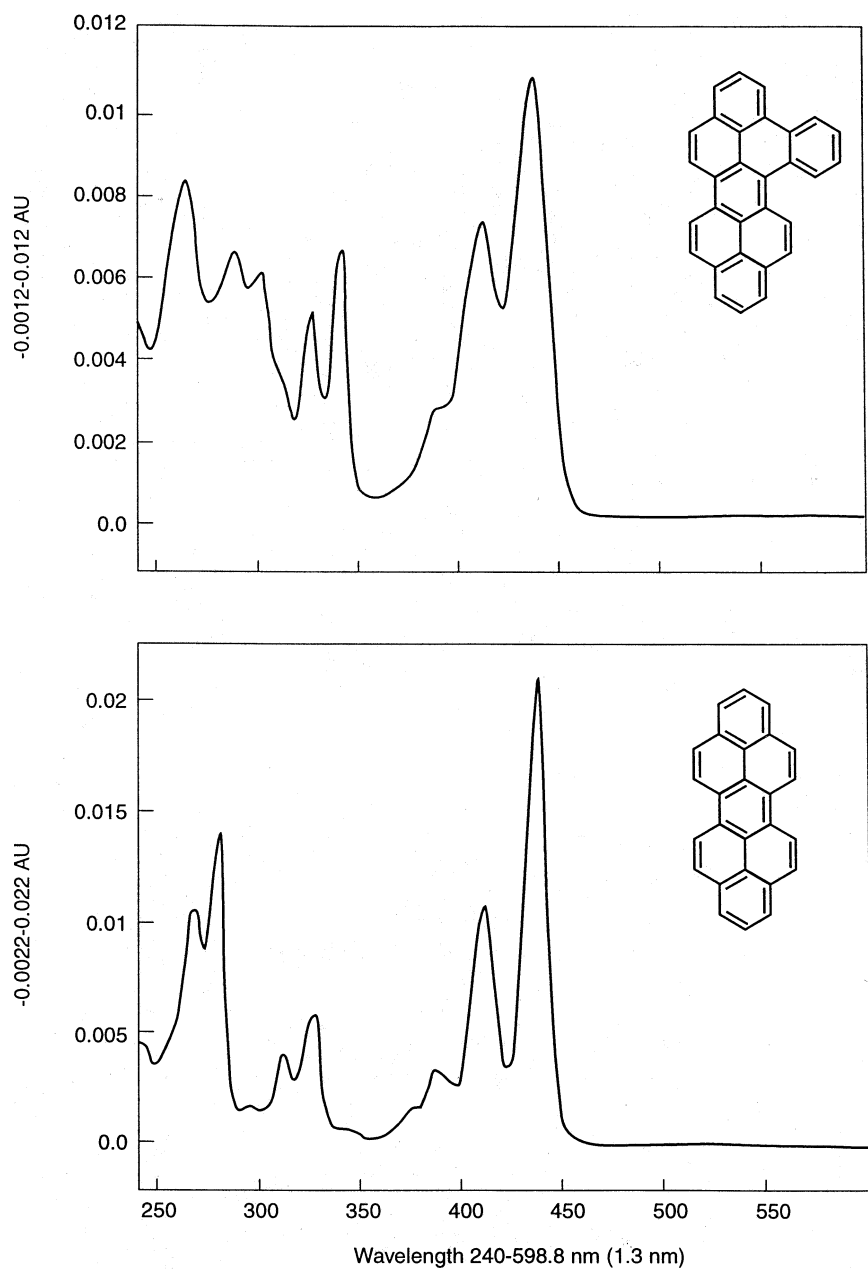


**Fig. 21.1** The UV absorbance spectra of tribenzo[a,cd,lm]perylene and dibenzo[cd,lm]perylene, showing the complexity inherent to the spectra of PAHs.

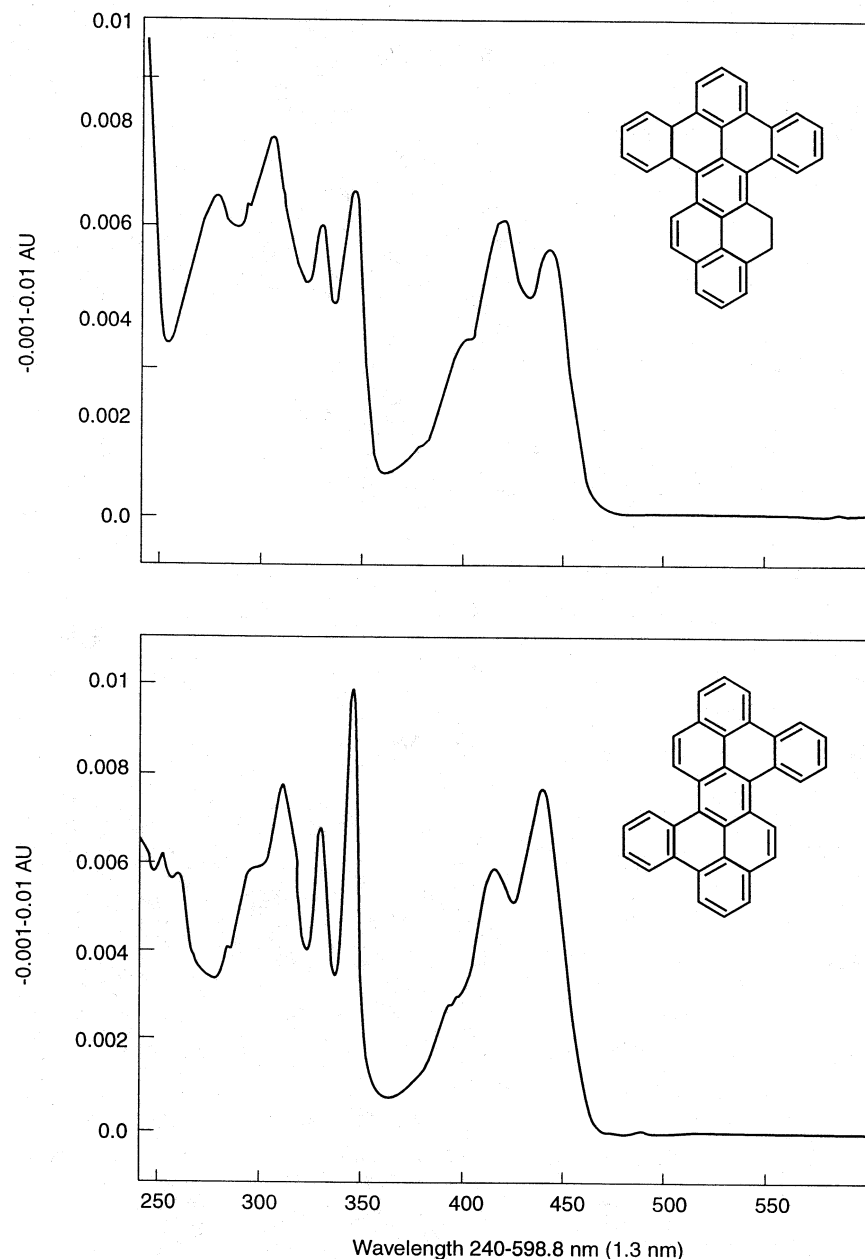


**Fig. 21.2** The UV absorbance spectra of the two isomers tetrabenzo[*a,cd,f,l*m]perylene and tetrabenzo[*a,cd,j,l*m]perylene. Note that these

spectra are not only different from each other, but are very different from those of the two similar structures shown in Fig. 21.1.

as compared to normal hydrogen atoms. This difference also results in the perdeutero versions having slightly shorter retention times than the unsubstituted versions in reversed-phase HPLC.

The DAD allows monitoring of all the wavelengths within a chosen spectral range. This makes it much more of a universal detector than the older single-wavelength designs. In those devices, major components could be assumed to be only minor constituents if the wavelength used was not at one of the compounds' stronger absorbance bands. If the wavelength was in a spectral region where a component did not absorb at all, it could be missed altogether. For example, since benzene absorbs strongly at 254 nm, this wavelength was often used to monitor for alkylbenzenes. High numbers of alkyl or fused saturated ring substituents will shift the spectrum to a very different maximum. The compound 1,2,3,4,5,6,7,8,9, 10,11,12-dodecahydrotriphenylene is such a compound [3]. It consists of a benzene ring with three saturated rings, fused at the 1,2; 3,4; and 5,6 faces. Its analogous most-intense absorbance maximum is at 273 nm, a shift of 19 nm because of the saturated ring substituents (Fig. 21.3). This band has a molar absorptivity of about 325. At 254 nm, the absorptivity is only 110. If equal amounts of benzene and this compound were injected, the chromatogram monitored at 254 nm would have two peaks. Their relative intensities would be 6.3 to 1.

Commercially available DADs usually acquire spectra from a low wavelength of 190 nm to an upper wavelength limit as high as 800 nm. For most applications, this high wavelength range is not needed. Most compounds absorb appreciably in the UV and lower visible range (350 nm to 500 nm, compounds appearing yellow or orange will absorb in this range). Metal complexes, dyes, and certain PAHs, are among the common compounds that absorb in the > 500 nm range (these compounds would appear to be red, green, purple, or blue to the human eye).

The HPLC separation of the higher fullerenes yielded one example of the advantage of monitoring at all absorbance wavelengths. Fetzer and Gallegos [4] initially performed a non-aqueous reversed-phase HPLC separation of a crude fullerene mixture. They also performed concurrent direct-probe MS analyses. All reports, at that time, of the composition of fullerene soot, reported only the major components C-60 (~ 90 %) and C-70 (~ 70 %). A series of small peaks in the DAD output after the expected two much larger ones of the C-60 and C-70 fullerenes was noticed. These small peaks had UV spectra that were characterized by almost monotonically increasing intensities when going to lower wavelengths, with very small shoulders and less intense bands at the high wavelengths. The absorbances, however, were not intense at either of the wavelengths of the two stronger bands of C-60 or for those of the many bands of C-70. Single-wavelength monitoring would either have missed these components or greatly underestimated the concentrations. Figure 21.4 shows the HPLC-DAD chromatogram with these small peaks appearing on the much more intense tail of the C-70 peak.

These small HPLC peaks corresponded to small peaks in the MS caused by C-76, C-78, C-80, C-82, and C-84 fullerenes. The total concentration of all these higher fullerenes is less than 1 %. The DAD easily observed these at wavelengths that were most sensitive for them, making their observation possible. Dieterich and

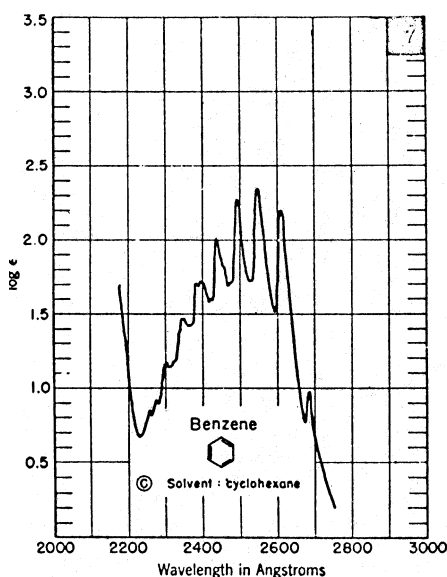
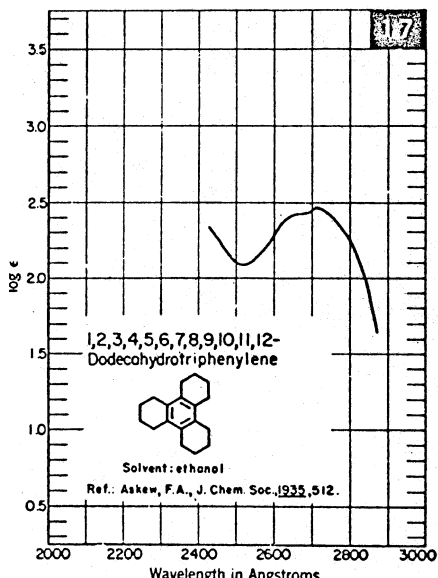


**Fig. 21.3** The UV absorbance spectra for benzene and 1,2,3,4,5,6,7,8,9,10,11,12-dodecahydronaphthalene, with both the loss in sharp energy levels and 20 nm red shift of the latter.



co-workers [5–7] then used this observation and the same separation method to isolate several of these larger fullerene species, which detailed molecular characterization, such as the mass spectrum in Fig. 21.5, showed to be C-76 fullerene, several C-78 isomers, and a wide variety of even larger fullerenes. Although these interesting carbon clusters would have eventually been discovered and isolated, the use of

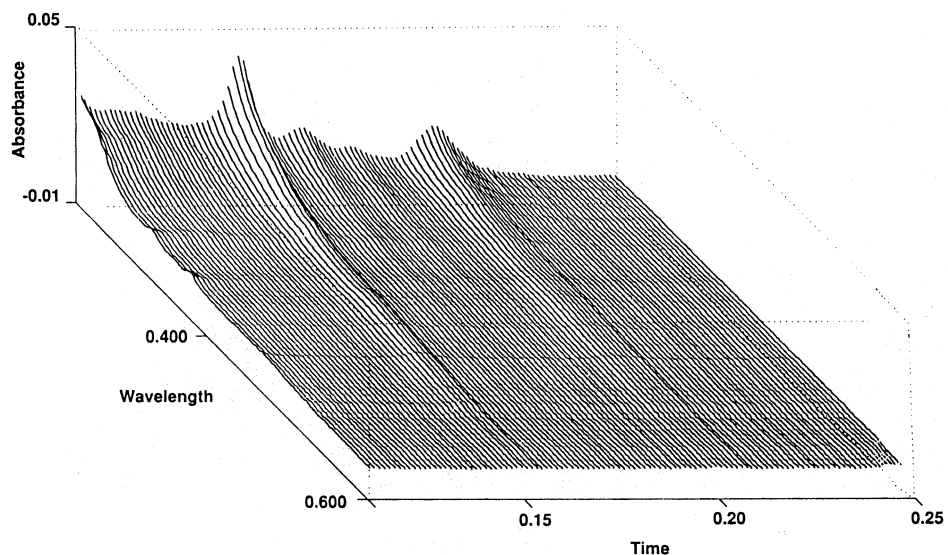


**Fig. 21.4** The later-eluting portion of the DAD chromatogram of a fullerene separation, showing several small peaks. These turned out to be heavier fullerenes.

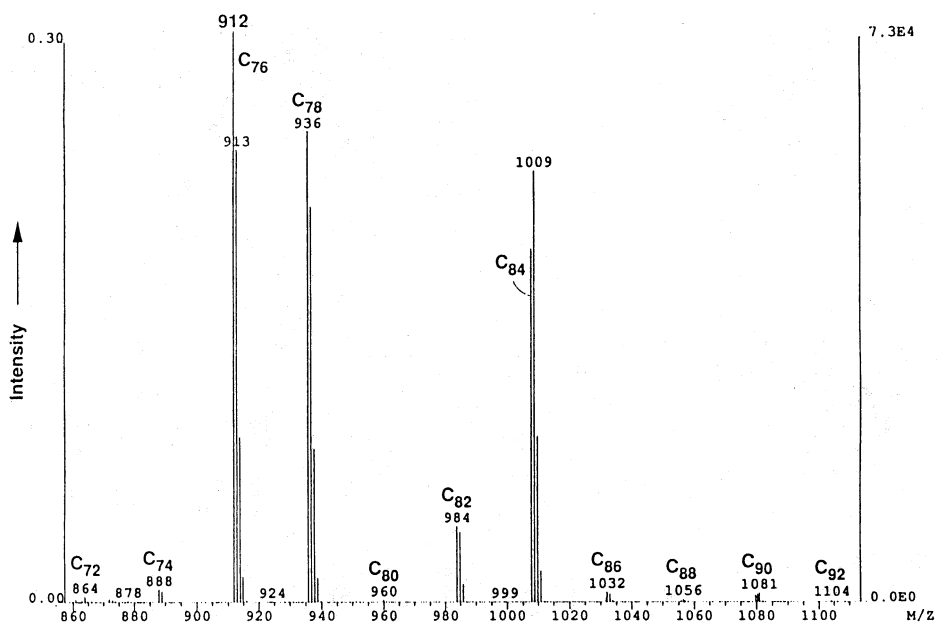


**Fig. 21.5** The mass spectrum of the material in Fig. 21.4 which showed that it was fullerenes larger than the C<sub>60</sub> and C<sub>70</sub> that predominate.

a DAD that enabled the observation of these minor peaks accelerated that discovery by several months.

Another example where using the DAD was advantageous was the unexpected discovery of a new eight-ring PAH [8–10]. A synthesis had been performed to make a certain other eight-ring isomeric PAH. This target PAH was preparatively separated by reversed-phase HPLC and a DAD was used to monitor the separation. After the isolation of the desired compound was completed, a very strong mobile phase of pure dichloromethane was used to clean off the column. After a short period of time, the column effluent showed a peak, which from the spectrum was obviously a PAH (the many bands clustered in packets of increasing intensity is characteristic of many PAH spectra, Fig. 21.6). This turned out to be a strongly retained isomer of the target PAH. It had a capacity factor of around 2 orders of magnitude greater than that of the dominant, but much earlier-eluting isomer (the upper spectrum of Fig. 21.1). The target PAH was a compact, non-planar structure and the unexpected one was elongated and planar, with these gross structural differences causing the retention difference.

The shift to slightly higher wavelengths described for the alkyl substitution of benzene is much more generic. It applies for all compound types and a large number of substituents. The classic Woodward–Hoffman additivity “rules” describe

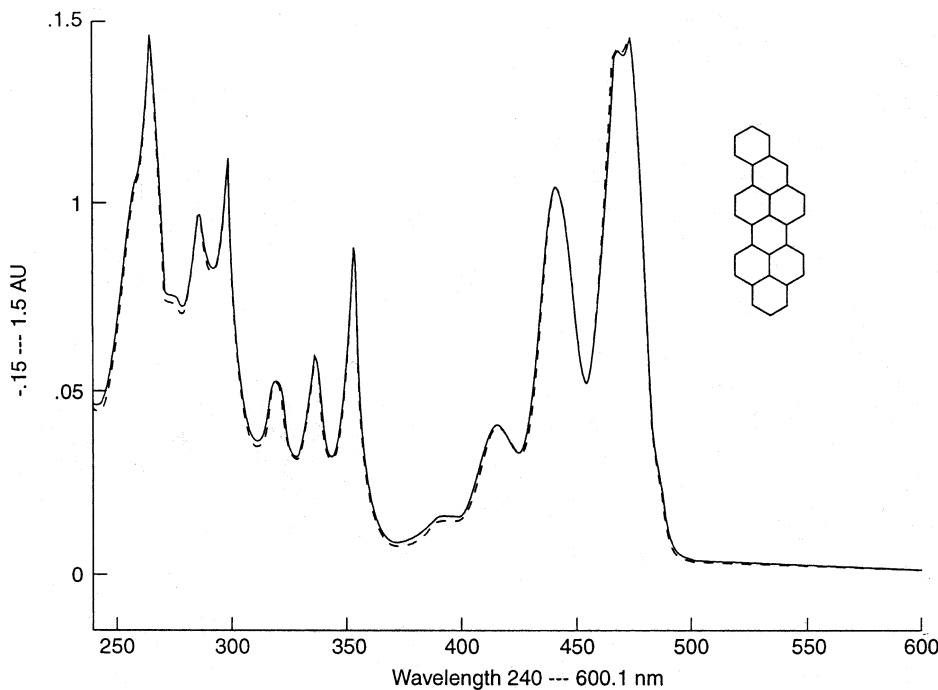


**Fig. 21.6** The UV absorbance spectrum of benzo[rst]-naphtho8,1,2-[cde]pentaphene, a new PAH unexpected discovery through the use of a DAD.

these and have been used to estimate the shifts for a wide variety of compound classes. These orderly trends in UV absorbance relative to structure can aid in identifying unknown peaks.

For simple compounds, such as either the unsubstituted compounds or their monomethyl derivatives, spectral matching programs that are included in the standard DAD data software usually work well. This is not true, on the other hand, for other more substituted compounds. Where the spectral shift due to alkyl-substitution is greater than 1–2 nm, the spectral shift is not recognized as such by the software. The currently available software does not work well [11, 12]. These programs generally work by spectral matching done on a point-to-point comparison, rather than by looking at the patterns of the spectral bands by comparison of the relative intensities of spectral features and the distance of each band from the others. The point-by-point method takes each wavelength intensity and, based on the Beer-Lambert law, normalizes the spectrum for comparison. Each wavelength's intensity is then compared to those in the standard spectra. Matches result from spectra with the smallest total of differences between the unknown peak and the reference spectra. Good matches may result because the unknown and a standard both contain a large absorbance band at the same wavelength, although numerous small bands in each may be very different.

With greater substitution, the common programs instead only see the large differences in location, due to the shift of the spectrum by the substitution, as altogether different peaks. They do not see the similarities in patterns because each band is examined separately. For example, the spectra, shown in Fig. 21.7, for unsubstituted PAH pyrene and for a highly alkyl-substituted pyrene (like the compound, 1,2,2a,3,4,4a,5,6-octahydrocoronene, with the dissimilarities accentuated for the spectral band at 305 nm due to residual impurity coronene) can be compared [3]. The similarity in the peak shapes and relative locations of the absorbance bands is obvious to the naked eye. A spectral matching program, however, cannot recognize the second compound as a pyrene-type species because the spectral shift is too large for the similarity to be found in a point-to-point comparison.

Co-elution of peaks is also not a serious problem with DADs because the spectra obey the Beer-Lambert law. The data computer, therefore, can examine the spectra across a peak for proportionality and yield a peak purity measurement. Since each co-eluting component contributes to the total absorbance at each wavelength, the changes in absorbance with retention time reflect the compositional changes. Software can assess these changes in the increase or decrease at specific wavelengths, and mathematically extract the contributions of each component. When recombedined for all wavelengths, individual spectra of each component are obtained [13]. These can then be compared to spectral libraries for identification (similar to the treatment of any of the spectra of any peak).

Since the DAD is a multiple-wavelength detector, data manipulations are possible with it that are impossible for single-wavelength detection. A simple example is co-elution of two components. If the retention times are slightly different, then the spectra from different times across the chromatographic peak will differ and show the co-elution. In the case where there is co-elution of a small number of compo-

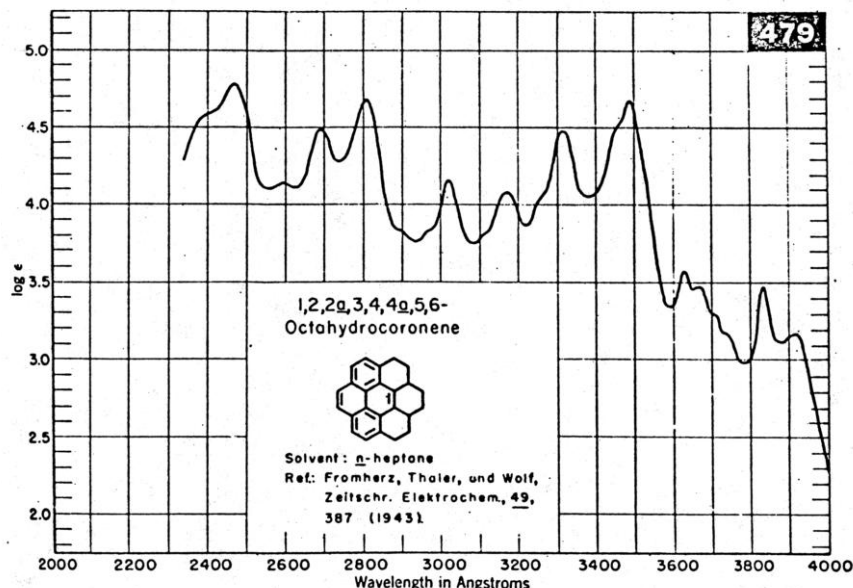
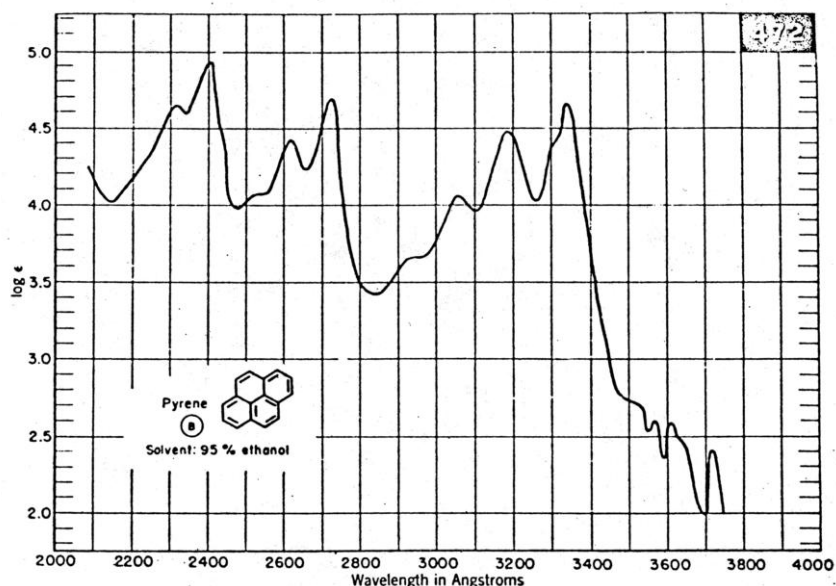


**Fig. 21.7** An example of the similar spectral pattern of highly alkyl-substituted PAHs. The peak in the lower spectrum at 305 nm is due to

some residual coronene from the starting material.

nents in a retention range, the overlapping peaks can be deconvoluted if there is any difference in retention times. For each wavelength, the intensity changes as the sum of the individual contributions due to each component (the Beer–Lambert Law). Across the peak of a single component, the spectra will all be proportional to each other. If two components with even slightly different retention times are within the peak, then the relative intensities will change. The contribution of the two components to each wavelength will be their individual absorbances based on their concentration at the retention time of the spectrum. Algorithms can separate the contribution from each and recreate the spectra of each component.

In the simplest case of two co-eluting compounds, the molar absorptivities need only be very different at two distinct wavelengths for deconvolution to be possible. The relative changes in intensity at these two wavelengths are enough to mathematically separate the spectral contributions of each compound at the different retention times. Both the retention times of the peak maxima of each component and their absorbance spectra can be separated from each other by the computer's algorithms.

Ramos et al. [13] first separated the individual spectra of benzo[*b*]fluoranthene and benzo[*k*]fluoranthene or chrysene and benz[*a*]anthracene from each other in a purposely created co-eluting peak of mixtures of each of the two pairs of PAHs. They were then able to deconvolute the individual spectra from a mixture of the isomers benzo[*e*]pyrene, benzo[*b*]fluoranthene, and benzo[*k*]fluoranthene in a similar fashion. In all cases they purposely generated peaks with severe overlap (greater than 90 % of each peak co-eluting with the other components) to show the power of deconvolution. Tauler et al. described another algorithm to deconvolute the individual spectra in co-eluting peaks and reviewed similar efforts by others. Multivariate curve resolution has been used as an alternative approach for peak deconvolution. It can identify minor impurity peaks and yield the "true" retention times [14, 15].

One problem arises in DAD use that was not as major in single-wavelength detection, the absorbance of the mobile phase. In single-wavelength detection under isocratic (constant composition) conditions, any absorbance due to the mobile-phase solvents only resulted in a constant increase in the baseline. This was easily overcome by normalizing the baseline output to zero. If gradient elution was used, the baseline rose in a continuous, readily accounted for fashion. With DADs, the total absorbance of the mobile-phase interferes with spectral collection in that range. Deconvolution software, however, can extract the spectra.

The advent of high-capability personal computers has fueled the growth in capabilities of the DAD. Early commercial versions of the diode-array absorbance detector (ca. 1982), for example, were operated off a small desktop computer with similar capabilities to today's hand-held calculators and data storage of only a few kilobytes. These instruments could only collect the spectra, determine peak purity, and match spectra from a small set of about 24 standards. Only a similar number of sample spectra could be collected because of the limited memory of such small computers. As the previous paragraphs highlight, the abilities of DAD software and data storage are much greater today. A typical 30 min HPLC-DAD run that col-

lects a spectrum every other second over a 250 nm range, might take several megabytes of storage.

Solvent selection with DADs must take the mobile-phase absorbance into account if the analytes have absorbances in the range of any of the potential choices. The choice of strong solvents for a gradient separation can be severely limited if some of the possibilities absorb in the wavelength regions of interest. For example, in aqueous reversed phase HPLC, methanol and acetonitrile have similar elution strengths and from a chromatographic standpoint one or the other can be used. Acetonitrile is much more favored, however, from a spectrometric standpoint because it does not absorb above 195 nm. Methanol has strong absorbance up to 230 nm and would mask any compounds that absorb below that wavelength.

Because of this much lower wavelength capability, acetonitrile allows detection of compounds containing sulfur, nitrogen, oxygen, and most other heteroatoms. Even the saturated alkanes absorb in the 210 to 220 nm range. Thus, aqueous acetonitrile gradients can be used for the analysis of sugars, amino acids, vitamins, and many other compounds that would be masked by the use of methanol.

Additionally, some solvent choices may require extra steps that must be taken to reduce the absorbing impurities of the solvent. Ethyl acetate and tetrahydrofuran (THF) are such solvents because they are unstable to hydrolysis or oxidation. UV absorbing impurities form when these solvents are exposed to water or oxygen prior to storage. Passage through freshly activated silica removes the impurities from ethyl acetate, while the peroxide that forms in the THF can be removed with sodium metal. These steps lower the UV wavelength cut-off for these solvents by 20 to 25 nm.

There have been many publications on the use of HPLC-DAD. As one set of examples that highlights both the growth and now-current wide application, is the analysis of the larger PAHs. This class of compounds has many, many isomers that have very similar structures and retention times. The collection of spectra by the DAD allows each HPLC peak to be monitored and compared to standard or reference spectra. PAH mixtures are usually very complex, so the separation and identification of these samples by using HPLC-DAD highlights the powerful capability possible with this combination.

One of the earliest works using HPLC-DAD for the identification of the large PAHs involved the analysis of a diesel particulate extract [16–18]. About a dozen LPAHs were found. The identifications made were later correlated to the observed mutagenicity of this diesel particulate. A carbon-black extract, obtained from the same carbon black was examined by HPLC-DAD. The DAD, as well as a much larger collection of standard compounds, allowed the identification of around 20 more LPAHs than in earlier studies of this same material.

McCarry et al. [19–25] performed a similar series of HPLC fractionations to determine the PAHs in sediment samples. They observed  $C_{24}H_{14}$  LPAHs similar to those found by Wise and co-workers in a coal-tar SRM. In later work, LPAHs of 26, 28, 30, and 32 carbons were found. Both a DAD and direct atmospheric-pressure chemical-ionization mass spectrometry were used for detection. To make the DAD less specific and more universal, the average response from 250 nm to 370 nm was collected as a total-absorbance chromatogram.

A new eight-ring PAH, phenanthro-5,4,3,2-[*efghi*]perylene, was observed in the HPLC-DAD analysis of a deposit from the catalytic hydrocracking of a petroleum-based feedstock [26]. This new PAH eluted close to the known isomer, benzo[*a*]coronene, but even with severe overlap of the two peaks, the DAD could deconvolute the combined spectra and yield one for each of the components. Preparative HPLC-DAD resulted later in the isolation of the pure new compound. A coal-tar pitch was separated and DAD spectra were used to identify the PAHs in it [27]. Several of the large PAHs, such as benzo[*a*]perylene and dibenzo[*a,j*]perylene, were found in this sample indicating that the formation mechanism included condensation of smaller PAHs through formation of bridging rings.

Some studies that focus on the formation of PAHs as a route to soots have relied heavily on HPLC-DAD analysis of the products of the pyrolysis of smaller PAHs [28, 29]. The analyses have found numerous larger PAHs that indicate that both condensation reactions and gross molecular rearrangements occur. The DAD allowed identification of several minor components, as well as some major ones that suffered from co-elution. Deep-sea hydrothermal vents, where magma seeps through faults and contacts ocean water and the detritus on the seafloor, have been shown to produce PAH-containing material. Several large PAHs were found by HPLC-DAD analyses in these complex mixtures [30, 31]. The use of on-line UV spectral collection allowed definitive identification through comparison with the retention times and spectra of standards. The identifications then led to ideas about the formation mechanisms. An example is found in the hydrothermal vent work. Several very condensed structures, including benzo[*ghi*]perylene, coronene, and ovalene, pointed to a formation through a series of one-ring additions. Other species seen could not form in this fashion, but their structures suggest formation through condensation reactions.

There have only been a few reports of gas-phase UV detection. The biggest drawbacks are that many volatile compounds have few characteristic chromophores and that gas-phase spectra differ dramatically from the solution spectra found in most references and in the published literature. In the gas-phase, the electronic transitions are better defined, whereas in solution the molecules have interactions and collisions with the molecules that spread out the energies, thus broadening the spectral bands.

For the sake of brevity we will use the acronym FSFD for full-spectrum fluorescence detector. There have been a few reports of FSFDs. There have been a variety of optical elements, including vidicons (television-type cameras with associated storage devices) and diode-arrays. There have been a few publications describing the use of FSFDs, many of which were used in PAH analyses. The PAHs are generally highly fluorescent and their spectra are very rich with many bands in both the excitation and the emission spectra. Two examples of PAH fluorescence spectral pairs are shown in Fig. 21.8 and 21.9. The first shows the common mirror-image pattern found for many PAHs, but the latter shows the asymmetrical one seen for many common highly condensed PAHs.

Jadamec et al. [32] reported an early FSSD that was based on a fast-scanning fluorometer with a flow cell. The output from the spectrometer was displayed on an

oscilloscope. The display was recorded by a vidicon (television-type) camera to collect spectra from an oscilloscope. They separated crude oil fractions from an oil spill sample and identified naphthalene and fluorene. Some of the later-eluting peaks were described as possible “polyphenyls”, but a lack of available standards could not preclude that these were not similar larger PAHs or other fluorescing heteroatom polycyclic compounds.

Gluckman and Novotny [33–35] and Cecil and Rutan [36] built two examples of in-lab assembled FSFDs that were based on diode-arrays as the detection element. The first group described a diode-array based emission monitor. They separated a variety of PAH standard mixtures and the carbon-black extract, identical to that used for the earlier GC-MS studies described above. Only a few of the PAHs were identified due to a lack of standard reference compounds or spectra, but two peaks were ascribed to non-alternant structures (containing five-member rings) to the large PAHs rubrene and decacyclene on the basis of similar patterns in their spectra.

Cecil and Rutan examined the corrections that need to be made in the fluorescence spectra gathered by diode arrays when there are differences in mobile-phase solvents. Normally, the changes in the strength of solvation between PAHs and different solvents lead to shifts in the spectra. Non-polar solvents, like

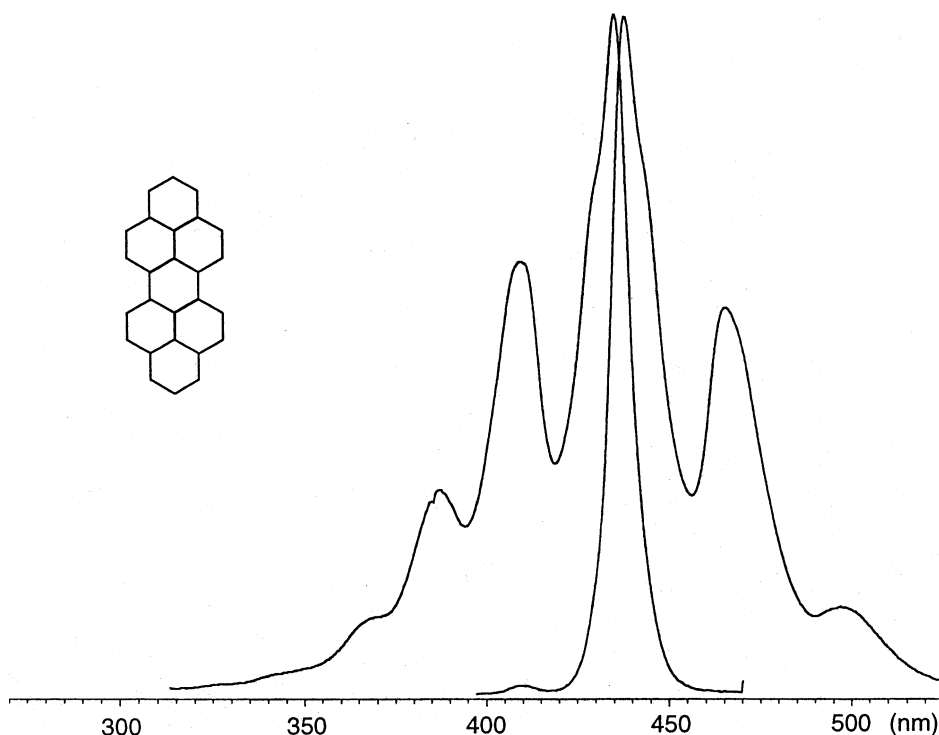


**Fig. 21.8** The excitation and emission spectra of dibenzo[cd,lm]perylene.

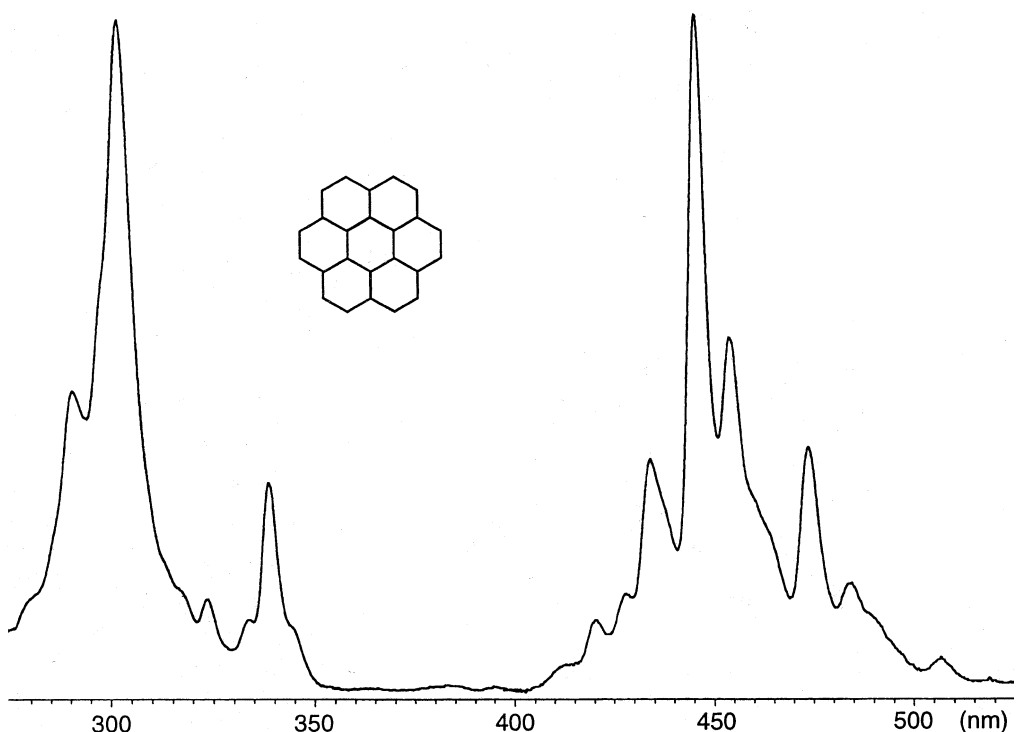


**Fig. 21.9** The excitation and emission spectra of coronene, showing their asymmetry.

n-hexane, iso-octane, or supercritical carbon dioxide, exhibit the lowest wavelength spectra because their solvation energies are the smallest. As solvents interact more strongly with the PAH, the fluorescence transition energy goes down. This leads to higher wavelength spectra. They found that both the wavelength shifts and band height changes are significant. Spectral matching to literature spectra (which would be the common mode since large collections of standard compounds are not practical) is made difficult. For example, perylene has a 6 nm higher wavelength when the solvent is changed from pure methanol to 20% water in methanol. The collection of a standard spectral library under set conditions was recommended, with algorithms dealing with the wavelength shifts. The second issue of relative changes in band heights was not addressed.

There is a recently introduced commercial FSFD [37]. Through the use of DAD-based optics, data can be collected as either the excitation spectra at a fixed emission wavelength or the emission spectra at a fixed excitation wavelength. The layout of this FSFD is shown in Fig. 21.10. The introductory brochure for this instrument gives examples of its use for PAHs, aflatoxins, vitamins, carbamates, and glyphosate and its main metabolite (the latter two examples were after appropriate derivatization to form fluorescent compounds). As the use of this detector increases, so too should literature reports of its application. Figures 21.11 and 21.12 are exam-

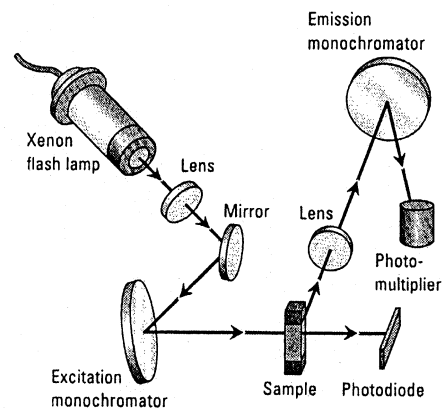


**Fig. 21.10** Schematic of a commercial FSFD. (Courtesy of Agilent Technologies Co.)

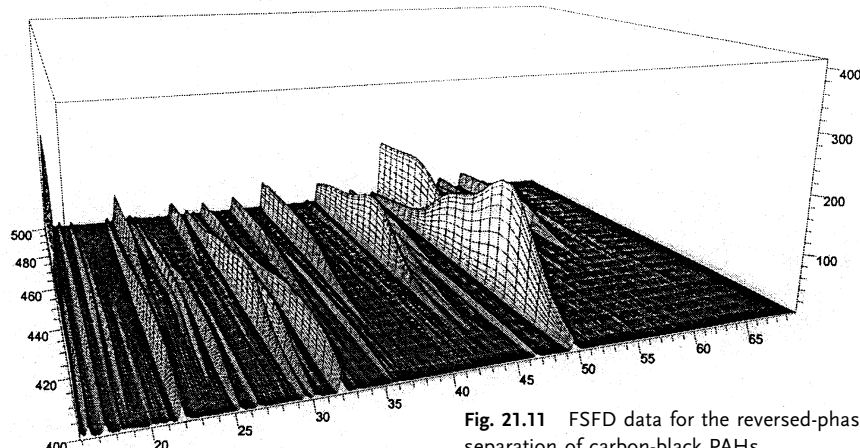


**Fig. 21.11** FSFD data for the reversed-phase separation of carbon-black PAHs.

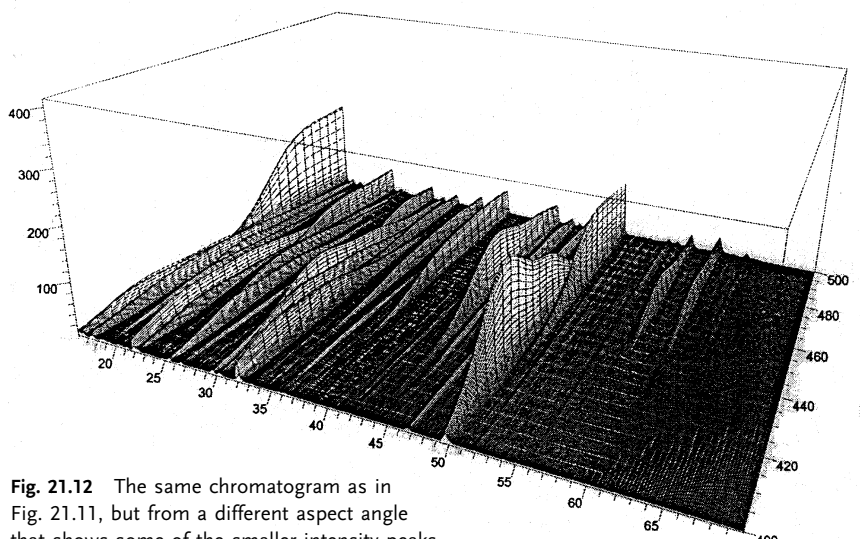


**Fig. 21.12** The same chromatogram as in Fig. 21.11, but from a different aspect angle that shows some of the smaller intensity peaks.

ples of the type of data available with this instrument. A carbon-black extract containing numerous large PAHs was separated by non-aqueous reversed-phase HPLC. The FSFD spots even minor components because it sees all of the fluorescence wavelengths. One unfortunate feature of this detector can be seen in these chromatograms. The designers chose to sacrifice spectral resolution for greater sensitivities by building in a wide spectral slitwidth (15 nm). The usually sharp multitude of peaks occurring in PAH spectra are not observed.

Burt et al. [38] coupled an HPLC to detect and identify several PAHs through measurement of their fluorescence decay lifetimes. Several wavelengths were monitored simultaneously to differentiate some closely eluting peaks.

Fogarty and co-workers [39, 40] used a dye-laser source and a videofluorometer, with a diode-array emission detector, to collect the complete three-dimensional excitation-emission map (EEM) of individual PAHs in a mixture of 18 standards. Their chromatographic data could be displayed as individual EEMs of peaks, or as the excitation or emission spectra as functions of the retention times.

Fluorescence detection has many inherent advantages and disadvantages. The major advantages include very high sensitivities, less interference from co-elution or chances for misidentification because only a small number of compounds fluoresce, and more selective detection because both the excitation and emission wavelengths are used [41]. The disadvantages are somewhat similar, by including too much selectivity so that wavelength selection for more than a single compound can be complicated (involving wavelength programs for retention windows), the higher sensitivity often requires more dilutions to get into the working range, quenching due to dissolved oxygen in the mobile phase or other components in the sample may unknowingly reduce the responses, and certain molecules (in particular some of the PAHs) have very solvent dependent responses.

One of the biggest advantages is the very high sensitivity. Since the signal of the sample's emitted light is measured directly (in contrast to UV absorbance measurement which measures small differences in the light beam intensities); there is little interference. This is accentuated by the measurement being at different wavelengths than the excitation and by the viewing optics being positioned at right angles to the incident excitation beam.

With this high sensitivity, the use of a DAD and a FSFD in series does not work well for highly fluorescent compounds. The analyte concentrations needed to yield DAD spectra of greater than 0.01 AU usually result in fluorescence emission peaks that are way off scale with the FSFD. The inherent sensitivities of a FSFD for PAHs, for example, are two or three orders of magnitude lower than those for a DAD. So, at the DAD limit of detection, the FSFD may have a signal a hundred or a thousand times larger in scale. In this case both spectral identification and quantitation with the DAD is more difficult. The regions of the absorbance spectrum that are off scale are, of course, unusable, but there are generally some wavelength ranges where less intense bands absorb. Integration of the chromatogram at the wavelength of one of these bands can also be used for quantitation.

For compounds that are weakly fluorescent, with quantum efficiencies of less than 0.1, the differences are much smaller and it might be possible to use these

two detectors in series. In this case, the FSFG would be in the emission spectral mode since the absorbance and excitation spectra are generally similar (because they arise from similar electronic transitions). This combination, however, is advantageous when both fluorescing and non-fluorescing analytes are targeted. One notable example is the EPA 16 priority-pollutant PAHs, where 15 fluorescence intensely. The three-ring acenaphthylene does not fluorescence, but the DAD can readily determine it.

The selectivity of detection is also very high, since few compounds will both elute in the retention range expected for a component of interest and excite and emit at the chosen set of wavelengths. The latter characteristic, however, can also be a disadvantage if the analyst is trying to determine the composition of an unknown mixture because the use of selective wavelengths may lead to missing components that fluoresce at other wavelengths or do not fluoresce at all.

An additional advantage inherent to the FSFDs is that the presence of co-eluting impurities can be observed. These compounds that would normally go undetected and affect quantitation should be readily seen, either as additional fluorescence if the compound does fluoresce or as reduced fluorescence or skewing of the spectrum if the compound only absorbs UV light. When working at typical analytical levels, the fluorescence signals from two compounds are additive, the first problem can be both spotted and corrected for.

The latter effect is known as inner-system filtering and is common in many “real world” samples. There are two types of inner-system filtering that reduce the fluorescence signal. In the first, the co-eluting species absorbs at the chosen excitation wavelength, thus reducing the incident beam intensity. The analyte then has a reduced excitation rate and the signal is diminished. In the second type, the emitted light from the analyte is absorbed by the co-eluting species, which would also diminish the signal. In either case, the effect should be proportional to the absorbance of the co-eluting species. This is extremely unlikely to match the spectral pattern of excitation or emission of the analyte (whichever occurs from one or the other type of inner-system filtering). Thus, the fluorescence spectrum would be altered non-uniformly and appear to be skewed relative to that of a standard injection of the same compound where no filtering occurs.

### 21.3 MS Detection

GC-MS is the most widely used hyphenated technique and there have been many comprehensive reviews. This description will only be a brief overview and touch on specific issues relevant to the coupling of the GC to the MS. The interfacing of the GC outlet to the MS inlet usually requires some type of selective carrier gas removal. Although direct connection of the GC to the MS is feasible (if large enough vacuum pumps are used), this is rarely done. This is because the vacuum at the outlet of the column can affect the separation efficiency, making most calculations of column retention parameter or efficiency calculations impossible, and the MS

system must be shut down for column switching. The large excess of carrier gas is inherently not compatible with the vacuum needed for MS.

Common interfaces include the molecular jet and flow splitters. The first uses the difference in momentum between the low-molecular weight carrier gas and the high-molecular-weight analytes. The column effluent passes into the separator inlet line, which is enclosed in a glass chamber that is under vacuum. A small gap separates this line from the outlet line. Sample molecules move preferentially from one line to the other by inertia, while much of the carrier gas is removed tangentially by the vacuum. The enrichment also increases the sensitivity of GC-MS.

In splitters, a narrow length of connecting tubing restricts the flow into the MS. The remainder of the GC effluent flows out as waste. Two types of splitter designs are used, open and direct. In open splitters, the mechanism is similar in concept to the jet separator. The column outlet butts into the restrictor, which is contained in a sheath. A stream of helium sweeps this area. The carrier gas is preferentially swept away from the restrictor, while the heavier analytes move toward the restrictor opening. In direct splitting, a simple tee connection results in only part of the flow passing through the restrictor.

The molecular jet and both types of splitter suffer from sample discrimination. In the jet separator and open splitter the enrichment varies with molecular weight. In the direct splitter, the ratio of the split changes as the temperature is ramped upwards in the commonly used gradient mode. The relative quantities of different analytes vary, making absolute quantitation impossible without tedious measurements of the enrichment or split flow ratios.

A few applications highlighting the power and limitations of GC-MS will be given, but the reader is directed to the reviews that focus on applications for a broader perspective of the use of GC-MS.

An example of the powerful combination of high-resolution GC with MS detection is shown in Fig. 21.13 to 21.19. Figure 21.13 is the total ion chromatogram of the separation of a commercial lubricating oil additive. Figures 21.14 to 21.19 are some of the individual peaks and the structures assigned to them by mass spectral interpretation of the fragmentations and mass losses. Note that certain peaks are identified as members of an isomeric set, with the other peaks yielding almost identical spectra.

The petroleum industry was one of the more important spawning grounds for GC-MS. The inherent nature of petroleum, and more importantly those of the much more valuable processed products derived from it, made this a natural occurrence. Petroleum products are almost totally composed of the non-polar or low-polarity compound classes of saturated hydrocarbons, olefinic hydrocarbons (those that contain an alkene double bond), and aromatic hydrocarbons. By being non-polar or only slightly polar, the volatilities of these compounds are very high. The inter-molecular interactions are primarily the weak van der Waal's and aromatic  $\pi$  bonding dipole-dipole interactions. Hydrogen bonding and acid-base interactions are only prevalent in the heavier materials such as residual (asphaltic) materials where the nitrogen and oxygen content is high. Processed material has

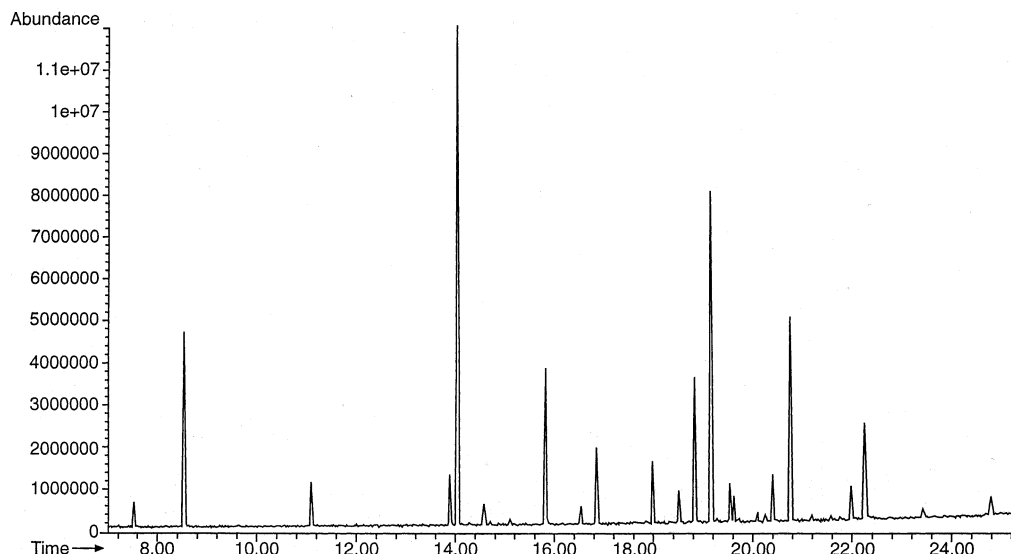


**Fig. 21.13** The total ion chromatogram of the GC separation of a commercial lubricating oil additive.

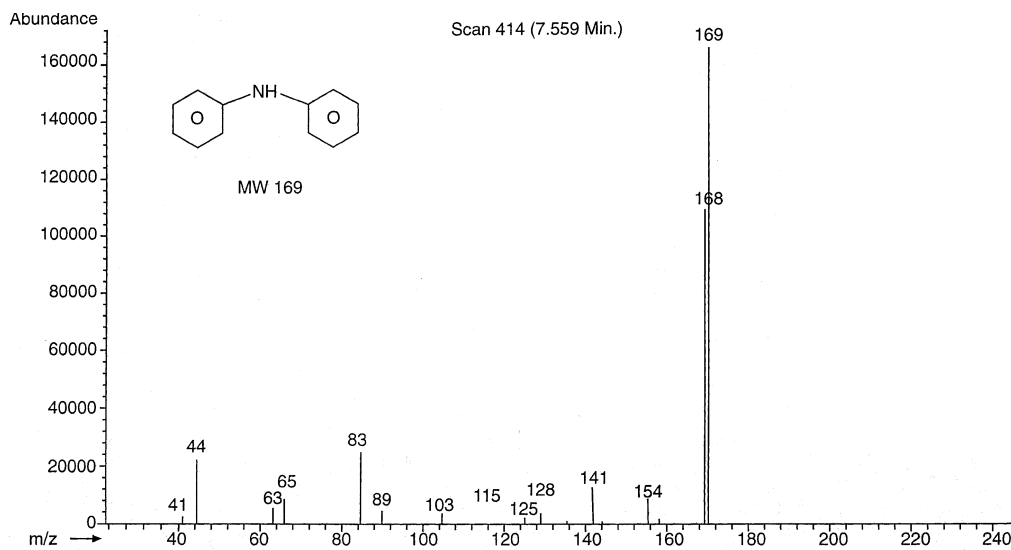


**Fig. 21.14**

**Fig. 21.14–19** The mass spectra of individual peaks in the chromatogram in Fig. 21.13. The numbers refer to the retention times. Courtesy of J. D. Hudson and M. T. Cheng, Chevron Research and Technology Co., Richmond, CA, USA.

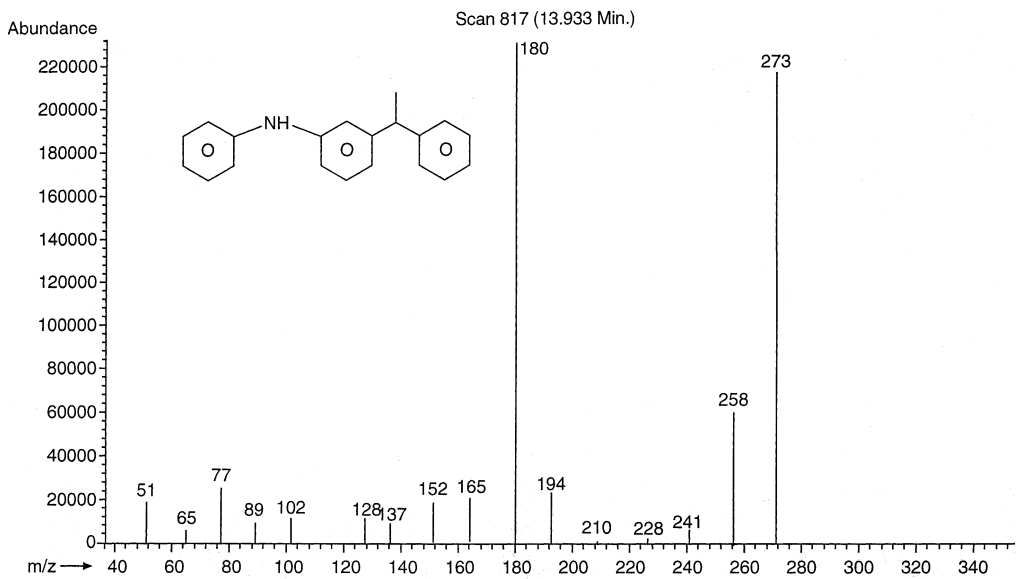


Fig. 21.15

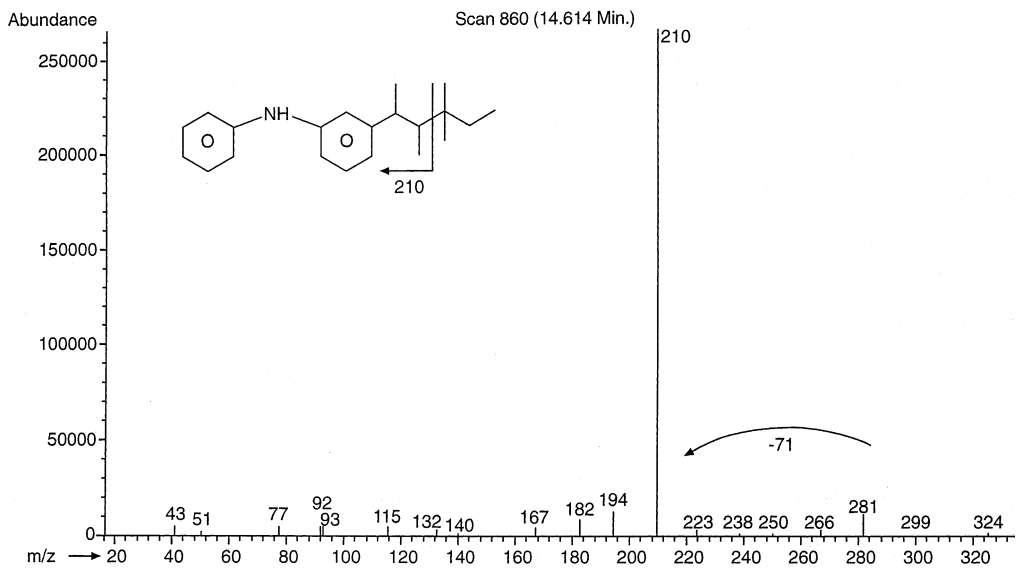


Fig. 21.16

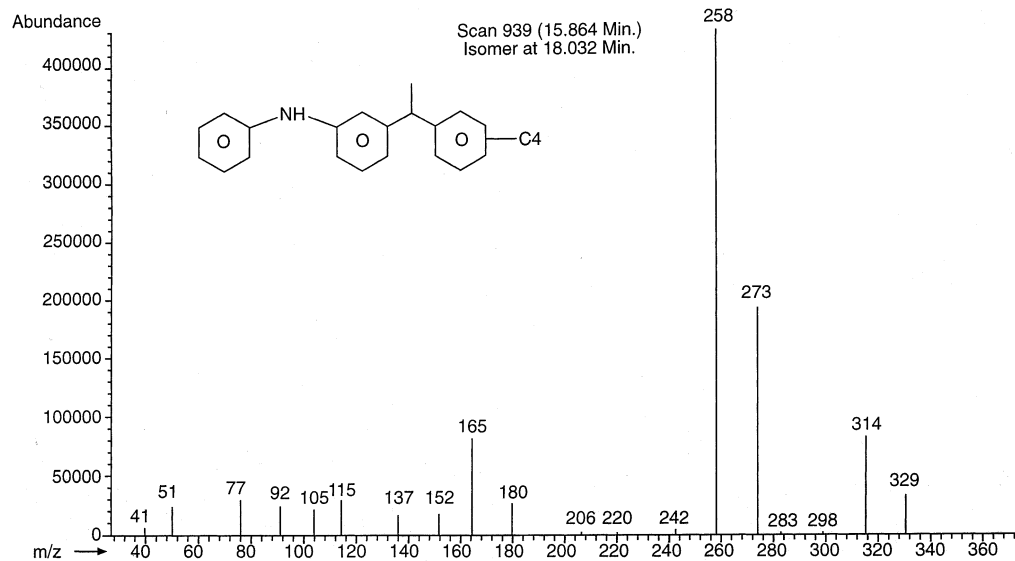


Fig. 21.17

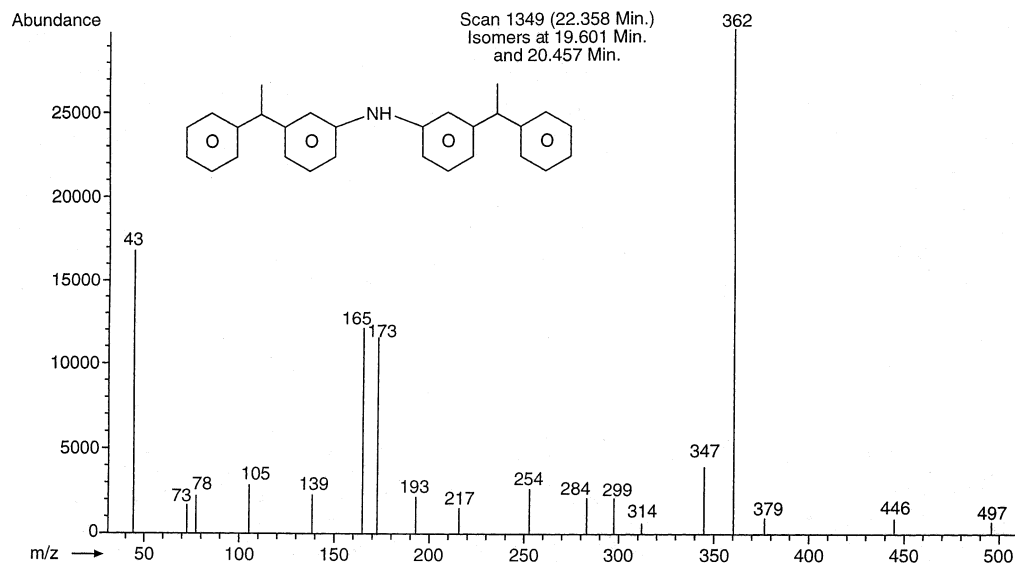


Fig. 21.18

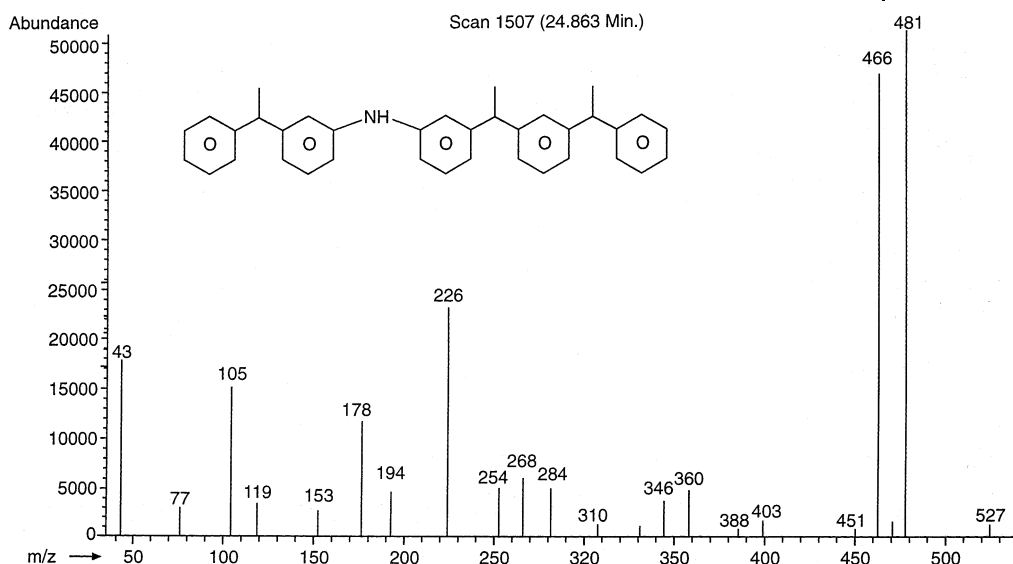


Fig. 21.19

undergone treatment to remove heteroatoms, so even the heavier fractions of lubricating base oil and wax are volatile enough for GC analysis.

The major impurities in these materials are the sulfur-containing analogues of these classes, which are also very non-polar. Due to the lack of polar functionalities, these compound classes are all relatively volatile. The only limitation to volatility is increasing molecular weight, but saturated hydrocarbons of at least 80 carbon atoms can be separated by high-temperature GC methods. The waxes and lubricating oil base stocks that are among the heavier processed products are lower than this carbon number. The most economically important materials, gasoline (petrol), diesel fuel, and aviation jet fuel (kerosene) all range from 5 to 20 carbon atoms.

Concurrently, there are large numbers of hydrocarbon compound isomers because of the presence of chain branching and saturated rings. The physical and chemical properties of each of these as components of the fuels determine the overall fuel properties. The high-resolution of GC, coupled to the carbon number and degree of saturation information from MS, can be used to predict these properties. The high efficiency of capillary GC is needed as the best separator of such complex mixtures, but the complexity is often so great that MS detection is a necessity in order to differentiate peaks. For the heavier products, the carbon number range and the proportions of linear and branched species affects the overall properties. For example, a motor oil base stock must have tight limits on its carbon number range. If it is too high, the oil will be too viscous at low temperatures to flow effectively at engine start-up. If it is too low, volatility will occur at high temperatures that can lead to uneven combustion in the engine. GC-MS is an almost ideal analytical tool for these types of samples.

One whole field of research relating to petroleum is dominated by GC-MS analyses: the use of biomarkers to characterize the location and origin of petroleum. Petroleum arises from a variety of organic material that is geologically aged and degraded [42]. The remnants of the original biological materials are reflected by a multitude of hydrocarbon species, including polyterpenes, steranes and hopanes (polycyclic saturated hydrocarbons whose cores resemble those of steroid compounds), and porphyrins. These generally result by defunctionalization and reduction of the ring systems to saturated and partially-hydrogenated forms of the ring structures. This field, initially spearheaded by researchers such as Seifert, Moldowan, and Gallegos, has grown to be a core tool in petroleum exploration because of its reliance on GC-MS.

High-resolution capillary GC can separate the myriad of saturated hydrocarbons found in petroleum. Correlations of individual components or classes of compounds have been made to a variety of variables. These included: whether the source material was originally terrestrial, marine, lacustrine (originating in lakes), etc.; the conditions (predominantly the temperature and the age) of the diagenesis, the period of transformation from biological material to the defunctionalized, predominantly hydrocarbon coal, shale oil, or petroleum; and the possible migration of the petroleum away from its source rocks to the ultimate pools where it is found. For example, the ratios of the stereoisomeric forms of a compound are used to determine racemization, which is then correlated to the age of the petroleum. This requires a GC separation capable of separating a multitude of very similar compounds, and the selectivity of MS to differentiate them. The geochemical literature is literally loaded with new uses of GC-MS to extract more information from each petroleum.

One common GC method for petroleum characterization is simulated distillation, sim-dist [43]. The GC retention times on a non-polar phase of a petroleum or processed material are correlated to the boiling points of the n-alkanes. These boiling point markers are then used to determine the amounts of material eluting in boiling point ranges. Sim-dist is a rapid method to estimate the yields from refinery distillation processes and is used to estimate the distribution of the various products from a process. Roussis and Fitzgerald reported a GC-MS method for sim-dist analysis of petroleum. The MS data were used to sub-divide the boiling point fractions into sub-classes of saturates, one-ring aromatics, two-ring aromatics, thiophenes, etc.

Another hydrocarbon class, the larger PAHs, those of 24 or more ring carbons, is also important in the analysis of petroleum and related materials in certain applications. These compounds elute at the upper temperature limit of current commercial capillary GC columns, but their isomeric complexity requires the higher resolution. Their separation and identification by GC-MS, however, has been very useful in a variety of analytical problems that highlight the power of high-resolution separations with highly selective detection. Schmidt et al. identified several 24-carbon PAHs in the effluent from burning hard coal by GC-MS with a methylphenyl polysoloxane column [44, 45]. Many peaks of 26 carbons eluted towards the end of their chromatograms, but were not identified. They later extended their identifica-

tions by synthesizing several more C<sub>24</sub>H<sub>14</sub> isomers. Wise and co-workers [46] used similar columns (DB-5) to separate the 24-carbon PAHs in extracts from a coal-tar standard reference material. They used GC-MS, and were unable to identify many peaks due to a lack of available standards for retention time comparisons. Simoneit and co-workers [47, 48] used high-temperature GC-MS to examine the PAHs in fractions obtained from alumina absorption chromatography fractions of the tar-like bitumens from deep-sea hydrothermal vent areas. They found PAHs of 24, 26, 28, and 30 carbons. Similarly to the other groups using only GC-MS, they were not able to identify any specific isomers.

One shortcoming of GC-MS for isomer analysis is that the “normal” electron impact (EI) ionization mechanism does not usually differentiate between isomers. The molecular ions, by definition, are the same and the fragmentation patterns through loss of substituent groups are also usually very similar. The ratios of ions are not reproducible enough to definitively distinguish between isomers. This leaves reliance on the separation and the resulting retention times as the only way to tell isomers apart.

For the PAHs, however, Simonsick and Hites [50] showed that special chemical ionization reagent gases could be used so that isomers will appear to have different fragmentation patterns. They used methane as the reagent and then used the M/M+1 ratio to compare to calculated ionization potentials (IPs) to assign structures to several LPAH peaks. They separated the same extract as had been earlier studied by Lee and Hites. They saw eight C<sub>28</sub>H<sub>14</sub> isomers and four C<sub>30</sub>H<sub>14</sub> isomers. The comparison of calculated IPs to ion ratios and the possession of two isomers from each set (which were used to compare retention times as well as ion ratios) let them assign probable structures to all 12 peaks. There was, however, a note of caution given. Even with the high resolution of capillary GC, they observed an ion ratio for one of their standards, benzo[pqr]naphtha-8,1,2-[bcd]perylene, that did not match the corresponding peak in the carbon-black separation. They relied on the GC retention time and a separate preparative HPLC separation and UV analysis of the peaks to confirm this component and assumed that there must be co-elution that changed the observed ion ratio.

This is just one example of the use of added reagents to cause selective ionization, commonly called chemical ionization (CI). The use of specific reagent gases for determining certain types of analytes in GC-MS is a rich field of study in itself [51]. Reagents are commonly chosen that aid in the selective ionization of target analytes through acid-base reactions or in the enhancement of the ionization of certain functional groups. For example, in negative ion CI, a reagent gas is chosen so that it has a slightly lower proton affinity than the target group. The target molecular type, as well as all others with a greater proton affinity, will ionize by giving up a proton to the reagent gas. Any molecules with a lower proton affinity than the reagent will not ionize. This specific mode is referred to as NICI, with the opposite approach of generating positive ions being PICI. In PICI, the reagent gas acts on electron affinity differences. For molecular classes with high proton affinities, such as the basic pyrroles, carbazoles, and aza-arenes, ammonia will selectively ionize them and many other common classes of compounds that

occur in the same samples (such as the PAHs, thiophenes, and furans) will remain neutral [52].

Suzuki et al. [53] used methanol chemical ionization to differentiate PAHs from similar-sized heteroatom-containing polycyclic aromatic compounds. They assigned example structures to the masses observed. Since neither were their methodologies for the LPAHs able to distinguish isomers nor did they use a large reference compound set, these structures can only be deemed to be possibilities among the huge number of isomers.

One of the many other areas in which GC-MS is widely used is in forensic analysis. Kaye [54] has reviewed many uses of GC-MS in his book dealing with the use of modern analytical methods of analysis in criminal investigations. He highlights GC-MS analyses of opiates, including heroin, codeine, and morphine characterization. Not only is this approach useful in identifying what a suspected substance might be, but if it is an illegal substance the pattern of components and impurities can aid in determining the source of the drugs. There are also examples given showing the widespread use of GC-MS as one of the preferred methods in the testing of athletes for use of performance-enhancing substances. There are a wide variety of compounds that can increase the performance of human (and equine) competitors, as well as a variety of measures and countermeasures described by both the analytical chemist responsible for monitoring any banned substances and athletes and trainers bent on circumventing the rules.

GC-MS has been widely used in environmental analyses. The U. S. Environmental Protection Agency's mandated methods for volatile and "semi-volatile" priority pollutants in effluent water call for GC-MS analyses for a wide variety of acid, base, and neutral compounds. An aqueous sample was sequentially extracted to give the various fractions after appropriate pH adjustments. Selected-ion monitoring of key ions for a pollutant during a range of time around its retention time is the required method. This requirement was one of the major driving forces in the sales of GC-MS equipment during the 1980s. Lacorte and co-workers [55] describe a similar method for a greatly expanded listing of environmental pollutants.

For LC-MS, the chemical ionization mode for the mass spectrometry is the most readily used since the large amounts of mobile-phase solvents naturally act as the chemical ionization reagent. This can limit the utility of LC-MS because the mobile-phase solvent choices are determined by the HPLC conditions. There is usually little flexibility in the choice of solvents. For example, the use of acetonitrile or methanol is a common variable in reversed-phase HPLC, but most other solvent switches lead to gross changes in the chromatographic separation. The most ideal chemical ionization reagents are very likely not usable for this reason. Rose-Mele et al. used this approach to identify the porphyrins, both free and bound to metals, in a shale oil.

The first interfaces between LC and MS were mechanical devices, such as the moving belt interface. In this interface, the column effluent was deposited onto a surface, which moved to collect the sequence of eluents. Solvent was then removed from the belt by heating, sometimes aided by vacuum. The belt then moved into the MS sample generation area where the deposited compounds

were volatilized by further heating and the very-high-vacuum conditions. Although this type of interface helped prove the utility of LC-MS, its cumbersome design and the presence of ghost peaks from previous runs were severe problems. With the advent of direct introduction methods, the mechanical interfaces became obsolete.

The most widely used modern interfaces between HPLC and MS are atmospheric-pressure ionization (API) using spray techniques. Thermospray, electrospray, ionspray are the three common modes. Each of these techniques utilizes the nebulization of the liquid stream with specific modes to increase the efficiency. Thermospray uses the inherent expansion of the solvents when they are exposed to a rough vacuum region (before the high vacuum of the MS), assisted by heating. Ionization is normally attained by the addition of ionic buffers, with the somewhat volatile ammonium acetate being a favorite. Subsequent conventional ionization with electron impact or high-charge fields of the stream may be used in addition, if there are an insufficient number of ions. Thermospray is most effective for HPLC mobile phases where no organic modifier is used (pure water with buffers, as in ion chromatography or an electrophoretic separation).

Electrospray ionization utilizes a high voltage field of several kV to ionize the droplets of the nebulized effluent. The charged droplets are accelerated and focused by ion optics into an area where a countercurrent of inert gas removes the uncharged droplets and vapor. Ionspray is similar, but a pressurized countercurrent of heated inert gas assists in the nebulization and evaporation of the mobile phase. Ionspray is more effective than electrospray with mobile phases with low levels of organic modifiers. Both approaches are relatively mild forms of ionization, so the molecular ions of the peaks are predominant. The slight degree of fragmentation can make the assignment of specific structures more difficult, especially for isomers, which would have different fragmentation patterns in their electron-impact spectra.

In a brochure describing their ionspray LC-MS interface [56], Waters shows examples of the separation and identification of several types of molecules, including polypeptides, bisphenol A polymer additives, and steroid anti-inflammatory drugs. Hewlett-Packard (now named Agilent Technology) describes similar applications for their commercially available electrospray LC-MS system [57]. This design differed from many by using an orthogonal flow stream in which the HPLC flow was dispersed and the ion inlet was perpendicular to it [58, 59]. This gave a better signal-to-noise and a more reproducible peak height. Charlwood and co-workers [60] used a microbore HPLC system with this interface to characterize derivatized oligosaccharides. The N-linked glycans of up to 10 sugars were separated, with the mass spectra of species being above 1800 Da. Peng and co-workers [61] used LC-MS-MS with an ionspray interface to determine candidate anti-arthritis drugs in human plasma and cartilage tissues. Mobile phase gradients of water, acetonitrile, and formic acid provided the chemical ionization reagent for positive ion MS. The target drugs were hydroxamic acid based protease inhibitors. The use of the selective MS-MS mode gave quantitation in plasma of sub-ng mL<sup>-1</sup> in plasma.

Suzuki and Yasumoto [62] used liquid chromatography-electrospray ionization mass spectrometry to measure the diarrhetic shellfish-poisoning toxins okadaic

acid, dinophysistoxin-1 and pectenotoxin-6 in bivalves. Holcapek and co-workers determined extremely low levels of several glycols, including ethylene glycol, using derivatization with benzoyl chloride [63]. HPLC-MS with an electrospray interface had limits of detection of 10 to 25 (g L<sup>-1</sup>). Boyer [64] used LC-MS with an electrospray interface to determine the pharmaceutical nortriptyline, a tricyclic antidepressant, and its metabolites. A mobile phase of water:methanol with 30 mM of ammonium acetate was used for selective ionization.

To highlight the on-going growth of LS-MS techniques, they were the subject of two chapters in a recent review volume [65, 66]. These dealt with the analysis of oligonucleotides by electrospray MS and the analysis for herbicides in aqueous media. The first, by Deforce and Van den Eeckhout, highlights the advantage of electrospray over other competing MS modes, such as matrix-assisted laser desorption/ ionization, time-of-flight (MALDI-TOF) MS. The easier coupling to an HPLC and the greater mass resolution at higher molecular weights are the main advantages cited. The resolution advantage is especially pronounced for oligonucleotides of more than 60 bases. In the herbicide review, D'Ascenzo and co-workers focus mainly on the use of thermospray interfaces and API. Besides giving detail descriptions of the interfaces, they emphasize the advantages of these approaches with aqueous samples.

The dietary flavonoids have been proposed as being beneficial in reducing the risk of contracting colon cancer and of heart attacks. The analysis of these very polar compounds in biological fluids has, therefore, received some attention. Nielsen et al. [67] monitored 12 of these compounds through reversed-phase HPLC analysis of urine. API-MS was used to measure the glycoside and aglycon forms of these polyphenolic compounds.

Hsu et al. [68] and Mao et al. [69] examined the nitrogen-containing heterocyclic compounds in diesel fuel and other processed petroleum products. A combination of normal-phase HPLC and chemical ionization MS showed the presence of indole, carbazole, and benzocarbazole with varying degrees of methylation up to four.

HPLC-MS has been heavily utilized to measure the “true” relationships between molecular size, molecular weight, and retention in size-exclusion chromatography (SEC) in polymer characterization. SEC separates a polymeric material through permeation differences as the sample passes through columns with pores with well-defined diameters. Permeation is based on the size of the molecules, but often the need is to know the molecular weights of the molecules. The relationship between the two is not straightforward, depending on structural factors that control the chain flexibility and intra-molecular interactions. The MS provides the absolute molecular weights. Its use for routine polymer characterization is not practical, however, so SEC with refractive index or evaporative light scattering detectors is used for its speed and simplicity of operation after the columns have been calibrated by SEC-MS.

Asserud et al. [70] used SEC with an electrospray interface to couple to a FTMS. They characterized a variety of poly(methyl methacrylate) polymers. This allowed them to accurately determine not only the molecular weight distribution, but also the end-group functionality and observe secondary polymer distributions

due to the formation of cyclic species. In the off-line mode (collection of the SEC effluent for subsequent FTMS), they were able to determine polymers with molecular weights of over 500,000 Da.

MALDI-MS has become increasingly popular as a tool to help calibrate SEC separations. In MALDI, the sample is trapped in a matrix. In this case, as the name implies, this matrix acts not only as a sample trap, but also takes an active role in the laser-induced ionization mechanism. The isolated polymer fractions are analyzed and molecular weight distributions based on the MS data are used to calibrate retention times on the SEC columns.

Pace and Betowski [71] used micro-column HPLC to introduce samples into a particle-beam MS. The separation was with a polymeric octadecylsilane bonded phase and methanol-tetrahydrofuran gradients. They examined a set of standard large PAHs, from 24 to 36 carbons, and compared those results to species seen in two extracts from soils collected at hazardous-waste sites. Generally their detection limits were approximately 1 ng.

Rosenberg et al. [72] used reversed-phase HPLC with atmospheric pressure chemical ionization MS to separate and measure several organotin species that had been extracted from sediments. These species were used as a fuel additive when organolead compounds were replaced. They are environmentally important because of their bioaccumulation and toxicities.

One interesting hybrid of LC-MS has been developed by Hercules and his research group: TLC-MS [73]. The MS approach utilizes MALDI MS. MALDI MS has much lower detection limits than many other MS approaches and can be used for both low and high molecular weight components. The TLC plate surface and the MALDI matrix are coupled. This is accomplished through pressing the TLC plate against a second plate coated with the MALDI matrix. Several cyclic peptides were separated and measured with this set-up.

One unique type of MS, ICP-MS, needs to be discussed separately because it does not deal with molecular species, but with atomic ones. The inductively coupled plasma is a common atomization source for atomic spectrometry. This “sample preparation/ sample introduction” mode has been coupled with an MS to yield an instrument capable of trace level elemental analysis. Each element has a unique set of isotopes in known proportions. These can be used to quantify the element. In the case of elements with overlapping isotopic mass numbers, simple deconvolution can be used to give results for each. ICPMS has very low detection limits.

GC- and LC-ICP-MS have been used as a means of separating species and then identifying individual peaks by their unique elemental mass spectra. Braverman [74] separated the rare-earth elements using HPLC-ICPMS. Schminke and Seubert, for example, used ion chromatography as the separations tool and the ICP-MS detector was used to measure bromate ion at  $\mu\text{g L}^{-1}$  levels in the presence of large excesses of sulfate and nitrate ions [75]. Organolead and organotin compounds have been analyzed with GC-ICPMS [76, 77]. The vanadium and nickel metalloporphyrins in a shale oil were examined by both GC-ICPMS and HPLC-ICPMS by Ebdon and co-workers [78]. They found that the HPLC approach gave much more reliable quantitative data.

There are a few issues that arise when a SFC is coupled to an MS that differ from those inherent to GC or HPLC. Since the fluid density in SFC is comparable to the liquid densities of HPLC, similar interfaces can be used to remove the large excess of mobile-phase molecules if there are slight modifications made. The most common SFC mobile phase is carbon dioxide. The task of removal of the excess is made even simpler because this fluid readily converts to the gas phase upon decompression. This, however, leads to one major problem. Expanding carbon dioxide gets very cold due to the Joule–Thompson effect. The interface area must be heated to prevent any sample deposition or co-precipitation on the interface surfaces of the cold carbon dioxide as dry ice. This problem of fluid expansion and rapid cooling is inherent to any type of detection where the detector is not maintained at high pressures. The thermospray interface is the most commonly used coupling device. As with HPLC-MS the vacuum system for SFC-MS must be of a much higher capacity than for GC-MS.

For the separation of very-polar phenolic Mannich bases, Fuchsluefer et al. used the novel fluid ethane with dimethyl ether as the modifier [79]. The normal carbon-dioxide-based mobile phases, even with polar modifiers, could not elute these compounds. They identified the main oligomeric products and several of the byproducts in the manufacture of these compounds, which are used as hardeners and accelerators in epoxy resins. They coupled their SFC outlet to a MS in the atmospheric-pressure chemical ionization mode.

## 21.4 NMR Detection

Nuclear magnetic resonance (NMR) is routinely used to determine the types of carbon and hydrogen present in molecular structures. NMR requires nuclei with  $\frac{1}{2}$  spins, and so is useful for other nuclei like silicon and phosphorus. The carbon-13 isotope is the NMR active one. It is present at about 1% in a bulk of inactive carbon-12. The reverse situation is present for hydrogen. The common hydrogen-1 isotope is most prevalent, and hydrogen-2 (deuterium) is the minor NMR-inactive isotope.

For observation of the hydrogen-1 in analytes, there must not be hydrogen-1 in the mobile phase or the strong solvent peaks will mask the small analyte ones. The requirement of the mobile phase containing only deuterated components is a severe limitation to the use of HPLC-NMR because these solvents are prohibitively expensive in the amounts used as mobile phases. Many perdeutero forms of solvents are hundreds of times more expensive. The more complex a solvent's structure, the more expensive and less available will be its perdeutero form (the same statement is true if carbon-13 versions are needed as NMR active versions of analytes). With the use of special radio-frequency pulse sequences and nuclear pre-saturation techniques, the proton signals due the mobile phases can be damped, but the use of deuterated solvents is still recommended. For carbon-13 NMR, the large signal peaks of the mobile-phase solvents will overwhelm the signals of the chro-

matographic peaks unless the sample components have been labeled with carbon-13. Labeling of the sample is convenient only in synthetic work and even then it can be very expensive to use labeled starting materials. For more exotic nuclei, like fluorine-19 and phosphorus-31, these limitations are not a problem because these nuclei are the most abundant and the common solvents do not interfere.

The residence time that a component must be in the NMR cavity in order to collect a spectrum with good signal-to-noise ratio (*S/N*) can be a limit on the chromatographic conditions or the flow rate. An individual NMR scan may only take small fractions of a second, but thousands (or even millions) of scans may be needed. Multiple scanning, even with the Fourier-transform based instruments in current use, can take several seconds or even minutes to acquire. For conventional HPLC, peak widths are of the order of several seconds. For microbore HPLC, peak widths are typically only a few seconds. Stop-flow methods are commonly used, since using slower flow rates increases the peak spreading due to diffusion leading to a loss in peak resolution. Stop-flow operation, however, results in a loss of accurate retention times for comparison (necessitating separate runs for collection of retention times and NMR spectra) and chromatographic resolution is degraded because of diffusion as the analytes sit on the column during the stop-flow periods.

Subramanian and co-workers [80] utilized a microbore HPLC with special connectors for coupling to a proton NMR. When the onset of a peak was detected, the flow was diverted to the NMR flow cell and the flow was stopped. The NMR spectrum of the peak was then collected. Flow was resumed, with repeated stoppages as each peak eluted. Mixtures of small amino acids and polypeptides were separated and identified. An example HPLC-NMR contour-map chromatogram is shown in Fig. 21.20. Figure 21.21 shows the three extracted NMR spectra of the components. A typical spectral collection time, for 5 µg of the peptide phenylalanine-alanine, was 3.5 h. Earlier work by this same group utilized a conventional, larger flow system (and thus larger sample sizes and shorter times needed for spectral acquisition). Typical total run times were 5 to 14 h for complex mixtures, even with the much larger sample volumes. The microbore system, however, was proportionally better because the higher separating power of microbore columns results in sharper peaks that are relatively more concentrated than those obtained with HPLCs of conventional flow rates. All types of spectrometric detection benefit from this advantage of microbore HPLC over conventional HPLC.

Preiss et al. [81] reported the use of stopped-flow HPLC-NMR to identify dyes and other pollutants in the effluent from a textile manufacturing plant. They utilized a mobile phase of gradient of acetonitrile and deuterium oxide. Although they used conventional volume equipment, stop-flow times of 0 min to 2 h were required to achieve good *S/N* for individual components. They identified 14 dyes, their degradation products, or other compounds (such as long-chain benzenesulfonates).

Levsen et al. [82] reviewed their research on the use of HPLC-NMR in the characterization of environmental samples. They examined a contaminated ground water from near a munitions plant, a leachate from a waste disposal site, and the effluent water from a textile mill. Since NMR detection is non-

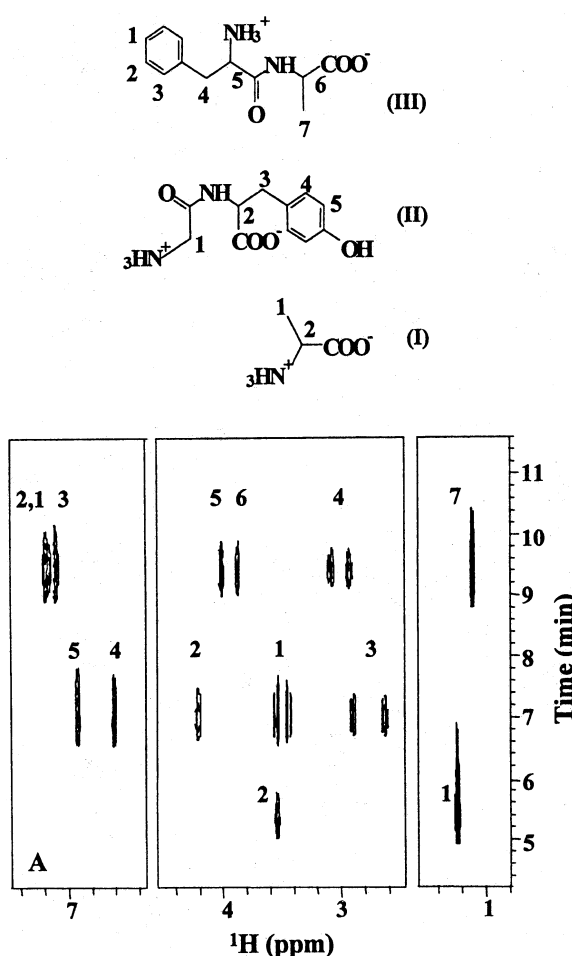


**Fig. 21.20** The three-dimensional contour map of a separation of simple polypeptides. From R. Subramanian, W.P. Kelley, P.D. Floyd, Z.J. Tan et al., *Anal. Chem.*, 1999, 71, 5335–5339.

destructive, they showed through subsequent off-line MS analysis of individually collected peaks that the two methods complement each other in helping to determine the structures of unknown compounds. They found carboxylic acids, aromatic sulfonates, aminoanthraquinones, and other compounds in these water samples.

SEC-NMR of stereo-regular poly(methyl methacrylate) (PEMA) polymers has been used by Kitayama and co-workers [83] to determine their tacticity (the orientation of functional groups relative to the polymer backbone). Since SEC uses much larger sample amounts than HPLC, this analysis could be done in real time. Each PEMA sample was separated on a single mixed-bed SEC column and

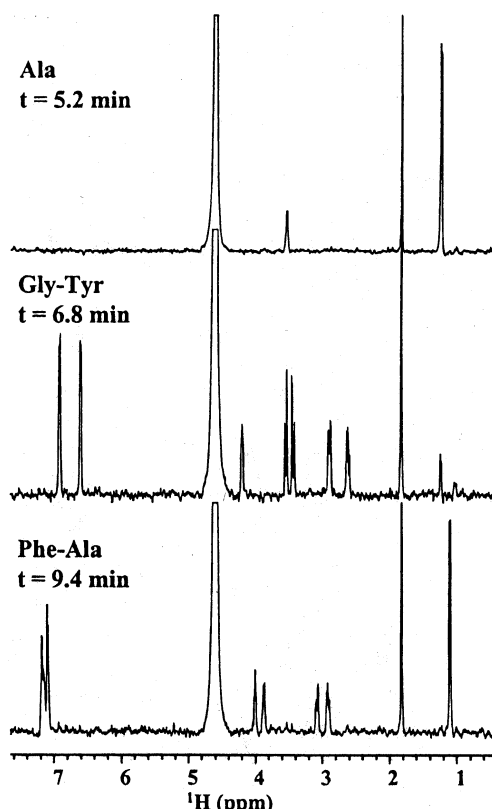


**Fig. 21.21** The extracted NMR spectra of the three polypeptides found in Fig. 21.20. From R. Subramanian, W. P. Kelley, P. D. Floyd et al., *Anal. Chem.*, 1999, 71, 5335–5339.

the proton NMR data was collected in a 1 h run time. The separation gave four peaks, which the NMR identified as the isotactic, heterotactic, predominantly syndiotactic, and syndiotactic forms.

## 21.5 FTIR Detection

FTIR detection can be a very useful tool in both the observation of a specific set of target compounds and in the elucidation of unknown ones. Infrared light causes molecules composed of a number of atoms to exhibit vibrational spectra. Some of the molecular motions are due to very complex contortions of the molecular structure, but many can be ascribed to the stretching of specific bond types or to certain motions within a functional group. Infrared radiation distorts the normal molecular bonding framework by stretching individual bonds or causing combina-

tions of bonds to undergo more complicated motions (such as the scissoring or wagging of two bonds linked to the same atom, the bending of a portion of an aromatic ring out of the plane, etc.).

In common practice, the units used are either of frequency, in  $\text{cm}^{-1}$ , or wavelength, in  $\mu\text{m}$ , with the first being more frequently used. When a spectrum is displayed with frequency as the  $x$ -axis, the low-energy molecular motions are at high  $\text{cm}^{-1}$  and are displayed to the left. The motions of larger atoms or groups of atoms that require more energy are at lower  $\text{cm}^{-1}$  values. This lower frequency region is not normally used for spectral interpretation of functionalities, but is useful for fingerprinting purposes when matching sample spectra to those of standards.

The molecular information that FTIR detection offers that MS, the other common hyphenated GC technique, cannot, includes elucidation of aromatic ring substitution (for example, with di-substitution, *ortho*, *meta*, or *para*), *cis* or *trans* or geminal substitution on a carbon–carbon double bond, the arrangement of rings in PAHs (benz[*a*]anthracene versus chrysene or triphenylene or benzo[*c*]phenanthrene or tetracene for the four-ring *ortho*-fused PAHs), alkyl-chain branching isomers, and alcohols, which often shows in the MS as the easily dehydrated product alkene [84].

There are two main types of FTIR detection for GCs, in the gas-phase using an in-stream optical system and through vapor deposition with detection being away from the GC flow stream. In the first, a light pipe that can transmit IR radiation is positioned on either side of a detection cell. Transparent windows pass the IR radiation into the flow cell. The whole assembly is maintained at temperatures of 250 °C to 350 °C to prevent deposition of sample molecules. Most interfaces for this type of GC-FTIR also have heated transfer lines to and from the flow cell to ensure that no deposition occurs before introduction into the spectrometer.

In the second mode, the eluting GC peaks are trapped and spectra of each component are collected offline. Cryogenic trapping of the GC eluent has become commonly available in recent years. An inert plate, often coated with a zinc selenide or a gold film, is positioned at the column outlet. This surface is cooled with either liquid nitrogen or helium. Stepper motors move it so that the eluting GC peaks are deposited and collected on the cold surface as a series of spots. These can then be individually examined by repositioning the plate in the FTIR optical path.

The spectra that are collected in this fashion have very narrow lines. The cooling reduces the inter-molecular interactions and collisional broadening that are found in KBr or solid phase spectra. These narrow-line spectra have both the bands useful in structural assignments and enough complexity in the patterns to be fingerprints. A broad band, such as the methyl-stretching band around 3000  $\text{cm}^{-1}$ , will typically collapse into two, three or more narrow bands when the sample is cooled. The locations and relative intensities of these sets of bands are fingerprints for many very common compounds. For example, each of the methylchrysene isomers gives a characteristic spectrum in the C–H stretching region, so that their separated peaks can be easily identified. Figure 21.22 shows the spectra of the two PAH isomers phenanthrene and anthracene, while Fig. 21.23 shows some of the spectra of the even more complex five-ring isomers set. These spectra were col-

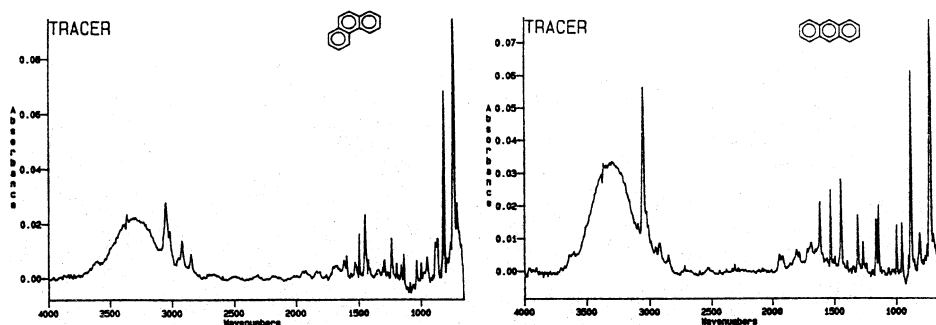


**Fig. 21.22** The GC-FTIR spectra of the three-  
ring PAH isomer phenanthrene and anthracene. Reproduced with permission from Gordon and Breach Science Publishers from A. M. H. Budzinski, J. R. Powell, P. Garrigues, *Polycyclic Aromat. Compd.*, 11, 334.

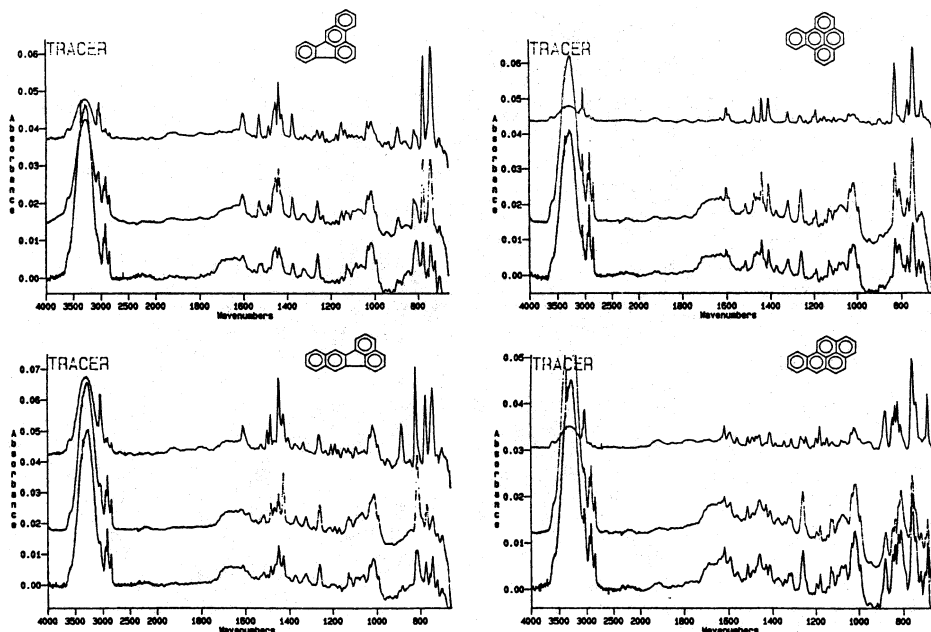


**Fig. 21.23** The GC-FTIR spectra of four iso-  
meric 20-carbon PAHs. Reproduced with per-  
mission from Gordon and Breach Science  
Publishers from A. M. H. Budzinski, J. R. Powell,  
P. Garrigues, *Polycyclic Aromat. Compd.*, 11,  
335.

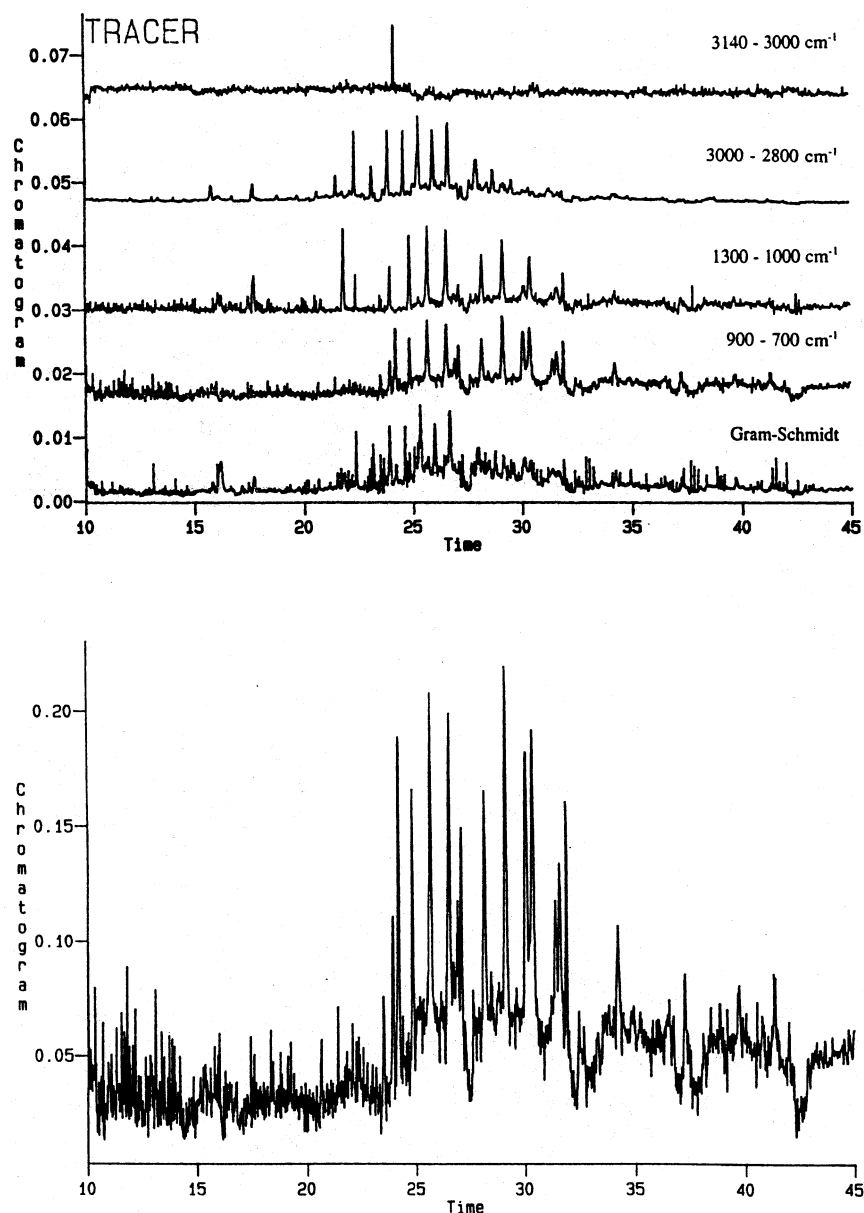


**Fig. 21.24** Selected wavenumber chromatograms of a sediment extract. Reproduced with permission from Gordon and Breach Science Publishers from A. M. H. Budzinski,

J. R. Powell, P. Garrigues, *Polycyclic Aromat. Compd.*, 11, 335.

lected during the analysis of a marine sediment sample. Figure 21.24 is an example of the use of selected wavenumber monitoring, showing the presence of certain structural features.

One major drawback of GC-FTIR is that the spectra collected are either in the gas phase at high temperatures or trapped at cryogenic temperatures. Most reference spectra in the literature, particularly for older synthetic work, were collected at room temperature as liquid films or as solid solutions in KBr pellets. These reference spectra have much broader bands and so spectral matching is not possible for gas-phase collection. Matrix effects, particularly for the more polar compounds, can occur in vapor deposition samples. These samples are undiluted, so that inter-molecular interactions can occur. Hydrogen bonding or acid–base interactions are minimized in the reference spectra because of the diluting KBr matrix. In spite of these possible problems, in a recent review article Bruno [85] estimated that GC-FTIR spectral matching was accurate around 95 % of the time. This contrasts with his estimate of only 75 % for correct GC-MS spectral identification. He attributed the difference mainly to the similarities in the mass spectra of isomers, which FTIR can differentiate.

As an example of the identifying power of GC-FTIR, a recent report is a good example. The PAHs in a marine harbor sediment were examined by Meyer et al. [86]. The sediment sample was extracted and compared to reference spectra obtained for the 24 PAHs in the reference mixture NIST SRM 1491. Although the PAHs are very similar structurally, being composed of ring aromatic carbons and peripheral hydrogen atoms, the relative arrangement of the rings and the number of hydrogen atoms and their positioning on each ring are the only variables. The overall spectrum, however, is a fingerprint, particularly in the lower frequency range as mentioned earlier. Of the 15 PAHs also detected by HPLC with fluorescence detection, GC-FTIR saw 13. Of these, 11 were identified, with only 2 being “not unequivocally” identified.

In an early report of the use of FTIR detection [87], Gurka and Betowski studied the volatiles from soil samples and from a commercial chemical still bottom sample using GC-FTIR and GC-MS. They found a wide variety of chlorinated compounds, particularly chlorobenzenes. Compton and Stout [88] reported the use of GC-FTIR to monitor the volatile compounds in coffee. Five selective functional group ranges were monitored in one example, the aromatic C–H stretching region of 3000–3140  $\text{cm}^{-1}$ , the aliphatic C–H stretching region of 2800–3000  $\text{cm}^{-1}$ , the carbonyl stretching region of 1680–1780  $\text{cm}^{-1}$ , the C–O region of 1000–1300  $\text{cm}^{-1}$ , and the C–N region of 900–1000  $\text{cm}^{-1}$ . Using the individual FTIR scans they identified over 40 components, including caffeine, pyridine, carbon disulfide, and a variety of carboxylic acids, ketones, and alcohols.

Wilkins et al. [89] describe the use of GC-FTIR to separate and identify some very similar cyclic alcohols, the pairs of *cis* and *trans*-menth-2-ene-1-ols, sabinene hydrates, and terpineols. The 800–1500  $\text{cm}^{-1}$  region gave distinct fingerprints that differentiated each isomer from the other.

HPLC-FTIR suffers greatly from the inherent interference of the large excess of mobile-phase solvent. Since the common solvents are only simple organic mole-

cules, such useful infrared regions as the C–H stretching one around  $3000\text{ cm}^{-1}$ , are lost. Other solvents have to be avoided if certain regions are of interest, which limits the choices for chromatographic optimization. For example, acetone or ethyl acetate cannot be used as the strong solvent in a reversed-phase separation if the carbonyl region is of interest. Many approaches have been utilized to surmount this limitation, including sample enrichment or solvent evaporation (as in GC-MS) or computer-generated solvent subtraction. The latter is inherently limited because it involves the, at-times, tenuous approach of subtracting a very large signal to observe a very small residual one.

Microbore HPLC can be coupled without modification to a conventional electrospray GC-MS type of interface for cryogenic trapping FTIR detection. A heated sheathing gas aided in solvent vaporization. A zinc selenide plate was used for sample spot collection.

Kaye [54] describes some examples of the use of HPLC-FTIR in identifying illicit drugs. He describes the characterization of heroin and lysergic acid samples by HPLC followed by identification from the FTIR spectra of isolated peaks. He highlights the advantage of HPLC methods over GC ones in that HPLC generates larger amounts of purified components that are in an easily collectable form. This allows subsequent definitive identification.

In a more general statement Kaye highlights that there is an inherently high need for validity of methods and confidence in the results for both identification of illegal drugs and their concentrations, so that the hyphenated techniques are widely used in drug testing and other forensics applications. Since many of these molecules are polar and water soluble, reversed-phase HPLC is the separation method of choice.

Huang and Sundberg [90] separated polyolefinic polymers by SEC, and FTIR detection was used to determine the variety of structures present in the resulting hydrocarbon polymers. Both the products of polymerization of a pure olefin and blends of two starting olefins were examined.

SFC-FTIR is also possible [91]. The carbon dioxide mobile phase that is most often used is relatively free of strong IR absorbances. It has two strong bands at  $2325\text{--}2375\text{ cm}^{-1}$  and  $3550\text{--}3650\text{ cm}^{-1}$ . French and Novotny [92] were the first to use supercritical fluid xenon as the mobile phase to observe throughout the IR range. This inert gas has no IR active bands. Through the use of microbore columns, the amount of xenon needed was relatively small since the flow rates were only a few microliters of fluid per minute. Since xenon gas can be expensive, this translated into only a few milliliters per minute of gaseous xenon being used. The use of the microbore system makes the cost of using xenon amenable. As a mobile phase, xenon is very non-polar and so behaves somewhat like carbon dioxide. Unlike carbon dioxide, however, it does not mix well with polar modifiers like methanol and, therefore, it is not as useful in the separation of polar analytes [93–96]. The use of xenon SFC has increased, being applied to the separation of sesquiterpenes and PAHs [97, 98]. The differences between supercritical fluid xenon spectra and those in the condensed phase have been assessed. Corrections are relatively simple.

Cryogenic trapping with SFC is also possible. Norton and Griffiths [99] report a typical detection limit of 1 to 10 ng injected, with the very strongly absorbing caffeine being seen at 500 pg injected. They found linear response for quantitation either from the FTIR spectrum or from the functional group wavelength chromatograms.

SEC, which is mainly used for high-molecular weight compounds like polymers and proteins, has been coupled to FTIR. Using SEC-FTIR, Liu and Dwyer [100] examined the types of branching in styrene–butadiene copolymers and Jordan and Taylor [101] measured the additives in several commercial polymers.

## 21.6

### Atomic Spectrometric Detection

There are a variety of atomic spectrometers, in addition to the ICP-MS already discussed, that have been coupled to chromatographs to give element specific monitoring. Generally the chromatographic stream is introduced into the plasma area of an atomic spectrometer. In this high-energy environment, all of the molecular bonds are ruptured and only free atoms are present. In this state the atoms can either absorb or emit light at characteristic wavelengths. Each element has a characteristic set of wavelengths, which are based on each element's unique atomic electron orbital energies.

The GC with atomic emission detection (AED) has become widely used during the past few years. The development of optical systems that can monitor several emission wavelengths simultaneously has made these systems both affordable and utilitarian. The interfacing of atomic spectrometers to GC is more straightforward than interfacing to HPLC or SFC. In GC, the helium carrier gas is in much lower amounts and can be an active component in the spectrometer plasma. The other two separation methods have large amounts of carrier that are not inherently compatible to the plasma and must be removed to ensure efficient atomization of the samples.

In GC-AED, the GC eluent stream is directly introduced into the plasma of an atomic emission spectrometer. The helium GC gas readily mixes with the helium or argon plasma that is normally used. This plasma is maintained in the plasma state at high energy through the use of several types of energy. Both AC and DC arcs have been used, as well as radio frequency and microwave radiation. Microwave plasmas are most common in commercial GC-AED instruments. Often volumes of reagent gases or a make-up gas are added to ensure optimum atomization of the molecules by the plasma.

Since the AED can detect carbon quantitatively, it is as universal a GC detector as the commonly used FID. The AED can also readily detect deuterium. This means that the same surrogates or sample spiking compounds useful in GC-MS can be used with GC-AED for estimation of extraction recoveries or sample handling losses. The detection of multiple elements simultaneously can yield approximate empirical formulae for the peaks. The precision and accuracy for all the common

# Gasoline

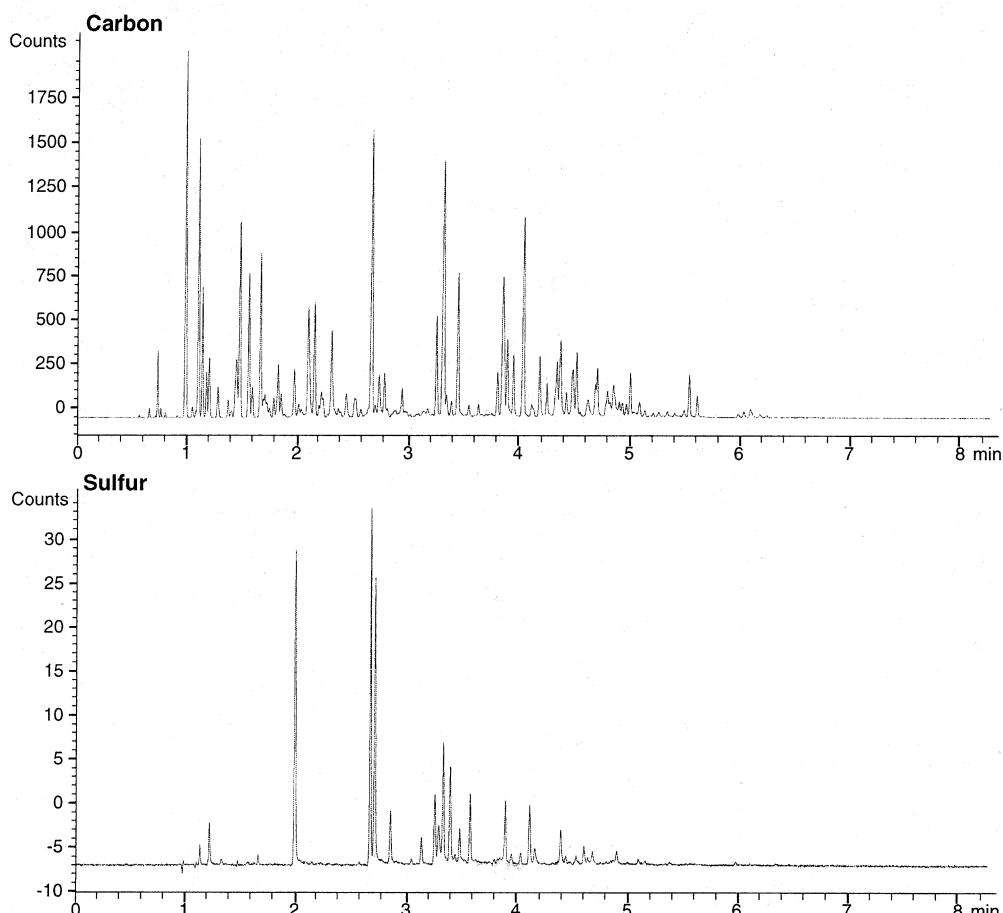


Fig. 21.25.

**Fig. 21.25–27** The GC-AED carbon and sulfur profiles of three different light processed petroleum distillates. Courtesy of J. Iwamoto, Chevron Research and Technology Co., Richmond, CA, USA.

elements, C, H, O, N, and S, are not good enough yet to give a true empirical formula for each peak that can then be used for absolute identification. They are, however, adequate to confirm peak identities. Figures 21.25–21.27 show the carbon and sulfur profiles obtained for three light petroleum distillates. While other GC detectors can detect the common heteroatoms nitrogen (the bead thermonic detector and the chemiluminescence detector) and sulfur (the flame photometric detector and the chemiluminescence detector), the GC-AED is the only common GC detector that is selective for oxygen. It is also the only detector that can simultaneously de-

## Jet

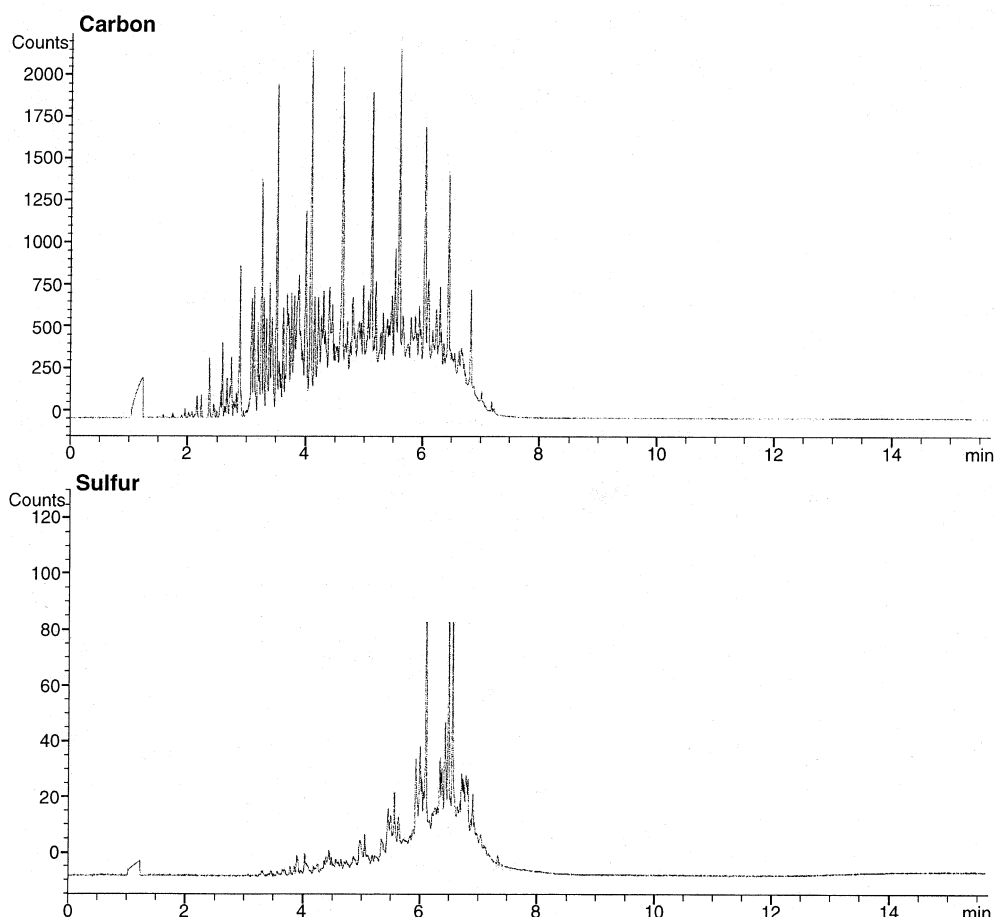


Fig. 21.26

tect more than one type of heteroatom, and commercial instruments commonly can detect 5 to 10 at a time. The capability of the GC-AED to analyze the volatile compounds of almost any element, makes its potential use very wide-ranging and valuable. Figure 21.28 shows such an example, with carbon, sulfur, nickel, and vanadium profiles for a heavy petroleum distillate sample.

Deuterium and carbon-13 have significantly different atomic emission spectra than the predominant normal-abundance isomers hydrogen-1 and carbon-12 so that the AED can be used for selective detection of labeled compounds. Quimby et al. [102] compare emission chromatograms collected for the 171.4 nm line of carbon-12, the analogous 171.0 nm line for carbon-13, and the 174.2 nm line for nitrogen. The chromatograms show that normal-abundance n-dodecane, n-tridecane, and n-tetradecane show at the first line, but at neither of the other two. Car-

# Diesel

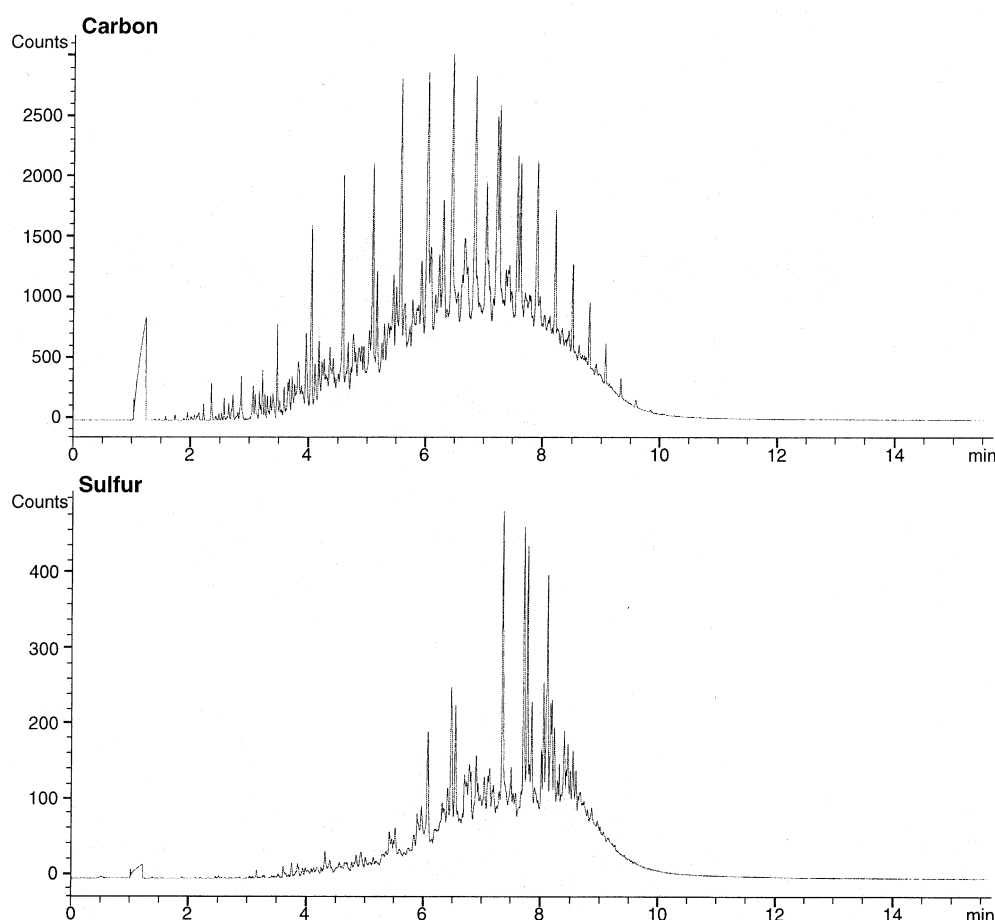
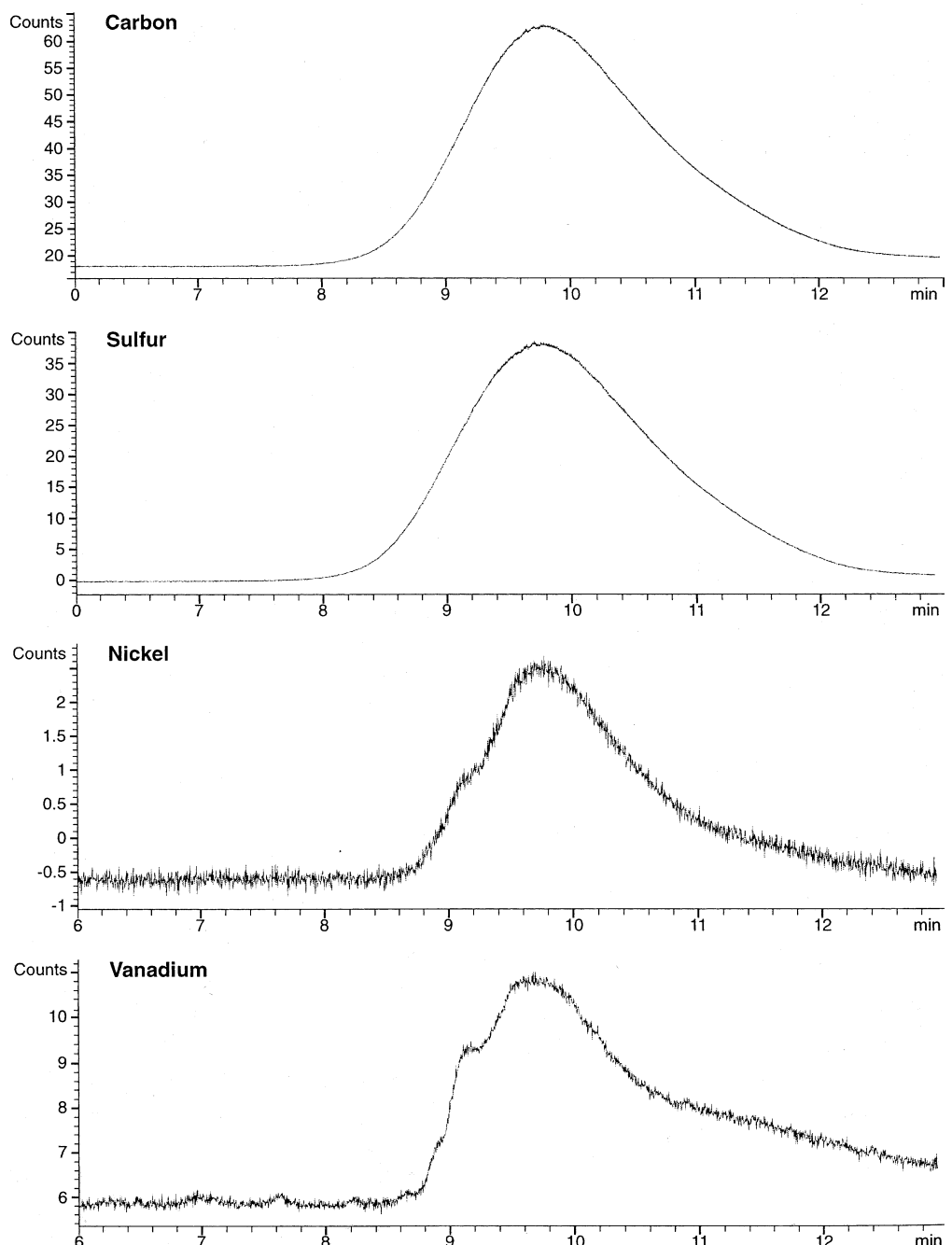


Fig. 21.27

Fig. 21.28 GC-AED profiles for carbon, sulfur, nickel, and vanadium of a vacuum gas oil distillation cut. Courtesy of J. Iwamoto, Chevron Research and Technology Co., Richmond, CA, USA. ►

## Heavy VGO



bon-13 labeled nitrobenzene shows a peak at the same retention time in the latter two, but not in the first.

GC-AED has been used to determine organomercury and organotin species in a variety of environmental samples, including marine sediments and several standard reference material samples of codfish oil, sediments, a variety of fish and other marine animal tissues [103–107]. Agilent Technologies highlights this application in their sales literature by showing the organotin compounds in a marine sediment standard reference material [108]. In another environmental analysis, Johnson et al. [109] use the chlorine, sulfur, and phosphorus lines to selectively detect pesticides such as chlorpyrifos. This work was part of a larger program to develop a method for the analysis of several hundred pesticides and suspected endocrine disrupters. Many pesticides contain two or more types of heteroatoms, so the simultaneous detection of these at the correct retention time and in the proper proportions is definitive for identification. Repetitive GC runs using MS detection [110] gave complementary information and allowed better identifications and comparisons of retention times between the two methods (the GC-MS retention times were perturbed by the outlet pressure being sub-ambient from the MS vacuum system).

Quimby et al. [111], Albro et al. [112], and Quimby et al. [113] used GC-AED to examine the nitrogen and sulfur species found in gasoline, diesel fuel, aviation fuel (kerosene), and heavier processed petroleum products. The species found were mainly carbazoles and thiophenes. A carbon emission line was used for universal detection. The selectivity and sensitivity of various emission lines were compared, as was the effect of reagent and make-up gas flows. The first paper also examined a variety of oxygen-containing species in gasoline. They used a test mixture that contained nine common alcohols and five ethers that are of some importance as gasoline additives (mandated by the US EPA for cleaner combustion). This is an important method in those areas that add alcohols or ethers to gasoline due to environmental regulation, since some of these are suspected carcinogens and their water solubility leads to build-up in the aqueous environment. This method selectively detects the oxygen-containing compounds. Other methods generally rely solely on chromatographic retention times for identification.

Boduszynski and co-workers [114] and Andersson and Sielex [115] have used GC-AED to examine the sulfur-containing molecules in petroleum and its heavier processed products. Both groups found a preponderance of thiophenic sulfur compounds in processed materials, in contrast to petroleum. The unprocessed petroleum had mercaptans, sulfides, thiophenes, as well as other species containing other heteroatoms in addition to the sulfur. These two studies also showed that this detector has the selectivity for sulfur that is attainable with the two older commonly used sulfur detectors, the flame photometric detector (FPD) and the chemiluminescent detectors. The first of these, however, suffers from a very non-linear response. This effect is very compound-class dependent. This is due to the fact that the light-emitting species that is detected is a two-sulfur atom one that results from recombination of the sulfur atoms in the combusted sample peak. The efficiency of combustion and the rate of recombination are both dependent on the

number of sulfur atoms and the structure of the sample molecules. This makes the AED a much more favored detection based just on its sulfur detecting capabilities.

The “volatile” porphyrins in crude oils (petroleum) were separated by high-temperature GC [116, 117]. The vanadium, nickel, and iron porphyrins were individually monitored. The optimum detection lines were chosen by looking at the emission spectra at the peaks of vanadyl octaethylporphyrin, nickel octaethylporphyrin, and ferrocene in individual runs of the standard compounds. The individual GC-AED chromatograms differed from each other in petroleum samples, but only a few peaks could be discerned on top of broad peak profiles. In some petroleum samples, no iron was seen.

As is the case with LC-MS, the solvent from an HPLC must be removed before the column output can be introduced into the spectrometer, or plasma conditions must be compatible to large amounts of organic solvents. For microwave or inductively-coupled plasmas (ICPs), the first must be done. Direct-current plasmas (DCPs) can accommodate direct solvent introduction. The high-molecular weight compounds when lead binds to human erythrocytes were separated by size-exclusion chromatography and ICP-AED was used to monitor the eluent.

Biggs and co-workers used a DC arc plasma detector to measure iron, nickel, vanadium, and sulfur profiles from SEC of petroleum and its distillation and adsorption chromatography fractions [118–123]. They found that the metal species were present as three distinct molecular sizes. They identified the low molecular weight ones as metalloporphyrins. They also measured the variety of silicon-containing species in polysiloxane polymers and synthetic alkyl- and arylsulfonates [124]. This combination of separation and elemental detection allowed them to see several oligomeric series of species in the polysiloxanes, which were compared with the retention times of standard compounds. The series proved to be linear chains, branched chains, and cyclic structures. The chromatographic method was able to give a baseline separation of each of the oligomers up to 60 units of trimethoxy-polydimethylsiloxane (silicone oils and greases are this type of polymer).

Slejkovec et al. [125] used HPLC-atomic fluorescence to separate and quantify the anionic arsenic compounds found in urban aerosol samples. The initial sample preparation produced aqueous extracts. These were found to contain only arsenate, although the separation worked for mixtures of arsenite, arsenate, monomethylarsonic acid, and dimethylarsonic acid. The detection limit for arsenate was  $80 \text{ pg mL}^{-1}$ .

Butcher et al. [126] coupled a diode-array based atomic absorption spectrometer to the output of an HPLC. They used this to determine the fuel additive methylcyclopentadienyl manganese tricarbonyl and the non-methylated species. They found a detection limit of  $2 \text{ ng(Mn) mL}^{-1}$ . They also examined the photolytic stability of these organomanganese compounds and found that samples should only be exposed to laboratory light during sample introduction.

**21.7****Other Types of Detection**

There have been a few reports of HPLC with Raman detection. Raman spectroscopy is complementary to FTIR and responds to those molecular motions that do not produce a change in a molecular dipole moment. Molecular motion such as stretching of an olefinic double bond or a sulfur–sulfur bond is not IR active, but is Raman active. Raman signals are inherently much weaker than FTIR ones, requiring laser sources and monitoring of small energy difference between the incident and observed light. Raman detection is usually done through the monitoring for a target analyte at a specific wavelength. Nguyen-Hong and co-workers [127] describe one such system. Cooper et al. [128] describe another which they used to detect nitrobenzene. The use of the more conventional approach of post-column trapping for Raman detection does not require cryogenic trapping. Silica plates (like those used in thin-layer chromatography) can collect the sample spots. The technique of surface-enhanced Raman spectrometry can then be readily performed on each spot. Calabin et al. [129] used this approach, with a post-collection application of colloidal silver as the surface-active agent. A commercial HC-Raman system is available as an option to a GC-FTIR one [130].

The optical activities of the eluting HPLC peaks can be monitored by using a circular dichroism spectrometer (CDS). In CDS, the effect that a sample solution has on the angle of a beam of polarized light is measured. Many organic compounds, particularly those involved in biological processes, show optical activity by exhibiting two forms. Light can either be polarized in a right-hand or a left-hand manner. Isolation of the biologically active form from a synthetic, racemic product mixture is a very important step for the organic chemist. In some materials of biological origin, like petroleum, the prevalent biological form racemizes, or starts to convert to an equilibrium mixture of the two forms, as soon as the biological process stops (for example, the organism dying). Measurement of the ratio of optical forms of certain of these pairs is an important tool in geochemistry.

Normally CDS requires the use of pure compounds, since the total change in the angle is measured and each component in a mixture adds to the total. Therefore, it is seldom used for real world analyses because it is useful only in determining the polarization of very pure compounds. The separating power of HPLC, however, makes CDS useful for certain applications. The chromatography separates a mixture into peaks, each of which is essentially a pure component as it flows through the sample cell. Yamamoto and co-workers [131] built a detector that readily measures the enantiomeric purity of separated peaks. They split the column effluent, with one part going to a regular absorbance detector and the other flowing into a cell using polarized light. Peak profiles and intensity ratios were used to assess the presence of any enantiomeric impurities.

Bringmann and co-workers used HPLC-CDS to determine the absolute stereo configurations of several plant metabolites [132]. They used identical chromatographic conditions for complementary HPLC-MS and HPLC-NMR data by coupling the same chromatograph and column to each type of spectrometer. Mistry

and co-workers [133] used HPLC-CDS and HPLC-NMR to identify and determine the stereo configuration of components of the neuromuscular blocking agent Atracurium Besylate. They used a chiral column and found 10 isomers, in four enantiomeric pairs and two meso compounds. This combination of complementary detectors helps assign the specific configurations and structural features of complex biological mixtures. Since chiral bonded phases, like the Pirkle columns, are specifically designed to separate optical isomers from each other, their use with subsequent CDS is potentially a very powerful tool in the characterization of natural products and other biological materials.

A variation on HPLC-CDS is based on magneto-optical rotation. In a longitudinal electric field, almost all molecules show optical activity [134]. The electrical field orients the molecules through their permanent dipole moments and/or through any anisotropic electrical polarizability. Kawazumi et al. [135] used this principle to build a detector for HPLC. Although the device was complicated, and prone to respond to minute changes in the refractive index or temperature of the mobile phase, it showed promise as a universal detector. This universality would only apply to detectability. Compounds with strong dipole moments and those that are easily polarizable would have more intense responses than compounds that do not.

The interesting combination of capillary electrophoresis-X-ray fluorescence detection was recently described as an element-specific detector [136]. A special plastic cell, which was both X-ray transparent and did not produce any interfering emission, was used. Vitamin B-12 (cyanocobalamin) and the cyclohexanediaminetetraacetic acid complexes of iron, zinc, cobalt, and copper were separated. Although the detection limits found were in the nanogram range, the authors estimate that with optimization that 2 or 3 orders of magnitude more sensitivity is likely.

Hill and Tarver [137] review the use of Fourier-transform ion-mobility spectroscopy with SFC. In this technique, sample molecules are placed in an atmospheric-pressure ionization chamber. The entrance and exit slits are rapidly and synchronously gated. This causes the drift times of the ions to be either in- or out-of-phase with the gates. The frequency of the gates can be ramped to control which ions are in-phase, and thus pass through to the ion detector. The real utility of this effect is the introduction of reagent gases, such as oxygen or ammonia. These gases selectively react with the sample molecular ions. The resulting arrangement is a selective detector for chemical reactivities.

In theory, almost every type of spectrometer can potentially be used as a chromatographic detector since the samples are most often in either the gas or liquid states. Given this fact, the number of hyphenated techniques is only bound to grow as more spectroscopists couple a chromatograph to their instruments.

## 21.8

### Serial or Parallel Multiple Detection

The combination of GC with FTIR and MS detection has been used for a variety of applications [138–142]. In all of these the GC effluent is split through a tee and each branch goes to one of the two detectors. Examples include a sample from suspected clandestine use of a chemical laboratory showed phenyl-2-propanone and other compounds indicative of methamphetamine production, the concentration of benzene, toluene, the xylene isomers, and 1,2,4-trimethylbenzene in a gasoline, the trace contaminants in solvents used in semiconductor manufacture, the three flavor essence isomers eugenol, and *cis*-and *trans*- isoeugenol (4-allyl-2-methoxyphenol and *cis*- and *trans*- 2-methoxy-4-propenylphenol), and the components in a perfume sample. In the last of these, the sample was previously run by GC-AED with C, H, O, and N detection to augment the other two types of detectors.

Unlike most of the other spectrometric detectors described here, the DAD and FSFD are non-destructive and can be readily used in a true flow-through mode (unlike NMR, which generally requires slower flow rates or stop-flow conditions). Therefore, the chromatographic eluent from them can easily be coupled to another subsequent detector. The commercial FSFD described earlier in fact typically is run in series with a DAD.

Destructive detectors, such as MS or AED, can be coupled to the output of the non-destructive detectors. This gives complementary and simultaneous information that can aid in peak identification. The retention data will show later retention times, but the sets of data can be reconciled for this lag through monitoring of standard compounds.

The series of DAD-MS detection has been the most commonly used. Quilliam and co-workers [143–145] determined polycyclic aromatic compounds and marine ecotoxins in this fashion. Their series of papers describes the coupling of a mass spectrometer to the outlet of the DAD. The MS mode was atmospheric-pressure chemical ionization, where the effluent was volatilized in a heated nebulizer. The mobile phase is preferentially removed, but the remaining solvent also acts as the chemical-ionization reagent. Both reversed-phase HPLC and supercritical fluid chromatography were used as the separation methods. This allowed separation of LPAHs of over 500 Da. This group was only able to identify a few of the LPAH peaks through the use of standards or reference UV absorbance spectra. These included coronene, benzo[*pqr*]naphtho [8,1,2-*bcd*]perylene, naphtho [8,1,2-*abc*]coronene, and ovalene. Bessant et al. used DAD and electrospray MS to measure hydroxypyridine isomers at different pHs. They noted peak shape difference, with the MS data showing much greater tailing. This was ascribed to the increased void volumes and the mechanism of solvent removal. The MS vacuum acts to effectively expand the void volume or increase post-column mixing because of the rapid expansion of the liquid volumes and the turbulence.

With the development of several commercial, commonly-available LC-MS interfaces, the combination of HPLC-DAD-MS is now becoming a routine sequential analytical approach. This should result in a burgeoning number of applications

in a wide variety of fields. Additionally, with the FSFD now also being commercially available, the combination of HPLC-FSFD-MS is easily possible. In a classic paper, Paeden et al. [146] separated the large PAHs from a carbon-black extract, collecting over 50 individual peaks. Fluorescence excitation and emission spectra and the mass spectrum of each fraction were then collected for characterization. Although the equivalent work has not yet been done, this same task of data collection would take less than a day by using the serial hyphenated technique approach in a few repetitive runs (to collect the two modes of fluorescence spectra at difference excitation and emission wavelengths). This would be in contrast to the several weeks required in the original work.

NMR is also a non-destructive technique, and a small number of sequential applications have been published. Wilson and co-workers [147] used HPLC-DAD-NMR-MS to characterize plant extracts. Hanson and co-workers [148] used a similar approach to examine another plant extract of pharmaceutical interest. In both cases, the complementary nature of the data provided quantitation of both major and minor constituents and aided in the structural identification of several of the minor components, including chiral isomers. Lommen et al. [149] describe a similarly configured system. The DAD and MS outputs were used to detect peaks, which were then transferred for NMR. They examined glycosides found in apple peel. They identified six quercetin glycosides and two phloretin glycosides, with the NMR data providing the definitive conformational data to differentiate the isomers.

## References

- 1 J. C. Fetzer, W. R. Biggs, *J. Chromatogr.*, 1993, 642, 319–327.
- 2 L. Huber, S. A. George, *Diode-Array Detection in HPLC*, Marcel Dekker, New York 1993.
- 3 R. A. Freidel, M. Orchin, *Ultraviolet Spectra of Aromatic Compounds*, John Wiley and Sons, New York, 1951, spectra 7 and 17.
- 4 J. C. Fetzer, E. J. Gallegos, *Polycyclic Aromat. Compd.*, 1992, 2, 245–251.
- 5 F. Dieterich, R. Ettl, Y. Rubin et al., *Science*, 1991, 252, 548–551.
- 6 R. Ettl, I. Chao, F. Dieterich, et al., *Nature (London)*, 1991, 353, 149–153.
- 7 F. Dieterich, R. L. Whetten, C. Thilgen et al., *Science*, 1991, 254, 1768–1770.
- 8 J. C. Fetzer, W. R. Biggs, *J. Chromatogr.*, 1984, 295, 161–169.
- 9 J. C. Fetzer, W. R. Biggs, *Org. Prep. Proced. Int.*, 1986, 18, 290–294.
- 10 J. C. Fetzer, *Polycyclic Aromat. Compd.*, 1999, 14/15, 1–10.
- 11 H. J. Boessenkoof, P. Cleij, C. E. Goewie et al., *Mikrochim. Acta*, 1986, 2, 71–92.
- 12 D. M. Demorest, J. C. Fetzer, I. S. Lurie et al., *LC/GC Mag.*, 1987, 5, 128–142.
- 13 L. S. Ramos, R. J. Stewart, B. G. Rohrback, *Chromatogr. (LC/GC)*, 1987, 2, 95–102.
- 14 R. Tauler, G. Durand, D. Barcelo, *Chromatographia*, 1992, 33, 244–254.
- 15 R. Gargallo, R. Tauler, F. Cuesta-Sanchez et al., *Trends Anal. Chem.*, 1996, 15, 279–286.
- 16 K. Jinno, J. C. Fetzer, W. R. Biggs, *Chromatographia*, 1986, 21, 274–276.
- 17 J. C. Fetzer, W. R. Biggs, K. Jinno, *Chromatographia*, 1986, 21, 439–442.
- 18 K. Jinno, Y. Miyashita, S. Sasaki et al., *Environ. Monit. Assess.*, 1991, 19, 13–25.
- 19 C. H. Marvin, L. Allan, B. E. McCarry et al., *Environ. Mol. Mutagenesis*, 1993, 22, 61–70.
- 20 C. H. Marvin, M. Tassaro, B. E. McCarry et al., *Sci. Total Environ.*, 1994, 156, 119–131.
- 21 A. E. Legzdins, B. E. McCarry, C. H. Marvin et al., *J. Environ. Anal. Chem.*, 1995, 60, 79–94.
- 22 C. H. Marvin, J. A. Lundrigan, B. E. McCarry et al., *Environ. Toxicol. Chem.*, 1995, 14, 2059–2066.
- 23 C. H. Marvin, B. E. McCarry, J. Villella et al., *Polycyclic Aromat. Compd.*, 1996, 9, 193–200.
- 24 C. H. Marvin, B. E. McCarry, J. A. Lundrigan et al., *Sci. Total Environ.*, 1999, 231, 135–144.
- 25 C. H. Marvin, R. W. Smith, D. W. Bryant et al., *J. Chromatogr.*, 1999, 863, 13–24.
- 26 J. C. Fetzer, W. R. Biggs, *Polycyclic Aromat. Compd.*, 1994, 5, 193–199.
- 27 J. C. Fetzer, J. R. Kershaw, *Fuel*, 1995, 74, 1533–1536.
- 28 M. J. Wornat, B. A. Vernaglia, A. L. LaFleur et al., *Twenty-Seventh International Symposium on Combustion*, The Combustion Institute, Pittsburgh, PA 1998, pp. 1677–1686.
- 29 M. J. Wornat, F. J. J. Vriesendorp, A. L. LaFleur et al., *Polycyclic Aromat. Compd.*, 1999, 13 221–240.
- 30 J. C. Fetzer, B. R. T. Simoneit, P. Garrigues et al., *Polycyclic Aromat. Compd.*, 1996, 9, 109–120.

- 31** B. R. T. Simoneit, J. C. Fetzer, in *Organic Geochemistry: Developments and Applications to Energy, Climate, Environment and Human History*, eds. J. O. Grimalt, C. Dorronsoro, A. I. G. O. A., Donostia, San Sebastian, Spain 1995, pp. 414–417.
- 32** J. R. Jadamec, W. A. Saner, Y. Talmi, *Anal. Chem.*, 1977, 49, 1316–1321.
- 33** J. C. Gluckman, M. Novotny, *J. High Resol. Chromatogr.*, 1985, 8, 672–677.
- 34** J. C. Gluckman, D. C. Shelly, M. Novotny, *Anal. Chem.*, 1985, 57, 1546–1552.
- 35** J. C. Gluckman, M. V. Novotny, *Chromatogr. Sci.*, 1989, 45, 145–173.
- 36** T. L. Cecil, PhD Thesis, Virginia Commonwealth University, 1990.
- 37** R. Schuster, H. Schulenberg-Schell, *A New Approach to Lower Limits of Detection and Easy Spectral Analysis*, Hewlett Packard Instruments (now Agilent Technology Co.), Waldbronn, Germany 1998.
- 38** J. A. Burt, M. A. Dvorak, G. D. Gillespie et al., *Appl. Spectrosc.*, 1999, 53, 1496–1501.
- 39** M. P. Fogarty, D. C. Shelly, I. M. Warner, *J. High Resol. Chromatogr.*, 1981, 4, 561–568.
- 40** D. C. Shelly, M. P. Fogarty, I. M. Warner, *J. High Resol. Chromatogr.*, 1981, 4, 616–626.
- 41** J. C. Fetzer, *The Chemistry and Analysis of the Large Polycyclic Aromatic Hydrocarbons*, John Wiley and Sons, New York 2000, ch. 4.
- 42** K. E. Peters, J. M. Moldowan, *The Biomarker Guide*, Prentice Hall, Englewood Cliffs, NJ 1993.
- 43** S. G. Roussis, W. P. Fitzgerald, *Anal. Chem.*, 2000, 72, 1400–1409.
- 44** W. Schmidt, G. Grimmer, J. Jacob et al., *Toxicol. Environ. Chem.*, 1986, 13, 1–16.
- 45** W. Schmidt, G. Grimmer, J. Jacob et al., *Fresenius J. Anal. Chem.*, 1987, 326, 401–413.
- 46** S. A. Wise, B. A. Benner, H. Liu et al., *Anal. Chem.*, 1998, 60, 630–637.
- 47** J. M. Gieskes, B. R. T. Simoneit, A. J. Magenheim et al., *Appl. Geochem.*, 1990, 5, 93–101.
- 48** B. R. T. Simoneit, W. D. Goodfellow, J. M. Franklin, *Appl. Geochem.*, 1992, 7, 257–264.
- 49** O. E. Kawka, B. R. T. Simoneit, *Org. Geochem.*, 1994, 22, 947–978.
- 50** W. J. Simonsick, R. A. Hites, *Anal. Chem.*, 1986, 58, 2114–2121.
- 51** J. T. Watson, *Introduction to Mass Spectrometry*, Lippincott-Raven Publishers, Philadelphia 1997, p. 219.
- 52** A. Rosele-Mele, J. F. Carter, J. R. Maxwell, *J. Am. Soc. Mass Spectrom.*, 1996, 7, 965–971.
- 53** S. Suzuki, T. Kaneko, M. Tsuchiya, *Kankyo Kagaku*, 1996, 6, 511–520.
- 54** B. H. Kaye, *Science and the Detective*, Wiley-VCH, Weinheim 1995, ch. 8.
- 55** S. Lacorte, I. Guiffard, D. Fraisse et al., *Anal. Chem.*, 2000, 72, 1430–1440.
- 56** Water Corporation, *Zspray Mass Detector for API LC/MS*, Milford MA 1999.
- 57** Hewlett-Packard, *Chemical Analysis*, 1999
- 58** K. Imatani, C. Smith, *Am. Lab.*, 1996, Nov.
- 59** Hewlett-Packard, *Development of a new Orthogonal Geometry Atmospheric Pressure Ionization Interface for LC-MS*, 1998
- 60** J. Charlwood, H. Birrell, E. S. P. Bouvier et al., *Anal. Chem.*, 2000, 72, 1469–1474.
- 61** S. X. Peng, S. L. King, D. M. Bornes et al., *Anal. Chem.*, 2000, 72, 1913–1917.
- 62** T. Suzuki, T. Yasumoto, *J. Chromatogr. A*, 2000, 874, 199–206.
- 63** M. Holcapek, H. Virelizler, J. Chamot-Rooke et al., *Anal. Chem.*, 1999, 71, 2288–2293.
- 64** A. Boyer, in *LCWorldTalk*, Shimadzu, Columbia MD, 2000
- 65** D. L. Deforce, E. G. Van den Eeckhout, in *Advances in Chromatography: Volume 40*, eds. P. R. Brown, E. Grushka, Marcel Dekker, New York, 2000, pp. 539–566.
- 66** G. d'Ascenzo, R. Curini, A. Gentili et al., in *Advances in Chromatography: Volume 40*, eds. P. R. Brown, E. Grushka, Marcel Dekker, New York 2000, pp. 567–598.
- 67** S. E. Nielsen, R. Freese, C. Cernett et al., *Anal. Chem.*, 2000, 72, 1503–1509.
- 68** C. S. Hsu, K. Kian, W. K. Robbins, *J. High Resol. Chromatogr.*, 1994, 17, 271–276.

- 69** J. Mao, C. R. Panchoco, D. D. Traficante et al., *Fuel*, **1995**, *74*, 880–887.
- 70** D. J. Afferud, L. Prokai, W. J. Simon-sick, *Anal. Chem.*, **1999**, *71*, 4793–4799.
- 71** C. M. Pace, L. D. Betowski, *J. Am. Soc. Mass Spectrom.*, **1995**, *6*, 597–607.
- 72** E. Rosenberg, V. Kmetov, M. Grasser-bauer, *Fresenius' J. Anal. Chem.*, **2000**, *366*, 400–407. (2000)
- 73** J. T. Mehl, D. M. Hercules, *Anal. Chem.*, **2000**, *72*, 68–73.
- 74** D. S. Braverman, *J. Anal. At. Spectrom.*, **1992**, *7*, 43–46.
- 75** G. Schminke, A. Seubert, *Fresenius' J. Anal. Chem.*, **2000**, *366*, 387–391.
- 76** T. De Smaele, L. Moens, R. Dams et al., *Fresenius' J. Anal. Chem.*, **1996**, *355*, 778–782.
- 77** M. Heisterkamp, T. De Smaele, J. P. Candelone et al., *J. Anal. At. Spectrosc.*, **1997**, *12*, 1077–1081.
- 78** L. Ebdon, E. H. Evans, W. G. Pretorius et al., *J. Anal. At. Spectrosc.*, **1996**, *9*, 939–943.
- 79** U. Fuchsluefer, G. Socher, H.-J. Grether et al., *Anal. Chem.*, **1999**, *71*, 2324–2333.
- 80** R. Subramanian, W. P. Kelley, P. D. Floyd et al., *Anal. Chem.*, **1999**, *71*, 5335–5339.
- 81** A. Preiss, N. Karfich, K. Levsen, *Anal. Chem.*, **2000**, *72*, 992–998.
- 82** K. Levsen, A. Preiss, M. Godejohann, *Trends Anal. Chem.*, **2000**, *19*, 27–48.
- 83** T. Kitayama, M. Janco, K. Ute et al., *Anal. Chem.*, **2000**, *72*, 1516–1522.
- 84** Bio Rad Laboratories, Cambridge MA, *Bio Rad's Infrared Detector*, 1999.
- 85** T. J. Bruno, *Sep. Sci. Technol.*, **1999**, *29*, 63–89.
- 86** A. Meyer, H. Budzinski, J. R. Powell et al., *Polycyclic Aromat. Compd.*, **1999**, *13*, 329–339.
- 87** D. F. Gurka, L. D. Betowski, *Anal. Chem.*, **1982**, *54*, 1819–1824.
- 88** S. Compton, P. Stout, *LC/ GC*, **1990**, *12*, 920–926.
- 89** K. Wilkins, I. Marr, B. B. Allen et al., *Differentiation of some Monoterpene alcohols in Organo Aromas*, Hewlett-Packard applications note IRD 91-3, 1991.
- 90** N. J. Huang, D. C. Sundberg, *Polymer*, **1994**, *35*, 5693–5698.
- 91** M. W. Raynor, K. D. Bartle, B. W. Cook, *J. High Resol. Chromatogr.*, **1992**, *15*, 361–366.
- 92** S. French, M. Novotny, *Anal. Chem.*, **1986**, *58*, 164–166.
- 93** H. Pichard, M. Caude, P. Sassiat et al., *Lab. Analysis*, **1988**, *16*, 131–133.
- 94** M. W. Raynor, G. F. Shilstone, K. D. Bartle et al., *J. High Resol. Chromatogr.*, **1989**, *12*, 300–302.
- 95** M. A. Healy, T. J. Jenkins, M. Polakoff, *Trends Anal. Chem.*, **1991**, *10*, 32–37.
- 96** M. W. Raynor, G. F. Shilstone, A. A. Clifford et al., *J. Microcolumn Sep.*, **1991**, *3*, 337–347.
- 97** T. J. Jenkins, G. Davidson, M. A. Healy et al., *J. High Resol. Chromatogr.*, **1992**, *15*, 819–826.
- 98** C. H. Kirschner, L. T. Taylor, *J. High Resol. Chromatogr.*, **1994**, *17*, 61–67.
- 99** K. L. Norton, P. R. Griffiths, *J. Chromatogr. A*, **1995**, *703*, 503–522.
- 100** M. X. Liu, J. L. Dwyer, *Appl. Spectrosc.*, **1996**, *50*, 349–350.
- 101** S. L. Jordan, L. T. Taylor, *J. Chromatogr. Sci.*, **1997**, *35*, 7–13.
- 102** B. Quimby, P. C. Dryden, J. J. Sullivan, *Anal. Chem.*, **1990**, *62*, 2509–2512.
- 103** G. W. Somsen, S. K. Coulter, C. Gooijer et al., *Anal. Chim. Acta*, **1997**, *349*, 189–197.
- 104** M. S. Jimenez, R. E. Sturgeon, *J. Anal. At. Spectrosc.*, **1997**, *12*, 597–601.
- 105** Y. Liu, V. Lopez-Avila, M. Alcaraz, *J. High Resol. Chromatogr.*, **1993**, *16*, 106–112.
- 106** Y. Lin, V. Lopez-Avila, M. Alcaraz et al., *J. AOAC Int.*, **1995**, *78*, 1275–1285.
- 107** M. K. Behlke, P. C. Uden, M. M. Schrantz et al., *Anal. Chem.*, **1996**, *68*, 3859–3866.
- 108** Agilent Technologies, *Sensitive and Selective Universal Element Detection for Routine or Research Analyses*, 1999
- 109** D. Johnson, B. Quimby, J. Sullivan, *Am. Lab.*, **1995**, Oct.
- 110** P. L. Wylie, B. D. Quimby, *A Method Used to Screen for 557 Pesticides and Suspected Endocrine Disrupters*, Agilent Technology, Wilmington, DE 1998.
- 111** B. D. Quimby, V. Giarrocco, J. J. Sullivan et al., *J. High Resol. Chromatogr.*, **1993**, *15*, 705–709.

- 112** T. G. Albro, P. A. Dreifuss, R. F. Wormsbecher, *J. High Resol. Chromatogr.*, **1993**, *16*, 13–17.
- 113** B. D. Quimby, D. A. Grudoski, V. Giarocco, *J. Chromatogr. Sci.*, **1998**, *36*, 435–443.
- 114** M. M. Boduszynski, D. A. Grudoski, C. E. Rechsteiner et al., in *Proceedings of the 6<sup>th</sup> INITAR International Conference*, 1995, vol. 2, pp.335–244.
- 115** J. T. Andersson and K. J. Sielex, *J. High Resol. Chromatogr.*, **19** 49–53 (1996)
- 116** L. A. Bergdahl, A. Schuetz, A. J. Grubb, *J. Anal. At. Spectrosc.*, **1996**, *11*, 735–738.
- 117** B. D. Quimby, P. C. Dryden, J. J. Sullivan, *J. High Resol. Chromatogr.*, **1991**, *14*, 110–116.
- 118** J. G. Reynolds, W. R. Biggs, J. C. Fetzer et al., *Collect. Colloq. Semin. (Inst. Fr. Pet.)*, **1984**, *40*, 153–159.
- 119** W. R. Biggs, J. C. Fetzer, R. J. Brown et al., *Liq. Fuels Technol.*, **1985**, *3*, 397–422.
- 120** J. G. Reynolds, W. R. Biggs, J. C. Fetzer, *Liq. Fuels Technol.*, **1985**, *3*, 423–447.
- 121** W. R. Biggs, R. J. Brown, J. C. Fetzer, *Energy Fuels*, **1987**, *1*, 257–262.
- 122** W. R. Biggs, J. G. Reynolds, J. C. Fetzer, *Cosmochim. Geochim. Acta*, **1988**, *52*, 2337–2341.
- 123** W. R. Biggs, J. C. Fetzer, R. J. Brown, *Anal. Chem.*, **1987**, *59*, 2798–2802.
- 124** W. R. Biggs, J. C. Fetzer, *Anal. Chem.*, **1989**, *61*, 236–240.
- 125** Z. Slejkovec, I. Salma, J. T. van Elteren et al., *Fresenius' J. Anal. Chem.*, **2000**, *366*, 830–834.
- 126** D. J. Butcher, A. Zybin, M. A. Bolshov et al., *Anal. Chem.*, **1999**, *71*, 5379–5385.
- 127** T. D. Nguyen Hong, M. Jouan, N. Quy Dao et al., *J. Chromatogr. A*, **1996**, *743*, 323–327.
- 128** S. D. Cooper, M. M. Robson, D. N. Batchelder et al., *Chromatographia*, **1997**, *44*, 257–262.
- 129** L. M. Calabrin, A. Ruperez, J. J. Laserna, *Anal. Chim. Acta*, **1996**, *318*, 203–210.
- 130** Bio-Rad Laboratories, Cambridge MA
- 131** A. Yamamoto, A. Matsunaga, K. Hayakawa et al., *J. Chromatogr. A*, **1996**, *727*, 55–59.
- 132** G. Bringmann, K. Messer, M. Wohlfarth et al., *Anal. Chem.*, **1999**, *71*, 2678–2686.
- 133** N. Mistry, A. D. Roberts, G. E. Tranter et al., *Anal. Chem.*, **1999**, *71*, 2838–2843.
- 134** J. Michl, E. W. Thulstrup, *Spectroscopy with Polarized Light*, Wiley-VCH, Weinheim 1986, p. 45.
- 135** H. Kawazumi, H. Nishimura, Y. Otsubo et al., *Anal. Sci.*, **1991**, *7*, 1479–1480.
- 136** S. E. Mann, M. C. Ringo, G. Shea-McCarthy et al., *Anal. Chem.*, **2000**, *72*, 1754–1758.
- 137** H. H. Hill, E. E. Tarver, in *Hyphenated Techniques in Supercritical Fluid Chromatography and Extract*, ed. K. Jinno, Elsevier, Amsterdam 1992, pp. 9–24.
- 138** *Clandestine Lab Reaction Mixture*, Hewlett-Packard GC-IR-MS application note IRD87-2, 1987.
- 139** *Analysis of Aromatics in Petroleum*, Hewlett-Packard GC-IR-MS application note IRD87-4, 1987.
- 140** *Semiconductor Solvents by GC/IR/MS*, Hewlett-Packard GC-IR-MS application note IRD86-4, 1986.
- 141** R. J. Leibrand, *The Power of the IRD: Isomer Differentiation*, Hewlett-Packard application note IRD88-7, 1988.
- 142** R. J. Leibrand, B. D. Quimby, M. Free, *The Use of Multispectral Analysis in the Characterization of Perfume*, Hewlett-Packard application note IRD 92-2, 1992.
- 143** P. G. Sim, M. A. Quilliam, S. Pleasance et al., *Polycyclic Aromat. Compd.*, **1993**, *3* (suppl.) 321–328.
- 144** J. F. Anacleto, L. Ramaley, R. K. Boyd et al., *Can. Rapid Commun. Mass Spectrom.*, **1991**, *5* 149–155.
- 145** A. L. LaFleur, K. Taghizadeh, J. B. Howard et al., *Am. Soc. Mass Spectrom.*, **1996**, *7*, 276–286.
- 146** P. A. Peaden, M. L. Lee, Y. Hirata et al., *Anal. Chem.*, **1980**, *52*, 2268–2271.
- 147** I. Wilson, E. D. Morgan, R. Lafont et al., *Chromatographia*, **1999**, *49*, 374–378.
- 148** S. H. Hansen, A. G. Jensen, C. Cornett et al., *Anal. Chem.*, **1999**, *71*, 5235–5241.
- 149** A. Lommen, M. Godejohann, D. P. Venema et al., *Anal. Chem.*, **2000**, *72*, 1793–1797.

## **Section XI**

### **General Data Treatment: Data Bases/Spectral Libraries**

## Introduction

*Kurt Varmuza*

Production, storage, treatment, evaluation, exploitation and interpretation of spectroscopic data is strongly connected with intensive use of computers. Modern spectroscopy – as many other disciplines – would not be possible without the tremendous developments in hardware and software during the last decades. Most of the mentioned aspects are treated in the three parts of this section, although the authors have focuses on different subjects.

Part *Optical Spectroscopy* by S. Thiele and R. Salzer for instance contains the topics basic data treatment, IR- and UV-databases and spectra similarity search methods. Emphasis is given to multivariate calibration methods that are now routinely used for quantitative analyses of compounds in complex matrices. Principles of the widely used chemometric methods, such as PCA, PCR, and PLS are explained together with their applications in IR spectroscopy.

Part *Nuclear Magnetic Resonance Spectroscopy* by W. Robien focuses on structure elucidation of organic compounds. Spectra similarity searches, spectrum prediction (from a given chemical structure), recognition of substructures and automatic isomer generation are the main topics; they are still areas of scientific research in computer-assisted structure elucidation.

Part *Mass Spectrometry* by A. N. Davies gives an overview from a user's point of view. Commercially available mass spectral databases and software products for library searches are characterized. A statement from section 24.1 is repeated here because it seems to be essential not only for mass spectral database systems: "... let the people who will be working with the systems have a major say in the testing and selection of the product to be purchased ...".

As a supplement to the more than 80 references given in the three parts an overview of books is presented here that are relevant to chemometrics [1] and its applications in spectroscopy. Two comprehensive standard books on chemometrics have been published by D. L. Massart et al. [2], and B. G. M. Vandeginste et al [3]. The predecessor of these books probably was the most used volume in chemometrics for many years [4]. Introductory and smaller books are from M. J. Adams (focus on analytical spectroscopy) [5], K. R. Beebe et al. (almost no mathematics) [6], R. G. Brereton [7], R. Kramer (focus on multivariate calibration) [8], and M. Otto [9]. The classical book on multivariate calibration in chemistry is from H. Mar-

tens and T. Naes [10], one on neural networks in chemistry from J. Zupan and J. Gasteiger [11].

- [1] K. Varmuza, in: P. v. R. Schleyer, N. L. Allinger, T. Clark, J. Gasteiger, P. A. Kollman, H. F. Schaefer III, P. R. Schreiner (Eds.), the Encyclopedia of Computation Chemistry, Wiley & Sons, Chichester, 1998, p. 346–366.
- [2] D. L. Massart, B. G. M. Vandeginste, L. C. M. Buydens, S. De Jong, J. Smeyers-Verbeke, Handbook of chemometrics and qualimetrics: Part A. Elsevier, Amsterdam, 1997
- [3] B. G. M. Vandeginste, D. L. Massart, L. C. M. Buydens, S. De Jong, J. Smeyers-Verbeke, Handbook of chemometrics and qualimetrics: Part B. Elsevier, Amsterdam, 1998.
- [4] D. L. Massart, B. G. M. Vandeginste, S. N. Deming, Y. Michotte, L. Kaufmann, Chemometrics: a textbook. Elsevier, Amsterdam, 1988.
- [5] M. J. Adams. Chemometrics in analytical spectroscopy. The Royal Society of Chemistry, Cambridge, 1995.
- [6] K. R. Beebe, R. J. Pell, M. B. Seasholtz, Chemometrics: A practical guide. Wiley & Sons, New York, 1998.
- [7] R. G. Brereton (Ed): Multivariate pattern recognition in chemometrics, illustrated by case studies. Elsevier, Amsterdam, 1992.
- [8] R. Kramer, Chemometric techniques for quantitative analysis. Marcel Dekker, New York, 1998.
- [9] M. Otto, Chemometrics. Wiley-VCH, New York, 1999.
- [10] H. Martens, T. Naes, Multivariate calibration. Wiley, Chichester, 1989.
- [11] J. Zupan, J. Gasteiger, Neural networks in chemistry and drug design. Wiley-VCH, Weinheim, 1999.

## **22**

# **Optical Spectroscopy**

*Steffen Thiele and Reiner Salzer*

### **22.1**

#### **Introduction**

The spectra measured by any method of optical spectroscopy may be subject to qualitative (what is it?) or quantitative (how much is it?) evaluation. We assume here that the basic rules described in other chapters for the overall analytical process are obeyed, in particular for sample selection and sample preparation. Errors during sample preparation or simply due to an incorrect positioning of the specimen in the optical beam can never be corrected for in the measured spectra. Restricted quality in the experimental spectra will lead to errors either in qualitative evaluation (e.g. ill-defined results in spectral search) or in quantitative evaluation (e.g. erroneous determination of concentration).

Modern spectrometer software offers a variety of mathematical tools for processing spectra. These tools provide powerful features to the experienced user but cause serious danger in the case of non-critical application. Some types of processing tools do not alter the information content of the spectra (cf. Tab. 22.1, Basic operations), others do (cf. Tab. 22.1, Manipulations). Particular attention has to be paid if the latter have to be used.

The evaluation of spectra will be discussed separately for qualitative and quantitative analysis. Particular emphasis will be laid (i) on state-of-the-art methods for searching spectra in spectral libraries or searching for spectroscopic information in data banks and on (ii) procedures for multivariate data analysis.

Two of the basic operations mentioned in Tab. 22.1 are of particular importance for the evaluation of spectra, centering and standardization. They will be considered first.

**Table 22.1** Types and objectives of spectra processing.

<b>Basic Operations</b>	<i>Prettier Display</i>	<i>Qualitative Evaluation</i>	<i>Quantitative Evaluation</i>
conversion transmission $T$ – absorbance $A$	X		X
conversion wavelength $\lambda$ – wavenumber $k$	X	X	X
background reduction	X	X	X
centering		X	X
standardization		X	X
spectra subtraction			X
<hr/>			
<b>Manipulations</b>			
background correction	X	X	
smoothing	X	X	X !
derivation	X	X	
deconvolution		X	
curve fitting		X	(X)
peak integration			X
generation of band tables		X	
spike correction (Raman spectra)	X	X	

## 22.2

### Basic Operations

#### 22.2.1

#### Centering

Centering is an important step in the pretreatment of spectral data prior to multivariate evaluation both for qualitative and for quantitative analysis. At first the mean spectrum  $\mathbf{a}_M^T$  is calculated from the set of measured spectra:

$$\mathbf{a}_M^T = (\bar{a}_1, \bar{a}_2, \dots, \bar{a}_p), \quad (1)$$

$$\text{where } \bar{a}_j = \frac{1}{n} \sum_{i=1}^n a_{ij} \quad j = 1, \dots, p. \quad (2)$$

The subscript  $j$  represents the number  $p$  of spectral data points, the subscript  $i$  the number  $n$  of measured spectra. Subsequently, the mean spectrum is subtracted from each measured spectrum:

$$\mathbf{a}_{C;i}^T = \mathbf{a}_i^T - \mathbf{a}_M^T \quad i = 1, \dots, n \quad (3)$$

As a result of the above data treatment the mean of the centered spectra  $\mathbf{a}_{C;i}^T$  amounts to zero, i.e. the center of the data set of  $n$  spectra has been shifted to the origin of the coordinate system (cf. Fig. 22.1). All subsequent matrix operations in

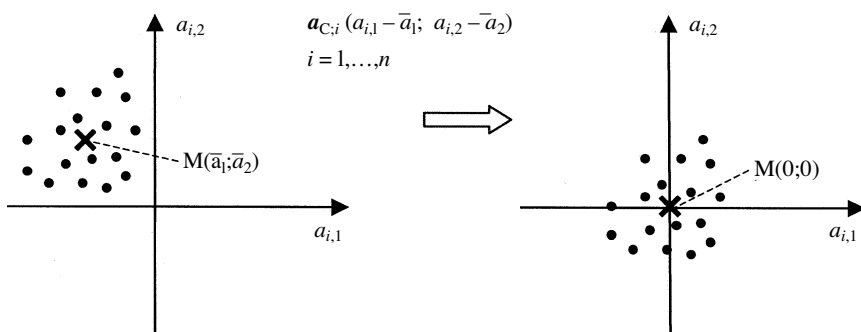


**Fig. 22.1** Effect of centering the measured absorbance values  $a_{i,1}$  and  $a_{i,2}$  illustrated for two spectral data points ( $p = 2$ ).

either qualitative or quantitative evaluation benefit from the centering, because the overlaid offset of the center has been removed and only the significant scattering of the measured spectra around the center is retained.

### 22.2.2

#### Standardization (Autoscaling)

Standardization is a method of pretreatment of spectral data prior to multivariate evaluation both for qualitative and for quantitative analysis, just like centering. In the case of standardization, the standard deviation  $s$  is calculated at each of the  $p$  spectral data points for all  $n$  measured spectra:

$$s_j = \sqrt{\frac{\sum_{i=1}^n (a_{ij} - \bar{a}_j)^2}{n-1}} \quad j = 1, \dots, p \quad (4)$$

The standardized absorbance value of each measured spectrum ( $i = 1, \dots, n$ ) at each spectral wavelength ( $j = 1, \dots, p$ ) is calculated by using

$$a_{sij} = \frac{a_{ij} - \bar{a}_j}{s_j} \quad (5)$$

The standardized set of spectral data shows a mean of zero and a variance of one. Standardization may also be useful for gathering and comparing multicollinearities in later evaluation steps (cf. Section 22.3).

One basic rule should be emphasized already here: the set of mathematical operations chosen for the calibration samples has to be applied in an absolutely identical manner to all subsequent test samples. This rule holds as well for the above-mentioned basic operations as for the more advanced operations described later in this chapter.

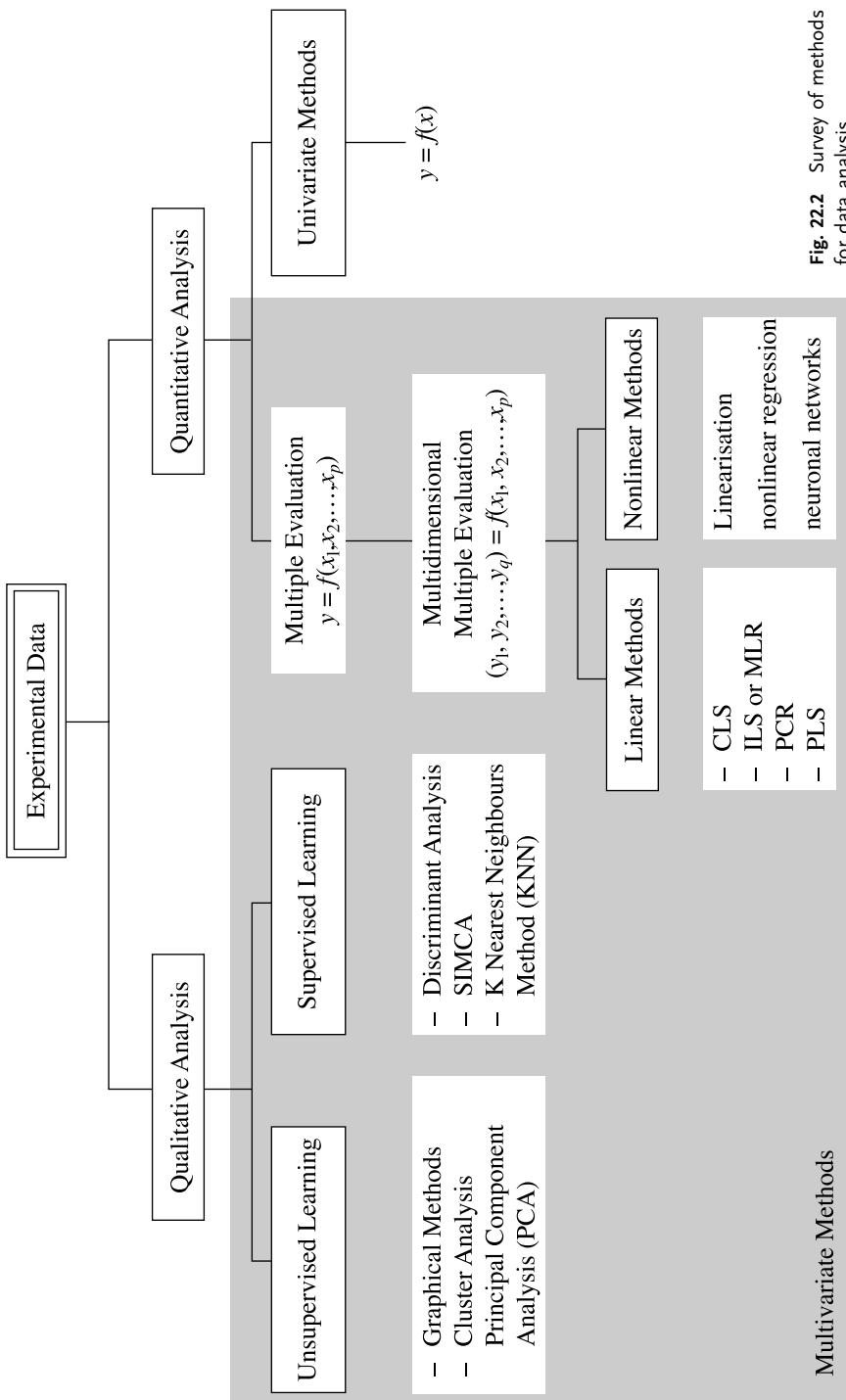
## 22.3 Evaluation of Spectra

### 22.3.1 Introduction

Contemporary spectrometers are able to produce huge amounts of data within a very short time. This development continues due to the introduction of array detectors for spectral imaging. The utilization of as much as possible of the enclosed spectral information can only be achieved by chemometric procedures for data analysis. The most commonly used procedures for evaluation of spectra are systematically arranged in Fig. 22.2 with the main emphasis on application, i.e. the variety of procedures was divided into methods for qualitative and quantitative analysis. Another distinctive feature refers to the mathematical algorithms on which the procedures are based. The dominance of multivariate over univariate methods is clearly discernible from Fig. 22.2.

In the case of qualitative analysis, unsupervised learning procedures are employed for explorative data analysis or for empirical investigation of samples with no additional information available. The analyst wants to sense the correlation within the data or the interrelation between the data and particular features or properties of the sample. Such information qualifies for structuring of data with respect to useful data range, property parameters and arrangement into classes. Excessive data amounts require reduction to a reasonable size by automated procedures prior to structuring. Principle Component Analysis (PCA) is an efficient method for such spectral data reduction. Supervised learning procedures are employed in order to assign new objects to already established classes (available additional knowledge). A simple case is the comparison of features between a new sample and previously characterized samples, e.g. during the search for an analyte spectrum in a spectral data base. The aim of this search is the elucidation of the composition or structure, respectively, of an unknown.

In the case of quantitative analysis, the amount of, or the exact relation between, the constituents of a compound or a mixture have to be established. The direct relation between the properties of a specimen and the concentration of its constituents could also be the aim of the quantitative investigation. In the latter case so-called calibration models have to be established, the corresponding model parameters have to be estimated, and they have to be confirmed by statistical methods. Calibration models established this way may then be used to determine, on a statistically verified basis, the concentration of constituents of an analyte within the calibrated range. All multivariate methods for quantitative analysis mentioned in Fig. 22.2 are employed for the evaluation of spectra.



Multivariate Methods

**Fig. 22.2 Survey of methods for data analysis**

## 22.3.2

**Qualitative Evaluation of Spectra****22.3.2.1 Spectral Data Banks**

Many digital spectral libraries have been transformed from printed spectra collections. Well known printed collections are the Aldrich spectra collection [1], the Sadler spectra collection [2–4], the Schrader–Meyer Atlas of IR and Raman spectra [5], the Hummel collection of IR spectra of polymers [6], the Merck IR Atlas [7] and the Buback collection of NIR spectra [8]. IR spectra have the largest share of digital optical spectra, followed at a clear distance by Raman spectra. Larger collections of UV/VIS spectra have not been established due to their missing fingerprint capability and to the strong sensitivity of the UV/VIS spectra to solvent interactions. A variety of dedicated spectra collections have been created in industrial laboratories without access to the public.

The difference between in-house and on-line versions of spectral libraries consists mainly in the fee, which depends upon the conditions of use. Usually, in-house versions have to be paid only once upon license acquisition and hardware purchase. Afterwards, the actual use is free of charge, regardless of its frequency. In certain cases an annual license fee has to be paid. Follow-up costs may occur if updates are demanded or if hardware service is needed. In the case of in-house systems running on UNIX workstations both initial costs as well as upkeep may be considerable. In contrast, the costs for on-line systems solely depend upon frequency of use. Both the reliability and speed of the internet connection may remarkably influence the cost. If only used occasionally the on-line version is certainly financially more viable than the in-house version. At best one is able to find free-of-charge internet offers, sometimes with restricted access to certain features (cf. Tab. 22.2).

Spectral data banks contain all sorts of information about a particular substance in the form of tables. The requested field of a table can be accessed by the user either via abbreviations (e.g., MF for molecular formula) or via input masks, which place the necessary denominations of the field at the user's disposal. Some fields may contain searchable information only as alphanumerical text (e.g., compound names), others may be searched only numerically (e.g., molecular weight). In the case of numerical fields, some numerical operators (e.g., <; =; > or – for area allocation) may also be applied.

It is often possible to search for bands of particular intensity in selected wavelength ranges. During the search all fields may be interconnected logically (search masks) or by logic operators (and; or; not; proximity operators). A summary of information contained in a spectral data bank for a given compound is given in Tab. 22.3.

The CAS number (Chemical Abstracts Service registry number) is of particular importance. This number went into a wide range of data banks (structural and factual data banks, bibliographic data banks, substance data banks) and may advantageously be used for fast access to information related to a particular substance. Data banks comprising information about several spectroscopic methods are of

**Table 22.2** Optical spectral data bases (according to provider specifications, 01.09.2000).

<b>Data Base</b>	<b>Type and Amount of spectra (if Available)</b>	<b>Availability</b>		<b>Charge</b>
		<i>In-house version</i>	<i>On-line version</i>	
<b>Aldrich</b>				
Condensed Phase	FT-IR: 18.500 FT-Raman: 14.000	X X		yes
Vapor Phase	FT-IR: 5.000	X		yes
<b>Environmental Protection Agency (EPA)</b>				
Vapor Phase	FT-IR: 3.300	X		yes
<b>Fiveash Data Manag., Inc.</b>				
Spectra of Drugs/ Canadian Forensic Spectra	FT-IR: 3.750	X		yes
Vapor Phase of Organic Compounds	FT-IR: 5.220	X		yes
Special Spectra	FT-IR: 2.600	X		yes
<b>Galactic Ind. Corp.</b> (URL:www.galactic.com)				
	IR, MS, NMR,UV/VIS, NIR: 6.000		X	no
<b>Galactic Ind. Corp. and Nicolet Instr. Corp.</b> (URL:FTIRsearch.com)				
	FT-IR: 71.000 Raman: 16.000		X X	yes yes
<b>Nicolet Instr. Corp.</b>				
Organic Chemical Library	FT-Raman: 1.000	X		yes
Vapor Phase Library (6.543 from Aldrich)	IR: 8.654	X		
Polymer Application Libraries and other special libraries	IR, Raman	X		yes
<b>NIST</b>				
WebBook (URL:webbook.nist.gov)	IR: 7.500 UV/VIS: 400	X X	X X	no
<b>Sadtler</b>				
Condensed Phase IR Standards	IR: 75.570	X		yes
Vapor Phase IR Standards	IR: 9.200	X		yes
Special Libraries	IR, Raman	X		yes
<b>SDBS</b>				
Organic compounds (URL:www.ilst.go.jp/RIODB/db004/menu-e.html)	FT-IR: 47.300 Raman: 3.500		X X	no no
<b>SpecInfo</b> (URL:www.chemicalconcepts.com/products.htm)				
	IR: 18.500	X	X	yes

**Table 22.3** Searchable information in spectral data banks.

Compound Identification	compound name incl. synonyms CAS number molecular formula molecular weight graphical structure representation additional data possible (e.g., melting point)
Acquisition of Spectra	sample source sample purity sample preparation spectrometer type spectral resolution additional data possible (e.g., special sample conditions; file format)
Spectrum	complete spectrum in numerical and graphical form band table

high value for structural elucidation if a combination of methods has to be applied (e.g., NIST, SDDBS, SpecInfo).

The spectral search itself is based on computation of similarity by comparison of full spectra or of peak tables. Necessary means are structural editors and spectral editors, which are usually applied off-line before the spectral search is started. Spectral editors may be used to erase existing peaks from or to generate new peaks into spectra. Spectral editors may also be used for the complete generation of new spectra. Structural editors are used to generate chemical 2D structures or to modify structures, which were previously obtained from chemical drawing programs. These structures can be searched in the data bank after they have been encoded by the structural editor. Substructure searches are uncommon in IR data banks because IR spectra are used for fingerprint identification of compounds rather than for assembling full structures from subunits.

In the case of a spectral search by comparison of peak tables, the system first computes the necessary peak table from the experimental spectrum of the analyte. For the subsequent search both the position and the intensity of the peaks in the spectrum of the unknown and in the spectra of the compounds contained in the data bank are compared. After the search has been completed, the top position in the hit list is assigned to the substance with least differences in peak positions and peak intensities.

In the case of a full spectra search, the complete set of spectral features (absorbance values at  $p$  wavelength positions) is compared between the spectrum of the unknown and all spectra contained in the data bank. So-called similarity measures are computed for each individual comparison. In the case of the mostly employed similarity measure, the Euclidean distance, the spectrum is regarded as a  $p$ -dimensional spectral vector (data points at  $p$  wavelength positions). The comparison

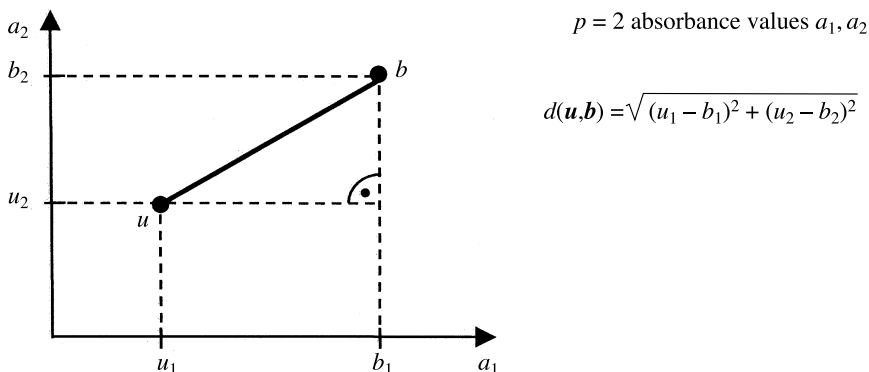


**Fig. 22.3** Euclidean distance between vector  $\mathbf{u}$  (spectrum of unknown substance) and vector  $\mathbf{b}$  (library spectrum) illustrated for absorbance values at two wavelengths.

between the spectral vector  $\mathbf{u}$  of the unknown and the vector  $\mathbf{b}$  of the data bank spectrum results in a value  $d(\mathbf{u}, \mathbf{b})$  (cf. Fig. 22.3):

$$d(\mathbf{u}, \mathbf{b}) = \sqrt{\sum_{i=1}^p (u_i - b_i)^2} \quad (6)$$

The library spectrum showing the minimal Euclidean distance  $d_{\min}$  from the spectrum of the unknown will be assigned the top position in the resulting hit list. In order to ensure comparability of the distances  $d$  each submitted spectrum has to be subjected to a particular normalization (cf. Fig. 22.4). At first, the lowest absorbance value across the spectrum is subtracted from all  $p$  data points of the spec-

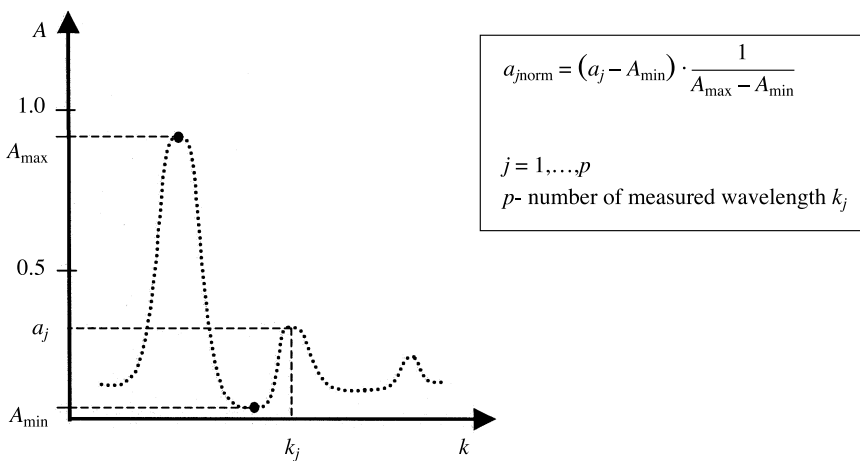


**Fig. 22.4** Normalization of a spectrum to the absorbance range between 0 and 1.

trum. Afterwards, the spectrum is normalized to the required absorbance maximum. The necessity of such a normalization constitutes a serious limitation of the search procedure.

In contemporary search algorithms each spectral vector is normalized to unit length (unit vector  $\mathbf{x}_E$ ). The length of a vector  $\mathbf{x}$  (also called absolute value or norm) is given by

$$\|\mathbf{x}\| = \sqrt{\mathbf{x}^T \mathbf{x}} \quad (7)$$

and the norm vector  $\mathbf{x}_E$  by

$$\mathbf{x}_E = \mathbf{x}/\|\mathbf{x}\| \quad . \quad (8)$$

By means of the definition of the scalar product of two vectors  $\mathbf{x}$  and  $\mathbf{y}$

$$\mathbf{x}^T \mathbf{y} = \|\mathbf{x}\| \|\mathbf{y}\| \cdot \cos(\mathbf{x}, \mathbf{y}) \quad , \quad (9)$$

the library search in the  $p$ -dimensional Euclidean space (where  $p$  is the number of measured wavelengths) results in the following distance value  $d_E$ :

$$d_E = 1 - \cos(\mathbf{u}, \mathbf{b}) = 1 - \frac{\mathbf{u}^T \mathbf{b}}{\sqrt{\mathbf{u}^T \mathbf{u}} \sqrt{\mathbf{b}^T \mathbf{b}}} \quad . \quad (10)$$

The calculated result corresponds to the cosine of the angle between the spectral vector  $\mathbf{u}$  of the unknown and the vector  $\mathbf{b}$  of the library spectrum. In the case of congruency of both vectors  $\mathbf{u}$  and  $\mathbf{b}$  we obtain  $\cos(\mathbf{u}, \mathbf{b}) = 1$ , thus  $d_E = 0$ .

A common problem for contemporary search algorithms, caused by varying baseline off-sets, can be overcome by centering the spectra (cf. Section 22.2). Centered spectra  $\mathbf{u}_Z$  are obtained by calculating the average  $\bar{u}$  of a spectral vector  $\mathbf{u}$  measured at  $p$  wavelengths:

$$\bar{u} = \frac{1}{p} \sum_{i=1}^p u_i \quad . \quad (11)$$

The average  $\bar{u}$  is subsequently subtracted from all components  $u_i$  of the vector  $\mathbf{u}$ :

$$\mathbf{u}_Z = (u_i - \bar{u})^T \quad \text{with} \quad i = 1, \dots, p \quad . \quad (12)$$

These centered vectors  $\mathbf{u}_Z$  are now used for the calculation of a correlated distance  $d_C$  as in Eq. (10)

$$d_C = 1 - \cos(\mathbf{u}_Z, \mathbf{b}_Z) = 1 - \frac{\mathbf{u}_Z^T \mathbf{b}_Z}{\sqrt{\mathbf{u}_Z^T \mathbf{u}_Z} \sqrt{\mathbf{b}_Z^T \mathbf{b}_Z}} \quad . \quad (13)$$

Based on mathematical definitions, Eq. (13) can be reformulated (corr stands for correlation)

$$\text{corr}(\mathbf{u}, \mathbf{b}) = \frac{\mathbf{u}_Z^T \mathbf{b}_Z}{\|\mathbf{u}_Z\| \|\mathbf{b}_Z\|} = \frac{\mathbf{u}_S^T \mathbf{b}_S}{p - 1} . \quad (14)$$

After introduction of the standardized vectors  $\mathbf{u}_S$  and  $\mathbf{b}_S$

$$\mathbf{u}_S = \frac{\mathbf{u}_Z}{s(\mathbf{u})} \quad \text{and} \quad \mathbf{b}_S = \frac{\mathbf{b}_Z}{s(\mathbf{b})} , \quad (15)$$

where  $s$  denotes the standard deviation of the vectors  $\mathbf{u}$  and  $\mathbf{b}$  (cf. Section 22.2):

$$s(\mathbf{u}) = \frac{\|\mathbf{u}_Z\|}{\sqrt{p-1}} \quad \text{and} \quad s(\mathbf{b}) = \frac{\|\mathbf{b}_Z\|}{\sqrt{p-1}} , \quad (16)$$

we obtain

$$\mathbf{u}_S = \frac{\mathbf{u}_Z}{\|\mathbf{u}_Z\|} \cdot \sqrt{p-1} \quad \text{and} \quad \mathbf{b}_S = \frac{\mathbf{b}_Z}{\|\mathbf{b}_Z\|} \cdot \sqrt{p-1} . \quad (17)$$

Equation (17) corresponds to Eq. (8) with the vectors now standardized to the length  $\sqrt{p-1}$ . In summary, the improvement in the correlated distance value is due to the removal of the baseline off-set and to the scale-invariance of the pre-treated vectors of the unknown and of the library spectrum. The following problems in searching for an unknown in a spectral library persist:

1. The spectrum cannot be satisfactorily normalized due to a non-horizontal or non-linear baseline.
2. The composition of the spectral library usually does not cover all necessary groups of chemical compounds.
3. The similarity scores which are used to construct the hit list are not necessarily significant measures for the similarity of structures.

A non-horizontal baseline may be corrected for by subtracting an angles straight line. In the case of a non-linear baseline, much experience is needed to minimize possible effects of a mathematical correction on the search results. Here, the computation of the second derivative of the spectrum might be the favorable option.

Even if an unknown belongs to a particular class of compounds, which is not represented in the library, the search will always result in a hit list with a number of entries. In general, entries with small scores are not relevant for an identification. In order to gain a feeling for the significance of an entry, with respect to its scores, one should experiment with the library, and a sound chemical knowledge is necessary.

### 22.3.2.2 Data Banks Containing Spectroscopic Information

Fields containing spectroscopic information can specifically be accessed in the data banks Beilstein (organic chemistry) and Gmelin (inorganic chemistry, organometallic chemistry) (cf. Tab. 22.4). Covered spectral ranges, measured spectral intensity maxima, and references, may be found. Data concerning the state of aggregation of the sample or the solvent may possibly be included as well. Of course, the full text option may be used in any data bank to search for spectroscopic data or experiments, e.g. in Chemical Abstracts or in Analytical Abstracts (example: raman spectrum AND ...).

If interdisciplinary matters are searched, bibliographic data banks like Biosis (biosciences, biomedicine), Medline (medicine), Inspec (physics, electroengineering, engineering) as well as all data banks containing patent information should be considered.

### 22.3.2.3 Interpretation of Spectra by Means of Group Frequencies and of Characteristic Bands

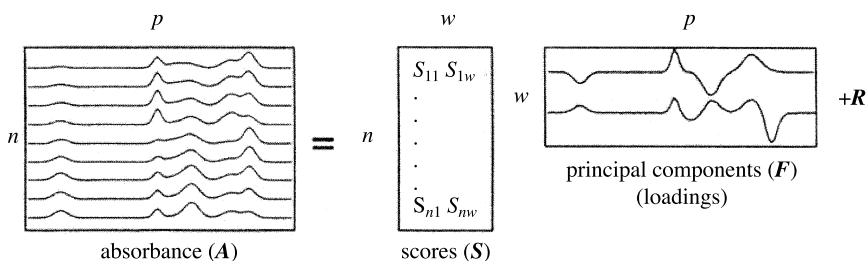
This topic has already been dealt with in Chapter 2. Currently there are numerous software products available on the market or under development, which are intended to support the task of spectra interpretation (e.g., IRMentor Pro [9], IR-Tutor [10], SpecTool [11] ). Certain tools even permit a spectrum simulation of the structure guessed [12]. Some spectrometer operation systems include tools to aid simple spectra interpretation.

### 22.3.2.4 PCA (Principal Component Analysis)

PCA is an efficient method for data reduction in particular in spectroscopy (cf. Fig. 22.5). It also has to be performed prior to quantitative evaluations by PCR (principal component regression).

**Table 22.4** Search fields for optical spectroscopy in the Beilstein and Gmelin data banks.

<b>Beilstein</b>		<b>Vibrational Spectrum (CTVIB)</b>
IRS	Infrared spectrum	Anisotropy of infrared bands
IRM	Infrared maximum	Degree of depolarization of Raman bands
RAS	Raman spectrum	Fermi resonance
RAM	Raman maximum	Fine structure of infrared bands
CTVIB	Vibrational spectrum	Intensity of infrared bands
 		Intensity of Raman bands
<b>Gmelin</b>		Polarization of infrared bands
IRS	Infrared spectrum	Reflection spectrum in the infrared region
UVS	UV/VIS spectrum	Resonance Raman effect



$n$  – number of spectra

$p$  – number of measured wavelengths = number of data points

$v$  – number of neglected principal components

$w$  – number of retained principal components  $w = p - v$

Fig. 22.5 Decomposition of the absorbance matrix  $A$ .

The mathematical background of PCA consists in the transformation of the initial coordinate system into a new one in order to display the variance of the experimental data much more clearly. To this aim the mathematical algorithms provide that

- the principal components consist of linear combinations (i.e. weighted sums) of the initial variables (i.e. absorbances at the measured wavelengths);
- the principal components are computed in such a way as to cover the largest amount of variance (e.g., the variance in spectral data due to the different properties of the measured samples);
- the linear combinations represent new, so-called latent variables (e.g., variables which cannot be assigned to a particular spectral band) with appropriate properties.

Initially, the  $n$  experimental spectra, each comprising  $p$  data points, are collected into a  $n,p$ -dimensional data matrix  $A$ . Any row of the matrix  $A$  comprises all  $p$  absorbance values of a particular spectrum. Any column consists of all  $n$  absorbance values at a particular wavelength. As a first step the data matrix is either centered ( $A_Z$ ) or standardized ( $A_S$ ) (cf. Section 22.2). In order to achieve the above stated aims, this pretreated matrix is afterwards split into two matrices by the chosen algorithm:

$$A_Z = S \cdot F^T \quad . \quad (18)$$

dimensions  $n, p \quad n, p \quad p, p$

Matrix  $S$  is called the score matrix. Its rows comprise the scaling coefficients. Matrix  $F$  may be called the loading matrix or principal components (PCs) or factors or eigenvectors. Its columns comprise the calculated principal components. By

multiplication of the matrices  $\mathbf{S}$  and  $\mathbf{F}$  we are able to reconstruct the centered or the standardized spectra.

Since the calculation of the principal components is based on the criterion of covering the largest amount of variance in the experimental data ( $\mathbf{A}_Z$  or  $\mathbf{A}_S$ ), the first principal component features the maximum variance. Subsequent PCs cover less and less variance. Distant PCs may be omitted for data reduction. In that case Eq. (18) may be rewritten as

$$\mathbf{A}_Z = \mathbf{S} \cdot \mathbf{F}^T + \mathbf{R} \quad , \quad (19)$$

dimensions  $n, p \quad n, w \quad w, p \quad n, p$

where  $w$  represents the number of retained PCs ( $w = p - v$ ),  $v$  is the number of neglected PCs,  $\mathbf{R}$  is the residual matrix (error matrix) (cf. Fig. 22.5). An analysis of the error matrix  $\mathbf{R}$  is necessary in order to chose  $w$ . Chemical knowledge has strictly to be applied during interpretation of the PCs, which are computed on pure mathematical considerations. Ideally,  $\mathbf{R}$  merely contains the spectral noise as well as unnecessary information from the experimental spectra.

One method in error analysis is the computation of residual variances. The shares of different PCs in the total variance are sketched in Fig. 22.6.

If 6 PCs are retained for further evaluation, a residual variance in the experimental values remains beyond consideration. Other methods for estimating a reasonable size of  $w$  are the eigenvalue-one criterion [13, 14], the Scree-test [13, 14], and cross validation (cf. Section 22.3.3).

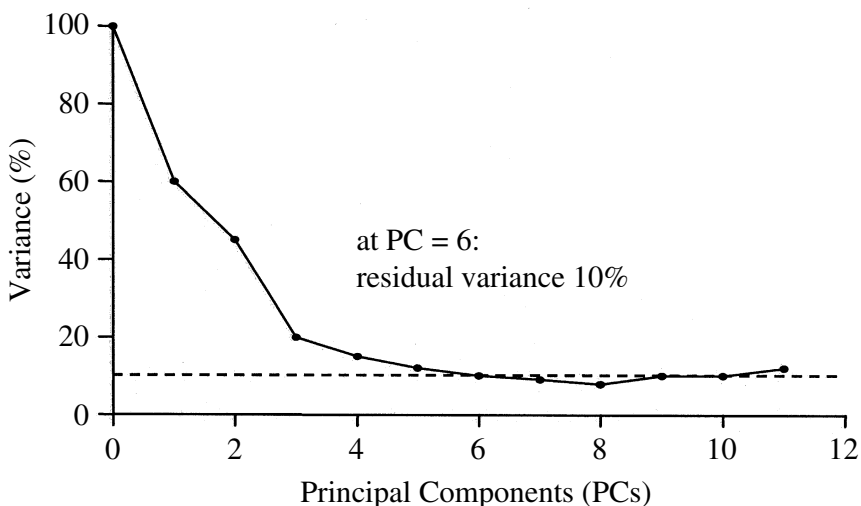


Fig. 22.6 Analysis of residual variance in PCA.

### 22.3.2.5 Cluster Analysis [13,14]

The aim of cluster analysis is the stepwise merger of objects (spectra) with respect to the similarity of their properties (absorbances at  $p$  measured wavelengths). A cluster comprises a group of objects whose similarity is closer than their similarity towards objects outside this group. The similarity of objects is assessed using the same distance measures as described earlier, e.g.

- Euclidean distance (cf. Fig. 22.3) or
- Mahalanobis distance [15, 16].

The calculation of the Mahalanobis distance is based on the interrelations between absorbance values at various wavelengths using their covariances. For this reason the Mahalanobis distance is of particular importance for assessing spectroscopic data.

Cluster analysis is often the preceding step for discriminant analysis.

### 22.3.2.6 Discriminant analysis [13, 14]

In the simplest case, a discriminant analysis is performed in order to check the affiliation (yes/no decision) of an unknown to a particular class, e.g. in case of a purity/quality check or a substance identification. A sample may equally well be assigned between various classes (e.g., quality levels) if a corresponding series of mathematical models has been established. Models are based on a series of test spectra, which has to completely cover the variations of particular substances in particular chemical classes. From this series of test spectra, classes of similar objects are formed by means of so-called discriminant functions. The model is optimized with respect to the separation among the classes. The evaluation of the assignment of objects to the classes of an established model is performed by statistically backed distance and scattering measures.

### 22.3.2.7 SIMCA Soft Independent Modeling of Class Analogy (SIMCA) [13,14]

In SIMCA, an independent principal component model (cf. PCA) is established for each individual class of the test data set. The evaluation of the assignment of objects to these classes of an established model is performed by statistically backed distance measures.

## 22.3.3 Quantitative Evaluation of Spectra

With respect to the applied mathematical algorithms, quantitative evaluation of spectra can be subdivided into univariate and multivariate methods (cf. Fig. 22.2). The independent variables  $x$  and  $x_i$ , respectively, are denoted regressors, whereas the dependent variables  $y$  and  $y_i$ , respectively, are denoted regressands. The basic sequence of a quantitative evaluation is always the same:

- Step 1: Choosing a model.
- Step 2: Choosing a training set.
- Step 3: Estimation of model parameters.
- Step 4: Validation of the model by statistical means.
- Step 5: Application of the model for prediction.

In the following sections the above sequence of steps will be discussed for all relevant methods used in evaluating optical spectra quantitatively.

#### 22.3.3.1 Univariate Methods

The only method considered is:

##### Least squares regression (LSR)

###### *Step 1: choosing a model*

The Beer–Lambert law is expressed by

$$A_k = C \cdot K_k , \quad (20)$$

$$\text{where } K_k = \varepsilon_k \cdot \log e \cdot l \quad (21)$$

$\varepsilon_k$  is the absorptivity coefficient at wavelength  $k$ , and  $l$  the thickness of the absorbing medium.

Within its application range, a linear calibration model can be established already by measuring at a single wavelength position

$$A = bC + a \quad (22)$$

The sample concentration  $C$  is calculated from the measured absorbance value  $A$  at the sensitivity  $b$  and the blank value  $a$ .

###### *Step 2: choosing a training set*

Spectra are measured with the analyte at  $n$  different concentrations. The absorbance values  $A_i$  are determined right at the maximum of a spectral band or peak, which is unambiguously assigned to the analyte.

The calibration based on peak area evaluation instead of a simple height determination might be advantageous. Likewise, rationing the heights or areas of two peaks might be useful to trace a concentration ratio. An initial baseline correction might be necessary. Preferably, a straight line should be employed for such corrections (cf. Fig. 22.7).

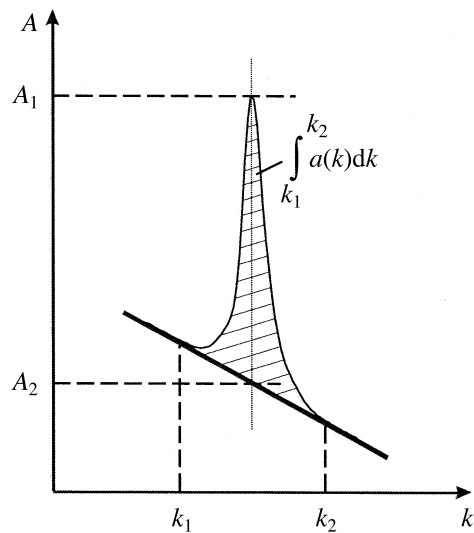


**Fig. 22.7** Quantitative evaluation of a baseline corrected spectral band.

*Step 3: estimation of model parameters*

A least squares regression is performed in order to estimate  $\hat{a}$  and  $\hat{b}$ :

$$\hat{a} = \frac{1}{n} \left( \sum_{i=1}^n A_i - \hat{b} \sum_{i=1}^n C_i \right); \quad \hat{b} = \frac{n \sum_{i=1}^n C_i A_i - \sum_{i=1}^n C_i \cdot \sum_{i=1}^n A_i}{n \sum_{i=1}^n C_i^2 - \left( \sum_{i=1}^n C_i \right)^2}. \quad (23)$$

*Step 4: validation of the model by statistical means*

This can be done in two ways

(a) Analysis of residuals

The analysis is performed by calculating

$$r_i = A_i - \hat{A}_i \quad i = 1, \dots, n. \quad (24)$$

using the absorbance values  $\hat{A}_i$ , which were calculated according to the model by

$$\hat{A}_i = \hat{b} C_i + \hat{a} \quad (25)$$

and subsequent graphic representation of  $r_i$  over  $C_i$  (cf. Fig. 22.8)

(b) Analysis of variance

The variances  $s_a$  and  $s_b$  of the estimated parameters  $\hat{a}$  and  $\hat{b}$  are calculated according to

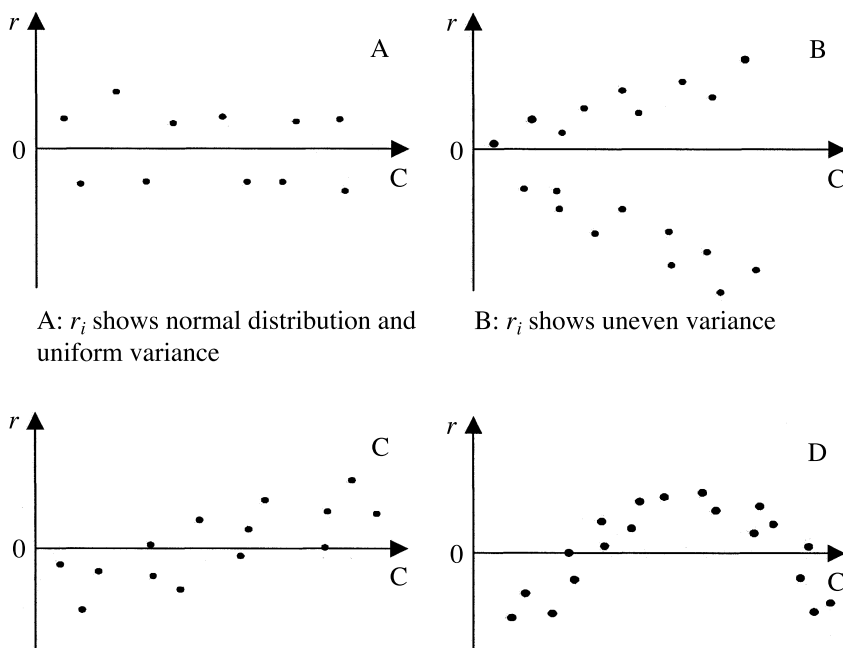


Fig. 22.8 Examination of a linear model by analyzing the residuals.

$$s_a^2 = \frac{s_0^2 \sum_{i=1}^n C_i^2}{n \sum_{i=1}^n (C_i - \bar{C})^2}; \quad s_b^2 = \frac{s_0^2}{\sum_{i=1}^n (C_i - \bar{C})^2}, \quad (26)$$

$$\text{where } s_0^2 = \frac{\sum_{i=1}^n (A_i - \hat{A}_i)^2}{n-2} \quad \text{and} \quad \bar{C} = \frac{1}{n} \sum_{i=1}^n C_i. \quad (27)$$

The confidence intervals  $\Delta a$  and  $\Delta b$  are calculated according to

$$\Delta a = \pm t(P, f)s_a \quad \text{and} \quad \Delta b = \pm t(P, f)s_b, \quad (28)$$

where  $t$  indicates a  $t$ -distribution,  $f$  the degree of freedom ( $f = n-2$ ) and  $P$  the requested probability for the confidence interval.

**Table 22.5** Advantages and disadvantages of least squares regression.

<b>Least Squares Regression</b>	
<b>Advantages</b>	<b>Disadvantages</b>
simple model fast calculation	analyte has to have an isolated spectral band no application to complex mixtures with overlaid spectral bands

*Step 5: application of the model for prediction* (cf. Tab. 22.5)

The predicted concentration  $C_{\text{pred}}$  may be calculated from measured absorbance values  $A_{\text{meas}}$  using the developed calibration model according to

$$C_{\text{pred}} = (A_{\text{meas}} - \hat{a})/\hat{b} \quad . \quad (29)$$

It should be mentioned here, that samples used for the estimation of the model parameters in steps 1–4 must not be re-used for prediction in step 5.

#### 22.3.3.2 Multivariate Methods [13, 14, 17]

From a mathematical point of view, applications of multivariate methods may be subdivided into the multiple case and the multidimensional multiple case (cf. Fig. 22.2). In the former case, several independent variables or features are mapped to merely one dependent variable or target value. In the second case, several independent variables or features are mapped to several dependent variables or target values. As a rule, linear models are used for such problems in optical spectroscopy. In the case of non-linear relations, the calibration range gets restricted, a linearizing data pretreatment is performed in order to get away with linear models, or non-linear methods (usually neural networks) have to be applied.

All models discussed below belong to the multidimensional multiple case.

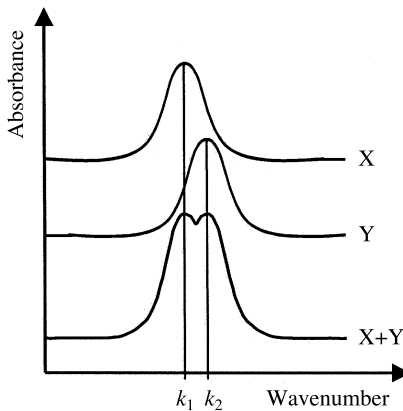
##### (a) **CLS Classical least squares (CLS), K-matrix**

*Step 1: choosing a model*

The generalized form of the Beer–Lambert law for mixtures containing  $m$  components may be written in matrix form (cf. Fig. 22.9) as

$$\begin{array}{l} A = C \cdot K \\ \text{dimensions } n, p \quad n, m \quad m, p \end{array} \quad . \quad (30)$$

The measured absorbance values of a spectrum ( $p$  data points) are contained in one row of the absorbance matrix  $A$ . The number of rows  $n$  in  $A$  corresponds to the number of measured spectra in the training set (cf. Fig. 22.5). In the concentration matrix  $C$ , a row contains the concentrations of the individual components of the



$$\begin{aligned} A_{k_1} &= C_X K_{X,k_1} + C_Y K_{Y,k_1} \\ A_{k_2} &= C_X K_{X,k_2} + C_Y K_{Y,k_2} \\ (A_{k_1} \quad A_{k_2}) &= (C_X \quad C_Y) \begin{pmatrix} K_{X,k_1} & K_{X,k_2} \\ K_{Y,k_1} & K_{Y,k_2} \end{pmatrix} \end{aligned}$$

**Fig. 22.9** Beer–Lambert law for a two component mixture.

particular training spectrum.  $\mathbf{K}$  represents the matrix of the absorptivity constants. A row contains these constants of a particular component for all  $p$  measured wavelength positions.

*Step 2: choosing a training set*

Preparation of  $n$  mixtures by variation of the concentration of all  $m$  components and subsequent measuring of their absorbance spectra.

*Step 3: estimation of model parameters*

Matrices  $\mathbf{A}$  (measured) and  $\mathbf{C}$  (prepared) in Eq. (30) are now known. Estimation of the calibration matrix  $\hat{\mathbf{K}}$  is performed by the equation

$$\hat{\mathbf{K}} = (\mathbf{C}^T \mathbf{C})^{-1} \mathbf{C}^T \mathbf{A} \quad . \quad (31)$$

*Step 4: validation of the model by statistical means*

This can be done in several ways, e.g.

(a) Analysis of residuals

The residual matrix  $\mathbf{R}$  is obtained by calculating the difference

$$\mathbf{R} = \mathbf{A} - \hat{\mathbf{A}} \quad (32)$$

$$\text{where } \hat{\mathbf{A}} = \mathbf{C} \hat{\mathbf{K}} \quad . \quad (33)$$

The  $n$  rows of  $\mathbf{R}$  contain difference spectra. Each difference spectrum can be assigned a particular error value

$$R_i = \sum_{j=1}^p r_{ij}^2 \quad i = 1, \dots, n \quad . \quad (34)$$

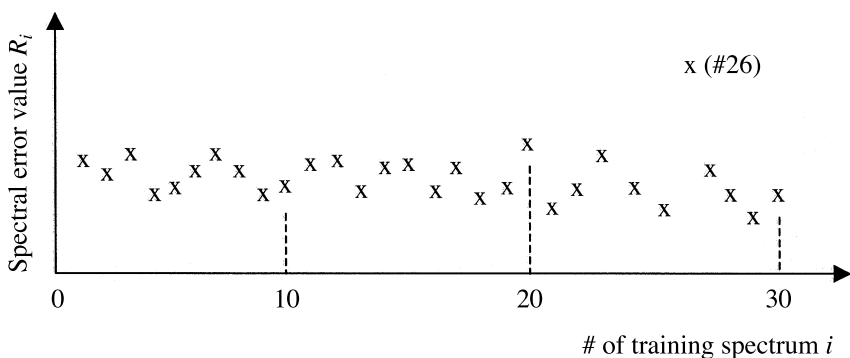


Fig. 22.10 Detection of outlier spectra.

These error values may be depicted graphically with the number  $n$  of the corresponding training spectrum on the abscissa (cf. Fig. 22.10). This graph permits an easy detection of outlier spectra.

#### (b) Cross validation

The following sequence has to be completed (leave-one-out strategy):

- Selection of a subset of  $n-1$  training spectra.
- Estimation of a model.
- Prediction of the concentration of the omitted sample.
- Repetition of the above sequence until each of the  $n$  training spectra has been omitted and predicted once.

After completion of the above cycle, all  $n$  experimentally prepared concentration values ( $C_{\text{exp}}$ ) are depicted graphically against the predicted concentration values

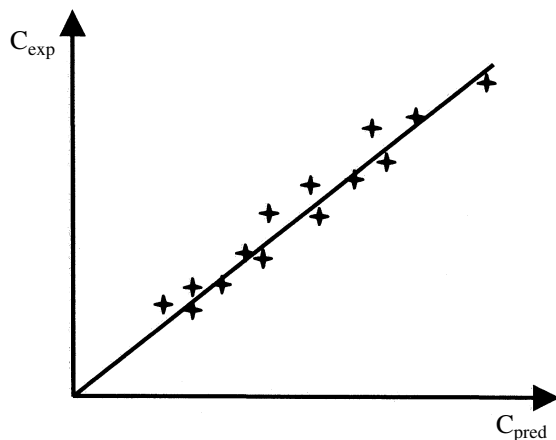


Fig. 22.11 Rating of the quality of the calibrated model for one of the  $m$  components.

**Table 22.6** Advantages and disadvantages of classical least squares regression.

<b>Classical Least Squares</b>	
<b>Advantages</b>	<b>Disadvantages</b>
relatively fast calculation	the components of the sample have to be known completely, all concentrations have to be varied during calibration
no wavelength selection necessary, complete spectrum applicable	during prediction all these and only these components have to be present in the sample fails in case of new impurities or components which were not present in the mixture during calibration
large number of data points per spectrum and large number of calibration spectra ensures low noise	matrix inversions necessary both during calibration and during prediction

( $C_{\text{pred}}$ ) for each of the  $m$  components (cf. Fig. 22.11). The quality of the calibrated model can be rated from this set of  $m$  diagrams.

The data couples ( $C_{\text{exp}}; C_{\text{pred}}$ ) in Fig. 22.11 may be evaluated by all statistical procedures. Cross validation is a very powerful method for outlier detection and optimization of calibration models. If the predicted concentrations obey the necessary quality standard for all but one training spectrum, the latter can be regarded as an outlier.

### (c) Set validation

The training spectra are randomly separated into two sets. The first set is used for calibration, the second set for validation. Set validation does not demand as much computing power as cross validation but is inferior in the quality of the results, and should be applied only for large data sets.

#### *Step 5: application of the model for predictions* (cf. Tab. 22.6)

The calibrated model is finally used to predict the concentrations of the  $m$  components (vector  $c^T$  comprising  $m$  concentration values) from the experimental spectrum (vector  $a^T$  comprising  $p$  absorbance values):

$$c^T = a^T \cdot (\hat{K}^T \hat{K})^{-1} \hat{K}^T \quad . \quad (35)$$

### (b) Inverse least squares (ILS), P-matrix or multiple linear regression (MLR, multidimensional)

#### *Step 1: choosing a model*

The generalized form of the Beer–Lambert law (cf. Eq. (30)) may be rearranged with respect to the concentration:

$$\begin{aligned} C &= A + P \\ \text{dimensions } n, m &\quad n, p \quad p, m \end{aligned} \quad . \quad (36)$$

The structure of matrices  $\mathbf{C}$  and  $\mathbf{A}$  was already described for CLS. The elements of the  $\mathbf{P}$  matrix are proportional to the reciprocal absorptivity constants. It is the crucial advantage of ILS over CLS, that only the concentrations of the components of interest have to be known during calibration.

*Step 2: choosing a training set*

Due to the mathematical requirement  $n>p$  (dimension of the matrix) a very large number of training spectra should be measured. This might evoke the problem of collinearity among the spectra, i.e. the spectra would no longer be completely independent of each other, as mathematically necessary. Instead, they might be transformed into each other by linear combinations. Linear dependences occur, e.g., if calibration mixtures are simply diluted without changing the concentration ratios between the constituents. Spectra of such diluted samples contain redundant information, which in turn causes mathematical instabilities. In order to keep  $p$  small one should restrict the calibration to spectral areas which comprise distinct contributions by the components of the mixture. Such decisions demand chemical knowledge as well as sure instinct.

*Step 3: estimation of model parameters*

Using the matrices  $\mathbf{A}$  (measured) and  $\mathbf{C}$  (prepared) (cf. Eq. (36)) one can now estimate the calibration matrix  $\hat{\mathbf{P}}$ :

$$\hat{\mathbf{P}} = (\mathbf{A}^T \mathbf{A})^{-1} \mathbf{A}^T \mathbf{C} \quad . \quad (37)$$

*Step 4: validation of the model by statistical means*

The validation of the model is performed in the same way as above for CLS.

*Step 5: application of the model for prediction (cf. Tab. 22.7)*

Based on a measured spectrum of an unknown (vector  $\mathbf{a}^T$  comprising  $p$  absorbance values) and on the calibration matrix, the concentrations of the  $m$  components can now be predicted (vector  $\mathbf{c}^T$  comprising  $m$  concentration values):

$$\mathbf{c}^T = \mathbf{a}^T \cdot (\mathbf{A}^T \mathbf{A})^{-1} \mathbf{A}^T \mathbf{C} \quad . \quad (38)$$

**Table 22.7** Advantages and disadvantages of inverse least squares regression.

<b>Inverse Least Squares</b>	
<b>Advantages</b>	<b>Disadvantages</b>
relatively fast calculation the calibration model may only be based on knowledge about the interesting components, impurities are not important only one matrix inversion during calibration complex mixtures may be analyzed	difficulty in choosing the right spectral areas Often a larger number of calibration samples necessary ( $n>p$ required for mathematical reasons) multi-collinearity may cause problems time-consuming calibration

### (c) Principal component regression (PCR)

#### *Step 1: choosing a model*

The main problem in the above described ILS is caused by possible multicollinearities between regressed spectra. This problem can be overcome by using a PCA (cf. Section 22.3.2) not only for data reduction but also to combine the data reduction with elimination of multicollinearities. The principal components computed this way are afterwards used as regressors in the ILS scheme.

#### *Step 2: choosing a training set*

- Full spectra or only spectral ranges showing contributions by the components of interest may be selected.
- Concentrations of the components of interest have to be known.
- Estimation of the principal components with respect to the chemical components to be calibrated (chemical knowledge!). This estimation based on chemical grounds ensures the closest relation between the variance represented in the principal components and the change in concentration of the chemical components of interest.

#### *Step 3: estimation of model parameters*

At first we introduce into the PCA (Eq. (18)) the equation  $\mathbf{F}^{-1} = \mathbf{F}^T$ , which is based on the orthogonality of  $\mathbf{F}$ :

$$\mathbf{S} = \mathbf{A}_Z \mathbf{F} \quad (39)$$

The second step yields in analogy to ILS ( $\mathbf{B}$  corresponds to  $\mathbf{P}$ )

$$\begin{array}{ccccccccc} \mathbf{C} & = & \mathbf{S} & \cdot & \mathbf{B} & = & \mathbf{A}_Z & \cdot & \mathbf{F} & \cdot & \mathbf{B} \\ \text{dimensions} & & n, m & & n, w & & w, m & & n, p & & p, w & & w, m \end{array} \quad (40)$$

$\mathbf{B}$  represents the matrix of coefficients of the regression of the PCA scores (regressors) versus the concentrations of the chemical components (regressands). All other symbols are identical to those already described above or in Section 22.3.2.

The estimation of the calibration matrix  $\hat{\mathbf{B}}$  yields

$$\hat{\mathbf{B}} = (\mathbf{S}^T \mathbf{S})^{-1} \mathbf{S}^T \mathbf{C} \quad . \quad (41)$$

#### *Step 4: validation of the model by statistical means*

The selection of the number of principal components has already been described for PCA (Section 22.3.2). The validation of the model is effected in analogy to CLS.

**Table 22.8** Advantages and disadvantages of principal component regression.

<b>Principal Component Regression</b>	
<b>Advantages</b>	<b>Disadvantages</b>
full spectrum or larger parts of a spectrum may be used	PCA demands much chemical knowledge and sure instinct
large number of spectral data points leads to noise reduction	large number of calibration samples necessary
only information about the components of interest necessary	large calibration effort necessary
rather complex mixtures may be analyzed	selection of non-significant principal components or neglect of important principal component possible
data reduction by PCA	

**Step 5: application of the model for prediction** (cf. Tab. 22.8)

The concentrations of all  $m$  components of interest (vector  $\mathbf{c}^T$  containing  $m$  concentration values) can be predicted based on the measured spectrum of an unknown mixture (vector  $\mathbf{a}^T$  containing  $p$  absorbance values), the principal component matrix  $\mathbf{F}$  and the calibration matrix  $\hat{\mathbf{B}}$ :

$$\mathbf{c}^T = \mathbf{a}^T \cdot \mathbf{F} \hat{\mathbf{B}} \quad . \quad (42)$$

**(d) Partial least squares (PLS)****Step 1: choosing a model**

The starting point is a model analogous to inverse calibration (ILS)

$$\begin{array}{l} \mathbf{C} = \mathbf{A} \cdot \mathbf{B} \\ \text{dimensions } n, m \quad n, p \quad p, m \end{array} \quad . \quad (43)$$

Like in PCA, both the concentration matrix  $\mathbf{C}$  and the absorbance matrix  $\mathbf{A}$  are decomposed into score and loading matrices  $\mathbf{S}_C$  and  $\mathbf{F}_C$  or  $\mathbf{S}_A$  and  $\mathbf{F}_A$ , respectively:

$$\mathbf{C} = \mathbf{S}_C \cdot \mathbf{F}_C^T; \quad \mathbf{A} = \mathbf{S}_A \cdot \mathbf{F}_A^T \quad . \quad (44)$$

The matrices  $\mathbf{C}$  and  $\mathbf{A}$  are decomposed interdependently with regard to their score matrices  $\mathbf{S}_C$  and  $\mathbf{S}_A$ , which maintains the close coherence between spectral information ( $\mathbf{A}$ ) and the component concentration ( $\mathbf{C}$ ) in the best possible manner.

**Step 2: choosing a training set**

Measurement of a large number  $n$  of training spectra, which cover as much of the concentration range as possible. The concentrations of the different components have to be varied independently.

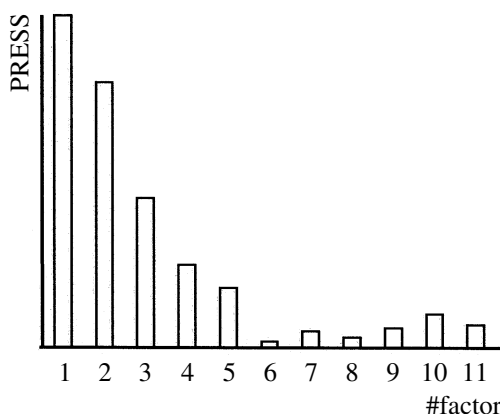


**Fig. 22.12** Estimation of the number of significant factors by means of the prediction residual error sum of squares (PRESS).

*Step 3: estimation of model parameters*

The estimation of the calibration matrix  $\hat{\mathbf{B}}$  yields

$$\hat{\mathbf{B}} = \hat{\mathbf{W}}(\mathbf{F}_A^T \hat{\mathbf{W}})^{-1} \mathbf{F}_C^T , \quad (45)$$

where  $\mathbf{W}$  represents the weight matrix, which is given a value during the decomposition.

*Step 4: validation of the model by statistical means*

The selection of an optimal number of factors (loadings) is a central point in PCR and PLS. In both methods the so-called prediction residual error sum of squares (PRESS) is calculated

$$\text{PRESS} = \sum_{i=1}^n \sum_{j=1}^m (C_{ij} - \hat{C}_{ij})^2 , \quad (46)$$

where  $n$  is the number of training spectra,  $m$  the number of components in the mixture,  $C_{ij}$  are the prepared and  $\hat{C}_{ij}$  the predicted concentrations. After a cross validation is performed, the prediction error (PRESS) can be depicted versus the number of employed factors in order to select an optimized number of factors.

In Fig. 22.12, the minimum for the prediction error is found at 6 factors. The following factors most render noise, their retention would deteriorate the quality of the model. Other validation is performed analogous to CLS.

**Table 22.9** Advantages and disadvantages of partial least squares regression.

<b>Partial Least Squares</b>	
<b>Advantages</b>	<b>Disadvantages</b>
full spectra may be used	abstract model
most robust calibration	large number of training spectra necessary
only information about components of interest necessary	extended computing time
very complex mixtures may be analyzed	determination of the optimal number of factors difficult
computation of factors and regression in a single step, projection of the features of interest (concentrations) onto the factors superior to PCR	

**Step 5: application of the model for prediction** (cf. Tab. 22.9)

The concentrations of all  $m$  components of interest (vector  $\mathbf{c}^T$  containing  $m$  concentration values) can be predicted based on the measured spectrum of an unknown mixture (vector  $\mathbf{a}^T$  containing  $p$  absorbance values) and the calibration matrix  $\hat{\mathbf{B}}$ :

$$\mathbf{c}^T = \mathbf{a}^T \hat{\mathbf{B}} \quad . \quad (47)$$

A survey of presently available software products for data analysis is given in Table 22.10.

**Table 22.10** Software products for data analysis.

<b>Product</b>	<b>Manufacturer</b>	<b>Methods Covered</b>
GRAMS/32, PLSplus/IQ Add-on	Galactic Ind. Corp.	LSR, PCA, PCR, PLS
MATLAB	MathWorks Inc.	
Chemometrics Toolbox	Applied Chemometrics Inc.	CLS, ILS, PCA, PCR, PLS
PLS_Toolbox	Eigenvector Research Inc.	
QuantIR	Nicolet Analytical Instruments	CLS, ILS, PLS
SCAN	Minitab Statistical Inc.	PCA, PCR, PLS and others
Statgraphics	Statistical Graphics Corp.	cluster analysis, discriminant analysis, PCA, linear and non-linear regression
Statistica	Stat Soft	cluster analysis, discriminant analysis, PCA, linear and non-linear regression
Unscrambler	Camo A/S	PCA, PCR, PLS

## References

- 1 C. J. Pouchert, *The Aldrich Library of Infrared Spectra*, Aldrich Chemical Co., Milwaukee, WI 1981.
- 2 W. W. Simons, *The Sadler Handbook of Infrared Spectra*, Sadler Research Laboratory, Philadelphia, PA 1978.
- 3 *Sadler Handbook of Ultraviolet Spectra*, Sadler Research Laboratory, Philadelphia, PA 1979.
- 4 J. R. Ferraro, *The Sadler Infrared Spectra Handbook of Minerals and Clays*, Sadler Research Laboratory, Philadelphia, PA 1982.
- 5 B. Schrader, *Raman/Infrared Atlas of Organic Compounds*, VCH, Weinheim 1989.
- 6 D. O. Hummel, *Atlas of Polymer and Plastic Analysis*, VCH, Weinheim 1991.
- 7 K.G.R. Pachler, F. Matlok, H.-U. Gremlich, *Merck FT-IR Atlas*, VCH, Weinheim 1988.
- 8 M. Buback, H. P. Vögele, *FT-NIR Atlas*, Wiley-VCH, Weinheim, 1993.
- 9 Bio-Rad Labor. Inc., Sadler Group, Philadelphia, USA.
- 10 C. Abrams, *IR Tutor*, Wiley-VCH, Weinheim 1998
- 11 *Spec-Tool*, Chemical Concepts, Weinheim, Germany.
- 12 URL:[www2.ccc.uni-erlangen.de/research/ir/index.html](http://www2.ccc.uni-erlangen.de/research/ir/index.html).
- 13 M. Otto, *Chemometrics*, Wiley-VCH, Weinheim 1999.
- 14 R. Henrion, G. Henrion, *Multivariate Datenanalyse*, Springer-Verlag, Berlin, 1995.
- 15 P. C. Mahalanobis, *Proc. Natl. Inst. Sci. India*, **1936**, 2, 49 (original reference).
- 16 R. De Maesschalck, D. Jouan-Rimbaud, D. L. Massart, *Chemom. Intell. Lab Syst.*, **2000**, 50(1), 1–18.
- 17 H. Martens, T. Naes, *Multivariate Calibration*, John Wiley & Sons, Chichester 1991.

## **23**

# **Nuclear Magnetic Resonance Spectroscopy**

*Wolfgang Robien*

### **23.1**

#### **Introduction**

Structure elucidation of organic compounds is mainly based on different types of spectroscopic techniques. Among the methods available NMR spectroscopy contributes a large amount of information; in many cases the spectral data are so rich in structural information content that the constitution, configuration and conformation of the unknown can be derived exclusively by the interpretation of such spectra. NMR spectroscopy is, in comparison to other techniques, an insensitive method leading to a low signal-to-noise ratio of the spectra obtained. This disadvantage has been circumvented by the introduction of the principle of Fourier-transformation leading to much shorter data acquisition times and the possibility of observing more insensitive nuclei than protons and therefore getting more detailed information about the sample under investigation. During the past three decades many sophisticated pulse techniques have been developed, which allow one, together with the use of highfield instrumentation, to investigate extremely small amounts of samples and additionally to get more complete information about them. In particular, the tremendous improvement based on two(three)-dimensional methods opened a new horizon in structure elucidation [1]. For all these reasons the earlier bottleneck of data acquisition as the most time-consuming step has been dramatically shifted to data interpretation, especially with the background of combinatorial chemistry and LC-NMR coupling.

Structure elucidation of a complex molecule from its spectral data without software support is a challenging and time-consuming procedure which can only be done by an expert in this field. In order to supply the expert with the necessary information during the spectrum interpretation and structure generation procedure, a large number of computer programs [2–4] and data collections have been developed [5].

**23.2****Comparison of NMR-Spectroscopy with IR and MS**

In order to understand the range of possibilities in computer-assisted structure elucidation methods it is essential to compare the different spectroscopic techniques with respect to their information content and their suitability for computer-assisted handling of their data. High resolution mass spectral data can lead to the molecular formula, which is a necessary parameter for most of the interpretation and isomer generation programs. MS is also well-suited to the detection of certain functional groups, as also is IR. The main disadvantage of MS is the extremely high dependence of the spectral pattern on the ionization technique applied; this effect can be used to get some more specific information about the unknown sample. Another reason why MS usually gives only supporting information during the structure elucidation process, is the complex and yet only partially understandable correlation between spectral and structural properties resulting in the absence of reliable methods to predict the MS spectrum for a given structure. Some work on this topic has been published [6], but the techniques developed have never been routinely applied. From IR spectra a large variety of functional groups and substitution patterns can be derived but the correlation between spectral behavior and structural property is not so well-defined as in NMR spectroscopy. For all these reasons MS and IR are not well-suited to rank a few hundred structural proposals as created by an isomer generation program, which is the usual case during computer-assisted structure elucidation, especially when dealing with molecules having a few non-carbon atoms which are only indirectly visible via the chemical shift values of the attached carbons.

NMR spectroscopy is an insensitive method compared to IR and MS, but it has been dramatically improved since its beginning. In organic chemistry  $^1\text{H}$ - and  $^{13}\text{C}$ -NMR-spectroscopies are usually routinely applied for structure elucidation purposes. The total shift range for protons spans roughly 12 ppm in typical organic compounds compared to 250 ppm for carbon. Solvent effects on protons are usually more pronounced, an effect – aromatic solvent induced shift (ASIS) – which is also systematically used in structure elucidation leads to the disadvantage that spectrum prediction by computer programs becomes more complicated. The comparison of a query spectrum against spectra in a reference library is also a more complex task for  $^1\text{H}$ -NMR spectra because of the field dependence of the spectral patterns. In carbon NMR spectroscopy the couplings between carbons at natural abundance are usually invisible and the couplings to protons are artificially suppressed by decoupling techniques leading to simplified spectral patterns. Furthermore carbon NMR spectroscopy allows direct insight into the skeleton of an organic sample. For all these reasons discussed above it can be concluded that  $^{13}\text{C}$ -NMR spectroscopy is the method of choice for computer-assisted structure elucidation, having the disadvantage of dealing with an insensitive nucleus, which is 5760 times more insensitive than a proton.

**23.3****Methods in NMR Spectroscopy**

The advantage of NMR spectroscopy is the large number of experimental techniques that allow one to derive a very specific piece of information about the unknown chemical structure. The parameters usually extracted from a NMR spectrum are:

- Chemical shift values
- Signal intensities
- Coupling constants

The chemical shift value reflects the electron density and therefore gives information about hybridization and the environment of the corresponding nucleus. The signal intensity is proportional to the number of nuclei and therefore gives information about symmetry. The coupling constants give information about spin systems and therefore insight into the relationship between different nuclei. Application of additional techniques allows one to determine the signal multiplicities in  $^{13}\text{C}$ -NMR spectra (for example: attached proton test (APT) and distortionless enhancement by polarization transfer (DEPT)) and to get more insight into the coupling network. The most prominent two-dimensional techniques used are:

- H–H correlation: Correlated spectroscopy (COSY)
- C–H correlation over one bond: Heteronuclear multiple quantum coherence (HMQC), heteronuclear single quantum coherence (HSQC)
- C–H correlation over multiple bonds: Heteronuclear multiple bond correlation (HMBC), correlation by long-range couplings (COLOC)
- C–C correlation: Incredible natural abundance double quantum transfer experiment (INADEQUATE)

Chemical shift values are the main information source for spectral similarity searches, whereas the correlation between spectral lines and the corresponding structural environment is the basis for spectrum prediction programs. The information derived from the correlation techniques is used by interpretation programs to prove the presence of certain structural fragments from a given set of correlation signals. These correlation signals are also used as distance constraints, in terms of number of bonds between two coupled nuclei, in the case of ambiguity, which occurs frequently in HMBC-type spectra, later on during the structure generation process.

**23.4****Spectral Similarity Search Techniques**

One very well-established method used in computer-assisted structure elucidation is the comparison of the spectrum of the unknown against a reference data collection. The largest databases available hold at the moment some 250,000 spectra of

the same method, corresponding to roughly 1% of the known chemical structures. The consequence for the design of the algorithms is that the procedure used for comparison must be able not only to detect the identical spectral pattern in any case, but it must also be able to retrieve similar patterns, which usually give a lot of information about partial structures and typical skeletons contained in the unknown.

The basic algorithms for spectral comparison use the Euclidian distance between corresponding data points when comparing curves or a given deviation when comparing peak lists in order to select compounds having similar resonances. The procedure for comparing peak lists can only be applied sequentially in some computer programs, leading to the unwanted effect that similar structures can be excluded when starting with an uncommon chemical shift value. The better approach handles the complete peak list of the unknown at the same time and afterwards allows the selection of lines which must be present in the reference spectrum. Different implementations of this basic algorithm allow the user to control the number of lines present in the reference spectrum compared to the number of lines available in the query spectrum allowing him to analyze the reference structure with respect to structural fragments present in the unknown or to derive components within a mixture.

The disadvantage of such a type of similarity search based on the comparison of a peak list against the reference data collection on a line-by-line basis is that regions without any line are completely neglected. Another approach which also takes into account regions without lines is the SAHO (spectral appearance in hierarchical order) search method [7]. The typical range of the chemical shift values is divided into smaller ranges (typically 10–15 ppm for carbon) and the number of signals within such a region is counted. In order to achieve a higher selectivity different multiplicities (either odd/even or singlet, doublet, triplet and quartet) can be counted separately, leading to an array of numbers describing the spectral pattern very well. The same procedure is applied to the reference data collection and the resulting arrays are stored. The comparison of the pattern of the unknown against the reference patterns is extremely fast, because only a small amount of data must be handled (typically 8 byte per spectrum) leading to a speed of  $10^5$  to  $10^6$  comparisons per second. This algorithm is an ideal tool to deduce at least the compound class of the unknown under the assumption that the reference data collection contains examples of similar structures. In any case it should be mentioned that the results from the similarity search based on line-by-line comparison and the SAHO method are usually complementary and the user is strongly advised to apply both methods when available. These spectral similarity search techniques are extremely fast and should therefore be applied first during the structure elucidation process in order to avoid more time-consuming techniques for solving trivial problems.

### 23.5

#### Spectrum Estimation, Techniques

For the reasons given in the Introduction  $^{13}\text{C}$ -NMR spectrum prediction is more popular than  $^1\text{H}$ -NMR spectrum prediction, moreover, some programs are known to perform at a reasonable level of precision [8–10]. The early work of collecting chemical shift values was severely influenced by the idea of predicting spectra for a given structure. The first very simple, but still useful approach of increment rules has been implemented into a large variety of computer programs. The central concept of this method is to use a parent structure (for example benzene [11]) and to start with this chemical shift value in the calculation. Increments are derived from the difference between the chemical shift value of the parent compound and the corresponding chemical shift value of the mono-substituted derivatives. Polysubstituted compounds are treated as “overlapping” mono-substituted derivatives and the tabulated increments are simply added to the base value of the parent compound neglecting therefore any substituent interaction. More sophisticated systems allow for additional correction parameters leading to improved results [12, 13]. The advantages of this method are the simple principle behind it and the good results for certain compound classes where other methods tend to fail (for example polysubstituted benzenes). One main disadvantage is that only a limited number of increment tables for a limited range of parent compounds is available in the literature.

A more elegant method has been developed to make use of all compounds in a large reference data collection. The increment table for a certain query structure is generated on-the-fly and therefore all reference spectra contribute to the solution of a particular problem. This method automatically includes substituent interactions if this information is available within the reference data. Furthermore a poly-substituted compound can be generated by formally overlapping only mono-substituted derivatives (as with the basic increment method), but also by selecting for example di- or tri-substituted derivatives, allowing different calculation pathways leading to an expectation range for the signals of the query structure. The disadvantage of this method is the long computing time and the complex algorithms behind using partial structure search technologies [14].

A different approach is called the HOSE (hierarchically ordered spherical description of environments) code [15] that is based on the extremely well pronounced correlation between a  $^{13}\text{C}$  chemical shift value and the corresponding carbon-centered substructural unit. The HOSE code starts at a carbon atom (focus atom) and describes its hybridization and multiplicity. The neighboring atoms are described in the same manner taking into account their atom type, hybridizations, number of directly bound hydrogens and the type of bonds between them. This scheme is applied to the first neighbors of the focus atom, then to the second neighbors and so on, leading to a spherical description of the structural environment. This carbon-centered fragment is sorted in a canonical way within each sphere giving a structure descriptor which is correlated to the known chemical shift value of its focus atom. This procedure is repeated for any carbon of any re-

ference structure available and stored on a file during database creation. The query structure is analyzed in the same way and the fragments generated are compared against the corresponding file of the database. Chemical shift values of coincident structure descriptors are taken for the calculation of the mean value, the total shift range and the standard deviation. The number of coincident spheres between the reference structures and the query structure determines the precision of the result obtained. For  $sp^3$  carbons at least three spheres ( $\gamma$ -effects) are necessary, in the case of conjugated systems four spheres usually give reliable results (effects of *para*-substituents). This basic principle has been implemented in a very similar way into several computer programs. Additionally, solvent induced effects can be added, leading to an improved spectrum prediction capability. The HOSE code was designed to handle a two-dimensional structure representation, therefore stereochemical effects were ignored. Consequently it was necessary to introduce a further extension which is able to describe steric interactions leading to an extreme improvement of the precision of the spectral prediction [16, 22].

A totally different approach is the utilization of neural network technologies as proposed by several authors [17–19]. The intellectual challenge of designing a neural network is the selection of the structure descriptors in order to reflect the correlation between structural and spectral properties in an optimal manner. Network optimization is a time-consuming task which must be done only once. The application of the trained network to a given structure is extremely fast and the prediction of the chemical shift values to be expected is performed within milliseconds, therefore giving an excellent tool for spectrum simulation and subsequent ranking of a large list of candidate structures.

## 23.6

### Spectrum Prediction, Quality Consideration

There is a strong relationship between the quality of the database, the level of sophistication of the algorithms used and the results obtained. General databases are usually built from literature data; despite most of the assignments given in the public domain literature being correct, a large number of either wrong structures and/or misassignments are known [20]. Even some very common functional groups (for example tosylate [21]) are known to be systematically assigned in two different ways. The assignment simply depends on the literature used for reference purpose, thus propagating the wrong assignment when using the wrong reference without checking. These data may appear later in some databases and will be used for further prediction leading to unreliable results. This type of error can be easily detected by analyzing a large reference collection by means of statistical methods and should be frequently applied by a database administrator.

As stated above, spectrum prediction is based on the correlation between structural environments and their corresponding chemical shift values. In order to simulate spectra by the methods described adequate reference material is necessary, which is not given in some journals, frequently, instead of assignments only peak-

lists (even without multiplicity information) as given by the spectrometer software have been published, diluting the basis for spectrum prediction of new classes of compounds.

In order to cover the enormous structural diversity it is necessary to have the most diverse database available. On the other hand it is necessary to fill gaps within the area of interest with ones own data. Usually a very small, but specifically dedicated database is much more powerful for solving a limited range of problems than a general database.

It is absolutely essential to have access to all parameters influencing the spectral simulation process; furthermore the typical parameters obtained as a result (mean value, range, deviation) are not sufficient to evaluate the result, because in many cases a visual inspection of the distribution is necessary in order to detect outliers or to understand stereochemical effects. Access to the original data contributing to a specific result must be possible in order to clarify any ambiguity.

Spectrum prediction is a frequently used technique during the structure elucidation process, but a detailed inspection of the results is necessary. Some programs offer the possibility to use different algorithms for spectrum prediction (usually HOSE code technology and neural networks). In such a situation both methods should be applied and the results obtained should be carefully compared [22]. At least in the case of different predictions a further critical evaluation of the result should be an obligation.

### 23.7

#### **Spectrum Prediction and Quality Control, Examples**

Spectrum prediction is an extremely decisive tool for verification of structural proposals and therefore the implementation of the algorithms and the quality of the reference database used cannot be discussed independently, because the results obtained are strongly connected to both parameters. The most severe limitation of the HOSE code is the availability of sufficient and correct reference material within the database, because a description of the query structure at a lower number of spheres dramatically influences the predicted chemical shift values. In Fig. 23.1 an assignment error on carbons 11 and 12 has been *artificially introduced* into the correct assignment as given in the literature in order to demonstrate the effect of accessing wrong entries within the reference database. The predicted spectrum as given in Fig. 23.2 using HOSE code technology with five coincident spheres (i.e. all neighbors up to five bonds) estimates 93.7 ppm and 94.3 ppm respectively for carbons 11 and 12 together with an expectation range of some 60 ppm which is totally useless for the spectroscopist. Estimation with two coincident spheres gives in this case the better mean values for carbon 11 and 12, again with extremely large expectation ranges as shown in Fig. 23.3. A comparison of the estimated values at one to five coincident spheres, as given in Fig. 23.4 demonstrates that there is only a small change in the mean values when increasing the number of coincident spheres, except for carbons 11 and 12 for which wrong reference material contributes heavily

## 12-HYDROXYCHILOSCYPHA-2,7-DIONE; COMPOUND-#4

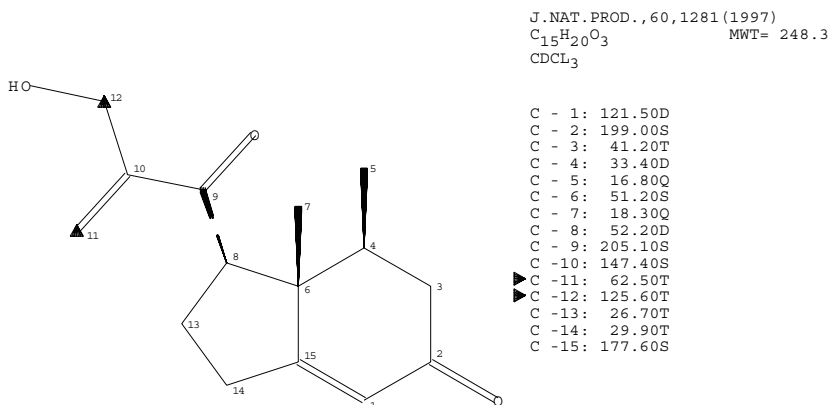


**Fig. 23.1** An entry from the reference database [22, 39] with an *artificially introduced* assignment error at carbons 11 and 12.

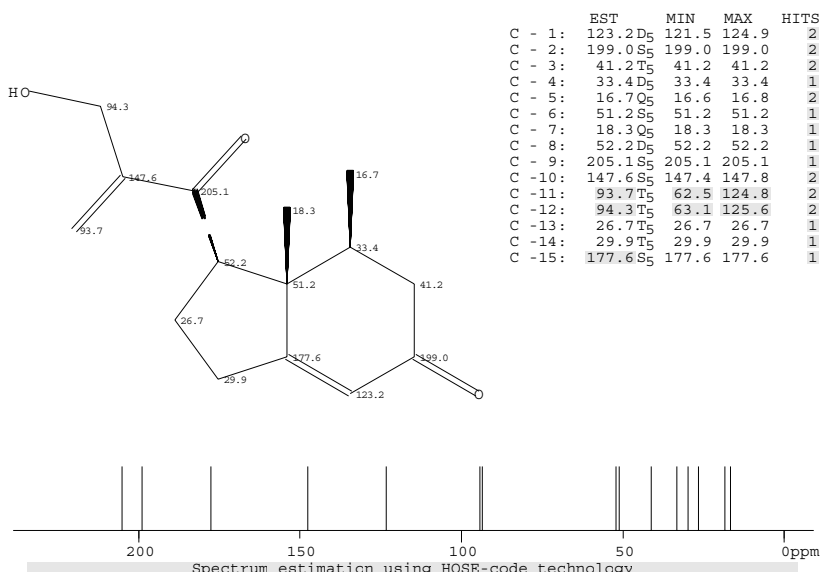


**Fig. 23.2** Spectrum estimation using 5 coincident spheres generating wrong predictions for carbons 11 and 12 at 93.7 and 94.3 ppm respectively, because of wrong reference material.

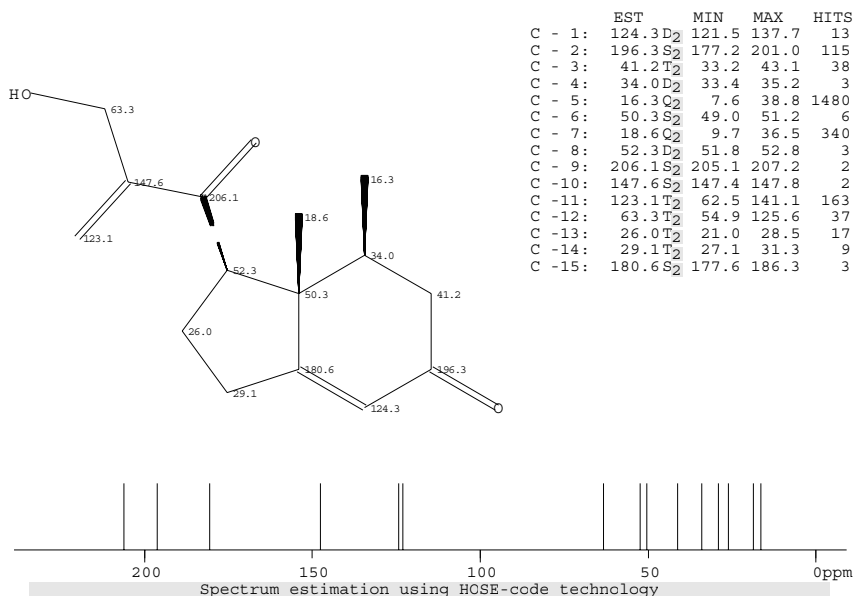


**Fig. 23.3** Spectrum estimation using two coincident spheres generating better predictions [123.1 ppm for C<sub>11</sub> and 63.3 ppm for C<sub>12</sub> respectively] than with five coincident spheres (see Fig. 23.4)

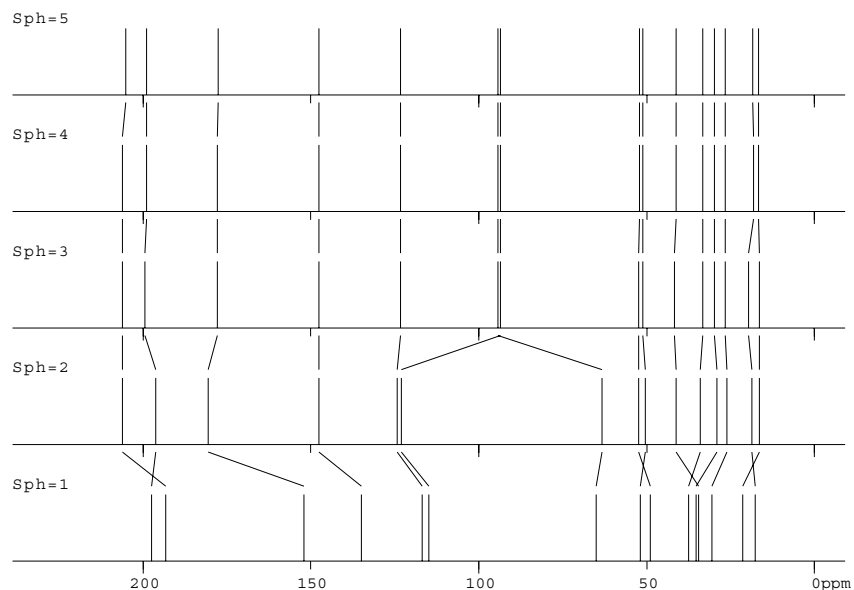


**Fig. 23.4** Dependence of the predicted chemical shift values on the number of coincident spheres, given on the left-hand side. The large change when increasing the number of coincident spheres from two to three is worth a more detailed investigation of the reference material used.

to the mean values. From this example it can be concluded that the HOSE code method is very sensitive to wrong assignments, leading to low-quality spectrum predictions in the case of wrong reference material. Neural network technology is far less sensitive to assignment errors, despite the wrong dataset being used during training reasonable chemical shift values are predicted, as given in Fig. 23.5.

Another important feature of spectrum prediction is the utilization of stereochemical information. Stereochemical effects may induce effects of up to *ca.* 30 ppm in typical organic compounds. The four isomeric tricyclo-octane derivatives as given in Fig. 23.6 demonstrate this clearly, especially at C<sub>8</sub> with a chemical shift range starting at 23 ppm in the exo,exo-derivative and going up to 53 ppm in the endo,endo-configurated isomer. The comparison of the corresponding carbon NMR spectra in Fig. 23.7 shows these large increments caused by steric interaction.

Implementation of steric interactions into the HOSE code and into neural networks improves spectrum prediction dramatically, as can be seen from the podocarpane example in Fig. 23.8. The diastereotopic methyl groups located at C<sub>4</sub> can be well predicted – 21.7 ppm for the axial and 33.4 ppm for the equatorial methyl group, which is in excellent agreement with the values found in the literature. The separation can be easily understood when inspecting the distribution of the entries contributing to the predicted values as given in Fig. 23.9. A total number of 34 entries selected from the reference database predicts a useless mean value at 28 ppm for *both* methyl groups when using the structural descriptors from the

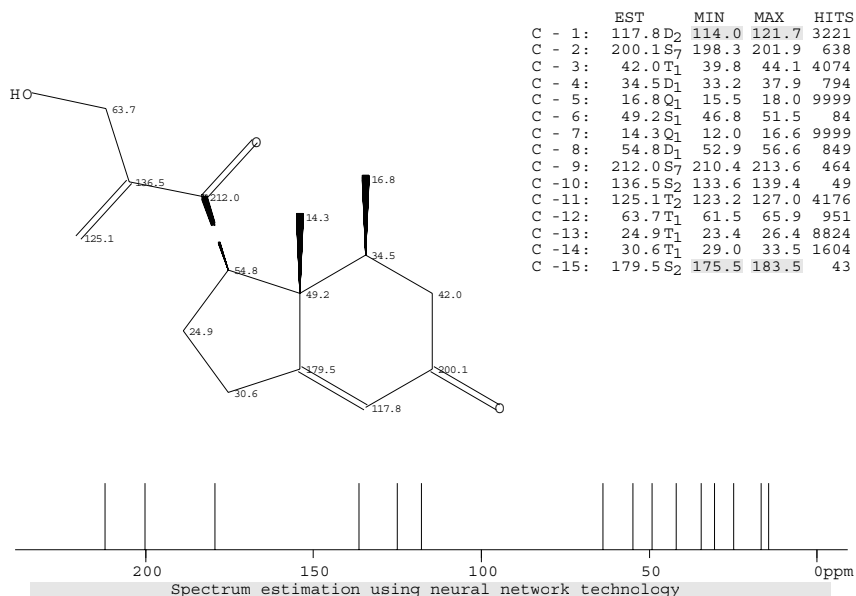


**Fig. 23.5** Predicted chemical shift values using neural network technology giving 125.1 ppm for C<sub>11</sub> and 63.7 ppm for C<sub>12</sub>, respectively.

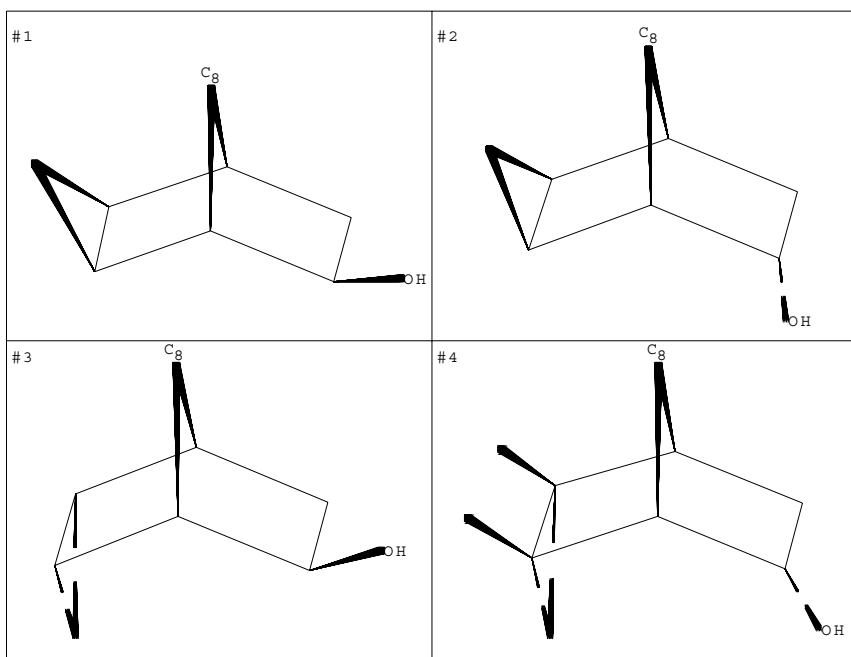


**Fig. 23.6** Four isomeric tricyclo-octane derivatives showing extremely pronounced effects of stereochemistry on chemical shift values (see Fig. 23.7).

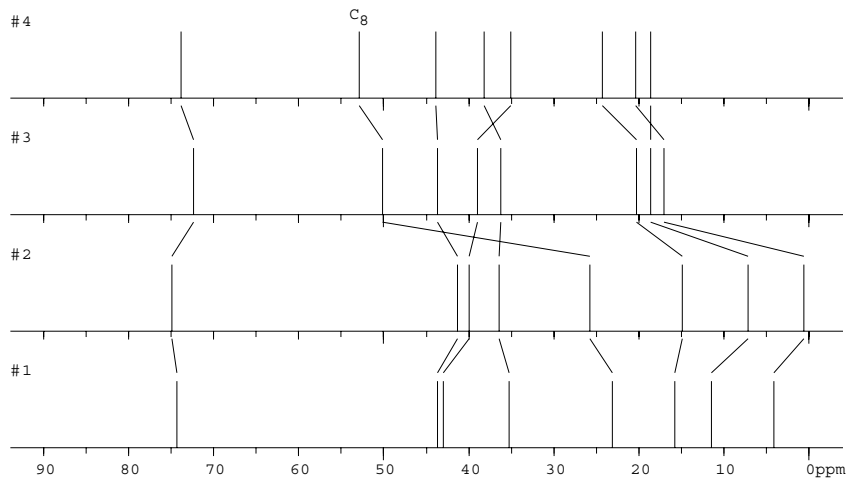


**Fig. 23.7** The  $^{13}\text{C}$ -NMR spectra of the four compounds given in Fig. 23.6 showing the effect of steric interactions on the chemical shift values.

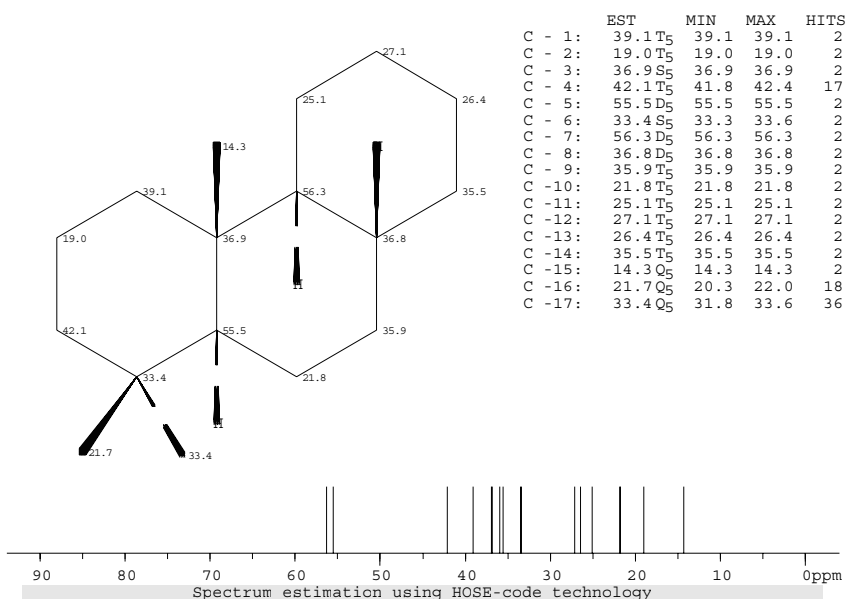


**Fig. 23.8** Spectrum prediction of podocarpane using HOSE-code technology with stereochemical information [22]. The chemical shift values of the methyl groups located at position 4 are predicted in good agreement with the literature data.

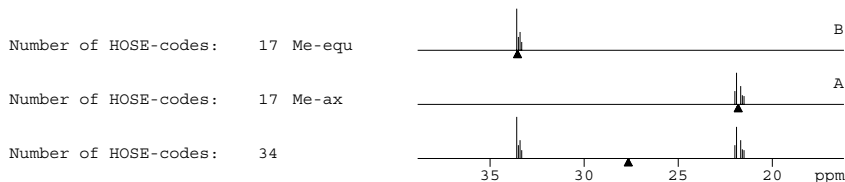


**Fig. 23.9** Distribution analysis of the entries contributing to the estimation of the methyl groups at position 4 of podocarpane. Bottom trace: stereochemical effects are ignored leading to a useless mean value around 28 ppm (small triangle); a total number of 34 reference data contribute to this mean value. Trace A and B: Utilization of stereochemical interactions separates the 34 reference data into two distinct sets of chemical shift values leading to a correct prediction for the axial and equatorial methyl group.

original HOSE code disregarding stereochemical effects. The introduction of the number of 1,3-diaxial interactions divides these 34 reference data into two groups of shift values estimating a chemical shift value of 21.7 ppm for the axial methyl group and 33.4 ppm for the equatorial one, which is shown in traces A and B of Fig. 23.9.

### 23.8

#### Spectrum Interpretation and Isomer Generation

Isomer generation is the well-defined task to generate, exhaustively and without redundancy, all possible chemical structures that are consistent with a given set of constraints [23, 24]. This combinatorial problem itself is optimally suited for computer application and this definition seems to be ready for easy implementation into a piece of computer software. A more detailed look into the background of isomer generation shows immediately the problems associated with this task. The enormous number of possible candidate structures when starting from only the molecular formula can be seen in Tab. 23.1.

Even a small molecular formula around C<sub>10</sub> produces a large number of possible chemical structures. The introduction of one heteroatom and/or a degree of unsaturation increases the size of the problem dramatically. The molecular formulae chosen in Tab. 23.1 represent comparably small compounds, far away from typical applications in modern organic chemistry. The main problem for making structure generation programs a common routine tool is the necessity to implement all available pieces of information from the most important spectroscopic techniques at the earliest possible step in order to avoid the “combinatorial explosion” and therefore

**Table 23.1** Number of possible isomers (without stereochemistry) depending on the molecular formula and constraints derived from NMR experiments.

Molecular formula	Additional information	Number of possible isomers [25]
C <sub>10</sub> H <sub>22</sub>		75
C <sub>15</sub> H <sub>32</sub>		4,347
C <sub>20</sub> H <sub>42</sub>		366,319
C <sub>10</sub> H <sub>22</sub>		75
C <sub>10</sub> H <sub>20</sub>		852
C <sub>10</sub> H <sub>18</sub>		5,568
C <sub>10</sub> H <sub>14</sub>		81,909
C <sub>10</sub> H <sub>12</sub>		201,578
C <sub>10</sub> H <sub>10</sub>		369,067
C <sub>10</sub> H <sub>10</sub>		369,067
C <sub>10</sub> H <sub>10</sub> O		7,288,733
C <sub>10</sub> H <sub>10</sub> O <sub>2</sub>		79,402,190
C <sub>10</sub> H <sub>10</sub> O <sub>2</sub>		79,402,190
C <sub>10</sub> H <sub>10</sub> O <sub>2</sub>	Signal multiplicity (4S, 3D, 2T, 1Q)	10,370,392
C <sub>10</sub> H <sub>10</sub> O <sub>2</sub>	Carbon hybridization (3sp <sup>3</sup> , 5sp <sup>2</sup> , 2sp)	240,751
C <sub>10</sub> H <sub>10</sub> O <sub>2</sub>	Signal multiplicity and hybridization as above	38,353
C <sub>10</sub> H <sub>16</sub>		24,938

long computing times during the structure generation process itself and during the necessary post-processing of the list of candidate structures. From Tab. 23.1 it can be seen that a powerful spectrum interpretation step is necessary even for a small molecular formula. The example  $C_{10}H_{10}$  gives 369,067 isomers when using only the molecular formula without further constraints. The introduction of one oxygen increases the size of the problem by a factor of 20, a further oxygen leads to roughly 80 million possible isomers. The utilization of multiplicity information which can be easily derived from DEPT spectra reduces the size of this particular problem by nearly one order of magnitude. Additionally the use of hybridization information as selected in Tab. 23.1 [26] reduces the number of possible isomers to 38,353 candidate structures. The determination of the multiplicity can be done by experimental techniques (usually DEPT) and is therefore information which is very secure. On the other hand the determination of the hybridization is based on the interpretation of chemical shift value together with further supporting information (for example  $^1J_{CH}$  couplings) therefore some ambiguity might remain, especially in the region around 100 ppm where  $sp^3$ ,  $sp^2$  and  $sp$ -carbon atoms have resonance lines.

The process of structure generation is a well-defined task based on graph theory, whereas spectrum interpretation, the translation from the spectral information into structural constraints, is based on heuristics. Even the selection of the hybridization state of a carbon atom cannot be performed with absolute security from its chemical shift value and some further information. A much more complex situation is encountered when deriving substructural fragments from spectral data, the interpretation of the data leads to a large amount of alternative possibilities for substructural units. This feature must be taken into account during the isomer generation process, making the programs more complex and slower.

There are two possible extreme situations which should be analyzed in further detail: The first approach uses a very detailed interpretation process based on a library of larger fragments as done for example by SPECSOLV [27], which makes structure generation working fast but with the disadvantage that only a part of the possible candidate structure compatible with the given constraints will be obtained, a situation which is less useful for natural product chemistry dealing with new classes of compounds. The other extreme approach is to take into account only absolutely safe pieces of information, for example signal multiplicities which can be determined experimentally. This situation uses only a very limited set of constraints for the structure generation process leading to an incredible number of candidates for further processing. In any case, ambiguity (for example with valencies and hybridizations) must be handled by the isomer generator which makes this tool much more complex. Usually there is a close connection between the interpretation and the isomer generation part of such systems.

A new horizon was introduced with the popularity of two-dimensional NMR methods giving information about coupled spin systems and therefore distance information (in terms of intervening bonds between coupled nuclei). The most useful experiments for organic structure elucidation are the methods for HH-, CH- and CC-correlation, the detailed experimental conditions (for example gradient-en-

hanced, normal-reverse detection) do not change the basic principle of these methods for computer application. The general information is always that correlation signals are translated into distance information between two atoms, which will be used either by the interpretation process leading directly to substructural units or, in the case of ambiguity (distance over 2 to  $n$  bonds) as a constraint during the structure generation process in order to exclude certain combinations of the substructural fragments. The COSY-type spectra give information about HH-correlations over two(geminal), three(vicinal) and four(allylic, W-coupling) bonds, but in many systems long-range couplings over more than four bonds are known, leading again to some ambiguity. The case of a  $^2J_{\text{HH}}$  coupling can be easily excluded by a heteronuclear correlation experiment. CH-correlation experiments over one bond (HMQC, HSQC) are able to detect exclusively this type of connection, because  $^1J_{\text{CH}}$ -couplings are much larger than any  $^nJ_{\text{CH}}$ -coupling. Long range correlation techniques have to deal with two problems. The first is the detection of artefacts from  $^1J_{\text{CH}}$ -correlations, which can be easily excluded from HMQC-type spectra. The second problem is a much more severe one, based on the fact that long-range  $J_{\text{CH}}$ -couplings are of similar size, in particular  $^2J_{\text{CH}}$  and  $^3J_{\text{CH}}$  cannot be distinguished in many cases. Prohibiting the differentiation between these two distances leads to an increased computing time during the structure generation process and in many cases to a larger set of candidate structures being produced. Frequently, signals corresponding to correlations over four to six bonds have also been observed adding a further order of magnitude to the complexity of structure generation, whereas ignoring this possibility leads to wrong structure proposals. Additionally, severe signal overlap may also increase the difficulties during the spectrum interpretation process [28]. CC-correlation techniques are well-suited for computer-assisted structure elucidation but they have the disadvantage of low sensitivity. Another well-known concept to restrict the number of generated candidate structures is to use a list of forbidden substructures within the candidates. This option should also be used with extreme care, because exotic structures, like highly strained or unexpected heterocyclic systems, will always be excluded [29].

From the scope of the problem of structure generation it can be seen that there is a demand for spectrum interpretation programs which work in a very carefully designed way, allowing the user access to all constraints and therefore selecting the correct set of constraints from the given experimental data. The basic idea of spectrum interpretation of NMR data is to correlate a certain chemical shift value with a set of functional groups used as building blocks for subsequent structure generation. In order to improve this basic idea of using a single line, a complete subspectrum can be correlated with a set of larger substructural fragments, leading to higher selectivity during the interpretation process and therefore faster post-processing. The approaches known work either with rule-based correlation tables (for example CHEMICS [30], DENDRAL [31], DARC [32]) or HOSE-code technology (SPEC SOLV[27]); atom-centered fragments (ACFs) are used in SESAMI [33, 34] and EPIOS [35], three-atom fragments are selected in CSEARCH [36, 37]. The basic principle behind these technologies remains always the efficient correlation between spectral and structural property; in any case these methods become slower

when using smaller fragments or they generate only partial solutions when starting from a too specific set of fragments. The latter effect is also extremely dependent on the database used for the generation of the subspectra–substructure correlation tables. In any case a high structural diversity within the reference database is obligatory.

### 23.9

#### Ranking of Candidate Structures

The usual case when applying an interpretation/isomer generation program to a real-world structure elucidation problem is not to obtain a single structural proposal to a specific set of constraints. Frequently a list of possible candidate structures will be generated, consisting either of only a few proposals or maybe a few thousands of proposals, depending on the number of constraints given. Therefore a ranking process based on spectrum prediction [37] is necessary to select proposals of higher probability. For  $^1\text{H}$ - and  $^{13}\text{C}$ -NMR-spectra well-established methods are available, which allow one to select a set of most probable candidate structures. It is strongly recommended not only to use a single best solution, but also to include useful alternatives for further investigation. Isomer generator programs also produce very uncommon structures, which are not well-represented by databases used for spectrum prediction purposes, leading to a biased evaluation of the hit list with the result that more common structures might be ranked better than uncommon ones. Spectrum prediction based on a database having a high degree of structural diversity is a fast and reliable method which can be applied to a hit list of a few thousand chemical structures within a reasonable time. In the case that more structures have been generated, the set of constraints should be refined and/or additional experimental data should be collected.

### 23.10

#### Conclusions

For the synthetic organic chemist spectrum simulation in order to verify a structural proposal is the most decisive task; in natural product chemistry the starting point is usually a spectral similarity search using the experimental spectrum of the unknown. Both methods are extremely fast and can be done automatically immediately after the measurement of the one-dimensional routine spectra. When these basic methods give no solution further spectroscopic experiments are usually performed, giving more detailed information about the unknown sample. Spectrum interpretation and subsequent isomer generation is mainly successful when a large amount of additional information is available. The most important pieces of information are the presence/absence of certain functional groups and the efficient use of distance constraints as derived from two-dimensional correlation spectroscopy. This information usually allows one to deduce the constitution of an or-

ganic compound, in order to determine the configuration and conformation a more specialized set of tools is available. Many of these techniques, either experimental or computational methods, have been developed to deal with specific classes of compounds, especially with biopolymers [38]. The typical application field of the computer-techniques described here is structure elucidation of organic compounds up to C<sub>50</sub>. Many steps during the structure elucidation process can be performed, or at least simplified and accelerated, by appropriate computational technologies, but the results must be critically evaluated by the expert. A large variety of algorithms and more or less integrated systems have been described in the literature and the field of computer-assisted structure elucidation is evolving dynamically. Numerous tools are commercially available and can support the chemist during the structure elucidation process, a critical evaluation of these tools with specific examples from his own field of application is strongly advised.

## References

- 1 Kessler H., Gehrke M., Griesinger C., *Angew. Chem. Int. Ed. Engl.*, **1988**, *27*, 490–536;
- Parella T., *Magn. Reson. Chem.*, **1998**, *36*, 467–495
- 2 Gray, N. A. B., *Computer-Assisted Structure Elucidation*, John Wiley and Sons, New York 1986.
- 3 Munk, M. E., *J. Chem. Inf. Comput. Sci.*, **1998**, *38*, 997–1009 and references cited therein.
- 4 Jaspars M., *Nat. Prod. Rep.*, **1999**, *16*, 241–248 and references cited therein.
- 5 <http://www.lohnninger.com/spectroscopy/dball.html>.
- 6 Gasteiger J., Hanebeck W., Schulz K. P., *J. Chem. Inf. Comput. Sci.*, **1992**, *32*, 264–271.
- 7 Bremser W., Wagner H., Franke B., *Org. Magn. Reson.*, **1981**, *15*, 178–187.
- 8 <http://www.biorad.com>.
- 9 <http://specinfo.wiley-vch.de>.
- 10 <http://www.acdlabs.com>.
- 11 Ewing D. F., *Org. Magn. Reson.*, **1979**, *12*, 499–524.
- 12 Höning H., *Magn. Reson. Chem.*, **1996**, *34*, 395–406.
- 13 Thomas S., Ströhle D., Kleinpeter E., *J. Chem. Inf. Comput. Sci.*, **1994**, *34*, 725–729; <http://www.chem.uni-potsdam.de/arosim/index.html>.
- 14 Chen L., Robien W., *Anal. Chem.*, **1993**, *65*, 2282–2287.
- 15 Bremser W., *Anal. Chim. Acta*, **1978**, *103*, 355–363.
- 16 [http://www.univie.ac.at/orgchem/csearch\\_server\\_info.html](http://www.univie.ac.at/orgchem/csearch_server_info.html).
- 17 <http://www.univie.ac.at/orgchem/wralpha.html>.
- 18 Klamt A., Hoever P., Bärmann F. et al., in *Software-Development in Chemistry 7*, ed. D. Ziessow, Gesellschaft Deutscher Chemiker, Frankfurt am Main 1993, pp. 39–44.
- 19 Meiler J., Meusinger R., Will M., *Mh. Chem.*, **1999**, *130*, 1089–1095.
- 20 Badertscher M., Bischofberger K., Pretsch E., *Trends Anal. Chem.*, **1980**, *16*, 234–241.
- 21 [http://www.acdlabs.co.uk/publish/nmr\\_485.html](http://www.acdlabs.co.uk/publish/nmr_485.html) and references cited therein.
- 22 Robien W., Purtuc V., Schütz V. et al., Lecture at 13th CIC-Workshop, 15 – 17. 11. 1998, Bad Dürkheim/Germany; <http://www2.chemie.uni-erlangen.de/external/cic/tagungen/workshop98/paper3.html>.
- 23 Shelley C. A., Hays T. R., Munk M. E. et al., *Anal. Chim. Acta*, **1978**, *103*, 121–132.
- 24 Masinter L. M., Sridharan N. S., Lederberg J., Smith D. H., *J. Am. Chem. Soc.*, **1974**, *96*, 7702–7714.
- 25 All calculations have been performed using MOLGEN-3.1, Benecke C., Grund R., Hohberger R. et al., *Anal. Chim. Acta*, **1995**, *314*, 141–147.
- 26 Rivera A. P., Arancibia L., Castillo M., *J. Nat. Prod.*, **1989**, *52*, 433–435.
- 27 Will M., Fachinger W., Richert J. R., *J. Chem. Inf. Comput. Sci.*, **1996**, *36*, 221–227.
- 28 Mukhopadhyay T., Nadkarni S. R., Bhat R. G. et al., *J. Nat. Prod.*, **1999**, *62*, 889–890.
- 29 Varmuza K., Jordis U., Wolf G., *ECHET96 - Electronic Conference on*

- Heterocyclic Chemistry*, 24.6.–22.7.1996,  
<http://www.ch.ic.ac.uk/ectoc/echet96>
- 30** Funatsu K., Sasaki S. I., *J. Chem. Inf. Comput. Sci.*, **1996**, *36*, 190–204.
- 31** Mitchell T. M., Schwenzer G. M., *Org. Magn. Reson.*, **1978**, *11*, 378–384.
- 32** Dubois J. E., Carabedian M., Ancian B., *C. R. Acad. Sci. (Paris)*, **1980**, *290*, 369–372, 383–386.
- 33** Razinger M., Balasubramanian K., Perdih M. et al., *J. Chem. Inf. Comput. Sci.*, **1993**, *33*, 812–825
- 34** Munk M. E., Madison M. S., Schulz K. P. et al., Lecture at 13th CIC-Workshop, 15–17.11.1998, Bad Dürkheim/Germany, <http://www2.chemie.uni-erlangen.de/external/cic/tagungen/workshop98/paper8.html>.
- 35** Carabedian M., Dagane I., Dubois J. E., *Anal. Chem.*, **1988**, *60*, 2186–2192.
- 36** Robien W., *Mikrochim. Acta [Wien]*, **1986**, *II*, 271–279.
- 37** Seger C., Jandl B., Brader G. et al., *Fresenius' J. Anal. Chem.*, **1997**, *359*, 42–45.
- 38** Zhu F. Q., Donne D. G., Gozansky E. K. et al., *Magn. Reson. Chem.*, **1996**, *34*, S125–S135.
- 39** All Figures have been generated using the CSEARCH-NMR-database system Kalchhauser H., Robien W., *J. Chem. Inf. Comput. Sci.*, **1985**, *25*, 103–108.

## **24**

### **Mass spectrometry**

*Antony N. Davies*

#### **24.1**

##### **Introduction**

The world of mass spectrometry is blessed with many advantages over the other fields of spectroscopy when it comes to data handling. Not only are mass spectroscopists able to call on the largest collections of high quality reference spectroscopic data of any technique but they are also required to pay out the least amount of money per data set for access! Furthermore, some of the most powerful data analysis tools available for the study of hyphenated data sets from, for example gas-chromatography/mass spectrometry are available for free over the Internet! Finally, most new mass spectrometers come delivered with a large reference data library with advanced competent search software installed as standard. Most scientists from other fields of spectroscopy would regard themselves as having an excellently equipped spectroscopic data handling software if they had access to the same high level of tools and well thought through data analysis packages as are available in a standard mass spectrometry laboratory.

In this chapter the various types of data to be found in mass spectrometry will be detailed. Some of the most common data analysis packages will be described and their strengths and weaknesses probed. The different spectroscopic data packages will be explained along with their differences.

As with all works of this nature it is essential to always go to the original source reference given to find out what the latest situation is for any given software package or reference library. Where a need or deficiency is identified here it might well be the case that the need has been satisfied or the deficiency been corrected by the time the handbook goes into print. Experience has however shown in recent years that this is probably not the case!

Finally, a note of warning: Where a particular opinion is expressed in this chapter it can only have been gained during the work of the author and more correctly his colleagues. This experiences is, by its nature and the nature of all research laboratories, restricted to work carried out in certain analytical problem areas and deals with a limited amount of sample matrices. It is very important for any reader intending to invest in the area of mass spectrometry data handling to test

the systems on real samples out of the day-to-day work of their laboratory. Finally, let the people who will be working with the systems have a major say in the testing and selection of the product to be purchased as they will have to be happy working with the new software systems and often possess many insights into the day-to-day running of the laboratory hidden to the average laboratory manager.

## 24.2

### Mass Spectrometry Databases

There are two major collections of mass spectrometry reference data in common use which will be described more fully below. Each has its own unique strategy for data collection and quality control as well as different spectral search options. However, many smaller but very high quality specialised collections can also be found [1]. In July 2000 the 25 millionth CAS registry number was assigned to a mutant epoxide hydrolyase. Figure 24.1 shows the dramatic increase in the number of substances registered. By the time this article appears in print this will of course be an old figure but anyone who looks at the Chemical Abstracts Service Web site can easily find the current numbers of compounds registered under <http://www.cas.org/cgi-bin/regreport.pl> [2].

Depressingly this number has increasingly outstripped the development of even the largest collection of reference spectroscopic data so that it is often the case that, even though an unknown substance may well have been fully documented in the scientific literature 20 or more years ago, if you rely on commercial reference data collections you may well not be able to identify the compound.

### CAS Statistics 1907 - 1999

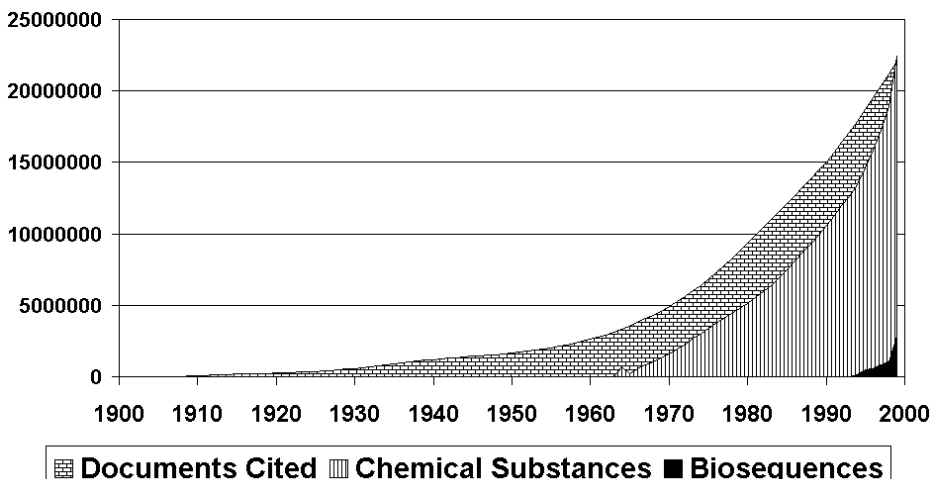


Fig. 24.1 Chemical Abstracts Service registry count changes 1907 to date.

This applies just as well when you are using reference data to carry out structure elucidation of completely new products such as new pharmaceutical agents. It is often the case that, regardless of the high level of intelligence now built into even the most modern of analytical spectroscopy tools, it is important to have added your own well characterised reference data to the knowledge base to ensure that for your particular chemistry the solution space is well populated. More simply put there is no point in trying to elucidate aromatic structures if your reference database only contains aliphatic compounds!

A superb example of such a strategy in action can be found in the description of the AMDIS program from NIST later in this chapter.

Finally, if your spectrometer comes with one of the commercial databases pre-installed it is well worthwhile checking which version has been installed as it could quite possibly be older than the current release and may well be easy to upgrade.

#### 24.2.1

##### NIST/EPA/NIH Mass Spectral Library

The smaller of the two largest collections is that administered by the US National Institute of Standards and Technology (NIST) more commonly known as NIST 02. This collection has been built up over many years from a number of mainly government backed initiatives in the UK and USA and is claimed to be the most widely used [3]. The US government agencies included the old National Bureau of Standards (NBS), the Environmental Protection Agency (EPA) and the National Institute of Health (NIH) who built on the initial work of the UK Atomic Weapons Research Establishment (AWRE) in Aldermaston [4]. Initially some of the data was only stored as an 8 peak data per compound which although saving storage space in an age when this was of primary importance gave spectra that are not useful in a modern environment. Since 1988 the responsibility for this collection has been with the NIST Mass Spectrometry Data Center. These spectra are now updated regularly and the most recent software release has been selected from over 175,000 spectra in the NIST archive. The latest release (January 2001) is known as the NIST 02 Mass Spectral Database and contains some 175,214 spectra of 147,350 compounds for which 107,105 have CAS numbers and virtually all (147,350) have chemical structures stored [3]. In this collection no radio-labelled substances were included and only a single representative spectrum per compound. A further 27,844 spectra of replicate (alternative) spectra for compounds in the main collection are also supplied. Considerable emphasis is placed on the quality of the spectra stored with each spectrum being critically evaluated [5].

Some of the data are available in the useful web-based reference collection of the National Institute of Standards called the WebBook (<http://webbook.nist.gov>). As with all such services any comment on the size of the collection will be out-of-date before this article goes to print but with over 10,000 mass spectra available on-line linked to a large amount of spectroscopic chemical and physical subsidiary data for the compounds of interest this is a reference data source which all analysts should have close to the top of their bookmarks!

#### 24.2.2

#### **Wiley Registry of Mass Spectral Data**

This data collection started out as the Mass Spectrometry Registry under the auspices of Stenhagen and Abrahamsson in Sweden and has grown in recent years out of the work of McLafferty and co-workers. This is the largest of the reference databases of mass spectrometric data which also makes it the largest collection of reference data available in any single field of spectroscopy [6]. The ethos of data inclusion is different in this reference library where multiple entries per compound were included if the spectra were significantly different from one another. Radio-labelled substances were also included.

The usefulness of any particular reference library is greatly enhanced by the availability of subsidiary data on the spectra stored and the Wiley Registry boasted Chemical Abstracts Service (CAS) registry numbers and chemical structure information at an early stage in its development. The Quality Index is in use here to assess candidate spectra for their fitness for use as reference data and this version is slightly different from that adopted by NIST. Unfortunately this has not been 100 percent successful in keeping out incorrect reference data sets. If you should spot what you regard as false data whilst using any collection you should report it to the collators as the best way to quality control any large reference library is to have as many people as possible with as wide an interest base as possible using the collections on a regular basis!

In 1991 this collection was already almost 140,000 spectra (139,859) but from only 118,114 compounds [7]. The fifth edition is available in book form and CD-ROM either with or without structures [8]. The current version is the 6th containing some 229,119 reference spectra from 200,500 compounds which can be combined with a version of the NIST database, increasing the total size to 275,821 spectra of 226,334 compounds. The version marketed by the Palisade Corporation is available with a useful data format conversion utility MASSTransit (<http://www.wileyregistry.com>). There is also the PC BenchTop/PBM search system described below which can be purchased for off-spectrometer data processing and analysis of GC/MS runs for example.

The 7th Edition contains over 390,000 electron impact mass spectra including the older NIST '98 database. Through use of the AccessPak it may be loaded into many Mass Spectrometer data systems.

#### 24.2.3

#### **SpecInfo/SpecData**

The SpecInfo databases from Chemical Concepts GmbH marketed as SpecData have the two databases mentioned above and also their own collection 'CC Mass Spectra 4th Edition' of some 40,000 spectra, although there will be some doubling up of the data available between the collections. The Chemical Concepts web site specifically indicates that, for example, the Industrial Chemicals Collection from Henneberg at the Max Planck Institut für Kohlenforschung, Mülheim, Germany

is also available in the NIST '98 database (<http://www.chemicalconcepts.com/p11343.htm>).

These collections have recently become available for searching through a web based client/server system called SpecSurf written by the company LabControl in Cologne, Germany. 'SpecInfo on the Internet' is hosted by the Wiley New York server at <http://specinfo.wiley.com/> [9]. In order to make proper use of the Java programming a small additional free program needs to be installed on your PC to enhance your browser but this is simple to carry out and well documented.

A further version of the SpecInfo database is also available through STN where the mass spectra along with other spectroscopic and chemical substance information can be found through the usual CAS type search options as well as single peak data such as base peak, base peak intensity, nominal mass, peak position etc. The 9th September 1999 upgrade reported over 65,900 mass spectra stored. For more details see: <http://www.cas.org/ONLINE/DBSS/specinfoss.html>.

#### 24.2.4

#### **SDBS, Integrated Spectra Data Base System for Organic Compounds**

This Japanese web-based database is freely available at <http://www.aist.go.jp/RIODB/SDBS/menu-e.html> and at the time of writing had last been updated on August 18 1999. The database is run by the NIMS National Institute of Materials and Chemical Research in Tsukuba.

The collection has NMR, IR, Raman and EPR data as well as MS data (approximately 19,600). Unfortunately the search options request only mass numbers and relative intensities (with a 50% error!) see Fig. 24.2.

A trial search carried out by inputting  $m/z$  values refused to show the initial hit list as it was deemed too long and a second  $m/z$  value was required to restrict the hit list.

The only active link in the results window is the SDBS registry number which will lead the user to the mass spectrum display window shown in Fig. 24.3.

#### 24.2.5

#### **Other Smaller Collections**

Depending on the instrument manufacturer a number of smaller specialised mass spectra databases are being made available, either as standard or as optional extras with the spectrometer data systems. A few of the more frequently found libraries are given below as well as collections of more unusual mass spectrometry techniques. Also included are a few references to data collection activities by some concerned organisations.

Search Compounds	Search NMR	Search MS	
<b>Compound Name:</b> <input type="text"/>	<b><sup>13</sup>C Peak Position (ppm)</b> <input type="text"/>	<b><sup>1</sup>H Chemical Shift (ppm)</b> <input type="text"/>	
<b>Molecular Formula:</b> <input type="text"/>	AND <input type="text"/> <input type="text"/>	AND <input type="text"/> <input type="text"/>	<b>Mass No.</b> <input type="text"/> <b>Intensity</b> <input type="text"/>
<b>Number of Atoms:</b>	AND <input type="text"/> <input type="text"/>	AND <input type="text"/> <input type="text"/>	<input type="text"/> <input type="text"/> <input type="text"/> <input type="text"/> <input type="text"/> <input type="text"/>
Carbon <input type="text"/> to <input type="text"/> Hydrogen <input type="text"/> to <input type="text"/> Oxygen <input type="text"/> to <input type="text"/> Nitrogen <input type="text"/> to <input type="text"/>	AND <input type="text"/> <input type="text"/> AND <input type="text"/> <input type="text"/> allowance $\pm 2.0$	AND <input type="text"/> <input type="text"/> AND <input type="text"/> <input type="text"/> allowance $\pm 0.2$	<input type="text"/> <input type="text"/> <input type="text"/> <input type="text"/> <input type="text"/> <input type="text"/>
<b>Molecular Weight:</b> <input type="text"/> to <input type="text"/>	NOT <input type="text"/> to <input type="text"/>	NOT <input type="text"/> to <input type="text"/>	<input type="text"/> <input type="text"/> <input type="text"/> <input type="text"/> <input type="text"/> <input type="text"/>
<b>CAS Registry No.:</b> <input type="text"/>	<input type="button" value="Clear"/>	<input type="button" value="Clear"/>	<input type="button" value="Clear"/>
<b>SDBS No.:</b> <input type="text"/>	<input type="button" value="Clear"/>		

Fig. 24.2 The SDMS database search mask.

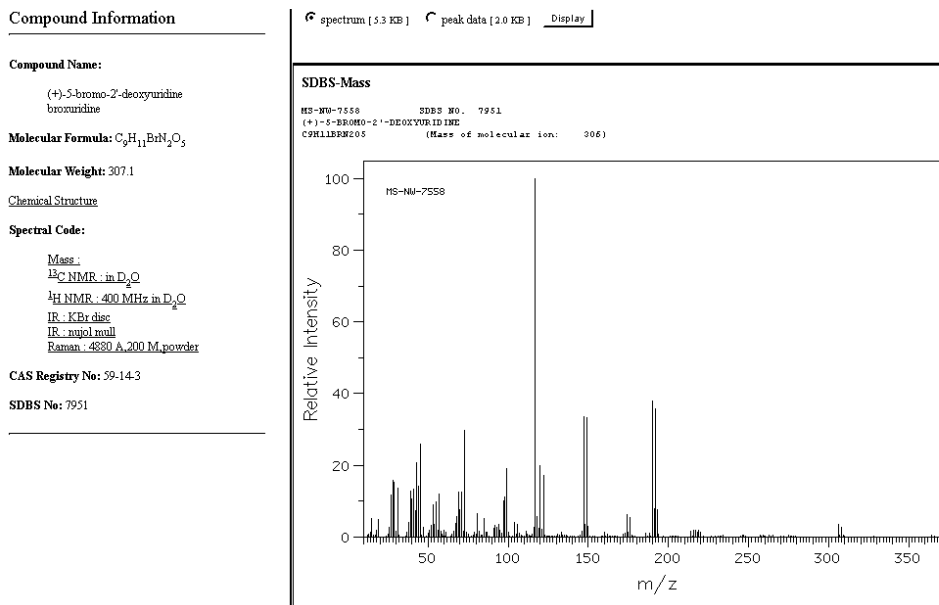


Fig. 24.3 The final SDMS mass spectrometry results window with cross-references linked.

#### 24.2.5.1 Pfleger/Maurer/Weber: Mass Spectral and GC Data of Drugs, Poisons, Pesticides, Pollutants and Their Metabolites

One of the smaller databases commonly delivered as standard with many GC/MS spectrometers is the PMW or Pfleger/Maurer/Weber. This database of about 4300 spectra is also published in book form with the 4th part bringing the database up to some 6300 spectra [10]. This is a good collection for those specialising in, for example, clinical toxicology, pharmacology, environmental chemistry and food analysis.

#### 24.2.5.2 Ehrenstorfer

Dr. Ehrenstorfer GmbH in Augsburg, Germany has been supplying analytical standards for many years and they have produced a mass spectra library of over 1450 spectra of pesticides and their metabolites, PCBs, PAHs explosives and other environmentally important compounds [11].

#### 24.2.5.3 Wiley-SIMS

A small CD-ROM based library of around 300 secondary ion mass spectra known as the Wiley-SIMS was created by Henderson and co-workers in Manchester UK. (see <http://www.surfacespectra.com>).

#### 24.2.5.4 American Academy of Forensic Sciences, Toxicology Section, Mass Spectrometry Database Committee

This group works to co-ordinate the generation of reliable mass spectra of new drugs and their metabolites see: <http://www.ualberta.ca/~gjones/msmlib.html>

The 1997 version of the data is available on-line for free as a demo library at the Galactic Industries web site. <http://www.galactic.com/> although to view the spectra you will need to have the spectra viewing program (also available for free) or another software program supporting Galactic's SPC format installed on your system.

This group is very interested in expanding the collection and would greet any approaches aimed at supplying standards for measurement.

#### 24.2.5.5 The International Association of Forensic Toxicologists (TIAFT)

Another effort to collect reference EI spectra to assist toxicologists in unknown substance identification has been started by this organisation. This small collection is available for free over the internet and specifically aims at gathering spectra of new upcoming or uncommon substances or less frequent derivatives of drugs. This group is interested in receiving new data and can be contacted through their web site at <http://www.tiaft.org>

### 24.3

#### Mass Spectrometry Search Software

Mass spectra are in themselves relatively simple data sets containing essentially simple lists of intensity against mass/charge ratio ( $m/z$ ). Unfortunately this hides the enormous complexity of the processes which the sample has undergone to yield such a signal. This can cause effects during the recording of mass spectra which, under often quite normal conditions, can deliver substantially different results for the same analyte. You could think that this would make the use of reference data collections for analyte identification effectively impossible unless representative data from all possible experimental conditions were available but fortunately there have been some rather clever algorithms developed. The reference databases themselves are standardised around low resolution electron ionisation mass spectra with a primary electron energy of 70 eV.

There have been several programs available for analysing multidimensional experiments in mass spectrometry such as the MassLib program developed by Henneberg and co-workers at the Max Planck Institute für Kohlenforschung in Mülheim, Germany or the more recent AMDIS package written by Stein and co-workers at the US National Institute of Standards and Technology at Gaithersburg [12].

Three different mass spectrometry search algorithms dominate the database searching systems commercially available today. The Cornell University 'Probability Based Matching' (PBM) software, The Integrated Control System (INCOS) and the MassLib system (see below) with the SISCOM search software.

These systems stem from original publications in the early 1970s but have been extensively copied, improved and adapted. They all use well thought out powerful algorithms and are surprisingly fast considering the size of the reference libraries through which they have to search. These systems initially reduce the size of the result space by the use of pre-searches, often using only a small fraction of the available data in the unknown spectrum and the reference libraries [13]. As only the pre-filtered reference data will be presented for more extensive comparison with the unknown spectrum the pre-search is a critical phase in the library search process and will be discussed again below.

The use of neural networks for mass spectral searching has also been successfully tested and reported recently [14].

Finally a word of warning, even though modern search software can produce superb results from what often looks like very poor starting data, it is also possible to produce hit lists of candidate solutions to a particular problem which are completely wrong. It is important not to rely solely on a computer generated hit list for your analysis but to approach the whole spectral searching task with a reasonable amount of healthy scepticism! On a slightly more positive note, if the first hit does not look right look further down the hit list your software presents you as often the correct hit may not have achieved the top ranking position. Nothing beats asking a friendly mass spectroscopist who knows your chemistry!

### 24.3.1

#### INCOS

The INCOS search algorithm originally developed by Finnigan involves the dot product calculation between the unknown spectrum and the library data [15]. An initial pre-search is carried out on a reduced number of peaks out of the unknown spectrum against a reduced peak number reference library. Having reduced the number of candidate hits through the pre-search a second more complete search is carried out through the surviving candidates to produce the final hit ranking. The search itself is weighted by the root of the product of the mass and intensity values giving preference to the higher  $m/z$  peaks due to their greater specificity in identifying the unknown. Sparkman has recently further qualified his assessment of the various current implementations of the INCOS algorithm amongst different spectrometer manufacturers by a criticism of the different pre-search algorithms which are a critical part of the complete software package [16].

Data reduction is carried out using a windowing technique. The main search under INCOS is similar in nature to how a scientist would compare two mass spectra in that, for a particular  $m/z$  region, the data are locally normalised, thereby ensuring that the search locates similar fragments in the reference library, irrespective of the varying intensity ratios between peaks of different fragments in the unknown. This makes the search system very robust against changes in the recorded data arising from slight changes in experimental set-up or conditions.

### 24.3.2

#### Probability Based Matching (PBM)

The probability based matching algorithm [17] and the self-training interpretive and retrieval system (STIRS) have been continuously improved over the last 20 years (see for example [18, 19]). The PBM system can carry out forward and reverse searches for pure analyte and mixture analysis. A forward search looks for the unknown spectrum in the reference database and the reverse search looks to find the best reference spectrum in the unknown data set. In a different strategy to the original INCOS algorithm the search is weighted linearly in favour of the peaks from molecular fragment ions.

The hit quality index (HQI) ranks the candidate reference spectra by their similarity to the unknown spectrum. As warned above it is not wise to take the hit list ranked by HQI at face value but to look down the hit list where it may well be possible to find what a human expert would regard as a better candidate solution to the search than the algorithm has picked out.

The forward search is the most rapid but demands unknown spectra of pure compounds to produce good results. If however the unknown spectrum includes peaks from unwanted impurities or of a mixture then it will not work correctly. The alternative reverse search strategy although slower is now required, whereby the resulting hit list shows the best reference spectrum in the library as found in the unknown data. Peaks in the unknown which do not appear in the library

spectrum do not downgrade the HQI as they would in the forward search as they may come from impurities or other substances in a mixture. Once the most significant component has been identified the reference spectrum of this component can be subtracted from the unknown mixture and the reverse search started again to identify, if possible, further compounds in the unknown sample.

#### 24.3.3

##### **MassLib/SISCOM**

The MassLib software package has been around in various forms for many years migrating from workstations to PCs as windowing became popular [13]. It was developed by Henneberg and co-workers at the Max Planck Institute in Mülheim, Germany for the analysis of GC/MS runs and is now into MassLib/PC version 8.5 [20].

The package uses fragment as well as neutral loss searching yielding hit lists useful for determining possible chemical structures for an unknown compound even when the compound is clearly not in the reference database. A limit of 500 spectra from the users own mass spectrometry database is currently in place for the basic package but this can be overcome with an upgrade.

For all such third party off-spectrometer data analysis packages it is important to be able to handle as many manufacturers' formats and international data transfer formats as possible and Tab. 24.1 typifies this with those formats currently supported by MassLib.

The full GC/MS trace is analysed to locate the various components and candidate unknown spectra generated for searching in the reference databases using SISCOM. The mass spectrum database search system which comes with the MassLib package detailed below is called SISCOM (Search for Identical and Similar Components) [21]. The Identity search option looks for the unknown in the reference libraries and can handle binary mixtures as unknowns provided both substances are represented in the reference database. The identity search swaps to the similarity search mode if no identical hits have been found in the reference databases where characteristic ions in the unknown are searched in the reference libraries. If this option is unsuccessful a related search option is available matching the library to the unknown.

Neutral loss masses from the  $M^+$  peak are also used via a special tool for spectral searching.

**Table 24.1** Data Formats currently supported by MassLib.

---

Balzers, Bear Instruments, DA5000, EPA I + II, EZ-Scan, GCQ, HP-Chemstation, HP-RTE, ICIS 1 + 2, INCOS, ITDS, ITS40, JCAMP-DX, Mach3, MassLab, MassLynx, MSD, MSS, NetCDF, Saturn, Shimadzu, Shrader, SSX, VG 11-250.

---

## 24.3.4

**AMDIS**

NIST have produced a freely available package called AMDIS (automated mass spectrometry deconvolution and identification system) for the analysis of GC/MS data sets. Developed to assist in the task of verifying the international Chemical Weapons Convention (<http://www.opcw.org/>) financially supported by the US Defense Special Weapons Agency (DSWA, US Department of Defense) the AMDIS program is also distributed with the NIST 02 Mass Spectral Library (see above).

The system comes with six speciality target libraries installed which consist of selected spectra from the 175,214 in the full NIST/EPA/NIH library (see Tab. 24.2).

These or user generated databases are the libraries in which the initial identification of the chromatographic peaks is carried out. In our work into pesticides in drinking and ground water for example we generated our own AMDIS library containing specifically the pesticides and their metabolites that we were working on ([http://www.spectroscopyeurope.com/td\\_col.html](http://www.spectroscopyeurope.com/td_col.html)).

In the latest release of the AMDIS package (v.2.1) it has been decided that computer speeds are now such that it is reasonable to allow searching of the whole of the NIST 02 database during the chromatography analysis phase.

Each single mass chromatogram is studied to identify the locations of the chromatographic peaks and all masses which have the same peak position are then extracted from the total ion chromatogram as a candidate spectrum for identification [22, 23]. If a candidate unknown spectrum has not been clearly identified it is possible to add this to the clipboard for transfer to the NIST MS Search package for individual searching through the NIST '98 database. If the automatic peak picking does not work to your satisfaction then it is possible to opt for manual mode in which the area of background and signal can be selected by use of the mouse and the candidate unknown spectrum generated in this way.

Unfortunately the requirement for only black and white images in this chapter makes it difficult to show the main features of AMDIS v2.1 which allows two different GC/MS runs to be displayed in the same window with their time axes tied. In Fig. 24.4 we have been studying PCBs in sewage sludge and have found the use of the top trace for the sludge sample analysed by flash-thermodesorption/GC/MS and the lower trace from our calibration runs using the DIN PCB mixture extremely useful due to the vast number of peaks seen in our complicated matrix.

**Table 24.2** Speciality target libraries installed in AMDIS.

- 
- NISTTOX 1251 spectra toxicological library,
  - NISTEPA is 1106 Environmental Protection Agency (EPA) target compounds,
  - NISTFF 993 flavours and fragrances
  - NISTDRUG is 778 drug analysis spectra,
  - NISTFDA 419 for Food and Drug Administration (FDA) analyses,
  - NISTCW is 62 chemical-weapons related data sets.
-

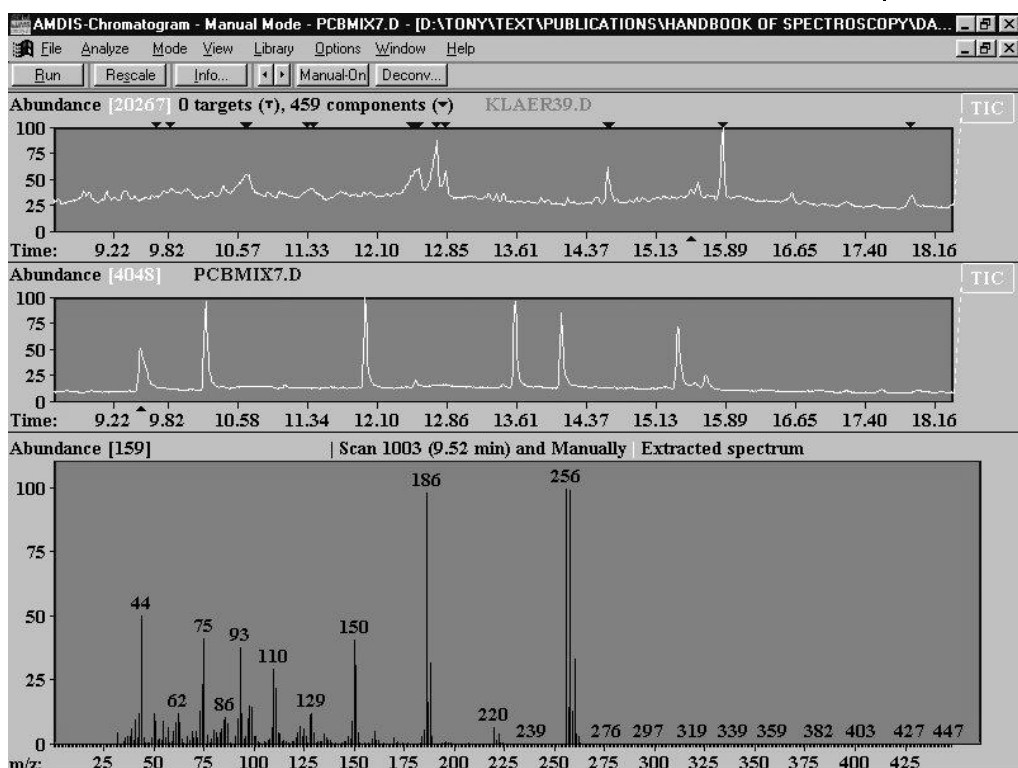


**Fig. 24.4** AMDIS 2.0 allows twin TIC windows to help comparisons between GC/MS runs. This figure shows a sewage sludge analysis (upper trace) compared to a reference PCB run (centre trace).

Since its introduction this package has become one of our major GC/MS data analysis tools finding favor with both scientists and laboratory technicians alike [12].

#### 24.3.5

##### Mass Frontier

A company established in 1997 in Bratislava, Slovakia has produced an interesting mass spectrometry data handling package called Mass Frontier (<http://www.high-chem.com>). The package is PC based and is modular containing a structure editor, spectra manager for spectra/structure databases (also user). The database search algorithm is that developed by NIST and a substructure search is also present. A fragments and mechanisms module can be used for consistency checking and analysis of mass spectra and as a help in MS/MS experiments. The new spectra to be analysed can come from the GC/LC/MS viewer where the TIC and single ion chromatograms can be used for peak location and candidate spectra generation.

## 24.3.6

**The WebBook**

One of the more useful free resources on the Internet for analytical chemists is the NIST WebBook <http://webbook.nist.gov>. The WebBook can be searched through a number of keys but unfortunately spectral searching is not one of them!

One of the most useful features of the NIST WebBook we have found is the name search, where a large selection of alternative names for a particular compound are available and searchable, greatly increasing the chance of finding the information you want on a particular substance if you do not know the IUPAC or CAS name or the CAS registry number and are not really too sure of the chemical structure. However it is possible to upload chemical structures for example (Fig. 24.5).

Amongst the various databases linked to the WebBook results page is that for mass spectrometry which will cause the spectrum to be presented to the user via a Java Applet which now allows direct printing from the browser (Fig. 24.6).

**Benzene, (trifluoromethyl) - Netscape**

Standard Reference Data Program      Online Databases      Chemistry WebBook

**Benzene, (trifluoromethyl)-**

- **Formula:**  $C_6H_5F_3$
- **Molecular Weight:** 146.11
- **CAS Registry Number:** 98-08-8
- **Chemical Structure:**

This structure is also available as a 2d Mol file.

- **Other Names:** Toluene,  $\alpha,\alpha,\alpha$ -trifluoro-;  $\alpha,\alpha,\alpha$ -Trifluorotoluene; (Trifluoromethyl)benzene; Benzyl fluoride; Benzo(trifluoride); Benzylidene fluoride; Phenylfluoriform;  $\alpha,\alpha,\alpha$ -Trifluorotoluene,  $\omega$ -Trifluorotoluene; USAF ma-16; UN 2338
- **Mass Spectrum**
- **References**
- **Notes / Error Report**
- **Other Data Available:**
  - Gas phase thermochemistry data
  - Condensed phase thermochemistry data
  - Phase change data
  - Reaction thermochemistry data
  - Henry's Law data

**Fig. 24.5** WebBook search results for trifluoromethylbenzene uploaded as in MDL molfile format.

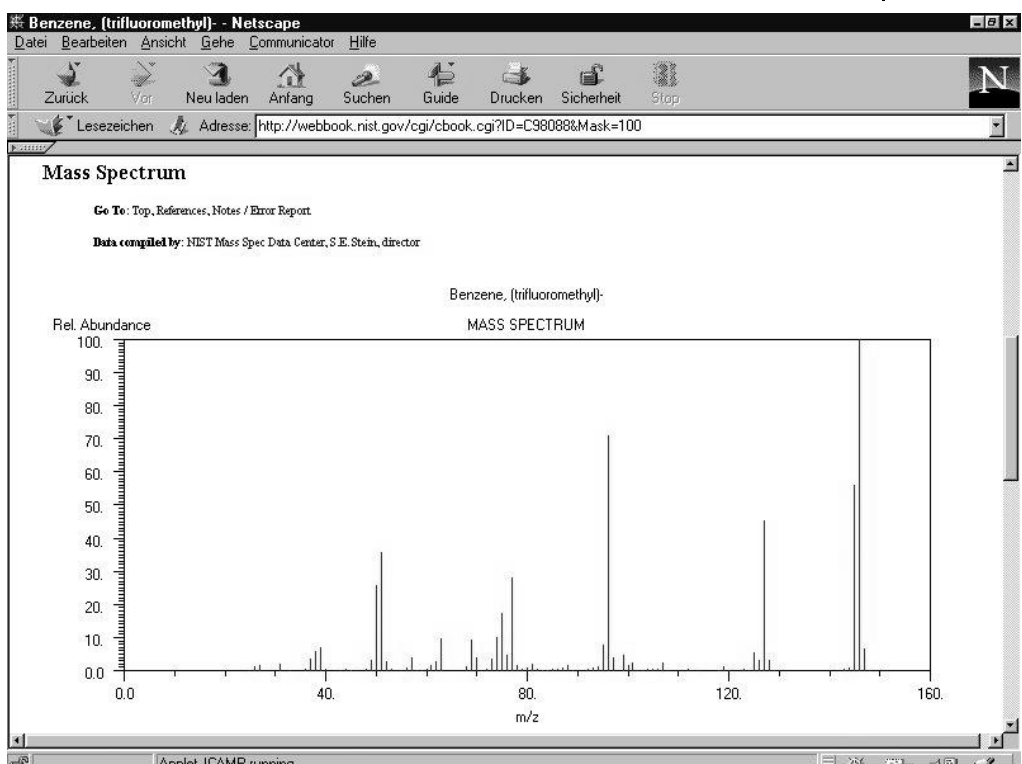


**Fig. 24.6** Mass spectrum hit results from a WebBook structure search. A Java Applet displays the JCAMP-DX file from NIST.

A static graphic file is also available in order to print off the spectrum in higher resolution than a screen capture if this is required. Additional information associated with this measurement is also displayed.

#### 24.3.7

#### General Spectroscopy Packages

The section would be incomplete if we were to leave out the general spectroscopy packages which are not MS specific but which have been receiving steady improvements over the years extending their capabilities to include mass spectrometry. Many of these packages originated in the optical spectroscopy or chromatography fields and have grasped the need to not only address but also be competent in other techniques (as have their users as this change has been demand led!).

Galactic Industries Corporation, famous for their ability to read a vast number of spectrometer manufacturer's data formats, has recently added a GC/MS Application Pack to its long-running GRAMS package (<http://www.galactic.com>).

The company creon LabControl mentioned above for their SpecSurf product also produces the versatile Spectacle package for many different types of spectroscopy including MS (<http://www.creonzlabcontrol.com>). As with Galactic their software can be found as an OEM product on several spectrometer control packages. They have also tackled the electronic records/electronic signatures rule and have a spectroscopic archiving product known as Q~DIS/R.

BioRad Sadtler have MS functionality built into their ChemWindow Spectroscopy package (<http://www.biorad.com>). This package is a reporting software with chemical/spectroscopic ability. The MS Tools are aimed at assisting mass spectra analysis by providing modules like producing lists of possible formulae or substructures for a given mass and fragmentation tool for studying fragmentation in proposed structures.

Last but not least ACDLabs have MS capability in their SpecManager product (<http://www.acdlabs.com>). Their MS module reads single spectra or GC/(LC)/MS data files and can be used for the subsequent analyses including ESI LC/MS minor components recovery, GC/MS separation of co-eluting components as well as structure/substructure formula generation from mass and ion data [24, 25].

#### 24.4

#### Biological Mass Spectrometry and General Works

Even within the scope of this chapter a quick discussion is required of the newest exciting field which has 'discovered' the power of linking mass spectrometric techniques with intelligent use of computerised data analysis which is biological mass spectrometry. Almost all of the systems above were developed with the analysis and characterisation of relatively uncomplicated chemical moieties in mind but rapid developments have been made especially in the application of mass spectrometric methods in the up-and-coming field of proteomics. For a review of the use of mass spectrometry and database searching in protein analysis for the identification of tryptic peptides see [26]. Additionally a review of electrophoretically separated enzyme digested protein analysis by peptide MS using under 1 pmol of sample and MALDI of electron ionisation methods has also been published [27].

Early attempts at applying chemometric methods to mass spectrometry data sets have been reported see for example [28, 29]. The potential and limitations of using multivariate classification methods for substructure analysis of low resolution mass spectra have also been published [30].

An interesting new reference work for practising mass spectroscopists is the new 'Desk Reference' by David Sparkman [16] which includes a substantial reference section entitled 'Correct and Incorrect Terms'. The information supplied here takes the form of sometimes quite extensive explanations on the correct and incorrect use of many of the phrases and terms in common use in mass spectrometry.

## References

- 1 A. N. Davies, P. S. McIntyre, Spectroscopic Databases, in *Computing Applications in Molecular Spectroscopy*, eds. W.O. George and D. Steele, 1995, The Royal Society of Chemistry, Cambridge 1995, pp. 41–59.
- 2 CAS, *Chemical Abstracts Service*, 2000, Columbus, OH 43210-0012, 2000.
- 3 NIST, *NIST '98 Mass Spectral Database*, National Institute of Standards and Technology, Gaithersburg, MD 1998.
- 4 S. R. Heller, Mass Spectrometry Databases and Search Systems, in *Computer Supported Spectroscopic Databases*, ed. J. Zupan, Ellis Horwood, Chichester 1986, pp. 118–132.
- 5 P. Ausloos, C. L. Clifton, S. G. Lias et al., *J. Am. Soc. Mass Spectrom.*, **1998**, *10*, 287–299.
- 6 Wiley, *Wiley Registry of Mass Spectral Data*, John Wiley & Sons, Chichester 1989.
- 7 F. W. McLafferty, D. B. Stauffer, A. B. Twiss-Brook et al., *J. Am. Soc. Mass Spectrom.*, **1991**, *2*(5), 432.
- 8 F. W. McLafferty, *Registry of Mass Spectral Data*, 5th edition, 1989, John Wiley & Sons, Chichester, 1989.
- 9 A. N. Davies, *Spectrosc. Eur.*, **2000**, *12*(1), 26–29.
- 10 K. Pfleger, H. Mauer, A. Weber, *Mass Spectral and GC Data of Drugs, Poisons, Pesticides, Pollutants and Their Metabolites*, 2nd edition, Wiley-VCH, Weinheim 1992, Vol. Parts 1–3 (Set).
- 11 D. Ehrenstorfer, *Library of Mass Spectra*, Dr. Ehrenstorfer GmbH: Augsburg, Germany 2000.
- 12 A. N. Davies, *Spectrosc. Eur.*, **1998**, *10*(3), 22–26.
- 13 A. N. Davies, *Spectrosc. Eur.*, **1993**, *5*(1), 34–38.
- 14 C. S. Tong, K. C. Cheng, *Chemometrics Intell. Lab. Syst.*, **1999**, *49*, 135–150.
- 15 S. Sokolow, J. Karnofsky, P. Gustafson, *Finnigan Application Report No. 2*, Finnigan, San Jose 1978.
- 16 O. D. Sparkman, *Mass Spectrometry Desk Reference*, 1st edition, Global View Publishing, Pittsburgh 2000, p.106.
- 17 F. W. McLafferty, R. H. Hertel, R.D. Villwock, *Org. Mass Spectrom.*, **1994**, *8*, 690–702.
- 18 K. S. Haraki, R. Venkataraghavan, F. W. McLafferty, *Anal. Chem.*, **1981**, *53*, 386–392.
- 19 F. W. McLafferty, S. Y. Loh, D. B. Stauffer, Computer Identification of Mass Spectra, in *Computer Enhanced Analytical Spectroscopy*, ed. H. L. C. Meuzelaar, Vol. 2. 1990, Plenum Press, New York 1990, Vol. 2, pp. 161–181.
- 20 F. Friedli, *MassLib. PC*, 2000, MSP KOFEL, Bindenhausstr. 46, CH-3098 Koeniz, Switzerland.
- 21 H. Damen, D. Henneberg, B. Weimann, *Anal. Chim. Acta*, **1978**, *103*, 289–302.
- 22 S. E. Stein, *J. Am. Soc. Mass Spectrom.*, **1999**, *10*, 770–781.
- 23 J. M. Halket, A. Przyborowska, S. E. Stein et al., *Rapid Commun. Mass Spectrom.*, **1999**, *13*, 279–284.
- 24 J. E. Biller, K. Biemann, *Anal. Lett.*, **1974**, *7*, 515–528.
- 25 A. Williams, *An Introduction to CODA: Integration into ACD/MS Manager*. Application Note , Advanced Chemistry Development, Toronto, Ontario 2000.

- 26** B. T. Chait, *Nat. Biotechnol.*, **1996**, *14*(11), 1544.
- 27** J. S. Cottrell, C. W. Sutton, *Methods Mol. Biol.*, **1996**, *61*, 67–82.
- 28** K. Varmuza, A. N. Davies, *Spectrosc. Int.*, **1990**, *3*(4), 14–17.
- 29** K. Varmuza, *Int. J. Mass Spectrom. Ion Processes*, **1992**, *118/119*, 811–823.
- 30** K. Varmuza, W. Werther, in *Advances in Mass Spectrometry*, eds. E. J. Karjalainen et al., Elsevier, Amsterdam 1998, Vol. 14, pp. 611–626.

## Index

### **a**

- 7-AAD 2/17
- absolute detection limit 1/378
- absorption 1/427
- absorption coefficient 1/40
- absorption index 1/74
- acceptor-donor-acceptor (A-D-A) dyes 2/58
- ACCORD-HMBC 1/244 ff
- accordion-optimized long-range heteronuclear shift correlation methods 1/244
- acetylcholine receptors 2/25
- acetylcholinesterase 2/21
- acyltransferase 2/21
- ACFs 2/483
- achievements 2/163 ff
  - atmospheric pressure chemical ionisation (APCI) 2/163
  - capillary electrophoresis (CE) 2/163
  - capillary zone electrophoresis (CZE) 2/163
  - electrospray ionisation (ESI) 2/163
  - obstacles 2/163 ff
  - TSP 2/163
- acquired immunodeficiency syndrome (AIDS) 2/47
- acridine orange 2/17
- acridinium ester 2/65
- acrylamide quenching 1/141
- actin
  - detection of cytoskeletal proteins 2/17
- activation energy
  - motional 1/278
  - rate constants 1/278
- active air collection methods 1/8
- active vs. passive sampling 1/8
- adenylate cyclase 2/24
- adrenergic receptors 2/25
- adsorbaste 1/553, 1/557
- adsorbate 1/508, 1/526 f, 1/560, 1/587, 1/591
- adsorption 1/519, 1/529, 1/531, 1/543, 1/545, 1/552, 1/580, 1/582
  - adsorption geometry 1/535
  - advantage
    - Connes 52
    - Felgett 1/52
    - and limitations 1/417
    - of TXRF 1/399
  - AEAPS (Auger electron appearance potential spectroscopy) 1/508
  - *Aequorea victoria* 2/58
  - aequorin 2/12
  - AES (Auger electron spectroscopy) 1/512, 1/591
  - affinity-proteomics 1/358
  - AIDS (acquired immunodeficiency syndrome) 2/47
  - Al<sup>3+</sup> 2/12
  - Aldrich 2/447
  - Alexa Fluor 2/15
  - Alexa Fluor dyes 2/51
  - alkaline phosphatase 2/50
    - enzyme labels 2/50
  - Alkemade 1/436
  - Alzheimer's disease 2/11, 2/13
  - amalgamation trap 1/451
  - AMDIS 2/495, 2/498
  - amino acid analysis 2/16
    - solid-phase synthesis 2/12
  - 9-amino-6-chloro-2-methoxyacridine 2/11
  - 7-aminocoumarins 2/20
  - 4-amino-5-methylamino-2',7'-difluoro-fluorescein (DAF) 2/14
  - aminopropylsilane 2/84
  - Amplex Red/resorufin 2/14
  - amplitude noise 1/405
  - amylase 2/20
  - analog-to-digital converter 1/387
  - analysis
    - of binding constants 2/128
    - environmental 2/152 ff
    - structural 1/98

- analytical sensitivity 1/376
- ANEП 2/19
- angiotensin II receptor 2/25
- angular dispersion 1/390
- anilides
  - groundwater 2/215
  - LC-MS/MS 2/215
  - natural waters 2/215
  - surface water 2/215
- anion receptors 2/69
- anisotropy 1/149, 1/151, 1/272
  - chemical shielding 1/271
  - dipolar coupling 1/271
- annexin V 2/26
- Anthozoa* species 2/58
- 9-anthroxyloxy 2/19
- n*-anthroxyloxy fatty acids 1/147
- antibody screening 2/6
- anticoagulant activity 2/24
- antifouling pesticides 2/225
  - LC-ICP-MS (inductive coupled plasma) 2/225
  - organotin 2/225
- antracene 2/70
- APCI (atmospheric pressure chemical ionisation) 2/183
  - anilides 2/192
  - antifouling 2/199
  - AEO 2/189
  - APEO
    - halogenated 2/191
  - biodegradation 2/195, 2/199
  - biological fluids 2/194
  - capillary zone electrophoresis (CZE) 2/186
  - carbamates 2/193
  - coconut diethanol amide (CDEA) 2/189
  - drugs
    - metabolites 2/184
  - drugs and diagnostic agents 2/184
  - dyes 2/186
  - estrogenic compounds 2/186
  - explosives
    - metabolites 2/187
  - FIA-MS 2/190
  - FIA-MS/MS 2/190
  - fruits 2/193, 2/197
  - fruit drinks 2/197
  - groundwater 2/192, 2/194, 2/196, 2/199
  - haloacetic acids 2/187
  - halogenated APEOs 2/191
  - herbicides 2/192
  - heterocyclic compounds 2/188
  - interlaboratory study 2/194
  - LAS 2/189, 2/191
- LC-MS 2/190
  - anilides 2/185
  - antifouling pesticides 2/185
  - carbamates 2/185
  - diagnostic agents 2/185
  - drugs 2/185
  - dyes 2/185
  - estrogenic compounds 2/185
  - explosives 2/185
  - fungicides 2/185
  - general 2/185
  - haloacetic acids 2/185
  - herbicides 2/185
  - industrial effluents 2/185
  - municipal wastewaters 2/185
  - organophosphorous compounds 2/185
  - pesticides 2/185
  - pharmaceuticals 2/185
  - phenoxy carboxylic acids 2/185
  - phenolic compounds 2/185
  - phenols 2/185
  - phenylureas 2/185
  - polycyclic aromatic hydrocarbons 2/185
  - quaternary amines 2/185
  - sulfonic acids 2/185
  - sulfonylureas 2/185
  - surfactants 2/185
  - thiocyanates 2/185
  - thioureas 2/185
  - toluidines 2/185
  - triazines 2/185
- LC-MS/MS 2/190
  - N-methyl carbamate pesticides 2/193
  - miscellaneous 2/199
  - MS/MS 2/195 f
  - MS/MS library 2/194
  - natural waters 2/198
  - NPEO 2/189
  - NPEO-sulfate 2/189
  - organophosphorus 2/194
    - biodegradation products 2/194
  - phenolic compounds 2/197
  - photodegradation 2/195
  - quantification 2/191 ff
  - pesticides 2/192
  - phenols 2/188
    - quantification 2/189
  - phenoxy carboxylic acids 2/195
  - phenylureas 2/196
  - polycyclic aromatic hydrocarbons (PAH) 2/187 f
  - quaternary amines 2/192
  - review
    - dyes 2/185

- general 2/185
- pesticides 2/185
- surfactants 2/185
- rivers 2/198
- river water 2/192 f, 2/199
- secondary alkane sulfonate (SAS) 2/189
- sediment 2/197
- sulfonylureas 2/196
- surface water 2/196, 2/198
- surfactants 2/189 f
- thiocyanates 2/192
- thioureas 2/196
- tin-containing pesticide 2/201
- toluidines 2/192
- triazines 2/197 ff
- triazole herbicides 2/199
- uncicides 2/192
- vegetables 2/193
- water 2/196 f, 2/198
- APCI-LC-MS/MS
- heterocyclic compounds 2/188
- phenols 2/188
- APD (avalanche photodiodes) 2/27
- APECS (Auger photoelectron coincidence spectroscopy) 1/557
- APFIM (atom probe field ion microscopy) 1/510
- API (atmospheric pressure ionization) 2/183 ff
- reviews 2/184
- apoptosis 2/11, 2/26
- applications
- special 1/103
- APS (appearance potential spectroscopy) 1/508
- aqueous matrices
- eluates of soil samples 2/153
- groundwater 2/153
- leachates 2/153
- surface waters 2/153
- wastewaters 2/153
- ARAES (angle resolved AES) 1/514
- Arc 1/477, 1/484
- ARC procedures 2/251
- argon ion laser 2/40, 2/27
- Argonne Protein Mapping Group 2/8
- ARIPES (angle resolved inverse photoemission spectroscopy) 1/536
- aromatic sulfonates 2/154
- ARPES (angle resolved photoelectron spectroscopy) 1/506
- artificial enzymes
- by molecular imprinting 2/71
- ARUPS (angle resolved ultraviolet photoemission spectroscopy) 1/506, 1/537, 1/584
- ARXPS (angle resolved X-ray photoelectron spectroscopy) 1/514, 1/587
- ascorbic acid 2/15
- atmospheric pressure chemical ionization (APCI) 2/183 ff
- atmospheric pressure ionization (API) 2/183 ff
- atom reservoir 1/434
- atomic absorption spectrometry 1/421 ff
- atomisation efficiency 1/441
- atomiser 1/440
- block diagram 1/437
- cold vapor generation technique 1/451 f
- direct sample introduction 1/452
- double beam spectrophotometer 1/453
- dynamic range 1/465
- electrothermal atomisation 1/443 ff
- external calibration 1/465
- flame atomisation 1/441
- flow injection 1/449
- instrumentation 1/436 ff
- laser ablation 1/452
- optical set-up 1/453
- quantitative analysis 1/465 ff
- quartz furnace 1/467
- quartz tube atomiser 1/449
- radiation sources 1/437 ff
- sample transfer efficiency 1/440
- single beam spectrophotometer 1/453
- solid sample introduction 1/452, 1/470
- standard addition technique 1/466
- transport efficiency 1/469
- vapour generation techniques 1/447 ff
- atomic spectroscopy, theory 1/421 ff
- atomisation 1/471
- atomiser 1/440
- ATP 2/20
- AT-Pases 2/20
- bioluminescent determination 2/20
- determination 2/65
- DNA 2/20
- GTPases 2/20
- in mitochondria 2/65
- RNA polymerases 2/20
- ATR (attenuated total reflection) 1/511
- correction 1/76
- technique 1/95
- -FTIR 2/92 ff
- in vivo monitoring of glucose 2/92
- attached proton test (APT) 2/471
- attenuated total internal reflection (ATR) 1/75, 2/75

- attenuation 1/402  
 Auger electron 1/369  
 Auger electron appearance potential spectroscopy (AEAPS) 1/508  
 Auger electron spectroscopy (AES) 1/512, 1/591  
 automatic gain control (AGC) 2/247  
 autoradiography 2/39  
 auxochrome 1/125  
 AV 2/29  
 avalanche photodiodes (APD) 2/27  
 avidin (AV) 2/29  
 azophenol 2/70
- b**  
 background correction 1/455 ff  
   – by wavelength modulation 1/462  
   – continuum source 1/456 f  
   – pulsed lamp 1/460  
   – self reversal 1/460 f  
   – Smith-Hieftje method 1/460 f  
   – two line 1/456 f  
   – Zeeman 1/458 ff  
 background emission 1/434  
 background interferences 2/252  
 bacterial luciferase genes ("Lux genes") 2/68  
 bacterial luciferases 2/65  
 bags 1/11  
 Balmer series 1/421  
 band shifts 1/109  
 bands  
   – characteristic 1/102  
 baseline 2/451  
 baseline correction 2/457  
   – batch processes 2/272  
   – continuous processes 2/272  
   – control charts 2/272  
   – feed-back control 2/269, 2/280  
   – feed-forward control 2/269, 2/280  
   – operational benefits 2/277  
   – statistical process control (SPC) 2/272  
 bathochromic effect 1/125  
 bathochromic shift 2/28  
 beenaker cavity 1/476  
 Beer-Lambert 1/89  
 Beer-Lambert law 1/40, 1/74, 2/75  
 bending modes 1/42  
 benz[e]indolium Sq660 2/35  
 benzindolium heptamethine cyanine dyes 2/34  
 benzofuranyl fluorophore 2/11  
 BHCT 2/56  
 BIA *see* real-time BioInteraction Analysis  
 BiaCore instrument 2/127
- BiaCore system 2/87  
 bioanalytical applications 1/344  
 bioinformatics 2/6  
 biological mass spectrometry 2/502  
 biological wastewater treatment  
   – alcohol ethoxylates (AOE) 2/175  
   – alkyl polyglucosides 2/175  
   – fluorine-containing surfactants 2/175  
 bioluminescent determination of ATP 2/20  
 bioluminescence 2/65  
 BioMEMS 2/131  
 biomolecular databases 2/8  
 biopolymer analysis 1/349  
   – sequence mutations 1/349  
 biosensor 2/3 ff  
   – calorimetric 2/5  
   – electrochemical 2/5  
   – optical 2/5  
   – piezoelectric 2/5  
   – technologies 2/5  
 biotin 2/29  
 BIS (Bremsstrahlung isochromat spectroscopy) 1/536  
 bis(alkylsiloxy)silyl complexes of naphthalocyanines (SiNPcs) 2/36  
 bisindolylmaleimides 2/24  
 bisoxonols 2/19  
 BLE (bombardment-induced light emission) 1/533  
 blood coagulation 2/4  
 blotting  
   – fluorescent strains for 2/15  
 blue-fluorescent N-methylanthraniloyl (MANT) 2/24  
 BODIPY 2/15 f, 2/16  
 BODIPY dyes 2/51  
 Bohr energy level 1/422  
 Boltzmann's law 1/426  
 boosted hollow-cathode lamp 1/438  
 Born-Oppenheimer approximation 1/41  
 Bremsstrahlung 1/372  
 Brewster angle 1/74, 2/83  
 bromacil 2/53  
 bromide  
   – ion, indicators for 2/13  
 Brookhaven protein data bank 2/7 f  
 bubblers 1/12  
 Bunsen 1/421, 1/436
- c**  
 Ca<sup>2+</sup> 2/12  
 Ca<sup>2+</sup> channel 2/25  
 CAE (capillary array electrophoresis) 2/39  
 calcein 2/12

- Calcium Green 2/12  
 calcium regulation 2/12, 2/23  
 calcium transport 2/12  
 calibration models 2/444  
 calibration tests 2/254  
 calibration  
   - Raman shift scale 1/60  
   - wavelength scale 1/65  
 calixarenes 2/69 f  
 calmodulin 2/23  
   - fluorescently labeled 2/23  
 Cambridge Crystallographic Database 2/8  
 candidate structures 2/481, 2/484  
 canisters 1/11  
 capacitively coupled microwave plasma (CMP) 1/476, 1/477  
 capillary array electrophoresis (CAE) 2/39  
 capillary column technology 2/255  
 capillary electrophoresis 1/346  
   - affinity chromatography 1/346  
   - atomic emission spectroscopy 1/492 ff  
   - capillary electrochromatography 1/346  
   - capillary isotachophoresis 1/346  
   - detection (CE-LIFP)  
     - laser-induced fluorescence polarisation 2/55  
   - mass spectrometry 1/348  
   - micellar electrokinetic chromatography 1/346  
 capillary gel electrophoresis 2/39  
 carbamates 2/177 ff, 2/193  
   - biological fluids 2/194  
   - drinking water 2/217  
   - estuarine waters 2/217  
   - groundwater 2/217  
   - hydrolytic degradation 2/217  
   - leaches of soil 2/217  
   - microbial degradation 2/217  
   - quantification 2/216 f  
   - natural waters 2/216  
   - river water 2/203, 2/217  
   - surface water 2/217  
 carbohydrate structures 1/351  
 carbon-centered fragment 2/473  
 carbonic anhydrase 2/13, 2/21  
 carboxyfluorescein 2/11  
 carriers 2/25  
 cartesian geometry 1/395  
 CAS 2/446  
 caspase protease activity 2/6  
 catalase 2/21  
 cation receptors 2/69  
 CBQCA 2/16  
 CCD (charge coupled device) 1/481  
 CCSD 2/9  
 CE *see* electrophoresis capillary  
 CEA *see* electrophoresis capillary array  
 CE-AES 1/492 ff  
 cell  
   - Alzheimer's disease 2/11  
   - apoptosis 2/11  
   - endocytosis 2/11  
   - gas 1/90  
   - homeostasis 2/11  
   - ion transport 2/11  
   - malignancy 2/11  
   - membrane-impermeant dyes, incl. stains for dead cells (SYTOX Dyes) 2/17  
   - muscle contraction 2/11  
   - multidrug resistance 2/11  
   - -permeant nucleic acid dye 2/17  
   - proliferation 2/11  
   - tracers  
     - microinjectable 2/57  
 cellular  
   - uptake of lipids 2/19  
   - diagnostics 2/15  
 cellulase 2/20  
 centering 2/442  
 CF-FAB 2/160 ff  
   - benzo[a]pyrene conjugates 2/161  
   - brominated surfactants 2/160  
   - carbamate 2/162  
   - collision-induced dissociation (CID) 2/162  
   - DNA adducts 2/161  
   - drinking water 2/160  
   - dyes 2/162  
   - explosives 2/161, 2/163  
   - flow injection analysis (FIA) 2/161  
   - metabolites of surfactants 2/160  
   - N-containing pesticides 2/162  
   - ozination 2/161  
   - PAH metabolites 2/162  
   - PAHs 2/163  
   - P-containing pesticides 2/162  
   - phenylurea 2/162  
   - products of surfactants 2/161  
   - raw 2/160  
   - seawater 2/160  
   - sulfonated azo dyes 2/161  
   - sulfonates 2/161  
   - surface water 2/160  
   - surfactants 2/160  
   - wastewater 2/160  
 chain conformation statistics 1/297  
 channeling-RBS 1/567  
 characteristic bands 2/452  
 charge coupled device (CCD) 1/481

- charge injection device (CID) 1/481  
charge structures 1/334  
charge transfer 2/251  
chemical abstracts service 2/489  
Chemical Concepts 2/491  
chemical exchange 2/111  
– in NMR 2/111  
chemical interferences 1/454, 1/462  
– in AES 1/487  
chemical ionization 1/331, 2/249, 2/261, 2/407  
chemical ionization process 2/262  
chemical modification 1/353  
chemical shift (CSA) 1/174, 1/272, 1/275, 1/281, 2/471  
chemical shift anisotropy (CSA) 1/174, 1/190, 1/270, 2/99  
– aromatic 1/190  
– dependence on bonding 1/190  
– interaction 1/187, 2/116  
– of  $^{15}\text{N}$  2/116  
– methyl sites 1/190  
– olefinic 1/190  
CHEMICS 2/483  
chemiluminescence 2/65  
Chemometrics Toolbox 2/467  
ChemWindow Spectroscopy 2/502  
chitinase 2/20  
chloride  
– ion, indicators for 2/13  
Cholera Toxin 2/21  
cholesterols 2/15, 2/69  
choline glutamate 2/21  
ChromaTide nucleotides 2/18  
chromoionophore 2/70  
chromophores 2/10, 1/125  
– UV/VIS 2/10  
– near-IR 2/10  
CI conditions 2/249 ff, 2/255  
CI ion source 2/261  
CI ionization processes 2/265  
CI mass spectrometry 2/260, 2/262  
CI process 2/250, 2/261  
CI techniques 2/260  
CID (charge injection device) 1/481  
CID procedure 2/257  
CID process 2/253 f  
CIGAR-HMBC 1/247  
circular dichroism (CD) 1/82, 2/6, 2/93 ff  
circulatory serine proteases 2/24  
classical least squares (CLS) 2/459  
clinical diagnostics 2/4  
CLS 2/459  
cluster analysis 2/455  
CMP 1/476  
 $\text{CN}^-$  2/14  
 $^{13}\text{C}$ -NMR spectrum prediction 2/473  
CODEX  $^{13}\text{C}$  NMR 1/292  
– correlation time 1/292  
– mobile segments 1/292  
– reorientation angle 1/292  
cold vapor generation technique 1/451 f  
collection and preparation of gaseous samples 1/4  
collection and preparation of liquid and solids 1/17  
collision induced dissociation (CID) 2/253  
collisional deactivation 2/250  
collisional quenching 1/45, 1/141, 1/157  
collisional-induced dissociation (CID) 1/337, 2/126  
colloidal gold 2/16, 2/89  
COLOC 2/471  
combinatorial chemistry 2/69  
combined rotation and multiple pulse decoupling (CRAMPS) 1/175, 1/287  
complexing agents 2/154  
compounds  
– atmospheric-pressure chemical ionisation 2/152  
– non-volatile 2/152  
– polar 2/152  
– thermolabile 2/152  
– volatile 2/153  
Compton equation 1/371  
Concanavalin A 2/21  
conclusions 2/226  
confocal 1/138, 1/155  
confocal microscopes 1/85  
conformation  
– molecular 1/578  
conformational states 1/349  
 $\alpha$ -conotoxin probes 2/25  
continuous flow FAB (CF-FAB) 2/160  
continuum source background correction 1/456 f  
continuum sources 1/439  
conventional mass spectrometers 2/251  
Coomassie Blue 2/16  
CoroNa Red 2/11  
correlated spectroscopy (COSY) 2/105, 2/471  
correlation 2/451  
correlation by long-range couplings (COLOC) 2/471  
COSY (homonuclear correlated spectroscopy) 1/173, 1/223 ff, 2/471  
COSY/GCCOSY 1/224  
COSY-type spectra 2/483

- coumarin's 2/15  
 coumarine 2/70  
 counting rate 1/405  
 counting statistics 1/404  
 coupling  
   – constants 2/471  
   – dipolar 1/276  
   –  $^2\text{H}$  quadrupolar 1/278  
   – quadrupolar 1/276  
 CP 1/281 f  
   – ramped 1/282  
 CP MAS 1/284  
 CPAA (charge particle activation analysis) 1/516  
 CRAMPS 1/175, 1/287  
 creatinine 2/69  
 critical angle of total reflection  $\emptyset_{\text{crit}}$  1/398  
 critical penetration depth 1/402  
 critical thickness 1/402, 2/79  
 croconine dyes 2/34  
 cross polarisation (CP) 1/281  
 cross validation 2/461  
 cross-relaxation experiments 2/110  
 cryogenic trapping 1/13  
 cryotrapping-AAS 1/468  
 crystal field 1/133  
 crystal spectrometer 1/391  
 crystallography  
   – chemical species specific 1/592  
   – chemical state specific 1/587  
   – element specific 1/587, 1/592  
 CSA (chemical shift) 1/272, 1/174, 1/275,  
   1/281, 2/471  
   – carboxyl group 1/272  
   – CODEX 1/291  
   – isotropic chemical shift 1/281  
   – isotropic spectra 1/281  
   – slow dynamic processes 1/291  
   – tensors 1/272  
 CSEARCH 2/483  
 cut-off thickness 2/79  
 Cy<sup>TM</sup>dyes 2/31  
 Cy3<sup>TM</sup> 2/31  
 Cy3NOS 2/31  
 Cy5<sup>TM</sup> 2/31  
 cyanide  
   – determination of 2/14  
   – in blood 2/14  
 cyanine dimers 2/17  
 cyanine dyes 2/17  
 cyclic AMP 2/71  
 cyclic nucleotides 2/24  
 cynine dyes 2/15  
 cysteine 2/15  
 cystic fibrosis 2/13  
 cysticercoisis 2/47  
 cytochrome c  
   – electron-transfer reaction in 2/86  
 cytochrome P-450 2/22  
 cytological staining 2/15
- d**
- Danish Center for Human Genome Research 2/9  
 dansyl chloride 2/16  
 dansyl fluorophores 2/19  
 DAPS (disappearance potential spectroscopy) 1/508  
 DARC 2/483  
 data analysis 2/445  
 data extraction in EDXRF 1/407  
 data extraction in WDXRF 1/406  
 data processing  
   – Fourier transformation 1/187  
   – phasing 1/187  
   – smoothing function 1/187  
 data treatment 1/404  
 databases  
   – spectral 1/99  
 DC arc 1/477, 1/484  
 DCIP 2/14  
 DCP 1/475  
 debsyl chloride 2/16  
 decomposition of organics 1/28  
   – ashing 1/28  
 deconvolution 2/391 f  
 decoupling 1/283  
   – CW 1/283  
   – TPPM 1/283  
 deformation vibrations 1/42  
 degeneration factor 1/428  
 DELFIA system 2/55  
 DENDRAL 2/483  
 density of states 1/537, 1/551  
 DEPT (distortionless enhancement polarization transfer) 1/215, 2/471, 2/482  
 depth profiling 1/512, 1/531, 1/546 f, 1/563,  
   1/565, 1/572, 1/589  
 descriptive proteomics 2/126  
 detection and determination limits 1/377  
 detection limits 1/418  
 detection of human IgG 2/53  
 detectors 1/59, 1/53, 1/389  
   – array 1/53  
   – DTGS 1/53  
   – MCT 1/53  
   – multichannel 1/61, 1/67  
   – single channel 1/57

- determination limit 1/378  
deuteration 2/98  
– in NMR 2/98  
deuterium effect 1/143  
deuterium lamp 1/439, 1/456 f  
2D exchange 1/303  
– isotactic polypropylene 1/303  
– tropolone 1/303  
DFT 2/28  
2D-gel electrophoresis 1/357  
diabetes 2/6  
diabetes mellitus 2/69  
diagnostic agents 2/154  
diagnostics  
– clinical 2/4  
– drug discovery 2/4  
2,3-diaminonaphthalene 2/13, 2/14  
dichlorodihydrofluorescein diacetate 2/26  
dichlorofluorescein 2/11  
2,4-dichlorophenoxyacetic acid (2,4-D)  
luminol/HRP system 2/65  
dielectric interface 2/72  
3,3'-diethyloxadicarbocyanine (DODC) 2/34  
difference interferometer 2/83  
diffuse reflection 1/78  
diffuse reflection infrared Fourier transform  
spectroscopy (DRIFTS) 1/518  
difluorofluoresceins (Oregon Green) 2/11  
dilute liquid crystals 2/99  
diode array UV *see* Photodiode array detection  
diode laser source 1/440  
diode lasers 2/10, 2/27  
1,2-dioxetane derivatives 2/65  
dioxins 2/257  
dipolar coupling (D) 1/174  
dipolar interaction 1/188 f  
– definition 1/188  
– Pake doublet 1/188  
– powder pattern 1/189  
direct (or second-element)  
enhancement 1/404  
direct current plasma 1/475  
direct-excitation configuration 1/393  
direct insertion 1/483  
direct liquid introduction (DLI) 2/153, 2/156  
direct sample introduction 1/452  
disappearance potential spectroscopy  
(DAPS) 1/508  
discoidal bilayered structures 2/99  
– in NMR 2/99  
*Discosoma* 2/58  
discriminant analysis 2/455  
dissociation energy 1/434  
dissociation equilibrium 1/463  
dissociation of molecules in a plasma 1/434  
distortionless enhancement polarization  
transfer (DEPT) 1/215, 2/471, 2/482  
5,5'-dithiobis-(2-nitrobenzoic acid) 2/14  
2D *J*-resolved NMR 1/219  
DLI  
– herbicides 2/156  
– pesticides 2/156  
2D MQMAS 1/317  
– glasses 1/317  
– isotropic shifts 1/317  
– microporous materials 1/317  
– minerals 1/317  
2D multiple quantum magic angle spinning  
(MQ/MAS) 1/176  
DNA 2/10  
– analysis 2/7  
– arrays and microarrays 2/18  
– polymerase 2/38  
– sequencing 2/10, 2/39  
2D NMR  
– homonuclear  $^{13}\text{C}$ - $^{13}\text{C}$  2D correlation  
experiments 1/293  
3D NMR 1/173, 1/204  
– connectivity information 1/206  
– HNCA pulse sequence 1/204  
DODC 2/33  
domain structure 1/569  
1D (one-dimensional) NMR 1/210  
donor/acceptor 1/152  
donor-acceptor-donor (D-A-D) dyes 2/58  
dopamines 2/15, 2/71  
doppler line broadening 1/430  
double beam atomic absorption  
spectrophotometer 1/453  
double bond  
– conjugated 1/129  
double rotation (DOR) 1/176  
double-focusing 1/336  
double-quantum filtered (2QF) COSY  
experiment 2/107  
double-quantum spectroscopy 1/295  
– BABA 1/295  
2D PASS 1/303  
DPH 1/151  
DQ spectroscopy 1/297  
–  $^{31}\text{P}$ - $^{31}\text{P}$  DQ MAS 1/297  
DRIFTS (diffuse-reflectance (or reflection)  
infrared Fourier transform  
spectroscopy) 1/518  
drinking water 2/256  
drug discovery 2/5  
drugs 2/154  
– ESI-LC-MS/MS 2/203

- MS/MS 2/204
- quantification 2/203 f
- wastewater 2/204
- X-ray contrast media 2/204
- DsRed 2/58
- DTNB 2/14
- dyes 2/154, 2/173, 2/205
- CZE 2/205
- MS/MS 2/206
- wastewater 2/206
- dynamic 1/140 f, 1/198
- -angle spinning (DAS) 1/176
- proteomics 2/126
- quenching 1/141
- range of motional 1/198
- solid-state  $^2\text{H}$  NMR 1/198
  
- e**
- easily ionisable element (EIE) 1/465
- echelle grating 1/439, 1/480
- echelle spectrograph 1/481 ff
- E-COSY 2/107
- edited experiments 2/117
- EDX (energy dispersive X-ray analysis) 1/524, 1/567
- ED-XRF instrumental configurations 1/393
- EEAES (electron excited Auger electron spectroscopy) 1/512
- EELFS, EXELFS (extended electron energy loss fine structure) 1/529, 1/535, 1/562
- EELS *see* HREELS
- effective path length 2/76
- EI conditions 2/253
- EI interferences 2/249
- EI scan program 2/248
- EI spectra 2/248
- EI/CI ion source 2/252
- Einstein coefficients 1/427 ff
- Einstein transition probability 1/427
- ejection techniques 2/252
- elastic or Rayleigh scattering 1/371
- electroanalysis 2/3
- electrochemically generated chemiluminescence (ECL) 2/65
- electrochemiluminescence 2/65
- electrodeless discharge lamp (EDL) 1/439
- electromagnetic spectrum 1/367
- electromagnetic wave 1/39 f
- electron ionisation 1/331
- electron pressure in a plasma 1/433
- electron temperature 1/435 f
- electronic states 1/508, 1/584
- electronic structure 1/539, 1/543, 1/571, 1/577
- electrophoresis
  - capillary 2/4
  - capillary array 2/4
  - gel 2/4
- electroreflectance 1/561
- electrospray (ESI) MS 2/122
- electrospray ionization (ESI) 1/329, 1/333, 2/201 ff
- electrospray ionization mass spectroscopy (ESI-MS) 2/123
- electrothermal atomisation 1/443 ff
- electrothermal vaporisation 1/483, 1/484
- element analysis *see* process analysis
- elemental composition 1/509 f, 1/513, 1/516, 1/524, 1/540, 1/543, 1/548, 1/556, 1/565 ff, 1/574, 1/589
- elemental distribution 1/548, 1/554, 1/569
- ELF *see* enzyme-labeled fluorescence
- ELISA (enzyme-linked immunosorbent assay) 2/50
- ellipsometric sensors 2/82
- ellipsometry 1/528, 2/82
- Ellman's reagent 2/14
- emission spectrum 1/382
- EMPA (electron microprobe analysis) 1/524
- EMS (electron momentum spectroscopy) 1/522
- end-fire coupling 2/82
- endocrine disrupting chemicals (EDC) 2/87
- endocytosis 2/11
- endogenous glycosidase activity 2/20
- endoplasmic reticulum 2/22
- probes for 2/22
- energy level diagram 1/425
- energy noise 1/405
- energy-dispersive XRF 1/393
- energy-gap law 1/143
- enhanced Raman scattering 1/119
- enhancement 1/403
- environmental analysis 2/254
- environmental monitoring 2/5
- Environmental Protection Agency 2/447
- environmental waters
  - antibiotic 2/203
  - sulfonamides 2/203
  - tetracyclines 2/202
- enzymatic exopeptidolytic cleavage 1/351
- enzyme-labeled fluorescence (ELF) 2/15
- enzyme-linked immunosorbent assay (ELISA) 2/50
- EPA methods 2/256
- EPECS (Auger photoelectron coincidence spectroscopy) 1/514
- epifluorescence 1/155

- epilepsy 2/13
- EPIOS 2/483
- epitope analysis 2/128
- epitope mapping 2/6
- EPMA (electron probe microanalysis) 1/524, 1/567
- EPXMA (electron probe X-ray Microanalysis) 1/524
- ERCS (elastic recoil coincidence spectroscopy) 1/522
- ERDA or ERD (elastic recoil detection (analysis)) 1/520
- ESCA [electron spectroscopy for chemical applications (originally analysis)] 1/587
- ESD (electron stimulated desorption) 1/525
- ESDIAD (electron stimulated desorption ion angular distributions) 1/526
- ESI (electrospray ionization) 1/329, 1/333, 2/200 ff
  - AEO 2/209 f
  - agricultural soil 2/222
  - alcohol ethoxylate (AEO) 2/213
  - alkyl etoxysulfates (AES) 2/211
  - alkylphenols 2/208
  - alkyl polyglucoside 2/212
  - alkyl sulfates (AS) 2/211
  - anilides 2/215
  - antibiotic 2/203
  - azo dyes 2/206
  - biodegradation 2/212
  - bisphenol A 2/208
  - CE-MS 2/213
  - chemical degradation 2/222
  - coastal waters 2/211
  - coconut diethanol amide (CDEA) 2/213
  - complexing agents 2/203
  - crop 2/222
  - CZE 2/205
  - degradation products 2/220, 2/222 f
  - diagnostic agents 2/203
  - disinfection byproducts 2/207
  - drinking water 2/203, 2/217 ff, 2/223
  - drugs 2/203
  - ditallow-dimethylammonium chloride (DTDMAC) 2/212
  - dyes 2/205
    - metabolites 2/205
  - EDTA 2/203
  - effluents 2/211
  - electropherogram 2/200
  - estrogenic compounds 2/206
  - estuaries 2/212
  - estuarine waters 2/217, 2/220 f
  - explosives 2/206
- fruits 2/222
- fungicides 2/215
- German Bight 2/212
- groundwater 2/217 ff, 2/223
- haloacetic acids 2/207
- halogenated APEO 2/211
- halogenated NPEO 2/210
- herbicides 2/215
- hydrolytic degradation 2/217
- imidazolinone herbicides 2/225
- insource-CID 2/211
- ion chromatograph 2/214
- LAS 2/212 f
- LC-MS 2/202, 2/213
  - anilides 2/202
  - antifouling pesticides 2/202
  - carbamates 2/202
  - complexing agents 2/202
  - drugs and diagnostic agents 2/202
  - dyes 2/202
  - estrogenic compound 2/202
  - explosives 2/202
  - fungicides 2/202
  - haloacetic acids and disinfection byproducts 2/202
  - herbicides 2/202
  - organoarsenic compounds 2/202
  - organophosphorus compounds 2/202
  - pesticides 2/202
  - phenols 2/202
  - phenolic pesticides 2/202
  - phenoxycarboxylic acids 2/202
  - phenylureas 2/202
  - polycyclic aromatic hydrocarbons 2/202
  - quaternary amines 2/202
  - sulfonic acids 2/202
  - sulfonylureas 2/202
  - surfactants 2/202
  - thiocyanate compounds 2/202
  - thioureas 2/202
  - toluidines 2/202
  - toxins 2/202
  - triazines 2/202
- leaches of soil 2/217
- metabolites 2/209 f, 2/222, 2/224
- N-methylglucamides 2/212
- microbial degradation 2/217
- miscellaneous 2/225
- MS/MS 2/204, 2/206 f, 2/209 ff, 2/216, 2/219, 2/221, 2/224 f
- natural waters 2/221
- neutral loss (NL) 2/209 f
- NPEO sulfates 2/213
- organoarsenic compounds 2/207

- perfluorooctanesulfonate (PFOS) 2/212
  - perfluorooctanoic acid (PFOA) 2/212
  - pesticides 2/215
  - phenols 2/208
  - photolysis products 2/222
  - quantification 2/203 ff
  - quaternary amines 2/215
  - quaternary ammonium compounds 2/214
  - neutral loss (NL) 2/209
  - nonylphenolpolyether carboxylate (NPEC) 2/210
  - North Sea 2/212
  - NPEO 2/209 ff
  - OPEO 2/211
  - photolysis 2/224
  - physicochemical degradation 2/224
  - review
    - dyes 2/202
    - general 2/202
    - pesticides 2/202
    - surfactants 2/202
    - sulfonates 2/202
    - toxines 2/202
  - river water 2/203, 2/217, 2/221, 2/223
  - sea water 2/212
  - secondary alkane sulfonates (SAS) 2/213
  - sediment 2/212
  - SFC-MS 2/223
  - sulfonamides 2/203
  - sulfonates 2/200
  - sulfonic acids 2/208
  - surface water 2/217 ff
  - surfactants 2/209
  - tetracyclines 2/202
  - thiocyanate compounds 2/215
  - toluidines 2/215
  - toxins 2/213
  - Waddensea marinas 2/212
  - wastewater 2/203, 2/204, 2/206, 2/210 f, 2/218
  - wastewater inflows 2/211
  - water 2/220
  - X-ray contrast media 2/204
  - ESI-LC-TOFMS
    - aromatic sulfonamides 2/204
    - sulfonates 2/204
    - textile wastewater 2/204
  - ESI-MS (electrospray ionization mass spectroscopy) 2/123
  - esters 2/11
  - estrone-3-glucuronide (E3G) 2/87
  - ethidium bromide 2/17
  - Euclidean distance 2/449, 2/472
  - eupropium chelates 2/56
  - evaluation of spectra 2/444
  - evanescent field 1/75 f
  - penetration depth 1/76
  - evanescent wave spectroscopy 2/71
  - evanescent wave-based techniques 2/69
  - EWCRDS (evanescent wave cavity ring-down spectroscopy) 1/530
  - EXAFS (extended X-ray absorption fine structure) 1/529, 1/535, 1/562, 1/584
  - excimer 1/154
  - excitation shift 1/146
  - excitation temperature 1/429, 1/435 f
  - EXELFS (extended energy loss fine structure) 1/529
  - ExPASy *see also* expert protein analysis system 2/8
  - expert protein analysis system 2/7
  - explorative data analysis 2/444
  - explosives 2/154
    - degradation 2/207
    - degradation products 2/206
    - groundwater 2/206
    - quantification 2/207
  - EXSY (EXchange SpectroscopY) 1/231
  - external ion sources 2/252 f
  - extraction and preparation of samples 1/14
- f**
- FAB (fast-atom bombardment mass spectrometry) 1/333, 1/574, 2/160 ff
  - benzo[a]pyrene conjugates 2/161
  - brominated surfactants 2/160
  - carbamate 2/162
  - collision-induced dissociation (CID) 2/162
  - DNA adducts 2/161
  - drinking water 2/160
  - dyes 2/162
  - explosives 2/161, 2/163
  - flow injection analysis (FIA) 2/161
  - metabolites of surfactants 2/160
  - N-containing pesticides 2/162
  - ozination 2/161
  - PAH metabolites 2/162
  - PAHs 2/163
  - P-containing pesticides 2/162
  - phenylurea 2/162
  - products of surfactants 2/161
  - raw 2/160
  - seawater 2/160
  - sulfonated azo dyes 2/161
  - sulfonates 2/161
  - surface water 2/160
  - surfactants 2/160
  - wastewater 2/160

- FAD 2/63
- FAM 2/40
- far-red 2/10
- fassel 1/473
- fast atom bombardment (FAB) 1/333, 1/574, 2/160 ff
- fatty acids 2/15
- FCS 2/19
- $\alpha$ -fetoprotein (AFP) 2/61
- FIA (flow injection analysis) 2/65
- FIA-AES 1/492 ff
- FIA-MS
  - surfactants 2/175
- FIA-MS/MS
  - surfactants 2/175
- fiber and waveguide SPR 2/88
- fiber optics 2/82
- fibronectin 2/24
- field desorption 1/332
- field effect transistor 1/387
- figures-of-merit 1/376
- films
  - Langmuir-Blodgett films 1/529, 1/560, 2/91
- filter
  - notch 1/62
  - Rayleigh 1/61
- filtered experiments (in NMR) 2/117
- FIM (field ion microscope) 1/541
- fingerprinting capabilities 2/255
- firefly luciferase 2/65
- FISH (fluorescence in situ hybridization) 2/18
- FITC see fluorescein isothiocyanate
- Fiveash Data 2/447
- flame AAS 1/441
  - burning velocity 1/443
  - gas mixtures 1/443
  - oxidising flame 1/443
  - reducing flame 1/443
- flame atomisation 1/441
- flame atomiser 1/471
- flavinmononucleotide (FMNH<sub>2</sub>) 2/65
- flow cytometry 1/135, 1/138, 1/153, 2/15
  - standardization reagents
- flow injection analysis (FIA) 2/65
- flow injection analysis and atomic emission spectroscopy 1/492 ff
- fluorescamine 2/16
- fluorescein casein 2/20
- fluorescein diacetate 2/11
- fluorescein isothiocyanate 2/29
- fluorescein's cyanines 2/15
- fluoresceins 2/28
- fluorescence 1/138
  - correlation spectroscopy (FCS) 1/155, 2/19
  - detection in HPLC 2/395 ff
  - enzyme-labeled 2/15
  - laser-induced 2/4, 2/39
  - lifetime 1/139, 2/28
  - polarisation 1/148, 1/151
  - polarisation immunoassay (FPIA) 2/55
  - polarisation spectroscopy 2/54
  - quencher 1/139
  - recovery after photobleaching (FRAP) 1/155, 2/19
  - resonance energy transfer (FRET) 1/152 f, 2/35, 2/56
  - sensors 1/156
  - spectroscopy 2/7
  - time-resolved 2/10
- fluorescent
  - dye loaded micro- and nanoparticles 2/15
  - dyes 2/7
  - enzymes 2/7
  - isothiocyanates 2/16
  - latex particles 2/15
  - polymixin B analogs 2/24
  - probes 2/10 f
  - proteins 2/7
- fluorescently labeled calmodulin 2/23
- fluoride
  - ion, indicators for 2/13
- fluorinated fluoresceins 2/51
- fluorophores 2/10
  - fluorophores
    - near-IR 2/10
    - visible 2/10
- FluoZin 2/13
- FMIR (frustrated multiple internal reflection) 1/511
- food analysis 2/5
- foot-and-mouth disease virus 2/87
- forbidden transition 1/375
- forward search 2/496
- Fourier transform infrared spectrometry (FTIR) 2/92 ff
- conformational changes in proteins 2/92
- protein unfolding 2/92
- secondary structure content 2/92
- Fourier transform ion cyclotron resonance (FTICR) detector 2/124
- Fourier transform ion cyclotron resonance instruments 2/124
- Fourier transform ion cyclotron resonance spectrometer (FT-ICR) 2/127

- FPA 1/53  
 fragmentations 1/350  
 Franck-Condon factor 1/45  
 Franck-Condon state 1/45, 1/144  
 FRAP 2/19  
 free induction decay (FID) 1/186  
 frequencies  
 – characteristic 1/99  
 – group 1/99  
 Fresnell equations 2/72  
 FRET 2/35  
 frustrated total internal reflection (FTR) 2/81  
<sup>19</sup>F solid-state NMR 1/287  
 – biomembranes 1/287  
 – fluoropolymers 1/287  
 FT RAIRS (Fourier transform reflection-absorption infrared spectroscopy) 1/559  
 FTIR (Fourier transform infrared spectrometry) 2/92 ff  
 – in vivo monitoring of glucose 2/92  
 FTIR microscopy 2/92 ff  
 – in vivo monitoring of glucose 2/92  
 FTIRRAS *see* IRRAS  
 full scan monitoring 2/251  
 full spectra search 2/448  
 full width at half of the maximum peak height (FWHM) 1/182  
 Fullerenes 2/387  
 functional genomics 2/3 ff  
 fundamental parameter method 1/414  
 fundamental parameter technique 1/410  
 fura-2 2/12  
 furans 2/257  
 Fura-Zin 2/13
- g**  
 GABA<sub>A</sub> receptor 2/25  
 galactic 2/447  
 galactose 2/21  
 gallium-aluminium-arsenide laser diode 2/27  
 gas chromatography and atomic emission spectroscopy 1/491 ff  
 gas chromatography-atomic absorption spectrometry (GC-AAS) 1/467 ff  
 gas chromatography coupled with mass spectrometric detection (GC-MS) 1/34, 2/251 f  
 gas chromatography/ion trap mass spectrometry (GC/ITMS) 2/244 ff, 2/251 ff, 2/255 ff, 2/262, 2/265  
 gas flow proportional counters 1/384  
 gas phase ionisation 1/331  
 gas temperature 1/435 f  
 GC ion trap mass spectrometer 2/245  
 GC/chemical ionization-ITMS 2/260  
 GC/CI MS 2/251  
 GC/EI MS 2/251  
 GC/EI-ITMS analyses 2/252  
 GC/ITMS 2/245, 2/247, 2/251 ff, 2/255 ff, 2/259, 2/262, 2/265  
 GC/MS 1/344, 2/251 f  
 GC/MS acquisition 2/247  
 GC/MS experiments 2/248  
 GC/MS quadrupole-based systems 2/244  
 GC/MS/MS 2/253  
 GC/MS/MS procedures 2/251  
 GC/MS/MS ion traps 2/254  
 GC-AES 1/491 ff  
 GC-MS (gas chromatography coupled with mass spectrometric detection) 2/152  
 – analysis 2/153  
 GCOSY 1/173  
 GDMS (glow discharge mass spectrometry) 1/533  
 GDOES (glow discharge optical emission spectrometry) 1/531  
 GE *see* electrophoresis gel  
 gel electrophoresis 2/39  
 gene expression 2/13  
 gene probes 2/10  
 genome 2/8  
 – map of the human 2/8  
 – project, human 2/3  
 genomics 2/3 ff  
 – functional 2/4  
 – polymorphism 2/4  
 gentamicin 2/87  
 GHMBC 1/173  
 GHMQC 1/173  
 GIS (grazing incidence spectroscopy) 1/559  
 GIXFR (grazing incidence X-ray fluorescence) 1/581  
 GIXFR (grazing-exit X-ray fluorescence) 1/581  
 glowbar 1/50  
 glow discharge 1/479  
 glucose 2/69  
 glucose oxidase 2/14  
 glucose-6-phosphate dehydrogenase 2/14  
 glucuronidase 2/20  
 β-glucuronidase 2/20  
 glutathione 2/14  
 glutathione transferase 2/14  
 glutathione 2/15  
 glycosidase 2/20  
 – endogenous activity 2/20  
 glycosylations 1/351  
 Golgi apparatus 2/22

- probes for 2/22
- gradient 1/232 f
- gradient 1D NOESY 1/255
- gradient experiments 1/233
  - GCOSY 1/233
  - GNOESY 1/233
  - GTOCSY 1/233
- GRAMS 2/467, 2/501
- graph theory 2/482
- graphite furnace (atomiser) 1/443 ff
- graphite furnace, L'vov platform 1/445
- graphite furnace, temperature profile 1/446
- graphite furnace, temperature program 1/447
- grating couplers 2/81, 2/83
- green fluorescent proteins 2/15, 2/58
- Greenfield 1/473
- Grimm 1/479
- Grotrian diagram 1/425
- group frequencies 1/44, 1/100, 2/452
  
- h**
- Hahn echo 2/104
- half width of atomic lines 1/437 f
- half-integer quadrupole nuclei 1/315
  - fourth-rank anisotropic broadening 1/315
  - second-order quadrupolar broadening 1/315
- haloacetic acids 2/154
- hard ionisation 1/331
- <sup>1</sup>H decoupling 1/282
  - TPPM 1/282
- <sup>1</sup>H DQ MAS
  - hydrogen-bonded protons 1/306
  - kinetics of hydrogen bond breaking and formation 1/306
  - order parameter 1/306
  - proton-proton distances 1/306
- HEIS (high energy ion scattering) 1/543, 1/565
- Helicobacter Pylori 2/54
- helium-neon laser 2/40
- hemicyanine dyes 1/143
- hemoglobin 2/69
- HeNe laser 2/31
- heparin 2/24
- heparin-binding growth factors 2/24
- 4,4'-bis (1',1',1',2',2',3',3',heptafluoro-4',6'-hexanedion-6'-yl)-chlorosulfo-o-terphenyl (BHHCT) 2/56
- herbicides
  - benzidines 2/154
  - carbamates 2/154
  - chlorinated 2/154
- quaternary ammonium 2/154
- phenoxyacetic acid 2/154
- triazine 2/154–
- heterogeneity 1/417
- heterogeneous catalysis 1/582
- heteronuclear 2D correlation (HETCOR) 1/176
- heteronuclear correlation (HETCOR) 1/307
  - <sup>1</sup>H-<sup>13</sup>C WISE (wideline separation) 1/307
- heteronuclear MQC (HMQC) 1/307
- heteronuclear SQC (HSQC) 1/307
- homonuclear decoupling in *t*<sub>1</sub> 1/307
- recoupled polarisation transfer (REPT) 307
- rigid and mobile chemical moieties 1/307
- heteronuclear correlation spectroscopy 2/96 ff
- heteronuclear dipolar couplings 1/310
  - dipolar couplings 1/310
  - internuclear distances 1/310
  - REPT 1/310
- heteronuclear multiple bond correlation (HMBC) 2/471
- heteronuclear multiple quantum coherence (HMQC) 2/114 ff, 2/471
- heteronuclear NMR experiments 2/94 ff, 2/113
- heteronuclear shift correlation 1/234
- heteronuclear single quantum coherence (HSQC) 2/471
  - <sup>1</sup>H-<sup>1</sup>H DQ MAS
- BABA recoupling sequence 1/305
- dipolar coupling constant 1/305
- spinning-sideband patterns 1/305
- HIAA (high energy ion activation analysis) 1/516
- high-performance liquid chromatography (HPLC) 2/10
- high-resolution gas chromatography (HRGC) 2/257
- high-resolution mass spectrometry (HRMS) 2/257
- high-resolution spectra
  - double rotation (DOR) 1/315
  - dynamic-angle spinning (DAS) 1/315
- hindered rotors 1/151
- histidine 2/15
- histochemistry 2/15
- hit list 2/451
- Hitachi Ltd. 2/266
- HIV-1 protease inhibitor 2/87
- <sup>1</sup>H MAS NMR 1/287
- HMBC (heteronuclear multiple bond correlation) 1/173, 1/242, 2/471
- HMQC (heteronuclear multiple quantum coherence) 1/173, 1/234, 2/471, 2/483

- hollow cathode discharge 1/479  
 hollow-cathode lamp (HCL) 1/437, 1/460 f  
 homeostasis 2/11  
 homonuclear 2D NMR 1/223  
 homonuclear dipolar coupling 1/285, 1/290  
 - BABA 1/290  
 - C71/290  
 - DRAMA 1/290  
 - DRAWS 1/290  
 - DREAM 1/290  
 - HORROR 1/290  
 - RFDR 1/290  
 homonuclear dipolar-coupled spins 1/290  
 - internuclear distance 1/290  
 homonuclear Hartmann-Hahn  
     (HOHAHA) 2/109  
 homonuclear TOCSY, total correlated  
     spectroscopy 1/226 ff  
 homonuclear two-dimensional  
 - double-quantum (DQ) coherence 1/294  
 - INADEQUATE 1/294 ff  
 HOMSTRAD (HOMologous STRucture  
     Alignment Database) 2/9  
 horseradish peroxidase (HRP) 2/16, 2/50,  
     2/65  
 - labelin immuno assay 2/50  
 HOSE code 2/473, 2/478, 2/483  
 HREELS, HEELS (high resolution electron  
     energy loss spectroscopy) 1/533  
 HRMS 2/258  
 HRP 2/15 f  
<sup>1</sup>H solid state NMR  
 - CRAMPS 1/299  
 - high-resolution 1/298  
 - windowless homonuclear decou-  
     pling 1/299  
 HSQC (heteronuclear single quantum  
     coherence) 1/173, 1/236, 2/471  
 human chorionic gonadotropin (hCG) 2/56  
 -  $\beta$ -subunit of 2/56  
 human creatine kinase MB (CK-MB) 2/87  
 human genome project 2/3  
 human IgG 2/53  
 human phenylalanine hydroxylase 2/87  
 human serum albumin (HSA) 2/56  
 Hybrid Q-TOF MS 2/124  
 hybrid time-of-flight mass spectro-  
     meters 1/340  
 hydride generation technique 1/448 ff  
 hybridization detection 2/18  
 hydrocarbons 2/261  
 hydroxy carbonyls 2/261  
 hydroxyl number 1/110  
 8-hydroxypyrene-1,3,6-trisulfonic acid 2/11  
 hydroxystilbamidine 2/17  
 hyperchromic effect 1/125  
 hyperfine structure line broadening 1/431  
 hypericin 2/24  
 hyphenated 2D NMR 1/174  
 hyphenated techniques 1/466 ff  
 hyphenated-2D NMR experiments 1/252  
 - GHSQC-TOCSY 1/252  
 - HC-RELAY 1/252  
 - HMQC-TOCSY 1/252  
 - HXQC-COSY 1/252  
 hypochromic effect 1/125  
 hypocrellins 2/24  
 hypsochromic effect 1/125  
 hypsochromic shift 2/28
- i*
- IASys system 2/85  
 IBIS biosensors 2/87  
 IBSCA (ion beam spectrochemical  
     analysis) 1/533  
 IC/MS 1/344  
 ICP (inductively coupled plasma) 1/473 ff  
 ICR mass spectrometry 2/252  
 identity search 2/497  
 IETS (inelastic electron tunneling  
     spectroscopy) 1/535  
 (IGF)-binding protein-2 2/87  
 illumination  
 - sample 1/113  
 ILS (inverse least square) 2/462  
 immunoaffinity extraction 1/345  
 immunoassay 2/7, 2/10, 2/15, 2/47  
 - competitive 2/47  
 - non-competitive 2/47  
 - sandwich 2/47  
 immunochemistry  
 - with NIR fluorophores 2/51  
 - with visible fluorophores 2/50  
 immunochromatography 2/15  
 immunohistochemistry 2/15  
 - stains for 2/15  
 immunosensor 2/53  
 IMPEACH-MBC 1/246  
 imprinted polymers 2/71  
*in situ* hybridization 2/16  
*in vivo* dynamics  
 - cytoskeleton 2/17  
*in vivo* glucose monitoring 2/69  
 INADEQUATE 1/232, 2/471  
 INCOS 2/496  
 indirect (or third-element)  
     enhancement 1/404  
 INDO 2/28

- indo-carbocyanines 2/19  
indolum heptamethine cyanine dyes 2/32  
indolum Sq635 2/35  
indolum-squarine dyes 2/34  
inductively coupled plasma (ICP) 1/473 ff  
inelastic or Compton scattering 1/371  
INEPT (insensitive nuclei enhanced by polarization transfer) sequence 1/214, 2/114  
infinitely thick or massive samples 1/402  
influence coefficient method 1/410, 1/413  
infrared and Raman spectroscopy 2/92 ff  
– in bioanalysis 2/92 ff  
infrared interfaces 2/416  
infrared microscopes 1/85  
infrared spectroscopy 1/41, 2/6  
in-house database 2/446  
in-plane 1/42  
INS (ion neutralisation spectroscopy) 1/538, 1/552  
instrumental tune-up tests 2/254  
instruments  
– single beam 1/64  
insulin 2/47  
intercalating dyes 2/18  
interface 1/529, 1/579, 2/152 ff  
– atmospheric pressure 2/155  
– atmospheric-pressure chemical ionisation (APCI) 2/152 f  
– continuous flow FAB (CF-FAB) 2/153, 2/160  
– direct liquid introduction (DLI) 2/152, 2/153, 2/156  
– electrospray (ESI) 2/153  
– environmental analyses 2/155  
– fast atom bombardment (FAB) 2/153, 2/160  
– hermospray (TSP) 2/153  
– ion spray 2/155  
– moving-belt (MBI) 2/152 f, 2/156  
– particle beam (PBI) 2/153, 2/157  
– soft ionisation 2/172  
interference 2/89  
– chemical 1/454  
– fringes 1/96  
– spectral 1/454 ff  
interferogram 1/51  
interferometer 1/50  
interferometry 2/83  
intermolecular ring current 1/297  
internal conversion 1/45, 1/138 f, 1/143  
internal energy 2/249  
internal standardization 1/412  
internal standards 1/410  
intersystem crossing 1/45, 1/138 f  
intracellular ion activity  
– chloride 2/13  
intracellular pH 2/11 f  
– estimating 2/11  
intramolecular processes 1/45  
intrinsic zone 1/387  
inverse 1/174  
inverse least squares (ILS) 2/462  
iodide  
– ion, indicators for 2/13  
ion association reactions 2/262  
ion attachment mass spectrometry (IAMS) 2/262  
ion attachment reactions 2/263  
ion current 2/247  
ion cyclotron resonance (ICR) spectrometers 2/249  
ion detection 1/340  
ion mobility spectrometry 2/123  
ion transport 2/11  
ion trap 2/247 ff, 2/250 f, 2/254 ff  
– mass spectrometry 2/244, 2/250, 2/265  
ionisation 1/432  
ionisation buffer 1/465  
ionisation in flames 1/464  
ionisation interference 1/433  
ionisation temperature 1/435 f  
ionisation, degree of in a plasma 1/432  
ionization method 2/249  
ionization modes 2/247  
ionization time 2/247 f  
ion-molecule processes 2/248  
ion-molecule reactions 2/247, 2/249, 2/251, 2/253  
ion-selective electrodes 2/70  
IPMA, SIMP (scanning ion microprobe) 1/539  
IPS, IPES (inverse photoelectron spectroscopy) 1/536  
IR spectroscopy 1/41, 2/6  
IRD™ dyes 2/32  
IRMentor Pro 2/452  
IRRAS (infrared reflection absorption spectroscopy) 1/75  
IRRAS, IRAS (infrared reflection-absorption spectroscopy) 1/559  
IR-Tutor 2/452  
isoluminol 2/65  
isomer generation 2/481  
isothiocyanates 2/16  
isotope labeling  
– in NMR 2/97  
Isotopic labeled compounds by atomic emission detection 2/423

- ISS (ion scattering spectrometry) 1/565  
 ITMS 2/261  
 IUPAC name of the X-ray line 1/373
- j**  
 $^2J$ ,  $^3J$ -HMBC 1/248  
 J-modulated spin echo experiments 1/213  
   - APT 1/213  
   - DEPT 1/213  
   - INEPT 1/213  
 JOE 2/40  
 jump ratio 1/371
- k**  
 $K^+$   
   - indicators for 2/10  
 Karplus equation 2/106  
 kinetic energy 1/336  
 Kirchhoff 1/421, 1/436  
 K-matrix 2/459  
 Kramers-Kronig relation 1/74  
 Kramers-Kronig transformation 1/81  
 Kretschmann configuration 2/85  
 KRIPIES ( $k$ -resolved inverse photoemission spectroscopy) 1/536  
 Kr laser 2/31  
 KRS-5 2/78  
 Kubelka-Munk relation 1/79
- l**  
 L'vov platform 1/445  
 labeling  
   - isotopic 2/38  
   - labelling 2/17  
   - detection 2/17  
   - quantitation 2/17  
 lactate 2/69  
 Lambert-Beer law 1/367, 1/429 f, 1/465, 2/75  
 laminin 2/24  
 laminar flow burner 1/441 ff  
 LAMMA, or LAMMS, or LMMS  
   (laser microprobe mass analysis or spectroscopy) 1/533  
 Langmuir-Blodgett 1/512  
 Langmuir-Blodgett films 1/529, 1/560, 2/91  
 lanthanide chelates 2/55  
 Larmor frequency 1/172  
 Larmor relation 1/172  
 laser ablation 1/452, 1/478, 1/484, 1/485  
 laser desorption 1/329, 1/334 ff  
 laser induced fluorescence (LIF) 2/39  
 laser induced fluorescence polarisation 2/55  
   - in capillary electrophoresis detection (CE-LIFP) 2/55
- laser plasma 1/478  
 latent variables 2/453  
 latex particles  
   - fluorescent 2/15  
 layered synthetic multilayers 1/391  
 LC-AES 1/492 ff  
 LC-MS 2/152 ff, 2/163, 2/226 f  
   - achievements 2/163 ff  
   - alkylpolyethersulfate 2/164  
   - capillary electrophoresis (CE) 2/163  
   - capillary zone electrophoresis (CZE) 2/163  
   - conclusions 2/226  
   - history 2/152 f  
   - library 27227  
   - non-ionic polyethylene glycol (PEG) surfactant 2/164  
   - non-ionic polypropylene glycol (PPG) surfactant 2/164  
   - obstacles 2/163 ff  
 least squares regression 2/456  
 leave-one-out strategy 2/461  
 lectins 2/21  
 LEED (low energy electron diffraction) 1/527  
 legionella pneumophila serogroup 1 (LPS1) 2/53  
 Leis (low-energy ion scattering spectroscopy) 1/542  
 library spectrum 2/450  
 Li-COR 4200 fluorescence microscope 2/53  
 Li-COR DNA sequencer 2/45  
 LIF *see* fluorescence, laser-induced lifetime 1/138  
   - luminescence 1/67  
   - of an excited state 1/428, 1/430  
 ligand field 1/133  
 limit of detection 1/378  
 line broadening 1/430  
   - Doppler 1/430  
   - hyperfine structure 1/431  
   - Lorentz 1/430  
   - pressure 1/430  
   - Stark 1/431  
 line profile 1/431, 1/461  
 linear absorption coefficient 367  
 linear dependences 2/463  
 linear models 2/459  
 linear Raman effect 1/43  
 lineshapes 1/272  
 linewidths 1/281, 1/430  
   - anisotropy 1/281  
   - asymmetry 1/281  
 lipase 2/21  
 lipid peroxidation 2/19

- lipids
  - HRP assay for 2/15
  - oxydation/peroxydation 2/15
  - metabolism 2/19
  - nalling 2/19
  - traffic 2/19
- LIPIDAT 2/9
- lipoprotein lipase 2/24
- liquid chromatography and atomic emission spectroscopy (LC-AES) 1/492 ff
- liquid chromatography-atomic absorption spectrometry (HPLC-AAS) 1/469
- liquid chromatography-mass spectrometry (LC-MS) 1/347, 2/152, 2/163, 2/226 f
- liquid crystals 1/529
- liquid samples 1/29
  - chromatographic separation 1/31
  - complexation 1/30
  - extraction 1/29
  - extraction/separation and preconcentration 1/29
- liquid-liquid extraction 1/344
- liquids 1/22
- lithium
  - determination of 2/70
  - in blood 2/70
- loading matrix 2/453
- local thermal equilibrium 1/433
- local thermal equilibrium (LTE) 1/427
- long-range heteronuclear chemical shift correlation 1/240
- Lorentz line broadening 1/430
- low-density lipoproteins 2/24
- low-viscosity solvents 1/146
- luciferase enzyme 2/65
- luciferase system
  - from the firefly *photinus pyralis* 2/65
- luciferin 2/65
- lucigenin 2/13, 2/22
- luminescence 1/44, 1/67
- luminol 2/65
- luminol/HRP system 2/65
- Lyman series 1/422
- lyotropic liquid crystals 2/101
- LysoSensor probes 2/11
  
- m**
- MAES (metastable atom electron spectroscopy) 1/551
- mag-fura-2 2/12
- magic angle spinning (MAS) 1/175, 1/94, 1/280
  - line narrowing 1/280
- magic-angle hopping (MAH) 1/300
- magic-angle turning (MAT) 1/300
- Magnesium Green 2/12
- magnesium
  - detection of Green, dye 2/12
- magnetic dipolar interaction 1/187
- magnetic domain 1/555
- magnetic domains 1/554
- magnetic field strengths 1/171
- magnetic materials 1/523, 1/537, 1/576 f
- magnetic moment 1/172
- magnetic resonance imaging (MRI) 1/199
  - image contrast control 1/199
- magnetic sector 1/335
- magnetoreflectance 1/561
- magnetron 1/476
- MALDI 2/502
- MALDI-TOF mass spectrometry 2/122
- MALDI-TOF-TOF MS 2/124
- malignancy 2/11
- maltose phosphorylase 2/14
- MAS 1/271, 1/280
  - anisotropic broadening 1/281
  - anisotropic lineshape 1/282
  - line narrowing 1/280
- MAS-J-HMQC 1/308
  - one-bond correlations 1/308
  - through-bond J couplings 1/308
- MAS-J-HSQC 1/308
  - one-bond correlations 1/308
  - through-bond J couplings 1/308
- mass analysis 1/335
- mass attenuation coefficient 1/367
- mass chromatogram 2/498
- mass frontier 2/499
- mass spectra quality indices 2/255
- mass spectral interfaces 2/401 f, 2/408 f
- mass spectrometry *see also* process
  - analysis 1/329, 1/338, 2/488
  - databases 2/489
  - search software 2/495
- mass spectroscopy (MS) 2/4, 2/122
  - in bioanalysis 2/122
- MassLib 2/495
- MassLib/SISCOM 2/497
- MASSTransit 2/491
- MATLAB 2/467
- matrices 2/253
- P-matrix 2/462
- matrix effects 1/401
- matrix modifier 1/463
- matrix-assisted laser desorption (MALDI)
  - MS 1/330, 2/122
- MBI
- pesticides 2/156

- polar pharmaceutical compounds 2/156
- polycyclic aromatic hydrocarbons 2/154
- surfactants 2/154
- measurements
  - reflection-absorption 1/94
- MEIS (medium energy ion scattering) 1/543, 1/565
- melatonin 2/63
- membrane chloride transport 2/13
- membrane fusion 2/19
- membrane potential 2/12
- membrane potential-sensitive probes 2/19
- membrane transport
  - chloride 2/13
- MEMS *see* microelectromechanical systems
- merocyanine 540 2/15, 2/19
- metal complexes 1/133
- metal ion association reactions 2/262
- metalloproteinas 2/13
- N-methyl-4-hydrazino-7-nitrobenzo-furazan 2/4
- 6-methoxyquinolinium derivatives 2/13
- Mg<sup>2+</sup> 2/12
- Michelson interferometer 1/50
- microinjectable cell tracers 2/57
- micromechanical systems in bioanalysis 2/131
- microparticles
  - fluorescent 2/15
- microscans 2/247, 2/249
- microscopic 1/84
- microscopic XRF 1/399
- microscopy 2/57
  - confocal 2/63
  - laser scanning, with MPE 2/63
  - standardization reagents 2/57
- microseparation methods 1/346
- microsomal dealkylase 2/21
- microsystems 2/3
  - microarray 2/3
  - microelectrophoresis 2/3
  - microfluidics 2/3
- microtubule
  - cell cycle-dependent 2/17
  - dynamics 2/17
  - polymerization 2/13
- microwave plasma 1/476
- microscan 2/246, 2/251
- MIES (metastable impact electron spectroscopy) 1/539, 1/551
- minor-groove binders 2/18
- MIP (multiple internal reflection) 1/476, 1/511
- mist chambers 1/13
- mitochondria
  - Na<sup>+</sup> gradients 2/11
  - probes for 2/22
  - sodium gradients in 2/11
- MitoFluor Probes 2/22
- mitotic spindle morphogenesis 2/17
- MitoTracker 2/22
- mixing chamber 1/441
- mixture rule 1/368
- MLR 2/462
- mode couplers (interferometers) 2/81
- modulation spectroscopy 1/561
- moisture 1/110
- molar ellipticity 1/82
- molecular film 1/536, 1/539
- molecular imprinting 2/69
- molecular interactions 1/580
- molecular orientation 1/535, 1/551
- molecular recognition structures 1/349
- moment
  - dipole 1/271
  - quadrupole 1/271
- monochromator
  - Czerny-Turner 1/58
- monolayer 1/501, 1/574
- Langmuir-Blodgett 1/512
- self-organised 1/536
- Moseley's law 1/374
- motion
  - rate constant 1/279
  - three site jump 1/279
- moving belt (MBI) 2/153, 2/156
- MPE laser scanning microscopy 2/63
- MQC 1/295
- MRI pulse sequence
  - echo planar sequence 202
  - spin-warp 1/200
- MS *see* mass spectroscopy
- MST *see* Microsystems
- mulls 1/92
- multichannel analyzer 1/387
- multichannel detection 1/470
- multichannel instruments 1/481 ff
- multichannel spectrometers 1/392
- multichannel wavelength-dispersive instruments 1/393
- multicollinearities 2/464
- multidrug resistance 2/11
- multi-element technique 1/470
- multi-frequency irradiation methods 2/254
- multilayer 1/501
- multi-photon 1/155
- multi-photon excitation 1/149

- multi-photon fluorescence excitation  
     (MPE) 2/59  
 multiphoton microscopy 1/138  
 multiple linear regression (MLR) 2/462  
 multiple magnetization transfers  
     (spin-diffusion) 2/111  
 multiple quantum spectroscopy 2/108  
 multiple-element techniques 1/413  
 multiple-frequency resonance ejection  
     methods 2/252  
 multistep elution 2/127  
     – as sample 2/127  
     – prep in MS 2/127  
 multivariate calibration in AES 1/489  
 multivariate calibration methods 2/69  
 multivariate methods 2/459  
 muscle contraction 2/11
- n**
- $\text{Na}^+$   
     – indicators for 2/10  
     – channel  
         – probes for the 2/25  
     – efflux in 2/11  
 NAA (neutron activation analysis) 1/518  
 NADH 2/15, 2/63  
 NADPH 2/15  
 $\text{Na}^+/\text{H}^+$  antiporter 2/25  
 $\text{Na}^+/\text{K}^+$ -ATPase 2/25  
 NanoOrange 2/16  
 nanoparticles  
     – fluorescent 2/15  
 naphthalene-2,3-dicarboxaldehyde 2/14  
 naphthalocyanine dyes  
     – bis(alkylsiloxy)silyl) complexes of  
         naphthalocyanines 2/36  
 naphthalocyanines 2/35  
 native-like structure 1/354  
 natural lifetime 1/138  
 NBD 2/19  
 NBT 2/14  
 near-field microscopes 1/86  
 near-field scanning optical microscopy 2/19  
 near-infrared (NIR) 1/42, 1/104, 2/10  
 nebuliser 1/441 f  
 negative ion chemical ionization (NICI)  
     experiments 2/253  
 neural network 2/474, 2/478  
 neuraminidase 2/20  
 neurokinin receptors 2/25  
 neuromedin C receptors 2/25  
 neutral loss searching 2/497  
 Newport Green 2/13
- NEXAFS (near edge X-ray absorption  
     spectroscopy) 1/544  
 NHS ester *see* *N*-hydroxysuccinimidyl ester  
*N*-hydroxysuccinimidyl (NHS) ester 2/28,  
     2/31  
 Nicolet 2/447  
 nicotinic acetylcholine receptors 2/91  
 Nile Blue 2/70  
 NIR 1/42, 1/104, 2/10  
     – absorbing chromophores 2/32  
     – absorption spectroscopy 2/68  
     – agriculture 1/110  
     – dye NN 382  
     – environmental monitoring 1/110  
     – fiber optic immunosensor 2/53  
     – food industry 1/110  
     – pharmaceutical industry 1/111  
     – polymer industry 1/111  
     – spectrometers  
         – miniaturised 2/68  
 NIST 2/447  
 NIST Mass Spectral Library 2/490  
 nitrate 2/70  
 nitric oxides 2/14  
 nitrobenzoxadiazole (NBD) 2/19  
 NIXSW (normal incidence X-ray standing  
     wave) 1/591  
 NMR *see also* nuclear magnetic resonance  
     spectroscopy 1/171, 2/297  
     – dynamic processes 1/277  
     –  ${}^2\text{H}$  1/278  
     – parameters  
         – chemical shift 1/181 ff  
         – detection frequency 1/181 ff  
         – gyromagnetic ratio 1/181 ff  
         – *J*-coupling constants 1/181 ff  
         – magnetic field 1/181 ff  
         – nuclear spin 1/181 ff  
     – resonance frequency 1/272  
         – orientational dependence 1/272  
     – single-crystal 1/273 f  
     – solid-state 1/275  
     – spectroscopy 2/6, 2/94 ff  
         – of proteins 2/94  
     – active nuclei 1/270  
         – magnetogyric ratios 1/270  
         – natural abundances 1/270  
         – nuclear spin quantum numbers 1/270  
 NOE (nuclear Overhauser effect) 1/173,  
     1/212  
 NOESY (nuclear Overhauser enhancement  
     spectroscopy) 1/228, 1/173, 2/110  
 noise levels  
     – in the NIR in visible regions 2/27

- non-covalent biopolymer complexes 1/349
- noncovalent supramolecular complexes 1/354
- non-invasive monitoring
  - of glucose 2/69
- non-linear least squares strategy 1/408
- non-linear methods 2/459
- non-linear Raman effect 1/43
- Non-RBS or n-RBS (Non-Rutherford backscattering spectrometry) 1/567
- Nonylphenolpolyglycoether (NPEO) 2/169 ff
  - in-source-CID 2/169
  - MS/MS CID 2/169
- normalization 2/449
- NRA (nuclear reaction analysis) 1/541, 1/563
- NSOM 1/86
- nuclear magnetic resonance (NMR) 1/171, 2/297
  - nuclear magnetic resonance spectroscopy 2/469
  - nuclear Overhauser effect (NOE) 1/173, 1/212
    - difference spectroscopy 1/212
    - distances between a pair of protons 1/212
    - stereochemical relationship 1/212
  - nuclear Overhauser enhancements (NOE) 2/98
- nuclear Overhauser enhancement spectroscopy (NOESY) 1/288, 1/173, 2/110
- nuclear spin quantum number 1/172
- nuclei
  - half-integer 1/271
  - integer 1/271
  - magnetogyric ratio 1/271
  - natural abundance 1/271
- nucleic acid analysis
  - by MS 2/130
- horseradish peroxidase (HRP) 2/16
- nucleotide-binding proteins 2/24
- number density (of absorbing atoms) 1/429
- number density (of excited particles) 1/428
  
- o**
- obstacles 2/163 ff
  - atmospheric pressure chemical ionisation (APCI) 2/163
  - capillary electrophoresis (CE) 2/163
  - capillary zone electrophoresis (CZE) 2/163
  - electrospray ionisation (ESI) 2/163
  - TSP 2/163
- off-resonance decoupling 1/216
- OliGreen 2/17
- one-dimensional NMR experiment 2/103
- operation
- continuous-scan 1/52
- ophthalddialdehyde 2/16
- opioid receptors 2/25
- optical activity 2/428
- optical density
  - in ATR 2/77
- optical rotatory dispersion (ORD) 1/81, 2/93
- optical spectral data bases 2/447
- optical spectroscopy *see also* process analysis 2/441
- optimization of ICP 1/490
- orbital angular momentum 1/423
- orbital quantum number 1/423
- organoarsenic compounds 2/154
- organophosphorus compounds 2/217 ff
  - biodegradation 2/195
  - drinking water 2/217
  - groundwater 2/194, 2/217
  - interlaboratory study 2/194
  - ion chromatography 2/217
  - MS/MS 2/217 f
  - photodegradation 2/195
  - quantification 2/218
  - stability 2/218
  - surface water 2/217
  - wastewater 2/218
- organophosphorus pesticides 2/179
- organotin compounds 2/258
- orientation
  - molecular 1/578
- orientational dependence 1/272
- oriented matrices 2/102
- in NMR 2/102
- oriented samples 1/313
- orthogonal injection
  - in ESI-MS 2/123
- outlier spectra 2/461
- out-of-plane 1/42
- overview
  - aromatic sulfonates 2/154
  - complexing agents 2/154
  - diagnostic agents 2/154
  - drugs 2/154
  - dyes 2/154
  - explosives 2/154
  - haloacetic acids 2/154
  - organoarsenic compounds 2/154
  - PAHs 2/154
  - pesticides 2/154
  - phenols 2/154
  - surfactants 2/154
  - toxins 2/154
  - xenoestrogens 2/154

- oxa-carbocyanines 2/19  
 oxazolium pentamethine cyanine dye (DODC) 2/33  
 oxidation state 1/585  
 oxidoreductase 2/21  
 OxyBURST technology 2/26  
 oxygen 2/15, 2/69
- p**
- PAES (positron annihilation auger electron spectroscopy) 1/555  
 PAH 2/154  
 – quantification 2/208  
 Pake doublet 1/192  
 parent structure 2/473  
 partial least squares (PLS) 2/465  
 particle beam (PBI) 2/153, 2/157  
 particle size 1/417  
 partition function 1/429, 1/433  
 PAS (photoacoustic spectroscopy) 1/552  
 Paschen series 1/422  
 passive sampling 1/13  
 pattern recognition  
 – FIA-MS 2/175  
 – FIA-MS/MS 2/175  
 PBI 2/157 ff  
 – alkylphenol carboxylates (APECs) 2/159  
 – alkylphenol ethoxylates (APEOs) 2/159  
 – anilides 2/158  
 – biochemical 2/157  
 – carbamate 2/158  
 – chlorinated phenoxy acid 2/158  
 – degradation products 2/157  
 – dyes 2/159  
 – herbicides 2/157  
 – isocyanates 2/158  
 – library-searchable EI spectra 2/159  
 – organo-phosphorus 2/158  
 – PAHs 2/159  
 – PAH metabolites 2/160  
 – pesticides 2/157  
 – phenylurea 2/158  
 – physiochemical 2/157  
 – quaternary ammonium 2/158  
 – triazines 2/158  
 P-COSY experiment 2/107  
 PCR 2/18, 2/464  
 PDT 2/36  
 2PE cross section 2/60  
 PED or PhD (photoelectron diffraction) 1/586  
 PEELS (parallel electron energy loss spectroscopy) 1/530, 1/535  
 PEEM (photemission electron microscopy) 1/553
- 2PE fluorescence polarization measurements 2/64  
 pelletized 1/417  
 pellets 1/92  
 penetration depth 1/402, 2/74  
 penicillin 2/87  
 peptidases 2/20  
 peptide  
 – analysis 2/16  
 – MS 2/502  
 perfluoro compounds 2/262  
 permeability  
 – of the dielectric media 2/72  
 permitivity 1/562, 2/72  
 peroxide 2/15  
 Perrin plots 1/150  
 perylene 2/19  
 PESIS (photoelectron spectroscopy of inner shell) 1/587  
 pesticides 2/154, 2/176 ff, 2/258  
 – anilides 1/176, 2/158, 2/192, 2/215  
 – antifouling 2/199  
 – benzidines 2/154  
 – biodegradation 2/199  
 – carbamate 2/154, 2/158, 2/177 ff, 2/193  
 – chlorinated 2/154  
 – phenoxy acid 2/158  
 – degradation pathways 2/182  
 – degradation products 2/182  
 – ESI-CZE-MS 2/215  
 – ESI-FIA-MS 2/215  
 – estuarine waters 2/182  
 – fruits 2/193, 2/197  
 – fruit drinks 2/197  
 – fungicides 2/215  
 – glyphosate 2/161  
 – groundwater 2/192, 2/196 f, 2/199  
 – herbicides 2/215  
 – isocyanates 2/158  
 – library 2/218  
 – N-methylcarbamate pesticides 2/193  
 – MS/MS 2/195 f, 2/216  
 – MS/MS library 2/194  
 – natural waters 2/198  
 – organophosphorus 2/158, 2/194  
 – biodegradation products 2/194  
 – organophosphorus compounds 2/179  
 – phenolic compounds 2/197  
 – phenoxyacetic acid 2/154  
 – phenoxyacrylic acids 2/179, 2/195  
 – phenylurea 2/158, 2/180, 2/196  
 – quantification 2/181, 2/192 ff, 2/215  
 – quaternary amines 2/176, 2/192, 2/215  
 – quaternary ammonium 2/154, 2/158

- rivers 2/198
  - river water 2/192 f, 2/199
  - sediment 2/197
  - soil samples 2/182
  - sulfonylureas 2/161, 2/180, 2/196
  - surface water 2/196, 2/198
  - thiocyanate 2/176, 2/192
    - compounds 2/215
  - thioureas 2/180, 2/196
  - tin-containing pesticides 2/201
  - toluidines 2/176, 2/192, 2/215
  - triazines 2/154, 2/158, 2/181, 2/197 ff
  - urea pesticides 2/180
    - quantification 2/180
  - vegetables 2/193
  - water 2/196 f
- Pfleger/Maurer/Weber database 2/494
- pH or PEH (photoelectron holography) 1/586
- pH
- indicators for 2/10
- phagocytosis 2/26, 2/68
- phallacidin 2/17
- phalloidin 2/17
- phallotoxins 2/17
- phase cycling routines 1/232
- CYCLOPS 1/232
  - EXORCYCLE 1/232
- phenanthridine dyes 2/17
- 2-phenetylamine 2/70, 2/71
- Phen Green FL 2/13
- phenobarbital 2/56
- phenols 2/154
  - quantification 2/208
- phenoxazine 2/70
- phenoxycarboxylic acids 2/179
  - drinking water 2/219
  - groundwater 2/219
  - MS/MS 2/219
  - quantification 2/219
  - surface water 2/219
- phenylureas
- agricultural soil 2/222
  - chemical degradation 2/222
  - crop 2/222
  - degradation products 2/220, 2/222
  - estuarine waters 2/220
  - fruit drinks 2/197
  - fruits 2/197, 2/222
  - groundwater 2/196 f
  - metabolites 2/222
  - MS/MS 2/221 f
  - natural waters 2/221
  - photolysis products 2/222
  - quantification 2/220 ff
- river water 2/221
  - sediment 2/197
  - surface water 2/196, 2/221
  - water 2/196 f
- phenytoin 2/56
- phosphatase-based signal amplification 2/15
- phosphate 2/14
- phospholipase activity 2/19
- phosphorescence 1/45
- phosphorylations 1/351
- photoacoustic 1/83 f
- sampling depth 1/84
- photobleaching 1/155, 1/157, 2/63
- photodiode array 2/381 ff
- photodiodes 2/10
- photodynamic therapy (PDT) 2/36
- photoelectric absorption 1/369
- photoelectric effect 1/369
- photomultiplier 1/386
- photomultiplier tubes (PMT) 2/27
- o-phthalodialdehyde 2/14
- phthalocyanines 2/10, 2/35
- phycobiliproteins 2/15, 2/57
- PicoGreen 2/17
- PIES (penning ionisation electron spectroscopy) 1/539, 1/551
- piezoreflectance 1/561
- PIGE or PIGME (particle induced gamma ray emission) 1/541, 1/546
- PISEMA (polarisation inversion with spin exchange at the magic angle) 1/313
- internuclear dipolar couplings 1/315
  - tilt angle of the polypeptide helix 1/315
- PIXE (particle induced X-ray emission) 1/541, 1/548
- plasma desorption 1/332
- PLS (partial least square) 2/465
- PLS\_Toolbox 2/467
- PLSplus 2/467
- PM (polarization modulation) 1/561
- PMB 2/496
- PMP (proton microprobe) 1/539
- PMT 2/27
- polarization 1/118, 1/383
- polarization excitation spectra 1/149
- polarized light 1/81
- polychromatic flow cytometry (PFC) 2/57
- polychromator 1/481 ff
  - Raman grating 1/61
- Polycyclic aromatic hydrocarbon (PAH) isomers
- by IR 2/417 ff
  - by UV 2/384 ff
- polyethylene glycols 2/101

- Polymer molecular weight, true value by  
 – LC-MS 2/410  
 polymethines 2/10  
 polymixin B  
 – analog 2/24  
 – fluorescent 2/24  
 population of excited levels 1/426  
 portable equipment 1/389  
 post-translational modifications 1/349  
 post-translational structure modifications 1/349  
 potential sensitive dyes 2/70  
 PPP MO 2/28  
 preamplifier 1/387  
 pregnancy-associated plasma protein A 2/56  
 preparation of gaseous samples 1/4  
 preparation of samples for analysis 1/24  
 presaturation method (NMR) 2/104  
 pre-search 2/495  
 PRESS 2/466  
 pressure line broadening 1/430  
 primary absorption 1/403  
 primary structures 1/349  
 principal component analysis 2/452  
 principal component regression (PCR) 2/464  
 principal quantum number 1/423  
 principle  
 – double-beam 1/49 f  
 Prion proteins 2/6  
 prism couplers 2/81  
 Probability Based Matching (PMB) 2/496  
 probes for Cl<sup>-</sup> channels 2/25  
 probes for K<sup>+</sup> channels 2/25  
 probes for mitochondria 2/22  
 process analysis 2/336 ff, 2/271 ff  
 – atomic emission spectrometry (AES) 2/336, 2/356  
 – gaseous effluents 2/357  
 – laser based techniques 2/362  
 – liquid streams 2/356  
 – plasma spectrometry 2/356  
 – reactive gases 2/360  
 – acoustic emission spectroscopy 2/276  
 – atomic spectrometry 2/336  
 – atomic spectroscopy 2/274  
 – chemical composition 2/273  
 – elemental analysis 2/336  
 – applications 2/336  
 – catalyst control 2/337  
 – corrosion monitoring 2/339  
 – on-stream/at-line analysis 2/343  
 – reducing environmental impact 2/341  
 – troubleshooting process problems 2/342
- inductively coupled plasma atomic emission spectrometry (ICPAES) 2/336  
 – inferential analysis 2/277  
 – infrared 2/274  
 – ion mobility spectrometry 2/276  
 – IR 2/279  
 – mass spectrometry 2/316 ff  
 – applications 2/330  
 – attributes 2/316  
 – calibration 2/327  
 – data analysis 2/325  
 – detectors 2/325  
 – fermentation off-gas analysis 2/331  
 – hardware 2/317  
 – ionization 2/231  
 – limitations 2/316  
 – maintenance 2/329  
 – mass analyzers 2/322  
 – operation 2/329  
 – sample collection and conditioning 2/319  
 – sample inlet 2/319  
 – vacuum system 2/325  
 – mass spectroscopy 2/274  
 – microwave 2/279  
 – microwave spectroscopy 2/274  
 – NMR (Nuclear Magnetic Resonance) 2/274, 2/279, 2/297 ff  
 – broadline NMR 2/301 ff  
 – calibration 2/299  
 – curing process applications 2/303  
 – food industry applications 2/303  
 – FT-NMR 2/307  
 – gasoline applications 2/309  
 – growth factor β<sub>3</sub> 2/313  
 – manufacturers 2/306  
 – petroleum refining 2/313  
 – polymer industry applications 2/306  
 – polymer production applications 2/303  
 – quantitation 2/297, 2/299  
 – sample 2/300  
 – sulfuric acid alkylation process 2/311  
 – optical spectroscopy 2/279 ff  
 – cavity ringdown spectroscopy 2/294  
 – chemiluminescence 2/280, 2/293  
 – Far-IR 2/279  
 – fluorescence 2/280, 2/293  
 – IR 2/279  
 – laser techniques 2/280  
 – laser diode techniques 2/291  
 – Mid-IR 2/279 ff  
 – Near-IR 2/279 f  
 – near-infrared spectroscopy 2/282 ff  
 – non-dispersive infrared analysers 2/280 f

- optical sensors 2/280, 2/294
  - Raman spectroscopy 2/280, 27287 ff
  - UV 2/279 f
  - UV/visible spectroscopy 2/280, 2/286
  - visible 2/279 f
  - physical characteristics 2/273
  - practical considerations 2/272
  - Raman spectroscopy 2/280
  - REMPI spectroscopy 2/275
  - sample 2/272 ff
  - spectroscopy 2/273
  - ultrasound 2/276
  - UV/visible 2/274, 2/279
  - X-ray fluorescence (XRF) 2/336, 2/344
    - corrosion monitoring 2/351
    - direct analysis of solids 2/354
    - liquid process streams 2/348
    - powders 2/352
    - slurries 2/352
    - trace analysis 2/351
  - X-ray techniques 2/279
  - process control 2/269 ff
  - process industry 2/5
  - process mass spectrometry 2/316
  - profile function 1/431
  - propidium iodide 2/17
  - proportionality 1/384
  - proteases 2/20
  - protective agent for AAS 1/463
  - protein 1/529
    - kinases 2/24
    - phosphatases 2/24
  - proteinase inhibitors 2/24
  - protein kinase 2/23
    - activators 2/24
    - inhibitors 2/24
  - protein quantitation 2/16
  - proteome 2/4
  - proteome analysis 1/356
  - proteomic databases 2/5
  - proteomics 1/356, 2/4
    - proteolytic degradation 1/356
    - sequence tags 1/356
  - proton transfer 2/251
  - pulsed field gradients (PFGs) 1/173, 2/102
  - pulsed lamp background correction 1/460
  - pulse-height selection 1/384
  - pulse methods 1/186
  - purple membranes (PM)
    - of *Halobacterium salinarum* 2/101
  - pyrene 1/154, 2/19
  - pyrophosphate 2/14
- q**
- quadrupolar coupling ( $C_Q$ ) 1/174
  - quadrupolar interaction 1/191
  - asymmetry parameter,  $\eta$  1/192
  - axially symmetric 1/278
  - definition 1/192
  - electric charge asymmetry of the nucleus 1/191
  - moments 1/191
  - nuclear electric quadrupole moment 1/192
  - quadrupolar coupling constant 1/192
  - tensor 1/192
  - quadrupolar nuclei
  - line shapes 1/195
  - quadrupole instruments 2/246
  - quadrupole ion trap 2/265
  - quadrupole ion trap mass spectrometry 2/244
  - quadrupole mass analyser 1/337
  - quadrupole mass spectrometry 2/258
  - qualitative evaluation of spectra, optical 2/446
  - QuantIR 2/467
  - quantitative calibration procedures 1/409
  - quantitative evaluation 2/455
  - quantitative proteomics 2/126
  - quantitative reliability 1/418
  - quantum number, orbital 1/423
  - quantum number, principal 1/423
  - quantum number, spin 1/423
  - quantum number, total 1/423
  - quantum yield 1/138 ff, 1/143, 2/28
  - quartz furnace-atomic absorption spectrometry 1/467
  - quartz T-tube atomiser (for AAS) 1/468
  - quartz tube atomiser 1/449
- r**
- radiation
    - scattered 1/97
  - radiationless relaxation 1/427
  - radiation source for AAS 1/434
  - radiative de-excitation 1/427
  - radiative transition 1/428
  - radio frequency (RF) 1/172
  - radio frequency (RF) generator 1/473
  - radioactive  $\alpha$ ,  $\beta$ , and  $\gamma$ -sources 1/382
  - radioactive sources 1/380
  - radioisotope XRF 1/397
  - radiotherapy 2/29
  - RAIRS (reflection absorption infrared spectroscopy) 1/75, 1/534, 1/559
  - Raman 2/428
    - mapping 1/117
    - microprobe 1/117

- scattering 2/27, 2/91
  - shift 1/43
  - spectroscopy 1/43, 1/557, 2/92 ff
    - near-infrared excitation 2/93
  - random and systematic error 1/415
  - RBS (Rutherford backscattering spectroscopy) 1/541, 1/565
  - R-COSY 2/108
  - reactive sites 1/353
  - real-time BioInteraction Analysis 2/5
  - receptor binding 2/25
  - recoupling methods 1/287 ff
    - REAPDOR 1/290
    - REDOR 1/287
    - TRAPDOR 1/290
  - red-edge 1/146
  - REDOR 1/310
    - dipolar couplings 1/310
    - distance determination 1/290
  - REELS, EELS (reflection electron energy loss spectroscopy) 1/535, 1/561
  - reflection 2/72
    - absorption 1/75
    - diffuse 1/97
    - measurements 1/73
    - off-axis 1/80
    - on-axis 1/80
  - reflectometric interference 2/81
  - reflectometric interference spectroscopy (RIfS) 2/89
  - refraction 2/72
  - refractive index
    - complex 1/74
  - region
    - fingerprint 1/102
  - regulations 2/256
  - relative detection limits 1/378
  - relative random counting error 1/405
  - relaxation 1/195
    - correlation times 1/196
    - methyl group rotation 1/196
    - spin-lattice  $T_1$  1/217
    - spin-spin  $T_2$  1/217
    - $T_1$ , spin-lattice relaxation 1/196
    - $T_{1p}$ , spin-lattice in the rotating frame relaxation 1/196
    - $T_2$ , spin-spin relaxation 1/196
    - times
      - $^{13}\text{C}$   $T_1$  1/285
      - $^1\text{H}$   $T_{1p}$  1/285
  - relayed COSY (R-COSY) 2/108
  - representative sample 1/117
    - REPT-HMQC 1/310
  - residual dipolar couplings (RDC) 2/99
  - residual variance 2/454
  - residuals 2/458
  - resolution 1/51
    - spectral 1/52
  - resonance 1/148
  - resonance energy transfer 1/45
  - resonance Raman scattering 1/119
  - resonant ejection frequencies 2/252
  - resonant mirror (RM) 2/83
  - reverse phase HPLC 2/45
  - reverse search 2/496
  - review
    - dyes 2/154
    - environmetal analysis 2/154
    - environmetal contaminants 2/154
    - general 2/154
    - surfactants 2/154
    - water analysis 2/154
  - RF level 2/254
  - RF ramping 2/248
  - RF voltages 2/252
  - rhodamine 1102/20
  - rhodamines 2/10, 2/15, 2/19, 2/28
  - RiboGreen 2/17
  - ribosomes 2/72
  - RNRA (resonant nuclear reaction analysis) 1/563
  - rocking modes 1/42
  - ROESY (rotating frame Overhauser enhanced spectroscopy) 1/173, 1/230
  - rosamines 2/22
  - Rose Bengal diacetate 2/15
  - rotating anode tubes 1/380
  - rotating-frame nuclear Overhauser effect spectroscopy (ROESY) 2/110
  - rotating-frame Overhauser effect (ROE) 2/109
  - rotational correlation time 1/149 f
  - rotational-echo double resonance (REDOR) 1/175
  - rotational resonance (RR) 1/290
  - rotational temperature 1/434, 1/436
  - Rowland circle 1/482
  - Rowland spectrometer 1/481 ff
  - ROX 2/40
  - RS (recoil spectroscopy) 1/520
  - ruthenium trisbipyridyl ( $\text{Ru}(\text{bpy})_3$ ) complexes 2/68
- s**
- Sadtler 2/447
  - Saha equation 1/432
  - SAHO 2/472
  - SALI (surface analysis by laser ionisation) 1/573

- SAM (scanning Auger microscopy) 1/567  
 sample preparation 1/105, 1/344  
 sample preparation for inorganic analysis 1/25  
 - acid digestion 1/25  
 - fusion reactions 1/27  
 - nonoxidizing acids 1/26  
 - oxidizing acids 1/26  
 samples  
 - liquid crystals 1/275  
 - neat solid 1/94  
 - oriented lipid bilayers 1/275  
 - polymer fibres 1/275  
 - powdered 1/275  
 sampling considerations 1/5  
 Sanger 2/37  
 Sanger method *see* DNA sequencing  
 SAv 2/29  
 SCAN 2/467  
 scan repetition rate 2/248, 2/251  
 SCANIIR (surface composition by analysis of neutral and ion impact radiation) 1/533  
 scanning modes 2/247  
 scattering 1/371  
 - in near-IR 2/10  
 - interactions 1/369  
 - Rayleigh 1/58  
 - Tyndall 1/58  
 schistosomiasis 2/47  
 scintillation counter 386  
 score matrix 2/453  
 SDBS 2/447, 2/492  
 sealed X-ray tubes 1/380  
 search for bands 2/446  
 secondary absorption 1/404  
 secondary ion mass spectrometry (SIMS) 2/125  
 secondary target EDXRF system 1/395  
 segmental mobility 1/151  
 selected-ion monitoring 2/251  
 selected-ion monitoring procedures 2/255  
 selection rules 1/373, 1/424  
 selective population transfer (SPT) 1/173, 1/213  
 - DEPT 1/213  
 - INEPT 1/213  
 - spin population inversion (SPI) 1/213  
 selenium  
 - ion, indicators for 2/13  
 self-absorption 1/431, 1/438  
 self-assembled biomembranes 2/91  
 self-chemical ionization 2/248  
 self-CI processes 2/253  
 self-decoupling 1/185  
 self-diffusion of 1/202  
 self-organizing monolayers 545  
 self-quenching 1/143  
 self-reversal 1/431, 1/460f  
 self-training interpretive and retrieval system (STIRS) 2/496  
 SEM (scanning electron microscopy) 1/567  
 semiconductor detectors 1/386  
 semiempirical quantum chemical methods 2/28  
 semiochemistry 2/70  
 SEMPA (scanning electron microscopy with polarisation analysis) 1/567  
 sensitivity 2/252  
 sensitivity AES 1/491  
 sensors 2/71  
 sequence data 2/8  
 sequence determinations 1/350  
 - sequencing 2/16  
 - synthesis 2/16  
 serotonin 2/63  
 SERS (surface enhanced Raman scattering) 1/557  
 SESAMI 2/483  
 SEW (surface electromagnetic waves spectroscopy) 1/574  
 SEXAFS (surface X-ray absorption fine structure) 1/527, 1/586  
 SFG (sum-frequency generation) 1/578  
 SHG (second harmonic generation) 1/579  
 shift correlation experiments 1/237ff  
 - accordion-HMQC experiment 1/239  
 - accordion-optimized direct correlation experiment ADSQC 1/239  
 - DEPT-HMQC 1/237  
 - multiplicity-edited GHSQC 1/238  
 sialidase 2/20  
 Siegbahn nomenclature 1/373  
 signal/background ratio 2/253  
 signal-to-background ratio 2/251f  
 SIM acquisition 2/251  
 SIM mode 2/260  
 SIM procedures 2/253  
 SIMCA 2/455  
 similarity measures 2/448  
 similarity search 2/497  
 SIMS (secondary ion mass spectrometry) 1/571  
 - dynamic mode 1/572  
 - state mode 1/571  
 simulated emission 1/427  
 simultaneous wavelength-dispersive spectrometers 1/393  
 single-channel instruments 1/392

- single-element techniques 1/412  
 single molecule detection 1/155  
 single nucleotide polymorphism studies  
   (SNP genotyping) 2/130  
 single quantum coherence (SQC) 1/176  
 singlet state 1/425  
 SiNPs 2/36  
 SLEELM (scanning low energy electron loss  
   microscopy) 1/562  
 slew-scan monochromator 1/480  
 slurry analysis 1/470  
 slurry nebulisation 1/483  
 small sample NMR 1/257 ff  
   – cryogenic NMR probe 1/260  
   – magic angle, liquid Nano-probe 1/258  
   –  $\mu$ -coil NMR probes 1/258  
   – SMIDG probe 1/258  
 Smith-Hieftje background correction  
   method 1/460 f  
 SNMS (secondary neutral mass  
   spectrometry) 1/533, 1/573  
 SNOM (scanning near-field optical  
   microscopy) 1/86, 1/571  
 sodium efflux  
   – in cells 2/11  
 sodium green 2/11  
 soft ionisation 1/332 ff  
   – interaces  
 – APCI 2/168  
 – ESI 2/168  
 – FAB 2/168  
 – TSP 2/168  
   – method 1/330  
 electrospray-ionisation 1/330  
 solid echo 1/278  
 solid phase extraction 1/345  
 solid sample introduction 1/452, 1/483 ff  
   – for AAS 1/470  
 solid samples 1/24  
 solid state NMR 1/174, 1/285  
   –  $^1\text{H}$  1/285  
 solid-phase microextraction 1/345, 2/127  
   – as sample 2/127  
   – prep in MS 2/127  
 solids 1/23  
 solid-state drift chamber 389  
 solid state NMR 1/173, 1/187  
 solute quenching 1/140 ff 1/141  
 solution state  $^1\text{H}$  NMR 1/171, 1/179  
 solvent quenching 1/143  
 solvent relaxation 1/144, 1/147  
 solvent suppression (in NMR) 2/104  
 sorbents 1/9 ff  
 space-charge effects 2/247 f, 2/249  
 SPAES (spin polarised Auger electron  
   spectroscopy) 1/512  
 spark 1/477, 1/484  
 speciation analysis 1/466  
 specimen preparation 1/416  
 SpecInfo 2/447, 2/491  
 SpecManager 2/502  
 SPECSOLV 2/482 f  
 SpecSurf 2/502  
 SpecTool 2/452  
 spectra library 2/247  
 spectra processing 2/442  
 spectra  
   – powder 1/276  
   – quantitative evaluation 2/455  
   – solid-state 1/277  
   – solution 1/277  
   – static powder 1/275 f  
 spectral buffering 1/455  
 spectral data bases, optical 2/447  
 spectral editing 1/283  
   – SS-APT 1/284  
 spectral interference in AES 1/486  
 spectral interferences 1/454 ff  
 spectral range  
   – MIR 1/89  
 spectral regions  
   – dead 1/49  
 spectral search 2/448  
 spectral similarity search 2/471  
 spectral simplification  
   – chemical modification 1/183  
   – selective decoupling 1/183  
   –  $^{13}\text{C}$  labeling 1/186  
   – deuteration 1/185  
   – self-decoupling 1/185  
 spectrometers  
   – AOTF 1/56  
   – diode array 1/56  
   – dispersive 1/48 f  
   – filter 1/56  
   – fluorescence 1/66  
   – Fouriertransform 1/50  
   – FT 1/48  
   – FT-NIR 1/55  
   – FT-Raman 1/61  
   – LED 1/56  
   – luminescence 1/66  
   – MIR 1/48  
   – multi-channel 1/63  
   – NIR 1/54  
   – Raman 1/57  
   – Raman grating 1/57  
   – scanning-grating 1/55

- UV/VIS 1/63
- vacuum 1/49
- spectroscopy
  - near-infrared 1/104
  - NIR 1/105
  - photoacoustic 1/97
  - Raman 1/112
- spectrum
  - emission 1/66
  - estimation 2/473
  - evaluation 1/405
  - excitation 1/66
  - prediction 2/474
- SPEELS (spin polarised electron energy loss spectroscopy) 1/575
- SPI (surface Penning ionisation) 1/551
- SPIES (surface Penning ionisation spectroscopy) 1/551
- spiking 1/412
- spin 1/172
  - spin angular momentum 1/423
  - spin decoupling 1/211
    - difference spectroscopy 1/212
    - selective population transfer (SPT) 1/211
    - spin ticking 1/211
  - spin-diffusion 2/111
  - spin-lattice 1/217
    - inversion-recovery 1/217
  - spin quantum number 1/423
  - spinning-sideband patterns
    - $^1\text{H}$ - $^1\text{H}$  DQ MAS 1/305
- SPIPES (spin polarised inverse photoelectron spectroscopy) 1/536 f
- spirobenzopyran 2/70
- SPMP (scanning proton microprobe) 1/539
- spontaneous decay 1/428
- spontaneous emission 1/427
- SPR biosensors 2/85 f
- SPR spectroscopy (surface plasmon resonance spectroscopy) 1/579
- Spreeta™ device 2/87
- SPUPS (spin polarised ultraviolet photo-electron spectroscopy) 1/508, 1/576, 1/584
- squaraine dyes 2/34
  - benz[e]indolium Sq660 2/35
- squarilium dyes
  - signal ransducing 2/71
- squaryliums 2/32
- SRPES (synchrotron radiation photoelectron spectroscopy) 1/588
- SRUPS (spin-resolved ultraviolet photo-emission spectroscopy) 1/537
- standard addition 1/410
- standard temperature 1/433
- standardization (autoscaling) 2/443
- standardization reagents
  - flow cytometry 2/57
  - microscopy 2/57
- Staphylococcus Aureus* (Cowan-1 strain) 2/84
- Stark line broadening 1/431
- Statgraphics 2/467
- static quenching 1/140
- Statistica 2/467
- statistics of sampling 1/18 ff
- step-scan 1/53
- stereochemical effects 2/478
- stereochemical interactions 2/480
- Stern-Volmer equation 1/141
- STIRS 2/496
- Stokes lines 1/43
- Stokes-shift 1/146, 2/10
- Stokes-Einstein 1/141
- storage ring 1/383
- streptavidin (SAv) 2/29
- streptomycin
  - residues in whole milk 2/87
- structural diversity 2/475
- structure elucidation 2/469
- STS (scanning tunneling spectroscopy) 1/570 ff
- styryl dyes (ANEP) 2/19
- $\beta$ -subunit of human chorionic gonadotropin (hCG) 2/56
- sulfide 2/14
  - probing of dynamic changes of red cell membrane 2/14
- 5-sulfofluorescein diacetate 2/11
- sulfonic acids 2/208
  - ion-pairing 2/209
  - leachates 2/208
  - MS/MS 2/208
  - plumes of landfills 2/209
  - quantification 2/208 f
  - textile wastewater 2/209
- sulfonylureas
  - agricultural soil 2/222
  - chemical degradation 2/222
  - crop 2/222
  - degradation products 2/220, 2/222
  - estuarine waters 2/220
  - fruits 2/222
  - metabolites 2/222
  - MS/MS 2/221 f
  - natural waters 2/221
  - photolysis products 2/222
  - quantification 2/220 ff
  - river water 2/221
  - surface water 2/221

- superconducting magnets 1/342
- supercritical-fluid extraction 1/346
- supervised learning 2/444
- surface
  - analysis technique
    - acronyms 1/594
    - classification 1/499
    - selection 1/501
    - type of information 1/505
  - cleanliness 1/514
  - concentration 1/501
  - contamination 1/506, 1/581, 1/590
  - definition 1/501
  - diffusion 1/555
  - enhanced fluorescence, SEF 2/91 ff
  - enhanced fluoroimmunoassay, SE-FIA 2/91
  - enhanced IR absorption, SEIRA 2/91
  - enhanced Raman scattering (SERS) 1/120, 2/93 ff
  - enhanced Raman spectroscopy (SERS) 2/93 ff
  - experimental 1/501
  - physical 1/501
  - plasmon 2/85
  - plasmon resonance (SPR) 2/81, 2/85
    - fiber and waveguide SPR 2/88
  - probe technique 1/499
  - resolution 1/502
  - selection rule 1/560
  - specificity 1/502
- surfactants 2/154, 2/189 f, 2/209 ff
- alcohol ethoxylate (AOE) 2/189 f, 2/209 f, 2/213
- alkylether carboxylates 2/190
- alkyl etoxysulfates (AES) 2/211
- alkyl polyglucamides 2/190
- alkyl polyglucosides 2/190, 2/212
- alkyl sulfates (AS) 2/211
  - APEO
    - halogenated 2/191
  - betaine 2/190
  - biodegradation 2/211 f
  - CDEA 2/190
  - coastal waters 2/211
  - coconut diethanol amide (CDEA) 2/189, 2/213
  - ditallow-dimethylammonium chloride (DTDMAC) 2/212
  - effluents 2/211
  - EO/PO compounds 2/190
  - estuaries 2/212
  - fatty acid polyglycol amines 2/190
  - gemini 2/190
- German Bright 2/212
- halogenated APEOs 2/191, 2/211
- halogenated NPEO 2/210
- ion chromatograph 2/214
- LAS 2/189, 2/211 ff
- NPEO 2/189 f
- NPEO-sulfate 2/189
- metabolites 2/209 f
- N-methylglucamides 2/212
- MS/MS 2/209 ff
- neutral loss (NL) 2/209 f
- nonylphenolpolyether carboxylate (NPEC) 2/210
- North Sea 2/212
- NPEO 2/209 ff
- NPEO sulfates 2/213
- OPEO 2/211
- perfluorooctanesulfonate (PFOS) 2/212
- perfluorooctanoic acid (PFOA) 2/212
- quantification 2/191, 2/210 ff
- quaternary ammonium compounds 2/214
- quaternary carboxoalkyl ammonium compounds 2/190
- sea water 2/212
- secondary alkane sulfonate (SAS) 2/189, 2/213
- sediment 2/212
- SPE concentrated analytes 2/190
- stability 2/190
- stability of SPE concentrated analytes 2/190
- sulfobetaine 2/190
- sulfosuccinates 2/190
- toxins 2/213
- Waddensea marinas 2/212
- wastewater 2/210 f
- wastewater inflows 2/211
- SXAPS (soft X-ray appearance potential spectroscopy) 1/508
- SXPS (soft X-ray photoelectron spectroscopy) 1/588
- SYBR 2/16
- SYBR Green 2/18
- synaptic transmission 2/13
- synchrotron radiation facilities 1/380
- SYPRO 2/16
- SYTO 2/16
- SYTOX Dyes 2/17

**t**

- TAG 2/33
- TAMRA 2/40
- tandem mass spectrometry (MS/MS) 2/122, 2/124, 2/168 ff, 2/257

- collision-induced dissociation (CID) 2/168
- discharge-on 2/169
- filament-on 2/169
- in-source-CID 2/169
- MS<sup>n</sup> 2/168
- TCS (total (or target) current spectroscopy) 1/510
- technique
- microsampling 1/98
- sampling 1/94
- TEELS (transmission electron energy loss spectroscopy) 1/535, 1/562
- TEM (transmission electron microscopes) 1/535, 1/562
- temperature of different excitation sources 1/436
- temperature, electron 1/435 f
- temperature, excitation 1/435 f
- temperature, gas 1/435 f
- temperature, ionisation 1/435 f
- temperature, rotational 1/434, 1/436
- tensors
  - quadrupolar 1/273
- term scheme 1/425
- tertiary structure 1/349
- tertiary structure characterisation 353
- tetracycline antibiotics 2/68
- tetraethylrhodamine derivatives 2/29
- tetramethylrhodamine isothiocyanata 2/29
- Texas Red 2/51
- thallium acid phthalate 1/391
- thermoelectrically cooled ED detectors 1/389
- thermometric probe 1/434
- Thermoquest 2/266
- thermoreflectance 1/561
- thermospray ionization (TSP) 2/172 ff
  - fungicides 2/172
  - herbicides 2/172
  - pesticides 2/172
  - sulfonated azo dyes 2/172
  - surfactants 2/172
- thia-carbocyanines 2/19
- thiazole green (TAG) 2/33
- thiazole orange 2/29
- thin film approach 1/412
- thin films 1/77
- thin samples 1/96
- thin-film samples 1/402
- thiol
  - indicatory for red cell membrane, probing 2/14
- thioureas
  - agricultural soil 2/222
  - chemical degradation 2/222
- crop 2/222
- degradation products 2/220, 2/222
- estuarine waters 2/220
- fruits 2/222
- metabolites 2/222
- MS/MS 2/221 f
- natural waters 2/221
- photolysis products 2/222
- quantification 2/220 ff
- river water 2/221
- surface water 2/196, 2/221
- water 2/196
- three-dimensional arrangement of elements 1/510
- three-photon excitation (3PE) 2/58
- thrombin 2/24
- thyroid-stimulating hormone (TSH) 2/83
- TIAFT 2/494
- time of flight 1/338
- time-resolved emission spectra 1/146
- time-resolved fluorescence 2/10, 2/55
- time-resolved fluorescence polarization 1/150
- time-resolved surface enhanced fluorescence 2/91
- Ti-Saphire laser 2/45
- titanium dioxide waveguide 2/83
- TMA-DPH 1/151
- TO 2/29
- tobacco mosaic virus (TMV) 2/101
- TOCSY 1/173
- TOF ERDA (time-of-flight ERDA) 1/522
- TOF-SIMS 2/125
- TO-PRO 2/17
- Torch 1/473, 1/474
- torsion modes 1/42
- torsional angle 1/298, 1/312
- total angular momentum 1/423
- total correlation spectroscopy (TOCSY)
  - [homonuclear Hartmann-Hahn (HOHAHA)] 2/109
- total internal reflection (TIR) 2/72 f
- total internal reflection fluorescence (TIRF) 1/155, 2/91 ff
- total quantum number 1/423
- total suppression of sidebands 1/282
- TOTO 2/17
- TOTO dimers
  - synthesis of 2/29
- toxicological analysis 1/344
- toxins 2/154, 2/213
  - CE-MS 2/213
  - LC-MS 2/213
  - MS/MS 2/213
  - seafood 2/213

- training set 2/456
- trans and gauche conformations 1/298
- TransFluorSpheres 2/57
- transformation
  - Fourier 1/51
  - Kubelka-Munk 1/97
- transition
  - charge transfer 1/132, 1/134
  - d-d 1/132
  - electronic 1/125
  - n→π\* 1/132
  - π→π\* 1/132
  - semiconductors 1/134
  - single-quantum 1/273
- transmissible spongiform encephalopathy (TSE) 2/6
- transmission measurements 1/71
- transmission spectroscopy 1/582
- transverse electric (TE) wave 2/72
- transverse magnetic (TM) wave 2/72
- transverse relaxation 2/98
- transverse relaxation optimized spectroscopy (TROSY) 2/95, 2/98
- transverse resonance condition 2/78
- trapped-ion mass analysers 1/339
  - dynamic traps 1/339
  - ion cyclotron resonance 1/339
  - static traps 1/339
- trapping efficiency 2/244
- TR-FIA 2/55
- triazine 2/88, 2/181f, 2/223
  - APCI-FIA-MS 2/199
  - APCI-FIA-MS/MS 2/199
  - APCI-LC-MS 2/199
  - degradation pathways 2/182
  - degradation products 2/182, 2/198, 2/223
  - drinking water 2/223
  - estuarine waters 2/182
  - groundwater 2/223
  - metabolites 2/224
  - MS/MS 2/224f
  - natural waters 2/198
  - photolysis 2/224
  - physicochemical degradation 2/224
  - quantification 2/223ff
  - rivers 2/198
  - river water 2/223
  - SFC-MS 2/223
  - soil samples 2/182
  - stability 2/198
  - surface water 2/198
  - water 2/198
- trifluorofluoresceins (Oregon Green) 2/11
- trinitrotoluene (TNT) 2/87
- triple resonance experiments (in NMR) 2/119
- triplet state 1/425
- TRITC *see* tetramethylrhodamine isothiocyanata
- trivial quenching 1/144
- TRXRFA (total reflection X-ray fluorescence analysis) 1/550
- tryptophans 1/141, 2/15
- TSE *see* transmissible spongiform encephalopathy
- TSP
  - alcohol ethoxylates (AOE) 2/175
  - alkyl polyglucosides 2/175
  - anilides 1/176
  - carbamates 2/177 ff
    - interlaboratory examination 2/178
    - quantification 2/177
  - degradation pathways 2/182
  - degradation products 2/182
  - dyes 2/173
  - EEC Drinking Water Directive 2/178
  - estuarine waters 2/182
  - explosives 2/174
  - fluorine-containing surfactants 2/175
  - fungicides 2/176, 2/183
  - herbicides 2/176, 2/183
  - miscellaneous 2/183
  - organophosphorus compounds 2/179
    - quantification 2/179
  - pesticides 2/176
  - phenoxyacrylic acids 2/179
  - phenylureas 2/180
  - polycyclic aromatic hydrocarbons (PAH) 2/174
  - quantification 2/180f
  - quaternary amines 2/176
  - seafood 2/176
  - soil samples 2/182
  - sulfonylureas 2/180
  - surfactants 2/175
  - thiocyanate 2/176
  - thioureas 2/180
  - toluidines 2/176
  - toxins 2/176
  - triazines 2/181
  - urea
    - interlaboratory study 2/181
  - urea pesticides 2/180
    - quantification 2/180
- TSP, LC-MS 2/172 ff
  - anilides 2/173
  - carbamates 2/173
  - dyes 2/173
  - explosives 2/173

- fungicides 2/173
- herbicides 2/173
- organophosphorus compounds 2/173
- pesticides 2/172 f
- phenoxycarboxylic acids 2/173
- phenylureas 2/173
- polycyclic aromatic hydrocarbons 2/173
- quaternary amines 2/173
- sulfonylureas 2/173
- surfactants 2/172
- thiocyanate 2/173
- thioureas 2/173
- toluidines 2/173
- toxins 2/173
- triazines 2/173
- TSP, review
  - dyes 2/173
  - general 2/173
  - pesticides 2/172
  - surfactants 2/172
- tubulin
  - conjugates 2/17
  - transport in neurons 2/17
- twisting 1/42
- two line background correction 1/456 f
- two-dimensional (2D) NMR 1/292
  - heteronuclear 1/292
  - homonuclear 1/292
- two-dimensional (2D) NMR experiment 2/105
- two-dimensional experiments
  - anisotropic-isotropic correlation 1/300
  - CSAs 1/300
- two-dimensional HPLC 2/127
  - as sample 2/127
  - prep in MS 2/127
- two-dimensional NMR 1/218
- two-photon excitation (2PE) 2/58
- two-photon fluorescence excitation 2/61
  - single step bioaffinity assays 2/58
- TXRF or TRXRF (total reflection X-ray fluorescence) 1/580
- type standardization 1/410, 1/412
- tyramide signal amplification (TSA) 2/16
- tyramide-labeled dyes 2/16
- tyrosine 2/15
  
- u**
- UHV (ultra high vacuum) 1/506
- Ulbricht sphere 1/79
- ULS 2/18
- ungicides 2/192
  - groundwater 2/192
  - river water 2/192
- univariate methods 2/456
- Universal Linkage System (ULS) 2/18
- Unscrambler 2/467
- unsupervised learning 2/444
- UPES, UVPES, UPS, UVPS (ultraviolet photoelectron spectroscopy) 1/583
- UPS (ultraviolet photoelectron spectroscopy) 1/508, 1/591
- urea 2/69
- urea pesticides
  - quantification 2/180
- uric acid 2/21
- UV shifts due to structure 2/382
- UV/VIS
  - absorption 1/44
  - spectroscopy 1/125
  - structural analysis 1/129
  
- v**
- vapour generation techniques 1/447 ff
- variable angle correlation spectroscopy (VACSY) 1/300
- Varian Inc. 2/266
- vibration
  - normal 1/99
- vibrational circular dichroism (VCD) 2/94
- vibrational mode 1/558, 1/578
- vibrational relaxation 1/45
- vibrations
  - combination 1/54, 1/104
  - overtone 1/54, 1/104
  - stretching 1/42
- VIS/NIR dyes 2/28
- volatile organic compounds (VOCs) 2/256
  
- w**
- wagging modes 1/42
- Walsh 1/436
- water analysis 2/154
- waveguides 2/78 f
  - monomodal 2/79
  - multimodal 2/79
- wavelength 1/367
- wavelength modulation background correction 1/462
- wavelength-dispersive XRF 1/390
- wavenumber 1/39
- weakly aligned systems 2/95
- WebBook 2/490, 2/500
- wheat germ agglutinin (WGA) 2/21
- white optics 1/91
- Wilatz 1/436
- Wiley Registry of Mass Spectral Data 2/491
- Wiley-SIMS database 2/494

- window material 1/71  
windowless homonuclear decoupling sequences  
– DUMBO-1 1/299  
– FSLG 1/299  
– PMLG 1/299  
WISE (wide line separation) 1/176  
Wollaston 1/436  
Woodward 1/125
- x**  
XAES (X-ray absorption fine structure) 1/584  
XANES (X-ray absorption near edge spectroscopy) 1/584  
xanthenes 2/10  
xantine 2/21  
XAPS (X-ray appearance potential spectroscopy) 1/508  
XCORFE 1/248  
XEAES (X-ray excited Auger electron spectroscopy) 1/512  
xenoestrogens 2/154  
xenon arc lamp 1/439
- Xenon for IR detection 2/420  
XNDO/S 2/28  
XPD (X-ray photoelectron diffraction) 1/586, 1/591  
XPS or XPES (X-ray photoelectron spectroscopy) 1/587  
X-ray crystallography 2/6  
X-ray detectors 1/384  
X-ray fluorescence 2/429  
XRF (X-ray induced fluorescence) 1/550  
XSW (X-ray standing wave) 1/591
- y**  
YO-PRO 2/17  
YOYO 2/17
- z**  
Zeeman background correction 1/458 ff  
Zeeman effect, anomalous 1/458  
Zeeman effect, longitudinal 1/460  
Zeeman effect, normal 1/458  
Zeeman effect, transverse 1/458  
zinc selenide 2/78